Volume 192 Number 1

THE BIOLOGICAL BULLETIN

FEBRUARY, 1997

Published by the Marine Biological Laboratory

Charles Baker Metz

As this issue of *The Biological Bulletin* went to press, we learned that Editorial Board Member and former Editor Charles B. Metz had passed away on 14 January 1997, in Homestead, Florida. He was 80 years old.

Biological Bulletin Publications

http://www.mbl.edu/BiologicalBulletin/

The home page for the electronic companion to *The Biological Bulletin—the Marine Models Electronic Record*—and other *Biological Bulletin* publications is available on the World Wide Web at the address shown above.

THE
BIOLOGICAL BULLETIN

PUBLISHED BY

THE MARINE BIOLOGICAL LABORATORY

FEBRUARY, 1997

Printed and Issued by
LANCASTER PRESS, Inc.
3575 HEMPLAND ROAD
LANCASTER, PA

THE BIOLOGICAL BULLETIN

THE BIOLOGICAL BULLETIN is published six times a year by the Marine Biological Laboratory, 7 MBL Street, Woods Hole, Massachusetts 02543.

Subscriptions and similar matter should be addressed to Subscription Manager, THE BIOLOGICAL BULLETIN, Marine Biological Laboratory, 7 MBL Street, Woods Hole, Massachusetts 02543. For 1997, a lower rate is available to individual subscribers (as distinguished from libraries and institutions). Single numbers: $40 for libraries; $20 for individuals. Subscription per volume (three issues): $97.50 for libraries; $50 for individuals. Subscription per year (six issues, two volumes): $195 for libraries; $100 for individuals.

Communications relative to manuscripts should be sent to Michael J. Greenberg, Editor-in-Chief, or Pamela L. Clapp, Managing Editor, at the Marine Biological Laboratory, 7 MBL Street, Woods Hole, Massachusetts 02543. Telephone: (508) 289-7428. FAX: 508-457-1924. E-mail: pclapp@mbl.edu.

http://www.mbl.edu/BiologicalBulletin/

The home page for the electronic companion to THE BIOLOGICAL BULLETIN—*the Marine Models Electronic Record*—and other BIOLOGICAL BULLETIN publications is available on the World Wide Web at the address shown above.

THE BIOLOGICAL BULLETIN is indexed in bibliographic services including *Index Medicus* and MEDLINE, *Chemical Abstracts, Current Contents*, and *CABS (Current Awareness in Biological Sciences)*.
Printed on acid free paper,
effective with Volume 180, Issue 1, 1991.

POSTMASTER: Send address changes to THE BIOLOGICAL BULLETIN, Marine Biological Laboratory, 7 MBL Street, Woods Hole, MA 02543.

Periodicals postage paid at Woods Hole, MA, and additional mailing offices.
ISSN 0006-3185

INSTRUCTIONS TO AUTHORS

The Biological Bulletin accepts outstanding original research reports of general interest to biologists throughout the world. Papers are usually of intermediate length (10–40 manuscript pages). A limited number of solicited review papers may be accepted after formal review. A paper will usually appear within four months after its acceptance.

Very short, especially topical papers (less than 9 manuscript pages including tables, figures, and bibliography) will be published in a separate section entitled "Research Notes." A Research Note in *The Biological Bulletin* follows the format of similar notes in *Nature*. It should open with a summary paragraph of 150 to 200 words comprising the introduction and the conclusions. The rest of the text should continue on without subheadings, and there should be no more than 30 references. References should be referred to in the text by number, and listed in the Literature Cited section in the order that they appear in the text. Unlike references in *Nature*, references in the Research Notes section should conform in punctuation and arrangement to the style of recent issues of *The Biological Bulletin*. Materials and Methods should be incorporated into appropriate figure legends. See the article by Lohmann *et al.* (October 1990, Vol. **179**: 214–218) for sample style. A Research Note will usually appear within two months after its acceptance.

The Editorial Board requests that regular manuscripts conform to the requirements set below; those manuscripts that do not conform will be returned to authors for correction before review.

1. ***Manuscripts.*** Manuscripts, including figures, should be submitted in triplicate. (Xerox copies of photographs are not acceptable for review purposes.) The submission letter accompanying the manuscript should include a telephone number, a FAX number, and (if possible) an E-mail address for the corresponding author. The original manuscript must be typed in no smaller than 12 pitch or 10 point, using double spacing (*including* figure legends, footnotes, bibliography, etc.) on one side of 16- or 20-lb. bond paper, 8½ by 11 inches. Please, no right justification. Manuscripts should be proofread carefully and errors corrected legibly in black ink. Pages should be numbered consecutively. Margins on all sides should be at least 1 inch (2.5 cm). Manuscripts should conform to the *Council of Biology Editors Style Manual*, 5th Edition (Council of Biology Editors, 1983) and to American spelling. Unusual abbreviations should be kept to a minimum and should be spelled out on first reference as well as defined in a footnote on the title page. Manuscripts should be divided into the following components: Title page, Abstract (of no more than 200 words), Introduction, Materials and Methods, Results, Discussion, Acknowledgments, Literature Cited, Tables, and Figure Legends. In addition, authors should supply a list of words and phrases under which the article should be indexed.

2. ***Title page.*** The title page consists of a condensed title or running head of no more than 35 letters and spaces, the manuscript title, authors' names and appropriate addresses,

and footnotes listing present addresses, acknowledgments or contribution numbers, and explanation of unusual abbreviations.

3. ***Figures.*** The dimensions of the printed page, 7 by 9 inches, should be kept in mind in preparing figures for publication. We recommend that figures be about 1½ times the linear dimensions of the final printing desired, and that the ratio of the largest to the smallest letter or number and of the thickest to the thinnest line not exceed 1:1.5. Explanatory matter generally should be included in legends, although axes should always be identified on the illustration itself. Figures should be prepared for reproduction as either line cuts or halftones. Figures to be reproduced as line cuts should be unmounted glossy photographic reproductions or drawn in black ink on white paper, good-quality tracing cloth or plastic, or blue-lined coordinate paper. Those to be reproduced as halftones should be mounted on board, with both designating numbers or letters and scale bars affixed directly to the figures. All figures should be numbered in consecutive order, with no distinction between text and plate figures. The author's name and an arrow indicating orientation should appear on the reverse side of all figures.

4. ***Tables, footnotes, figure legends, etc.*** Authors should follow the style in a recent issue of *The Biological Bulletin* in preparing table headings, figure legends, and the like. Because of the high cost of setting tabular material in type, authors are asked to limit such material as much as possible. Tables, with their headings and footnotes, should be typed on separate sheets, numbered with consecutive Roman numerals, and placed after the Literature Cited. Figure legends should contain enough information to make the figure intelligible separate from the text. Legends should be typed double spaced, with consecutive Arabic numbers, on a separate sheet at the end of the paper. Footnotes should be limited to authors' current addresses, acknowledgments or contribution numbers, and explanation of unusual abbreviations. All such footnotes should appear on the title page. Footnotes are not normally permitted in the body of the text.

5. ***Literature cited.*** In the text, literature should be cited by the Harvard system, with papers by more than two authors cited as Jones *et al.*, 1980. Personal communications and material in preparation or in press should be cited in the text only, with author's initials and institutions, unless the material has been formally accepted and a volume number can be supplied. The list of references following the text should be headed Literature Cited, and must be typed double spaced on separate pages, conforming in punctuation and arrangement to the style of recent issues of *The Biological Bulletin*. Citations should include complete titles and inclusive pagination. Journal abbreviations should normally follow those of the U. S. A. Standards Institute (USASI), as adopted by BIOLOGICAL ABSTRACTS and CHEMICAL ABSTRACTS, with the minor differences set out below. The most generally useful list of biological journal titles is that published each year by BIOLOGICAL ABSTRACTS (BIOSIS List of Serials; the most recent issue). Foreign authors, and others who are accustomed to using THE WORLD LIST OF SCIENTIFIC PERIODICALS, may find a booklet published by the Biological Council of the U.K. (obtainable from the Institute of Biology, 41 Queen's Gate, London, S.W.7, England, U.K.) useful, since it sets out the WORLD LIST abbreviations for most biological journals with notes of the USASI abbreviations where these differ. CHEMICAL ABSTRACTS publishes quarterly supplements of additional abbreviations. The following points of reference style for THE BIOLOGICAL BULLETIN differ from USASI (or modified WORLD LIST) usage:

A. Journal abbreviations, and book titles, all underlined (for *italics*)

B. All components of abbreviations with initial capitals (not as European usage in WORLD LIST *e.g., J. Cell. Comp. Physiol.* NOT *J. cell. comp. Physiol.*)

C. *All* abbreviated components must be followed by a period, whole word components *must not* (*i.e., J. Cancer Res.*)

D. Space between all components (*e.g., J. Cell. Comp. Physiol.*, not *J.Cell.Comp.Physiol.*)

E. Unusual words in journal titles should be spelled out in full, rather than employing new abbreviations invented by the author. For example, use *Rit Vísindafjélags Islendinga* without abbreviation.

F. All single word journal titles in full (*e.g., Veliger, Ecology, Brain*).

G. The order of abbreviated components should be the same as the word order of the complete title (*i.e., Proc.* and *Trans.* placed where they appear, not transposed as in some BIOLOGICAL ABSTRACTS listings).

H. A few well-known international journals in their preferred forms rather than WORLD LIST or USASI usage (*e.g., Nature, Science, Evolution* NOT *Nature, Lond., Science, N.Y., Evolution, Lancaster, Pa.*)

6. ***Reprints, page proofs, and charges.*** Authors receive their first 100 reprints (without covers) free of charge. Additional reprints may be ordered at time of publication and normally will be delivered about two to three months after the issue date. Authors (or delegates for foreign authors) will receive page proofs of articles shortly before publication. They will be charged the current cost of printers' time for corrections to these (other than corrections of printers' or editors' errors). Other than these charges for authors' alterations. *The Biological Bulletin* does not have page charges.

ERRATUM

The Biological Bulletin, Volume **191**, Number 3, page 409

The following correction should be made in the article by Fraser M. Shilling, Ove Hoegh-Guldberg, and Donal T. Manahan, titled "Sources of energy for increased metabolic demand during metamorphosis of the abalone *Haliotis rufescens* (Mollusca)" (*Biol. Bull.* **191:** 402–412).

In Table II on page 409, the value for "Energy balance: Ratio of available to required energy" should be a percentage; that is, it should read 38.7%, not 38.7.

Reference: *Biol. Bull.* **192**: 1–16. (February, 1997)

Coelenterate Cnidae Capsules: Disulfide Linkages Revealed by Silver Cytochemistry and Their Differential Responses to Thiol Reagents

WALTER M. GOLDBERG AND GEORGE T. TAYLOR

Electron Microscopy Laboratory, Department of Biological Sciences, Florida International University, University Park, Miami, Florida 33199

Abstract. The sulfur cytochemistry of cnidae from the Portuguese man-of-war *Physalia physalis*, the scyphozoan *Cassiopeia xamachana*, and the black coral *Cirrhipathes luetkeni* was evaluated on the basis of electron microscopy, X-ray microanalysis, amino acid analysis, and response to disulfide reducing agents. The cnidae examined included large and small holotrichous isorhizas in *P. physalis*, another small isorhiza in *C. xamachana*, and both spirocysts and microbasic mastigophore nematocysts in *C. leutkeni*. A strong reaction with methenamine-silver reagent was characteristic of all cnidae capsules, but the pattern and extent of that argentophilia was dependent upon the type of cnida and its state of maturity. The large isorhizas of *P. physalis* reacted primarily in the outermost capsule layers, but in *C. xamachana* isorhizas, silver stained the entire capsule with the exception of the outermost region. The small isorhizas of *P. physalis* and the mastigophore capsules of *C. leutkeni* stained throughout, whereas the spirocyst capsules were outlined by silver, clearly delineating the inner and outer layers. All of these reactions were abolished with alkylation, but only after treatment with disulfide reducing agents; alkylation alone diminished silver staining only slightly, indicating that the argentophilic response was due primarily to disulfide linkages. The cystine content of these cnidae varied from 4.1 to 4.7 mole percent for a given species, but amino acid analyses did not separate components of the cnidom.

Cnidae, both within and among species, exhibited differential responses to the disulfide reducing agent dithiothreitol (DTT). Isolated, unfixed, large isorhizas of *P. physalis* discharged and appeared to dissolve rapidly in the presence of this reagent, whereas small isorhizas from both *P. physalis* and *C. xamachana* discharged, but dissolved slowly if at all. The discharge and solution responses of the capsule coincided with the complete development of the tubule. Cnidae containing an undeveloped or partially developed tubule were resistant to DTT, displayed a weak capsular argentophilia, and contained background levels of sulfur; these results suggest that formation of disulfide linkages is one of the final steps in capsular maturation. In contrast, mature nematocyst and spirocyst capsules in *C. leutkeni* tentacles were resistant to DTT among other reagents, despite the presence of disulfides. This suggests that other types of covalent, intermolecular linkages could play a prominent role in the development of capsular stability in this species.

Received 17 July 1996; accepted 16 October 1996.

Introduction

Coelenterate cnidae are among the most complex intracellular secretion products known (Gupta and Hall, 1984). Each is composed of a double-walled capsule containing an inverted tubule. During eversion the tubule discharges explosively, completing the process within 3 ms, one of the fastest mechanical events known in the biological sciences (Holstein and Tardent, 1984). More than 30 types of cnidae have been described, and they are classified into three groups: nematocysts, spirocysts, and ptychocysts (*e.g.*, Mariscal, 1974, 1984). Hydrozoans have the greatest variety of nematocysts, and scyphozoans have the least, but only anthozoans produce all three types. Ptychocysts occur only in cerianthid anemones and are the most phylogenetically restricted of the cnidae. Spirocysts are also limited in their distribution,

occurring only in the tentacles of various anthozoans; but spirocysts are also quite common, often outnumbering tentacular nematocysts (Mariscal and McLean, 1976; Goldberg and Taylor, 1989).

Nematocysts in particular have been examined closely, yielding details of structure and function relationships. For example, upon discharge, the capsule must withstand internal pressures of up to 140 bar during eversion (Lubbock and Amos, 1981; Tardent, 1988), a feat requiring enormous tensile strength. Recent work has shown that disulfide-linked, woven mini-collagens composing the internal wall of the nematocyst capsule (Kurz *et al.*, 1991) may be the key structural element in the resistance of these cnidae to such pressures. The tensile strength derived from this capsule structure is estimated to be nearly as high as that of steel (Holstein *et al.*, 1994).

The occurrence of disulfide-linked collagens in nematocysts was first established by Blanquet and Lenhoff (1966) after the suggestion by Brown (1950), and subsequently by Yanagita and Wada (1954), that since coelenterate cnidae are soluble in disulfide reducing agents, they might be composed of keratins. Hamon (1955) confirmed the earlier observations of disulfide linkages by demonstrating the presence of cystine histochemically. However, Blanquet and Lenhoff clearly showed that cystine is responsible for stabilizing collagenous proteins, the dominant components of the nematocyst capsule. They also showed that the cnidae at their disposal dissolved in a number of disulfide reducing agents including dithiothreitol, sodium thioglycolate, and mercaptoethanol.

Disulfide linkages have since been shown to be widespread in nematocyst capsules judging from amino acid composition (Fishman and Levy, 1967; Blanquet, 1988; Brand *et al.*, 1993) and X-ray microanalysis revealing the presence of sulfur (Mariscal, 1980, 1984, 1988). However, although the nematocysts from a variety of cnidarians dissolve quickly in disulfide reducing agents as might be predicted, some nematocysts and spirocysts appear to be resistant to such treatment (Mariscal and Lenhoff, 1969; Mariscal, 1971). Despite a number of subsequent chemical studies (see review by Blanquet, 1988; Brand *et al.*, 1993), little progress has been made in answering the questions raised by Mariscal and Lenhoff's original observations. To this end, we have examined the chemistry of cnidae capsules in three coelenterates, each representing a class within the phylum. The sulfur cytochemistry of each type of cnida is confirmed by X-ray microanalysis and correlated with amino acid composition, degree of maturity, and response to disulfide reducing agents.

Materials and Methods

Microscopy

Three species were collected for this study, including *Physalia physalis* Lamarck (Hydrozoa: Siphonophora) from various localities in southeast Florida; *Cassiopeia xamachana* Bigelow (Scyphozoa: Rhizostomae) from several nearshore locations in the Florida Keys, and *Cirrhipathes luetkeni* Brook (Anthozoa: Antipatharia) from a depth of 25 m off Hollywood, Florida.

Nematocyst batteries separated from fixed tentacles of *P. physalis*, individual tentacles isolated from *C. luetkeni* polyps, and oral vesicles—the baglike, oval structures associated with the oral arms (see Bigelow, 1900)—from *C. xamachana* were dissected using iridectomy scissors under low-power microscopy. All of these cnidae-containing structures, referred to as tentacles or tentacular tissues, were prepared for transmission electron microscopy (TEM) by fixation at room temperature for 2–4 h in an artificial seawater solution containing 2.5% glutaraldehyde and 1.0% paraformaldehyde in 0.1 *M* cacodylate buffer at pH 8.0. The tissue was then stored in 0.1 *M* cacodylate buffer at 4°C. Post-fixation with osmium is incompatible with silver staining (*e.g.*, Hayat, 1993) and was omitted. Tentacular tissues were dehydrated through ethanols and embedded in Spurr resin. Thick sections examined in the light microscope were contrasted with 0.1% toluidine blue in 1% borax. For TEM we used a Philips EM 300 electron microscope operated at 60 kv. No contrast agents other than silver were employed in transmission microscopy.

Cnidae fixed as above were also examined by scanning electron microscopy (SEM). Aldehyde fixation was followed by osmication using 1% OsO_4 in 0.1 *M* cacodylate buffer, pH 8.0, for 1 h at room temperature. Dehydration in ethanols was followed by critical point drying (CPD) with CO_2 as the transitional fluid, or by cryofracture from 100% ethanol in liquid nitrogen prior to CPD. Tentacles were then sputter-coated with Au-Pd and examined in an ISI Super 3A scanning electron microscope operated at 10 or 15 kv.

Silver staining for disulfide groups

The methenamine-silver stain (Rambourg 1967; Locke and Krishnan, 1971) was employed for general electron contrast and sulfur cytochemistry. All reagents were made fresh daily using double-distilled, deionized (ddd) water, and all steps employed constant agitation on an orbital rotator. Fixed tentacular tissues were rinsed several times in ddd-water, then treated with 5% sodium metabisulfite for 10 min to block pre-existing aldehyde groups or those introduced by the fixative. After washing in three additional changes of ddd-water, tissues were immersed in methenamine-silver reagent and placed in closed 1.5-ml polypropylene microcentrifuge tubes in a 70°C oven for 30 min. After a brief ddd-water rinse, all tissues were treated with 5% sodium thiosulfate to remove unreduced silver deposits, then rinsed with ddd-water again before dehydration and embedment.

Cytochemical control procedures

Before silver staining, additional aldehyde-fixed tentacles were treated with the disulfide reducing agent dithiothreitol (=DTT, Cleland's reagent) 0.2 *M* in 0.05 *M* phosphate buffer pH 8.0 at 37°C for 90 min. Some samples were stained with methenamine-silver and examined without further treatment; others were treated with iodoacetic acid to alkylate naturally occurring sulfhydryl groups as well as those produced by disulfide reduction (alkylation blockade). Iodoacetic acid (0.1 *M*) was prepared with 0.2 *M* boric acid in 50% *N*-propanol according to the method of Swift (1968). Because we used tissue rather than sections, the reaction time for this blockade was extended from 4 h at room temperature to 18 h. Blockaded tissues were rinsed first with 20% *N*-propanol, then several times with ddd-water, and treated with methenamine-silver as above. Samples treated with iodoacetic acid alone prepared as above, or with the boric acid–propanol solvent alone, were also examined both with and without silver treatment, as were tissues treated with DTT alone. Parallel experiments employed alkaline 0.3 *M* thioglycolic acid prepared and used under the same conditions as DTT for disulfide reduction, and 0.1 *M N*-ethyl maleimide prepared according to Kiernan (1990) to block sulfhydryl groups. These sequential control treatments (disulfide reduction followed by alkyl bockade) will be referred to as post-reduction alkylation.

Elemental composition

Sections about 100-nm thick (dark gold interference color) from tissues treated with methenamine-silver were mounted on carbon-coated copper grids and examined in a Philips EM 300 transmission electron microscope operating at 100 kv. X-ray microanalysis employed a Link Analytical EDS system. The goniometer was tilted at 36° and counts were obtained using a spot size of 250 nm over an interval of 600 s real time. Count rates were 1800–2500 cps; dead time varied from 20% to 25%. No fewer than four undischarged cnidae of each type (described below) were scanned, including two types of nematocysts from *P. physalis* tentacle, one from *C. xamachana*, and both a nematocyst and a spirocyst from *C. huetkeni*. In all but *C. huetkeni*, the spot was moved every 50–60 s to another location on the same nematocyst capsule. In the latter species, the spot was moved every 30–50 s and changed to a new cnida every 150 s due to the small size of the capsules. Thus each 600-s count for each type of cnida in *C. huetkeni* was a composite of four nematocysts and four spirocysts; four such 600-s counts were taken from a total of 16 cnidae in this species. X-ray spectra of Spurr resin (blank sections) served as a means of determining background. A composite peak showing maximum, minimum, and mean net counts was constructed for each type of cnida

Isolation of cnidae and amino acid analysis

Freshly collected *P. physalis* tentacles, *C. xamachana* oral vesicles, and whole segments of *C. huetkeni* colonies were allowed to autolyze in seawater at 4°C over a period of 2–7 days. Debris was removed by filtration through a coarse nylon mesh, and the filtrate was treated briefly with a sonicator probe to disperse the remaining material. Recovery of undischarged cnidae from *P. physalis* required an initial low-speed centrifugation (200 × *g*) for 4 h over concentrated sucrose (approximately 2.5 *M*). The sucrose layer was diluted and cnidae were concentrated by centrifugation, then resuspended in a small volume of 0.1 *M* cacodylate buffer, pH 8.0. The crude, buffered autolysate was layered over 2.0 *M* sucrose and centrifuged at 10 × *g* for an additional 60 min, or allowed to settle at 4° overnight. A clean nematocyst preparation was obtained after repeating this process. The filtered *C. xamachana* autolysate was separated from debris by centrifigation into 1.25 *M* sucrose for 1 h at 1000 × *g*. Cnidae in the sucrose layer were concentrated, resuspended in cacodylate buffer, and briefly sonicated after addition of 1 μl ml^{-1} Triton X-100. The crude cnidae were filtered through a 10-μm nylon mesh, layered onto a discontinuous gradient of 1.75, 2.0, 2.25, and 2.5 *M* sucrose, and spun for 1 h with a swinging bucket rotor at 2000 × *g*. Cnidae were in the 2.25 and 2.5 *M* layers. This process was repeated 2–3 times. The *C. huetkeni* autolysate contained a considerable amount of mucus and was treated with 0.5% cetylpyridinium chloride in addition to Triton X-100. The treatment and procedure was otherwise the same as for *C. xamachana*.

Clean, isolated cnidae from each species were taken from buffer to distilled water and disrupted with a sonicator probe. The fragments were recovered by brief centrifugation, rinsed with distilled water, then dehydrated in ethanols and oven-dried. Cnidae fragments yielding 1–2 μg of protein were oxidized in 95% performic acid for 30 min to convert cystine into cysteic acid and were subsequently hydrolyzed by microwave digestion in 6 *N* HCl for 18 min under an atmosphere of nitrogen. Amino acids were derivitized with Edman's reagent (phenylisothiocyanate—see Heinrickson and Meredith, 1984) and quantitated by reverse-phase high-performance liquid chromatography at Florida State University Analytical Laboratories, using a detection wavelength of 254 nm. Analyses of each species were performed in triplicate, with the cnidae of each replicate representing a single individual or colony.

Effects of DTT, thioglycolic acid, and collagenase

Isolated cnidae stored in 0.1 *M* cacodylate buffer were taken to distilled water. The effects of disulfide reduction

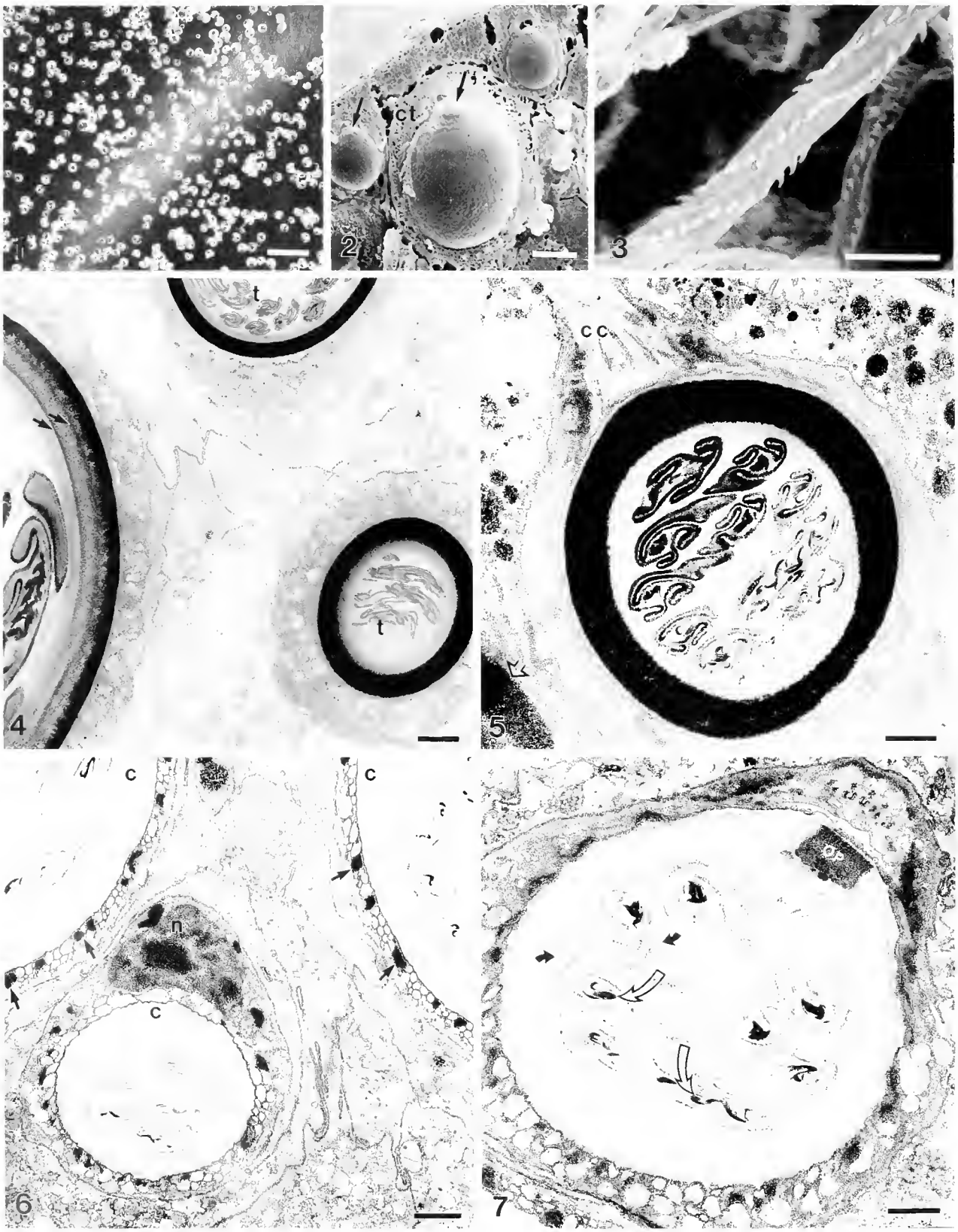

Figures 1–7. Cnidae from *Physalia physalis*

were examined for 15 min after placing a 10-μl drop containing several hundred cnidae on a slide, followed by 25 μl of 0.2 *M* DTT or 0.3 *M* thioglycolic acid in 0.2 *M* bicarbonate buffer, pH 10.3 (Brand *et al.*, 1993). Isolated cnidae were also tested with collagenase (Type 1A: 320 units mg^{-1} and 1.7 units mixed protease, Sigma Chemical Co., St. Louis, MO) by exposing them to 1500 enzyme units in TES buffer, pH 7.5 (10:1 enz:cnidae vol), for 5 h at 37°C. Cnidae were recovered by centrifugation, washed in distilled water, and again exposed to DTT or thioglycolic acid as above.

Results

Isolated cnidae and electron microscopy

Physalia physalis. Clean, largely undischarged nematocyst preparations were obtained from *P. physalis* (Fig. 1). Cnidae isolated in sucrose were remarkably difficult to discharge and, in contrast to results reported by Lane (1960), were often unresponsive to centrifugation or to immersion in distilled water, 50 m*M* sodium citrate, *N*-HCl or *N*-NaOH, despite capsular permeability to toluidine blue. Two size classes (diameters 8–12 μm and 20–35 μm) were obtained from tentacles (Fig. 2). These ranges are in general agreement with the measurements obtained by Lane and Dodge (1958), Hulet *et al.* (1974), and Cormier and Hessinger (1980). The larger of the two was characterized by a uniform tubule diameter of about 2.5 μm, with spines of about equal size (0.9–1.2 μm), uniformly distributed along its length in three rows (Fig. 3). The smaller cnidae contained similar tubules and spination, but these were not examined in the discharged condition. The designation of these nematocysts as holotrichous isorhizas seems appropriate and is consistent with identifications made previously (Mariscal, 1974; Brand *et al.*, 1993).

Cnidae from *P. physalis* tissues treated with methenamine-silver demonstrated a clear and consistent pattern of argentophilia. The large isorhizas were always strongly silver-positive, but only in the outermost portion of the capsule (Fig. 4). Deeper regions, delineated by what appeared to be fibrous annuli, were only lightly stained. These electron-opaque annuli subdivided the capsule into as many as five distinct layers. In contrast, the small isorhiza capsules were most often completely blackened with metallic silver (Figs. 4, 5). In less intensely stained capsules, one or two electron-opaque annuli could be distinguished, but in small isorhizas these layers did not react differentially with silver. The annuli were present in isorhizas that were untreated except for aldehyde fixation, and were therefore unrelated to the silver stain.

In *P. physalis* and all other species examined, the background stain varied in intensity, probably due in part to variations in temperature during the 30-min interval at 70°C. Figure 4 shows a low-background preparation in which some generalized staining of membranes is evident. However, nothing in the tissue compares to the intensity of the capsule stain. Figure 5 shows a small isorhiza with typically strong capsular argentophilia but with higher background staining of membranes and small vesicles. Nuclei and mucus cell secretory inclusions were also stained. The nematocyst tubule was quite variably electron-opaque (*cf.* Figs. 4 and 5), and silver deposits were often observed on the tubule periphery. Al-

Figure 1. Large and small isorhizas isolated from tentacular tissue in sucrose. Darkfield microscopy. Scale bar = 100 μm.

Figure 2. Freeze-fracture SEM of nematocyst battery cross-section showing large isorhiza and surrounding cnidocyte (cl) flanked by two small isorhizas. The opercula (arrows) are visible at the top of each; battery surface is at the upper left. Scale bar = 5 μm.

Figure 3. Everted tubule of large isorhiza showing arrangement of three spiral rows of spines. Scale bar = 5 μm.

Figure 4. Low-magnification overview of methenamine-silver preparation showing two small isorhizas (top and right) with surrounding tissue, and a section of a large isorhiza (left). Note that small cnidae capsules are completely invested with electron-opaque silver deposits, whereas the large isorhiza is primarily reactive in the outer capsule; annuli marking inner capsule layers are noted by arrows. The tubule (t) of small isorhizas displays little reactivity toward silver. Scale bar = 2 μm.

Figure 5. Detail of methenamine-silver reaction on small isorhiza and surrounding cnidocyte. The capsule is clearly delineated from surrounding cellular material by the degree of argentophilia. A tangential section through the cnidocil complex (cc) is shown at the upper left. Extracellular vesicles (upper right) are silver-positive, as is mucus secretory material (clear arrow). Tissue was treated with iodoacetic acid, but not with disulfide reducing agent. Scale bar = 1 μm.

Figure 6. Low-magnification overview of tentacular tissue after DTT-iodoacetic acid blockade of methenamine silver reaction. Note that nucleus (n), numerous cnidocyte vesicles (arrows), and membranes are reactive, but the capsular (c) response is all but completely blocked by alkylation. Scale bar = 2 μm.

Figure 7. Detail of blockade on small isorhiza. Note that the operculum (op), the periphery of the tubule (solid, curved arrows), and the cnidocyte cytoplasm are reactive, but the capsule is not. Electron-opaque spines visible in the tubule center (clear, curved arrows) are not argentophilic. Scale bar = 1 μm.

though the opacity of the spines in the center of the tubule could be confused with silver stain, they were present in unstained controls (see also micrographs in Hulet *et al.*, 1974, and Hessinger and Ford, 1988) and were therefore unrelated to argentophilia.

Control procedures using DTT or thioglycolic acid followed by iodoacetate or ethyl maleimide alkylation essentially eliminated capsular argentophilia, while background staining remained on nuclei, cnidocyte membranes, and many extracapsular vesicles (Fig. 6). At higher magnification some nonspecific silver was still visible around the tubule periphery, and the operculum was also stained (Fig. 7), suggesting that these structures may have a different chemical composition from that of the capsule. Tissues treated with DTT or thioglycolic acid alone exhibited a somewhat less intense capsular argentophilia and a higher background, but were otherwise not significantly different from untreated tissues. Treatment with disulfide reducing agents alone, however, removed the electron-opaque annuli that subdivided the capsule, resulting in the uniformly electron-lucent appearance of capsules in Figures 6 and 7. Control tissues treated with propanol and boric acid, or iodoacetic acid (as in Fig. 4), or ethyl maleimide alone were indistinguishable from experimental groups.

Cassiopeia xamachana. The nematocysts in the tentacles of this scyphozoan were divided into two distinct regions. The free edges of the oral arms were white and digitate (called "digitella" by Bigelow, 1900; "tentacles" by Smith, 1937) and contained primarily ovoid nematocysts 12–15 μm long, tentatively identified as euryteles. The oral vesicles, on the other hand, contained primarily small (6–9 μm), round cnidae. Clean nematocysts obtained from *C. xamachana* oral vesicles are shown in Figure 8. The smaller cnidae contained a tubule about 1 μm in diameter narrowing gradually (Fig. 9). Spines could not be measured in our SEM material, but appeared uniform in TEM preparations. These cnidae were identified by Mariscal and Bigger (1976) as holotrichous isorhizas, and this diagnosis is consistent with our observations. A smaller number of the eurytele nematocysts were also present in these preparations and were not separated by our isolation procedure. In addition, the oral vesicles contained developmental stages of these cnidae, some of which were included in our samples.

The capsules of mature isorhizas from *C. xamachana* tentacular tissue were 0.4–0.5 μm thick and were strongly argentophilic throughout, except for the ~0.1 μm thick outermost region (Fig. 10). As in the small isorhizas of *P. physalis*, one or two electron-opaque annuli could be distinguished, but these were obscured unless the silver stain was omitted. The tubule of mature isorhizas was electron-opaque in part due to nonspecific silver deposits and in part due to naturally occurring electron-opaque material in the tubule center.

Mature isorhizas were often closely accompanied by various stages of their development. The most common of these were capsules containing an electron-opaque matrix in which the tubule had not yet developed, or in which an incipient tubule could be observed (Fig. 10). We refer to the former as immature cnidae and the latter as submature. In both cases, the capsule was substantially less argentophilic than the mature cnidae. The immature stages reacted variably with silver; reactions ranged from diffuse and nonlocalized deposits to no reaction at all. The submature cnidae also exhibited variation in capsular argentophilia, which ranged from diffuse deposits to more concentrated metallic silver, but was always less than in the mature cnidae. In addition to acquiring argentophilia during the transition from submature to the mature condition, the capsule exhibited a 20%–50% decrease in thickness. Moreover, the electron-lucent tubule of submature cnidae and their contrasting electron-opaque matrix (Figs. 10, 11 inset) changed to an electron-opaque tubule in an electron-gray matrix during maturation. The latter change was the most consistent indicator of capsules most likely to exhibit a strong argentophilic reaction. The background reactivity of tissue from the oral vesicles was similar to that of *P. physalis* tentacle and included generalized membrane, nucleus, and vesicle staining.

Post-reduction alkylation of mature and submature nematocyst capsules resulted in a virtually complete silver blockade, except in the outermost capsule layer at the cnidocyte membrane interface (Fig. 11) and in the operculum. Immature nematocysts in blockaded tissues continued to exhibit a weak response to methenamine-silver. This response could not be distinguished from the same weak reactivity in unblocked tissues, suggesting that it may not be due to sulfur. The response of submature cnidae to capsular silver was variable. In some cases, argentophilia was like that of the immature cnidae; in others, a greater amount of silver was deposited. In the latter case, silver was effectively blocked by post-reduction alkylation (Fig. 11 inset), although the silver at the capsule periphery could not be blocked. Mature nematocyst capsules treated with disulfide reducing agents alone or with iodoacetate or ethyl maleimide alone were still strongly argentophilic, but they were less intensely blackened and were accompanied by greater amounts of background silver.

Cirrhipathes luetkeni. Clean cnidae preparations from whole colonies (Fig. 12) yielded spindle-shaped nematocysts and cylindrical spirocysts, both of which were 15–18 μm long and about 3–4 μm at the widest diameter. A small number of nematocysts measuring about 22 × 5 μm were also present. Nematocysts outnumbered spirocysts about 2:1 because whole colonies were used to ob-

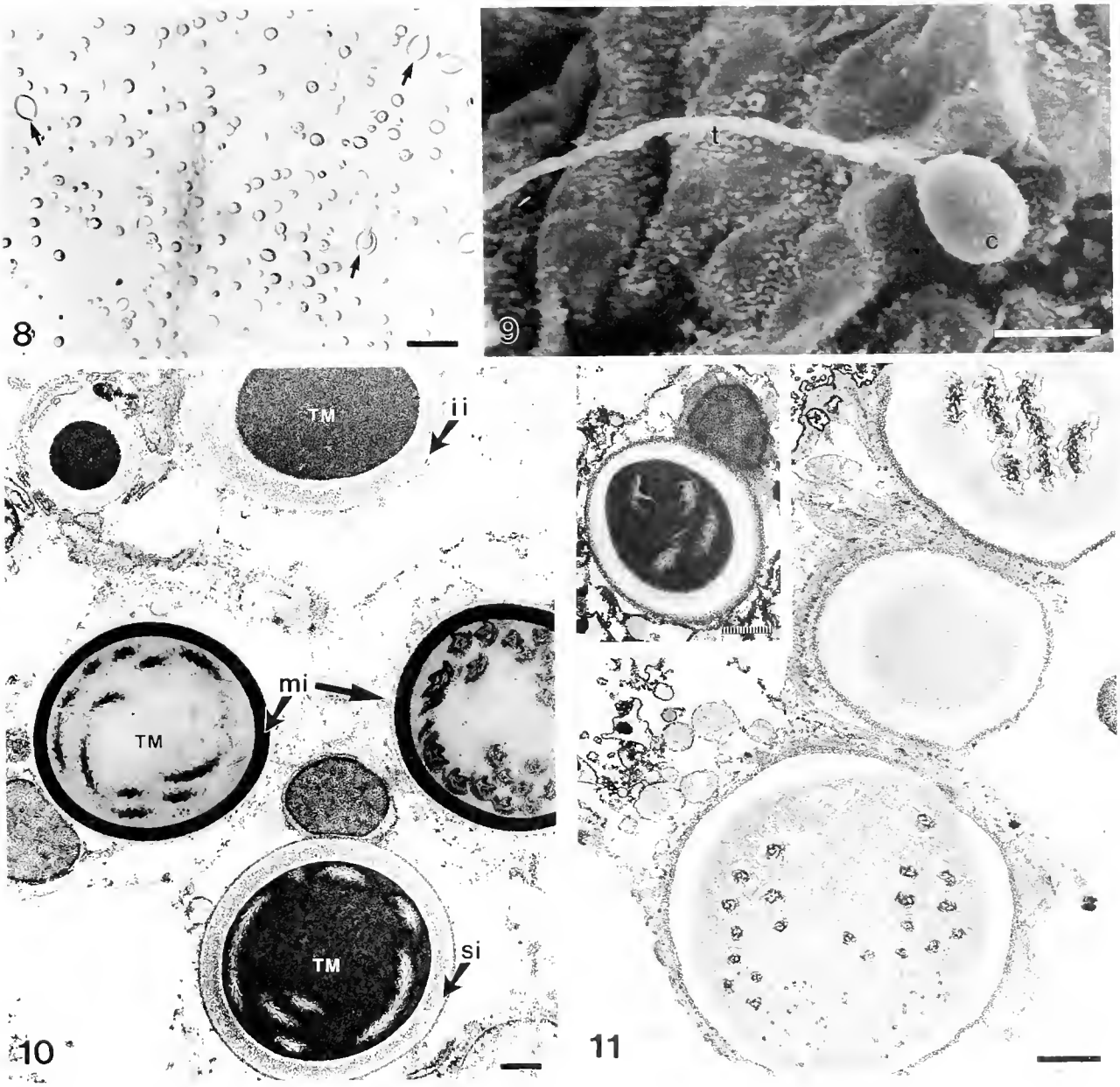

Figures 8–11. Cnidae from *Cassiopeia xamachana*

Figure 8. Cnidae isolated from oral vesicles are primarily small isorhizas with a small percentage of euryteles (arrows). Scale bar = 25 μm.

Figure 9. SEM preparation of small isorhiza capsule (c) and everted tubule (t). Spines are appressed to the tubule and are not visible. Scale bar = 5 μm.

Figure 10. Small isorhizas in various stages of development. Immature isorhizas (ii) at top, mature isorhizas (mi) in center, and submature isorhiza (si) at bottom. Note diffuse silver deposits on capsules of immature isorhizas and the electron-opaque tubule matrix (TM) in their centers. Central electron-opaque matrix of (si) surrounds electron-lucent tubule, whereas in (mi) the tubule is electron-opaque and the matrix (TM) is electron-gray. Note differences in capsular argentophilia: ii = diffuse, si = slightly greater, mi = intense. Scale bar = 1 μm.

Figure 11. DTT-iodoacetic acid blockade of mature isorhizas blocks capsular argentophilia; cytoplasm is still reactive. Inset: submature capsular silver is also occasionally blocked except for the outer capsule layer. Scale bar = 1 μm.

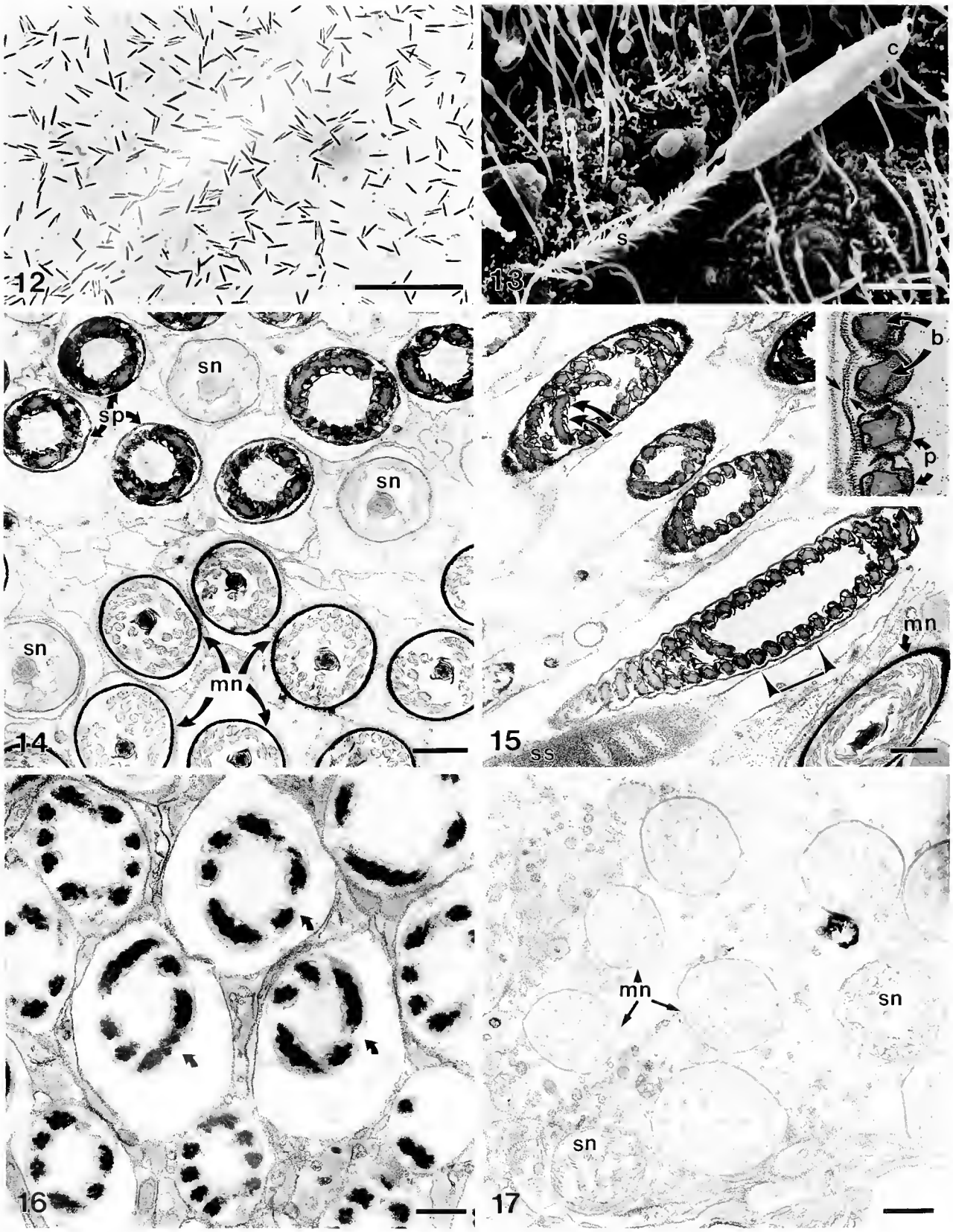

Figures 12–17. Cnidae from *Cirrhipathes luetkeni*.

tain cnide; tentacles alone would have yielded a greater proportion of spirocysts. Nematocysts and spirocysts could not be separated and were included in the final product employed for observation and chemical analysis. Many but not all spirocysts were recovered without capsules. Isolated nematocysts were resistant to discharge, and unless they were disintegrated by probe sonication, most were left intact by the isolation procedure. Those found in the discharged state (Fig. 13) were consistent with the description of microbasic b-mastigophores (Mariscal, 1974).

The capsules of both nematocysts and spirocysts in fixed material were strongly argentophilic. Tentacular cross-sections at low magnification were quite striking when the silver-blackened outlines of the cnidae were compared to the rest of the tissue (Fig. 14). The inner and outer surfaces of the spirocyst capsule were separately outlined by silver deposits (Fig. 15 and inset). The tubule wall in *C. huetkeni* spirocysts was thin, folded at intervals into pleats, and strongly argentophilic (Fig. 15 and inset). The tubule interior was essentially solid, and thus typical of the antipatharians examined by Goldberg and Taylor (1996). The unstained *C. huetkeni* tubule contained four helically arranged bundles of electron-gray material. In cross-section, the bundles were separated by electron-lucent, cruciform partitions, but in contrast to the tubule wall and its pleats, none of the material within the tubule (bundles or partitions) was argentophilic (Fig. 15 inset).

Unlike spirocysts, the nematocyst capsules were strongly silver-positive across the entire capsule cross-section (Fig. 14). Nematocyst tubules, on the other hand, displayed an inconsistent pattern of silver deposition. Often in the same section, the entire tubule was outlined with silver in one area, but in other areas only the shaft was argentophilic, or the tubule failed to stain at all.

The silver reactivity of the cnidae capsules in *C. huetkeni* is persistent. We have tested this species (as well as four other antipatharian species of the genus *Antipathes*—see Goldberg and Taylor, 1996) using specimens that had been fixed and stored in ethanol for years, and they display essentially the same reactivity as freshly collected material.

Post-reduction alkylation treatment of tissue stored in cacodylate buffer eliminated all silver reactivity from the nematocyst capsule, and most but not all reactivity from the spirocysts. Unfortunately, the background staining after blockade treatment increased considerably, particularly on the cell membranes. However, when we employed fixed material stored in ethanol rather than in cacodylate, the membrane background was substantially reduced. No capsular silver was deposited in the spirocyst controls (Fig. 16), but electron-opaque deposits (Ag?) formed within the tubules. Since tubule precipitates were absent in all other preparations, we suspect that they are artifacts in this case. The nematocysts were completely free of silver deposits after blockade treatment (Fig. 17). In *C. huetkeni* cnidae as in those of *C. xamachana*, treatment with disulfide reducing agents (DTT or thioglycolic acid) or sulfhydryl blocking agents (iodoacetate or ethyl maleimide) alone did not significantly reduce argentophilia cnidae, but increased background silver deposits.

Argentophilia of immature cnidae

The relationship between argentophilia and maturity was evident in *C. xamachana* nematocysts because of the

Figure 12. Isolated cnidae from whole colonies are a mixture of nematocysts and spirocysts, with many more of the former. Scale bar = 100 μm.

Figure 13. Discharged microbasic b-mastigophore nematocyst on tentacular surface showing shaft (s) about the same length of capsule (c) with gradual transition to tubule at lower left. Tentacular cilia are bulbous with pointed tips, possibly artifacts. Scale bars = 5 μm.

Figure 14. Methenamine-silver response of spirocyst capsules (sp) and mature microbasic mastigophore nematocyst capsules (mn) in tentacular cross-section. Note that capsules in submature nematocysts (sn) are weakly argentophilic and the tubules within are surrounded by an electron-gray matrix. Mature nematocyst tubules are matrix-free; their capsules are strongly argentophilic. Scale bar = 2 μm.

Figure 15. Tangential view of spirocysts treated as above showing uniform silver reactivity of capsule wall. The tubule and pleats (curved arrows) are also silver-positive; internal portions of the tubule are not. Note submature spirocyst (ss), lower left, with diffuse silver over electron-opaque matrix; capsule wall is indistinct and is not argentophilic. Mature nematocyst (mn) is shown at lower right. Scale bar = 2 μm. **Inset:** Detail of argentophilia in tubule wall and pleats from area of bar-connected arrowheads in Fig. 15. Note distinct staining of inner and outer layers of the capsule (straight arrows). The tubule wall is continuous with the pleats (p), and both are silver-positive. The tubule interior is not argentophilic and contains four bundles (b) of electron-gray material partitioned in an electron-lucent, cruciform pattern. Scale = 3.0 × Fig. 15 scale bar.

Figure 16. DTT-iodoacetic acid blockade of mature spirocysts blocks capsular argentophilia (arrows); pleats are also blocked; electron-opaque deposits in tubule are most likely artifacts. Scale bar = 1 μm.

Figure 17. Treatment as above showing complete silver blockade of mature nematocysts (mn) and submature nematocysts (sn). Scale bar = 1 μm.

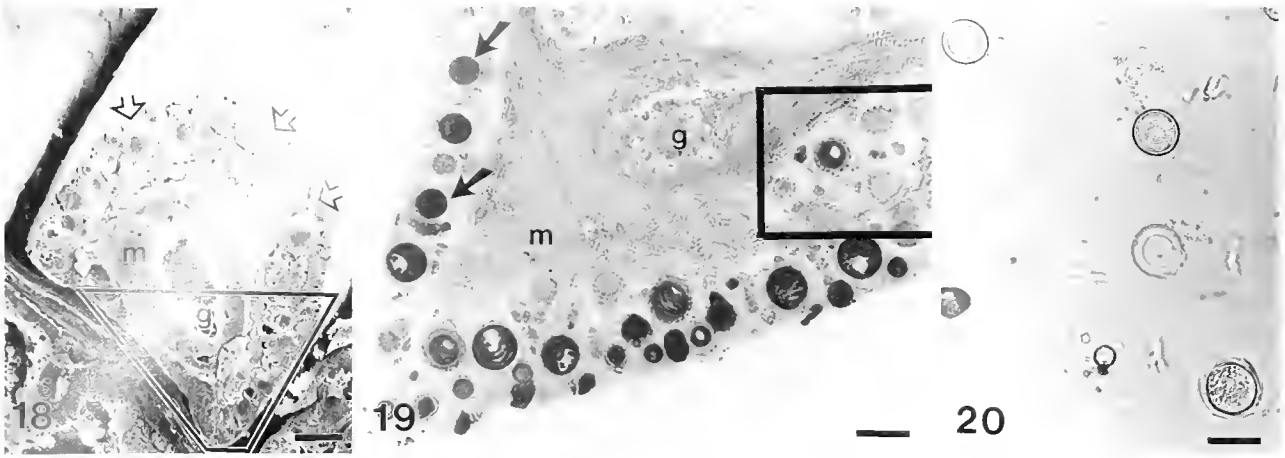

Figures 18–20. Immature nematocysts in *Physalia physalis*

Figure 18. SEM cross-section of freeze-fractured nematocyst battery showing mature cnidae at the outer face (clear arrows). Immature cnidae are formed in the deeper layers of the battery. Mesoglea (m) supports the inner battery; gastroderm (g) lines the center of the tentacle (t) and extends into each battery. Scale bar = 25 μm.

Figure 19. Toluidine blue-stained thick section taken in plane of trapezoid (Fig. 18) with corresponding locations of mesoglea (m) and gastroderm (g). Mature cnidae at the periphery of the battery contain a tubule with no matrix. These occur along with capsules containing a basophilic matrix (arrows), possibly representing submature isorhizas. Immature cnidae (boxed area) are only weakly basophilic. Scale bar = 25 μm.

Figure 20. Large, immature or submature isorhizas treated with 0.2 *M* DTT, pH 10.3, are resistant to depolymerization in contrast to mature stages. Scale bar = 25 μm.

proximity of various stages of development. As noted above, silver deposition in the capsule corresponded with the extent of tubule development. In *P. physalis* almost all of the cnidae on the outer face of the battery were mature (Fig. 18). Immature isorhizas, located deeper within the battery, were only weakly reactive toward toluidine blue and were virtually unresponsive to methenamine-silver reagent. However, with the development of the submature stage, the tubule matrix and capsule became strongly basophilic (Fig. 19). Because the tubule matrix apparently was not rendered electron-opaque with aldehyde fixation alone, we were unable to determine whether the basophilia coincided with silver deposition. Thus, in the electron microscope, the submature cnidae could not be distinguished with certainty from mature isorhizas.

Developing spirocysts in *C. luetkeni* occurred just below the outermost, mature cysts. Submature spirocysts were filled with a granular, naturally electron-opaque matrix surrounding the nascent tubule. The matrix also contained a diffuse silver-reaction product. The spirocyst capsule was not clearly developed as a double-walled structure at this stage (Fig. 15), and it exhibited affinity for silver only when the electron-opaque tubule matrix had almost completely disappeared.

Submature nematocyst capsules were most often located within clusters of mature mastigophores and were readily distinguished from mature nematocysts by their weak argentophilia. In every case, the weak staining of the capsules was associated with the presence of some remaining electron-gray matrix surrounding the tubule (Fig. 14). This matrix did not occur in mature nematocysts, suggesting that strong argentophilia in the capsule of these cnidae occurs coincidentally with the complete maturation of the tubule.

Response of unfixed cnidae to DTT

The large isorhizas of *P. physalis* discharged within about 10–15 s of exposure to DTT. After discharge the capsule dissolved rapidly, followed by the tubule. The time from discharge to complete solution was generally 30–60 s. Brand *et al.* (1993) also observed rapid solution in DTT, and found that *P. physalis* capsules and tubules dissolved almost simultaneously. It should be noted, however, that these authors employed discharged cnidae in their study. Our results contrast with those of Mariscal and Lenhoff (1969), who noted that disulfide reducing agents solubilize only fully discharged nematocysts. Solubility in DTT was typical of the mature isorhizas only. Those with clearly developed cysts but lacking a developed tubule failed to dissolve in this reagent. Most of these immature, DTT-resistant cysts in our *P. physalis* samples were the larger isorhizas (Fig. 20), but our isola-

tion procedure favored the larger cnidae. We also found that some of the large, mature isorhizas with an apparently well-developed tubule were resistant to DTT. However, these constituted <0.5% of that population, and we cannot be certain from light microscopic observations that they were completely mature.

The smaller isorhizas of both *P. physalis* and *C. xamachana* required 30–60 s for discharge after DTT treatment. Upon discharge, the tubules dissolved slowly over a period of several minutes, and in some cases failed to dissolve at all. Many of the small isorhiza capsules were only partially dissolved and could still be recognized after 15 min. In contrast, the euryteles in *C. xamachana* tentacles discharged and began to dissolve immediately on exposure to DTT; the tubule dissolved within 30 s. Small, immature isorhizas in both species were as resistant to DTT as the larger, immature ones in *P. physalis*.

Unlike the other cnidae in this study, isolated, undischarged mastigophores and spirocysts in *C. luetkeni* failed to respond to DTT: they did not discharge and the capsule did not dissolve. Efforts to dissolve these cnidae in collagenase were unsuccessful, although it should be noted that all cnidae in this study were collagenase-resistant, consistent with observations made by Blanquet and Lenhoff (1966). We followed our collagenase treatment with DTT, again without effect. These cnidae also failed to discharge or disintegrate after 30 min at room temperature in the presence of 0.5 *M* thioglycolic acid, 3 *M* HCl, 1 *M* NaOH, or 0.2 *M* borohydride.

X-ray microanalysis

The spectra presented in Figure 21 range from 1.2 to 5.0 keV. The zinc peak at 1.0 keV and the copper and zinc peaks above 5.0 keV originated from the grids and were eliminated from the analysis, as were traces of chromium and iron that originated from the microscope pole-pieces. We found no elements in these energy ranges that were natural constituents of nematocysts or spirocysts. Elements that were consistently present are depicted in the figure as a solid peak followed by a dashed line. Mean counts are indicated by a bar at the apex of the solid peak. The highest and lowest counts are indicated by the highest and lowest bars. Elements not consistently present are shown as peaks without bars or dashes.

Small amounts of silicon (1.7 keV) were found in all cnidae except *C. xamachana* nematocysts, and small amounts of chlorine (2.8 keV) were found in all but *C. luetkeni* nematocysts. In addition, trace amounts of aluminum (1.5 keV) were found both in spirocysts and in nematocysts of *C. luetkeni*. Sulfur (2.3 keV), on the other hand, was present in all cnidae, and was the dominant naturally occurring element. Nonetheless, since sulfur counts were often 1 per s or less, we employed samples that had been treated with methenamine-silver (3.1 and 3.3 keV) in case a consistent multiple of silver to sulfur could be demonstrated. However, silver-to-sulfur ratios were often inconsistent among individual cnidae. The ratios were generally in the range of 3:1 for all but spirocysts, which were closer to 2:1. The large isorhizas from *P. physalis* and the small isorhizas of *C. xamachana* had the highest sulfur and silver counts. The immediately adjacent submature cnidae (those without completely differentiated tubules) exhibited only background levels of sulfur, corresponding to the cytochemical results. The second-highest levels of sulfur were found in mature, large *P. physalis* isorhizas. Submature capsules could not be distinguished for separate X-ray examination. Surprisingly, the lowest sulfur counts were found in mature, small *P. physalis* isorhizas, followed closely by the microbasic mastigophores of *C. luetkeni*. Spirocyst sulfur counts were unexpectedly higher than those of the small nematocysts. However, since the spot size was wider than the diameter of the spirocyst capsule, sulfur counts were unavoidably collected from both the capsule and the tubule. This was also the case with the mastigophores, but the tubule alone appeared to contribute little sulfur to the spectrum. Immature cnidae of both types from *C. luetkeni* displayed only background sulfur counts.

Amino acid analysis

The amino acid analysis included a mixture of cnidae types, along with various stages of maturity that were unavoidable with the procedure employed. These results (Table I), while not ideal, provide a general impression of capsule chemistry and are instructive where they corroborate information obtained by cytochemistry and X-ray microanalysis.

In *P. physalis* nematocysts, levels of glycine, proline, and hydroxyproline were consistently high among the three colonies examined. Cysteic acid was the dominant sulfur amino acid. In *C. xamachana* nematocysts, proline and hydroxyproline were substantial constituents, although levels of these amino acids were not as high as those of *P. physalis*. The high levels of sulfur found in X-ray microanalysis were reflected in the total S-amino acids found in this species (6.84% ± 1.30%) but about 45% of these occurred as metsulfone. When cysteic acid and the small amount of residual cystine alone were considered, the total was not significantly different from that of *C. xamachana* cnidae.

Levels of proline and hydroxyproline in *C. luetkeni* cnidae were similar to those found in *C. xamachana*, and the total S-amino acid was similar to totals found in *P. physalis*. Cysteic acid residues were highest (3.00 ±

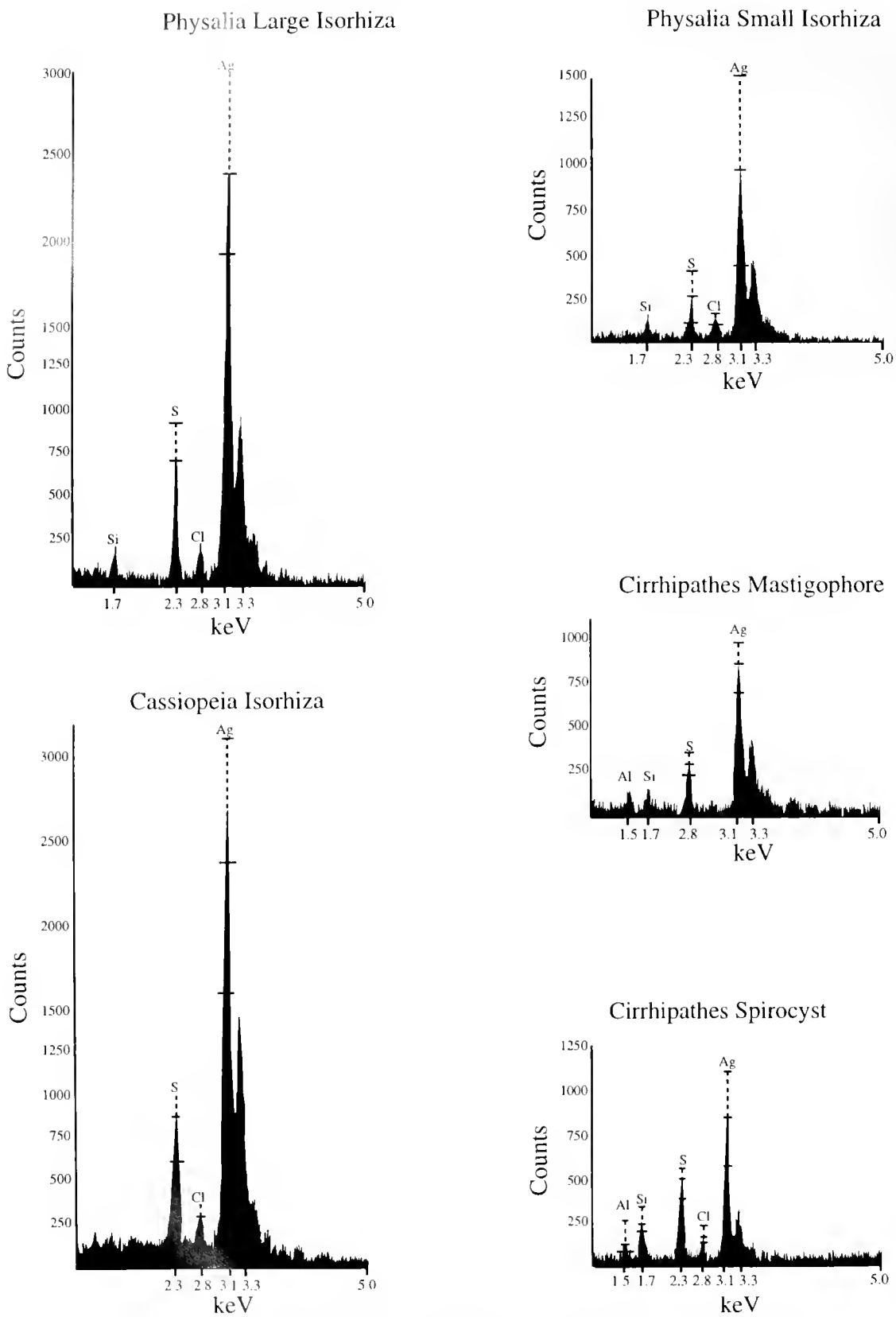

Figure 21. Composite TEM X-ray spectra of cnidae capsules. Methenamine-silver preparations show relative amounts of silver compared to natural constituents of the capsule. Mean counts for each element

Table I

Glycine, proline/hydroxyproline and S-amino acid content of cnidae as mole.% (pmoles amino acid as a percent of total pmoles ± std dev of 3 samples)

Amino acid	*Physalia physalis*	*Cassiopeia xamachana*	*Cirrhipathes luetkeni*
Gly	20.56 ± 0.15%	18.4 ± 3.9%	19.49 ± 1.97%
Pro	23.94 ± 0.06%	12.79 ± 3.55%	11.28 ± 2.6%
Hypro	10.72 ± 0.04%	1.81 ± 0.81%	1.70 ± 0.45%
Cys*	4.36 ± 0.17%	4.72 ± 1.13%	4.14 ± 0.61%
Met**	0.25 ± 0.01%	2.12 ± 0.29%	0.44 ± 0.06%

* Cys is the combined result of cysteic acid and small amounts of residual cystine, unconverted by performic acid.

** Met is methionine converted by performic acid to metsulfone.

0.48 mole.%), whereas metsulfone never constituted more than 0.49 mole.%. However, in contrast to the other types of cnidae examined, in *C. luetkeni* cnidae a substantial amount of cystine (1.14% ± 0.23% of the amino acids or 27.5% of the S-amino acids) was left unhydrolyzed by performic acid.

Discussion

Alkaline silver solutions have long been used to demonstrate neurofibrils, reticulum, Golgi, and other components of tissues and cells. The nature of the reaction is complex, and the degree of specificity often depends upon the type of fixation employed, the counter ion of the silver (nitrate, hydroxide, carbonate, methenamine, etc.) and the post-silver treatment of the tissue (*e.g.*, Humason, 1979). Specificity is further complicated by the action of silver as both an oxidizing stain and a redox reagent (Hayat, 1993). Methenamine-silver, introduced by Gomori (1946), was initially adapted for electron microscopy as a periodic acid–Schiff reagent. Despite nonselective staining of nuclear chromatin, melanin granules and ribosomes, neutral carbohydrate could be specifically demonstrated by periodic acid oxidation along with aldehyde blockade reactions (see reviews by Kiernan, 1990; Hayat, 1993). Methenamine-silver has also been employed to demonstrate disulfides in keratin and in other cystine-containing tissues. The mechanism probably involves alkaline hydrolysis of the disulfide and subsequent reduction of an undescribed methenamine-silver complex to metallic silver (Swift, 1968, 1973; Thompson and Colvin, 1970). The specificity of the reagent is dependent upon site-specific silver reduction in tissues that have been aldehyde-blocked and extracted with thiosulfate to eliminate unreduced silver. In addition, disulfide reduction and subsequent alkylation must prevent deposition of reduced silver at those previously reactive sites. Finally, the method should be employed in conjunction with parallel chemical techniques to confirm the cytochemical results (Thompson and Colvin, 1970). The silver cytochemistry of cnidae capsules is consistent with the results of post-reduction alkylation controls, X-ray microanalysis, and amino acid analysis. All of these data suggest that the argentophilia in the cnidae we have studied is due to the presence of capsular disulfides.

We know of only one other study in which electron cytochemistry has been used to detect disulfides in cnidae. Watson and Mariscal (1984) used performic acid oxidation coupled with alcian blue staining to study nematocyst development in the anemone *Haliplanella luciae*. They found that nematocyst maturation in that species is characterized by a 50% reduction in the thickness of the capsule wall, coincident with the formation of disulfide linkages. Both of these conclusions are in accordance with our observations of *Cassiopeia xamachana*. Capsule thinning also occurs with maturity in *Physalia physalis*, judging from the differences between immature and mature isorhizas. We did not attempt to study maturational changes in *Cirrhipathes luetkeni* cnidae.

If the alcian blue technique has an advantage over methenamine-silver, it is in the capacity to distinguish sulfhydryl from disulfide groups. We were not able to directly determine the contribution of either group specifically because both are argentophilic. The application of iodoacetic acid as a blockade prevented pre-existing sulfhydryl groups from reacting with silver, but increased the background in all but *P. physalis*. No differences were noted in this species between mature cnidae treated with iodoacetic acid and those left unblocked, suggesting that their argentophilia may be due entirely to disulfide groups. In *C. xamachana* and *C. luetkeni*, on the other hand, there was a small decrease in capsular argentophilia with iodoacetate controls, suggesting that some reactivity was contributed by sulfhydryl groups, although significantly less than that contributed by disulfides. In either case, the weak reactivity of developing cnidae in our study strongly suggests that neither sulfhydryl nor disulfide groups are present until very late in the process of capsular maturation.

The amino acid composition of coelenterate cnidae has been examined by a number of authors (Phillips,

Figure 21. (*Continued*) are represented by bar atop solid peaks; dashed lines indicate highest counts; lowermost bar represents lowest counts. Peaks without bars or dashes represent elements that were not consistently present.

1956; Lenhoff *et al.*, 1957; Lenhoff and Kline, 1958; Lane and Dodge, 1958; Fishman and Levy, 1967; Lane, 1968, 1974; Phelan and Blanquet, 1985; Blanquet, 1988) or the patterns of their constituent proteins (Kurz *et al.*, 1991; Brand *et al.*, 1993; Holstein *et al.*, 1994); but the universe of species examined is surprisingly small, representing only four genera with nematocysts (*Hydra* spp., *Physalia physalis*, *Aiptasia pallida*, *Metridium* spp.) and *Pachycerianthus torreyi*, a species with ptychocysts. Elevated levels of glycine, proline, and hydroxyproline are characteristic of collagen, and all cnidae analyzed thus far, including those in the present study, appear to contain these structural proteins. Glycine in nematocyst protein varies from 31.2–19.2 mole percent (Fishman and Levy, 1967; Stone *et al.*, 1970; Lane, 1974; Phelan and Blanquet, 1985). Glycine in our study is within this range, albeit at the lower limits. In *P. physalis* the proline content we reported is consistent with levels given by Lane (1968; 1974). Proline levels in *C. xamachana* and *C. luetkeni* cnidae were not unlike those of *P. physalis*. Hydroxyproline in *P. physalis*, at 10.7 mole percent, is slightly higher than the range of 6.9–9.2 mole percent reported by Fishman and Levy (1967) and Phelan and Blanquet (1985). However, hydroxyproline levels have also been reported as 20%, 8.5%, and 5.4% of the nematocyst protein (Kline, 1961; Blanquet and Lenhoff, 1966; Stone *et al.*, 1970, respectively). Conversion of our data to this form yields 12.5% hydroxyproline for *P. physalis*, but only 1.9% for *C. luetkeni* and 1.0% for *C. xamachana*. Thus a considerable range of this imino acid appears to occur in the proteins of the capsule and the tubule. However, these figures have not taken into account the ratio of collagen to the total nematocyst protein, and we cannot state with certainty that all of the cnidae pooled in our analyses (*e.g.*, spirocysts in *C. luetkeni*) contain collagen.

The amount of cystine in cnidocysts is only occasionally reported, and the range is considerable. Phelan and Blanquet (1985) found 7.24 and 2.39 mole percent cysteine in *Aiptasia pallida* and *Pachycerianthus torreyi* respectively, and Fishman and Levy (1967) reported 25.7 mole percent in *Metridium marginatum*. The most frequent and readily obtainable observation of cnidocyst chemistry is by X-ray microanalysis. In every case in which such analyses of capsule composition have been performed, sulfur has been the dominant element (Mariscal, 1980; Lubbock *et al.*, 1981, 1988; Gupta and Hall, 1984; Tardent *et al.*, 1990; Zierold *et al.*, 1991; this study). In addition, each author has suggested that disulfide linkage of collagen is the most likely role of that element. Several studies have shown that certain nematocysts dissolve in thiol reagents (*e.g.*, Yanagita, 1959; Blanquet and Lenhoff, 1966; Fishman and Levy, 1967; Mariscal, 1980; Phelan and Blanquet, 1985; Brand *et al.*, 1993). Yet it is not clear from this database whether the presence of sulfur alone in nematocysts, or even the presence of cystine, means that the capsule will be dissolved by disulfide reducing agents. This uncertainty was first indicated by Mariscal and Lenhoff (1969) who tested the solubility in dithiothreitol of 16 nematocysts from squash preparations of 10 coelenterate species. Five of the nematocysts from four species failed to depolymerize in this reagent, as did spirocyst preparations from two additional species. Phelan and Blanquet (1985) found that ptychocysts from the cerianthid *P. torreyi* were similarly resistant to the effects of disulfide reducing agents, although cysteic acid residues were present in their hydrolysates.

In light of these results, reasonable questions have been raised as to whether this insolubility might be due to (a) the absence of disulfide bonds in some cnidae, (b) the interference of reducing agent activity by mucus in the fresh preparations used by Mariscal and Lenhoff (1969), or (c) the inaccessibility of disulfides to reducing agent activity resulting from the tertiary structure of the capsule proteins (Blanquet, 1988). As in Phelan and Blanquet's observations of ptychocysts, our study has shown that cnidae from *C. luetkeni* contain cysteic acid residues. In addition, electron cytochemistry and X-ray microanalysis strongly suggest that in spite of their resistance to DTT and thioglycolate, nematocysts and spirocysts of this species both possess disulfide linkages. Our use of clean cnidae preparations rules out chemical interference with disulfide reduction in this study. With respect to the last suggestion (c) above, disulfide linkages located deep within hydrophobic regions of the protein could account for the relatively large amount of cystine remaining after performic acid hydrolysis in this species. However, since disulfide reducing agents fail to cause capsular depolymerization in *C. luetkeni*, it is possible that disulfides occur within rather than between peptide chains, or that disulfides are secondary to other types of covalent, intermolecular linkages as they are in bivalve byssus (*e.g.*, Benedict and Waite, 1986; Van Ness *et al.*, 1988) and dogfish egg capsule (*e.g.*, Rusaouën *et al.*, 1976). A lesser degree of dependence on disulfides as a means of capsule protein stabilization may also account for the partial depolymerization responses noted in the small isorhizas of *P. physalis* and *C. xamachana* (this study) and in nematocysts of the sea nettle (Goldner *et al.*, 1969; Stone *et al.*, 1970).

Spirocysts have long been considered a separate class of cnidae (*e.g.*, Hyman, 1940), a perspective reinforced by their distinctive tubule structure (*e.g.*, Mariscal *et al.*, 1977; Rifkin, 1991; Goldberg and Taylor, 1996). The chemistry of the spirocyst capsule is essentially unknown, except that, like some nematocysts, those of two actiniarians are resistant to disulfide reducing agents

(Mariscal and Lenhoff, 1969). Despite this property, Mariscal (1984) found that sulfur was the most strongly represented element in the spirocyst capsule of the anemone *Haliplanella luciae*, as it was in the nematocyst capsules of that species. Our study of *C. luetkeni* not only shows that sulfur is the principal element of the capsule (as well as the tubule wall and pleats), but electron cytochemistry strongly suggests that capsular sulfur occurs primarily in the form of disulfide linkages, as it does in nematocysts.

Surprisingly, the presence of disulfide linkages in spirocyst capsules is not entirely new information. Hamon (1955) observed that spirocysts from *Anemonia sulcata* reacted more strongly to nitroprusside after disulfide reduction than did the basitrichs of the same species. Unfortunately, the effects of disulfide reducing agents on unfixed cnidae were not investigated. Further study will be necessary to determine the distribution of resistance to disulfide reduction among coelenterate cnidae generally, and spirocysts specifically. Additional work should also focus on the characterization of spirocyst capsule proteins and the alternative forms of capsular stabilization reflected in their resistance to thiol reagents.

Acknowledgments

We thank P. Blackwelder of E.M. Analytical, Inc., for assistance with and use of X-ray analytical equipment, and C. Bigger and B. Fry for assistance in collecting specimens. This work benefited from discussions with K. Downum and D. Kuhn. We thank R. N. Mariscal (Florida State University) for helpful critique of the manuscript. Support from Florida International University is gratefully acknowledged.

Literature Cited

Benedict, C. V., and J. H. Waite. 1986. Location and analysis of byssal structural proteins of *Mytilus edulis*. *J. Morphol.* **189:** 171–181.

Bigelow, R. P. 1990. The anatomy and development of *Cassiopeia xamachana*. *Mem. Boston Soc. Nat. Hist.* **5:** 191–236.

Blanquet, R. S. 1988. The chemistry of cnidae. Pp. 407–425 *The Biology of Nematocysts*, D. A. Hessinger and H. M. Lenhoff, eds. Academic Press, New York.

Blanquet, R. S., and H. M. Lenhoff. 1966. A disulfide-linked collagenous protein of nematocyst capsules. *Science* **154:** 152–153.

Brand, D. D., R. S. Blanquet, and M. A. Phelan. 1993. Collagenous, thiol-containing proteins of cnidarian nematocysts: a comparison of the chemistry and protein distribution patterns in two types of cnidae. *Comp. Biochem. Physiol.* **106B:** 115–124.

Brown, C. H. 1950. Keratins in invertebrates. *Nature* **166:** 439.

Cormier, S. M., and D. A. Hessinger. 1980. Cellular basis for tentacle adherence in the Portuguese Man-of-War (*Physalia physalis*). *Tissue Cell* **12:** 713–721.

Fishman, L., and M. Levy. 1967. Studies on the nematocyst capsule protein from the sea anemone *Metridium marginatum*. *Biol. Bull.* **133:** 464–465.

Goldberg, W. M., and G. T. Taylor. 1989. Cellular structure and organization of the black coral *Antipathes aperta* 1. Organization of the tentacular epidermis and nervous system. *J. Morphol.* **202:** 239–253.

Goldberg, W. M., and G. T. Taylor. 1996. The structure of the spirocyst tubule in black corals (Anthozoa: Antipatharia) and its taxonomic significance. *Mar. Biol.* **125:** 655–662.

Goldner, R., J. W. Burnett, J. S. Stone, and M. S. Dilaimy. 1969. The chemical composition of sea nettle nematocysts. *Proc. Soc. Exp. Biol. Med.* **131:** 1386–1388.

Gomori, G. 1946. The study of enzymes in tissue sections. *Am. J. Clin. Pathol.* **16:** 347–352.

Gupta, B. L., and T. A. Hall. 1984. Role of high concentrations of Ca, Cu, and Zn in the maturation and discharge in situ of sea anemone nematocysts as shown by X-ray microanalysis of cryosections. Pp. 77–95 in *Toxins, Drugs, and Pollutants in Marine Animals*. L. Boils *et al.*, eds. Springer-Verlag, Berlin.

Hamon, M. 1955. Cytochemical research on coelenterate nematocysts. *Nature* **176:** 357.

Hayat, M. A. 1993. *Stains and Cytochemical Methods*. Plenum Press, New York. 455 pp.

Heinrickson, R. L., and S. C. Meredith. 1984. Amino acid analysis by reverse-phase high-performance liquid chromatography: precolumn derivitization with phenylisothiocyanate. *Anal. Biochem.* **136:** 65–74.

Hessinger, D. A., and M. T. Ford. 1988. Ultrastructure of the small cnidocyte of the Portuguese Man-O-War (*Physalia physalis*) tentacle. Pp. 75–94 in *The Biology of Nematocysts*, D. A. Hessinger and H. M. Lenhoff, eds. Academic Press, New York.

Holstein, T. W., and P. Tardent. 1984. An ultrahigh-speed analytical exocytosis: nematocyst discharge. *Science* **223:** 830–833.

Holstein, T. W., M. Benoit, G. v. Herder, G. Wanner, C. N. David, and H. E. Gaub. 1994. Fibrous mini-collagens in *Hydra* nematocysts. *Science* **265:** 402–404.

Hulet, W. H., J. L. Belleme, G. Musil, and C. E. Lane. 1974. Ultrastructure of *Physalia* nematocysts. Pp. 99–114 in *Bioactive Compounds from the Sea*. H. J. Humm and C. E. Lane, eds. Marcel Dekker, New York.

Humason, G. L. 1979. Pp. 162–207 in *Animal Tissue Techniques*. W. H. Freeman, San Francisco.

Hyman, L. H. 1940. Pp. 365–661 in *The Invertebrates: Protozoa through Ctenophora*. McGraw-Hill, New York.

Kiernan, J. A. 1990. *Histological and Histochemical Methods: Theory and Practice*. Pergammon Press, New York. 433 pp.

Kline, E. S. 1961. Chemistry of nematocyst capsule and toxin of *Hydra littoralis*. Pp. 153–168 in *The Biology of* Hydra *and of Some Other Coelenterates*. H. M. Lenhoff and W. F. Loomis, eds. University of Miami Press, Coral Gables, FL.

Kurz, E. M., T. W. Holstein, B. M. Petri, J. Engel, and C. N. David. 1991. Mini-collagens in *Hydra* nematocysts. *J. Cell Biol.* **115:** 1159–1169.

Lane, C. E. 1960. The Portuguese Man-of-War. *Sci. Am.* **13:** 371–393.

Lane, C. E. 1968. Coelenterata: chemical aspects of ecology: pharmacology and toxicology. Pp. 263–284 in *Chemical Zoology* v. 2, M. Florkin and B. T. Scheer, eds. Academic Press, New York.

Lane, C. E. 1974. Nematocyst toxins of coelenterates. Pp. 123–137 in *Bioactive Compounds from the Sea*. H. J. Humm and C. E. Lane, eds. Marcel Dekker, New York.

Lane, C. E., and E. Dodge. 1958. The toxicity of *Physalia* nematocysts. *Biol. Bull.* **115:** 219–226.

Lenhoff, H. M., E. S. Kline, and R. Hurley. 1957. A hydroxyproline-rich, intracellular, collagen-like protein of *Hydra* nematocysts. *Biochim. Biophys. Acta* **26:** 204–205.

Lenhoff, H. M., and E. S. Kline. 1958. High imino acid content of the capsule from *Hydra* nematocysts. *Anat. Rec.* 130: 425.

Locke, M., and N. Krishnan. 1971. The distribution of phenoloxidases and polyphenols during cuticle formation. *Tissue Cell* **3:** 103–126.

Lubbock, R., and W. B. Amos. 1981. Removal of bound calcium from nematocyst causes discharge. *Nature* **290:** 500–501.

Lubbock, R., B. L. Gupta, and T. A. Hall. 1981. Novel role of calcium in exocytosis: mechanism of nematocyst discharge as shown by X-ray microanalysis. *Proc. Natl. Acad. Sci. USA* **78:** 3624–3628.

Mariscal, R. N. 1971. The effect of a disulfide reducing agent on the nematocyst capsules from some coelenterates with an illustrated key to nematocyst classification. Pp. 157–168 in *Experimental Coelenterate Biology*, H. M. Lenhoff, L. Muscatine, and V. Davis, eds. Univ. Hawaii Press, Honolulu.

Mariscal, R. N. 1974. Nematocysts. Pp. 129–178 in *Coelenterate Biology: Reviews and New Perspectives*, L. Muscatine and H. M. Lenhoff, eds. Academic Press, New York.

Mariscal, R. N. 1980. The elemental composition of nematocysts as determined by X-ray microanalysis. Pp. 337–342 in *Developmental and Cellular Biology of Coelenterates*, P. Tardent and R. Tardent, eds. Elsevier/North-Holand, Amsterdam.

Mariscal, R. N. 1984. Cnidaria. Pp. 57–67 in *Biology of the Integument* vol. 1 Invertebrates, J. Bereiter-Hahn, A. G. Matolsky, and K. S. Richards, eds. Springer-Verlag, Berlin.

Mariscal, R. N. 1988. X-ray microanalysis and perspectives on the role of calcium and other elements in cnidae. Pp. 95–114 in *The Biology of Nematocysts*, D. A. Hessinger and H. M. Lenhoff, eds. Academic Press, New York.

Mariscal, R. N., and H. M. Lenhoff. 1969. Effect of a disulfide reducing agent on coelenterate nematocyst capsules. *Experientia* **25:** 330–331.

Mariscal, R. N., and C. H. Bigger. 1976. A comparison of putative sensory receptors associated with nematocysts in an anthozoan and a scyphozoan. Pp. 559–567 in *Coelenterate Ecology and Behavior*, G. O. Mackie, ed. Plenum, New York.

Mariscal, R. N., and R. B. McLean. 1976. The form and function of cnidarian spirocysts 2. Ultrastructure of the capsule tip and wall and mechanism of discharge. *Cell Tissue Res.* **169:** 313–321.

Mariscal, R. N., R. B. McLean, and C. Hand. 1977. The form and function of cnidarian spirocysts 3. Ultrastructure of the thread and function of spirocysts. *Cell Tissue Res.* **178:** 427–432.

Phelan, M. A., and R. S. Blanquet. 1985. Characterization of nematocyst proteins from the sea anemones *Aiptasia pallida* and *Pachycerianthus torreyi* (Cnidaria: Anthozoa). *Comp. Biochem. Physiol.* **81B:** 661–666.

Phillips, J. H. 1956. Isolation of active nematocysts of *Metridium senile* and their chemical composition. *Nature* **178:** 932.

Rambourg, A. 1967. An improved silver-methenamine technique for the detection of periodic acid reactive complex carbohydrates with the electron microscope. *J. Histochem. Cytochem.* **15:** 409–412.

Rusaouën, M., J-P. Pujol, L. Bocquet, A. Veillard, and J-P. Borel. 1976. Evidence of collagen in the egg capsule of the dogfish, *Scyliorhinus canicula*. *Comp. Biochem. Physiol.* **53B:** 539–543.

Rifkin, J. F. 1991. A study of the spirocytes from the Ceriantharia and Actiniaria (Cnidaria: Anthozoa). *Cell Tissue Res.* **266:** 365–393.

Smith, H. G. 1937. Contribution to the anatomy and physiology of *Cassiopeia frondosa*. Carnegie Inst. Wash. Pub. #475, *Pap. Dry Tortugas Lab.* **31:** 17–52.

Stone, J. H., J. W. Burnett, and R. Goldner. 1970. The amino acid content of sea nettle (*Chrysaora quinquecirra*) nematocysts. *Comp. Biochem. Physiol.* **33:** 707–170.

Swift, J. A. 1968. The electron histochemistry of cystine-containing proteins in thin transverse sections of human hair. *J. R. Microsc. Soc.* **88:** 449–460.

Swift, J. A. 1973. The electron cytochemical demonstration of cystine disulfide bonds using the silver-methenamine reagent. *Histochemie* **35:** 307–310.

Tardent, P. 1988. History and current state of knowledge concerning discharge of cnidae. Pp. 309–332 in *The Biology of Nematocysts*, D. A. Hessinger and H. M. Lenhoff, eds. Academic Press, New York.

Tardent, P., K. Zierold, M. Klug, and J. Weber. 1990. X-ray microanalysis of elements present in the matrix of cnidarian nematocysts. *Tissue Cell* **22:** 629–643.

Thompson, E., and J. R. Colvin. 1970. Electron cytochemical localization of cystine in plant cell walls. *J. Electron Microsc.* **91:** 87–98.

Van Ness, K. P., T. J. Koob, and D. R. Eyre. 1988. Collagen cross-linking: distribution of hydroxypyridinium cross-links among invertebrate phyla and tissues. *Comp. Biochem. Physiol.* **91B:** 531–534.

Watson, G. M., and R. N. Mariscal. 1984. Ultrastructure and sulfur cytochemistry of nematocyst development in catch tentacles of the sea anemone *Haliplanella luciae* (Cnidaria: Anthozoa). *J. Ultrastruct. Res.* **87:** 159–171.

Yanagita, T. M. 1959. Physiological mechanism of nematocyst responses in sea-anemone 1. Effects of trypsin and thioglycolate upon the isolated nematocysts. *Jpn. J. Zool.* **12:** 361–375.

Yanagita, T. M., and T. Wada. 1954. Effects of trypsin and thioglycolate upon the nematocysts of the sea anemone. *Nature* **173:** 171.

Zierold, K., P. Tardent, and S. V. Buravakov. 1991. Elemental mapping of cryosections from cnidarian nematocytes. *Scanning Microsc.* **5:** 439–444.

Reference: *Biol. Bull.* **192:** 17–26. (February, 1997)

Ovarian Development in the Class Holothuroidea: a Reassessment of the "Tubule Recruitment Model"

M. A. SEWELL[1], P. A. TYLER[2], C. M. YOUNG[1], AND C. CONAND[3]

[1]*Department of Larval Ecology, Harbor Branch Oceanographic Institution, 5600 U.S. 1 North, Fort Pierce, Florida 34946;* [2]*Department of Oceanography, University of Southampton, Southampton SO17 1BJ, United Kingdom; and* [3]*Laboratoire de Biologie Marine, Université de la Réunion, 97715 Saint-Denis Cedex, La Réunion, France*

Abstract. The "tubule recruitment model" for the development of the holothurian gonad was proposed (a) to connect the stages of oogenesis with ovarian morphology in holothurians throughout the reproductive season and (b) to emphasize the potential for the holothurian ovary as a model system for cytological and biochemical study of echinoderm oogenesis. To reassess the evidence for this model, we have examined published accounts and unpublished observations on gonad development in holothurians from both temperate and tropical habitats, in shallow water and in the deep sea. A very limited number of species were found to conform to the predictions of the tubule recruitment model. The patterns of gonad development vary substantially in holothurians, even at the individual level, and with taxonomic position, geographical location, and habitat. The tubule recruitment model can be applied to only a small subset of holothurians, specifically those in the families Stichopodidae and Holothuriidae that have gonad morphology similar to that of *Parastichopus californicus.* However, the tubule recruitment model is invalid for many other aspidochirotes, and does not have wider applicability within the class Holothuroidea.

Introduction

Fundamental concepts of reproduction can often be addressed and tested most easily in marine invertebrates, where the diversity of reproductive modes is greater than among terrestrial animals (Giese *et al.,* 1987). Comparative studies within the marine invertebrates can be used to recognize unifying patterns of reproduction and to assist in the development of robust theory (Giese *et al.,* 1987). An example is the "tubule recruitment model" proposed by Smiley (1988) to describe gonad development in the class Holothuroidea (phylum Echinodermata). This conceptual model, based on a careful and impressive study of ovarian development in the aspidochirote sea cucumber *Parastichopus californicus,* was proposed to connect the stages of oogenesis with the ovarian morphology of holothurians throughout the reproductive season (Smiley, 1988, 1994; Smiley *et al.,* 1991), and to accentuate the usefulness of the holothurian ovary as a model system for cytological and biochemical study of echinoderm oogenesis (Smiley, 1988, 1990, 1994; Smiley *et al.,* 1991).

Since the tubule recruitment model was first published, several studies have documented apparent exceptions to the model. Moreover, our own work with a variety of holothurians from throughout the world, and from depths ranging from the intertidal zone to the deep sea, casts additional doubt on the broad applicability of the model. Here we reexamine both the published literature and our own unpublished data to test the applicability of the tubule recruitment model to the class Holothuroidea in general, and particularly to the aspidochirote holothurians.

Background

Holothurians differ from other extant echinoderms in having a single gonad located dorsally in interambulacrum CD (Hyman, 1955). The gonad consists of many blind-ending tubules that are united at the anterior end in a fleshy, saddle-shaped gonad basis in the dorsal suspensor mesentery of the gut. The gonoduct exits anterio-

Received 22 December 1995; accepted 6 November 1996.

dorsally from the gonad basis and leads to single or multiple external gonopores located between or near the tentacles in interradius CD.

In contrast to the highly conservative gonad morphology found in other echinoderm classes, there is considerable variability among the gonads of different holothurians (Hyman, 1955). Although most species are gonochoric, three of the six holothurian orders have hermaphroditic representatives (Smiley *et al.*, 1991). It is overall gonad morphology, however, that exhibits the most extreme degree of variability. The tubules attached to the gonad basis vary in shape (*e.g.*, tubules, nodules, globose sacs), length, degree of branching, and thickness—even between species in the same family (*e.g.*, the Stichopodidae; Conand, 1993a—fig. 2). For illustrations of tubule variability, see the following figures: figs. 64, 67, 68, 72–76 (Hyman, 1955); figs. 4, 6 (Conand, 1981); fig. 1 (Tyler and Gage, 1983); fig. 1 (Tyler *et al.*, 1985b); fig. 1 (Tyler and Billett, 1987); fig. 2 (Tyler *et al.*, 1992); fig. 2 (Conand, 1993a); fig. 6 (Conand, 1993b); fig. 1 (Hamel *et al.*, 1993); fig. 3 (Sewell, 1994).

In holothurians with an annual cycle, the reproductive season can generally be divided into five "stages of maturity" as first described for *Stichopus japonicus* by Tanaka (1958). After spawning, the spent tubules are usually resorbed and the gonads are defined as being in a post-spawning, or resting, stage (Stage I). The later stages of gonad maturity are defined based on the stage of development of gametes within the gonad tubules (Recovery, Growth, Mature, Shedding; Stages II to V). There is not an equal division of time in each maturity stage; in some species a considerable portion of the reproductive cycle may be spent in the resting stage, with little or no gonad material present. Observations of the presence, size, and appearance of tubules in the resting-stage gonad are crucial for assessment of the tubule recruitment model in holothurians.

The Tubule Recruitment Model

Overview

The tubule recruitment model of gonad development was based on histological and ultrastructural observations of oogenesis in *Parastichopus californicus* (as *Stichopus californicus*). These observations are described in Smiley and Cloney (1985); Smiley (1988, 1990, 1994); and Smiley *et al.* (1991). In *P. californicus* the ovarian tubules are present as three distinct cohorts on the gonad basis: the smallest or primary tubules most anterior; intermediate-sized secondary tubules in a medial position; and the largest fecund tubules at the posterior end (Fig. 1). Central to the model is the progressive recruitment of primary tubules, which originate in the anterior gonad basis in Year N, to become the secondary tubules of Year N+1 and the fecund tubules of Year N+2 (Fig. 2).

In simple terms, the entire process of ovary development and oogenesis in *Parastichopus californicus* can be viewed as a slowly moving conveyor belt carrying containers of maturing oocytes to the posterior end of the gonad basis (Fig. 2). After spawning, the spent fecund tubules are resorbed until only a pigmented plaque remains on the posterior of the gonad basis. Some of the nutrients obtained from phagocytosis of the spent tubules are transferred to the primary and secondary tubules, where they may provide energy for gamete proliferation and vitellogenesis respectively. For a more complete description of the processes that occur within each tubule cohort, see the detailed discussions of the model in Smiley and Cloney (1985); Smiley (1988, 1990); Smiley *et al.* (1991); and Smiley (1994).

A number of assumptions were made in the formulation of the tubule recruitment model: (1) that other holothurians would, like *Parastichopus californicus*, have a gonad consisting of distinct tubule cohorts; (2) that resorption of the spent tubules, as suggested by Hyman (1955), is a general feature of holothurian reproduction; (3) that only the recently fecund tubules are completely resorbed, and (4) that more than one year is required to produce mature oocytes.

Support for the tubule recruitment model (Smiley, 1988) was drawn from descriptions of gonad morphology in the aspidochirotes *Stichopus japonicus* (Mitsukuri, 1903), *Holothuria parvula* (Kille, 1942), *Neostichopus grammatus* (Deichmann, 1948), and the dendrochirote *Sclerodactyla (Thyone) briareus* (Kille, 1939). The presence of several size classes of tubules on the gonad basis in the aspidochirote *Mesothuria intestinalis* (Théel, 1901), the dendrochirote *Cucumaria laevigata* (Ackermann, 1902), and other unspecified species (Delage and Hérouard, 1903; Deichmann, 1930, 1948) were used in a subsequent review to provide support for the proposed model (Smiley *et al.*, 1991). Gonad index studies on the aspidochirotes *Stichopus japonicus* (Tanaka, 1958), *Thelenota ananas* and *Holothuria nobilis* (Conand, 1981) were also considered to provide data consistent with the tubule recruitment described in *Parastichopus californicus* (Smiley, 1988).

Evidence for the tubule recruitment model was limited to holothurians of the orders Aspidochirotida and Dendrochirotida. Comparative information on oogenesis in other holothurian orders was considered too limited to assess the model's general applicability (Smiley, 1988). However, in subsequent reviews it was suggested that the model had broad-scale applicability to ovarian development throughout the class Holothuroidea (Smiley, 1990; Smiley *et al.*, 1991; Smiley, 1994). Several groups of holothurians were considered to be problematic to the tubule recruitment model; these included male holothurians of any order, small hermaphroditic or

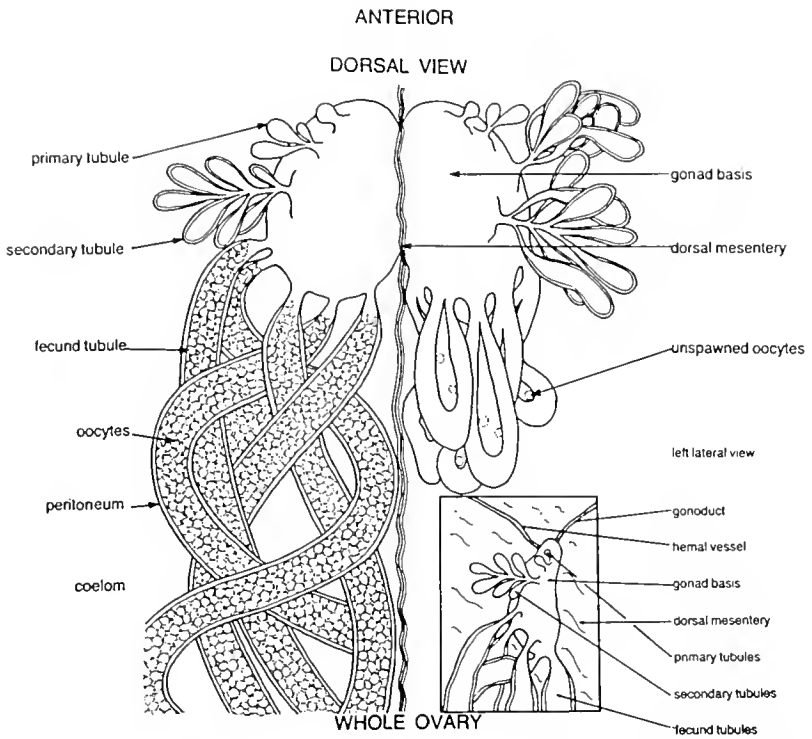

Figure 1. The tubule recruitment model as proposed by Smiley (1988) in *Parastichopus californicus*. The whole ovary of *P. californicus* is shown. The left side of the figure represents the prespawning condition with mature oocytes in the fecund tubule and earlier oocyte development in the primary and secondary tubules. The right side shows the post-spawning, or resting-phase, gonad. The fecund tubules are in the process of resorption, and the primary and secondary tubules are larger preparatory to posterior migration on the gonad basis. In this model, three cohorts of tubules are present on the gonad basis at any one time. Diagram reprinted from Smiley and Cloney (1985) with permission.

short-lived holothurians, and species with more than one spawning per year or with continuous reproduction (*e.g.*, polar and deep-sea species; Smiley, 1988; Smiley *et al.*, 1991; Smiley, 1994).

Testing

For a species to conform to the tubule recruitment model it must have gonad tubules that develop in distinct primary, secondary, and fecund cohorts, with each cohort of tubules having synchronous development of oocytes. After spawning, the relict fecund gonad tubules are resorbed, but the primary and secondary tubules persist on the gonad basis and migrate posteriorly as new primary tubules are formed. Consequently, the gonad in the resting stage following spawning must contain primary tubules as well as secondary tubules that will develop into the fecund tubules for the next reproductive season.

The tubule recruitment model would not apply to situations in which a single tubule or a single cohort of similar-sized tubules is attached to the gonad basis and resorbed partially or totally after the reproductive period. It would also not apply where immature previtellogenic and mature vitellogenic oocytes are found in the same ovarian tubule (overlapping generations of oocytes), because this would be evidence that the same "container," or cohort of tubules, is being used for multiple reproductive seasons.

Our survey of the published literature is confined to those papers on holothurian reproduction that describe in detail the gross morphology of the gonad during the reproductive period. We assess the validity of the tubule recruitment model in two ways. First, we consider studies in which sufficient information is provided to test for the distinct gonad morphology required by the model (*i.e.*, primary, secondary, and fecund tubules). Second, we describe the reproductive studies published after 1988 that explicitly test the tubule recruitment model. Our examination of those studies, in combination with our own unpublished observations, leads us to suggest that the applicability of the tubule recruitment model is relatively limited in holothurians, even within the family Stichopodidae in which it was initially proposed.

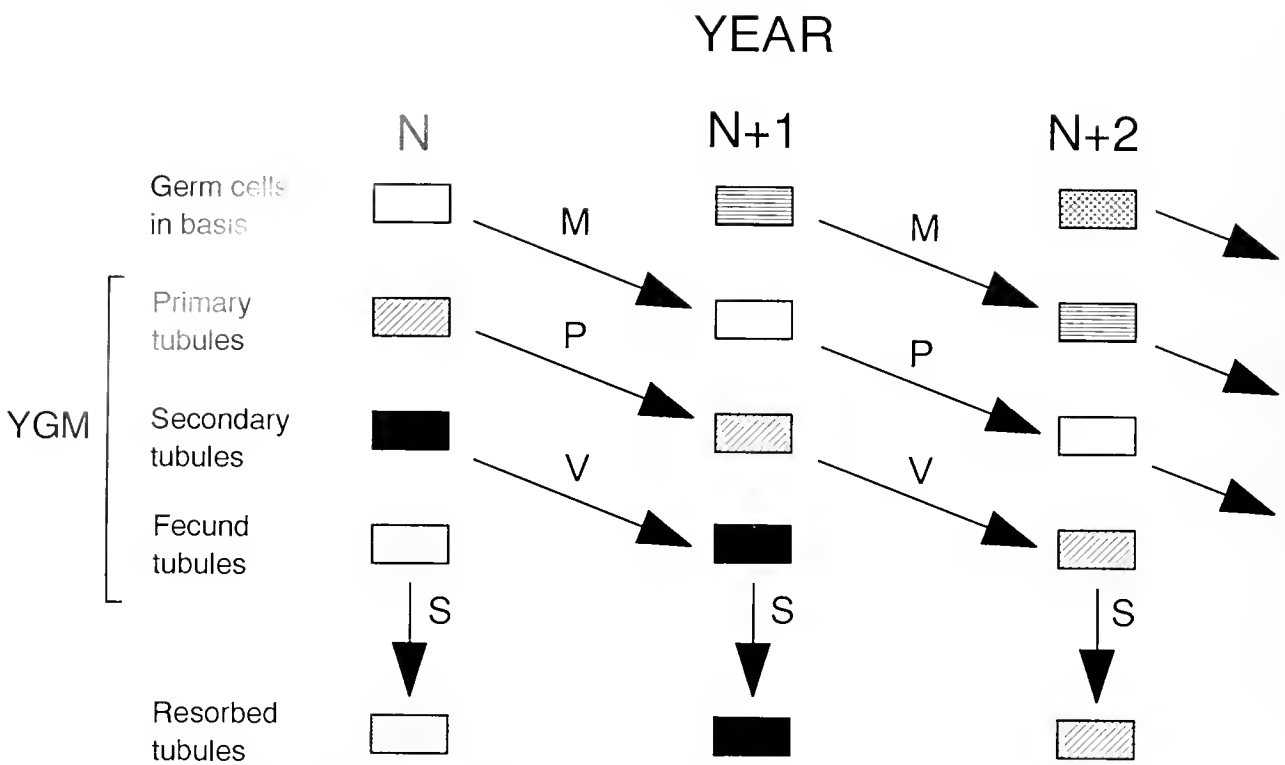

Figure 2. Schematic diagram to show progressive recruitment of tubules in the ovary of *Parastichopus californicus*. The gonad morphology is shown for three consecutive years: N, N+1, N+2. In each year the gonad has three cohorts of tubules (YGM = year-round gonad morphology), as well as primary germ cells at the very anterior and the remains of resorbed tubules at the posterior end of the gonad basis. Tubule cohorts derived from the same primary germ cells are shown with the same pattern (open, hatched, filled, etc.). The germ cells of year N migrate on the gonad basis (M) to become the primary tubules of year N+1. Oogonial proliferation (P) in this year results in secondary tubules in Year N+2. Vitellogenesis (V) in the secondary tubules results in fecund tubules whose gametes are spawned (S) and the empty tubules resorbed in Year N+3. Consequently, the gametogenic process in *P. californicus* from primary germ cells to spawning takes 4 years.

Evidence from Gonad Morphology

Order Aspidochirotida

A priori we might expect that the strongest support for the tubule recruitment model would be found in aspidochirote holothurians, considering that the model was based on *Parastichopus californicus* (Family Stichopodidae). The model can be tested in many aspidochirotes because of reproductive studies prompted by their importance as beche-de-mer fisheries (Conand and Byrne, 1993).

In holothurians of the family Stichopodidae (30 species; Smiley, 1994) the gonad is present as two tufts of tubules, one on each side of the dorsal mesentery. Although tubule morphology varies considerably in species of this family, none of the other species examined are described as having distinct size classes of tubules on the gonad basis (*Stichopus variegatus*—Conand, 1993a; *S. mollis*—Sewell, 1992; *Thelenota ananas*—Conand, 1993a). Variability in the pattern of gonad development is, however, apparent in species with broad geographical ranges (*S. japonicus*—Tanaka, 1958; Choe, 1963; *S. mollis*—Sewell, 1992). In these species there are differences in the amount of gonad material found during the resting stage.

Sewell (1992) in a study of gonad development of the temperate *Stichopus mollis* in New Zealand showed that the tubule recruitment model may be applicable in only some populations. Detailed study of a population of *S. mollis* in northern New Zealand found complete resorption of the gonad after spawning, with no gonad material present during the winter months (Sewell and Bergquist, 1990; Sewell, 1992). In contrast, *S. mollis* from southern New Zealand retained a large volume of tubules in the resting period, and the tubules contained developing oocytes (Sewell, 1992). The evidence for progressive recruitment of tubules is, however, equivocal because the southern population examined was from a greater depth

than the northern one (Sewell, 1992) and the specimens were preserved and eviscerated, with unattached gonads (M. A. Sewell, unpub. obs.).

A similar pattern of gonad development with latitude is observed in the temperate Japanese sea cucumber *Stichopus japonicus*. A resting-phase gonad with shrunken tubules observed in *S. japonicus* at Hokkaido (Tanaka, 1958) was not seen in this species in southern Japan by Choe (1963). In Atsumi Bay the gonads in *S. japonicus* completely disappear after spawning, and a condition corresponding to the resting stage of Tanaka (1958) was not found (Choe, 1963).

Differences in the resting-phase gonad in distantly separated populations of *S. japonicus* and *S. mollis* are also reflected on a smaller scale in two other stichopodids. In the tropical *Stichopus variegatus* and *Thelenota ananas*, a high variability has been observed in the resting stage maintained in individual sea cucumbers. After spawning, the gonad tubules were entirely resorbed, and only the gonad basis remained in some individuals (C. Conand, unpub. obs.). A similar pattern was recently reported in the South African stichopodid *Neostichopus grammatus* (Foster and Hodgson, 1995). Although Smiley (1988) considered that to be a species showing progressive tubule recruitment, Foster and Hodgson (1995) reported that the tubules are either resorbed completely after spawning or are reduced to a few very short fine threads.

Almost 50% of the aspidochirote holothurians are within the Family Holothuriidae (Smiley, 1994). In this family, gonad tubules are present only on the right side of the dorsal mesentery. Two species of this family were considered by Smiley (1988) to provide support for the tubule recruitment model—*Holothuria parvula* (Kille, 1942) and *H. nobilis* (Conand, 1981). In *H. parvula* the ovary has distinct tubule cohorts, with small immature tubules at the anterior, a distinct cohort of mature tubules, and the resorption of the most posterior tubules after spawning (Kille, 1942). Evidence for tubule recruitment in *H. nobilis* is more limited, however, under the criteria defined earlier. The gonad in this species has one tuft of tubules; the length and diameter of these tubules vary during the reproductive cycle, but no tubule cohorts are described (Conand, 1981).

Cohorts of tubules with differing stages of oocyte development have been observed in individuals of the tropical species *Holothuria atra* (Pearse, 1968); *H. leucospilota* (Viet Nam and Britaev, 1992); *H. floridana* and *H. mexicana* (Engstrom, 1980); and the temperate *H. forskali* (Tuwo and Conand, 1992). However, the number of tubule cohorts varies between species (*H. atra*—3; *H. leucospilota*—2; *H. floridana* and *H. mexicana*—2 or 3; *H. forskali*—5). More importantly for the assessment of the tubule recruitment model, tubule cohorts are not consistently seen in all individuals (Pearse, 1968; Engstrom, 1980), and in *H. leucospilota* they are seen in the summer spawning period but not the spring one (Viet Nam and Britaev, 1992). Furthermore, in studies of *Holothuria* species at other locations, many resting-stage individuals have no gonads (*H. tubulosa*—Coulon, 1994; *H. leucospilota*—Ong Che, 1990; *H. atra*—Chao *et al.*, 1994; C. Conand, unpub. obs.) or only one tubule cohort (*H. mexicana*—Hyman, 1955, fig. 64). We, therefore, conclude that in the genus *Holothuria*, evidence for the tubule recruitment model is provided by some individuals of selected species, but only at some geographical locations and some times.

The tropical holothurid *Actinopyga* shows a pattern similar to that of the genus *Holothuria*. The ovary in *A. echinites* consists of a single tuft of tubules (Conand, 1982). However, after spawning in *A. echinites* and *A. mauritiana* only a few resting individuals possessed gonad tubules (Conand, 1993a; C. Conand, unpub. obs.), suggesting that tubule recruitment does not generally occur.

The family Synallactidae comprises 143 species (42% of the order Aspidochirotida; Smiley, 1994), which are found at bathyal depths. The hermaphroditic *Mesothuria intestinalis*, which shows distinct variation in size and arrangement of male and female gonad tubules (Théel, 1901; Hyman, 1955 fig. 77C), was considered to provide evidence for the tubule recruitment model (Smiley *et al.*, 1991). The gonad of a full-grown individual consists of tufts of sexually differentiated tubules, with male and female gametes reaching their maturation in different, successive tufts (Théel, 1901). There is evidence in this species for the progressive recruitment of tubules on the gonad basis: the youngest tubules at the anterior are followed posteriorly by tufts of alternating male and female tubules, and the marks of resorbed tubules from previous reproductive periods are visible at the most posterior position (Théel, 1901). The female tuft does not, however, contain cohorts of tubules with oocytes in different stages of development (Théel, 1901). In terms of the tubule recruitment model, there is evidence for progressive recruitment of tubule tufts, but the arrangement of primary, secondary, and fecund female tubules seen in *Parastichopus californicus* is lacking.

The gonad structure of the hermaphroditic *Paroriza pallens* and *P. prouhoi* differs from that of other synallactids: the gonad is composed of nodules along a central tube that connects to the gonoduct (Tyler *et al.*, 1992). Each nodule contains oocytes in various stages of development; there are no distinct areas with the same oogenic stage (Tyler *et al.*, 1992). Among gonochoric synallactids, the gonad tubules of female *Benthothuria funebris* and *Palaepatides grisea* show evidence of size variation (P. A. Tyler, unpub. obs.), but the very distinctive gonad tubules in *Bathyplotes natans* do not (Tyler *et al.*, 1994). In the

ovaries of *Mesothuria verrilli* and *M. lactea* the size of the tubules is uniform, but in the testis of the latter, the tubule size varies (P. A. Tyler, unpub. obs.).

Order Dendrochirotida

The order Dendrochirotida is the most speciose in the class Holothuroidea, with 553 of the 1427 species (Smiley, 1994). At this point, however, sufficient information to test the tubule recruitment model is available for a relatively small number of temperate dendrochirotes.

The only species that shows cohorts of gonad tubules as predicted by the tubule recruitment model is *Sclerodactyla (Thyone) briareus* (Kille, 1939); although Coe (1912) did not describe an obvious size differentiation in the gonad tubules of this species (see Hyman, 1955, fig. 67). There is no evidence for variation in tubule size in the ovaries of *Cucumaria planci* (Hérouard, 1889; Hyman, 1955, fig. 72B), *Cucumaria glacialis* (Mortensen, 1894; Hyman, 1955, fig. 76H), or *Aslia lefevrei* (Costelloe, 1985; Tuwo and Conand, 1994).

In dendrochirotes for which there have been seasonal studies of reproduction, there is no evidence for progressive tubule recruitment. In *A. lefevrei* and *Pawsonia saxicola*, relict gametes are resorbed after spawning, but the tubules themselves are not (Tuwo and Conand, 1994). A similar pattern is observed in *Psolus fabricii*, which has new oocytes present in its tubules after spawning (Hamel *et al.*, 1993). Although the ovary of *P. fabricii* has two sizes of gonad tubules, the large and small tubules are intermixed within the gonads (Hamel *et al.*, 1993). Because the tubules are not resorbed after spawning, large tubules become small tubules due to oocyte release (Hamel *et al.*, 1993). In these species the same tubules, or "containers," are being used for more than one reproductive season.

Examination of reproduction in the temperate *Cucumaria frondosa* along the Atlantic coast of Canada and the northern United States showed differing gonad morphology with latitude (Hamel and Mercier, 1996). In northern latitudes the gonad is divided into two distinct classes of tubules; south of New Brunswick the tubules are of a uniform size (Hamel and Mercier, 1996). In the St. Lawrence estuary, where large and small tubules are present, the gonad tubules are not resorbed after spawning. As in *Psolus fabricii*, the small tubules contain earlier stages of gamete development; mature oocytes are found in the large tubules (Hamel and Mercier, 1996). In contrast, at more southern latitudes the gonad tubules are in the same stage of development and attain maturity after a single year (Hamel and Mercier, 1996). Thus, in *Cucumaria frondosa* the gonad morphology and pattern of gametogenesis might be related to differing environmental conditions associated with latitude, rather than being characteristic of the species throughout its range.

In the hermaphroditic species *Cucumaria laevigata*, the developing tubules at the gonad basis are sexually indifferent but become female and release eggs as they lengthen (Ackermann, 1902; Hyman, 1955). With continuing growth the remaining female tissue is phagocytosed and the same tubules produce sperm (Hyman, 1955). Thus, the gonad of *C. laevigata* consists of small basal undifferentiated tubules, larger female tubules, and very long male tubules (see Hyman, 1955, fig. 76G). Again, contrary to the tubule recruitment model, the same tubules are used for more than one reproductive period.

Order Dactylochirotida

Although there are 31 species of dactylochirote holothurian (Smiley, 1994), reproduction has been described in only one species, the lower bathyal *Ypsilothuria bitentaculata* (as *Y. talismani*). In this species Tyler and Gage (1983) showed that a cluster of small similar-sized tubules are present throughout the year.

Order Molpadida

The few reproductive studies that have been conducted in molpadid holothurians reveal no evidence of size cohorts within the gonad tubules. The ovaries of *Paracaudina chilensis* (Kawamoto, 1927; see Hyman, 1955, fig. 75) and *Molpadia roretzii* (Hatanaka, 1939) consist of elongated tubules of the same size. In the only dedicated study of gonad morphology, Tyler *et al.* (1987) showed that *Cherbonniera utriculus* has a gonad with fewer than 10 small, even-sized tubules.

Order Apodida

The few reproductive studies in the apodids are restricted to species within the family Synaptidae, the majority being in hermaphroditic species. In the simultaneous hermaphrodite *Leptosynapta tenuis*, oocytes and developing sperm are found in the two branching tubules. In reproductively active animals the tubules are extensively branched; after spawning the tubules are shrunken, with little branching (Green, 1978). Oocytes are present in these tubules throughout the year (Green, 1978). In the protandric hermaphrodite *Leptosynapta clarki*, after spawning the relict gametes are resorbed from the posterior ends of the two gonad tubules (Sewell and Chia, 1994). New gametes for the next reproductive season form in the anterior end of each gonad tubule, adjacent to the gonad basis (Sewell and Chia, 1994). The type of gametes (oocytes or sperm) formed at the gonad basis is dependent on the previous sex, animal size, and other undetermined factors (Sewell, 1994).

The simultaneous hermaphrodite *Synaptula hydri-*

formis similarly shows continued development of gametes within the same gonad tubule (Frick *et al.*, 1996). Gametes of many different stages are found simultaneously within the two tubules of the ovotestis, and the entire tubule is not resorbed after reproduction. Progressive tubule recruitment, therefore, does not occur in this species (Frick *et al.*, 1996).

In the only study of a gonochoric apodan, *Rhabdomolgus ruber*, the ovary is an unpaired tubule (Menker, 1970). Tubule growth occurs from the gonad basis, the youngest eggs being most anterior and the older oocytes occupying positions at the posterior end (Menker, 1970). Unspawned eggs are resorbed in the posterior part of the gonad in the autumn and winter (Menker, 1970), suggesting that the same tubule is retained year-round.

Order Elasipoda

There has been considerable research on the gonad morphology of the deep-sea elasipodid holothurians. Early studies of the gonads were made from the collections of the *Challenger* (Théel, 1882, plate XLVI; see Hyman, 1955, fig. 76D–F) and *Galathea* expeditions (Hansen, 1975). These data, together with more recent studies of the families Laetmogonidae (Tyler *et al.*, 1985b), Deimatidae (Tyler and Billett, 1987), Psychropotidae (Tyler and Billett, 1987), and Elpidiidae (P. A. Tyler, unpub. obs.), provide no evidence for the progressive recruitment of tubules. In most species the ovarian tubules contain one or more large vitellogenic oocytes, together with a large number of smaller previtellogenic oocytes. In addition, because most species probably show continuous reproduction, the seasonal, synchronous development of tubules as proposed in the tubule recruitment model is considered unlikely. The one exception to this pattern is in species of *Peniagone* in which there is a progressive increase in the size of the gonadal tubules from anterior to posterior (Tyler *et al.*, 1985a).

Conclusions from gonad morphology

Review of the gonad morphology of more than 45 holothurians suggests that size division and progressive recruitment of gonad tubules in *Parastichopus californicus* is the exception, rather than the rule, in holothurian reproduction. Holothurian species may show different patterns of gonad development between individuals and locations, and the use of the same tubule for oocyte growth in more than one reproductive period is seen in species of the orders Dendrochirotida, Apodida, and Elasipoda.

Our conclusions many be challenged on the grounds that the authors of some of the studies we analyzed may not have specifically looked for the small primary and secondary tubules on the gonad basis. We, however, maintain that when reports of primary or secondary tubules are lacking (either because of true absence or an incomplete examination of gonad morphology), the observation of the various stages of oogenesis in the same tubule "container" is, in itself, sufficient to cast doubt on the tubule recruitment model. Consequently, from morphological evidence alone, we question the general applicability of the tubule recruitment model to describe reproduction in the class Holothuroidea.

Evidence From Explicit Tests

The tubule recruitment model has been explicitly addressed in nine holothurian species from three of the six orders (Table 1). These include species from different regimes of depth (shallow water or deep sea) and temperature (temperate or tropical), and in both gonochoric and hermaphroditic forms.

In the order Aspidochirotida, support for the tubule recruitment model is found in only one species (*Holothuria forskali*), and perhaps in southern New Zealand populations of *Stichopus mollis* (Table 1). The other three aspidochirote species studied do not show cohorts of tubules or the progressive recruitment of tubules during ovarian development (Table 1).

In *Holothuria forskali*, the tubules attached to the gonad basis can be subdivided into five classes (T_1–T_5), and the tubules show progressive recruitment (Tuwo and Conand, 1992). Although there are some minor differences in tubule recruitment between *H. forskali* and *Parastichopus californicus* (*e.g.*, resorption in the T_5 tubules takes several months, and it can also occur in some T_3 and T_4 tubules; Tuwo and Conand, 1992), this species conforms well to the predictions of the tubule recruitment model.

A more problematic species is *Stichopus mollis*, which exhibits different patterns of gonad development in populations from the North and South Island of New Zealand (Sewell, 1992). Detailed visual and microscopical examination of individuals showed the complete resorption of the gonad tubules after spawning in northern New Zealand; *i.e.* no tubule recruitment (Sewell, 1992). Preserved samples sent from the South Island in June and August had a large mass of resting-phase gonad tubules (Gonad Index for June: 0.00% in North Island, 0.11% in South Island; Sewell, 1992), with the largest tubules containing previtellogenic oocytes (Sewell, 1992). Examination of the gonad basis for primary and secondary tubules was hindered by poor preservation and evisceration of the gonads in most females (M. A. Sewell, unpub. obs.). Consequently, although we can be certain that a resting phase gonad is present in southern New Zealand populations of *Stichopus mollis*, an explicit test of the tubule recruitment model for these populations awaits further research.

Table I

Studies of holothurian reproduction published after 1988 in which the tubule recruitment model is explicitly tested

Order Family		Sex[1]	Seasonality of reproduction[2]	Habitat[3]	Study location	Tubule recruitment model[4]	Reference
Aspidochirotida							
Stichopodidae	*Stichopus mollis*	G	A	S, T, Sub	northern New Zealand	No	Sewell (1992)
					southern New Zealand	?	Sewell (1992)
	Stichopus variegatus	G	A	S, Tr, Sub	New Caledonia	No	Conand (1993a); C. Conand (unpub. obs.)
	Thelenota ananas	G	A	S, Tr, Sub	New Caledonia	No	Conand (1993b); C. Conand (unpub. obs.)
Holothuriidae	*Holothuria forskali*	G	A	S, T, Sub	Brittany, France	Yes	Tuwo and Conand (1992)
Synallactidae	*Bathyplotes natans*	G	C	D, T, Sub	Bahamas	No	Tyler *et al.* (1994)
Dendrochirotida							
Psolidae	*Psolus fabricii*	G	A	S, T, Sub	St. Lawrence Estuary, Canada	No	Hamel *et al.* (1993)
Cucumariidae	*Cucumaria frondosa*	G	A	S, T, Sub	St. Lawrence Estuary, Canada	No	Hamel and Mercier (1996)
Apodida							
Synaptidae	*Leptosynapta clarki*	PH	A	S, T, Int	Bamfield, Canada	No	Sewell and Chia (1994)
	Synaptula hydriformis	SH	C	S, Tr, Sub	Florida Keys	No	Frick *et al.* (1996)

[1] G = gonochoric; PH = protandric hermaphrodite; SH = simultaneous hermaphrodite.
[2] A = 1 reproductive period per year; C = continuous reproduction.
[3] S = Shallow; D = deep sea; T = temperate; Tr = tropical; Sub = subtidal; Int = intertidal.
[4] No = tubule recruitment model not supported; Yes = tubule recruitment model supported; ? = further research required.

The three other aspidochirotes (*Stichopus variegatus, Thelenota ananas, Bathyplotes natans*) do not conform to the predictions of the tubule recruitment model (Table I). The discrepancy may be partly a result of the difference in gonad morphology from *Parastichopus californicus* (Fig. 1). These species do not have distinct primary, secondary, and fecund tubule tufts, but instead have a number of similar-length tubules attached to the gonad basis. Each tubule is surrounded with clusters of gonadal saccules, reminiscent of a bunch of grapes (see Conand, 1993a, fig. 2; Tyler *et al.*, 1994, fig. 2). In *Stichopus variegatus* and *Thelenota ananas*, many individuals have no tubules at all in the resting phase (C. Conand, unpub. obs), suggesting that in these individuals all gonad material is resorbed after spawning. In *Bathyplotes natans*, individual tubules produce and resorb oocytes on a nonseasonal basis; the entire tubule is not resorbed (Tyler *et al.*, 1994).

Sea cucumbers in the orders Dendrochirotida and Apodida also fail to support the tubule recruitment model (Table I). Although both dendrochirotes have large and small tubules, the same "container" is used to make oocytes for the next reproductive season (Hamel *et al.*, 1993; Hamel and Mercier, 1996). The apodids, which have only two gonad tubules, similarly use these containers for more than one reproductive season (Sewell and Chia, 1994; Frick *et al.*, 1996). In both species different developmental stages of gamete (oocyte in *Leptosynapta clarki* and oocytes and sperm in *Synaptula hydriformis*) are found within each tubule (Sewell and Chia, 1994; Frick *et al.*, 1996).

The tubule recruitment model is, therefore, not generally upheld in those holothurians where gonad morphology and development have been critically examined. Of the nine species annotated in Table I, only one (*Holothuria forskali*) provides direct support for the tubule recruitment model.

Conclusions and Recommendations for Future Research

The aim of this review has been to assess the applicability of the tubule recruitment model to species from all orders of the class Holothuroidea, and the validity of this conceptual model as a general paradigm for ovarian development in holothurians. The reproductive studies considered here show that gonad development varies in holothurians as a function of taxonomic position, geographical location, and habitat, and even within individ-

uals at the same location. We conclude that the tubule recruitment model may be appropriate for a number of species in the aspidochirote families Stichopodidae and Holothuriidae. However, it is not valid for many other aspidochirotes and does not have wider applicability within the holothurians.

The tubule recruitment model may prove to be applicable only to those species that, like *Parastichopus californicus,* have tufted tubular-type gonads. In recent research on species with saccular gonads (*e.g., Bathyplotes natans*) or without distinct tufts of tubules (*e.g., Synaptula hydriformis*), the authors have questioned the generality of the tubule recruitment model (Tyler *et al.,* 1994; Frick *et al.,* 1996). The pattern of ovarian development in *Parastichopus californicus,* with synchronous development of all gametes in discrete subsets of the gonad tubules, is apparently not the rule for holothuroid oogenesis (Frick *et al.,* 1996).

It is apparent from our review that the tubule recruitment model can be applied only to a small subset of holothurians, specifically those in the families Stichopodidae and Holothuriidae that resemble *Parastichopus californicus* in gonad morphology. The tubule recruitment model is useful for such animals and can serve to focus attention on details of gametogenesis such as ultrastructure and physiological control. Nevertheless, it is also important to acknowledge and carefully study the gonads of species that do not fit the predictions of the tubule recruitment model. This will lead to a better understanding of the various mechanisms underlying the wide diversity of gametogenic processes that are found in the class Holothuroidea.

Acknowledgments

The germ cells of this review were conceived during a dinner at the 8th International Echinoderm Conference in Dijon in September 1993. We thank our colleagues and the conference organizers for providing a forum for this discussion. We also thank J. Pearse for later discussion, J. Frick for comments on an earlier version of the manuscript, and J-F. Hamel for providing pre-published data. Harbor Branch Oceanographic Institution Contribution No. 1174.

Literature Cited

Ackermann, A. 1902. Uber die anatomie und zwittrigkeit der *Cucumaria laevigata. Z. Wiss. Zool.* **72:** 721–749.

Chao, S-M., C-P. Chen, and P. S. Alexander. 1994. Reproduction and growth of *Holothuria atra* (Echinodermata: Holothuroidea) at two contrasting sites in southern Taiwan. *Mar. Biol.* **119:** 565–570.

Choe, S. 1963. *Namako No Kenkyu (Biology of the Japanese Common Sea Cucumber* Stichopus japonicus *Selenka).* Pusan National University, Japan. 226 pp.

Coe, W. R. 1912. Echinoderms of Connecticut. *Conn. State Geol. Nat. Hist. Surv.* **19:** 1–147.

Conand, C. 1981. Sexual cycle of three commercially important holothurian species (Echinodermata) from the lagoon of New Caledonia. *Bull. Mar. Sci.* **31:** 523–543.

Conand, C. 1982. Reproductive cycle and biometric relations in a population of *Actinopyga echinites* (Echinodermata: Holothuroidea) from the lagoon of New Caledonia, western tropical Pacific. Pp. 437–442 in *Proceedings of the International Echinoderm Conference, Tampa Bay,* J. M. Lawrence, ed. A. A. Balkema, Rotterdam.

Conand, C. 1993a. Reproductive biology of holothurians from the major communities of the New Caledonia Lagoon. *Mar. Biol.* **116:** 439–450.

Conand, C. 1993b. Ecology and reproductive biology of *Stichopus variegatus* an Indo-Pacific coral reef sea cucumber (Echinodermata: Holothuroidea). *Bull. Mar. Sci.* **52:** 970–981.

Conand, C., and M. Byrne. 1993. A review of recent developments in the world sea cucumber fisheries. *Mar. Fish. Rev.* **55:** 1–13.

Costelloe, J. 1985. The annual reproductive cycle of the holothurian *Aslia lefevrei* (Dendrochirota: Echinodermata). *Mar. Biol.* **88:** 155–165.

Coulon, P. 1994. Role du macrobenthos detritivore dans la écosystèmes littoraux: etude de l'holothurie *Holothuria tubulosa,* espece commune des herbiers de posidonie en Mediterrance. Ph.D. thesis, Universite Libre de Bruxelles, Brussels.

Deichmann, E. 1930. The holothurians of the western part of the Atlantic Ocean. *Bull. Mus. Comp. Zool.* **71:** 41–226.

Deichmann, E. 1948. The holothurian fauna of South Africa. *Ann. Natal Mus.* **11:** 325–376.

Delage, Y., and E. Hérouard. 1903. *Les Echinodermes.* Traité de Zoologie Concrète. Yome III. Librarie C. Reinwald. Schleicher Frères et Cie, editeurs, Paris.

Engstrom, N. A. 1980. Reproductive cycles of *Holothuria (Halodeima) floridana, H. (H.) mexicana* and their hybrids (Echinodermata: Holothuroidea) in southern Florida, U.S.A. *Int. J. Invertebr. Reprod.* **2:** 237–244.

Foster, G. G., and A. N. Hodgson. 1995. Annual reproductive cycles of three sympatric species of intertidal holothurians (Echinodermata) from the coast of the Eastern Cape Province of South Africa. *Invertebr. Reprod. Dev.* **27:** 49–59.

Frick, J. E., E. E. Ruppert, and J. P. Wourms. 1996. Morphology of the ovotestis of *Synaptula hydriformis* (Holothuroidea: Apoda): an evolutionary model of oogenesis and the origin of egg polarity in echinoderms. *Invertebr. Biol.* **115:** 46–66.

Giese, A. C., J. S. Pearse, and V. B. Pearse, eds. 1987. *Reproduction in Marine Invertebrates, Vol. IX, General Aspects: Seeking unity in diversity.* Blackwell Scientific Publications, Palo Alto, CA.

Green, J. D. 1978. The annual reproductive cycle of an apodous holothurian, *Leptosynapta tenuis:* a bimodal breeding season. *Biol. Bull.* **154:** 68–78.

Hamel, J-F., and A. Mercier. 1996. Gonad morphology and gametogenesis of the sea cucumber *Cucumaria frondosa.* Pp. 22–33 in *Beche-de-mer Information Bulletin, Number 8 (April 1996).* South Pacific Commission, New Caledonia.

Hamel, J-F., J. H. Himmelman, and L. Dufresne. 1993. Gametogenesis and spawning of the sea cucumber *Psolus fabricii* (Duben and Koren). *Biol. Bull.* **184:** 125–143.

Hansen, B. 1975. Systematics and biology of the deep-sea holothurians. *Galathea Report* **13:** 1–262.

Hatanaka, M. 1939. A study of the caudate holothurian, *Molpadia*

roretzii (V. Marenzeller). *Sci. Rep. Tohuku Univ. Fourth Ser.* **14:** 155–190.

Hérouard, E. 1889. Recherches sur les holothuries des côtes de France. *Arch. Zool. Exp. Gén. Ser. 2* **7:** 535–704.

Hyman, L. H. 1955. *The Invertebrates. Echinodermata, The Coelomate Bilateria* McGraw Hill Book Company, New York. 763 pp.

Kawamoto, N. 1927. The anatomy of *Caudina chilensis* with especial reference to the perivisceral cavity, the blood and the water vascular systems in their relation to the blood circulation. *Sci. Rep. Tohuku Univ. Fourth Ser.* **2:** 239–264.

Kille, F. R. 1939. Regeneration of the tubules following extirpation in the sea cucumber *Thyone briareus*. *Biol. Bull.* **76:** 70–79.

Kille, F. R. 1942. Regeneration of the reproductive system following binary fission in the sea cucumber *Holothuria parvula* (Selenka). *Biol. Bull.* **83:** 55–66.

Menker, D. 1970. Lebenszyklus, jugendentwicklung und geschlechtsorgane von *Rhabdomolgus ruber* (Holothuroidea: Apoda). *Mar. Biol.* **6:** 167–186.

Mitsukuri, K. 1903. Notes on the habits and life-history of *Stichopus japonicus* Selenka. *Annot. Zool. Jpn.* **5:** 1–21.

Mortensen, T. 1894. Zur Anatomie und Entwicklung der *Cucumaria glacilis* (Ljungman). *Z. Wiss. Zool.* **57:** 704–732.

Ong Che, R. G. 1990. Reproductive cycle of *Holothuria leucospilota* Brandt (Echinodermata: Holothuroidea) in Hong Kong and the role of body tissues in reproduction. *Asian Mar. Biol.* **7:** 115–132.

Pearse, J. S. 1968. Patterns of reproductive periodicities in four species of Indo-Pacific echinoderms. *Proc. Indian Acad. Sci. Sect. B* **68:** 247–279.

Sewell, M. A. 1992. Reproduction of the temperate aspidochirote *Stichopus mollis* (Echinodermata: Holothuroidea) in New Zealand. *Ophelia* **35:** 103–121.

Sewell, M. A. 1994. Small size, brooding and protandry in the apodid sea cucumber *Leptosynapta clarki*. *Biol. Bull.* **187:** 112–123.

Sewell, M. A., and P. R. Bergquist. 1990. Variability in the reproductive cycle of *Stichopus mollis* (Echinodermata: Holothuroidea). *Invertebr. Reprod. Dev.* **17:** 1–7.

Sewell, M. A., and F-S. Chia. 1994. Reproduction of the intraovarian brooding apodid sea cucumber *Leptosynapta clarki* (Echinodermata: Holothuroidea) in British Columbia. *Mar. Biol.* **121:** 285–300.

Smiley, S. 1988. The dynamics of oogenesis and the annual ovarian cycle of *Stichopus californicus* (Echinodermata: Holothuroidea). *Biol. Bull.* **175:** 79–93.

Smiley, S. 1990. A review of Echinoderm oogenesis. *J. Electron Microsc. Tech.* **16:** 93–114.

Smiley, S. 1994. Holothuroidea. Pp. 401–471 in *Microscopic Anatomy of Invertebrates, Vol. 14, Echinodermata*, F. W. Harrison and F-S. Chia, eds. Wiley-Liss, New York.

Smiley, S., and R. A. Cloney. 1985. Ovulation and the fine structure of the *Stichopus californicus* (Echinodermata: Holothuroidea) fecund ovarian tubules. *Biol. Bull.* **169:** 342–364.

Smiley, S., F. S. McEuen, C. Chaffee, and S. Krishnan. 1991. Echinodermata: Holothuroidea. Pp. 663–750 in *Reproduction of Marine Invertebrates, Volume VI, Echinoderms and Lophophorates*, A. C. Giese, J. S. Pearse, and V. B. Pearse, eds. The Boxwood Press, Pacific Grove, CA.

Tanaka, Y. 1958. Seasonal changes occurring in the gonad of *Stichopus japonicus*. *Bull. Fac. Fish. Hokkaido Univ.* **9:** 29–36.

Théel, H. 1882. Holothuroidea. *Challenger Reports (Zoology) IV (8).* 176 pp.

Théel, H. 1901. On a singular case of hermaphrodism in holothurids. *Bihang till Kungl. Svensk. Vetensk-acad. Handl. 27: Afd. 4* **No. 6:** 1–38.

Tuwo, A., and C. Conand. 1992. Reproductive biology of the holothurian *Holothuria forskali* (Echinodermata). *J. Mar. Biol. Assoc. U.K.* **72:** 745–758.

Tuwo, A., and C. Conand. 1994. Fécondité de trois holothuries tempérées à développement pélagique. Pp. 561–568 in *Echinoderms Through Time, Proceedings of the 8th International Echinoderm Conference, Dijon, France*, B. David, A. Guille, J-P. Feral, and M. Roux, eds. A. A. Balkema, Rotterdam.

Tyler, P. A., and D. S. M. Billett. 1987. The reproductive ecology of elasipodid holothurians from the N. E. Atlantic. *Biol. Oceanogr.* **5:** 273–296.

Tyler, P. A., and J. D. Gage. 1983. The reproductive biology of *Ypsilothuria talismani* (Holothuroidea: Dendrochirota) from the N. E. Atlantic. *J. Mar. Biol. Assoc. U.K.* **63:** 609–616.

Tyler, P. A., J. D. Gage, and D. S. M. Billett. 1985a. Life-history biology of *Pentagone azorica* and *P. diaphana* (Echinodermata: Holothurioidea) from the north-east Atlantic Ocean. *Mar. Biol.* **89:** 71–81.

Tyler, P. A., A. Muirhead, D. S. M. Billett, and J. D. Gage. 1985b. Reproductive biology of the deep-sea holothurians *Laetmogone violacea* and *Benthogone rosea* (Elasipoda: Holothurioidea). *Mar. Ecol. Prog. Ser.* **23:** 269–277.

Tyler, P. A., D. S. M. Billett, and J. D. Gage. 1987. The ecology and reproductive biology of *Cherbonniera utriculus* and *Molpadia blaki* from the N. E. Atlantic. *J. Mar. Biol. Assoc. U.K.* **67:** 385–397.

Tyler, P. A., C. M. Young, D. S. M. Billett, and L. A. Giles. 1992. Pairing behaviour, reproduction and diet in the deep-sea holothurian genus *Paroriza* (Holothurioidea: Synallactidae). *J. Mar. Biol. Assoc. U.K.* **72:** 447–462.

Tyler, P. A., K. Eckelbarger, and D. S. M. Billett. 1994. Reproduction in the holothurian *Bathyplotes natans* (Holothurioidea: Synallactidae) from bathyal depths in the northeast and eastern Atlantic Ocean. *J. Mar. Biol. Assoc. U.K.* **74:** 383–402.

Viet Nam, N., and T. A. Britaev. 1992. Reproductive cycle of the sea cucumber *Holothuria leucospilota* in Nha Trang Bay (Southern Viet Nam). *Russ. J. Mar. Biol.* **18:** 185–191.

Reference: *Biol. Bull.* **192**: 27–40. (February, 1997)

Energy Use During the Development of a Lecithotrophic and a Planktotrophic Echinoid

O. HOEGH-GULDBERG[1] AND R. B. EMLET[2]

[1]*School of Biological Sciences, Building A08, University of Sydney, 2006 NSW, Australia; and*
[2]*Institute of Marine Biology and Department of Biology, University of Oregon, Charleston, OR 97420*

Abstract. The energy required for development was measured in two closely related echinoids with differing modes of development. *Heliocidaris tuberculata* hatches from a 95-μm egg ($\sim$0.1 μg dry organic mass) and develops *via* a planktotrophic larva over 21–30 days into a juvenile (5.3–7.5 μg). *H. erythrogramma* hatches from a $\sim$400 μm egg (11.6–19.0 μg) and develops over 3.5–4 days *via* a lecithotrophic larva into a juvenile with a mass not detectably different from that of the egg. Oxygen consumption increased exponentially in *H. tuberculata* and peaked at about 200–500 pmol indiv^{-1} h^{-1}, whereas the oxygen consumption of *H. erythrogramma* increased rapidly, reaching a plateau at about 800 pmol indiv^{-1} h^{-1} on the second day. Metabolic energy expenditure for development to metamorphosis was twofold higher for *H. tuberculata* (52–60 mJ indiv^{-1}) than for *H. erythrogramma* (26–35 mJ indiv^{-1}). The interspecific comparison suggests that about half the metabolic expenditure for planktotrophic development goes toward building and operating the larval feeding apparatus and that the return on this investment is 400%–600% over the larval period. When the energy equivalents of the organic masses of the juveniles are included, the energy for constructing a juvenile on a per mass basis is essentially the same for both species (*cf. H. tuberculata:* 37–42 mJ μg^{-1}; *H. erythrogramma:* 34–36 mJ μg^{-1}) and implies the absence of developmentally based energetic barriers or benefits to changes in modes of development. Substantial amounts of metabolically inactive material may be present in embryos with nonfeeding development and should be considered in physiological measurements and comparisons.

Introduction

Most marine invertebrates have life cycles that include a pelagic larva (Thorson, 1950) which may feed (planktotrophic) or not feed (lecithotrophic) on food particles. Nonfeeding larval development has evolved repeatedly in echinoderms and many other marine invertebrate phyla (*e.g.,* Strathmann, 1978a, 1993; Emlet, 1990, 1994; Wray, 1995) and is associated with increased size of eggs. With sufficient materials and energy in the larger eggs, lecithotrophic development is relatively rapid, and morphogenesis can be quite modified from that of related taxa with feeding larval development (*e.g.,* asteroids: Byrne, 1991, 1995; McEdward, 1992; Janies and McEdward, 1993; echinoids: Raff, 1987; Wray and Raff, 1989, 1990; nemerteans: Martindale and Henry, 1995). Among echinoids, studies on species with feeding and nonfeeding larval development have demonstrated remarkable changes in early embryology and larval form. Patterns of cell cleavage (Raff, 1987), cell lineages (Wray and Raff, 1989, 1990), and mechanisms of blastulation and gastrulation (Henry *et al.,* 1991; Wray and Raff, 1991; Schatt and Feral, 1996) have apparently changed. The timing of expression of larval and juvenile traits has been rearranged (*e.g.,* Raff, 1987; Wray and Bely, 1994; Emlet, 1995); larval shape and degree of retention of the ancestral larval structures varies (*e.g.,* Amemiya and Emlet, 1992; Olson *et al.,* 1993; Emlet, 1995; Morris, 1995). The length of the larval period and the size at metamorphosis can change (Lawrence *et al.,* 1984; McClintock and Pearse, 1986; Emlet *et al.,* 1987; Emlet and Hoegh-Guldberg, 1997).

Our understanding of how development evolves is particularly enhanced by comparisons between closely related taxa with differing modes of development. One area in which we lack such comparative data is the energy required for development. Energy required for development includes (a) the maternal energy contributed in the egg, (b) the total metabolic expenditure during development, and (c) the energy in the mass change between fertilization and metamorphosis. Larger eggs do

Received 26 April 1996; accepted 14 November 1996.

contain more energy, but few studies have been able to provide precise estimates of the energy required for different developmental modes (Jaeckle, 1995). We know little about whether metabolism changes when development changes. Because lecithotrophic species have their own energy supply and usually develop relatively rapidly, how does their metabolic activity change after fertilization? If rates are adjusted for mass-specific metabolism, how do planktotrophs and lecithotrophs compare? The large yolky eggs of many lecithotrophs may contain metabolically inert materials; how might this confound interpretations of mass-specific metabolism? Do lecithotrophic larvae, which have a finite maternal energy supply, require more or less energy to produce a juvenile than is required by planktotrophic larvae that must gather materials and energy through feeding? Although the evidence suggests that nonfeeding development has evolved repeatedly and a considerable effort has been made to understand this in terms of life-history evolution (*e.g.*, Vance, 1973; Strathmann, 1985; Roughgarden, 1989; Havenhand, 1993, 1995), we know of no studies (or theories) that have searched for developmentally based energetic differences associated with particular modes of development.

The present study compares the energy use by two closely related species with differing modes of development. By providing several genera that include both planktotrophic and lecithotrophic species, the echinoderm fauna of southeast Australia presents an unusual opportunity to minimize evolutionary distance and environmental differences. The echinoid genus *Heliocidaris* includes two species that co-exist in the Sydney region. The adult distributions partially overlap in shallow, subtidal, rocky habitats, and in general both species experience similar thermal and other environmental regimens during their life cycles. Laegdsgaard *et al.* (1991) found different seasons of reproduction for the two species, but viable gametes of both species were readily obtained for this study during Austral summers. *H. tuberculata* (Lamarck) hatches from a small egg (diameter ~95 μm) and completes development *via* a feeding larva over 21–30 days at 22°C (this study). *H. erythrogramma* (Valenciennes) hatches from a relatively large egg (~400 μm) and completes development in 3.5 to 4 days at 22°C (Williams and Anderson, 1975; Raff, 1987; Emlet, 1995). The divergence time for the two species has been estimated as 5–8 million years, on the basis of differences in mitochondrial DNA (McMillan *et al.*, 1992), and as 10–13 million years, on the basis of DNA hybridization methods (Smith *et al.*, 1990). The small genetic distance (*ca.* 10 million years *vs.* 10's to 100's of millions of years), and the similarity of adult habitats and physical regimens of the life cycles between sibling *Heliocidaris* species minimizes the influence of factors unrelated to the comparison of developmental mode.

This study utilizes the close relationship yet contrasting developmental modes of sibling species of *Heliocidaris* to compare biomass changes and metabolism from fertilization through metamorphosis. With this information, differences in the energy budgets of a lecithotroph and a planktotroph are analyzed. We also take advantage of the fact that the blastocoelic lipid reserves of *H. erythrogramma* can be largely removed (Emlet and Hoegh-Guldberg, 1997) and use this manipulation to provide a perspective on the partitioning of energy use in the two types of development. Comparison between the two species of the total energy required for development yields a quantitative measure of the maternal contribution of energy required to produce a juvenile. This interspecific comparison also permits us to estimate of the cost of building and maintaining a larval feeding apparatus and its efficiency for accumulating the energy required to construct a juvenile echinoid.

Materials and Methods

Collection, maintenance, and culture of embryos and larvae

The experiments described here were conducted over three reproductive seasons (primarily December 1992–January 1993 and January–February 1994, but also January–February 1996). *Heliocidaris erythrogramma* and *H. tuberculata* were collected, under permit, from Shelly Beach, Fairy Bower, and Clovelly near Sydney, Australia. Adults were maintained at the University of Sydney in recirculating aquaria for up to a week. Animals were spawned by coelomic injection with 0.5 *M* KCl. Eggs were washed with several changes of 1-μm filtered seawater and fertilized with dilute concentrations of sperm. Fertilized eggs were placed in dishes without stirring for the first day, and gentle stirring of cultures began on day 2.

Embryos and larvae were cultured at 22°C and culture water was changed every 2–3 days. Cultures of *H. erythrogramma* were checked for juveniles beginning on the third day. Cultures of *H. tuberculata* were fed algal cells (*Chaetoceros gracilis* or *Rhodomonas lens*, CSIRO, Hobart) at final concentrations of 20–50 × 10^3 cells ml^{-1}, and the first individuals completed development in 21–30 days. Larvae of both species either metamorphosed spontaneously or were induced to metamorphose with scrapings from algal-encrusted rocks.

Removal of blastocoelic lipid from embryos of Heliocidaris erythrogramma

Lipid-rich vesicles are extruded into the blastocoel of *H. erythrogramma* during the first 8–12 h of development and prior to hatching (Henry *et al.*, 1991). These blastocoelic vesicles were removed from newly hatched

blastulae (12–14 h post-fertilization) by centrifuging blastulae for two 15-s intervals in a microcentrifuge (Beckman Microfuge E). Blastocoelic lipid extrudes through tiny rips in the blastoderm of the blastulae during centrifugation. Embryos at this stage do not have mesenchyme cells and hence the loss of cells from the blastula is minimal. This manipulation removes almost all the blastocoelic lipid, which occupies about 40% of the volume of the blastula (Emlet and Hoegh-Guldberg, 1997), and embryos treated in this manner develop normally to the juvenile stage in the same time as untreated larvae (Emlet and Hoegh-Guldberg, 1997). We refer to this as the "reduced-lipid" treatment.

Dry organic mass

Dry organic mass was measured for eggs, embryos, and larvae of the two *Heliocidaris* species at various developmental stages. These measurements were used to follow changes in biomass during development and to make calculations on energy use. Five or six replicate determinations of biomass based on 15–200 (*H. erythrogramma*) or 300–2800 (*H. tuberculata*) individuals per determination were made for eggs, embryos, and larvae. Individuals for organic-mass determination were concentrated by removing seawater around the embryos or larvae. Initial samples were frozen in small amounts of seawater, but later (and most) samples were rinsed for a few seconds in distilled water (McEdward, 1984) prior to being frozen (−20°C). Frozen larvae were added to small aluminum dishes (pre-ashed at 458°C for 6 h) and were dried at 80°C to constant mass (which occurred between 5 and 10 d). Samples were then weighed (total dry mass) to the nearest microgram on a mass-calibrated electrobalance (Cahn 25, Cahn/Ventron), and subsequently ashed at 458°C for 6 h. Ashed samples were weighed (ash mass) on the same balance, and dry organic mass was calculated as the difference between the total dry mass and the ash mass, and expressed as dry organic mass per larva.

Polarographic respirometry of growing and differentiating larvae

Polarographic respirometry was used to measure the metabolic rate of embryos and larvae at various stages during development and for embryos in which lipid reserves had been removed. Microrespirometry chambers (100-μl and 500-μl) and polarographic oxygen electrodes (Strathkelvin Instruments, Glasgow, U.K., OM780 and SI1302) connected to a data acquisition and analysis system (DATACAN IV, Sable Systems, Los Angeles, CA) were used to measure the metabolic rate of the embryos and larvae. Chamber temperature was 22°C and was controlled to within ±0.1 C° by a temperature-controlled water bath (HAAKE 6) connected to the water jacket of each microrespirometer cell. Respirometry chambers contained known numbers of individuals (range 5–175, usually 10–30 for *H. erythrogramma,* and range 20–1179, usually 50–150 for *H. tuberculata*) for each measure of oxygen consumption. The highest numbers were for eggs and cleavage stages, which had low rates of oxygen consumption, and the lowest numbers were for larval stages. Metabolic rate was calculated as oxygen consumption in pmol O_2 individual^{-1} h^{-1}. Specific metabolic rates (SMR = metabolic rates standardized to mass) were calculated by dividing respiratory rates by the mean dry organic mass of samples of embryos or larvae taken within ±1 day of each reported SMR.

Calculation of energy budgets and the maternal investment of each species in its eggs

Energy budgets for the entire development of each species were constructed to compare energy use between the two types of development. Energy values for biomass and oxygen consumption were calculated with data collected from two to four cultures. Biomass of eggs and changes in biomass during development were converted into units of energy, joules (J), by using the energy equivalents for combustion enthalpy for each fraction (lipid = 39.5 kJ g^{-1}, protein = 24.0 kJ g^{-1}, and carbohydrate = 17.5 kJ g^{-1}; Gnaiger, 1983). For changes in biomass, the material laid down was assumed to have the same composition as that of eggs. The composition of eggs (percent lipid, protein, and carbohydrate) of the two *Heliocidaris* species was estimated from data collected for a wide range of planktotrophic and lecithotrophic echinoderm species (table 6 in Jaeckle, 1995). These data indicate that the eggs of lecithotrophic and planktotrophic species have characteristically distinct percentages of constituents. Assuming that the remainder fraction of the egg resembles the composition of the measured portion, the mean composition of the eggs of lecithotrophic species is 57.0% lipid, 40.0% protein, and 3.0% carbohydrate and of planktotrophic species is 28.6% lipid, 65.6% protein and 5.8% carbohydrate. Our use of these estimates is supported by preliminary biochemical analyses of the composition of eggs of *H. erythrogramma;* the results indicate that larvae with a normal complement of blastocoelic lipid consist of 58% lipid, 39% protein, and 3% carbohydrate (A. Moran, unpubl. data). The composition of gonadal tissue from *H. tuberculata* and *H. erythrogramma* (Lawrence and Byrne, 1994) also supports these values estimated from Jaeckle (1995). The respective percentages of lipid, protein, and carbohydrate in tissues of the ripe ovaries were as follows: *H. erythrogramma*—50%, 38%, and 8%; *H. tuberculata*—27%, 54%, and 12% (table 3 in Lawrence and Byrne, 1994).

For each species, total metabolic expenditure for development was calculated from the total amount of oxygen taken up over the entire course of development. To-

tal oxygen consumption was determined by integrating 3rd or 4th order polynomial equations fitted to respirometry data (instantaneous metabolic rates) with a curve-fitting program (Solver, Microsoft, USA $r^2 > 0.95$). The total oxygen was converted into energy units, J, by assuming that the substrate being combusted was a mixture of lipid, protein, and carbohydrate and by using the oxyenthalpic equivalent for this mixture (480 kJ/mol O_2) determined from Gnaiger (1983).

The maternal investment of energy into the eggs of the two species was compared using calculations of the energy contained within the eggs and the energy required for complete larval development (see above). Some calculations of the energy content of the eggs of *H. erythrogramma* also took into consideration the fact that about half the egg (Table I) consists of a blastocoelic lipid-rich component that is used primarily for juvenile development (Emlet and Hoegh-Guldberg, 1997). In this case, egg energy content was calculated by excluding the proportion of the egg mass removed by centrifugation of blastulae and assuming that the rest of the egg has the same lipid, protein, and carbohydrate fractions as the original egg. This last assumption was made because the biochemical composition of the reduced-lipid embryos was not measured and will cause an overestimate of energy content of reduced-lipid embryos by as much as 15% if centrifugation produced embryos with a composition similar to that of planktotrophic eggs.

Results

Changes in dry organic mass

Heliocidaris tuberculata. Three cohorts of larvae were raised through metamorphosis with the first individuals metamorphosing on days 21, 29, and 30 for the separate cultures. Dry organic mass was measured for these cohorts and for others not raised through metamorphosis. The eggs from two cohorts of *Heliocidaris tuberculata* had estimated dry organic masses of 0.12 ± 0.01 μg egg^{-1} and 0.22 ± 0.02 μg egg^{-1} (mean ± 1 SEM), respectively. The egg masses of these cohorts are significantly different (*t*-test: $T = 4.82$, df = 10, $P = 0.001$), but the higher value for one cohort may be in error because it was based on samples frozen in small amounts of seawater and these may have absorbed moisture upon initial weighing. The value of 0.12 μg egg^{-1} falls on the regression line of egg volume and dry organic weight for eggs of echinoderm species with lecithotrophic and planktotrophic development (fig. 1 in Jaeckle, 1995) and is used for calculations throughout this study.

Larval masses increased exponentially during feeding larval development. Competent larvae, recognized by well-developed juvenile rudiments including definitive spines and shortened larval arms, had masses of 4.18 ± 0.93 μg $larva^{-1}$ to 5.97 ± 0.34 μg $larva^{-1}$ (mean ± 1 SEM), representing a 35- to 50-fold increase from a 0.12 μg egg^{-1} over the 21–30-day larval period (Fig. 1A). The calculated change in dry organic weight ranged between 4.06 and 5.86 μg $larva^{-1}$. Two-day-old juveniles of two cohorts had dry organic masses of 5.26 ± 0.24 μg $juvenile^{-1}$ (mean ± 1 SEM) and 7.49 ± 0.39 μg $juvenile^{-1}$, respectively.

Heliocidaris erythrogramma. The dry organic mass of the eggs of *Heliocidaris erythrogramma* differed significantly among seven cultures (ANOVA, $F = 8.83$, df = 6, $P < 0.001$) and ranged from 11.59 ± 0.93 μg egg^{-1} to 18.97 ± 1.03 μg egg^{-1} (mean ± 1 SEM). Ovoid eggs had equivalent, mean spherical diameters of 369 to 418 μm for six cultures. The dry organic mass of embryos of *H. erythrogramma* from which the blastocoelic contents had been removed by centrifugation was measured to estimate the percentage of the egg mass that was contributed to the blastocoelic contents (Table IA). The mean percentage that was blastocoelic contents was $52.2 \pm 5.1\%$ (mean ± 1 SEM) and ranged from 39.8 to 64.7% (= mean ± 95% CI).

The mean dry organic masses of *H. erythrogramma* remained unchanged in one culture, increased in another, and decreased in two others after 4 days of larval development (Fig. 1B). Three of these cohorts showed nonsignificant changes in mass, and one showed a significant drop over this interval (*t*-tests, Table IB). Larvae of *H. erythrogramma* from which the blastocoelic lipid had been removed developed normally to the juvenile stage in the same time (3.5–4 d) as control echinoids (see also Emlet and Hoegh-Guldberg, 1997).

At metamorphosis, control juveniles of *H. erythrogramma* had substantially greater organic mass than reduced-lipid juveniles. One-day-old control juveniles from four cohorts had mean dry organic masses of 12.4, 16.5, 18.9, and 19.4 μg $individual^{-1}$ ($n = 3$ to 6 replicate samples per cohort). Sibling reduced-lipid juveniles from the same cohorts had mean dry organic masses of 4.4, 7.2, 10.2, and 13.8 μg $individual^{-1}$, respectively ($n = 2$ to 5 replicate samples per cohort). These values for reduced-lipid juveniles range from 0.8 to 1.8 times the dry organic mass of juvenile *H. tuberculata.* Because metabolic studies were conducted on cohorts of *H. erythrogramma* from the upper part of the egg-mass distribution, even reduced-lipid juveniles from these cohorts had masses greater than those of *H. tuberculata.* These values indicate that juveniles of the two species differ in mass and energy content even after blastocoelic lipid materials are taken into account. See Emlet and Hoegh-Guldberg (1997) for comparisons of juvenile size and growth between the control and reduced-lipid treatments of *H. erythrogramma* and between the congeners.

Metabolic rates during development

Heliocidaris tuberculata. The metabolic rate of *H. tuberculata* increased from near zero (1.99 to

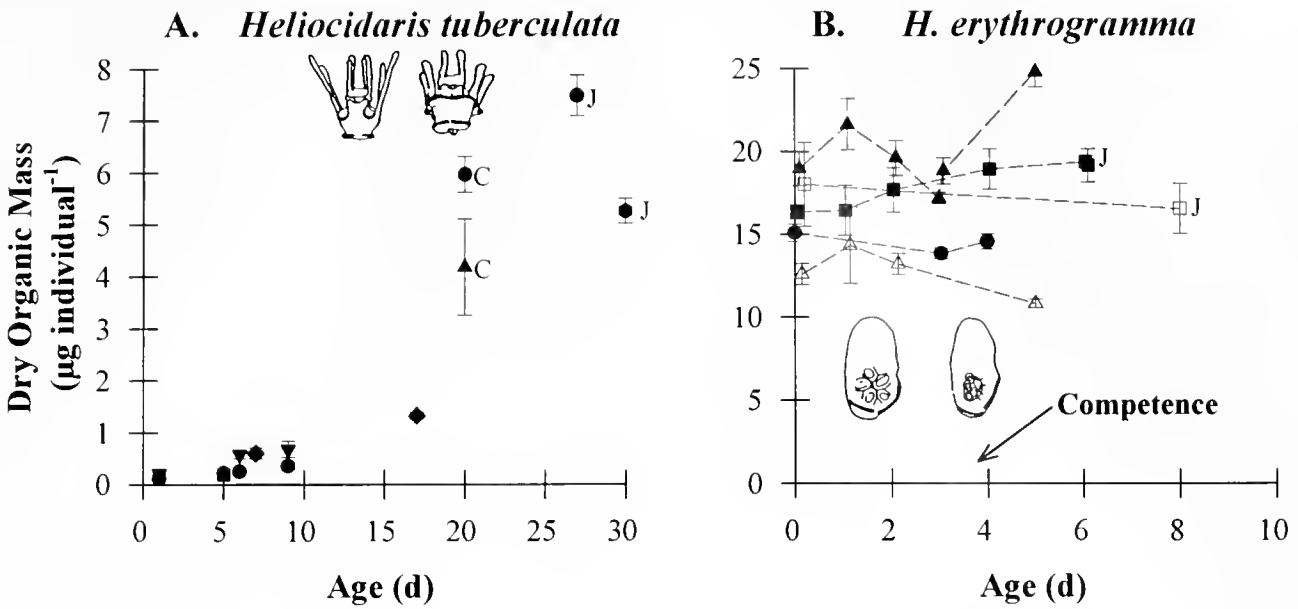

Figure 1. Changes in dry organic mass as a function of time for the embryos and larvae of the planktotrophic echinoid, *Heliocidaris tuberculata* (A), and the lecithotrophic echinoid, *H. erythrogramma* (B). Shown are means ± 1 SEM (n = 5–6 replicate weight determinations at a given age), with different symbol types representing cultures derived from separate parental pairs. Drawings indicate the morphology of larvae at various stages during development (adapted from Emlet, 1995). C, competent larval stages; J, juveniles. The arrow indicates the approximate age at which *H. erythrogramma* reaches metamorphic competence.

4.75 pmol O_2 larva^{-1} h^{-1}) to metabolic rates that ranged between 200 and 500 pmol O_2 larva^{-1} h^{-1} (Fig. 2A). Metabolic rates generally followed changes in biomass. However, specific metabolic rates (SMR) indicated that this was not strictly so. Three distinct phases could be identified (Fig. 3A): (1) An initial increase in specific metabolic rate over the first 2 days; (2) a relatively stable phase from days 2 to 10 in which the SMR ranged between 150 and 250 pmol O_2 μg^{-1} h^{-1}; and (3) a final phase (days 10–22) in which the SMR dropped to between 50 and 150 pmol O_2 μg^{-1} h^{-1}.

Heliocidaris erythrogramma. The metabolic rate of *H. erythrogramma* showed some dramatic changes during development. Metabolic rates increased steadily from 17 to 27 pmol O_2 larva^{-1} h^{-1} just after fertilization to approximately 600–800 pmol O_2 larva^{-1} h^{-1} at 36 h (22°C, Fig. 2B). A transient spike in the metabolic rate was seen in some cultures between 25 and 31 h after fertilization (corresponding to late gastrulation, early vestibule formation). This spike was not seen in all cultures, however. Metabolic rates ranged from 600 to 1000 pmol O_2 larva^{-1} h^{-1} from 1.5 days after fertilization until metamorphosis and then declined with time after metamorphosis (Fig. 2B). Two days after metamorphosis, juveniles (two cohorts), for example, had metabolic rates that ranged between 200 and 400 pmol O_2 larva^{-1} h^{-1} (Fig. 2B).

Specific metabolic rates of *H. erythrogramma* larvae were lower than those of *H. tuberculata* for most of their development (*cf.* SMR ranges, *H. erythrogramma:* 0–100 pmol O_2 μg^{-1} h^{-1}, Fig. 4; and *H. tuberculata:* 0–300 pmol O_2 μg^{-1} h^{-1}, Fig. 3A). However, if SMRs are calculated using dry organic masses from which the blastocoelic lipid fraction has been removed, SMR values showed a greater resemblance to those of *H. tuberculata* (Figs. 3A and B, 5). The metabolic rates of embryos with and without blastocoelic lipid were measured in order to investigate the metabolic activity of the blastocoelic fraction of *H. erythrogramma* embryos. Removal of lipid rich contents from embryos in five separate cultures revealed that larval metabolic rates were not different between uncentrifuged (control) and reduced-lipid embryos (Fig. 6, Nested ANOVA, testing for effects of removing lipid contents $F_{5,28} = 0.25$, $P = 0.94$).

Energy budgets, maternal investment, and the energy required to produce a juvenile

Energy budgets were constructed to provide precise measurement of the energy required for development in both species. Calculated totals were then used together with the energetic contents of eggs to provide estimates of the proportion of energy for development that was provided as maternal investment in the egg.

Table I

Dry organic mass (micrograms per individual) for Heliocidaris erythrogramma

A. Embryos (24–30 h) with (Control) and without (Reduced Lipid) blastocoelic lipid from 7 independent cultures

	Control embryos		Reduced lipid embryos		
Culture ID (*n**)	Mean	1 SEM	Mean	1 SEM	Blastocoelic Contents (%)†
HE013 (5,6)	17.7	1.4	10.5	1.3	40.8
HE016 (6,6)	18.6	1.4	11.9	1.1	35.9
HE017 (6,6)	18.9	0.8	10.2	0.8	46.1
HE94/3 (4,5)	12.4	0.5	4.4	0.5	64.3
HE94/4 (5,5)	14.4	2.3	4.4	0.8	69.1
HE94/5 (6,6)	12.7	0.7	4.4	0.3	65.0
HE94/6 (5,5)	18.0	2.5	10.0	1.6	44.4
Mean	16.1		8.0		52.2
SEM	1.1		1.3		5.1
Min (95% CI)	13.4		4.9		39.8
Max (95% CI)	18.7		11.1		64.7

B. Eggs and competent larvae from cultures shown in Figure 1B

	Eggs		Competent larvae		*t*-tests (df 10)
Culture ID (*n**)	Mean	1 SEM	Mean	1 SEM	*T*, prob.
HE010 (6,6)	15.10	0.52	14.61	0.47	0.70, $P = 0.50$
HE013 (6,6)	16.35	0.42	18.96	1.21	2.03, $P = 0.07$
HE017 (6,6)	18.97	1.03	18.62	0.80	0.82, $P = 0.94$
HE94/4 (6,6)	12.59	0.64	10.85	0.25	2.53, $P = 0.03$

* The number of replicate samples for each treatment.

† The blastocoelic contents (%) is the percent of the original mass removed by centrifugation of blastulae.

Heliocidaris tuberculata. During the course of development *H. tuberculata* accumulated biomass that represented between 114 and 164 mJ individual^{-1} (Table IIA). Between 108.9 and 124.6 nmol of oxygen or 52 and 60 mJ individual^{-1} was utilized in routine metabolism during this same period (Table IIB). Excluding maternal investment in the egg, the energy for development is approximately equal to the sum of these two components and ranged between 174 mJ individual^{-1} and 216 mJ individual^{-1}. If one includes the energy invested into the egg, the energy for development is slightly higher and is equal to 177–220 mJ individual^{-1}. On a per weight basis, the energy for producing a juvenile of *H. tuberculata* ranges from 37–42 mJ μg^{-1}.

The proportion of energy for producing a juvenile that comes from maternal investment in the egg can be calculated by dividing the energy invested into an egg by the total energy for development. Values calculated in this way yielded estimates of maternal investment by *H. tuberculata* of less than 2% of the total energy required to produce a juvenile (1.3% and 1.6% for two cohorts).

Heliocidaris erythrogramma. For three of four cultures, changes in the biomass were not significant over the 3.5–4 days it took *H. erythrogramma* to develop into a juvenile (Table IB). Based on the integrated metabolic rate of *H. erythrogramma* over the time course of development, the expected decline in biomass (total energy burned in respiration divided by 27 kJ g^{-1}, the energy released per gram of a mixture of protein, carbohydrate, and lipid aerobically combusted; Gnaiger, 1983) was between 0.9 and 1.3 μg individual^{-1}. This is below the precision of the method used to measure dry organic weight.

H. erythrogramma utilized 55.2 to 74.1 nmol O_2 individual^{-1} (range of means from four cultures) to develop into a juvenile. In energetic equivalents this is 26 to 35 mJ individual^{-1} (Table IIIB). The energy required for *H. erythrogramma* to develop into a juvenile (excluding maternal investment in the egg) was therefore 29 ± 6 mJ individual^{-1} (mean ± 95% CI; Table IIIC). If the maternal investment in the egg was added (including that used for juvenile development), the total energy for *H. erythrogramma* to develop into a juvenile was 571 ± 87 mJ individual^{-1} (mean ± 95% CI; Table IIID). If one takes into account that about 52.2% of the *H. erythrogramma* egg is used for juvenile development and is not an investment in embryonic and larval development (Emlet and Hoegh-Guldberg, 1997), the energy for development is 325 ± 68 mJ individual^{-1} (mean ± 95% CI; Table IIID).

The energy for producing a juvenile was estimated by dividing the total energy for development by the mass of juvenile produced. The estimated energy for development per microgram of juvenile body produced ranged between 34.1 and 34.8 mJ μg^{-1} across the four cohorts examined. The mass-specific energy for producing a juvenile of *H. erythrogramma* was similar even when the blastocoelic contents were excluded from the calculation of both the total energy required for development and the total energy supplied to the egg (range 35.4–36.3 mJ μg^{-1}, Table IIIE).

Maternal investment including the lipid-rich blastocoelic component was 94.8% ± 1.3% (mean ± 95% confidence interval, $n = 4$) of the total energy required to make a juvenile. Maternal investment by *H. erythrogramma* excluding this blastocoelic component was 90.8% ± 1.6%. In either case this was many times greater than the maternal investment by *H. tuberculata* (<2%).

Discussion

Despite the active discussion for more than 50 years on larval life-history patterns of marine invertebrates (*e.g.*, Thorson, 1950; Crisp, 1976; Strathmann, 1985; Havenhand, 1995), precise estimates of the energetics of development are lacking for invertebrates with differing

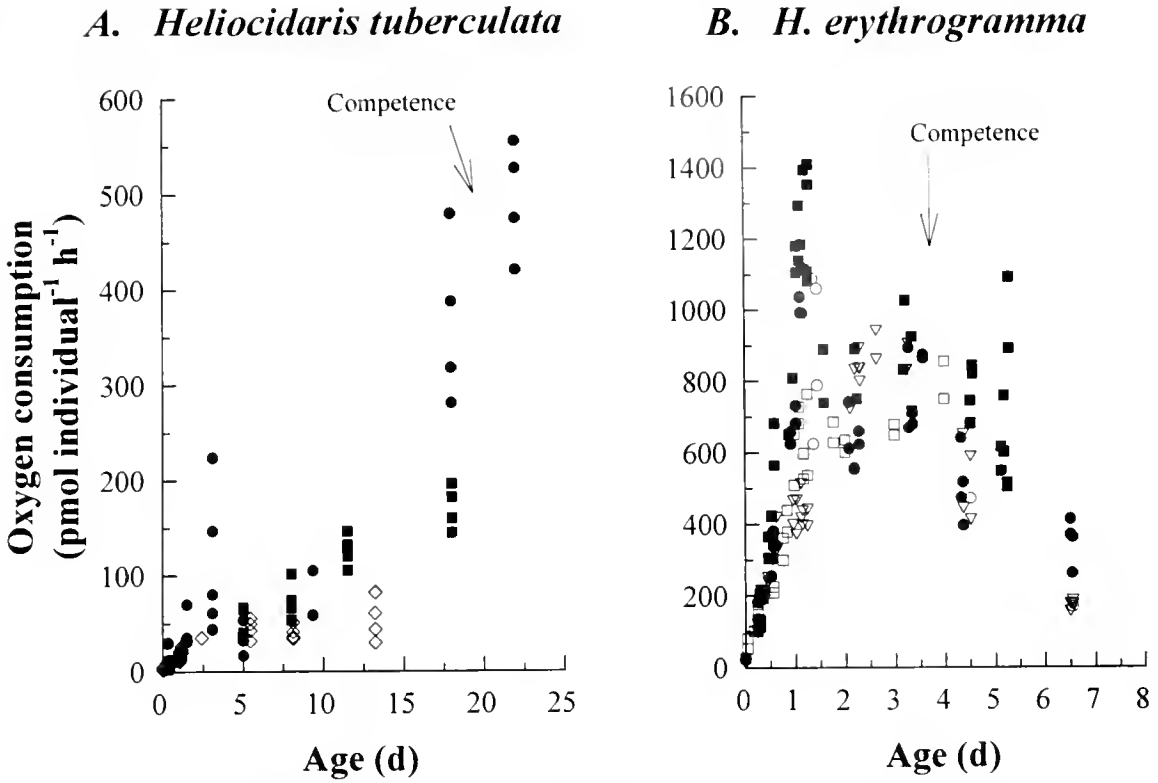

Figure 2. The oxygen consumption of embryos and larvae of the planktotrophic echinoid, *Heliocidaris tuberculata* (A), and the lecithotrophic echinoid, *H. erythrogramma* (B). Symbols represent individual respirometry measurements (a chamber of larvae at a given stage) with different symbol types representing individual cultures derived from separate parental pairs. Arrows indicate the approximate ages at which metamorphic competence occurred in each species.

modes of development. This study addresses this issue for two species of congeneric urchins, estimating the energy required for development, the energy required to build and operate a feeding larva and that required to transform an egg into a juvenile, and the percentage of the total energy required for development that is invested into the two egg types by the mother. The key observation of the present study is that although the two species differ greatly in terms of developmental mode, metabolic expenditures, and maternal investment, the energy required to make a juvenile is essentially the same when scaled to juvenile mass.

Changes in metabolic rates as a function of developmental stage

A rapid increase in the metabolic rate of both species of sea urchins characterizes the first 2 days of development. The egg rapidly differentiates into the cellular components required for further development during this period. For *Heliocidaris tuberculata*, this involves the formation of the feeding apparatus required to accumulate further resources over the 3–4-week period of development. *H. erythrogramma* develops directly into a juvenile sea urchin over 3.5–4 days at 22°C. In this case, the differentiation presumably results in a minimal swimming apparatus and the juvenile rudiment. Although comparisons are complicated by the differences in the duration of development between the two species, some interesting trends are revealed.

The rapid rise in metabolic activity slows at the end of the second day in both species and leads to a period in which the metabolic activity per gram of tissue (specific metabolic rate, SMR) remains relatively constant (Figs. 3, 4). In the case of *H. tuberculata*, the SMR during this second phase ranges between 150 and 250 pmol O_2 μg^{-1} h^{-1}. *H. erythrogramma* had SMR values ranging between 30 and 70 pmol O_2 μg^{-1} h^{-1}. Part of the difference between the SMR of the two species is due to the presence of a large amount of blastocoelic lipid in the larvae of *H. erythrogramma*. This lipid-rich store, representing about 50% of the dry organic mass of the larva, does not appear to influence the success or timing of larval development (Emlet and Hoegh-Guldberg, 1997), and its removal does not affect the metabolic activity of larvae (Fig. 6). The SMR of *H. erythrogramma* was corrected for the presence of non-metabolically active lipid by standardizing rates to masses excluding blastocoelic

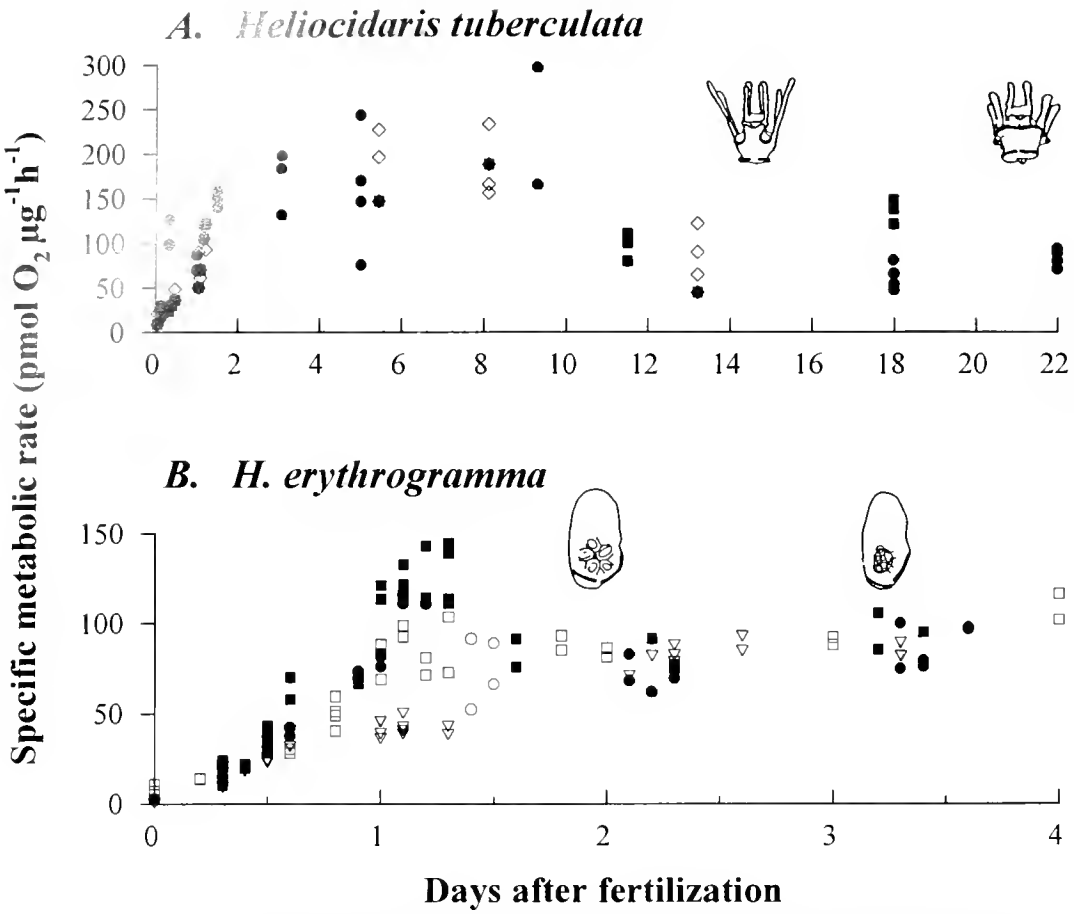

Figure 3. The specific metabolic rate of *Heliocidaris tuberculata* (A) and *H. erythrogramma* (B) as a function of age. The SMRs for *H. erythrogramma* were calculated by dividing larval metabolic rates by the dry organic mass of the reduced-lipid embryos for a given culture. This "corrected" SMR assumes that not all embryo or larval mass is metabolically active and is corroborated by data presented in Fig. 6. Symbols represent individual respirometry measurements (a chamber of larvae at a given stage), and different symbol types represent cultures derived from separate parental pairs. Drawings indicate the morphology of larvae at various stages during development (adapted from Emlet, 1995).

contents (*cf.* Figs. 3B, 4). SMR values of *H. erythrogramma* larvae corrected to active metabolic tissue were similar to the SMR of *H. tuberculata* over the last 10 days of its development (*cf.* Ht: 50–150 pmol O_2 μg^{-1} h^{-1}; He: 50–100 pmol O_2 μg^{-1} h^{-1}).

The slower and more stable growth of the feeding larva during the last part of development of *H. tuberculata* suggests that the increased SMR earlier in the development of this species (~250 pmol O_2 μg^{-1} h^{-1} as opposed to 50–150 pmol O_2 μg^{-1} h^{-1}; Fig. 3) is associated with the greater amount of metabolic activity required to form larval arms, skeleton, and associated feeding structures. Coeloms are also growing during this period of increased metabolism, but the vestibule or amniotic invagination has not yet formed (Emlet, pers. obs.). In this case, the difference between the larval structures of the early larval stages of *H. tuberculata* and those seen later in this species and in *H. erythrogramma* is that *H. tuberculata* does not have a significant amount of rudiment tissue early in development. This difference implies that metabolic rates of young *H. tuberculata* larvae are being standardized to smaller masses of relatively more active tissue and that rudiment tissues are relatively less active metabolically. If the SMR of rudiment tissues is lower than that of functioning larval tissues, then (in the presence of ample food or energy reserves) energetic savings might be gained by forming rudiment tissues early in development rather than investing in more expensive larval tissues.

The SMR values reported here are at the lower end of a large range of values published for feeding and growing invertebrate larvae (268–893 pmol O_2 μg^{-1} h^{-1} dry organic mass), which were reviewed by Hoegh-Guldberg and Manahan (1995), based on numbers presented by Crisp (1976). The viability of larvae during respirometry measurements was also investigated during experiments

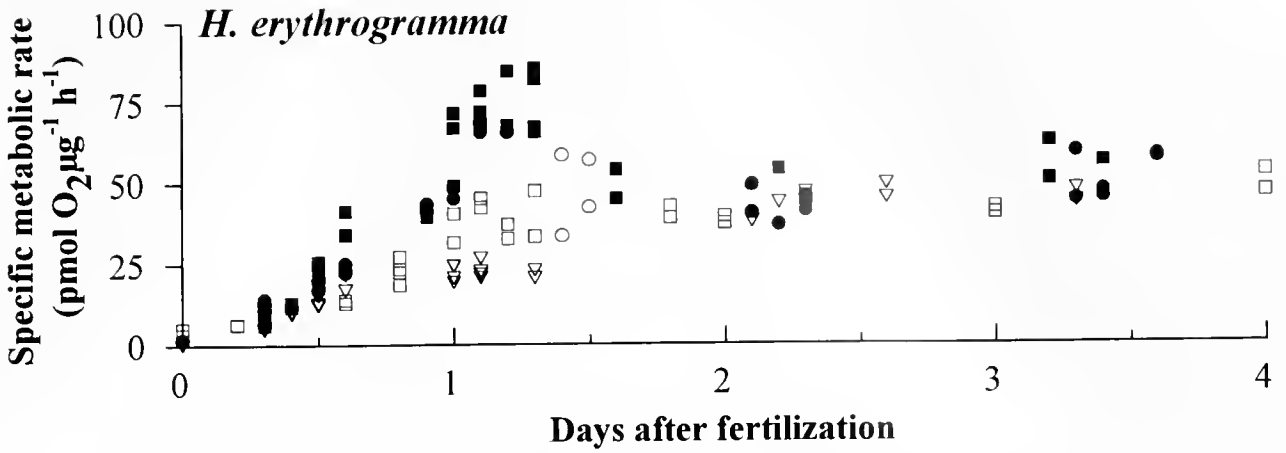

Figure 4. The "uncorrected" specific metabolic rate of the echinoid *Heliocidaris erythrogramma* standardized to the mass of the egg (including blastocoelic lipid). These uncorrected SMRs are roughly half those reported in Fig. 3B. However, the relative positions of some measurements have shifted between Figs. 3B and 4 because the % blastocoelic lipid varies among larvae from different cultures. Metamorphic competence occurred at 3.5–4 days.

reported here. Larvae were always intact and swimming normally after respirometry measurements. Ongoing work by Moreno and Hoegh-Guldberg (unpublished) has revealed that the problems reported by Hoegh-Guldberg and Manahan (1995) are probably the result of the small chambers used in the latter experiments rather than an inherent problem with the polarographic oxygen technique (leaking of KCl, effect of electric fields, etc.).

Energy budgets, maternal investment, and the energy for producing a juvenile

H. tuberculata increases in size at an average rate of between 0.20 and 0.27 µg d^{-1} over its developmental period of 3+ weeks. During the same time, between 108.9 and 124.6 nmol of oxygen were consumed. By comparison, *H. erythrogramma* did not increase in size. In this case, the decrease in mass was probably in the range of 1–1.5 µg individual^{-1} (based on its metabolic rate) over its short developmental period and hence was too small to detect with the methods used here. The embryos and larvae of *H. erythrogramma* also consumed about half as much (45%–68%) oxygen as *H. tuberculata* (between 55.2 and 74.1 nmol individual^{-1}, range of means from four cultures of *H. erythrogramma*).

Although the oxygen consumption of *H. erythrogramma* was lower, its maternal investment was higher than that of *H. tuberculata*. In echinoids, the energy reserves of the egg are used by embryos and larvae as sources of both nutrients and energy. *H. tuberculata* produces eggs that are 95 µm in diameter and contain about 3.3 mJ of energy (assuming a mixture of lipid, protein, and carbohydrate that is typical of planktotrophic eggs; Jaeckle, 1995). By comparison, *H. erythrogramma* produces eggs that are 370 to 420 µ in diameter and contain between 490 and 619 mJ of energy (assuming typical lecithotrophic egg composition; Jaeckle, 1995) or 241 and 334 mJ of energy when blastocoelic lipid is excluded.

The difference in the size of egg energy reserves between *H. tuberculata* and *H. erythrogramma* contributed to the difference in energy required to make a juvenile in the two species. Results from two separate cultures revealed that it takes between 177 and 220 mJ of energy to make a juvenile of *H. tuberculata*. These values are both below the lower 95% confidence interval (257 mJ) of the energy required for making a juvenile of *H. erythrogramma* (mean = 325 mJ, see Table IIID). When the lipid-rich component is removed from embryos of *H. erythrogramma*, the resulting juveniles have test and overall dimensions at settlement that are similar to those of *H. tuberculata* (Emlet and Hoegh-Guldberg, 1997), but in some instances the dry organic masses of these juveniles were still greater than those for juveniles of *H. tuberculata*. Thus part of the absolute difference in energy for development is reflected in different masses of the resulting juveniles, even when blastocoelic lipids are excluded.

If the total energy to make a juvenile is standardized to the mass of juvenile produced, the difference between the two species largely disappears (*cf.* values for *H. tuberculata*: 37, 42 mJ µg^{-1} and *H. erythrogramma*: 34, 35, 35, 34 mJ µg^{-1} when blastocoelic contents are included and 35, 36, 36, 36 mJ µg^{-1} when they are excluded). This result means that the energy to make a juvenile *via* feeding larval development is essentially the same as the energy to make one directly from reserves added to the egg. This suggests that larval acquisition of materials from the environment to produce a juvenile may be nearly as

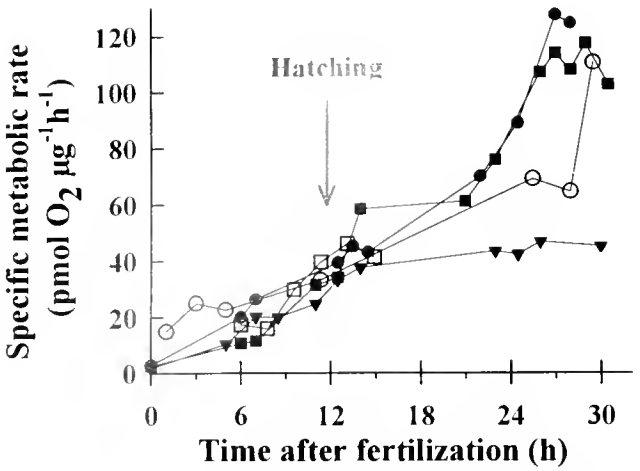

Figure 5. The specific metabolic rate of *Heliocidaris tuberculata* (open symbols) and *H. erythrogramma* (closed symbols) during early development. The SMRs of *H. erythrogramma* were calculated using masses excluding blastocoelic lipids. Symbols represent individual respirometry measurements. The arrow indicates the approximate point at which hatching occurred.

efficient as the "pre-packaging" of materials provided in the lecithotrophic egg. Comparable calculations of energy per microgram for planktotrophic larval development of the crown-of-thorns seastar, *Acanthaster planci* (from table 1 in Hoegh-Guldberg, 1994; measurements done at 27°C), and for the lecithotrophic larvae of the red abalone, *Haliotis rufescens* (from tables 2 and 3 of Jaeckle and Manahan, 1989, at 16°–17°C), yield values of 37 mJ μg^{-1} and 36–38 mJ μg^{-1} respectively, suggesting that the energy for development corrected for organic mass is strikingly similar among echinoids, asteroids, and gastropods. Further studies that include both planktotrophic and lecithotrophic comparisons are required and are in progress to substantiate this generalization and these studies (Moreno and Hoegh-Guldberg, unpublished).

The interspecific comparisons of metabolism and energy requirements allow some measure of the effectiveness with which feeding larvae acquire energy. Metabolic expenditures (measured as oxygen consumed) by larvae of *H. tuberculata* were roughly twice those measured for *H. erythrogramma* over their respective developmental intervals. Because eggs of *H. erythrogramma* contain all the necessary reserves for juvenile construction, the metabolism measured can be considered to be the metabolic cost to turn these reserves into a juvenile and maintain it (range for four cohorts = 26 to 35 mJ). If one assumes that half of the metabolic expenditure of *H. tuberculata* goes (ultimately) toward the same purpose, then the remaining half of the metabolic expenditure is used to build and power the larval feeding apparatus and digestive system to acquire these reserves. In return for this investment in larval feeding (half of the metabolic expenditure was 26 to 30 mJ individual^{-1}), the offspring increases 35- to 50-fold in organic matter, representing an increase in energy content of 114 to 164 mJ individual^{-1}. These numbers suggest that for every millijoule expended to power the feeding systems there is roughly a return of 5 to 7 mJ (1 mJ used to power the feeding systems and 4 to 6 mJ that supply materials for juvenile construction). In other words, return on the investment is 400% to 600% over the 21- to 30-day interval! These numbers may be high for several reasons. If our measurements of metabolic rates are low, then the actual investment in feeding is higher and the relative return lower. Our studies were conducted at high food concentrations under laboratory conditions. High food concentrations reduce the time for development and minimize the energy required by restricting the period over which metabolic expenditures occur. The developmental period for pluteus larvae can be extended by weeks to months on limited food (*e.g.*, Paulay *et al.*, 1985; Fenaux *et al.*, 1988, 1994; Pedrotti and Fenaux, 1993), in which time larvae are metabolically active but not gaining biomass at maximal rates (see Strathmann, 1978b, 1987, for examples of the varying planktonic durations). Under situations of food limitation with prolonged development, the return on the investment in the feeding apparatus would be expected to drop.

The values for the effectiveness of the larval feeding were based on a congeneric, interspecific study of energy for development, and we know of no similar studies for comparison. Similar measurements on other congeners with differing modes of development should permit comparisons of effectiveness of different kinds of feeding larvae. In a recent comparison of feeding rates among 11

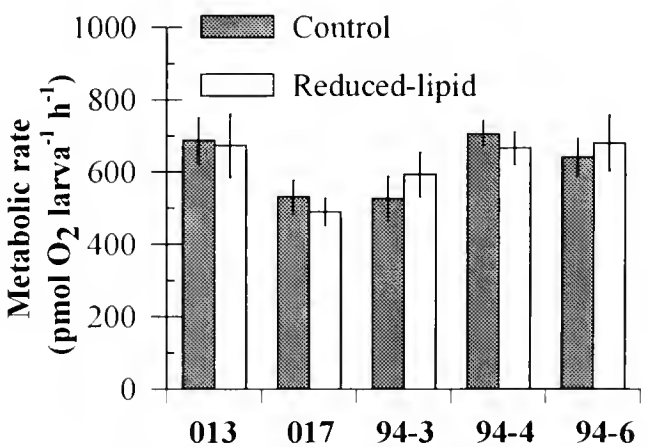

Figure 6. Metabolic rates of larvae of *Heliocidaris erythrogramma* with (control) and without blastocoelic lipid reserves (reduced-lipid). Each bar represents the mean ± 1 SEM and is based on three or four chambers of larvae. Each pair of bars is identified by a culture ID, representing separate parental pairs.

Table II

Mass and energy summaries for the entire development of Heliocidaris tuberculata *constructed from data collected from two independent cultures*

Culture ID	HT004	HT-CK1
A. Changes in biomass during development.		
(1) Biomass of egg (μg egg^{-1})	0.12	0.12
(2) Biomass at end of development (μg larva^{-1})	5.97	4.18
Biomass change (μg larva^{-1})	+ 5.86	+ 4.06
(3) Energy equivalents of biomass change (J larva^{-1})	0.164	0.114
B. Metabolic expenditure		
Total oxygen consumption (pmol individual^{-1})	108,908	124,571
(4) Energy expenditure (J individual^{-1})	0.052	0.060
C. Energy for development excluding maternal investment (J larva^{-1})		
(5 = 3 + 4) J larva^{-1}	0.216	0.174
D. Energy for development including maternal investment (J larva^{-1})		
(6) Egg investment (J egg^{-1})	0.0033	0.0033
(7 = 5 + 6) J larva^{-1})	0.220	0.177
E. Energy for development per mass of juvenile (J μg^{-1})		
(8 = 7/2)	0.037	0.042

See Materials and Methods for the basis by which biomass and oxygen consumption were converted into units of energy.

species of echinoderm larvae, representing four classes (and two body forms), Hart (1996) suggested that the pluteus body plan might be "an energetically inexpensive adaptation for suspension feeding in the plankton" (Hart, 1996, p. 42). He based his suggestion on the observations that pluteus larvae (both echinoid and ophiuroid larvae) developed and grew faster than non-pluteus larvae (asteroids and holothuroids) under similar feeding conditions, and that even though the maximal clearance rates are lower overall for the pluteus than for non-pluteus forms, the pluteus larvae also had a higher maximal clearance rate for a given number of cells in the ciliary feeding apparatus. Measurements of the energy for development of planktotrophic larvae of *Acanthaster planci* allow a partial and heuristic comparison with the values for larvae of the *Heliocidaris* species. With the same assumptions for *A. planci* as were used for planktotrophic *H. tuberculata*, the mean egg energy = 28.6 mJ, the range of energy of the added biomass = 39.3–44.3 mJ, and the range of energy expended during respiration = 16.3–29.2 mJ (calculated from table 1 of Hoegh-Guldberg, 1994). Like the values for *H. tuberculata* (Table II), the energy expended in respiration was roughly half the value of the energy equivalents calculated for the biomass added during the larval period. In the absence of a comparison with nonfeeding development in a related seastar, it is not clear how much of the respiratory costs to associate with juvenile formation versus building and running the larval feeding apparatus of the seastar larva. If we assume that these costs partition as they did for *Heliocidaris* (50% to juvenile formation and 50% to operation of the feeding system), then larvae of *Acanthaster* may experience about 270% to 540% return on investment in the feeding apparatus. This range extends lower than but overlaps the return estimated for pluteus larvae and hence is consistent with Hart's (1996) suggestion of difference in effectiveness of larval body plans. Obviously the data are limited and many assumptions are untested within this comparison. Its greatest use, however, is demonstrating the potential for inferences if appropriate comparisons are made.

Comparison of the amount of energy invested into the egg with the total energy required to produce a juvenile permits the calculation of the maternal investment in each species. *H. tuberculata* invests 3.3 mJ of organic energy into each egg; this amounts to less than 2% of the total energy needs of embryonic and larval development (177 and 220 mJ individual^{-1}, Table IIC). In comparison, *H. erythrogramma* invests between 241 and 334 mJ into each egg; this contributes 90.8% ± 1.6% (mean ± 95% CI) of the total energy required to make a juvenile *H. erythrogramma* (325 ± 68 mJ individual^{-1}, Table IIID). This study verified that a planktotrophic egg contains only a small contribution to the total energy required by a developing larva, whereas the opposite is true with a lecithotrophic egg, which makes a huge contribution to the energy for development.

Implications for the evolution of development and metabolic studies

The values for energy required to produce a juvenile imply that there are no developmentally based energetic barriers or benefits to changes in modes of development. The total energy for development (per individual) in the species with planktotrophic larvae is essentially the same as that in the species with pelagic, lecithotrophic larvae, once juvenile body size is taken into account. Selection for the increase in egg size, the loss of feeding function, and the reorganization of morphogenesis do not require increases or decreases in the overall energy required to produce a juvenile beyond those that are considered in life-history theory. The additional comparison that we offer is for the energy required for development of *H. erythrogramma* with and without the blastocoelic lipid components. This comparison not only demonstrates that this species invests materials that are not used in larval development (see also Emlet and Hoegh-Guldberg, 1997), but also corroborates the observation that similar energy for development is involved when juvenile size is

Table III

Mass and energy summaries for the early development of Heliocidaris erythrogramma *constructed from data collected from four independent cultures*

Culture ID	HE007	HE010	HE013	HE017
A. Changes in biomass during development				
(1) Egg biomass (μg egg^{-1})	16.09	15.10	16.35	18.97
(1′) Est. biomass, excl. blastocoelic cont. (μg egg^{-1})	7.37	9.0	9.68	10.22
(2) Biomass of at end of development (μg larva^{-1})	—	14.61	18.96	18.86
Biomass change (μg larva^{-1})	—	−0.49	+ 2.61	− 0.11
(3) Energy equivalents of biomass change (J larva^{-1})*	0	0	0	0
B. Metabolic expenditure				
Total Oxygen consumption (pmol individual^{-1})	55,156	62,643	74,107	59,627
(4) Energy expenditure (J individual^{-1})	0.026	0.029	0.035	0.028
C. Energy for development excluding maternal investment				
(5 = 3 + 4) J larva^{-1}	0.026	0.029	0.035	0.028
	Mean	95% CI	Lower	Upper
	0.029	0.006	0.023	0.036
D. Energy for development including maternal investment (J larva^{-1})				
(6) Egg investment (complete egg)	0.525	0.490	0.534	0.619
(6′) Egg investment (without blastocoelic contents)	0.241	0.292	0.316	0.334
(7 = 5 + 6) Energy for development (complete egg)	0.551	0.519	0.569	0.647
	Mean	95% CI	Lower	Upper
	0.571	0.087	0.485	0.658
(7′ = 5 + 6′) Energy for development	0.267	0.321	0.351	0.362
(excluding blastocoelic contents)	Mean	95% CI	Lower	Upper
	0.325	0.068	0.257	0.393
E. Energy for development per mass of juvenile (J μg^{-1})				
(8 = 7/1) Juvenile with blastocoelic contents	0.0343	0.0346	0.0348	0.0341
(8′ = 7′/1′) Juvenile without blastocoelic contents	0.0362	0.0359	0.0363	0.0354

See Materials and Methods for the basis by which biomass and oxygen consumption were converted into units of energy.
* Changes in biomass were not significant, see Table IB.
—, no data.

taken into account. A bigger juvenile can be made with increased maternal investment, but the energy for development per individual does not change from that of a juvenile developing from planktotrophic larvae when corrected for juvenile size.

Though the overall energy for development per mass of juvenile appears unchanged, there are substantial differences in the magnitude and patterns of metabolism. Having sufficient energy reserves to fuel development appears to permit the lecithotrophic species to rapidly increase metabolic activity and sustain it at a high rate throughout development. In comparison, the metabolic rate of *H. tuberculata*, after its initial increase during embryogenesis, only increases further as larval mass and tissues are acquired. As stated before, this can take time and depends on local conditions (phytoplankton concentrations, etc.). Although these differences are in part attributable to a greater number of cells present earlier in development for *H. erythrogramma* relative to *H. tuberculata*, these patterns indicate that greater numbers of cells are metabolically active in *H. erythrogramma* soon after gastrulation.

That lecithotrophs may contain a substantial amount of metabolically inactive biomass is an important finding of this study. If this material were not excluded from our estimates of specific metabolic rate, the differences between species would be far greater. For example, the specific metabolic rates of the planktotrophic and lecithotrophic echinoid show roughly similar patterns and absolute values when inert materials are excluded from the calculations of specific metabolic rate. If we had neglected to exclude the metabolically inert blastocoelic components present in *H. erythrogramma*, however, we would have come to quite different conclusions. In that

case, the lower SMR of *H. erythrogramma* compared to that of *H. tuberculata* would have led us to conclude that specific metabolic rates are inversely related to larval size, as appears to be the case for a large proportion of the kingdom Animalia (Zeuthen, 1947). The presence of metabolically inert materials in the egg, embryos, and larvae of invertebrates is likely to be a problem in any comparison of species with differing egg size, especially in cases where the measurement and removal of these energy reserves is not as easy as for *H. erythrogramma*. Two other sea urchins, *Asthenosoma ijimai* (Amemiya and Emlet, 1992) and *Holopneustes purpurescens* (V. Morris, pers. comm; Emlet, pers. obs.), are known to extrude at least some lipid-rich material into their blastocoels, but this has not been reported for most other echinoderms with large, "yolky" eggs (*e.g., Patiriella exigua,* Cerra and Byrne, 1995).

Acknowledgments

Supported by an A.R.C. small grant and a University (of Sydney) Research Grant to O.H.-G and by NSF grants INT-9114655 and IBN-9396004 to R.B.E. We thank G. Moreno, C. King, and S. Dove, and especially P. Selvakumaraswamy for help throughout this research effort. M. Byrne and V. Morris provided many helpful comments during discussion. Comments by B. Hentschel, A. Moran, R. Strathmann, and two anonymous reviews helped us improve the manuscript. This is contribution number 97-01 from the Oregon Institute of Marine Biology.

Literature Cited

Amemiya, S., and R. B. Emlet. 1992. The development and larval form of the echinothurioid echinoid, *Asthenosoma ijimai,* revisited. *Biol. Bull.* **182:** 15–30.

Byrne, M. 1991. Developmental diversity in the starfish genus *Patiriella* (Asteroidea: Asterinidae). Pp. 499–508 in *Biology of Echinodermata,* T. Yanagisawa, I. Yasumasu, C. Ogura, N. Suzuki, and T. Motokawa, eds. A. A. Balkema, Rotterdam.

Byrne, M. 1995. Changes in larval morphology in the evolution of benthic development by *Patiriella exigua* (Asteroidea: Asterinidae), a comparison with the larvae of *Patiriella* species with planktonic development. *Biol. Bull.* **188:** 293–305.

Cerra, A., and M. Byrne. 1995. Cellular events of wrinkled blastula formation and the influence of the fertilization envelope on wrinkling in the seastar *Patiriella exigua. Acta Zool.* **76:** 155–165.

Crisp, D. J. 1976. The role of the pelagic larva. Pp. 145–155 in *Perspectives in Experimental Biology,* P. Spencer Davies, ed. Pergamon Press, Oxford.

Emlet, R. B. 1990. World patterns of developmental mode in echinoid echinoderms. Pp. 329–334 in *Advances in Invertebrate Reproduction, Vol 5,* M. Hoshi and O. Yamashita, eds. Elsevier, Amsterdam.

Emlet, R. B. 1994. Body form and patterns of ciliation in nonfeeding larvae of echinoderms: functional solutions to swimming in plankton? *Am. Zool.* **34:** 570–585.

Emlet, R. B. 1995. Larval spicules, cilia, and symmetry as remnants of indirect development in the direct developing sea urchin *Heliocidaris erythrogramma. Dev. Biol.* **167:** 405–415.

Emlet, R. B., and O. Hoegh-Guldberg. 1997. Effects of egg size on post-larval performance: experimental evidence from a sea urchin. *Evolution* **51** (in press).

Emlet, R. B., L. R. McEdward, and R. R. Strathmann. 1987. Echinoderm larval ecology viewed from the egg. Pp. 55–136 in *Echinoderm Studies, Vol. 2,* M. Jangoux and J. M. Lawrence, eds. A.A. Balkema, Rotterdam.

Fenaux, L., C. Cellario, and F. Rassoulzadegan. 1988. Sensitivity of different morphological stages of the larva of *Paracentrotus lividus* (Lamarck) to quantity and quality of food. Pp. 259–266 in *Echinoderm Biology, Proc. 6th Intn'l Echinoderm Conf., Victoria,* R. D. Burke, P. V. Mladenov, P. Lambert, and R. L. Parsley, eds. Balkema, Rotterdam.

Fenaux, L., M. F. Strathmann, and R. R. Strathmann. 1994. Five tests of food-limited growth of larvae in coastal waters by comparisons of rates of development and form of echinoplutei. *Limnol. Oceanogr.* **39:** 84–98.

Gnaiger, E. 1983. Calculation of energetic and biochemical equivalents of respiratory oxygen consumption. Pp. 337–345 in *Polarographic Oxygen Sensors. Aquatic and Physiological Applications,* E. Gnaiger and H. Forstner, eds. Springer-Verlag, Berlin.

Hart, M. F. 1996. Variation in suspension feeding rates among larvae of some temperate, eastern Pacific echinoderms. *Invertebr Biol.* **115:** 30–45.

Havenhand, J. N. 1993. Egg to juvenile period, generation time, and the evolution of larval type in marine invertebrates. *Mar. Ecol. Prog. Ser.* **97:** 247–260.

Havenhand, J. N. 1995. Evolutionary ecology of larval types. Pp. 79–122 in *Marine Invertebrate Larvae,* L. McEdward, ed. CRC Press, Boca Raton, FL.

Henry, J. J., G. A. Wray, and R. A. Raff. 1991. Mechanism of an alternate type of echinoderm blastula formation: the wrinkled blastula of the sea urchin *Heliocidaris erythrogramma Dev. Growth Differ.* **33:** 317–328.

Hoegh-Guldberg, O. 1994. Uptake of dissolved organic matter by larval stage of the crown-of-thorns starfish *Acanthaster planci. Mar. Biol.* **120:** 55–63.

Hoegh-Guldberg, O., and D. T. Manahan. 1995. Coulometric measurement of oxygen consumption during development of marine invertebrate embryos and larvae. *J Exp. Biol.* **198:** 19–30.

Jaeckle, W. B. 1995. Variation in the size, energy content, and composition of invertebrate eggs: correlates to the mode of larval development. Pp. 49–77 in *Marine Invertebrate Larvae,* L. McEdward, ed. CRC Press, Boca Raton, FL.

Jaeckle, W. B., and D. T. Manahan. 1989. Growth and energy imbalance during the development of a lecithotrophic molluscan larva *(Haliotis rufescens). Biol. Bull.* **177:** 237–246.

Janies, D. A., and L. R. McEdward. 1993. Highly derived coelomic and water-vascular morphogenesis in a starfish with pelagic direct development *Biol. Bull.* **185:** 56–76.

Laegdsgaard, P., M. Byrne, and D. T. Anderson. 1991. Reproduction of sympatric populations of *Heliocidaris erythrogramma* and *H. tuberculata* (Echinoidea) in New South Wales. *Mar. Biol.* **110:** 359–374

Lawrence, J. M., and M. Byrne. 1994. Allocation to body components in *Heliocidaris erythrogramma* and *Heliocidaris tuberculata* (Echinodermata: Echinoidea). *Zool. Sci* **11:** 133–137.

Lawrence, J. M., J. B. McClintock, and A. Guille. 1984. Organic level and caloric content of eggs of brooding asteroids and an echinoid (Echinodermata) from Kerguelen (South Indian Ocean). *Int. J Invertebr. Reprod. Dev.* **7:** 249–257.

Martindale, M. Q., and J. Q. Henry. 1995. Modifications of cell fate specification in equa-cleaving nemertean embryos: alternate patterns of spiralian development. *Development* **121:** 3175–3185.

McClintock, J. B., and J. S. Pearse. 1986. Organic and energetic content of eggs and juveniles of Antarctic echinoids and asteroids with lecithotrophic development. *Comp. Biochem. Physiol.* **85A:** 341–345.

McEdward, L. R. 1984. Morphometric and metabolic analysis of the growth and form of an echinopluteus. *J. Exp. Mar. Biol. Ecol.* **82:** 259–287.

McEdward, L. R. 1992. Morphology and development of a unique type of pelagic larva in the starfish *Pteraster tesselatus* (Echinodermata: Asteroidea). *Biol. Bull.* **182:** 177–187.

McMillan, W. O., R. A. Raff, and S. R. Palumbi. 1992. Population genetic consequences of developmental evolution in sea urchins (Genus Heliocidaris). *Evolution* **46:** 1299–1312.

Morris, V. B. 1995. Apluteal development of the sea urchin *Holopneustes purpurescens* Agassiz (Echinodermata: Echinoidea:Euechinoidea). *Zool. J. Linn. Soc.* **114:** 349–364.

Olson, R. R., J. L. Cameron, and C. M. Young. 1993. Larval development (with observations on spawning) of the pencil urchin *Phyllacanthus imperialis*: a new intermediate larval form? *Biol. Bull.* **185:** 77–85.

Paulay, G., L. Boring, and R. R. Strathmann. 1985. Food limited growth and development of larvae: experiments with natural sea water. *J. Exp. Mar. Biol. Ecol.* **93:** 1–10.

Pedrotti, M. L., and L. Fenaux. 1993. Effects of food diet on the survival, development and growth rates of two cultured echinoplutei (*Paracentrotus lividus* and *Arbacia lixula*). *Invertebr. Reprod. Dev.* **24:** 59–70.

Raff, R. A. 1987. Constraint, flexibility, and phylogenetic history in the evolution of direct development in sea urchins. *Dev. Biol.* **119:** 6–19.

Roughgarden, J. 1989. The evolution of marine life cycles. Pp. 270–300 in *Mathematical Evolutionary Theory*, M. W. Feldman, ed. Princeton Univ. Press.

Schatt, P., and J. P. Feral. 1996. Completely direct development of *Abatus cordatus*, a brooding schizasterid (Echinodermata: Echinoidea) from Kerguelen, with a description of perigastrulation, a hypothetical new mode of gastrulation. *Biol. Bull.* **190:** 24–44.

Smith, M. J., J. D. G. Boom, and R. A. Raff. 1990. Single-copy DNA distance between two congeneric sea urchin species exhibiting radically different modes of development. *Mol. Biol. Evol.* **7:** 315–326.

Strathmann, M. F. 1987. *Reproduction and Development of Marine Invertebrates of the Northern Coast.* Univ. Washington Press, Seattle.

Strathmann, R. R. 1978a. The evolution and loss of feeding larval stages of marine invertebrates. *Evolution* **32:** 894–906.

Strathmann, R. R. 1978b. Length of pelagic period in echinoderms with feeding larvae from the northeast Pacific. *J. Exp. Mar. Biol. Ecol.* **34:** 23–27.

Strathmann, R. R. 1985. Feeding and nonfeeding larval development and life-history evolution in marine invertebrates. *Ann. Rev. Ecol. Syst.* **16:** 339–361.

Strathmann, R. R. 1993. Hypotheses on the origins of marine larvae. *Ann. Rev. Ecol. Syst.* **24:** 89–117.

Thorson, G. 1950. Reproductive and larval ecology of marine bottom invertebrates. *Biol. Rev.* **25:** 1–45.

Vance, R. R. 1973. On reproductive strategies in marine benthic invertebrates. *Am. Nat.* **107:** 339–352.

Williams, D. H. C., and D. T. Anderson. 1975. The reproductive system, embryonic development, larval development and metamorphosis of the sea urchin *Heliocidaris erythrogramma* (Val.) (Echinoidea: Echinometridae). *Aust. J. Zool.* **23:** 371–403.

Wray, G. A. 1995. Evolution of larvae and developmental modes. Pp. 413–447 in *Marine Invertebrate Larvae*, L. McEdward, ed. CRC Press, Boca Raton, FL.

Wray, G. A., and A. E. Bely. 1994. The evolution of echinoderm development is driven by several distinct factors. *Dev. Suppl.* **1994:** 97–106.

Wray, G. A., and R. A. Raff. 1989. Evolutionary modification of cell lineage in the direct-developing sea urchin. *Heliocidaris erythrogramma Dev. Biol.* **132:** 458–470.

Wray, G. A., and R. A. Raff. 1990. Novel origins of lineage founder cells in the direct-developing sea urchin *Heliocidaris erythrogramma Dev. Biol.* **141:** 41–54.

Wray, G. A., and R. A. Raff. 1991. Rapid evolution of gastrulation mechanisms in a sea urchin with lecithotrophic larvae. *Evolution* **45:** 1741–1750.

Zeuthen, E. 1947. Body size and metabolic rate in the animal kingdom with special regard to the marine microfauna. *C. R. Trav. Carlsberg, Ser. Chim.* **26:** 17–161.

Reference: *Biol. Bull.* **192:** 41–52. (February, 1997)

Stages of Larval Development and Stem Cell Population Changes During Metamorphosis of a Hydrozoan Planula

VICKI J. MARTIN AND WILLIAM E. ARCHER

Department of Biological Sciences, University of Notre Dame, Notre Dame, Indiana 46556

Abstract. Scanning electron microscopy and light histology were used to reveal the changes in overall morphology and in stem cell differentiation and distribution that occur as a free-swimming, solid hydrozoan planula larva is transformed into a sessile, hollow adult polyp. Eight stages of development are described: young 10-hour planula, mature 48-hour planula, attaching planula, disc, pawn, crown, immature polyp, and primary adult polyp. The larval interstitial stem cell population (interstitial cells, nematocytes, ganglion cells) undergoes dramatic changes during metamorphosis: (1) distribution patterns change, (2) certain larval derivatives disappear, (3) new types of derivatives differentiate, and (4) migration patterns become more complex. This study is the first to examine how a stem cell system develops in an organism that goes from embryo to larva to adult.

Introduction

The stem cell, found in metazoans from sponges to vertebrates, is an intriguing but little understood cell type. Stem cells, by definition, are not terminally differentiated: they have the ability to divide, not only generating more stem cells (self renewal) but also yielding a variety of differentiated cell types. The mechanisms by which stem cells differentiate into different phenotypes and arrive at the appropriate location are some of the most important questions in developmental biology and metazoan evolution. Three major migratory stem cell systems have been extensively studied: vertebrate neural crest cells, vertebrate hematopoietic cells, and invertebrate cnidarian interstitial cells (Bode and David, 1978; LeDouarin, 1979; Heimfeld and Bode, 1986; Martin and Archer, 1986; Lumsden, 1988; Bronner-Fraser and Fraser, 1988; Potten and Loeffler, 1990; Weston, 1991; Martin, 1991; Medvinsky *et al.*, 1993).

The study of stem cells in evolutionarily primitive metazoans may reveal some of the earliest mechanisms used for setting up patterns of cell distribution and overall morphology. Certain marine cnidarians have characteristics that make them ideal for such a study. Embryogenesis and metamorphosis are relatively rapid and, more importantly, both embryos and adults contain a population of migratory stem cells, making it possible to compare stem cell behavior during embryogenesis with behavior in the adult.

To date, studies on cnidarian metamorphosis are few and virtually nothing is known about the behavior of the interstitial cell system during metamorphosis (Martin *et al.*, 1983; Berking, 1984; Thomas *et al.*, 1987; Weis and Buss, 1987; Plickert *et al.*, 1988; Schwoerer-Böhning *et al.*, 1990; Sommer, 1990). Thus it is not known how the interstitial stem cell lineage develops in an organism that goes from an embryo to a larva to an adult.

The embryonic interstitial cell system of the marine hydrozoan *Pennaria tiarella* has been characterized by Martin and associates (Martin and Thomas, 1977, 1980, 1981a, b; Martin and Archer, 1986; Martin, 1988a, 1990, 1991). Embryos possess a well-defined population of migratory interstitial stem cells that either divide to replenish the population or differentiate into ganglion cells or nematocytes. The adult stem cell system of this hydrozoan has also been examined, though in less detail (Martin, 1988b). Because embryos and adults of *Pennaria tiarella* are easy to obtain and manipulate, develop quickly, and are small and transparent, the interstitial stem cell system can be examined continuously starting from the moment it arises in the embryo, progressing

Received 13 October 1995; accepted 15 November 1996.

through embryogenesis and formation and metamorphosis of the planula larva, and continuing in the adult.

In this study we used both scanning electron microscopy and light histology to examine the changes in overall morphology and in stem cell differentiation and distribution that occur as the free-swimming, solid planula larva of *Pennaria tiarella* is transformed into the sessile, hollow adult polyp. Our results show that the larval interstitial cell system is extensively modified during metamorphosis to produce the adult pattern.

Materials and Methods

Culture of Pennaria *adults and embryos*

Mature colonies of *Pennaria tiarella* were collected from pier pilings in Wilmington and Morehead City, North Carolina. Fronds from male and female colonies were mixed together in large finger bowls of filtered seawater; these bowls were placed in the dark at 1800 hours, and returned to the light at 2100 hours. Within 1 h after exposure to light, early cleavage stages were observed in the bottoms of the dishes. These embryos were transferred to small dishes of filtered seawater and reared at 23°C to the desired planular stage.

Forty-eight-hour planulae were incubated in cesium chloride to initiate metamorphosis (Archer and Thomas, 1983). A stock solution containing 9.76 g CsCl/100 ml distilled water was mixed with Millipore-filtered seawater at a ratio of 1 (stock):10 (seawater). Planulae were placed in 4 ml of this mixture for 3 h; some of these animals were fixed for scanning electron microscopy (SEM) immediately after the cesium treatment. Planulae placed in cesium for 3 h were also returned to dishes of Millipore-filtered seawater and allowed to continue their development. Treated planulae were fixed for SEM after a recovery period of 2 (disc stage), 6 (pawn stage), 12 (crown stage), 14 (immature polyp), or 18 (primary polyp) h.

Scanning electron microscopy (SEM)

For SEM, 10- and 48-h control planulae, cesium-treated planulae immediately after treatment, and cesium-treated planulae allowed to recover for various times were fixed for 1 h in 2.5% glutaraldehyde in 0.2 *M* Millonig's phosphate buffer, pH 7.4. Samples were rinsed three times in the phosphate buffer, postfixed for 1 h in 2% osmium tetroxide in 1.25% sodium bicarbonate buffer, pH 7.2, then rinsed three times in the sodium bicarbonate buffer. Animals were dehydrated through a graded series of ethanols to 100%, critical-point dried using CO_2, mounted on metal stubs, and sputter coated with gold palladium for 1 min in a Denton sputter coater. Samples were viewed and photographed with a JEOL JSM T-300 scanning electron microscope operated at 25 kV.

Light microscopy

Control planulae (various ages) and stages of metamorphosis comparable to those processed for SEM were fixed for 1 h in 10% formalin in seawater. Samples were dehydrated for 15 min each through an ascending alcohol series (25%–100% ethanol), followed by a 20-min rinse in 100% ethanol: 100% tertiary butyl alcohol (1:1), and an overnight incubation in 100% tertiary butyl alcohol. After being infiltrated and embedded in Paraplast Plus paraffin, animals were serially sectioned at 8 μm. The sections were mounted on glass slides and stained with azure B, which specifically stains the interstitial cells and their derivatives (Martin, 1991). Slides were viewed and photographed using a Zeiss standard research microscope.

Results

Planular morphology and stages of metamorphosis: General observations

Between 8 and 10 h postfertilization the gastrula of *Pennaria tiarella* elongates in an anterior-posterior direction to produce a fat, ciliated, free-swimming planula larva (Fig. 1). This 10-h larva has a distinct enlarged anterior apical pole and a narrower posterior basal pole. The surface cells are numerous, small, and uniform in size. By 24 h postfertilization 10-h planulae narrow and elongate to form mature, metamorphosis-competent planulae. Although planula larvae are competent to metamorphose at 24 h, as shown by induction with cesium chloride (Archer and Thomas, 1983), many planulae swim in the water column for 2 to 3 days before attaching and metamorphosing. During this swimming period the larvae continue to elongate. The 48-h hydrozoan planula is solid, elliptical, and moves in the water column with its enlarged apical end directed forward (Fig. 2).

During metamorphosis the solid, nonfeeding, motile planula is transformed into a hollow, sessile, feeding adult polyp (Figs. 3–9); this process takes about 18–20 h. The apical end of the planula forms the base of the polyp, the middle region forms the stalk, and the basal end forms the hypostome and tentacles. As planulae metamorphose their morphology changes dramatically, in distinct stages known as shortening planula (Fig. 3), disc (Fig. 4), pawn (Fig. 5), crown (Fig. 6), immature polyp (Fig. 7), and primary polyp (Figs. 8 and 9).

Mature planulae of *Pennaria* attach to substrates, usually pier pilings in the wild, *via* their anterior, apical poles; shortly thereafter metamorphosis begins.

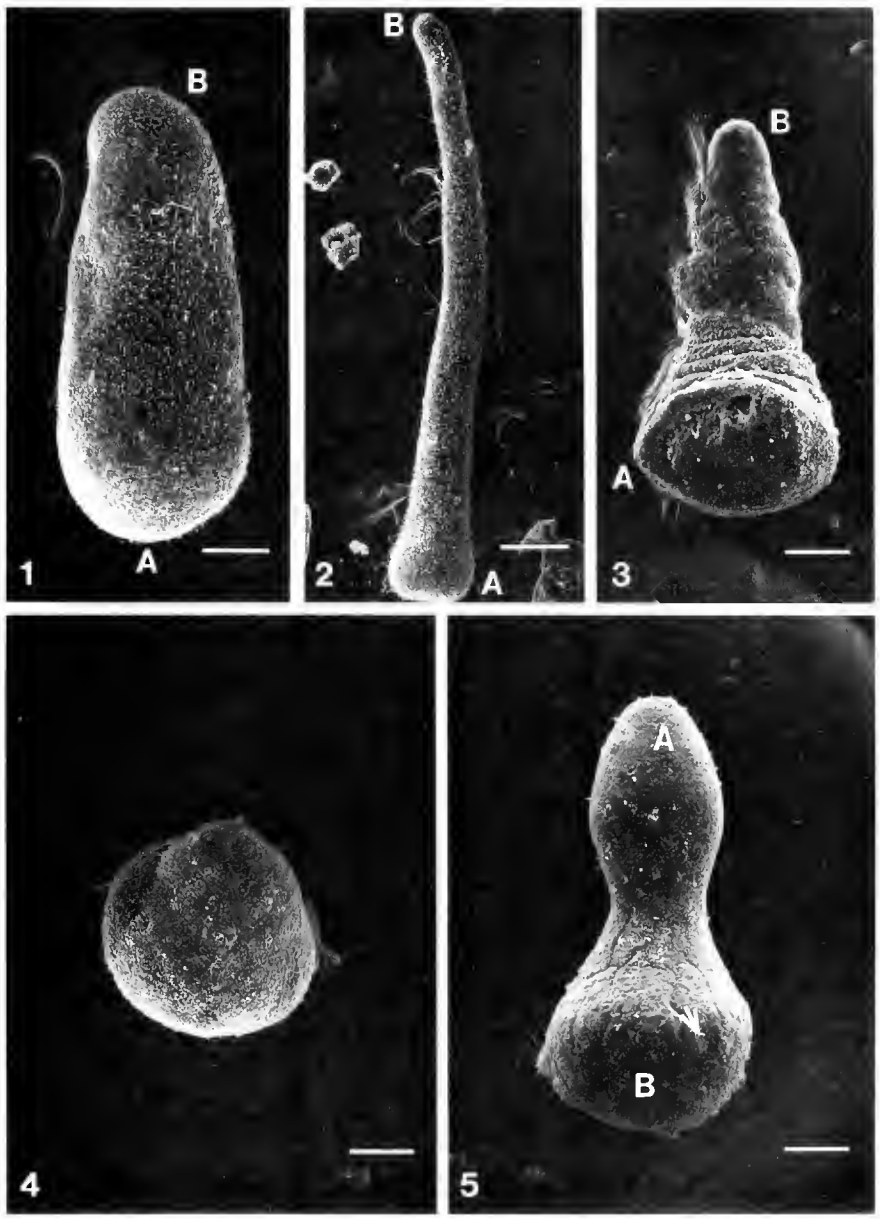

Figure 1. Ten-hour planula. The young larva is 350 μm long and 170 μm wide. A, apical end; B, basal end. Bar = 50 μm.

Figure 2. Forty-eight-hour pre-metamorphic planula. The ciliated larva moves with its enlarged apical end (A) directed forward. It is 900 μm long, 130 μm wide in the apical region, 70 μm wide in the mid area, and 50 μm wide at the basal end. B, basal. Bar = 100 μm.

Figure 3. Attached metamorphosing planula. The original anterior, apical end (A) of the larva attaches to the substrate and flattens over it while the original basal end (B) contracts towards the attached end. Thus the animal becomes short and fat, measuring 320 μm long, 160 μm wide in the apex, 93 μm wide in the middle, and 45 μm wide in the basal region. Bar = 50 μm.

Figure 4. Disc stage. The disc is a flattened ball, 180 μm in diameter, on the substrate. Bar = 50 μm.

Figure 5. Pawn stage. The base (B) of the pawn, now considered the posterior end of the animal, arises from the apical end of the planula. The anterior, apical region (A) of the pawn, derived from the basal region of the planula, forms the head and tentacles of the primary polyp. Small amounts of perisarc material (arrow) are deposited at the base. The pawn is 350 μm tall, 160 μm wide in the anterior head, 73 μm wide in the mid-stalk, and 106 μm wide at the posterior base. Bar = 50 μm.

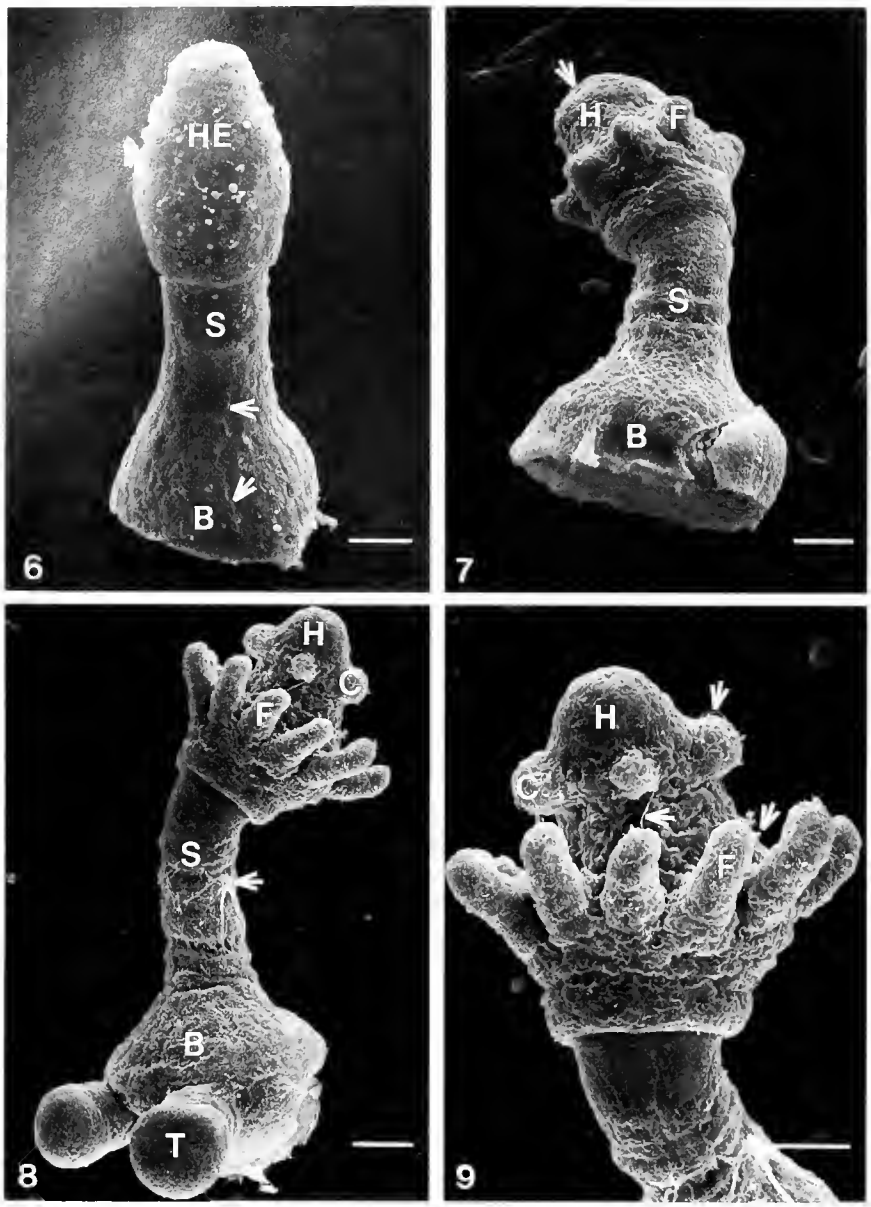

Figure 6. Crown stage. A distinct head region (HE), stalk (S), and base (B) are evident. Perisarc material (arrows) covers the surface. The crown is 427 μm tall, 125 μm wide in the apical crown region, 80 μm wide in the stalk region, and 166 μm wide at the base. Bar = 50 μm.

Figure 7. Immature polyp. The head region consists of a conical mound, the hypostome (H), a mouth (arrow), and a ring of forming filiform tentacles (F). A stalk (S) connects the head to the base (B). The polyp is 340 μm tall, 120 μm wide in the anterior hypostome region, 73 μm wide in the mid-stalk area, and 206 μm wide in the posterior base. Bar = 50 μm.

Figure 8. Primary polyp. The head is composed of the hypostome (H), short capitate tentacles (C), and the longer filiform tentacles (F). A narrow stalk (S), covered by perisarc (arrow), extends from the head to the base (B) of the adult. Stolons (T) emerge from the base. The primary polyp is 500 μm tall, 200 μm wide in the crown area, 70 μm wide in the mid-stalk area, and 200 μm wide in the basal area. Bar = 50 μm.

Figure 9. Enlarged head region of a primary polyp showing hypostome (H) with capitate (C) and filiform (F) tentacles. These tentacles are armed with nematocytes (arrows). Bar = 50 μm.

Shortening planula (Fig. 3). Once attached the apical planula end flattens and expands over the substrate while the basal end contracts down towards the expanded apical pole. Thus the attached larva becomes short and fat.

Disc (Fig. 4). Within 2 h of attachment the basal end of the larva has completely contracted and a round disc shape is formed. The animal appears as a small, flattened ball on the surface of the substrate; apical and basal ends

are not discernible. Cilia are absent and the surface is relatively smooth.

Pawn (Fig. 5). Six h after attachment a tiny bleb appears in the center of the disc and begins to elongate in an upright direction to form a shape that resembles the pawn of a chess set. The formation of the pawn from the disc stage requires 4 h. The original apical end of the planula forms the base of the pawn and the original basal end of the planula forms its head. The surface of the pawn is smooth and the first beginnings of a perisarc, an outer noncellular protective coating, are seen at the base.

Crown (Fig. 6). During the next 6 h the pawn elongates; the anterior head widens, forming a crown; and a sharp demarcation appears between the head and the stalk. This crown stage is formed 12 h after attachment, and it is during this stage that general features of the adult polyp begin to take shape: crown (future hypostome), stalk, base. The surface at this stage is smooth and covered with perisarc material.

Immature polyp (Fig. 7). After 2 h, 14 h after attachment, an immature polyp is formed. Its head region consists of a hypostome, a conical mound bearing the mouth at its tip, and a ring of forming filiform tentacles. These tentacles arise as tiny evaginations of the body wall at the base of the crown and lengthen to achieve the adult tentacle morphology. A clear division between the polyp head and the narrowing stalk is evident. The stalk connects the head to an enlarging base. The surface of the immature polyp below the region of the head is covered with perisarc.

Primary polyp (Figs. 8,9). Within 4 h, 18 h after attachment, a primary polyp is formed. A row of long, filiform tentacles and a new row of short, evaginating capitate tentacles, just above the filiform tentacles, characterize the crown region, constituting the fully formed adult hypostome (Fig. 9). A mouth is present at the very tip of the hypostome just above the whorl of capitate tentacles, a perisarc covers the stalk and basal region of the polyp, and stolon formation has begun in the basal region of the polyp (Fig. 8). These stolons produce additional polyps that remain attached to the original primary polyp, thus creating a colony.

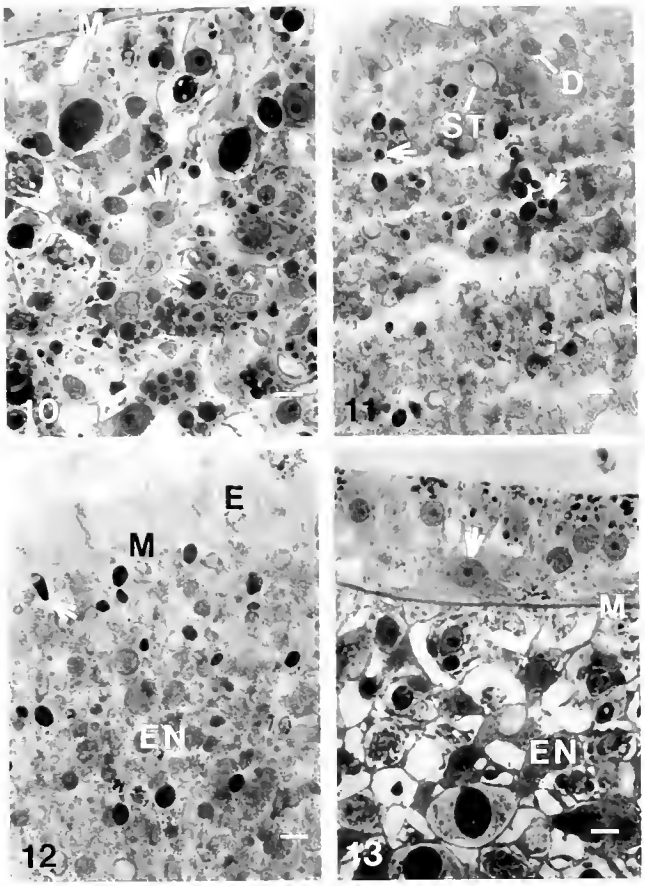

Figure 10. Interstitial cells (arrows) in the central endoderm of a mature planula. Each cell has a lightly stained cytoplasm plus a nucleus with a darkly stained nucleolus. M, mesoglea. Bar = 10 μm.

Figure 11. Nematoblasts with large dark capsules (D), small dark capsules (arrows), or large clear capsules (ST) in the endoderm of a mature planula. Bar = 10 μm.

Figure 12. Nematoblast with a bullet-shaped capsule (arrow) in the endoderm of a mature planula. Developing desmonemes (large dark capsules) and microbasic heterotrichous b-mastigophores (small dark capsules) are also seen. E, ectoderm; EN, endoderm; M, mesoglea. Bar = 10 μm.

Figure 13. Bipolar ganglion cell (arrow) in the ectoderm of a mature planula. The endoderm lacks neurons. EN, endoderm; M, mesoglea. Bar = 10 μm.

Interstitial stem cell system

Planulae of *Pennaria tiarella* contain a population of migratory stem cells, interstitial cells, that either divide to replenish the population or differentiate into two classes of somatic products: nematocytes (stinging cells) or ganglion cells (neurons). Early differentiating intermediates of the nematocyte lineage are called nematoblasts, and intermediates of the neural lineage are referred to as neuroblasts. Interstitial cells and their derivatives are easily identified in larval and adult tissue at the light microscopic level (Figs. 10–13). In the following sections we describe the behaviors of the interstitial cells, the nematoblasts and nematocytes, and the neuroblasts and ganglion cells during embryogenesis, in the metamorphosis-competent planula, during metamorphosis, and in the adult polyp.

Interstitial cells

Interstitial cells are small round cells measuring 7.5 μm in diameter (Fig. 10). They contain a centrally located nucleus with one or more darkly stained nucleoli.

These cells arise during gastrulation (8–10 h postfertilization), in the central core of the endoderm along the entire length of the young planula (Table I). They divide in the endoderm and by 13–14 h postfertilization begin to emigrate to the ectoderm, migrating as single cells through the interstitial spaces of the endoderm and through the mesoglea. By 15 h postfertilization, the interstitial cells reach the base of the ectoderm. Migration occurs along the entire apical-basal axis of the young planula. As planulae age, the numbers of interstitial cells in both the ectoderm and endoderm increase, and migration from the endoderm to the ectoderm continues along the entire planular axis. Thus the metamorphosis-competent planula has many interstitial cells at the base of its ectoderm and in the endoderm along its entire body axis (Table I).

During metamorphosis, as the apical pole of the planula attaches to a substrate and the basal end contracts towards the attached end, the interstitial cells located in the mid to basal regions of the larva move into the ectoderm and endoderm of the attachment region (Figs. 14–16; Table I). Their mechanism of movement is unknown but probably involves active cellular migration. The ectoderm and the endoderm of the remaining, still contracting basal portion of the attached larva become devoid of interstitial cells (Fig. 15; Table I). Once the disc stage is formed, interstitial cells fill both the ectoderm and the endoderm (Table I). As the center of the disc elongates in an upright direction, a pawn is produced (Fig. 17). The growing, apical upright tissue of the pawn, destined to form the head and stalk of the adult polyp, is devoid of interstitial cells (Fig. 17; Table I). These cells remain in the attached, now basal, end of the metamorphosing animal (Fig. 18); where the upright portion of the pawn connects to the basal disc is a sharp demarcation between presence of interstitial cells in the base and absence of these cells above the base. The distribution pattern of interstitial cells in the base of the pawn remains unchanged from that of the disc.

By the time the crown stage has formed, the interstitial cells have migrated out from the basal attachment site to populate the entire body axis of the animal (Fig. 19; Table I). In the attachment area (basal disc) a few interstitial cells are found in both the ectoderm and the endoderm. Along the body stalk, the region of the animal that connects the basal disc to the head, are scattered ectodermal interstitial cells and a few endodermal interstitial cells (Table I). The head of the crown stage has interstitial cells in both the ectoderm and the endoderm (Fig. 19; Table I). This same distribution pattern of interstitial cells is maintained in the immature polyp and in the adult primary polyp (Table I). In the primary polyp many interstitial cells are seen at the base of each filiform tentacle, but none are seen within the tentacles.

Nematoblasts and nematocytes

Nematoblasts, immature nematocytes, range from 10 to 12.5 μm in diameter and form distinctive dark-staining or light-staining capsules (Figs. 10–12); each capsule contains a nematocyst thread that may possess barbs and spines. Nematoblasts are found in both the ectoderm and the endoderm throughout embryogenesis, metamorphosis, and in the adult polyp. Once nematoblasts move to the outer surface of the ectoderm or project into a forming gastric cavity, they complete their differentiation and are considered functional nematocytes. A few nematoblasts with dark capsules are first detected in the apical endoderm of the young 10-h planula (Table I). Migration of the nematoblasts begins by 13 h postfertilization, and these cells are the first of the interstitial cell system to appear in the ectoderm (by 14 h postfertilization) of the planula. Nematoblasts in the apical endoderm migrate as single cells into the apical ectoderm; they do not divide and syncytial clusters of nematoblasts are not observed at any stage of the life cycle. As planulae mature the nematoblasts increase in number in both the ectoderm and the endoderm and are largely confined to the apical two-thirds of the planular axis (Table I). At least four types of capsules have been observed in the mature planula (Figs. 10–12): a large clear capsule (stenoteles), a large dark capsule (desmonemes), a small dark capsule (microbasic heterotrichous b-mastigophores), and a metachromatic bullet-shaped capsule (microbasic heterotrichous b-mastigophores with inclusions). Stenoteles and desmonemes predominate; only a few microbasic heterotrichous b-mastigophores with inclusions are seen.

Fully differentiated nematocytes are found only at the surface of the mature planula, the majority in an area extending from the apical end of the planula to the mid planula (Table I); only a few nematocytes are found at the surface in the basal (posterior) region. Fully differentiated nematocytes of planulae contain either a large clear capsule (stenoteles), a large dark capsule (desmonemes) or a bullet-shaped capsule (microbasic heterotrichous b-mastigophores with inclusions); no fully differentiated nematocytes housing the small dark capsules (microbasic heterotrichous b-mastigophores) are found in the planula.

As planulae attach to substrates, all nematoblasts move into the ectoderm and endoderm of the apical attachment region (Figs. 14 and 15). Nematocytes are confined to the outer surface of the ectoderm of the attachment area. Hence, the contracting basal portion of the attached larva is devoid of nematoblasts and nematocytes in both the ectoderm and the endoderm (Table I). All four types of nematoblast capsules are detected in the ectoderm and endoderm of the attachment area. The bulk of these cells are differentiating stenoteles, desmonemes, and microbasic

Table I

Distribution of the interstitial cell system during development of Pennaria tiarella

Stage	Interstitial cells	Nematoblasts	Nematocytes	Ganglion cells
10-Hour Planula				
Apical Ectoderm	—	—	—	—
Mid Ectoderm	—	—	—	—
Basal Ectoderm	—	—	—	—
Apical Endoderm	+	+	—	—
Mid Endoderm	+	—	—	—
Basal Endoderm	+	—	—	—
48-Hour Planula				
Apical Ectoderm	++	++	++	++
Mid Ectoderm	++	++	++	++
Basal Ectoderm	++	+	+	++
Apical Endoderm	++	++	—	—
Mid Endoderm	++	++	—	—
Basal Endoderm	++	+	—	—
Attaching Planula				
Apical Ectoderm (Attachment site)	++	++	+	—
Mid Ectoderm	—	—	—	—
Basal Ectoderm	—	—	—	—
Apical Endoderm	++	++	—	—
Mid Endoderm	—	—	—	—
Basal Endoderm	—	—	—	—
Disc Stage				
Ectoderm	++	++	+	—
Endoderm	++	++	—	—
Pawn Stage				
Apical Ectoderm (Head and Stalk)	—	—	—	—
Basal Ectoderm (Foot)	++	++	+	+
Apical Endoderm (Head and Stalk)	—	—	—	—
Basal Endoderm (Foot)	++	++	—	—
Crown Stage				
Apical Ectoderm (Head)	+	+	+	—
Mid Ectoderm (Stalk)	+	+	+	+
Basal Ectoderm (Foot)	+	++	+	++
Apical Endoderm (Head)	+	+	—	—
Mid Endoderm (Stalk)	+	+	—	—
Basal Endoderm (Foot)	+	+	—	—
Immature Polyp				
Apical Ectoderm (Head)	+	+	+	++
Apical Ectoderm (Tentacle)	—	+	++	++
Mid Ectoderm (Stalk)	+	+	+	+
Basal Ectoderm (Foot)	+	++	+	++
Apical Endoderm (Head)	+	+	—	—
Apical Endoderm (Tentacle)	—	—	—	—
Mid Endoderm (Stalk)	+	+	—	—
Basal Endoderm (Foot)	+	+	—	—
Primary Polyp				
Apical Ectoderm (Head)	+	+	+	++
Apical Ectoderm (Tentacle)	—	+	++	++
Mid Ectoderm (Stalk)	+	+	+	+
Basal Ectoderm (Foot)	+	++	+	++
Apical Endoderm (Head)	+	+	—	—
Apical Endoderm (Tentacle)	—	—	—	—
Mid Endoderm (Stalk)	+	+	—	—
Basal Endoderm (Foot)	+	+	—	—

Table Key: ++ = Abundant to moderate in number. + = A few present. — = Absent.

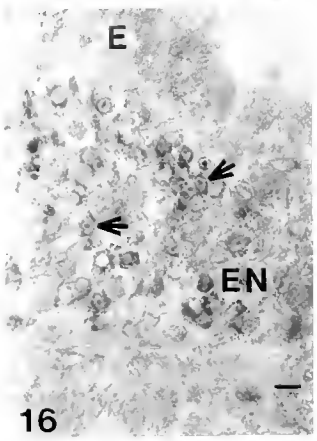

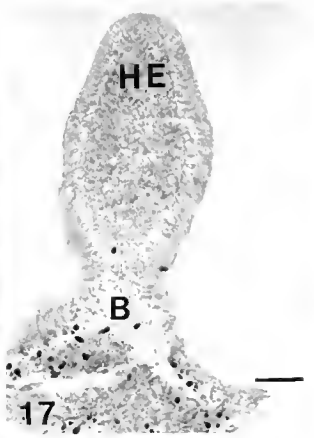

Figure 14. Apical region of an attaching planula. The interstitial cell system has moved into the attachment area; note the large number of dark nematoblast capsules in this region. E, ectoderm; EN, endoderm; M, mesoglea. Bar = 50 μm.

Figure 15. Mid to basal region of an attaching planula. Note the absence of the interstitial cell system in the basal portion (B) of the animal. E, ectoderm, EN, endoderm; M, mesoglea. Bar = 50 μm.

Figure 16. Interstitial cells (arrows) in the attachment region of a metamorphosing planula. E, ectoderm; EN, endoderm. Bar = 10 μm.

Figure 17. Pawn. The apical head region (HE) is devoid of the interstitial cell system. These cells remain in the basal region (B) of the pawn. Dark nematoblast capsules are abundant in the base. Bar = 50 μm.

heterotrichous b-mastigophores; only a few developing microbasic heterotrichous b-mastigophores with inclusions are found. Once the disc stage is reached, the four types of nematoblasts fill the ectoderm and endoderm (Fig. 20); a few nematocytes (stenoteles and desmonemes) are observed around the ectodermal surface of the disc (Table 1). As the center of the disc elongates to form the pawn, the nematoblasts and nematocytes remain in the attachment disc (Figs. 17 and 21). Thus, the upright growing tissue is devoid of nematoblasts and nematocytes. These cells are confined to the substrate-attached basal disc region of the metamorphosing animal and resemble the pattern described for the disc stage (Table 1). By the time the crown stage has formed, the interstitial cell system has migrated from the basal attachment site to populate the entire body axis of the animal. Nematoblasts are the first of the line to appear apically (Figs. 22–24), and distinct patterns of nematoblast and nematocyte distribution are observed. In the ectoderm of the attachment area are all four types of nematoblasts and two types of nematocytes (stenoteles and desmonemes). On either side of the basal disc just above the substrate attachment zone, the perisarc is connected to the basal disc and lower body column. In these regions of perisarc attachment to the ectoderm, the ectoderm has an abundance of nematoblasts (desmonemes and stenoteles) (Fig. 22). Along the body stalk of the crown in the ectoderm are the four types of

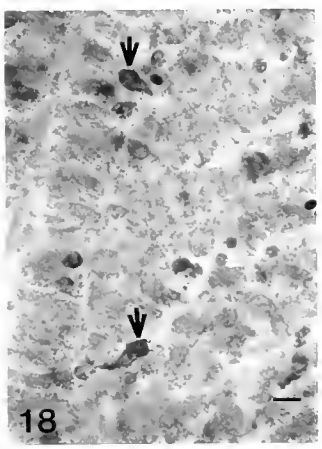

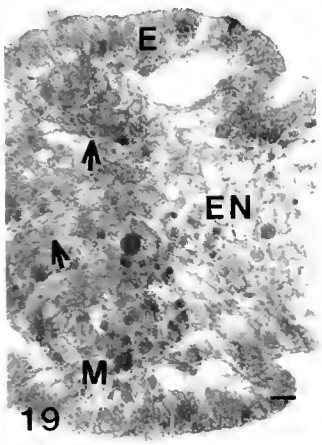

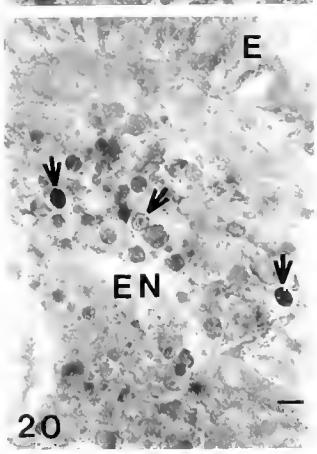

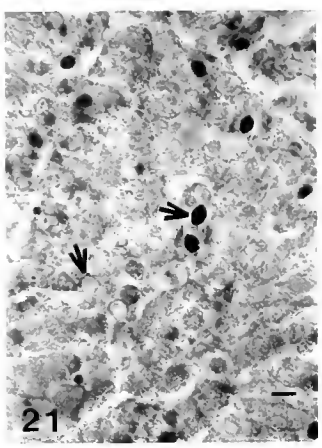

Figure 18. Interstitial cells (arrows) in the endoderm at the base of the pawn. These cells are migrating as indicated by the presence of a single filopodial-like extension. Bar = 10 μm.

Figure 19. Head region of the crown stage. Interstitial cells (arrows) are detected; however, ganglion cells are absent in this area. E, ectoderm; EN, endoderm; M, mesoglea. Bar = 10 μm.

Figure 20. Disc stage. Nematoblasts (arrows) are abundant in the endoderm; ganglion cells are absent. E, ectoderm; EN, endoderm. Bar = 10 μm.

Figure 21. Nematoblasts (arrows) in the endoderm at the base of the pawn. Bar = 10 μm.

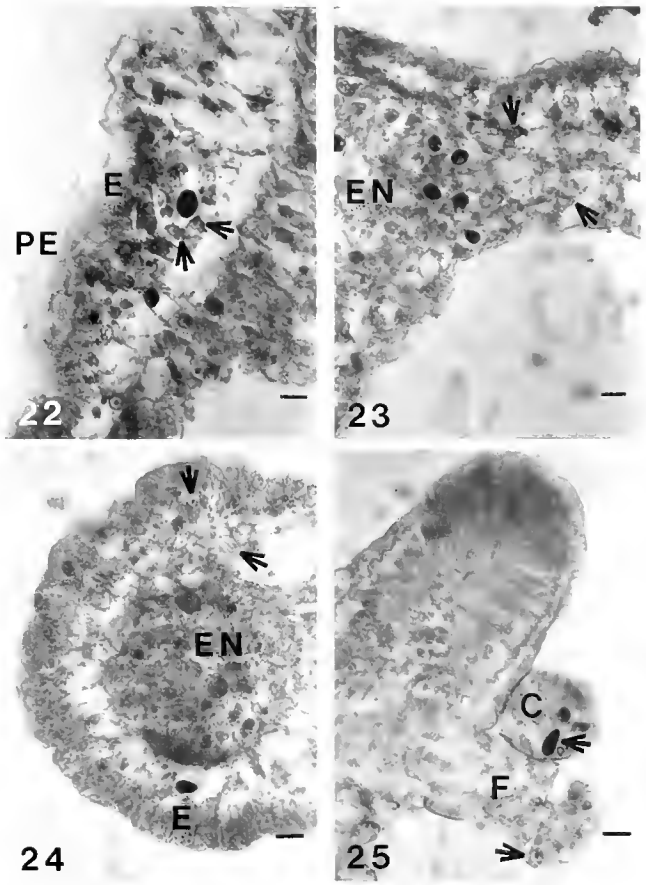

Figure 22. Crown stage. The perisarc (PE) is attached to the ectoderm (E) just above the foot region of the forming polyp. This region is rich in ganglion cells (arrows) and nematoblasts. Bar = 10 μm.

Figure 23. Stalk region of the crown stage showing multipolar ganglion cells (arrows) and nematoblasts. EN, endoderm. Bar = 10 μm.

Figure 24. Stenoteles (arrows) and a nematoblast with a dark bullet-shaped capsule in the head region of the crown stage. E, ectoderm; EN, endoderm. Bar = 10 μm.

Figure 25. Head region of a primary polyp showing nematoblasts (arrows) in a capitate tentacle (C) and a filiform tentacle (F). Bar = 10 μm.

nematoblasts and at the surface a few nematocytes (stenoteles and desmonemes). The endoderm of the stalk has a few nematoblasts (desmonemes and stenoteles) (Fig. 23). In the head of the crown in both the ectoderm and the endoderm are three types of nematoblasts: desmonemes, stenoteles, and microbasic heterotrichous b-mastigophores with inclusions (Fig. 24). Three kinds of nematocytes, the same varieties as the head nematoblasts, project from the ectodermal surface of the head. Prior to the crown stage, the nematoblasts with bullet-shaped capsules (microbasic heterotrichous b-mastigophores with inclusions) are seen sparingly along the whole body axis of metamorphosing animals; however, by the crown stage many nematoblasts of this type have accumulated in the head.

As the crown stage transforms into the immature polyp, the ectoderm of the forming filiform tentacles becomes filled with three types of nematoblasts and nematocytes: stenoteles, desmonemes, and microbasic heterotrichous b-mastigophores with inclusions. Other than this change, the distribution pattern of the nematoblasts and nematocytes is the same as seen in the crown stage.

As immature polyps form primary adult polyps, a second group of short tentacles, the capitate tentacles, appears just above the whorl of filiform tentacles (Fig. 25). These capitate tentacles are populated with the same three types of nematoblasts and nematocytes that occupy the filiform tentacles (Fig. 25). Along the body column mature nematocytes with small dark capsules (microbasic heterotrichous b-mastigophores) are visible. Other than these changes, the nematoblast and nematocyte system of the primary polyp resembles that of the immature polyp. Thus in the primary polyp the concentration of nematoblasts and nematocytes is high in the head and in the foot and scattered in the stalk. The distribution pattern of nematocytes is specific: in the head are stenoteles, desmonemes, and microbasic heterotrichous b-mastigophores with inclusions; along the body column are stenoteles, desmonemes, and microbasic heterotrichous b-mastigophores; and in the foot are desmonemes and stenoteles.

Neuroblasts and ganglion cells

Differentiating neuroblasts are detected as early as 16–20 h postfertilization in both the ectoderm and endoderm of the planula (Brumwell and Martin, 1996). These first neuroblasts arise in the apical region of the larva; shortly thereafter they are found along the entire length of the planula. Neuroblasts are small round cells, similar in size to interstitial cells, that contain cytoplasm rich in neurosecretory vesicles (Brumwell and Martin, 1996). These differentiating intermediates migrate as single cells from the endoderm to the base of the ectoderm; neuroblasts are positioned closer to the mesoglea than are the interstitial cells of the ectoderm. Neuroblasts seemingly emigrate in a straight path from the endoderm to the ectoderm; there is no evidence that they migrate in an apical or basal direction in the larva. Once neuroblasts reach the basal ectoderm they stop moving and complete their differentiation by extending neural processes. These processes are filled with neural vesicles and form an extensive neural plexus of transversely and longitudinally oriented processes throughout the length of the planula. As the planula ages additional ganglion cells differentiate and incorporate into the larval network. Fully differentiated larval ganglion cells are 5 μm in diameter, bipolar, spindle-shaped, and positioned in the ectoderm just above the mesoglea along the entire apical, basal axis of the planula (Fig. 13; Table I).

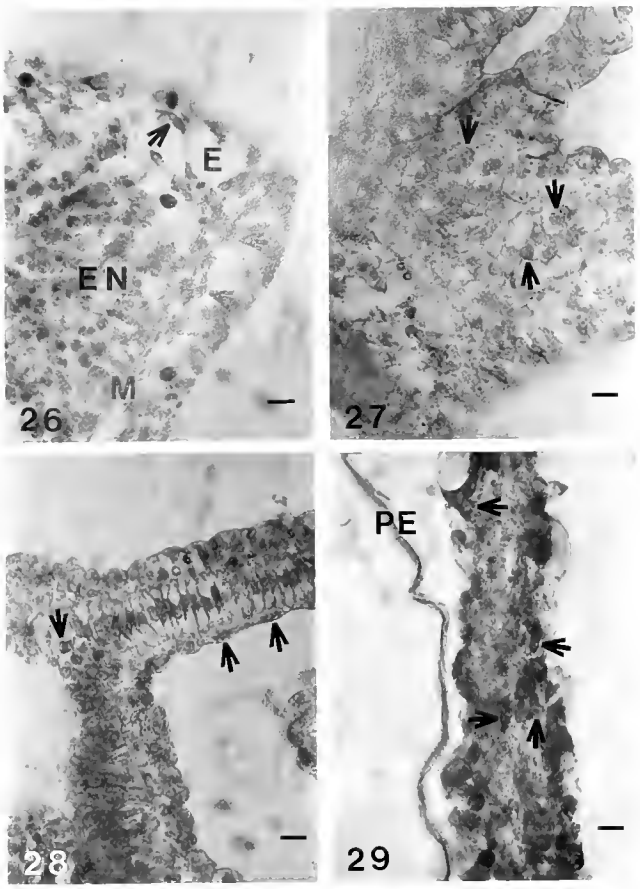

Figure 26. Neurons (arrows) and nematoblasts with dark capsules in the basal disc of the crown stage. E, ectoderm; EN, endoderm; M, mesoglea. Bar = 10 μm.

Figure 27. Ganglion cells (arrows) in the head region of a primary polyp. Bar = 10 μm.

Figure 28. Filiform tentacle of a primary polyp. Note the abundance of neurons (arrows) at the base of the tentacle and along its length. Bar = 10 μm.

Figure 29. Stalk of a primary polyp. Note the ganglion cells (arrows) in the ectoderm. PE, perisarc. Bar = 10 μm.

During attachment and the early stages of metamorphosis, the larval ganglion cells disappear; by the disc stage they are gone (Table I). In the pawn a few ganglion cells differentiate in the basal disc (Table I). These neurons are found in the ectoderm just above the mesoglea; they are triangular or star-shaped and are multipolar. These neurons have smaller cell bodies and thinner processes than did the planular ganglion cells. By the crown stage ganglion cells are found in the ectoderm of the basal disc and the body stalk (Table I). The basal disc contains a large number of ectodermal bipolar and multipolar ganglion cells (Fig. 26), and multipolar ganglion cells are abundant in the region of perisarc attachment to the basal disc and lower body column (Fig. 22). Along the body stalk in the ectoderm are at least three types of ganglion cells: triangular-, star- or spindle-shaped (Fig. 23). Ganglion cells are not detected in the head of the crown stage. As the crown stage develops into the immature polyp, many ganglion cells (bipolar, multipolar) appear in the head ectoderm and tentacles (Table I). By the primary polyp stage, the head of the animal is enriched in ganglion cells, especially around the mouth (Fig. 27). Ganglion cells are found at the base of each filiform tentacle and in the ectoderm along the lengths of the tentacles (Fig. 28). In the ectoderm of the body stalk are scattered ganglion cells (Fig. 29), and the distribution pattern in the basal disc mimics that of the immature polyp (Table I). Thus in the primary polyp there is a high concentration of ganglion cells in the ectoderm of the head and basal disc and some scattered ganglion cells in the ectoderm of the body column (Table I). The ganglion cells of the polyp are three types: spindle-shaped bipolar, star-shaped multipolar, and triangular-shaped multipolar.

Discussion

The transformation of the cnidarian planula larva into the adult phenotype is rapid, taking only 18–20 h in the hydrozoan *Pennaria tiarella*, and is characterized by general body reorganization and modification of the stem cell system. During metamorphosis the hydrozoan planula ceases swimming, loses its cilia, and attaches to the substrate by its apical (aboral) pole. Both glandular secretions and nematocytes may be used for securing planulae to a substrate (Martin *et al.*, 1983). Shortly after attachment the basal (oral) end of the larva contracts down towards the apical pole until it disappears into the attached pole. A tiny circular disc is formed. Next, a tiny bleb appears in the center of the disc and begins to elongate in an upright direction forming a pawn shape. Three distinct regions of the pawn are evident: an apical head, a mid-stalk region, and a basal disc. The pawn grows and reshapes to produce a crown stage, in which general features of the adult polyp begin to take shape: head, stalk, and base, with a clear separation between the head and the stalk. Tentacles evaginate from the head region and a mouth breaks through at the tip of the head, producing an immature polyp. This stage becomes a primary polyp when a row of long filiform tentacles and a row of short capitate tentacles adorn the head. A mouth is present at the very tip of the head just above the whorl of capitate tentacles, and a perisarc covers the stalk and basal region of the polyp. To form a colony, the polyp extends stolons from the base and asexually buds additional polyps, all of which remain connected together.

Four major changes occur in the interstitial cell system during metamorphosis: (1) the distribution pattern of the cells along the body axis changes, (2) certain larval derivatives disappear, (3) new types of derivatives differenti-

ate, and (4) migration patterns become more complex. Comparisons of the distribution patterns of the interstitial cell system in the planula and in the adult clearly show that these cells undergo dramatic reorganization during metamorphosis. This is not surprising given the fact that the entire polarity of the animal changes as a planula forms an adult: the apical end of the planula becomes the basal end of the polyp, and the mid-to-basal end of the planula forms the stalk and hypostome of the adult. In the planula, interstitial cells and ganglion cells are found along the entire apical-basal axis, whereas the majority of the nematoblasts and nematocytes are confined to the apical two-thirds of the planula. During metamorphosis this whole larval pattern is lost; from the disc stage onward a new adult pattern of the interstitial cell system is established. By the time the primary polyp has formed interstitial cells, nematoblasts and ganglion cells are found along the entire body axis; the concentration of ganglion cells and nematoblasts is high in the foot; the concentration of ganglion cells is high in the hypostome; the concentration of ganglion cells and nematocytes is high in the tentacles; and specific types of nematocytes are confined to distinct regions of the polyp.

In the mature planula two major kinds of derivatives differentiate from interstitial cells: a single type of bipolar ganglion cell and four types of nematoblasts. Of the latter only three types (desmonemes, stenoteles, and microbasic heterotrichous b-mastigophores with inclusions) complete differentiation in the planula; only a few nematocytes with bullet-shaped capsules (microbasic heterotrichous b-mastigophores with inclusions) were ever found in the planula. The other variety (microbasic heterotrichous b-mastigophores) begins development in the planula but completes differentiation only during metamorphosis. The larval bipolar ganglion cells disappear during planular attachment, suggesting that these neurons play a role in the attachment of the planula to the substrate. A subpopulation of these larval ganglion cells contain a RFamide-like peptide that may be used to initiate metamorphosis, to propagate it, or both (Brumwell and Martin, 1996). In fact, several investigators have previously proposed that the larval neurons are involved in propagating the metamorphic signal to other cells in the planula (Martin and Thomas, 1981b; Thomas *et al.*, 1987; Plickert, 1988; Leitz *et al.*, 1994; Leitz and Lay, 1995; Gajewski *et al.*, 1996; Brumwell and Martin, 1996).

In the adult polyp two types of somatic derivatives arise from interstitial cells: ganglion cells, of which there are at least three varieties, and nematocytes, of which there are four kinds. These new neurons begin to appear at the pawn stage and are found throughout the remaining phases of metamorphosis. Three types of nematocytes (desmonemes, stenoteles, and microbasic heterotrichous b-mastigophores with inclusions) first appear in the planula and are found throughout metamorphosis, whereas microbasic heterotrichous b-mastigophores, which begin but never complete differentiation in the planula, appear at the ectodermal surface between the crown stage and the polyp stage. Furthermore, by the polyp stage, fully differentiated microbasic heterotrichous b-mastigophores with inclusions have increased in number and are abundant in the head. The appearance of new somatic stem cell derivatives during metamorphosis, notably the three kinds of ganglion cells, indicates that the interstitial cells have a greater differentiative potential than demonstrated in the planula.

The migration patterns of the interstitial cell system are more complex in the adult than in the planula. In the planula the interstitial cells, nematoblasts, and neuroblasts emigrate from the endoderm to the ectoderm. There is no evidence that once in the ectoderm, these cells migrate in an apical-basal direction (Martin and Archer, 1986)—they appear to stay close to the site at which they entered the ectoderm. During metamorphosis this changes: interstitial cells, nematoblasts, and possibly neuroblasts migrate apically in large numbers. As the pawn stage arises from the disc, the emerging stalk and head of the pawn form and initially are completely devoid of a stem cell system. Between the pawn stage and the crown stage, the stem cells migrate apically in large numbers and populate the stalk and head of the crown. The first cells of the stem cell line to appear anteriorly are nematoblasts, followed by interstitial cells and lastly by ganglion cells. Interestingly, this is the order of appearance of interstitial cell types in the ectoderm of the planula shortly after larval interstitial cell migration begins (Martin and Archer, 1986). The introduction of the stem cell system into the forming apical region of the crown may be essential for shaping of the hypostome and for tentacle formation. Coincidentally, it is during the crown stage that general features of the adult hypostome begin to take shape and the stem cell system first appears in the apical end of the metamorphosing animal. Because interstitial cells and nematoblasts are found in the endoderm of adult polyps, it is possible that these cells can move from the endoderm to the ectoderm. Thus in the adult, multiple directions of migration are probable. Furthermore, since specific types of cells accumulate in specific regions of the polyp—for example, neurons are abundant in the head and the foot—some sort of directed migration must occur during metamorphosis.

Acknowledgments

This research was supported by National Science Foundation Grants DCB-8702212, DCB-8942149, DCB-9046094, DUE-9552116 and Career Advancement Award DCB-8711245 and a John Yarborough Me-

morial Undergraduate Research Grant from the North Carolina Academy of Science, Inc.

Literature Cited

Archer, W., and M. Thomas. 1983. An SEM study of morphological changes during metamorphosis in *Pennaria tiarella*. *Proc. Southeast Electron Microc. Soc.* **7:** 21.

Berking, S. 1984. Metamorphosis in *Hydractinia echinata*. Insights into pattern formation in hydroids. *Wilhelm Roux's Arch. Dev. Biol.* **193:** 370–378.

Bode, H., and C. David. 1978. Regulation of a multipotent stem cell, the interstitial cell of hydra. *Prog. Biophys. Mol. Biol.* **33:** 189–206.

Bronner-Fraser, M., and S. Fraser. 1988. Cell lineage analysis reveals multipotency of some avian neural crest cells. *Nature* **335:** 161–164.

Brumwell, G., and V. Martin. 1996. Ultrastructural localization of RFamide-like peptides in neuronal dense-cored vesicles of a enidarian planula larva. *Invertebr. Biol.* **115:** 13–19.

Gajewski, M., T. Leitz, J. Schloßherr, and G. Plickert. 1996. LWamides from enidaria constitute a novel family of neuropeptides with morphogenetic activity. *Dev. Biol.* **205:** 232–242.

Heimfeld, S., and H. Bode. 1986. Growth regulation of the interstitial cell population in *Hydra*. *Dev. Biol.* **116:** 51–58.

LeDouarin, N. 1979. *Cell Lineage, Stem Cells and Cell Determination.* Elsevier/North Holland, Amsterdam.

Leitz, T., and M. Lay. 1995. Metamorphosin A is a neuropeptide. *Wilhelm Roux's Arch. Dev. Biol.* **204:** 276–279.

Leitz, T., K. Morand, and M. Mann. 1994. Metamorphosin A: a novel peptide controlling development of the lower metazoan *Hydractinia echinata* (Coelenterata, Hydrozoa). *Dev. Biol.* **163:** 440–446.

Lumsden, A., 1988. Multipotent cells in the avian neural crest. *Trends Neurosci* **12:** 81–83.

Martin, V. 1988a. Development of nerve cells in hydrozoan planulae. I. Differentiation of ganglionic cells. *Biol. Bull.* **174:** 319–329.

Martin, V. 1988b. Development of the interstitial cell system in a marine hydrozoan polyp. *Am. Zool.* **28:** 95A.

Martin, V. 1991. Development of nerve cells in hydrozoan planulae. III. Some interstitial cells traverse the ganglionic pathway in the endoderm. *Biol. Bull* **178:** 10–20.

Martin, V. 1991. Differentiation of the interstitial cell line in hydrozoan planulae. I. Repopulation of epithelial planulae. *Hydrobiologia* **216/217:** 75–82.

Martin, V., and W. Archer. 1986. Migration of interstitial cells and their derivatives in a hydrozoan planula. *Dev. Biol.* **116:** 486–496.

Martin, V., and M. Thomas. 1977. A fine-structural study of embryonic and larval development in the gymnoblastic hydroid *Pennaria tiarella*. *Biol. Bull.* **153:** 198–218.

Martin, V., and M. Thomas. 1980. Ultrastructure of the nervous system in the planula larva of *Pennaria tiarella*. *J. Morphol.* **166:** 27–36.

Martin, V., and M. Thomas. 1981a. The origin of the nervous system in *Pennaria tiarella* as revealed by treatment with colchicine. *Biol. Bull.* **160:** 303–310.

Martin, V., and M. Thomas. 1981b. Elimination of the interstitial cells in the planula larva of the marine hydrozoan *Pennaria tiarella*. *J. Exp. Zool* **217:** 303–323.

Martin, V., F. Chia, and R. Koss. 1983. A fine-structural study of metamorphosis of the hydrozoan *Mitrocomella polydiademata*. *J. Morphol.* **176:** 261–287.

Medvinsky, A., N. Samoylina, A. Müller, and E. Dzierzak. 1993. An early preliver intraembryonic source of CFU-S in the developing mouse. *Nature* **364:** 64–67.

Plickert, G., 1988. Proportion altering factor (PAF) stimulates nerve cell formation in *Hydractinia echinata*. *Cell Differ. Dev.* **26:** 19–28.

Plickert, G., M. Kroiher, and A. Munck. 1988. Cell proliferation and early differentiation during embryonic development and metamorphosis of *Hydractinia echinata*. *Development* **103:** 795–803.

Potten, C., and M. Loeffler. 1990. Stem cells: attributes, spirals, pitfalls and uncertainties. Lessons for and from the crypt. *Development* **110:** 1001–1020.

Schwoerer-Böhning, B., M. Kroiher, and W. Müller. 1990. Signal transmission and covert prepattern in the metamorphosis of *Hydractinia echinata* (Hydrozoa). *Wilhelm Roux's Arch. Dev. Biol.* **198:** 245–251.

Sommer, C. 1990. Post-embryonic larval development and metamorphosis of the hydroid *Eudendrium racemosum* (Cavolini) (Hydrozoa, Cnidaria). *Helgol. Meeresunters.* **44:** 425–444.

Thomas, M., G. Freeman, and V. Martin. 1987. The embryonic origin of neurosensory cells and the role of nerve cells in metamorphosis of *Phialidium gregarium* (Cnidaria, Hydrozoa). *Int. J. Invertebr. Reprod. Dev.* **11:** 265–287.

Weis, V., and L. Buss. 1987. Ultrastructure of metamorphosis in *Hydractinia echinata*. *Postilla* **199:** 1–20.

Weston, J. 1991. Sequential segregation and fate of developmentally restricted intermediate cell populations in the neural crest lineage. *Curr. Top. Dev. Biol.* **25:** 133–153.

Reference: *Biol. Bull.* **192:** 53–61. (February, 1997)

Subcuticular Rejection: an Advanced Mode of the Allogeneic Rejection in the Compound Ascidians *Botrylloides simodensis* and *B. fuscus*

EUICHI HIROSE[1], YASUNORI SAITO[2], AND HIROSHI WATANABE[3]

[1]*Biological Laboratory, College of Bioresource Sciences, Nihon University, Fujisawa, Kanagawa 252, Japan;* [2]*Shimoda Marine Research Center, University of Tsukuba, Shimoda, Shizuoka 415, Japan; and* [3]*Tokyo Kasei Gakuin Tsukuba College, Tsukuba, Ibaraki 305, Japan*

Abstract. Allogeneic rejection between colonies (colony specificity) was described by electron microscopy in two compound ascidians, *Botrylloides simodensis* and *B. fuscus*. When two incompatible colonies are brought into contact at their growing edges, the tunic cuticle dissolves and the tunics of the colonies partially fuse. Alloreactive, humoral factors may diffuse to the opposite colony through the partially fusing tunic, and the tunic cells (free cells distributed in the tunic) possibly recognize these factors and induce a rejection reaction. Then, blood cells—mainly morula cells—infiltrate into the tunic, while tunic cells are disintegrating near where the partial fusion of the tunic is occurring. The infiltrating blood cells aggregate, disintegrate, and discharge electron-dense materials in the tunic at the subcuticular regions where the tunics have partially fused. Since the rejection lesion is restricted to the subcuticular area, some regulatory systems may be involved in this restriction. At the end, new walls are formed in the tunic matrix to separate the rejection lesion from the contacting colonies. The new wall is a continuous layer composed of electron-dense fibers and is structurally identical to the regenerating tunic cuticle. The mode of occurrence of colony specificity (Hirose *et al.*, 1994) and the present results indicate that tunic cells are the only allorecognition sites in *B. fuscus*.

Introduction

Self or non-self recognition is one of the most fundamental interactions among individuals, and its occurrence has been observed in many animal phyla. For instance, rejection or acceptance of grafted tissues among allogeneic individuals (histocompatibility) is one of the immediate examples of its occurrence. Whereas a tissue graft is an artificial treatment, a kind of tissue transplantation occurs naturally in many colonial forms of sessile animals, from sponges to ascidians. This phenomenon is known as colony specificity; when a sessile colony grows on a substratum and comes in contact with another conspecific colony, the two colonies either fuse to form a single colony, or they do not fuse. The outcome depends on allogeneic recognition between the two colonies. In some ascidians, the genetic control of this allorecognition has been demonstrated and is thought to be an ancestor of the major histocompatibility complex in vertebrates (Oka and Watanabe, 1957, 1960; Sabbadin, 1962; Scofield *et al.*, 1982; Weissman *et al.*, 1990).

Studies on colony specificity in colonial ascidians have been focused on species of the family Botryllidae (botryllid ascidians), and every botryllid ascidian studied has exhibited colony specificity (reviewed in Saito *et al.*, 1994). These species all form sheetlike colonies in which the zooids are connected with a vascular network, and the whole of the colony is embedded in a gelatinous tunic, an integumentary matrix that covers the epidermis. Free cells (tunic cells) of a few different kinds are distributed throughout the tunic (Hirose *et al.*, 1991), and a cuticular layer overlaying the tunic matrix is the outermost structure of the colony (Hirose *et al.*, 1990a).

When two compatible colonies are brought into contact at their growing edges, they fuse into a single colony. The course of the fusion reaction is fundamentally the same in all botryllids, as follows: (1) contact of the tunic

Received 26 January 1996; accepted 23 October 1996.

surfaces (= cuticle); (2) dissolution of the tunic cuticle at the contact area; (3) penetration of ampullae (termini of the blood vessels at colony periphery) into the opposite colony; (4) contact between the penetrating ampullae and those of the opposite colony; (5) ampullar fusion and establishment of vascular connection between the two colonies. In contrast, the rejection reaction in each species is initiated at a specific stage of the fusion process. In *Botryllus primigenus*, for example, rejection is initiated after the penetration of ampullae (Taneda, 1985).

Some *Botrylloides* species show a subcuticular rejection (SCR) that begins at the earliest step in the fusion process—immediately after the partial fusion of the tunic. The rejection reaction in SCR involves blood cell infiltration and occurs in only a small area of the tunic contacting an allogeneic colony. The loss of tissue is minimized in this rejection, which seems, therefore, to be the most advanced mode of rejection found thus far among botryllid ascidians. In other ascidians, such as *Botryllus primigenus*, all of the ampullae interacting with their allogeneic counterparts disintegrate and are cut off the colony (Taneda *et al.*, 1985, for review).

Among species of *Botrylloides* that show SCR, two different reactions are elicited when incompatible colonies are brought into contact at artificial cut surfaces. Whereas intensive rejection occurs at the contacting boundaries in *B. simodensis* (Hirose *et al.*, 1990b), vascular connections are established between incompatible conspecifics (surgical fusion) in *B. fuscus* and *B. violaceus* (Hirose *et al.*, 1988, 1994). Surgical fusion indicates that the effector system inducing the rejection in the latter two species is not distributed in the vascular system. During SCR, therefore, allorecognition is probably carried out in the tunic. We have used light and electron microscopy to examine the process of SCR in *B. simodensis* and *B. fuscus*. This study should provide a better understanding of the mechanisms of allogeneic rejection and bring essential insights to the questions: when is self or non-self recognized; and what is the agent of recognition?

Materials and Methods

Animals

Colonies of *Botrylloides simodensis* and *B. fuscus* were collected in the vicinity of Shimoda (Shizuoka Prefecture, Japan). The colonies were attached on glass plates and reared in culture boxes immersed in Nabeta Bay near the Shimoda Marine Research Center.

The fusibility of colonies was tested with fusion experiments, as follows: Two pieces of colony of the same size were brought into contact at their growing edges on a glass slide. After 1–2 h in a moisture chamber, the colonies attached to the glass slide and were then reared in running seawater in an aquarium in the laboratory; they were observed every day under a binocular stereomicroscope. Within several days, either a fusion or a rejection reaction occurred between the paired colonies. Here 'fusion' means establishment of a common vascular system between the two colonies, and 'rejection' means its interruption or prevention.

Light microscopy

The specimens were fixed with 2.5% glutaraldehyde solution containing 0.45 *M* sucrose buffered with 0.1 *M* cacodylate at pH 7.4. The fixed specimens were then dehydrated through a butanol series, embedded in Paraplast, sectioned at 5 μm, and stained with Congo red, Delafield's hematoxylin, and eosin-orange G.

Scanning electron microscopy

To observe the structures of internal tissues, the method of Armstrong (1971) was applied, as follows: Specimens embedded in Paraplast were cut with a razor blade or a microtome blade to expose the inner structures. The specimens were washed in xylene (1 h, three changes) to remove the Paraplast and then cleared with absolute ethanol. These specimens were dried in a critical point dryer and sputter-coated with gold-palladium. They were examined with a Hitachi S-570 scanning electron microscope at 20 kV.

Transmission electron microscopy

The specimens were fixed at room temperature in a 2.5% solution of glutaraldehyde containing 0.45 *M* sucrose and buffered with 0.1 *M* cacodylate at pH 7.4. An alternative fixation, on ice for 2 h, was in a 2.5% solution of glutaraldehyde containing 2% NaCl buffered with 0.1 *M* Millonig's phosphate buffer at pH 7.4. The latter medium is essentially the same as that of Sugino *et al.* (1987). These prefixed specimens were rinsed in the same buffer, and then postfixed with 1% osmium tetroxide in the same buffer for 1 to 2 h. After dehydration through an ethanol series, the specimens were cleared with *n*-butyl glycidyl ether and embedded in epoxy resin. Thin sections were double-stained with uranyl acetate and lead citrate. They were examined with a Hitachi HS-9 transmission electron microscope at 75 kV.

Results

General features of subcuticular rejection

In both *Botrylloides simodensis* and *B. fuscus*, when incompatible colonies are brought firmly into contact at their growing edges, they never fuse (Fig. 1). Yet the signs of inflammatory rejection are barely observable under a

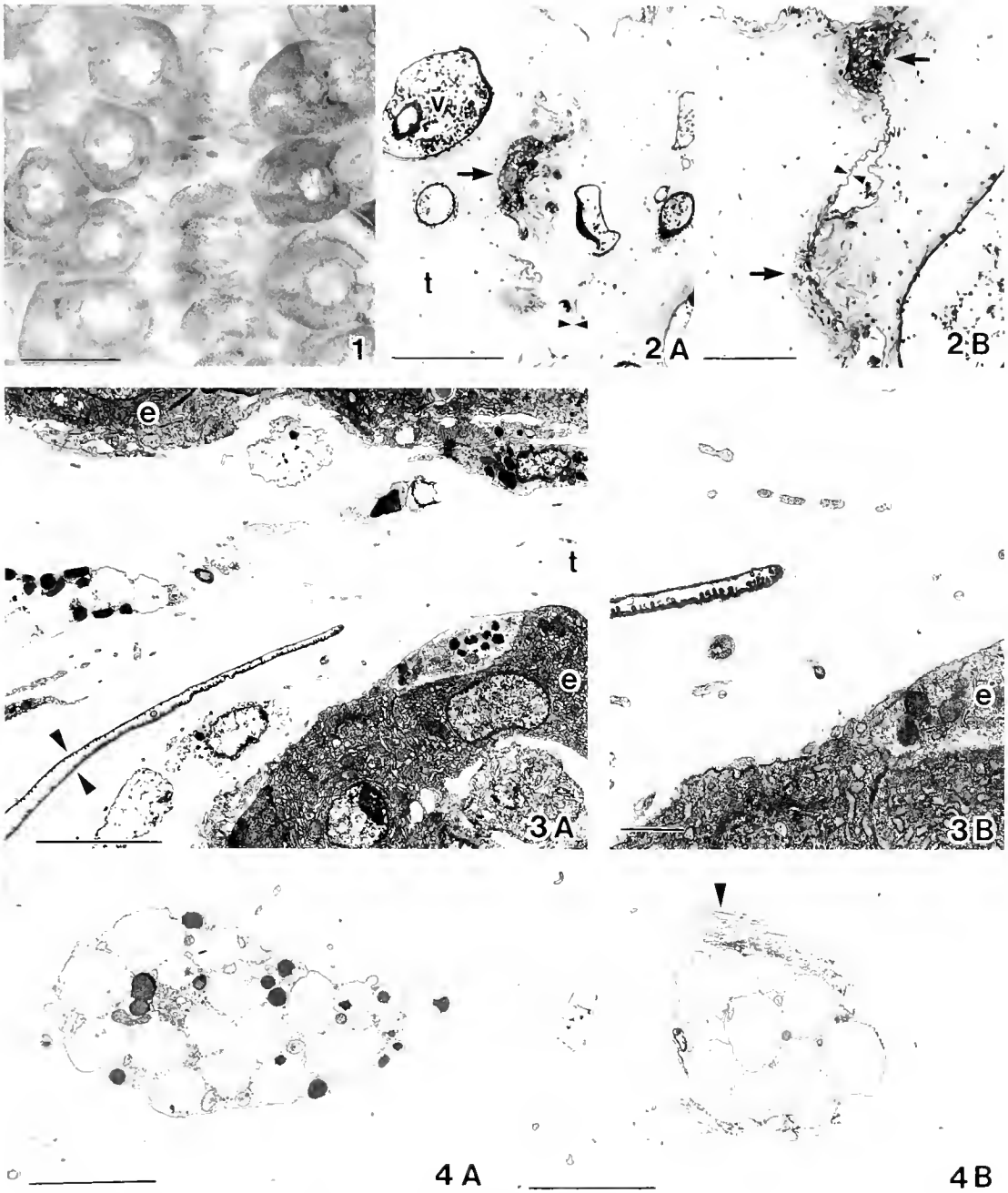

Figure 1. Subcuticular rejection in *Botrylloides simodensis*. Two incompatible colonies (right and left) are contacted at their growing edges. Rejection lesions are barely seen under the stereomicroscope. Bar = 0.5 mm.

Figure 2. Histological sections of subcuticular rejection in *Botrylloides simodensis* (A) and *B. fuscus* (B). Arrows, rejection lesions; arrowheads, tunic cuticle; t, tunic matrix; v, vascular vessel. Bar = 200 μm (A) and 100 μm (B).

Figure 3. Fusion of the tunic between incompatible colonies of *Botrylloides fuscus* (A) and an enlargement (B). Arrowheads, tunic cuticle of each colony; e, epidermis of vascular ampulla; t, tunic matrix. Bar = 5 μm (A), 1 μm (B).

Figure 4. Vacuo-granular tunic cells of *Botrylloides fuscus*. Intact cell with vacuoles and granules (A), and a disintegrating one discharging electron-dense materials that produce filamentous structures (arrowhead, B). Bar = 5 μm.

binocular stereomicroscope. In histological sections, rejection lesions are restricted to a limited part of the subcuticular region in the contact area (Fig. 2). In this rejection, infiltrating blood cells—mainly eosinophilic morula cells—aggregate and disintegrate in the tunic at the subcuticular region; thus the lesion is also well stained by eosin. The morphological process of SCR is fundamentally the same in *B. simodensis* and *B. fuscus*.

In this report, SCR is divided into the following three stages: (1) partial fusion of the tunic at the contact area; (2) blood cell infiltration, migration, and disintegration in the tunic; (3) separation of rejection lesion from the colonies. Since we cannot observe these processes in living specimens, the time course is difficult to define with precision. When actively growing colonies were brought into contact and reared at about 20°C, the time course could be estimated on the basis of histological data, as follows: (1) partial fusion of the tunic cuticle occurs 1 to 2 days after contact; (2) blood cell infiltration and disintegration begins shortly after partial fusion (2 to 3 days after contact) and continues until the rejection lesion is separated from the colony; (3) separation of the lesion is usually completed within 4 to 7 days after contact. The time course depends on the growth rate of the colonies as well as on temperature.

Partial fusion of the tunic

The first stage of SCR between the two colonies is the partial fusion of the contacting tunics; in other words, the dissolution of the tunic cuticles (Fig. 3). Partial fusion occurs in 1 to 2 days after the contact of the colonies. The tunic cuticle is a continuous, electron-dense sheet with minute protruberances (Hirose *et al.*, 1990a), and it is a boundary between the two contacting colonies. At the contact area, the tunic cuticles of both colonies adhere closely to each other. Thereafter, the cuticles dissolve here and there, and the tunic matrices of both colonies become continuous. In these areas, the edges of the adhering tunic cuticles become continuous and have a hairpin form (Fig. 3B). At this stage, the reaction between incompatible colonies shows no sign of a rejection reaction.

Blood cell infiltration, migration, and disintegration

The first signs of a rejection reaction are the infiltration of blood cells and the disintegration of tunic cells (vacuogranular tunic cells; see Hirose *et al.*, 1991) in the subcuticular regions where the partial tunic fusion is occurring (Figs. 4–6); we are not sure which of these events occurs earlier. Many of the infiltrating blood cells are morula cells that have several vacuoles filled with electron-dense material. The disintegrating tunic cells discharge electron-dense materials that probably originate from their granules. The discharged materials seem to bind to the filamentous components of the tunic matrix and form electron-dense filaments around the cells (arrows in Fig. 4). Afterward, the infiltrating blood cells migrate around the regions of partial tunic fusion (Fig. 7), and then they disintegrate (Fig. 8). The disintegrating morula cells discharge electron-dense materials, as seen around disintegrating tunic cells, and electron-dense filamentous structures are also formed in the tunic (Fig. 8).

The infiltrating blood cells increase in number, and they disintegrate and discharge their contents in the tunic (Figs. 9 and 10). Electron-dense fibers appear around the disintegrating cells (arrows in Fig. 10). This inflammatory-like reaction occurs in a limited area, because the infiltrating cells usually disintegrate after migrating to a subcuticular location where the tunics have partially fused. The cell infiltration, migration, and disintegration proceed further, and eventually the migrating cells form an aggregate in those subcuticular regions where the tunics of the allogeneic colonies have partially fused (Figs. 11 and 12). Within the cell aggregates, disintegrating cells discharge their contents, *i.e.*, electron-dense, eosinophilic materials. Around them is some electron-dense substance that may be derived from the discharged materials.

Separation of the rejection lesion

When the rejection is complete, a dense continuous layer appears in the tunic matrix, and it separates both colonies from the rejection lesion (Figs. 13–16). This new wall consists of aggregates of electron-dense fibers (arrows in Figs. 14 and 16).

Discussion

When colonies are brought into contact at their growing edges, the first interaction is a dissolution of the cuticles of the contacting tunics. Due to the cuticle dissolution, the tunics of the two colonies undergo partial fusion. Even when rejection is induced by contact between cut surfaces, the tunic matrixes of the two colonies appear to fuse shortly after the contact (Hirose *et al.*, 1990b). The tunic matrices facing each other probably fuse without allorecognition. At this stage, morphological differences are not observed between compatible and incompatible combinations, but the signs of rejection soon appear. Allorecognition probably occurs shortly after the tunics partially fuse. Blood plasma induces the allospecific reaction in both *Botryllus primigenus* (Taneda and Watanabe, 1982) and *Botrylloides simodensis* (Saito and Watanabe, 1984). Probably, alloreactive factors diffuse into the opposite colony through sites of partial fusion, and the alloreactive cells respond to these factors. Furthermore, the allorecognition sites are

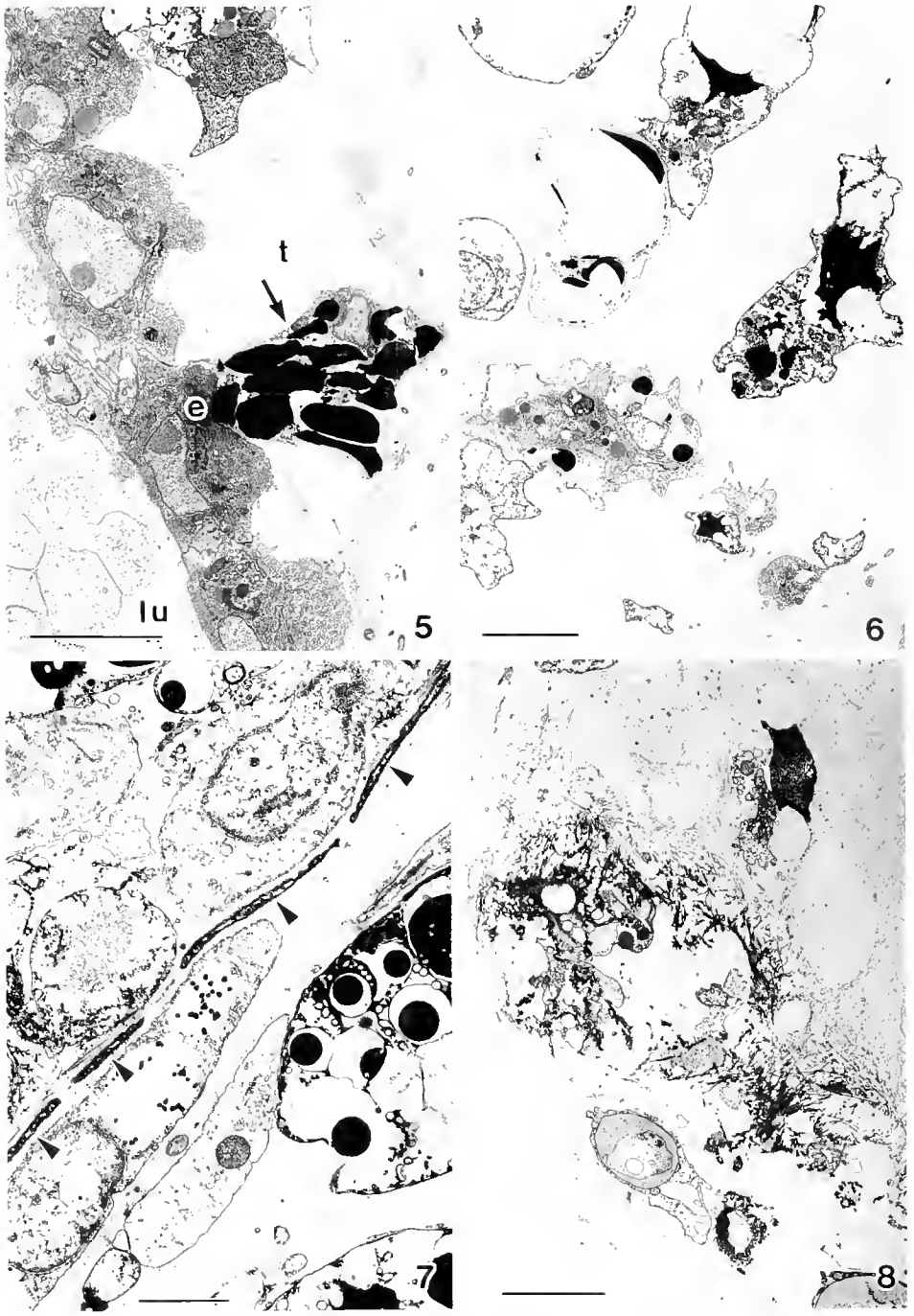

Figure 5. Blood cell infiltration (*Botrylloides simodensis*). Arrow, infiltrating blood cell (morula cell); e, epidermis of blood vessel; lu, vascular lumen; t, tunic matrix. Bar = 5 μm.

Figure 6. Blood cells infiltrating in the tunic (*Botrylloides fuscus*). Bar = 5 μm.

Figure 7. Blood cells migrate in an area of partial tunic fusion (*Botryllodes simodensis*). Arrowheads indicate tunic cuticle. Bar = 2 μm.

Figure 8. Disintegration of infiltrating blood cells (morula cells) in the tunic (*Botryllodes fuscus*). Electron-dense materials are discharged in the tunic. Bar = 5 μm.

probably restricted to the tunic, particularly in species in which surgical fusion occurs, *i.e., B. fuscus;* moreover, the tunic cells may well be the sole allorecognition sites. On the other hand, the ampullar epithelia or some kinds of blood cells may also be alloreactive in *B. simodensis,* because an intensive rejection occurs between incompatible colonies that make contact at artificial cut surfaces.

The first signs of SCR are the disintegration of vacuo-

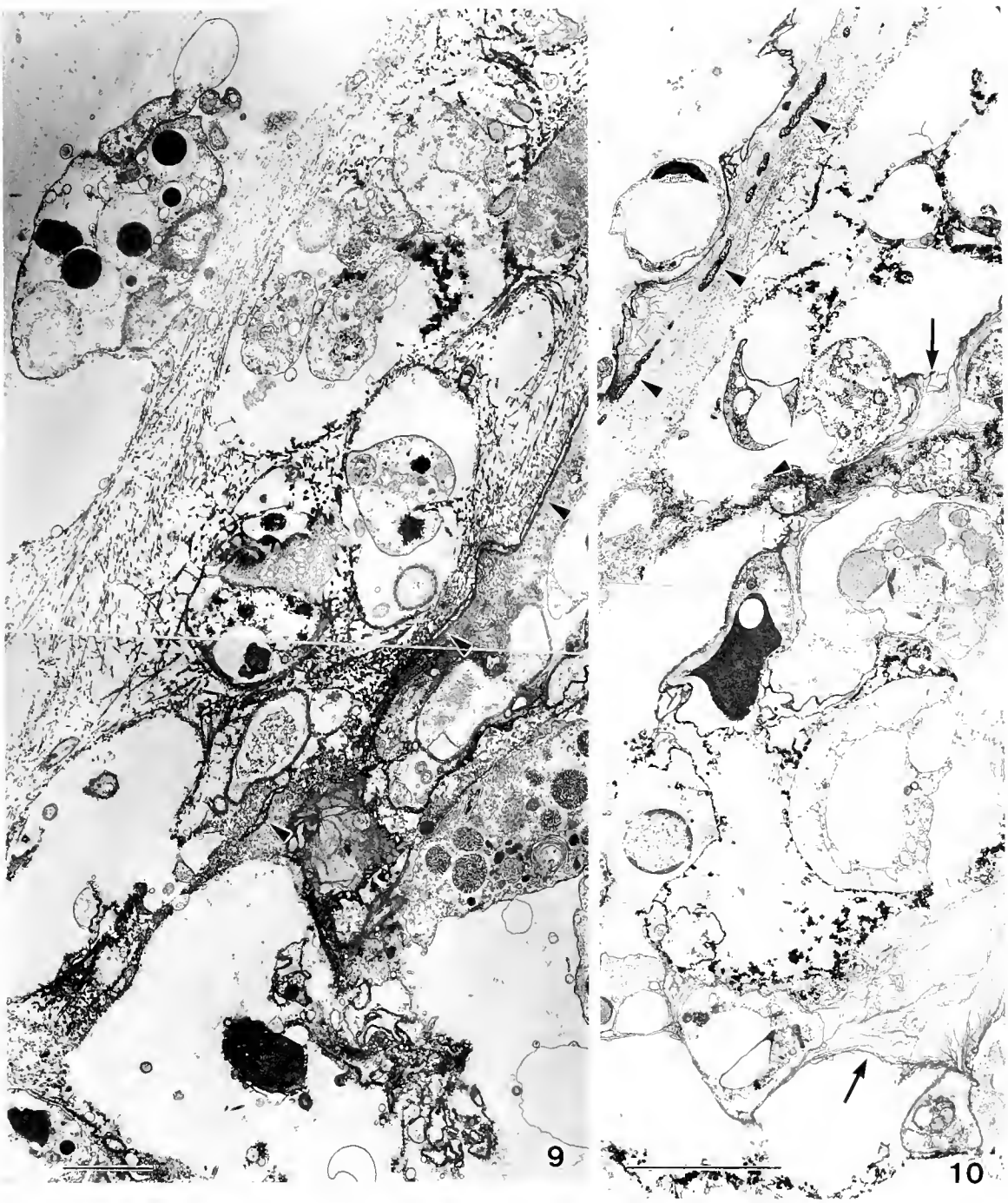

Figures 9 and 10. Disintegration of blood cells in the vicinity of a partial fusion of tunic cuticles (Fig. 9, *Botryllodes simodensis*, Fig. 10, *B. fuscus*). Electron-dense fibers are formed in the tunic (arrows in Fig. 10). Arrowheads, tunic cuticle. Bar = 2 μm, Fig. 9; 5 μm, Fig. 10.

granular tunic cells and the infiltration of blood cells, mainly morula cells. The disintegrating tunic cells may release chemotactic factors that induce blood cell infiltration. Whether the tunic cell disintegration is a primary response to the allorecognition or an induced one remains uncertain. The infiltrating blood cells migrate and disintegrate at limited sites in the subcuticular region during SCR; the discharged contents from blood cells might also contain chemotactic factors that induce blood cell infiltration and disintegration.

The disintegrating tunic cells and morula cells discharge electron-dense materials, and these materials ap-

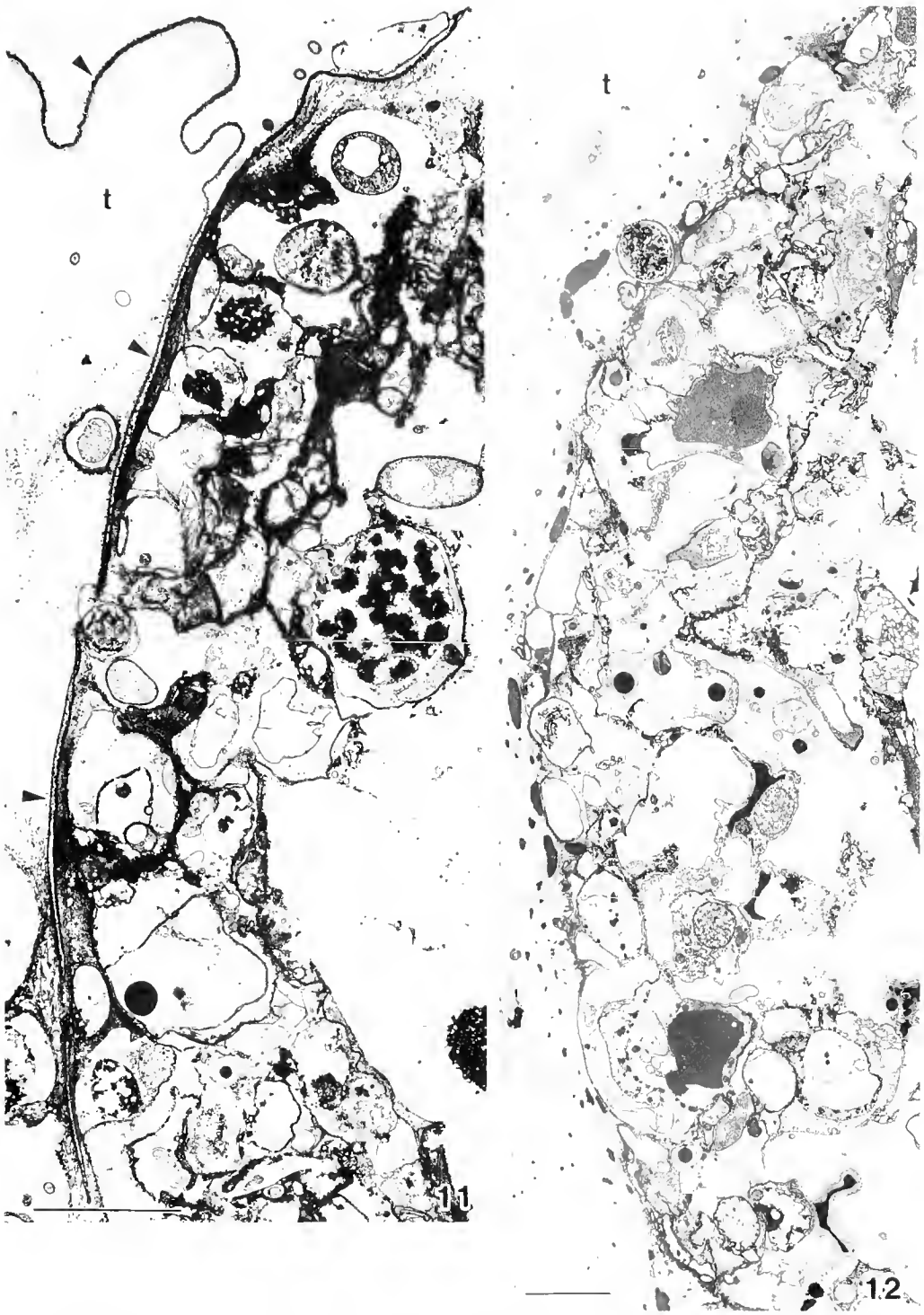

Figures 11 and 12. Cell aggregates at the rejection lesion (Fig. 11, *Botrylloides simodensis;* Fig. 12, *B. fuscus*). Arrowheads, tunic cuticle; t, tunic matrix. Bar = 5 μm.

pear to bind to the tunic matrix to form filamentous structures around the disintegrating cells. The discharged contents probably rearrange the tunic matrix and induce the disintegration of the tunic structures. The formation of filaments in the tunic around the disintegrating cells was reported in the allogeneic rejection of *Botryllus primigenus* (Tanaka, 1973; Tanaka and Watanabe, 1973). In some solitary ascidians, morula cells (or

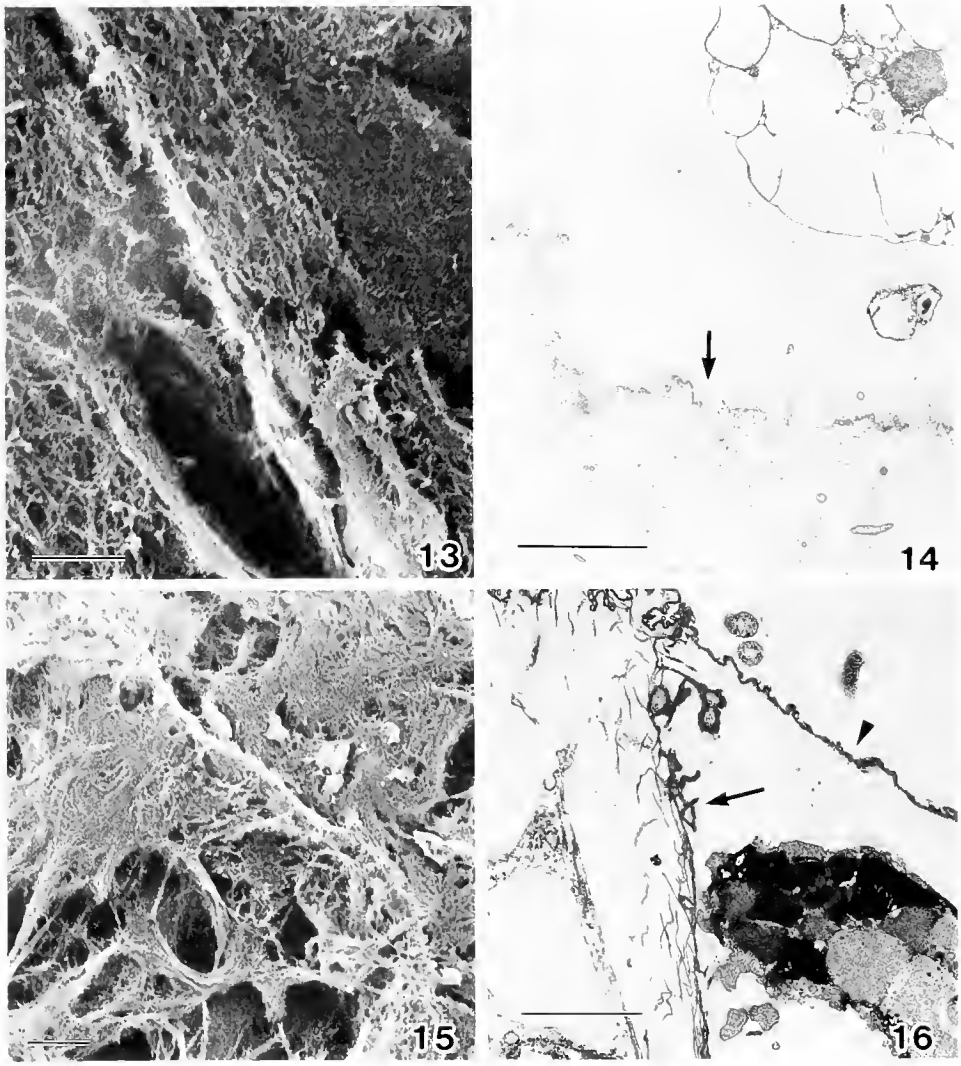

Figures 13–16. New wall separating the colony from the rejection lesion (Figs. 13 and 14, *Botrylloides simodensis*, Figs. 15 and 16, *B. fuscus*). Figures 13 and 15 are scanning and Figures 14 and 16 are transmission electron micrographs. Lower left parts are lesion areas in these figures. Arrows, new wall; arrowheads, tunic cuticle. Bar = 5 μm, Figs. 13 and 14; 10 μm, Fig. 15; 2 μm, Fig. 16.

vacuolated cells) contain phenoloxidase, which has cytotoxic activity (Jackson *et al.*, 1993), and they release the enzyme in response to allogeneic blood cells (Akita and Hoshi, 1995). In *Botryllus schlosseri*, a botryllid ascidian, Ballarin *et al.* (1993) showed that the morula cells contain phenoloxidase, as well as peroxidase and arylsulfatase; and these authors also showed that phenoloxidase is involved in the allogeneic rejection reaction (Ballarin *et al.*, 1994, 1995). In the SCR of *Botrylloides* species, the discharged substances from morula cells also probably contain phenoloxidase.

In the SCR, the infiltrating blood cells form aggregates in the subcuticular region where partial fusion occurs. There may be a regulatory system to restrict the rejection reaction to the limited areas. In contrast, when rejection is induced by contact between cut surfaces in *B. simodensis*, the infiltrating cells disintegrate at random around the cut surface facing the incompatible colony, and the rejection lesion is large enough to be observed as a clear, black line (Hirose *et al.*, 1990b). In this case, the regulatory system proposed above would not work.

After the rejection reaction, the new wall appears, separating the rejection lesion from the colonies. The synthesis of the new wall was first described in the allogeneic rejection in *B. primigenus* (Tanaka, 1973; Tanaka and Watanabe, 1973), and the same structures were also reported in the rejection induced by the contact of allogeneic colonies of *B. simodensis* at cut surfaces (Hirose *et*

al., 1990b). Since the fine structure of the new wall is the same as that of regenerating tunic cuticle (Hirose *et al.*, 1995), the new wall should eventually become a tunic cuticle. During cuticle regeneration, the electron-dense fibers are probably produced from the aggregates of tunic matrix, and proteolysis is probably involved. In SCR, the disintegrating cells may release factors that induce the aggregation of tunic matrix and lead to the production of the electron-dense fibers. The new wall is supposed to act as (1) a barrier that prevents the migration of cells to the disintegrating tissue, (2) a barrier preventing the diffusion of factors into the colony from the allogeneic colony and disintegrating cells, (3) an outer covering of the tunic once the rejection lesion has been cleared.

What cell types in a colony discriminate self from nonself? The most likely candidates are the tunic cells, particularly in *B. fuscus* where surgical fusion occurs between incompatible colonies at the cut surface (Hirose *et al.*, 1994). In this species, surgical fusion indicates that the distribution of allorecognition sites is restricted to the tunic, and thus tunic cells may be the sole allorecognition sites. The morphological changes that occur during the fusion and rejection reactions also suggest that the allorecognition is carried out only in the subcuticular region of the tunic that is partially fused with the contacting colony.

Acknowledgments

The present study was partly supported by Grants-in-Aid to EH and YS from the Ministry of Education, Science and Culture of Japan. Most of this study was performed at the Shimoda Marine Research Center (SMRC), University of Tsukuba, and we thank the staff members. We wish to express our gratitude to Dr. Y. Sugino (Tosa Women's High School) for providing advice on electron microscopy and to anonymous referees for their valuable comments and suggestions. This study includes the contribution no. 599 from SMRC.

Literature Cited

Akita, N., and M. Hoshi. 1995. Hemocytes release phenoloxidase upon contact reaction, an allogeneic interaction, in the ascidian *Halocynthia roretzi*. *Cell Struct. Func.* **20:** 81–87.

Armstrong, P. B. 1971. A scanning electron microscope technique for study of the internal microanatomy of embryos. *Microscope* **19:** 281–284.

Ballarin, L., F. Cima, and A. Sabbadin. 1993. Histoenzymatic staining and characterization of the colonial ascidian *Botryllus schlosseri* hemocytes. *Bol. Zool.* **60:** 19–24.

Ballarin, L., F. Cima, and A. Sabbadin. 1994. Phenoloxidase in the colonial ascidian *Botryllus schlosseri* (Urochordara: Ascidiacea). *Anim. Biol* **3:** 41–48.

Ballarin, L., F. Cima, and A. Sabbadin. 1995. Morula cell and histocompatibility in the colonial ascidian *Botryllus schlosseri*. *Zool. Sci. (Tokyo)* **12:** 757–764.

Hirose, E., Y. Saito, and H. Watanabe. 1988. A new type of manifestation of colony specificity in the compound ascidian, *Botrylloides violaceus* Oka. *Biol. Bull.* **175:** 240–245.

Hirose, E., Y. Saito, K. Hashimoto, and H. Watanabe. 1990a. Minute protrusions of the cuticle: fine surface structures of the tunic in ascidians. *J. Morphol* **204:** 67–73.

Hirose, E., Y. Saito, and H. Watanabe. 1990b. Allogeneic rejection induced by cut surface contact in the compound ascidian, *Botrylloides simodensis*. *Invertebr. Reprod. Dev.* **17:** 159–164.

Hirose, E., Y. Saito, and H. Watanabe. 1991. Tunic cell morphology and classification in botryllid ascidians. *Zool. Sci. (Tokyo)* **8:** 951–958.

Hirose, E., Y. Saito, and H. Watanabe. 1994. Surgical fusion between incompatible colonies of the compound ascidian, *Botrylloides fuscus*. *Dev. Comp. Immunol.* **18:** 287–294.

Hirose, E., Y. Saito, and H. Watanabe. 1995. Regeneration of the tunic cuticle in the compound ascidian, *Botrylloides simodensis*. *Dev. Comp. Immunol.* **19:** 143–151.

Jackson, A. D., V. J. Smith, and C. M. Peddie. 1993. *In vitro* phenoloxidase activity in the blood of *Ciona intestinalis* and other ascidians. *Dev. Comp. Immunol.* **17:** 97–108.

Oka, H., and H. Watanabe. 1957. Colony-specificity in compound ascidians as tested by fusion experiments (a preliminary report). *Proc. Jpn. Acad* **33:** 657–659.

Oka, H., and H. Watanabe. 1960. Problems of colony-specificity in compound ascidians. *Bull. Mar. Biol. Stn. Asamushi* **10:** 153–155.

Sabbadin, A. 1962. Le basi genetiche della capacità di fusione fra colonie in *Botryllus schlosseri* (Ascidiacea). *Rend. Accad. Naz. Lincei* **32(Ser. 8):** 1031–1035.

Saito, Y., and H. Watanabe. 1984. Partial biochemical characterization of humoral factors involved in the nonfusion reaction of a botryllid ascidian, *Botrylloides simodensis*. *Zool. Sci. (Tokyo)* **1:** 229–235.

Saito, Y., E. Hirose, and H. Watanabe. 1994. Allorecognition in compound ascidians. *Int. J. Dev. Biol.* **38:** 237–247.

Scofield, V. L., J. M. Schlumpberger, L. A. West, and I. L. Weissman. 1982. Protochordate allo-recognition is controlled by a MHC-like gene system. *Nature* **295:** 499–502.

Sugino, Y. M., A. Tominaga, and Y. Takashima. 1987. Differentiation of the accessory cells and structural regionalization of the oocyte in the ascidian *Ciona savignyi* during early oogenesis. *J. Exp. Zool.* **242:** 205–214.

Tanaka, K. 1973. Allogeneic inhibition in a compound ascidian, *Botryllus primigenus* Oka. II. Cellular and humoral responses in "nonfusion" reaction. *Cell. Immunol.* **7:** 427–443.

Tanaka, K., and H. Watanabe. 1973. Allogeneic inhibition in a compound ascidian, *Botryllus primigenus* Oka. I. Processes and features of "nonfusion" reaction. *Cell. Immunol.* **7:** 410–426.

Taneda, Y. 1985. Simultaneous occurrence of fusion and nonfusion reaction in two colonies in contact of the compound ascidian, *Botryllus primigenus*. *Dev. Comp. Immunol.* **9:** 371–375.

Taneda, Y., Y. Saito, and H. Watanabe. 1985. Self or non-self discrimination in ascidians. *Zool. Sci. (Tokyo)* **2:** 433–442.

Taneda, Y., and H. Watanabe. 1982. Studies on colony specificity in the compound ascidian, *Botryllus primigenus* Oka. II. *In vivo* bioassay for analyzing the mechanisms of "nonfusion" reaction. *Dev. Comp. Immunol.* **6:** 243–252.

Weissman, I. L., Y. Saito, and B. Rinkevich. 1990. Allorecognition histocompatibility in a protochordate species: Is the relationship to MHC semantic or structural? *Immunol. Rev.* **113:** 227–241.

Reference: *Biol. Bull.* **192:** 62–72. (February, 1997)

Effects of Common Estuarine Pollutants on the Immune Reactions of Tunicates

DAVID RAFTOS AND AIMEE HUTCHINSON

School of Biological Sciences, Macquarie University, North Ryde, NSW, 2109, Australia

Abstract. Tunicates are filter-feeding estuarine and marine animals that are frequently exposed to chronic environmental pollution. This study demonstrates that exposure to low-level (*i.e.*, below the threshold of acute lethality) contamination with tributyltin, creosote, and copper can have substantial effects on natural immune reactions in tunicates. Sublethal doses of toxicants administered either *in vitro* or *in vivo* profoundly affected phagocytosis, cellular cytotoxicity, and hematopoietic cell proliferation. Effects were not always inhibitory, and responses often varied depending on the route of toxicant administration. The data suggest that pollutants can activate cascades of cellular processes and compensatory mechanisms, as well as directly inhibiting some of the responses tested. Some evidence indicates that toxicants exert their effects by altering the relative frequencies of circulatory hemocytes.

Introduction

Marine invertebrates can be profoundly affected by aquatic pollution. Detrimental effects have been identified using tests for acute lethality (*e.g.*, 96-h LD_{50}), toxicant bioaccumulation, anatomical and biochemical aberration, or altered biodiversity and abundance (Giam and Ray, 1987; Landis and Yu, 1995; Peakall, 1992). However, there is relatively little information regarding the effects of environmental contamination on natural immune reactions in invertebrates, even though modulation of the immune system may dramatically alter populations by affecting their resistance to infection (Anderson *et al.*, 1990; McCarthy and Shugart, 1990; Roales and Perlmutter, 1977; Sarot and Perlmutter, 1976; Stebbing, 1985). Some evidence suggests that the effects of decreased disease resistance resulting from low-level, chronic pollution may not be reflected accurately in assays that test acute lethality. For instance, heavy metal or polychlorinated biphenyl contamination in worms can significantly inhibit lysozyme activity, wound healing, phagocytosis, rosette formation, and tissue transplantation rejection at concentrations that are not acutely lethal (Cooper and Roch, 1992; Fitzpatrick *et al.*, 1992; Rodrigues-Grau *et al.*, 1989).

The aim of the current study is to demonstrate that subacute contamination with three common estuarine pollutants—the antifouling agents tributyltin (TBT), copper, and creosote—can significantly affect the immunological defenses of tunicates. Tunicates (Urochordata, Ascidiacea) are aquatic filter-feeding invertebrates that are ubiquitous components of estuarine and coastal marine systems (Berrill, 1950; Goodbody, 1974). They occur in large populations on marinas, moorings, and wharves that are often subjected to chronic pollution, particularly from antifouling treatments. The effects of pollution are likely to be compounded in tunicates by their filter-feeding lifestyle. Large volumes of potentially polluted water pass over the sensitive endothelial surfaces of the pharynx (up to 100 l of water per day), greatly increasing the propensity of tunicates to absorb toxicants (Goodbody, 1974).

Here, we test the effects of toxicants on a number of well-characterized assays of immunological reactivity in tunicates. Those assays quantify hemopoietic cell proliferation (Raftos and Cooper, 1991; Raftos *et al.*, 1991), phagocytosis (Beck *et al.*, 1993; Kelly *et al.*, 1993), and cellular cytotoxicity (Parrinello *et al.*, 1993; Peddie and Smith, 1993, 1994). Tunicates lack adaptive antipatho-

Received 17 May 1995; accepted 24 October 1996.

Abbreviations: FSW, filtered seawater; MAC, marine anticoagulant; MS, marine saline; PAH, polycyclic aromatic hydrocarbon; RRBC, rabbit red blood cells; TBT, tributyltin; TBS, Tris-buffered saline.

genic defense mechanisms that are analogous to the mammalian adaptive immune system (Raftos, 1994). Hence, innate (or natural) immunological reactions, such as phagocytosis and cellular cytotoxicity, are probably the major protective responses of these animals.

Materials and Methods

Tunicates

Specimens of *Styela plicata* were collected from two sites on Sydney Harbor, Australia (Balmoral Beach and Birkenhead Point). After collection, tunicates were maintained in 40-l aquaria filled with seawater. Aquaria were held at 14°C under constant aeration. These conditions can maintain *S. plicata* for up to 2 months with limited mortality. *In vivo* exposures were conducted in partitioned aquaria containing 40 l of seawater per compartment.

Toxicants

Tributyltin oxide and copper sulfate were purchased from ICN Chemicals (Sydney, NSW, Australia) and creosote was obtained from BBC Pty Ltd (Chatswood, NSW, Australia). Tributyltin and copper were diluted directly in filtered seawater (FSW; 0.45-μm filtration). Creosote was prepared as a saturated stock solution in FSW by vigorously agitating 1% v/v creosote in toxicant-free, filtered seawater overnight and then filtering the solution (0.45-μm) to remove insoluble material. Concentrations of creosote are cited as percentages (v/v) of filtered, saturated creosote solutions. Chemical analysis (Australian Analytical Laboratories, Asquith, NSW, Australia) revealed that 5% v/v of a saturated solution of creosote contained 1 mg/l total polycyclic aromatic hydrocarbons (PAH) (napthalene, 280 μg/l; anthracene, 250 μg/l; phenanthrene, 150 μg/l; acenapthene, 93 μg/l; remaining PAHs < 80 μg/l). No PAHs (practical quantitation limit = 1 μg/l) were detected in the normal seawater used in aquaria.

Treatment protocols

Two forms of toxicant treatment were applied. Tunicate cells were exposed to toxicants *in vitro* to assess effects on isolated tissues, and live tunicates were exposed to toxicants in aquaria to identify effects that were derived from interactions between organ or physiological systems. Where possible, the effects of toxicants were tested over a range of doses and at a number of time points for exposure periods of up to 9 days. For brevity, only representative data reflecting trends in both dose response and kinetic analysis are presented here.

Dosages

The ranges of doses used for the three toxicants were selected to incorporate concentrations that yielded significant differences from nontreated controls in at least one of the assays tested. Copper was the only compound that proved to be acutely toxic at high doses. All tunicates ($n = 8$) died within 8 days of exposure to ≥ 5 μg/ml copper. Mortality was assessed by the sensitivity of tunicates to touch (failure to retract siphons) and by an analysis of hemocyte (blood cell) viability. None of the other doses tested, including <5 μg/ml copper, caused mortality within 20 days ($n = 4$ per dose).

Hemocyte harvesting and manipulation

Hemocytes were harvested from incisions in the buccal siphons of *S. plicata*. The exuded hemolymph (blood) was collected in equal volumes of ice-cold marine anticoagulant buffer (MAC; 0.1 *M* glucose, 15 m*M* trisodium citrate, 13 m*M* citric acid, 10 m*M* EDTA, 0.45 *M* NaCl, pH 7.0; Peddie and Smith, 1994) or FSW. Debris and cell aggregates were removed from the hemolymph by sedimentation for 5 min ($1 \times g$). As required, hemocytes were washed by centrifugation ($400 \times g$, 5 min, 4°C) through either MAC or FSW.

Cell viability and morphology

Hemocyte viabilities and the relative frequencies of distinct hemocyte subpopulations were determined using a FACScan flow cytometer with an argon-ion laser tuned to 488 nm (Becton Dickenson, Mountain View, CA). Hemocytes for flow cytometry were obtained either by bleeding tunicates that had been exposed to toxicants in aquaria or by harvesting cells that had migrated from cultured pharyngeal explants during *in vitro* exposures ("emigrant hemocytes"; see *Proliferative activity of toxicant-treated tunicate cells* section). In viability studies, hemocytes (1×10^6/ml) were stained with ethidium bromide (0.1% v/v) immediately prior to analysis. Dead cells were detected by their increased red (800 nm) fluorescence reflecting the intercalation of ethidium bromide into cellular DNA. The relative frequencies of distinct hemocyte subpopulations were determined by analyzing forward angle versus 90° light-scatter plots.

Proliferative activity of toxicant-treated tunicate cells

To quantify hemopoietic cell proliferation, tunicate tissue cultures were established by excising small portions (2×2 mm) of the pharynx for explant culture in tunicate tissue culture medium (T-RPMI; Raftos and Cooper, 1990). Each 100 ml of T-RPMI contained 10 ml RPMI-1640 tissue culture medium (with sodium bicar-

bonate, without L-glutamine; Sigma Chemicals, St. Louis, MO), 1 ml 20% w/v NaCl, 1 ml antibiotic stock solution (4 mg/ml streptomycin sulfate, 10^3 IU/ml penicillin sulfate), 100 μl 1 *M* L-glutamine, and 88 ml FSW. Cultures were maintained at 15°C without CO_2 supplementation. Under these conditions explant cultures normally maintain cell viability and function for up to 70 days (Raftos and Cooper, 1990).

For *in vitro* exposure trials, explants were cultured for up to 8 days in 96-well flat-bottomed tissue culture plates containing 200 μl/well T-RPMI and various concentrations of toxicants. Explants were moved to fresh medium every 2–4 days. After appropriate exposure periods of up to 8 days, explants were incubated (overnight, 15°C) with 18.5 MBq/ml ^{3}H-thymidine (Amersham, NSW, Australia, 740 GBq/mmol). Non-incorporated ^{3}H-thymidine was removed after incubation by extensive washing in FSW. Explants were then digested (37°C, overnight) in 2.0% w/v trypsin (Sigma Chemicals) to facilitate liquid scintillation counting in Ecolite scintillation cocktail (ICN, Seven Hills, NSW, Australia) (Raftos *et al.*, 1991).

Explants from tunicates exposed to toxicants in aquaria were excised, incubated immediately in T-RPMI containing 18.5 MBq/ml ^{3}H-thymidine (overnight, 15°C), and then washed and digested as described above.

Phagocytic activity of toxicant-exposed hemocytes

To test the phagocytic activity of tunicates that had been exposed to toxicants in aquaria, hemocytes from treated tunicates were harvested into FSW and their densities adjusted to 3×10^6 cells/ml without washing. For *in vitro* exposures, toxicants were added to hemocyte suspensions harvested from nonexposed tunicates (3×10^6 cells/ml in T-RPMI). Aliquots (200 μl) of hemocyte suspensions were cultured (15°C) on autoclaved glass coverslips (22 × 22 mm) for either 2 h (aquarium exposures) or overnight (*in vitro* exposures). Adherent hemocytes were washed with 400 μl FSW before being overlaid with 50 μl yeast (Baker's yeast type II, Sigma Chemicals; 5×10^6 yeast/ml) that had been prepared and opsonized with *S. plicata* plasma according to the method of Beck *et al.* (1993). Noningested yeast were removed by extensive washing with FSW after a 30-min incubation (15°C), and phagocytic activity was quantified microscopically (Beck *et al.*, 1993; Kelly *et al.*, 1993).

Cytotoxic activity of treated cells

Hemocytes from tunicates that had been exposed to toxicants in aquaria were harvested in MAC and tested immediately in cytotoxicity assays. For *in vitro* exposures, hemocytes were harvested from nontreated tunicates and cultured overnight (15°C) in T-RPMI containing various concentrations of toxicants before being tested for cytotoxic activity.

Cytotoxic activities of hemocytes were tested in two assays that used either K562 human chronic myelogenous leukemia cells or rabbit red blood cells (RRBC) as targets. The capacity of hemocytes to kill K-562 cells was assessed by a modification of the method of Peddie and Smith (1993). Hemocyte suspensions were adjusted to 4×10^7 cells/ml in MAC; 50–100 μl of these hemocyte suspensions were then mixed in round-bottomed 5-ml flow cytometry tubes with equal volumes of K-562 cells (4×10^6 cells/ml) suspended in marine saline (MS; 12 m*M* $CaCl_2 \cdot 6H_2O$, 11 m*M* KCl, 26 m*M* $MgCl_2 \cdot 6H_2O$, 45 m*M* Tris, 38 m*M* HCl, 400 m*M* NaCl, pH 7.4). The cell mixtures were incubated at 15°C for 90 min, stained with ethidium bromide and then immediately tested, using a FACScan flow cytometer, for the uptake of red fluorescence (800 nm). Specific cytotoxic activities were calculated as the percentage of dead K562 cells in a particular sample minus the percentage of dead cells in controls that contained K562 cells but no hemocytes. K562 cells were obtained from the American Type Tissue Culture Collection (Rockville, MD) and were grown in RPMI-1640 tissue culture medium. Immediately prior to their use in cytotoxicity assays, K562 cells were conditioned to the high tonicity of MS by incubation (30 min, 20°C) in an intermediate saline solution (12 m*M* $CaCl_2 \cdot 6H_2O$, 11 m*M* KCl, 26 m*M* $MgCl_2 \cdot 6H_2O$, 45 m*M* Tris, 38 m*M* HCl, 300 m*M* NaCl, pH 7.4; Peddie and Smith, 1993).

The ability of hemocytes to lyse RRBC was quantified by the method of Parrinello *et al.* (1993). Hemocytes were washed once through Tris-buffered saline (TBS; 10 m*M* Tris, 150 m*M* NaCl, pH 7.4) and resuspended in TBS supplemented with 10 m*M* $CaCl_2$ (TBS-Ca) to yield 2×10^6 cells/ml. One-hundred microliters per well of the suspensions were then incubated (60 min, 37°C) with an equal volume of RRBC (4×10^7 cells/ml in TBS-Ca) in 96-well round-bottomed tissue culture plates. After incubation the plates were centrifuged and 100 μl of the resulting supernatant was transferred to flat-bottomed plates so that the absorbance (405 nm) of hemoglobin released from lysed cells could be quantified on a microplate spectrophotometer. Specific cytotoxic activities were calculated as percentages relative to maximum release (4×10^6 RRBC/well in H_2O) and spontaneous release (4×10^6 RRBC/well in TBS-Ca, no hemocytes) values.

Statistical analysis

Nontreated controls were included in all experiments. A minimum of four tunicates were tested for each dose

Table I

Percentage viabilities of hemocytes after 8 days of in vitro *or aquarium exposure to a variety of toxicants*

Treatment	% viable cells ± SEM ($n \geq 4$)	
	In vitro	Aquarium
Control (no treatment)	87.3 ± 1.6	95.0 ± 0.6
TBT (10 μg/l)	89.3 ± 3.4	94.3 ± 1.2[a]
Cu (0.5 μg/ml)	75.1 ± 2.1[#]	93.1 ± 2.3
Creosote (1%)	72.6 ± 4.8[#]	96.6 ± 0.7

[a] Tested after 6-day exposure.
[#] $P < 0.05$ *vs.* nontreated control.

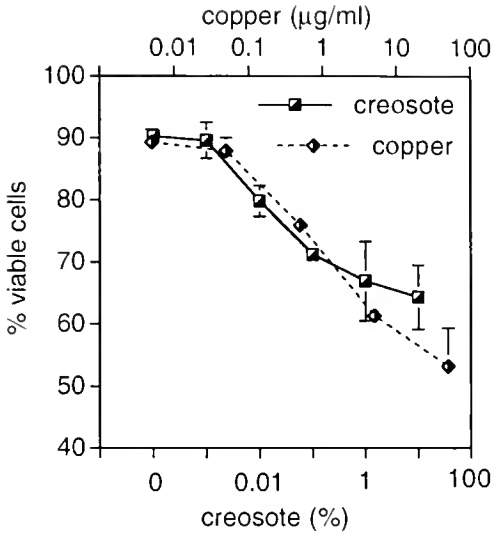

Figure 1. The percentage of viable cells (±SEM, $n \geq 4$) in the population of hemocytes that had emigrated from tunicate pharyngeal explants after 8 days of *in vitro* exposure to various doses of creosote and copper.

and time point in aquarium trials. More than three replicates were tested for each dose and time point during *in vitro* exposures. The statistical significance of differences between treatments was determined by Student's two-tailed *t*-test using the Statview SE+ (Abacus Concepts Inc, Berkeley, CA) and Statworks (Cricket Software Inc., Philadelphia, PA) statistical packages.

Results

Effects of toxicants on hemocyte viability

The viability of hemocytes emigrating from *in vitro* pharyngeal cultures was decreased by exposure to copper or creosote (Table I). Decreases in viability were dose-dependent, with concentrations greater than 0.001% creosote or 0.05 μg/ml copper significantly lowering hemocyte survival after 8 days of exposure ($P < 0.05$ *vs.* nontreated controls; Fig. 1). Ten percent creosote or 50 μg/ml copper decreased viability by 37% and 48% relative to nontreated controls.

In contrast, TBT did not significantly alter hemocyte viability at any of the doses or times tested during *in vitro* exposures ($P > 0.05$). Moreover, the viabilities of hemocytes harvested from tunicates that had been exposed to creosote, copper, or TBT for up to 9 days in aquaria did not differ significantly from those of nontreated controls ($P > 0.05$; Table I).

Alteration of proliferative activity

Exposure to toxicants profoundly affected the uptake of ^{3}H-thymidine by pharyngeal explants (Table II). Exposure to TBT *in vitro* was the only treatment that did not significantly alter proliferation at any of the doses or times tested ($P > 0.05$; Fig. 2A). TBT treatment in aquaria reduced proliferative activity by as much as 62% after 6 days of exposure (10 μg/l; Fig. 2A) and copper inhibited ^{3}H-thymidine incorporation by up to 82% (0.5 μg/ml, day 8; Table II) when compared to nontreated controls.

The effects of creosote on proliferation were both time- and dose-dependent. After 4 days of exposure to high doses of creosote in aquaria (≥1%), proliferative activity was significantly increased relative to nontreated controls ($P < 0.05$; Fig. 2B). In contrast, treatment with 0.5% creosote had no effect after 4 days of exposure but significantly enhanced ^{3}H-thymidine uptake (252% *vs.* controls) after 8 days. At this latter time point, proliferative activity in tunicates exposed to high doses (≥1% creosote) had subsided. Significant effects of TBT on proliferation were evident after 4 days of exposure and did not subside over time (Fig. 2A).

Table II

Effect on hematopoietic cell proliferation of exposure for 8 days to various toxicants either in vitro *or in aquaria; data are represented as percentages of ^{3}H-thymidine uptake detected in nontreated controls*

Treatment	% of nontreated control[γ] ± SEM ($n \geq 6$)	
	In vitro	Aquarium
TBT (10 μg/l)	124.1 ± 23.2[a]	38.8 ± 7.1[#]
Cu (0.5 μg/ml)	31.6 ± 4.2	17.7 ± 4.8
Creosote (0.5%)	71.3 ± 8.0	252.1 ± 2.1

[a] $P > 0.05$ *vs.* nontreated controls.
[#] 6-day exposure.
[γ] Mean ^{3}H-thymidine uptake by nontreated controls = 987 ± 23 cpm.

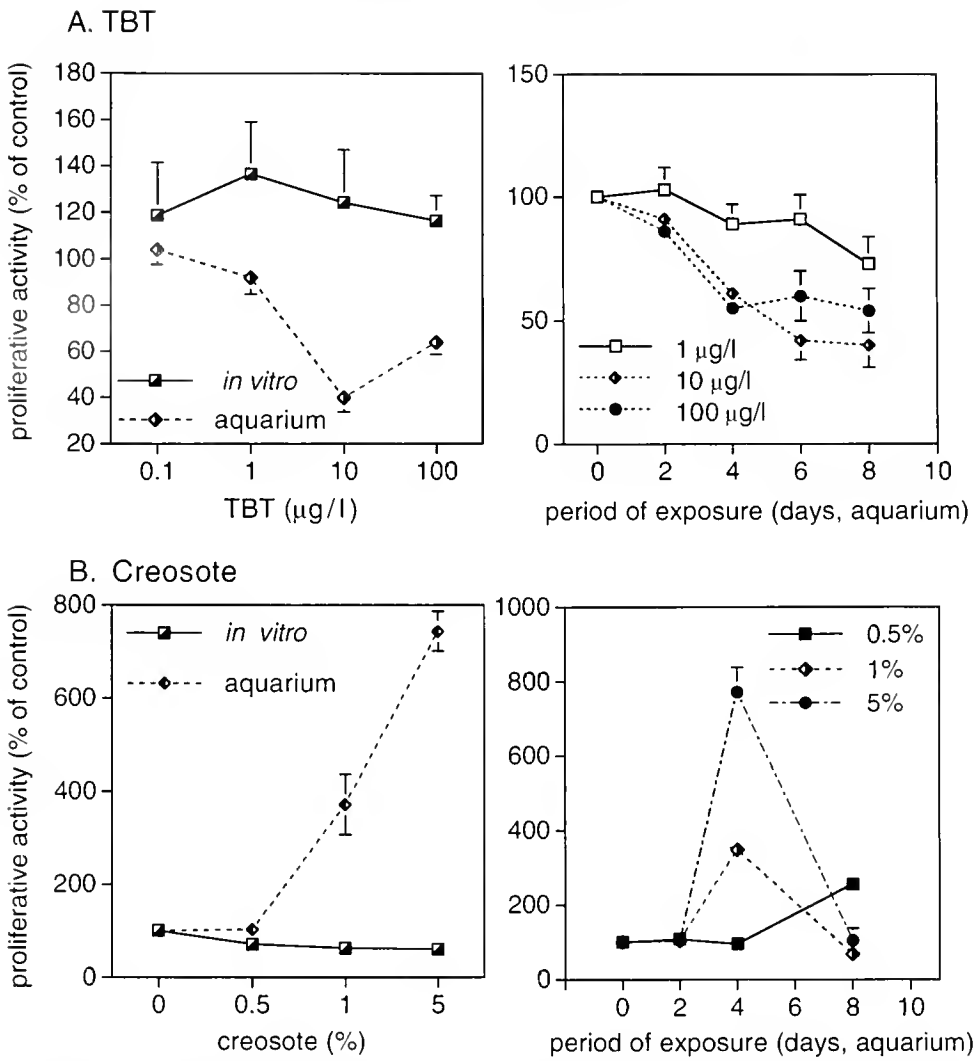

Figure 2. Proliferative activity (percentage of nontreated control values ± SEM, $n \geq 4$) in pharyngeal explants that were treated with various concentrations of (A) TBT or (B) creosote by either *in vitro* or aquarium exposure and harvested from tunicates after various periods of exposure. Uptake by controls: Day 2 = 322 ± 47 cpm; Day 4 = 874 ± 71 cpm; Day 8 = 944 ± 79 cpm.

Effects of toxicants on phagocytosis

Incubation of hemocytes with copper *in vitro* did not significantly ($P > 0.05$) alter phagocytic activity (Table III). However, copper substantially decreased phagocytosis (62% *vs.* control, 8 days, 0.5 µg/ml) during aquarium exposures. Exposure to 10 µg/l TBT *in vitro* significantly ($P < 0.05$) stimulated phagocytosis, whereas hemocytes taken from tunicates that had been treated with TBT in aquaria had lower phagocytic activities than those of nontreated controls (Table III). Creosote exposure significantly reduced phagocytosis after *in vitro* treatment, but greatly enhanced the phagocytic activity of hemocytes from tunicates exposed in aquaria (Table III).

The effects of *in vitro* TBT treatment on phagocytosis were dose-dependent (Fig. 3A). *In vitro* doses of TBT ranging from 1 to 10 µg/l enhanced phagocytosis by up to 220% relative to nontreated controls ($P < 0.05$), whereas a higher dose (100 µg/l) reduced phagocytic activity to 51% of its normal level ($P < 0.05$ *vs.* control). Other treatments consistently enhanced (creosote in aquaria) or inhibited (creosote *in vitro*, TBT in aquaria) phagocytosis over the range of doses tested (Fig. 3A).

Modulation of phagocytic activity by toxicants was also time-dependent (Fig. 3B). Alterations of phagocytosis resulting from treatment with both TBT and creosote in aquaria were most pronounced after short periods of exposure (creosote = 314% of control value, day 2; TBT

Table III

Phagocytic activities, relative to nontreated controls, of tunicate hemocytes that had been exposed to various toxicants for either 24 h in vitro *or 8 days in aquaria*

Treatment	% of nontreated control[γ] ± SEM ($n \geq 4$)	
	In vitro	Aquarium
TBT (10 μg/l)	220.1 ± 3.2	75.6 ± 3.1[α]
Cu (0.5 μg/ml)	89.2 ± 8.4[β]	37.4 ± 15.7
Creosote (1%)	56.8 ± 12.5	196.5 ± 21.1

[α] 6-day exposure.
[β] $P > 0.05$ *vs.* nontreated controls.
[γ] Mean phagocytic activity in nontreated controls = 0.43 ± 0.11 yeast ingested per hemocyte.

= 69.4% of control value, day 3) and returned to levels similar to control values after longer treatment times (creosote = 148% of control, 8 days; TBT = 105% of controls, 9 days).

Cytotoxic activities after toxicant treatment

Creosote was the only toxicant that significantly affected the cytotoxic activity of hemocytes toward either K562 or RRBC targets (Table IV). Exposure to creosote in aquaria inhibited cytotoxic activity toward K562 cells in a dose-dependent fashion (Fig. 4A). Treatment with 5% creosote for 8 days reduced anti-K562 cytotoxicity to levels that did not differ significantly from those of negative controls in which hemocytes and K562 cells were mixed at 4°C ($P > 0.05$; Fig. 4A). Significant ($P < 0.05$) inhibition of cytotoxic responses toward K562 cells was evident at all of the creosote doses tested (Fig. 4A). A different pattern emerged in assays that used RRBC as targets. Exposure to creosote doses greater than 0.5% for 8 days significantly enhanced the cytotoxic activity of hemocytes toward RRBC (Fig. 4A).

Figure 4B shows that the inhibitory effect of creosote on cytotoxicity toward K562 cells was reversible. The cytotoxic activity of hemocytes from tunicates that had been exposed to 5% creosote for 4 days and then transferred to toxicant-free seawater for a further 4 days (13.9% specific cytotoxicity) did not differ significantly from those of nontreated controls (15.3% specific cytotoxicity; $P > 0.05$). However, it was significantly greater than the cytotoxic activities evident among hemocytes taken from tunicates that had been exposed to 5% creosote continuously for 8 days (5.4% specific cytotoxicity; $P < 0.05$).

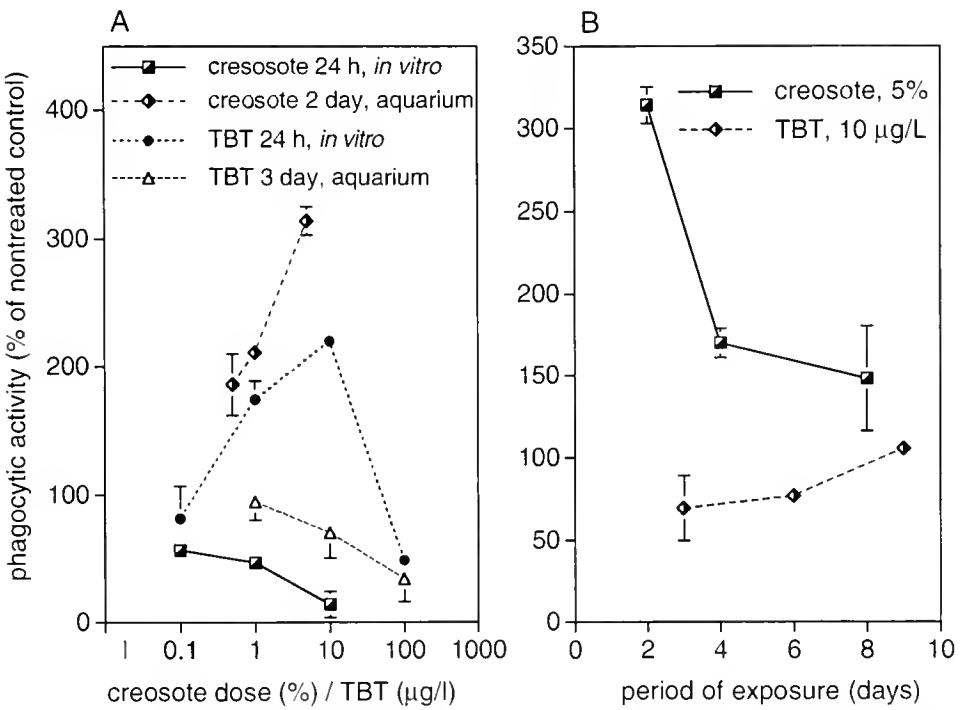

Figure 3. Phagocytic activities (percentage of nontreated control values ± SEM, $n \geq 4$) of tunicate hemocytes that were (A) exposed to various doses of creosote or TBT overnight *in vitro* or harvested from tunicates that had been treated with creosote or TBT for 2 or 3 days in aquaria, or (B) harvested from tunicates after various periods of exposure to 5% creosote or 10 μg/l TBT in aquaria.

Table IV

Effect of treatment with various toxicants either overnight (in vitro exposure) or for 8 days (aquarium exposures) on cytotoxic activity of tunicate hemocytes toward K-562 or rabbit red blood cells (RRBC)

	% of nontreated control[γ] ± SEM ($n \geq 4$)		
Treatment	*In vitro*/ K562	Aquarium/ RRBC	Aquarium/ K562
TBT (10 μg/l)	nt[α]	121.1 ± 14.3	119.0 ± 26.9[β]
Cu (0.5 μg/ml)	85.8 ± 5.2	96.8 ± 6.4	108.1 ± 21.3
Creosote (1%)	nt	138.9 ± 6.9[δ]	53.6 ± 15.4[δ]

[α] Not tested.
[β] 6-day exposure.
[δ] $P < 0.05$ *vs.* nontreated control.
[γ] Mean cytotoxic activities for nontreated controls = 43.6 ± 6.1 for K562 and 21.2 ± 3.1 for RRBC.

Effect of creosote on the frequency of hemocyte subpopulations

Creosote was the only toxicant that affected the frequencies of hemocyte subpopulations in tunicates exposed to toxicants in aquaria (Fig. 5). Three distinct subpopulations of hemocyte were identified by analysis of forward angle *vs.* 90° light-scatter plots. They were designated small (low forward scatter), large (high forward scatter, low 90° scatter) and large granular (high forward and high 90° scatter) hemocytes. Treatment with creosote significantly decreased the frequency of large granular hemocytes relative to the other hemocyte subpopulations. The frequency of large granular hemocytes was reduced by two-thirds relative to nontreated controls after 4 days of exposure ($P < 0.05$; Fig 5A). This effect was apparent within 2 days of exposure to high doses of creosote (5%) and was evident for all of the doses tested within 4 days (Fig 5A). There was a corresponding increase in the frequency of small hemocytes: after 4 days about two times more small hemocytes were present within treated tunicates than in nontreated controls (Fig 5B). The frequency of large hemocytes did not vary from control levels at any of the doses or times tested (Fig 5B).

Discussion

This study has demonstrated that sublethal contamination by common estuarine pollutants can significantly alter innate immunological reactions in tunicates. The three compounds tested here (TBT, copper, and creosote) are particularly relevant. All three are major components of antifouling films that are used to prevent the growth of sessile invertebrates. TBT can leach from marine paints and accumulate to hazardous levels in harbors and marinas (Bryan *et al.*, 1986; Huggett *et al.*, 1986). It is known to inhibit chemiluminescence responses, chemotactic activity, phagocytic oxidative bursts and phagocytosis by fish leukocytes (Rice and Weeks, 1991; Warinner *et al.*, 1988; Weeks *et al.*, 1986).

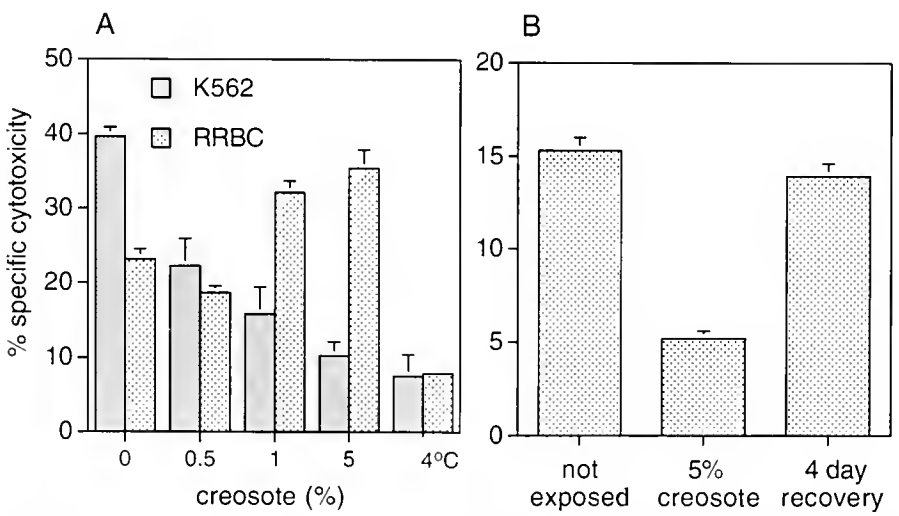

Figure 4. (A) Cytotoxic activities (percentage of nontreated control values ± SEM, $n = 4$) of hemocytes taken from tunicates that were exposed to various doses of creosote in aquaria for 8 days; 4°C represents hemocytes from nontreated controls that were mixed with targets at 4°C to suppress cytotoxic activity. (B) Cytotoxic activities (percent specific cytotoxicity toward K562 cells ± SEM, $n = 4$) of hemocytes harvested from tunicates that had either been held in aquaria without creosote (not exposed), exposed to 5% creosote in aquaria for 8 days (5% creosote), or exposed to 5% creosote in aquaria for 4 days and then transferred to fresh seawater without creosote for a further 4 days (4-day recovery).

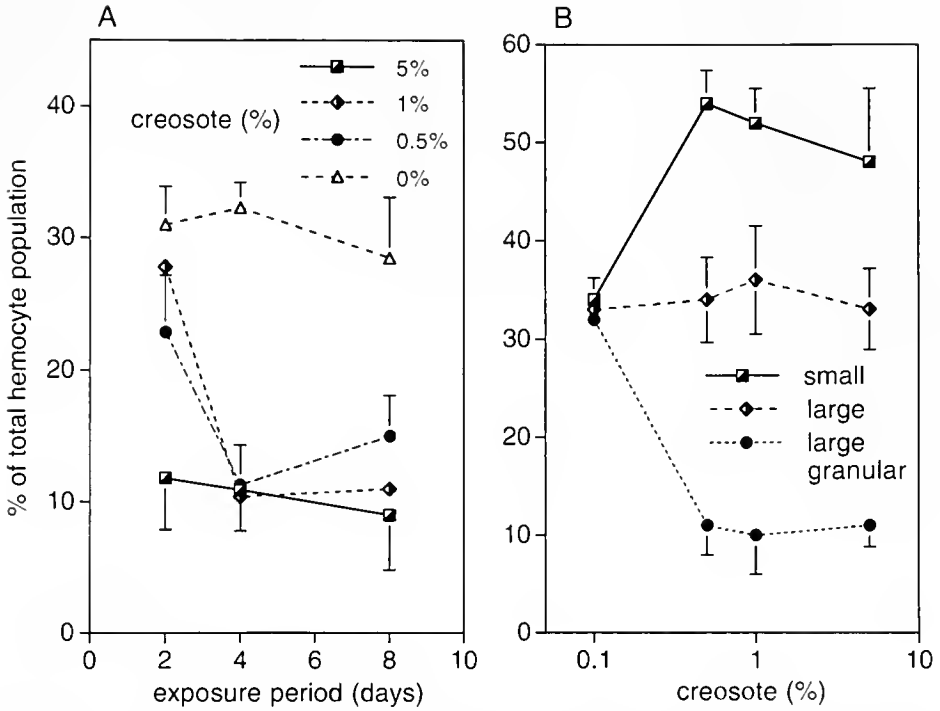

Figure 5. Frequencies (percentages of the total hemocyte population ± SEM, $n = 4$) of (A) large granular hemocytes in hemolymph harvested from tunicates after various periods of exposure to a range of creosote concentrations in aquaria, or (B) small, large, and large granular hemocytes harvested from tunicates that been exposed to various doses of creosote for 4 days in aquaria.

Although the use of TBT on pleasure craft is now prohibited widely, it is still applied to larger vessels and remains a common harbor contaminant (NSW Environment Protection Authority, pers. comm.; Stebbing, 1985). For use on small craft, TBT has been superseded by copper-based antifouling products. Like TBT, copper is known to have substantial immunological effects on aquatic organisms at subacute doses (Roales and Perlmutter, 1977). Creosote is a hydrocarbon-based protective coating that is frequently used on pylons, wharves, and netting. It is composed of about 85% PAH, 10% phenolic compounds, and 5% heterocyclic compounds (Faisal *et al.*, 1991). PAHs in particular have been associated with a variety of physiological effects including carcinogenesis and the alteration of immune reactivity in humans and other animals (Faisal *et al.*, 1991; National Research Council, USA, 1972). In fish, PAHs are responsible for the development of eye lens cataracts, gill necrosis, degeneration of renal epithelia, and neoplasia. They can also inhibit macrophage function, cellular cytotoxicity, and cellular proliferation (Faisal *et al.*, 1991). The range of doses that were tested in this study include levels that can frequently be found in the environment. TBT concentrations >2 μg/l have been detected in marine areas (Waldcock and Miller, 1983). PAH levels greater than 10 times the maximum dose used here are reportedly common for harbor waters, and levels of copper up to 2.5 μg/ml have been detected in heavily utilized environments (Hyland and Scheider, 1976; Pluarg International Joint Commission, 1978; Waldhauer *et al.*, 1978).

Only high doses of copper (≥5 μg/ml) were acutely lethal to tunicates. However, all of the toxicants tested here exerted powerful effects on at least some immunological reactions (summarized in Table V). The ability of toxicants, particularly creosote, to simultaneously affect a variety of apparently unrelated parameters, such as phagocytosis, proliferation, and cellular cytotoxicity, does not simply reflect general morbidity or metabolic downturn resulting from toxicant poisoning. The observation that toxicants enhanced some hemocyte-mediated responses but inhibited or had no effect on others confirms that tunicate cells were not generally inactivated by toxicant treatment. There is also no evidence that any of the toxicants affected the viability of cells from tunicates that were exposed in aquaria (except after death at lethal doses of copper), even though both creosote and copper decreased hemocyte viability *in vitro*. This discrepancy has three plausible explanations. First, the observed differences in hemocyte viabilities may

have been due to the rapid clearance of dead hemocytes *in vivo*. Those dead cells may not have appeared in the circulating hemolymph, and so may not have been detected in viability assays. Second, tunicates could possess mechanisms to detoxify, sequester, or prevent the penetration of copper and creosote *in vivo*. This possibility is not, however, supported by the observation that some immunological reactions were similarly affected by identical doses of toxicants applied *in vitro* and in aquaria (*e.g.*, copper's inhibitory effect on cell proliferation). Third, differences between *in vitro* and aquarium trials might have been due to the existence of compensatory or interactive mechanisms that cannot operate in isolated *in vitro* systems.

The latter explanation is supported by differences that were evident between the effects of *in vitro* and aquarium exposures on immunological parameters such as phagocytosis, cell proliferation, and cytotoxicity. For instance, *in vitro* creosote treatment inhibited phagocytic activity and cell proliferation, whereas tunicates treated with creosote in aquaria had an enhanced capacity for phagocytosis and a transient increase in proliferative activity. Such contrasting results indicate that some effects *in vivo* may result from interactive mechanisms rather than from direct toxicity toward the response being examined. Creosote poisoning, for instance, may have stimulated regulatory activity that specifically enhanced phagocytosis and proliferation. Mechanisms that are capable of such cellular regulation are well characterized in tunicates. Regulatory molecules in the hemolymph can enhance phagocytosis and cell proliferation in a manner analogous to the activities of vertebrate cytokines (Beck *et al.*, 1993; Raftos, 1994; Raftos *et al.*, 1991).

The data also suggest that tunicates have mechanisms that can confer some degree of adaptive protection, and allow recuperation, from the effects of toxicants. The existence of mechanisms for adaptive protection is indicated by the kinetics of toxicant poisoning. Alterations in the levels of phagocytosis among tunicates treated with creosote or TBT in aquaria were short lived. Phagocytic activity returned to more-or-less normal levels after 8 days of continuous exposure. This amelioration can be explained in two ways. First, creosote and TBT may have become detoxified over the 8-day exposure period. Second, adaptive mechanisms that reduced the effect of toxicants on phagocytosis may have been activated. The latter possibility is supported by evidence indicating that both creosote and TBT retain their toxicity toward other immunological reactions for at least 8 days. The existence of processes that allow recuperation from the effects of toxicants is indicated by the rapid recovery of cytotoxic activity when tunicates are transferred from contaminated to fresh seawater. There are many possible mechanisms by which toxicants could gain their effects, or by which tunicates might adaptively ameliorate those effects. For instance, the observed recuperation of some reactions from poisoning may reflect the existence of inducible detoxication mechanisms that directly affect toxicant bioavailability. Inducible low molecular weight metal-binding proteins (metallothioneins) that can bind and detoxify a variety of metals such as copper and tin have been identified in many species (George, 1990).

An alternative explanation for the varied effects of toxicants is that alterations in the frequencies of specific effector cells are responsible both for altering immune functions and for the later recovery of those immune reactions from poisoning. In fish, it has been reported that the frequencies of specialized, ion-transporting chloride cells vary significantly during copper poisoning as those cells migrate to and from fixed tissues (Pelgrom *et al.*, 1995). Similarly, the frequency of large granular hemocytes in *S. plicata* decreased rapidly upon exposure to creosote. The large granular hemocyte population includes vesiculated cell types that have been implicated in wound repair and that become localized in fixed tissues during inflammation-like responses (Goodbody, 1974; Wright, 1981). These cells may have been sequestered in fixed tissues damaged during creosote treatment, and so may have altered the relative mix of hemocyte types in the hemolymph. The loss of large granular hemocytes from the circulation may also have activated compensatory hematopoietic cell proliferation. Such hematopoietic proliferation was detected directly by increased ^{3}H-thymidine uptake and is also indicated by the specific increase observed in the frequency of small hemocytes, a population that includes immature hemoblasts derived from hematopoiesis (Ermak, 1982; Rinkevich and Rab-

Table V

Summary of the effects of different toxicants on a variety of responses that were tested either in vitro (vit) *or by aquarium exposure* (aqu)

	Toxicant/treatment					
	TBT		Creosote		Copper	
Responses tested	vit	aqu	vit	aqu	vit	aqu
Cell viability	0	0	↓	0	↓	0
Phagocytosis	↔	↓	↓	↑	0	↓
Proliferation	0	↓	↓	↔	↓	↓
Cytotoxicity (K562)	—	0	—	↓	0	0
Cytotoxicity (RRBC)	—	0	—	↑	—	0

↑ = enhanced by toxicant treatment; ↓ = inhibited by toxicant treatment; ↔ = enhanced or suppressed depending upon dose or time of exposure; 0 = no significant alteration relative to nontreated controls; — = not tested.

inowitz, 1993; Wright, 1981). The regulatory activity that may have activated cell proliferation might also have affected phagocytic activity. Tunicate cytokine-like molecules have pleiotropic effects that include the simultaneous activation of phagocytosis and proliferation (Beck *et al.*, 1993; Raftos, 1994; Raftos *et al.*, 1991). This role of altered hemocyte frequencies on immune functions remains speculative, but is currently being tested.

In conclusion, it is clear that environmental contaminants have profound effects on immunological reactions in tunicates. Those effects are unlikely to be the result of general morbidity, and they are not reflected by acute lethality. However, because of the implicit relationship between innate immune reactions and antipathogenic defenses, it is likely that the effects demonstrated here alter the capacity of tunicates to defend themselves against infection. The relevance of these effects to the viability of tunicate populations remains unclear. Little is known about the level of surveillance that is required by tunicates for survival. We are investigating that relationship between innate or natural immunological competance and long-term population health by testing the effects of environmental toxicants on the ability of tunicates to deal with artificial and natural infections.

Acknowledgments

This study was funded in part by a grant from the Australian Research Council and an Internal Research Grant from the University of Technology, Sydney. We thank Monika Burandt for help with field work and for other technical assistance.

Literature Cited

Anderson, D. P., G. W. Bryan, P. E. Gibbs, L. C. Hummerstone, and G. R. Burt. 1990. Immunological indicators: effects of environmental stress on immune protection and disease outbreaks. *Am. Fish. Soc. Symp.* **8:** 38–50.

Beck, G., R. F. O'Brien, G. S. Habicht, D. L. Stillman, E. L. Cooper, and D. A. Raftos. 1993. Invertebrate cytokines III: Interleukin-1-like molecules stimulate phagocytosis by tunicate and echinoderm cells. *Cell. Immunol.* **146:** 284–299.

Berrill, N. J. 1950. *The Tunicata* The Ray Society, London.

Bryan, G. W., P. E. Gibbs, L. C. Hummerstone, and G. R. Burt. 1986. The decline of the gastropod, *Nucella lapidus*, around South-Western England: evidence for the effect of tributyltin from antifouling paints. *J. Mar. Biol. Assoc. U.K.* **66:** 611–640.

Cooper, E. L., and P. Roch. 1992. The capacities of earthworms to heal wounds and to destroy allografts are modified by polychlorinated biphenyls (PCBs). *J. Invertebr. Pathol.* **60:** 55–63.

Ermak, T. H. 1982. The renewing cell populations of ascidians. *Am. Zool.* **22:** 795–805.

Faisal, M., M. S. M. Marzouk, C. L. Smith, and R. J. Huggett. 1991. Mitogen induced proliferative responses from spot exposed to polycyclic aromatic hydrocarbon contaminated environments. *Immunopharmacol. Immunotoxicol.* **13:** 311–327.

Fitzpatrick, L. C., R. Sassani, B. J. Venables, and A. J. Goven. 1992. Comparative toxicity of polychlorinated biphenyls to the earthworms *Eisenia foetida* and *Lumbricus terrestris*. *Environ. Pollut.* **77:** 65–79.

George, S. G. 1990. Biochemical and cytological assessments of metal toxicity in marine animals. Pp. 123–142 in *Heavy Metals in the Environment*, R. W. Furness and P. S. Rainbow, eds. CRC Press, Boca Raton, FL.

Giam, G. S., and L. E. Ray. 1987. *Pollution Studies in Marine Animals.* CRC Press, Boca Raton, FL.

Goodbody, I. 1974. The physiology of ascidians. Pp. 1–149 in *Advances in Marine Biology*, F. S. Russel and M. Yonge, eds. Academic Press, London.

Hyland, J. L., and E. D. Schneider. 1976. Petroleum hydrocarbons and their effects on marine organisms, populations, communities and ecosystems. Pp. 61–76 in *Sources, Effects, and Sinks of Hydrocarbons in the Aquatic Environment.* Proc. Symp. AIBS, Washington, DC.

Huggett, R. J., M. E. Bender, and D. J. Westbrook. 1986. Organotin concentrations in the Southern Chesapeake Bay. Pp. 12–62 in *Oceans 86 Proceedings, Organotin Symposium.* IEEE Publishing, New York.

Kelly, K., E. L. Cooper, and D. A. Raftos. 1993. A humoral opsonin from the solitary urochordate, *Styela clava*. *Dev. Comp. Immunol.* **17:** 29–39.

Landis, W. G., and M.-H. Yu. 1995. *Introduction to Environmental Toxicology.* Lewis, Boca Raton, FL.

McCarthy, J. F., and L. R. Shugart. 1990. *Biomarkers of Environmental Contamination.* CRC Press, Boca Raton, FL.

National Research Council, U.S.A. 1972. *Particulate Polycyclic Organic Matter.* U.S. National Academy of Sciences, Washington, DC.

Parrinello, N., V. Arizza, M. Cammarata, and D. M. Parrinello. 1993. Cytotoxic activity of *Ciona intestinalis* hemocytes: properties of the *in vitro* reaction against erythrocyte targets. *Dev. Comp. Immunol.* **17:** 19–27.

Peakall, D. 1992. *Animal Biomarkers as Pollution Indicators.* Chapman and Hall, New York.

Peddie, C. M., and V. J. Smith. 1993. *In vitro* spontaneous cytotoxic activity against mammalian target cells by hemocytes of the solitary ascidian, *Ciona intestinalis*. *J. Exp. Zool.* **269:** 616–623.

Peddie, C. M., and V. J. Smith. 1994. Blood cell mediated cytotoxic activity in the solitary ascidian, *C. intestinalis*. *Ann. N.Y. Acad. Sci.* **712:** 332–340.

Pelgrom, S. M. G. J., R. A. C. Lock, P. H. M. Balm, and S. E. Wendelaar Bonga. 1995. Integrated physiological response of tilapia, *Oreochromis mossambicus*, to sublethal copper exposure. *Aquat. Toxicol.* **32:** 303–320.

Pluarg International Joint Commission. 1978. Environmental management strategy for the Great Lakes. International Reference Group on Great Lakes Pollution from Land Use Activities. Windsor, Ontario, Canada.

Raftos, D. A. 1994. Allorecognition and humoral immunity in tunicates. *Ann. N.Y. Acad. Sci.* **712:** 227–243.

Raftos, D. A., and E. L. Cooper. 1990. *In vitro* culture of tissues from the solitary tunicate, *Styela clava*. *In Vitro Cell. Dev. Biol.* **26:** 962–970.

Raftos, D. A., and E. L. Cooper. 1991. Proliferation of lymphocyte-like cells from the solitary tunicate, *Styela clava*, in response to allogeneic stimuli. *J. Exp. Zool.* **260:** 391–400.

Raftos, D. A., E. L. Cooper, G. S. Habicht, and G. Beck. 1991. Tunicate cytokines: tunicate cell proliferation stimulated by an endogenous hemolymph factor. *Proc. Natl. Acad. Sci. U.S.A.* **88:** 9518–9522.

Rice, C. D., and B. A. Weeks. 1991. Tributyltin stimulates reactive oxygen formation in toadfish macrophages. *Dev. Comp. Immunol.* **15:** 431–436.

Rinkevich, B., and C. Rabinowitz. 1993. *In vitro* culture of blood cells from the colonial protochordate *Botryllus schlossen*. *In Vitro Cell. Dev. Biol.* **29A:** 79–85.

Roales, R. R., and A. Perlmutter. 1977. The effects of sub-lethal doses of methyl mercury and copper, applied singly and jointly on the immune response of blue gourami to viral and bacterial antigens. *Arch. Environ. Contam. Toxicol.* **5:** 325–331.

Rodrigues-Grau, J., B. J. Venables, L. C. Fitzpatrick, and A. J. Goven. 1989. Suppression of secretory rosette formation by PCBs in *Lumbricus terrestris*: an earthworm assay for humoral immunotoxicity of xenobiotics. *Environ. Toxicol. Chem.* **8:** 1201–1207.

Sarot, D. A., and A. Perlmutter. 1976. The toxicity of zinc to the immune response of the zebra fish (*Brachydanio rario*) injected with viral and bacterial antigens. *Trans. Am. Fish. Soc.* **105:** 456–459.

Stebbing, A. R. D. 1985. Organotins and water quality—some lessons to be learned. *Mar. Pollut. Bull.* **10:** 383–390.

Waldcock, M. J., and D. Miller. 1983. The determination of total and tributyltin in seawater and oysters in areas of high pleasure craft activity. *ICES Papers CM 1983/E:12* (mimeograph). International Council for the Exploration of the Sea, Copenhagen.

Waldhauer, R. A., A. Matte, and R. E. Tucker. 1978. Lead and copper in the waters of Raritan and Lower New York Bays. *Mar. Pollut. Bull.* **9:** 38–42.

Warinner, J. E., E. S. Mathews, and B. A. Weeks. 1988. Preliminary investigations of the chemiluminescent response in normal and pollutant-exposed fish. *Mar. Environ. Res.* **24:** 281–284.

Weeks, B. A., P. L. Warinner, J. Mason, and D. S. McGinnis. 1986. Influence of toxic chemicals on the chemotactic responses of fish macrophages. *J. Fish Biol.* **28:** 653–658.

Wright, R. K. 1981. Urochordates. Pp. 565–627 in *Invertebrate Blood Cells*. N. A. Ratcliffe and A. F. Rowley, eds. Academic Press, London.

Reference: *Biol. Bull.* **192:** 73–86. (February, 1997)

Prey Capture by the Sea Anemone *Metridium senile* (L.): Effects of Body Size, Flow Regime, and Upstream Neighbors

KENNETH R. N. ANTHONY*

The Royal Swedish Academy of Sciences, Kristineberg Marine Research Station, Kristineberg 2130, S-450 34 Fiskebäckskil, Sweden

Abstract. The sea anemone *Metridium senile* is a quantitatively important passive suspension feeder in hard-bottom communities on the west coast of Sweden and occurs in aggregations with different size distributions. This study tests the hypothesis that different polyp sizes have different optimal flow regimes maximizing prey capture. Results showed that prey capture by *M. senile* is a function of both flow regime and polyp size, and different optimal flow regimes exist for different size classes. Large anemones had a maximum feeding efficiency at the slowest flow, medium-sized anemones at moderate flow, and small anemones at moderate- to high-flow regimes. Small anemones showed consistently higher feeding rates (per unit of biomass and area of tentacle crown) at all velocities above 10 cm s^{-1} and exhibited less flow-induced deformation of the tentacle crown, suggesting that small anemones are better at feeding in moderate- to high-flow habitats. Different vertical projections of large and small anemones in the boundary layer could only partly account for differences in feeding success among size classes. Feeding rate was also a function of upstream conspecifics, declining asymptotically to 30% of the maximum rate. The negative effects of neighbors on feeding in aggregations with clonal rather than polyp growth appear to be compensated for by the generally higher feeding efficiency of small polyps.

Introduction

Flow habitat and body size are both important factors in the feeding biology of benthic, passive suspension feeders. Due to the nature of near-bottom hydrodynamics, however, flow exposure and body size are inseparable factors (Koehl, 1977a; Vogel, 1981). As suspension feeders grow taller they become exposed to faster currents within and beyond the substratum-associated boundary layer, and consequently to both greater drag and higher flux of potential prey (Wainwright and Koehl, 1976; Vogel, 1981). The height of a passive suspension feeder in a given flow habitat is therefore likely to involve a trade-off between maximizing food availability and minimizing flow forces and physical stress. In soft-bodied passive suspension feeders such as sea anemones, limitations as to how tall an individual can grow in a high-flow environment may, in part, be governed by the extent to which flow forces cause deformation of the feeding apparatus (Koehl, 1976, 1977a), reducing prey capture and thus energy for growth and reproduction (Sebens, 1979, 1981, 1982; Lesser *et al.*, 1994). Vertically oriented passive suspension feeders of different sizes are therefore likely to have different ranges of optimal flow velocities at which the physical stress is minimized and potential for prey capture is maximized. Many sessile cnidarians are, however, capable of polyp degrowth and indeterminate growth of the genet, in part through variable extents of asexual proliferation such as pedal laceration (Bucklin, 1987; Anthony and Svane, 1995), polyp fission (Francis, 1979; Sebens, 1980), and colony fission (McFadden, 1986). These capabilities result in size plasticity of the polyp (or colony) as well as of the clone. Small clones of large polyps (or colonies) in low-flow habitats and large clones of small polyps (or colonies) in high-flow habitats constitute alternative solutions for maximizing prey capture and the positive energy balance of the genet. In the latter case, however, the extent to which the relationship between polyp size, flow, and prey capture is modified by the presence of neighbor-

Received 18 October 1995; accepted 25 October 1996.

* Current address: James Cook University of North Queensland, Department of Marine Biology, Townsville Qld. 4811, Australia.

ing conspecifics (or clone members produced by asexual reproduction) has been demonstrated in only a few passive (octocorals: McFadden, 1986) and active (phoronids: Johnson, 1990; bryozoans: Okamura, 1992) suspension feeders.

In this paper, the sea anemone *Metridium senile* is used for testing the effects of flow, polyp size, and upstream neighbors on the feeding success of soft-bodied, passive suspension feeders. Five features render *M. senile* a good model for such studies: (1) The projected area of the tentacle crown increases more-or-less isometrically with body size (Sebens, 1981); (2) new tentacles of a determined size are added to the tentacle crown as the anemone grows (Sebens, 1979), so that the spacing and size of filtering elements are the same for large and small anemones; (3) the size of prey (zooplankton) taken does not increase significantly with anemone size (Purcell, 1977; Sebens, 1981; Sebens and Koehl, 1984); (4) it is capable of polyp degrowth (in part through asexual reproduction by pedal laceration) and thus has an intrinsic potential for adjusting its body size to the flow environment; and finally (5) it often forms dense, clonal aggregations (Anthony and Svane, 1994) in which prey capture per polyp is likely to be influenced by the presence of adjacent clonemates.

Metridium senile is a ubiquitous member of the hard-bottom community of most northern waters (Hoffmann, 1976; Fautin *et al.*, 1989) and occurs in different size distributions in different flow environments (Hoffmann, 1976, 1986; Shick *et al.*, 1979; Shick and Hoffmann, 1980; Anthony and Svane, 1994). For example, in high-flow channels on the west coast of Sweden where the current velocity frequently exceeds 100 cm s^{-1}, the walls and bottoms are carpeted by dense populations of small (2–3-cm-high) *M. senile*. Conversely, in low-flow habitats where the current rarely exceeds 5 cm s^{-1}, large (20–30-cm-high) *M. senile* predominate (Anthony and Svane, 1994, 1995). In moderate-flow habitats, populations of *M. senile* are generally composed of intermediate-sized anemones (Shick, 1991; and pers. obs.). Previous studies have suggested that differences in size distributions of *M. senile* can be attributed to the physical effects of flow on the anemone body plan (Koehl, 1977a; Shick and Hoffmann, 1980); genetic differences between local populations or clones (Shick *et al.*, 1979; Shick and Dowse, 1985; Hoffmann, 1986; Anthony and Svane, 1994); and effects of substratum instability, which influence the rate of laceration and thereby inversely affect polyp and clone size (Anthony and Svane, 1995). Trade-offs between polyp size and prey capture in different flow regimes are likely to structure populations of this ecologically and morphologically plastic species (Shick, 1991). Nevertheless, no studies have experimentally tested the hypothesis that different polyp sizes of *M. senile* have different optimal flow regimes that reflect the size distributions in natural populations.

The objectives of this study are to (1) quantify prey capture in *M. senile* at a range of polyp sizes and flow velocities, (2) test whether combinations of polyp size and flow regime that maximize prey capture reflect size-frequency distributions found in different flow habitats *in situ*, and (3) test whether prey capture in *M. senile* is, in part, a function of the number of upstream conspecifics.

Materials and Methods

All experiments were conducted in a laboratory flume (300-cm long, 47-cm wide, 18–20-cm water depth), designed as described by Vogel (1981). A constant flow was ensured by controlling revolutions of the propeller by a Panasonic 501 inverter. Flow straighteners were mounted at the entrance of the flume channel to reduce turbulence to a level resembling near-bed field conditions. Prey used in all experiments were newly hatched nauplii of *Artemia salina*, which measure about 600 μm in length and are within the mid-range of prey sizes reported to be taken by *M. senile* in the field (Sebens and Koehl, 1984). *Artemia* nauplii do not show the escape responses characteristic of some natural prey (Trager *et al.*, 1994), so their use may produce overestimates of prey-capture rates *in situ*. That potential drawback was outweighed by the advantages that the non-evasive *Artemia* nauplii are less likely to confound flow effects on capture rates and can be reared in replicable batches.

Flow measurements

Feeding experiments were carried out at six preset flow regimes: 4, 10, 17, 20, 28, and 44 cm s^{-1}, measured at 10 cm above the flume floor by visually tracking and timing particles over a 25-cm trajectory within the working section of the flume. To determine the local flow velocity experienced by each anemone size class in a given flow regime, the vertical flow profile between 0.2 and 15 cm above the flume floor (1-cm intervals) was determined from a matrix of 16 × 6 point samples taken within a plane normal to flow. These local flow velocities were measured with a thermistor probe (LaBarbera and Vogel, 1976) calibrated according to the method described by Vogel (1981, p. 316). The development of a turbulent boundary layer was evident at all flow regimes, and the local flow velocities measured at 0.2–1 cm above the flume floor were generally 50% of those measured at a height of 10 cm (U_{10}). The flow profiles obtained in the flume at the six experimental flow regimes are depicted in Figure 1.

Distribution of nauplii in the flume

A comparison of the prey-capture success of different size classes of passive suspension feeders requires the as-

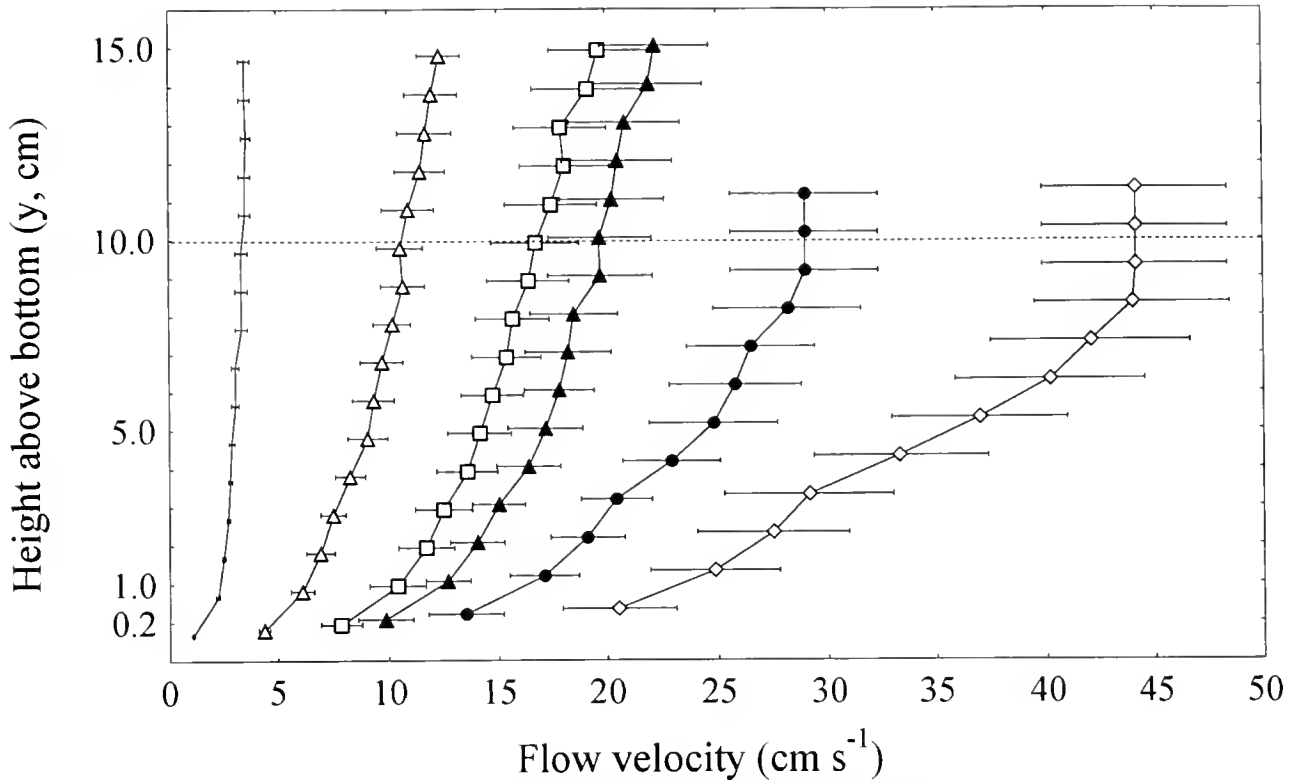

Figure 1. Flow profile as a function of flow regime in the working section of the flume. Flow regime is referred to as the velocity measured at 10 cm above the flume floor (U_{10}). Error bars represent ±1 SE of 6 isobath measurements.

sumption of a uniform and constant distribution of prey items in the water column. Therefore, deviations from an even, vertical distribution of *Artemia* due to nauplii swimming or hydrodynamic sorting were determined by simultaneous sampling from 10 different heights above the bottom in the working section of the flume. Samples were collected with a comb of 4-mm acrylic pipes spaced 15 mm apart and pointing into the current, each pipe connected to a silicone tube (see Muschenheim, 1987). One-liter samples were taken at each height, and sampling was replicated three times (1-h intervals) for every flow regime. The numbers of nauplii were standardized to a percentage distribution and tested using a replicated *G*-test for goodness-of-fit (Sokal and Rohlf, 1981). Significantly higher concentrations of nauplii were found close to the bottom of the flume channel at U_{10} = 4 cm s^{-1} (G_p = 55.4, $P < 0.0001$) and U_{10} = 10 cm s^{-1} (G_p = 20.1, $P < 0.01$), but the vertical distribution was uniform at U_{10} = 17, 20, 28, and 44 cm s^{-1} ($P > 0.05$).

Vertical feeding zone and tentacle-crown deformation

The height range of the tentacle crown above the flume floor (measured at the uppermost (y_U) and lowermost (y_L) tentacle tips) was determined for each group of anemones during experiments. These values were used to compare vertical feeding zones and local flow velocities experienced by different size classes and to calculate feeding efficiencies. Furthermore, the ratio of tentacle-crown surface area (S) to ash-free dry weight of individual polyps (AFDW) was used to indicate and compare the degree of tentacle-crown deformation caused by flow forces. Ash-free dry weight was used as denominator rather than a linear dimension because it provides the least variable measure of size. During each feeding experiment, tentacle-crown diameter (TCD, mean of two diameters taken at right angles to each other and described by the outermost tentacle tips) for each anemone was measured with callipers and used in calculating tentacle-crown area ($S = \pi(\mathrm{TCD}/2)^2$).

Feeding experiments: sampling and experimental design

Three size classes of anemones within the full size range of *M. senile* were sampled in the Gullmarsfjord on the west coast of Sweden, from three sites that experience different prevailing current regimes. Large anemones

(6.0–6.5-cm pedal disc diameter, pdd) were collected in the central Gullmarsfjord where the current is generally low (<5 cm s^{-1}), medium-sized anemones (2.5–3.0-cm pdd) were collected in a sound experiencing an intermediate current regime (10–15 cm s^{-1}), and small anemones (1–2 cm pdd) were sampled in a narrow channel where the current frequently exceeds 100 cm s^{-1} (see also Anthony and Svane, 1994). In the laboratory, the anemones were allowed to attach to panels (terracotta tiles measuring 10 by 20 cm, 3 mm thick) submerged in seawater tables. Excess anemones were removed from the panels so that a single row of 2–4 contiguous anemones was established on each panel.

Prior to each experiment the flume was filled with filtered (<20 μm) seawater freshly collected at 30-m depth in the fjord (31–33‰ salinity and 8–11°C). The volume of the system when full (20-cm depth) was 400 ± 2 l. Two panels with anemones attached were placed aligned on the bottom of the flume in the working section, so that a single row of 3–8 anemones was oriented perpendicular to flow. The anemones were allowed 12–24 h to acclimate to the selected flow regime and to fully expand before the feeding experiment was run. Immediately before an experiment, a standardized initial concentration (C_0) of 150 ± 20 *Artemia* nauplii l^{-1} was obtained by carrying out dilution series in 2000-ml beakers and calculating batch concentrations and C_0. This concentration was assumed to be below that causing saturation of the anemones, since only a small percentage (<5%) of the tentacles were occupied in prey capture at any given time. The overall prey capture obtained in the experiments was therefore assumed to be insignificantly affected by the C_0 chosen.

So that concentration of prey could be plotted as a function of time, five 140-ml water samples were taken simultaneously from the upstream section of the tank at $t = 0$ and after every 10 min during the following 70–90 min. Because the total sampling volume was less than 3% of the system volume, sampling volume was not replaced or corrected for in the analysis. Samples were taken using a rack of fixed pipettes (2 mm thick and 20 cm long) arranged along a horizontal transect normal to the direction of flow and connected by silicone tubes to a rack of syringes on the outside of the tank. Sampling was done manually and isokinetically during 30 ± 3 s to minimize variation due to prey patchiness. The samples were immediately filtered through a plankton mesh (60-μm) to give 50-ml concentrated suspensions, and the nauplii in each sample were counted directly using a dissecting microscope. The proportion of nauplii damaged by handling and by the flume propeller was less than 5%. To determine feeding relative to anemone biomass, the anemones were dislodged from the panels 24 h after each experiment, any food boluses were removed with a syringe, and anemones were frozen and freeze-dried for 48 h. After weighing, the dried anemones were combusted for 12 h at 500°C and the ash-free dry weight (AFDW) was obtained by subtracting ash weight from dry weight.

Analysis of feeding experiments

The natural logarithm of prey concentration was plotted with time, and the expected relationship

$$\mathrm{Ln}(C_t) = -Ft + \mathrm{Ln}C_0 \qquad (1)$$

was fitted to the data using linear regression analysis and tested using Pearson's product-moment correlation (Sokal and Rohlf, 1981). The relationship is a linearization of the function

$$C_t = C_0 e^{-Ft} \qquad (2)$$

describing the exponential decrease in prey concentration with time in a closed system (Leversee, 1976) where C_t and C_0 are the concentrations of prey (nauplii l^{-1}) at the times t and t_0, respectively, and F is the clearance rate (min^{-1}) of the suspension feeder. F depends on the features of the feeding structures such as the size and density of tentacles per square centimeter of tentacle-crown area (Sebens, 1981), orientation relative to flow (Leversee, 1976; Johnson and Sebens, 1993), height above the substratum (Muschenheim, 1987), and prey availability. The total clearance rate of the group of anemones (F_{tot}) was the slope of the regression line ±95% CL, and the maximum feeding rate was determined as $F_{tot}C_0V$ (nauplii min^{-1}), where V is the water volume (l) of the system. To account for settlement and accumulation of prey that could not be explained by anemone feeding, control experiments were conducted using anemone mimics. To be able to compare the retention of prey among anemone size classes in a given flow regime, feeding rates were expressed based on ash-free dry weight (AFDW) and square centimeter of tentacle-crown area (S) at t_0. The empirical, maximum feeding rate per square centimeter of tentacle-crown area was thus determined as

$$\text{Feeding rate}_{\text{Max,cm}^{-2}} = \frac{C_0V(F_{\text{tot}} - F_{\text{control}})}{S} \qquad (3)$$

and the maximum feeding rate per gram of ash-free dry weight was calculated as

$$\text{Feeding rate}_{\text{Max,AFDW}^{-1}} = \frac{C_0V(F_{\text{tot}} - F_{\text{control}})}{\text{AFDW}} \qquad (4)$$

Only the control experiment run at the lowest flow velocity (4 cm s^{-1}) produced a significant depletion rate ($F_{control}C_0V$ ± CL (nauplii min^{-1}) = 0.36 ± 0.18, P = 0.02), and this was accordingly subtracted from feeding

experiments run at this flow speed. Feeding rates of different size classes at a given flow regime were compared using an unplanned comparison (the Tukey-Kramer method; Sokal and Rohlf, 1981).

Feeding efficiencies (E) are useful in comparing feeding performance among size classes as well as in comparing feeding performance of a size class among flow regimes, and were calculated as the number of prey items captured relative to the number that would pass through the space occupied by the feeding appendages if the latter were not there (see Patterson, 1991). The maximum number of prey items passing the projected feeding surface perpendicular to flow ($S_{f,\mathrm{pr}}$, cm^2) per unit time is a product of the concentration of prey at t_0(C_0, nauplii l^{-1}) and the flow velocity (U_y, cm s^{-1}) at the level of the feeding structures (y), hence

$$N_{\mathrm{passing}} = S_{f,\mathrm{pr}} C_0 U_y \frac{1}{1000\ \mathrm{cm}^3} \times \frac{60\ \mathrm{s}}{\mathrm{min}} \qquad (5)$$

$S_{f,\mathrm{pr}}$ was calculated as an ellipsoid described by the height and width ranges of the tentacle crown (perpendicular to the flow direction), from which the projected, transverse sectional area of the uppermost part of the column (the parapet; see Manuel, 1988) was subtracted. The feeding efficiency (E) was then expressed as

$$E = \frac{N_{\mathrm{captured}}}{N_{\mathrm{passing}}} = \frac{FV}{S_{f,\mathrm{pr}} U_y} 16.7 \frac{\mathrm{cm}^3\ \mathrm{l}^{-1}}{\mathrm{s\ min}^{-1}} \qquad (6)$$

where $N_{\mathrm{captured}} = C_0 VF$ (nauplii min^{-1}).

Effect of upstream neighbors

To determine the effect of upstream neighbors on the feeding rate per square centimeter of tentacle crown area, a series of experiments analogous to the above were conducted using six patch sizes of anemones. Patch size was expressed as the number of parallel rows of anemones aligned perpendicular to flow on the bottom of the flume. To exclude variation caused by flow and anemone size, all experiments were conducted using anemones within an intermediate size range (3–4-cm pdd), and run at the flow speed at which this size class had its maximum feeding efficiency (see Results). Effect of upstream neighbors on prey capture per square centimeter of tentacle crown was tested using the Tukey-Kramer method (Sokal and Rohlf, 1981).

Results

Vertical feeding zone and tentacle-crown deformation

The height of tentacle crowns above the flume floor (y, from lowermost to uppermost tentacle tips), and thus vertical feeding zone, of large anemones was 2–3 times that of medium and small anemones, and showed a consistent decline with increasing flow regime (Fig. 2). The feeding zone of large anemones was especially affected by flow—their mean height at the highest flow ($y_{\mathrm{Mean}} \pm$ SE = 4.2 ± 0.2 cm) was only 50% of that recorded at the lowest flow regime ($y_{\mathrm{Mean}} \pm$ SE = 8.2 ± 0.9 cm). A pronounced downstream bending of anemone columns with increasing flow occurred (Fig. 2). The three size classes experienced different local flow velocities (U_y, estimated from flow profiles in Fig. 1) in a given flow regime because of their different positions in the boundary layer. The uppermost tentacles of large anemones experienced about twice the flow velocity of medium and small anemones, which were positioned deeper in the turbulent boundary layer (Figs. 1 and 2). Differences in local flow speeds were less noticeable among medium and small anemones.

Tentacle-crown deformation, indicated by a decreasing ratio of projected tentacle-crown area to ash-free dry weight (S/AFDW) with increasing flow, was most pronounced for large anemones (Table 1). The projected prey-capture surface of large anemones at U_{10} = 44 cm s^{-1} was only one-third of that recorded at U_{10} = 4 cm s^{-1}. Tentacle-crown deformation of small and medium-sized anemones was noticeable only at flows between 4 and 17 cm s^{-1}. In that range they showed an initial increase in S/AFDW, presumably indicating incomplete tentacle-crown extension at the lowest flow velocity. Moreover, the generally lower S/AFDW ratios of large relative to small anemones corroborates earlier findings (Sebens, 1981) that larger *M. senile* have a smaller prey-capture surface per unit of biomass.

Feeding rates

Feeding rates of the three size classes of *M. senile* showed drastic changes with increasing flow, regardless of unit (per polyp, square centimeter of tentacle-crown area, or gram of ash-free dry weight, Fig. 3). Feeding rates tended to increase linearly and monotonically with flow over the range 4–17 cm s^{-1} for all size classes, indicating that the availability of prey is a function of flow in low to moderate flow regimes. On a per-polyp basis, large anemones captured 3–10 times more nauplii than small and medium-sized anemones within the flow range 4–17 cm s^{-1} (Fig. 3A). Above 20 cm s^{-1}, however, the feeding rate of large anemones declined rapidly with flow and converged with those of small and medium anemones, which remained constant above 20 cm s^{-1}. On a per-biomass basis, the pattern was partly reversed: small anemones showed 2–3 times higher feeding rates than medium-sized anemones, which in turn showed higher feeding rates than large anemones, over the flow range 10–44 cm s^{-1} (Fig. 3B). At the slowest flow, medium-sized anemones showed significantly lower feeding rates

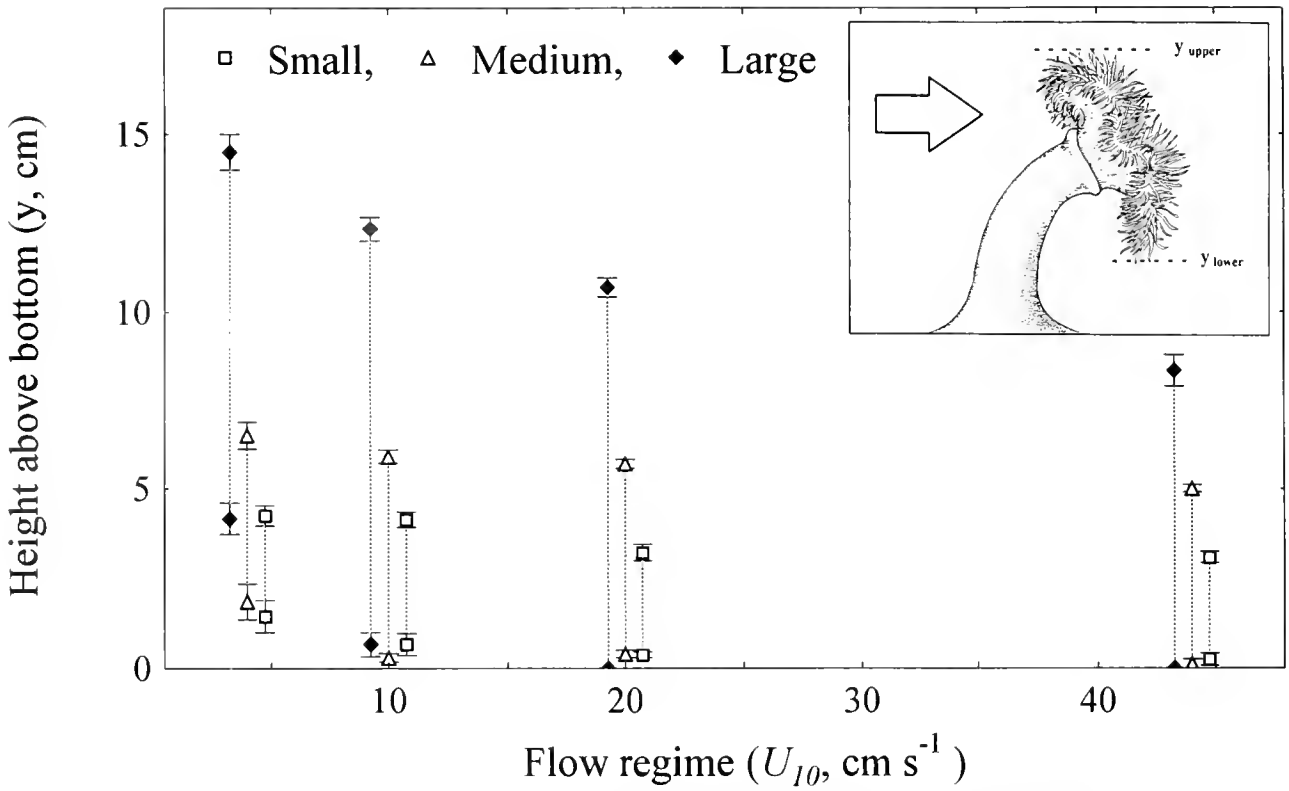

Figure 2. Vertical feeding zone (range of tentacle-crown heights) of the three size classes of *Metridium senile* as a function of flow regime. Error bars are ±1 SE of 3 to 9 anemones. The inset shows the typical posture of a medium-sized anemone at moderate flow; the arrow indicates flow direction. Small anemones: 1.0–2.0 cm in pedal disc diameter (pdd), medium: 2.5–3.0 cm pdd, and large: 6.0–6.5 cm pdd.

than did both small and large anemones. Interestingly, feeding rates based on feeding-surface area (S, Fig. 3C) and on anemone biomass displayed the same general patterns, perhaps reflecting isometric growth (Sebens, 1981). One noticeable difference among the sets of data is, however, that large anemones showed a significant decrease in prey capture per unit biomass at $U_{10} >$ 17 cm s^{-1}.

Feeding efficiencies

The three size classes of *M. senile* demonstrated three distinct flow optima, inversely related to size class, at

Table I

Flow-induced tentacle-crown deformation and anemone biomass in three size classes of Metridium senile

	Small (1.0–2.0 cm pdd)			Medium (2.5–3.0 cm pdd)			Large (5.5–6.0 cm pdd)	
U_{10} (cm s^{-1})	n	S/AFDW ± SE (cm^2 g^{-1})	AFDW ± SE (g)	n	S/AFDW ± SE (cm^2 g^{-1})	AFDW ± SE (g)	n	S/AFDW ± SE (cm^2 g^{-1})	AFDW* ± SE (g)
4	9	64.99 ± 6.24	0.156 ± 0.019	7	43.86 ± 2.44	0.635 ± 0.048	3	56.31 ± 7.14	2.827 ± 0.403
10	6	84.09 ± 3.18	0.148 ± 0.009	5	49.52 ± 3.31	0.682 ± 0.052	3	53.67 ± 7.48	2.827 ± 0.403
17	8	52.48 ± 3.99	0.159 ± 0.022	5	40.86 ± 3.31	0.663 ± 0.058	3	43.39 ± 3.92	2.827 ± 0.403
20	8	47.80 ± 2.83	0.160 ± 0.020	5	36.48 ± 1.92	0.650 ± 0.061	3	29.61 ± 3.17	2.827 ± 0.403
28	7	47.80 ± 3.61	0.101 ± 0.015		—	—		—	—
44	6	44.74 ± 3.96	0.148 ± 0.009	4	36.37 ± 1.09	0.541 ± 0.016	3	20.56 ± 4.16	2.827 ± 0.403

Size classes were based on measurement of pedal disc diameter (pdd). The degree of tentacle-crown deformation is quantified as the decrease in ratio of tentacle crown area (S) to ash-free dry weight (AFDW) with increasing flow (U_{10}). SE denotes standard error of n = 3 to 9 anemones.

* The same three large anemones were exposed to all flow regimes.

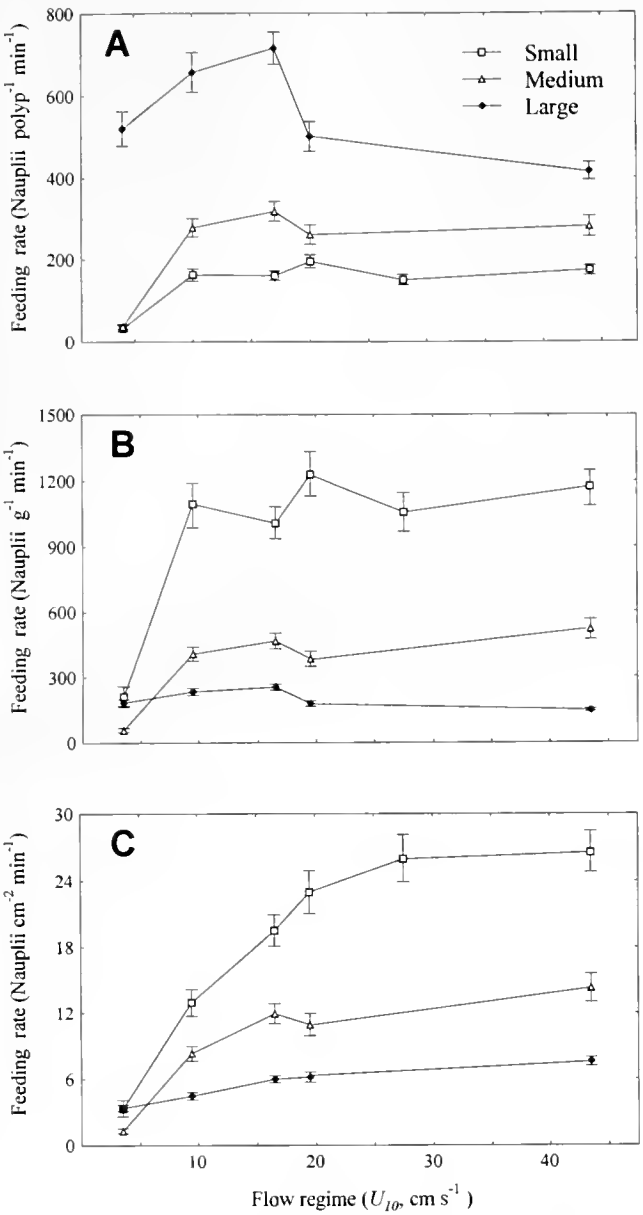

Figure 3. Feeding rates (nauplii min^{-1}) per (A) polyp, (B) gram of ash-free dry weight, and (C) unit area of tentacle crown of *Metridium senile* as a function of body size and flow regime. Error bars are ±95% confidence limits. All comparisons among size classes are significant at any given flow regime except at U_{10} = 4 cm s^{-1}. Groups with overlapping error bars are not significantly different by the Tukey-Kramer test. Regressions for the determination of F were highly significant in all experiments ($P < 0.001$, $R > 0.88$).

which the feeding efficiency (E) was maximized (Fig. 4). Large anemones showed a maximum feeding efficiency at the slowest flow (U_{10} = 4 cm s^{-1}), medium-sized anemones at low to moderate flows (10–17 cm s^{-1}), and small anemones at moderate to high flows (10–20 cm s^{-1}). Small anemones were able to capture and retain up to 25.7 ± 2.0% of the nauplii passing the projected area of the tentacle crown at their optimal flow speed (U_{10} = 20 cm s^{-1}). The feeding efficiency of all size classes decreased monotonically beyond their optimum. At all flow velocities except the lowest one, small anemones were significantly (2–3 times) more efficient than medium-sized anemones, which in turn were about twice as efficient as large anemones; these results are analogous to the pattern of feeding rates based on biomass and area of feeding surface.

Effect of upstream neighbors

The feeding rate per unit area of tentacle crown of medium-sized *M. senile* declined significantly with increasing numbers of conspecifics upstream (6.45 ± 0.45 to 2.25 ± 0.30 nauplii min^{-1} cm^{-2}, both ±95% CL) (Fig. 5). The effect of upstream neighbors was most pronounced within small aggregations of anemones (2–4 rows). Increasing the number of aligned rows of anemones from 7 to 16 did not reduce the feeding rate per unit area of tentacle crown, and thus indicated a threshold at which the feeding rate per polyp was unaffected by the addition of upstream neighbors.

Discussion

Feeding rates and efficiencies

The combinations of polyp size and flow regime at which prey capture of *Metridium senile* is maximized are in good agreement with the pattern of population structures and flow habitats observed in the field, suggesting that size distributions of *M. senile* are, in part, based on the ability to utilize seston flux. Interestingly, small anemones were generally more efficient at retaining prey than both medium and large anemones over the full flow range. Large anemones were, however, more than twice as efficient as medium-sized anemones at the slowest flow, but this relationship was reversed at moderate to high flow. The generally higher feeding rate per unit area and per unit biomass of small anemones may allow rapid growth to a size at which they can better compete for space, avoid size-selective predation (Harris, 1986), and reproduce sexually (Anthony and Svane, 1994), provided that the energy input is used in polyp growth rather than in clonal growth by pedal laceration (see below). The maximized feeding at a high flow speed of small *M. senile* is inconsistent with other studies on prey capture (*e.g.*, Okamura, 1984, 1985; McFadden, 1986; Best, 1988; Leonard *et al.*, 1988, Dai and Lin, 1993) and growth (Okamura, 1992; Eckman and Duggins, 1993) of tentaculate suspension feeders. In these studies maximum rates of feeding, growth, or both were generally associated with low flow speeds. A direct comparison

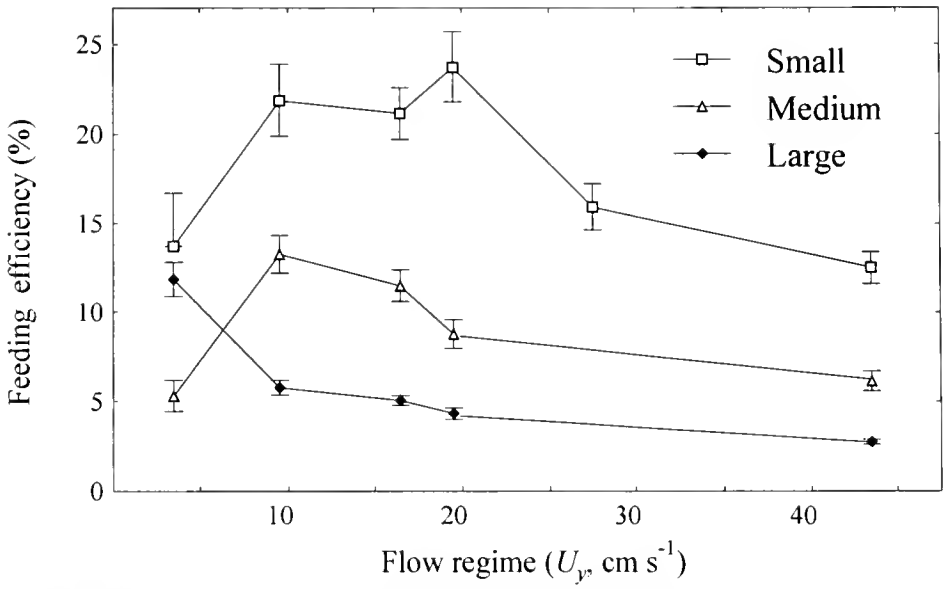

Figure 4. Feeding efficiency (number of nauplii captured per number of nauplii passing, see Eq. 5 and 6) as a function of flow regime in three size classes of *Metridium senile*. Error bars are ±95% confidence limits. All comparisons among size classes are significant at any given flow regime except between small and large anemones at $U_{10} = 4$ cm s^{-1}. Groups with overlapping error bars are not significantly different by the Tukey-Kramer test.

among studies of flow, body size, and prey capture is difficult, however, because different ranges of size and flow regime are used in different studies. Also, comparisons of size *per se* among different taxa of suspension feeders are complicated by differences in their structural organization.

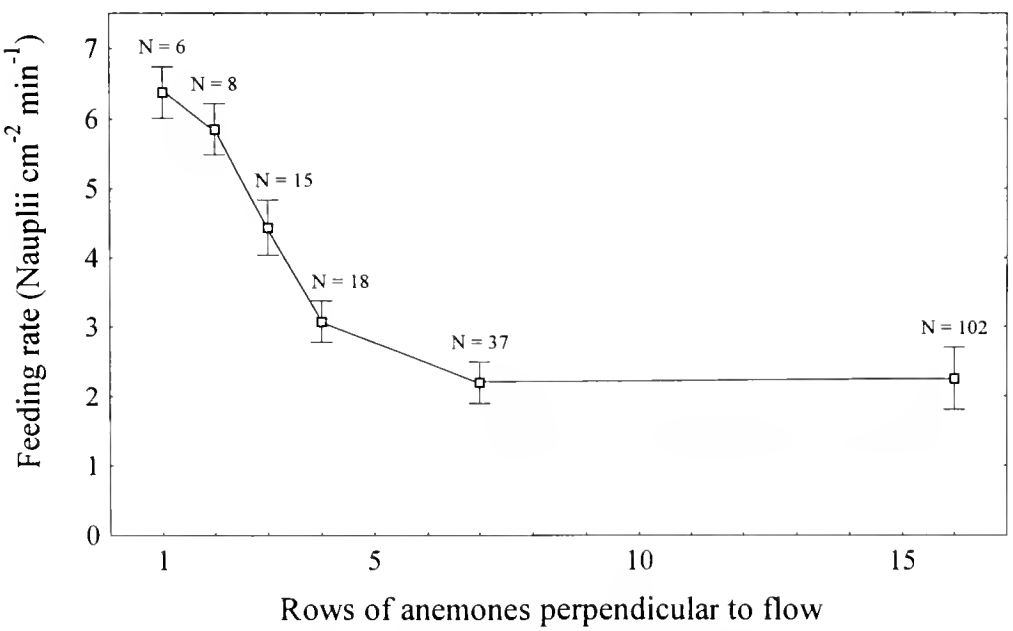

Figure 5. Effects of upstream neighbors in *Metridium senile*. Feeding rate (nauplii min^{-1}) per square centimeter of tentacle crown as a function of the number of upstream conspecifics. Error bars are ±95% confidence limits. Groups underlined at the same level are not significantly different by the Tukey-Kramer test.

The maximum prey-capture efficiency of *M. senile* from the Gullmarsfjord (25.6 ± 2.0%, small anemones) is only half of that reported by Lesser *et al.* (1994) for *M. senile* from the Gulf of Maine (40% for offshore and 52% for coastal anemones). Data on prey capture were, however, not given in relation to flow speed although a significant tentacle-crown deformation (50%) at increasing flow was recorded, as also found in this study. The feeding efficiencies determined for *M. senile* in this study are also generally lower than those of the sea pen *Ptilosarcus gurneyi* (Best, 1988) which were up to 42%, decreasing with flow to 30% within a narrow low-flow range (1.5–5.0 cm s^{-1}), but are comparable with whole-colony efficiencies of the octocoral *Alcyonium siderium* (Patterson, 1991) in moderate flow regimes. However, the feeding efficiency of *A. siderium* is inversely related to both colony size and flow speed (Patterson, 1991), whereas the relationship between feeding, size, and flow shows a more complex pattern in *M. senile*. These different patterns may, in part, be due to the different filtering structures and tentacular organizations between solitary and colonial anthozoans, and to differences in structural flexibility.

The increasing feeding rates as a function of ambient flow within the low to moderate flow range corroborates earlier assumptions that moderate-flow habitats provide higher seston availability than low-flow habitats (Shick and Hoffmann, 1980; Sebens, 1984; Shick, 1991). The flow range at which food intake per polyp or per biomass is maximized, however, is different between size classes. Large anemones showed a relatively distinct maximum at 10–17 cm s^{-1}, whereas small and medium anemones maintained a constant food intake above 10 cm s^{-1}. These different responses to flow are likely to explain, in part, the differences in size distribution of *M. senile* across flow habitats. In high-flow habitats *M. senile* typically forms dense aggregations of small anemones monopolizing vast areas of rock wall and consisting of only a few clones, whereas populations in low-flow habitats often comprise large and usually more scattered individuals from numerous clones (Anthony and Svane, 1994).

Only at the slowest flow were large anemones able to achieve feeding rates and feeding efficiencies comparable to those of small and medium-sized anemones. Large anemones had a significant feeding disadvantage relative to small and medium anemones at flows greater than 10 cm s^{-1}, and displayed a per-biomass food intake only one-eighth that of the small anemones in very high flow regimes. One explanation for this pattern is based on differences in the geometry of the tentacle crown of large and small anemones. Although the tentacles of large and small *M. senile* have comparable geometry and size (Sebens, 1981), the relative size of the oral disc increases with body size. Therefore, the proportion of tentacle crown effective in upstream capture (the circumference of tentacles facing upstream or perpendicular to flow) when the anemone is bent downstream relative to the total tentacle crown area is likely to be greater for small anemones. Subtracting the projected area of the upper part of the column from the surface area of the tentacle crown accounted to some extent for such geometric differences. However, size-related differences in the spacing of openings in the capitulum at the base of the tentacles were not accounted for. If such differences exist, mainly as a result of differential convolutions of the tentacle crown, they are likely to affect the size-specific feeding efficiencies (J. M. Shick, pers. com.).

In moderate to high flow velocities, a great proportion of the tentacle crown of large anemones is hidden from the upstream flux and is thus engaged in wake feeding, which is likely to be less effective than upstream feeding (Shimeta and Jumars, 1991). Small anemones may benefit from both upstream and wake feeding at comparable flow rates, whereas wake feeding is likely to be the predominant mode of feeding for large anemones in moderate to high flow. However, due to the higher Reynolds number associated with large animals (Shimeta and Jumars, 1991), downstream vortex formation is more pronounced for large anemones. This effect may, in part, be beneficial in providing a leeward region of enhanced retention efficiency through reduced flow velocities (Patterson, 1984).

Although the probability of prey encounter increases with flow, so does the risk of dislodgement of captured prey, and an optimum local velocity must be within the range over which retention significantly exceeds dislodgement of encountered prey. Both the capacity for retention by and the risk of dislodgement from the tentacles of sea anemones and of passive suspension feeders in general may vary among size classes and among genotypes. The small *M. senile* from high-flow habitats may be better adapted to feeding in a high-flow environment by being equipped with a more efficient cnidom for both subduing and retaining intercepted prey. Effects of flow forces on dislodgement of intercepted prey in cnidarian suspension feeders are, however, poorly understood (Patterson, 1984; Shimeta and Jumars, 1991).

Vertical feeding zone and tentacle-crown deformation

The prey availability can for some passive suspension feeders be adjusted to a given flow regime by means of behavior or change of posture, for example by regulating the height and orientation of the feeding appendages (ophiuroids: Warner and Woodley (1975); crinoids: Holland *et al.* (1987), Leonard (1989); sea anemones: Robbins and Shick (1980), this study; polychaetes: Muschenheim (1987), Shimeta and Jumars, (1991)) or by vertical,

oriented locomotion of the whole animal (Anthony and Svane, 1995). Differences in prey capture among small, medium, and large *M. senile* in this study could not be explained fully by different local flow velocities at different heights in the boundary layer. In fact, the local flow velocities experienced at the mean level of the tentacle crown of the three size classes in low to moderate flow regimes did not differ by more than 1–2 cm s^{-1}. Contrasting local flow velocities due to differences in vertical position were found only between large and small or medium-sized anemones at the highest flow regime (6–8 cm s^{-1}). A higher degree of downstream bending of medium-sized and especially large anemones due to proportionately greater drag (Koehl, 1977a) explains the overlapping, vertical feeding zones of different size classes. Flow forces thus act in moving the feeding apparatus of large anemones into the boundary layer and away from the maximum exposure, enabling some, though reduced, prey capture at even the highest ambient flow.

Tentacle-crown deformation, and thereby a reduced prey-capture area normal to flow, could to some extent account for the significantly lower feeding success of large anemones in regimes of moderate to high flow. Prey-capture surface per unit biomass decreased by more than 50% when altering the flow regime from 4 to 44 cm s^{-1}, affecting the volume of water filtered and the rate of potential prey encounter accordingly, and probably also the spacing between tentacles (see also Lesser *et al.*, 1994). Best (1988) also found that the deformability of the sea pen *Ptilosarcus gurneyi* strongly affected filtration efficiency and volume of water filtered. The effectiveness of the feeding apparatus of a large, soft-bodied suspension feeder is intrinsically apt to be more constrained by flow forces than is that of a small suspension feeder, because large animals are subject to proportionately greater drag (Koehl, 1977a) and shear stresses (Koehl, 1977b) than are small animals in similar flow conditions. Since the potential prey capture of, for example, a sea anemone is a function of the surface area of the feeding apparatus (Sebens, 1981), the *S*/AFDW ratio is likely to be a useful indicator of flow-habitat suitability.

Feeding rates vs. metabolic cost

To determine flow optima of passive suspension feeders, information on both energy intake and metabolic cost is necessary for every flow regime (Sebens, 1979, 1982). Although the pattern of feeding rates per unit of biomass suggests that small anemones generally have a greater energy surplus than large and medium-sized anemones regardless of flow regime, energy demand is likely to vary among size classes as well as among flow regimes. Gas exchange, and thus metabolic cost, in cnidarians is largely governed by the thickness and characteristics of the boundary layer surrounding the organism, which in turn are functions of organism size and flow regime (Patterson, 1992a). For example, Patterson and Sebens (1989) found that the rate of respiration in large specimens of *Metridium* doubled over the flow range 7–15 cm s^{-1} due to the effect of water motion. A useful method for comparing metabolic cost across flow regimes as well as size classes is the relationship between Sherwood number and Reynolds number (Patterson and Sebens, 1989; Patterson, 1992a, b). Sherwood number (Sh) is a dimensionless index of metabolism, defined as the ratio of mass flux per unit surface area assisted by convection (F_{conv}, μ cm^{-2} h^{-1}) to that which would occur if diffusion through a stagnant layer of water was the only mechanism of gas exchange. Reynolds number (Re) is the ratio of inertial to viscous forces acting on the flowing water, and is an index of the strength of flow experienced by the organism. For *Metridium*, the functional relationship between Sh and Re is $Sh = 0.28\ Re^{1.04}$ as found by Patterson and Sebens (1989). Since Re is a function of body size and flow [$Re = U_y \times TCD/v$, where U_y is local flow speed (cm s^{-1}), TCD is tentacle-crown diameter (cm), and v is the kinematic viscosity of seawater (1.04×10^{-2} cm^2 s^{-1})], Sh can be readily obtained for all combinations of flow regime and size class in this study. Expected (flow-assisted) metabolic cost can be derived from Sh as the convective mass flux (F_{conv}, the numerator of Sh), normalized to biomass by multiplying with the ratio of surface area to biomass (SA/AFDW, cm^2 g^{-1}), where SA is the sum of tentacle surface area [see regressions in Sebens (1981)] and surface area of the column. According to Patterson (1992b) convective mass flux can be calculated as $F_{conv} = Sh \times D(C_e - C_i)/TCD$, where D is the diffusion coefficient for oxygen (7.2×10^{-2} cm^2 h^{-1}), C_e is the oxygen concentration in the surrounding water ($\approx$7 mg l^{-1}), and C_i is the oxygen concentration at the site of metabolism. For azooxanthellate cnidarians, C_i can be regarded as negligible (pers. com., Mark Patterson). Expected metabolic rate per unit biomass ($R_{exp} = Sh \times D \times C_e \times SA/[TCD \times AFDW]$, μg (g dry wt)$^{-1}$ h^{-1}) as a function of flow regime for the three size classes of *M. senile* is shown in Figure 6.

Expected metabolic rate for all size classes increases as a linear function of flow regime, with a 10-fold increase in metabolic rate between lowest and highest flow speeds. In accordance with allometric studies (*e.g.*, Sebens, 1981), metabolic rate is greater for small and medium-sized compared to large anemones, by a factor of about ½. Interestingly, expected metabolic rate is higher for medium-sized compared to small anemones at flow regimes greater than 10 cm s^{-1}, probably due to the higher local flow speeds (and hence Sh) experienced by medium-sized anemones (Figs. 1 and 2). Although energy

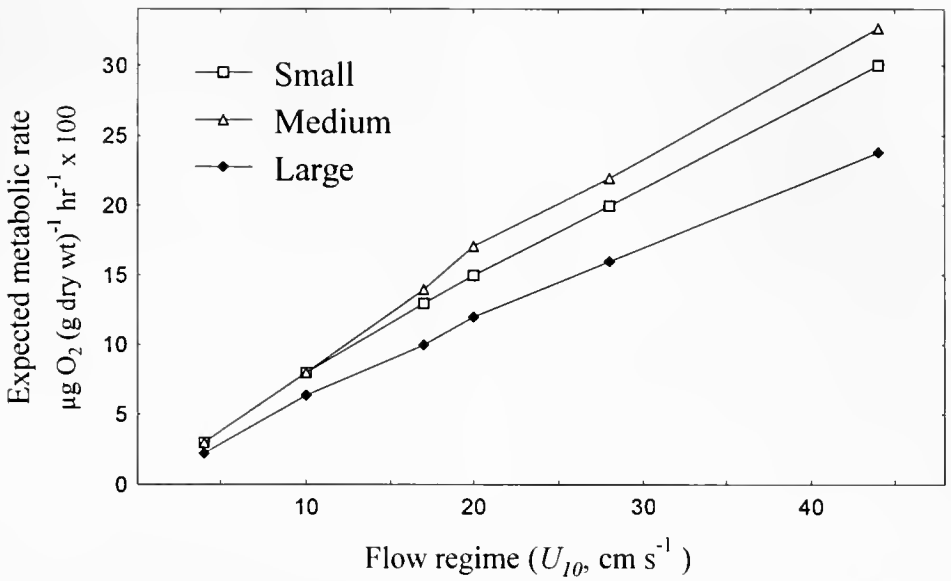

Figure 6. Expected metabolic rate as a function of flow regime for the three size classes of *Metridium senile*, based on mean Reynolds numbers for the study anemones and empirical mass-transfer relations from Patterson and Sebens (1989). See text for calculations.

balance also depends on local food availability, food quality, and absorption efficiency (*e.g.*, Zamer, 1986), the patterns of potential food intake (feeding rate) and expected metabolic cost provide a basis for relative comparisons of potential flow optima among size classes. The flow speed at which energetic cost counterbalances food intake will be highest for the small anemones, intermediate for medium-sized anemones, and lowest for large anemones. Due to very high feeding rates, small anemones are able to maintain a more positive energy balance than both medium and large anemones at all flow speeds $\geq$10 cm s^{-1}. The almost 10-fold increase in feeding rate of small anemones in the flow range 4–10 cm s^{-1} amply exceeds the concomitant increase in metabolic cost over this flow interval, and is likely to allow rapid growth of juvenile anemones and lacerates in low-to-moderate flow regimes. At higher flow speeds, however, feeding rate remains constant, whereas metabolic rate increases linearly with flow. If the feeding rate of small anemones at 4 cm s^{-1} is sufficient to meet basic energy demands, so is the feeding rate at 44 cm s^{-1} because both feeding rate and metabolic cost increase 10-fold between lowest and highest flow. At the lowest flow speed, however, large anemones are likely to have a more positive energy balance than the smaller size classes, given the comparable feeding rates of small and large anemones but the lower mass-specific metabolic cost of large anemones. Since large anemones only showed low weight-specific feeding rates without a convincing maximum, any energetic optimum of this size class must be confined to low-flow regimes because of the rapid increase in metabolic rate with flow. The flow optimum of medium-sized anemones, on the other hand, is likely to be located in the range 10–20 cm s^{-1}, as their feeding rate is minimal at 4 cm s^{-1} ($^1/_3$ of large and small anemones) and their expected metabolic cost increases with flow at a relatively higher rate than for the two other size classes.

Use of mass-transfer theory to compare metabolic cost between individual *M. senile* in different flow regimes does not, however, take into account the differences in spatial distributions between large and small anemones. Large anemones are often widely separated from one another, whereas small anemones (due to their pronounced clonality) form dense patches structurally resembling coral colonies (Anthony and Svane, 1994). Flow around individual polyps in such patches is likely to be further reduced, resulting in a thicker diffusive boundary layer and a lower gas exchange than for small, spatially isolated individuals in similar flow habitats (see also Patterson and Sebens, 1989).

Effects of flow and feeding on reproductive patterns

One way in which *M. senile* might maintain an energetically optimal polyp size in the prevailing current regime is by altering the rate of pedal laceration. Laceration is a loss of tissue to the individual polyp (facilitating degrowth), but also an effective means of clonal growth, so differential rates of laceration between local populations may have consequences for their size distributions. The generally higher rates of laceration in populations of small *M. senile* from high-flow habitats relative to popu-

lations of large anemones from low-flow habitats support this hypothesis (Shick and Hoffmann, 1980; Anthony and Svane, 1994). Since large anemones cannot maintain a positive energy balance in high-flow habitats, whereas small anemones can, any excess energy acquired by high-flow anemones is likely to be allocated to clonal growth (through pedal laceration) rather than to polyp growth. Laceration is also stimulated by feeding (Bucklin, 1987), suggesting that asexual reproduction is one pathway by which energy surplus is translated into a greater genet biomass. Effects of feeding and ambient flow on laceration are, however, apt to be closely linked due to the direct proportionality between flow and seston flux, and hence potential particle encounter. By obtaining an optimal polyp size in a given flow habitat through growth or degrowth (*via* laceration), the energy available for clonal growth, sexual reproduction, and hence genet fitness can be further enhanced. Clonal growth as opposed to polyp growth in high-flow habitats creates the energetic potential for the genet to grow indefinitely without size-energy constraints, because the addition of new polyps to the clone increases feeding surface and energetic cost linearly (Sebens, 1979). Conversely, growth to a maximum polyp size in low-flow habitats enables maximum feeding and thus energy input (this study), and also a maximum per-biomass reproductive output (Anthony and Svane, 1994).

Effect of upstream neighbors

Considering the clonal nature and high polyp densities of most populations of *M. senile*, the presence of upstream neighbors is likely to be an important factor affecting the energy input of both the polyp and the clone. Furthermore, the effect of upstream neighbors on near-bed prey availability downstream may select for large size in some flow habitats, despite a relatively greater food intake in small anemones, and thereby contribute to structuring local populations. The asymptotic relationship between feeding rate per unit area of tentacle crown and number of upstream conspecifics, on the other hand, indicated that the potential feeding capacity was not reduced to below about 30% of the situation without neighbors upstream. A likely explanation for this threshold is that individual anemones function as roughness elements, increasing turbulence and eddy diffusivity downstream (Denny, 1988), thereby reducing local particle depletion around tentacle crowns by mixing mainstream water into the turbulent boundary layer. In high-flow habitats, the generally higher density of anemones may also provide shelter for individual anemones by moving the turbulent boundary layer outward. As suggested by Patterson (1984), particle lift in the boundary layer over the tentacle-crown canopy may be responsible for reduced downstream concentrations, and thereby, in part, account for the asymptotic rather than linear reduction in retention with increasing number of upstream neighbors (see also Fréchette *et al.*, 1989). Furthermore, gravitational deposition is likely to be more important in dense clones than in populations of scattered individuals on horizontal substrata, providing a "rain" of seston that is independent of the number of upstream neighbors. Overall, these results suggest that increased clonal growth of *M. senile* in high-flow habitats at the expense of polyp growth (see review by Shick, 1991) may negatively affect net prey capture by the genet through feeding interaction between clonemates. Conversely, predominant polyp growth and reduced clonal growth in low-flow habitats is likely to enhance prey capture by excluding the effect of neighbors. The generally higher feeding efficiency of small polyps of *M. senile* may, however, compensate for the negative effects of neighbors in dense, clonal aggregations if the prevailing flow conditions provide a correspondingly higher flux of prey.

Acknowledgments

I thank the administration and staff of Kristineberg Marine Research Station for providing laboratory facilities and technical assistance. Thanks are especially due to Ken Sebens for reviewing the penultimate draft, and to Terry Hughes, Bette Willis, The Coral Discussion Group at James Cook University, Henrik Glenner, Pia Anthony, and Robert George for valuable discussions and comments on earlier versions of the manuscript. I am grateful to Mark Patterson for his advice on calculations of expected metabolic cost. Malcolm Shick, William Zamer, and Barbara Best improved the final manuscript. Thanks are also due to Walt Doyle for assistance in the laboratory. This work was supported by the Nordic Council for Marine Biology, Nordic Academy for Advanced Studies, the Axel Hemmingsen Grant, and the Hierta-Retzius Foundation (Royal Swedish Academy of Sciences).

Literature Cited

Anthony, K. R. N., and I. Svane. 1994. Effects of flow-habitat on body size and reproductive patterns in the sea anemone *Metridium senile* (L.) in the Gullmarsfjord, Sweden. *Mar. Ecol. Prog. Ser.* **113:** 257–269.

Anthony, K. R. N., and I. Svane. 1995. Effects of substratum instability on locomotion and pedal laceration in *Metridium senile* L. (Anthozoa: Actiniaria). *Mar. Ecol. Prog. Ser.* **124:** 171–180.

Best, B. A. 1988. Passive suspension feeding in a sea pen: effects of ambient flow on volume flow rate and filtering efficiency. *Biol. Bull.* **175:** 332–342.

Bucklin, A. 1987. Growth and asexual reproduction of the sea anemone *Metridium*: comparative laboratory studies of three species. *J. Exp. Mar. Biol. Ecol.* **110:** 41–52.

Dai, C.-F., and M.-C. Lin. 1993. The effects of flow on feeding of three gorgonians from southern Taiwan. *J. Exp. Mar. Biol. Ecol.* **173:** 57–69.

Denny, M. 1988. *Biology and the mechanisms of the wave-swept environment.* Princeton University Press, Princeton.

Eckman, J. E., and D. O. Duggins. 1993. Effects of flow speed on growth of benthic suspension feeders. *Biol. Bull.* **185:** 28–41.

Fautin, D. G., A. Bucklin, and C. Hand. 1989. Systematics of the sea anemones belonging to genus *Metridium* (Coelenterata: Actiniaria), with a description of *M. giganteum* new species. *Wasmann J. Biol.* **47(1–2):** 77–85.

Francis, L. 1979. Contrasts between solitary and clonal lifestyles in the sea anemone *Anthopleura elegantissima*. *Am. Zool.* **19:** 669–681.

Fréchette, M., C. A. Butman, and W. R. Geyer. 1989. The importance of boundary-layer flows in supplying phytoplankton to the benthic suspension feeder *Mytilus edulis* L. *Limnol. Oceanogr.* **34:** 19–36.

Harris, L. G. 1986. Size-selective predation in a sea anemone, nudibranch, and fish food chain. *Veliger* **29:** 38–47.

Hoffmann, R. J. 1976. Genetics and asexual reproduction of the sea anemone *Metridium senile*. *Biol. Bull.* **151:** 478–488.

Hoffmann, R. J. 1986. Variation in contributions of asexual reproduction to the genetic structure of populations of the sea anemone *Metridium senile*. *Evolution.* **40(2):** 357–365.

Holland, N. D., A. B. Leonard, and J. R. Strickler, 1987. Upstream and downstream capture during suspension feeding by *Oligometra serripinna* (Echinodermata: Crinoidea) under surge conditions. *Biol. Bull.* **173:** 552–556.

Johnson, A. S. 1990. Flow around phoronids: consequences of a neighbor to suspension feeders. *Limnol. Oceanogr.* **35:** 1395–1401.

Johnson, A. S., and K. P. Sebens, 1993. Consequences of a flattened morphology: effects of flow on feeding rates of the scleractinian coral *Meandrina meandrites*. *Mar. Ecol. Prog. Ser.* **99:** 99–114.

Koehl, M. A. R. 1976. Mechanical design in sea anemones. Pp. 23–31 in *Coelenterate Ecology and Behavior*, G. O. Mackie, ed. Plenum Press, New York.

Koehl, M. A. R. 1977a. Effects of sea anemones on the flow forces they encounter. *J. Exp. Biol.* **69:** 87–105.

Koehl, M. A. R. 1977b. Mechanical organisation of cantilever-like sessile organisms: sea anemones. *J. Exp. Biol.* **69:** 127–142.

LaBarbera, M. J., and S. Vogel. 1976. An inexpensive thermistor flowmeter for aquatic biology. *Limnol. Oceanogr.* **21:** 750–756.

Leonard, A. B. 1989. Functional response in *Antedon mediterranea* (Lamarck) (Echinodermata: Crinoidea): the interaction of prey concentration and current velocity on a passive suspension feeder. *J. Exp. Mar. Biol. Ecol.* **127:** 81–103.

Leonard, A. B., J. R. Strickler, and N. D. Holland, 1988. Effects of current speed on filtration during suspension feeding in *Oligometra serripinna* (Echinodermata: Crinoidea). *Mar. Biol.* **97:** 111–125.

Lesser, M. P., J. D. Witman, and K. P. Sebens. 1994. Effects of flow and seston availability on scope for growth of benthic suspension-feeding invertebrates from the Gulf of Maine. *Biol. Bull.* **187:** 319–335.

Leversee, G. J. 1976. Flow and feeding in the fan-shaped colonies of the gorgonian coral, *Leptogorgia*. *Biol. Bull.* **151:** 344–356.

Manuel, R. L. 1988. *Synopsis of the British Fauna. New Series 18, British Anthozoa.* Academic Press, London.

McFadden, C. S. 1986. Colony fission increases particle capture rates of a soft coral: advantages of being a small colony. *J. Exp. Mar. Biol. Ecol.* **103:** 1–20.

Muschenheim, D. K. 1987. The dynamics of near-bed seston flux and suspension-feeding benthos. *J. Mar. Res.* **45:** 473–496.

Okamura, B. 1984. The effects of ambient flow velocity, colony size, and upstream colonies on the feeding success of Bryozoa. I. *Bugula stolonifera* Ryland, an arborescent species. *J. Exp. Mar. Biol. Ecol.* **83:** 179–193.

Okamura, B. 1985. The effects of ambient flow velocity, colony size, and upstream colonies on the feeding success of Bryozoa. II. *Conopeum reticulum* L., an encrusting species. *J. Exp. Mar. Biol. Ecol.* **89:** 69–80.

Okamura, B. 1992. Microhabitat variation and patterns of colony growth and feeding in a marine bryozoan. *Ecology* **73(3):** 1502–1513.

Patterson, M. R. 1984. Patterns of whole colony prey capture in the octocoral *Alcyonium siderium*. *Biol. Bull.* **167:** 613–629.

Patterson, M. R. 1991. Passive suspension feeding by an octocoral in plankton patches: empirical test of a mathematical model. *Biol. Bull.* **180:** 81–92.

Patterson, M. R. 1992a. A mass transfer explanation of metabolic scaling relations in some aquatic invertebrates and algae. *Science* **255:** 1421–1423.

Patterson, M. R. 1992b. A chemical engineering view of cnidarian symbioses. *Am. Zool.* **32:** 566–582.

Patterson, M. R., and K. P. Sebens. 1989. Forced convection modulates gas exchange in cnidarians. *Proc. Natl. Acad. Sci. USA* **86:** 8833–8836.

Purcell, J. E. 1977. The diet of large and small individuals of the sea anemone *Metridium senile*. *Bull. S. C. Acad. Sci.* **76:** 168–172.

Robbins, R. E., and J. M. Shick. 1980. Expansion-contraction behavior in the sea anemone *Metridium senile*: environmental cues and energetic consequences. Pp. 101–116 in *Nutrition in the Lower Metazoa*, D. C. Smith and Y. Tiffon, eds. Pergamon Press, Oxford.

Sebens, K. P. 1979. The energetics of asexual reproduction and colony formation in benthic marine invertebrates. *Am. Zool.* **19:** 683–697.

Sebens, K. P. 1980. The regulation of asexual reproduction and indeterminate body size of the sea anemone *Anthopleura elegantissima* (Brandt). *Biol. Bull.* **158:** 370–382.

Sebens, K. P. 1981. The allometry of feeding, energetics, and body size in three sea anemone species. *Biol. Bull.* **161:** 152–171.

Sebens, K. P. 1982. The limits to indeterminate growth: an optimal size model applied to passive suspension feeders. *Ecology* **63(1):** 209–222.

Sebens, K. P. 1984. Water flow and coral colony size: interhabitat comparisons of the octocoral *Alcyonium siderium*. *Proc. Natl. Acad. Sci. USA* **81:** 5473–5477.

Sebens, K. P., and M. A. R. Koehl. 1984. Predation on zooplankton by the benthic anthozoans *Alcyonium siderium* (Alcyonacea) and *Metridium senile* (Actiniaria) in the New England subtidal. *Mar. Biol.* **81:** 255–271.

Shick, J. M. 1991. *A Functional Biology of Sea Anemones.* Chapman & Hall, London.

Shick, J. M., R. J. Hoffmann, and A. N. Lamb. 1979. Asexual reproduction, population structure, and genotype-environment interactions in sea anemones. *Am. Zool.* **19:** 699–713.

Shick, J. M., and R. J. Hoffmann. 1980. Effects of the trophic and physical environments on asexual reproduction and body size in the sea anemone *Metridium senile*. Pp. 211–216 in *Developmental and Cellular Biology of Coelenterates*, P. Tardent and R. Tardent, eds. Elsevier/North Holland Biomedical Press, Amsterdam.

Shick, J. M., and H. B. Dowse. 1985. Genetic basis of physiological variation in natural populations of sea anemones: intra- and interclonal analyses of variance. *Proc. 19th European Marine Biology Symposium*, Cambridge, P. E. Gibbs, ed. Cambridge University Press, UK.

Shimeta, J., and P. A. Jumars. 1991. Physical mechanisms and rates

of particle capture by suspension feeders. *Oceanogr. Mar. Biol. Ann. Rev.* **29**: 191–257.

Sokal, R. R., and F. J. Rohlf. 1981. *Biometry* 2 ed. W. H. Freeman & Co, San Francisco.

Trager, G., Y. Achituv, and A. Genin. 1994. Effects of prey escape ability, flow speed, and predator feeding mode on zooplankton capture by barnacles. *Mar. Biol.* **120**: 251–259.

Vogel, S. 1981. *Life in Moving Fluids, the Physical Biology of Flow* Willard Grant Press, Boston, Massachusetts.

Wainwright, S. A., and M. A. R. Koehl. 1976. The nature of flow and the reaction of benthic cnidaria to it. Pp. 5–21 in *Coelenterate Ecology and Behavior*, G. O. Mackie, ed. Plenum Press, New York.

Warner, G. F. and J. D. Woodley. 1975. Suspension feeding in the brittle star *Ophiotrix fragilis*. *J. Mar. Biol. Assoc. U.K.* **55**: 199–210.

Zamer, W. E. 1986. Physiological energetics of the intertidal sea anemone *Anthopleura elegantissima*. I. Prey capture, absorption efficiency and growth. *Mar. Biol.* **92**: 299–314.

Reference: *Biol. Bull.* **192:** 87–97. (February, 1997)

Patterns and Consequences of Whole Colony Growth in the Compound Ascidian *Polyclinum planum*

ALAN R. HOLYOAK

Department of Biology, University of California, Santa Cruz, California 95064

Abstract. The size and shape of colony-forming modular animals can convey ecological advantages, but many patterns and consequences of colony-level growth are not well understood. I carried out a longitudinal study on an intertidal population of the pedunculate ascidian *Polyclinum planum* to determine the patterns and consequences of its colony growth. I found that each *P. planum* colony is a nonfragmenting genet, and that colony size is limited by water-flow forces and reproductive state. *P. planum* mitigates the effects of water-flow forces by having an attenuating pattern of growth and by producing a laterally flattened, zooid-bearing lobe atop its tough flexible peduncle. Growth slows as the colony nears a size limit set by the environment and as it becomes reproductively active. The laterally flattened lobe allows colonies to increase their surface-to-volume ratio, to house increased numbers of zooids (thereby increasing reproductive potential), and to minimize the effects of the acceleration reaction of water. *P. planum*'s growth pattern fits predictions for colonies living in wave- or surge-impacted environments. The growth of *P. planum* provides insight into how indeterminate modular growth conveys ecological and reproductive advantage, even amidst a physically stressful environment.

Introduction

Theories describing the indeterminate growth of colony-forming modular organisms suggest that the colonies have the potential to grow linearly or exponentially throughout their postlarval lives (Jackson, 1977; Sebens, 1987). Sebens (1987) defines three patterns of indeterminate growth, two of which (Indeterminate Growth Types II and III from his paper) are applicable to colony-forming modular organisms. In Sebens' (1987) Indeterminate Growth Type II (Plastic Exponential Growth), energy intake and expenditures occur at the level of each member (module) of a colony, thus allowing each module to contribute independently to the colony and producing continuous linear or exponential growth—a growth pattern reported by Hughes and Jackson (1985) for stony corals, by Karlson (1988) for a zoanthid, by Pätzold *et al.* (1987) for a bryozoan, and by Bak *et al.* (1981) for a compound ascidian. In Sebens' (1987) Indeterminate Growth Type III (Plastic Attenuating Growth), colony growth rates decrease as colony size increases, growth being limited largely by environmental factors before internal energetic constraints take effect—a growth pattern reported by Hughes and Connell (1987) for stony corals, by Karlson (1988) for a zoanthid, and by Denny *et al.* (1985) for a hydrocoral.

External factors therefore constrain growth in some situations, but internal constraints are also known to be limiting in some taxa. For example, Millar (1952, 1971) and Bak *et al.* (1981) report that ascidian colonies grow rapidly when they are not reproductive, but that growth slows or ceases during reproduction. For at least some modular species, colony growth and reproduction are physiologically incompatible processes.

To evaluate the applicability of growth predictions for a colony-forming modular organism, one must understand how environmental effects (external factors) and life-history constraints (internal factors) affect colony growth. It is, unfortunately, difficult to collect those kinds of life-history data for many colony-forming modular species. The difficulty arises because there is often no way of knowing whether a colony encountered in the field developed directly from a larva or was one of many ramets produced by fragmentation (for examples, see Hughes, 1984; Hughes and Jackson, 1985; Karlson,

Received 24 July 1995; accepted 24 October 1996.

Current Address: Department of Biology, Manchester College, North Manchester, Indiana 46962.

1986, 1988; Rosen, 1986; Lasker, 1990; McFadden, 1991; Stocker, 1991). That uncertainty eliminates the possibility of measuring age-related effects at the level of genets. To further complicate matters, ramets of some modular species can fuse with other ramets of the same or different genotype (Hughes and Jackson, 1985; Rinkevich and Weissman, 1987a, b; Stocker, 1991; Pancer *et al.*, 1995). One way to be sure of the origins, ages, and fates of colonies of modular organisms is to conduct longitudinal site surveys, as suggested by Berrill (1950) when he stated that "the age of (compound) ascidians is practically impossible to estimate, unless a certain inhabited area is followed closely through seasons and years." That is sound advice if one hopes to understand the life histories of modular species, because age, size, and shape of modular colonies may not be as tightly linked as those parameters are to body size among unitary organisms (Hughes and Jackson, 1980; Jackson and Coates, 1986; Hughes and Connell, 1987).

In the present study I use monthly site surveys conducted over 2.5 years to describe the pattern of whole colony growth and the consequences of that growth for intertidal *Polyclinum planum* growing *in situ*. In so doing I try to determine whether the growth pattern of *P. planum* colonies more closely approximates Sebens' (1987) Type II or III pattern of growth, or some other pattern, and to discern what factor or factors constrain whole colony growth in this species.

I hypothesize that the growth pattern of *P. planum* will be more similar to Sebens' (1987) Growth Type III (Plastic attenuating growth) than to his Growth Type II (Plastic exponential growth). I chose Type III rather than Type II because the colonies at my study sites live in a wave- and surge-impacted environment, and the associated water-flow forces may impose limits to colony size.

Water-flow forces present an obvious ecological risk to erect, though flexible, intertidal *P. planum* colonies. Denny *et al.* (1985) demonstrated how the water-flow forces of drag, lift, and, most importantly, acceleration can dislodge or limit the size of intertidal organisms. Because the *P. planum* colonies at my sites are constantly subjected to water-flow forces, they should have adaptations for dealing with those forces that will be evidenced as the colonies increase in size.

I also hypothesize that the onset of reproduction in *P. planum* colonies will limit growth, and that large colonies will show more evidence of reproductive activity than small colonies. A *P. planum* colony grows by strobilation of its zooids. Strobilation, however, precludes gonadogenesis and larval brooding by the zooid because gonads develop only in its post-abdomen and larvae are brooded only in its atrial chamber—structures that become disorganized during strobilation (Holyoak, 1992).

P. planum, an aplousobranch ascidian, is well suited to a longitudinal investigation of colonial growth. It has a distinctive colony form—a fleshy, zooid-bearing lobe supported by a tough and flexible peduncle—that makes it readily identifiable in the field even when colonies are small (Fig. 1). *P. planum* colonies are not believed to fragment, so a single colony represents an entire genet (Pearse *et al.*, 1989). The nonfragmenting growth of these colonies eliminates the confounding effects of not knowing whether a colony is a ramet or an unfragmented genet. The loss of a *P. planum* colony is consequently a greater loss to the population, from an evolutionary perspective, than the loss of one ramet from a population of fragmenting genets. Since a genet of *P. planum* does not spread its genes across several physiologically isolated ramets, one would expect this species to display strategies that allow individual colonies to minimize ecological risks and to maximize reproductive productivity.

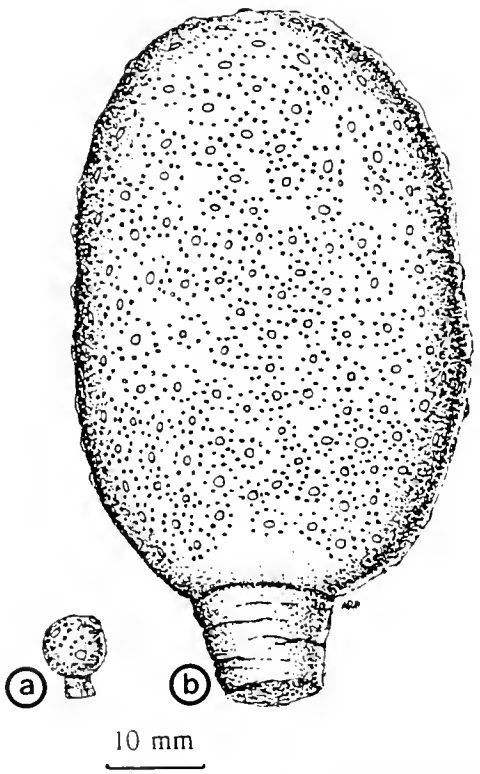

Figure 1. (a) Small "recruit-sized" *Polyclinum planum* colony with a spheroidal zooid-bearing lobe atop its zooid-free peduncle. (b) Large *P. planum* colony with a laterally flattened lobe. Note: Silhouette shapes of larger colonies are highly variable.

Materials and Methods

Between December 1989 and May 1992, I monitored the whole colony growth of intertidal *Polyclinum planum in situ* at the Hopkins Marine Station (HMS), Pacific Grove, California. The colonies there live attached

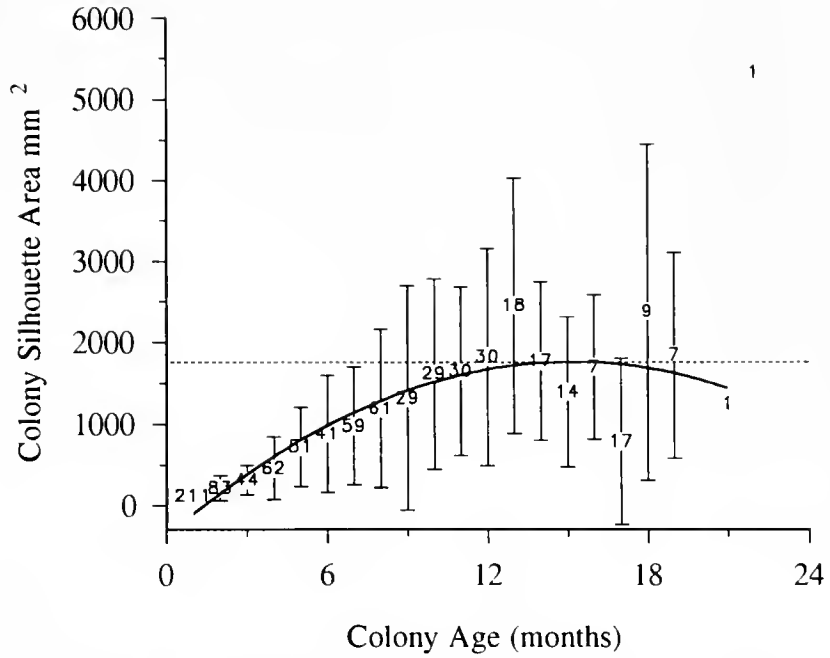

Figure 2. Mean growth trajectory of *Polyclinum planum*. A quadratic regression provides a significant fit to the data ($Y = -377.06 + 283.09x - 9.38x^2$; $r^2 = 0.734$; $t = -3.59$; df = 17; $P < 0.005$). Numbers indicate the number of observations included in each age class, error bars are standard deviations, and the horizontal dashed line indicates the maximum size (colony-silhouette area in mm^2) of the growth trajectory. The single outlier at month 23 was not included in the curve-fitting analysis. Discrepancies between numbers of colonies indicated for each age class (month) on this figure compared to Figure 7 are due to the fact that I was typically able to map all colonies at my sites each month, even with marginal tide conditions, but I was not able to photograph all colonies in months with marginal tides.

to granitic substrates below about −0.3 m MLLW (Mean Lower Low Water tide) and are most abundant in areas where granitic outcrops covered by surfgrass (*Phyllospadix* sp.) are protected from direct wave action. The highest density of *P. planum* I encountered during preliminary surveys prior to establishing my study sites was 95 colonies in a single 0.25-m^2 quadrat, though the mean of 7.8 colonies per 0.25-m^2 quadrat (SD = 14.95 colonies; n = 45 0.25-m^2 quadrats surveyed in the intertidal zone at HMS) was more representative of *P. planum* densities at HMS.

I established three study sites, each about 1 m^2, at −0.3 m MLLW; all had *P. planum* colonies present at the beginning of the study. The sites were within 10 m of each other and all of them had a dense canopy of surfgrass covering a mosaic of encrusting organisms, foliose algae, and bare rock surfaces. The three sites were on the inshore side of massive granitic outcroppings along the outermost reaches of the HMS intertidal zone. Most of the force produced by waves was typically expended on those rocks. *P. planum* colonies were nevertheless subjected to surge conditions as water from breaking waves flowed over and around the outcroppings during all but the lowest tides. Because *P. planum* lives low in the intertidal zone, my study sites were accessible for only hours at a time and only in months with sufficiently low tides. This somewhat limited access occasionally hampered data collection. For this paper describing patterns of colony growth, data from the three sites were pooled.

Three lag bolts were anchored at each site and used to locate the sites and to aid in mapping the locations of all *P. planum* colonies. A colony's position was mapped monthly by measuring the distance between its peduncular point of attachment and the three lag bolts. A mapped colony was then manipulated gently so that the full silhouette view of its zooid-bearing lobe (along with a 15-cm ruler, for scale) could be photographed. Colonies thus censused could thereafter be identified by their map coordinates and photorecords. Colonies that appeared on the study sites for the first time and were large enough to be positively identified as *P. planum* (with a lobe-silhouette area typically between 50 and 200 mm^2) were referred to as "recruits." A colony's post-recruitment life span ended when it was dislodged from its mapped location.

Photographs of colonies were digitized, and the silhouette areas of zooid-bearing lobes were measured by means of video imagery analysis (Image version 1.43).

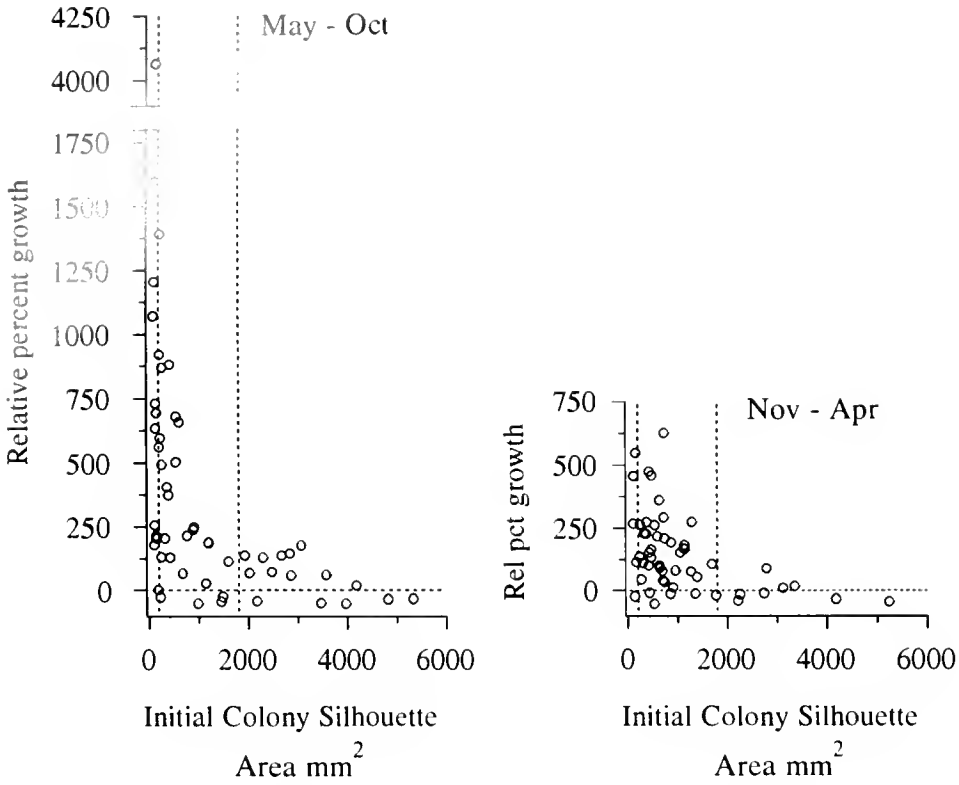

Figure 3. Relative percent growth of *Polyclinum planum* colonies by size and season. The graph on the left shows growth of 55 colonies during calm, warm-water months; the graph on the right shows growth of 53 colonies during months with colder, rough sea-state conditions. Vertical dashed lines delineate colony size classes (small = <200 mm^2 lobe-silhouette area; medium = 200–1800 mm^2; large = >1800 mm^2).

Lobe silhouette areas were used to generate a mean growth trajectory for *P. planum*. I used stepwise polynomial regression (Zar, 1984) as a descriptive tool to fit a curve to the mean growth data. That curve should not be used to make statistical comparisons, however, because the monthly data included individual colonies that were sampled multiple times (*i.e.*, in consecutive months), and therefore violate the assumptions of independence required for regression analysis. Consequently, comparisons of *P. planum*'s mean growth trajectory to theoretical growth curves are unavoidably qualitative.

To determine where new material (zooids and tunic) is added to zooid-bearing lobes of growing colonies, I manipulated eight of the colonies on my sites. I tied loops of cotton-wrapped nylon thread through three points on their lobes—one loop through the lobe near the peduncle, one loop through the center of the lobe, and one loop through the lobe near the lobe tip. In successive months I measured distances between those marks, and between the marks and lobe edges.

In April 1991 I began measuring the thickness of lobes and calculating a lobe flatness value for each colony by dividing a lobe's maximum width by its maximum thickness. Spheroidal lobes had flatness values of 1.0, and colonies with lobes wider than they were thick had flatness values greater than 1.0. Those values were used to generate a mean trajectory of lobe flattening for *P. planum*. I again used stepwise polynomial regression to fit a curve to the trajectory of lobe flattening.

At the end of my study, in May 1992, I collected 77 *P. planum* colonies from the study sites to test for relationships between colony age, size, and reproductive state. Those colonies ranged from 66 mm^2 to 5661 mm^2 in size (colony-silhouette area) and from 1 to 24 months in age.

I determined the reproductive state of those colonies by cutting three wedge-shaped pieces from the lobe of each colony—one from the lobe tip and one from each lateral edge of the colony. I counted the total number of exposed zooids on one side of each wedge, the number of those zooids undergoing strobilation, and the total number of larvae brooded by the nonstrobilating zooids. I also dissected the post-abdomen from four nonstrobilating zooids per wedge and measured the largest oocyte from each one. I used chi-square analyses to test for effects of colony age and colony size on reproductive

condition of *P. planum*. I also used linear regression to test for the effect of colony age on colony size.

Results

Polyclinum planum colonies were present on the research sites throughout the study. Recruitment and dislodgement of colonies occurred year-round, as did colony growth. The colonies did not fragment: each recruit produced only one pedunculate colony. During the study 211 *P. planum* colonies appeared at the study sites as recruits and became dislodged between 1 and 23 months later. The mean value for maximum lobe-silhouette area attained by those colonies was 803.0 mm^2 (SD = 1224.4 mm^2; n = 211 colonies). The largest of those colonies had a lobe-silhouette area of 8511 mm^2 at 17 months of age.

The mean post-recruitment life span of *P. planum* was 5.52 months (SD = 5.49 months; n = 211 colonies). The longest-lived colony on my sites persisted an exceptional 24 months. That colony did not become dislodged during the course of this study, so it was not used in analyses that included data only from colonies that did become dislodged.

Mean growth trajectory

Mean colony size was plotted against age in months to generate a growth trajectory for *P. planum* (Fig. 2). The mean growth trajectory included a period of rapid growth throughout the first 10–12 months, followed by a period of attenuating growth to a mean maximum size of 1759 mm^2 at month 15. The growth trajectory also indicated a decline in colony size among older colonies. Most colonies aged 14 months or older (21 of 27 colonies = 77.8%) decreased in lobe-silhouette area before being dislodged. The 21 colonies that experienced a size decrease lost an average of 42.4% (SD = 25.5%) of their maximum lobe-silhouette area prior to dislodgement. Some colonies decreased in size gradually, by abrasion; others lost larger pieces of their lobes, presumably in a single event, the explanation of which remains problematic.

The growth data also revealed increasing size variability within age classes throughout the first 9 months. After the 9th month standard deviations were so wide in some age classes that they overlapped the mean values of virtually all other age classes (for example, see Fig. 2, months 9, 12, 13, and 18). This trend suggests that colony age and size were not as tightly linked among larger colonies as among smaller ones, thus demonstrating the indeterminate nature of *P. planum* colony growth.

Relative percent growth of *P. planum* colonies, comparing colony-silhouette area at the beginning and end of 6-month intervals—May through October (months with calmer sea-state conditions) or November through April (months with rougher sea-state conditions)—confirmed the general trends of size-specific growth indicated by the mean growth trajectory. Smaller colonies grew more rapidly than larger colonies (Fig. 3). Those growth data also suggest a seasonal effect on growth rates: the smallest size class of colonies exhibited much greater increases in relative percent growth during periods of calmer and warmer sea-state conditions (between May and October) than did colonies of similar initial size during rougher and cooler sea-state conditions (between November and April).

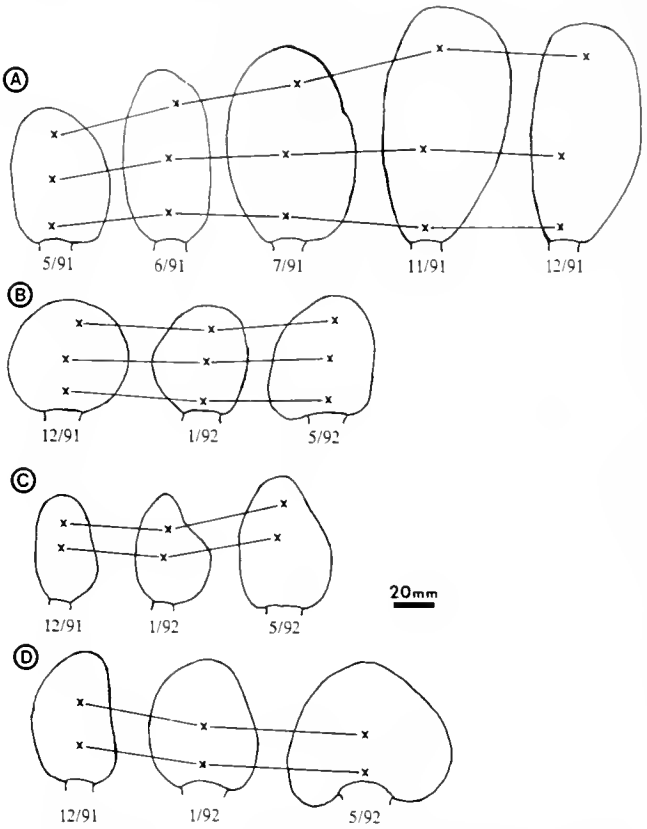

Figure 4. Patterns of lobe expansion for four colonies with marked lobes. An "X" indicates the location where a loop of thread was tied through the zooid-bearing lobe.

To test for seasonal effects on size-specific relative percent growth, I assigned colonies to three size classes: (1) small (<200 mm^2 colony-silhouette area; the size of most recruits); (2) medium (200–1800 mm^2; colonies larger than recruits but smaller than the maximum size indicated by the growth trajectory); and (3) large (>1800 mm^2; colonies larger than the maximum colony area indicated by the growth trajectory). T-tests showed a significant seasonal effect on growth of medium-sized colonies (t = 3.309; df = 65; P = 0.0014). There was no seasonal effect on growth of large colonies (t = 1.874; df

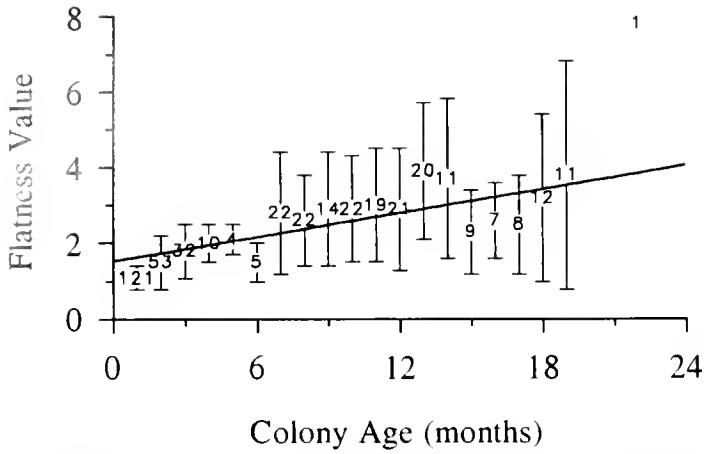

Figure 5. Mean trajectory of lobe flattening for *Polyclinum planum*. A linear regression provides a significant fit to the data ($Y = 1.528 + 0.106x$; $r^2 = 0.568$; $t = 4.73$; df = 17; $P < 0.001$). Error bars are standard deviations, and numbers indicate the number of observations included in each age class. The single outlier at month 23 was not included in the curve-fitting analysis. The numbers of colonies indicated per month on this figure differ from those of Figure 2 because I began measuring lobe thicknesses in April 1991, and I began measuring lobe silhouette areas (shown in Fig. 2) in December 1989.

= 22; $P = 0.074$) or small colonies ($t = 1.246$; df = 15; $P = 0.232$). The lack of a seasonal effect on small colonies is probably due to the extremely wide variability of growth displayed by small colonies in the May–October group (Fig. 3).

Intra-colony growth

Four of eight colonies with marked lobes persisted long enough to show where *P. planum* can add new material to the zooid-bearing lobe (Fig. 4). Colony A added new material in a diffuse manner throughout the length and width of its lobe. More material was added between the middle mark and the mark furthest from the peduncle than between the middle and proximal marks. After July 1991, colony A also added more material along its right side than along its left side. Colony B decreased slightly in size in January 1991, after which material was added to the left side of the colony. Colony C added more material to the lobe proximal to the peduncle than distally, causing the two marked spots on this colony to move away from the peduncle but not much farther from each other. Colony C also added material along the left and right sides of the lobe. Colony D added material along the right and left sides of its lobe, producing a spade-shaped silhouette. The peduncle of that colony also expanded upward into the lobe, causing the marked spots to appear to move closer to the peduncle.

Mean trajectory of lobe flattening

Zooid-bearing lobes of small colonies changed gradually from a spheroidal shape to a laterally flattened discoidal shape as they grew (Fig. 5), becoming what were essentially bilayered sheets of zooids. Lobes of recruits had a mean cross-sectional flatness value of 1.1 (SD = 0.3; $n = 121$ recruits appearing between April 1991 and May 1992). The flattest colony measured was 20 months old; it had a lobe width of 113.5 mm and a flatness value of 12.6. Stepwise polynomial regression showed that a linear function best described changes in colony flatness. The mean flatness value of the regression was 2.53. The linear function of the regression shows that ratios of lobe width to thickness typically increase throughout a colony's life span. Increases in lobe-flatness values are largely the result of the expansion of lobe width, because lobe thickness typically did not decrease during a colony's life span.

Recruitment and survivorship

Simple (least squares) linear regression showed that the number of *P. planum* recruits appearing at the study sites each month was not significantly dependent upon surface water temperatures (Fig. 6; $r^2 = 1.46 \times 10^{-6}$; df = 1,21; $P > 0.75$) (seawater temperatures were measured daily by HMS staff). Likewise, the number of recruits appearing monthly at the study sites was not dependent upon the number of days of strong surge conditions per month ($r^2 = 0.022$; df = 1,21; $P = 0.5$). Seawater temperature and surge conditions were measured by HMS staff. Linear regression of the number of colonies dislodged per month on water temperature did, however, indicate a significant relationship ($r^2 = 0.345$; df = 1,21; $P < 0.005$), as did the regression of the number of colonies dislodged per month on the number of days of strong surge per month ($r^2 = 0.256$; df = 1,21; $P < 0.025$).

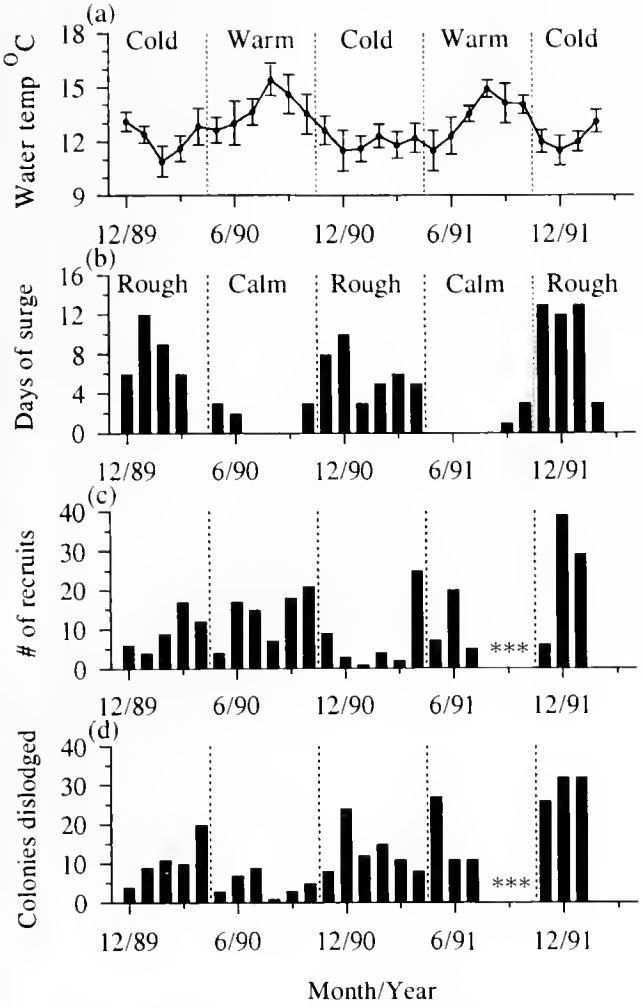

Figure 6. (a) Mean monthly surface seawater temperature at Hopkins Marine Station (HMS); (b) number of days of strong surge conditions per month at HMS; (c) number of recruits appearing at the research sites per month; (d) and number of colonies dislodged from research sites per month. Vertical dashed lines indicate break points between warm months with calm sea-state conditions and colder water months with rougher sea-state conditions. Asterisks on the two lower graphs indicate months during which data could not be collected. Data on seawater temperature and sea-state condition were collected by and provided courtesy of HMS staff.

Significantly more colonies were dislodged from the study sites during months with rough (as defined by HMS staff) sea-state conditions (Nov–Apr; $\bar{x}$ = 7.2 days of strong surge per month; SD = 3.7 days) than during months with calmer sea-state conditions (May–Oct; $\bar{x}$ = 1.0 day of strong surge per month; SD = 1.3 days), as indicated in Table 1.

For both small and large colonies, the proportion of colonies dislodged was significantly larger during rough months than during calm months (Table 1). There was, however, no statistical difference between the proportion

Table 1

The number of Polyclinum planum *colonies dislodged per size class by season*

	Colony size class (colony-silhouette area in mm^2)		
	0–200	200–1800	>1800
Strong surge (Nov–Apr)	75 (62.5)	74 (69.9)	44 (31.4)
Calm (May–Oct)	21 (33.5)	39 (43.1)	13 (25.6)
Column χ^2 values	7.16*	0.63 NS	11.26***
Contingency table χ^2 value = 19.05***			

The results of a chi-square analysis of this 2 × 3 contingency table and the results of chi-square tests for each column are indicated. Numbers in parentheses are the expected values for each cell.
* = $P < 0.01$; *** = $P < 0.001$; NS = not significant.

of medium-sized colonies dislodged in rough *versus* calm months. The medium-sized colonies had survived early post-recruitment mortality but had not grown large enough to exceed the maximum growth trajectory.

Age- and size-dependent survivorship data (Fig. 7) showed that the greatest mortality occurred among the youngest colonies (39.3%—83 of 211 colonies) and among the smallest colonies (47.9%—101 of 211 colo-

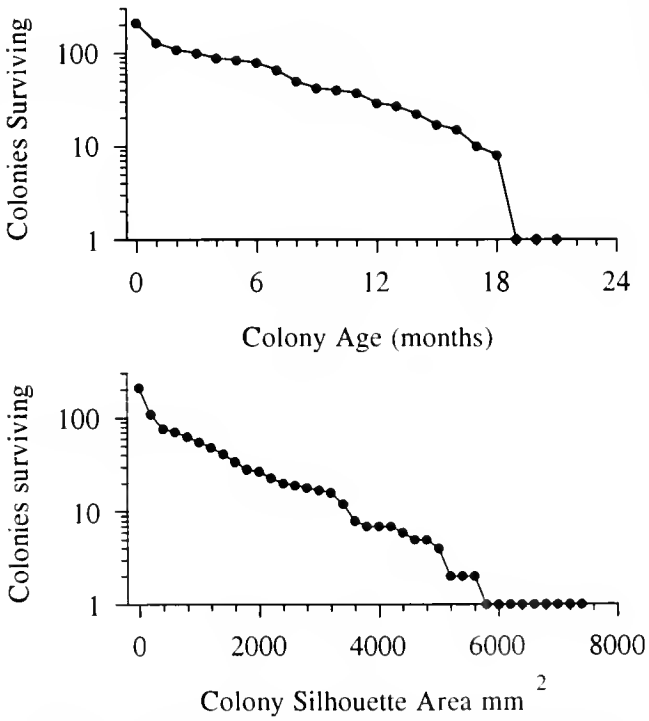

Figure 7. Age-dependent and size-dependent survivorship curves for *Polyclinum planum*.

Table II

Comparisons of number of colonies in each size class with zooids undergoing strobilation, bearing oocytes, and brooding larvae

	Colony size classes (colony silhouette area in mm^2)		
	0–200	200–1800	>1800
Strobilation			
100% zooid strobilation	11 (5.45)	23 (23.64)	1 (5.91)
<100% zooid strobilation	1 (6.55)	29 (28.36)	12 (7.09)
Column χ^2 values	10.35**	0.18 NS	7.48*
Contingency table χ^2 value = 18.01***			
Oocytes			
Oocytes present	0 (2.03)	7 (8.78)	6 (2.19)
Oocytes not present	12 (9.97)	45 (43.2)	7 (10.81)
Column χ^2 values	2.44 NS	0.47 NS	7.97**
Contingency table χ^2 value = 10.88**			
Brooded Larvae			
Brooded larvae present	0 (0.94)	2 (4.05)	4 (1.01)
Larva not present	12 (11.06)	50 (47.95)	9 (11.99)
Column χ^2 values	1.02 NS	1.12 NS	9.60**
Contingency table χ^2 value = 11.74**			

The results of a chi-square analysis of this 2 × 3 contingency table and the results of chi-square tests for each column are indicated. Numbers in parentheses indicate the expected values for each cell. * = $P < 0.01$; ** = $P < 0.005$; *** = $P < 0.001$; NS = not significant.

nies with silhouette areas smaller than 200 mm^2). After those initial losses, both age- and size-specific survivorship curves indicated a nearly constant rate of mortality, with possible increased mortality among the largest colonies.

Reproductive state

Results of chi-square analyses of the effects of colony size and colony age on reproductive state of colonies collected in May 1992 are shown in Tables II and III, respectively. For colonies of the smallest size class (<200-mm^2 colony-silhouette area), the frequencies of colonies bearing strobilating zooids were higher than expected; in medium-sized colonies (200–1800 mm^2) the frequencies did not differ from expected values; and in large colonies (>1800 mm^2) the frequencies were lower than expected. The large size class also had higher-than-expected frequencies of colonies with developing oocytes and of brooding larvae, whereas the other size classes did not differ significantly from expected values for those parameters (Table II).

Results of chi-square analyses on colony age class and reproductive state showed a significant age effect on the frequency of strobilating colonies among the youngest age class (colonies 1 month old), but the other age classes did not differ significantly from expected values for strobilation. Age-class comparisons of the frequency of colonies bearing developing oocytes or brooded larvae did not differ from expected values (Table III). There was, however, a significant relationship between colony age and colony size (Fig. 8). Colony size appears to be a better predictor of reproductive state that colony age, but colony size is affected by colony age, because the smallest colonies tend to be young, and larger colonies tend to be older.

I used multiple regression analysis to ascertain the relative effects of colony size and colony age on oocyte size. That analysis was significant, explaining 36.87% of observed variability ($F = 21.96$; df = 2,75; $P < 0.001$). Colony size accounted for 99.9% of the variability explained by the regression, whereas colony age contributed only an additional 0.01% to the explanation ($F = 0.035$ *NS;* df = 1,75; $P > 0.75$). Colony size may thus be invoked as a primary determinant of oocyte size; colony age has a secondary effect on oocyte size because it affects colony size.

Discussion

Polyclinum planum colonies do not fragment into physiologically isolated ramets as they grow. This observation bears out the assumption made by Pearse *et al.*

Table III

Comparisons of number of colonies in each age class with zooids undergoing strobilation, bearing oocytes, and brooding larvae

	Colony age classes (months)		
	1	2–15	>15
Strobilation			
100% zooid strobilation	10 (4.85)	23 (27.38)	1 (1.76)
<100% zooid strobilation	1 (6.15)	39 (34.62)	3 (2.24)
Column χ^2 values	9.78**	1.25 NS	0.59 NS
Contingency table χ^2 value = 11.62**			
Oocytes			
Oocytes present	0 (1.85)	12 (10.47)	1 (0.68)
Oocytes not present	11 (9.15)	50 (51.53)	3 (3.32)
Contingency table χ^2 value = 3.20 NS			
Brooded larvae			
Larvae present	0 (0.86)	6 (4.83)	0 (0.31)
Larvae not present	11 (10.14)	56 (57.17)	4 (3.69)
Contingency table χ^2 value = 1.57 NS			

The results of a chi-square analysis of this 2 × 3 contingency table, and, when the contingency test is significant, the results of chi-square tests for each column are indicated. Numbers in parentheses indicate expected values for each cell. ** = $P < 0.005$; NS = nonsignificant.

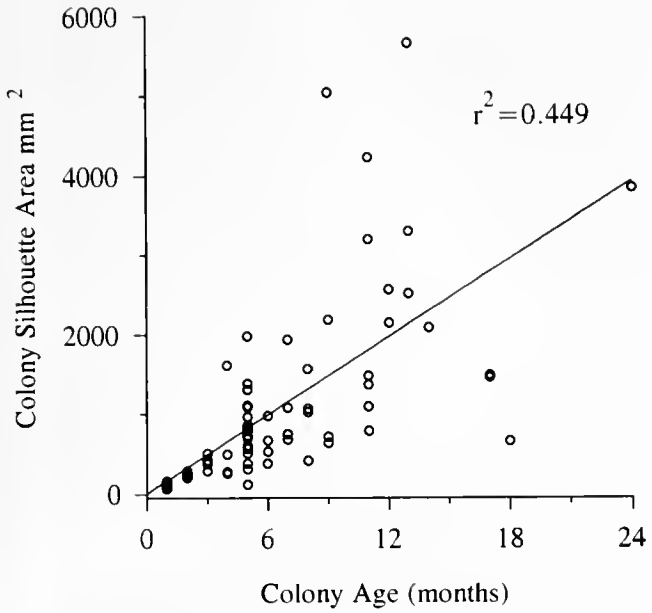

Figure 8. The relationship between colony age and colony size for *Polyclinum planum* collected in May 1992 ($n = 77$ colonies). The solid line indicates the linear regression, which was significant at $\alpha = 0.05$.

(1989) that this is a nonfragmenting species and means that each *P. planum* colony represents an entire genet. As such, the loss of a *P. planum* colony is a greater loss, in an evolutionary sense, than if it were only one of several physiologically isolated ramets. *P. planum* has consequently developed growth-related adaptations that increase the chances of colony survivorship even in physically stressful intertidal environments.

The most obvious ecological risk to erect, though flexible, intertidal colonies of *P. planum* is dislodgement by water-flow forces. Denny *et al.* (1985) demonstrated how such forces can dislodge or limit the size of intertidal organisms living in wave-impacted environments. Since intertidal *P. planum* colonies are subjected to those kinds of water flow forces, it is not surprising that this species exhibits growth-related adaptations for dealing with stresses associated with water flow. The pattern of *P. planum* colony growth reveals two strategies for mitigating the effects of water flow: (1) an attenuating pattern of growth; and (2) allometric expansion of the zooid-bearing lobe into a laterally flattened structure.

Attenuating growth, like that demonstrated by *P. planum* (see Fig. 2), is common among colony-forming modular organisms such as corals (Hughes and Connell, 1987; Karlson, 1988; Lasker, 1990), bryozoans (Hughes, 1990; Kauffman, 1981), and ascidians (Ryland *et al.*, 1984; Stoner, 1989; Stocker, 1991). In the case of *P. planum*, it appears that environmental stress limits colony size. The general pattern of *P. planum*'s attenuating growth is several months of rapid growth followed by slowing and eventual cessation of growth. A few colonies did, however, grow continuously until they were dislodged. The typical pattern of *P. planum* growth does not differ markedly from Sebens' (1987) predictions for Indeterminate Growth Type III (Plastic Attenuating Growth), but the growth pattern of a few colonies approximated Sebens' Indeterminate Growth Type II (Plastic exponential growth).

The maximum size for a *P. planum* colony is set, at least in part, by water-flow forces. This is evidenced by the fact that some colonies, probably in protected microhabitats, produced lobes much larger than 1800 mm^2 (colony-silhouette area—the maximum colony size indicated by *P. planum*'s mean growth trajectory—see Fig. 2), even though susceptibility to dislodgement increased for other colonies when their silhouette areas exceeded 1800 mm^2 (see Table I). Similar water-flow-induced size restrictions have been suggested or demonstrated for colony-forming modular organisms such as sea fans (Birkeland, 1974) and coral (Denny *et al.* 1985), and for unitary organisms including sea urchins, limpets, mussels, and snails (Denny *et al.*, 1985).

Life-history constraints also limit colony growth. As *P. planum* colonies increase in size, they tend to become reproductively active (see Table II). The onset of reproduction is a critical event in the life history of any organism (Lloyd, 1980; Sebens, 1982; Kozlowski and Weigert, 1986). A shift from growth to reproductive activity in *P. planum* appears to occur as the rate of colony growth slows. This relationship between growth and reproduction apparently occurs not only in colonies of *P. planum* but among colonies of some other ascidians (Bak *et al.*, 1981; Brunetti *et al.*, 1988). For some clonal taxa, however, the event triggering the onset of reproductive activity can vary greatly and may include colony age, size, or environmental stimuli; in other cases neither colony age nor size is a good predictor of the onset of reproduction (Harvell and Grosberg, 1988).

Slowed growth at the onset of reproductive activity in *P. planum* is a consequence of life-history constraints on individual zooids. *P. planum* zooids are hermaphroditic, producing sperm and oocytes in gonads housed in the post-abdomen (Ritter and Forsyth, 1917). Iterative production of new zooids (*i.e.*, colony growth) involves strobilation of the post-abdomen, where gonads develop, and disorganization of the atrial chamber (Holyoak, 1992), where larvae are brooded. As a result, a *P. planum* zooid cannot simultaneously undergo strobilation and produce gametes or brood larvae.

The second growth-related strategy that *P. planum* uses to minimize the effects of water flow involves morphogenesis of the zooid-bearing lobe from a small spheroidal structure into a large laterally flattened one. Changes in the silhouette shape of marked colonies sug-

gest that *P. planum* is able to add material to just about any part of a growing lobe, thereby producing a wide range of colony shapes (see Fig. 4).

The ecological advantage of lobe flattening is evident when the morphology of *P. planum* colonies is considered in light of the acceleration of water, which, according to Denny *et al.* (1985), is the water-flow force with the greatest ability to dislodge sessile organisms. The impact of the acceleration reaction of water is directly proportional to an object's volume, not to its exposed surface area (Denny, 1993). If the spheroidal lobe of a *P. planum* recruit were to increase in size isometrically, producing a large spherical lobe, the stress from the acceleration reaction and the chance of dislodgement would hypothetically be greater for that colony than for one with a flattened lobe having the same frontal silhouette area.

Increased reproductive potential is a direct benefit of colony growth and lobe flattening. A flattened lobe has a greater surface-to-volume ratio than a spheroidal lobe. Because zooids are located only at the surface of *P. planum* colonies (Abbott, 1987), a flat lobe can house more zooids than a spheroidal lobe with the same volume. And since each zooid has the potential to produce gametes and brood larvae, the reproductive capacity of a colony is directly proportional to the number of zooids it contains. *P. planum* is therefore able to increase its surface area, maximize the number of zooids it can bear, and simultaneously minimize the effects of the water acceleration reaction by producing a flattened lobe.

One final consequence of growth is its impact on the mortality rate of recruits (Table 1). Though growth beyond an environmentally imposed size limit puts the largest colonies at risk, the greatest observed mortality occurred among the smallest and youngest colonies (Fig. 7). Birkeland (1974) reported a similar trend of high mortality among smaller members of a population of sea fans growing in heavy surf. High mortality among the smallest size class of *P. planum* colonies is almost certainly a function of site selection by larvae at settlement. The long-term suitability of a site is not tested until colonies grow large enough to extend beyond the boundary layer. Only colonies with the best settlement sites and the firmest peduncular attachments will survive to grow into the larger size classes. Mortality among small colonies is almost certainly a consequence of growth because *P. planum* has no known predators, and I saw no evidence of predation on any colonies during this study.

In conclusion, colony-level growth and morphogenesis of modular organisms are large-scale effects of self-assembly processes. Those processes include the temporal and spatial iteration and arrangement of modules (Rosen, 1986; Ryland and Warner, 1986). The result of those processes is colony morphology that can convey ecological advantage (*e.g.*, Ryland and Warner, 1986, and references therein). Though we are learning more about the complexities and significance of modular growth, we are still largely ignorant of the mechanisms that regulate it. My data suggest that growth in *P. planum* may be regulated by a combination of external and internal factors. As we unravel the rules of colony-level modular growth, we may gain insights into the processes that regulate and drive development at other levels of biological organization.

Acknowledgments

I thank A. T. Newberry, J. S. Pearse, C. M. Young, B. Rinkevich, and two anonymous reviewers for their helpful comments on drafts of the manuscript. Support for this study was provided by the Department of Biology, University of California at Santa Cruz; Friends of the Long Marine Laboratory; the American Museum of Natural History (Lerner-Gray Fund for Marine Research); the Earl and Ethel Myers Oceanographic and Marine Biology Trust; and Manchester College.

Literature Cited

Abbott, D. P. 1987. *Observing Marine Invertebrates.* Stanford Univ. Press, Stanford.

Bak, R. P. M., J. Sybesma, and F. C. vanDuyl. 1981. The ecology of the tropical ascidian *Tridemnum solidum.* II. Abundance, growth and survival. *Mar. Ecol. Prog. Ser.* **6:** 43–52.

Berrill, N. J. 1950. *The Tunicata.* The Ray Society, London.

Birkeland, C. 1974. The effect of wave action on the population dynamics of *Gorgonia ventalina* Linnaeus. *Stud. Trop. Oceanogr.* **12:** 115–126.

Brunetti, R., M. Bressan, M. Marin, and M. Libralato. 1988. On the ecology and biology of *Diplosoma listerianum* (Milne Edwards, 1841) (Ascidiacea, Didemnidae). *Vie Milieu* **38:** 128–131.

Denny, M. W. 1993. *Air and Water: The Biology and Physics of Life's Media.* Princeton Univ. Press, Princeton.

Denny, M. W., T. L. Daniel, and M. A. R. Koehl. 1985. Mechanical limits to size in wave-swept organisms. *Ecol. Monogr.* **55:** 69–102.

Harvell, C. D., and R. K. Grosberg. 1988. The timing of sexual maturity in clonal animals. *Ecology* **69:** 1855–1864.

Holyoak, A. R. 1992. Morphogenetic movements and assembly of strobilae into zooidal systems in early colony development of the compound ascidian *Polyclinum planum.* *Biol. Bull.* **183:** 432–439.

Hughes, T. P. 1984. Population dynamics based on individual size rather than age: a general model with a reef coral example. *Am. Nat.* **123:** 778–795.

Hughes, T. P. 1990. Recruitment limitation, mortality, and population regulation in open systems: a case study. *Ecology* **71:** 12–20.

Hughes, T. P., and J. B. C. Jackson. 1980. Do corals lie about their age? Some demographic consequences of partial mortality, fission, and fusion. *Science* **209:** 713–715.

Hughes, T. P., and J. B. C. Jackson. 1985. Population dynamics and life histories of foliaceous corals. *Ecol. Monogr.* **55:** 141–166.

Hughes, T. P., and J. H. Connell. 1987. Population dynamics based on size or age? A reef coral analysis. *Am. Nat.* **129:** 818–829.

Jackson, J. B. C. 1977. Competition on marine hard substrata: the adaptive significance of solitary and colonial strategies. *Am. Nat.* **111:** 743–767.

Jackson, J. B. C., and A. G. Coates. 1986. Life cycles and evolution

of clonal (modular) animals. *Phil. Trans. R. Soc. Lond. B* **313:** 7–22.

Karlson, R. H. 1986. Disturbance, colonial fragmentation, and size-dependent life history variation in two coral reef cnidarians. *Mar. Ecol. Prog. Ser.* **28:** 245–249.

Karlson, R. H. 1988. Size-dependent growth in two zoanthid species: a contrast in clonal strategies. *Ecology* **69:** 1219–1232.

Kauffman, K. W. 1981. Fitting and using growth curves. *Oecologia* **49:** 293–299.

Kozlowski, J., and R. G. Weigert. 1986. Optimal allocation of energy to growth and reproduction. *Theor. Popul. Biol.* **29:** 16–37.

Lasker, H. R. 1990. Clonal propagation and population dynamics of gorgonian coral. *Ecology* **71:** 1578–1589.

Lloyd, D. G. 1980. Benefits and handicaps of sexual reproduction. *Evol. Biol.* **13:** 69–111.

McFadden, C. S. 1991. A comparative demographic analysis of clonal reproduction in a temperate soft coral. *Ecology* **72(5):** 1849–1866.

Millar, R. H. 1952. The annual growth and reproductive cycle in four ascidians. *J. Mar. Biol. Assoc. U. K.* **31:** 41–61.

Millar, R. H. 1971. The biology of ascidians. *Adv. Mar. Biol.* **9:** 1–100.

Pancer, Z., H. Gershon, and B. Rinkevich. 1995. Coexistence and possible parasitism of somatic and germ cell lines in chimeras of the colonial urochordate *Botryllus schlosseri*. *Biol. Bull.* **189:** 106–112.

Pätzold, J., H. Ristedt, and G. Wefer. 1987. Rate of growth and longevity of a large colony of *Pentaflora foliacea* (Bryozoa) recorded in their oxygen isotope profiles. *Mar. Biol.* **96:** 535–538.

Pearse, J. S., V. B. Pearse, and A. T. Newberry. 1989. Telling sex from growth: dissolving Maynard Smith's paradox. *Bull. Mar. Sci.* **45:** 433–446.

Rinkevich, B., and I. L. Weissman. 1987a. Chimeras in colonial invertebrates: a synergistic symbiosis or somatic- and germ-cell parasitism? *Symbiosis* **4:** 117–134.

Rinkevich, B., and I. L. Weissman. 1987b. A long-term study on fused subclones in the ascidian *Botryllus schlosseri*: the resorption phenomenon (Protochordata: Tunicata). *J. Zool. (Lond.)* **213:** 717–733.

Ritter, W. E., and R. A. Forsyth. 1917. Ascidians of the littoral zone of southern California. *Univ. Calif. Publ. Zool.* **16:** 439–512.

Rosen, B. R. 1986. Modular growth and form of corals: a matter of metamers? *Phil. Trans. R. Soc. Lond. B* **313:** 115–142.

Ryland, J. S., and G. F. Warner. 1986. Growth and form in modular animals: ideas on the size and arrangement of zooids. *Phil. Trans. R. Soc. Lond. B* **313:** 53–76.

Ryland, J. S., R. A. Wigley, and A. Muirhead. 1984. Ecology and colonial dynamics of some Pacific reef flat Didemnidae (Ascidiacea). *Zool. J. Linn. Soc.* **80:** 261–282.

Sebens, K. P. 1982. The limits of indeterminate growth: an optimal size model applied to passive suspension feeders. *Ecology* **63:** 209–222.

Sebens, K. P. 1987. The ecology of indeterminate growth in animals. *Ann. Rev. Ecol. Syst.* **18:** 371–407.

Stoner, D. S. 1989. Fragmentation: a mechanism for the stimulation of genet growth rates in an encrusting colonial ascidian. *Bull. Mar. Sci.* **45:** 277–287.

Stocker, L. J. 1991. Effects of size and shape of colony on rates of fission, fusion, growth and mortality in a subtidal invertebrate. *J. Exp. Mar. Biol. Ecol.* **149:** 161–175.

Zar, J. H. 1984. *Biostatistical Analysis, 2nd ed.* Prentice-Hall, Inc., Englewood Cliffs, NJ.

Reference: *Biol. Bull* **192:** 98–110. (February, 1997)

Conflicting Morphological and Reproductive Species Boundaries in the Coral Genus *Platygyra*

KAREN MILLER[1,*] AND RUSSELL BABCOCK[2,†]

[1]*Marine Biology Dept, James Cook University of North Queensland, Townsville, QLD 4811, Australia; and* [2]*Australian Institute of Marine Science, PMB 3, Townsville, QLD 4810, Australia*

Abstract. In mass-spawning corals, potential exists for gametes of a number of species to mix in the water column. The existence of morphologically distinct sympatric coral populations despite such an event implies the presence of isolating mechanisms to prevent hybridization and maintain species boundaries. Over 380 fertilization trials were conducted to determine the extent of reproductive isolation among the seven morphologically defined species (morphospecies) of the scleractinian coral genus *Platygyra*, on the Great Barrier Reef. Results from these experiments demonstrate that fertilization between-morphospecies can occur at rates equivalent to within-morphospecies fertilizations, indicating that no gametic-level barriers to fertilization exist among these morphological species. Observations of spawning times both in the field and in the laboratory have shown that all seven morphospecies spawn on the same night and that there is considerable overlap in the hour of spawning among them. These data indicate that few, if any, temporal barriers to fertilization exist among morphospecies of *Platygyra* on the Great Barrier Reef. In addition, larvae resulting from between-morphospecies crosses are capable of settlement and subsequent growth equivalent to that of within-morphospecies larvae. Our results reveal a discontinuity between reproductive and morphological species boundaries within the scleractinian genus *Platygyra* and challenge species definitions within the Scleractinia. It is not yet clear what mechanisms might maintain morphological boundaries in *Platygyra* in the face of the clear potential for gamete mixing. The disjunct distributions of certain morphospecies along latitudinal and habitat boundaries, and the small levels of variation in reproduction may be two such mechanisms.

Received 18 July 1996; accepted 21 November 1996.

* Present address: National Institute of Water and Atmospheric Research, PO Box 14-901, Kilbirnie, Wellington, New Zealand.

† Present address: University of Auckland, Leigh Marine Laboratory, P.O. Box 349, Warkworth, New Zealand.

Introduction

Species boundaries in scleractinian corals are primarily based on skeletal morphology (*e.g.*, Ellis and Solander, 1786; Vaughan and Wells, 1943; Veron *et al.*, 1977; but see Lang, 1984). It is generally assumed that morphological differences between coral species are highly correlated with reproductive incompatibility (*i.e.*, biological species boundaries) (Willis, 1990) and that traditional theories of hierarchical evolution and speciation (*e.g.*, Darwin, 1859) will apply to corals.

Recognition that most of the corals on the Great Barrier Reef reproduce annually during a mass spawning event (Harrison *et al.*, 1984; Willis *et al.*, 1985; Babcock *et al.*, 1986) has prompted an examination of assumptions that morphological species boundaries reflect biological species boundaries within the Scleractinia (Wallace and Willis, 1994). The persistence of morphologically distinct species groups (*e.g.*, Veron *et al.*, 1977) coupled with mass spawning events, whereby gametes of many species become mixed within the water column, implies the presence of some mechanism to prevent hybridization and hence maintain species boundaries (Willis, 1990). The benefit of such mechanisms was supported by results from experimental crosses in the genus *Montipora*, in which hybridization was documented but considered to be maladaptive due to arrested development in hybrid embryos (Hodgson, 1988). More recently, however, fertilization experiments have indicated that successful fertilization *in vitro* is possible among some morphological coral species (Willis *et al.*, 1992), although how experimental fertilization relates to field fertilization is unknown.

The coral genus *Platygyra* includes morphological species (morphospecies) from the Great Barrier Reef; *Platygyra daedalea, P. sinensis, P. pini, P. lamellina, P. ryukyuensis, Platygyra* 'B', and *Platygyra* 'H' (see Miller, 1994a, b). These morphological species have been recognized by traditional taxonomy (*e.g.,* Chevalier, 1975; Veron *et al.,* 1977; Veron, 1993) and numerical taxonomy (Miller, 1994a), although both approaches have recognized a continuum of separate characters among the species. Based on the occurrence of morphologically distinct species of *Platygyra,* it seems highly likely that mechanisms exist that promote reproductive incompatibility and subsequently maintain species differences within the genus.

Contrary to expectations, genetic comparisons show no differentiation between the morphological species of *Platygyra* (Miller and Benzie, in press). The high genetic similarity of *Platygyra* morphospecies may reflect recent speciation events following which little genetic divergence has taken place (Miller and Benzie, in press). Alternatively, gene exchange may occur naturally between the morphological species groups, and hence the morphological boundaries in this genus may not necessarily represent reproductive isolation between species. The relationship between reproductive and morphological species boundaries within *Platygyra* and the presence or absence of reproductive isolation between the morphological species therefore need to be established.

A number of mechanisms, including pre- and post-zygotic barriers, could mitigate reproductive isolation between coral species. In *Platygyra,* there is some indication of temporal differences (in the order of hours) in spawning times among some of the morphospecies (Babcock *et al.,* 1986), although these observations involved only a few colonies, and variability in spawning times within morphospecies has not been documented. Coral gametes remain viable for at least 5 h in the water column (Oliver and Babcock, 1992), and it is not known whether these short temporal differences in spawning act as a complete isolating mechanism.

Sperm chemotaxis is used by a variety of marine invertebrates to attract conspecific sperm (*e.g.,* Miller, 1979, 1985), and may well be important in reducing potential for hybridization, for example, in pelagic communities of hydromedusae (Miller, 1979). Chemical sperm attractants have also been implicated as a mechanism to reduce hybridization in the coral genus *Montipora* (Coll *et al.,* 1994). However, even in *Montipora,* where sperm attractants have actually been identified, chemotaxis is not completely specific, and heterospecific attractants may still elicit a degree of chemotactic behavior between species (Coll *et al.,* 1994; Richard Miller, pers. comm.). At this point, the role of sperm chemotaxis as an effective isolating mechanism during mass spawning is still speculative.

Species-specific gamete-binding proteins have been described in some marine invertebrates, including abalone (Vacquier *et al.,* 1990) and sea urchins (Palumbi, 1992; Metz and Palumbi, 1996). Similar proteins may play an important role in the reproductive isolation of many free-spawning invertebrates, including scleractinian corals.

The high predictability of spawning in *Platygyra* species on the Great Barrier Reef (Babcock *et al.,* 1986) makes it possible to explore reproductive relationships and potential isolating mechanisms between these corals at the gamete level. In this paper, we document results from more than 380 trials that show potential for fertilization between the morphological species of *Platygyra.* Parallel field observations of spawning times suggest that few if any temporal reproductive barriers exist between the morphological species. This evidence suggests there are no pre-zygotic isolating mechanisms between the morphological species of *Platygyra.* Furthermore, we found no differences in the ability of larvae from within-morphospecies and between-morphospecies crosses to settle and grow. We also examined the effects of gamete aging, sperm dilution, and parental genotype on fertilization success.

The discovery that successful fertilization can occur between morphological species of *Platygyra* calls into question the previous assumption that morphological species boundaries equate with reproductive isolation and subsequently with evolutionary units. Our results prompt a reexamination of species definitions within the Scleractinia and indicate that species groupings based solely on morphology are clearly not always "biological" species (Mayr, 1942). Our data, combined with other recent findings in this field (Knowlton *et al.,* 1992; Van Veghel and Bak, 1993; Van Veghel, 1994; Wallace and Willis, 1994), suggest that species definitions in the Scleractinia should perhaps be based on a range of criteria, rather than solely on reproductive or morphological evidence. In addition, we suggest that in *Platygyra,* even with genetic exchange, discrete morphological groups will be maintained through a combination of spatial and temporal variability in reproductive processes and fitness in a variety of habitats.

Materials and Methods

We conducted fertilization experiments and observed spawnings over a 3½-year study period during seven consecutive spawnings at three reefs in the central Great Barrier Reef: Magnetic Island—19°10′ S, 146°51′ E (1990, 1991, 1992, 1993); Davies Reef—18°50′ S, 147°39′ E (1990, 1991); and Orpheus Island—18°35′ S, 146°29′ E

(1992). On the afternoon of the predicted mass spawning, gravid *Platygyra* colonies were transferred from the reef into separate containers and kept under natural light to simulate normal conditions. Colonies generally commenced spawning from dusk onwards. Once a colony had spawned, gamete bundles were collected from the surface of the water and sperm and eggs were separated by gentle agitation and use of a 105-μm sieve. Sperm were stored at room temperature (about 27°C) in a concentrated form to reduce aging (see Chia and Bickell, 1983; Oliver and Babcock, 1992) until required for fertilization. Eggs were taken through a series of 8 to 10 washes of 'sperm-free water' (collected half a kilometer from the edge of the reef on the afternoon before the commencement of spawning) to ensure the absence of any trace sperm. Eggs were stored in glass jars with gentle agitation until needed for experiments.

Eggs and sperm from different colonies were combined experimentally in 20-ml glass scintillation vials to examine fertilization success between colonies of different morphologies. Morphological species identification of all colonies used in fertilization trials was based on Miller (1994a). Concentrations of the stored sperm were estimated by five replicate hemacytometer counts and, just before fertilization, diluted to a concentration of approximately 2.5×10^6 sperm/ml. This sperm concentration has been shown to give optimum rates for fertilization in trials with *Platygyra sinensis* and other coral species (Oliver and Babcock, 1992). About 100 eggs were added to 20-ml aliquots of diluted sperm in a vial. Each cross was replicated either two or three times. Sperm concentrations within experimental vials were checked randomly and found to be within 10% of estimated concentrations.

Experiments were designed in a matrix system in which all colonies were crossed reciprocally with all other colonies (eggs A × sperm B and eggs B × sperm A, etc.), although trials between some morphological species have not yet been conducted due to the time constraints associated with coral spawning. All colonies were tested for their ability to self-fertilize (eggs A × sperm A, eggs B × sperm B, etc.). Replicate controls were prepared by placing eggs from each colony in 20 ml of sperm-free water to determine whether there had been any sperm contamination of washed eggs. Glass vials containing eggs and sperm were kept at ambient sea temperature with gentle agitation to allow fertilization to take place.

Fertilization in all replicate vials was recorded after 2–3 hours and again after 6–8 hours by censusing the first 100 eggs sampled from any one vial. Fertilization was scored as the initiation of cleavage, 2–3 h after fertilization (Babcock and Heyward, 1986). After about 7 h most of the embryos were blastulae. The condition of eggs and embryos in all crosses was recorded as either 'regular'—with even, symmetrical cleavages and apparently normal development (see Babcock and Heyward, 1986); or 'irregular'—with uneven, asymmetrical cleavages and abnormal development.

Analysis of fertilization data

Percent fertilization in crosses after 2–3 h and 6–8 h was based on the total number of eggs censused in each vial. Percent fertilization after 6–8 h was calculated to detect any increase in fertilization over egg-sperm contact time. The percentage of fertilized eggs developing to blastulae between the two counts for each vial was calculated as the number fertilized after 6–8 h (including cleavages and embryos) expressed as a percentage of the number of fertilized eggs after 2–3 h. Mean percent fertilization of the three replicate vials in each cross (colony pairing) was used for the analyses. Any crosses for which the controls showed sperm contamination of eggs during the washing process were not used in the analyses. Results from the seven spawnings at three reefs were combined at the level of morphological species for analysis.

A two-way analysis of variance (ANOVA) based on the percent fertilization data after 2–3 h was carried out to determine whether fertilization rates differed either between between-morphospecies and within-morphospecies fertilizations or between the different morphospecies (based on maternal colony type). The main effects were fertilization type (2 treatments; within and between morphospecies) and egg species (7 treatments; *Platygyra* B, *P. daedalea*, *Platygyra* H, *P. lamellina*, *P. pini*, *P. ryukyuensis*, *P. sinensis*). The analysis was repeated using the percent fertilization data after 6–8 h. A further two-way ANOVA was carried out to compare the development of cleaved eggs through to blastulae in within- and between-morphospecies crosses. All of these analyses were done using both arcsine-transformed and raw data. Both methods produced similar results and only results from analyses of raw data are presented here.

A one-way ANOVA comparing fertilization rates after 2–3 h between morphospecies combinations was also done to determine whether there were significant differences in fertilization between morphological species-pair crosses. Replication was too low to compare all morphospecies-pair crosses; consequently this analysis was carried out only on crosses in which *P. daedalea* was the maternal colony, and for the sperm of *P. daedalea*, *P. lamellina*, *P. pini*, *P. ryukyuensis*, *P. sinensis* and selfs. The incidence of irregular and regular embryos was compared between crosses to determine whether irregular embryos were more common in between-morphospecies crosses.

Effect of sperm concentration on fertilization rates

To determine whether fertilization success was an artifact of using optimal sperm concentrations in experi-

Table 1

Mean fertilization rates from fertilization trials between morphological species of Platygyra *based on all crosses tried over the 3½-year study period*

	Eggs							
Sperm	PD	PH	PL	PP	PR	PS	PB	Selfs
PD	**45.2** (0–100) $n = 49$	18.3 (0–58.9) $n = 5$	66.8 (41–90) $n = 13$	65.4 (0–100) $n = 11$	36.3 (0–84.1) $n = 8$	52.6 (0–99.1) $n = 18$	1.3 (0–6.3) $n = 2$	3.1 (0–6) $n = 28$
PH	47.5 (0–94.2) $n = 5$	**51.5** (9–95.8) $n = 2$	—	24.6 (0–62.5) $n = 4$	—	77.1 (0–100) $n = 2$	—	1.4 (0–4.1) $n = 2$
PL	68.2 (1–100) $n = 13$	—	**58.1** (41–84) $n = 6$	—	63.8 (40–77) $n = 2$	72.3 (41–91) $n = 2$	—	2.7 (0–6.2) $n = 4$
PP	66.6 (6.5–99) $n = 10$	17.4 (0–41.8) $n = 4$	—	**58.6** (1–96.7) $n = 4$	—	77.4 (26–98) $n = 2$	—	8.9 (0–15) $n = 5$
PR	66.1 (7–100) $n = 8$	—	90.5 (90–92) $n = 2$	—	**57.7** (31–71) $n = 2$	70.6 (27–92) $n = 4$	—	6.2 (0–14.3) $n = 2$
PS	71.7 (0–100) $n = 50$	26.6 (13–44) $n = 2$	45.4 (0–90.8) $n = 2$	7.3 (0–27.7) $n = 2$	65.3 (7–100) $n = 4$	**50.1** (0–100) $n = 8$	—	3.7 (0–11) $n = 6$
PB	43.5 (31–57) $n = 1$	—	—	—	—	—	—	—

n = total number of crosses between morphospecies (*i.e.*, colony pairs). All crosses between colony pairs were replicated three times and the range of % fertilization over all replicates of all crosses is presented in parentheses. Conspecific crosses are in bold and crosses between morphospecies in normal type. '—' denotes cross not yet tried. 'Selfs' are crosses using eggs and sperm from the same colony. PD—*P. daedalea*, PL—*P. lamellina*, PP—*P. pini*, PR—*P. ryukyuensis*, PS—*P. sinensis*, PB—*Platygyra B*, PH—*Platygyra H*.

mental crosses, a sperm dilution series was carried out using two colonies each of *Platygyra daedalea* and *P. ryukyuensis* from Orpheus Island. Sperm was diluted to 10^5, 10^4, and 10^3 per ml and used in reciprocal crosses between all four colonies (within-morphospecies, between-morphospecies, selfs, and controls). Percent fertilization in all crosses was calculated after 2–3 h as described above.

Effect of egg age on fertilization rates

Due to the complex washing procedures and the nature of the experiments described above, it can be up to 6 h after spawning before eggs and sperm are combined in fertilization trials. Sperm kept in a concentrated form has been shown to age slowly (Chia and Bickell, 1983; Oliver and Babcock, 1992), although nothing is known about the effect of aging on the egg—particularly with regard to its ability to be fertilized with foreign sperm.

To test whether egg aging was influencing the results of fertilization trials, an experiment was carried out to look at fertilization rates in eggs of varying ages. Three colonies each of *P. daedalea* and *P. sinensis* from Magnetic Island were used. Once two colonies had spawned, gametes were washed as described above and immediately crossed with each other. As each successive colony spawned, gamete bundles were washed and immediately crossed with all other colonies that had already spawned. This was repeated until all six colonies had spawned, after which all crosses were repeated at 2-h intervals until eggs were 8-h old. All crosses were reciprocal and each cross was replicated twice at each time interval. Controls with sperm-free water were done at all stages of the experiment. Percent fertilization of within- and between-morphospecies crosses at various egg ages was compared for both *P. daedalea* and *P. sinensis*, and regression analysis was used to detect general trends associated with the effect of egg age on fertilization success for all cross types (within-morphospecies, between-morphospecies, self, and control).

Fertilization success as a function of genotype

Tissue samples from all colonies used in the fertilization trials in 1991 and 1992 were collected for genetic analysis to determine whether any genetic structuring, independent of morphology, was associated with breeding groups within the genus and whether incompatible

colonies were clonemates. Colonies were screened using allozyme electrophoresis at nine polymorphic loci (PGM*, MPI*, CK*, LP*, LT-1*, LT-2*, LG-1*, LG-2*, and GPI*; see Miller, 1994b; Miller and Benzie, in press, for further details of electrophoretic techniques). The genetic difference between mated colonies, based on the nine-loci genotype, was calculated as a percentage based on the number of different alleles (*i.e.*, alleles not shared by the two colonies). The fertilization success between any two colonies and the genetic difference between them was then compared.

Larval rearing

In addition to the fertilization experiments described above, large numbers (>1000) of larvae from both within- and between-morphospecies crosses were reared and allowed to settle so that their subsequent development could be monitored through planulae to polyp. Larvae were raised using the methods described by Babcock and Heyward (1986). After 4–5 days, larvae were transferred from plastic jars (2–4 l) to closed aquaria in which settlement substrata (either coral rubble or terracotta paving tiles) were provided. Once all larvae had settled, settlement plates were transferred to a flow-through aquarium system where they were maintained to obtain specimens for examination of colony morphology.

Results

Fertilization trials

The fertilization trials among colonies of *Platygyra* showed that fertilization took place between all the morphological species tested (Table I). The gametes of the seven morphological species crossed were highly compatible, and mean fertilization rates among different morphospecies were similar (between 50% and 70%, Table I). In total, 389 crosses were conducted including 1140 separate vials. Although variability within replicate vials was sometimes high (Table II), the controls indicated no contamination of trials by foreign sperm. The high levels of fertilization (>50%) measured in crosses demonstrates that colonies were reproductively compatible. Interestingly, self-fertilization rates were low in all morphospecies (Table I).

Fertilization success was highly variable both among and within morphological species, with most differences occurring at the level of individual crosses. For example, fertilization success between any two *P. daedalea* colonies ranged from 9.8% to 67.1% in crosses carried out on 17 October 1992 (Table II) and between 0% and 81% between *P. sinensis* colonies on the same night (Table II). Similarly, the success of between-morphospecies crosses seems largely dependent on colony compatibility (Table II). No colony had consistently low fertilization with all other colonies (*e.g.*, Table II), so variability was not due simply to low overall viability of the gametes in any one colony.

Table II

Mean fertilization rates (± standard deviation) between three colonies of Platygyra daedalea *and three colonies of* P. sinensis *from fertilization trials carried out at Magnetic Island on 17 October 1992*

	Eggs					
Sperm	PD1	PD2	PD3	PS1	PS2	PS3
PD1	—	31.6 (0.0)	24.8 (14.07)	3.4 (1.84)	7.1 (3.82)	0.0 (0.00)
PD2	9.8 (0.21)	—	67.1 (3.96)	68.9 (0.0)	40.1 (3.18)	7.7 (1.98)
PD3	27.5 (6.51)	47.5 (15.63)	—	70.6 (1.13)	43.1 (15.91)	16.7 (23.55)
PS1	72.0 (5.66)	67.7 (1.34)	91.6 (4.74)	—	45.1 (3.04)	7.15 (10.11)
PS2	73.2 (3.25)	56.1 (6.79)	95.4 (0.0)	73.3 (2.69)	—	0.0 (0.00)
PS3	23.1 (11.24)	18.2 (4.31)	74.9 (0.71)	81.2 (2.05)	10.7 (7.00)	—

Self-fertilization rates (eggs and sperm from the same colony, denoted by "—") were <1% in all colonies except PD1 which was <3%. All controls (eggs in sperm-free water) had 0% fertilization.

In crosses for which *P. daedalea* was the maternal colony, ANOVA indicated significant variability in fertilization rates with different sperm types ($df = 5$, $MS = 19043.31$, $F = 25.65$, $P < 0.001$). However, the source of most of this variability lay in differences between rates of self fertilization rather than in crosses within and between morphological species. Tukey's HSD test showed no differences between fertilization rates for within-morphospecies crosses [PD × PD ($\bar{x} = 45.2$, $n = 49$)] and between-morphospecies crosses [PD × PS ($\bar{x} = 71.7$, $n = 50$), PD × PL ($\bar{x} = 68.2$, $n = 13$), PD × PP ($\bar{x} = 66.6$, $n = 10$), PD × PR ($\bar{x} = 66.1$, $n = 8$)]. These fertilization rates were, however, significantly different from rates of self fertilization in *P. daedalea* ($\bar{x} = 3.1$, $n = 28$).

Fertilization success between some morphological species was low. Crosses between *Platygyra* H eggs and *P. daedalea* sperm ($n = 5$ pairs), *Platygyra* H eggs and *P. pini* sperm ($n = 3$ pairs), *P. pini* eggs and *P. sinensis* sperm ($n = 2$ pairs) and *Platygyra* B eggs and *P. daedalea* sperm ($n = 1$ pair) had fertilization rates below 20% (Table I). However, the low fertilization rates between these morphospecies are within the range observed between colonies of the same morphospecies (Table I) and may not reflect species incompatibility. Larvae produced by crosses with low fertilization rates were regular in appearance and seemed to develop normally.

Reciprocal crosses between different morphological

Table III

Results from multiple two-way analyses of variance to compare fertilization success (in both within- and between-morphospecies crosses) for the seven different morphological species of Platygyra

Experimental data analyzed	Source of variation	df	*F*	Pr > *F*
2–3 h	fertilization type	1	0.08	0.77 (ns)
	egg species	6	1.64	0.13 (ns)
	fert-type × egg species	5	1.75	0.12 (ns)
6–8 h	fertilization type	1	0.53	0.46 (ns)
	egg species	6	2.20	0.04*
	fert-type × egg species	5	0.42	0.83 (ns)
Development	fertilization type	1	1.03	0.31 (ns)
	egg species	6	4.60	0.00***
	fert-type × egg species	5	0.59	0.71 (ns)

'Fertilization type' is within/between morphospecies crosses; 'egg species' is the morphological species from which eggs in crosses originated. Analyses were performed on data from both counts at 2–3 h and 6–8 h following fertilization, and to compare the development of embryos from both within- and between-morphospecies crosses. (ns)–not significant, * $P < 0.05$, *** $P < 0.001$.

species generally produced similar fertilization rates (*i.e.*, eggs and sperm from two different morphological species readily fertilized each other) (Table I). In some cases, however, compatibility in reciprocal crosses was asymmetrical. For example, *P. sinensis* eggs were readily fertilized by *P. pini* sperm (77.4% fertilization), whereas *P. pini* eggs were poorly fertilized by *P. sinensis* sperm (7.3% fertilization; Table I). A similar pattern existed between *Platygyra* B and *P. daedalea* (Table I), but replication was too low to determine if these differences were significant.

The overall rates of between-morphospecies crosses (all morphospecies pooled) were not significantly different from the rates of within-morphospecies fertilization ('fertilization type'—Table III; Fig. 1a, b), nor was there any difference in within- or between-species fertilizations among the different morphospecies ('fert-type × egg species'—Table III). These results indicate that fertilization can occur at the same rate both within and between morphological species of *Platygyra*.

There were no differences in mean fertilization rates in either within- or between-morphospecies crosses between 2–3 h and 6–8 h (Fig. 1a, b); therefore percent fertilization did not increase with egg-sperm contact time. About 80% of all eggs fertilized after 2–3 h had developed into blastulae after 6–8 h, and survival rates were the same in both within- and between-morphospecies crosses (Fig. 1c).

A comparison of regular *versus* irregular cleavages and embryos, at both 2–3 h and 6–8 h following fertilization, showed that the number of irregular cleavages was similar in both within- and between-morphospecies crosses and between 2–3 and 6–8 h (Fig. 2). Irregular embryos made up about 10%–15% of the 100 eggs counted (fertilized and unfertilized) after both 2–3 h and 6–8 h, whereas regular cleavages were, on average, 40%–50% of the 100 counted. The occurrence of irregular embryos does not appear to be related to differing morphology of

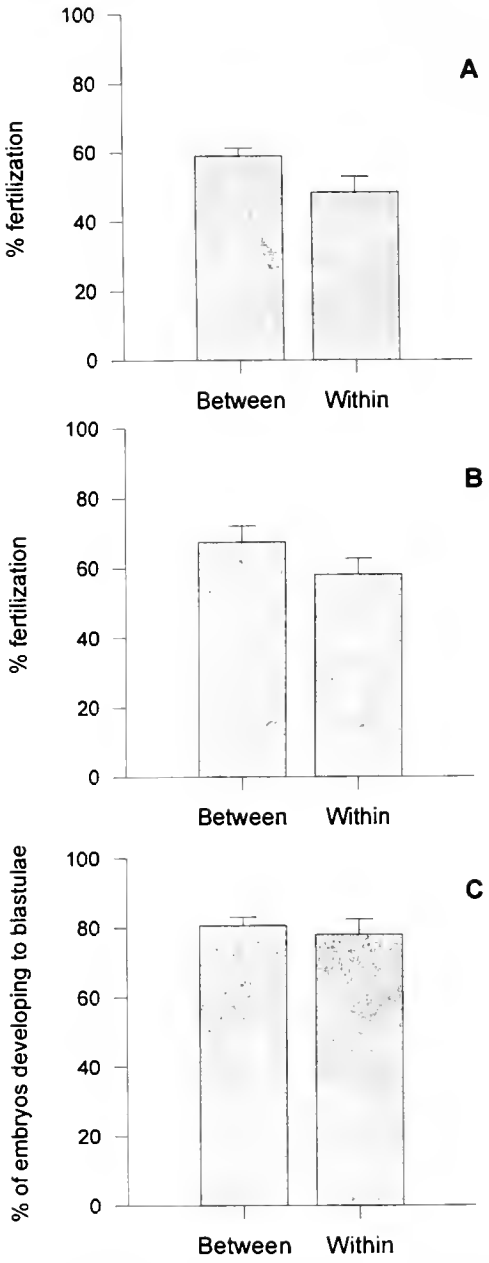

Figure 1. Fertilization success. Mean within- and between-morphospecies fertilization rates in fertilization trials between morphological species of *Platygyra*. Bars denote standard errors. (A) 2–3 h following gamete mixing; (B) 6–8 h following gamete mixing; (C) development of embryos after 6–8 h.

parent colonies but may be a consequence of the experimental method (see Oliver and Babcock, 1992).

Effects of sperm concentration on fertilization rates

There were no effects of sperm concentration on fertilization rates in either *P. daedalea* or *P. ryukyuensis* crosses. Fertilization rates for *P. daedalea* colonies fertilized with conspecific sperm did not differ significantly at sperm concentrations ranging from 10^3 to 10^5 per ml (Fig. 3). Similarly, sperm concentration did not affect fertilization rates in crosses of *P. daedalea* eggs with *P. ryukyuensis* sperm (Fig. 3) or in crosses of *P. ryukyuensis* eggs with conspecific sperm and with *P. daedalea* sperm (Fig. 3).

Effects of egg age on fertilization rates

The ability of an egg to be fertilized by sperm from a different morphological species does not appear to be a function of egg age. There was no significant change in within-morphospecies or between-morphospecies fertilization rates with egg age in either *P. daedalea* or *P. sinensis*. Regression analysis of percent fertilization with egg age was not significant for either *P. daedalea* or *P. sinensis* for any fertilization type (Fig. 4): within-morphospecies (r^2 = 0.005, 0.05 respectively), between-morphospecies (r^2 = 0.04, 0.1 respectively), self (r^2 = 0.07, 0.1 respectively), or controls (r^2 = 0.0004, 0.0 respectively). Although r^2 was not significant (possibly due to high variation in fertilization rates; see Fig. 4), fertilization (both within- and between-morphospecies) showed an overall decrease with egg age in *P. daedalea* and a general increase with egg age in *P. sinensis* (Fig. 4). Between-morphospecies fertilization rates were generally higher than within-morphospecies fertilization rates in *P. daedalea*, whereas between-morphospecies fertilization rates were lower than within-species fertilizations in *P. sinensis* (Fig. 4); however, neither difference was significant.

Fertilization success as a function of genotype

Fertilization success in colonies of *Platygyra* was not related to the genetic difference between parent colonies. No two colonies used in fertilization trials had identical nine-locus genotypes (*i.e.*, none were clonemates). Colonies that were between 40% and 60% different genetically had fertilization rates varying between 0% and 100% (Fig. 5). No evidence of what might be considered a self-recognition allele (Grosberg, 1988) was seen on the basis of the nine-locus genotypes of incompatible colonies. Colony pairs exhibiting low levels of fertilization did not possess consistent allelic or genotypic characteristics.

Temporal separation in spawning times

There was some evidence of temporal separation of spawning times between some morphological species of *Platygyra* (Fig. 6). However, this separation was not clearly defined and an overlap in spawning time existed between the different morphospecies. Although *Platygyra daedalea* colonies have been observed spawning throughout the night, *P. lamellina* and *P. pini* tend to spawn earlier in the evening (spawning 50 to 200 minutes after sunset), while *P. sinensis*, *P. ryukyuensis*, and *Platygyra* H generally spawn later (more than 200 minutes after sunset) (Fig. 3). The ranges of spawning times observed in the field and laboratory show that there was considerable overlap in spawning, and that the gametes of different morphological species were often released simultaneously.

Larval rearing

The embryos of within- and between-morphospecies crosses developed into ciliated planulae larvae within 2 days of fertilization and were competent to settle 4–5 days after spawning. Metamorphosed larvae from both fertilization types gained zooxanthellae within 2 days after settlement and subsequently began skeletal construction. After 5 months, recruits ranged in diameter from 2 to 10 mm. In March 1993 the oldest colony from a between-morphospecies cross had reached 3½ years of age, and colony diameters ranged between 2 and 5 cm. Unfortunately, all colonies died in 1993 because of a prob-

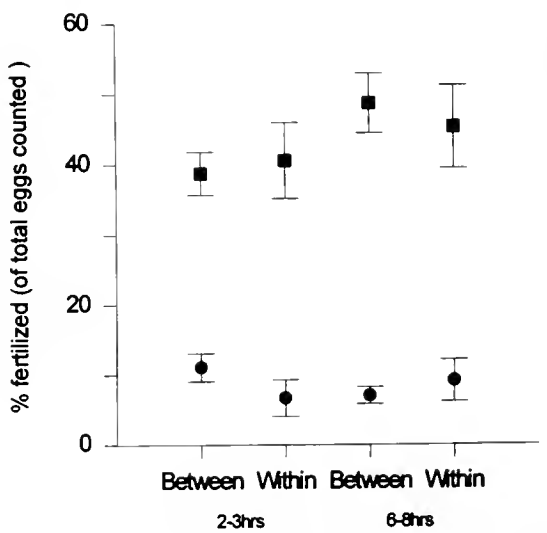

Figure 2. Embryo condition. Occurrence of regular and irregular embryos in both within- and between-morphospecies fertilization trials expressed as a percentage of the first 100 eggs counted per vial (all morphospecies pooled). Bars represent 95% confidence limits. ■—regular embryos; ●—irregular embryos.

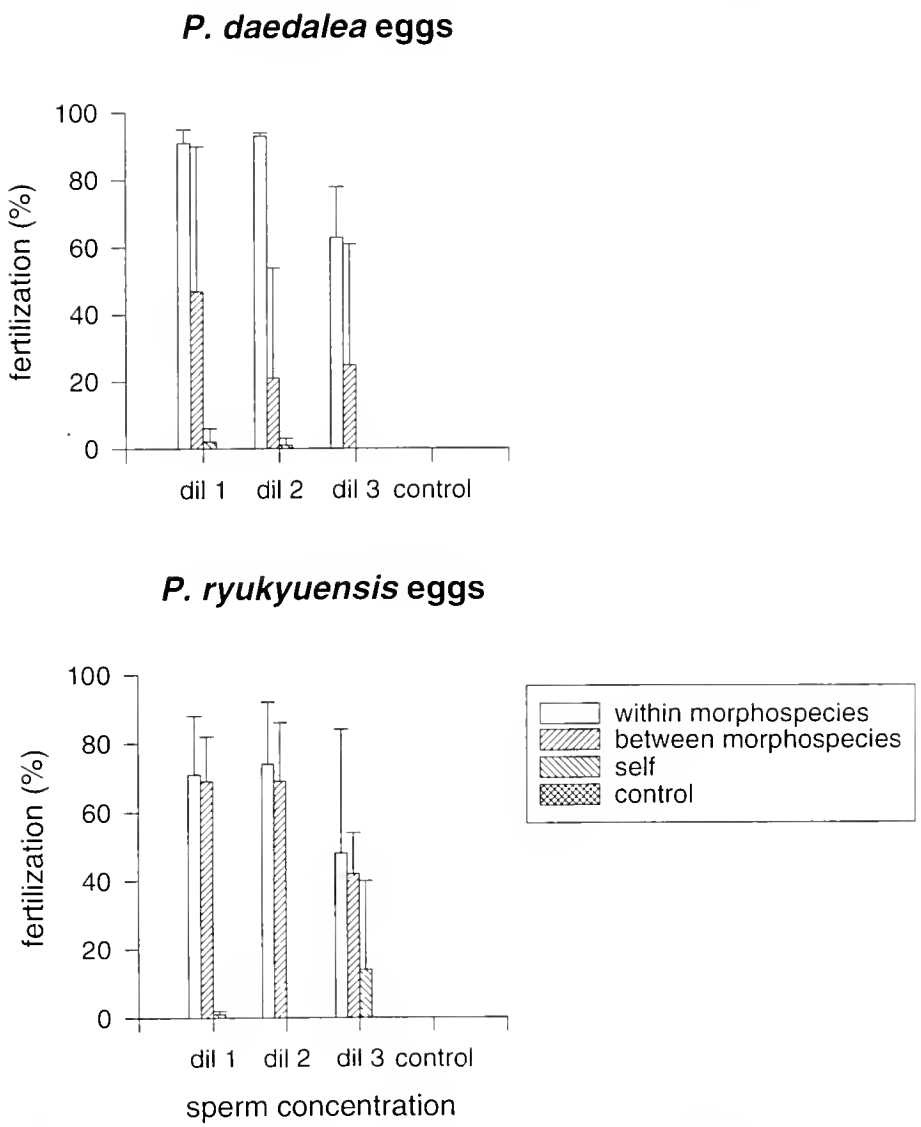

Figure 3. Effects of varying sperm concentration. Results from crosses between two colonies each of *Platygyra daedalea* and *P. ryukyuensis* in which sperm concentrations were varied 100-fold. Sperm concentrations: Dil 1 = 1×10^5 ml $^{-1}$, Dil 2 = 1×10^4 ml^{-1}, Dil 3 = 1×10^3 ml^{-1}. Error bars are standard deviations. Controls are with sperm-free water.

lem with the seawater system. Development of colonies from between-morphospecies crosses appeared to be normal up to that point, although their skeletal characteristics were not well enough developed to reveal whether they resembled any of the predefined morphological species or perhaps were intermediate in morphology between the parent colonies.

Discussion

Fertilization is clearly possible between the different morphological species of *Platygyra in vitro*. There appeared to be no relationship between morphology and reproductive compatibility since fertilization was recorded in all crosses. Fertilization occurred between most morphological *Platygyra* species at rates equivalent to within-species fertilizations (Table I, Fig. 1a, b). Nonsignificant differences in fertilization rate for comparisons among crosses in which *P. daedalea* was the maternal colony probably reflect widespread gametic compatibility within the genus. The low fertilization rates in some crosses between morphological species may reflect small sample sizes and differences in compatibility between individual colonies (Table III, Fig. 1a, b) rather than overall morphospecies incompatibility. Embryos resulting from between-morphospecies

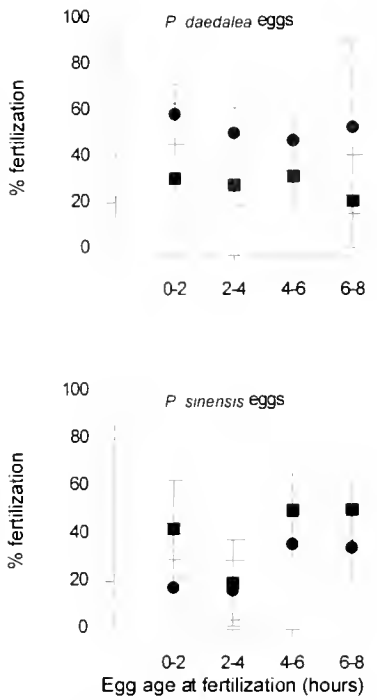

Figure 4. Effects of egg aging. Mean fertilization rates with increasing egg age in crosses between three colonies each of *Platygyra daedalea* and *P. sinensis*. Bars represent 95% confidence limits. ■—within-morphospecies crosses, ●—between-morphospecies crosses.

crosses apparently did not have reduced survivorship (Fig. 1c).

Percent fertilization was high after 2 h (the minimum time after fertilization in which cleavage becomes evident), and fertilization rates did not increase with egg-sperm contact time. This suggests that fertilization between gametes occurred promptly after the eggs were introduced into the vials, irrespective of the morphotype of the parent colonies. Variations in egg age, sperm dilution, and parental genotype failed to affect patterns of fertilization in crosses within or among morphospecies.

No evidence of pre-zygotic barriers to fertilization was detected among the morphological species of *Platygyra*. The seven morphological species have overlapping spawning times (Fig. 6), and high levels of fertilization in trials indicate that no species-specific gamete recognition systems (*e.g.*, Uehara *et al.*, 1990; Vacquier *et al.*, 1990; Palumbi, 1992) are operating in *Platygyra*. Preliminary investigations of sperm chemotaxis in *Platygyra* showed limited evidence of sperm attraction, but no evidence of species-specificity of sperm attraction in *Platygyra* (K. Miller and R. Miller, unpubl. data). Even if present, species-specific sperm chemotaxis could not be completely effective as a barrier to fertilization without membrane-level recognition or selectivity.

Mixed parentage does not appear to affect the development of *Platygyra* larvae or the competence of larvae to settle, metamorphose, and grow. Sterility of these offspring may be a post-zygotic isolating mechanism between morphological species of *Platygyra*, although costs associated with sterile progeny (*e.g.*, gamete wastage, loss of resources) may be high. However, in histological studies all mature-sized colonies of *P. sinensis* had gonads (Babcock, 1986) and in the 389 fertilization trials carried out, no colony was ever found that did not fertilize with at least one other colony, suggesting that sterile *Platygyra* are either rare or nonexistent.

Results from this study, combined with genetic studies (Miller and Benzie, in press), lead us to believe that fertilization and gene flow will occur between morphological "species" of *Platygyra*. This raises a number of perplexing questions. First, should these morphological groups within the genus *Platygyra* (Miller, 1994a) be considered true species, or is there simply one highly polymorphic species (*e.g.*, Skulason and Smith, 1995) within the genus? And second, if gene exchange occurs freely between all morphological types, how can the morphologically distinct groups be maintained in this genus?

Morphological species boundaries within the genus *Platygyra* are clear (Miller 1994a), and morphological differences appear to be far greater between *Platygyra* spp. than between other controversial species groups: for example, the three morphological variants of *Montastraea annularis* that are now considered sibling species (Knowlton *et al.*, 1992; Weil and Knowlton, 1994); the two morphs of *Montipora digitata* that have been identified as reproductively isolated species (Stobart and Benzie, 1994); and *Acropora cuneata* and *A. palifera*, which are difficult to distinguish by morphology but are genetically distinct (Ayre *et al.*, 1991). Hence it is not surprising that the seven morphological variants of *Platygyra* have been considered separate species in the past.

However, genetic and reproductive data indicate that *Platygyra* morphospecies are much more closely related than the *Montastrea* spp., the *Montipora* spp., or the two *Acropora* species. Furthermore, many groups of corals show discrepancies between species characters including morphology, genetics, and reproduction (Potts and Garthwaite, 1986; McMillan *et al.*, 1991; Willis *et al.*, 1992; Wallace and Willis, 1994; Romano and Palumbi, 1996). Defining species boundaries in corals is clearly a controversial issue. Nonetheless, our results show that in the case of *Platygyra*, it is inappropriate to consider the taxonomic unit as the minimal evolutionary unit and that evolutionary processes in different morphological species of *Platygyra* will be linked.

The maintenance of seven morphologically distinct entities in *Platygyra* in spite of genetic interchange poses a challenging question. Progeny from between-morphospecies crosses may be expected to have morphological

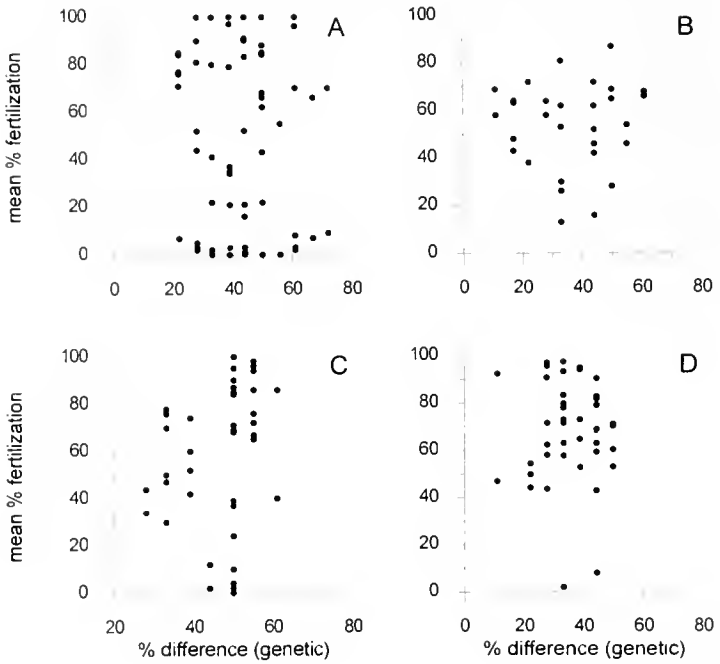

Figure 5. Fertilization success as a function of genotype. Comparison of percent fertilization (based on the mean of three replicates) and allelic differences between colonies used in fertilization trials. (A) Magnetic Island, 1991; (B) Magnetic Island, 1992; (C) Davies Reef, 1991; (D) Orpheus Island, 1992.

characters intermediate between those of the parent colonies and, with continued interbreeding, distinctions between the morphological species would be likely to break down. However, nothing is known of the mechanisms that produce skeletal differences in corals; if morphology is linked to dominance alleles, then between-morphospecies progeny may display the skeletal characteristics of only one parent (*e.g.*, Strathmann, 1981; Byrne and Anderson, 1994). Alternatively, processes such as introgression may play a role in the maintenance of morphological differences in *Platygyra* (Miller and Benzie, in press).

Reproductive and distributional variation may also provide some level of segregation between the morphospecies, thus helping to maintain morphological differences. There is some separation among spawning times of *Platygyra* morphospecies on the Great Barrier Reef, but these do not constitute complete temporal barriers to fertilization (Fig. 6). Nevertheless, most egg-sperm interactions take place in the first few seconds after mature eggs are in contact with a sperm suspension (Fig. 1a; Denny and Shibata, 1989; Mundy *et al.*, 1994), and colonies are more likely to be fertilized by close neighbors (Oliver and Babcock, 1992). These factors in combination could result in a degree of temporal reproductive segregation, if not total isolation.

Sophisticated egg-sperm recognition systems are clearly operational at several levels in *Platygyra*. Colonies of *Platygyra* do not frequently self-fertilize (Table I), unlike *Goniastrea favulus*, which commonly self-fertilizes (Heyward and Babcock, 1986; Stoddart *et al.*, 1988). In addition, the high variability in fertilization rates both within and between morphological species also indicates some level of incompatibility or individual recognition between certain pairs of individuals. This degree of reproductive separation in combination with small differences in the timing of spawning is probably insufficient to produce fixed allelic differences in the populations, but it may produce the indications of nonrandom mating present in the genotypic structure of *Platygyra* populations (Miller and Benzie, in press).

No clear-cut habitat separation is apparent in *Platygyra*, where all morphospecies can be found in various habitats on a single reef (Miller, 1994a). At large scales, however, trends in the distribution of morphospecies are apparent. For example, *P. lamellina* is rare on mid-shelf and shelf-edge reefs in the central Great Barrier Reef; *P. pini* is rare on coastal reefs; *P. ryukyuensis* is most common on coastal fringing reef flats; and *P. lamellina*, *P. ryukyuensis*, and *Platygyra* H are rare or absent on the reefs from the southern Great Barrier Reef (Miller, 1994b). Across even larger scales, further discontinuities in species distributions are evident (Veron, 1993), and observations of spawning times of *Platygyra* in other regions (*e.g.*, Okinawa: Heyward *et al.*, 1987; Hayashibara *et al.*, 1993) indicate that on geographical scales segregation of spawning times among *Platygyra*

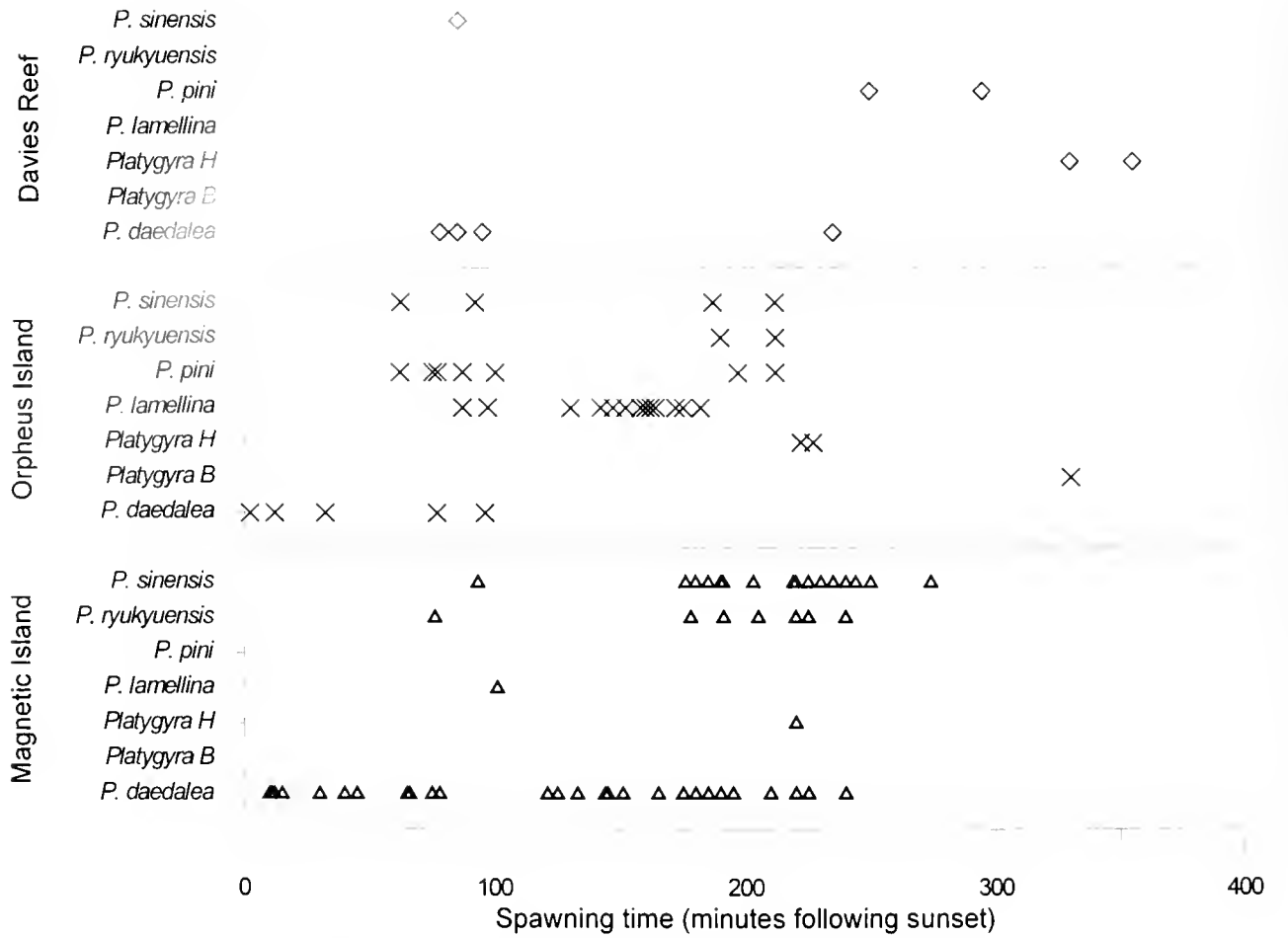

Figure 6. Temporal separation in spawning. Spawning times of *Platygyra* colonies at three reefs on the Great Barrier Reef. Spawning times include observations made by scuba divers *in situ*, spawning times of experimental colonies in aquaria (these have been shown not to differ from *in situ* spawning times, see Miller, 1994b), and spawning times recorded by Babcock *et al.* (1986).

morphospecies could result in reproductive isolation. The distribution of the morphological species of *Platygyra* clearly exhibits some habitat-level differences that may contribute to the continued coexistence of the morphospecies, specifically through differential fitness in various habitats and the subsequent spatial and temporal reproductive isolation in certain habitats.

It has recently been proposed that reticulate evolution occurs within the Scleractinia (Veron, 1995). *Platygyra* morphospecies are widespread throughout the Indo-Pacific (Veron, 1993) and, as we have discussed, there are varied levels of differentiation and connectedness between the morphological and genomic units. Surface-circulation vicariance mechanisms (Veron, 1995) and reticulate evolution may well be the basis for the morphological and genetic variation in *Platygyra* populations across both local and geographic scales, and the likelihood of this linkage among morphological species of *Platygyra* should be accepted.

Acknowledgments

We thank Craig Mundy, Annabel Miles, and Dick Miller for invaluable assistance during coral spawning trips; we are also grateful to the many other people who helped out during fertilization experiments. Also thanks to Maria Byrne, Alina Szmant, and Charlie Veron, who provided many useful comments on this manuscript. This work was financed by grants to K. Miller from The Australian Coral Reef Society and The Australian Museum, ARC grants to T. Hughes and to B. Willis/K. Miller/B. Stobart, and a James Cook University Post-graduate research award. Support was also provided by the Australian Institute of Marine Science. This is contribution 149 from the James Cook University Coral Group.

Literature Cited

Ayre, D. J., J. E. N. Veron, and S. L. Dufty. 1991. The corals *Acropora palifera* and *Acropora cuneata* are genetically and ecologically distinct. *Coral Reefs* **10:** 13–18.

Babcock, R. C. 1986. The population ecology of reef flat corals of the family Faviidae (*Goniastrea, Platygyra*). Doctor of Philosophy Thesis, James Cook University, Townsville. 163 pp.

Babcock, R. C., and A. J. Heyward. 1986. Larval development of certain gamete spawning scleractinian corals. *Coral Reefs* **5:** 111–116.

Babcock, R. C., G. D. Bull, P. L. Harrison, A. J. Heyward, J. K. Oliver, C. C. Wallace, and B. L. Willis. 1986. Synchronous spawnings of 105 scleractinian coral species on the Great Barrier Reef. *Mar. Biol.* **90:** 379–394.

Byrne, M., and M. J. Anderson. 1994. Hybridization of sympatric *Patiriella* species (Echinodermata: Asteroidea) in New South Wales. *Evolution* **48:** 549–577.

Chevalier, J. P. 1975. *Les scleractinaires de la Melanesie Francaise (Nouvelle Caledonie, Iles Chesterfield, Iles Layaute, Nouvelles Hebrides).* 2eme Partie. Exped. Francaise recifs corallens Nouvelle Caledonie. Edn. Fond. Singer-Polignac, Paris. 507 pp.

Chia, F. S., and L. R. Bickell. 1983. Echinodermata. Pp. 545–620 in *Reproductive Biology of Invertebrates,* Vol. 2: Spermiogenesis and sperm function. John Wiley & Sons, New York.

Coll, J. C., B. F. Bowden, G. V. Meehan, G. M. Konig, A. R. Carroll, D. M. Tapiolas, P. M. Alino, A. Heaton, R. De Nys, P. A. Leone, M. Maida, T. L. Aceret, R. H. Willis, R. C. Babcock, B. L. Willis, Z. Florian, M. N. Clayton, and R. L. Miller. 1994. Chemical aspects of mass spawning in corals. 1. Sperm attractant molecules in the eggs of the scleractinian coral *Montipora digitata. Mar. Biol.* **118:** 177–182.

Darwin, C. 1859. *On the Origin of Species.* John Murray, London. 513 pp.

Denny, M. W., and M. F. Shibata. 1989. Consequences of surf zone turbulence for settlement and external fertilization. *Am. Nat.* **134:** 859–889.

Ellis, J., and D. Solander. 1786. *The Natural History of Many Curious and Uncommon Zoophytes.* Benjamin White and Peter Elmsly, London. 208 pp.

Grosberg, R. K. 1988. The evolution of allorecognition specificity in clonal invertebrates. *Q. Rev. Biol.* **63:** 377–412.

Harrison, P. L., R. C. Babcock, G. D. Bull, J. K. Oliver, C. C. Wallace, and B. L. Willis. 1984. Mass spawning in tropical reef corals. *Science* **223:** 1186–1189.

Hayashibara, T., K. Shimoike, T. Kimura, S. Hosaka, A. Heyward, P. Harrison, K. Kudo, and M. Omori. 1993. Patterns of coral spawning at Akajima Island, Okinawa, Japan. *Mar. Ecol. Prog. Ser.* **101:** 253–262.

Heyward, A. J., and R. C. Babcock. 1986. Self- and cross-fertilization in scleractinian corals. *Mar. Biol.* **90:** 191–195.

Heyward, A., K. Yamazato, T. Yeemin, and M. Minei. 1987. Sexual reproduction of corals in Okinawa. *Galaxea* **6:** 331–343.

Hodgson, G. 1988. Potential gamete wastage in synchronously spawning corals due to hybrid inviability. *Proc. 6th Int. Coral Reef Symp.* **2:** 707–714.

Knowlton, N., E. Weil, L. A. Weight, and H. M. Guzman. 1992. Sibling species in *Montastrea annularis,* coral bleaching, and the coral climate record. *Science* **255:** 330–333.

Lang, J. C. 1984. Whatever works: the variable importance of skeletal and of non-skeletal characters in scleractinian taxonomy. *Palaeontogr. Am.* **54:** 18–44.

Mayr, E. 1942. *Systematics and the Origin of Species.* Dover publications Inc., New York. 334 pp.

McMillan, J., T. Mahoney, J. E. N. Veron, and D. J. Miller. 1991. Nucleotide sequencing of highly repetitive DNA from seven species in the coral genus *Acropora* (Cnidaria: Scleractinia) implies a division contrary to morphological criteria. *Mar. Biol.* **110:** 323–327.

Metz, E. C., and S. R. Palumbi. 1996. Positive selection and sequence rearrangements generate extensive polymorphisms in the gamete recognition protein bindin. *Mol. Biol. Evol.* **13:** 397–406.

Miller, K. J. 1994a. Morphological species boundaries in the coral genus *Platygyra*: environmental variation and taxonomic implications. *Mar. Ecol. Prog. Ser.* **110:** 19–28.

Miller, K. J. 1994b. The *Platygyra* species complex: implications for coral taxonomy and evolution. Ph.D. Dissertation, James Cook University of North Queensland. 164 pp.

Miller, K. J., and J. A. H. Benzie. In press. No clear genetic distinction between morphological species within the coral genus *Platygyra. Bull. Mar. Sci.* **60:** ???

Miller, R. 1979. Sperm chemotaxis in the hydromedusae. 1. Species specificity and sperm behaviour. *Mar. Biol.* **53:** 99–114.

Miller, R. 1985. Demonstration of sperm chemotaxis in the Echinodermata: Holothuroidea, Ophiuroidea. *J. Exp. Zool.* **234:** 383–414.

Mundy, C., R. Babcock, I. Ashworth, and J. Small. 1994. A portable, discrete-sampling submersible plankton pump and its use in sampling starfish eggs. *Biol. Bull.* **186:** 168–171.

Oliver, J., and R. Babcock. 1992. Aspects of the fertilization ecology of broadcast spawning corals: sperm dilution effects and *in situ* measurements of fertilization. *Biol. Bull.* **183:** 409–417.

Palumbi, S. R. 1992. Marine speciation on a small planet. *TREE* **7:** 114–118.

Potts, D. C., and R. L. Garthwaite. 1986. Population genetics of the genus *Porites. Abstr. Annu. Meet. Int. Soc. Reef Stud.* p. 38.

Romano, S. L., and S. R. Palumbi. 1996. Evolution of Scleractinian corals inferred from molecular systematics. *Science* **271:** 640–642.

Skulason, S., and T. B. Smith. 1995. Resource polymorphisms in vertebrates. *TREE* **10:** 366–370.

Stobart, B., and J. A. H. Benzie. 1994. Allozyme electrophoresis demonstrates that the scleractinian coral *Montipora digitata* is two species. *Mar. Biol.* **118(2):** 183–190.

Stoddart, J. A., R. C. Babcock, and A. J. Heyward. 1988. Self-fertilization and maternal enzymes in the planulae of the coral *Goniastrea favulus. Mar. Biol.* **99:** 489–494.

Strathmann, R. R. 1981. On barriers to hybridization between *Strongylocentrotus drobachiensis* (O. F. Muller) and *S. pallidus* (G. O. Sars). *J. Exp. Mar. Biol. Ecol.* **55:** 39–47.

Uehara, T., H. Asakura, and Y. Arakaki. 1990. Fertilisation blockage and hybridisation among species of sea urchins. Pp. 305–310 in *Advances in Invertebrate Reproduction 5.* Elsevier Science, Amsterdam.

Vacquier, V. D., K. R. Carner, and C. D. Stout. 1990. Species-specific sequences of abalone lysin, the sperm protein that creates a hole in the egg envelope. *Proc. Natl. Acad. Sci. USA* **87:** 5792–5796.

Van Veghel, M. L. J. 1994. Reproductive characteristics of the polymorphic Caribbean reef building coral *Montastrea annularis.* 1. Gametogenesis and spawning behavior. *Mar. Ecol. Prog. Ser.* **109:** 209–219.

Van Veghel, M. L. J., and R. P. M. Bak. 1993. Intraspecific variation of a dominant Caribbean reef building coral, *Montastrea annularis:* genetic behavioural and morphometric aspects. *Mar. Ecol. Prog. Ser.* **92:** 255–265.

Vaughan, T. W., and J. W. Wells. 1943. Revision of the sub-orders, families and genera of the Scleractinia. *Geol. Soc. Am. Spec. Pap.* **44:** 1–363.

Veron, J. E. N. 1993. Biogeography of hermatypic corals. *Australian Institute of Marine Science Monograph Series Volume 10.* Townsville. 433 pp.

Veron, J. E. N. 1995. *Corals in Space and Time.* University of New South Wales Press, Sydney. 321 pp.

Veron, J. E. N., M. Pichon, and M. Wijsman-Best. 1977. Scleractinia of eastern Australia, Part 2, Families Faviidae, Trachyphyllidae. *Australian Institute of Marine Science Monograph Series Volume 3*, Townsville. 233 pp.

Wallace, C. C., and B. L. Willis. 1994. The systematics of the coral genus *Acropora* implications of the new biological findings for species concepts. *Annu. Rev. Ecol. Syst.* **25:** 237–262.

Weil, E., and N. Knowlton. 1994. A multi-character analysis of the Caribbean coral *Montastaea annularis* (Ellis and Solander, 1786) and its two sibling species, *M. faveolata* (Ellis and Solander, 1786) and *M. franksi* (Gregory, 1895). *Bull. Mar. Sci.* **55:** 151–175.

Willis, B. L. 1990. Species concepts in extant scleractinian corals: considerations based on reproductive biology and genotypic population structures. *Syst. Bot.* **15:** 136–149.

Willis, B. L., R. C. Babcock, P. L. Harrison, J. K. Oliver, and C. C. Wallace. 1985. Patterns in the mass spawning of corals on the Great Barrier Reef from 1981 to 1984. *Proc. 5th Int. Coral Reef Symp.* **4:** 343–348.

Willis, B. L., R. C. Babcock, P. L. Harrison, and C. C. Wallace. 1992. Experimental evidence of hybridisation in reef corals involved in mass spawning events. *Proc. 7th Int. Coral Reef Symp.* **Abstracts:** 109.

The Future of Aquatic Research in Space: Neurobiology, Cellular and Molecular Biology

Proceedings
of a workshop
sponsored by
THE CENTER FOR ADVANCED STUDIES
IN THE SPACE LIFE SCIENCES
AT THE MBL

13–15 May 1996

Marine Biological Laboratory,
Woods Hole, Massachusetts

Funded by
THE NATIONAL AERONAUTICS
AND SPACE ADMINISTRATION
under Cooperative Agreement
NCC 2-896

CONTENTS

The Future of Aquatic Research in Space: Neurobiology, Cellular and Molecular Biology

Reference: *Biol. Bull.* **192:** 115–116. (February, 1997)

Introduction

The Center for Advanced Studies in the Space Life Sciences at the Marine Biological Laboratory was established through a cooperative agreement between the MBL and the National Aeronautics and Space Administration. This NASA-sponsored Center serves as an interface between NASA and the basic life science community, addressing issues of mutual interest. A series of symposia, workshops, and seminars will be held at the MBL to advise NASA on a wide variety of topics in the life sciences, including cell biology, developmental biology, molecular biology, neurobiology, plant biology, and systems biology. Special attention will be directed at examining how gravity affects biological processes, and how variation in gravity can be utilized as a probe to better understand such processes. This setting provides a forum for scientists to think about and discuss, often for the first time, the role that gravity may play in fundamental cellular and physiological processes.

"The Future of Aquatic Research in Space: Neurobiology, Cellular and Molecular Biology" held at the MBL from May 12 to 15, 1996, is the first workshop sponsored by the new Center. This meeting was chaired by George Langford, who participated in the overall planning of the sessions on mechanosensation, developmental biology, neurobiology, and cell biology. Fred Sack was responsible for organizing the session on plant biology.

Although the gravitropic and gravitactic responses of plants to changes in gravity were discussed at this meeting, the responses of animal cells to gravity are not well documented. Yet mechanical force can affect both eukaryotic and prokaryotic cells. At this workshop, Gillespie described how a mechanically sensitive hair bundle serves the hair cell in mechano-electrical transduction. Furthermore, specific ion channels are activated by stretch. Exciting developments in this area, described at this meeting, include the genetic analysis of mechanosensation in *C. elegans* and the identification, purification, and reconstitution of a mechanosensitive channel from *E. coli*. Studies on related channels in neurons and *Xenopus* oocytes were also discussed. Mechanical force can also be generated within the cell by the action of molecular motors; the subject of the final session at this workshop.

The potential effects of microgravity on sensory systems were considered in the discussion and remain to be explored. The notion that the microgravity environment might influence the development of *Xenopus* eggs by altering the rotation of the entire egg cortex after fertilization appears to have been dispelled by direct experimentation. *Xenopus* eggs develop normally during spaceflight. In his presentation, Elinson suggested that this finding might reflect the control of cortical movement by a microtubule-based mechanism that is insensitive to changes in gravity. He further suggested that larger eggs, such as those from the Puerto Rican terrestrial-breeding frog *coqui*, might lack this microtubule-based mechanism and could therefore exhibit altered development in microgravity.

Several theoretical studies indicate that the effects of microgravity would be minuscule at the subcellular level, but Baxter, in his abstract, cites empirical evidence that gravity does affect cellular processes such as signal transduction. To reconcile this apparent contradiction, Baxter presents the intriguing hypothesis that nonlinear molecular systems within the cell provide the amplification required for cells to sense gravity. This controversy underscores the complexities that must be considered in predicting potential responses of cells to changes in gravity; it must also be a central consideration in the planning of future studies on the effects of microgravity.

Scott Brady provided the following remarks at the conclusion of the workshop. He pointed out the unique experimental environments afforded by spaceflight, which will lead to new approaches for addressing fundamental questions in biology: "The emphasis in this workshop and in much of the life sciences research supported by NASA has been on the effects of microgravity and the ways in which an organism responds to microgravity. This is appropriate, and such questions will continue to

This paper was originally presented at a workshop titled *The Future of Aquatic Research in Space: Neurobiology, Cellular and Molecular Biology*. The workshop, which was held at the Marine Biological Laboratory, Woods Hole, Massachusetts, from 13 to 15 May 1996, was sponsored by the Center for Advanced Studies in the Space Life Sciences at MBL and funded by the National Aeronautics and Space Administration under Cooperative Agreement NCC 2-896.

be important. However, we should not forget that the conditions of spaceflight include other parameters that may affect biological processes, and we may be able to use the unique environment to address a wider range of biological questions.

For example, the unique behavior of fluids under conditions of microgravity suggests that the conditions of spaceflight may help us understand how fluid mechanics are important for biological processes. Activities that might be altered include membrane currents and second messenger signaling, among others. Differences in fluid mechanics have already led to at least one practical application, as seen in the current interest in production of protein crystals that cannot be grown on earth and lead to new insights into the structure of biologically important molecules.

Several people have remarked about the effects of radiation encountered during spaceflight. An understanding of the biological hazards associated with this radiation is clearly important for people, animals, and plants during the extended periods of spaceflight expected for the space station or a trip to Mars. There are surely other environmental factors that will also be important to evaluate during extended exposure to spaceflight.

Finally, a critical challenge for any organism is achieving homeostasis in response to a changing environment. Much remains to be understood about the homeostatic mechanisms that living organisms employ to assure their continued survival as an individual entity and as a species. The conditions of spaceflight, including microgravity, represent a profound perturbation of the normal environment. By observing the responses of an organism to this perturbation and defining the molecular mechanisms that underlie these responses, we have a rare occasion to explore biological homeostasis. As opportunities to conduct long term studies of different organisms under conditions of spaceflight increase, we must be more creative in identifying important questions and devising experimental models."

E. A. DAWIDOWICZ
Director
Center for Advanced Studies
in the Space Life Sciences
Woods Hole
July 1996

Reference: *Biol. Bull.* **192:** 117. (February, 1997)

Mechanosensitive Channels: Introduction

WERNER R. LOEWENSTEIN

Laboratory of Cell Communication, Marine Biological Laboratory, Woods Hole, Massachusetts 02543

Our subject in this session is mechanoreception, a function that is at the bottom of much of what goes on in an organism—from the basic sensing of cell movements, osmotic changes, and touch, to the elaborate sensing of gravity, balance, hearing, and so on. The hub of this function is a class of tubular membrane proteins that lets ions in or out of cells. Very little is known yet about the molecular makeup of this mechanosensitive class of proteins. Their better-known cousins, the membrane channels that transduce chemical or electrical stimuli, fall into three basic building plans: arrangements of four, five, or six subunits with a central axis of symmetry forming an aqueous passageway through the lipid bilayer of the cell membrane—the channel pore. The channel I have been playing with—the cell-to-cell channel—belongs to the latter class; here polar α-helical stretches from the neighboring subunits line a 16–18 Å pore. This channel is quite large, and we are just beginning to understand what configurational changes in the subunits are involved in the closing and opening of the pore. The narrower and more selective ion channels have fewer subunits, and the polar space between the helices is smaller.

This paper was originally presented at a workshop titled *The Future of Aquatic Research in Space: Neurobiology, Cellular and Molecular Biology*. The workshop, which was held at the Marine Biological Laboratory, Woods Hole, Massachusetts, from 13 to 15 May 1996, was sponsored by the Center for Advanced Studies in the Space Life Sciences at MBL and funded by the National Aeronautics and Space Administration under Cooperative Agreement NCC 2-896.

We should keep our eyes peeled on this polar space. Here is where much of the action in the channel takes place—the opening and closing of the pore, or "channel gating," as it is called. So, the overarching question is how the mechanical stimulus, namely strain on the cell surface, is coupled to gating—how that strain is converted into an electrical current. The mechanosensory channels are probably among the oldest channel entities, and so we may hope that the conversion is relatively simple. The prospect of that simplicity—perhaps, a rather direct transducer mechanism—has attracted many of us here to try our hand at this channel modality. But what nature actually holds in store for us remains to be seen. We will get a firsthand feel for the problem; the speakers in this morning session will offer us a broad range of mechanosensitive proteins, from unicellular organisms to vertebrates.

Cathy Morris will start things off with a picture of how neurons sense their mechanical state—a low-rate sensing that comes into play during the vagaries of their long lives. Owen Hamill will deal with the transduction and gating mechanisms of mechanosensitive channels in *Xenopus* oocytes. Martin Chalfie will tell us about his genetic dissections of a channel in nematodes, and center on the role of the extracellular- and intracellular matrix in the coupling between stimulus and gating. And Ching Kung ends the session with a look at a mechanosensory channel in *E. coli*, which he has managed to put into liposomes and to analyze both genetically and chemically.

Reference: *Biol. Bull.* **192:** 118–120. (February, 1997)

How Do Neurons Monitor Their Mechanical Status?

CATHERINE E. MORRIS[1], HOWARD LESIUK[1], AND LINDA R. MILLS[2]

[1]*Loeb Institute, Ottawa Civic Hospital, Ottawa K1Y 4E9, Canada, and* [2]*Playfair Institute, Toronto Western Hospital, Toronto M5T 2S8, Canada*

Neurons lead mechanically active lives. In consequence, the neuronal plasma membrane must mechanically adjust itself as it is subjected to a multitude of internally and externally generated forces. Neuronal arborizations are not fixed structures; they are plastic and can be refashioned and repaired. Neuronal cytoplasm churns with motor-driven axonal transport and with the to-and-fro of membrane trafficking. Neurites continually generate tension while they are growing (see Heidemann and Buxton, 1994); nonadherent neurites cannot sustain tension and are retracted. Neural processes cope with stretching and compressive forces from surrounding tissues, and they cope with osmotically induced swelling and shrinking. Arborizations of a given neuron extend in many directions and may traverse many environments. While some processes are only micrometers long, others can be meters long. In spite of the potentially hazardous nature of their arborized geometry and the abundance of mechanical perturbations they experience, individual neurons evidently survive for 100 years or more! And to survive, they must ensure that the continuity of their plasma membrane is never breached.

How is it that, always and at all locations in a neuron, there is sufficient membrane to prevent rupture? We can rule out two possibilities *a priori*. First, "wrinkles," or microvilli, cannot be maintained everywhere; the excess capacitance would appreciably compromise fast neuronal signaling. Second, central directives from the soma to add or subtract plasma membrane globally would be grossly inappropriate for a highly arborized cell.

For effective regulation of cell surface area, the neuronal plasma membrane must detect and respond to tension in a local fashion. We hypothesize that membrane area is regulated by a sensor-effector system of *mechanosensitive membrane disposition—i.e.*, a system which assures that cytoplasmic stores of membrane are rapidly recruited to the plasma membrane when tension rises, then restored to the cytoplasm when membrane tension falls. If exocytosis and endocytosis are tension-sensitive, this should make the disposition of membrane mechanosensitive, but this example does not exhaust the possibilities. Although it is possible to imagine how mechanosensitive ion channels might contribute tension-sensitive regulation of plasma membrane area, the most streamlined system would respond to tension with no intermediary chemical or voltage signals. The system would be in greatest demand during neural development (which involves both outgrowth and retraction of processes) and subsequently could provide an emergency response system to prevent rupture, membrane excess, or both whenever local stresses changed.

In molluscan and mammalian neurons, we have been examining membrane dynamics that seem to reflect the exaggerated workings of such a sensor-effector system, *i.e.*, a system of mechanosensitive membrane disposition (Wan *et al.*, 1995; Reuzeau *et al.*, 1995). Osmomechanical perturbations of cultured neurons induce Vacuole Like Dilations (VLDs). VLDs, which can grow to about 10 μm across, form when neurons *shrink* (Fig. 1a, stages B to C, D, or Fig. 1b) and disappear as they *swell* (Fig. 1a, stages D to B). It seems counterintuitive for a membranous cytoplasmic structure to swell as the cell itself shrinks. The explanation is that, initially, VLDs are not true vacuoles. VLDs start as invaginations of membrane

This paper was originally presented at a workshop titled *The Future of Aquatic Research in Space. Neurobiology, Cellular and Molecular Biology.* The workshop, which was held at the Marine Biological Laboratory, Woods Hole, Massachusetts, from 13 to 15 May 1996, was sponsored by the Center for Advanced Studies in the Space Life Sciences at MBL and funded by the National Aeronautics and Space Administration under Cooperative Agreement NCC 2-896.

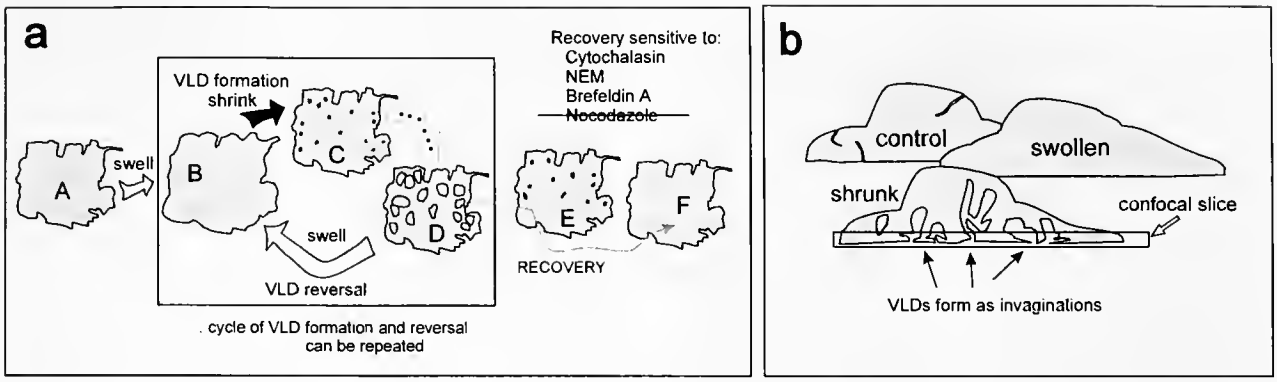

Figure 1. (a) Schematic showing that VLDs form (B to C) when neurons shrink and that VLDs reverse (D to B) upon subsequent reswelling. Repeated cycles of VLD formation and reversal (B–C–D–B . . . etc.) can be effected repeatedly with about 2 min between solution exchanges. If neurons with VLDs are left in isosmotic medium (D to E), the VLDs disappear by a drug-sensitive process termed recovery (D to F). The schematic depicts experiments in which neurons first swell (A to B), so that return to an isosmotic medium (B to C) constitutes a shrinking stimulus. Between C and D, the VLDs enlarge to full size, then recovery (post-D) begins. For VLD formation, the critical stimulus is shrinkage; for VLD reversal, the critical stimulus is swelling. Accordingly (though not depicted), VLDs also form when neurons shrink by going from isosmotic to hyperosmotic medium; *these* VLDs reverse when the neurons are returned to isosmotic medium. (b) Vertical section schematic to show how VLDs form: when the neuron shrinks, VLDs are initiated as invaginations from the adherent surface; then, as recovery proceeds, they pinch off near the adherent surface, yielding true vacuoles. A confocal slice (in cross section) made through a cell shortly after VLDs form is depicted, as in the image in Figure 2, bottom.

at discrete sites on the substrate-adherent surface. Confocal microscopy using membrane dyes (Figs. 1b and 2) and aqueous-phase dyes (Reuzeau *et al.*, 1995) reveals that VLD membrane and VLD contents are initially contiguous with plasma membrane and with extracellular fluid, respectively. VLD formation and reversal are rapid, occurring over tens of seconds. If stimuli that elicit VLD formation and reversal are given repeatedly (repeated cycles of swelling and shrinking, as depicted in Fig. 1a), then VLD formation and reversal occurs repeatedly at the same site. In cells left in normal saline to recover, VLD membrane is reprocessed and the VLDs disappear on a time scale of tens of minutes (at room temperature); this recovery is blocked by cytochalasin, by *N*-ethylmaleimide, and by Brefeldin A, but not by nocadazole. By contrast, these drugs do *not* block the osmomechanically driven formation and reversal of VLDs. During recovery (*i.e.*, the drug-sensitive set of events), VLDs can pinch off and become true vacuoles. This pinching-off, which involves actin rearrangements, internalizes membrane so that it is no longer, strictly speaking, plasma membrane.

Although the perturbations we use are osmomechanical, our evidence indicates that the membrane dynamics of VLD formation and reversal (but not VLD recovery dynamics) are driven predominantly by the mechanical rather than the chemical aspects of the perturbations. The evidence: absolute osmolarity is not important (VLDs form with shrinking stimuli whether the perturbations are hyposmotic-to-normal or normal-to-hyperosmotic), and extracellular calcium and other ions are not required.

Gastropod neurons are mechanically robust in the face of extreme swelling stimuli (Wan *et al.*, 1995). Though solute loss and the mechanics of the cortical cytoskeleton may reduce the rate of swelling, neurons can swell enormously and survive; 5-fold volume increases are tolerated. In effect, *compliance*, in the form of recruitment of additional membrane, appears to protect the cell from rupture when swelling is excessive (Wan *et al.*, 1995; Fejtl *et al.*, 1995). The membrane capacitance of these neurons increases with swelling and subsequently decreases with shrinking (Wan *et al.*, 1995). Membrane tension (see Dai and Sheetz, 1995) in *Lymnaea* neurons (J. Dai, M. Sheetz, and C. Morris, 1996. Am. Soc. Cell Biol. abstract) exposed to 0.5× normal osmolarity increased significantly, but to a level well below lytic tension, then was redressed upon return to normal saline. The return from 50% to normal osmolarity also elicited VLDs; hence, VLD formation occurred when the cell was reshrinking and membrane tension was falling back to normal. Taken together, the VLD, capacitance, volume, and tension observations are consistent with the possibility that neurons have a sensor-effector system

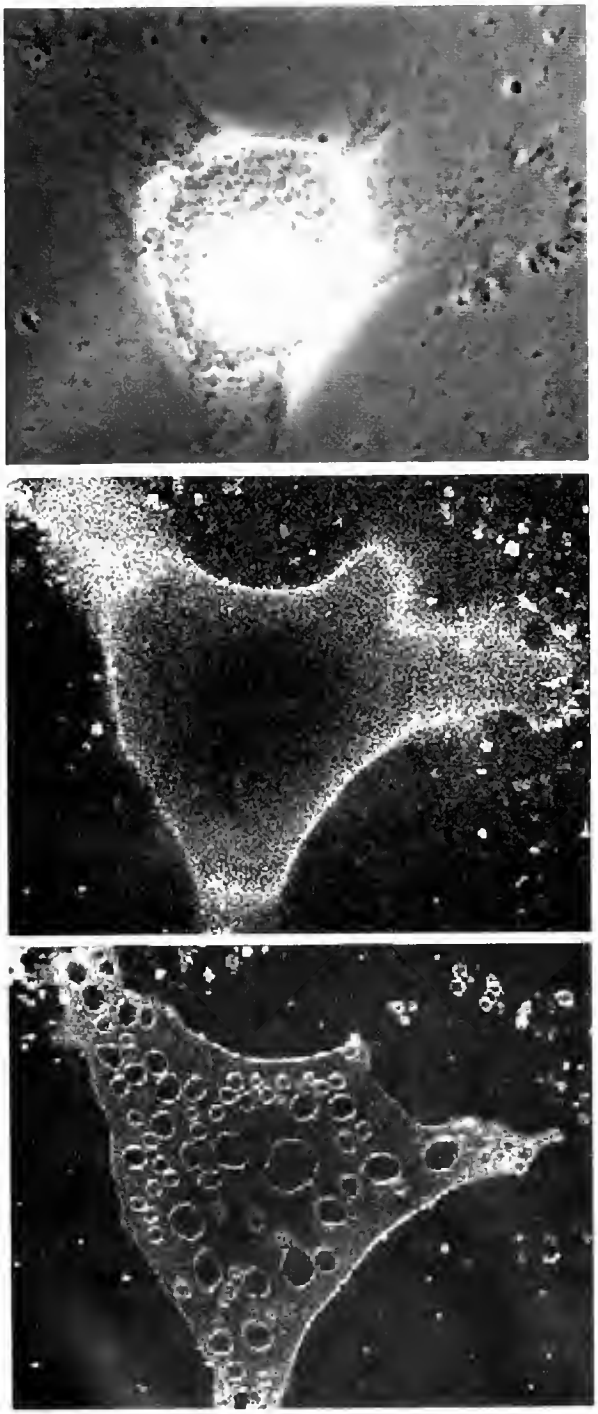

Figure 2. Phase contrast (top) and confocal fluorescence (middle, bottom) images of a cultured *Lymnaea stagnalis* neuron before (top, middle) and 1.5. min after) a solution change that elicited VLDs (bottom). The fluorescence images are confocal slices near the substrate. Fluorescence is from the membrane dye, dil. Neurons were stained (and made to swell) by adding distilled water plus dil (yielding a swelling medium osmolarity of about 0.2× normal) for 2 min. Excess dye was removed by several washes with the isosmotic saline. These washes shrank the swollen neuron, eliciting VLDs, bottom. (Because only a single confocal slice of the cell near the substrate is seen, volume changes are not evident.) Before eliciting VLDs (middle), dil stains only the plasma membrane. Its subsequent presence in VLD membrane (bottom) indicates that VLD membrane is contiguous with plasma membrane. Scale: phase contrast image is 140 μm high.

that enables them, in the face of changing mechanical stresses, to regulate their cell surface area and to keep membrane tension close to a set point.

So, how do neurons monitor their mechanical status? Adhesion to a substrate is critical to the VLD events we observe. Therefore, we suggest that neurons monitor and adjust their membrane tension and their surface area by using a sensor-effector system (*i.e.*, mechanosensitive membrane disposition) that works in concert with a cytoskeletal adhesion-based sensor-effector system (see Wang *et al.*, 1993). Although the popular idea of a monitoring role for mechanosensitive neuronal channels is not completely ruled out, evidence suggests that ion channel mechanosensitivity is deployed effectively in specialized receptor neurons (Oliet and Bourque, 1996), whereas it is suppressed in general-purpose neurons (Morris and Horn, 1991; Small and Morris, 1994; Paoletti and Ascher, 1994).

Acknowledgments

Supported by grants from NSERC, Canada, and by the Heart and Stroke Foundation of Ontario.

Literature Cited

Dai, J., and M. P. Sheetz. 1995. Mechanical properties of neuronal growth cone membranes studied by tether formation with laser optical tweezers. *Biophys. J.* **68:** 988–996.

Fejtl, M., D. H. Szarowski, D. Decker, K. Buttle, D. O. Carpenter, and J. N. Turner. 1995. Three-dimensional imaging and electrophysiology of live *Aplysia* neurons during volume perturbation: confocal light and high-voltage electron microscopy. *JMSA* **1:** 75–85.

Heidemann, S. R., and R. E. Buxton. 1994. Mechanical tension as a regulator of axonal development. *Neurotoxicology* **15:** 95–108.

Morris, C. E., and R. Horn. 1991. Failure to elicit neuronal macroscopic mechanosensitive currents anticipated by single channel studies. *Science* **251:** 1246–1249.

Oliet, S. H. R., and C. W. Bourque. 1996. Gadolinium uncouples mechanical detection and osmoreceptor potential in supraoptic neurons. *Neuron* **16:** 175–181.

Paoletti, P., and P. Ascher. 1994. Mechanosensitivity of NMDA receptors in cultured mouse central neurons. *Neuron* **13:** 645–655.

Reuzeau, C., L. R. Mills, J. A. Harris, and C. E. Morris. 1995. Discrete and reversible vacuole-like dilations induced by osmomechanical perturbations of neurons. *J. Membr. Biol.* **145:** 33–47.

Small, D. R., and C. E. Morris. 1994. Delayed activation of single mechanosensitive channels in *Lymnaea* neurons. *Am. J. Physiol.* **267:** C598–606.

Wang, N., J. P. Butler, and D. E. Ingber. 1993. Mechanotransduction across the cell surface and through the cytoskeleton. *Science* **260:** 1124–1127.

Wan, X., J. A. Harris, and C. E. Morris. 1995. Responses of neurons to extreme osmomechanical stress. *J. Membr. Biol.* **145:** 221–31.

Reference: *Biol. Bull.* **192:** 121–122. (February, 1997)

Mechanogated Channels in *Xenopus* Oocytes: Different Gating Modes Enable a Channel to Switch From a Phasic to a Tonic Mechanotransducer

OWEN P. HAMILL AND DON W. MCBRIDE JR.

Department of Physiology and Biophysics, The University of Texas Medical Branch, Galveston, Texas 77555

Critical to the survival of any cell is its ability to sense and respond appropriately to changes in its environment. In the case of the mechanical environment, there are both static and dynamic components that the cell may be required to selectively detect. Such detection takes place in the presence of a dynamic background of mechanical stimulation arising from Brownian motion, gravitational force, and various forces generated within a cell (*e.g.*, due to molecular motors and cycles of cytoskeletal polymerization and depolymerization) that maintain cell shape and also mediate shape changes during growth and adhesion. In addition to such background forces, a cell may experience other mechanical perturbations, ranging from steady indentations to high-frequency vibrations, and from osmotic challenges to fluid shear stresses. Detection and appropriate responses to such perturbations may be critical for the function and, perhaps, survival of the cell. Therefore, cells require biological mechanotransducers that can extract specific information regarding relevant mechanical stimuli while filtering out irrelevant stimuli.

A variety of mechanosensitive processes have been identified including (i) mechanosensitive enzymes such as adenylate cyclase (Watson, 1990) and phospholipase A_2 (Jukka *et al.*, 1995), (ii) mechanosensitive transmitter release (Chen and Grinnell, 1995), (iii) mechanosensitive gene activation (Sadoshima *et al.*, 1992), and (iv) the widely expressed class of mechanogated (MG) membrane ion channels (Martinac, 1992). Of these different processes, the MG channels have proven the most amenable to detailed biophysical study. This has been due, in part, to the development of high-resolution patch-clamp recording (Hamill *et al.*, 1981) and fast pressure-clamp stimulating techniques (McBride and Hamill, 1992, 1993, 1995; Hamill and McBride, 1995a). We have used these techniques to study the dynamic properties of single MG channels, mainly focusing on the cation-selective channel endogenously expressed in *Xenopus* oocytes (Hamill and McBride, 1992, 1994, 1995b, 1996a; Zhang *et al.*, 1996). This channel is blocked by amiloride and its analogs, aminoglycoside antibiotics and gadolinium (for review see Hamill and McBride, 1996b). One of the most interesting kinetic features of the channel is that its gating mode can be shifted from a highly nonstationary, phasic or "high pass" mode to a stationary, tonic or "low pass" mode (*i.e.*, the input-filter characteristics change). When in the phasic mode the MG channel activity exhibits rapid and complete adaptation (*i.e.*, the channels close) despite the presence of maintained mechanical stimulation. This adaptation is highly voltage dependent and is similar to that seen in audiovestibular hair cells (Crawford *et al.*, 1991). For example, at −100 mV the decay time constant of adaptation is about 100 ms, while at +100 mV it is more than 2 s. However, unlike the hair cell, this adaptation does not depend on either extracellular or intracellular Ca^{++} nor on the polarity of stimulation (*i.e.*, suction or pressure). We find that the adaptation in the oocyte MG channel is due to a shift of the stimulus-response relation (Boltzmann) to the right (*i.e.*, towards higher pressures) with no change in shape of the relation. This adaptation reduces response saturation

This paper was originally presented at a workshop titled *The Future of Aquatic Research in Space: Neurobiology, Cellular and Molecular Biology*. The workshop, which was held at the Marine Biological Laboratory, Woods Hole, Massachusetts, from 13 to 15 May 1996, was sponsored by the Center for Advanced Studies in the Space Life Sciences at MBL and funded by the National Aeronautics and Space Administration under Cooperative Agreement NCC 2-896.

while preserving the differential sensitivity to transient changes in mechanical stimulation.

When the MG channel is in the tonic mode, the open channel probability becomes time independent but increases with increasing suction or pressure stimulation. However, the sensitivity of the MG channel to mechanical activation is decreased. Although voltage-dependent adaptation is clearly absent in this mode, the voltage dependence of MG channel lifetime is preserved and single channel conductance and ion selectivity remain unaltered. The switching between gating modes can be mechanically induced in the patch-clamp configuration and is most likely due to a physical decoupling of the membrane from the underlying cytoskeleton, which presumably contains the required viscoelastic elements. This idea of decoupling is supported by the observed development of a clear space within the patch pipette between the membrane and the underlying cytoplasm; development of this space accompanies the mechanically induced channel mode switching.

The channel mode switching from phasic to tonic, as studied here, probably reflects a pathological situation associated with patch-clamp recording (Hamill and McBride, 1997). Nevertheless, it does indicate a mechanism by which a single molecular mechanotransducer may alter its input filter characteristics (*i.e.*, go from a transient to a steady-state detector) of mechanical signals. It remains to be determined whether the remodeling of the cortical cytoskeleton that occurs during cell development and differentiation (*e.g.*, see Vale, 1991; Sardet *et al.*, 1994) may also modulate membrane mechanosensitivity by such a mechanism.

Acknowledgments

Our research is supported by grants from the National Institute of Arthritis and Musculoskeletal and Skin Diseases, Grant RO1-AR42782, the National Science Foundation, and the Muscular Dystrophy Association.

Literature Cited

Chen, B.-M., and A. D. Grinnell. 1995. Integrins and modulation of transmitter release from motor terminals by stretch. *Science* **269:** 1578–1580.

Crawford, A. C., M. G. Evans, and R. Fettiplace. 1991. The action of calcium on the mechanoelectrical transducer current of turtle hair cells. *J. Physiol.* **434:** 369–398.

Hamill, O. P., A. Marty, E. Neher, B. Sakmann, and F. Sigworth. 1981. Improved patch clamp techniques for high current resolution from cells and cell-free membrane patches. *Pflugers Arch. Eur. J. Physiol.* **391:** 85–100.

Hamill, O. P., and D. W. McBride, Jr. 1992. Rapid adaptation of the mechanosensitive channel in *Xenopus* oocytes. *Proc. Natl. Acad. Sci. USA* **89:** 7462–7466.

Hamill, O. P., and D. W. McBride, Jr. 1994. Molecular mechanisms of mechanoreceptor adaptation. *News in Physiological Sciences* **9:** 53–59.

Hamill, O. P., and D. W. McBride, Jr. 1995a. Pressure/patch-clamp methods. Pp. 75–87 in *Patch Clamp Techniques and Protocols,* A. A. Boulton, G. B. Baker, and W. Walz, eds. Humana Press, New Jersey.

Hamill, O. P., and D. W. McBride, Jr. 1995b. Mechanoreceptive membrane ion channels. *Am. Sci.* **83:** 30–37.

Hamill, O. P., and D. W. McBride, Jr. 1996a. Voltage and tension sensitivity of a mechanogated channel. *Biophys. J.* **70:** A348.

Hamill, O. P., and D. W. McBride, Jr. 1996b. The pharmacology of mechanogated channels. *Pharmacol. Rev.* **48:** 231–252.

Hamill, O. P., and D. W. McBride, Jr. 1997. Induced membrane hypo/hyper-mechanosensitivity: a limitation of patch-clamp recording. *Annu. Rev. Physiol.* **59:** 621–631.

Jukka, Y., A. Lehtonen, and P. K. J. Kinnunen. 1995. Phospholipase A_2 as a mechanosensor. *Biophys. J.* **68:** 1888–1894.

Martinac, B. 1992. Mechanosensitive ion channels: biophysics and physiology. Pp. 327–352 in *Thermodynamics of Cell Surface Receptors,* M. B. Jackson, ed. CRC Press, Boca Raton, FL.

McBride, D. W., Jr., and O. P. Hamill. 1992. Pressure clamp: a method for rapid step perturbation of mechanosensitive channels. *Pflugers Arch. Eur. J. Physiol* **421:** 606–612.

McBride, D. W. Jr., and O. P. Hamill. 1993. Pressure-clamp technique for measurement of the relaxation kinetics of mechanosensitive channels. *Trends Neurosci.* **16:** 341–345.

McBride, D. W. Jr., and O. P. Hamill. 1995. A fast pressure-clamp technique for studying mechanogated channels. Pp. 329–340 in *Single Channel Recording,* 2nd Edition, B. Sakmann, and E. Neher, eds. Plenum Press, New York.

Sadoshima, J-I., T. Takahashi, L. Jahn, and S. Izumo. 1992. Roles of mechano-sensitive ion channels, cytoskeleton, and contractile activity in stretch-induced immediate-early gene expression and hypertrophy of cardiac myocytes. *Proc. Natl. Acad. Sci. USA* **89:** 9905–9909.

Sardet, C., A. McDougall, and E. Houliston. 1994. Cytoplasmic domains in eggs. *Trends Cell Biol.* **4:** 166–172.

Vale, R. D. 1991. Severing of stable microtubules by a mitotically activated protein in *Xenopus* egg extracts. *Cell* **64:** 827–839.

Watson, P. A. 1990. Direct stimulation of adenylate cyclase by mechanical forces in S49 mouse lymphoma cells during hyposmotic swelling. *J. Biol. Chem.* **265:** 6569–6575.

Zhang, Y., F. Gao, D. W. McBride, and O. P. Hamill. 1996. On the nature of mechano-gated channel activity in cytoskeleton deficient vesicles shed from *Xenopus* oocytes. *Biophys. J.* **70(2):** A349, 1996.

Reference: *Biol. Bull.* **192:** 123–124. (February, 1997)

Discussion

MORRIS: I would like to ask Owen Hamill a question. Both my laboratory (in collaboration with Rick Elinson) and now your laboratory have shown that, if you use pharmacological agents to block these channels, embryogenesis of the oocyte is not impeded. Is this a fair statement? Could you comment on what it means?

HAMILL: Frogs eggs have been taken up on the space shuttle, where they can be happily fertilized, and embryogenesis occurs normally in the microgravity environment. Once the oocytes are out of the animal, they don't seem to be especially dependent on mechanical stimuli, at least as reflected by mechanogated channels. For example, you can block the mechanosensitive channel and still watch the whole process, from fertilization to a developed embryo. Apparently the tadpoles also develop normally in microgravity. But of course all of the mechanically interesting events of oocyte development occur before fertilization and are associated with the growth of the oocyte from 10^{-9} grams to 1 mg. This involves enormous expansion of the oocyte with enormous cytoskeletal rearrangement, and it's our bet that that's dependent on the mechanogated channel.

LOEWENSTEIN: Dr. Morris, what you call the adhesion portion seems to start out with an invagination process. What structures do you actually see or suspect might be initiating this?

MORRIS: We haven't actually any clue about that as yet. We know that once the VLDs form, actin accumulates around them. However, if you treat the cells with cytochalasin, you can still make these VLDs. It's clear that the cytochalasin has worked because the phalloidin staining is wildly different. We need to look at spectrin staining and things like that. I don't want to do this with the molluscan cells; so we are going to try it in skeletal muscle fibers, because they make very big cells in culture and we can use the antibodies with them. A recent paper from Brad Amos and Jack Lucy's lab in Cambridge (*J. Muscle Res. Cell Motil.* 1995. **16:** 401–11) has shown basically the same thing: reversible vacuolation in skeletal muscle. In their case, it's the entotubular system that's involved, which originates at the Z-line. They don't know either whether any other structures are associated with this. The only structural detail that they have is that it's associated with the Z-line. We don't have any molecular information.

LOEWENSTEIN: How do you define adhesion?

MORRIS: It's the attached surface; and we know the cells are adherent. I don't mean that there are specific adhesion molecules associated with this. I don't know that. It's not happening on the upper surface of these cultured cells, which is a very low-level definition of adhesion.

LOEWENSTEIN: What do you suggest for the mechanism of reversibility here?

MORRIS: I suspect that the membrane is flowing back out and up over the surface when swelling is occurring. That's the reversibility. I am amazed that membrane would then flow back into the same site, but it does. I presume that some structure there is acting as a scaffold to support it, but we have no idea yet about what it is.

QUESTION: Rick Steinhart has recently been describing how cells rupture and reseal very quickly with membrane vesicles. I wonder whether you are looking at rupture that occurs upon swelling at the sites of attachment, where the maximal mechanical force would be experienced. Recruitment of membrane vesicles to seal that rupture could be what makes your internal vacuoles.

MORRIS: If so, we are not picking up any of the extracellular dyes into the cell.

QUESTION: How big are these dyes?

MORRIS: We used Rhodamine 3000. The structures that we see are not tiny vesicles; they grow to be an average of 10 μm across once they are fully formed.

QUESTION: What happens to the membrane voltage during the swelling?

MORRIS: I don't know what happens to the membrane voltage. We

know that we can activate the potassium channels with slow swelling, and we think that these channels may actually be the stretch-activated channels. We don't know whether they are being stretch-activated. We could be getting additional conductance because we've added more membrane carrying the channels, or because they are getting second messenger signals. Since slow swelling is activating these potassium currents, I would imagine that, like *Aplysia* neurons, ours hyperpolarize with swelling. We haven't actually measured them.

CHALFIE: You showed what happens after 2-min changes. What happens when the cells reach osmotic equilibrium after the change? Do the vacuoles go away?

MORRIS: Yes, that's in recovery.

ELINSON: Owen (Hamill), those oocytes have an animal and vegetal difference. Do you see any disparity in the presence of those channels on the animal or vegetal pole? Or if you look at oocytes early in oogenesis, when things are moving, do you see any differences in these mechanical channels?

HAMILL: No, we don't.

ELINSON: So we still have no role for these channels in the oocyte?

HAMILL: We don't know the role yet.

QUESTION: Dr. Morris, is contact with a cover slip required for formation of VLDs?

MORRIS: Not necessarily. We have images of hippocampal cells growing on glial cells and they make VLDs, but these are hard to image. So I don't think that contact with a cover slip is critical, but mechanical contact of some sort is.

HAMILL: Do you see these VLDs with mild osmotic changes, or do you really have to stress the cells?

MORRIS: You see them if you step them down from normal to 70% normal osmotic concentration.

LOEWENSTEIN: Dr. Hamill, in your interesting model there seem to be two components: one is nonmechanical and the other, superimposed on that, is mechanical and acting somewhere in the coupling process. Could you elaborate on the latter? I could easily see an adaptation process being promoted mechanically, but I can't quite visualize a process in which adaptation is abolished mechanically, as in your case.

HAMILL: If the viscoelastic element is in the cytoskeleton and that's decoupled, adaptation would be abolished. You can think of this in terms of a gating spring and a dashpot in series. Normally, when you pull on the dashpot the spring stretches. Then the dashpot relaxes the spring, and you get adaptation. What we imagine in the oocyte is that the adaptation occurs because the underlying cytoskeleton relaxes. Once the cytoskeleton is decoupled, or one element (the viscous element) is decoupled, you can still have gating, but not the relaxation. We have tried to dissect out the viscous from the elastic elements. At one point we thought that one might be the microtubule and the other actin, but they don't seem to be very sensitive to either colchicine or cytochalasin.

CHALFIE: What is the effect of fertilization in activating these channels?

HAMILL: There certainly are potential changes associated with the block to polyspermy. We have tried very hard to see effects of all these mechanosensitive channels on polyspermy, fertilization, and even maturation. Up to maturation there is no sensitivity blocking of the mechanogated channel. But that's only half the story because many events precede maturation, and we have not yet examined them.

Reference: *Biol. Bull.* **192:** 125. (February, 1997)

A Molecular Model for Mechanosensation in *Caenorhabditis elegans*

MARTIN CHALFIE

Department of Biological Sciences, 1012 Fairchild, Columbia University, Mail Code 2446, 1212 Amsterdam Avenue, New York, NY 10027

Sensory signaling by chemicals and light are fairly well understood in molecular terms, but the molecules needed for mechanical signaling, which underlies the senses of touch, hearing, and balance, are not known. By analyzing the genes needed for mechanosensation in the nematode *Caenorhabditis elegans*, we hope to gain this molecular understanding. Six touch receptor neurons respond to gentle touch in *C. elegans*. Mutations producing touch insensitivity have identified 12 *mec* (mechanosensory abnormal) genes needed for touch cell function (Chalfie and Sulston, 1981; Chalfie and Au, 1989). Eight of these genes have been cloned by ourselves and others. Two genes (*mec*-4 and *mec*-10) encode similar subunits (degenerins) of a channel needed for mechanosensation (Driscoll and Chalfie, 1991; Huang and Chalfie, 1994). Gene interaction studies suggest that many of the remaining *mec* genes interact with this channel (Huang and Chalfie, 1994; Gu *et al.*, 1996).

Predicted protein sequences, gene interactions, and ultrastructural studies of the touch receptor neurons suggest the following model for mechanosensation in these cells (Gu *et al.*, 1996). Mechanosensation requires the degenerin channel formed from MEC-4, MEC-10, and probably MEC-6. This channel is attached to the extracellular matrix, perhaps through interactions with MEC-5 (a collagen) and possibly MEC-1 and MEC-9 (Du *et al.*, 1996). Intracellularly, the channel is attached to the microtubules formed by MEC-12 (α-tubulin) and MEC-7 (β-tubulin), through an interaction with the stomatin-like protein MEC-2 (Huang *et al.*, 1995). The other *mec* genes may be modifying the conductance of this channel. In this model, physical manipulation of the channel either by displacement of the cuticle or the microtubules opens the channel.

This paper was originally presented at a workshop titled *The Future of Aquatic Research in Space: Neurobiology, Cellular and Molecular Biology*. The workshop, which was held at the Marine Biological Laboratory, Woods Hole, Massachusetts, from 13 to 15 May 1996, was sponsored by the Center for Advanced Studies in the Space Life Sciences at MBL and funded by the National Aeronautics and Space Administration under Cooperative Agreement NCC 2-896.

Literature Cited

Chalfie, M., and M. Au. 1989. Genetic control of differentiation of the *C. elegans* touch receptor neurons. *Science* **243:** 1027–1033.

Chalfie, M., and J. Sulston. 1981. Developmental genetics of the mechanosensory neurons of *Caenorhabditis elegans*. *Dev. Biol.* **82:** 358–370.

Driscoll, M., and M. Chalfie. 1991. The *mec*-4 gene is a member of a family of *Caenorhabditis elegans* genes that can mutate to induce neuronal degeneration. *Nature* **349:** 588–593.

Du, H., G. Gu, C. William, and M. Chalfie. 1996. Extracellular proteins needed for *C. elegans* mechanosensation. *Neuron* **16:** 183–194.

Gu, G., G. A. Caldwell, and M. Chalfie. 1996. Genetic interactions affecting touch sensitivity in *Caenorhabditis elegans*. *Proc. Natl. Acad. Sci. USA* **93:** 6577–6582.

Huang, M., and M. Chalfie. 1994. Gene interactions affecting mechanosensory transduction in *Caenorhabditis elegans*. *Nature* **367:** 467–470.

Huang, M., G. Gu, E. L. Ferguson, and M. Chalfie. 1995. A stomatin-like protein necessary for mechanosensation in *C. elegans*. *Nature* **378:** 292–295.

Reference: *Biol. Bull.* **192:** 126–127. (February, 1997)

Mechanosensitive Channels of *E. coli:* A Genetic and Molecular Dissection

PAUL BLOUNT[1], SERGEI I. SUKHAREV[1], PAUL MOE[1,2], AND CHING KUNG[1,3]

[1]*Laboratory of Molecular Biology and* [2]*Departments of Bacteriology and* [3]*Genetics, University of Wisconsin, Madison, Wisconsin 53706*

Our understanding of mechanosensation is poor, especially at the level of molecule. There is no shortage of phenomena, from the sensation of gravity, touch, balance, and hearing in animals, gravitropism and thigmomorphogenesis in plants, to the detection of osmotic forces in all cells including microbes. Yet to name a protein or gene that is responsible for these sensations is difficult. This knowledge vacuum is all the more striking given that we know, in exquisite detail, the structure and function of a myriad of ligand receptors, and even the receptors of light, rhodopsins.

One class of "receptors" are ion channels. These are integral membrane proteins that line gated pores. By "gated," physiologists mean that the pore is usually closed until the channel protein "senses" a stimulus. There are ion channels gated by external ligands (*e.g.*, neurotransmitters), second messengers (Ca^{2+}, cyclic nucleotides), or membrane potentials (*i.e.*, transmembrane voltage drop) (Hille, 1992). Channel pores, when open, allow passive fluxes of permeant ions. The advent of the patch clamp has greatly enhanced our capability to monitor these ion fluxes: even the ion current through a single channel protein can clearly be registered and analyzed (Sakmann and Neher, 1995). Activities of channels that open when the membrane patch in a patch-clamp pipette is mechanically stretched were first observed in muscle cells (Guharay and Sachs, 1984; Brehm *et al.*, 1984). This kind of activity has now been reported from studies of neurons, oocytes, heart cells, lens cells, blood cells, and plant cells (Sackin, 1995). Moreover, mechanosensitive (MS) channel activities have also been observed in microbes: budding yeast, fission yeast, bean-rust fungus, and the bacteria *Escherichia coli* and *Bacillus subtilis.*

When *E. coli* is cultured in the presence of cephalexin, the cells do not remain septate but continue to grow into filaments, some reaching 100 μm in length. They can be digested with lysozyme and EDTA and then collapsed into spheres 3 to 10 μm in diameter. Patch-clamp experiments on such giant spheroplasts revealed two types of MS-channel activities, one with a very large conductance (2.5 nS) and one with a smaller conductance (0.8 nS). These activities are observed as the appearance and disappearance of unitary currents indicative of channel opening and closing. The open probability increases with the suction applied to the patch-clamp pipette (Martinac *et al.*, 1987; Sukharev *et al.*, 1993). The MS channels of *E. coli* can be reconstituted. In other words, bacterial membrane vesicles, even after solubilization in a mild detergent, can be placed in liposomes made of foreign lipids and the MS channels remain functional (Delcour *et al.*, 1989). We followed the activity of the 2.5-nS MS conductance through different series of column chromatographic enrichments by reconstituting the column fractions into soybean liposomes and examining patches excised from them with the patch clamp. By tracing the activities in the more and more enriched fractions, a protein of about 17,000 molecular weight was identified. From the N-terminal sequence of this protein, the corresponding gene, *mscL,* was cloned (Sukharev *et al.*, 1994a). Disrupting *mscL* by a marker insertion removed the 17-kD membrane protein and the 2.5-nS conductance. Replenishing this null strain with *mscL* on a plasmid restored both. The *mscL* gene, subcloned into appropriate plasmids, has been functionally expressed in two heterologous systems: rabbit reticulocyte lysate and yeast. Therefore *mscL* alone is necessary and sufficient

This paper was originally presented at a workshop titled *The Future of Aquatic Research in Space: Neurobiology, Cellular and Molecular Biology.* The workshop, which was held at the Marine Biological Laboratory, Woods Hole, Massachusetts, from 13 to 15 May 1996, was sponsored by the Center for Advanced Studies in the Space Life Sciences at MBL and funded by the National Aeronautics and Space Administration under Cooperative Agreement NCC 2-896.

for the 2.5-nS MS-channel activities (Sukharev *et al.*, 1994a, b).

Conceptual translation of *mscL* yields a protein of 136 amino-acid residues. The first three-quarters of the MscL protein is highly hydrophobic according to its hydrophobicity plot. Four lines of recent evidence have indicated that each MscL peptide traverses the membrane twice, with both the N- and the C-terminus in the cytoplasm. Cross-linking and other experiments showed that MscL monomers assemble into a hexamer that probably encloses the pore. A number of deletions and point substitutions have been made and tested for MS-channel properties. These results indicate the importance of both the transmembrane domains and the linking loop between these domains. Substitutions of certain hydrophilic residues changed the channel kinetics, the mechanosensitivity, or both (Blount *et al.*, 1996a, b). Well-conserved *mscL* homologs have recently been found in several bacteria, including gram-positive bacteria (Moe *et al.*, unpub. data).

Our current effort is directed toward (1) understanding the molecular basis of mechanosensitivity by applying forward and reverse genetics on *E. coli mscL*, (2) elucidating the function of these MS channels in bacterial physiology, and (3) searching for mscL homologs in other species, including plants and animals.

Acknowledgments

Work in our laboratory was supported by NIH GM47856.

Literature Cited

Blount, P., S. I. Sukharev, P. C. Moe, M. J. Schroeder, H. R. Guy, and C. Kung. 1996a. Membrane topology and multimeric structure of a mechanosensitive channel protein of *Escherichia coli*. *EMBO (Eur. Mol. Biol. Organ.) J.* **15:** 4798–4805.

Blount, P., S. I. Sukharev, M. J. Schroeder, S. Nagle, and C. Kung. 1996b. Single residue substitutions that change the gating properties of a mechanosensitive channel in *Escherichia coli*. *Proc. Natl. Acad. Sci. USA* **93:** 11652–11657.

Brehm, P., R. Kullberg, and F. Moody-Corbett. 1984. Properties of non-junctional acetylcholine receptor channels on innervated muscle of *Xenopus laevis*. *J. Physiol. (Lond.)* **350:** 631–648.

Delcour, A. H., B. Martinac, J. Adler, and C. Kung. 1989. Modified reconstitution method used in patch-clamp studies of *Escherichia coli* ion channels. *Biophys. J.* **56:** 631–636.

Guharay, F., and F. Sachs. 1984. Stretch-activated single ion channel currents in tissue-cultured embryonic chick skeletal muscle. *J. Physiol. (Lond.)* **352:** 685–701.

Hille, B. 1992. *Ionic Channels of Excitable Membranes.* Sinauer Associates Inc., Sunderland, MA.

Martinac, B., M. Buechner, A. H. Delcour, J. Adler, and C. Kung. 1987. Pressure-sensitive ion channel in *Escherichia coli*. *Proc. Natl. Acad. Sci. USA* **84:** 2297–2301.

Sackin, H. 1995. Mechanosensitive channels. *Annu. Rev. Physiol.* **57:** 333–353.

Sakmann, B., and E. Neher. 1995. *Single-Channel Recording.* 2nd Edition. Plenum Press, New York.

Sukharev, S. I., B. Martinac, V. Y. Arshavsky, and C. Kung. 1993. Two types of mechanosensitive channels in *Escherichia coli* cell envelope: solubilization and functional reconstitution. *Biophys. J.* **65:** 177–183.

Sukharev, S. I., P. Blount, B. Martinac, F. R. Blattner, and C. Kung. 1994a. A large-conductance mechanosensitive channel in *E. coli* encoded by *mscL* alone. *Nature* **368:** 265–268.

Sukharev, S. I., B. Martinac, P. Blount, and C. Kung. 1994b. *Methods: A Companion to Methods in Enzymology.* **6:** 51–59.

Reference: *Biol. Bull* **192:** 128–130. (February, 1997)

Discussion

CHALFIE (in response to an inaudible question): We have been able to identify 17 genes in the screen for touch-insensitive genes. If you mutate them, you get a selectively defective animal that just doesn't respond to touch. Of the five genes required for cell differentiation that we have identified, three are transcription factors that are needed to make either precursors or the cell itself, another appears to be a transcription factor needed to maintain the differentiated state, and the fifth is a splicing factor needed to process one or more of the function genes. This last gene is the work of Lundquist *et al.* (*Development* 1996. **122:** 1601–1610).

We also know that there are genes whose products act negatively in the touch system, but we would not have been able to screen for mutations in these genes, because we were not looking for touch supersensitive animals. We are trying to develop ways to look at such mutants. For example, the touch circuit is one that requires gap junctions between the interneurons and the touch receptor cells. At the same time as the posterior touch cells are making gap junctions to one set of interneurons, they are also making chemical synapses to another set of interneurons to which the anterior cells are making gap junctions. Getting rid of the chemical synapses wouldn't produce touch insensitivity, but others have identified genes needed for chemical transmission.

QUESTION: Twelve seems to be a small number for what seems to be a saturation screen.

CHALFIE: As I tried to indicate, we have over 500 mutations in 17 genes, quite a number of alleles for every single one of those genes that we study. So we have probably saturated for genes that can be mutated to the touch-insensitive phenotype. In addition, we have done an experiment to get dominantly enhancing mutations with two different function genes, and we have not been able to find any new players. That says that no dosage-dependent gene is involved. We have not been able to eliminate genes that may be important for the mechanosensory apparatus (for example microtubule-associated protein) and that also produce lethality or are perhaps redundant.

HAMILL: By analogy to the hair cell, your model envisages gating being mediated by the cytoskeleton. In the hair cell, the tip links are directly gated. What do you see as a role for MEC-5 in your system?

CHALFIE: The three products that we think are important in the extracellular matrix are MEC-1, MEC-5, and MEC-9. *mec-1* is not cloned, but when you get rid of it genetically there is no extracellular matrix for those cells, and the animals are touch insensitive. Both *mec-5* and *mec-9* have been cloned: *mec-5* encodes a collagen that's made by the cells that surround the touch cells, and MEC-9 is a secreted protein made by the touch cells. We have very strong genetic interactions between the two of them, so we think they are coupled. We have somewhat weaker evidence for an interaction between the *mec-5* collagen and the *mec-4* and *mec-6* genes whose products we think contribute to the channel. So a collagen is associated with the channel. There's also another one of this family of channel proteins, the product of the *unc-105* gene, that's being worked on by J. D. Liu in Bob Waterston's lab in St. Louis (Liu *et al.* 1996. *Science* **273:** 361–364). What they have found is that a suppressor of *unc-105* activity is also a collagen. So this family of channel proteins seems to interact with collagens.

Let me address one other thing that you said. I don't think that the models are very different. It's like the distinction between pulling and holding on, and to what. We're saying that whether you're holding on with the tip link or the extracellular matrix, you are also tethered to the actin cytoskeleton or the microtubule cytoskeleton in the two systems. In fact, the question is, Does the tip link move to open that channel, or does the hair cell move and pull the channel away from the tip link? I don't think that there is any evidence bearing on which element is actually the moving component. Peter (Gillespie) may have more to say about that. It seems to me that it would be easier for the microtubules to float within the cell than for the extracel-

lular matrix to be moved. In fact, if you hit the matrix hard enough, that will jar the microtubules. It's hard to know who is pulling on whom; I just think that the microtubules are a little more liable to be moved relative to the matrix.

LOEWENSTEIN: When you mentioned the inside sensor, did you really mean *sensor* or *coupling?* The actual sensor is the transducer. I think you probably meant coupling, and that is what makes your system different from Kung's.

CHALFIE: We don't know how these things are interacting. One of the things that we have tried to explain in the model is the morphology of the cell with the microtubules situated within the processes. In fact, the microtubules are not needed for the outgrowth of the cells or any other function of the cell that we can find; but the microtubules are absolutely essential for those cells functioning as touch receptors. In addition, the association with the MEC-2 protein and genetic interactions all suggest that the microtubules are actually part of the apparatus. This model is very difficult to test by trying to reconstitute all of these components in some sort of heterologous system.

KAWASAKI: You find these touch receptors in *E. coli* and hair cells. How ubiquitous are they?

CHALFIE: Owen Hamill probably has a better handle on this in terms of the pharmacology of channels examined with cells in culture. Mechanically activated and mechanically inactivated channels have been found in a wide variety of cell types. If you are asking whether channel proteins similar to the *E. coli* or *C. elegans* proteins can be found in vertebrates, the answer is that Ching Kung and I both hope so. Our channel proteins are certainly found in nematodes, and there are similar members of what could be a superfamily of proteins in vertebrates. Whether these proteins act as mechanosensory channel components in vertebrates is not known.

KUNG: If I may add to the matter of ubiquity: By the criterion of the patch clamp these channels are all over the place. You can take just about any cell membrane, attach a patch pipette, apply suction and you will see something open. If you do not use the patch clamp as a criterion, but look for the genes, then we are looking for *mec-4, mec-10,* or *mscL* homologues. That's in progress. When you say homologue, you must be careful because you do not know how much of the region is crucial to mechanosensation. One doesn't know how to search the database at this point, because our knowledge of these molecules is fairly primitive.

LOEWENSTEIN: Dr. Kung, a comment on your model propsing a hexamer. A hexameric channel implies a mechanistic possibility that I think is quite attractive in a mechanosensing device. If your six subunits are slanted, as in the channel I have been working with, you might get a direct coupling in a rather simple way. A hexamer with slanted units can switch between an open and closed configuration by a slight change in the tilt of the subunits. A very small movement, due to a pressure change in the lipid bilayer of the cell membrane, would change the angle of tilt, making the channel go into the open configuration—a coupling as direct as you are proposing. With this model, one could easily imagine that a minute strain perpendicular to the membrane could be amplified by the lever action of the slanted subunits and be transduced into a current—a channel opening or closing produced in the most directly coupled way.

KUNG: I have to point out that I don't propose, I prove. That's not a proposal, that's actually an observation. You ask me whether this is a possible model. I certainly think that this is a possible model. My position is that I believe in experiments.

BARLOW, R.: I have a question regarding degenerins. You said that three mutations cause cell death, cell lysis. As I understood it, your interpretation is that faulty operation of the channel leads to cell death. I am curious about an analogous situation, in vision, where multiple mutations of rhodopsin lead to retinal degeneration. Retinal degeneration may not necessarily be caused by rhodopsins not working well, but rather that the mutated proteins trigger natural cell death, apoptosis. Could something similar be happening with these mutations?

CHALFIE: That's a great question. In *C. elegans* there is some beautiful work, primarily by people in Bob Horvitz's lab, on genes that are needed for programmed cell death in the animal. A cell that's dying by programmed cell death in *C. elegans* becomes very condensed and very refractile in the light microscope. Mutations in the genes *ced-3* and *ced-4* abolish these cell deaths, so the cells persist. The deaths that we see in the *mec-4* and *mec-10* animals, and in mutants defective in one other gene, *deg-1* (all three genes encode proteins we call degenerins), are very different. The cells don't become refractile; they swell up to many cell diameters and vacuolate. Genetically, mutations in *ced-3* and *ced-4* genes have absolutely no effect that we have been able to discern on the degenerations caused by mutations in *mec-4* or *deg-1*, and so on. In addition, any of the mutations that prevent the cell deaths from the pre-

sumed channel mutations have no effect on programmed cell death, so they seem to be two independent systems. Rather than apoptotic cell death, a better analogy might be to some of the defects that are seen in hypocalemic periodic paralysis in humans and other mammals in which a defect in the dihydropyridine calcium channel leads to defects in muscle with a fair amount of vacuolization and ultrastructural changes, such as membrane infolding and multilamellar bodies. We see these defects in *mec-4* and *deg-1* animals. Because of the similarities in morphology, we think that the channel defect causes the degeneration.

Reference: *Biol. Bull.* **192:** 131–133. (February, 1997)

Gravitaxis in Flagellates

DONAT-PETER HÄDER

Institute for Botany and Pharmaceutical Biology, Staudtstr. 5, D-91058 Erlangen, Germany

The green, unicellular flagellate *Euglena gracilis* orients itself in the water column by responding to external stimuli such as light and gravity (Häder, 1987; Häder *et al.*, 1995). While the photoreceptor has been characterized spectroscopically and biochemically in this organism, our knowledge of gravity-dependent orientation mechanisms has been rather limited. Earlier hypotheses assumed that the cell has an asymmetric mass distribution and is passively oriented in the water column like a buoy. However, we found that the cells change their orientation with age: young cells (up to 4 days after inoculation) show positive gravitaxis, but older cells show a negative one. Another indication that the cells use an active receptor and a physiological sensory transduction chain for graviperception is the finding that positive gravitaxis (in young cells) can be reversed by the addition of micromolar concentrations of certain heavy metal ions (cadmium, mercury, lead).

During a recent space flight on the American shuttle *Columbia* the cells could be subjected to increasing accelerations on a centrifuge microscope (NIZEMI) (Häder *et al.*, 1995). These experiments indicated that the threshold for gravitaxis in *Euglena* is at about $0.16 \times g$; above $0.64 \times g$ the precision of orientation saturates. The dose response curve has a typical sigmoidal shape, again indicating the involvement of a physiological gravireceptor in contrast to a passive orientation in the water column.

One option for an active gravireceptor is an intracellular statolith exerting pressure on a sensor, as has been proposed for gravitropism in higher plants. This assumption could be ruled out by the following experiment. The density of the outer medium was increased with Ficoll. At low Ficoll concentrations (2.5%), negative gravitaxis was only slightly impaired compared to the control (Fig. 1a, b). With increasing concentrations, the density of the medium approached the density of the *Euglena* cell body (1.04 g ml^{-1}), and negative gravitactic orientation was strongly affected (Fig. 1c, d). At higher concentrations, the cells showed positive gravitaxis (Fig. 1e) because the direction of the pressure of the cell body on its outer membrane is reversed, and so the direction of orientation also reverses. Changing the density of the medium cannot affect an intracellular gravisensor. Therefore it was assumed that the whole cell—being heavier than the surrounding medium—exerts pressure on the lower cell membrane which has also been suggested for the ciliate *Paramecium* (Machemer and Bräucker, 1992). This could be sensed by stretch-sensitive ion channels which have been demonstrated in a number of different biological systems.

Stretch-sensitive ion channels can be inhibited by gadolinium ions (Franco *et al.*, 1991; Lacampagne *et al.*, 1994; Sukharev *et al.*, 1993). At low concentrations, Gd^{3+} (100 μM) strongly affected graviorientation, which was totally inhibited after 90 s. This result indicates strongly that Ca^{2+}-conducting, stretch-sensitive ion channels in the cell membrane of *Euglena gracilis* are involved in gravitaxis; and a further indication is that a modulation of the electrical membrane potential is one element in the signal transduction chain. $TPMP^+$, a lipophilic cation, passes through membranes driven by the existing membrane potential and thus neutralizes the potential. $TPMP^+$ strongly impaired graviorientation even at low concentrations (10 μM), indicating that the membrane potential plays a crucial role in gravitactic orientation. In addition, sudden changes of the ionic composition of the outer medium had drastic effects on gravitac-

This paper was originally presented at a workshop titled *The Future of Aquatic Research in Space: Neurobiology, Cellular and Molecular Biology*. The workshop, which was held at the Marine Biological Laboratory, Woods Hole, Massachusetts, from 13 to 15 May 1996, was sponsored by the Center for Advanced Studies in the Space Life Sciences at MBL and funded by the National Aeronautics and Space Administration under Cooperative Agreement NCC 2-896.

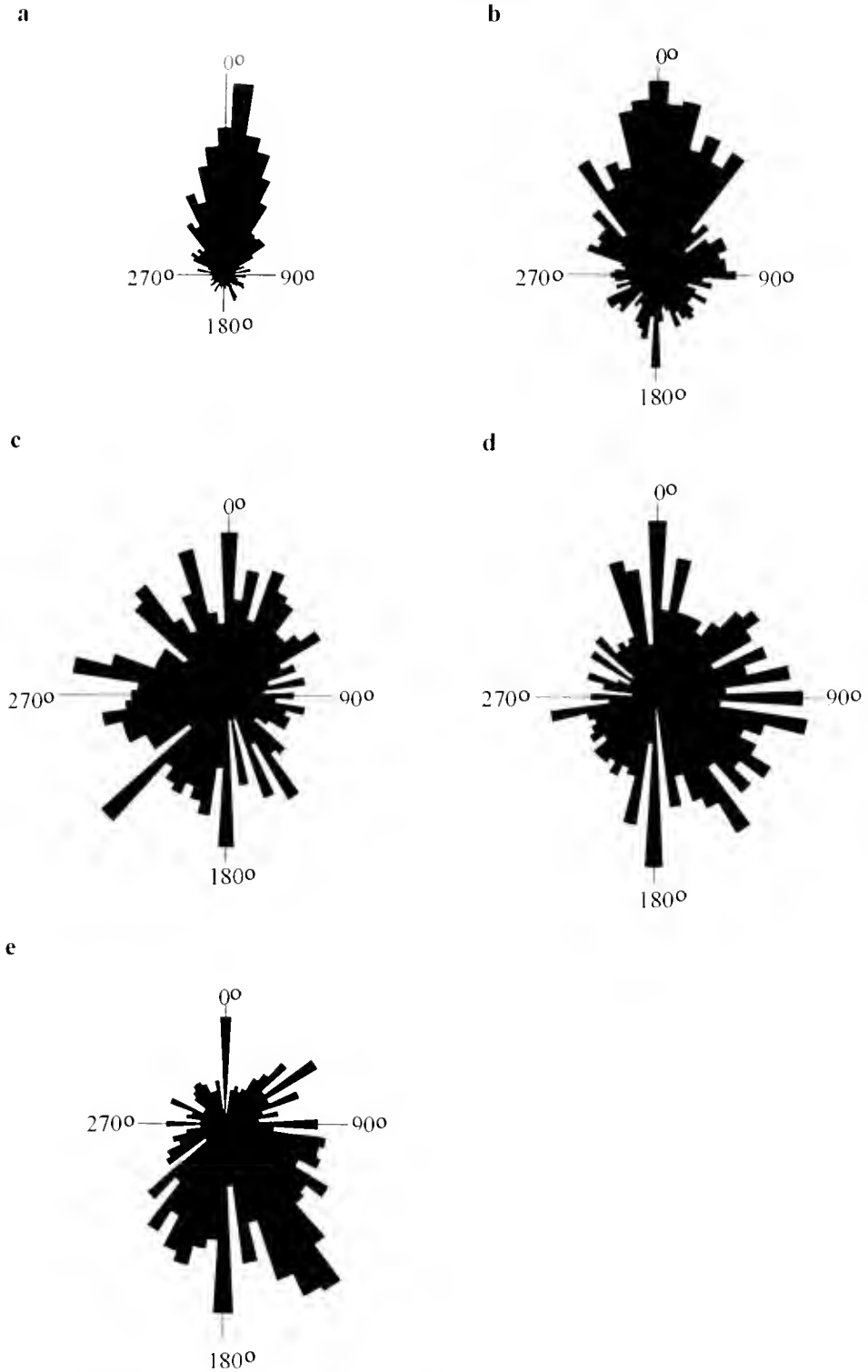

Figure [illegible] histograms of gravitactic orientation of *Euglena gracilis* cells in different Ficoll concentrations [illegible] 2.5% (b), 5% (c), 7.5% (d) and 10% (e). 0° indicates upwards. The swimming directions of [illegible] have been binned in 64 sectors of 5.6° each; the length of each sector indicates the normalized number of cells swimming in the respective direction.

tic orientation. Another interpretation could be based on localized ion fluxes and Ca^{2+} gradients.

Based on these results, the following model was proposed for gravitaxis in *Euglena:* The cell has a higher density than the surrounding medium, and depending on the position of the cell, the resulting pressure deforms different parts of the cell membrane. These deformations activate stretch-sensitive ion channels; the resulting change in the ion flux alters the membrane potential, which is the primary event of gravity sensing. Another assumption of the hypothesis is that stretch-sensitive ion channels are not evenly distributed over the cell. Most likely, channels are concentrated at the front pole of the cell. Modulation of the membrane potential would be minimal only during vertical upward swimming.

In preparation for future experiments on the space station, a terrestrial bioreactor that allows the long-term, stable culture of unicellular algae (CEBAS) has been developed and tested. A fully automatic monitoring system determines all important physical and chemical parameters, such as temperature, light, oxygen, pH, nitrogen, and ammonia. Furthermore, absorption spectra are recorded demonstrating changes in pigmentation. Cell density, motility, velocity, and graviorientation were measured frequently with a real-time, computer-controlled image analysis system developed for this purpose. This bioreactor has been running for more than 500 days.

Literature Cited

Franco, A., Jr., B. D. Winegar, and J. B. Lansman. 1991. Open channel block by gadolinium ion of the stretch-inactivated ion channel in mdx myotubes. *Biochem. J* **59:** 1164–1170.

Häder, D.-P. 1987. Polarotaxis, gravitaxis and vertical phototaxis in the green flagellate, *Euglena gracilis*. *Arch. Microbiol.* **147:** 179–183.

Häder, D.-P., A. Rosum, J. Schäfer, and R. Hemmersbach. 1995. Gravitaxis in the flagellate *Euglena gracilis* is controlled by an active gravireceptor. *J. Plant Physiol.* **146:** 474–480.

Lacampagne, A., F. Gannier, J. Argibay, D. Garnier, and J.-Y. Le Guennec. 1994. The stretch-activated ion channel blocker gadolinium also blocks L-type calcium channels in isolated ventricular myocytes of the guinea-pig. *Biochim. Biophys. Acta* **1191:** 205–208.

Machemer, H., and R. Bräucker. 1992. Gravireception and gravireponses in ciliates. *Acta Protozool.* **31:** 185–214.

Sukharev, S. I., B. Martinac, V. Y. Arshavsky, and C. Kung. 1993. Two types of mechanosensitive channels in the *Escherichia coli* cell envelope: solubilization and functional reconstitution. *Biophys. J.* **65:** 177–183.

Reference: *Biol. Bull.* **192:** 134–136. (February, 1997)

Gravitropism in the Rhizoids of the Alga *Chara:* A Model System for Microgravity Research

JOHN Z. KISS

Department of Botany, Miami University, Oxford, Ohio 45056

Gravitropism in plants can be divided into the following stages: perception, transduction, and response (Evans *et al.*, 1986). In higher plants, there is a cellular and spatial separation between the perception of and response to gravity, and a signal must be transmitted over a relatively large distance. However, the rhizoid (a rootlike extension) of the alga *Chara* is a model system in which all stages of gravitropism can be analyzed in a single cell (Braun and Sievers, 1994; Kiss, 1994; Sievers *et al.*, 1996). The cell biology of gravitropism is therefore much more readily analyzed in such single-celled systems than in multicellular organisms.

Chara rhizoids have a distinctive structural polarity, with a group of 50–60 vesicles near the apex (Fig. 1). The bulk of the cell consists of a large vacuole, and the nucleus is located immediately adjacent to this zone (Kiss and Staehelin, 1993). Like pollen tubes and root hairs, these rhizoids can be characterized as tip growing cells since all extension occurs at the extreme apex (Sievers and Volkmann, 1979). The *Chara* rhizoid is an ideal single-celled subject for space biology studies because (1) a great deal of background information is available about its structure and gravitropic kinetics; (2) rhizoid formation can easily be induced under controlled conditions; and (3) these cells have already been successfully flown aboard the U.S. Space Shuttle and in sounding rockets (*e.g.*, Volkmann *et al.*, 1991).

Gravity perception in plants is hypothesized to be mediated by the interaction between dense organelles (termed statoliths) and other cytoplasmic structures (Sack, 1991; Salisbury, 1993). In higher plants, much evidence suggests that amyloplasts function as statoliths (Kiss *et al.*, 1989, 1996). But, in *Chara* rhizoids, the membrane-bound vesicles that are located close to the rhizoid apex appear to serve this function (Fig. 1). These vesicles sediment to the lower wall within minutes of horizontal reorientation (Figs. 2, 3), and this sedimentation precedes gravitropic curvature (Sievers and Volkmann, 1979).

Research in our laboratory has focused on three major areas. First, we have been characterizing the statolith compartment and its membrane to determine their potential roles in mechanisms of gravitropism (Wang-Cahill and Kiss, 1995). Statoliths in *Chara* rhizoids are very distinctive in that they contain barium sulfate (Sievers and Volkmann, 1979) in an organic matrix consisting of protein and carbohydrate (possibly 3-linked polysaccharides) moieties. Second, we have been manipulating the number of statolith vesicles in *Chara* rhizoids (by altering the growth medium) and have found that the response to gravity is correlated with the number of statoliths (Kiss, 1994). These results are comparable to studies with higher plants in which it was found that starch-deficient mutants (*i.e.*, less total mass of statoliths per cell) were not as sensitive to gravity as their respective wild-types (Kiss *et al.*, 1989, 1996; Kiss and Sack, 1990).

We also have been investigating the potential role of integrin-like proteins in gravity perception and subsequent transduction mechanisms in both *Chara* and in higher plants. Integrins are a large family of integral plasma membrane proteins that link the extracellular matrix to the cytoskeleton in animal cells (Hynes, 1992). They exist as heterodimers of α and β subunits and have been shown to activate intracellular signaling cascades involved in both "inside-to-out" and "outside-to-in" signaling. While several studies have shown that integrin-like proteins are present in plant and fungal cells (Mar-

This paper was originally presented at a workshop titled *The Future of Aquatic Research in Space: Neurobiology, Cellular and Molecular Biology*. The workshop, which was held at the Marine Biological Laboratory, Woods Hole, Massachusetts, from 13 to 15 May 1996, was sponsored by the Center for Advanced Studies in the Space Life Sciences at MBL and funded by the National Aeronautics and Space Administration under Cooperative Agreement NCC 2-896.

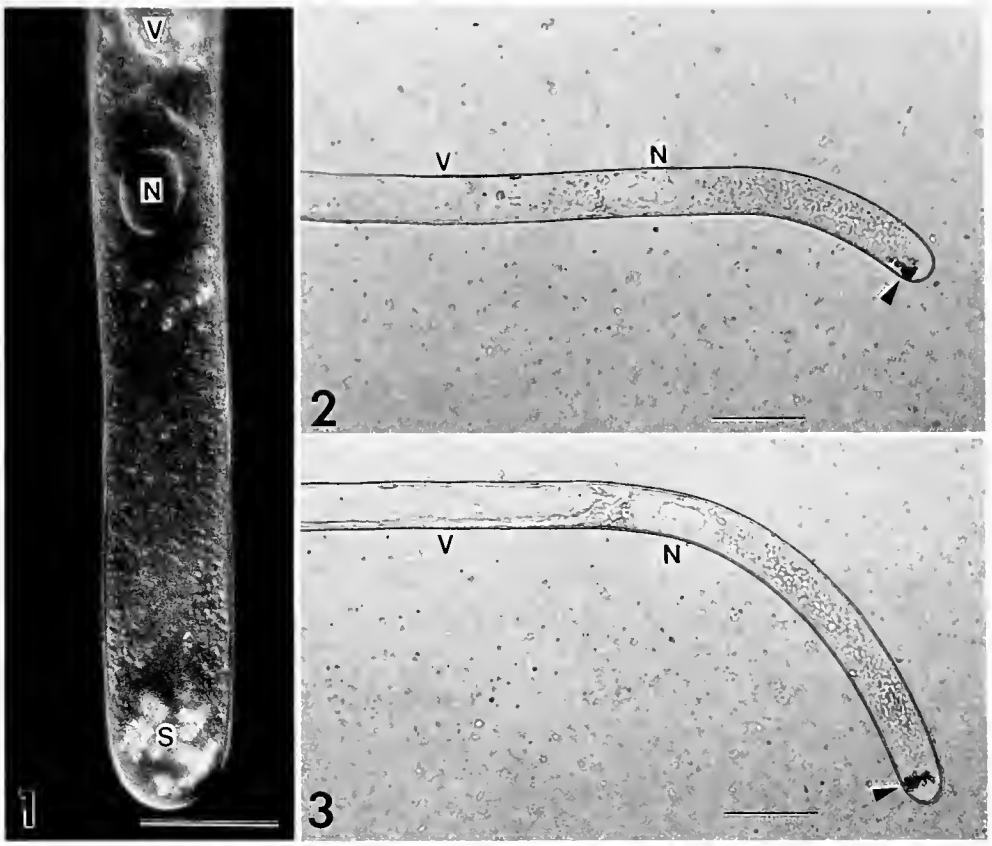

Figures 1–3. Light microscopy of *Chara* rhizoids. N = nucleus; S = statolith vesicles; V = vacuole. (1) A rhizoid imaged with differential-interference-contrast optics. This cell has a distinctive structural polarity in which statolith (S) vesicles are located near the apex, and the nucleus (N) is near the vacuole (V) region. Scale bar = 40 μm. (2) A rhizoid viewed with brightfield optics through agar (that was used in the growth medium). After reorientation of the rhizoid, statolith vesicles (arrowhead) sediment to the lower wall. This sedimentation is followed by gravitropic curvature in the rhizoid. Scale bar = 80 μm. (3) A rhizoid at a latter stage of gravitropic curvature. Note the position of the statolith vesicles, which are indicated by an arrowhead. Scale bar = 80 μm.

cantonio and Hynes, 1988; Quatrano *et al.*, 1991; Kaminskyj and Heath, 1995), unequivocal evidence for integrins in plant cells is still lacking. Nevertheless, there is some evidence that integrin-like proteins may play a role in gravity perception in characean algae, particularly in the gravity-regulated cytoplasmic streaming in internodal cells (Wayne *et al.*, 1992).

As a first step in determining whether integrin-like proteins are involved in the gravitropic signal transduction pathway in plant cells, we have investigated their distribution in *Chara*. Western blot analyses and immunofluorescence microscopy were used to gain information about the size, abundance, and location of integrin-like proteins in plants (Katembe *et al.*, 1997). Several different polypeptides in the rhizoids and internodal cells of *Chara* are recognized by a chicken anti-integrin antibody (against the β_1 subunit; see Marcantonio and Hynes, 1988). These cross-reactive polypeptides appear to be associated with cellular membranes, a feature which is consistent with the known location of integrins in animal systems. In immunofluorescence studies of rhizoids, the antibody stained throughout *Chara* rhizoids, but the highest density of immunolabel was at the tip. Furthermore, the anti-integrin antibody cross-reacted with the higher plant *Arabidopsis* in both roots and shoots and in a specific manner. Based on our data and given the central role that integrins play in cell-cell interactions and cell signaling in animal cells, they are strong candidates for a mediating role in gravity signal transduction in plant cells.

Acknowledgments

The author thanks his colleagues at Miami University who have supported this project: Chris Makaroff, Fan Wang-Cahill, Jira Katembe, and Lucinda Swatzell. Financial support was provided by grants to JZK from the

National Aeronautics and Space Administration (NAGW-3783 and NAG 2-[illegible]), the Research Challenge Program (Ohio Board of Regents), and the Committee for Faculty Research (Miami University).

Literature Cited

Braun, M., and A. Sievers. 1994. Role of the microtubule cytoskeleton in gravisensing *Chara* rhizoids. *Eur. J. Cell Biol.* **63:** 289–298.

Evans, M. L., R. Moore, and K.-H. Hasenstein. 1986. How roots respond to gravity. *Sci. Am.* **255:** 112–119.

Hynes, R. O. 1992. Integrins: versatility, modulation, and signaling in cell adhesion. *Cell* **69:** 11–25.

Kaminskyj, S. G., and I. B. Heath. 1995. Integrin and spectrin homologues, and cytoplasm-wall adhesion in tip growth. *J. Cell Sci.* **108:** 849–856.

Katembe, W. J., L. J. Swatzell, C. A. Makaroff, and J. Z. Kiss. 1997. Immunolocalization of integrin-like proteins in *Arabidopsis* and *Chara*. *Physiol. Plant.* **99:** in press.

Kiss, J. Z. 1994. The response to gravity is correlated with the number of statoliths in *Chara* rhizoids. *Plant Physiol.* **105:** 937–940.

Kiss, J. Z., J. Hertel, and F. D. Sack. 1989. Amyloplasts are necessary for full gravitropic sensitivity in roots of *Arabidopsis thaliana*. *Planta* **177:** 198–206.

Kiss, J. Z., and F. D. Sack. 1990. Severely reduced gravitropism in dark-grown hypocotyls of a starch-deficient mutant of *Nicotiana sylvestris*. *Plant Physiol.* **94:** 1867–1873.

Kiss, J. Z., and L. A. Staehelin. 1993. Structural polarity in the *Chara* rhizoid: a reevaluation. *Am. J. Bot.* **80:** 273–282.

Kiss, J. Z., J. B. Wright, and T. Caspar. 1996. Gravitropism in roots of intermediate-starch mutants of *Arabidopsis*. *Physiol. Plant.* **97:** 237–244.

Marcantonio, E. E., and R. O. Hynes. 1988. Antibodies to the conserved cytoplasmic domain of the integrin β-1 subunit react with proteins in vertebrates, invertebrates and fungi. *J. Cell. Biol.* **106:** 1756–1772.

Quatrano, R. S., L. Brian, J. Aldridge, and T. Schultz. 1991. Polar axis fixation in *Fucus* zygotes: components of the cytoskeleton and extracellular matrix. *Dev. Suppl.* **1:** 11–16.

Sack, F. D. 1991. Plant gravity sensing. *Int. Rev. Cytol.* **127:** 193–252.

Salisbury, F. B. 1993. Gravitropism: changing ideas. *Hortic. Rev.* **15:** 233–278.

Sievers, A., and D. Volkmann. 1979. Gravitropism in single cells. Pp. 567–572 in *Encyclopedia of Plant Physiology*, Vol. 7, W. Haupt and M. Feinleib, eds. Springer-Verlag, Berlin.

Sievers, A., B. Buchen, and D. Hodick. 1996. Gravity sensing in tip-growing cells. *Trends Plant Sci.* **1:** 273–279.

Volkmann, D., B. Buchen, Z. Hejnowicz, M. Tewinkel, and A. Sievers. 1991. Oriented movement of statoliths studied in a reduced gravitational field during parabolic flights of rockets. *Planta* **185:** 153–161.

Wang-Cahill, F., and J. Z. Kiss. 1995. The statolith compartment in *Chara* rhizoids contains carbohydrate and protein. *Am. J. Bot.* **82:** 220–229.

Wayne, R., M. P. Staves, and A. C. Leopold. 1992. The contribution of the extracellular matrix to gravisensing in characean cells. *J. Cell Sci.* **101:** 611–623.

Discussion

NICK: Is it possible to purify the statoliths?

KISS: Our group and others have tried for some while, but it does seem to be difficult. The problem is that they are almost too dense and there are many technical difficulties.

NICK: If they are so very dense, they should be more easily isolated.

KISS: Yes and no. The density of pure barium sulfate is about 4.5, and it goes through every gradient. We would be more interested in isolating the statoliths with the membrane around them, and that is certainly very difficult because you have this solid rock in a membrane. The membrane is lost somewhere in the gradient. So although I agree with you, there may also be a problem of quantity.

JACOBS: Dr. Kiss, you implied that the statoliths in *Chara* are not active themselves, but just diverting material to the upper side of the cell. Do you think that is the case, and if so, what's the evidence for this as opposed to a more direct effect?

KISS: The model I presented is primarily from the Sievers group. I think that other things are involved besides Golgi vesicles being physically displaced.

QUESTION: Has anyone measured the two sides of the curving rhizoid to see which of them is bowed more than normal?

KISS: There have been detailed studies with beads and particles. It's a bowing rather than a bulging mechanism.

NICK: I have a small contribution to the question of this diversion hypothesis. There's an old paper (unfortunately forgotten because it's written in German) by Friedrich and Hertel (see Nick abstract). They have shown that, when you apply different strengths of acceleration, the curvature goes with the dose even if the sedimentation is already saturated. This speaks against a pure proximity mechanism.

KISS: I would agree with you on that.

ROUX: Have either one of you tried to use RGDS to try to inhibit your gravity responses? [Ed: RGDS is the tetrapeptide Arg-Gly-Asp-Ser contained in the integrin recognition site of many protein ligans (Schwartz *et al.* 1995. *Annu. Rev. Cell. Biol.* **11**: 549–599.)]

KISS: Randy Wayne has done that with the internodal cells (Wayne *et al.* 1992. *J. Cell. Sci.* **101(3):** 611–623). This indicates that the gravireceptor in *Chara* may be an integrin-like protein. The approach that we are trying now is to microinject anti-integrin antibodies into the rhizoid. We have not done the RGDS experiments with the rhizoids.

BARLOW, R.: Dr. Häder, you presented a model indicating that the direction of motion is dependent on the location of channels in the membrane. You placed the channels in one part of the cell so that it would move in one particular direction. It isn't clear to me why you impose that restriction on the model.

HÄDER: The problem in the mechanism of reorientation is that, at a given point in time, the cell swings out its flagellum, which brings the front end over. This has been shown to be the case in both graviorientation and phototaxis. When the cell is swimming on a helical path, it is not only moving conically, it is really rotating, so the flagellum moves all the way around. Whenever you have a light source from one side, and this stimulus hits the cell in the right direction, the flagellum will swing out on the other side and turn the front end stepwise in the direction of the light. By analogy, for graviorientation you need to have the cell in a certain position when it swings out its flagellum. When you have the channels all the way around, some channels would be activated all the time. This would be independent of whether the cells are swimming horizontally, downwards, or upwards. So we assume that the channels are in a certain position, and the cell aims for minimal modulation of the signal. This occurs when the channels are at the top. When the cell is swimming upwards, the whole pressure goes downwards where there are no channels, or fewer channels. Each time the cell deviates from that course, moving either horizontally or downwards, it will activate the channels. This will then lead to reorientation

of the flagellum, which will bring the cell upwards again.

BARLOW, R.: I can understand why having channels uniformly located all over the cell leads to a problem, but it's not at all clear to me, even with your explanation, why having the channels on one part or the other of the cell would lead to the directionality you observe. It seems to me that you could develop a workable model with channels at either pole of the cell. Am I missing something important?

HÄDER: We did that by running a model. When the channels are at either pole, the cells would go up or down equally well. That might explain the crossover that is observed between the young and the old cells. One thing that we cannot distinguish in that model is whether the channels are distributed symmetrically round the top of the cell, or whether they are oriented only on the same side as the flagellum.

QUESTION: How did you rule out the presence of channels in the flagella?

HÄDER: The flagellum moves with a frequency of 50 Hz in this flagellate, and it will be in various positions; so the flagellum is not a good choice for positioning the channels. One possibility is that the front end of the cell has an invagination, referred to as a reservoir. The flagellum doesn't sit on the tip of the flagellate, but rather inside the reservoir. This reservoir does not have the pellicule, which consists of proteinaceous strips going round the cell, and could be a candidate for the location of the channels.

QUESTION: Did you look at the effect of the RGDS peptide on your cells?

HÄDER: We did not try this peptide with *Euglena.*

QUESTION: Dr. Kiss, did you try any buoyancy experiments with the rhizoid?

KISS: No, these were done with internodal cells by Randy Wayne and his colleagues (in the *Chara* internode).

MORRIS: Dr. Häder, I have a question about your experiments with Ficoll. Presumably this is also going to have an osmotic effect. Do you know the general effects of the osmotic perturbation? Also, can you just take the flagella off these *Euglena?* If so, what happens to the cells, do they just sink? I wondered if you could address the problem of using gadolinium, because it also blocks calcium channels, and that is going to have enormous effects on motility and so on. Finally, have you tried any other inhibitors to block the mechanoresponses?

HÄDER: In answer to your first question, the Ficoll we were using has a molecular weight of 400,000. We checked osmotic effects with Ficolls of lower molecular weight and could find no effect on graviorientation. As I mentioned, we did all the experiments with phototaxis and gravitaxis in parallel. Another potential concern to us was that Ficoll was also changing the viscosity of the medium. As a control for this, we used methyl cellulose, which has much higher viscosity. Our concern was that there could be a disturbance of the timing in an organism that rotates, where it might take a certain time between the application of a stimulus and the response. During this time, the flagellum could be one quarter or half way round the cell. However, when we used higher concentrations of methyl cellulose in an attempt to decrease the velocity of this movement, we saw no effect. In answer to the next question, we can distinguish very easily between effects on motility or swimming velocity and on orientation. Even when the cells are swimming very slowly, we can determine whether they are moving up or down. Thus we can distinguish whether we are affecting gravipereception or anything in the cellular metabolism that could slow the cell down. As long as the cells are swimming in a specific direction, we can detect this.

Reference: *Biol. Bull.* **192**: 139–140. (February, 1997)

The Influence of Gravity and Light on Developmental Polarity of Single Cells of *Ceratopteris richardii* Gametophytes

ERIN SWINT EDWARDS AND STANLEY J. ROUX

Department of Botany, The University of Texas, Austin, Texas 78713

The gametophyte generation of *Ceratopteris richardii* is being used in a number of laboratories as a model plant system for developmental studies (Chasan, 1992). It is an especially valuable system for the study of the effect of gravity on plants in that the detection and response to gravity take place in the single-celled spore during its germination. The most visible evidence of the control of *C. richardii* spore polarity by gravity is that the direction of growth of the primary rhizoid, when it emerges, is downward, in line with the vector of gravity (Edwards and Roux, 1994). However, the direction of rhizoid growth is determined prior to its actual emergence through the spore coat. The influence of gravity on this growth polarity is, in fact, determined irreversibly during a "polarity-determination window"—a period that occurs after germination has been initiated by exposure of spores to light, but before the first cellular division. Gravity does not appear to have an independent effect on the later events of prothallus and secondary rhizoid growth in the gametophyte, for the growth of prothallial cells follows the same direction as that of the first prothallial cell, and the growth of secondary rhizoids follows the same direction as that of the primary rhizoid, no matter how the gametophyte is oriented.

The polarity-determination window is specified by a simple assay in which the spore position is changed by 180° at various times after the initiation of germination by light, but before rhizoid emergence, and then the subsequent direction of rhizoid emergence and growth is recorded (Edwards and Roux, 1994). Turning the spore upside down before the window opens will also change the direction of rhizoid emergence by 180°: the rhizoid will grow downward in accord with its second position of down. But, if the orientation of a spore is changed 180° after the polarity-determination window closes for that *individual* spore, the primary rhizoid will grow up, in accord with what was down before the orientation change. If the orientation of a population of spore is changed *during* the polarity-determination window for that population, some of the primary rhizoids grow in the first direction of down, while the others grow in the second direction of down. Thus, the closing of the polarity-determination window for a population of spores can be determined as the time at which the orientation change has no effect on the orientation of primary rhizoid growth; *i.e.*, the direction of rhizoid growth has already been fixed by gravity prior to this time. The exact time of opening this window for a population of spores and the duration of the open state vary from spore lot to spore lot and can be influenced by growth conditions (Edwards, 1996).

The direction of rhizoid growth is not the earliest visible response of germinating spores to gravity. Before the first cellular division, but after the polarity-determination window, the first indication of cell polarity is migration of the nucleus down (with respect to gravity) along the proximal face of the spore (Edwards and Roux, 1994). This downward migration of the nucleus sets up an asymmetric first cell division, determining the developmental fate of the two daughter cells, one giving rise to the primary rhizoid, and the other giving rise to the prothallus. Thus, in dictating the direction of nuclear migration, gravity also dictates the developmental polarity of the spore. When spores are germinated on a clinostat, the direction of nuclear migration is random, as is the direction of rhizoid growth. However, in each case, the direction of nuclear migration predicts the direction of rhizoid emergence and elongation (Edwards, 1996).

This paper was originally presented at a workshop titled *The Future of Aquatic Research in Space: Neurobiology, Cellular and Molecular Biology*. The workshop, which was held at the Marine Biological Laboratory, Woods Hole, Massachusetts, from 13 to 15 May 1996, was sponsored by the Center for Advanced Studies in the Space Life Sciences at MBL and funded by the National Aeronautics and Space Administration under Cooperative Agreement NCC 2-896.

Although nuclear migration is the most obvious nuclear movement, it is not the first nuclear movement. During the polarity-determination window, the nucleus exhibits random excursions centered around the middle of the spore. These excursions can be visualized through the transparent spore coat, and followed in reference to a fixed trilete marking on the spore coat called the laesura (Edwards, 1996). They can be clearly described in plots showing change in nuclear position over time (Fig. 1). Since the nucleus is the only organelle clearly visible through the intact spore coat by light microscopy, the very likely possibility remains that other organelles move during the polarity-determination window in response to gravity as well. However, nuclei possess sufficient mass to contribute significantly to gravity detection (Sack, 1991). Their centered movements prior to their migration may play some role in the sensing of the vector of gravity, for, as described by Mesland (1992), nuclei are typically tethered to the cell periphery by cytoskeletal elements, and these elements could convey tension and compression forces as the nucleus moves in various directions. Both the centered movements of the nucleus and its directional migration exhibit the same periodic variance in speed (Edwards, 1996). The cause for this is not clear at this time, but may indicate that the same kind of molecular motor machinery is driving both movements.

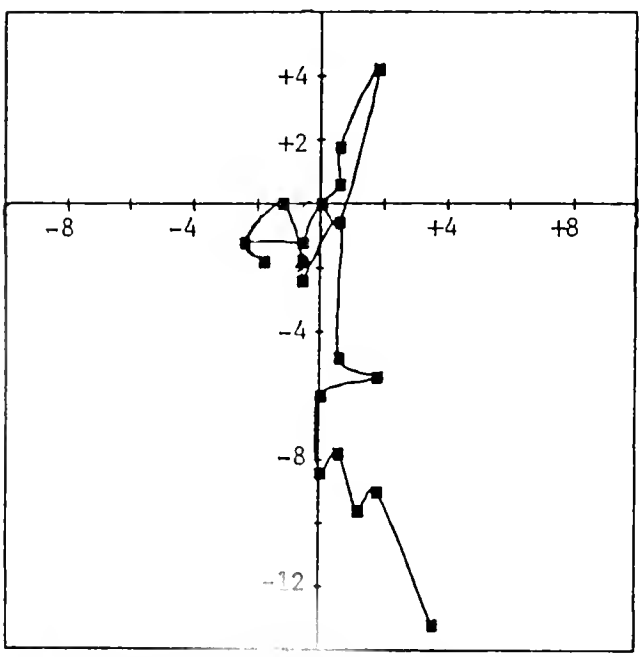

Figure 1. Path of nuclear migration in a representative spore germinating on a vertically oriented side. The position of the nucleus was recorded every half hour. The original position of the nucleus is assigned the position 0,0. Its initial movement is restricted to a region near the center of the spore before it starts its migration downward 15 h after exposure to light. All number values are in micrometers.

Another environmental gradient used to control the polarity of fern spore development is unilateral light (Raghaven, 1989). Light gradients do affect polarity of *C. richardii* spores, but initial experiments using total fluences of about 100 μmol/m^2 of unilateral white light indicate that the influence of light gradients is secondary to that of gravity.

Tests of the effects of agonists and antagonists on the gravity and light responses are impeded by the limited permeability of the thick spore coat. To overcome this problem, prothallus protoplasts may be used as an alternate experimental system for studying processes related to development of cell polarity. A protocol has been developed that consistently yields viable protoplasts that are capable of regeneration, development into fertile gametophytes, and production of sporophytes. Furthermore, the protoplasts follow a path of regeneration in which a primary rhizoid is formed with the first cell division, thus resembling spore germination. As in spores, polarity of regenerating protoplasts is influenced by unidirectional light and gravity (Edwards, 1996).

The gametophyte generation of *C. richardii* has many advantages that make it ideal for spaceflight studies. Its small size and easy culture mean that large numbers of individuals can be utilized in a single experiment. Since germination is initiated by light, samples can easily be prepared ahead of time, and germination initiated only after launch with its attendant hyper-*g* and strong vibrational stimuli. In addition, the primary gravity response, fixing the polarity of nuclear migration and rhizoid growth, occurs in a relatively synchronized population of cells relatively soon after light-induced initiation of germination, and it can be visualized easily through the clear spore coat of *Ceratopteris* with video microscopy equipment already developed and used in previous shuttle experiments (STL-B). The simplicity of these single isolated cells should facilitate discoveries that will be applicable to more complicated systems and thus lead to advances in the study of the effects of gravity and light stimuli on a wide range of organisms.

Literature Cited

Chasan, R. 1992. *Ceratopteris*, a model plant for the 90s. *Plant Cell* **4:** 113–115.

Edwards, E. S., and S. J. Roux. 1994. Limited period of graviresponsiveness in germinating spores of *Ceratopteris richardii*. *Planta* **195:** 150–152.

Edwards, E. S. 1996. The influence of gravity and light on developmental polarity of single cells of *Ceratopteris richardii* gametophyes. Ph.D. dissertation, The University of Texas at Austin.

Mesland, D. 1992. Possible actions of gravity on the cellular machinery. *Adv. Space Res.* **12:** 15–25.

Raghaven, V. 1989. *Developmental Biology of Fern Gametophytes* Cambridge Univ. Press, Cambridge.

Sack, F. D. 1991. Plant gravity sensing. *Int. Rev. Cytol* **127:** 193–251.

Reference: *Biol. Bull.* **192:** 141–143. (February, 1997)

Probing Rice Gravitropism With Cytoskeletal Drugs and Cytoskeletal Mutants

PETER NICK[1], REA GODBOLE[2], AND QI YAN WANG[1]

[1]*Institut für Biologie II, Schänzlestrasse I, 79104 Freiburg, Germany, and*
[2]*Institut für Biologie III, Schänzlestrasse I, 79104 Freiburg, Germany*

In multicellular organs, phototropic sensing is based upon gradients in stimulus strength across the entire tissue. The differences in the strength of the gravitational field between the two flanks of a plant are certainly too small to be sensed. This implies that each cell, individually, must align its polarity with the direction of gravity. As the first step in gravity sensing, the gravitational field must be translated into a mechanical force that can then be perceived in the second step. It is generally believed that statoliths of some kind are the targets of the gravitational field. In plants, sedimentable amyloplasts have been conceived of, since the turn of the century, as potential statoliths (Haberlandt, 1900; Nemec, 1900).

In principle statolith sedimentation might be transduced into a new alignment of cell polarity in two ways. Displacement of the statolith could interfere with diffusible molecules, causing a concentration gradient that can then direct the new cell polarity (proximity mechanism). Alternatively, the statoliths could be pressed into a structure that is sensitive to mechanical stress, triggering a signal cascade that would cause a reorientation of cell polarity (pressure mechanism). The observation that the gravitational response is pressure dependent, even for accelerations where amyloplast sedimentation already seems to be saturated, favors a pressure mechanism at least for higher plants (Rawitscher, 1932; Johnsson, 1965; Friedrich and Hertel, 1973). The pressure-perceiving structure must embody some kind of directionality, if it is to interact with a transducing mechanism and alter cell axis and polarity. Cytoskeletal elements, actin microfilaments and microtubules, are good candidates for the pressure-perceiving system (Table 1): they have a distinct axis and polarity, and microtubules have repeatedly been found to be highly sensitive to mechanical stress. Polymerization and depolymerization of tubulin into microtubules is one of the few biochemical processes that have been reported to respond directly to the direction of gravity (Tabony and Job, 1992).

With these considerations as background, we tried to assess the role of microtubules and microfilaments in the gravitropic response of rice coleoptiles. The rice coleoptile is highly sensitive to gravity, and the abundance of amyloplasts can be controlled by submerged growth. The cuticle of rice is very thin, so the cells are more accessible to drugs than are coleoptiles from other species. The coleoptile grows exclusively by cell elongation, and there is a wealth of old physiological data about this process. Accessibility of molecular techniques and a very small genome also make rice an excellent system for molecular studies.

Several steps of the gravitropic response chain were probed with cytoskeletal drugs (Table 1). Ethyl-*N*-phenylcarbamate (EPC) and oryzalin block tubulin polymerization and rapidly eliminate microtubules. Taxol blocks depolymerization of tubulin, yielding an increased number of microtubules, and cytochalasin D rapidly eliminates actin microfilaments. The drugs were found to be effective within 15–30 min after application to the gravity-sensing tissue of the Japanese rice cultivar Nihonmasari.

Amyloplast sedimentation, the putative first step of the response chain (Sack, 1991), was investigated in vi-

This paper was originally presented at a workshop titled *The Future of Aquatic Research in Space: Neurobiology, Cellular and Molecular Biology*. The workshop, which was held at the Marine Biological Laboratory, Woods Hole, Massachusetts, from 13 to 15 May 1996, was sponsored by the Center for Advanced Studies in the Space Life Sciences at MBL and funded by the National Aeronautics and Space Administration under Cooperative Agreement NCC 2-896.

Table I

Elements of the plant cytoskeleton and [illegible] drugs used in this study

Cytoskeletal element	Co[illegible]	Drug
Microtubles	[illegible]ulin	Elminating:
		Ethyl-*N*-phenylcarbamate (EPC)
		Oryzalin
		Colchicin
		Stabilizing:
		Taxol
Microfilaments	Actin	Eliminating:
		Cytochalasin D (CD)

bratome sections after starch was stained with Lugol solution. Sedimentation was not affected by cytochalasin D, only slightly promoted by microtubule elimination, and strongly inhibited by taxol. In this system, therefore, microtubules, but not microfilaments, are in physical contact with the statoliths. The gravity-induced reorientation of microtubules in the gravity-sensing tissue was analyzed, after paraformaldehyde fixation, in vibratome sections by immunofluorescence and confocal laser microscopy. The usual reorientation from transverse to longitudinal was inhibited by taxol. Cytochalasin D promoted this reorientation, even in the absence of gravitropic stimulation. The gravitropically induced lateral transport of auxin was followed by measuring the asymmetry of radioactively labeled auxin fed to the coleoptile tip. Lateral transport was inhibited by suppression of both tubulin polymerization and depolymerization. This inhibition could be separated from effects on longitudinal transport. Cytochalasin D inhibited auxin transport *per se,* yet we failed to observe a specific inhibition of lateral transport. Gravitropic bending was delayed by the microtubule drugs (irrespective of whether they inhibit polymerization or depolymerization of tubulin), whereas cytochalasin D caused a precocious onset of bending at a slower rate. It should be emphasized that gravitropism occurs, although at low efficiency, in the absence of microtubules and microfilaments. Furthermore, the gravitropic response could be inhibited at concentrations that would permit phototropism (as internal control for differential growth) to proceed.

These data favor the idea that microtubules interact with the gravity-perceiving system in the rice coleoptile. It is not enough that microtubules are present to fulfill this task, they must also be dynamic. Reorientation of microtubules from transverse to longitudinal is a prerequisite for the establishment of a new (radial) cell polarity resulting in a lateral transport of auxin. This would explain why cytochalasin D, promoting such a reorientation, causes a precocious gravitropic response.

To test this hypothesis further, the gravitropic response was analyzed in two cytoskeletal rice mutants. In the mutant *ER31,* the reorientation response of microtubules to the auxin signal is interrupted, although auxin *per se* is perceived normally, and microtubules are able to respond to other signals (Nick *et al.,* 1994). In this mutant, gravity can reorient microtubules, and gravitropism functions with about the same bending rate as in the wild type, but the bending is delayed by several hours. In the mutant *Yin-Yang,* the auxin-induced stimulation of actin polymerization is disturbed, resulting in the partial decay of actin microfilaments and the formation of nuclear actin baskets in response to auxin (Wang and Nick, unpubl. data). In this mutant, gravitropism begins earlier than in the wild type, but develops at a slower rate. The gravitropic behavior of the mutant *ER31* can be mimicked by treatment with antimicrotubular drugs; the gravitropic behavior of the mutant *Yin-Yang* is similar to that of the wild type after application of cytochalasin D.

The data can be discussed in terms of a physical contact between amyloplasts and microtubules during gravity perception. Microtubules serve as amplifiers for the mechanical stress exerted by the amyloplasts. This stress is then perceived by mechanosensitive channels that are probably located in the endoplasmic reticulum and causes the establishment of a new cell polarity. For this polarity shift, reorientation of microtubules seems to be a time-limiting step. The shifted polarity then causes a shift of auxin transport in the transverse direction and, eventually, gravitropic bending. Parallel to this pathway, a second, slower gravitropic pathway that is independent of microtubules seems to exist. This pathway might function independently of auxin. The observation that rice can respond gravitropically under submerged conditions (when amyloplasts are small) opens up the possibility that two completely different gravitropic pathways exist. The extremely high gravitropic sensitivity of the rice coleoptile might have evolved in response to a situation in which amyloplasts, due to submergence, are small. This high sensitivity might be the result of two mutually enhancing signal chains. We can ask whether the two chains can be separated under conditions of microgravity, when only the more sensitive of the two chains contributes to the gravitropic response.

Acknowledgments

The authors thank Wolfgang Michalke and Rainer Hertel for technical advice and valuable discussions. This work has been supported by a grant of the Graduierten-

kolleg to R.G. and by a fellowship of the Deutsche Forschungsgemeinschaft (Habilitandenprogram) to P.N.

Literature Cited

Friedrich, U., and R. Hertel. 1973. Abhängigkeit der geotropischen Krümmung der *Chara*—rhizoide von den Zentrifugalbeschleunigung. *Z. Pflanzenphysiol.* **70:** 173–184.

Haberlandt, G. 1900. Über die Perzeption des geotropischen Reizes. *Ber. Dtsche. Bot. Ges.* **18:** 261–272.

Johnsson, A. 1965. Investigation of the reciprocity rule by means of geotropic measurements. *Physiol. Plant.* **18:** 945–967.

Nemec, B. 1900. Über die Art der Wahrnehmung des Schwerkraftreizes bei den Pflanzen. *Ber. Dtsche. Bot. Ges.* **18:** 241–245.

Nick, P., O. Yatou, M. Furuya, and A. M. Lambert. 1994. Auxin dependent microtubule responses and seedling development are affected in a rice mutant resistant to EPC. *Plant J.* **6:** 651–663.

Rawitscher, F. 1932. Der Geotropismus der Pflanzen. Gustav Fischer Verlag, Jena.

Sack, F. D. 1991. Plant gravity sensing. *Int. Rev. Cytol.* **127:** 193–252.

Tabony, J., and D. Job. 1992. Gravitational symmetry breaking in microtubular dissipative structures. *Proc. Natl. Acad. Sci. USA* **89:** 6948–6952.

Reference: *Biol. Bull.* **192:** 144–145. (February, 1997)

Discussion

KISS: Do you think that detection by proximity and detection by pressure are mutually exclusive?

NICK: No, of course not. If you think about pressure perception, you must consider stretch-activated channels. Although such channels seem to exist in plants, we don't know anything about them, and it's easier to think about proximity mechanisms.

LOMAX: Peter (Nick), it seems that there's something circular going on here, because you have the microtubules reorienting in response to auxin. You also have auxin reorienting in response to microtubules. Are you saying that all of this is going on in one cell, or in different cell types?

NICK: The cells I have shown here are really those that perceive gravity. This means that they are not the cells of the epidermis, but below. The story is more complex because, in the epidermis where gravity is not perceived, the auxins induce a reorientation of microtubules. So we have two components. I don't know the exact relationship, in those gravity-perceiving cells, between the direction of auxin transport and the direction of the microtubules. In regenerating tissues, the direction of auxin flow and the direction of the microtubules are perpendicular to each other. However, it's difficult to sort out what's the cause and what's the effect. At this point, it's a correlation. It's also a correlation when you reorient the microtubules by some other means, either dilatation or with cytochalasin B, before you get gravitropism. At the moment, I do not understand what the causal relationship is.

QUESTION: In dicots at least, those cells in which the amyloplasts are sedimenting are also the cells where the major polar auxin transport is taking place. Consequently, there should be high concentrations there holding the microtubules in an orientation.

NICK: It is probably in those cells where auxin is actually transported, but in the end the epidermis is the response site.

LOMAX: Stan (Roux), what kind of light does it take to change the orientation?

ROUX: We have used only white light so far.

LI: Have you isolated any genes by your differential display?

ROUX: We have perfected the method to the point that we have been able to eliminate some false positives. We now have 17 candidates; the primers are amplified, and we are using them to probe Northern blots during that period.

LI: Peter (Nick), did you check auxin transport in the late phase for cytochalasin-treated rice?

NICK: In cytochalasin-treated rice coleoptiles, auxin transport (both lateral and longitudinal transport) is reduced to the same degree by this drug. We checked auxin transport at 2.5 h after the onset of stimulation, somewhere in the middle of curvature development.

LI: Do you see some reduction in polar auxin transport?

NICK: We see some reduction in the rate of bending.

LI: But not completely blocked for polar auxin transport.

NICK: No, we can't block polar auxin transport completely with cytochalasin. We tried various concentrations, but could never block more than about 60%.

MANDOLI: Stan (Roux), your first graph showed that 20% of the population of the *Ceratopteris* spores are not responding, or they are not in the population at all. Could you comment on that? Were you talking about the time to respond to fixed polarity determination? The data come down to 20% and then stop.

ROUX: That means that 20% can still reorient even at that time point. Some cells, apparently, do not show complete fixation of the polarity by gravity within that window. That may reflect a little bit of asynchronization within the population that's not perfectly synchronized. We are just looking at a window. If you went out another 7 or 8 h, you might see that drop down.

MANDOLI: I am wondering what information you have about the extreme variability (mentioned in your abstract) from spore lot to spore lot, and the exact timing of the window

for a population of spores that you say is very variable. In your model, you have a polarity determination window just before nuclear migration. (Roux: It's always just before nuclear migration. The sequence never changes.) Do you see that when you analyze an individual spore, and is that invariant from spore lot to spore lot? I'm confused by such extreme variability from population to population.

ROUX: On an individual spore base, the sequence is always the same. So the fixation always occurs before nuclear migration. However, that time of fixation will vary from spore lot to spore lot. It's related to ripening. After the spores are harvested, they have to ripen for some period. That phenomenon also occurs in seeds. The longer the ripening, the shorter the window. We may actually be looking at synchronization of the population. That is, as ripening lengthens, more and more of the spores are synchronized so that they are fitting into a sharper window. We have also found out recently that we can shrink that window by temperature modulation, which is very exciting. If we incubate them at a low temperature (20°C) for about five h, and then switch to the high temperature, we shrink the window by half. Maybe that's another way of better synchronizing the population.

MANDOLI: That sounds very similar to what Lew Feldman has published on changing the phytochrome response of corn seeds. He imbibed the seeds in cold and could switch them from a low to a very low fluence response by the temperature of imbibition. That might suggest a membrane property, or such.

Peter (Nick), I have a question on gravitropism where we have statoliths settling. What's really known, in either of these systems, about the membranes surrounding the particles? In amyloplasts, people have talked for decades about the fact that the starch granule itself is settling. Maybe we have been looking at the wrong thing; maybe it's the membrane that is settling, but as I understand from John (Kiss), it is very difficult to purify membranes from *Chara*. What would happen if you took amyloplasts out of plants and put them into *Chara*, or purified the membrane from amyloplasts and started looking there instead?

NICK: I think that some people have tried to make antibodies against the amyloplast surface. I don't know where this is published, but there have been attempts like this, and you can stain amyloplasts with the antibodies. However, the problem is that amyloplasts are quite sticky, and when you really look carefully with all of the negative controls, you find that you can stain it with any secondary antibody you want. It's quite difficult to work with amyloplasts because they have all this carbohydrate sticking out. I think that it would be very difficult to get some specific response.

MANDOLI: So if the response is dose dependent, does that help you at all to correlate the numbers of statoliths or amyloplasts with the graviresponse?

NICK: I think it's difficult to use a biochemical approach on amyloplasts. But it will be necessary, of course.

KISS: I don't think I can answer the question any better. Our original goal was to try to isolate the statolith vesicles with the membrane. The statoliths are very dense, and we could not get a membrane fraction isolated. It would be very interesting to look at interactions, possibly with cytoskeleton, that way. I think Fred Sack had done some work along these lines.

SACK: We isolated amyloplasts but were unable to purify the membrane. The question is, What would your assay be for a functional protein? How would you reconstitute this, and how would you identify something special?

NICK: I would like to throw one remark into this debate. There is some old work (quoted in 1932 in a book by Rawitscher on Geotropismus) [see Nick abstract] pointing out that you don't necessarily need the action of sedimentation; something is already going on even if the moving particles just drag or pull on some element.

Reference: *Biol. Bull.* **192:** 146–149. (February, 1997)

Mauthner System Discrimination of Stimulus Direction From the Acceleration and Pressure Components at Sound Onset

ROBERT C. EATON, AUDREY L. GUZIK, AND JANET L. CASAGRAND

Center for Neuroscience, University of Colorado, Boulder, Colorado 80309-0334

When an animal turns away from an aversive stimulus, what are the underlying neurophysiological processes that extract the correct sensory information and produce an appropriate motor output? The goal of our research program has been to use the Mauthner system as a model neural network to understand such sensorimotor processes (Eaton *et al.*, 1991). The Mauthner cells are a bilateral pair of brain stem neurons. They receive acoustic and other sensory inputs and connect directly to spinal motoneurons. Together with other reticulospinal cells, the Mauthner cells trigger the C-start, a characteristic escape movement of fishes. This behavior occurs when the animal is presented with a sudden aversive stimulus, such as is produced by a predator during an attack. Previously my laboratory focused on the production of the escape movement and the role of the Mauthner neurons in organizing the descending flow of motor signals that activate escape. Now, however, we have an excellent idea of other candidate neurons that participate in the escape response (Foreman and Eaton, 1993; Lee *et al.*, 1993; Fetcho *et al.*, 1995). To further understand the underlying sensorimotor process, we recently began studying how the Mauthner system computes the direction of sounds so that the animal makes the correct initial decision to turn left or right away from the stimulus (Eaton *et al.*, 1995a). In this paper we present the rationale, the theoretical background, and some of our preliminary findings from these recent studies.

The end organs of the inner ear are conserved in vertebrate evolution and convey information about translational acceleration and gravity (Davis *et al.*, 1995). Teleost fishes, such as the goldfish, use the otolithic end organs to detect sounds ranging from very low frequencies to more than 1 KHz (Popper and Fay, 1993). These end organs are experimentally accessible. Moreover, the saccule of some teleosts has about an order of magnitude more receptors than the human saccule (Corwin, 1981). Finally, some central neural networks that receive afferent input from these organs are well studied. One of these is the Mauthner system.

The Mauthner system consists of the two Mauthner cells, their sensory afferents, controlling interneuronal networks, and output cells to motor circuits both in the brain stem and spinal cord. The Mauthner axons cross the midline and descend into the spinal cord on the side opposite the Mauthner soma. When one Mauthner cell fires, the animal turns toward the side opposite the activated Mauthner neuron. The other Mauthner cell is inhibited from firing.

Fishes can detect the direction of underwater sounds, particularly those that activate Mauthner-initiated escape responses (Eaton *et al.*, 1995a). But they probably do not use the same mechanisms as terrestrial animals, which obtain their major cues of sound direction by analyzing interaural time and intensity differences. Instead, as proposed by Schuijf (1981) on the basis of the physics of underwater sound propagation, sound direction can be determined if the fish compares the phase of the particle acceleration component and the phase of the pressure component of the sound wave. Experimental evidence supports this theory (Buwalda *et al.*, 1983). We

This paper was originally presented at a workshop titled *The Future of Aquatic Research in Space: Neurobiology, Cellular and Molecular Biology*. The workshop, which was held at the Marine Biological Laboratory, Woods Hole, Massachusetts, from 13 to 15 May 1996, was sponsored by the Center for Advanced Studies in the Space Life Sciences at MBL and funded by the National Aeronautics and Space Administration under Cooperative Agreement NCC 2-896.

have recently shown that the physical basis of this *phase model* is most readily apparent for the sounds that the Mauthner system is specialized to detect; that is, the onset of a sound that originates relatively close to the fish (Guzik and Eaton, 1994; Eaton *et al.*, 1995a). This is because the Mauthner-initiated escape response is adapted to detecting ambush attacks from predators that strike from within a short distance.

Let us assume that the predator is on the left side of the fish and lunges forward to bite. This causes particle acceleration from left to right and positive sound pressure. But the source location cannot be computed from the acceleration component alone. Particles moving left to right *could* be caused by a source beginning with compression (positive pressure) on the left, or a source beginning with rarefaction (negative pressure) on the right, as would be caused by a predator on the right trying to suck the prey into its mouth. This ambiguity is resolved by referring to the pressure component.

For instance, consider the phase polarity from the perspective of the left Mauthner cell. Left-to-right acceleration will be registered as a *positive* phase relative to this cell. If acceleration is from left to right, and the source is on the left, pressure will be *increasing*. The left Mauthner cell will detect the phase of these two components as both being positive, and thus it should fire. This would cause the animal to correctly turn to the right.

Alternatively if the acceleration were from left to right, but the pressure was *decreasing*, this could be caused only by a sound source on the right beginning with rarefaction (negative pressure). Thus, the acceleration and pressure components are of opposite phase (or polarity), and the left Mauthner cell should not fire. Using these conventions, the components from the perspective of the right Mauthner cell would both be positive, or in-phase, and the cell should fire, causing the animal to turn correctly to the left.

In the most general terms, whenever the initial components of the aversive sound stimulus are in-phase with respect to one Mauthner cell (either both positive or both negative), that cell should fire; and whenever they are out-of-phase, the cell should not fire. This is equivalent to the logical operator known as the equivalence function, EXCLUSIVE-NOR or XNOR (Guzik and Eaton, 1994). Whenever its inputs are the same, it is ON; whenever they are different it is OFF (Guzik and Eaton, 1994; Eaton *et al.*, 1995a). This is the problem that must be solved by the two Mauthner cell networks to detect the direction of impulse sounds created by predators.

How might the Mauthner system perform XNOR and compute sound direction? The acceleration component is detected as a translational motion of the body, which has roughly the same density as the water. The end organs of the inner ear contain otoliths that have high density and act as inertial devices to cause a shearing motion on the underlying sensory epithelium whenever the body accelerates in phase with the water. In the goldfish, experimental evidence shows that these accelerations are detected by all three end organs of the inner ear, saccule, utricle and lagena (Fay, 1984), though it has been argued that the utricle and lagena are most important for this detection (Schellart and Popper, 1992). The pressure component is transduced by the swimbladder, a gas-filled chamber in the abdomen. The swimbladder changes in size as a result of changes in the impinging sound pressure field. These vibrations are conveyed through a series of ossicles to the fluids of the inner ear where they vibrate the otoliths, most likely in the saccule, and activate the sensory epithelium of the inner ear. This leads to the firing of the acoustic afferents that activate the Mauthner cells (Canfield and Eaton, 1990).

We have performed neurocomputational simulations to give insights into how the underlying neurons might be implementing the XNOR function. If the Mauthner cell can solve XNOR, it must receive all four combinations of sensory afferents (positive and negative pressure, left-to-right and right-to-left acceleration) but fire only to those combinations appropriate for sound from the "correct" direction. This would require a nonlinear interaction of these inputs, perhaps through an appropriate spatial arrangement of synapses on the dendritic membrane.

Alternatively, the XNOR solution might emerge from interactions of the Mauthner network as a whole. Mathematically, XNOR can be solved by an indefinite number of equivalent circuits made of various types of logical operators that together perform the overall XNOR function. Thus, each neural element could be performing a subsidiary function that contributes to the overall XNOR logic. Our simulation studies show that the PHP neurons may be playing an essential role in this directional computation (Eaton *et al.*, 1995a).

The PHP cells were discovered and extensively investigated by Faber and Korn (Faber and Korn, 1978; Faber *et al.*, 1991), who showed that these neurons operate in a feed-forward manner to regulate the firing threshold of the Mauthner cell to sound. These cells are strongly activated by low-level acoustic stimulation and strongly inhibit the Mauthner cell. However, at higher levels of activation appropriate for eliciting escape, the PHP cells saturate, whereas the Mauthner neuron becomes progressively excited and eventually exceeds the PHP cell inhibition, thus leading to an action potential (Faber *et al.*, 1991).

How might the PHP cells be performing part of the XNOR function? In the simplest simulations, these cells are divided into two populations, both synapsing on each Mauthner cell (Eaton *et al.*, 1995a). Each population of

PHP cells is turned on by the two, out-of-phase, pressure and acceleration combinations that should not activate the associated Mauthner cell on that side of the brain. Thus, the left Mauthner cell would be turned off by PHP cells whenever the sound was originating on the right, regardless of whether it began with compression or rarefaction. This would allow the right Mauthner cell to fire off its pressure input, while the right PHP cell populations would not be activated. In these simulations, the PHP cells act as AND gates. Other more complex simulations more closely duplicate the feed-forward dynamics of Faber and Korn. In these models, the PHP cells perform an OR function (Guzik *et al.*, 1995).

We are currently doing neurophysiological and behavioral experiments to evaluate the XNOR model. We have devised an experimental test chamber based on a design of Fay (Fay, 1984); ours produces accelerations at 90 degrees to the long axis of the fish. In the center of this chamber is a sound pressure null; a fish at this location perceives only the acceleration component. We can artificially control the polarity of sound pressure at the null point by producing a sound pulse in the air above the tank. Thus, we can independently control the initial phase of the acceleration, and the sound pressure components, and thereby artificially influence the apparent direction of the sound stimulus. In preliminary behavioral trials, the fish escapes in the directions predicted by the phase model (Eaton *et al.*, 1995b). In our trials, the ratio of amplitude of acceleration to pressure is higher than for typical monopole or dipole sound sources.

The test chamber can also be used for fishes restrained for neurophysiological recording from the Mauthner system neurons. So far, we know that the Mauthner cell is widely tuned to sound pressure frequencies from 100 to 2 KHz (Casagrand *et al.*, 1995). We are currently investigating Mauthner responsiveness to acceleration alone, and to combinations of acceleration and pressure, to determine whether the Mauthner cell itself performs the XNOR function. If the Mauthner cell performs XNOR, this should be detectable as differences in amplitude or timing of EPSPs evoked to different acceleration and pressure combinations of our artificial sounds. If it does not, we would expect to see differences in the timing or amplitude of the EHP, the extracellular field potential generated by the PHP cells. This will indicate that the PHP cells are solving XNOR.

Although our experiments are still in the preliminary stage, enough is already known about the Mauthner system so that we can use it to understand how a computational problem like the phase model is being solved in neurophysiological terms with identified cells. In many types of experiments involving central auditory or vestibular processing, the relevance of a neuron's response to a particular component of the stimulus is often difficult to know. The Mauthner system has important advantages. We have a good physical theory of the problem being solved by the system. Also, we can access the output state of the system both neurophysiologically and behaviorally. We therefore know that the system has interpreted the stimulus as having a particular salience: a predator attacking from a certain location relative to the body axis of the fish. This makes possible concrete statements about the real importance of the underlying neurophysiological events. We therefore believe that such work may provide new insights into understanding basic principles of central vestibular and auditory functions.

Acknowledgments

Work described in this paper was supported by grants from NIH and ONR.

Literature Cited

Buwalda, R. J. A., A. Schuijf, and A. D. Hawkins. 1983. Discrimination by the cod of sounds from opposing directions. *J. Comp. Physiol. A* **150:** 175–184.

Canfield, J. G., and R. C. Eaton. 1990. Swimbladder acoustic pressure transduction initiates Mauthner-mediated escape. *Nature* **347:** 760–762.

Casagrand, J. L., A. L. Guzik, and R. C. Eaton. 1995. Frequency dependence of auditory PSPs in the goldfish Mauthner cell. *Soc. Neurosci. Abstr.* **21:** 399.

Corwin, J. T. 1981. Postembryonic production and aging of inner ear hair cells in shark. *J. Comp. Neurol.* **201:** 541–553.

Davis, J. G., J. C. Oberholtzer, F. R. Burns, and R. I. Greene. 1995. Molecular cloning and characterization of an inner ear-specific structural protein. *Science* **267:** 1031–1034.

Eaton, R. C., R. DiDomenico, and J. Nissanov. 1991. Role of the Mauthner cell in sensorimotor integration by the brain stem escape network. *Brain Behav. Evol.* **37:** 272–285.

Eaton, R. C., J. G. Canfield, and A. L. Guzik. 1995a. Left-right discrimination of sound onset by the Mauthner system. *Brain Behav. Evol* **46:** 165–179.

Eaton, R. C., A. L. Guzik, and J. L. Casagrand. 1995b. The neural mechanism for directional escape in the goldfish. *J. Acous. Soc. Am.* **98:** 2940.

Faber, D. S. and H. Korn. 1978. Electrophysiology of the Mauthner cell: basic properties, synaptic mechanisms and associated networks. Pp. 47–131 in *Neurobiology of the Mauthner Cell*, D. S. Faber and H. Korn eds. Raven Press, New York.

Faber, D. S., H. Korn, and J.-W. Lin. 1991. The role of medullary networks and presynaptic membrane properties in regulating Mauthner cell responsiveness to sensory excitation. *Brain Behav. Evol* **37:** 286–297.

Fay, R. R. 1984. The goldfish ear codes the axis of acoustic particle motion in three dimensions. *Science* **225:** 951–954.

Fetcho, J. R., Y.-H. Kao, and D. M. O'Malley. 1995. Functional roles of serially homologous reticulospinal neurons studies by *in vivo* confocal calcium imaging in the zebrafish. *Soc. Neurosci. Abstr.* **21:** 687.

Foreman, M. B., and R. C. Eaton. 1993. The direction change concept for reticulospinal control of the goldfish escape. *J. Neurosci.* **13:** 4101–4113.

Guzik, A. L., and R. C. Eaton. 1994. Directional hearing by the Mauthner system. *Adv. Neural Inf. Process. Syst.* **6:** 574–581.

Guzik, A. L., R. C. Eaton, and D. W. Mathis. 1995. A backpropagation model of the Mauthner system. *Soc. Neurosci. Abstr.* **21:** 147.

Lee, R. K. K., R. C. Eaton, and S. J. Zottoli. 1993. Segmental arrangement of reticulospinal neurons in the goldfish hindbrain. *J. Comp. Neurol.* **327:** 1–18.

Popper, A. N., and R. R. Fay. 1993. Sound detection and processing by fish: critical reviews and major research questions. *Brain Behav. Evol.* **41:** 14–38.

Schellart, N. A. M., and A. N. Popper. 1992. Functional aspects of the evolution of the auditory system of actinopterygian fish. Pp. 295–322 in *The Evolutionary Biology of Hearing*, D. B. Webster, R. R. Fay, and A. N. Popper, eds. Springer, New York.

Schuijf, A. 1981. Models of acoustic localization. Pp. 267–310 in *Hearing and Sound Communication in Fishes*, W. N. Tavolga, A. N. Popper, and R. R. Fay, eds. Springer, New York.

Reference: *Biol. Bull.* **192:** 150–153. (February, 1997)

Imaging Neural Activity With Single Cell Resolution in an Intact, Behaving Vertebrate

JOSEPH R. FETCHO, KINGSLEY J. A. COX, AND DONALD M. O'MALLEY

Department of Neurobiology and Behavior, State University of New York at Stony Brook, Stony Brook, New York 11794-5230

Introduction

Most behaviors are produced by activity in populations of neurons, but the physiological approaches commonly used to study neural circuits allow the activity of only one or very few neurons to be monitored at a time. What is needed are approaches that allow the monitoring of activity in a group of cells—preferably a large group—while simultaneously permitting the identification and the recording of activity from each cell. Progress along these lines has been made with the use of electrode arrays (Wilson and McNaughton, 1994). An alternative, very promising approach—*i.e.*, imaging—offers an easy determination of both the activity and the identity of cells (Wu *et al.*, 1994; O'Donovan *et al.*, 1993). In this method, the neurons are labeled with an indicator dye that signals their activity, and the dye is then used to monitor the cells that are active during a particular behavior. The ideal situation would be one in which a population of neurons could be labeled and their activities observed with single-cell resolution in an intact, behaving animal. This ideal is difficult to achieve with vertebrates because most of them are opaque, so the neurons cannot be seen in the intact animal. Notable exceptions are the larvae of many fishes, which are transparent and thus especially suitable for imaging neurons. We have developed approaches in which a fluorescent calcium indicator is used to monitor neural activity in intact fish. Neurons that are labeled with the indicator increase in brightness due to the calcium influx associated with their activity. Thus, neural activity during behavior can be determined by watching for the increase in brightness in particular cells (O'Donovan *et al.*, 1993; Fetcho and O'Malley, 1995; Fetcho *et al.*, 1995; Cox and Fetcho, 1996; O'Malley *et al.*, 1996). The transparency of the fish has allowed us to image activity in neuronal populations with single-cell resolution in an intact vertebrate. Our work so far has focused on the neuronal populations involved in the escape behavior. This behavior has been the subject of intensive study with single-cell recording techniques in the past (Faber and Korn, 1978; Fetcho and Faber, 1988; Fetcho, 1992), but the ability to monitor groups of neurons is providing a new view of the relationships between neural activity and the escape behavior.

This paper was originally presented at a workshop titled *The Future of Aquatic Research in Space: Neurobiology, Cellular and Molecular Biology*. The workshop, which was held at the Marine Biological Laboratory, Woods Hole, Massachusetts, from 13 to 15 May 1996, was sponsored by the Center for Advanced Studies in the Space Life Sciences at MBL and funded by the National Aeronautics and Space Administration under Cooperative Agreement NCC 2-896.

Labeling

Central neurons were labeled with a calcium indicator, calcium green dextran. Neuronal activity causes an influx of calcium through voltage-dependent calcium channels, so the calcium levels sensed by the indicator can be used as a measure of activity. The neurons in larval, post-hatching zebrafish (*Danio rerio*) were labeled in two ways. In the first, the indicator was injected into muscle or into the central nervous system, backfilling the neurons of interest. Calcium green dextran is taken up by the damaged processes of neurons, resulting in both retrograde and anterograde labeling (O'Donovan *et al.*, 1993; Fetcho and O'Malley, 1995). This approach led to a very robust labeling of populations of neurons. The neurons could be observed and individually identified in the spinal cord and in the brain of the living fish either by confocal microscopy or enhanced video imaging. The labeling was very similar to that seen in material that had

been cleared and stained with horseradish peroxidase (HRP). We could see many of the individually identifiable neurons of zebrafish (Bernhardt *et al.*, 1990), including the three primary motoneurons (rostral, middle, and caudal—RoP, MiP, and CaP, respectively) located in spinal segments, and the Mauthner cell and its two serially homologous neurons (MiD2cm, MiD3cm) located in the hindbrain. Other identifiable spinal neuronal types (*e.g.*, secondary motoneurons, Rohon Beard cells, dorsal root ganglion cells, circumferential descending (CiD) cells, commissural posterior ascending (CoPa) cells) and brain neurons (*e.g.*, vestibulospinal neurons, nucleus of the medial longitudinal fasciculus) were also evident. The relatively high fluorescence of calcium green at basal calcium levels produced well-labeled dendrites and axons. The quality of the labeling, and the high resolution and optical sectioning ability of the confocal microscope, allowed the collection of serial optical sections through the neurons of interest. Three-dimensional reconstructions of the cells from live fish were produced from optical sections using the VolVis program (Sobierajski *et al.*, 1995). The reconstructions allowed a detailed examination of the neurons whose physiology was being studied optically. This allowed the unambiguous identification of the cells and also provided information about the relationships of the axons and dendrites of the imaged neurons.

Although labeling by injection into the larval fish produced well-labeled neurons, the injection may in some instances disrupt portions of the neural circuits of interest. To circumvent this problem, we also labeled neurons by injecting calcium green dextran into blastomeres of one-, two-, four-, or eight-celled embryos. In this procedure, the indicator is labeling the progeny of the blastomere, just as lineage tracers are used in developmental studies. The fish were then raised to post-hatching larval stages. These injections produced larval fish in which a large fraction of cells contained the calcium indicator; from one-eighth to all of the cells should be labeled, depending on the number of blastomeres that had been formed at the time of injection. The proportion of labeled cells, in our experience, was roughly consistent with this expectation, although the intensity of the labeling of individual cells varied. The confocal microscope effectively removed fluorescence that was out of focus, and allowed visualization of the labeled cells in the intact animal. This approach has the advantage of not disrupting the neural circuitry, at least so far as we can tell. The lack of damage is evidenced by our ability to raise such blastomere-labeled fish to adulthood after imaging their neural activity. The labeling produced by blastomere injections is not, however, as intense as that by injection into larvae, so the type of each cell is more difficult to identify. Nevertheless, we have been able to observe identifiable classes of spinal neurons (*e.g.*, Rohon Beard cells) and some neurons, such as olfactory epithelial cells, are very brightly labeled (Cox and Fetcho, 1996).

Responses of Neurons

We initially used electrical stimuli to determine whether the indicator was responsive in the neurons and to demonstrate that we could resolve differential responses in adjacent cells (Fetcho and O'Malley, 1995). Motoneurons in larval fish, typically 3–5-days old, were backfilled by injections of calcium green dextran into muscle and then, a day or more later, were embedded in agar and observed with a Biorad MRC 600 confocal imaging system using a Zeiss IM 35 inverted microscope. The fish remain healthy in the agar, probably because they depend on cutaneous respiration at these early stages. An electrical stimulus applied to the skin overlying the muscle near the site of calcium green injection could increase the fluorescence of the labeled motoneurons. A single stimulus typically produced increases of 5%–10%; additional stimuli, applied in rapid succession, further increased the fluorescence (over 100% change for a train of 40 stimuli in some cells) consistent with the accumulation of calcium expected upon repeated activation of the motoneurons. By varying the strength of the electrical stimulus, we could detect differential responses in adjacent motoneurons, with one cell showing a large increase in fluorescence (*e.g.*, 70%) and an immediately adjacent one showing none. Thus, we could resolve differences in adjacent cells which were roughly 10 μm diameter and only about 1 μm apart.

Having confirmed that the cells behaved as expected to electrical stimulation, we examined their responses during escapes (Fetcho and O'Malley, 1995). Escape behaviors were elicited by an abrupt touch applied to the head or tail with a piezoelectric tapping device. In the escape behavior, a touch on one side of the head leads to a massive, rapid C-bend to the opposite side of the body, which turns the fish away from a threatening stimulus. When we imaged spinal motoneurons on the side of a C-bend during the escape, we found a massive activation, with every cell that we imaged responding during the escape bend. In individual cells, the increases in fluorescence ranged from 16% to 151%. The activated motoneurons included the larger primary motoneurons, as well as the smaller secondary ones. Most of our observations were obtained with low temporal resolution, usually 400 ms for each image. However, we could achieve resolutions on the millisecond time scale of synaptic events by taking advantage of the line-scanning ability of the confocal microscope. This allowed us to look at one line through a group of cells every 2 ms, and revealed a synchronous activation of the motoneurons. The pri-

mary motoneurons innervate extensive regions of the axial muscle and are known to be important in escapes, based upon evidence that they receive a monosynaptic input from the reticulospinal Mauthner cell that initiates the escape (Myers *et al.*, 1986; Westerfield *et al.*, 1986; Fetcho and Faber, 1988; Liu and Westerfield, 1988). The secondary motoneurons are more numerous and their role in escapes has been less clear. Our data indicate that the motoneurons activated in escapes include both primary and secondary pools (Fetcho and O'Malley, 1995). We observed a similar massive activation of cells in ventral cord that had been labeled by blastomere injections and imaged in the larval fish (Cox and Fetcho, 1996). The identity of these cells in the blastomere-labeled fish was not certain because of the less complete filling of cells from blastomere injections. But, based upon their locations, they were most likely motoneurons. The observations from backfills and blastomere injections are consistent with the massive activation of muscle that occurs during the escape bend. The most powerful C-bends occur in response to stimulation of the head (Eaton *et al.*, 1984; Foreman and Eaton, 1993). These bends are the most forceful motor behavior produced by the fish, so such a large recruitment of motoneurons is not surprising.

We began our imaging studies with motoneurons, because enough was known about their activity patterns that we could use previous data to evaluate the reliability of the approach. More recently we have begun to study other, less well understood systems, including the olfactory system, reticulospinal neurons, and spinal interneurons. Our studies of reticulospinal neurons, for example, have demonstrated that the brain as well as the spinal cord, can be examined by *in vivo* imaging. We have used the approach to evaluate predictions about the pattern of activation of the Mauthner cell and its serially homologous neurons in hindbrain (Fetcho *et al.*, 1995; O'Malley *et al.*, 1996). The hindbrain consists of a series of segments that contain repeated, morphologically similar neurons in successive segments. One of these sets of serially repeated cells includes the reticulospinal Mauthner cell (in hindbrain segment 4), which is known to play a role in escapes, and two reticulospinal cells (MiD2cm, MiD3cm in segments 5 and 6 respectively) that are very like the Mauthner cell in their dendritic structure and axonal projection. The functional role of the Mauthner-like cells was unknown, but Foreman and Eaton (1993) predicted that the observed variability in the strength of the C-bend, in response to sensory stimuli at different locations relative to the fish, might be determined in part by variability in the activation neurons in the set (including the Mauthner cell, MiD2cm, and MiD3cm). We have examined and confirmed their predictions by calcium imaging, which has allowed us to study the function of a set of cells that has been difficult to study with more conventional techniques (Fetcho *et al.*, 1995; O'Malley *et al.*, 1996). Our observations suggest that the hindbrain consists of serial sets of functionally similar neurons that may act together in various combinations to produce behavioral variability.

Conclusions

Although still in its infancy, the use of calcium imaging in the larval zebrafish offers the possibility of studying the activity of populations of neurons with single-cell resolution anywhere in the brain or spinal cord of an intact, behaving vertebrate. This will provide important information about the relationships between the activity of neuronal populations and behavior in the normal animal, but there are other advantages of the zebrafish as well. Thousands of mutant lines of zebrafish have now been generated by saturation mutagenesis, including many with sensory and motor deficits (Mullins *et al.*, 1994; Driever *et al.*, 1994). The calcium imaging approach should prove useful in analyzing the functional deficits of these mutant lines. The transparency of the fish will also facilitate the optical killing of particular, fluorescently labeled neurons. The behavior and neuronal activity of the fish can be studied both before and after particular neurons or sets of neurons have been killed, allowing a more causal link between neurons and behavior. It may also be possible to use local optical uncaging of neuroactive substances to activate or inhibit neurons. This would allow noninvasive perturbations of activity. The combination of imaging activity, genetics, and cell ablation will permit a powerful analysis of the neural basis of behavior in a vertebrate.

Acknowledgments

Supported by NIH NS26539, NS-09113, and the Howard Hughes Medical Institute.

Literature Cited

Bernhardt, R. R., A. B. Chitnis, L. Lindamer, and J. Y. Kuwada. 1990. Identification of spinal neurons in the embryonic and larval zebrafish. *J. Comp. Neurol.* **302:** 603–616.

Cox, K. J. A., and J. R. Fetcho. 1996. Labeling blastomeres with a calcium indicator: a non-invasive method of visualizing neuronal activity in zebrafish. *J. Neurosci. Methods* **68:**185–191.

Driever, W., D. Stemple, A. Schier, and S. Solinica-Krezel. 1994. Zebrafish: genetic tools for studying vertebrate development. *Trends Genet.* **10:** 152–159.

Eaton, R. C., J. Nissanov, and C. M. Wieland. 1984. Differential activation of Mauthner and non-Mauthner startle circuits in zebrafish: implications for functional substitution. *J. Comp. Physiol.* **155:** 813–820.

Faber, D. S., and H. Korn, eds. 1978. *Neurobiology of the Mauthner Cell.* Raven Press, New York.

Fetcho, J. R. 1992. Excitation of motoneurons by the Mauthner axon in goldfish: complexities in a "simple" reticulospinal pathway. *J. Neurophysiol.* **67:** 1574–1586.

Fetcho, J. R., and D. S. Faber. 1988. Identification of motoneurons and interneurons in the spinal network for escapes initiated by the Mauthner cell in goldfish. *J. Neurosci.* **8:** 4192–4213.

Fetcho, J. R., and D. M. O'Malley. 1995. Visualization of active neural circuitry in the spinal cord of intact zebrafish. *J. Neurophysiol.* **73:** 399–406.

Fetcho, J. R., Y.-H. Kao, and D. M. O'Malley. 1995. Functional roles of serially homologous reticulospinal neurons studied by *in vivo* confocal calcium imaging in zebrafish. *Soc. Neurosci. Abstr.* **21:** 687.

Foreman, M. B., and R. C. Eaton. 1993. The direction change concept for reticulospinal control of goldfish escape. *J. Neurosci.* **13:** 4101–4113.

Liu, D. W., and M. Westerfield. 1988. Function of identified motoneurons and coordination of primary and secondary motor systems during zebrafish swimming. *J. Physiol. (Lond.)* **403:** 73–89.

Mullins, M. C., M. Hammerschmidt, P. Haffter, C. Nusslein-Volhard. 1994. Large-scale mutagenesis in the zebrafish: in search of genes controlling development in a vertebrate. *Curr. Biol.* **4:** 189–202.

Myers, P. Z., J. S. Eisen, and M. Westerfield. 1986. Development and axonal outgrowth of identified motoneurons in the zebrafish. *J. Neurosci.* **6:** 2278–2289.

O'Donovan, M. J., S. Ho, G. Sholomenko, and W. Yee. 1993. Real-time imaging of neurons retrogradely and anterogradely labeled with calcium-sensitive dyes. *J. Neurosci. Methods* **46:** 91–106.

O'Malley, D. M., Y.-H. Kao, and J. R. Fetcho. 1996. Imaging the functional organization of zebrafish hindbrain segments during escape behaviors. *Neuron* **17:**1145–1155.

Sobierajski, L. M., R. S. Avila, D. M. O'Malley, S. Wang, and A. E. Kaufmann. 1995. Visualization of calcium activity in nerve cells. *IEEE Comp. Graph. Appl.* **15:** 55–61.

Westerfield, M., J. V. McMurray, and J. S. Eisen. 1986. Identified motoneurons and their innervation of axial muscles in the zebrafish. *J. Neurosci.* **6:** 2267–2277.

Wilson, M. A., and B. L. McNaughton. 1994. Reactivation of hippocampla ensemble memories during sleep. *Science* **265:** 676–679.

Wu, J.-Y., L. B. Cohen, and C. X. Falk. 1994. Neuronal activity during different behaviors in *Aplysia*: a distributed organization? *Science* **263:** 820–823.

Reference: *Biol. Bull.* **192:** 154–156. (February, 1997)

Discussion

KAWASAKI: It appeared that the image you showed lasted for a second or so. Does this reflect the time course of the calcium concentration?

FETCHO: That's a good question. The recovery time is slow: the rise is very fast, but the recovery time takes many seconds. This time course occurs in a number of different cells. There's quite a bit of debate about the basis for that time course. Some people think that the dye might be affecting the time course of the calcium increase. We think that the calcium returns slowly to resting levels; but this is a very difficult issue to resolve, and one that is not my main focus. I just want an indication of which cells are active.

WIEDERHOLD: How many action potentials have been fired in the Mauthner cell to get that much of a rise?

FETCHO: As far as we know, in these teleost fishes, the Mauthner cell fires only a single action potential. That's a big change that we see. It turns out there's some variability in the size of the observable changes. In the course of an experiment, the cell changes the way it responds. It will start out with relatively modest responses and then, with repeated trials, will convert to these larger responses. We think that there are some interesting things going on, perhaps with respect to intracellular calcium being released, perhaps from stores.

BAKER: I have a question to either of you. First, I totally reject the hypothesis that there are iterative, homologous, reticular spinal neurons in the hindbrain. For three or four hundred million years, each hindbrain segment has had an independent evolutionary history. Don't you think that your evidence demonstrates that the reticulospinal neurons are not iteratively homologous, because they each exhibit their own physiological sensitivity, properties, and projections? Wouldn't it be more useful to think about each of these segments containing reticulospinal neurons having their own independent role in the escape behavior?

FETCHO: The issue is the distinction between homology and iterative homology; what was the origin of these cells? Surely they arose a long time ago, and they have been independently evolving for a long time. However, they might at first have been the result of a duplication event that (to me) would represent a serial homologous type of organization. I would agree that they have independently evolved for a long time. This certainly is the case.

BAKER: Joe (Fetcho), Model T's can be duplicated, but they will never become Cadillacs. In other words, duplication and divergence occurred so long ago that iterative homology is not a useful physiological tool.

FETCHO: They have both morphological similarities and reasonable functional similarities as well, at least to the extent that they seem to be involved in the escape behavior. It remains to be seen whether the homologues are involved in other things as well. We haven't explored that very much.

EATON: I don't know if either one of us wants to get caught in a debate about homology and analogy. From my point of view, I mean only what has been stated in the previous papers that have come before us; these particular cells have similar genetics, developmental history, immunohistochemistry, and so on. That doesn't have to imply that there aren't going to be functional differences between the cells as well. In fact, we would expect that once the cells are determined, they will go off on different paths and different features of their function will be emphasized. That's as far as I would like to go on that.

BAXTER: I wonder if you have looked at the ability of the Mauthner circuit to adapt. For example, if you turn the animal upside down, must it now reverse its reactions?

EATON: That's a very good question. We don't know anything about that yet.

BAXTER: Some of the synapses in your circuit were electrotonic, and one doesn't typically think of those as being very plastic.

EATON: The inputs to the Mauthner cell from the inner ear fibers are mixed chemical-electrotonic junctions. The important point here is that the fish is using its vestibular organs to hear. Or, to put it in the

other perspective, humans don't use their vestibular organs to hear in the same way. As far as I know, there's not much known about how the fish discriminates between those two components—the gravitational field and the acoustic particle acceleration—at the same time. What happens then, when you disturb that process by putting the fish in zero gravity or by turning it upside down in a gravitational field, would be most interesting to evaluate. I don't think anyone has started to look at that, but it's certainly an issue that could be evaluated.

BASS: Do those PHP cells encode sound intensity? Joe (Fetcho) are you able to visualize those cells?

EATON: We don't know that they encode sound intensity *per se*. In the only very controlled experiments, electrical shocks were applied to the eighth nerve. As the intensity increased, the nerves fired more robustly. We don't know how they respond to controlled sound pulses. None of that has been evaluated.

FETCHO: The short answer is that we don't know whether we can visualize the PHP cells. We think that we can look at any neurons anywhere in the brain; it's just a matter of getting the dye into them without messing up the circuits that you're interested in. We haven't tried to label the PHP cells.

MORRIS: I want to get back to this business of up and down in your experiments. I was assuming that the fish was lying on its side—in the confocal experiments anyway—while you were stimulating and imaging. Is this correct?

FETCHO: That depends on the experiments. In the reticulospinal experiments, the fish is actually lying on its back, so that we are looking through the entire head to see the cells at the bottom of the brain. That's why we can look anywhere in the brain; basically we are looking through the whole brain to see those images. When we are looking at spinal neurons, we look from the side because it's very transparent from that angle. There's a lot of pigment at the top of the fish.

BARLOW, R.: Joe (Fetcho), I would like to get a better feel for what you were seeing in your calcium measurements. It appeared that there is a signal without stimulation. Is there background activity—that is, free intracellular calcium without stimulation?

FETCHO: That's right.

BARLOW, R.: And when you stimulate, there's an increase in calcium?

FETCHO: That's right. Calcium green dextran has fairly good fluorescence at basal calcium levels, which is very important for us, because we would like to know what cells we are looking at. If you can't see them at rest, then you might have trouble.

BARLOW, R.: Where is the action potential fired with regard to the increased free calcium in the cell? Where's the axon hillock region? Does your imaging data make sense as to where the major conductance changes are taking place?

FETCHO: In goldfish, where it's best understood, the spikes are initiated right where you might expect—at the initial segment region. You get a fairly substantial depolarization of the soma as well, but it's passively invaded by the spike. We don't know much about the distribution of calcium channels in the cell.

In the case of the auditory inputs, they come in on the lateral dendrite. The big lateral dendrite that goes out to the ear is passive, and postsynaptic potentials are passively conducted to the initial segment. The spikes originate at the initial segment right near where the axon goes off, and then it's passively propagated back into the soma.

BARLOW, R.: But you are detecting calcium changes mainly in the cell body.

FETCHO: Well, that's all we've looked at. We haven't explored what's happening out in the dendrite. We don't see much in the cell body, unless the cell fires an action potential. We can do thresholding experiments where we are stimulating right near the threshold for escapes. Under those conditions, we would expect a massive subthreshold synaptic input to the cell. In cases where the fish doesn't carry out an escape, you don't see any change. You only see the change when you get the escape—when the Mauthner cell has fired a spike.

COMMENT: One possibility may be that the channels in the larval Mauthner cell are different from those in the adult, in what is being experienced. In fact, that's the case in some embryonic amphibian neurons which show calcium spikes that don't appear later in development. That's certainly a possibility here.

HIGHSTEIN: I have a comment. I don't think that fish can tell the difference between hearing sound and vibration. It's all vibrational energy with different frequencies. In fact, there's good evidence that the mammalian saccule transduces so-called auditory stimuli. I have heard anecdotal reports of sound underwater so intense that it rattles paper on a clipboard used for writing underwater. *A propos* of that, I wonder what the parties here think they are stimulating to make the fish escape. I doubt that he's using his lateral line to hear.

EATON: Both of us have avoided saying anything about the lateral line, because we don't know what possible role it plays in these responses. We have some circumstan-

tial evidence suggesting that both the lateral line and the ear are involved in the responses to tail stimulation. We don't have any good direct evidence though. The lateral line could certainly contribute to the resolution of acoustic directionality in adult fish in ways that are very similar to what the inner ear would be doing. I should also mention that the accelerations we use are somewhat higher than you would expect for a standard classical monopolar or dipole sound source. But as you say, it's sort of a continuum of intensities of accelerations that vary from normal acoustic levels to levels that are higher than those you might call vibration. But in the fish, how can you distinguish which is which?

SACK: I have a question of a technical nature. Dr. Fetcho, what concentration of calcium green did you inject without affecting the intracellular calcium concentration?

FETCHO: We inject about five nanoliters of a 5% w/v solution into blastomeres. If you inject too much, they die. If you inject too little, the dye gets diluted. If you get the right amount in, the cells are visible in the larvae and their responses can be imaged. The fish can be taken out of the agar after imaging and raised to adulthood. The dye does not cause any obvious problems.

Reference: *Biol. Bull.* **192**: 157. (February, 1997)

Complex Signal Processing by Weakly Electric Fishes

MASASHI KAWASAKI

Department of Biology, University of Virginia, Gilmer Hall, Charlottesville, Virginia 22903

How does the nervous system extract meaningful information from complex sensory stimuli in order to perform appropriate behaviors? The jamming avoidance response of weakly electric fishes, such as *Gymnarchus niloticus*, provides an attractive model system with which to study the neuronal substrate of pattern recognition.

The African electric fish *Gymnarchus* generates electric organ discharges at an individually fixed frequency for electrolocation. But when two fish with slightly different discharge frequencies meet, they shift their discharge frequencies away from each other and thus avoid effects of jamming on their electrolocation capabilities. To produce the correct jamming avoidance response, *Gymnarchus* must extract information about the sign of the frequency difference between its own discharge and its neighbor's. This stimulus feature, the sign of frequency difference, is concealed in the temporal pattern of amplitude and phase modulation in the sensory stimulus. The amplitude modulation and the phase modulation are sampled by different classes of electroreceptors and processed in parallel by the hindbrain (Rose *et al.*, 1988; Kawasaki, 1993, 1996; Kawasaki and Guo, 1996).

This paper was originally presented at a workshop titled *The Future of Aquatic Research in Space: Neurobiology, Cellular and Molecular Biology*. The workshop, which was held at the Marine Biological Laboratory, Woods Hole, Massachusetts, from 13 to 15 May 1996, was sponsored by the Center for Advanced Studies in the Space Life Sciences at MBL and funded by the National Aeronautics and Space Administration under Cooperative Agreement NCC 2-896.

Literature Cited

Kawasaki, M., and Y.-X. Guo. 1996. Neuronal circuitry for comparison of timing in the electrosensory lateral line lobe of an African wave-type electric fish, *Gymnarchus niloticus*. *J. Neurosci.* **16**: 380–391.

Kawasaki, M. 1996. Comparative analysis of the jamming avoidance response in African and South American wave-type fishes. *Biol. Bull.* **191**: 103–108.

Kawasaki, M. 1993. Independently evolved jamming avoidance responses employ identical computational algorithms: a behavioral study of the African electric fish, *Gymnarchus niloticus*. *J. Comp. Physiol.* **173**: 9–22.

Rose, G. J., M. Kawasaki, and W. Heiligenberg. 1988. 'Recognition units' at the top of a neuronal hierarchy? Prepacemaker neurons in *Eigenmannia* code the sign of frequency differences unambiguously. *J. Comp. Physiol.* **162**: 759–772.

Reference: *Biol. Bull.* **192:** 158–160. (February, 1997)

From Neurons to Behavior: Vocal-Acoustic Communication in Teleost Fish

ANDREW H. BASS, DEANA A. BODNAR, AND JESSICA R. McKIBBEN

Section of Neurobiology and Behavior, Cornell University, Ithaca, New York 14853

Overview

Sound communication is not unique to humans and other mammals, but rather, is a trait shared with most nonmammalian vertebrates. The focus of our studies has been one species of sound-producing teleost fish, the plainfin midshipman (*Porichthys notatus*). Our research program has taken three principal directions: (1) functional organization of the vocal organ and brain circuitry establishing the physical attributes of vocalizations; (2) development of, and hormonal influences on, the expression of sexually dimorphic vocal traits; and (3) encoding of vocal signals by the peripheral and central auditory system.

Midshipman Fish: Spawning and Vocal Behaviors

The plainfin midshipman has a wide distribution along the western coastline of northern California and on into southern Canada. There are two male reproductive morphs, *type I* and *type II*, with distinct spawning and vocal behaviors (Brantley and Bass, 1994). Type I males build nests under rocks in the intertidal and subtidal zones where they fertilize and then guard eggs deposited on the roof of their nest by females. In contrast, type II males gain access to gravid females and their eggs by essentially parasitizing the type I male's reproductive tactic. Thus, type II males lie perched outside of, or sneak into, a type I male's nest and shed sperm in an attempt to compete with the type I male for eggs; they do *not* build nests or guard eggs.

This paper was originally presented at a workshop titled *The Future of Aquatic Research in Space: Neurobiology, Cellular and Molecular Biology*. The workshop, which was held at the Marine Biological Laboratory, Woods Hole, Massachusetts, from 13 to 15 May 1996, was sponsored by the Center for Advanced Studies in the Space Life Sciences at MBL and funded by the National Aeronautics and Space Administration under Cooperative Agreement NCC 2-896.

Nesting type I males generate two classes of vocalization. Trains of short duration 150-ms grunts are produced at intervals of about 400 ms during defense of a nest against potential intruder males. Type I males also produce long-duration (minutes to over 1 hour), quasi-sinusoidal calls known as hums. The hum has a simple harmonic structure; the fundamental frequency is near 90–100 Hz with one or two prominent higher harmonics. During the breeding season, nesting males often cluster in groups of two or more and produce hums simultaneously. Observations of captive populations of nesting type I males, together with playbacks of natural or computer-synthesized acoustic signals through underwater loudspeakers, show that hums, but not grunts, can attract females to an artificial nest site (Brantley and Bass, 1994; McKibben *et al.*, 1995). Type II males and females have only been observed to produce isolated, low-amplitude grunts in nonspawning contexts.

Vocal Motor Circuitry

Anatomical and neurophysiological studies have identified a vocal control system in midshipman (Bass and Baker, 1990; Bass *et al.*, 1994, 1996a). The vocal organ consists of a pair of sonic muscles attached to the lateral walls of the swimbladder. Each sonic muscle is innervated by a single nerve formed by branches of the ventral occipital nerve roots that exit the hindbrain just caudal to the vagus nerve. The occipital nerves carry motor axons originating from two clusters (nuclei) of vocal motoneurons extending along the midline of the caudal hindbrain (medulla oblongata) and rostral spinal cord. Each motoneuron cell body (soma) has a single, unbranched axon that innervates muscle fibers located on the same (ipsilateral) side of the body axis, and a dendritic arbor that extends throughout both motor nuclei. Intracellular

recording and staining studies have identified vocal pacemaker neurons that are ventrolateral to the motoneurons. The firing frequency of the pacemaker neurons is matched 1:1 with that of the sonic motoneurons and, in turn, to the fundamental discharge frequency of the vocal motor volley as recorded intracranially from the occipital nerve roots. A single pacemaker neuron innervates the neurons in both motor nuclei, consistent with the hypothesis that their role is to synchronize the firing of motoneurons positioned on both sides of the brain. The latter, in turn, leads to the simultaneous contraction of both sonic muscles at a fundamental discharge frequency that establishes the fundamental frequency of vocalization. Hence, there is a direct relationship between the rhythmic, patterned output of a pacemaker-motoneuron circuit and the physical attributes of vocalization. Sex- and morph-specific vocal behaviors are reflected in a divergence of neurobiological and endocrinological traits, ranging from the size of the sound-producing (sonic) muscles to the rhythmic firing properties of vocal neurons (Bass, 1992, 1996).

Encoding of Species-Specific Acoustic Signals

Among many species of teleost fish, acoustic signals are primarily encoded by fibers that innervate the sacculus division of the inner ear (Popper and Fay, 1993). The most extensive studies of auditory coding in teleost fish have been carried out in the goldfish, *Carassius auratus* (Popper and Fay, 1993). Although goldfish have served as a useful model for identifying the general coding mechanisms utilized by the vertebrate auditory system, their lack of obvious vocal behavior makes it difficult to examine the coding and processing of behaviorally relevant stimuli, such as communication signals. A practical way to address questions of vocal signal coding has been to identify neural mechanisms in nonmammalian species that utilize acoustic communication signals in their social behavior; one such species is the midshipman fish.

A fundamental problem faced by the auditory system of any vocalizing species is the segregation and recognition of two concurrent vocal signals from independent sources. Midshipman are routinely faced with the acoustic problem of segregating concurrent signals when numerous males congregate during the breeding season and vocalize simultaneously. Within a natural population, the fundamental frequencies (F0s) of individual hums differ within a range of about 10 Hz. The summation of two concurrent multiharmonic signals, such as hums that differ in their F0s, results in a complex sinusoidal waveform with multiple envelope periodicities at difference frequencies (dF) between (1) the F0s of each signal; (2) their higher harmonics; and (3) the F0s and higher harmonics. So far, we have assessed the encoding of simple beats produced by the summation of two tones near the F0s of natural hums with dFs less than 10 Hz. Playback experiments suggest that midshipman can discriminate and choose between two concurrent hums that differ in F0 (McKibben *et al.*, 1995). Hence, midshipman must have a neural mechanism for segregating and discriminating between two signals on the basis of F0.

Peripheral Coding (McKibben and Bass, 1996; McKibben *et al.*, 1995): Acoustic stimuli were used to evoke single-unit responses in primary afferent fibers of the VIIIth cranial nerve that innervate the sacculus. At intensity levels comparable to those of natural signals (100–130 dB, re: 1 μPa), auditory fibers respond to pure tones over a frequency range of 60–300 Hz by changes in their average spike rate. Fibers respond best to frequencies below 120 Hz within the range of F0s of midshipman vocalizations. Phase-locking of spikes begins at lower intensity levels and seems to better encode signal frequency. Two tones at slightly different F0s (dFs of 2–20 Hz) were added to generate stimuli that mimic the simple acoustic beats that result from the overlap between the hums of Type I males. In response to simple beats, auditory afferents synchronize best to one of the two tones, usually the one with the lower F0. In general, synchronization to dF was much lower than to either of the two tones comprising the beat stimulus.

Auditory midbrain (Bass *et al.*, 1996b; Bodnar and Bass, 1996; Bodnar *et al.*, 1996): In midshipman, as in other teleosts, the midbrain's torus semicircularis includes a nucleus centralis that receives input from hindbrain nuclei encoding acoustic information. Multi- and single-unit recordings in the nucleus centralis show that the majority of auditory units exhibit changes in their spike rate with changes in frequency from 70 to 200 Hz. At least two types of units, tonic and phasic, are present. Tonic units respond throughout the duration of the stimulus, while phasic units respond only at stimulus onset. In response to simple beats with combinations of primary tones in the range of 80–100 Hz, a subset of tonic units are tuned to low frequency dFs (4–10 Hz); units exhibit low synchronization to individual tones. About half of the dF encoding neurons exhibit no significant change in their dF tuning with different primary tones. Thus, some units appear to be tuned to a specific dF, while in others, coding of dF and the F0s may be coupled.

In summary, the results suggest that a peripheral periodicity code of the individual components of a beat waveform is transformed into a midbrain dF code.

Acknowledgments

Research support from NSF, NIH, NIMH, Cornell University, U. C. Bodega Marine Laboratory, and New York State Hatch Grant.

Literature Cited

Bass, A. H. 1992. Dimorphic [illegible] and alternative reproductive tactics in a vocalizing [illegible] *Neurosci* **15:** 139–145.

Bass, A. H. 1996. Shapin[illegible] exuality. *Am Sci* **84:** 352–363.

Bass, A. H., and R. Baker [illegible]. Sexual dimorphisms in the vocal control system of a t[illegible] morphology of physiologically identified neurons. *J* [illegible] **21:** 1155–1168.

Bass, A. H., M. A. Marchaterre, and R. Baker. 1994. Vocal-acoustic pathways in a teleost fish. *J Neurosci* **14:** 4025–4039.

Bass, A. H., D. A. Bodnar, and M. A. Marchaterre. 1996b. Auditory pathways in a vocal fish: inputs to a midbrain nucleus encoding acoustic beats. *Soc Neurosci Abstr* **22:** 447.

Bass, A. H., B. J. Horvath, and E. B. Brothers. 1996a. Non-sequential developmental trajectories lead to dimorphic vocal circuitry for males with alternative reproductive tactics. *J Neurobiol* **30:** 493–504.

Bodnar, D. A., and A. H. Bass. 1996. The coding of concurrent signals (beats) within the auditory midbrain of a sound producing fish, the plainfin midshipman. *Association for Research in Otolaryngology,* No. 617.

Bodnar, D. A., J. R. McKibben, and A. H. Bass. 1996. Temporal computation of the difference frequency of concurrent acoustic signals in the central auditory system of a vocal fish. *Soc. Neurosci. Abstr* **22:** 447.

Brantley, R. K., and A. H. Bass. 1994. Alternative male spawning tactics and acoustic signals in the plainfin midshipman fish, *Porichthys notatus* (Teleostei, Batrachoididae). *Ethology* **96:** 213–232.

McKibben, J. R., and A. H. Bass. 1996. Peripheral encoding of behaviorally relevant acoustic signals in a vocal fish. *Soc. Neurosci. Abstr.* **22:** 447.

McKibben, J. R., D. A. Bodnar, and A. H. Bass. 1995. Everyone's humming, but is anyone listening? Acoustic communication in a marine teleost fish. *4th Int Neuroethol. Congr. Abstr* p. 351.

Popper, A. N., and R. R. Fay. 1993. Sound detection and processing by fish: critical review and major research questions. *Brain Behav Evol.* **41:** 14–38.

Reference: *Biol. Bull.* **192:** 161–163. (February, 1997)

Discussion

QUESTION: Dr. Bass, is one hum better than the other? Why should a female care which male's nest she goes into? What's the value of it?

BASS: Certainly that is a critical question which we are pursuing. I don't have the answer to it. In acoustic systems that have been studied in terms of female choice, a fundamental frequency of the signal can often be predictive of body size; in this system, however, we have found no such correlate. In fact, this goes back to work that I did with Bob Baker, here at the MBL, where we were recording from the CNS. I found no correlation between the fundamental frequency of the motor discharge and an animal's body size. So body size is not a cue in that context.

QUESTION: Didn't you say that the population in this range is all within the same temperature?

BASS: Actually I don't know that. Unfortunately the temperature was not monitored in those experiments for each of the individual nests. This is a critical issue that we hope to investigate.

HIGHSTEIN: Obviously, these fish are fairly deaf because the noise is so loud. Maybe this is just some variation in frequency, so they know whether to go in one direction or another. If all the frequencies were the same, they might get confused about the sources. By having slight differences in frequency the sources might become clearer and lead them in one direction or the other.

BASS: So you're suggesting that the frequency differences could play a role in localization. This may very well be the case. As you can imagine, working in an aquatic environment is extremely difficult. Furthermore, doing those field experiments has proven extremely difficult, and we are still pursuing them. I wish I had the answer to your question. All I know is that you see that variation in the natural signal. It just so happens that there are units in the midbrain that perfectly encode the difference frequency.

MORRIS: I have a question for Masashi (Kawasaki). I was really intrigued by the fact that in neither of these different evolutionary lines was the internal reference information used. It seems sort of amazing not to make use of that readily available piece of information. Do you have any notions from an evolutionary engineering point of view? What's the point?

KAWASAKI: To make it more amazing, there is a species related to the African fish that does process the internal reference system for gating. This was a double shock to us because the African species is functionally similar to the unrelated fish and dissimilar from the fish that belongs to the same family. I think that the timing comparison involved in the systems that I described is very accurate. The threshold for the timing comparison is sub-microsecond, yet the fish can perform the behavior when the only available phase is 100 ns. The internal reference mechanisms, the sort of mechanism that predicts feedback timing and gating, may not be accurate enough to do this. For internal reference mechanisms, for this gating, only millisecond accuracy may be enough. However, when you are interested in microsecond and sub-microsecond timing differences, using parallel systems and subtracting between the two channels could be a good idea. In the bat's echolocation system, there is an internal reference mechanism that is also not used as a reference for some aspects. In the echo delay comparison, the system computes a timing difference between outgoing cry and returning echo, but without using the internal reference system. But, for blocking self stimulation, it does use the internal reference system.

BAKER: Do either of you believe that the role of electrotonic coupling has been either overemphasized or overstressed in your system analysis? Do either of you have any evidence that it's necessary for these behaviors?

BASS: No. As you know, Bob (Baker), we did electron microscopy on sonic motor system early on. Although I did find gap junctions, I remember being amazed in the beginning when I didn't see a lot of them.

BAKER: Is this also true in your system, Masashi (Kawasaki)? Is electronic coupling absolutely necessary for the behavior?

KAWASAKI: We have done staining of calcium-binding proteins (calbindin or calretinin) in this differential phase coding circuitry. Not all of the elements are labeled. Although I haven't done any electron microscopy on this system, we have seen that the giant cell, which is one of the components of this system, doesn't light up with calretinin. This might indicate that this neuron does not use gap junctions.

BAKER: In this particular case, what role does the cerebellum play? Is it essential for the behavior?

KAWASAKI: Lesion of the cerebellum doesn't abolish the behavior.

QUESTION: Andy (Bass), were the differential frequency responses recorded in males or females? Is there any difference, and do two males sitting side by side try to separate their frequencies?

BASS: We have no evidence that there is anything like a jamming avoidance response. In answer to your question, let me first say that females do not generate signals. They generate grunts—very isolated grunts—infrequently, and the fundamental frequency of their signal is on the order of 15%–20% lower, which is matched by a difference in the CNS output. Nevertheless, if you sample a single, hour-long hum from males at different intervals, the standard deviation is on the order of 1 Hz. It is a highly stable behavior. In all the experiments on the CNS that Bob (Baker) and I have done over the years, we've never seen any evidence that the animals can modulate their central frequency. Although males may be trying to jam each other in this behavior, there is no evidence that they can actively produce something like a jamming avoidance response as a social response.

QUESTION: Are those differential frequency responses from the responding neurons present in both males and females?

BASS: Everything I've mentioned so far occurs in both males and females. We haven't seen anything that's obviously sexually dimorphic. Another interesting issue here is that it is important to understand the difference between the responses of the auditory and electrosensory systems. The fish that Masashi (Kawasaki) is studying are more or less continuously generating an output. Our fishes do not continuously generate. There are two conditions under which it would be useful for a neuron to produce a difference frequency. One is when the animal is actively vocalizing, trying to detect a neighbor whose pulse is essentially superimposed on its own. This is distinct from the case in which an individual is silent, but is listening to two other animals out there. It would seem that both males and females would want to do that. We've only studied the situation in which an animal is essentially listening to two other pulses.

QUESTION: Dr. Kawasaki, do the fish turn to maximize their signal?

KAWASAKI: This system cannot use propagation time. There is no propagation time associated with an electric field. Therefore, no distances could be encoded into time *per se*. The whole system is concerned more with dynamics than with stationary steady-state levels. So the fish will always operate in a moving situation. The majority of neurons respond to modulation of amplitude or phase.

ATEMA: Andy (Bass), you have eliminated so many possibilities for the real value of the signal. Wouldn't it be helpful to consider the cost to the sender of producing the signal? Perhaps the female is assessing the male's ability to maintain a constant and powerful sound for a long time. The female may be going around and comparing constancy between different males. Is there any evidence, on either the part of the sender or the receiver, that sound constancy and power are the parameters that constitute signal value? All your data seem to point in that direction, including temperature compensation.

BASS: That's an excellent point. We haven't really assessed our data carefully to determine whether the intensity coding in the CNS involves signal value and power output. There is a lot of power output from an individual male. We just don't have enough data yet—it's very hard to collect—but we are looking at intensity at an individual nest and how that might vary with male size. One would predict that the larger males might be able to produce a signal for a longer time. But it also might be a louder signal, and part of the goal in the field work this summer is to collect more data on that particular issue. The neurobiology is ahead of the behavior, as is the case in so many systems. What's beautiful about this system is that we can directly correlate male vocal signals with reproductive success. We can count the number of eggs in a male's nest, and we can in fact assess the number of clutches the individual male has. That's where the field work is going. Your question is excellent. Clearly the issue is identifying the value of the signal to an individual female.

BARLOW, R.: Andy (Bass), one of your slides indicates that the playback experiment was performed at night. What happens during the day?

BASS: We were really surprised. Basically this is a nocturnal behavior—that's when you pick up the humming. To get a decent video of the behavior, we decided to see what happens at 4 o'clock in the afternoon, instead of 8 at night. Although they do show the response, it is not as robust and consistent as at earlier hours. It's remarkably locked into some sort of circadian rhythm.

BARLOW, R.: Did you do experi-

ments in constant dark throughout the day and night?

BASS: These experiments are performed outdoors in those circular tanks. We have no control over the lighting.

BASS: Another issue we need to assess here is a female's initial approach to the signal. The way a female makes that decision may not be the same as when she makes her decision when she is close to the signal. This vocal signal could function merely as a beacon to let females know where males are breeding. If the female can assess on the basis of the beat frequency, she might be able to extract the number of males that are in a cluster, and that's why she goes to that cluster. But when she gets close to the cluster, how she makes the decision between different males could involve an entirely different set of rules. This could involve olfactory stimuli. Maybe at that point, the lateral line plays an important role in terms of intensity coding of that signal, which as you say is a very intense vibrational signal. I think we have such a long way to go in teasing apart those two things. These fish differ from the toadfish here at Woods Hole. If you listen to the calls of the toadfish, there is not much overlap in their signals. What's going on in these fish is different. We have done some recordings in toadfish and have not found any units that appear to be encoding DF. So the toadfish here at Woods Hole and our midshipman fish may have very different strategies.

COMMENT: The toadfish at Woods Hole undergo a huge temperature range. Presumably, as the muscle gets warmer, it's able to operate at a higher frequency, and the call frequency goes up with temperature. If we went to the west coast and there was also a large temperature range there (which is probably not the case), the call frequency would also increase with increasing temperature. One might imagine the case in which a cold female cannot hear a warm male, because the warm male is sounding out frequencies at 200 Hz and the female is, let's say, at 15 degrees, where her neurons only operate at 100–110 Hz. The suggestion is that the difference in temperature sensitivity, or the selection of different frequencies by the female, may just be a temperature effect on their neurons. That would be a necessity if they were to operate over a large temperature range.

BASS: That reminds me of some experiments that I did here at the MBL with the motor system, where the temperature and the firing frequency of the motor neurons were tightly coupled. The fundamental frequency of the hum varies directly with temperature. Your point is well taken that there is temperature coupling between the receiver and the sender. (Comment: There has to be or else it would not be heard!) Well, the caveat to that is, if you look at tuning curves in these animals, they are pretty broad, even if you are shifting temperature. Within the range of variation of the animal's experience, rather than our own artificial manipulations, things are still falling pretty much within their tuning curve, given the intensity of the signal.

Reference: *Biol. Bull.* **192:** 164–166. (February, 1997)

Activity-Dependent Regulation of Neural Networks: The Role of Inhibitory Synaptic Plasticity in Adaptive Gain Control in the Siphon Withdrawal Reflex of *Aplysia*

THOMAS M. FISCHER AND THOMAS J. CAREW

Department of Psychology, Yale University, New Haven, Connecticut 06520

Neural networks can be dynamic systems that enable organisms to adapt to, and learn about, complex and variable environments. The broad objective of our research program is to understand the nature of this type of adaptive process by examining the functional significance of neural plasticity observed at both cellular and network levels during adaptive behavioral modifications. Our primary goal is to characterize the role of inhibitory modulation in network function and plasticity, by focusing upon a recurrent synaptic circuit formed by the L29 excitatory interneurons and the L30 inhibitory interneurons within the siphon withdrawal reflex (SWR) network of *Aplysia californica*. Recurrent inhibitory circuits such as this are a common feature of motor networks, providing a mechanism for rapid control of behavioral output. Moreover, intrinsic and extrinsic modulation of recurrent inhibitory circuitry can endow motor networks with a high degree of flexibility and an enhanced capability for adaptive modification. By focusing upon identified inhibitory elements within a well-defined circuit with direct behavioral relevance, and performing experiments ranging from cellular to behavioral levels of analysis, we are beginning to define a functional role for inhibitory processing in mediating adaptive gain control of the SWR in response to changing environmental conditions.

This paper was originally presented at a workshop titled *The Future of Aquatic Research in Space: Neurobiology, Cellular and Molecular Biology*. The workshop, which was held at the Marine Biological Laboratory, Woods Hole, Massachusetts, from 13 to 15 May 1996, was sponsored by the Center for Advanced Studies in the Space Life Sciences at MBL and funded by the National Aeronautics and Space Administration under Cooperative Agreement NCC 2-896.

Our cellular experiments have demonstrated that dynamic interactions between the L29s and L30s can significantly regulate reflex input to the LFS-type siphon motor neurons (MNs). The L29s (5 total) and L30s (3 total) are reciprocally interconnected by both chemical and electrical synapses: the L29s directly excite the L30s which, in turn, directly inhibit the L29s. The L29 excitatory interneurons, which are known to act as facilitatory neuromodulatory neurons (Hawkins *et al.*, 1981), also provide substantial excitatory input to LFS MNs; a single L29 can account for as much as 50% of reflex input to these MNs evoked by siphon stimulation. Yet surprisingly, direct intracellular activation of the L29s causes a significant, transient *decrement* of reflex input to the MNs. The mechanism of this inhibition is through the recruitment and enhancement of recurrent L30 inhibitory synaptic transmission. Activation of the L30s, either directly through current injection or indirectly by means of activation of the L29s, results in a significant potentiation of the L30 synapse. This activity-dependent potentiation (ADP) of the L30s occurs at low, behaviorally relevant activation frequencies (2 to 10 Hz), and has a time course of expression matching that of the reflex inhibition produced by activation of the L29s (Fischer and Carew, 1993). The recurrent interactions between L29 and L30 interneurons can thus provide a mechanism for activity-dependent regulation of excitatory input to the siphon motor neurons.

Our identification of the dynamic network interactions described above raised the important issue of the functional significance of the L29/L30 circuit. To address this question, we performed a series of experiments in which we first examined the kinds of behaviorally rel-

evant stimuli that activate the L29/L30 circuit, and then how this activation modulates reflex responding. These experiments were performed in a reduced preparation consisting of the tail, mantle (siphon and gill), and central nervous system; this preparation provides a useful interface between behavioral experiments in intact animals and analysis of cellular events. We found that weak (non-noxious) tactile input readily activates the L30s, and that this activation is sufficient to potentiate the L30 inhibitory synapse onto L29 neurons. This same stimulus also produces significant inhibition of siphon-evoked reflex responses in both L29 interneurons and siphon MNs, with a time course corresponding closely to the time course of L30 ADP (Fischer and Carew, 1995). Similar results were obtained when intact, freely moving animals were used (Blazis *et al.*, 1994). Finally, we directly tested the role of the L30s in mediating this inhibitory process by reversibly inactivating (hyperpolarizing) them during tactile stimulation; this significantly attenuates the inhibition of siphon-evoked responses (Fischer and Carew, 1995).

These results led us to propose an adaptive role for L30-mediated inhibition in regulating SWR responsiveness under conditions of different levels of ambient (tactile) environmental stimulation. Specifically, we hypothesize that activation of the L30s by weak tactile input from the environment transiently increases the strength of L30-mediated inhibition in the SWR network. To produce a siphon response in the face of this increased inhibition, a stronger input from the siphon would be required. In this fashion, the increase in L30-mediated inhibition caused by weak tactile stimulation can elevate the effective threshold for evoking a motor neuron response based upon the recent tactile experience of the animal (Fischer and Carew, 1995). Recent behavioral experiments, which are discussed below, provide support for this model (Yuan *et al.*, 1996).

In contrast to the effects of weak tactile stimulation on L30 inhibitory processing, we found that a more intense stimulus, tail shock, selectively attenuates specific forms of L30 ADP. At least two temporally separate forms of ADP can be distinguished: (1) frequency facilitation (FF), which is a short-term enhancement that is expressed during L30 activation; and (2) augmentation (AUG), which is a longer-term form of enhancement that persists for up to 60 s following activation. We found that a single tail shock selectively attenuates AUG with no effect on FF. This suppression of AUG lasts for hours, and is mimicked by bath application of the monoamine serotonin, a neuromodulator implicated in behavioral sensitization. The mechanism of this suppression is due to a reduction in calcium influx during L30 activation, to a level at which FF is fully expressed, but below the level required for AUG (Fischer and Carew, 1994). These findings were extended in a series of cellular experiments examining the calcium dependence of the different forms of synaptic potentiation exhibited by the L30s. Using the photo-activated calcium chelator diazo-4, we demonstrated that all forms of L30 ADP require presynaptic elevation of free calcium for their expression (Fischer *et al.*, 1996). The selective suppression of different components of L30 ADP by tail shock suggests that L30-mediated effects on reflex responsiveness should be differentially expressed following shock depending upon the recent activation history of the L30s. Under conditions in which L30 is active, L30 mediated inhibition should be normal, since FF is relatively unaffected. Conversely, at time points tens of seconds following L30 activity, inhibition should be attenuated, since the prominent form of ADP at these time points (AUG) is suppressed. We are currently carrying out both behavioral and computational analysis to examine the implications of these cellular predictions.

The findings described above provided us with an opportunity to examine the behavioral implications of the functional suppression of a specific form of synaptic plasticity. In separate experiments utilizing both reduced preparations and intact animals, we found that a single tail shock of the same intensity used in our cellular experiments abolished the inhibition normally produced following weak tactile input. Further, we found that the level of shock used to abolish the inhibition was insufficient to produce sensitization of the reflex, suggesting that low levels of tail shock may induce a lower threshold component of sensitization by reducing L30 inhibitory modulation within the SWR circuitry (Blazis *et al.*, 1994). A corollary of this view is that the low-threshold component of sensitization may be expressed not by an increase in reflex amplitude, but rather by a reduction in the threshold of reflex activation under stimulus conditions that normally induce L30-mediated behavioral inhibition. Recent behavioral experiments support this view (discussed below). Thus, tail-shock-induced suppression of L30 ADP may be viewed as an initial step in behavioral sensitization; it would also have secondary effects such as allowing greater levels of activity in facilitatory neuromodulator neurons such as the L29s. Previous work in other laboratories has demonstrated that sensitization of the SWR may be accompanied by a reduction in network inhibition (Frost, 1987; Trudeau and Castellucci, 1993). Our work is consistent with, and an extension of, these results.

Our results to date thus show that L30-mediated inhibition can provide for a dynamic regulation of the SWR that is dependent upon the recent tactile experience of the animal. To further test our cellular predictions, we examined the effects of changing environmental conditions on SWR responsiveness in intact animals by induc-

ing a low-level tactile stimulus, artificial turbulence (mimicking tidal wave action) into the animal's home aquarium. We found that turbulence produced two main effects on the SWR: a significant decrease in the duration of the SWR response to a siphon stimulus of fixed intensity, and a significant increase in the siphon stimulus intensity (threshold) required to elicit a siphon response. Both of these effects were manifest within 1 min of the change in conditions, and remained stable for the 10 min in which the turbulent conditions were maintained. Rapid recovery dynamics were revealed when calm conditions were restored; both measures returned to baseline (pre-turbulence) values within 1 min upon restoration of calm conditions. The overall characteristics of this adaptive response were consistent with the dynamics of L30 ADP. We next investigated the effects of tail shock on turbulence-induced adaptation. Tail shock did not alter the behavioral inhibition produced during turbulence, which is consistent with observations that L30 is active during turbulence, and that the FF component of L30 ADP is intact following shock. We have yet to systematically examine the recovery dynamics following turbulence, where effects on the AUG component of L30 ADP would be manifest. Further, we found that following shock, the threshold stimulus intensity for evoking a siphon response in calm conditions was significantly decreased. Turbulent conditions still induced an increase in reflex threshold, but this increase was significantly smaller than in nonshocked animals. These results are again consistent with previous cellular predictions. We plan to perform additional cellular experiments to directly test the role of L30 ADP in mediating this adaptive process.

Taken collectively, our results indicate that activity-dependent inhibition in the SWR network promotes a rapid and dynamic adjustment of reflex behavior in response to changing environmental conditions. Future experiments will be directed at examining how this inhibitory system may interact with the cellular and network processes underlying learning, and how modifications of inhibition through tail shock may modulate this interaction.

Acknowledgments

This work was supported by NIH grants MH48672 to TJC and MH10334 to TMF.

Literature Cited

Blazis, D. E. J., N. J. Priver, T. M. Fischer, and T. J. Carew. 1994. Modulation of tail-induced inhibition of the siphon withdrawal reflex of *Aplysia*. *Soc. Neurosci. Abstr.* **20:** 814.

Fischer, T. M., and T. J. Carew. 1993. Activity dependent recurrent inhibition: a mechanism for dynamic gain control in the siphon withdrawal reflex of *Aplysia*. *J. Neurosci.* **13:** 1302–1314.

Fischer, T. M., and T. J. Carew. 1994. Tail shock differentially modulates two forms of synaptic plasticity in inhibitory interneuron L30 of *Aplysia*. *Soc. Neurosci. Abstr.* **20:** 1072.

Fischer, T. M., and T. J. Carew. 1995. Cutaneous activation of the inhibitory L30 interneurons provides a mechanism for regulating adaptive gain control in the siphon withdrawal reflex of *Aplysia*. *J. Neurosci.* **15:** 762–773.

Fischer, T. M., R. S. Zucker, and T. J. Carew. 1996. Activity-dependent potentiation of synaptic transmission from L30 inhibitory interneurons of *Aplysia* depends upon residual calcium. *Soc. Neurosci. Abstr.* **22:** 327.

Frost, W. N. 1987. Mechanisms contributing to short- and long-term sensitization in *Aplysia*. Ph.D. thesis, Columbia University.

Hawkins, R. D., V. R. Castellucci, and E. R. Kandel. 1981. Interneurons involved in mediation and modulation of gill-withdrawal reflex in *Aplysia*. I. Identification and characterization. *J. Neurophysiol.* **45:** 304–314.

Trudeau, L.-E., and V. R. Castellucci. 1993. Functional uncoupling of inhibitory interneurons plays an important role in short-term sensitization of *Aplysia* gill and siphon withdrawal reflex. *J. Neurosci.* **13:** 2126–2135.

Yuan, J. W., T. M. Fischer, and T. J. Carew. 1996. Dynamic regulation of the siphon withdrawal reflex of *Aplysia* in response to changing environmental conditions. *Soc. Neurosci. Abstr.* **22:** 1403.

Reference: *Biol. Bull.* **192:** 167–169. (February, 1997)

Complex Oscillations in Simple Neural Systems

DOUGLAS A. BAXTER AND JOHN H. BYRNE

Department of Neurobiology and Anatomy, The University of Texas Medical School at Houston, Houston, Texas 77030

One of the goals of this workshop is to explore how research on aquatic plants and animals can improve our understanding of the basic mechanisms underlying the effects of gravity on biological processes. In general, the focus of "gravitational biology" has been to investigate gravitational effects at the organismal level rather than at the cellular, subcellular, or molecular levels. Indeed, previous theoretical studies have indicated that the effects of gravity would be minuscule at the subcellular level (Albrecht-Buehler, 1991; Nace, 1983; Pollard, 1965, 1971; Todd, 1989). However, recent spaceflight and ground-based experiments have demonstrated that a broad range of basic cellular properties can be influenced by gravity, including cytoskeletal structure and cell morphology, cell-cell interactions, cellular metabolism, exocytosis and endocytosis, concentrations of electrolytes, voltage-gated channels, intracellular levels of second messengers, and enzymatic activities (Cogoli *et al.*, 1990; Cogoli and Gmünder, 1991; Edgerton and Roy, 1994; Gruener and Hoeger, 1990, 1991; Hughes-Fulford, 1991; Hymer *et al.*, 1994; Krasnov, 1994; Morrison, 1994; Reitstetter *et al.*, 1991; Rijken *et al.*, 1994; Sato *et al.*, 1992; Schatz *et al.*, 1994; Sibonga *et al.*, 1989; Todd, 1989). Thus, perturbations in the gravitational environment can induce modifications in cellular activities, which in turn may contribute to gravity-dependent changes at the organismal level.

How is it possible to resolve the theoretical and empirical findings? An intriguing explanation for the influence of gravity on cells was derived, in part, from nonlinear dynamical systems theory (Kondepudi and Prigogine, 1983; Kondepudi and Strom, 1992; Mesland, 1987, 1990, 1992a, 1992b). Specifically, even if the force of gravity at the subcellular level is extremely weak by comparison with other forces, the nonlinearities of most molecular systems may provide the amplification required to allow a weak signal to influence subcellular processes. Thus, gravity may be a bifurcation parameter capable of inducing state transitions. Since nonlinear dynamical systems are the rule rather than the exception in biology, the application of these principles may help us to design new experiments that will provide insights into basic cellular physiology and the molecular basis of gravitational effects on cells.

In the present paper, we describe how some of the concepts and analytical techniques of nonlinear dynamical systems have been applied to computational and experimental analyses of single-cell and multicellular neuronal oscillators (Baxter *et al.*, 1996; Butera *et al.*, 1995; Byrne *et al.*, 1994; Canavier *et al.*, 1991, 1993, 1994; Lechner *et al.*, 1996). Our analysis has focused on the R15 neuron, which is located in the abdominal ganglion of the marine mollusc *Aplysia*. R15 has intrigued neurobiologists for decades, principally because of its intrinsic ability to produce complex bursting activity. This cell also exhibits many different modes of oscillatory activity.

Previous experimental studies have demonstrated two conventional methods of shifting the activity of R15 between different modes of activity. First, the activity can be altered by intracellularly injecting a constant bias current. Sufficiently large depolarizing bias currents shift the activity of R15 from bursting to beating (*i.e.*, tonic spiking activity), whereas sufficiently large hyperpolarizing bias currents shift R15 into a silent mode. Second, the activity of R15 can be altered by applying modulatory transmitters, such as serotonin (5-HT). By modulating biophysical parameters (*e.g.*, membrane conductances)

This paper was originally presented at a workshop titled *The Future of Aquatic Research in Space: Neurobiology, Cellular and Molecular Biology*. The workshop, which was held at the Marine Biological Laboratory, Woods Hole, Massachusetts, from 13 to 15 May 1996, was sponsored by the Center for Advanced Studies in the Space Life Sciences at MBL and funded by the National Aeronautics and Space Administration under Cooperative Agreement NCC 2-896.

various concentrations of 5-HT can shift the electrical activity of R15 between a variety of bursting modes, which vary in the intensity of spiking during the burst and the duration of the interburst interval.

We have used a Hodgkin-Huxley type model of the R15 neuron and computer simulations to investigate a novel method for shifting the electrical activity of R15 among different modes of oscillatory activity. This novel method does not rely on alterations in model parameters, but rather exploits the intrinsic nonlinear properties of the cell. The simulations indicated that, for a single set of parameter values, the model cell can generate up to eight distinct modes of oscillatory activity. These modes of electrical activity corresponded to multiple stable attractors, whose coexistence in phase space was an emergent property of the nonlinear dynamics of the cell. Brief perturbations, which were simulated postsynaptic potentials (PSPs), could switch the activity of R15 between different modes. These mode transitions did not require any changes in the biochemical or biophysical parameters of the neuron and provided an enduring response to a transient input. Moreover, the nature of the mode shift, as well as whether the mode shift occurred at all, was dependent upon the timing of the PSP (*i.e.*, perturbation) relative to the ongoing activity, thus providing a mechanism for phasic sensitivity (*i.e.*, temporal specificity). Finally, the multistability of this neuronal oscillator was regulated by modulatory transmitters. The actions of modulatory transmitters were simulated by systemically altering the conductances of specific membrane currents within physiological ranges (*e.g.*, ±20% of control values). Changing these parameters regulated the number of coexisting modes of electrical activity, such that at control values eight modes coexisted, at intermediate values two or three modes coexisted, and at the maximum and minimum values only a single mode existed. Thus, by modulating membrane conductances, transmitters could position the neuronal oscillator in different regions of its parameter space; some regions supported multistability, whereas others did not.

Recently, we have begun to extend our analyses of the dynamics of neuronal oscillators to include multicellular oscillators (Baxter *et al.*, 1996, 1997; Canavier *et al.*, 1995). These analyses have focused on a ring network composed of identical cellular and synaptic elements. The individual cells consist of modeled R15 neurons. The parameter values that were used in these simulations positioned the cells in a region of their parameter space that supported only a single attractor, which was a bursting limit cycle. Thus, the individual circuit elements by themselves did not support multistability. We found, however, that the ring network exhibited multistability. Simulations also illustrated that, as the number of cells in the ring network was increased, the number of coexisting patterns also increased. Similarly, if the parameter values for the individual cells were modified such that the cells themselves became multistable, then the number and diversity of coexisting oscillatory patterns increased dramatically.

Electrophysiological experiments have tested several key predictions of the computational studies. First, we examined whether the oscillatory electrical activity of individual R15 neurons exhibited multistability. Second, we examined whether modulatory transmitters regulated the multistability. Finally, we examined whether networks of R15 neurons that were artificially connected into a ring network could support multistability. The results of these electrophysiological experiments were consistent with the predictions of the computational studies and indicated that nonlinear processes may endow individual cells with a richer repertoire of cellular state transitions than has been previously appreciated.

In summary, the data described above indicate that there are two fundamentally different methods of producing an enduring change in the mode of oscillatory activity in R15. One method is parameter dependent (*e.g.*, application of a bias current or a modulatory transmitter), whereas the second method is parameter *in*dependent. Parameter-independent changes in the mode of activity emerge from the proliferation of attractors in the phase space of this nonlinear system. Each of these attractors correspond to a different pattern of oscillatory activity, and brief perturbations (*e.g.*, synaptic inputs) can switch the electrical activity from one stable pattern of oscillation to another. These mode transitions do *not* require any changes in the parameters of the model, and such parameter-independent transitions can provide an enduring response to a transient input. These studies have provided novel insights into the ways in which nonlinear dynamics at the cellular level might be exploited in the generation and control of oscillatory patterns of electrical activity and to process and store information.

Note, finally, that electrical activity is only one of the nonlinear dynamical activities in cells. The interactions among most, if not all, biochemical reactions and second messenger systems are highly nonlinear. Thus, nonlinear state transitions (*i.e.*, bifurcations) at the molecular level might function to amplify relatively weak signals (*e.g.*, gravity) above the level of random thermal noise, and the weak signals could thus be manifest at the cellular level. R15 may provide a useful model system with which to investigate these possibilities. For example, R15 can be maintained *in vitro* for many days while its electrical activity is being monitored by means of a number of noninvasive techniques (*e.g.*, Parsons *et al.*, 1991). Moreover, the parameter-independent mode transitions that we have characterized could serve as a very sensitive measure of the effects of gravity on cellular processes.

Literature Cited

Albrecht-Buehler, G. 1991. Possible mechanisms of indirect gravity sensing by cells. *ASGSB Bull.* **4:** 25–34.

Baxter, D. A., C. C. Canavier, R. J. Butera, J. W. Clark, and J. H. Byrne. 1996. Complexity in individual neurons determines which patterns are expressed in a ring circuit model of gait generation. *Soc. Neurosci. Abstr.* **22:** 1437.

Baxter, D. A., C. C. Canavier, H. A. Lechner, R. J. Butera, A. A. DeFranceschi, J. W. Clark, and J. H. Byrne. 1997. Coexisting stable oscillatory states in single cell and multicellular neuronal oscillators. In press, in *Oscillations in Neural Systems*, D. Levine, V. Brown, and T. Shirey, eds. Lawrence Erlbaum Assoc., Hillsdale, NJ.

Butera, R. J., J. W. Clark, C. C. Canavier, D. A. Baxter, and J. H. Byrne. 1995. Analysis of the effects of modulatory agents on a modeled bursting neuron: dynamic interactions between voltage and calcium dependent systems. *J. Comput. Neurosci.* **2:** 19–44.

Byrne, J. H., C. C. Canavier, H. Lechner, J. W. Clark, and D. A. Baxter. 1994. Role of nonlinear dynamical properties of a modeled bursting neuron in information processing and storage. *Neth. J. Zool.* **44:** 339–356.

Canavier, C. C., J. W. Clark, and J. H. Byrne. 1991. Simulation of the bursting activity of neurons R15 in *Aplysia*: role of ionic currents, calcium balance, and modulatory transmitters. *J. Neurophysiol.* **66:** 2107–2124.

Canavier, C. C., D. A. Baxter, J. W. Clark, and J. H. Byrne. 1993. Nonlinear dynamics in a model neuron provide a novel mechanism for transient synaptic inputs to produce long-term alterations of postsynaptic activity. *J. Neurophysiol.* **69:** 2252–2257.

Canavier, C. C., D. A. Baxter, J. W. Clark, and J. H. Byrne. 1994. Multiple modes of activity in a model neuron suggest a novel mechanism for the effects of neuromodulators. *J. Neurophysiol.* **72:** 872–882.

Canavier, C. C., R. J. Butera, D. A. Baxter, J. W. Clark, and J. H. Byrne. 1995. Networks of physiologically based neuronal oscillators may provide improved models of pattern generation. *Soc. Neurosci. Abstr.* **21:** 147.

Cogoli, A., and F. K. Gmünder. 1991. Gravity effects on single cells: techniques, findings and theory. *Adv. Space Biol. Med.* **1:** 183–248.

Cogoli, A., B. Bechler, and G. Lorenzi. 1990. Responses of cells to microgravity. Pp. 97–112 in *Fundamentals of Space Biology*, M. Asashima and G. M. Malacinski, eds. Japan Scientific Societies Press, Tokyo.

Edgerton, V. R., and R. R. Roy. 1994. Neuromuscular adaptation to actual and simulated weightlessness. *Adv. Space Biol. Med.* **4:** 33–67.

Gruener, F., and G. Hoeger. 1990. Vector-free gravity disrupts synapses formation in cell culture. *Am. J. Physiol.* **27:** C489–C494.

Gruener, F., and G. Hoeger. 1991. Vector-averaged gravity alters myocyte and neuron properties in cell culture. *Aviat. Space Environ. Med.* **56:** 1159–1165.

Hughes-Fulford, M. 1991. Altered cell function in microgravity. *Exp. Gerontol.* **26:** 247–256.

Hymer, W. C., K. Shellenberge, and R. Grindeland. 1994. Pituitary cells in space. *Adv. Space Res.* **14:** 61–70.

Kondepudi, D. K., and I. Prigogine. 1983. Sensitivity of nonequilibrium chemical systems to gravitational field. *Adv. Space Res.* **3:** 171–176.

Kondepudi, D. K., and P. B. Strom. 1992. Gravity detection through bifurcation. *Adv. Space Res.* **12:** 7–14.

Krasnov, I. B. 1994. Gravitational neuromorphology. *Adv. Space Biol. Med.* **4:** 85–110.

Lechner, H. A., D. A. Baxter, J. W. Clark, Jr., and J. H. Byrne. 1996. Bistability and its regulation by serotonin in the endogenously bursting neuron R15 in *Aplysia*. *J. Neurophysiol.* **75:** 957–962.

Mesland, D. A. M. 1987. *Biorack* experiments in *Spacelab D-1* and *IML-1*: further developments in gravitational biology. Pp. 305–312 in *Proceedings of the Third European Symposium on Life Sciences Research in Space*, J. Hunt, ed. **ESA SP-271**, Noordwijk, The Netherlands.

Mesland, D. A. M. 1990. Gravity effects on cells. Pp. 221–227 in *Proceedings of Fourth Symposium on Life Sciences Research in Space*, **ESA SP-307**, Trieste, France.

Mesland, D. A. M. 1992a. Mechanisms of gravity effects on cells: are there gravity-sensitive windows? *Adv. Space Biol. Med.* **2:** 211–228.

Mesland, D. A. M. 1992b. Possible actions of gravity on the cellular machinery. *Adv. Space Res.* **12:** 15–26.

Morrison, D. R. 1994. Cellular changes in microgravity and the design of space radiation experiments. *Adv. Space Res.* **14:** 1005–1019.

Nace, G. W. 1983. Gravity and positional homeostasis in the cell. *Adv. Space Res.* **3:** 159–168.

Parsons, T. D., B. M. Salzberg, A. L. Obaid, F. Raccuia-Behling, and D. Kleinfeld. 1991. Long-term optical recordings of patterns of electrical activity in ensembles of cultured *Aplysia* neurons. *J. Neurophysiol.* **66:** 316–333.

Pollard, E. C. 1965. Theoretical considerations on living system in the absence of mechanical stress. *J. Theor. Biol.* **8:** 113–123.

Pollard, E. C. 1971. Physical determinants of receptor mechanism. Pp. 25–34 in *Gravity and the Organism*, A. Gordon and M. Cohen, eds. The University of Chicago Press, Chicago.

Reitstetter, R., A. Schatz, A. Linde-Hommes, and W. Briegleb. 1991. Changes in ion channel properties related to gravity. *Physiologist* **34, Suppl. 1:** S68–S69.

Rijken, P. J., J. Boonstra, A. J. Verkleij, and S. W. de Laat. 1994. Effects of gravity on the cellular response to epidermal growth factor. *Adv. Space Biol. Med.* **4:** 159–188.

Sato, A., T. Nakajima, Y. Kumei, T. Hongo, and K. Ozawa. 1992. Gravitational effects on mammalian cells. *Physiologist* **35, Suppl. 1:** S43–S46.

Schatz, A., R. Reitstetter, A. Linke-Hommes, W. Briegleb, K. Slenzka, and H. Rahamann. 1994. Gravity effects on membrane processes. *Adv. Space Res.* **14:** 35–43.

Sibonga, J. D., T. N. Fast, P. X. Callahan, and C. M. Winget, eds. 1989. *Cells in Space.* NASA **SP-10034**, Moffett Field, CA.

Todd, P. 1989. Gravity-dependent phenomena at the scale of the single cell. *ASGSB Bull.* **2:** 95–113.

Reference: *Biol. Bull.* **192:** 170–171. (February, 1997)

Discussion

MORRIS: Dr. Baxter, I wonder whether a system that has so many attractors in it is subject to knocking between one attractor and the next by noise.

BAXTER: We have addressed that issue. The EPSP that we typically used as a perturbation was modeled from experimental measurements of the giant EPSP onto R15. That's the largest EPSP that R15 receives. We found that these mode transitions were fairly insensitive to low amplitude noise. If you had large amplitude inputs, activity of R15 could be bounced between modes. Another consideration is that the phase-portraits I showed were two-dimensional, which implies a nice linear relationship between the location of these attractors; however, that's not the case. These attractors have 11 dimensions to them, and even though they may look far apart on this two-dimensional plot, they could be right next to each other. One attractor could be very large, whereas another attractor could be very small. It's a very complex question, and there is no simple answer. Noise can be a problem.

NICK: What happens to your isolated cell when you turn it by 90 degrees?

BAXTER: We have not examined the response of R15 to changes in direction of the gravity vector. However, we can induce shifts between bursting activity and beating activity in the isolated cell by perturbing the cell with brief current pulses.

BAXTER: Tom (Fischer), what's the effect of serotonin on the L30 synapse?

FISCHER: Serotonin has the same effect as tail shock; it inhibits a calcium channel. We don't know what type of calcium channel at this point. However, if you look at other indices of calcium conductance, it just decreases the amount of calcium influx. We need to see what kind of channels are being regulated, using the appropriate voltage clamp experiment. It seems that there is a direct interaction with that channel to decrease its conductance.

BAXTER: You say directly. Are there no second messengers involved?

FISCHER: No, I didn't mean that. It probably acts through cyclic AMP. This was shown through the work of Bill Frost at Texas—Houston.

BARLOW, R.: It may be of interest to point out that in the *Limulus* lateral eye there is a possibly analogous situation to R15 bursting. Theoretical analyses by Hartline, Ratliff, and Knight showed that the system of equations that describe the response of the eye does not have a unique solution, and for a long time it wasn't clear what that meant. In our experiments we found that the sensitivity of the cells to inhibition depended on the cell's own level of excitation. This introduced a striking nonlinearity into the formulation, which indicates that the eye will go into oscillation. All receptors in the eye are responding in synchrony, oscillating at about 5/s. This is a network property rather than the property of an individual cell. It's almost exactly as you describe for R15.

BAXTER: We have extended our analysis to small networks of R15, from both a computational and experimental standpoint. In the computer simulations, we can take R15s, hook them together and manually "position" them in a region of their parameter space, where the individual cells do not support multistability, yet the network can. If one combines multistability at the cellular level with the network level, the combinations and perturbations become quite complex.

ELINSON: Dr. Baxter, I'm quite unfamiliar with this kind of thing, but all of those phases seem rather scary. It seems as though any hypothesis would be possible. Is there some way of predicting which is the strongest track and which are less likely?

BAXTER: I guess what you are getting at is the question, How attractive is an attractor? How strong is one attractor as compared to another? That's very difficult to answer with the full model because it's such a high-dimensional system, so we have addressed the question in two ways. One is to reduce the model. We have reduced it down to a four-variable model, which allows us to do analytical system analysis and quantitatively evaluate the attractors. Second, with the full system,

one can do a random search of the state space by just creating, for example, 1000 random combinations of initial conditions, and then running simulations with each set of values and determining the relative frequency with which the system stabilizes in a given attractor. Our thinking is that, if you have a very big attractor or a very strong attractor, you'll end up there most often. So you can get some feeling for how large an attractor is. I don't remember, when I showed you the eight or so attractors, what their relative strengths are. I think the beating and the outer bursting were very strong attractors, but that's going to vary under conditions of modulation as well.

BAKER: Dr. Fischer, how do you envision the tail shock acting to block that response?

FISCHER: We think that the tail shock affects calcium channels on the presynaptic terminals of the L30s and thus regulates presynaptic facilitation. We have carried out a number of studies to show that the enhancement in the L30s is strictly dependent upon the levels of intracellular calcium. What's important is how much calcium you get in the cell per activity. Tail shock and serotonin seem to act on a calcium channel, such that less calcium gets in per unit activity.

MORRIS: Dr. Baxter, when you reduce the system from 11 to 4 dimensions to be able to look at it analytically, you still have very serious decision making to do. Which seven parameters are you going to make instantaneous and which are you going to let run?

BAXTER: We don't do this arbitrarily. This was an important part of Robert Butera's Ph.D. thesis. In general terms, what we did was to divide the system into slow and fast systems. The slow system comprises the conductances underlying oscillations, and the fast system comprises the conductances underlying the action potentials. We then collapsed the fast system into a single variable that represents the perturbation of the fast onto the slow system. Thus, the reduced model has three variables describing the slow system, and one variable represents this lumped effect of the fast onto the slow. We then tested the reduced model and compared its output to that of the full model. The reduced model responded to modulatory transmitters in the same way as the full system and also manifested multistability. Thus, the reduced model captured many of the salient features of the full system.

COMMENT: I want to say for the record that Jim Blankenship's lab has shown that serotonin facilitates motor activity in feeding behaviors in *Aplysia*. Dr. Fischer, has serotonin been shown to facilitate motor activity in vertebrates in contrast to invertebrates?

FISCHER: I can't really speak for the vertebrate work. Serotonin has a lot of effects within the feeding circuits, where it can facilitate both ends of the neuromuscular junction. It also affects siphon withdrawal reflex facilitation, which is probably the most famous form of plasticity studied in this animal; but you see inhibition of inhibitory interneurons as well as facilitation of sensory neurons as a result of serotonin application. Thus, one neuromodulatory system seems to perform whatever function it has to do to get the response up. It can up regulate sensory neuron transmission and motorneuron activity in this system, but conversely it decreases inhibition. I don't think it's appropriate to speak of serotonin as having a net facilitory or net inhibitory role, it just produces reflex facilitation and, at least in our hands, does what it has to do to accomplish this.

Reference: *Biol. Bull* **192**: 172–174. (February, 1997)

Getting a Head in Frog Development

RICHARD P. ELINSON

Department of Zoology, University of Toronto, 25 Harbord Street, Toronto, Canada M5S 3G5

The development of a head in frog embryos depends on the vegetal cortex of the egg. This at first seems odd because the head develops on the opposite side of the egg, close to the animal cortex. Nonetheless, the vegetal cortex not only is the repository of interesting localized RNAs, but it also causes the cytoplasmic movement that initiates a chain of events, culminating in the head.

During oogenesis, RNAs are specifically transported to the vegetal cortex (Forristall *et al.*, 1995; Kloc and Etkin, 1995). These RNAs are of two types. One type is involved in formation of germ cells and the other in formation of the head and other dorsoanterior structures. Germ cells arise from germ plasm, located in the vegetal cortex. Xcat-2 RNA is localized to the germ plasm, and like nanos RNA in *Drosophila*, with which it has sequence similarity, it may be involved in germ cell formation (Mosquera *et al.*, 1993). Other RNAs, such as Vg1 and Xwnt-11, are spread more evenly along the vegetal cortex. Processed Vg1 protein is an inducer of dorsal mesoderm, and both it and Xwnt-11 RNA can cause the formation of a dorsoanterior axis experimentally (Thomsen and Melton, 1993; Ku and Melton, 1993). These or other RNAs are the likely source of a dorsalizing activity found at the vegetal cortex in the mature egg, ready for fertilization (Fujisue *et al.*, 1993; Holowacz and Elinson, 1993).

The Cortical Rotation, Gravity, and Dorsoanterior Development

An hour or so after fertilization, the entire egg cortex rotates by 30° relative to the cytoplasm. This rotation establishes the dorsoanterior axis and depends on a transient array of parallel microtubules at the vegetal cortex (Elinson and Rowning, 1988; Larabell *et al.*, 1996). A kinesin-like protein is associated with the microtubules and is thought to move the cortex along the microtubules, which are anchored in the cytoplasm (Houliston *et al.*, 1994).

This critical rotation can be influenced by gravity in several ways. First, extremes of gravity, caused by centrifugation, can overcome the microtubule mechanism and produce a dorsoanterior axis on the centripetal side (Black and Gerhart, 1985). Second, gravity, acting alone, can produce a dorsoanterior axis in the absence of the microtubule mechanism (Scharf and Gerhart, 1980). Third, gravity alone can orient the microtubules prior to their formation, thereby directing where the dorsoanterior axis will form (Ziseking and Elinson, 1990). Gravity in these cases acts by moving the heavy yolk-rich cytoplasm downwards, producing a cytoplasmic rearrangement.

These gravity effects have led to repeated attempts to place frog eggs in space to see how they develop in zero gravity. In the most successful of such experiments, there was little or no perturbation of the dorsoanterior axis (Souza *et al.*, 1995). A normal head formed, indicating that some form of cytoplasmic rearrangement occurred. This arrangement was probably due to the functioning of the parallel microtubule mechanism. One would guess, although it has not been shown, that the various cytoplasmic regions of different densities retained their identity (Smith and Neff, 1986) thanks to the egg cytoskeleton.

Dorsalizing Activity and the Dorsoanterior Axis

When cytoplasm is withdrawn from the vegetal cortex of the fertilized egg and microinjected into the ventral side of a cleaving embryo, an extra head and other dorsoanterior structures form. There is some connection be-

This paper was originally presented at a workshop titled *The Future of Aquatic Research in Space: Neurobiology, Cellular and Molecular Biology*. The workshop, which was held at the Marine Biological Laboratory, Woods Hole, Massachusetts, from 13 to 15 May 1996, was sponsored by the Center for Advanced Studies in the Space Life Sciences at MBL and funded by the National Aeronautics and Space Administration under Cooperative Agreement NCC 2-896.

tween this dorsalizing activity in the fertilized egg and the components of the vegetal cortex of the oocyte, since UV irradiation of the oocyte eliminates the later dorsalizing activity (Holowacz and Elinson, 1993). An attractive model is that an RNA, localized to the vegetal cortex of the oocyte, is translated during oocyte maturation to produce a protein with dorsalizing activity in the vegetal cortex of the fertilized egg.

Induction of a dorsoanterior axis, such as occurs with injected vegetal cortex, can be due to one of two activities: mesoderm induction or competence modification (Elinson and Holowacz, 1995). Some molecules, such as processed Vg1 protein or activin, are mesoderm inducers. They induce the formation of dorsal mesoderm, thus generating a dorsoanterior axis. Other molecules, such as Xwnt-8 RNA, are competence modifiers. They convert ventral mesoderm to dorsal mesoderm, and in so doing, they can create a complete dorsoanterior axis, including a head. The teratogen lithium acts in this way. The dorsalizing activity of the vegetal cortex behaves more like a competence modifier than a mesoderm inducer (Holowacz and Elinson, 1995).

The cortical rotation moves the dorsalizing activity to an asymmetric equatorial position in the egg (Fujisue *et al.*, 1993), where its activity specifies the dorsoanterior axis. The way that the dorsalizing activity is brought into position is not important, because microinjection or gravity-mediated rearrangements can substitute for the normal microtubule mechanism. In zero gravity, the microtubule mechanism should still function.

Why Can Gravity Substitute for the Microtubule Mechanism?

After fertilization, the whole frog egg rotates in its jelly capsule (note this involves the whole egg, not just the cortex, and occurs earlier than the cortical rotation). As a result, the animal-vegetal axis of the fertilized frog egg is perpendicular to gravity, and there is no asymmetry of gravitational force on the yolk mass to produce the cytoplasmic rearrangement required for specifying the dorsoanterior axis. If gravity normally plays no role in this specification, why can it have an effect? One possibility is that gravity-induced rearrangement is an evolutionarily primitive mechanism, which has been superseded by the microtubule mechanism. If there are any frogs lacking the microtubule mechanism, their eggs would be interesting objects to put in space, with zero gravity.

We have limited knowledge of the mechanism of cortical rotation in different species, but one place to look would be in frogs with large eggs (Elinson *et al.*, 1990). Most terrestrially breeding frogs have eggs greater than 3 mm in diameter, more than 10 times the volume of the 1.3-mm egg of *Xenopus laevis*, the current model for frog development. The way that these species specify dorsoanterior development is unknown, but it is easy to imagine a role for gravity. First, it seems unlikely that these huge eggs could quickly set up a large microtubule-based system powerful enough to cause a massive cortical movement. Second, a slight asymmetry of the huge yolk mass is all that would be needed to shift the cytoplasm and set up a dorsoanterior axis.

Frogs with large eggs usually breed on land, so they are out of the domain of this conference on aquatic research in space. The eggs can, however, develop in water (Elinson, 1987) and may be intriguing to examine under zero gravity conditions.

Literature Cited

Black, S. D., and J. C. Gerhart. 1985. Experimental control of the site of embryonic axis formation in *Xenopus laevis* eggs centrifuged before first cleavage. *Dev. Biol.* **108:** 310–324.

Elinson, R. P. 1987. Fertilization and aqueous development of the Puerto Rican terrestrial-breeding frog, *Eleutherodactylus coqui*. *J. Morphol* **193:** 217–224.

Elinson, R. P., and T. Holowacz. 1995. Specifying the dorsoanterior axis in frogs: 70 years since Spemann and Mangold. *Curr. Top. Dev. Biol.* **30:** 253–285.

Elinson, R. P., and B. Rowning. 1988. A transient array of parallel microtubules in frog eggs: potential tracks for a cytoplasmic rotation that specifies the dorso-ventral axis. *Dev. Biol.* **128:** 185–197.

Elinson, R. P., E. M. Del Pino, D. S. Townsend, F. C. Cuesta, and P. Eichhorn. 1990. A practical guide to the developmental biology of terrestrial-breeding frogs. *Biol. Bull.* **179:** 163–177.

Forristall, C., M. Pondel, L. Chen, and M. L. King. 1995. Patterns of localization and cytoskeletal association of two vegetally localized RNAs, Vg1 and Xcat-2. *Development* **121:** 201–208.

Fujisue, M., Y. Kobayakawa, and K. Yamana. 1993. Occurrence of dorsal axis-inducing activity around the vegetal pole of an uncleaved *Xenopus* egg and displacement to the equatorial region by cortical rotation. *Development* **118:** 163–170.

Holowacz, T., and R. P. Elinson. 1993. Cortical cytoplasm, which induces dorsal axis formation in *Xenopus*, is inactivated by UV irradiation of the oocyte. *Development* **119:** 277–285.

Holowacz, T., and R. P. Elinson. 1995. Properties of the dorsal activity found in the vegetal cortical cytoplasm of *Xenopus* eggs. *Development* **121:** 2789–2798.

Houliston, E., R. Le Guellec, M. Kress, M. Philippe, and K. Le Guellec. 1994. The kinesin-related protein Eg5 associates with both interphase and spindle microtubules during *Xenopus* early development. *Dev. Biol.* **164:** 147–159.

Kloc, M., and L. D. Etkin. 1995. Two distinct pathways for the localization of RNAs at the vegetal cortex in *Xenopus* oocytes. *Development* **121:** 287–297.

Ku, M., and D. A. Melton. 1993. Xwnt-11: a maternally expressed *Xenopus wnt* gene. *Development* **119:** 1161–1173.

Larabell, C., B. A. Rowning, J. Wells, M. Wu, and J. C. Gerhart. 1996. Confocal microscopy analysis of living *Xenopus* eggs and the mechanism of cortical rotation. *Development* **122:** 1281–1289.

Mosquera, L., C. Forristall, Y. Zhou, and M. L. King. 1993. A mRNA localized to the vegetal cortex of *Xenopus* oocytes encodes a protein with a nanos-like zinc finger domain. *Development* **117:** 377–386.

Scharf, S. R., and J. C. Gerhart. 1980. Determination of the dorsal-

ventral axis in eggs of *Xenopus laevis*: complete rescue of uv-impaired eggs by oblique orientation before first cleavage. *Dev. Biol.* **79:** 181–198.

Smith, R. C., and A. W. Neff. 1986. Organisation of *Xenopus* egg cytoplasm: response to simulated microgravity. *J. Exp. Zool.* **239:** 365–378.

Souza, K. A., S. D. Black, and R. J. Wassersug. 1995. Amphibian development in the virtual absence of gravity. *Proc. Natl. Acad. Sci. U.S.A.* **92:** 1975–1978.

Thomsen, G. H., and D. A. Melton. 1993. Processed Vg1 protein is an axial mesoderm inducer in *Xenopus*. *Cell* **74:** 433–441.

Ziseking, N., and R. P. Elinson. 1990. Gravity and microtubules in dorsoventral polarization of the *Xenopus* egg. *Dev. Growth Diff.* **32:** 575–581.

Reference: *Biol. Bull.* **192:** 175–177. (February, 1997)

Fate Specification Along the Sea Urchin Embryo Animal-Vegetal Axis

ROBERT C. ANGERER AND LYNNE M. ANGERER

Department of Biology, University of Rochester, Rochester, New York 14627

Introduction

Like those of a large majority of taxa, sea urchin embryos establish a spatial coordinate system for the initial body plan from one axis, the animal-vegetal (A-V), that is fixed during oogenesis by asymmetric deposition of maternal molecules (the embryologists' "determinants") and a second axis, dorsal-ventral (or, more descriptively, oral-aboral), that is specified sometime during the first few cleavage divisions (reviewed by Davidson, 1989). The ability of sea urchin embryos to establish these axes while continuously reorienting in culture suggests that neither axis is sensitive to the earth's gravitational field. In embryos of many sea urchin species, A-V polarity is evidenced by the unequal sizes of blastomeres of the 16-cell embryo, which consists of tiers of eight mesomeres, four macromeres, and four micromeres. Classical experimental micromanipulations of embryos (reviewed by Hörstadius, 1973), have established that the fates of micromeres are determined by inheritance of maternal molecules. In addition, the micromeres provide a vegetal focus of inductive influence that is critical in the normal embryo for appropriate specification of fates of overlying animal blastomeres, and that can induce vegetal differentiation (gut, secondary mesenchyme) in cells of more animal tiers when micromeres are transplanted to ectopic sites (Khaner and Wilt, 1991; Ransick and Davidson, 1993). Thus, specification of fates along the AV axis utilizes both major mechanisms familiar to developmental biologists—inheritance of maternally provided positional information, and communication among cells, presumably by ligand-receptor interactions.

This paper was originally presented at a workshop titled *The Future of Aquatic Research in Space: Neurobiology, Cellular and Molecular Biology*. The workshop, which was held at the Marine Biological Laboratory, Woods Hole, Massachusetts, from 13 to 15 May 1996, was sponsored by the Center for Advanced Studies in the Space Life Sciences at MBL and funded by the National Aeronautics and Space Administration under Cooperative Agreement NCC 2-896.

Studies with the Very Early Blastula Gene Set

The Very Early Blastula (VEB) gene set provides an entree to the mechanism of maternal determination of the AV developmental axis. Several years ago, we used subtractive cDNA screening methods to identify a set of mRNAs encoded by four different genes expressed transiently in the very early blastula (~150 cells), and absent from both the maternal pool of mRNAs and the message complement of later differentiated cells (Reynolds *et al.*, 1992). Surprisingly, the mRNAs identified by this simple temporal screen accumulate in the embryo with congruent spatial patterns and very similar temporal patterns. These genes, which we named the VEB genes, have two important features. First, the messages they encode accumulate asymmetrically along the AV axis, being present throughout the animal ~85% of the embryo but absent from the region around the vegetal pole. Second, the messages accumulate in embryonic blastomeres that are continuously separated beginning at the 2-cell stage. This latter property strongly suggests that activation of VEB gene expression, and consequently the asymmetry of accumulation, is regulated by a corresponding asymmetric distribution of maternal regulatory activities that corresponds to part of the molecular mechanism that establishes this axis. Our approach is to investigate the *cis*-acting elements in the regulatory apparatus of the VEB genes, and the *trans*-acting factors that drive their expression, to identify these critical molecular components.

Regulatory regions of the SpHE *and* SpAN *genes identify multiple positively acting factors that drive nonvegetal expression.* We have analyzed the regulatory regions of two of the VEB genes: *SpHE*, which encodes the hatching enzyme (Wei *et al.*, 1995), and *SpAN* (Kozlow-

ski *et al.*, 1996), which encodes an astacin-family protease that is likely to be involved in regulating the activities of cell signaling molecules (see below). These analyses include functional assays of expression of VEB promoter-driven transgenes microinjected into sea urchin eggs that are then allowed to develop into embryos, as well as standard *in vitro* assays of interaction of VEB promoter *cis* elements with proteins in nuclear extracts.

These studies have demonstrated that about 300 bp of sequence upstream of the transcription initiation site of *SpHE* and *SpAN* are each sufficient to drive expression of a β-galactosidase reporter in the correct nonvegetal pattern—*i.e.*, expression of the transgene is never observed in primary mesenchyme cells (PMCs) derived from the vegetal micromeres. Despite the congruence of expression of *SpAN* and *SpHE*, and the similar, compact structure of their regulatory regions, the repertoire of positively acting factors regulating these genes is rather different. On the basis of rate of accumulation of transcripts, the endogenous SpHE promoter is very strong. Reflecting this characteristic, it carries an apparent excess of positive regulatory sites (Wei *et al.*, 1995): The region within 300 bp of the transcription start site contains at least nine sites of protein binding which interact with six different factors. No one *cis* element appears to be critical for expression since replacement or deletion of individual sites decreases promoter activity no more than about twofold. Mutation of combinations of *cis* elements has little effect until three or four are inactivated. In contrast, the *SpAN* promoter contains fewer sites of protein-DNA interaction, two of which are essential for high transgene transcriptional activity (Kozlowski *et al.*, 1996).

The multiplicity of positive factors driving VEB gene transcription argues against the simple hypothesis that a single spatially restricted, positive factor regulates the nonvegetal accumulation of VEB mRNAs. At least three mechanisms could achieve spatial regulation of the VEB genes: (1) the presence of a vegetal negative regulator sufficient to prevent expression; (2) exclusion of the majority of positive regulators from vegetal pole cytoplasm; and (3) repression of the VEB genes in vegetal cells by means of a unique chromatin structure. To test for a negative regulator operating in the vegetal region, we made a series of deletions across the −300 *SpHE* promoter. None of these led to ectopic expression in PMCs, indicating that if a negative mechanism operates, it must involve multiple, independently sufficient regulatory sites. A vegetal-specific repressive chromatin structure might be established in micromeres which, as a result of unequal cleavage at 16-cell stage, would inherit a lower quantity of any uniformly distributed positively acting factors that were stockpiled in the egg cytoplasm. Consistent with this hypothesis, micromeres have a distinctive bulk chromatin structure that is less accessible to nuclease digestion than is that of the larger blastomeres (Cognetti and Shaw, 1981). Furthermore, these small vegetal cells are believed to contain a special cytoplasmic domain, as reflected by a loss of the pigment granules that are tethered in the egg cortical cytoskeleton (Schroeder, 1980). Experiments are underway to discriminate among these possibilities by examining the DNA-binding proteins present in separated animal and vegetal blastomeres, as well as by using *in vivo* footprinting coupled with ligation-mediated PCR to examine actual occupancy of *cis* elements in animal and vegetal blastomeres.

SpAN *may function to convert maternal gene regulatory information asymmetrically arrayed along the AV axis into spatial regulation of cell-cell interactions.* Because the sea urchin embryo cellularizes rapidly, and because the fates of all but the most vegetal blastomeres (micromeres) are context-dependent, the maternal AV asymmetry must be translated into, or supplemented by, extensive cell-cell interactions. Interestingly, one of the VEB genes, *SpAN*, encodes a member of the astacin protease family. Other members of this family include *Drosophila tolloid* (Schimell *et al.*, 1991) and *tolloid related* (Nguyen *et al.*, 1994; Finelli *et al.*, 1995). These metalloendoproteases consist of an astacin protease module linked to domains expected to be involved in protein-protein interactions (complement C1r/s; EGF), implying that they may function as tethered proteases. *Tolloid* has been shown to interact genetically with *decapentaplegic* (Ferguson and Anderson, 1992a, b), a member of the TGFβ superfamily of signaling molecules, and both of these genes are essential for regulating the fates of cells along the dorsal-ventral axis in the early *Drosophila* embryo. The only vertebrate astacin protease identified to date, BMP-1, has recently been shown to be a collagen-processing enzyme (Kessler *et al.*, 1996). However, a member of the TFGβ superfamily, BMP4 (which is functionally homologous to *dpp;* Padgett *et al.*, 1993), has been strongly implicated in regulating mesodermal patterning along the DV axis of *Xenopus* embryos (reviewed by Hogan *et al.*, 1994). Because BMP4 is synthesized as a pro-protein, like other members of the TGF-β family, it presumably requires activation by proteolytic cleavage, and astacin proteases are potential candidates. We have therefore explored the effect of over- or misexpressing *Xenopus* BMP4 and sea urchin SpAN in early sea urchin embryos by injecting the corresponding mRNAs into unfertilized eggs. Both proteins cause similar and dramatic phenotypic effects, interpreted most simply as suppression of differentiation of vegetal structures. Misexpression in *Xenopus* embryos of both BMP4 and SpAN also perturbs the dorsal-ventral axis leading to ventralized phenotypes. We hypothesize that SpAN

operates in sea urchin embryos in a BMP4-like pathway which functions to limit the range of inductive influence emanating from the vegetal pole. In this way, the *SpAN* gene, through its regulation by maternal factors, could convert maternal spatial information into regulation of cell signaling along the AV-axis.

Acknowledgments

This work was supported by NIGMS grant GM25553.

Literature Cited

Cognetti, G., and B. R. Shaw. 1981. Structural differences in the chromatin from compartmentalized cells of the sea urchin embryo: differential nuclease accessibility of micromere chromatin. *Nucleic Acids Res.* **9:** 5609–5621.

Davidson, E. H. 1989. Lineage specific gene expression and the regulative capacities of the sea urchin embryo: a proposed mechanism. *Development* **105:** 421–445.

Ferguson, E. L., and K. V. Anderson. 1992a. *Decapentaplegic* acts as a morphogen to organize dorsal-ventral pattern in the *Drosophila* embryo. *Cell* **71:** 451–461.

Ferguson, E. L., and K. V. Anderson. 1992b. Localized enhancement and repression of the activity of the TGF-β family member, *decapentaplegic*, is necessary for dorsal-ventral pattern formation in the *Drosophila* embryo. *Development* **114:** 583–597.

Finelli, A. L., T. Xie, C. A. Bossie, R. K. Blackman, and R. W. Padgett. 1995. The tolkin gene is a tolloid-BMP-1 homologue that is essential for *Drosophila* development. *Genetics* **141:** 271–281.

Hogan, B. L., M. Blessing, G. E. Winnier, N. Suzuki, and C. M. Jones. 1994. Growth factors in development: the role of TGF-beta related polypeptide signaling molecules in embryogenesis. *Dev. Suppl.*: 53–60.

Hörstadius, S. 1973. Chapter 6 in *Experimental Embryology of Echinoderms*. Oxford Univ. Press (Clarendon), New York.

Kessler, E., K. Takahara, L. Biniaminov, M. Brusel, and D. S. Greenspan. 1996. Bone morphogenetic protein-1: the type I procollagen C-proteinase. *Science* **271:** 360–362.

Khaner, O., and F. Wilt. 1991. Interactions of different vegetal cells with mesomeres during early stages of sea urchin development. *Development* **112:** 881–890.

Kozlowski, D. J., M. L. Gagnon, J. Marchant, L. M. Angerer, S. D. Reynolds, and R. C. Angerer. 1996. Characterization of a *SpAN* promoter sufficient to mediate correct spatial regulation along the animal-vegetal axis of the sea urchin embryo. *Dev. Biol.* **176:** 95–107.

Nguyen, T., J. Jamal, M. J. Shimell, K. Arora, and M. B. O'Connor. 1994. Characterization of tolloid-related-1: a BMP-1-like product that is required during larval and pupal stages of *Drosophila* development. *Dev. Biol.* **166:** 569–586.

Padgett, R. W., J. M. Wozney, and W. M. Gelbart. 1993. Human BMP sequences can confer normal dorsal-ventral patterning in the *Drosophila* embryo. *Proc. Natl. Acad. Sci. USA* **90:** 2905–2909.

Ransick, A., and E. H. Davidson. 1993. A complete second gut induced by transplanted micromeres in the sea urchin embryo. *Science* **259:** 1134–1138.

Reynolds, S. D., L. M. Angerer, J. Palis, A. Nasir, and R. C. Angerer. 1992. Early mRNAs, spatially restricted along the animal-vegetal axis of sea urchin embryos, include one encoding a protein related to tolloid and BMP-1. *Development* **114:** 769–786.

Schroeder, T. E. 1980. Expression of the prefertilization polar axis in sea urchin eggs. *Dev. Biol.* **79:** 428–443.

Shimell, M. J., E. L. Ferguson, S. R. Childs, and M. B. O'Connor. 1991. The *Drosophila* dorsal-ventral patterning gene *tolloid* is related to human bone morphogenetic protein-1. *Cell* **67:** 469–481.

Wei, Z., L. M. Angerer, M. L. Gagnon, and R. C. Angerer. 1995. Characterization of the *SpHE* promoter that is spatially regulated along the animal-vegetal axis of the sea urchin embryo. *Dev. Biol.* **171:** 195–211.

Reference: *Biol. Bull.* **192:** 178. (February, 1997)

Expression and Regulation of a Sea Urchin *Msx* Class Homeobox Gene: Insights Into the Evolution and Function of a Gene Family That Participates in the Patterning of the Early Embryo

ROB MAXSON, HONGYING TAN, SONIA L. DOBIAS, HAILIN WU, JEFFERY R. BELL, AND LIANG MA

Department of Biochemistry and Molecular Biology, K. R. Norris Cancer Hospital, University of Southern California School of Medicine, 1441 Eastlake Avenue, Los Angeles, California 90033

Inductive tissue interactions, in which signals from one tissue alter the fate of another, are an essential feature of the development of all metazoans. Secreted and membrane-bound signaling molecules, their receptors, and a series of intracellular signal transducers are key molecular components of inductive interactions. Equally important are systems of transcription factors that respond to and regulate such intracellular signaling pathways (Davidson, 1990). Among these transcription factors are the *Msx* proteins. Named for the Drosophila *msh*, the *Msx* proteins are homeodomain-containing DNA-binding proteins that can function as both transcriptional activators and repressors (Davidson, 1995). Characterized by a distinct and highly conserved homeodomain, *Msx* proteins have been identified in a wide variety of metazoans from vertebrates to coelenterates. Although there is evidence that they participate in inductive tissue interactions that underlie vertebrate organogenesis, including those that pattern the neural crest, there is little information about their function in simple deuterostomes.

To learn more about the ancient function of *Msx* genes, to shed light on the evolution of developmental mechanisms within the lineage that gave rise to vertebrates, and finally, to provide a molecular baseline for assessing the effects of microgravity on key regulatory events of embryonic patterning, we have isolated and characterized *Msx* genes from ascidians and echinoderms (Ma *et al.*, 1995; Dobias *et al.*, 1996). We demonstrate that portions of the *Msx* protein sequence, including the homeodomain and flanking amino acids, are highly conserved across wide phylogenetic distances. Also conserved, particularly among echinoderms, ascidians, and vertebrates, are aspects of *Msx* expression patterns during early embryogenesis. In an analysis of *Msx* gene function, we show that overexpression of a sea urchin *Msx* gene (*SpMsx*) causes profound anomalies in gastrulation and spiculogenesis, but does not alter the specification of the major embryonic territories. Further, *SpMsx*, like its mammalian congeners, is regulated by members of the BMP family (TGF-β superfamily) of signaling molecules, and that the downstream targets of *SpMsx* likely includes components of the extracellular matrix. We conclude that *Msx* genes function in signaling processes that underlie patterning of early embryos. We suggest that *Msx* gene activity may provide a useful marker for inductive interactions that may be perturbed during the stresses of space flight.

This paper was originally presented at a workshop titled *The Future of Aquatic Research in Space: Neurobiology, Cellular and Molecular Biology*. The workshop, which was held at the Marine Biological Laboratory, Woods Hole, Massachusetts, from 13 to 15 May 1996, was sponsored by the Center for Advanced Studies in the Space Life Sciences at MBL and funded by the National Aeronautics and Space Administration under Cooperative Agreement NCC 2-896.

Literature Cited

Davidson, D. 1995. The function and evolution of *Msx* genes: pointers and paradoxes. *Trends Genet.* **11:** 405–411.

Davidson, E. H. 1990. How embryos work: a comparative view of diverse modes of cell fate specification. *Development* **108:** 365–369.

Dobias, S. L., L. Ma, J. R. Bell, and R. Maxson. 1996. Expression and regulation of a sea urchin *Msx* class homeobox gene: insights into the evolution of *Msx* gene function. *Mech. Dev.* In press.

Ma, L., B. J. Swalla, J. Zhou, J. Chen, R. Maxson, and W. Jeffery. 1995. Expression of an *Msx* homeobox gene in ascidians: developmental insights into the origin and evolution of vertebrates. *Dev. Dyn.* **205:** 308–318.

Reference: *Biol. Bull.* **192**: 179–180. (February, 1997)

Discussion

NICK: Dr. Elinson, you have shown that the microtubules may not be necessary for establishing the dorsal-ventral axis, that gravity alone can do the job. Maybe the arrangement of the microtubules is responding to gravity, and by this we have a sort of self-enhancing loop. It may not be a cause of the axis, but it may be the means of perceiving the effect of gravity in this system.

ELINSON: I showed that when you irradiate with UV and then tilt the egg, the microtubules don't re-form. So that's a microtubule-free system that's working. I do know that there is a model by Tabony and Job that you cited on microtubule patterning by gravity. The time course of that model just doesn't fit here. The whole array forms in a couple of minutes, and I think it took hours for Tabony and Job to get some kind of array generating. I don't think that's involved here.

ANGERER, R.: I want to ask Rick (Elinson) about the big-egg–little-egg experiment. It seemed to me that one interpretation for the lack of dependence on gravity for *Xenopus* development in space is simply that the motor lies between the cortex and deeper layers. It's just ratcheting one against the other, whereas the experimental embryologist needs gravity to hold the center in place while he rotates the outside. This means that gravity will never be sufficient. Even the big egg is going to require some kind of microtubule motor, and would be likely to work the same way in space (as in a small egg).

ELINSON: The normal *Xenopus* egg is, in effect, suspended in space, because it's floating in a capsule. I think that's why you're able to get this cortex to move relative to the cytoplasm. If you have it pinned down, then yes the cytoplasm will be driven relative to the cortex. I don't think that driving can occur in very large eggs; I would be amazed if it did. Nonetheless, in the very large egg, it would just have to be a tiny bit off center, and you would get a shift of cytoplasm due to gravity. So why not take advantage of that opportunity? That's why I might imagine that such a huge egg may work with a gravity mechanism rather than with a microtubule mechanism.

ANGERER, R.: Don't you think that you will still need some cytoplasmic localization event to make a shift? The egg pops out and now has an orientation; nothing is moving. Now you're saying that something has to move, so gravity alone couldn't be sufficient under that circumstance.

ELINSON: I guess what I'm assuming is that the likelihood of an egg ending up perfectly vertical—animal-vegetal—is very small. Just a tiny little shift off-axis of such a huge egg would be enough to move some cytoplasm around and provide the net effect of an axis. No one knows anything about these eggs in that regard.

HAMILL: Richard (Elinson), you said that the cytoplasmic factor you extracted was only from the cortical layer. Did you get any effect with material removed from deeper layers?

ELINSON: The only way we get this activity is if the pipette is put down onto the surface of the egg and the surface is drawn into the pipette, breaking the membrane. When you do that, the cortical cytoplasm flows into the pipette. If you stick your needle into the egg and remove material, you don't get activity.

CASSIDY: Richard (Elinson), has the embryogenesis and the whole developmental sequence of the *coqui* been well established already?

ELINSON: Yes, we have a reproductive colony of these frogs in the laboratory. We are doing embryological and molecular experiments on them, so I'm suggesting that maybe we should look at their eggs as well. The stages have all been worked out; the egg develops into a little frog within 3 weeks.

QUESTION: Dr. Maxson, it seems that when you disrupted the *msx* gene in the mice you got several deficits, but evidently that's not the case in the humans. Can you address this point?

MAXSON: In many cases mice have supernumerary digits. Some humans with this disease have triphalangeal thumbs. So there does seem to be a limb defect in humans. Some of the people in this family have visual field defects, so it's possible that there's an eye connection. As far as anybody knows, they have nor-

mal hearing and normal vestibular function.

ELINSON: Rob (Angerer), if you move the micromeres around, do they inhibit this SpAN expression?

ANGERER, R.: Christian Gache has done that experiment, and the answer is no, they don't. The micromeres are not antagonistic to SpAN, as near as we can tell.

QUESTION: (Dr. Angerer) You get this mosaic expression with DNA; do you get it with RNA?

ANGERER, R.: The reason for the mosaic expression with DNA is this: The first thing that happens when you inject the DNA is that 2000 copies concatenate into a single particle which integrates sometime in the first few cell divisions. One person that I know of, Andy Cameron in Eric Davidson's lab, injected mRNA that was labeled and followed it. That message went uniform rapidly.

Reference: *Biol. Bull.* **192:** 181–182. (February, 1997)

Actin-Dependent Pigment Granule Transport in Retinal Pigment Epithelial Cells

BETH BURNSIDE AND CHRISTINA KING-SMITH

Department of Molecular and Cell Biology, 335 LSA-3200, University of California, Berkeley, California 94720-3200

Introduction

Since diffusion of particles as large as vesicles or organelles is constrained by the high viscosity of cytoplasm, directed translocation of these particles from one cytoplasmic site to another must be achieved by cytoskeletal intervention. In most cases, this is achieved by attaching the particle to a molecular motor which then navigates along a microtubule or an actin filament track (Fath and Burgess, 1994). Although microtubule-dependent transport in animal cells has been more extensively studied, important roles for actin-dependent transport have also recently been recognized (Langford, 1995).

Results and Discussion

Our laboratory has been using the migration of membrane-bound melanin pigment granules in the teleost retinal pigment epithelium (RPE) as a model system for studying intracellular particle transport (Burnside *et al.*, 1983; King-Smith *et al.*, 1995, 1996). The RPE is a simple epithelium that lines the back of the vertebrate eye and lies between the photoreceptors and the choroidal blood supply. In the fish RPE, pigment granules undergo dramatic migrations in response to changes in light condition: they aggregate into the RPE cell body in the dark and disperse into the cell's long apical projections in the light, migrating distances as great as 100 μm. Several properties of RPE cells make them technically advantageous for a study of particle transport. In these cells, pigment granules migrate within fixed apical projections; thus transport-related cytoskeletal dynamics can be examined in the absence of change in cell shape. Either pigment granule aggregation or dispersion can be triggered at will by incubating RPE cells with cAMP or dopamine, respectively, and pigment granule translocation is slow enough to permit experimental intervention or biochemical isolation while granules are traveling in either direction (Burnside and Basinger, 1983; Dearry and Burnside, 1988). Pure preparations of RPE sheets (containing a single cell type) can be isolated in different functional states in sufficient amounts to permit both molecular and biochemical analyses. Finally, normal aggregaton and dispersion can be induced in single isolated cells *in vitro*, thereby permitting analysis of transport kinetics under different experimental conditions by time-lapse videomicroscopy (King-Smith *et al.*, 1995, 1996).

Video analysis has shown that pigment granule movements in RPE cells are slower but otherwise similar to those previously reported for dermal melanophores (unpubl. obs.). During dispersion, pigment granule movement is saltatory and bidirectional, with individual pigment granules moving independently; mean centrifugal and centripetal velocities were 3.2 and 1.5 μm/min respectively. The net pigment dispersion rate in isolated cells (1.8 μm/min) is similar to that observed *in vivo* (2.2 μm/min). After full dispersion is achieved, bidirectional saltations of pigment granules continue within the apical projections. When aggregation is triggered by cAMP, all granules undergo a coordinated, smooth, nonsaltatory centripetal movement, with a mean velocity of 3.6 μm/min, which is comparable to the mean *in vivo* velocity of 3.4 μm/min. In the time-lapse movies, other forms of motility are visible in the apical projections, including bidirectional translocations of mitochondria,

This paper was originally presented at a workshop titled *The Future of Aquatic Research in Space: Neurobiology, Cellular and Molecular Biology*. The workshop, which was held at the Marine Biological Laboratory, Woods Hole, Massachusetts, from 13 to 15 May 1996, was sponsored by the Center for Advanced Studies in the Space Life Sciences at MBL and funded by the National Aeronautics and Space Administration under Cooperative Agreement NCC 2-896.

formation and migration of cytoplasmic bridges between projections, and modest extensions and retractions of the tips of the projections.

To identify the cytoskeletal mechanisms of RPE pigment migration, we investigated whether disruption of microtubules with nocadozole would block pigment granule movement in isolated sunfish RPE cells *in vitro*. Neither aggregation nor dispersion was inhibited by the complete disruption of the microtubules of the apical projections (unpubl. obs.). Microtubule disruption had no effect on the mean velocities of individual granules, or on the rate or extent of pigment granule aggregation or dispersion. Maintenance of the aggregated or dispersed states was also unaffected by microtubule disruption. These observations strongly suggest that microtubules are not required for pigment granule migration in isolated RPE cells.

As a first step toward evaluating the role of actin filaments in RPE pigment granule transport, we also investigated the effects of cytochalasin D on pigment granule migration in isolated RPE cells (unpubl. obs.). Net pigment granule aggregation and dispersion were both strongly and reversibly inhibited by cytochalasin D, the IC50 for dispersion (0.5 μM) being lower than that for aggregation (2.5 μM). Video analysis revealed that cytochalasin has a surprising effect on the movements of individual pigment granules. Although most granules stopped moving altogether within minutes of exposure to cytochalasin, several granules in each projection began to undergo very rapid (up to 40 μm/s), bidirectional excursions. When cytochalasin was applied to isolated RPE cells in which the microtubules had been previously disrupted by nocodazole, all pigment granule movement stopped, suggesting that the very rapid bidirectional excursions observed in cytochalasin-treated cells are microtubule-dependent.

These inhibitor studies suggest that actin filaments play important roles in both aggregation and dispersion, although the mechanism of actin filament participation is not clear. Since the effects of cytochalasin D on aggregation and dispersion have different IC50s, the force-producing mechanisms of the two processes may differ. The low IC50 for dispersion suggests that interfering with plus-end assembly of actin filaments is sufficient to block centrifugal transport. The higher IC50 for aggregation, on the other hand, suggests that additional effects of cytochalasin, such as disruption of actin filament organization, may be necessary to block motility in this case. The implication that both centrifugal and centripetal pigment granule movements are actin-dependent is somewhat surprising, since all known myosin motors move only toward the plus ends of actin filaments. The roles of myosin motors and actin filament dynamics in pigment granule transport are not yet clear.

In parallel with physiological analyses of RPE transport, we have also identified myosin motor proteins expressed in fish RPE cells (unpubl. obs.). Using degenerate primers based on conserved sequences in the myosin motor domain for RT-PCR, we have identified 11 myosin motor proteins that are expressed in teleost RPE. These include one apparently novel myosin selectively expressed in RPE and retina, and two selectively expressed in RPE. We are currently making isotype-specific antibodies to these motors for isolation of native proteins and subcellular localization of each myosin isotype. Ultimately we plan to analyze the roles of these myosin motors in pigment granule transport and other motile processes of RPE cells.

Acknowledgments

Supported by NIH grant R37-EY03575.

Literature Cited

Burnside, B., R. A. Adler, and P. O'Connor. 1983. Retinomotor pigment migration in the teleost retinal pigment epithelium. I. Roles for actin and microtubules in pigment granule transport and cone movement. *Invest. Ophthalmol. Vis. Sci.* **24:** 1–15.

Burnside, B., and S. Basinger. 1983. Retinomotor pigment migration in the teleost retinal pigment epithelium. II. Cyclic adenosine 3′, 5′-monophosphate induction of dark-adaptive movement in vitro. *Invest. Ophthalmol. Vis. Sci.* **24:** 16–23.

Dearry, A., and B. Burnside. 1988. Stimulation of distinct D2 dopaminergic and alpha2-adrenergic receptors induces light-adaptive pigment dispersion in teleost retinal pigment epithelium. *J. Neurochem.* **51:** 1516–1523.

Fath, K. R., and D. R. Burgess. 1994. Membrane motility mediated by unconventional myosin. *Curr. Opin. Cell Biol.* **6:** 131–135.

King-Smith, C., L. Bost-Usinger, and B. Burnside. 1995. Expression of kinesin heavy chain isoforms in retinal pigment epithelial cells. *Cell Motil. Cytoskeleton* **31:** 66–81.

King-Smith, C., P. Chen, D. García, H. Rey, and B. Burnside. 1996. Calcium-independent regulation of pigment granule aggregation and dispersion in teleost retinal pigment epithelial cells. *J. Cell Sci.* **109:** 33–43.

Langford, G. M. 1995. Actin- and microtubule-dependent organelle motors: interrelationships between the two motility systems. *Curr. Opin. Cell Biol.* **7:** 82–88.

Reference: *Biol. Bull.* **192**: 183–185. (February, 1997)

Myosin Drives Retrograde F-Actin Flow in Neuronal Growth Cones

C. H. LIN*, E. M. ESPREAFICO#, M. S. MOOSEKER† AND P. FORSCHER†

*†Dept. Biology, Yale University, New Haven, Connecticut 06511; #Dept. Morphology, Faculdade de Medicina de Ribeirão Preto-USP, SP, Brazil; *National Yang-Ming University, Taipei, Taiwan*

Neuronal growth cones guide axons in the developing nervous system toward distant target sites. Recent evidence suggests that growth cones decode both diffusible and substrate-bound molecular signals during the guidance process (Kennedy and Tessier-Lavigne, 1995; Tessier-Lavigne, 1992), which involves pathfinding, branching, and ultimately target recognition. All of these behaviors depend on precise regulation of growth cone motility. Bray pioneered the investigation of growth cone motility and was the first to observe that inert particles placed on the growth cone surface would move in a retrograde direction, suggestive of an underlying centripetal membrane or actin filament flux (Bray, 1970). Early studies also demonstrated that growth cone motility depends on actin filament assembly (Yamada and Wessells, 1973), and a critical role for actin assembly in axonal guidance emerged when axons in the developing grasshopper nervous system were shown to lose all pathfinding capabilities upon treatment with cytochalasin (Bentley and Toroion-Raymond, 1986). Later, studies characterizing actin dynamics in *Aplysia* growth cones *in vitro* suggested that the retrograde flux mentioned above is actually due to actin filament assembly at nucleation sites along the leading edge, followed by retrograde translocation and filament disassembly or recycling by means of severing at a proximal site. This process was referred to as "retrograde flow" (Forscher and Lin, 1991; Forscher and Smith, 1988; Smith, 1988).

The peripheral actin ultrastructure of the growth cone has also been well characterized as being composed of two distinct structural domains: filopodia containing arrays of uniformly polarized (barbed end distal) actin filaments, and intervening lamellipodium domains with less polarized filament structure (*cf.* figure 6a; Lewis and Bridgman, 1992). Both domains appear to exhibit uniform retrograde flow relative to an external substrate reference as judged by actin fluorescence photobleaching studies (Lin and Forscher, 1995). Assembly of actin filaments, followed by centripetal displacement relative to the leading cell margin, has been observed in a wide variety of motile cells and appears to be a fundamental property of directed growth processes and cell migration (Cramer *et al.*, 1994; Bray and White, 1988; Fisher *et al.*, 1988; Abercrombie *et al.*, 1970).

In our initial characterization of actin filament dynamics in *Aplysia* growth cones, we noted that when cones were treated with 2–5 μM cytochalasin, retrograde flow did not appear to be markedly affected. Continued retrograde flow in the absence of new actin assembly resulted in formation of an F-actin-free gap along the growth cone margin and eventual clearance (typically in about 3 min) of F-actin from lamellipodia and filopodia. This persistent retraction of actin filament networks in the *absence* of actin assembly demonstrated that polymerization could not be supplying the driving force for retrograde F-actin flow; therefore, we suggested that a myosin-like molecular motor might be involved (Forscher and Smith, 1988). Despite recent molecular cloning of several brain myosins (Bahler *et al.*, 1994; Ruppert *et al.*, 1993; Cheney *et al.*, 1993) and localization of myosins to growth cones (Rochlin *et al.*, 1995; Espreafico *et al.*, 1992; Cheng *et al.*, 1992; Miller *et al.*, 1992), little or no information about the functional role of myosins in growth cone motility has emerged (*cf.* Tanaka and Sabry, 1995).

This paper was originally presented at a workshop titled *The Future of Aquatic Research in Space: Neurobiology, Cellular and Molecular Biology*. The workshop, which was held at the Marine Biological Laboratory, Woods Hole, Massachusetts, from 13 to 15 May 1996, was sponsored by the Center for Advanced Studies in the Space Life Sciences at MBL and funded by the National Aeronautics and Space Administration under Cooperative Agreement NCC 2-896.

Given the functional implications of our previous work, we designed experiments aimed at global inhibition of myosin activity to test whether *any* myosin was in fact involved in driving retrograde F-actin flow in growth cones. All known myosins have an evolutionarily conserved N-terminal head domain containing the site for ATP and F-actin binding as well as force generation (Mooseker and Cheney, 1995). Chymotryptic digestion of muscle myosin results in cleavage of a head domain subfragment (S1) from the rest of the molecule (Margossian and Lowey, 1982). S1 exhibits ATP-dependent actin-filament binding, but lacking the C-terminal tail, is incapable of generating force unless artificially tethered (*e.g.*, by an antibody) to a substrate. In addition, further treatment of S1 with the sulfhydryl reagent, *N*-ethylmaleimide (NEM), results in a myosin head species (NEM-S1) that remains tightly bound to actin filaments, even in the presence of ATP, and thus can serve as a potent specific inhibitor of actomyosin function (Cande, 1986; Meeusen and Cande, 1979). Our first experimental approach then was to competitively inhibit myosin function by injection of purified S1 or NEM-S1 and to look at effects on growth cone motility, actin dynamics, and structure.

We compared the results of S1 or NEM-S1 injection with those obtained after treatment with 10–30 m*M* 2,3-butanedione-2-monoxime (BDM), a pharmacological inhibitor of endogenous myosin ATPase activity (Fig. 1B). BDM has previously been shown to affect cross-bridge kinetics and to inhibit both conventional muscle and nonmuscle myosin ATPases including myosin V, platelet myosin II, and a drosophila myosin ATPase fraction without affecting kinesin ATPase activity or actin assembly (Cramer and Mitchison, 1995; Backx *et al.*, 1994; McKillop *et al.*, 1994; Schramm *et al.*, 1994; Zhao and Kawai, 1994). We found that both types of myosin

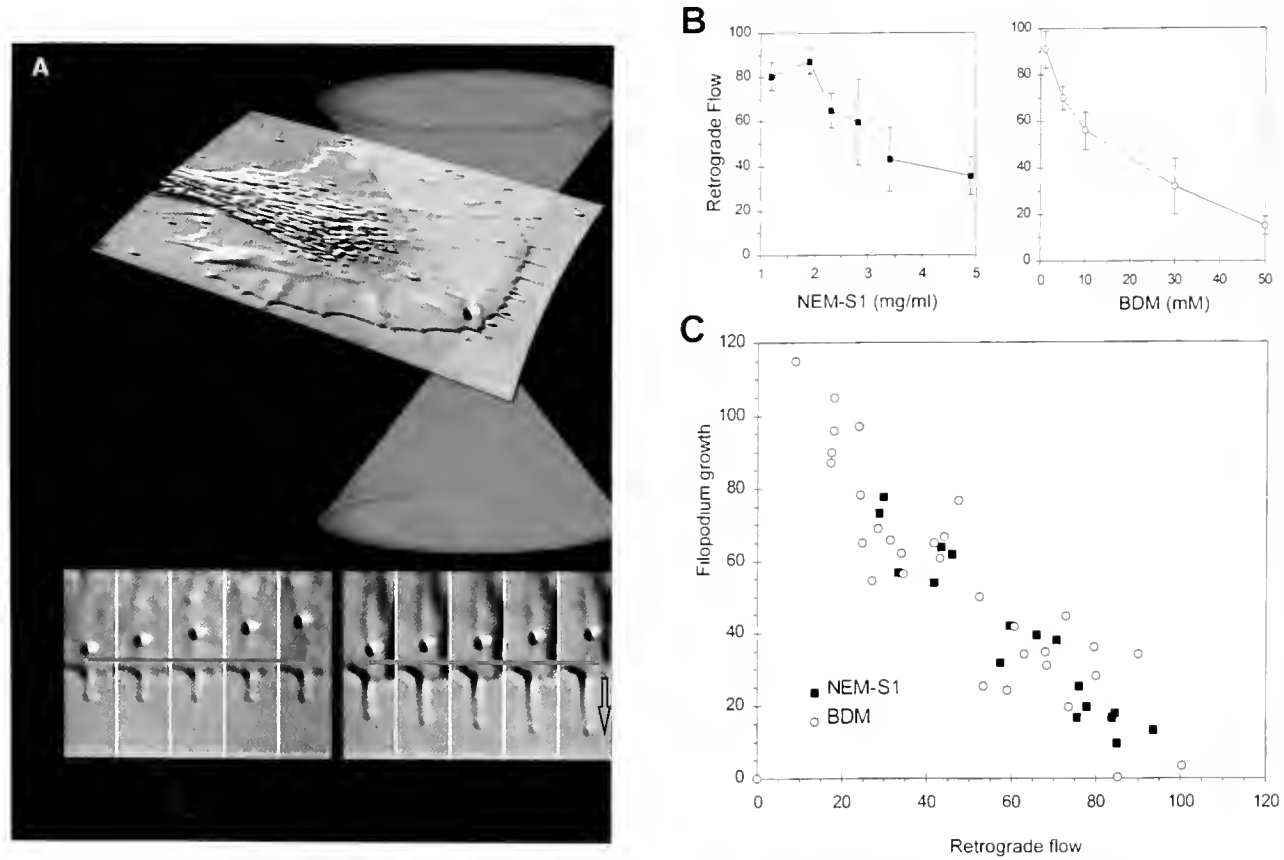

Figure 1. Rates of filopodium growth and retrograde F-actin flow are inversely proportional. (A) Silica beads (200-nm diameter) derivatized with Con-A were applied to the growth cone surface with a single-beam gradient IR laser trap (red graphic top) and used as a noninvasive tool to quantify F-actin flow rates. Video sequence shows bead displacement over time (15-s intervals) under control conditions (green arrow) and immediately after myosin inhibition with 10 m*M* BDM (red arrow). Yellow arrow denotes filopodial growth. (B) Dose-response curves for NEM-S1 and BDM treatments. Rates are % control retrograde flow. (C) Rates of filopodium elongation *versus* retrograde flow. Data from different experiments (growth cones) were normalized by control retrograde flow rates.

inhibition produced essentially the same effects: dose-dependent attenuation of retrograde F-actin flow accompanied by filopodial and leading edge extension at rates directly proportional to the degree of flow inhibition (Fig. 1C). Filopodial growth stimulated by the myosin antagonists was cytochalasin sensitive, indicating that it is due to barbed end filament assembly. These experiments demonstrate that retrograde actin flow is indeed driven by a myosin ATPase, and that actin filament assembly and myosin motors function independently. Our results suggest that simple superimposition of actin polymerization and the action of myosin motors underlie the process of retrograde F-actin flow.

Literature Cited

Abercrombie, M., J. E. M. Heaysman, and S. M. Pegrum. 1970. The locomotion of fibroblasts in culture. III. Movement of particles on the dorsal surfaces of leading lamella. *Exp. Cell Res.* **62:** 389–398.

Backx, P. H., W. D. Gao, M. D. Azon-Backx, and E. Marban. 1994. Mechanisms of force inhibition by 2,3-butanedione monoxime in rat cardiac muscle: role of calcium and crossbridge kinetics. *J. Physiol.* **476:** 487–500.

Bahler, M., R. Kroschewski, H. E. Stoffler, and T. Behrmann. 1994. Rat myr 4 defines a novel subclass of myosin I: identification, distribution, localization, and mapping of calmodulin-binding sites with differential calcium sensitivity. *J. Cell Biol.* **126:** 375–389.

Bentley, D., and A. Toroian-Raymond. 1986. Disordered pathfinding by pioneer neuron growth cones deprived of filopodia by cytochalasin treatment. *Nature* **323:** 712–715.

Bray, D. 1970. The surface movement during growth of single explanted neurons. *Proc. Natl. Acad. Sci. USA* **65:** 905–910.

Bray, D., and J. G. White. 1988. Cortical flow in animal cells. *Science* **239:** 883–888.

Cande, W. Z. 1986. Preparation of *N*-ethylmaleimide-modified heavy meromyosin and its use as a functional probe of actomyosin-based motility. *Methods Enzymol.* **134:** 473–477.

Cheney, R. E., M. A. O'Oshea, J. E. Heuser, M. V. Coelho, J. S. Wolenski, E. M. Espreafico, P. Forscher, R. E. Larson, and M. S. Mooseker. 1993. Brain myosin-V is a two-headed unconventional myosin with motor activity. *Cell* **75:** 13–23.

Cheng, T. P., N. Murakami, and M. Elzinga. 1992. Localization of myosin IIB at the leading edge of growth cones from rat dorsal root ganglionic cells. *FEBS Lett.* **311:** 91–94.

Cramer, L. P., T. J. Mitchison, and J. A. Theriot. 1994. Actin-dependent motile forces and cell motility. *Curr. Opin. Cell Biol.* **6:** 82–86.

Cramer, L. P., and T. J. Mitchison. 1995. Myosin is involved in postmitotic cell spreading. *J. Cell Biol.* **131:** 179–189.

Espreafico, E. M., R. E. Cheney, M. Matteoli, A. A. Nascimento, P. V. De Camilli, R. E. Larson, and M. S. Mooseker. 1992. Primary structure and cellular localization of chicken brain myosin-V (p190), an unconventional myosin with calmodulin light chains. *J. Cell Biol.* **119:** 1541–1557.

Fisher, G. W., P. A. Conrad, R. L. DeBiasio, and D. L. Taylor. 1988. Centripetal transport of cytoplasm, actin, and the cell surface in lamellipodia of fibroblasts. *Cell Motil. Cytoskeleton* **11:** 235–247.

Forscher, P., and C. Lin. 1991. Polycationic bead translocation driven by actin assembly in neuronal growth cones. *J. Cell. Biol.* **115:** 368a.

Forscher, P., and S. J. Smith. 1988. Actions of cytochalasins on the organization of actin filaments and microtubules in a neuronal growth cone. *J. Cell Biol.* **107:** 1505–1516.

Kennedy, T. E., and M. Tessier-Lavigne. 1995. Guidance and induction of branch formation in developing axons by target-derived diffusible factors. *Curr. Opin. Neurobiology* **5:** 83–90.

Lewis, A. K., and P. C. Bridgman. 1992. Nerve growth cone lamellipodia contain two populations of actin filaments that differ in organization and polarity. *J. Cell Biol.* **119:** 1219–1243.

Lin, C.-H., and P. Forscher. 1995. Growth cone advance is inversely proportional to retrograde F-actin flow. *Neuron* **14:** 763–771.

Margossian, S. S., and S. Lowey. 1982. Preparation of myosin and its subfragments from rabbit skeletal muscle. *Meth. Enzymol.* **85:** 55–71.

McKillop, K. F., N. S. Fortsne, K. W. Ranatunga, and M. A. Geeves. 1994. The influence of 2,3-butanedione-2-monoxime on the interactions between actin and myosin in solution and skinned muscle fibers. *J. Muscle Res. Cell Motil.* **15:** 309–318.

Meeusen, R. L., and W. Z. Cande. 1979. N-Ethylmaleimide modified heavy meromyosin: a probe for actomyosin interactions. *J. Cell Biol.* **82:** 57–65.

Miller, M., E. Bower, P. Levitt, D. Li, and P. D. Chantler. 1992. Myosin II distribution in neurons is consistent with a role in growth cone motility but not synaptic vesicle mobilization. *Neuron* **8:** 25–44.

Mooseker, M. S., and R. E. Cheney. 1995. Unconventional myosins. *Annu. Rev. Cell Dev. Biol.* **11:** 633–675.

Roehlin, M. W., K. I. Itoh, R. S. Adelstein, and P. C. Bridgman. 1995. Localization of myosin II A and B isoforms in cultured neurons. *J. Cell Sci.* **108:** 3661–3670.

Ruppert, C., R. Kroschewski, and M. Bahler. 1993. Identification, characterization and cloning of myr 1, a mammalian myosin-I. *J. Cell Biol.* **120:** 1393–1403.

Schramm, M., H. G. Klieber, and J. Daut. 1994. The energy expenditure of actomyosin ATPase, calcium-ATPase and sodium-potassium-ATPase in guinea pig cardiac ventricular muscle. *J. Physiol.* **481:** 647–662.

Smith, S. J. 1988. Neuronal cytomechanics: the actin-based motility of growth cones. *Science* **242:** 708–715.

Tanaka, E., and J. Sabry. 1995. Making the connection: cytoskeletal rearrangements during growth cone guidance. *Cell* **83:** 171–176.

Tessier-Lavigne, M. 1992. Axon guidance by molecular gradients. *Curr. Opin. Neurobiology* **2:** 60–65.

Yamada, K. M., and N. K. Wessells. 1973. Cytochalasin B: effects on membrane ruffling, growth cone and microspike activity, and microfilament structure not due to altered glucose transport. *Dev. Biol.* **31:** 413–420.

Zhao, Y., and M. Kawai. 1994. BDM affects nucleotide binding and force generation steps of the crossbridge cycle in rabbit psoas muscle fibers. *Am. J. Physiol.* **266:** C437–C447.

Reference: *Biol. Bull.* **192:** 186–190. (February, 1997)

Multiple Myosin Motors and Mechanoelectrical Transduction by Hair Cells

PETER G. GILLESPIE

Departments of Physiology and Neuroscience, The Johns Hopkins University, Baltimore, Maryland 21205

Hair cells are exquisitely specialized mechanoreceptors, responding only to specific frequencies of sound or to distinct head movements (reviewed in Hudspeth, 1989, 1992). A hair cell carries out mechanoelectrical transduction with its mechanically sensitive hair bundle, a beveled collection of stereocilia and one solitary kinocilium. Although the kinocilium is a true cilium, with the familiar 9 + 2 arrangement of microtubule doublets, stereocilia are actin-based. Stereocilia contain several hundred cross-linked actin filaments, so they are quite rigid. A stereocilium pivots at its flexible basal insertion point, where only a few dozen actin filaments penetrate the cell. Deflection of the bundle causes adjacent stereocilia to slide along each other, stretching elastic gating springs that tug open transduction channels located at the top of the bundle.

Hair cells adapt to sustained stimuli; for example, hair cells in the bullfrog's sacculus can detect transient vertical accelerations of less than 10^{-5} *g*, despite a constant 1 *g* stimulus from gravity (Koyama *et al.*, 1982). Gating-spring tension, and hence channel open probability, is controlled by adaptation motors, which likely contain myosin molecules (reviewed in Hudspeth and Gillespie, 1994; Gillespie, 1995). During an excitatory stimulus, when gating-spring tension is high, Ca^{2+} entering through open transduction channels triggers the adaptation motors to slip down the cytoskeleton and reduce tension (Fig. 1). By contrast, during inhibitory bundle deflections that slacken the gating springs, the motors climb towards the apical ends of the stereocilia and restore tension. The adaptation motor thus acts as a negative-feedback control mechanism that ensures that gating-spring tension remains at its optimal level.

To prove that adaptation is carried out by myosin molecules and to identify the responsible isozyme, we have taken advantage of years of intensive study of the properties of skeletal-muscle myosin. We have applied general principles derived from muscle actomyosin to design of experiments for hair cells. The ATPase cycle of myosin is illustrated in a simplified form in Figure 2. Are the properties of skeletal-muscle myosin II likely to resemble those of a hair-cell myosin, even one of an unusual class? Recent results have suggested that this is so. Detailed kinetic characterization of two *Acanthamoeba* myosin-I isozymes indicates that ATPase hydrolysis utilizes the same mechanism as vertebrate myosin II. Furthermore, the rate and equilibrium constants defining the amoeba myosin-I cycle are nearly identical to those of vertebrate myosin II (Ostap and Pollard, 1996). These results give us confidence that the same will hold true for the myosin molecules of hair bundle.

To provide evidence that myosin mediates adaptation in hair cells, we dialyzed hair cells of the bullfrog's sacculus with tight-seal, whole-cell recording electrodes filled with compounds that should interfere with the ATPase cycle. In one series of experiments, we introduced into hair cells adenine nucleoside diphosphates, such as ADP and the metabolism-resistant analog ADPβS, expecting that they would promote the population of the diphosphate-bound state of myosin (Gillespie and Hudspeth, 1993). We saw the expected results: adaptation was blocked, but the transduction currents remained robust, as if the adaptation motors were arrested along the actin

This paper was originally presented at a workshop titled *The Future of Aquatic Research in Space: Neurobiology, Cellular and Molecular Biology*. The workshop, which was held at the Marine Biological Laboratory, Woods Hole, Massachusetts, from 13 to 15 May 1996, was sponsored by the Center for Advanced Studies in the Space Life Sciences at MBL and funded by the National Aeronautics and Space Administration under Cooperative Agreement NCC 2-896.

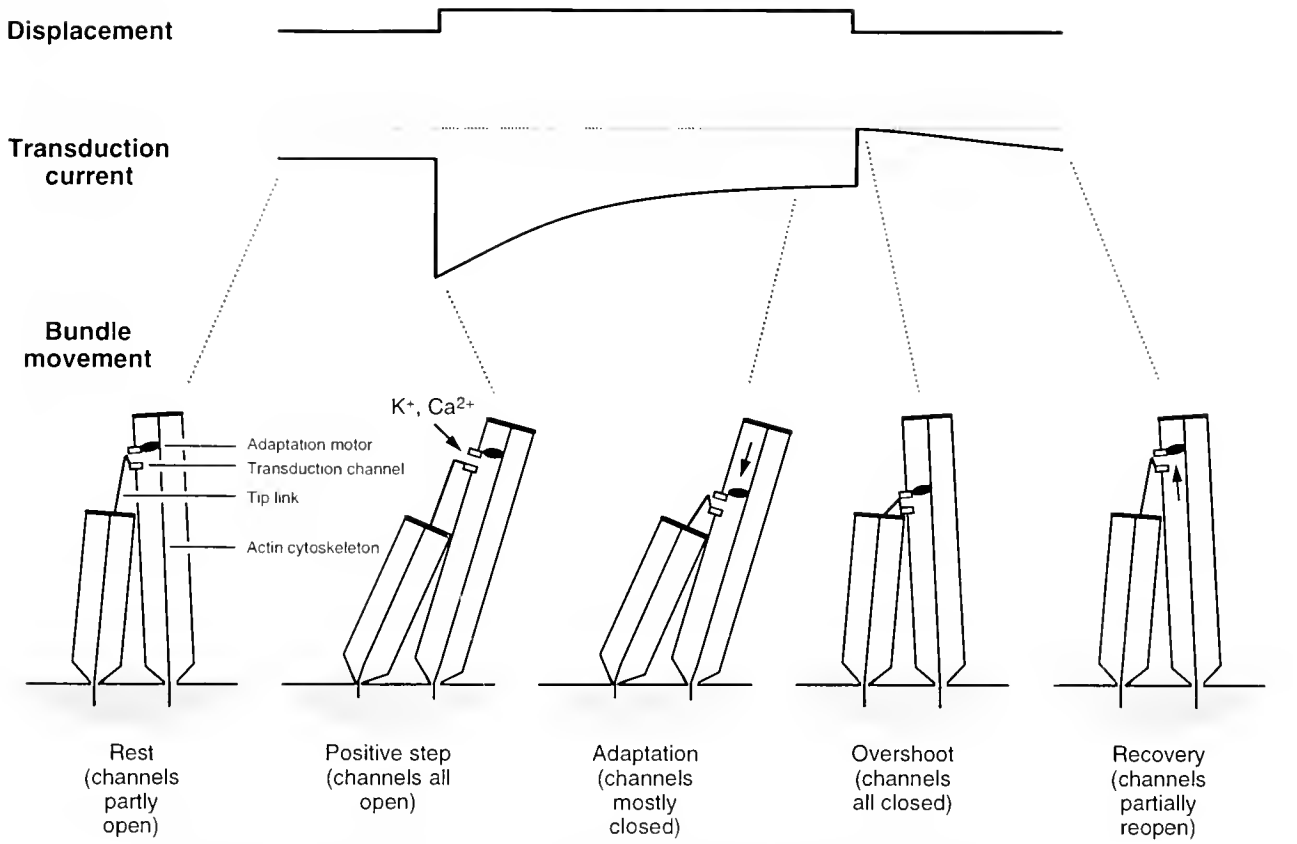

Figure 1. Transduction-channel gating and adaptation by hair cells. The response of a hair cell's transduction apparatus to a 100-ms, excitatory displacement is depicted. Transduction channels are gated by tension in tip links, and tension in tip links is controlled both by bundle position and by adaptation-motor position. When the displacement is applied, transduction channels open and a large inward current develops. In response to high tip-link tension and the influx of Ca^{2+}, however, the adaptation motor slips down the actin cytoskeleton. As it does so, tension in the tip link diminishes and channels close. When the bundle is returned to its rest position, the adaptation motor is caught below its rest position, so tip-link tension drops precipitously and transduction channels close completely. Responding to the reduced tension, the adaptation motor restores resting tip-link tension by reascending the actin cytoskeleton. Modified from Hudspeth and Gillespie (1994).

filaments, unable to climb or slip. In addition, channel open probability increased, as the number of myosin molecules in force-producing states increased. These results are entirely analogous to the effects of ADP on isometrically contracting muscle fibers, where ADP blocks both shortening and lengthening, as well as increasing isometric tension (Cooke and Pate, 1985).

In a second series of experiments, we filled hair cells with phosphate analogs, reasoning that this should lead to decreased actin-myosin interaction (Yamoah and Gillespie, 1996). Phosphate analogs such as vanadate, beryllium fluoride, and sulfate eliminated motor-force production, blocked climbing adaptation, and slowed slipping adaptation. The effects of phosphate analogs on slipping adaptation were quantitatively explained by a simple model that uses parameter values obtained from skeletal-muscle myosin.

The remarkable similarity of the effects of adenine nucleoside diphosphates and phosphate analogs on hair-cell adaptation with their effects on skeletal-muscle behavior lends strong support to the hypothesis that myosin molecules mediate adaptation. To date, no other model for adaptation fits more than a fraction of these and other data.

The evidence that myosin molecules probably mediate adaptation has triggered a search for isozymes of myosin expressed in hair cells. Early evidence that hair bundles contain myosin (Macartney *et al.*, 1980) was later disputed (Drenckhahn *et al.*, 1982), and may have been due to anti-actin-antibody contamination of anti-myosin polyclonal antisera (Gillespie *et al.*, 1993). Because of the large number of myosin isozymes (Cheney *et al.*, 1993) and lack of antibodies that recognize all myosin isozymes, we developed a photoaffinity-labeling ap-

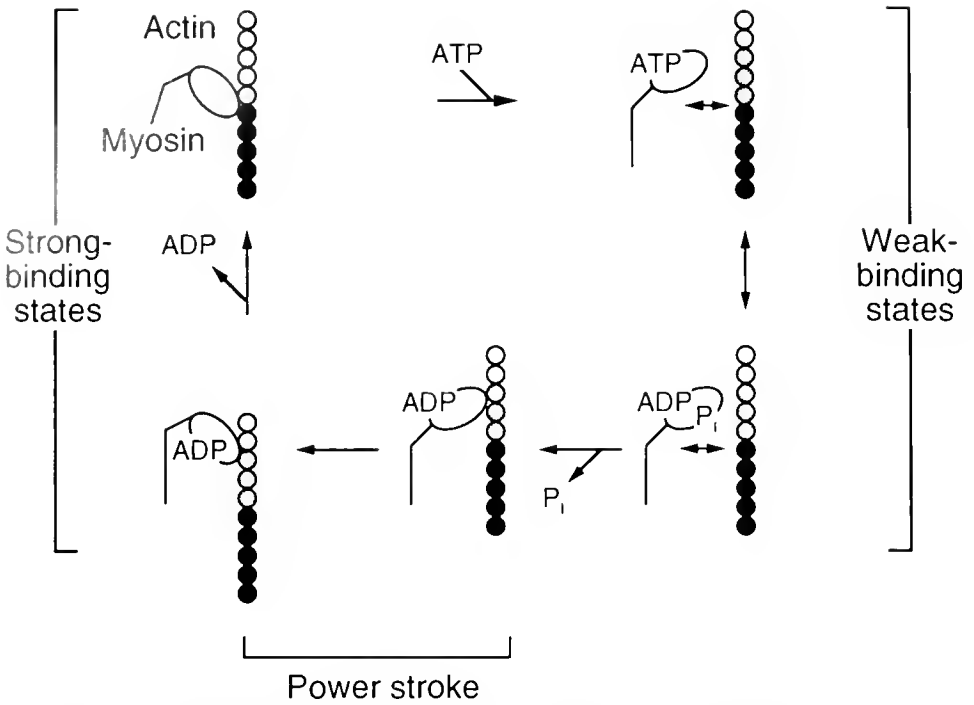

Figure 2. ATP hydrolysis by myosin. In the absence of bound nucleotide, myosin is bound tightly to actin. The consequence of ATP binding is a dramatic decrease in the affinity of myosin for actin; the complex then enters several so-called "weak-binding states," in which myosin only transiently interacts with actin. ATP is hydrolyzed to ADP and P_i in a readily reversible step, then P_i is released and myosin rebinds actin. Following P_i release, a kinetically irreversible step is surmounted, which is probably associated with the power stroke that generates forces and displaces actin and myosin filaments. When ADP is bound, like the subsequent nucleotide-free state, myosin is bound tightly to actin. The effect of adenine nucleotide diphosphates like ADP and ADPβ should be to lock the myosin in a tightly bound complex with actin; adaptation motors would therefore be unable to release from actin or carry out power strokes. By contrast, phosphate analogs like vanadate, beryllium fluoride, and sulfate should increase the population of weakly bound states, decreasing force production and inhibiting climbing by the adaptation motors.

proach that relies on the properties of myosin's ATPase cycle. In this method, purified hair bundles (Gillespie and Hudspeth, 1991) are incubated with a radioactive nucleotide, such as [α-^{32}P]UTP, and a trapping phosphate analog, such as vanadate. After the nucleotide is hydrolyzed and P_i is released, vanadate binds to myosin and traps the nucleotide in a slowly dissociating state. Thorough washing eliminates nucleotides bound to other bundle proteins, then radioactive nucleotides are covalently crosslinked to myosin molecules by UV irradiation. We found that three myosin isozymes, of 120, 160, and 230 kD, were most consistently labeled in purified hair bundles (Gillespie *et al.*, 1993). Although all three proteins have properties that suggest they are myosin molecules, the behavior of the 120-kD protein was most consistent with that of an adaptation motor. Labeling of the 120-kD protein was blocked by antagonists of myosin, including ADP, ADPβS, and NANTP, and the rank order of effectiveness of three trapping analogs (vanadate, beryllium fluoride, and aluminum fluoride) was identical to the order of stability of the corresponding myosin II-analog complexes in the presence of actin (Gillespie *et al.*, 1993; Yamoah and Gillespie, 1996). The 120-kD protein bound calmodulin, which is the Ca^{2+}-binding mediator of adaptation (Walker and Hudspeth, 1996). The other photolabeled proteins shared some, but not all, of these characteristics. The data thus argue that bundles contain three myosin isozymes, and that the 120-kD myosin has the most appropriate behavior for an adaptation-motor myosin.

We have used selective antibodies to identify and localize three myosin isozymes in saccular hair bundles. Two of these isozymes, myosin VI and myosin VIIa, have been shown, by genetic methods, to play essential roles in hair cells (Avraham *et al.*, 1995; Gibson *et al.*, 1995). Using an anti-myosin-VI antiserum, we showed that an unusually high-mass form of this isozyme is found exclusively in hair bundles (T. Hasson, P. G. Gillespie, and D. P. Corey, unpubl. data). This 160-kD form probably corresponds to the 160-kD photoaffinity-labeled protein. The location of myosin VI in bullfrog hair cells is complex. A large amount of myosin VI was found

in the cytoplasm, and it can readily diffuse out of permeabilized hair cells. Another fraction was apparently tightly bound within the cuticular plate. In hair bundles, myosin VI was associated with basal tapers of a fraction of stereocilia (only 10%–25%). In other bundles, usually small bundles from newly formed hair cells, myosin VI was found throughout the bundle. We suspect that myosin VI may be playing a structural role in hair bundles.

Myosin VIIa was abundant in purified hair bundles, and it comigrated with the 230-kD photoaffinity-labeled protein (T. Hasson, P. G. Gillespie, and D. P. Corey, unpubl. data). In frog bundles, myosin VIIa was largely concentrated in a band 1–2 μm in height just above the basal tapers. Because one class of intersterecociliary linkages is found in that location, we suspect that myosin VIIa serves as the intracellular anchor for these basal linkages. This localization is entirely consistent with its distributed localization in cochlear hair bundles (Hasson *et al.*, 1995), where this class of linkages appears to be found along the length of the stereociliary opposition.

Finally, myosin Iβ appears to be the 120-kD photoaffinity-labeled bundle protein. Myosin Iβ has been definitively localized to hair bundles by using two antibodies. The first antibody, mT2, is selective for this isozyme over all other known myosin-I isozymes (Metcalf, 1996). In immunoblots, mT2 identified a 120-kD protein present at 100–200 molecules per stereocilium (Gillespie *et al.*, 1993). A polyclonal antiserum raised against the tail of cloned myosin Iβ also detected, on immunoblots, a 120-kD protein of similar abundance (T. Hasson, P. G. Gillespie, and Corey, D. P., unpubl. data). Both antibodies are selective, but additional confirmation of the responsible isozyme derives from separation, on SDS-PAGE, of the 120-kD protein from myosin Iα (unpubl. data), the only other myosin-I isozyme known to be expressed in hair-cell-containing tissues (Solc *et al.*, 1994).

Both antibodies labeled stereociliary tips, as expected for an adaptation-motor myosin (Gillespie *et al.*, 1993; T. Hasson, P. G. Gillespie, and D. P. Corey, unpubl. data). But only a fraction of tips were labeled, and a substantial amount of myosin was found below the stereociliary tips; this observation is consistent with a recent demonstration that the transduction apparatus is highly dynamic and can re-form after the tip links are broken (Zhao *et al.*, 1996). In fixed cells observed with anti-myosin-Iβ antibodies, myosin molecules may be immobilized while carrying transduction channels and tip links to their proper locations.

Proof that myosin Iβ is indeed the adaptation motor will come from three classes of experiments, all in progress. Because the adaptation motor is thought to reside in the insertional plaque found at the upper end of a tip link (Hudspeth and Gillespie, 1994), immunolocalization of myosin Iβ at the plaque by immunoelectron microscopy will provide one level of proof. More convincing would be the inhibition of adaptation by isozyme-selective inhibitors of myosin Iβ, such as inhibitory antibodies or selective peptides. Most definitive would be introduction of a mutated myosin gene into the genome of an animal with its myosin-Iβ gene deleted; if the properties of the reintroduced myosin gene were sufficiently distinctive, adaptation would be affected in a predictable manner.

Acknowledgments

This work was supported by the NIH (R01 DC02368 and P60 DC00979). P.G.G. is a Pew Scholar in the Biomedical Sciences.

Literature Cited

Avraham, K. B., T. Hasson, K. P. Steel, D. M. Kingsley, L. B. Russell, M. S. Mooseker, N. G. Copeland, and N. A. Jenkins. 1995. The mouse *Snell's waltzer* deafness gene encodes an unconventional myosin required for structural integrity of inner ear hair cells. *Nature Genetics* **11:** 369–375.

Cheney, R. E., M. A. Riley, and M. S. Mooseker. 1993. Phylogenetic analysis of the myosin superfamily. *Cell Motil. Cytoskeleton* **24:** 215–223.

Cooke, R., and E. Pate. 1985. The effects of ADP and phosphate on the contraction of muscle fibers. *Biophys. J.* **48:** 789–798.

Drenckhahn, D., J. Kellner, H. G. Mannherz, U. Gröschel-Stewart, J. Kendrick-Jones, and J. Scholey. 1982. Absence of myosin-like immunoreactivity in stereocilia of cochlear hair cells. *Nature* **300:** 531–532.

Gibson, F., J. Walsh, P. Mburu, A. Varela, K. A. Brown, M. Antonio, K. W. Beisel, K. P. Steel, and S. D. M. Brown. 1995. A type VII myosin encoded by the mouse deafness gene *shaker-1*. *Nature* **374:** 62–64.

Gillespie, P. G. 1995. Molecular machinery of auditory and vestibular transduction. *Curr. Opin. Neurobiol.* **5:** 449–455.

Gillespie, P. G., and A. J. Hudspeth. 1991. High-purity isolation of bullfrog hair bundles and subcellular and topological localization of constituent proteins. *J. Cell Biol.* **112:** 625–640.

Gillespie, P. G., and A. J. Hudspeth. 1993. Adenine nucleoside diphosphate block adaptation of mechanoelectrical transduction in hair cells. *Proc. Natl. Acad. Sci. USA* **90:** 2710–2714.

Gillespie, P. G., M. C. Wagner, and A. J. Hudspeth. 1993. Identification of a 120-kD hair-bundle myosin I located near stereociliary tips. *Neuron* **11:** 581–594.

Hasson, T., M. B. Heintzelman, J. Santos-Sacchi, D. P. Corey, and M. S. Mooseker. 1995. Expression in cochlea and retina of myosin VIIa, the gene product defective in Usher syndrome type 1B. *Proc. Natl. Acad. Sci. USA* **92:** 9815–9819.

Hudspeth, A. J. 1989. How the ear's works work. *Nature* **341:** 397–404.

Hudspeth, A. J. 1992. Hair-bundle mechanics and a model for mechanoelectrical transduction by hair cells. Pp. 357–370 in *Sensory Transduction*, D. P. Corey and S. Roper, eds. Rockefeller University Press, New York.

Hudspeth, A. J., and P. G. Gillespie. 1994. Pulling springs to tune transduction: adaptation by hair cells. *Neuron* **12:** 1–9.

Koyama, H., E. R. Lewis, E. L. Leverenz, and R. A. Baird. 1982. Acute seismic sensitivity in the bullfrog ear. *Brain Res.* **250:** 168–172.

Macartney, J. C., S. D. Comis, and J. O. Pickles. 1980. Is myosin in the cochlea a basis for active motility? *Nature* **288**: 491–492.

Metcalf, A. B. 1996. Molecular characterization of amphibian myosin IB, a candidate for the hair bundle's adaptation motor. Ph.D. thesis. University of Texas Southwestern Medical Center, Dallas, TX.

Ostap, E. M., and T. D. Pollard. 1996. Biochemical kinetic characterization of *Acanthamoeba* myosin-I ATPase. *J. Cell Biol.* **132**: 1053–1060.

Sole, C. K., B. H. Derfler, G. M. Duyk, and D. P. Corey. 1994. Molecular cloning of myosins from bullfrog saccular macula: a candidate for the hair cell adaptation motor. *Auditory Neurosci.* **1**: 63–75.

Walker, R. G., and A. J. Hudspeth. 1996. Calmodulin controls adaptation of mechanoelectrical transduction by hair cells of the bullfrog's sacculus. *Proc. Natl. Acad. Sci. USA* **93**: 2203–2207.

Yamoah, E. N., and P. G. Gillespie. 1996. Phosphate analogs block hair-cell adaptation by inhibiting adaptation-motor force production. *Neuron* **17**: 523–533.

Zhao, Y.-d., E. N. Yamoah, and P. G. Gillespie. 1996. The hair cell's tip links rapidly regenerate. *Proc. Natl. Acad. Sci. USA* **93**: 15469–15474.

Reference: *Biol. Bull.* **192:** 191–196. (February, 1997)

Discussion

LANGFORD: Beth (Burnside), it was very exciting to see those results with particle motion on actin filaments. You used the decoration of the actin filaments with the S1 heads to show directionality. You mentioned that, to prepare the cells for this experiment, you have to extract a great deal, so you may have lost the actin.

BURNSIDE: That was done with intact sheets of RPE with attached retina, not on isolated cells. And the distribution was that 75% of the actin filaments in apical projections were oriented with plus ends towards the tips of the projections, and 25% were oriented otherwise. We have not repeated the procedures with isolated cells, because they are rather tenuously attached to their cover slips. With the intact retina/RPE preparations, we have to permeabilize rather drastically to get the myosin subfragments into the region of the apical projections, since they are not exposed. Thus some of the apical projections may have been mechanically disrupted enough to stir around their actin filaments. I am more inclined to believe the 75+% with plus ends distal; the other ±25% may have been produced by tissue disruption.

LANGFORD: Do you ever see evidence of bundles of actin, or do they always appear as single filaments?

BURNSIDE: There are no bundles in these fish. In other fish that I've looked at, there are really tight bundles. Parrot fish and chick RPE cells have bundles, but they don't move their granules.

QUESTION: (Dr. Burnside) What is the source of the dopamine?

BURNSIDE: Dopamine is released from interplexiform cells located in the inner retina. This dopamine would have to diffuse 50–100 μm to reach the RPE cells and thus is acting as a diffusible neuromodulator in this case. We have shown that the dopamine receptors located on the photoreceptors are D4 receptors, with binding constants for dopamine in the nanomolar range. We have not specifically characterized the receptors on RPE cells, but they have similar affinities for dopamine.

ELINSON: Paul (Forscher), without the myosin inhibition we see this tremendous retrograde flux. If you showed us a time lapse of that same effect under myosin inhibition, would we see the same speed of extension forward due to the actin polymerization?

FORSCHER: That's exactly what you see. There is an inverse proportional relationship between growth and flow. If you incrementally slow the flow, you get incremental growth by exactly the same amount.

ELINSON: So the myosin is actually competing against growth?

FORSCHER: I wouldn't say it's competing; there's a steady state. There are two processes going on: Under the conditions of these experiments, where the growth cone isn't really interacting with anything in the outside world, there's a futile cycle that is essentially assembling actin, and the myosins are pulling it back. The rate of assembly is matched by the rate of myosin action, and that's the retrograde flow rate. Superimposed on that, you can see fluctuations of the leading edge and fillopodia. This means that the rate of assembly is fluctuating slightly above and below the rate of retrograde flow, but they are not coupled. Basically the point of my talk was that, if you slow retrograde flow by an increment, you'll get extension that's perfectly proportional to that.

QUESTION: Does that mean that retrograde flow is an artifact of not being able to grasp?

FORSCHER: That's a second seminar. Briefly, we have measured retrograde flow and growth cone target interactions with neuronal substrates. When the growth cone can grab on to something with its myosin intact, it grabs on. The microtubules go toward the contact site, and the growth cone starts moving forward. There's a perfect correlation between growth and slowing of retrograde flow. But in this case, instead of turning the motor off, the motor is intact, and the actin inside is interacting through some adhesion proteins to grab onto the outside world.

BRADY: Growth cones don't normally go across glass cover slips, or for that matter, sheets of cells. They are often going through three-dimensional matrices of extracellular

matrix. That would probably fit more with the specific interactions with a substrate.

FORSCHER: One of the problems is that we've put these cells into an extremely artificial environment. In fact, *Aplysia* growth cones also look and behave somewhat differently when cultured on a more physiological substrate.

LANGFORD: Peter (Gillespie), I have a question about the other myosins. You mentioned that myosin Iβ is probably the adaptation motor. You have identified other myosins: what do you think they are doing?

GILLESPIE: One of the more striking localizations of myosin VI is in the cuticular plate, to which the stereocilia insert. The myosin seems to be rigidly associated there. In the cuticular plate there's an actin meshwork that's cross linked together, perhaps by myosin VI; maybe myosin VI is involved in forming the cuticular plate. There's more to it than that. I have looked at newly formed bundles from the cells most recently turned into hair cells. These cells have a lot of myosin VI in the stereocilia—not concentrated down at the tapers, but actually throughout the stereocilia. I don't know what it's doing there, but it's striking. My guess is that the bundle needs myosin VII for these linkages to hold the stereocilia together, so that the whole bundle can move, even when displacement is applied to only one part of the bundle. The nature of the linkages is unknown, but they probably also need an intracellular anchor, and this could be myosin VII. That's our hypothesis for the time being.

BURNSIDE: (Dr. Gillespie) In your preparations, do you think you have myosin without actin?

GILLESPIE: There's a tremendous amount of the myosin—both myosin VI and myosin VII—that's not particularly localized in any way. If you look at the hair-cell bodies, they have a ton of both myosin VI and myosin VII in the cytoplasm. If you permeabilize fixed cells with streptolysin O, most of the myosin VI diffuses away. It seems to be just sitting there, presumably not interacting with actin filaments. We don't know whether this is a reservoir, or what it's doing.

GILLESPIE: David Corey has shown that there are multiple splice-variants of myosin VI. We saw a 160-kD form in the hair bundle, whereas in the cell body there is the 150-kD form. We don't know what the source of that difference is, but it's intriguing.

GILLESPIE: We haven't done systematic studies in too many organisms. Most of the work is in frog and guinea pig. Unfortunately, labeling of myosin Iβ hasn't been done yet in a mammal. Labeling of myosin VI and myosin VII is consistent in the frog and the guinea pig, although it's not identical. With myosin VII you get labeling up and down the stereocilia—where these linkages are. Myosin VI is not at all prominent in stereocilia in guinea pig, and it took unusual experiments to see this labeling associated with tapers in frogs.

QUESTION: Peter (Gillespie), what's the evidence that the actin in the stereocilia is dynamic in any way; or is it always stable?

GILLESPIE: As far as we can tell it's stable, in the sense that the structure is not sensitive to cytochalasin. The actin is heavily crosslinked, and there's no evidence for any rapid turnover. On the other hand, it seems very unlikely that you make the actin when you build a hair cell, and that's it. There's got to be some mechanism for turning over the actin filaments or actin monomers, but there have been no systematic approaches to studying that yet. So we really don't know. I'm sure it's dynamic on some time scale.

BRADY: Beth (Burnside), your results quite clearly show that actin and myosins were involved in both directions of movement for your pigment granules.

BURNSIDE: We don't absolutely know that it's myosin.

BRADY: It certainly isn't microtubule-based, which is the point of the question. It's also true that the pigment-granule movement that you see looks very similar to pigment-granule movement in a wide variety of cell types; yet there's a very large literature arguing that microtubule-based transport occurs in these other cells. Would you like to comment on that?

BURNSIDE: We were shocked when we did the experiments. I talked to Leah Haimo who studies a fish dermal melanophore in which the microtubules are very clearly involved in the pigment migration. The literature of pigment migration in melanophores is extremely variable. So there really just may be a variety of different ways that cells move. One thing is that the speed of movement in the dermal melanophores is much faster. In our case, this is very slow and occurs at a rate that's similar to what happens in frog dermal melanophores. The evidence for the involvement of microtubules in frog dermal melanophores is not very good at all. I think it may be an adaptation to a slower movement, but I don't know why you should see saltation out, and smooth movement in. That's the same in both the microtubule-based system and in our system. I don't understand why that's the case.

BRADY: The other possibility is connected with the point you made about the organization. When you get rid of the microtubules in these cells, the processes stay pretty much the same. That's not necessarily true in some other cell types in which the

disruption of cytoplasm may be more pronounced.

BURNSIDE: That's a good point. Experiments in which microtubules are disrupted *in vivo* are much more difficult to interpret because neighboring cell types are also affected and indirect effects, for example, on signaling, cannot be ruled out. When we disrupted microtubules in isolated RPE-retina preparations, pigment aggregation was inhibited. I interpret that to mean that when the RPE apical projections are interdigitated with the photoreceptors as they are *in situ*, then microtubules are needed, perhaps for structural purposes such as maintaining a patent pathway for granule transport. Once the apical projections are stuck down to a cover slip, microtubules are not needed for normal pigment migration in either direction, suggesting that the structural support may be provided by the substrate under these conditions. In fact, when we disrupt microtubules in isolated, unattached RPE sheets, the apical projections disappear. We do not know whether they retract or become too fragile to withstand our handling procedures, but they are gone, suggesting that microtubules are needed for structural support when the projections are not attached to a substrate.

MANDOLI: Peter (Gillespie), you said that the sacculus was involved in orienting the frog. I was wondering whether you think that you would see an atrophy of the hairs in microgravity?

GILLESPIE: People have actually looked, and others could probably comment better on that than I can. Most species use the sacculus as a true vertical-acceleration detector for vestibular information. The frog uses it as a specialized detector for ground-borne vibration. When you sneak up and try to grab that frog for dinner, it feels you from 30 yards away, because it has adapted its sacculus to detect ground-borne vibration. I don't know what happens to the hair cells in space, but I know that it's been looked at.

MANDOLI: These linkages between the stereocilia, you said that they run all the way up and down?

GILLESPIE: You see the crosslinks between adjacent stereocilia from top to bottom.

MANDOLI: Is the localization of myosin VII consistent with that linkage?

GILLESPIE: The answer is yes, although that hasn't really been looked at systematically. It will be very informative to look at the chicken, where those linkages have been mapped out in different regions of different auditory and vestibular organs. We know what to expect there, so that will be a strong test of the hypothesis.

MORRIS: In mammals at least, hair cells have to last a lifetime. It's kind of intriguing to think of how you maintain this really nifty three-dimensional system and do repairs. I was wondering if there are any thoughts on whether a modification of the mechanism that's used for adaptation is used for getting new tip-link structures with the channels out to the tip.

GILLESPIE: That's exactly how I think of it. We've been recently doing experiments in which we break tip links with calcium chelators and watch them regenerate over a number of hours. As far as we can tell, the tip links seem to be coming from below the tips; we see evidence of linkages from below the tips. Transduction comes back over the same time course as tip links. Interestingly, there's much less adaptation after 24 h of regeneration in the chelator-treated regenerated cells than in the controls. I think that the adaptation motor or another myosin is involved in assembling everything together. This makes sense from a lot of points of view. We also have a strong suspicion that the stereociliary surface has much more than just one tip-link monomer per stereocilia. We have some indirect evidence that there's a reserve of that protein. One simple model is that you have a hemi-tip link on each stereocilium, and that these can come together and form an intact tip link. Each hemi-tip link is controlled by a motor. I don't actually believe that hypothesis for a number of reasons, but at least it's plausible. I think it's more likely that the extended part of the tip link is solubilized when we treat with calcium chelators, and that it has receptors on either stereocilia. But we don't know how it's all put together.

QUESTION: What is the tip link made of?

GILLESPIE: We have direct and relatively indirect evidence that it's glycoprotein. Regeneration is not blocked by cyclohexamide, so new protein synthesis is not needed, at least over 12 h. We don't know whether the tip link is stored in some reserve in the cell body and then brought out, or (as I have suggested before) whether there's a lot of the tip-link protein on the stereociliary surface that's brought together. We are interested in getting back to the myosin story. In the case of myosin Iβ, we always see fewer than every single stereocilia lit up at the tip by either of the myosin Iβ antibodies. That correlates with what is seen with scanning electron microscopy, particularly in the frog hair cell, where there are relatively few tip links. I think there's evidence that there is less than a full set of tip links at any given time in a frog's hair cell, perhaps because there's much more dynamic turnover of the transduction apparatus than we initially thought. The balance between tip link, transduction-apparatus insertion, and retrieval is affected.

BARLOW, R.: You show extreme changes in the angle of the stereocilia in your cartoons. How much movement actually takes place?

GILLESPIE: Very little. The stereocilia here are 8000 nm tall, and in the cochlear hair cell the stereocilia are 4000 nm tall. At the limits of human hearing you can detect displacement of the stereocilia of about 0.1 nm. You can show a pretty robust displacement of transduction current in response to a 1-nm displacement with mammalian cochlear hair cells *in vitro*. So the movements that are needed for gating the transduction channels are very small.

QUESTION: Is there any evidence as to exactly what type of glycoprotein makes up the tip link?

GILLESPIE: Not at the moment. There's a protein in muscle called titin that's involved in connecting the myosin filaments to the Z-line. Titin has the right properties to be a tip-link protein. It's an elastic, long and elongated (1 μm long), 4 MDa protein. Actually I don't think that the tip link is a titin homologue.

BARLOW, R.: The tip link would not work well if it were elastic.

GILLESPIE: We know that the element that gates the transduction channels is elastic. We need to have some elasticity in it. We do know whatever gates the transduction channel that we measure has a stiffness of about 0.5 mN/m.

BARLOW, R.: Being elastic, wouldn't the tip link lend itself to adaptation?

GILLESPIE: Not really. If you move the bundle, you want the displacement to supply a force to the transduction channel.

BARLOW, R.: But you don't want the tip link to stretch, rather you want it to be inelastic.

GILLESPIE: No, you actually want it to stretch some because you want the channels gate to respond to the tension in the gating spring, rather than to the displacement of the channel. We know that is how it works. Whether you want that or not is another matter.

BARLOW, R.: Beth (Burnside), you mentioned that the movement of these granules and the movement of the photoreceptors is to place the photoreceptors in what appears to be the preferred position. What's the evidence that this lends itself to sensitivity changes in the retina?

BURNSIDE: There isn't any evidence. Maureen Powers did a sabbatical in my lab and we used ERGs to try to ascertain whether changes in sensitivity could be correlated with changes in retinomotor position. In the whole fish it is extremely difficult to be sure you have produced a change in retinomotor position without changing anything else in the retina. We did show changes in sensitivity, but we could not convince ourselves that we were looking at specific effects of retinomotor position. We tried to look at isolated A-waves by knocking out photoreceptor synaptic transmission, but most of the effect we could detect was on B-waves, and thus possible contributions of altered signaling pathways in the inner retina could not be ruled out.

BARLOW, R.: Paul (Forscher), in the first experiment, was concanavalin A on the beads?

FORSCHER: In our initial experiments we used polycationic beads that were derivatized with polyethyleneimine. To our surprise we found that with highly charged polycationic beads you'd get triggering of new actin assembly. A bead that was moving retrograde would suddenly start whizzing around on a little jet of newly assembled actin. Since we didn't want that, we screened a battery of lectins and found that ConA binds to many *Aplysia* membrane proteins. If we derivatize a bead with ConA, we get a flow-coupled bead every time.

BARLOW, R.: When actin moves under the membrane, are membrane proteins moving with it?

FORSCHER: That's a very interesting question, but I didn't say that. We don't know whether the membrane proteins that bind ConA are actually moving with the actin before they bind to the bead. We have studied the detailed dynamics of the protein apCAM, which is an N-CAM analog. When a bead that's derivatized with an antibody against an extracellular epitope for that protein initially binds, it diffuses freely in the plane of the membrane. As the bead accumulates more and more of that protein over time, it couples to the actin flow. If you have enough density of antibody on the bead, it will trigger actin assembly by crosslinking apCAM. So it's complicated. We also know that unligated apCAM is normally a freely diffusible membrane protein; it doesn't tend to aggregate.

KUNG: Peter (Gillespie), if you cut the tip link and then stain for Iβ, does this protein still stay on top?

GILLESPIE: I haven't done that systematically, but I have done it over a short period of time, then treated with chelators and looked to see if there are any changes. There's nothing obvious. On the other hand, now that we know about the time course for tip-link regeneration and are also starting to get an idea about the time course of tip-link retrieval, we know that we are going to have to do those experiments over longer time periods.

BRADY: One point that didn't come out quite as much in these talks as it could have is that a lot of times different systems of motors do

interact with each other, and different cytoskeletal elements also interact with each other. Paul's (Forscher) work showed some of that, as did Beth's (Burnside) to some extent. There are examples in which actions or a mutation in a myosin has a suppressor that is a kinesin-like protein. This has boggled the imagination of people working on microtubule and microfilament motors. There are also examples in which knocking out one motor disrupts the mitotic spindle, and knocking out a second motor that happens to have a similar localization suppresses the initial mutation and restores function. Finally, there is an example that may be relevant to the comment about the dynamics of the stereocilia. Molecular dissections of regenerating cilia in *Chlamydomonas* have used genetic approaches to identify a number of motor proteins, in addition to the dyneins, that are important for assembly of cilia and apparently, in some cases, for the delivery of protein to construct a cilium. There are particles analogous to what Paul (Forscher) sees moving along the outside of cilia on the membrane, and there are kinesins in the center portion of the flagella. It's not clear what all of these different interactions may do. One thing that we probably want to consider is that many motors may serve not for movement, but for generating a dynamic tension on a structure necessary for function, or for mediating shape changes, or for assembly and disassembly of structures like the mitotic spindle.

SACK: I realize this may not be trivial. If one were to be able to place a microscope in a horizontal orientation and maintain the optics with a vertical stage, you might actually be able to test whether gravity affects the motility processes you described. This has been described in plant (*Chara*) cells—for example, in terms of the streaming rate. If you put the cell in a vertical orientation you can see differences in motility, downward-directed *versus* upward-directed. We don't know why that's important to the particular cells in which it occurs. The cytoskeleton certainly evolved to prevent stratification, but in plant cells motility is found to be under control. There's lots of signaling controlling it, and it's not a simple question of passive drag. I don't know if anybody has looked for this in animal systems. It would take a horizontal microscope, but it might uncover interactions of gravity with cytoskeleton.

FORSCHER: There is recent evidence that the localization of adhesion proteins may actually be influenced by tension generated by either tyrosine kinase dependent phosphorylation or myosin. This means that you can biochemically alter a protein's state by applying the appropriate force.

FORSCHER: (Dr. Burnside) Have you looked at particle movement on the surface of your cells?

BURNSIDE: We tried to do that using your derivatized-bead approach with positively charged beads, but we could never get them to stick.

QUESTION: I have one comment and a question about the sacculus in the frogs. First of all, it is known that the sacculus of frogs also has acoustic sensitivity, just as it serves as a gravistatic organ. There's evidence not only in mammals, but in frogs, and of course in fishes, where the sacculus can function as an acoustic organ, a gravistatic organ, or both. My question to Dr. Gillespie is, How confident can we be that what you've found about the sacculus is going to be true of other otolithic end organs, or even of what's going on in hair cells in the cochlea?

GILLESPIE: That's something that has concerned us for many years, and Jim Hudspeth in particular who has developed the molecular approach to hair cells with the frog sacculus. Although that question is continuously raised, every time that we have found something interesting and important in the frog hair cell—be it adaptation or gating compliance in the transduction channel apparatus, or what have you—it turns out to have a parallel in every other system that's been looked at. We've started looking at myosin Iβ in utricular hair cells, in collaboration with Richard Baird. It seems to be there with a relatively similar distribution. We are particularly interested in what's going on in the utricular cells. Richard has shown that different cell types in the utriculus, which has a much less uniform population of cell types, have different adaptation kinetics. We are wondering whether that will give us any more clues as to the identity and properties of the adaptation. I think that the sacculus is a very useful model system in which many of the basic principles will apply. There are going to be some differences, and there are going to be some specializations for its particular role, but by and large I think that it's a useful system to work on.

QUESTION: Dr. Gillespie) what is your opinion on why the hair cells in the cochlea of mammals don't have kinocilium?

GILLESPIE: The hypothesis that makes the most sense to me is that cochlear hair cells respond to extremely high frequencies, and a microtubule-based cilium may be an impediment to very fast movement of a hair bundle. The stereocilia may be moved very readily and faster, because they are tapered and pivot readily at their bases.

HIGHSTEIN: Another hypothesis that might be more appropriate is that the inner hair cells are not directly attached to the tectorial mem-

brane. The difference in these hair-cell systems seems to be the accessory apparatus, rather than the hair cells themselves. Depending on how the bundle is coupled into the accessory apparatus, this energy is coupled into the accessory apparatus; you can sense angular acceleration, linear acceleration, and so forth. In the cochlea the frequency argument has been put forward. Another possibility is that there is no direct attachment to the tectorial membrane in the inner hair cells, and the fluid movement itself may be what's deviating the cilia.

GILLESPIE: That's true. Outer hair cells do seem to be attached, and they have no kinocilia either. You are absolutely right.

Reference: *Biol. Bull.* **192:** 197–199. (February, 1997)

Chairs and Speakers

Workshop Chair
GEORGE M. LANGFORD, Ph.D.
Department of Biological Sciences
6044 Gilman Labs
Dartmouth College
Hanover, NH 03755
603-646-1331
Fax: 603-646-1347
E-mail: George.M.Langford@Dartmouth.EDU

ROBERT C. ANGERER, Ph.D.
Department of Biology
University of Rochester
Rochester, NY 14627
716-275-8715
Fax: 716-275-2070
E-mail: rangerer@rca.biology.rochester.edu

LYNNE M. ANGERER, Ph.D.
Department of Biology
University of Rochester
Rochester, NY 14627
716-275-3215
Fax: 716-275-2070
E-mail: langerer@la.biology.rochester.edu

ANDREW H. BASS, Ph.D.
Department of Neurobiology and Behavior
Seeley G. Mudd Hall
Cornell University
Ithaca, NY 14853-2702
607-254-4340
Fax: 607-254-4308
E-mail: ahb3@cornell.edu

DOUGLAS A. BAXTER, Ph.D.
Department of Neurobiology and Anatomy
University of Texas Medical School at Houston
Houston, TX 77030
713-792-5720
Fax: 713-500-0621
E-mail: dbaxter@nba19.med.uth.tmc.edu

SCOTT T. BRADY, Ph.D.
Department of Cell Biology and Neuroscience
Southwestern Medical Center at Dallas
5323 Harry Hines Blvd.
Dallas, TX 75235
214-648-1830
Fax: 214-648-1801
E-mail: SCOTT.BRADY@EMAIL.SWMED.EDU

BETH BURNSIDE, Ph.D.
Department of Molecular and Cell Biology
335 LSA-3200
University of California
Berkeley, CA 94720
510-642-3200
Fax: 510-643-6791
E-mail: burnside@violet.berkeley.edu

MARTIN CHALFIE, Ph.D.
Department of Biological Sciences
1012 Sherman Fairchild
Columbia University
New York, NY 10027
212-854-8870
Fax: 212-865-8246
E-mail: chalfie@cubsps.bio.columbia.edu

ROBERT C. EATON, Ph.D.
Center for Neuroscience
Department of Biology (EPO Box 334)
University of Colorado
Boulder, CO 80309

303-492-6536
Fax: 303-492-8699
E-mail: mauthner@colorado.edu

RICHARD P. ELINSON, Ph.D.
Department of Zoology
University of Toronto
25 Harbord Street
Toronto, M5S 3G5 Canada
416-978-4445
Fax: 416-978-8532
E-mail: elinson@zoo.utoronto.ca

JOSEPH R. FETCHO, Ph.D.
Department of Neurobiology and Behavior
State University of New York at Stony Brook
Stony Brook, NY 11794-5230
516-632-8698
Fax: 516-632-6661
E-mail: JFetcho@ccmail.sunysb.edu

THOMAS M. FISCHER, Ph.D.
Department of Psychology
P.O. Box 208205
Yale University
New Haven, CT 06520-8205
203-432-4676
Fax: 203-432-4690
E-mail: fischer@compuslug.psych.yale.edu

PAUL FORSCHER, Ph.D.
Department of Biology KBT 338
P.O. Box 208103
Yale University
New Haven, CT 06520
203-432-6344
Fax: 203-432-6161
E-mail: paul.forscher@yale.edu

PETER GILLESPIE, Ph.D.
Department of Physiology
The Johns Hopkins University School of Medicine,
WBSB 205
725 N. Wolfe Street
Baltimore, MD 21205-2185
410-614-3083
Fax: 410-955-0461
E-mail: Peter_Gillespie@qmail.bs.jhu.edu

EDWARD M. GOOLISH, Ph.D.
Space Station Biological Research Project
NASA Ames Research Center
T20G-2
Moffett Field, CA 94035
415-604-1961
Fax: 415-604-1701
E-mail: ed_goolish@qmgate.arc.nasa.gov

DR. DONAT-PETER HÄDER
Institute for Botany and Pharmaceutical Biology
Staudtstrasse 5, D-91058
Erlangen, Germany
49-9131-858216
Fax: 49-9131-858215
E-mail: dphaeder@biologie.uni-erlangen.de

OWEN HAMILL, Ph.D.
Department of Physiology & Biophysics
University of Texas Medical Branch
Galveston, TX 77555-0641
409-772-5464
Fax: 409-772-3381
E-mail: ohamill@beach.utmb.edu

MASASHI KAWASAKI, Ph.D.
Department of Biology
Gilmer Hall, Room 277
University of Virginia
Charlottesville, VA 22903
804-982-5763
Fax: 804-982-5626
E-mail: mk3u@virginia.edu

JOHN Z. KISS, Ph.D.
Department of Botany
Miami University
Oxford, OH 45056
513-529-5428
Fax: 513-529-4243
E-mail: kissjz@muohio.edu

CHING KUNG, Ph.D.
Laboratory of Molecular Biology
R. M. Bock Laboratories
University of Wisconsin
1525 Linden Drive
Madison, WI 53706-1596
608-262-2059
Fax: 608-262-4570
E-mail: ckung@macc.wisc.edu

WERNER R. LOEWENSTEIN, Ph.D.
Laboratory of Cell Communication
Marine Biological Laboratory
7 MBL Street
Woods Hole, MA 02543
508-289-7430
Fax: 508-548-2003
E-mail: lhoward@mbl.edu

ROBERT E. MAXSON, Ph.D.
633 Norris Hospital
USC Medical School
1441 Eastlake Avenue
Los Angeles, CA 90033
213-764-0633
Fax: 213-342-2764
E-mail: maxson@zygote.hsc.usc.edu

CATHERINE E. MORRIS, Ph.D.
Neurosciences Department—Loeb Institute
Ottawa Civic Hospital
1053 Carling Avenue
Ottawa, Ontario, K1Y 4E9 Canada
613-761-5073
Fax: 613-761-5330
E-mail: morris@civich.ottawa.on.ca

DR. PETER NICK
Institut für Biologie II/Botanik
Schänzlestrasse 1
D-79104 Freiburg, Germany
49-761-203-2646
Fax: 49-761-203-2612
E-mail: pnick@ruf.uni-freiburg.de

SIMON OSTRACH, Ph.D.
Mechanical and Aerospace Engineering
Case Western Reserve University
Cleveland, OH 44106
216-368-2940
Fax: 216-368-6445
E-mail: sxo3@po.cwru.edu

STANLEY J. ROUX, JR., Ph.D.
Department of Botany
University of Texas at Austin
Austin, TX 78713-7640
512-471-5858
Fax: 512-471-3878
E-mail: sroux@uts.cc.utexas.edu

FRED D. SACK, Ph.D.
Department of Plant Biology
Ohio State University
182 Botany and Zoology Bldg.
1735 Neil Avenue
Columbus, OH 43210
614-292-0896
Fax: 614-292-6345
E-mail: fsack@magnus.acs.ohio-state.edu

Reference: *Biol. Bull.* **192**: 200–201. (February, 1997)

Participants

JELLE ATEMA, Ph.D.
B.U. Marine Program
Marine Biological Laboratory
Tel: 508-289-7499
E-mail: atema@bio.bu.edu

MEL AVERNER, Ph.D.
NASA Headquarters
E-mail: maverner@gm.olmsa.hq.nasa.gov

ROBERT BAKER, Ph.D.
New York University Medical Center
Tel: 212-263-5402

ROBERT BARLOW, Ph.D.
Marine Biological Laboratory
Tel: 508-289-7356

FR. J. D. CASSIDY, O.P., Ph.D.
Providence College

MARY ANNE FREY, Ph.D.
NASA Headquarters
E-mail: mafrey@gm.olmsa.hq.nasa.gov

CHANDLER FULTON, Ph.D.
Brandeis University
Tel: 617-736-3150
E-mail: fulton@binah.cc.brandeis.edu

STEPHEN M. HIGHSTEIN, M.D., Ph.D.
Washington University
St. Louis
E-mail: highstein@WUMS.WUSTL.EDU

WILLIAM P. JACOBS, Ph.D.
Department of Molecular Biology
Princeton University
Tel: 609-924-2[illegible]

CELESTE JARVIS
Information Dynamics
Tel: 202-488-5126
E-mail: cjarvis@hq.nasa.gov

YI LI, Ph.D.
Kansas State University
Tel: 913-532-6360
E-mail: yili@ksu.ksu.edu

TERRI LOMAX, Ph.D.
Oregon State University
E-mail: lomaxt@bcc.orst.edu

BRIAN LOWE
Boston University
Tel: 508-548-5169
E-mail: btlowe@bio.bu.edu

DINA MANDOLI, Ph.D.
University of Washington
E-mail: mandoli@u.washington.edu

ALLEN MENSINGER, Ph.D.
Washington University
St. Louis
E-mail: MENSINA@TFNEURON.WUSTL.EDU

ENRICO NASI, Ph.D.
Boston University School of Medicine
Tel: 617-638-4347
E-mail: enasi@acs.bu.edu

KENNA PEUSNER, Ph.D.
George Washington University
Tel: 202-994-3489

D. MARSHALL PORTERFIELD
Louisiana State University
Tel: 504-388-1464
E-mail: MPFIELD@AOL.COM

JOHN D. RUMMEL, Ph.D.
Marine Biological Laboratory
Tel: 508-289-7218

TOM SCOTT, Ph.D.
NASA Headquarters
Tel: 202-488-5145
E-mail: tscott@gm.olmsa.hq.nasa.gov

ROBERT B. SILVER, Ph.D.
Marine Biological Laboratory
Tel: 508-548-3705
E-mail: rsilver@mbl.edu

RAQUEL SUSSMAN, Ph.D.
Marine Biological Laboratory
Tel: 508-289-7241

DANIEL TOMSIC, Ph.D.
NIH
Tel: 301-496-3868
E-mail: TOMSIC@CODON.NIH.GOV

PEI-LAN TSOU
Department of Botany
North Carolina State University
Tel: 919-515-3345
E-mail: ptsou@unity.ncsu.edu

CHARLES E. WADE, Ph.D.
NASA Ames Research Center
Tel: 415-604-3943

NORMAN WAINWRIGHT, Ph.D.
Marine Biological Laboratory
Tel: 508-289-7343
E-mail: nwainwri@mbl.edu

RON J. WHITE, Ph.D.
NASA Headquarters
Tel: 202-358-2194
E-mail: rjwhite@gm.olmsa.hq.nasa.gov

MICHAEL WIEDERHOLD, Ph.D.
University of Texas Health Science Center
San Antonio
E-mail: WIEDERHOLD@UTHSCSA.EDU

SARAH WYATT, Ph.D.
Department of Botany
North Carolina State University
E-mail: Sarah_Wyatt@ncsu.edu

STEVE ZOTTOLI, Ph.D.
Williams College
E-mail: Steven.J.Zottoli@williams.edu

CONTENTS

Volume 192 Number 2

THE BIOLOGICAL BULLETIN

APRIL, 1997

Published by the Marine Biological Laboratory

We've Turned the World of Confocal Microscopy

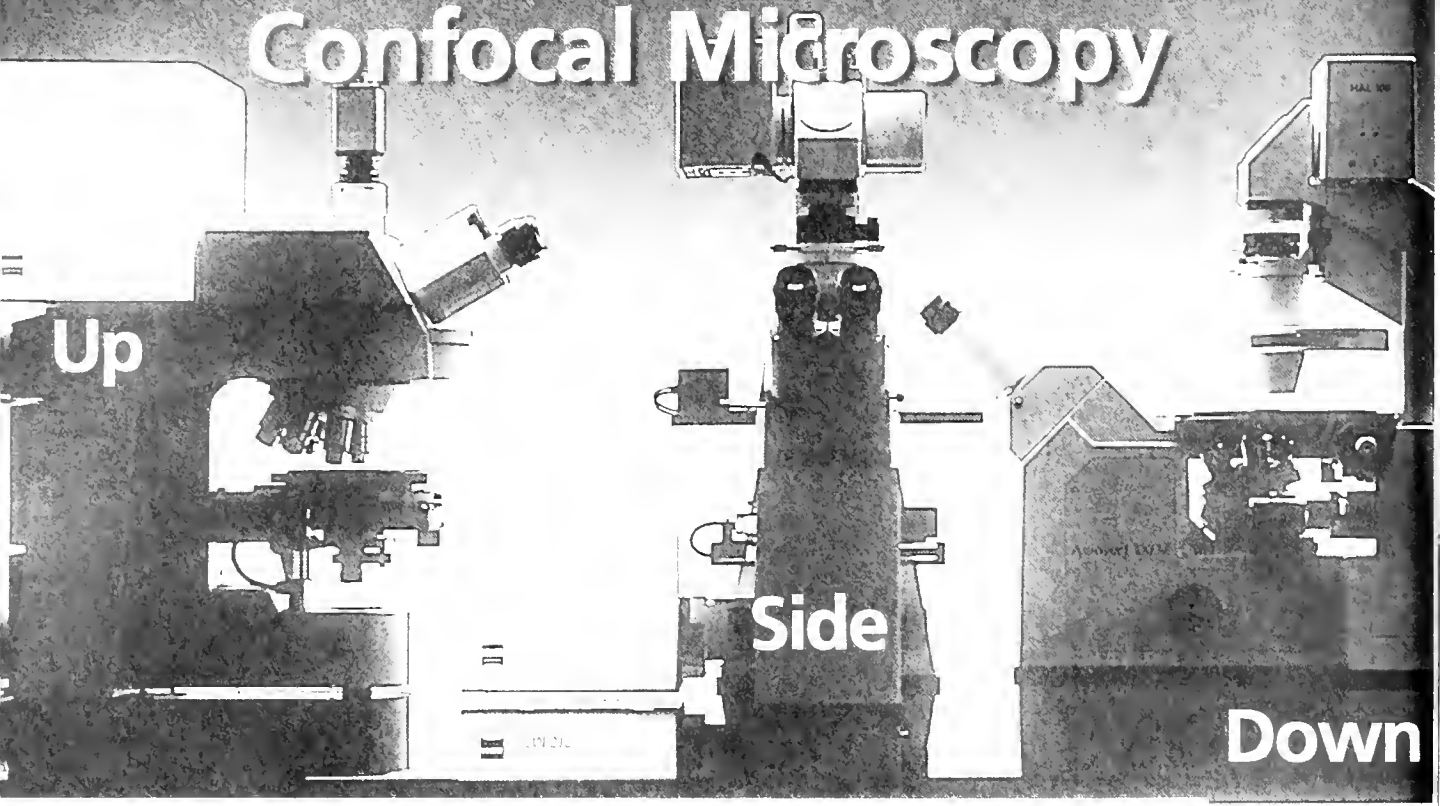

Confocal perfection. Are first-class technology and flexibility your prime concerns in choosing a confocal microscope? The new LSM 510 Laser Scan Microscope has it all: innovative high-end technology; unparalleled ease of operation with advanced software; compact scanning module that fits both inverted and upright microscopes.

Scanning flexibility. Unique scanning capabilities open up new possibilities. Significant specimen characteristics are no longer hidden. 3D imaging, interactive XY scanning. What you've always wanted in a confocal microscope is now a reality.

Images of a new quality. Four simultaneous fluorescence channels, each with computer-controlled pinhole. Scanning fields up to 2048 x 2048 pixels, plus 4 x 12 bit resolution. Integration, oversampling, quasi-photon counting. See what you're missing - with the new LSM 510. It is confocal imaging at its best.

ZEISS

Zeiss Optical Systems, Inc. · Thornwood, NY 10594
(800) 982-6493 · Fax 914-681-7446 · micro@zeiss.com · www.zeiss.com

THE BIOLOGICAL BULLETIN

PUBLISHED BY
THE MARINE BIOLOGICAL LABORATORY

APRIL, 1997

Printed and Issued by
LANCASTER PRESS, Inc.
3575 HEMPLAND ROAD
LANCASTER, PA

THE BIOLOGICAL BULLETIN

THE BIOLOGICAL BULLETIN is published six times a year by the Marine Biological Laboratory, 7 MBL Street, Woods Hole, Massachusetts 02543.

Subscriptions and similar matter should be addressed to Subscription Manager, THE BIOLOGICAL BULLETIN, Marine Biological Laboratory, 7 MBL Street, Woods Hole, Massachusetts 02543. For 1997, a lower rate is available to individual subscribers (as distinguished from libraries and institutions). Single numbers: $40 for libraries; $20 for individuals. Subscription per volume (three issues): $97.50 for libraries; $50 for individuals. Subscription per year (six issues, two volumes): $195 for libraries; $100 for individuals.

Communications relative to manuscripts should be sent to Michael J. Greenberg, Editor-in-Chief, or Pamela L. Clapp, Managing Editor, at the Marine Biological Laboratory, 7 MBL Street, Woods Hole, Massachusetts 02543. Telephone: (508) 289-7428, FAX: 508-457-1924, E-mail: pclapp@mbl.edu.

http://www.mbl.edu/BiologicalBulletin/

The home page for the electronic companion to THE BIOLOGICAL BULLETIN—*the Marine Models Electronic Record*—and other BIOLOGICAL BULLETIN publications is available on the World Wide Web at the address shown above.

THE BIOLOGICAL BULLETIN is indexed in bibliographic services including *Index Medicus* and MEDLINE, *Chemical Abstracts, Current Contents, CABS (Current Awareness in Biological Sciences),* and *Geo Abstracts.*

Printed on acid free paper,
effective with Volume 180, Issue 1, 1991.

POSTMASTER: Send address changes to THE BIOLOGICAL BULLETIN, Marine Biological Laboratory, 7 MBL Street, Woods Hole, MA 02543.

Periodicals postage paid at Woods Hole, MA, and additional mailing offices.
ISSN 0006-3185

INSTRUCTIONS TO AUTHORS

The Biological Bulletin accepts outstanding original research reports of general interest to biologists throughout the world. Papers are usually of intermediate length (10–40 manuscript pages). A limited number of solicited review papers may be accepted after formal review. A paper will usually appear within four months after its acceptance.

Very short, especially topical papers (less than 9 manuscript pages including tables, figures, and bibliography) will be published in a separate section entitled "Research Notes." A Research Note in *The Biological Bulletin* follows the format of similar notes in *Nature.* It should open with a summary paragraph of 150 to 200 words comprising the introduction and the conclusions. The rest of the text should continue on without subheadings, and there should be no more than 30 references. References should be referred to in the text by number, and listed in the Literature Cited section in the order that they appear in the text. Unlike references in *Nature,* references in the Research Notes section should conform in punctuation and arrangement to the style of recent issues of *The Biological Bulletin.* Materials and Methods should be incorporated into appropriate figure legends. See the article by Lohmann *et al.* (October 1990, Vol. **179:** 214–218) for sample style. A Research Note will usually appear within two months after its acceptance.

The Editorial Board requests that regular manuscripts conform to the requirements set below; those manuscripts that do not conform will be returned to authors for correction before review.

1. ***Manuscripts.*** Manuscripts, including figures, should be submitted in triplicate. (Xerox copies of photographs are not acceptable for review purposes.) The submission letter accompanying the manuscript should include a telephone number, aFAX number, and (if possible) an E-mail address for the corresponding author. The original manuscript must be typed in no smaller than 12 pitch or 10 point, using double spacing (*including* figure legends, footnotes, bibliography, etc.) on one side of 16- or 20-lb. bond paper, 8½ by 11 inches. Please, no right justification. Manuscripts should be proofread carefully and errors corrected legibly in black ink. Pages should be numbered consecutively. Margins on all sides should be at least 1 inch (2.5 cm). Manuscripts should conform to the *Council of Biology Editors Style Manual,* 5th Edition (Council of Biology Editors, 1983) and to American spelling. Unusual abbreviations should be kept to a minimum and should be spelled out on first reference as well as defined in a footnote on the title page. Manuscripts should be divided into the following components: Title page, Abstract (of no more than 200 words), Introduction, Materials and Methods, Results, Discussion, Acknowledgments, Literature Cited, Tables, and Figure Legends. In addition, authors should supply a list of words and phrases under which the article should be indexed.

2. ***Title page.*** The title page consists of a condensed title or running head of no more than 35 letters and spaces, the manuscript title, authors' names and appropriate addresses,

and footnotes listing present addresses, acknowledgments or contribution numbers, and explanation of unusual abbreviations.

3. ***Figures.*** The dimensions of the printed page, 7 by 9 inches, should be kept in mind in preparing figures for publication. We recommend that figures be about 1½ times the linear dimensions of the final printing desired, and that the ratio of the largest to the smallest letter or number and of the thickest tothe thinnest line not exceed 1:1.5. Explanatory matter generally should be included in legends, although axes should always be identified on the illustration itself. Figures should be prepared for reproduction as either line cuts or halftones. Figures to be reproduced as line cuts should be unmounted glossy photographic reproductions or drawn in black ink on white paper, good-quality tracing cloth or plastic, or blue-lined coordinate paper. Those to be reproduced as halftones should be mounted on board, with both designating numbers or letters and scale bars affixed directly to the figures. All figures should be numbered in consecutive order, with no distinction between text and plate figures and cited, in order, in the text. The author's name and an arrow indicating orientation should appear on the reverse side of all figures.

Color: The Biological Bulletin will publish color figures and plates, but must bill authors for the actual additional cost of printing in color. The process is expensive, so authors with more than one color image should—consistent with editorial concerns, especially citation of figures in order—combine them into a single plate to reduce the expense. On request, when supplied with a copy of a color illustration, the editorial staff will provide a pre-publication estimate of the printing cost.

4. ***Tables, footnotes, figure legends, etc.*** Authors should follow the style in a recent issue of *The Biological Bulletin* in preparing table headings, figure legends, and the like. Because of the high cost of setting tabular material in type, authors are asked to limit such material as much as possible. Tables, with their headings and footnotes, should be typed on separate sheets, numbered with consecutive Roman numerals, and placed after the Literature Cited. Figure legends should contain enough information to make the figure intelligible separate from the text. Legends should be typed double spaced, with consecutive Arabic numbers, on a separate sheet at the end of the paper. Footnotes should be limited to authors' current addresses, acknowledgments or contribution numbers, and explanation of unusual abbreviations. All such footnotes should appear on the title page. Footnotes are not normally permitted in the body of the text.

5. ***Literature cited.*** In the text, literature should be cited by the Harvard system, with papers by more than two authors cited as Jones *et al.*, 1980. Personal communications and material in preparation or in press should be cited in the text only, with author's initials and institutions, unless the material has been formally accepted and a volume number can be supplied. The list of references following the text should be headed Literature Cited, and must be typed double spaced on separate pages, conforming in punctuation and arrangement to the style of recent issues of *The Biological Bulletin*. Citations should include complete titles and inclusive pagination. Journal abbreviations should normally follow those of the U. S. A. Standards Institute (USASI), as adopted by BIOLOGICAL ABSTRACTS and CHEMICAL ABSTRACTS, with the minor differences set out below. The most generally useful list of biological journal titles is that published each year by BIOLOGICAL ABSTRACTS (BIOSIS List of Serials; the most recent issue). Foreign authors, and others who are accustomed to using THE WORLD LIST OF SCIENTIFIC PERIODICALS, may find a booklet published by the Biological Council of the U.K. (obtainable from the Institute of Biology, 41 Queen's Gate, London, S.W.7, England, U.K.) useful, since it sets out the WORLD LIST abbreviations for most biological journals with notes of the USASI abbreviations where these differ. CHEMICAL ABSTRACTS publishes quarterly supplements of additional abbreviations. The following points of reference style for THE BIOLOGICAL BULLETIN differ from USASI (or modified WORLD LIST) usage:

A. Journal abbreviations, and book titles, all underlined (for *italics*)

B. All components of abbreviations with initial capitals (not as European usage in WORLD LIST *e.g., J. Cell. Comp. Physiol.* NOT *J. cell. comp. Physiol.*)

C. *All* abbreviated components must be followed by a period, whole word components *must not* (*i.e., J. Cancer Res.*)

D. Space between all components (*e.g., J. Cell. Comp. Physiol.*, not *J.Cell.Comp.Physiol.*)

E. Unusual words in journal titles should be spelled out in full, rather than employing new abbreviations invented by the author. For example, use *Rit Vísindafjélags Islendinga* without abbreviation.

F. All single word journal titles in full (*e.g., Veliger, Ecology, Brain*).

G. The order of abbreviated components should be the same as the word order of the complete title (*i.e., Proc.* and *Trans.* placed where they appear, not transposed as in some BIOLOGICAL ABSTRACTS listings).

H. A few well-known international journals in their preferred forms rather than WORLD LIST or USASI usage (*e.g., Nature, Science, Evolution* NOT *Nature, Lond., Science, N.Y.; Evolution, Lancaster, Pa.*)

6. ***Reprints, page proofs, and charges.*** Authors receive their first 100 reprints (without covers) free of charge. A $25 surcharge will be added for each 100 reprints (including the first 100) of articles that include color illustrations. Additional reprints may be ordered at time of publication and normally will be delivered about two to three months after the issue date. Authors (or delegates for foreign authors) will receive page proofs of articles shortly before publication. They will be charged the current cost of printers' time for corrections to these (other than corrections of printers' or editors' errors). Other than these charges for authors' alterations, *The Biological Bulletin* does not have page charges.

Reference: *Biol. Bull.* **192:** 203–207. (April, 1997)

Choreography of the Squid's "Nuptial Dance"

WARWICK H. H. SAUER[1], MIKE J. ROBERTS[2], MAREK R. LIPINSKI[2], MALCOLM J. SMALE[3], ROGER T. HANLON[4], DALE M. WEBBER[5], AND RON K. O'DOR[5]

[1]*Department of Ichthyology and Fisheries Science, Rhodes University, P.O. Box 94, Grahamstown 6140, South Africa;* [2]*Sea Fisheries Research Institute, Cape Town 8012, South Africa;* [3]*Port Elizabeth Museum, Humewood 6013, Port Elizabeth, South Africa;* [4]*Marine Biological Laboratory, Woods Hole, Massachusetts 02543, USA; and* [5]*Dalhousie University, Halifax, Canada B3H 4J1*

A mass spawning of squid resembles, at first glance, a chaotic "nuptial dance" (1). But for the first time, we have applied 3-D, radio-linked acoustic positioning (RAP) to this confusing process, and our early results now reveal a choreography that is, in fact, well organized in time and space. Remote tracking with RAP of individual Loligo vulgaris reynaudii *off South Africa has provided insights into the daily sequence of behaviors that lead these animals to aggregate for sexual selection. Each dawn, the squid navigate for several kilometers, toward the shore, to small, well-defined zones near egg beds on the substrate. After several hours of circling above these egg beds, a pelagic, 3-D lek-like aggregation of large males forms; females are drawn in, and the aggregation condenses as the females and males pair, mate, and lay eggs. Smaller "sneaker males" remain on the periphery of the mating arena and, from this station, attempt extra-pair copulations (EPCs). The mating system of squids is thus unexpectedly complex, rivaling those of mammals and birds (2, 3). Commercial squid-jigging fishermen in South Africa have recently been attracted to the spawning grounds, and they have been successful. Moreover, their activities may be selective for large males. Thus, attention should be devoted to ensuring that such targeted fishing does not alter the characteristics of squid population genetics. Remote tracking and video observations, in combination with genetic analyses, may offer a new opportunity to monitor mating effort and reproductive success, and thus to manage the fishery.*

Determining the reproductive behavior of highly mobile marine animals is challenging, but the results can be rewarding, particularly in situations in which the species is the target of a fishery that is conducted directly on the spawning grounds. Collaborative efforts between the fishermen's cooperatives and the government's Sea Fisheries Research Institute led to the present study, which was conducted in November 1993 and November 1994 in Oyster Bay, South Africa. Underwater visibility was limited and diving conditions were treacherous, thus the observations of squid behavior by divers during these periods were substantially complemented by an analysis of data collected by remote tracking.

Eight squid were fitted with acoustic transmitters that produced pulses of 50–80 kHz "pings." The devices were placed within the mantle cavity and attached to the mantle wall by a hypodermic needle that was thrust through the wall, crimped, and secured with silicone washers (see 4). Four of the eight squid were large males (430 g; mantle length [ML] about 32 cm), two carrying Vemco V16T-3H telemetry tags with a thermistor-controlled pulse interval, one a V16-3H pinger (all, 70 × 16 mm diameter), and one a V8-2L pinger with a constant pulse interval of about 1 s (35 × 8 mm diameter). These transmitters encoded temperatures in the intervals between pings (as the data on depth and jet pressure had been telemetered in previous studies; 4). In addition, two small "sneaker" males (70 g; about 15 cm ML) and two females (180 g; about 21 cm ML) each carried V8-2L pingers. The data supplied by all of these transmitters are equivalent to those provided by long-term, focal sampling of animal behavior (5).

The acoustic transmitters borne by the squids were tracked for 14 days by four hydrophone-equipped RAP buoys (Vemco Ltd., Shad Bay, NS, Canada) moored in Oyster Bay in a 45-m square over two small egg beds (each about 1 × 2 m) located 1 km offshore. The buoys monitored the arrival times of signals from the tagged

Received 23 May 1996; accepted 29 January 1997.

squid and transmitted them by radio to a base station, which used a triangulation routine (6) to calculate 3-D positions. The eight squid were tracked for a total of 54 animal-days (maximum for one individual, 14 d). They produced 35 megabytes of positional data, and the four large male squid produced temperature data as well.

Data from transmitters fixed to the substrate were compared with data from diver-transported units so that the accuracy of the software in its present state of development could be evaluated. These tests showed position accuracy of less than 1 m inside the array of RAP buoys, decreasing to 5–10 m at a 150-m radius from the center of the array (note Fig. 2). Full resolution of point-by-point tracks requires a complex post-analysis that is still in progress, but 10-20 s averaging gave reasonable, real-time tracks for typical squid speeds of 10-50 cm s^{-1}. At worst, a squid moving 50 cm s^{-1}, signaling its position every 20 s, produces points 10 m apart at 150 m from the center of the array; smaller movements are usually recorded at slower speeds.

The eight squid being tracked were consistently present near the array during the day. The diel rhythmicity with which the three types of squid appeared on the egg beds is illustrated in Figure 1. These behavioral observations are limited in number, but they are consistent; this consistency, together with our previous experience (4), indicates that acoustically tagged squid show the normal range of movement.

At dawn, the squid arrived in the vicinity of the egg beds. The large males made circles (50–150 m radius) around the area (records of these and subsequent movements are shown in Fig. 2). Females and other males gradually joined the large males as they coalesced into a 3-D mating arena that was generally situated within 10 m of the substrate (typical depths were 20–30 m). Agonistic behavior among males was very striking and

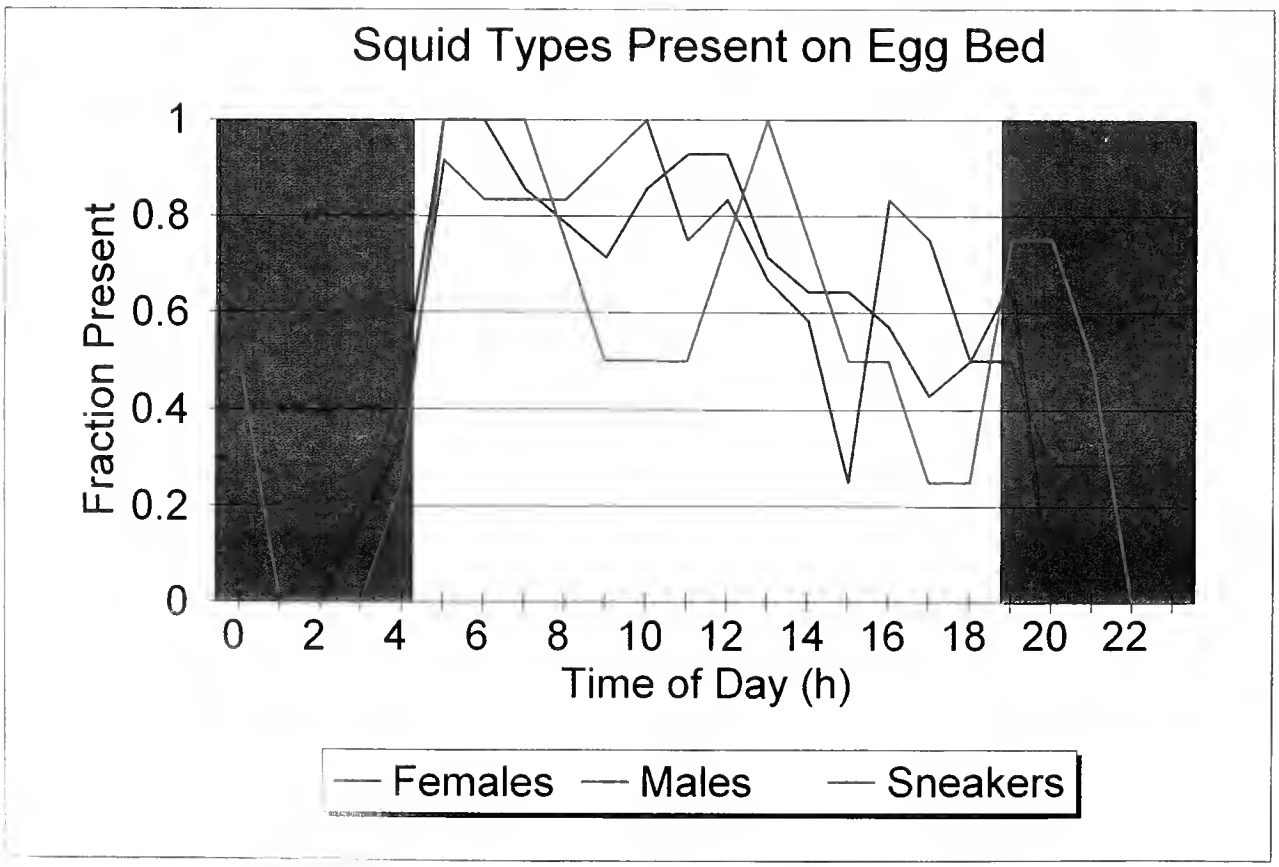

Figure 1. Diel patterns of squid visitations to the egg bed, shown as the ratio of hours present to hours monitored. Three large males (blue, 32 cm mantle length) were monitored over 8 full days, two females (green, 21 cm ML) over 7 days, and two small "sneaker" males (red, 15 cm ML) over 2 days. Females and sneakers from offshore appear at dawn and often remain past dusk. Large males also appear at dawn, although numbers peak later; they often disappear by noon and make brief return visits before moving offshore at dusk. A trade-off between detailed tracking of individuals and continuous monitoring of all frequencies makes statistical analysis of daytime data difficult, but continuous monitoring at night (1800 h–0400 h) did not indicate the presence of large males or females, so patterns are clearly distinct.

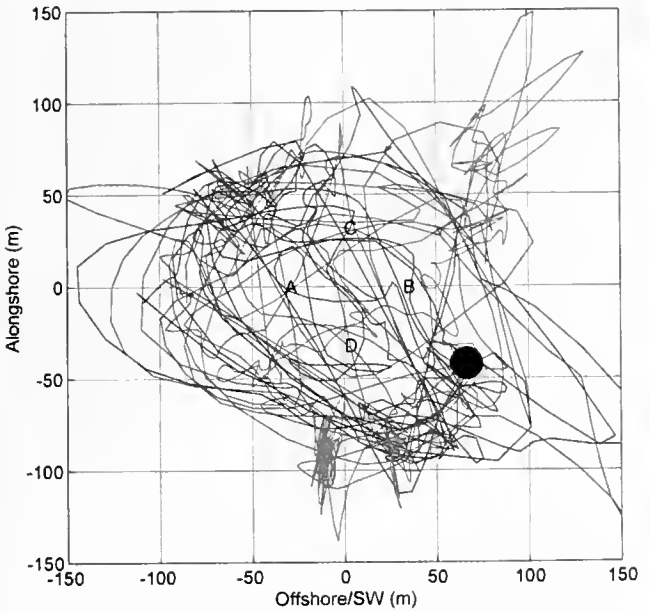

Figure 2. Overhead view of a typical full day of tracks for a large male (blue), a female (green), and a sneaker male (red); full details of behaviors can be replayed on computer animations. The black dot identifies an egg mass confirmed by divers; video surveys also showed numerous squid and scattered egg fingers beneath the area of heavy tracks on the opposite side of the array. Ten days of similar records show that males and females begin at dawn making circles of 50–150 m radius, high in the water column, around the sonobuoy array (A,B,C,D). Circling decreases by mid-morning, and in the afternoon females spend more time near bottom at individual egg patches. Sneaker males remain outside the main arena, low in the water column and near egg patches; direct observations show that they rush in to intercept pairs. Speeds average 18 cm s^{-1} for females, 14 cm s^{-1} for large males, and 17 cm s^{-1} for small sneakers.

common as they competed for temporary pairings with females (7; unpubl. results). The paired large males and females mated, and the female then moved with her partner to the substrate to deposit her "egg fingers" (Fig. 3). Although these squid need adjacent bottom for egg-finger attachment, criteria for such beds are not stringent. Lone large males often waited near the egg beds to intercept pairs moving to and from the communal egg beds.

This activity—repeated mating and egg laying with a series of temporary partners—often continued for 1–2 h after sunset (Fig. 1). Meanwhile, the sneaker males remained all day at the periphery of the arenas (Figs. 1 and 2). In this station, presumably, they are maximizing their opportunities for extra-pair copulations (EPCs): that is, watching for females temporarily paired with larger males; then, after the pair has mated, swimming rapidly into the arena to mate briefly with those females (Fig. 4). The mean duration of a sneaker male's mating was only 6 s; in contrast, large males mated for 16–20 s (7). Large males occasionally left during the day, and one

Figure 3. Photo of a large male escorting a female squid (*Loligo vulgaris reynaudii*) as she attaches an "egg finger" of about 100 eggs to an egg bed. Photo by MJS.

was tracked manually by boat to another mating arena 1.5 km alongshore. Tagged large males were apparently unsuccessful in mating, as evidenced by the short time they spent near the egg beds. In contrast, paired males escort female mates to the egg beds and guard them as their eggs are deposited (Fig. 3). This does not necessarily imply that tags interfered with normal behavior, because males outnumber females.

Most squid moved offshore at dusk; one large male was tracked 2 km offshore, where he remained relatively stationary (perhaps feeding or resting) until his return at dawn. During this male's onshore migration, his mean swimming speed was, as expected, 1 body length per second (45 cm s^{-1}), three times his speed in the mating arena. In contrast, sneakers were smaller and faster, averaging nearly 1 body length per second for the whole day; their tactic of avoiding large males and achieving sneak EPCs requires swift swimming.

Figure 4. This enhanced video image of a "sneaker" male (left) intercepting a temporary pair and attaching a sperm package to the female with no response by the escort (right) is direct evidence of sneaking in squid mating systems. Video by RTH.

Males of various terrestrial and aquatic taxa assemble in large leks or lek-like aggregations to attract females and then compete for mating access (2, 3, 8, 9). Among loliginid squids, however, the tactic that appears to be primary is the intensive sexual selection that occurs in these nearshore mating arenas, with many of the requisites for leks (2). We suggest that the daily offshore-to-inshore movements and circling aggregation of male squid draw in new male and female schools from offshore, increasing the size of the aggregation and the number of females. Our picture of the dynamics of these lek-like aggregations suggests that high-biomass mating arenas ensure that most eggs are deposited in locations with a high probability of hatching success. Other potential benefits of larger aggregations are more intensive competition for mates and more gene mixing in the population.

Overall, the squid mating system first includes a period of offshore mating that provides sperm to most females before the onset of the inshore migration. This sperm is stored and, as an alternative tactic, can be used by individual females that never make it to inshore mating arenas. Females that do participate in the inshore mating aggregations probably use the sperm of the large males with which they pair and mate in these arenas (10, 11). In the end, then, females that mate with large males and sneakers, as well as with males while offshore, have at least three sources of sperm (7, 11, 12). Therefore, the potential for genetic mixing—already increased by the spawning aggregation—will be further augmented. This type of mating system may be typical of loliginid squids, and assessment of paternity by some molecular technique will help resolve this possibility (12).

The fishery for the squid *Loligo vulgaris reynaudii* in South Africa began when fishermen located squid aggregations by sonar and jigged them intensively. At the outset, low-intensity jigging often yielded tons of squid daily for several months, primarily during what we now recognize as the early morning period of circling and pairing over mating arenas (13). Previous sporadic diving observations confirmed that the aggregated squid were spawning around communal egg beds (14, 15). At present fishing levels, the aggregations seem more transitory and isolated, and offshore spawning may have increased.

By now, the fishery, although relatively new, has become the third most valuable in South Africa (16); this fits the worldwide trend in which cephalopods have risen to third in dollar value (behind shrimp and tuna) as finfish stocks have declined due to fishing pressure (17). But this fishery clearly targets spawning squid. Therefore, fishery biologists and fisherman's cooperatives are keen to avert both biological and commercial disaster; thus they have been supporting the acquisition of baseline data on population dynamics, especially as it is influenced by reproductive behavior. Field trials combining molecular genetic and behavioral observations with experimental fishing are planned to develop management strategies that will avoid alteration or breakdown of the critical spawning aggregations. In addition to the potential for altering the mating dynamics (and thus gene distribution) on the mating arenas, recruitment could also be adversely affected by increases in the alternative tactic of mating and spawning offshore, where development temperatures and success may be lower (18).

The novel remote tracking project reported here is part of a larger program that includes videography of behaviors recorded by divers, analysis of the recapture of previously tagged squid, bottom surveys carried out by video using the Global Positioning Systems for location, and biomass assessments from sonar and trawl samples.

In summary, the use of an unorthodox technique (tagging and monitoring with RAP) led to the surprising conclusion that the squid's "nuptial dance" seems to be choreographed by the large males each morning, and that the nature of the interactions is reminiscent of lek aggregations of birds and mammals. Because the annual life cycle of squid is brief (19), and because the fishery has only recently developed, the system has great potential as a model of genetic shifts in populations that are subjected to natural selection from predators, sexual selection due to squid behavior, and selective fishing pressure from human behavior. Fishery managers might take advantage of this useful model system.

Acknowledgments

We acknowledge the advice of Mart Gross and support from the Foundation for Research and Development (South Africa), South African Squid Management Industrial Association (South Africa), Sea Fisheries Research Institute (South Africa), National Institutes of Health grant RR01024 (USA), and National Sciences and Engineering Research Council (Canada).

Literature Cited

1. **Cousteau, J.-Y., and P. Diolé. 1973.** Last dance on the mating ground. *Nat. Hist.* **82(4):** 45–48.
2. **Höglund, J., and R. V. Alatalo. 1995.** *Leks* Princeton Univ. Press, Princeton, NJ.
3. **Widemo, F., and I. P. F. Owens. 1995.** Lek size, male mating skew and the evolution of lekking. *Nature* **373:** 148–151.
4. **O'Dor, R. K., J. A. Hoar, D. M. Webber, F. G. Carey, S. Tanaka, H. Martins, and F. M. Porteiro. 1994.** Squid (*Loligo forbesi*) performance and metabolic rates in nature. *Mar. Fresh. Behav. Physiol.* **25:** 163–177.
5. **Martin, P., and P. Bateson. 1993.** *Measuring Behaviour: An Introductory Guide,* 2nd edition. Cambridge University Press, Cambridge, U.K.
6. **O'Dor, R. K., D. M. Webber, W. H. H. Sauer, M. Roberts, and M. Smale. 1996.** High-resolution, 3-D tracking of squid on spawning grounds. Pp. 193–198 in *Proc. 13th Int. Symp. Biotelemetry,* C. Cristalli, C. J. Amlaner, Jr., and M. R. Neuman, eds. Univ. Arkansas Press, Fayetteville.

7. **Hanlon, R. T., M. J. Smale, and W. H. H. Sauer. 1994.** An ethogram of body patterning behavior in the squid *Loligo vulgaris reynaudii* on spawning grounds off South Africa. *Biol. Bull.* **187:** 363–372.
8. **McKaye, K. R., S. M. Londa, and J. F. Stauffer. 1990.** Bower size and male reproductive success in a cichlid fish lek. *Am. Nat.* **135:** 597–613.
9. **Colin, P. L., and L. J. Bell. 1991.** Aspects of the spawning of labrid and scarid fishes (Pisces: Labroidei) at Eniwetok Atoll, Marshall Islands with notes on other families. *Environ. Biol. Fishes* **31:** 229–260.
10. **Hanlon, R. T., and J. B. Messenger. 1996.** *Cephalopod Behaviour.* Cambridge Univ. Press, Cambridge, U.K.
11. **Boyle, P. R., G. J. Pierce, and L. C. Hastie. 1995.** Flexible reproductive strategies in the squid *Loligo forbesi*. *Mar. Biol.* **121:** 501–508.
12. **Hanlon, R. T. 1996.** Evolutionary games that squids play: fighting, courting, sneaking, and mating behaviors used for sexual selection in *Loligo pealei*. *Biol. Bull.* **191:** 309–310.
13. **Sauer, W. H. H. 1993.** The ecology of spawning squid *Loligo vulgaris reynaudii* in the inshore waters of the Eastern Cape. Ph.D. Thesis, U. of Port Elizabeth. 121 pp.
14. **Sauer, W. H. H., M. J. Smale, and M. R. Lipinski. 1992.** The location of spawning grounds, spawning and schooling behaviour of the squid *Loligo vulgaris reynaudii* (D'Orbigny) (Cephalopoda: Myopsida) off the eastern Cape coast. *Mar. Biol.* **114:** 97–107.
15. **Sauer, W. H. H., and M. J. Smale. 1993.** Spawning behavior of *Loligo vulgaris reynaudii* in shallow coastal waters of the southeastern Cape, South Africa. Pp. 489–498 in *Recent Advances in Cephalopod Fisheries Biology*, T. Okutani, R. K. O'Dor, and T. Kubodera, eds. Tokai University Press, Japan.
16. **Stuttaford, M. 1994.** *Fishing Industry Handbook, South Africa, Namibia and Mosambique* Pub: Marine Information, Stellenbosch, S. A. 434 pp.
17. **FAO Fisheries Department. 1993.** Fisheries and the Law of the Sea: A Decade of Change. *FAO Fisheries Circular*, **No. 853:** Rome. 66 pp.
18. **Roberts, M. J., and W. H. H. Sauer. 1994.** Environment: the key to understanding the South African chokka squid (*Loligo vulgaris reynaudii*) life cycle and fishery. *Antarct. Sci.* **6(2):** 249–258.
19. **Augustyn, C. J., M. R. Lipinski, W. H. H. Sauer, M. J. Roberts, and B. A. Mitchell-Innes. 1994.** Chokka squid on the Agulhas Bank: life history and ecology. *S. Afr. J. Sci.* **90:** 143–154.

Reference: *Biol. Bull.* **192:** 208–216. (April, 1997)

Uptake and Persistence of Homologous and Heterologous Zooxanthellae in the Temperate Sea Anemone *Cereus pedunculatus* (Pennant)

SIMON K. DAVY*, IAN A. N. LUCAS, AND JOHN R. TURNER

School of Ocean Sciences, University of Wales, Bangor, Marine Science Laboratories, Menai Bridge, Anglesey, LL59 5EY, UK

Abstract. The uptake and persistence of symbiotic dinoflagellates (zooxanthellae) were measured in the temperate sea anemone *Cereus pedunculatus* (Pennant). Aposymbiotic specimens of *C. pedunculatus* were inoculated with zooxanthellae freshly isolated from a range of temperate and subtropical Anthozoa. Each inoculate consisted of zooxanthellae from a single host species and was either homologous (zooxanthellae from a host of the same species as the one being inoculated) or heterologous (from a host of a different species than the one being inoculated). The densities of zooxanthellae in host tissues were determined at regular intervals. *C. pedunculatus* took up homologous and heterologous zooxanthellae to similar degrees, except for zooxanthellae from the temperate *Anthopleura ballii*, which were taken up to a lesser extent. The densities of all zooxanthellae declined between 4 hours and 4 days after uptake, indicating that zooxanthellae were expelled, digested, or both during this period. The densities of all zooxanthellae increased between 2 and 8 weeks after inoculation, indicating zooxanthella growth. Over the entire 8-week period after uptake, densities of homologous zooxanthellae were always greater than those of heterologous zooxanthellae. Between 8 and 36 weeks after infection, densities of homologous zooxanthellae declined markedly and densities of some heterologous zooxanthellae increased further, resulting in homologous and heterologous zooxanthella densities being the same at 36 weeks. These densities were the same as those in naturally infected *C. pedunculatus* of similar size. The results suggest that zooxanthellae from a range of host species and environments can establish symbioses with *C. pedunculatus* and that, over long periods under laboratory conditions, heterologous zooxanthellae may populate *C. pedunculatus* to the same extent as homologous zooxanthellae.

Received 12 January 1996; accepted 9 January 1997.

* Present address: Department of Symbiosis and Coral Biology, Division of Marine Science, Harbor Branch Oceanographic Institution, 5600 U.S. 1 North, Fort Pierce, Florida 34946.

Introduction

Many benthic marine Cnidaria possess endosymbiotic dinoflagellates (zooxanthellae) of the genus *Symbiodinium*. These Cnidaria may lose zooxanthellae entirely (*i.e.*, become aposymbiotic) when under environmental stress (Williams and Bunkley-Williams, 1990; Glynn, 1991) or when zooxanthellae are not inherited maternally (Trench, 1987; Shick 1991). Consequently, they may be susceptible to reinfection and colonization by zooxanthellae released from a range of host species (Schoenberg and Trench, 1980c; Rowan and Powers, 1991b; Buddemeier and Fautin, 1993). Despite this susceptibility and the high diversity of hosts and symbionts (Trench, 1987; Rowan and Powers, 1991b; Trench, 1993; McNally *et al.*, 1994), many species of Cnidaria have been reported to harbor just one strain or species of *Symbiodinium* (Schoenberg and Trench, 1980a, b; Rowan and Powers, 1991a, b; Trench, 1993). Other hosts have been found to contain more than one strain or species of zooxanthella, but even in these cases the algae are the same across the host's geographical range (Trench and Winsor, 1987; Rowan and Powers, 1991b; Rowan and Knowlton, 1995).

The uptake and persistence of zooxanthellae following

inoculation of aposymbiotic hosts has been investigated in a range of tropical marine Cnidaria (Kinzie, 1974; Kinzie and Chee, 1979; Schoenberg and Trench, 1980c; Trench, 1981; Trench *et al.*, 1981; Colley and Trench, 1983; Fitt and Trench, 1983a, b; Berner *et al.*, 1993). The zooxanthellae were either homologous (from a host of the same species of cnidarian as the one being inoculated) or heterologous (from a host of a different species than the one being inoculated). In contrast, similar work has been performed using just one species of temperate marine Cnidaria, the North American sea anemone *Anthopleura elegantissima* (Trench, 1969, cited in Trench, 1971; Muller-Parker, 1996; Weis and Levine, 1996).

The temperate sea anemone *Cereus pedunculatus* (Pennant) (family Sagartiidae) is locally abundant around the south and west coasts of Europe, where it is found partially buried in sand and mud from the midshore to a depth of 25 m (Manuel, 1981). *C. pedunculatus* may reproduce by oviparity, but frequently it is hermaphroditic or parthenogenetic and viviparous (Rossi, 1975; Schäfer, 1981; Shick, 1991). The zooxanthellae of *C. pedunculatus* are located within the host's endodermal cells and have been identified as *Symbiodinium* sp. (Davy *et al.*, in press). Oocytes may contain up to 300 zooxanthellae, suggesting that *C. pedunculatus* acquires its symbionts through maternal inheritance (Turner, pers. obs.). Brooded and recently released juvenile *C. pedunculatus* always harbor zooxanthellae, but densities in recently released individuals may be less than 10% of those in adult anemones (Darmayati, 1993; Davy *et al.*, 1996). The fact that *C. pedunculatus* produces offspring that lack a full complement of zooxanthellae means that they may be susceptible to infection by zooxanthellae released from other Anthozoa.

The sea anemones *Anthopleura ballii* (Cocks) (family Actiniidae) and *Anemonia viridis* (Forskäl) (family Actiniidae), and the zoanthid *Isozoanthus sulcatus* (Gosse) (family Parazoanthidae) are frequently found in the same localities as *C. pedunculatus*, and also harbor *Symbiodinium* sp. (Davy *et al.*, in press). *A ballii* and *A. viridis* regularly expel zooxanthellae in large boluses, as well as in mucous strands (Davy, pers. obs.); it is also probable that *I. sulcatus* releases zooxanthellae, but this has not been observed. This expulsion suggests that zooxanthellae from a variety of sources are available to infect new hosts.

This research therefore aimed to determine whether heterologous zooxanthellae can infect *C. pedunculatus*, and to compare the persistence of homologous and heterologous zooxanthellae after infection. From this information the potential for heterologous zooxanthellae to establish a lasting symbiosis with *C. pedunculatus* in the field could be inferred.

Materials and Methods

Collection and maintenance of symbiotic Anthozoa

The sea anemones *Cereus pedunculatus* (Pennant), *Anemonia viridis* (Forskäl), and *Anthopleura ballii* (Cocks), and the zoanthid *Isozoanthus sulcatus* (Gosse) were collected from Lough Hyne Marine Nature Reserve, Eire (51°29′ N; 9°18′ W). All four species are exclusively subtidal at this location. The anemones were all collected from a depth of 1 to 3 m, and the zoanthids from 5 to 9 m. Specimens of *A. viridis* were also collected from the intertidal zone at Shell Island, North Wales (52° 47′ N; 004° 06′ W). For comparative purposes, specimens of the subtropical sea anemone *Aiptasia pallida* (Verrill), cloned from one individual, were obtained from Dr. Ç. B. Cook, Bermuda Biological Station. The *A. pallida* had originally been collected from a mangrove root in Walsingham Pond, Bermuda.

Adult Anthozoa were kept in seawater from the Menai Strait, North Wales. They were maintained at 21°C, illuminated at 80 μmol photons m^{-2} s^{-1} on a cycle of 12 h light:12 h dark, and fed twice weekly with *Artemia* sp. (Bonneville *Artemia* International Inc.). The light and temperature regimes were comparable to those experienced during a warm summer in Lough Hyne (Turner, 1988, and his pers. obs.).

Preparation of aposymbiotic Anthozoa

Juvenile specimens of *C. pedunculatus* were squeezed from the enterons of brooding adult anemones and placed in a dark-box to render them aposymbiotic. Seawater from the Menai Strait, at the ambient temperature (10–18°C), flowed through the dark-box continuously. It is unlikely that zooxanthellae were present in this seawater because Anthozoa-zooxanthella associations do not occur locally. In addition, the examination of dark-treated anemones suggested that infections had not occurred under these conditions (see below). The juveniles were collected on two occasions, with the first batch (n = 250) remaining in the dark for more than 3 years and the second batch (n = 120) remaining in the dark for 5 months. After collection, the anemones were fed every 2 months with *Artemia* sp; the anemones also received planktonic food *via* the flow-through seawater system. It is likely that the juveniles were genetically related to one another because all adult anemones were collected from the same site and spawning of gametes has not been observed in this population (Davy and Turner, pers. obs.).

Prior to use, 3-year dark-treated anemones (n = 180) with oral disc diameters of about 2 to 3 mm were placed in 100-ml containers filled with filtered (0.45 μm) seawater (FSW). Five anemones were placed in each container.

These anemones were maintained at 21°C, illuminated at 80 μmol photons m^{-2} s^{-1} on a cycle of 12 h light:12 h dark, and fed weekly with *Artemia* sp. for 2 weeks. The anemones were never observed to change from white to brown over this period and so were assumed to be aposymbiotic. This assumption was checked by squashing a subsample of five anemones (anemones sampled from the same container; *n* was limited by anemone availability) and examining their tissues under bright-field and epifluorescent illumination using a Leitz Orthoplan microscope. Neither zooxanthellae nor chlorophyll *a* were detected, confirming that the 3-year dark-treated anemones were aposymbiotic. Therefore, immediately after being maintained in the light for 2 weeks, these anemones were used for monitoring patterns of long-term infection by zooxanthellae. Non-inoculated control polyps used in these experiments remained zooxanthella-free over a period of 36 weeks, reconfirming that the anemones were aposymbiotic.

In contrast, squashes made of 5-month dark-treated polyps ($n = 5$) before they were placed in the light revealed a small number of residual zooxanthellae (less than 1000 zooxanthellae per polyp). These anemones were therefore used for short-term monitoring of infection patterns, where densities of residual zooxanthellae were negligible in comparison to densities of phagocytosed zooxanthellae. To keep residual zooxanthellae to a minimum, these anemones were maintained in the dark until inoculation.

Infection of aposymbiotic Cereus pedunculatus *when coexisting with symbiotic* C. pedunculatus

Under nonstressful conditions, *C. pedunculatus* regularly releases a small percentage (<0.3% per hour) of its zooxanthellae (Darmayati, 1993). A motile stage has yet to be observed in the life history of these zooxanthellae, either following release or when in culture (Davy *et al.*, in press; Davy, pers. obs.). To establish whether zooxanthellae released by one anemone could infect another anemone, 3-year dark-treated *C. pedunculatus* ($n = 5$) were placed in a container with symbiotic *C. pedunculatus* ($n = 5$). Three-year dark-treated *C. pedunculatus* ($n = 5$) in a second container acted as controls. All anemones were illuminated at 80 μmol photons m^{-2} s^{-1} on a cycle of 12 h light:12 h dark, maintained at 21°C, and fed weekly with *Artemia* sp. After 8 weeks, the presence or absence of zooxanthellae in the formerly aposymbiotic polyps (which were still distinct due to their lighter pigmentation) was determined. This involved squashing the polyps and using bright-field and epifluorescent microscopy to search their tissues. Densities of zooxanthellae were not quantified.

Persistence of homologous and heterologous zooxanthellae

To investigate the extent to which zooxanthellae from different host species could establish a symbiosis with *C. pedunculatus*, the uptake and persistence of homologous and heterologous zooxanthellae following inoculation were measured.

Three oral discs plus attached tentacles of *C. pedunculatus*, 5 tentacles from each of 10 individuals of *A. ballii* and *A. viridis*, 30 polyps of *I. sulcatus*, and 10 complete *A. pallida* were collected for isolation of zooxanthellae. Host tissue for each host species was pooled, homogenized in 10 ml FSW in a glass tissue-grinder, and centrifuged for 10 min at 1200 rpm. The supernatant was discarded, and the algal pellet was resuspended in 5 ml FSW and centrifuged for a further 5 min at 1200 rpm. The supernatant was again discarded and the algal pellet adjusted with FSW to give a concentration of 2×10^7 cells ml^{-1}. Isolates from different host species were kept separate.

Dark-treated specimens of *C. pedunculatus* ($n = 150$ and $n = 90$ for anemones maintained in darkness for 3 years and 5 months, respectively) with oral disc diameters of about 2 to 3 mm were maintained in 100-ml containers (five anemones of the same dark-treatment per container) and inoculated with homologous or heterologous zooxanthellae. Anemones in each container were inoculated with zooxanthellae from just one source, thus preventing cross-infection by zooxanthellae from different sources. A 1-ml hypodermic syringe was used to deposit 0.2 ml of suspension (*i.e.*, 4×10^6 zooxanthellae) onto the oral disc of each aposymbiotic anemone. This number of zooxanthellae was sufficient to saturate the uptake sites of these anemones (Davy, 1994). Once the anemones had expanded again, 0.1 ml of an *Artemia* sp. suspension was pipetted onto each oral disc. This suspension enhanced ingestion of zooxanthellae (Davy, 1994). To remove any zooxanthellae and *Artemia* sp. not captured by the anemones, the FSW was then changed. Uninoculated 3-year and 5-month dark-treated anemones ($n = 25$ and $n = 15$, respectively; five anemones per 100-ml container) acted as controls for spontaneous infection. All anemones were maintained at 21°C, illuminated with 80 μmol photons m^{-2} s^{-1} on a cycle of 12 h light:12 h dark, and fed weekly with *Artemia* sp. The densities of zooxanthellae in 5-month dark-treated anemones were measured after 4 h, 2 days, and 4 days, and the densities of zooxanthellae in 3-year dark-treated anemones were measured after 2, 4, 6, 8, and 36 weeks.

Following the incubation period, polyps ($n = 4$ or 5 for each group; replicate anemones sampled from the same container) were narcotized in 7.5% magnesium chloride

in FSW. Oral disc diameters were then measured using an ocular micrometer, and oral disc areas were calculated. This method (i) facilitated measurement of large numbers of polyps; (ii) was repeatable; and (iii) gave units (square millimeters of oral disc) proportional to the protein content of the polyp ($r^2 = 0.97$ for anemones with disc diameters of 1.0 to 3.0 mm; Davy, 1994). Polyps examined between 4 hours and 4 days after reinfection were cut longitudinally, and residual *Artemia* sp. and zooxanthellae were washed from their enterons; this step was not necessary for anemones examined after 2 weeks or more. Each polyp was then homogenized in 1 ml FSW, and the number of zooxanthellae in the homogenate was counted using a Fuchs Rosenthal hemacytometer. The density of zooxanthellae in the anemone's tissues was expressed as zooxanthellae per square millimeter of oral disc.

The same method was used to determine the densities of zooxanthellae in five similarly sized, naturally infected *C. pedunculatus*. These values were compared with those from the infection experiments.

Statistical analysis

Significant differences ($P < 0.05$) were identified using one-way analysis of variance (ANOVA) followed by Bonferroni pair-wise comparisons. When variances were not homogeneous (as determined using Bartlett's statistic), data were logarithmically transformed.

Results

Infection of aposymbiotic Cereus pedunculatus *when co-existing with symbiotic* C. pedunculatus

All aposymbiotic *Cereus pedunculatus* maintained in the presence of symbiotic *C. pedunculatus* turned brown after 2 months. Light microscopy revealed that this change in color resulted from the presence of zooxanthellae in the endodermal cells. In contrast, control anemones remained white and free of zooxanthellae after 2 months.

Short-term persistence of zooxanthellae

Figure 1 summarizes the patterns of infection of *C. pedunculatus* by homologous zooxanthellae and by zooxanthellae from *Anthopleura ballii*, *Anemonia viridis*, *Isozoanthus sulcatus*, and *Aiptasia pallida* over the first 4 days (*i.e.*, over the short-term).

The densities of homologous zooxanthellae were not significantly different from the densities of any of the heterologous zooxanthellae at 4 h (Bonferroni *post-hoc* ANOVA, $P > 0.05$); but note that the homologous zooxanthellae were 2.5 times denser than the zooxanthellae

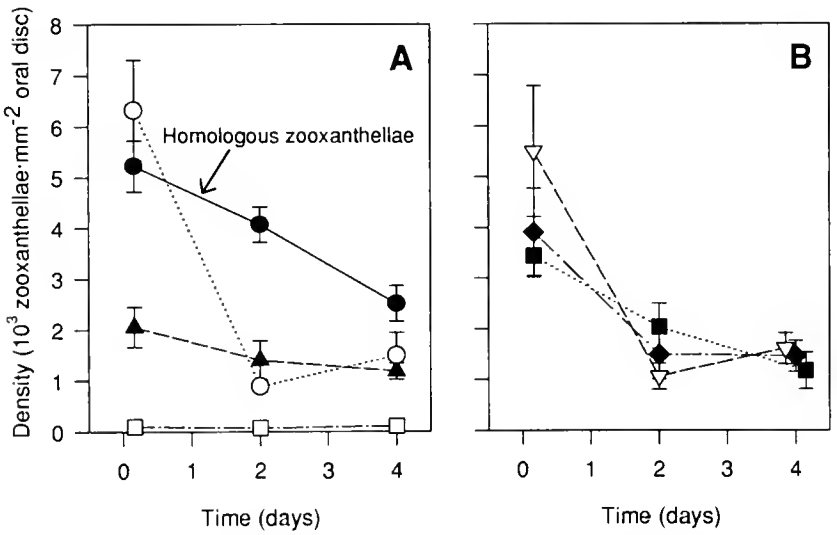

Figure 1. Short-term persistence patterns of homologous and heterologous zooxanthellae in infected *Cereus pedunculatus*. All anemones dark-treated for 5 months prior to infection and unfed over period shown. $n = 5$. Points at 4 days offset for clarity. All values are means ± 1 SE. (A) Persistence of homologous zooxanthellae from *C. pedunculatus* (● — ●), and heterologous zooxanthellae from *Anthopleura ballii* (▲ – – – ▲) and *Isozoanthus sulcatus* (○ · · · ○). □ – · – □ represents zooxanthellae in non-inoculated dark-treated controls. (B) Persistence of heterologous zooxanthellae from *Anemonia viridis* from Lough Hyne (◆ – · – ◆) and Shell Island (▽ – – – ▽), and *Aiptasia pallida* (■ · · · ■).

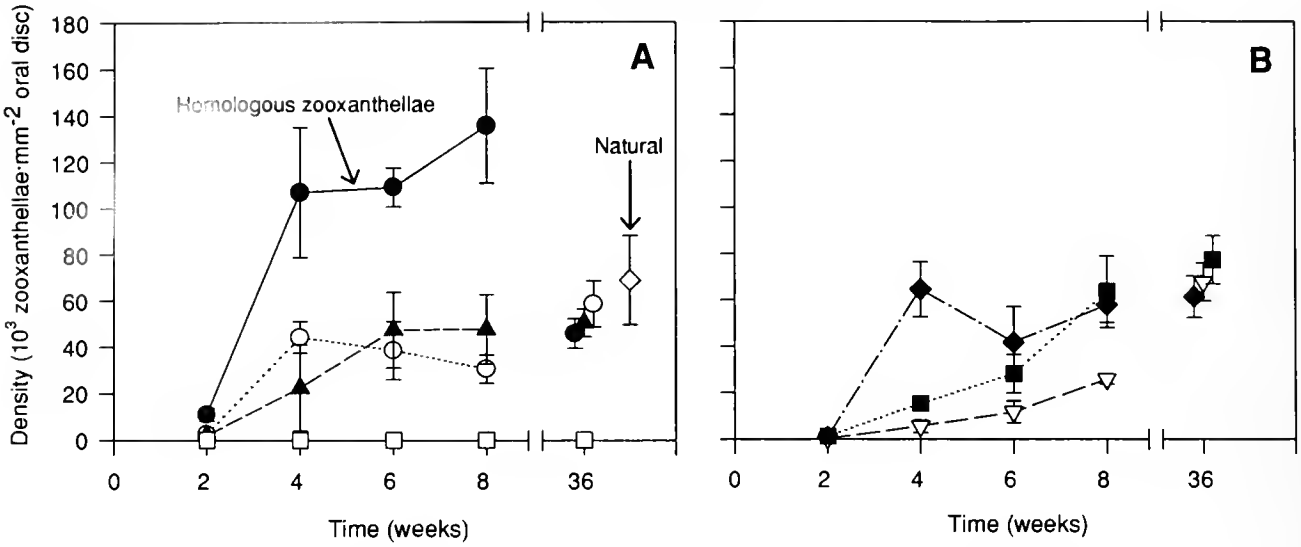

Figure 2. Long-term persistence patterns of homologous and heterologous zooxanthellae in infected *Cereus pedunculatus*. All anemones dark-treated for more than 3 years prior to infection and fed weekly over period shown. $n = 5$, except $n = 4$ for zooxanthellae from *Anthopleura ballii* and *Isozoanthus sulcatus* at 36 weeks. Points at 36 weeks offset for clarity. All values are means ± 1 SE. (A) Persistence of homologous zooxanthellae from *C. pedunculatus* (● — ●), and heterologous zooxanthellae from *A. ballii* (▲ - - - ▲) and *I. sulcatus* (○ · · · ○). □ - · - □ represents zooxanthellae in non-inoculated dark-treated controls, and white diamond represents zooxanthellae in naturally infected *C. pedunculatus*. (B) Persistence of heterologous zooxanthellae from *Anemonia viridis* from Lough Hyne (♦ - · - ♦) and Shell Island (▽ - - - ▽), and *Aiptasia pallida* (■ · · · ■).

from *A. ballii* (Fig. 1A). Subsequently, homologous zooxanthellae persisted at the highest densities. Homologous zooxanthellae were present at significantly greater densities than any of the heterologous strains at 2 days (Bonferroni *post-hoc* ANOVA, $P < 0.01$).

Short-term infection patterns by heterologous zooxanthellae were similar to one another, with the only major difference being the relatively low uptake of zooxanthellae from *A. ballii*. Zooxanthellae from *A. ballii* were present at significantly lower densities than zooxanthellae from *I. sulcatus* at 4 h (Bonferroni *post-hoc* ANOVA, $P < 0.05$).

Long-term persistence of zooxanthellae

Figure 2 summarizes the densities of zooxanthellae 2, 4, 6, 8, and 36 weeks after reinfection (*i.e.*, over the long-term), and the density of zooxanthellae in naturally infected *C. pedunculatus*.

Homologous zooxanthellae persisted at significantly greater densities than any of the heterologous zooxanthellae at 2 and 6 weeks (Bonferroni *post-hoc* ANOVA, $P < 0.05$). Homologous zooxanthellae also persisted at significantly greater densities than zooxanthellae from *A. ballii, A. viridis* (Shell Island), and *A. pallida* at 4 weeks, and zooxanthellae from *A. ballii, A. viridis* (Shell Island), and *I. sulcatus* at 8 weeks (Bonferroni *post-hoc* ANOVA, $P < 0.05$). However, at 36 weeks, the densities of homologous zooxanthellae, heterologous zooxanthellae, and zooxanthellae in naturally infected *C. pedunculatus* were not significantly different (ANOVA, $P > 0.05$).

Zooxanthellae from *A. pallida* were present at significantly lower densities than zooxanthellae from *A. viridis* (Lough Hyne) at 4 weeks (Bonferroni *post-hoc* ANOVA, $P < 0.05$). Zooxanthellae from *A. viridis* (Shell Island) were present at significantly lower densities than any other heterologous zooxanthellae at 2 and 4 weeks, and zooxanthellae from *A. ballii* and *A. viridis* (Lough Hyne) at 6 weeks (Bonferroni *post-hoc* ANOVA, $P \leq 0.02$). No other significant differences were evident between the densities of heterologous zooxanthellae (Bonferroni *post-hoc* ANOVA, $P > 0.05$).

Anemone size

Prior to infection, anemones had oral disc diameters of about 2 to 3 mm. At the end of the 36-week experimental period, all anemones infected with either homologous or heterologous zooxanthellae still had oral disc diameters of 2 to 3 mm and were not significantly differ-

ent in size (average diameter 2.39 ± 0.03 mm; ANOVA, $P > 0.95$). As oral disc area is proportional to polyp protein content (see Materials and Methods), these results suggest that changes in anemone biomass were minimal during the experimental period, presumably reflecting the limited feeding regime (once per week). Thus the substantial changes in zooxanthella densities were most likely due to changes in the number of zooxanthellae rather than in the normalizing parameter (oral disc area).

Discussion

The results reveal that zooxanthellae from a range of host species, localities, and environments can establish symbioses with *Cereus pedunculatus*. In the short-term, homologous zooxanthellae persist to a greater extent than heterologous zooxanthellae, but over the long-term the two types of zooxanthellae achieve similar densities. The possible reasons for these infection patterns and their implications will be discussed.

Short-term persistence

C. pedunculatus took up zooxanthellae from *Anthopleura ballii* at a lower rate than zooxanthellae from the other host species, perhaps indicating discrimination based upon the surface characteristics of the zooxanthellae. However, uptake rates of zooxanthellae from the other host species were similar. This suggests that during the initial phases of infection *C. pedunculatus* was unable to discriminate between these zooxanthellae, perhaps because of the similarity of their surface characteristics or the host material contaminating their surfaces (Trench *et al.*, 1981; Colley and Trench, 1983).

Following phagocytosis, all populations of zooxanthellae declined, with the homologous populations declining less rapidly than most of the heterologous populations. Symbiont populations also declined following infections of *Hydra viridissima* (Jolley and Smith, 1980) and the jellyfish *Cassiopeia xamachana* (Colley and Trench, 1983), but did not do so following infections of a number of other species of Cnidaria (Muscatine *et al.*, 1975; Schoenberg and Trench, 1980c; Berner *et al.*, 1993). The decline may represent the nonselective elimination of a proportion of the phagocytosed zooxanthellae or the selective elimination of unhealthy and incompatible zooxanthellae. Elimination may occur *via* expulsion or digestion. Regular expulsion of zooxanthellae is a common feature of Anthozoa-zooxanthella symbioses (Steele, 1975; Høegh-Guldberg *et al.*, 1987; Stimson and Kinzie, 1991; McCloskey *et al.*, 1996), and the production of zooxanthella-containing boluses was observed during the course of experiments. In contrast, digestion is thought not to play a major role in the regulation of populations of zooxanthellae (Colley and Trench, 1985).

The elimination of some zooxanthellae more quickly than others has also been observed in *C. xamachana* (Colley and Trench, 1983). This trend may indicate differences in zooxanthella survivorship following isolation or discrimination among genotypically distinct zooxanthellae by means of post-phagocytotic recognition (Colley and Trench, 1983; Trench, 1988, 1992, 1993; Markell *et al.*, 1992; Markell and Trench, 1993). If zooxanthellae were being discriminated against by post-phagocytotic recognition, it is curious that a small number of zooxanthellae always persisted. Perhaps there was some variation within the source populations, with the retained zooxanthellae being the few that possessed certain appropriate characteristics.

Long-term persistence of zooxanthellae

Homologous zooxanthellae repopulated *C. pedunculatus* much more rapidly and achieved higher densities than did heterologous zooxanthellae. Similar patterns have been observed in *C. xamachana* (Colley and Trench, 1983) and *Aiptasia tagetes* (= *pallida*) (Schoenberg and Trench, 1980c). In contrast, zooxanthellae from *Anemonia viridis* from Shell Island repopulated *C. pedunculatus* more slowly than did any of the other zooxanthellae. These repopulation trends may result from host-algal recognition and greater expulsion or digestion of some types of zooxanthellae than others. However, the repopulation patterns could also be determined by differing growth rates of zooxanthellae; changes in host biomass (either growth or shrinkage), which could cause the 'dilution' or 'concentration' of zooxanthella populations, were probably not responsible for the density changes. Comparison of growth and expulsion rates of homologous and heterologous zooxanthellae during repopulation of aposymbiotic anemones would be an interesting topic for future work.

Several factors could influence the growth of zooxanthellae during repopulation. Firstly, the light and temperature regimes may favor growth by one type of zooxanthellae over another. However, this possibility is not supported by the similarity of the specific growth rates (0.25–0.29 d^{-1}) of zooxanthellae from *C. pedunculatus*, *A. ballii*, and *A. viridis*, when cultured *in vitro* under the same light and temperature regimes as those used here (Davy, 1994). Secondly, the growth of zooxanthellae may depend upon the ability of a particular strain or species to survive in the intracellular environment of the host (Rahat and Reich, 1988). But this hypothesis is inconsistent with evidence from analogous plant-microbial symbioses (Trench, 1993). Thirdly, hosts may be

able to control the growth of zooxanthellae directly (Smith and Muscatine, 1996). It is therefore possible that *C. pedunculatus* was able to exercise more control over some types of zooxanthellae than others. Finally, the growth of zooxanthellae may be limited by the intracellular space available within the host, with small zooxanthellae achieving greater densities than large zooxanthellae. It seems unlikely that this hypothesis can explain the densities achieved by zooxanthellae from *A. viridis* (Lough Hyne) and *A. pallida* (Fig. 2B), given that these zooxanthellae are similar in size to zooxanthellae from *C. pedunculatus* when in their original hosts, after residing in reinfected *C. pedunculatus* for 36 weeks, and when cultured *in vitro* (Davy, 1994; Davy *et al.*, 1996, and in press). It is unknown, though, whether these zooxanthellae maintained similar sizes throughout the repopulation process.

In spite of previous differences, at 36 weeks the densities of homologous and heterologous zooxanthellae, and zooxanthellae in naturally infected *C. pedunculatus*, were similar. The decline in the density of homologous zooxanthellae to a "normal" level is unique. If the population of zooxanthellae was unialgal, then the decline may result from the population being "brought under control." However, why this occurred only several months after the establishment of the symbiosis is unknown. One possibility is that control mechanisms become repressed in aposymbiotic anemones and are restored during the repopulation process. Alternatively, if the homologous population contained a mixture of zooxanthella types, then the decline may result from an initially successful type becoming unstable and being replaced by a type better suited to the culture conditions.

The ultimate success of heterologous zooxanthellae that were initially slow to establish a symbiosis with *C. pedunculatus* can also be interpreted in different ways depending upon the nature of the zooxanthella populations. Firstly, if the populations were unialgal, then host-symbiont adjustment over time may have enhanced the compatibility of the partners (Roughgarden, 1975; Smith, 1980). It would be interesting to re-isolate heterologous zooxanthellae or make reinfected anemones aposymbiotic again, and determine whether the repopulation process is faster when repeated. In a comparable experiment, however, the growth of heterologous zooxanthellae in *A. tagetes* was not enhanced by their previous association with the same host species (Schoenberg and Trench, 1980c). Alternatively, if the populations contained a mixture of zooxanthella types, then the "normal" densities achieved by heterologous zooxanthellae at 36 weeks may represent the proliferation of a small number of zooxanthellae identical to those usually harbored by *C. pedunculatus*. But such a mechanism is unlikely to explain the gradual increase in the density of zooxanthellae from *A. pallida*. This anemone is found at subtropical latitudes in the western Atlantic, and so probably contains zooxanthellae that are quite different from those in *C. pedunculatus*. In fact, the zooxanthellae of this anemone are believed to be a single species, *Symbiodinium bermudense* (Banaszak *et al.*, 1993). Furthermore, evidence from carbon-flux studies suggests that the homologous and heterologous zooxanthella populations were not identical at 36 weeks (Davy, 1994).

Host-symbiont recombination in the field

Molecular genetic techniques must be employed to determine the precise nature of the source populations of zooxanthellae and whether heterologous zooxanthellae actually establish symbioses with *C. pedunculatus* in the field. The long-term infection patterns (Fig. 2) suggest that host-symbiont recombination may be possible—if, that is, the new symbiosis is competitive under the prevailing environmental conditions and the heterologous zooxanthellae are not overgrown by homologous zooxanthellae in the short-term (Schoenberg and Trench, 1980c; Colley and Trench, 1983). The ability to establish symbioses with zooxanthellae from a range of sources may enable *C. pedunculatus* to adapt to different environmental regimes, as has been suggested for corals (Buddemeier and Fautin, 1993; Rowan and Knowlton, 1995). Alternatively, it may simply increase the anemone's chances of survival should it lose all of its zooxanthellae and have to acquire new symbionts. There are, however, no reports of "bleached" *C. pedunculatus* in the field. How zooxanthellae behave in mixed homologous-heterologous inoculations and the ecological advantages of maintaining heterologous zooxanthella populations are important questions for future research, both in temperate and tropical systems.

Acknowledgments

We thank Drs. R. K. Trench and C. B. Cook, and several anonymous reviewers for valuable comments on earlier drafts of the paper. We also thank the Irish Wildlife Service for permission to work and collect specimens in Lough Hyne Marine Nature Reserve. This work was carried out whilst SKD was in receipt of a SERC award.

Literature Cited

Banaszak, A. T., R. Iglesias-Prieto, and R. K. Trench. 1993. *Scrippsiella velellae* sp. nov. (Peridiniales) and *Gloeodinium viscum* sp. nov. (Phytodiniales), dinoflagellate symbionts of two hydrozoans (Cnidaria). *J. Phycol.* **29:** 517–528.

Berner, T., G. Baghdasarian, and L. Muscatine. 1993. Repopulation of a sea anemone with symbiotic dinoflagellates: analysis by in vivo fluorescence. *J. Exp. Mar. Biol. Ecol.* **170:** 145–158.

Buddemeier, R. W., and D. G. Fautin. 1993. Coral bleaching as an adaptive mechanism: a testable hypothesis. *Bioscience* **43:** 320–326.

Colley, N. J., and R. K. Trench. 1983. Selectivity in phagocytosis and persistence of symbiotic algae by the scyphistoma stage of the jellyfish *Cassiopeia xamachana*. *Proc. R Soc. Lond Ser. B* **219:** 61–82.

Colley, N. J., and R. K. Trench. 1985. Cellular events in the re-establishment of a symbiosis between a marine dinoflagellate and a coelenterate. *Cell Tissue Res.* **239:** 93–103.

Darmayati, Y. 1993. The effect of elevated temperature on the symbiosis between the sea anemone *Cereus pedunculatus* Pennant and *Symbiodinium* sp. M.Sc. thesis, University of Wales. 54 pp.

Davy, S. K. 1994. The specificity of temperate anthozoan-dinoflagellate symbioses. Ph.D. thesis, University of Wales. 546 pp.

Davy, S. K., I. A. N. Lucas, and J. R. Turner. 1996. Carbon budgets in temperate anthozoan-dinoflagellate symbioses. *Mar. Biol.* **126:** 773–783.

Fitt, W. K., and R. K. Trench. 1983a. Infection of coelenterate hosts with the symbiotic dinoflagellate *Symbiodinium microadriaticum*. Pp. 675–681 in *Endocytobiology II*, W. Schwemmler and H. E. A. Schenk, eds. Walter de Gruyter, Berlin.

Fitt, W. K., and R. K. Trench. 1983b. Endocytosis of the symbiotic dinoflagellate *Symbiodinium microadriaticum* Freudenthal by endodermal cells of the scyphistomae of *Cassiopeia xamachana* and resistance of the algae to host digestion. *J. Cell Sci.* **64:** 195–212.

Glynn, P. W. 1991. Coral bleaching in the 1980's and possible connections with global warming. *Trends Ecol. Evol.* **6:** 175–179.

Hoegh-Guldberg, O., L. R. McCloskey, and L. Muscatine. 1987. Expulsion of zooxanthellae by symbiotic cnidarians from the Red Sea. *Coral Reefs* **5:** 201–204.

Jolley, E., and D. C. Smith. 1980. The green hydra symbiosis. II. The biology of the establishment of the association. *Proc. R. Soc. Lond. Ser. B* **207:** 311–333.

Kinzie, R. A. 1974. Experimental infection of aposymbiotic gorgonian polyps with zooxanthellae. *J. Exp. Mar Biol. Ecol.* **15:** 335–345.

Kinzie, R. A., and G. S. Chee. 1979. The effect of different zooxanthellae on the growth of experimentally reinfected hosts. *Biol. Bull.* **156:** 315–327.

Manuel, R. L. 1981. *British Anthozoa.* Academic Press, London. 241 pp.

Markell, D. A., R. K. Trench, and R. Iglesias-Prieto. 1992. Macromolecules associated with the cell walls of symbiotic dinoflagellates. *Symbiosis* **12:** 19–31.

Markell, D. A., and R. K. Trench. 1993. Macromolecules exuded by symbiotic dinoflagellates in culture: amino acid and sugar composition. *J. Phycol.* **29:** 64–68.

McCloskey, L. R., T. G. Cove, and E. A. Verde. 1996. Symbiont expulsion from the anemone *Anthopleura elegantissima* (Brandt) (Cnidaria; Anthozoa). *J. Exp. Mar. Biol. Ecol.* **195:** 173–186.

McNally, K. L., N. S. Govind, P. E. Thomé, and R. K. Trench. 1994. Small subunit ribosomal DNA sequence analyses and a reconstruction of the inferred phylogeny among symbiotic dinoflagellates (Pyrrophyta). *J. Phycol.* **30:** 316–329.

Muller-Parker, G. 1996. A comparison of temperate and tropical algal-anemone associations. *8th Int. Coral Reef Symp.* **Abstracts:** 139.

Muscatine, L., C. B. Cook, R. L. Pardy, and R. R. Pool. 1975. Uptake, recognition and maintenance of symbiotic *Chlorella* by *Hydra viridis*. *Symp. Soc. Exp. Biol.* **29:** 175–203.

Rahat, M., and V. Reich. 1988. The establishment of algal/*Hydra* symbioses—a case of recognition or preadaptation? Pp. 297–310 in *Cell to Cell Signals in Plant, Animal and Microbial Symbioses*, NATO ASI Series H17, S. Scannerini, D. C. Smith, P. Bonfante-Fasolo and V. Gianinazzi-Pearson, eds. Springer-Verlag, Berlin.

Rossi, L. 1975. Sexual races in *Cereus pedunculatus* (Boad.). *Pubbl. Staz. Zool. Napoli (Suppl., VIII Eur. Mar. Biol. Symp.)* **39:** 462–470.

Roughgarden, J. 1975. Evolution of marine symbiosis—a simple cost-benefit model. *Ecology* **56:** 1201–1208.

Rowan, R., and N. Knowlton. 1995. Intraspecific diversity and ecological zonation in coral-algal symbiosis. *Proc. Natl. Acad. Sci. USA* **92:** 2850–2853.

Rowan, R., and D. A. Powers. 1991a. Molecular genetic identification of symbiotic dinoflagellates (zooxanthellae). *Mar. Ecol. Prog. Ser.* **71:** 65–73.

Rowan, R., and D. A. Powers. 1991b. A molecular genetic classification of zooxanthellae and the evolution of animal-algal symbioses. *Science* **25:** 1348–1351.

Schäfer, W. 1981. Fortpflanzung und Sexualität von *Cereus pedunculatus* und *Actinia equina* (Anthozoa, Actiniaria). Helgol. Meeresunters. **34:** 451–461.

Schoenberg, D. A., and R. K. Trench. 1980a. Genetic variation in *Symbiodinium* (= *Gymnodinium*) *microadriaticum* Freudenthal, and specificity in its symbiosis with marine invertebrates. I. Isoenzyme and soluble protein patterns of axenic cultures of *S. microadriaticum*. *Proc. R. Soc. Lond. Ser. B* **207:** 405–427.

Schoenberg, D. A., and R. K. Trench. 1980b. Genetic variation in *Symbiodinium* (= *Gymnodinium*) *microadriaticum* Freudenthal, and specificity in its symbiosis with marine invertebrates. II. Morphological variation in *S. microadriaticum*. *Proc. R. Soc. Lond. Ser. B* **207:** 429–444.

Schoenberg, D. A., and R. K. Trench. 1980c. Genetic variation in *Symbiodinium* (= *Gymnodinium*) *microadriaticum* Freudenthal, and specificity in its symbiosis with marine invertebrates. III. Specificity and infectivity of *S. microadriaticum*. *Proc. R. Soc. Lond Ser. B* **207:** 445–460.

Shick, J. M. 1991. *A Functional Biology of Sea Anemones.* Chapman and Hall, New York. 395 pp.

Smith, D. C. 1980. Principles of colonisation of cells by symbionts as illustrated by symbiotic algae. Pp. 317–332 in *Endocytobiology I*, W. Schwemmler and H. E. A. Schenk, eds. Walter de Gruyter, Berlin.

Smith, G. J., and L. Muscatine. 1996. Why don't symbiotic dinoflagellates overgrow their cnidarian hosts? 8th Int. Coral Reef Symp. **Abstracts:** 183.

Steele, R. D. 1975. Stages in the life history of a symbiotic zooxanthella in pellets extruded by its host *Aiptasia tagetes* (Duch. and Mich.) (Coelenterata, Anthozoa). *Biol. Bull* **149:** 590–600.

Stimson, J., and R. A. Kinzie. 1991. The temporal pattern and rate of release of zooxanthellae from the reef coral *Pocillopora damicornis* (Linnaeus) under nitrogen-enrichment and control conditions. *J. Exp Mar. Biol. Ecol.* **153:** 63–74.

Trench, R. K. 1971. The physiology and biochemistry of zooxanthellae symbiotic with marine coelenterates. III. The effect of homogenates of host tissues on the excretion of photosynthetic products *in vitro* by zooxanthellae from two marine coelenterates. *Proc. R. Soc. Lond. Ser. B* **177:** 251–264.

Trench, R. K. 1981. Cellular and molecular interactions in symbioses between dinoflagellates and marine invertebrates. *Pure Appl. Chem.* **53:** 819–835.

Trench, R. K. 1987. Dinoflagellates in non-parasitic symbioses. Pp. 530–570 in *The Biology of Dinoflagellates*, F. J. R. Taylor, ed. Blackwell Scientific, Oxford.

Trench, R. K. 1988. Specificity in dinomastigote-marine invertebrate symbioses: an evaluation of hypotheses of mechanisms involved in producing specificity. Pp. 325–346 in *Cell to Cell Signals in Plant, Animal and Microbial Symbioses*, NATO ASI Series H17, S. Scannerini, D. C. Smith, P. Bonfante-Fasolo and V. Gianinazzi-Pearson, eds. Springer-Verlag, Berlin.

Trench, R. K. 1992. Microalgal-invertebrate symbiosis, current trends. Pp. 129–142 in *Encyclopedia of Microbiology*, Vol. 3, J. Lederberg, ed. Academic Press, New York.

Trench, R. K. 1993. Microalgal-invertebrate symbioses: a review. *Endocytobiosis Cell Res* **9:** 135–175.

Trench, R. K., N. J. Colley, and W. K. Fitt. 1981. Recognition phenomena in symbioses between marine invertebrates and "zooxanthellae"; uptake, sequestration and persistence. *Ber. Deutsch. Bot Ges Bd* **94:** 529–545.

Trench, R. K., and H. Winsor. 1987. Symbiosis with dinoflagellates in two pelagic flatworms, *Amphiscolops* sp. and *Haplodiscus* sp. *Symbiosis* **3:** 1–22.

Turner, J. R. 1988. The ecology of temperate symbiotic Anthozoa. D. Phil. thesis, University of Oxford, 484 pp.

Weis, V. M., and R. P. Levine. 1996. Differential protein profiles reflect the different lifestyles of symbiotic and aposymbiotic *Anthopleura elegantissima*, a sea anemone from temperate waters. *J. Exp. Biol.* **199:** 883–892.

Williams, E. H., and L. Bunkley-Williams. 1990. The world-wide coral reef bleaching cycle and related sources of coral mortality. *Atoll Res Bull* **335:** 1–71.

Reference: *Biol. Bull.* **192:** 217–230. (April, 1997)

p58, a Cytoskeletal Protein, Is Associated With Muscle Cell Determinants in Ascidian Eggs

WILLIAM R. BATES

Bamfield Marine Station, Bamfield, British Columbia, Canada V0R 1B0, and the Department of Biology, University of Victoria, Victoria, British Columbia, Canada V8W 2Y2

Abstract. The theory that p58, a cytoskeletal protein, has an important role in ascidian muscle cell development was tested by altering normal distributions of orange-pigmented myoplasm in *Boltenia villosa* embryos and determining if muscle development is correlated with the presence of p58. Removal of the animal region of fertilized *Boltenia* eggs resulted in the redistribution of myoplasm into the anterior endoderm cells of the embryo. Despite alterations in the normal distribution of myoplasm, these embryos developed into larvae. However, when four-celled embryos that exhibited altered distributions of pigmented myoplasm were stained with NN18, an antibody that stains p58, a maximum of two blastomeres were stained, as in control embryos. Compression of *Boltenia* embryos at the four-celled stage caused the myoplasm to be partitioned into four blastomeres of an eight-celled embryo, instead of into two blastomeres. Compressed and cleavage-arrested eight-celled embryos developed myosin and muscle actin RNA in a maximum of four blastomeres, compared to a maximum of two blastomeres in control embryos. When compressed eight-celled embryos were stained with NN18, p58 was present in a maximum of four blastomeres. These results support the idea that the cytoskeletal protein p58 is associated with muscle cell determinants in ascidian eggs.

Introduction

Egg cytoskeletons are known to have important roles in the determination of embryonic cells (Jeffery, 1982; Jeffery, 1989; Elinson, 1990; Hill *et al.*, 1990). Experiments performed by Jeffery and Meier (1983), Jeffery and Swalla (1990a), Swalla *et al.* (1991), and Marikawa (1995) support the idea that cytoplasmic factors required for the development of larval muscle cells are associated with myoplasmic cytoskeletal domain (MCD) of ascidian eggs. The MCD consists of two distinct, yet integrated, cytoskeletal systems: a plasma membrane lamina (PML) and a deep filamentous lattice (DFL). The PML is an actin-containing skeleton, sensitive to DNase I treatment, that contracts towards the vegetal pole during ooplasmic segregation (Jeffery and Meier, 1983). The DFL (Jeffery and Meier, 1983; Swalla *et al.*, 1991) is situated beneath the PML; contains pigment granules, mitochondria, and other components; and co-segregates with the PML during ooplasmic segregation. Swalla *et al.* (1991) have shown that a protein termed p58, which binds to a vertebrate intermediate filament antibody, is a component of the DFL. In ascidian species that produce tadpoles, the DFL was present in the cortical cytoplasm of the unfertilized egg and was partitioned exclusively into embryonic muscle progenitor cells. Eggs produced by direct-developing ascidians, which do not produce larvae with muscular tails, lack p58 (Swalla *et al.*, 1991; Bates, 1995).

Normal distributions of myoplasm were altered in ascidian embryos by using a microcompression technique (Whittaker, 1980). Whittaker positioned four-celled *Styela* embryos between glass plates during the third cell cycle and applied pressure that resulted in the reorientation of mitotic spindles according to Hertwig's Rule. In compressed eight-celled embryos, all of the blastomeres were in the same plane, instead of four animal blastomeres being positioned over four vegetal blastomeres. Furthermore, in compressed embryos, myoplasm was present in four blastomeres, instead of in two blastomeres. Compressed and non-compressed eight-celled embryos were then treated with cytochalasin B to pre-

Received 23 September 1996; accepted 3 January 1997.

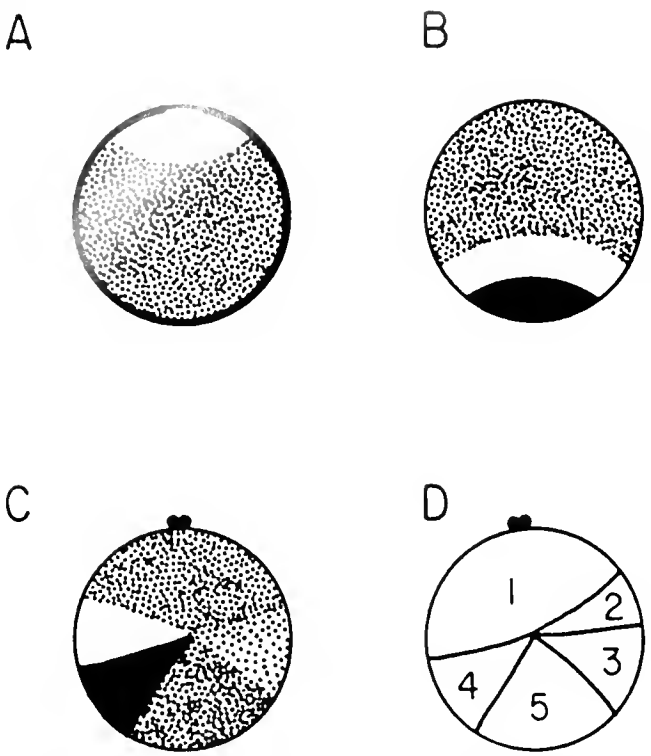

Figure 1. A schematic drawing showing the distribution of cytoplasmic determinants in unfertilized and fertilized ascidian eggs. (A) In the unfertilized egg, the myoplasm (bold line) is situated in the egg periphery. The ectoplasm (white region) is located inside the germinal vesicle, and the endoplasm (stipled region) fills the inner egg region. (B) After an egg is fertilized, the myoplasm moves into the vegetal pole region. The ectoplasm forms a band of cytoplasm above the myoplasm, and the endoplasm resides above the ectoplasm. (C) During the second phase of ooplasmic segregation, the myoplasm and ectoplasm shift into the equatorial region. At the end of the second phase of ooplasmic segregation, the egg cytoplasm is divided into five regions: (1) ectoplasm; (2) neuroplasm; (3) notochord plasm; (4) myoplasm; and (5) endoplasm (based on Conklin, 1905).

vent subsequent cell divisions. Treatment with cytochalasin facilitated the identification of myoplasm-containing blastomeres in eight-celled embryos after they were cultured for the time required for control embryos to develop into hatched larvae. When these embryos were examined for the activity of acetylcholinesterase (AchE), a muscle-specific enzyme, a maximum of four blastomeres comprising a compressed embryo expressed AchE activity, whereas in non-compressed eight-celled embryos a maximum of two blastomeres exhibited AchE activity. These elegant experiments performed by Whittaker provide rigorous support for Conklin's idea, published in 1905, that ascidian eggs contain muscle cell determinants.

Bissection of fertilized eggs has also been used to alter the normal distributions of myoplasm in ascidian embryos. When the animal hemispheres of fertilized eggs were removed, myoplasm was partitioned into more than the normal number of blastomeres (Bates, 1988). During the first phase of ooplasmic segregation, fertilized eggs were bissected into vegetal fragments that contained all of the egg myoplasm, termed myoplasm-enriched (ME) fragments, and into animal fragments that lacked myoplasm. ME fragments composed of 40%–50% of the total egg volume usually cleaved normally, completed gastrulation, and in some cases developed into larvae. At each developmental stage, it was shown that more than the normal number of blastomeres contained myoplasm. In larvae derived from ME fragments, most of the myoplasm was contained in tail muscle cells, although significant quantities of myoplasm were present in some of the head endoderm cells.

When the spatial expressions of tissue-specific markers were examined in ME larvae, each marker was normally expressed. For example, AchE activity and myosin were expressed in the cytoplasm of tail muscle cells, and alkaline phosphatase (AP) activity was expressed in the cytoplasm of endoderm cells situated in the head region. In another set of experiments, smaller ME fragments composed of 10%–30% of the total egg volume were produced from the vegetal pole region of fertilized eggs at the first stage of segregation, and these fragments could sometimes undergo several rounds of cleavage before cell division stopped. When cleavage-arrested four-celled ME embryos composed of 10%–30% of the total egg volume were tested for AchE activity after the controls developed into larvae, in some cases AchE activity was detected in all four blastomeres. In cleavage-arrested control four-celled embryos and ME four-celled embryos composed of 40%–50% of the total egg volume, AchE

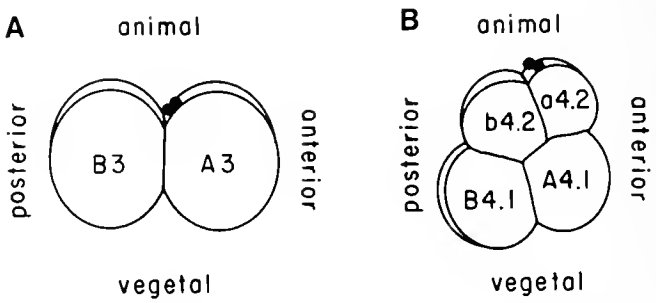

Figure 2. Schematic drawings showing the designation of blastomeres composing four-celled and eight-celled ascidian embryos. (A) The A3 blastomeres of a four-celled embryo lack myoplasm, whereas the B3 blastomeres contain myoplasm and develop muscle cell features when isolated from the rest of the embryo. (B) B4.1 blastomeres contain myoplasm and produce most of the tail muscle cells, mesenchyme cells, and some of the endoderm cells and notochord cells. A4.1 blastomeres produce spinal cord cells, endoderm, notochord, and distal tail muscle cells. a4.2 blastomeres produce epidermal and brain cells. b4.2 blastomeres produce epidermis, spinal cord cells, and distal tail muscle cells (Conklin, 1905; Nishida and Satoh, 1983).

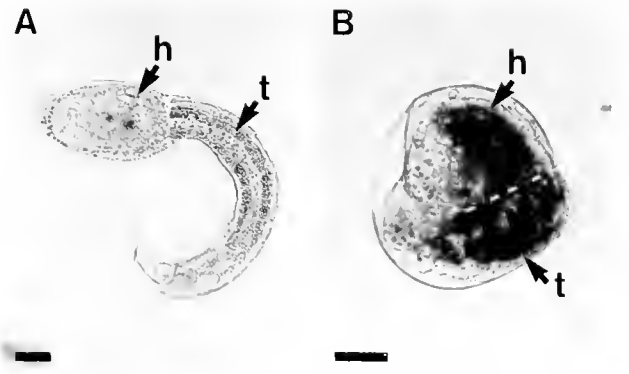

Figure 3. Light photomicrographs of detergent-extracted larvae. (A) A control larva showing the pigmented myoplasm within tail muscle cells (t). Endoderm cells situated within the head region (h) do not contain myoplasm. (B) A myoplasm-enriched (ME) larva showing the pigmented myoplasm within tail muscle cells (t) and the pigment granules evident within some of the endoderm cells situated in the head region (h). The dotted white lines shown in (A) and (B) designate the boundary between the larval head and and tail regions. Scale bars equal 50 μm.

activity was detected in a maximum of two blastomeres that corresponded to the posterior B3 muscle progenitor cells.

The contrasting results obtained from these two kinds of myoplasm redistribution experiments present an intriguing paradox. Why were muscle cell fates altered in compressed embryos and in small ME embryos produced from the vegetal pole region, whereas muscle cell fates were normal in ME embryos composed of 40%–50% of the total egg volume? The present study resolves this paradox by examining the distribution of MCD components in ME and compressed *Boltenia villosa* embryos and provides experimental support for the idea that p58 anchors ascidian muscle cell determinants.

Materials and Methods

Adult ascidians and embryo cultures

Boltenia villosa (Stimpson 1864) adults were purchased from Westwind Sealab Supplies, Victoria, British Columbia, Canada. Adults were maintained under conditions of constant light to prevent spawning (West and Lambert, 1975). Eggs and sperm were dissected from the gonads of two or more individuals. The eggs were cross-fertilized, washed several times with large volumes of seawater, and cultured at 11°C until the desired developmental stages were obtained.

Surgical methods

The spatial patterns of five kinds of cytoplasmic factors present in unfertilized and fertilized ascidian eggs are shown in Figure 1. These factors determine epidermal, muscle, endoderm, notochord, and nerve cell fates. The present study is focused on muscle cell factors localized in the myoplasm of ascidian eggs. Prior to fertilization, the myoplasm is present in the cortical cytoplasm that surrounds the egg. Within minutes of fertilization, the myoplasm is dramatically segregated into the vegetal hemisphere by a series of precisely controlled cytoplasmic movements, termed ooplasmic segregation. A fixed cleavage pattern subsequently partitions the myoplasm into specific blastomeres of the embryo (Fig. 2). In four-celled embryos, the posterior B3 blastomeres contain myoplasm, whereas the anterior A3 blastomeres lack it. At the eight-cell stage, the B4.1 blastomeres contain myoplasm, and these cells produce most of the tail muscle cells of the larva (Conklin, 1905; Nishida and Satoh, 1983).

The normal distribution of myoplasm within embryonic progenitor cells was altered using a surgical method previously described by Bates and Jeffery (1987). Eggs were fertilized and allowed to undergo the first phase of ooplasmic segregation, in which the cortical myoplasm is moved into the vegetal hemisphere and surrounds the vegetal pole. At a position corresponding to the animal pole, a tear was made in the follicular envelope (FE) that surrounds the egg. In some cases, 50%–60% of the total egg was extruded through the torn FE, leaving the my-

Figure 4. Light photomicrograph of a thick section through a myoplasm-enriched (ME) larva showing pigment granules (pg) in tail muscle cells and in the cytoplasm of endoderm cells situated in the head region (h). The notochord (n) is displaced into a more anterior position than normal. Scale bar equals 100 μm.

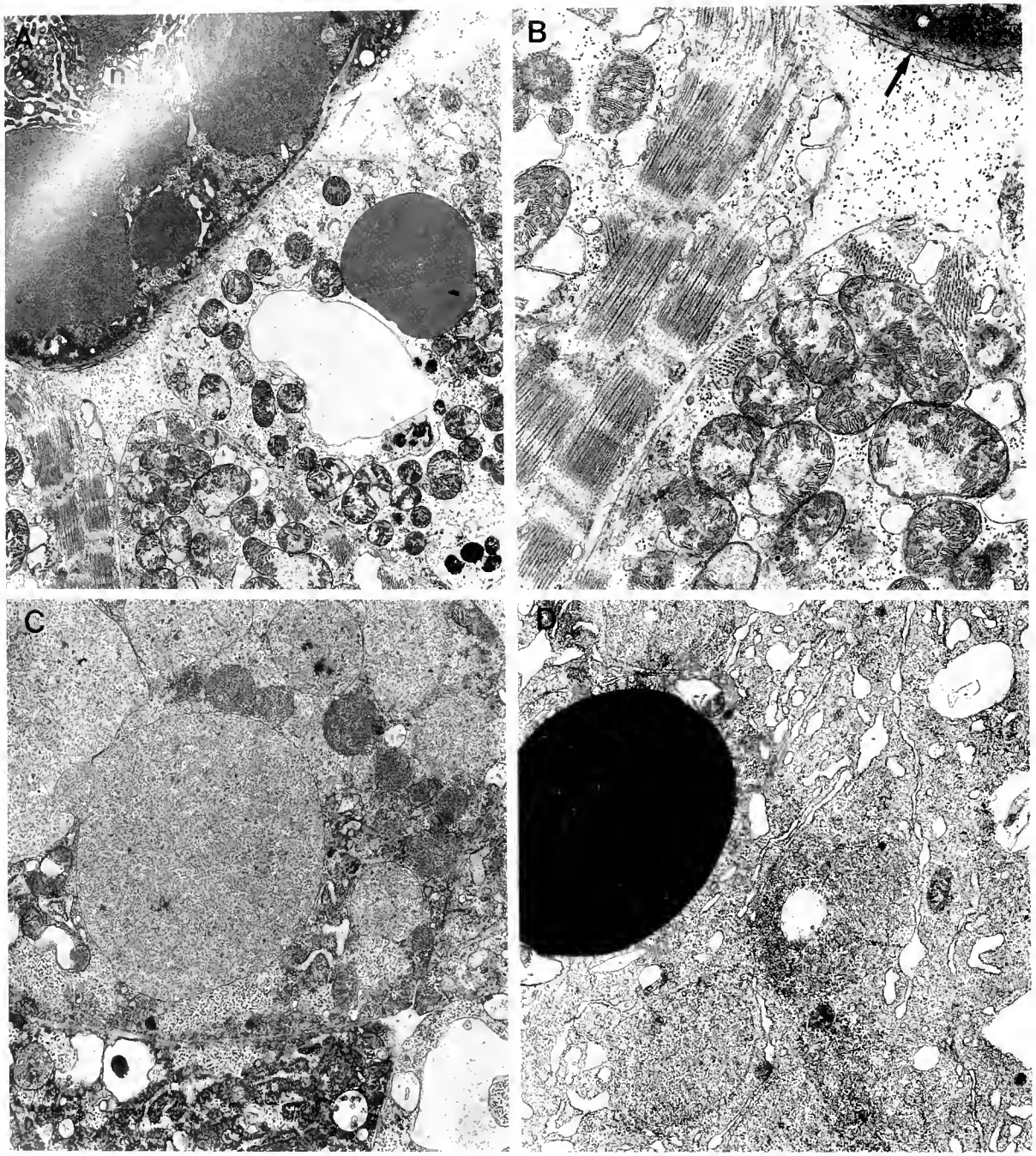

Figure 5. Transmission electron micrographs showing the ultrastructural features of muscle and endoderm cells of a myoplasm-enriched (ME) larva. (A) Sacromeres are evident in tail muscle cells near the notochord (n). Magnification equals 6,300×. (B) A higher magnification of (A) showing well-developed sacromere structure. Magnification equals 13,500×. Arrow points to the notochord sheath that surrounds the notochord (n). (C) Fine structure of yolky endodermal cells situated in the head region. Magnification equals 10,500×. (D) Features of endoderm and epidermal cells in the head region. Magnification equals 10,500×.

oplasm-containing vegetal hemisphere within the FE. The cytoplasmic bridge connecting the extruded egg region with the myoplasmic region was cut using a fine needle. In other cases, 70%–90% of the total egg volume was extruded through the tear, and the cytoplasmic bridge was cut leaving the vegetal pole ME fragment

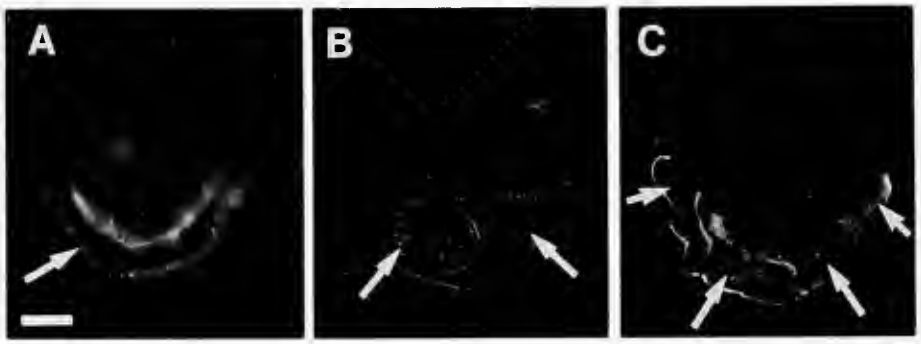

Figure 6. Photomicrographs showing myosin heavy chain expression in a control larva, a cleavage-arrested eight-celled embryo, and a compressed and cleavage-arrested eight-celled embryo. (A) Section of a control larva showing the expression of myosin heavy chain protein in tail muscle cells (arrow) situated along the notochord. (B) Section of a cleavage-arrested eight-celled embryo showing myosin in the peripheral cytoplasm of B4.1 blastomeres (long arrows). (C) Section of a compressed and cleavage-arrested eight-celled embryo showing myosin in the peripheral cytoplasm of B4.1 blastomeres (long arrows) and two additional blastomeres (short arrows). Scale bar in (A) equals 50 μm. Same magnifications in (B and C) as in (A).

within the FE. ME fragments of both size classes were either fixed for electron microscopy or immunocytochemistry, or they were transferred to tissue culture wells containing filtered seawater and cultured until the desired developmental stages were obtained.

Microcompression of embryos

Whittaker (1980) modified T. H. Morgan's microcompression technique (1910) to reorient mitotic spindles of eight-celled *Styela* embryos. Compression resulted in the partitioning of the myoplasm of eight-celled *Styela* embryos into four blastomeres instead of two blastomeres. A compression method similar to Whittaker's was used to alter the normal distributions of myoplasm in *B. villosa* embryos. Microcompression chambers were prepared by positioning strips of lens paper about 20 mm apart on a glass microscope slide. A drop of seawater containing four-celled embryos was positioned between the paper strips, and a coverslip was placed over the embryos. Seawater was gradually withdrawn from beneath the coverslip by capillary action to exert a gentle pressure on the embryos. The extent of compression was monitored under a microscope. Pressure was applied to embryos for about 15 to 20 min. Next, the coverslip was floated away from the compressed embryos and the embryos were transferred to a well containing 2 μg/ml cytochalasin B (CB; Sigma Chemical Co., St. Louis, MO) dissolved in seawater. CB treatment inhibits cell division, as previously described by Whittaker (1980). Control and compressed eight-celled CB embryos were cultured until the control eggs developed into hatched larvae. CB embryos were subsequently processed for *in situ* hybridization or immunocytochemistry.

Identification of myoplasm

Orange pigment granules embedded in the cortex of *B. villosa* eggs were used to produce myoplasm-enriched (ME) egg fragments. Some specimens were treated with 0.5% Triton X-100 detergent to make the myoplasm-containing cells more visible in photographs (Jeffery and Meier, 1983; Bates, 1988).

Transmission electron microscopy

Larvae were fixed with 2% glutaraldehyde in 0.1 *M* phosphate buffer, pH 7.4, for 30 min at room temperature, as previously described by Jeffery and Meier (1983). Specimens were rinsed with phosphate buffer and post-fixed in 1% osmium tetroxide dissolved in 0.1 *M* phosphate buffer, pH 7.4, for 1 h at room temperature. After the samples were rinsed with the phosphate buffer, they were dehydrated through a graded series of ethanol. Following gradual infiltration with Spurr's resin, specimens were embedded. Thick sections (0.5 μm) and thin sections were cut. The thin sections were stained with 2% aqueous uranyl acetate and lead citrate and viewed using a Phillips 420 electron microscope at 80 kV.

Scanning electron microscopy

Specimens were prepared for scanning electron microscopy (SEM) using a modification of a method previously described by Jeffery and Meier (1983). Specimens were extracted with 0.5% Triton X-100 detergent dissolved in seawater for 45 to 60 min at room temperature and then washed in seawater. Triton X-100 detergent removes cell membranes to expose the underlying MCD for SEM (Jeffery and Meier, 1983). Specimens

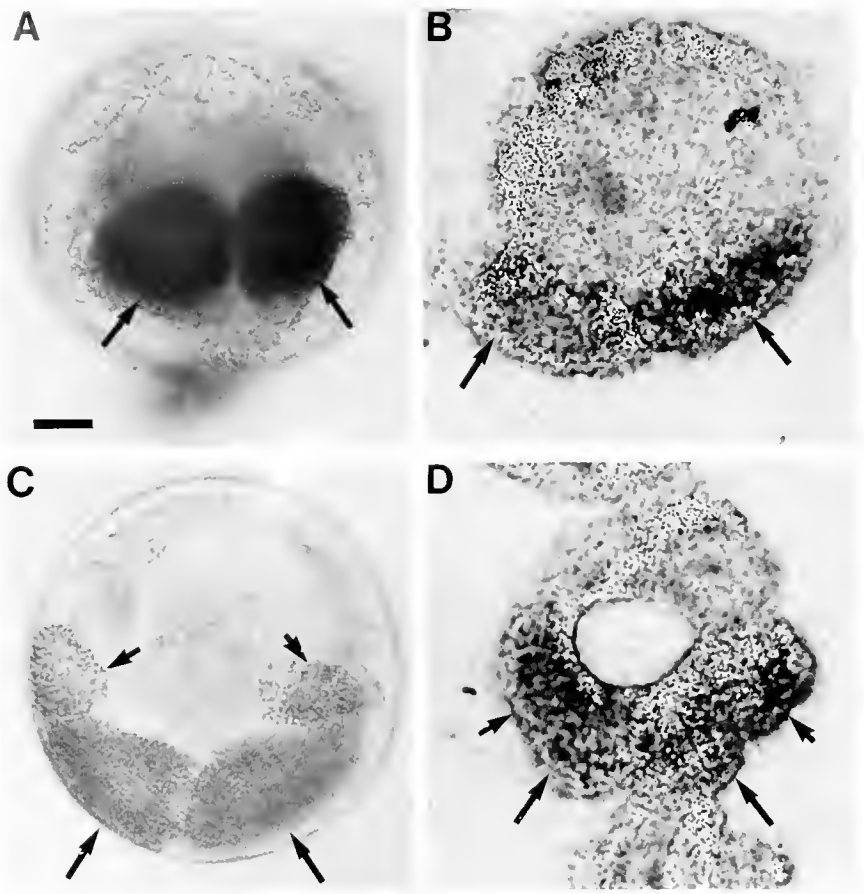

Figure 7. Light photomicrographs showing the spatial distribution of myoplasm in control and compressed eight-celled embryos and *in situ* hybridizations of sectioned control and compressed cleavage-arrested eight-celled embryos using SpMA3C anti-sense RNA. (A) A detergent-extracted control embryo showing myoplasm contained in the B4.1 blastomeres (long arrows). (B) Bright-field image of a cleavage-arrested embryo showing the hybridization of SpMA3C probe to the cytoplasm of B4.1 blastomeres (long arrows). (C) A detergent-extracted, compressed embryo showing myoplasm in the B4.1 blastomeres (long arrows) and in two additional blastomeres (short arrows). (D) Bright-field image of a compressed and cleavage-arrested eight-celled embryo showing the hybridization of SpMA3C probe to the cytoplasm in the B4.1 blastomeres (long arrows) and in two additional blastomeres (short arrows). Scale bar in (A) equals 50 μm. Same magnification for (B–D) as (A).

were rinsed with PBS and then fixed in 2% glutaraldehyde in 0.1 *M* sodium phosphate buffer, pH 7.4, for 30 min at room temperature. Samples were washed three times in 0.1 *M* sodium phosphate buffer. Fixed specimens were immersed in 1% osmium in the same buffer for 1 h at room temperature, followed by dehydration through a grade I series of ethanol (10%, 30%, 50%, 70%, 100%) for 10 min at each step.

Specimens were transferred into a specimen holder and inserted inside a Tousimis Autosamdri-814 critical point drying chamber. Dried specimens were attached to double-sided tape on an aluminum stub and coated inside a Sputtering System, Hummer VII coating machine. A 20-nm gold/palladium metal alloy coating was applied to the surface of each specimen, and the specimens were viewed using a JSM-6400 scanning electron microscope.

In situ *hybridization*

The *in situ* hybridization method previously described by Tomlinson *et al.* (1987) was used in the present study. Normal and compressed eight-celled embryos, cultured in seawater containing cytochalasin B until the controls developed into larvae, were fixed for 20 min in 3:1 ethanol-glacial acetic acid at −20°C. After the fixed embryos were dehydrated in a graded series of ethanol, they were gradually infiltrated with Paraplast and embedded in BEEM capsules. Specimens were sectioned at 7 μm and dried on gelatin-coated slides. SpMA3C DNA cloned

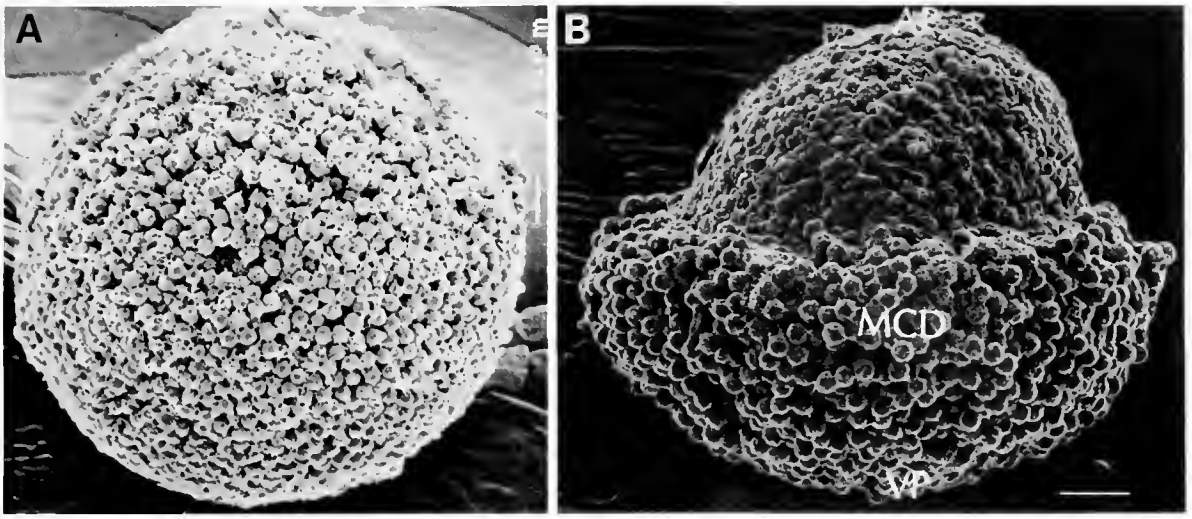

Figure 8. Scanning electron micrographs of detergent-extracted unfertilized and fertilized eggs. (A) An unfertilized egg showing the myoplasmic cytoskeletal domain (MCD) in the peripheral egg cytoplasm. (B) A fertilized egg at the first stage of ooplasmic segregation showing the segregation of the MCD in the cytoplasm of the vegetal hemisphere. AP—animal pole; VP—vegetal pole. Same magnification for (A) and (B); Scale bar in (A) equals 10 μm.

into Bluescribe vector was linearized using EcoR1 or Hind III to serve as templates for anti-sense and sense RNA probes respectively. Linearization was checked by running some of the cut and uncut DNA on 1% agarose gels followed by ethidium bromide staining. SpMA3C DNA cut with EcoRI was transcribed in the presence of 50 μCi of ^{3}H-UTP (Amersham) or ^{35}S-UTP (Amersham) and cold ATP, CTP, and GTP (400 μM of each nucleotide) using T3 polymerase. SpMA3C DNA was cut with Hind III and transcribed with T7 polymerase to produce sense probes.

The hybridization buffer contained 50% formamide, 10% w/v dextran, 0.01 *M* Tris, 0.3 *M* NaCl, 0.001 *M* EDTA, 500 μg/ml tRNA, Denhardt's solution (1:10 dilution of 50× stock), and 500 μg/ml polyadenylic acid. Slides were probed at low stringency (washed in 1× SSC for 30 min at room temperature) or at high stringency (washed in 1× SSC for 30 min at 45°C), air dried, dipped in Kodak NTB-2 nuclear track emulsion, and exposed for up to 6 weeks.

Immunocytochemistry

Specimens were fixed and embedded in polyester (Steedman's) wax, as previously described by Mita-Miyazawa *et al.* (1987). Specimens were fixed for 20 min in absolute methanol and then immersed in cold absolute ethanol for 20 min. Specimens were infiltrated in 50% polyester wax in absolute ethanol for 1 h at 42°C, then infiltrated in 100% polyester wax for 1 h at 42°C. Specimens were embedded in BEEM capsules, sectioned at 7 μm, and mounted on gelatin-coated stripes of coverslips. Sections were de-waxed in 100% ethanol, rehydrated, and washed in PBS prior to treatment with the primary antibody.

Myosin was detected using Mu-2 antibody (Mita-Miyazawa *et al.*, 1987) diluted 1:300 with PBS. Sections were immersed in the primary antibody for 1 h at room temperature, washed in PBS at room temperature, and immersed in FITC-conjugated anti-mouse IgG (Sigma Chemical Company, St. Louis, MO) diluted 1:60 with PBS. After a 30-min incubation at room temperature, sections were washed in PBS for 30 min, mounted in 80% glycerol in PBS, and viewed with an Olympus fluorescence microscope. Stained sections were photographed using Tri X film, ASA 400.

Monoclonal anti-neurofilament 160 antibody (clone NN18; Sigma Chemical Company, St. Louis, MO) was the primary antibody used to detect p58 in embryos (Swalla *et al.*, 1991). Sections were immersed in NN18 diluted 1:25 with PBS for 1 h at room temperature. Sections were washed with PBS and treated for 1 h at room temperature with anti-mouse IgG-POD (Sigma Chemical Company, St. Louis, MO) diluted 1:60 with PBS. Peroxidase activity was detected using Sigma FAST DAB peroxidase substrate tablets. Sections were incubated in the substrate solution for 10 min, washed in PBS, and viewed with a Zeiss Axioplan microscope.

Results

The myoplasm of an ascidian egg is normally partitioned into the embryonic progenitor cells that produce

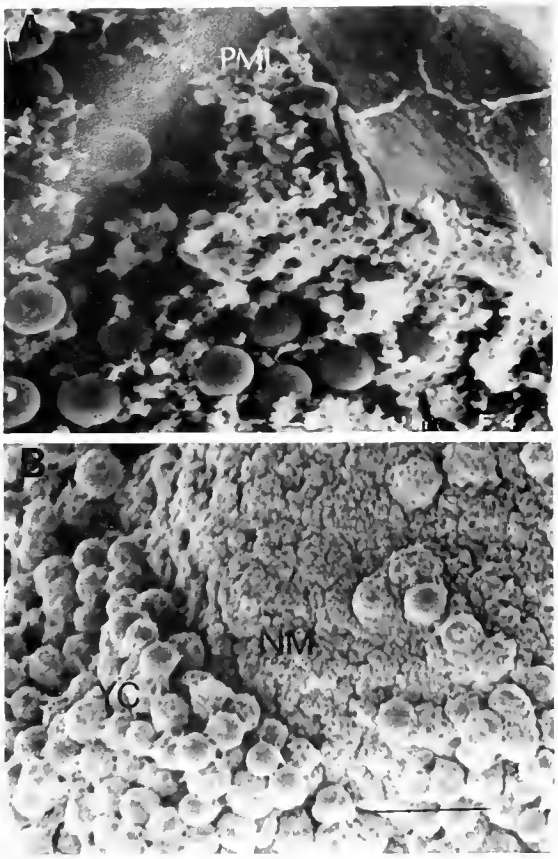

Figure 9. Higher magnification scanning electron micrographs of myoplasmic and non-myoplasmic egg regions. (A) The plasma membrane lamina (PML) of the myoplasmic cytoskeletal domain (MCD) is evident beneath a small patch of plasma membrane that was not dissolved by Triton X-100 treatment. Numerous pigment granules are evident. Scale bar equals 1 μm. (B) A distinct boundary is evident between the MCD and non-MCD regions of a fertilized egg. Scale bar equals 10 μm.

muscle cells situated in the larval tail region (Fig. 3A). When the animal hemisphere region was surgically deleted from fertilized eggs at the first stage of ooplasmic segregation, the nucleated vegetal merogons that contained segregated myoplasm developed into myoplasm-enriched (ME) larvae (Fig. 3B). In striking contrast to normal larvae, in which the pigmented myoplasm was present only in the tail muscle cells, in ME larvae myo- lasmic pigment granules were present in tail muscle ls and many of the endoderm cells situated in the lar- ead region (Fig. 3B). To determine more precisely cell types of ME larvae contained pigmented my- thick sections of ME larvae were examined, as Fig. 4. Pigmented myoplasm was evident in the of many endoderm cells situated in the head tioned ME larvae, whereas myoplasmic pig- me s were not evident in the cytoplasm of epi- derm otochord cells. Thick sections of ME larvae also revealed that their notochords were displaced into more anterior positions, as compared to normal larvae.

Can endoderm cells of ME embryos that contain pigmented myoplasm develop muscle cell features? This important question was addressed by using transmission electron microscopy to examine the cytoplasm of head-region endoderm cells of ME larvae for myofilaments. Twelve ME larvae were sectioned and thick sections were produced to identify head and tail regions prior to cutting thin sections. The ultrastructural features of ME tail muscle cells and head endoderm cells are shown in Figure 5. Sacromeres were evident in the peripheral cytoplasm of tail muscle cells (Fig. 5A, B); however, there was no evidence for the development of myofilaments in the head region of ME larvae in the more than 300 sections that were examined (Fig. 5C, D).

Next, the expressions of two muscle-specific markers, myosin and muscle actin RNA, were examined in cleavage-arrested control (non-compressed) and compressed eight-celled embryos. Figure 6 shows the expression patterns of myosin heavy chain protein in a control larva (Fig. 6A), in a cleavage-arrested eight-celled embryo (Fig. 6B), and in a compressed and cleavage-arrested eight-celled embryo (Fig. 6C). Myosin development was restricted to the tail muscle cytoplasm in normal larvae (in all 40 larvae tested). In cleavage-arrested eight-celled embryos, a maximum of two blastomeres expressed myosin (40 larvae tested). In contrast, compressed and cleavage-arrested eight-celled embryos developed myosin in a maximum of four blastomeres (40 embryos tested).

In another set of experiments, the development of muscle-specific actin RNA was studied in control and compressed cleavage-arrested eight-celled embryos (Fig. 7). A maximum of two blastomeres in control embryos showed hybridization signals (50 embryos examined; Fig. 7B), whereas a maximum of four blastomeres exhibited hybridization signals in the compressed embryos (40 embryos examined; Fig. 7D). The redistribution of pigmented myoplasm into more than the normal number of blastomeres by compression (compare A and C in Fig. 7) promoted the ectopic development of these muscle cell markers.

Why were muscle cell fates altered in compressed *Boltenia* embryos, whereas cell fates were normal in ME *Boltenia* embryos? This question was examined by studying the distribution of MCD components in normal embryos compared to ME embryos and compressed embryos.

Spatial distributions of the myoplasmic cytoskeletal domain and p58

The structure of the pigmented MCD of an unfertilized *Boltenia* egg treated with Triton X-100, as revealed

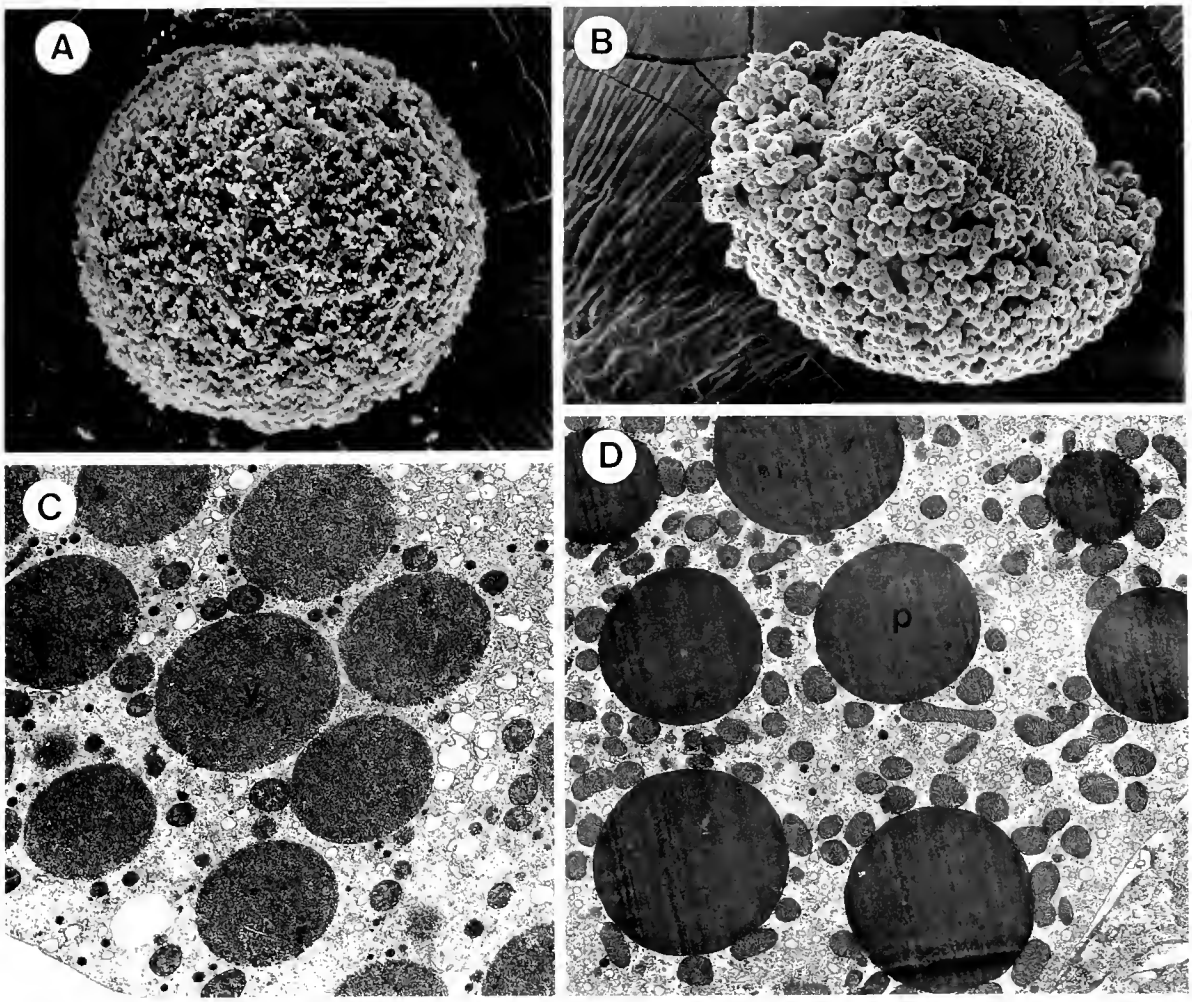

Figure 10. Scanning electron micrographs (SEM) and transmission electron micrographs (TEM) of myoplasm-deficient and myoplasm-enriched egg fragments. (A) SEM of a detergent-extracted myoplasm-deficient egg fragment. The pigmented myoplasmic cytoskeletal domain (MCD) is absent. Scale bar equals 10 μm. (B) SEM of a detergent-extracted myoplasm-enriched egg fragment. The pigmented MCD covers about 60%–70% of the surface. Scale bar equals 10 μm. (C) TEM of cytoplasm of a myoplasm-deficient egg fragment. Yolk granules and a few scattered mitochondria are evident. Magnification equals 6,300×. (D) TEM of cytoplasm of a myoplasm-enriched egg fragment. Pigment granules surrounded by many mitochondria. Magnification equals 6,300×.

by scanning electron microscopy, is shown in Figure 8A. After fertilization, the MCD segregated into the vegetal hemisphere and covered about 40%–50% of the total egg perimeter (Fig. 8B). The animal hemisphere region lacked the MCD and contained only a few scattered pigment granules. Higher magnification SEM images of the animal and vegetal hemisphere regions of a fertilized egg are shown in Figure 9. A small patch of plasma membrane that was not dissolved by Triton X-100 is evident in Fig. 9A. The distinct edge of the MCD in a fertilized egg is shown in Fig. 9B.

Animal fragments produced from fertilized eggs during the first phase of ooplasmic segregation lacked the MCD (Fig. 10A) and contained fewer mitochondria than found in the ME fragments (compare C and D in Fig. 10). The MCD surrounded about 60%–70% of the perimeter of ME fragments (Fig. 10B), and the MCD contained more mitochondria than did the egg fragments produced from the animal hemisphere (Fig. 10D). Removal of the animal hemisphere resulted in a 10%–20% increase in the surface area of an ME fragment composed of MCD (compare Figs. 8B and 10B). This increase in the surface area that contained the pigmented MCD resulted in the development of orange-headed larvae (Fig. 3B).

Seasonal variations in the distribution of myoplasmic

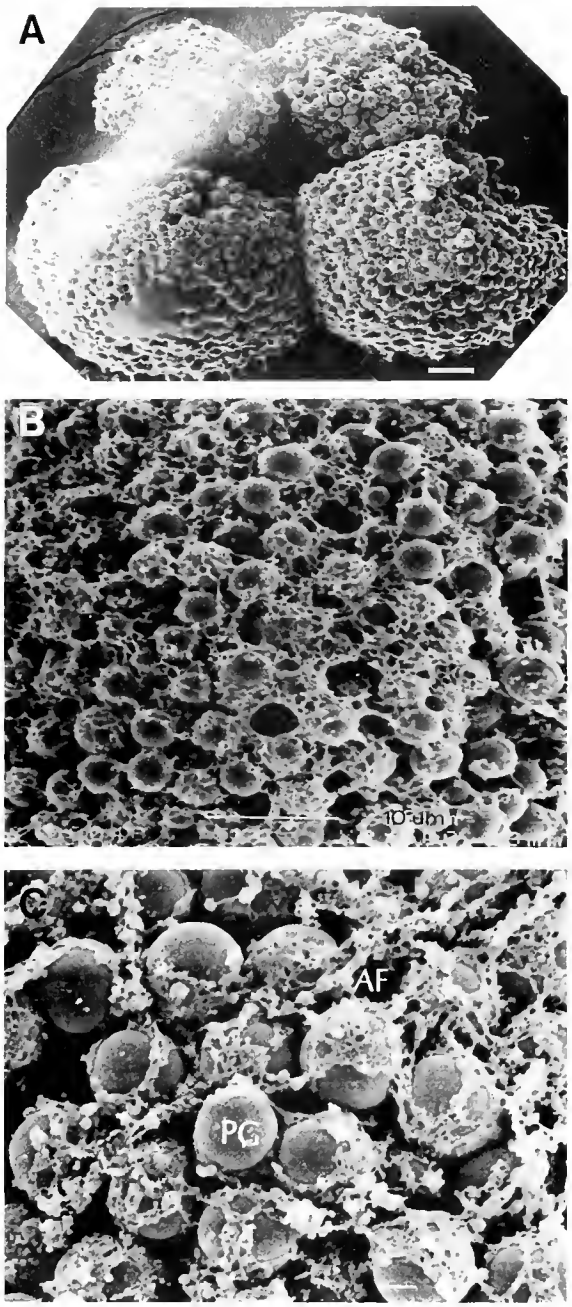

Figure 11. Scanning electron micrographs of a four-celled embryo showing the pigmented myoplasmic cytoskeletal domain (MCD) present in all four blastomeres. (A) The MCD is present in the cytoplasm of posterior B3 blastomeres and in the cytoplasm of anterior A3 blastomeres. Scale bar equals 10 μm. (B) Higher magnification showing the structure of the MCD in B3 cytoplasm. The MCD consists of a network of filaments with underlying pigment granules. Scale bar equals 10 μm. (C) Higher magnification of the MCD in the posterior region of an A3 blastomere. Actin filaments (AF) composing the plasma membrane component of the MCD cover the underlying pigment granules (PG) that are embedded in the deep filamentous lattice (PG). Scale bar equals 1 μm.

Table I

Distribution of the myoplasmic cytoskeletal domain (MCD) in the blastomeres of four-celled embryos produced in the autumn that showed pigment granules in all blastomeres

Number of blastomeres containing MCD	Number of embryos
0	0
1	0
2	0
3	1
4	29

pigment granules in *Boltenia villosa* embryos were observed. In late autumn, about one-quarter of the *B. villosa* adults produced clutches of eggs in which orange pigment granules were present in the cortical cytoplasm of all four blastomeres in four-celled embryos, as compared to clutches of eggs produced at other times of the year in which pigment granules were restricted to the cortical cytoplasm of B3 blastomeres of four-celled embryos. Most of the embryos that exhibited altered pigmentation patterns developed into normal larvae. The spatial distributions of the MCD were mapped in four-celled embryos; SEM was used to determine if the MCD was restricted to the B3 blastomeres or was also found in A3 cytoplasm. These results are shown in Figure 11 and Table I. Whereas most of the pigmented MCD was con-

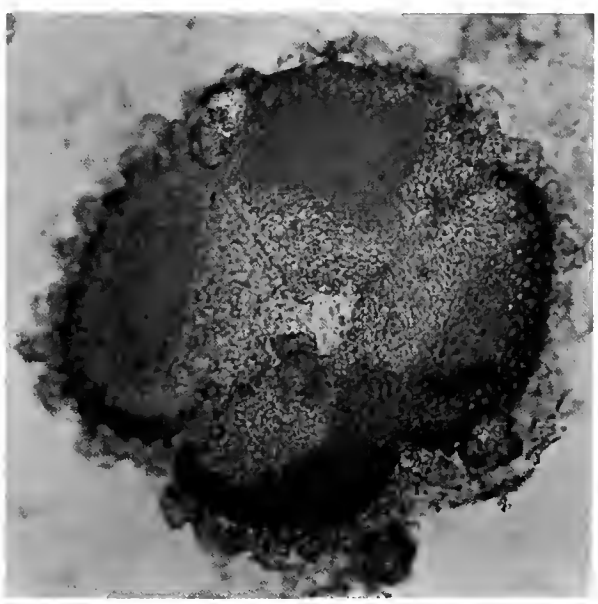

Figure 12. Light photomicrograph of a four-celled embryo stained with NN18 antibody in which the myoplasmic cytoskeletal domain is present in all four blastomeres. Two blastomeres are stained with NN18 antibody. Scale bar equals 100 μm.

Table II

Distribution of p58 in unoperated and myoplasm-enriched (ME) four-celled embryos

Specimens	Maximum number of blastomeres stained with NN18 antibody				
	0	1	2	3	4
'Autumn' embryos	8	7	25	0	0
ME embryos composed of 40%–50% of total egg volume	2	4	15	0	0
ME embryos composed of 20%–30% of total egg volume	0	0	1	8*	10

* Three blastomere per embryo were in the plane of section.

tained in the B3 blastomeres, A3 blastomeres contained significant quantities of the pigmented MCD.

The spatial distributions of p58, a protein associated with the DFL component of the MCD, were examined using NN18 antibody in four-celled embryos that contained pigmented MCD in all blastomeres. A maximum of two blastomeres per embryo were stained with NN18 antibody (Fig. 12 and Table II). Therefore, although A3 blastomeres contained the anteriormost region of the MCD, this region of the MCD lacked p58.

In another set of experiments, four-celled ME embryos composed of 40%–50% and 20%–30% of the total egg volume were stained with NN18 antibody. In embryos made up of 40%–50% of the total egg volume, a maximum of two blastomeres were stained with NN18 as in control four-celled embryos (Fig. 13A and Table II). In contrast, when four-celled embryos derived from smaller ME fragments produced from the vegetal pole region were stained with NN18, in most cases (95%; n = 19) more than two blastomeres reacted with the antibody (Fig. 13B and Table II). When compressed eight-celled embryos were stained with NN18, a maximum of four blastomeres reacted with this antibody (Fig. 13C and Table III). In control eight-celled embryos, a maximum of two blastomeres were stained with NN18.

Discussion

The results of the present study demonstrate that (1) compression of four-celled *Boltenia villosa* embryos increased the number of blastomeres of eight-celled embryos that could develop muscle cell features; (2) the development of muscle cell features in compressed embryos was correlated with the presence of the cytoskeletal protein p58; (3) p58 was restricted to the cytoplasm of posterior B3 blastomeres of four-celled ME embryos composed of 40%–50% of the total egg volume; (4) p58 was present in the cytoplasm of anterior A3 and posterior B3 blastomeres of four-celled embryos that were derived from small ME fragments produced from the vegetal pole region of fertilized eggs at the first stage of ooplasmic segregation; and (5) p58 was concentrated in the vegetal pole region of the MCD at the first stage of ooplasmic segregation.

The present results provide rigorous experimental support for the idea, first suggested by Swalla *et al.* (1991), that the cytoskeletal protein p58 is associated with muscle cell determinants in ascidian eggs. Another cytoskeletal protein, myoplasmin-C1, is localized in ascidian myoplasm (Nishikata *et al.*, 1987), and it has been suggested that myoplasmin-C1 may interact with p58 through α-helical rod regions formed by hydrophobic heptad repeats present in both of these proteins (Nishikata and Wada, 1996; B. J. Swalla, pers. comm.). Therefore, α-helix coiled-coil complexes composed of p58 and my-

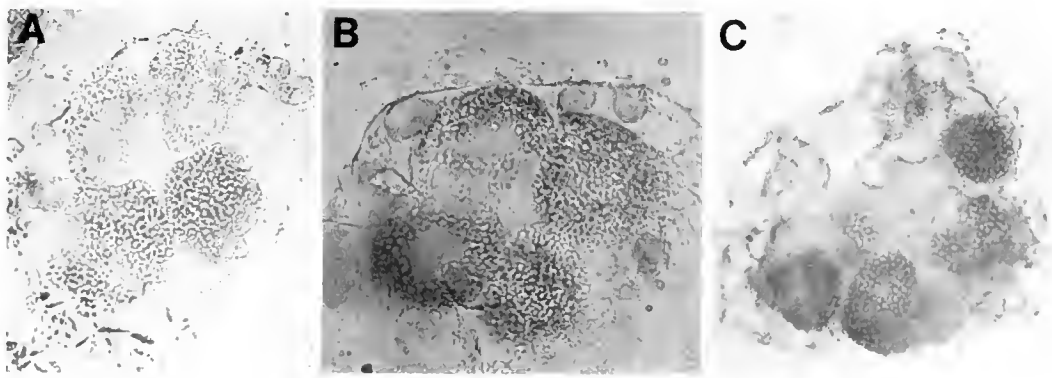

Figure 13. Light photomicrographs of NN18 staining patterns of myoplasm-enriched (ME) and compressed embryos. (A) A section of a four-celled ME embryo composed of 40% of the total egg volume that shows two blastomeres stained with NN18. (B) A section of a four-celled ME embryo composed of 30% of the total egg volume in which four blastomeres reacted with NN18. (C) A section of a compressed embryo showing four blastomeres stained with NN18. Scale bars equal 50 μm.

Table III

Distribution of p58 in normal and compressed eight-celled embryos

Specimens	Maximum number of blastomeres per embryo stained with NN18 antibody								
	0	1	2	3	4	5	6	7	8
Normal embryos	2	2	24	0	0	0	0	0	0
Compressed embryos	3	1	1	0	22*	0	0	0	0

* In five embryos, five or six blastomeres were in the plane of section.

oplasmin-C1 may be the cytoskeletal scaffold that anchors muscle cell determinants.

The expression of a muscle actin promoter-*lacZ* reporter gene construct, MocuMA1/*lacZ*, was recently examined in the tailless larvae of *Molgula occulta*. In these larvae, which lack p58 and do not develop functional muscle cells, low levels of β-galactosidase activity were detected in a few posterior cells (Kusakabe *et al.*, 1996). This result and the presence of insertions, deletions, and codon substitutions in the coding regions of orthologous larval muscle actin genes isolated from the urodele species *Molgula oculata* suggest that mutations in muscle genes rather than changes in trans-acting regulatory factors are responsible for the regression of muscle cells. These investigators also reported that MocuMA1/*lacZ* constructs are expressed in mesenchyme and other nonmuscle cell types in urodele larvae and that the *M. occulta* cells expressing β-galactosidase activity did not correspond to the cells expressing low levels of vestigial AchE activity. Therefore, these results suggest that the activity of the MocuMA1 promoter is somewhat "leaky" in some cell types, as is the transcription of AchE genes in vestigial muscle cells of several anural ascidian species (Whittaker, 1979; Jeffery and Swalla, 1990b; and Bates and Mallett, 1991). The results obtained by Jeffery and Meier (1983), Swalla *et al.* (1991), Nishikata and Wada (1996) and those reported in the present study suggest that determinants associated with the myoplasmic cytoskeleton are required for the normal promoter activities of muscle genes.

Mapping the distributions of p58 in ME and compressed embryos has resolved the paradox of why cell fates were normal in embryos derived from ME fragments composed of 40%–50% of the total egg volume (Bates, 1988), but muscle cell fates were altered in compressed embryos (Whittaker, 1980; and the present study) and small ME embryos produced from the vegetal pole region of fertilized eggs (Bates, 1988). Removal of the animal hemisphere of a fertilized egg during the first stage of ooplasmic segregation resulted in a 10%–20% increase in the cortical cytoplasm of an ME fragment that contained the MCD. Increasing the surface area of MCD would produce larger than normal myoplasmic crescents after the second phase of ooplasmic segregation. These enlarged crescents would position the anteriormost MCD into the endodermal determinant domain of the egg (Conklin, 1905; Nishida, 1994). The normal cleavage pattern of an ME embryo (Bates, 1988) would then partition the anterior MCD into endoderm cells, resulting in the development of larvae in which some of the head endoderm cells contain pigmented cytoplasm.

When the regional expressions of three muscle-specific markers, myosin heavy chain (Bates, 1988), AchE activity (Bates, 1988), and myofilaments (present study) were examined in ME larvae, only tail muscle cells were able to develop these markers. The endoderm cells present in

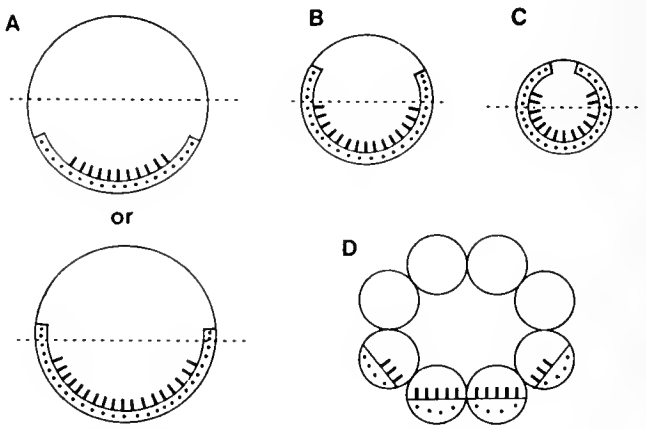

Figure 14. A summary of the present results. (A; top) The myoplasmic cytoskeletal domain (MCD) resides in the more posterior cytoplasm of a fertilized egg at the second stage of ooplasmic segregation (anterior—top; MCD is outlined). The MCD contains pigment granules (dots), proteins, RNA, and mitochondria. The posterior region of the MCD contains p58 (short lines). (A; bottom) In late autumn, some adults produce eggs in which some of the MCD was extended into the anterior cytoplasm, yet p58 was restricted to the more posterior MCD. (B) In myoplasm-enriched (ME) fragments composed of 40%–50% of the total egg volume, there was an increase in cortical cytoplasm that contained the MCD. As in autumn eggs that exhibited altered pigmentation patterns (Fig. 14A; bottom), some of the pigmented MCD was extended into the more anterior cytoplasm. This pigmented MCD was partitioned into some of the head endoderm cells of the larva; however, endoderm cell fates remained normal because p58 was localized in the more posterior region of the MCD. (C) In smaller ME fragments produced from fertilized eggs, MCD that contained p58 was present in the anterior cytoplasm as well as in the posterior cytoplasm. After two cell divisions, the resulting four blastomeres contained p58, and all four blastomeres of cleavage-arrested smaller ME embryos expressed AchE activity (Bates, 1988). (D) Compression of four-celled embryos resulted in the partitioning of MCD that contained p58 into four blastomeres of eight-celled embryos, in contrast to normal eight-celled embryos that have p58 in the two B4.1 blastomeres. The presence of p58 in four blastomeres of a compressed and cleavage-arrested eight-celled embryo promoted the development of myosin and muscle actin RNA in four blastomeres.

Table IV

Summary of results

Type of embryo[1]	Maximum number of cells/embryo expressing a muscle cell marker	Distribution of p58
Cleavage-arrested four-celled control embryos	two cells expressed AchE activity[2]	two cells
Cleavage-arrested four-celled ME embryos 40%–50% TEV	two cells expressed AchE activity[2]	two cells
Cleavage-arrested four-celled ME embryos 10%–30% TEV	four cells expressed AchE activity[2]	four cells
Cleavage-arrested eight-celled embryos	two cells expressed myosin and muscle actin RNA	two cells
Cleavage-arrested and compressed eight-celled embryos	four cells expressed myosin and muscle actin RNA	four cells

[1] ME = myoplasm-enriched; TEV = total embryo volume.
[2] From Bates (1988).

the head region of ME larvae developed an endoderm-specific marker, alkaline phosphatase activity, as did the control larvae (Bates, 1988). The detection of p58 in the cytoplasm of B3 blastomeres of four-celled ME embryos but not in A3 blastomeres explains why muscle cell fates in these embryos were normal.

Two observations described in the present study indicate the probable distribution of p58 in the MCD in fertilized eggs just prior to first cleavage. During most of the year, *Boltenia* adults produce clutches of eggs that develop into four-celled embryos in which the MCD resides exclusively in the cytoplasm of the B3 blastomeres (Jeffery and Meier, 1983). However, in late autumn some animals produce four-celled embryos in which the MCD is present in A3 blastomeres and in B3 blastomeres. When these embryos were stained with NN18, only two blastomeres contained p58. These results suggest that p58 may be more concentrated in the posterior region of the MCD prior to first cleavage than in the more anterior region of the MCD. This idea is further supported by the detection of p58 in the cytoplasm of all four blastomeres of four-celled ME embryos produced from the vegetal pole region of fertilized eggs (see Fig. 14).

The present results indicate that the distribution of the cytoskeletal protein p58 is correlated with the ectopic development of muscle cell features in compressed ascidian embryos. Whittaker (1980) observed that the maximum number of blastomeres that can develop AchE activity is four in compressed and cleavage-arrested eight-celled *Styela* embryos, but only two in non-compressed and cleavage-arrested embryos. The present results have confirmed and extended Whittaker's findings by showing that compression can alter muscle cell fates in *Boltenia villosa* embryos and that p58 is present in four, instead of two, blastomeres of compressed eight-celled embryos.

The results of the present study are summarized in Figure 14 and in Table IV. During the first phase of ooplasmic segregation following fertilization, the MCD is moved towards the vegetal pole. The MCD is then secondarily shifted into the equatorial-vegetal region of the egg prior to first cleavage (Fig. 14A, top), and this region designates the future posterior region of the larva (Conklin, 1905). Embedded within the MCD are pigment granules, mitochondria, RNA, and proteins. The cytoskeletal protein p58 is concentrated in the deep filamentous lattice of the MCD (Swalla *et al.*, 1991). In some clutches of eggs produced in late autumn, the surface area of an egg containing pigmented MCD was greater than in eggs produced at other times of the year (Fig. 14A, bottom). This increase resulted in the development of four-celled embryos in which the MCD was present in the cytoplasm of all four blastomeres. However, staining with NN18 showed that only the primary muscle progenitor B3 cells contained p58. These observations suggest that p58 is associated with the posterior MCD contained within the cytoplasm of B3 blastomeres, but absent from the anterior region of the MCD contained in A3 blastomeres.

In ME fragments composed of 40%–50% of the total egg volume, there was an increase in the surface area that contained the pigmented MCD (Fig. 14B). This increase resulted in the redistribution of some of the pigmented MCD into the anterior blastomeres. When four-celled ME embryos derived from this size class of egg fragments were immersed in NN18, a maximum of two blastomeres were stained. These results demonstrate that p58 distributions were not altered in the ME embryos and explains why the fates of embryonic ME cells were normal. In contrast, nearly the entire cortical cytoplasm of smaller ME fragments produced from the vegetal pole region of fertilized eggs contained the MCD (Fig. 14C). When four-celled ME embryos derived from these fragments were stained with NN18, p58 was detected in all four blastomeres. This observation explains why AchE activity was sometimes detected in all four blastomeres of small cleavage-arrested ME embryos, as compared to a maximum of two blastomeres in the control cleavage-arrested four-celled embryos (Bates, 1988). Compression of four-celled embryos caused p58 to be partitioned into four, rather than two, blastomeres of an eight-celled embryo (compare Figs. 2B and 14D). The presence of p58 in four blastomeres was correlated with the development of myosin and muscle actin RNA in four blastomeres of compressed and cleavage-arrested eight-celled embryos.

In conclusion, mapping the distribution of p58 has resolved the paradox of why cell fates were normal in ME embryos composed of 40%–50% of the total egg volume, but muscle cell fates were altered in small ME embryos and in compressed embryos. Immunoprecipitation experiments, now in progress, will coprecipitate muscle cell determinants with p58 for microinjection into non-muscle lineage blastomeres of urodele ascidian embryos and injection into anural ascidian eggs.

Acknowledgments

Monica Lovis and Mike Swallow are thanked for their technical assistance. SpMA3C DNA was kindly provided by Dr. William Jeffery, and Mu-2 antibody was kindly provided by Dr. N. Satoh. The comments provided by the reviewers were most helpful in preparing this manuscript. The author is most thankful for the award of an operating grant by the Natural Sciences and Engineering Research Council (NSERC) of Canada. This paper is dedicated to the memory of Dr. Rick Brodeur.

Literature Cited

Bates, W. R. 1995. Direct development in the ascidian *Molgula retortiformis* (Verrill, 1871). *Biol. Bull.* **188:** 16–22.

Bates, W. R. 1988. Development of myoplasm-enriched ascidian embryos. *Dev. Biol.* **129:** 241–252.

Bates, W. R., and W. R. Jeffery. 1987. Localization of axial determinants in the vegetal pole region of ascidian eggs. *Dev. Biol.* **124:** 65–76.

Bates, W. R., and J. E. Mallett. 1991. Ultrastructural and histochemical study of anural development in the ascidian *Molgula pacifica* (Huntsman). *Roux's Arch. Dev. Biol.* **200:** 193–201.

Conklin, E. G. 1905. The organization and cell lineage of the ascidian egg. *J. Acad. Natl. Sci. (Philadelphia)* **13:** 1–119.

Elinson, R. P. 1990. Cytoskeleton and embryo polarity. *Curr. Opin. Cell Biol.* **2:** 43–48.

Hill, D. P., S. Strome, and G. P. Radice. 1990. The cytoskeleton in development. Pp. 177–200 In *Cytoplasmic Organization System*, G. M. Malacinski, ed. McGraw-Hill, New York.

Jeffery, W. R. 1982. Messenger RNA in the cytoskeletal framework: analysis by *in situ* hybridization. *J. Cell Biol.* **95:** 1–7.

Jeffery, W. R. 1989. Localized mRNA and the egg cytoskeleton. *Int. Rev. Cytol.* **119:** 151–195.

Jeffery, W. R., and S. Meier. 1983. A yellow crescent cytoskeletal domain in ascidian eggs and its role in early development. *Dev. Biol.* **96:** 125–143.

Jeffery, W. R., and B. J. Swalla. 1990a. The myoplasm of ascidian eggs: a localized cytoskeletal domain with multiple roles in embryonic development. *Semin. Cell Biol.* **1:** 373–381.

Jeffery, W. R., and B. J. Swalla. 1990b. Anural development in ascidians: evolutionary modification and elimination of the tadpole larva. *Semin. Dev. Biol.* **1:** 253–261.

Kusakabe, T., B. J. Swalla, N. Satoh, and W. R. Jeffery. 1996. Mechanism of an evolutionary change in muscle cell differentiation in ascidians with different modes of development. *Dev. Biol.* **174:** 379–392.

Marikawa, Y. 1995. Distribution of myoplasmic cytoskeletal domains among egg fragments of the ascidian *Ciona savignyi*: the concentration of deep filamentous lattice in the fragment enriched with muscle determinants. *J. Exp. Zool.* **271:** 348–355.

Mita-Miyazawa, I., T. Nishikata, and N. Satoh. 1987. Cell- and tissue-specific monoclonal antibodies in eggs and embryos of the ascidian *Halocynthia roretzi*. *Development* **99:** 155–162.

Morgan, T. H. 1910. The effects of altering the position of the cleavage planes in eggs with precocious specification. *Wilhelm Roux' Arch. Entwicklungsmechanik Org.* **29:** 205–224.

Nishida, H. 1994. Localization of egg cytoplasm that promotes differentiation to epidermis in embryos of the ascidian *Halocynthia roretzi*. *Development* **120:** 235–243.

Nishida, H., and N. Satoh. 1983. Cell lineage analysis in ascidian embryos by intracellular injection of tracer enzyme. I. Up to the eight-cell stage. *Dev. Biol.* **99:** 382–394.

Nishikata, T., and M. Wada. 1996. Molecular characterization of myoplasmin-C1: a cytoskeletal component localized in the myoplasm of the ascidian egg. *Dev. Genes Evol.* **206:** 72–76.

Nishikata, T., I. Mita-Miyazawa, T. Deno, and N. Satoh. 1987. Monoclonal antibodies against components of the myoplasm of eggs of the ascidian *Ciona intestinalis* partially block the development of muscle-specific acetylcholinesterase. *Development* **100:** 577–586.

Swalla, B. J., M. R. Badgett, and W. R. Jeffery. 1991. Identification of a cytoskeletal protein localized in the myoplasm of ascidian eggs: localization is modified during anural development. *Development* **111:** 425–436.

Tomlinson, C. R., R. L. Beach, and W. R. Jeffery. 1987. Differential expression of a muscle actin gene in muscle cell lineages of ascidian embryos. *Development* **101:** 751–765.

West, A. B., and C. C. Lambert. 1975. Control of spawning in the tunicate *Styela plicata* by variations in a natural light regime. *J. Exp. Zool.* **195:** 265–270.

Whittaker, J. R. 1979. Development of vestigial tail muscle acetylcholinesterase in embryos of an anural ascidian species. *Biol. Bull.* **156:** 393–407.

Whittaker, J. R. 1980. Acetylcholinesterase development in extra cells caused by changing the distribution of myoplasm in ascidian embryos. *J. Embryol. Exp. Morphol.* **55:** 343–354.

Reference: *Biol. Bull.* **192:** 231–242. (April, 1997)

Embryonic Coat of the Grass Shrimp *Palaemonetes pugio*

PATRICIA S. GLAS[1], LEE A. COURTNEY[2,*], JAMES R. RAYBURN[1], AND WILLIAM S. FISHER[2]

[1] *National Research Council Associates and* [2] *U.S. Environmental Protection Agency, National Health and Environmental Effects Research Laboratory, Gulf Ecology Division, 1 Sabine Island Dr., Gulf Breeze, Florida 32561*

Abstract. The embryo of the grass shrimp, *Palaemonetes pugio,* is surrounded during development by a protective extracellular coat designated as the embryonic coat (EC). At hatching, this EC is composed of four embryonic envelopes (EE), each of which is composed of multiple layers. The outermost layer of the EC, the outer investment coat (OIC), is derived primarily, if not completely, from pleopods of the female. The first envelope (EE1) forms as a bilayered envelope, $EE1_a$ and $EE1_b$, immediately after oviposition. The OIC becomes closely associated with EE1 and remains in close contact with EE1 until hatching occurs. An additional layer, $EE1_c$, is added to the inner side of EE1 between 3 and 5 d after oviposition. Three more embryonic envelopes, EE2, EE3, and EE4, are formed between the embryo and EE1 by 7 d after oviposition. Formation of embryonic envelopes continues until 10 d after oviposition; by this time each envelope is morphologically distinct in composition, with "outer" and "inner" sides clearly identifiable. All but the innermost embryonic envelope (EE4) are shed by the embryo about 6 h before hatching. Permeability of the EC during the 12-d incubation period is found to decrease between 0 and 5 d after oviposition, and then increase until hatching. Fluorescently labeled lectins react positively with the OIC, indicating the presence of glucose and *N*-acetylglucosamine residues. Thus, the palaemonid EC is a dynamic structure throughout embryonic development.

Received 19 August 1996; accepted 20 December 1996.

Abbreviations: embryonic coat (EC); embryonic envelope (EE); outer investment coat (OIC); scanning electron microscopy (SEM); transmission electron microscopy (TEM); fluorescein isothiocyanate (FITC); Tris[hydroxymethyl]aminomethane (Tris).

Mention of commercial products does not constitute endorsement by the U.S. Environmental Protection Agency.

* Author to whom correspondence should be addressed.

Introduction

Grass shrimp, *Palaemonetes pugio,* inhabit estuaries in the coastal regions of the eastern United States. During mating, the male places a spermatophore on the thorax of a mature female, near the opening of the gonopores. As eggs are extruded from the oviduct, they pass across the spermatophore and are fertilized externally. Eggs are deposited, or oviposited, on setae of the pleopods of the female. After about 2 weeks of incubation, the embryos hatch as zoeal larvae (Broad, 1957). During this time, the embryonic coat (EC) must protect the embryos from microbial, physical, and possibly chemical conditions of the ambient water while allowing passage of gases and other metabolites.

Various nomenclature has been used to describe the embryonic coat in marine decapods. Lobsters have a fertilization envelope or chorion (Talbot, 1981; Talbot and Goudeau, 1988); crabs have an extra-cellular capsule or fertilization envelope (Goudeau and LaChaise, 1980a, b; Goudeau and Becker, 1982), penaeid shrimp have a hatching envelope (Clark and Lynn, 1977; Pillai and Clark, 1987), and *Palaemon* has an extracellular capsule (Goudeau *et al.,* 1991). Investigations have revealed at least one additional "coat" besides the fertilization or hatching envelope as part of the protective covering of the developing embryo. Lynn *et al.* (1993) reported the presence of three or more "envelopes" during later stages of development in the penaeid shrimp *Sicyonia ingentis.* Goudeau and LaChaise (1983) and Goudeau *et al.*

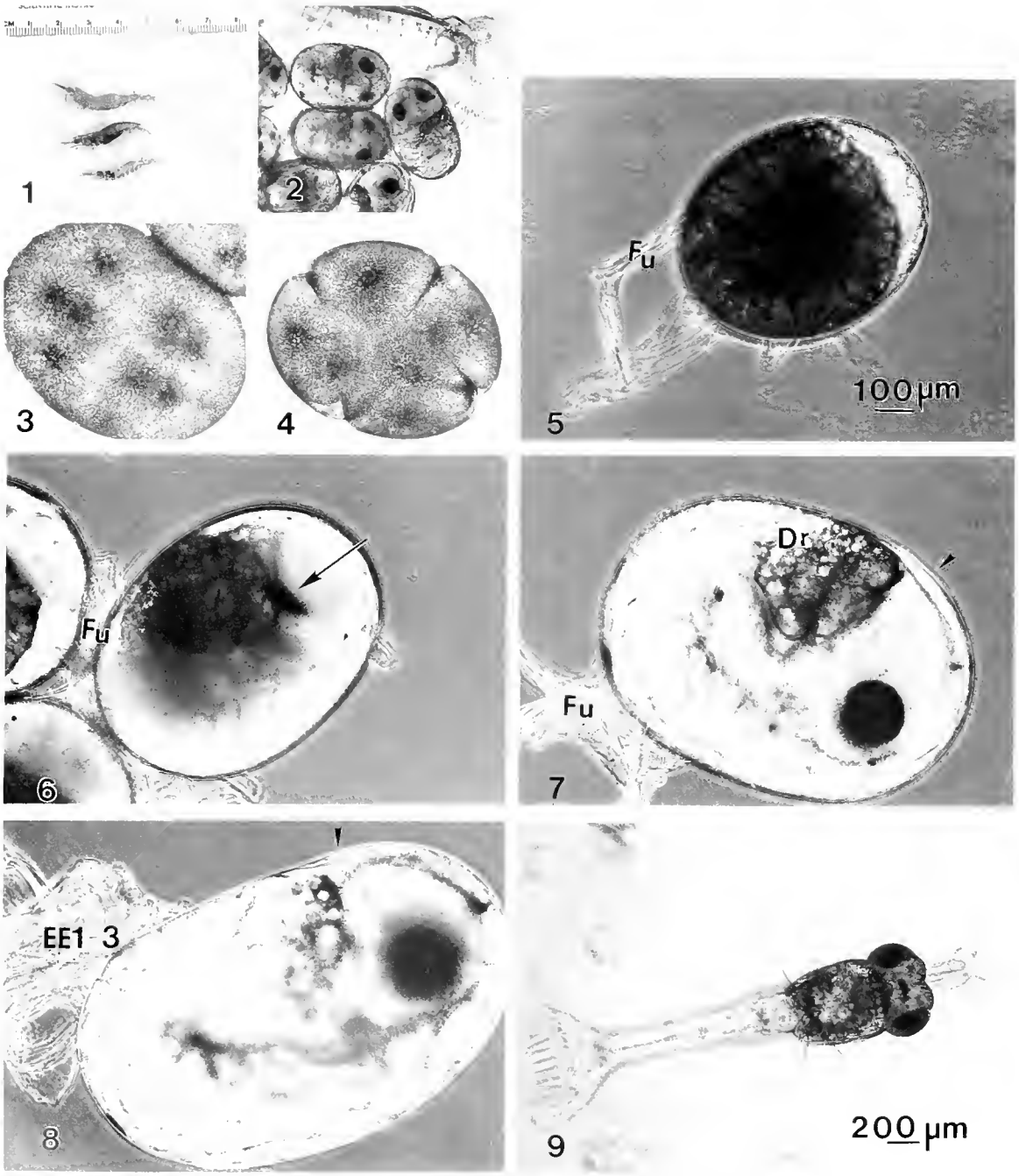

Figures 1–9. Adult and embryonic stages of the grass shrimp, *Palaemonetes pugio*

Figure 1. Photograph of *P. pugio* adults. Top, mature female; middle, ovigerous female; bottom, mature male.

Figure 2. Embryos 8 d after oviposition are shown attached to the ventral abdomen of a female. The embryos were attached to setae on the female pleopod by a cement that also forms the outer investment coat (OIC) of the embryonic coat.

Figure 3. Phase contrast micrograph of fertilized eggs on Day 0 within 4 h of ovipositioning. The embryo had progressed through karyokinetic divisions without cytokinesis.

Figure 4. Cytokinesis began after the embryos had completed three karyokinetic divisions.

Figure 5. The tissue cap stage was seen 3 d after oviposition. The tissue cap (clear area at the animal pole) is the developing embryo. The attachment of the egg by the funiculus, Fu, may provide spatial orientation for embryo development.

Table I

Development of Palaemonetes pugio *at 27°C and 20‰ salinity*

Embryonic stage	Day of development	Diameter (mm)	Standard deviation
Oviposition/karyokinesis/ cytokinesis	0	0.59	0.026
Late cleavage/early gastrulation	1	0.62	0.021
Gastrulation	2	0.67	0.028
Tissue cap	3	0.66	0.027
Cephalothorax delineation	4	0.66	0.021
Heartbeat initiation	5	0.69	0.020
Eye pigmentation	6	0.72	0.016
Embryonic eye	7	0.76	0.021
Early compound eye	8	0.80	0.019
Completed compound eye	9	0.84	0.048
Protozoeal embryo	10	0.84	0.030
Protozoeal embryo	11	0.82	0.047
Protozoeal embryo/pre-hatch	12	0.98	0.030
Hatch—1st zoeal larva	12	2.28	0.340

For each stage, the diameter is the mean value for 24 embryos measured across the longer axis of the oval-shaped egg. The hatch length is the "unfolded" length of the zoeal stage larva. Days of development represent 24-h periods at 27°C and 20‰ salinity.

(1990) reported five "coats" in the brachyuran crab *Carcinus maenas* and six "coatings" in the lobster *Homarus gammarus*. Morphological studies of the EC in palaemonid shrimp have been published (Sandifer and Lynn, 1980; Fisher and Clark, 1983; Lynn and Clark, 1983; Goudeau *et al.*, 1991), but none of these studies have examined embryos beyond the first few hours after oviposition.

On the basis of observations of development in *Palaemonetes pugio,* we have adapted terminologies from Talbot and Goudeau (1988) for the lobster and from Lynn *et al.* (1993) for penaeid shrimp. Crustacean decapods, in general, have an embryonic coat (EC) surrounding the developing embryo. This coat comprises one or more embryonic envelopes (EE) plus, in animals that brood their young, an outer investment coat (OIC) or cement that attaches the embryos to the female. Each EE, in turn, may be formed of several different layers. Thus, EEs are defined as layers that generally appear together as a single unit. The layers are morphologically distinct regions of the envelope. The origin of the layers that form the EE is usually embryonic, whereas the OIC origin may be maternal, embryonic, or both. In this study, we show that the EC is morphologically and functionally dynamic throughout embryogenesis.

Materials and Methods

Grass shrimp, *Palaemonetes pugio,* were collected from waters in east Escambia Bay, Pensacola, Florida, during the summer and fall of 1995. Adults were maintained at 24°C temperature and 20‰ salinity in flow-through aquaria. Animals were held in these conditions for 2 weeks before ovigerous females were removed. This period ensured that eggs removed from the females were oviposited under laboratory conditions. Embryos were gently removed from females and their ages were determined by using developmental stages as indications of approximate times postextrusion, *i.e.*, after oviposition (Tyler-Schroeder, 1978). A method modified from Fisher and Foss (1993) was used to culture the embryos. Each embryo was placed in a separate well of a 24-well plastic tissue culture plate. The plates were incubated at 27°C and 20‰ salinity with continual agitation at 60 rpm on a rotary shaker. Under these conditions, hatching was consistently 11–13 d after oviposition, with most embryos hatching after 12 d (Fisher and Foss, 1993).

Embryo development

Embryos at different developmental stages were removed from culture plates, placed on glass slides in seawater in a ring of petroleum jelly, covered with glass coverslips, and photographed using phase microscopy on an inverted microscope. Embryo lengths were obtained using a Microcomp particle analysis system attached to a video capture system mounted on a dissecting microscope. Twenty-four embryos were measured daily throughout the course of development. Mean embryo lengths and standard deviations were calculated for each day of development.

Figure 6. At 7 d after oviposition, eye development (arrow) was well advanced. The cephalothorax and abdominal regions were well defined. Fu, funiculus.

Figure 7. By 10 d after oviposition, eye formation appeared complete. The telson (arrowhead) was wrapped around the cephalothorax of the embryo. Lipid droplets (Dr) were seen in the region of the developing hepatopancreas. Fu, funiculus.

Figure 8. At 12 d after oviposition, about 6 h before hatch, EE1–EE3 were shed (EE1–3), remaining attached only at the point of the funiculus. Only EE4 remained around the embryo. Arrowhead indicates the telson still within EE4. Figures 3–8 are presented at the same magnification to demonstrate the increase in embryo size during development. Bar equals 100 μm.

Figure 9. The first zoeal larvae hatched 12 d after oviposition. Bar equals 200 μm.

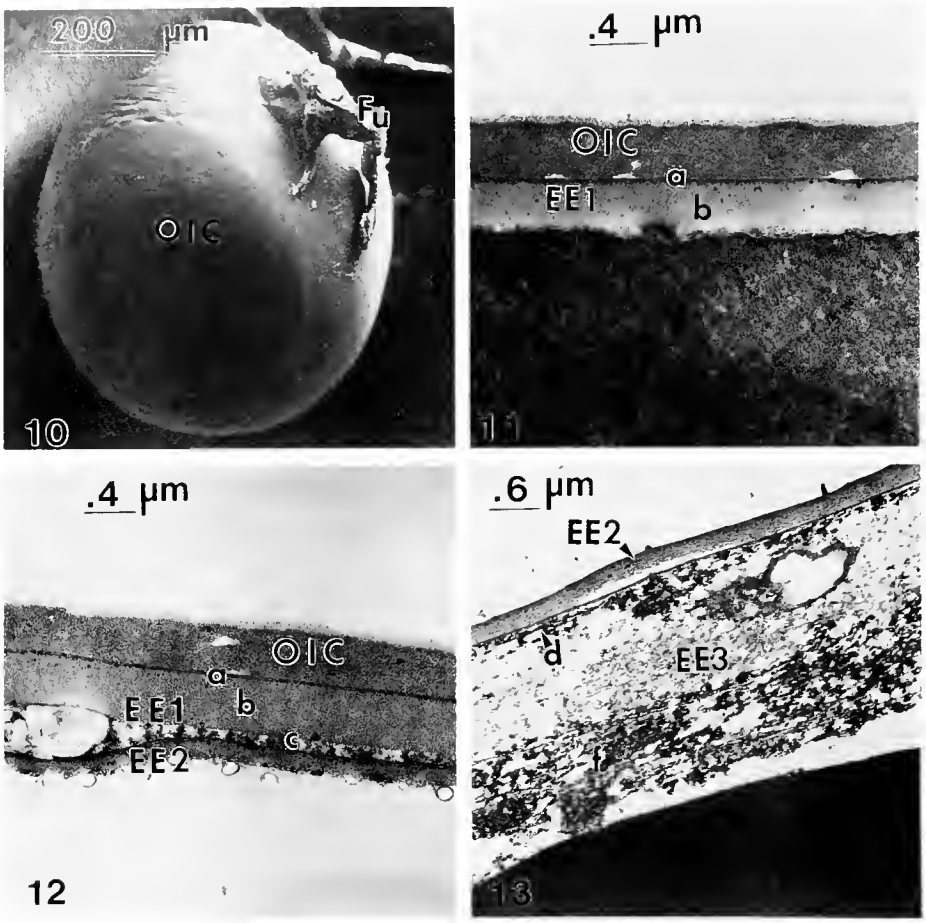

Figures 10–19. Electron micrographs of *Palaemonetes pugio* embryos showing the development of the embryonic coat.

Figure 10. A scanning electron micrograph of an embryo at 3 d after oviposition shows the smooth outer surface of the outer investment coat (OIC) with the funiculus, Fu. The funiculus was the point of attachment of the embryo to a seta of the female pleopod.

Figure 11. At 3 d after oviposition, the OIC and first embryonic envelope (EE1) were the only parts of the EC seen with TEM. EE1 had two layers, a thin, electron-dense layer, "a," and a thicker, less electron-dense layer, "b."

Figure 12. By 5 d after oviposition, EE1 had 3 layers, "a" and "b" as defined above, and layer "c," a flocculent, loosely defined layer. A second envelope, EE2, had formed and, in some areas, elevated to just below EE1.

Figure 13. In a section of another embryo 5 d after oviposition, EE2 (arrow) remained close to the embryo. The third envelope, EE3, was seen forming internally to EE2 and had a thin, electron-dense outer layer (d) and a looser, inner fibrillar layer (f).

Embryonic coat development

Morphological changes in the embryonic coat (EC) were examined using scanning electron microscopy (SEM) and transmission electron microscopy (TEM). Embryos for SEM and TEM were fixed for 24 h in 1.6% formaldehyde and 0.8% glutaraldehyde in seawater. Alternatively, embryos were fixed for 4 h in 3% glutaraldehyde, then 24 h in Bouin's fixative. Samples were washed three times with 0.2 *M* phosphate buffer and post-fixed in 1% osmium tetroxide in phosphate buffer, then washed in distilled water. SEM samples were then frozen in liquid nitrogen, loaded into the Zeiss DSM 962 scanning electron microscope, sublimated, then sputter-coated with palladium-gold. For freeze-fracture samples, the embryos were fractured before sublimation. Samples for TEM analysis were dehydrated with acetone, infiltrated with Spurr's resin, and then embedded in fresh resin. Thin sections were cut, double stained with lead citrate (Venable and Coggeshall, 1965) and aqueous uranyl acetate, and observed with TEM.

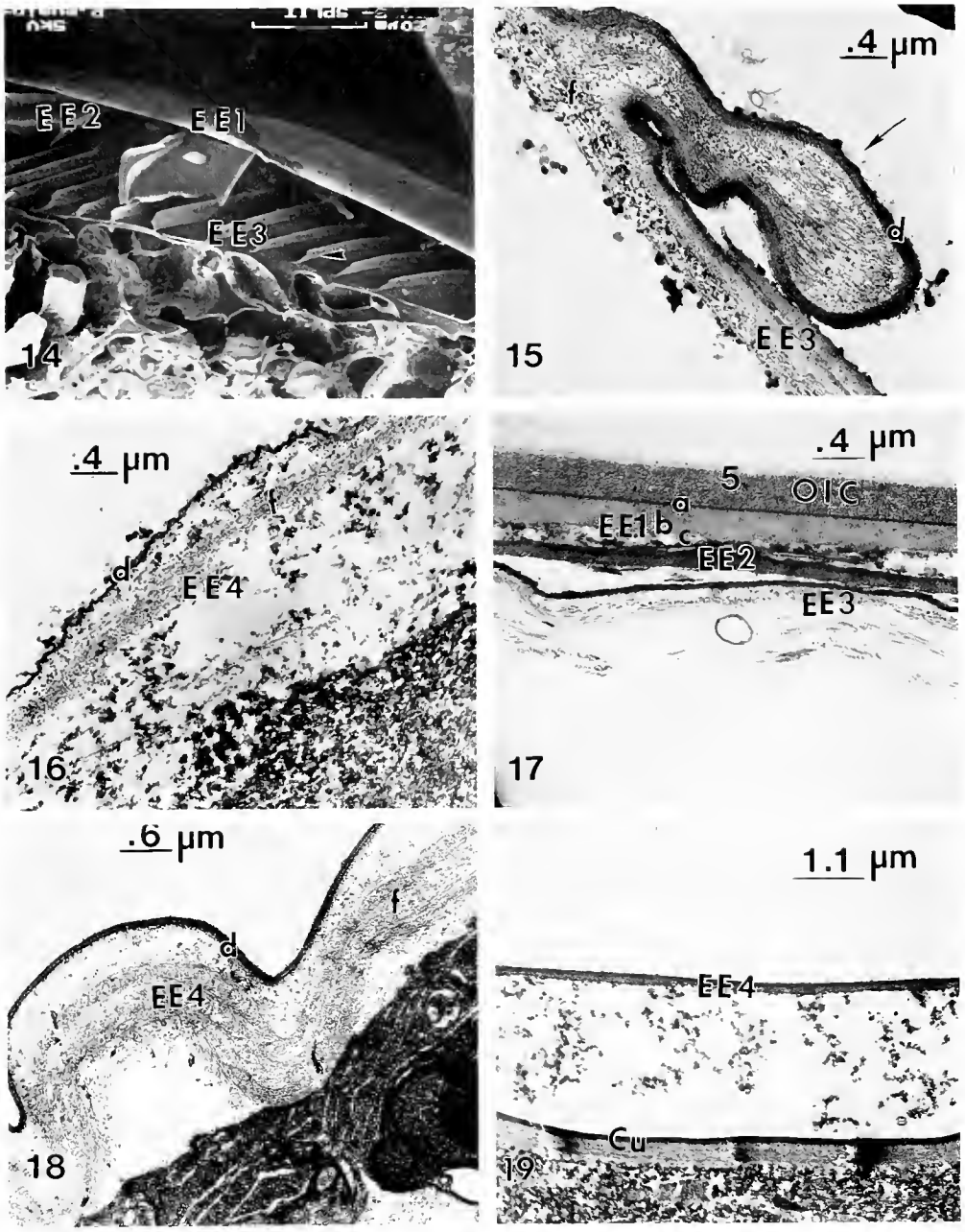

Figure 14. Between 5 and 7 d after oviposition, multiple envelopes of the EC had formed and are visible in this SEM of a freeze-fractured 7-d embryo. Three of the envelopes, EE1, EE2, and EE3, were seen, with EE3 having an elaborate system of ridges (arrowhead).

Figure 15. A cross-section of a ridge (arrow) in EE3 was seen in TEM from a 7-d embryo. The dense layer (d) and fibrillar layer (f) of EE3 were better organized than in earlier micrographs.

Figure 16. By 7 d after oviposition, a fourth envelope had formed interiorly to EE3. This envelope, EE4, remained close to the embryo and developed a thin, electron-dense outer bilayer (d) and a fibrillar inner layer (f).

Figure 17. By 10 d after oviposition, four EE surrounded the embryo, with EE1–EE3 found juxtaposed and relatively distant from EE4 and the embryo. This micrograph of the EC at 10 d shows all the layers of EE1 (a, b, and c), as well as EE2 and the two layers of EE3.

Figure 18. At 10 d after oviposition, EE4 was still found close to the embryo. The dense outer layer (d) had a bilaminar, railroad-track appearance, while the inner fibrillar layer (f) had become more organized. EE4 formed large folds with a wavelike appearance.

Figure 19. Before hatching from EE4, the embryo formed the cuticle (Cu) of the exoskeleton. This cuticle had a trilaminar appearance in contrast to the bilaminar appearance of EE4. The characteristic layering of the cuticle had already begun.

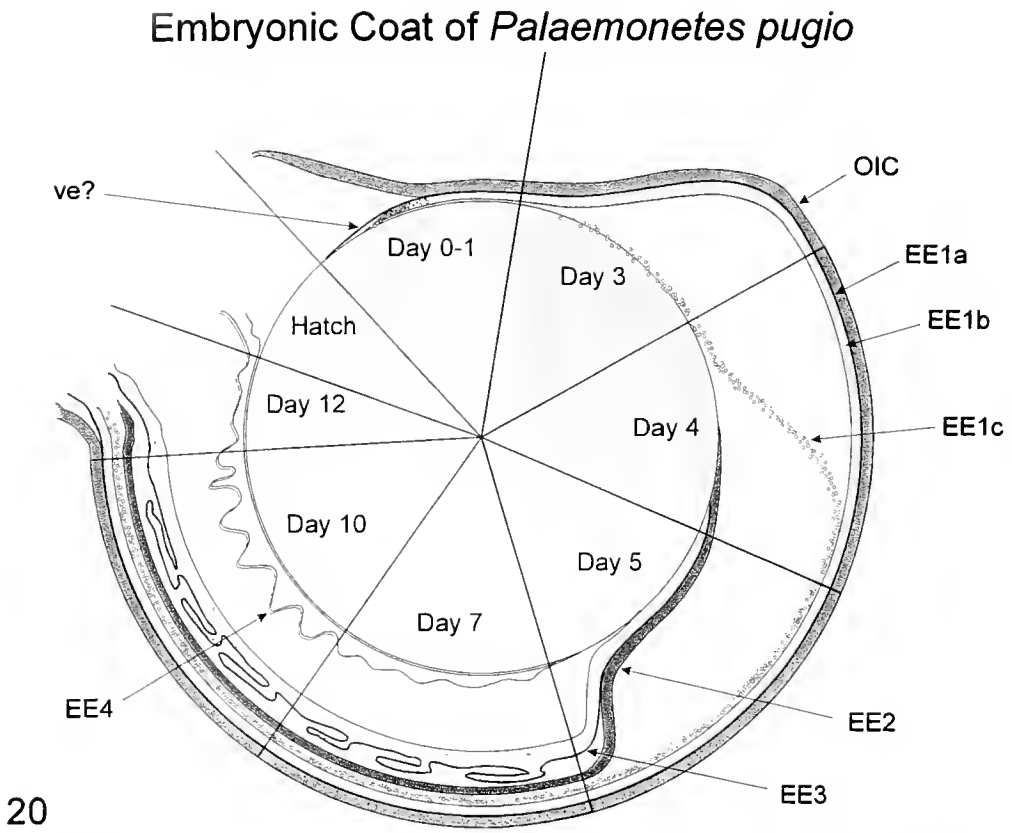

Figure 20. A schematic presentation of the sequence of formation of the embryonic coat of *Palaemonetes pugio*, including the embryonic envelopes (EE) and layers. ve, vitelline envelope; OIC, outer investment coat; $EE1_a$, $EE1_b$, and $EE1_c$, the three layers of the first embryonic envelope; EE2, EE3, EE4, the second, third and fourth embryonic envelopes, respectively. The layers and distance from the embryo are not to scale.

Embryonic coat permeability

Permeability assays were performed as reported by Glas *et al.* (1995) and Legge (1995). Embryos at various stages of development were incubated with fluorescein isothiocyanate (FITC)-labeled dextrans of five molecular weights (Sigma Chemical Co.) by adding 10 μl of fluorescently labeled dextran (stock = 50 mg/ml in distilled water) to individual wells containing embryos and seawater at 20‰ salinity. After 30 min incubation in the dark at 27°C, embryos were rinsed three times with filtered seawater and examined for dextran penetration beneath the EC using UV filters on an inverted microscope. At least ten embryos were observed for each concentration of dextran. Penetration of the EC by the dextran was determined by focusing through the embryo. For illustration, embryos were examined and photographed using confocal microscopy. The embryos were scanned using the same settings for laser intensity (488 nm blue laser), detector gain.

Lectin-binding affinity

Embryos with intact ECs at 8 d and 12 d after oviposition were incubated with FITC-labeled lectins. The lectins (and their affinities for oligosaccharides) used in this study were Concanavalin A agglutinin (Con A), α-D-glucosyl residues, especially glucose and *N*-acetylglucosamine; *Limulus polyphemus* bacterial agglutinin (LPA), *N*-acetylated D-hexosamines, especially D-glucuronic acid and *N*-acetylneuraminic acid; and *Triticum vulgaris* agglutinin (wheat germ agglutinin, WGA), *N*-acetyl-β-D-glucosaminyl residues, especially *N*-acetyl-β-D-glucosamine oligomers. Lectin stock solutions, 1 mg/ml for LPA and WGA and 2 mg/ml for Con A, in 0.05 *M* Tris (pH 7.2), with 0.01 *M* calcium, magnesium, and manganese chlorides as trace metals, were made according to the procedures of Kiernan (1990); 10 μl of stock solution was added to individual wells containing embryos in 1.0 ml seawater at 20‰ salinity. The embryos were incubated in the dark for 1 h at 27°C, then rinsed three times

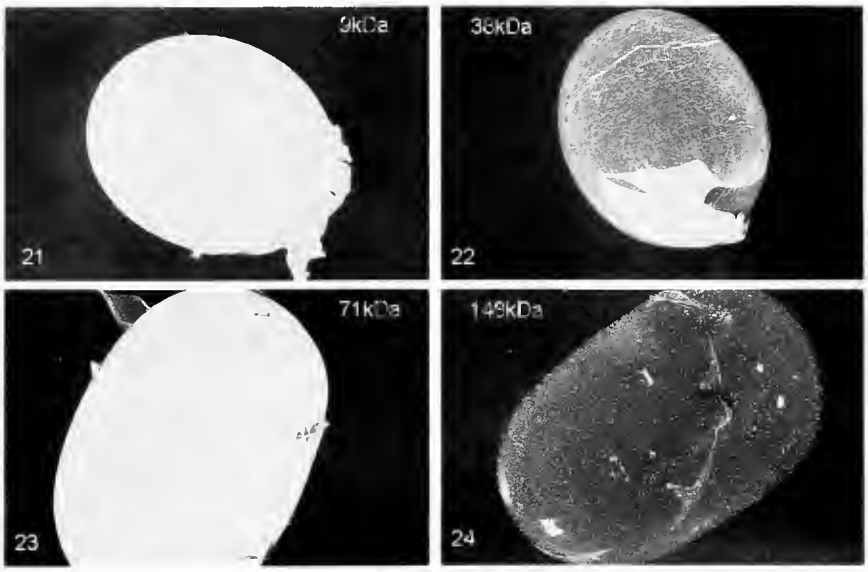

Figures 21–24. Permeability of the embryonic coat (EC) of *Palaemonetes pugio* was determined using FITC-labeled dextrans. Embryos were viewed using confocal microscopy.

Figure 21. At 3 d after oviposition, the embryo EC was permeable to FITC-labeled dextrans weighing 9 kDa. The dextran inside the EC showed the entire embryo as a bright image.

Figure 22. An example of an embryo 3 d after oviposition incubated with dextrans weighing 38 kDa. The dextran does not remain in the inside of the EC so the outline of the embryo is visible.

Figure 23. Embryo EC was permeable to the FITC-labeled dextran weighing 72 kDa at 10 d after oviposition, so the embryo appears as a bright oval.

Figure 24. Embryo EC was impermeable to the dextran weighing 148 kDa at 10 d after oviposition.

with seawater. The embryos were then observed for fluorescence on the outside of the OIC. To block for nonspecific binding, embryos were pretreated for 30 min with 1 mg/ml bovine serum albumin in the Tris buffer, then rinsed with seawater. As sugar controls, lectins were incubated with 1 *M* solutions (0.3 *M* for *N*-acetylneuraminic acid) of specific oligosaccharides before being added to the wells (Kiernan, 1990). Sugars used were sucrose, glucose, and *N*-acetylglucosamine (for Con A); D-glucuronic acid and *N*-acetylneuraminic acid (for LPA); and *N*-acetylglucosamine and *N*-acetylneuraminic acid (for WGA).

Table II

Permeability of the embryonic coat of Palaemonetes pugio *to FITC-labeled dextrans*

Day of development	FITC-labeled dextran molecular weight (kDa)					
	4.3	9.3	19.6	38.9	71.2	148.3
3	+	+	+	±	−	−
4	+	+	−	−	−	−
5	+	+	−	−	−	−
7	+	+	+	±	−	−
10	+	+	+	+	+	−
12	+	+	+	+	+	+

Permeability is recorded as + (permeable) or − (nonpermeable) on the basis of the presence or absence of fluorescent dye in the perivitelline space; ± indicates that fluorescence was found in the perivitelline space of 50% of the eggs. Each symbol represents the observation of at least four embryos.

Results

Embryo development

Development and hatching of *P. pugio* closely followed the sequence of events described by Broad (1957), Davis (1965), and Thomas (1970). Ova of *P. pugio* were released from the female oviduct and passed over the male spermatophore, fertilized, and attached to the female pleopods during oviposition (Figs. 1 and 2). At the time of attachment, the zygotes were single celled, carrying both male and female pronuclei. After pronuclear fusion, the zygote proceeded through three karyokinetic divisions (Fig. 3) before cytokinesis (Fig. 4). The orientation of the embryo within the EC remained the same, with the funiculus, or attachment stalk, at the distal edge of the presumptive cephalothorax.

By 3 d, or 72 h after oviposition, embryos reached the tissue cap stage as described by Tyler-Shroeder (1978): the clear region was at the animal end of the embryo, and yolk filled much of the remainder of the egg (Fig. 5). Af-

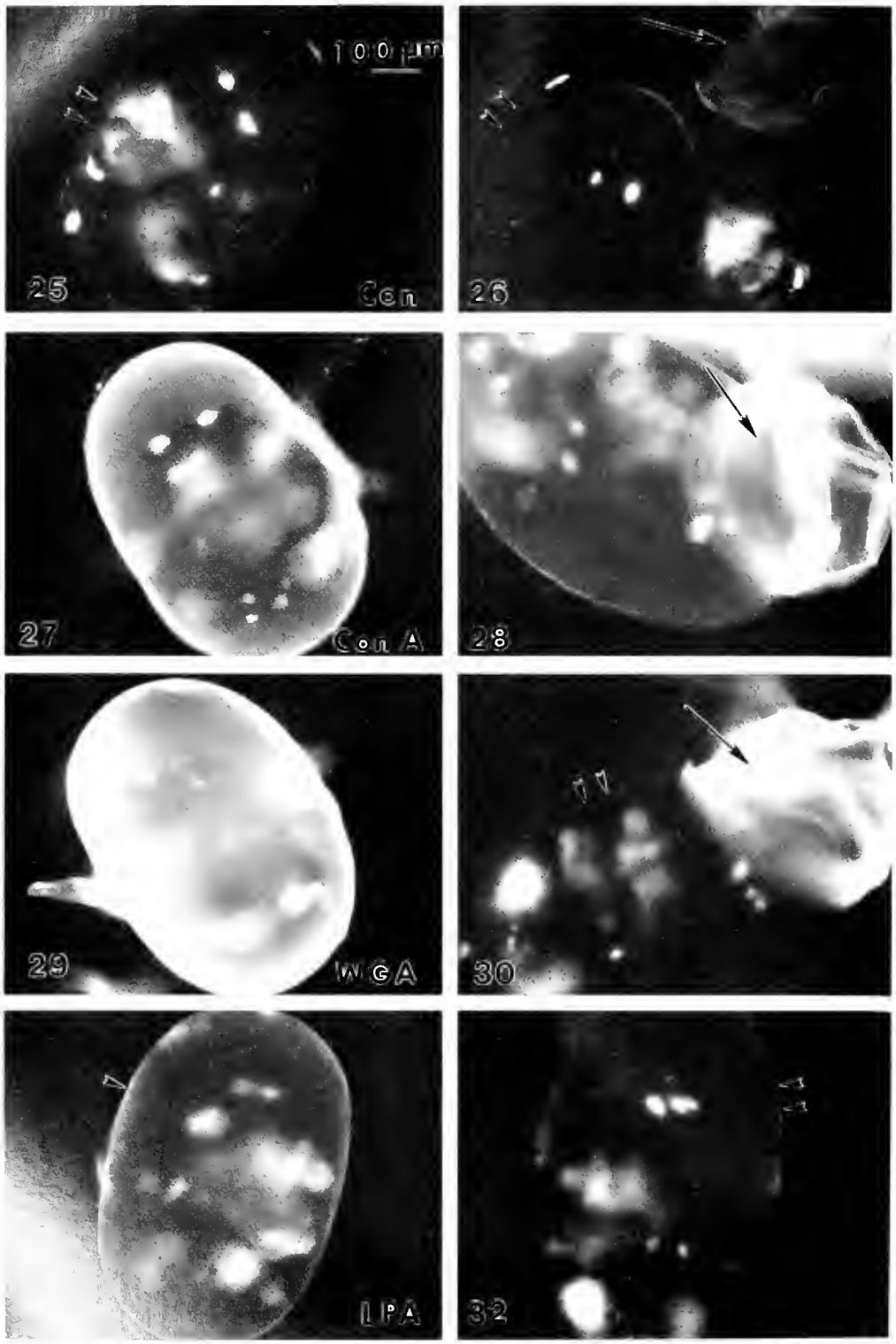

Figures 25–32. Embryos at 8 d and 12 d after oviposition were exposed to FITC-labeled lectins.
Figures 25–26. Control embryos. Con, at 8 d after oviposition had some autofluorescence, especially in the eyes, [illegible] darker pigmented areas. Arrowheads indicate the outline of the embryo.
Figure 27. Con A, the outer LE1–EE3 were shed (arrow), the remaining inner coat (arrowheads) also did not show any fluorescence.

ter 5 d of development, the heart had begun beating, and segmentation was apparent as the embryos were elongating. Eye pigmentation was evident by 7 d after oviposition (Fig. 6), with development continuing until 9 d, when the compound eye was fully formed. At this time, the embryos appeared to be completely formed externally. At 10 d (Fig. 7), lipid "droplets" were visible in the region destined to become the hepatopancreas, and the amount of dark yolk had greatly diminished.

The size of *P. pugio* embryos cultured at 27°C and 20‰ salinity increased throughout development (Table I). After 12 d of development and about 6 h before hatching, the embryos shed the outer portion of the EC (Fig. 8) and rapidly increased in size from 0.82 mm to 0.98 mm within 24 h (Table I). The embryos finally broke through the remaining envelope to hatch as first zoeal larvae (Fig. 9). Development was consistent with that described by Fisher and Foss (1993) so that hatching consistently occurred after 11–13 d of incubation.

Embryonic coat formation

During oviposition, the female released a "cement" that coated the newly fertilized eggs in a sticky layer for attachment to setae on the pleopods (Figs. 2 and 10). By 4 h after oviposition, the cement had formed an outer investment coat (OIC) that surrounded the embryo (Fig. 10) and also comprised the attachment strands, or funiculi, which connected the embryos to the pleopods. The embryos were always attached in the same relative position; *i.e.,* the funiculus was always at the position that became the posterior end of the carapace on the dorsal side (see Davis, 1965). The funiculus and attachment points to other embryos were continuous with the OIC surface. Externally, the OIC had no distinguishing features other than the funiculus attachments (Fig. 10). The smooth exterior surface of the embryos sometimes had bacterial growth during later stages of embryonic development, a common occurrence for externally brooded decapod embryos (Fisher, 1983). Otherwise, no dramatic external changes occurred until the outer envelopes were shed. The stickiness of the cement was no longer noticeable by 3 d after oviposition as the eggs no longer clumped together on contact.

Four hours after oviposition, the embryo was surrounded by the OIC and a bilayered embryonic envelope, EE1. Transmission electron micrographs revealed that the OIC comprised the outermost layer of the coat surrounding the embryo and was about 0.4 μm thick (Fig. 11). The first EE initially consisted of a thin, outer layer, $EE1_a$, and a thick, inner layer, $EE1_b$. The thickness of the $EE1_b$ had increased to 0.38–0.4 μm by 3 d after oviposition (Fig. 11), after which no further increase was seen. Within 3–5 d after oviposition, a third layer, $EE1_c$, was added to the previous two layers. This layer was composed of an electron-dense, filamentous material with a loosely organized structure (Fig. 12). This layer did not always stain well, appearing as a sparsely filled space between EE1 and EE2 after its formation. Usually EE1 was closely associated with the OIC.

The second envelope, EE2, began to appear late in the 4th d after oviposition. At 5 d after oviposition, EE2 elevated to remain closely associated with EE1 (Fig. 12). In a section of another 5-d embryo, EE2, which had not yet elevated could be seen as a dense envelope outside the newly forming EE3 (Fig. 13). When stained for electron microscopy, EE2 measured about 0.12–0.2 μm, with a thin, dense outer layer and a less dense inner layer.

A third envelope, EE3, appeared by 5 d after oviposition. This envelope consisted of an electron-dense, thin outer layer and a wide band of heterogeneous electron-dense and lucent regions (Fig. 13). By 7 d, this envelope had condensed and formed ridges in some parts of the embryo (Fig. 14). The ridges did not circumscribe the embryo. In section, a ridge was seen as an area where EE3 had folded back on itself (Fig. 15). The condensed EE3 had an outer electron-dense layer about 0.13 μm thick and a fibrillar, less dense inner layer about 0.26 μm

Figure 27. The lectin Concanavalin A (Con A) had a high affinity for the outer investment coat (OIC) of the 8-d embryo.

Figure 28. After the outer EEs were shed immediately prior to hatching, the Con A lectin had only a slight affinity for the remaining envelope, EE4. The discarded EE1–EE3 and OIC (arrow) still reacted strongly with the lectin.

Figure 29. The wheat germ agglutinin lectin, WGA, had a very strong affinity for the OIC of the 8-d embryo.

Figure 30. At 12 d after oviposition, after the outer EE1–EE3 and OIC were shed, the WGA lectin had no affinity for EE4, which remained around the embryo (arrowheads). The discarded EE1–EE3 and OIC (arrow) still reacted to the lectin.

Figure 31. *Limulus polyphemus* agglutinin showed only low nonspecific affinity for the OIC of the 8-d embryo (arrowhead).

Figure 32. At 12 d after oviposition, after EE1–EE3 and the OIC were shed immediately before hatching, the LPA lectin had no affinity for EE4 (arrowheads), which remained around the embryo. Bar equals 100 μm.

thick (Fig. 15). The fibrils tended to lay parallel to the embryo surface. By 10 d after oviposition, this envelope was about 0.5 μm wide and, in regions where EE3 had not formed ridges, was found subjacent to EE2 (Fig. 17).

The final envelope, EE4, was first seen at 7 d after oviposition. The morphology of EE4 was initially similar to EE3 during formation in that the outer layer was electron-dense and the inner layer was fibrillar and irregular (Fig. 16). The layers were near the embryo surface and measured about 0.5 μm thick. By this time, EE3 had moved away from the embryo toward the outer envelopes that were layered beneath the OIC (Fig. 17). At 10 d after oviposition, EE4 had large wave-shaped folds (Fig. 18) and measured about 1.2 μm thick. The outer layer of EE4 had formed a bilaminar "railroad-track" appearance, and the inner fibrillar layer was oriented parallel to the embryo surface. The developing embryo was seen immediately below the waves of EE4 (Fig. 18). EE4 remained near the embryo surface throughout the rest of embryonic development.

Six hours before hatching, the OIC and the outer envelopes, EE1–EE3, were shed, remaining attached to the embryo only at a point on the posterior dorsal edge of the cephalothorax (Davis, 1965). The innermost envelope, EE4, no longer had folds in it, but was found close to the embryo (Fig. 19). The thickness of the envelope was greatly reduced, as though stretched. The fibrils were scattered throughout the space between the dense outer layer and the embryo. At this time, the cuticular layer of the embryonic exoskeleton had formed (Fig. 19). The cuticular layer could be distinguished from EE4 by the morphology of the dense outer layer. In EE4, this layer was bilaminar, or "railroad track," in appearance, whereas the dense layer of the forming cuticle had a trilaminar appearance.

The sequence of events for the formation of the extraembryonic coat is summarized in Figure 20. The relative widths of the embryo, envelopes, layers, and perivitelline space are not drawn to scale. The origin of EE1 from a precursor layer or "vitelline envelope" is speculative at this time.

FITC-labeled dextrans indicate permeability change with time

When embryos were incubated with FITC-labeled dextrans 3 d after oviposition, only those dextrans weighing less than 39 kDa were able to penetrate the EC (Figs. 21 and 22). Permeability became more restrictive by 7 d after oviposition, when only the dextrans weighing less than 9 kDa could penetrate the EC. This restriction continued until 7 d after oviposition, when larger size dextrans were able to penetrate the EC. As the embryos aged further, the permeability to dextrans increased, with only the largest dextran (148 kDa) being excluded from the EC by 10 d after oviposition (Figs. 23 and 24). Immediately prior to hatching, 12 d after oviposition, all dextrans tested penetrated the inner envelope, EE4 (see Table II).

Lectin specificity indicates β-glucoside saccharides

The OICs of embryos were exposed to three lectins—Concanavalin A (Con A), *Limulus polyphemus* agglutinin (LPA), and wheat germ agglutinin (WGA)—at 8 d and 12 d after oviposition to test for the presence of specific terminal oligosaccharides (Figs. 25–32). Embryos without any lectins added showed slight autofluorescence in pigmented regions (see Thomas, 1970, for description) but no fluorescence in the EC (Figs. 25 and 26). The OICs of embryos incubated with Con A 8 d after oviposition gave a positive fluorescent reaction (Fig. 27), indicating terminal sucrose, D-glucosyl and *N*-acetyl-D-glucosamine residues. After the EEs were shed at 12 d after oviposition, there was little fluorescent reaction with EE4 (Fig. 28), but the discarded EEs and OICs still reacted strongly. At 8 d after oviposition, the OIC had a strong fluorescent reaction with WGA (Fig. 29), indicating terminal *N*-acetyl-D-glucosaminyl residues as well as β-*N*-acetylglucosamine oligomers. Embryos 12 d after oviposition had little fluorescent reaction with EE4 when treated with WGA (Fig. 30), although the discarded EEs and OICs still reacted. At 8 d after oviposition, LPA showed only nonspecific binding with the OIC (Fig. 31). At 12 d after oviposition, when the outer EE and OIC were shed, EE4 showed no affinity for the LPA lectin (Fig. 32). When blocked for nonspecific binding using bovine serum albumin, the Con A and WGA lectins continued to react strongly with the OIC, but LPA lectin showed no reaction with the OIC. When each lectin was preincubated with the corresponding sugars, fluorescence was blocked in all treatments (data not shown).

Discussion

The formation of the EC within the first four hours after oviposition has been documented in the prawn *Palaemon serratus* by Goudeau *et al.* (1991) and in *Macrobrachium* by Sandifer and Lynn (1980) and by Lynn and Clark (1983). The formation of additional coats after the EC has formed has also been reported in other species such as penaeid shrimp (Lynn *et al.*, 1993) and lobster (Talbot and Goudeau, 1988). What has not been described in previous studies is that formation of the EC may continue, as in *P. pugio*, for up to 10 d or so after oviposition. In *P. pugio* during this time, at least three additional EEs are formed around the developing embryo that are not present at 3 d after oviposition. These envelopes show distinct morphological character-

istics that allow each to be identified during development. The EEs form and mature morphologically for 10 d after oviposition of the embryos. Together, the OIC and all the EEs form the protective EC of the palaemonid shrimp. At 12 d after oviposition, the outer envelopes, EE1–EE3, are shed; only the innermost envelope, EE4, remains around the embryo. Hatching occurs when the embryo emerges from EE4. The hatching of *P. pugio* is described by Davis (1965). However, the role of the funiculus in the development of the embryo has not been closely examined.

Broad (1957) states that a prezoeal molt takes place before hatching. We saw no evidence of a molt that, as Helluy and Beltz (1991) have seen in lobster, conforms to the surface of the embryo before hatching. The cuticle layer seen at 12 d conformed to the surface of the embryo, but was clearly separate from EE4. Although the innermost envelope, EE4, was morphologically similar to the adult crustacean exoskeleton, there were distinct morphological differences when compared to the embryonic exoskeleton (compare Fig. 18 and Fig. 19).

Changes in permeability of the EC to labeled dextrans coincide with the formation of the envelopes. As EEs were added, the permeability of the EC decreased. After all the envelopes had formed and the embryo had developed further, the permeability increased. The permeability was greatest as the embryo approached hatching; *i.e.*, after the OIC and EE1–EE3 had been shed and only EE4 remained around the embryo. Some of these results may explain in part the difficulty in embryo fixation reported by Thomas (1970) and also seen in this laboratory.

Lectin affinity studies lend some insight into the composition of the EC. The lectins are too large in molecular weight to penetrate the EC. Only Con A may be small enough to pass in and out of the EC; however, it appears to bind to the EC, as indicated by the strong fluorescent image. The strong Con A and WGA lectin affinity indicates the presence of a terminal glucosyl and *N*-acetylglucosamine residues. Contrast the binding of lectin to the OIC with the lack of binding to EE4 after the outer coat has been shed.

The results of this study are important to those using *P. pugio* for bioassays to understand the effects of toxicants and microorganisms on the developing embryo. The changing morphological and functional aspects of the EC throughout the development of the embryo profoundly affect the stage-specific sensitivity and susceptibility of the embryo. Further research is needed to address the importance of the OIC and funiculus in successful development, the functional roles of the different layers of each EE, and the effects of physical and chemical stressors on the progression of EC formation.

In this paper, we propose terminology to describe a complex protective structure. We use terms that are descriptive yet familiar, avoiding commonly used terms such as "extracellular coat" because we feel they are misleading. Because we are studying the envelopes around an embryo with multicellular organization, not just the newly fertilized zygote, the word "extracellular" could be misleading to those unfamiliar with the historical usage. We use "coat" to encompass the entire protective structure, since normally we think of only one coat being used at a time. We have continued to use "envelope" since it is now widely accepted in several species. Ideally, this usage will further promote the standardization of terminology among developmental biologists.

Acknowledgments

The authors give special thanks to Steve Foss, EPA, for assistance with the embryo cultures. John Lynn and Prudence Talbot were helpful with pertinent discussions on *Macrobrachium* reproduction and lobster development, respectively. Jeff Green and Gerry Cripe provided valuable criticism of the manuscript. This work was performed while PSG and JRR held National Research Council–EPA, Gulf Ecology Division Research Associateships. This is EPA, Gulf Ecology Division contribution No. 979.

Literature Cited

Broad, A. C. 1957. Larval development of *Palaemonetes pugio* Holthius. *Biol. Bull.* **112:** 144–161.

Clark, W. H., Jr., and J. W. Lynn. 1977. A Mg^{++} dependent cortical reaction in the eggs of penaeid shrimp. *J. Exp. Zool.* **200:** 177–183.

Davis, C. C. 1965. A study of the hatching process in aquatic invertebrates. XIV. An examination of hatching in *Palaemonetes vulgaris* (Say). *Crustaceana* **8:** 233–238.

Fisher, W. S. 1983. Eggs of *Palaemon macrodactylus:* II. Association with aquatic bacteria. *Biol. Bull.* **164:** 201–213.

Fisher, W. S., and W. H. Clark, Jr. 1983. Eggs of *Palaemon macrodactylus:* I. Attachment to the pleopods and formation of the outer investment coat. *Biol. Bull.* **164:** 189–200.

Fisher, W. S., and S. S. Foss. 1993. A simple test for toxicity of number 2 fuel oil and oil dispersants to embryos of grass shrimp, *Palaemonetes pugio*. *Mar. Pollut. Bull.* **26:** 385–391.

Glas, P. S., J. D. Green, and J. W. Lynn. 1995. Oxidase activity associated with the elevation of the penaeoid shrimp hatching envelope. *Biol. Bull.* **189:** 13–21.

Goudeau, M., and J. Becker. 1982. Fertilization in a crab. II. Cytological aspects of the cortical reaction and fertilization envelope elaboration. *Tissue Cell* **14:** 273–282.

Goudeau, M., H. Goudeau, and D. Guillaumin. 1991. Extracellular Mg^{2+} induces a loss of microvilli, membrane retrieval, and the subsequent cortical reaction, in the oocyte of the prawn *Palaemon serratus*. *Dev. Biol.* **148:** 31–50.

Goudeau, M., and F. Lachaise. 1980a. 'Endogenous yolk' as the precursor of a possible fertilization envelop in a crab (*Carcinus maenas*). *Tissue Cell* **12:** 503–512.

Goudeau, M., and F. Lachaise. 1980b. Fine structure and secretion of the capsule enclosing the embryo in a crab (*Carcinus maenas (L)*). *Tissue Cell* **12:** 287–308.

Goudeau, M., and F. Lachaise. 1983. Structure of the egg funiculus and deposition of embryonic envelopes in a crab. *Tissue Cell* **15:** 47–62.

Goudeau, M., F. Lachaise, G. Carpentier, and B. Goxe. 1990. High titers of ecdysteroids are associated with the secretory process of embryonic envelopes in the European lobster. *Tissue Cell* **22:** 269–281.

Helluy, S. M., and B. S. Beltz. 1991. Embryonic development of the American lobster (*Homarus americanus*): Quantitative staging and characterization of an embryonic molt cycle. *Biol. Bull.* **180:** 355–371.

Kiernan, J. A. 1990. *Histological and Histochemical Methods: Theory and Practice.* Permagon Press, Oxford.

Legge, M. 1995. Oocyte and zygote zona pellucida permeability to macromolecules. *J. Exp. Zool.* **27:** 145–150.

Lynn, J. W., and W. H. Clark, Jr. 1983. A morphological examination of sperm-egg interaction in the freshwater prawn, *Macrobrachium rosenbergii*. *Biol. Bull.* **164:** 446–458.

Lynn, J. W., P. S. Glas, Q. Lin, and J. D. Green. 1993. Assembly of extracellular envelopes around the eggs and embryos of the marine shrimp, *Sicyonia ingentis*. *J. Reprod. Dev.* **39:** 90–91.

Pillai, M. C., and W. H. Clark, Jr. 1987. Oocyte activation in the marine shrimp, *Sicyonia ingentis*. *J. Exp. Zool.* **24:** 325–329.

Sandifer, P. A., and J. W. Lynn. 1980. Artificial insemination of caridean shrimp. Pp. 271–288 in *Advances in Invertebrate Reproduction, Vol II*, W. H. Clark, Jr. and T. S. Adams, eds. Elsevier/North Holland, New York.

Talbot, P. 1981. The ovary of the lobster, *Homarus americanus*. II. Structure of the mature follicle and origin of the chorion. *J. Ultrastruct. Res.* **76:** 249–262.

Talbot, P., and M. Goudeau. 1988. A complex cortical reaction leads to formation of the fertilization envelope in the lobster, *Homarus*. *Gamete Res.* **19:** 1–18.

Thomas, M. B. 1970. A descriptive morphological and electrophoretic study of the embryonic development of *Palaemonetes pugio* (Crustacea: Decapoda). M. S. Thesis. Department of Zoology, University of North Carolina, Chapel Hill.

Tyler-Shroeder, D. B. 1978. Culture of the grass shrimp (*Palaemonetes pugio*) in the laboratory. Pp. 69–72 in *Bioassay Procedures for the Ocean Disposal Permit Program*, EPA/600/9-78-010, U.S. EPA, Environmental Research Laboratory, Gulf Breeze, FL.

Venable, J. H., and R. Coggeshall. 1965. A simplified lead citrate stain for use in electron microscopy. *J. Cell Biol.* **25:** 407–408.

Reference: *Biol. Bull.* **192:** 243–252. (April, 1997)

Morphology and Development of *Odostomia columbiana* Dall and Bartsch (Pyramidellidae): Implications for the Evolution of Gastropod Development

RACHEL COLLIN[1,*] AND JOHN B. WISE[2]

[1] *Department of Zoology, University of Washington, Box 351800, Seattle, Washington 98195; and*
[2] *Houston Museum of Natural Science, 1 Herman Circle Drive, Houston, Texas 77030*

Abstract. Although pyramidellid gastropods are a phylogenetically important group of diverse and abundant ectoparasites, little is known about their life histories. Herein, we describe the adult morphology and development of the pyramidellid *Odostomia columbiana,* which parasitizes the scallops *Chlamys hastata* and *C. rubida* in the Northeast Pacific. Anatomically, adult *O. columbiana* resemble other known pyramidellids although they lack the tentacular pads typical of other *Odostomia* species. Embryonic development is similar to that described for other pyramidellids: cleavage is unequal, gastrulation is partially by invagination, and considerable growth occurs before hatching. However, embryonic and larval development are much slower than for other described species. The planktotrophic larvae hatch after 19 days of intracapsular development and metamorphose about 2 months later. *O. columbiana* veligers have a large black pigmented mantle organ to the right of the midline, a distinct metapodial tentacle, and three or four long bristles that project over the operculum from behind the foot. Observations of newly metamorphosed juveniles suggest that previous disagreements regarding the development of heterostrophy are due to variation in the degree of heterostrophy among species. Our observations also generally corroborate certain scenarios explaining the evolution of gastropod cleavage type and larval heterochrony. Unequal cleavage and larvae that hatch without well-developed eyes and tentacles may be characteristic of the common ancestor of pyramidellids and opisthobranchs; however, late development of the larval heart is probably a derived condition of opisthobranchs.

Received 16 August 1996; accepted 17 December 1996.

* Address for correspondence: Committee on Evolutionary Biology, Culver Hall, 1025 E. 57th Street, Chicago, IL 60637; e-mail: rcollin@midway.uchicago.edu

Abbreviations: PMO = pigmented mantle organ; bp1 = anterior buccal pump; bp2 = posterior buccal pump; VCSGL = ventral ciliated strip gland.

Introduction

Pyramidellids are common ectoparasites in many marine communities, but little is known about their biology and life histories (Haszprunar, 1988; Wise, 1996). In particular, data concerning their development and larval biology are lacking. As in many benthic marine invertebrates with limited adult dispersal, the duration of a planktonic larval stage may be a key factor influencing pyramidellid distribution and population dynamics. Long-lived planktonic stages may increase colonization of patchily distributed hosts, whereas species that hatch as crawling juveniles may have lower probabilities of local extinction (Thorson, 1950; White *et al.,* 1984; Cumming, 1993). Therefore, knowledge of pyramidellid development and larval biology is key to understanding their life histories and host-parasite interactions, and to planning effective pest-control strategies for aquaculture.

Pyramidellid development is also particularly informative when viewed in a phylogenetic context. Generally, pyramidellids are placed, with other families in the order Heterostropha, at the base of the heterobranch clade (Haszprunar, 1988). Although the relationships among these families are poorly resolved, pyramidellids clearly represent basal members of the clade that in-

cludes opisthobranchs and pulmonates, and which is the sister group of the Caenogastropoda (Haszprunar, 1988; Bieler, 1992; Mikkelsen, 1996). Knowledge of such basal groups can be useful in tracing evolutionary transitions, determining ancestral character states, and testing evolutionary scenarios. This knowledge may be particularly useful in gastropod development, where evidence for evolutionary scenarios is often available from derived representatives of only a few clades. For example, van den Biggelaar (1996) found a trend in cleavage type and D-quadrant specification from equal cleavage and late specification in "archaeogastropods" to unequal cleavage and early specification in opisthobranchs and pulmonates. Additionally, Page (1994) suggested that heterochronic shifts in gastropod development decelerated the formation of larval and adult structures in opisthobranch larvae relative to prosobranchs. These scenarios were generated primarily from observations of derived caenogastropods, opisthobranchs, and pulmonates. Moreover, detailed descriptions of pyramidellid development could be used to further support or refute these types of scenarios.

To date, accounts of pyramidellid reproduction and embryology are brief and limited to a small number of European (Lebour, 1932, 1936; Rasmussen, 1944, 1951; Fretter and Graham, 1949), eastern North American (Robertson, 1978; White *et al.*, 1985), and Indo-Pacific (Amio, 1963; Nishino *et al.*, 1983; Cumming, 1993) species (Table I). Although more than 50 species have been reported from western North America (Dall and Bartsch, 1909), there exists only a single account of pyramidellid development from the region (LaFollette, 1979). No detailed embryological studies of pyramidellids have been published, and larvae that do not metamorphose immediately after hatching are seldom reared through settlement (see Robertson, 1967, for an exception). Consequently, the details of early development, the duration of the planktonic period, and the events at metamorphosis have been the subject of much speculation (Thorson, 1946; Fretter *et al.*, 1982).

Published accounts of pyramidellid reproduction and development are often obscured by taxonomic confusion within the group. Criteria used to identify species are often not explicitly stated in published reports, or the taxonomy is so conjectural that species cannot be identified with much certainty. For example, Clark (1971) and Hoffmann (1979) did not state how they identified their [illegible] as *Odostomia columbiana*, and Cumming (1993) [illegible]able to definitely identify "*Turbonilla* sp." to ge[illegible]pecies. This taxonomic uncertainty makes it di[illegible] interpret comparative reproductive and de[illegible]l data.

R[illegible] `poecilogony, a rare condition in gastropods (Hoag[illegible]d Robertson, 1988; Bouchet, 1989) in which two or more developmental modes occur in one species, may be an example of such taxonomic confusion. *Boonea impressa* has been reported to have planktotrophic development in North Carolina and lecithotrophic development in Texas. However, these populations may not represent the same species (Bouchet, 1989). Both small eggs that develop into planktotrophic larvae and large eggs with direct development have also been reported for *Brachystomia rissoides* in areas of different salinities in Europe (Pelseneer, 1914; Rasmussen, 1944, 1951; Thorson, 1946).

This paper adds to the data on pyramidellid development while avoiding the taxonomic confusion of previous studies by describing both the adult morphology and the development of the pyramidellid *Odostomia columbiana* Dall and Bartsch, 1907. This new information is discussed in the context of the general characteristics of pyramidellid development and its implications for the evolution of development within the gastropods.

Materials and Methods

Mature *Odostomia columbiana* were found on the scallops *Chlamys hastata* and *C. rubida* dredged from 90–130 m in San Juan Channel, Washington (48°34′10″ N, 123°2′0″ W) during March 1995. Both the snails and their hosts were kept at ambient sea temperature (8°–12°C) in flow-through sea-tables at Friday Harbor Laboratories, Washington. Snails ranged from 5 to 8 mm in length and were identified as *O. columbiana* on the basis of the original description of the shell provided by Dall and Bartsch (1907) and by comparison with the holotype and five syntypes on deposit at the National Museum of Natural History (lot #126658). Voucher specimens have been deposited at the Field Museum of Natural History (FMNH 293334: dry shells; FMNH 293334: formalin-fixed animals).

Adult morphology

Adult snails were extracted for dissection by first cracking their shells with a vise. Snails were dissected whole, and structures of the gut and reproductive tract were routinely stained with toluidine blue (Wise, 1993, 1996).

Development

Egg masses were present on the scallops when they were collected, and adult snails continued to produce egg masses in the laboratory until May 1996. Scallop shells were checked for new egg masses several times a month to determine whether reproduction was seasonal. Individual egg masses were removed from the scallop shells and kept in small glass dishes while their development

was observed. Although we did not observe egg laying, several egg masses were collected before the beginning of first cleavage. Observations of these egg masses were used to produce a developmental timetable. Eggs and egg capsules were measured prior to first cleavage, and measurements were taken in the plane of the chalazae. After hatching, larvae were transferred to filtered (0.45 μm) seawater in small glass dishes. They were fed *Isochrysis galbana* and *Rhodomonas* sp. *ad libitum*, and the water was changed every 2 to 3 days. Because the larval shells are hydrophobic, flakes of cetyl alcohol were added to the surface of the cultures to prevent larvae from becoming trapped in the surface tension. When the veligers began to spend time crawling, juvenile scallops were added to the cultures to induce metamorphosis and as food for newly metamorphosed juveniles. All observations reported are of animals reared or maintained in the laboratory.

Larval shells were prepared for scanning electron microscopy by rinsing them in dilute bleach and distilled water following the procedure of Hickman (1995). They were mounted on stubs with double-sided tape, coated with gold and palladium, and examined with a JEOL JM35 scanning electron microscope.

Results

Adult morphology

The following is given in the concise style of a species description.

Shell: Relatively thin, elongate conical, chalky white, 5–8 mm in length, composed of 5 to 6 adult whorls. Adult whorls with numerous fine spiral growth lines. Whorl shoulders rounded, with moderately deep sutures. Shell etched and pitted, particularly above body whorl. Lenticular aperture, with flared lower portion. Single, short, acute columellar fold on upper half of columella perpendicular to columellar axis. Smooth, sinistrally heterostrophic protoconch oriented 130 degrees to teleoconch axis, with 40% submerged within first adult whorl. Operculum brown, lenticular, with subcentric nucleus.

Head-Foot: White to yellow, with numerous scattered white cells. Propodium with slight medial indentation and rounded lateral edges. Foot narrows posterior to propodium, then widening to gradually taper to a blunt apex. Pedal gland opens in middle of groove extending along posterior half of ventral surface of foot. Attachment thread present. Tentacles subtriangular, connate, ventrolaterally folded; tentacular pads apparently absent. Black round eyes beneath epithelium on median side of tentacles. Mentum unnotched, not bifurcate.

Alimentary Tract: Retracted introvert-proboscis extending posteriorly from its aperture on ventral side of head, dorsal to mentum base and entering cephalic hemocoel (Fig. 1). Introvert joining buccal sac (containing buccal sucker, stylet, and stylet bulb), which is connected to buccal pump. Buccal pump divided into anterior (bp1) and posterior (bp2) sections, with bp2 one-third longer than bp1; bp1 narrow, round in cross-section; bp2 wider, laterally flattened, distally rounded. Short, straight anterior esophagus originating on ventral surface of alimentary tract at bp1–bp2 juncture, extending posteriorly to join posterior esophagus and paired salivary glands, forming a four-way junction. Long, highly coiled posterior esophagus extending posteriorly to enter visceral mass and join stomach. Long, narrow salivary glands equal to bp2 in length. Salivary gland ducts highly folded and attached to anterior esophagus. Ducts penetrating alimentary tract just anterior to bp1–bp2 juncture, extending parallel to one another within walls of bp1 and entering stylet bulb without exiting gut. Salivary glands not attached distally to esophagus.

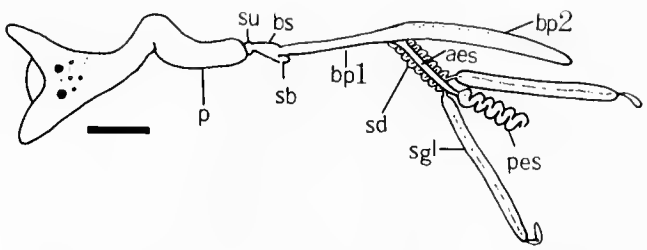

Figure 1. Diagram of alimentary tract of *Odostomia columbiana*. aes = anterior esophagus, bp1 = buccal pump 1, bp2 = buccal pump 2, bs = buccal sac, p = proboscis, pes = posterior esophagus, sb = stylet bulb, sd = salivary gland duct, sgl = salivary gland, su = sucker. Scale bar is 500 μm.

Pallial Cavity: Mantle and mantle organs typical of members of the Odostominae, with exception of position of ventral ciliated strip gland (=VCSGL). Small, spherical, yellow VCSGL underlying 20% of ventral ciliated strip about halfway from anterior edge of mantle floor. Ventral and dorsal ciliated strips joining on mantle roof posterior end of mantle cavity. Small, round-to-oblong pigmented mantle organ (=PMO), composed primarily of cells containing a bright yellow exudate, framed by numerous brown cells. A thick, bright yellow exudate is released when snail is disturbed.

Reproductive System: Opaque-to-transparent reproductive organs located on columellar side. Common pallial gonoduct extends anteriorly from visceral mass to open on right side of head just anterior and beneath the right tentacle.

Reproduction and development

Our observations of reproduction and larval development of *O. columbiana* generally agree with previous accounts of pyramidellid development (Pelseneer, 1914;

Table I

Review of pyramidellid development

Species	Egg size (μm)	Capsule size (μm)	Days to hatching	Larval duration (days)	Temp. (°C)	Reference
Boonea im[illegible]	130*	180–280*	3–5	7	~25	White *et al.*, 1985
Brachyst[illegible]issoides	120	500	25	0	?	Rasmussen, 1951
Brachyst[illegible]ia rissoides	60	200	?	?	?	Thorson, 1946
Brachystomia rissoides	70	200	6	?	~20	Rasmussen, 1944
Brachystomia rissoides	100	380	25	0	?	Pelseneer, 1914
Chrysallida cincta	?	320	22–27	0	20	LaFollette, 1979
Chrysallida decussata	90–120†	240–350	?	?	?	Lebour, 1936
Menestho diaphana	80*	200	16	? >8	11	Kristensen, 1970
Odostomia acuta	~80*	160 × 200	a few	?	?	Høisæter, 1989
Odostomia columbiana	**72–74**	**153–178**	**19**	**~70**	**12**	**this study**
Odostomia desimana	80	130 × 160	14	?	?	Amio, 1963
Odostomia eulimoides	?	?	10–12	3–4	18	Fretter and Graham, 1949
Odostomia eulimoides	90*	160	?	?	?	Lebour, 1932
Odostomia fujitaii	?	?	15–16	8–12	15	Minichev, 1971
Odostomia sp.	~100*	~200*	7	3 (?)	22	Nishino *et al.*, 1983
Odostomia omaensis	60	120 × 150	8	?	?	Amio, 1963
Turbonilla sp.	130	300 × 400	10–11	3–5 or 0	23	Cumming, 1993

* Measured from figures.
† 4–8 eggs per capsule.

Lebour, 1932, 1936; Rasmussen, 1944, 1951; Fretter and Graham, 1949; White *et al.*, 1985). However, both embryonic (used here to refer to development prior to hatching) and larval development are much slower than reported for other species (Tables I and II). Although we searched for spermatophores like those described by Robertson (1978), at no time did we find any attached to the shells or bodies of these snails. Egg masses each containing up to several hundred eggs were deposited on the hosts' shells continually from March 1995 until May 1996 when the last of the snails died. Irregular egg masses are often deposited in groups, making it difficult to distinguish individual masses. Each snail generally produced several egg masses per week.

Table II

Developmental time table for O. columbiana *at 10–12°C*

Age	Stage
~6 h	First cleavage
18 h	4 cells
24 h	8 cells
48 h	Round blastula
2–3 days	Gastrulation: blastula flattens and then forms a horseshoe-shaped gastrula
3–7 days	Gastrula
8 days	Foot and head rudiments begin to differentiate, some trochal ciliary motion; the shell is not yet present
10 days	Shell, cilia, and foot with operculum and statocysts present, light red PMO just visible
17 days	Heartbeat and ciliary motion in gut visible
19 days	Veligers hatch, PMO is black
72–80 days	Veligers begin to crawl
~90 days	Settlement and metamorphosis

Individual eggs are white and range from 71 to 77 μm in diameter (mean = 74.5; SD = 1.61; n = 23). Egg size did not differ between summer (July) and winter (January). Each round egg, surrounded by an oval layer of opaque albumin, is enclosed in a thick transparent gelatinous capsule (Fig. 2A–F). The length of the space enclosing the albumin is 154–170 μm (mean = 162.5; SD = 4.6; n = 23) and the outer length of the capsule is 193–222 μm (mean = 211; SD = 6.9; n = 23). In some previous accounts of pyramidellid development (*e.g.*, White *et al.*, 1985), capsular length has been reported as egg size, whereas other studies measure the egg cell. In this paper "egg" is used to denote the actual egg cell, and "capsule" refers to the egg and the albumin contained in one gelatinous covering. The capsules are connected to one another by thin strands called chalazae. In *O. columbiana*, chalazae are composed of a thin extraembryonic layer that surrounds the albumin layer beneath the capsule, traverses the capsule, and continues between capsules as a thin tubular strand (Fig. 2C). The egg, albumin, and capsular covering are embedded in a transparent gelatinous matrix that is often covered with diatoms.

All eggs within a single egg mass develop synchro-

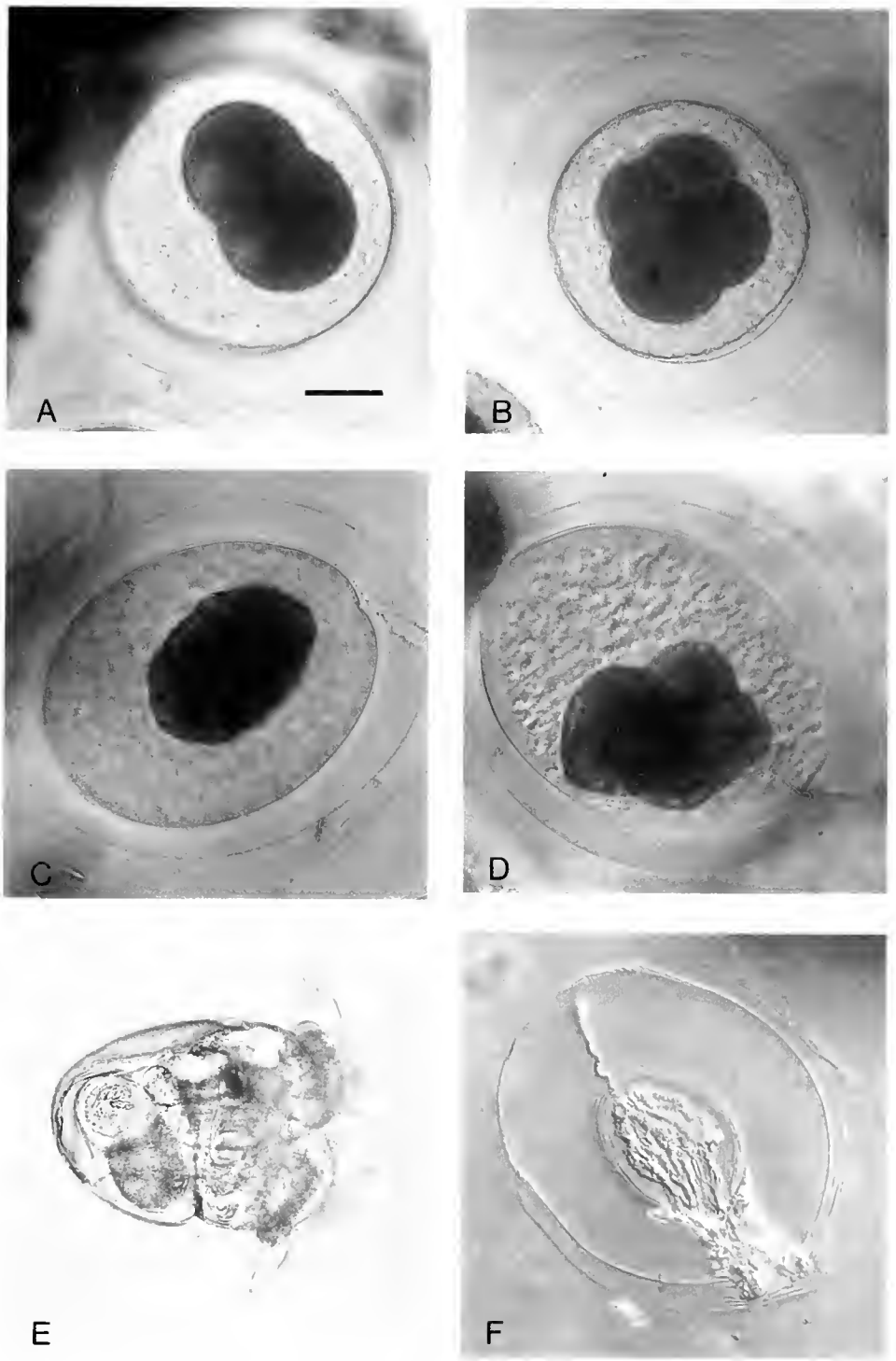

Figure 2. Stages in *Odostomia columbiana* development. (A) Two-cell stage; (B) four-cell stage; (C) blastula; (D) beginning of differentiation of the foot, velum, and shell; (E) hatchling veliger; (F) empty egg capsule. In A and B the capsule appears round because it is viewed end on. Chalazae are clearly visible in the upper right of C and the upper left of F. All figures are to the same scale, and scale bar is A is 40 μm.

nously, and the initial cleavages are simultaneous. First cleavage is clearly unequal (Fig. 2A), but the second cleavage appears to be more-or-less equal. This results in a four-cell stage with two relatively large cells and two small cells (Fig. 2B). Third cleavage is also unequal. Because the polar bodies are initially obscured by the

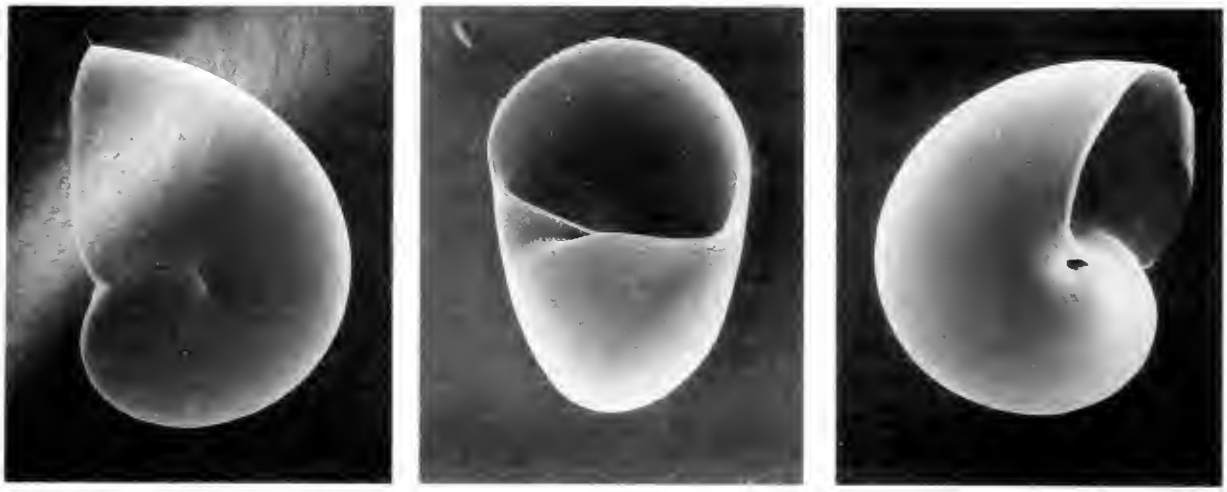

Figure 3. Scanning electron micrograph of *Odostomia columbiana* larval shell at hatching. Apical, apertural, and umbilical views, from left to right. Shell length is 150–160 μm for these three shells.

opaque albumin, the polarity and direction of this division could not be determined.

After 2 days the initially spherical blastula flattens (Fig. 2C) and in the next few days develops into a heart-shaped or cup-shaped gastrula. Thus gastrulation occurs at least partially by invagination, as is typical of many opisthobranchs. After 8 days the foot, head, and velum anlangen appear (Fig. 2D), and short cilia present on the velar lobes beat weakly. Even after the cilia are fully formed the embryos rotate very slowly, if at all, within the capsules. After 10 days the shell and statocysts are clearly visible, and the pigmented mantle organ begins to develop. As the PMO grows it darkens and changes from dark red to black before the larvae hatch. At 17 days the beating heart is visible, and the cilia of the gut are active. The embryo continues to absorb the surrounding albumin and grows until it eventually fills the capsule. At no time during development did we observe paired larval kidneys similar to those described by Pelseneer (1914). Additionally, methods used to demonstrate protein uptake in morphologically similar caenogastropod larval kidneys (Collin, unpubl. data) did not detect protein uptake in decapsulated embryos. Inspection of capsules, after hatching, shows that larvae hatch through an opening in the capsule along one of the chalazal strands (Fig. 2F).

At hatching the smooth, sinistral protoconch comprises nearly an entire whorl (Fig. 3) and is 150–160 μm in length (n = 7; Fig. 3). Newly hatched larvae have a black PMO just to the right of the midline, a small bilobed velum, and no eyes, tentacles, or obvious apical tuft (Fig. 2E). Except for the PMO and the stomach and digestive gland, whose color reflects larval diet, the veliger is entirely transparent. Although larvae retracted into their shells when placed under the microscope, the foot points slightly to the animal's right when they swim. As the foot grows, the metapodial tentacle, the posterior protuberance of the foot (distinct from adult metapodial tentacles) and its terminal cilia, which extend over the operculum, become more obvious. On each side of the foot, three or four bristles, which seem to originate behind the foot, project radially over the edge of the operculum. Veligers develop eyes within 18–23 days of hatching. After 2 months, the velum shrinks and the larvae, which are about 290 μm in shell length, begin to crawl. Larvae at this stage settle and metamorphose within days of the addition of juvenile scallops to the culture. Larvae that were the same age but had not begun to crawl did not settle in response to scallops. Water in which scallops had been kept overnight did not induce metamorphosis in crawling larvae. The PMO remained dark for at least 1 month after metamorphosis (Fig. 4), but had turned yellow after 6 months.

Discussion

Taxonomic note

The snails used in this study were identified as *O. columbiana* on the basis of the original description of the shell (Dall and Bartsch, 1907, 1909) and by comparison with the type specimens. All animals were collected attached to *Chlamys* spp. However, previous papers have described *O. columbiana* found on *Trichotropis cancellata* in Puget Sound, but did not state how the snails were identified (Clark, 1971; Hoffmann, 1979). Pyramidellid snails on *T. cancellata* are much smaller (2–4 mm, pers. obs., RC) than the snails used in this study and those described by Dall and Bartsch (up to 8 mm). The differences in size and host suggest that these may be two

Figure 4. Juvenile *Odostomia columbiana* at the edge of a scallop shell about 1 month after settlement. The black PMO is visible through the shell in the middle of the body whorl. Shell length is about 700 μm.

different species. Nevertheless, the adult shell shape, sculpture, protoconch morphology, and adult anatomy are quite similar.

Previous studies have reported that some pyramidellids may not be host specific, or their preference may change as they grow (Boss and Merrill, 1965; Powell *et al.*, 1987), suggesting that the association of small animals with *T. cancellata* and large animals with *Chlamys* spp. may represent an ontogenetic host shift. This is unlikely because juvenile *O. columbiana* raised in this study did not move onto *T. cancellata* when given the choice between juveniles of *Chlamys* spp. or *T. cancellata*. No egg masses were discovered on *T. cancellata*, so it is unclear whether the pyramidellids from these hosts were sexually mature. Our preliminary results suggest that these are closely related species.

Adult morphology

The morphology of *O. columbiana* is very similar to that of other members of the family. However, it differs in several ways from the morphology of known species of the genus *Odostomia*. *Odostomia columbiana* lacks tentacular pads, and its gut arrangement is similar to that found in members of the genus *Boonea* except that the salivary gland ducts are attached to the anterior esophagus, which with the posterior esophagus and paired salivary glands form a four-way junction (Fig. 1). *Odostomia columbiana*, as well as other members of the subfamily Odostominae, will ultimately be relegated to other genera (Wise, in prep.).

Pyramidellid development

The reproduction and development of *O. columbiana* is similar to that previously described for other pyramidellids (Lebour, 1932, 1936; Rasmussen, 1944, 1951; Fretter and Graham, 1949; White *et al.*, 1985), although most of these descriptions are brief and small differences may have been overlooked. Eggs of *O. columbiana* are relatively small, but not unusually so (Table I). Because embryos grow to fill the capsule before hatching, capsule size is a good predictor of larval size in pyramidellids. *O. columbiana* deposits a single egg per capsule, as do other pyramidellids except *Chrysallida decussata* (Table I). Development of *O. columbiana* is slower than in other species with comparable egg size; only species with large eggs and direct development have a similarly long embryonic period (Table I). Because water temperatures were either not reported or varied considerably in several previous studies, it is difficult to determine whether these differences in development rate were due to temperature.

In *O. columbiana* the long embryonic period is followed by an unusually long planktonic larval stage. Although times to metamorphosis may be different in the laboratory than in nature, veligers in two non-overlapping cultures settled at the same age. Furthermore, recent improvements in larval culture technique and larval diet have reduced the time to metamorphosis in cultures of other invertebrate larvae (Strathmann, 1987). This suggests that the longer larval period of *O. columbiana* in comparison to other laboratory-reared pyramidellid species from previous studies is real (Table I). Unfortunately these studies did not indicate if the larvae studied were planktotrophic or if food was added to the larval cultures. A distinctive characteristic of the *O. columbiana* veligers is the presence of bristles extending over the operculum from the side of the foot. These are not figured or mentioned in any other description of pyramidellid larvae.

Our observations increase the data on the distribution of several developmental characters that are used in heterobranch systematics. Robertson (1985) suggested that chalazae may be a useful synapomorphy shared by pyramidellids, architectonicids, and opisthobranchs. Chalazae are clearly present in egg masses of *O. columbiana* and many other pyramidellids. Høisæter (1989), however, suggests that some pyramidellids lack chalazae and that their presence may be a useful systematic character within the pyramidellids. He did not find chalazae in *O. acuta*, and they were not mentioned in descriptions of egg masses from *Brachystomia eulimoides* (Lebour,

1932) and *Odostomia* sp. (Nishino *et al.*, 1983). Additionally, the shape and thickness of the chalazae of *O. fujitanii* figured by Minichev (1971) are clearly different from those in *O. columbiana* and other pyramidellids. Spermatophores have also been used as a systematic character within pyramidellids to define the genus *Boonea* (Robertson, 1978). *O. columbiana* apparently lacks spermatophores; however, this character has been observed in some other species occurring in the northeastern Pacific (A. J. Kohn, pers. comm.).

Our observations of pyramidellid development from hatching to metamorphosis illuminate several points that have been the subject of much conjecture. At hatching, veligers of *O. columbiana* are morphologically similar to veligers of other planktotrophic pyramidellid species, all of which seem to have small, nonpigmented velums. Previous studies that failed to rear larvae to metamorphosis often concluded that the larval period is short because the velum is small (*e.g.*, Thorson, 1946). This is not the case for *O. columbiana,* which has a long planktonic period during which its velum remains small. Small velar lobes are also typical of planktotrophic opisthobranch larvae (pers. obs., RC), although caenogastropods with long-lived feeding larvae often have large complex velar lobes (Thorson, 1946).

Confusion exists as to how differential shell growth around the aperture results in heterostrophy (the change of coiling direction from a left-handed protoconch to a right-handed teleoconch). Thorson (1946) illustrated several pyramidellid shells near metamorphosis and stated that the outer apertural margin of the larval shell thickens to become a new columella at metamorphosis. Fretter *et al.* (1982) disagreed and suggested that the protoconch's outer lip is continuous with the outer lip of the teleoconch. In *O. columbiana,* the position of the columella shifts clockwise around the aperture as the coiling direction changes, but not to the extent described by Thorson (1946). These conflicting observations of changes in shell shape at metamorphosis may be due to variation in degree of heterostrophy among pyramidellid species. Although the coiling direction reverses in all cases, there is considerable variation in the displacement of the coiling axis of the teleoconch relative to that of the protoconch. In most of the species figured by Thorson (1946), the displacement is offset roughly perpendicular to the teleoconch axis. However, in *O. columbiana* and *Odostomia* sp. (one species studied by Fretter and Graham, 1962), the angle between the coiling axes of the protoconch and teleoconch often appears to be close to 140 degrees (Fretter *et al.*, 1982).

Evolution of gastropod development

Detailed studies of embryology and larvae of "archaeogastropods," caenogastropods, and opisthobranchs reveal several trends in gastropod development. Among gastropods there is a trend in both caenogastropods and opisthobranchs toward unequal cleavage and early D-quadrant specification (Freeman and Lundelius, 1992; van den Biggelaar, 1996; van den Biggelaar and Haszprunar, 1996). Equal cleavage with 4d cell formation at the 64-cell stage as in "archaeogastropods" is assumed to be the ancestral condition. In opisthobranchs, the first one or two cleavages are unequal, and the 4d cell is produced by the 24-cell stage. Intermediate conditions occur in the Architaenioglossa and the Valvatoidea, and there is considerable variation in basal opisthobranchs (van den Biggelaar, 1996). Although Pelseneer (1914) and van den Biggelaar and Haszprunar (1996, citing Pelseneer) report equal cleavage in pyramidellids, first cleavage in *O. columbiana* is clearly not equal. In addition, White *et al.* (1985) figured an unequal two-cell stage of *Boonea impressa* in the process of division. This suggests that either cleavage varies among pyramidellids (an unusual occurrence in gastropod groups) or Pelseneer's account is inaccurate. Regardless, it is interesting that early cleavage divisions in pyramidellids are similar to those in anaspideans and some other opisthobranchs.

Page (1994) suggested that heterochronic shifts in the timing of development of larval and adult organs account for some of the variation in gastropod larval development. In "archaeogastropods" the adult organs develop directly from the embryo, whereas in caenogastropods the larva hatches with well-formed larval organs and subsequently develops the definitive adult structures. Development is retarded in opisthobranchs, and they hatch at a stage of morphogenesis similar to that of unhatched caenogastropods: some larval organs develop after hatching, and the definitive adult organs develop during late larval life or at metamorphosis (Page, 1994). Page (1994) paid particular attention to the stage of formation of the eyes, tentacles, and larval heart. Caenogastropod veligers hatch with well-formed eyes and tentacles, and the larval heart develops long before hatching (Page, 1994, and pers. obs). In opisthobranchs, the larvae hatch before the eyes or tentacles have formed, and the larval heart usually forms during the last half of the planktonic stage (Page, 1994). The observations of *O. columbiana* reported here suggest that pyramidellid larval development may combine characters of opisthobranch and caenogastropod development. As in opisthobranchs, the eyes and tentacles did not appear until well into larval development; as in caenogastropods, the heart began to beat well before hatching.

These observations support recognized trends in the evolution of gastropod development and suggest ancestral character states. Unequal cleavage is characteristic of pyramidellids and some basal opisthobranchs, whereas caenogastropods have a polar lobe; thus unequal cleav-

age may be a heterobranch synapomorphy. However, additional groups at the base of this clade must be examined to rule out parallel evolution of unequal cleavage from an equally cleaving ancestor, because many other opisthobranchs and pulmonates have equal cleavage. Additionally, larvae that hatch before the development of eyes and tentacles were probably ancestral for pyramidellids and opisthobranchs. On the other hand, early appearance of the larval heart relative to hatching in pyramidellids and caenogastropods suggests that late development of the heart is a derived feature of the opisthobranchs. It is clearly necessary to have detailed descriptions of more phylogenetically intermediate groups and to formulate robust phylogenetic hypotheses before any firm conclusions regarding the evolution of these characters can be drawn.

Acknowledgments

We thank A. Kabat (US National Museum of Natural History) for lending us the type specimens of *O. columbiana*, R. Bieler (Field Museum of Natural History, Chicago) for accepting the voucher specimens, E. Kozloff for translating Minichev (1971), and D. Willows and the staff of Friday Harbor Laboratories for their support. B. Pernet and R. Strathmann made useful comments on the manuscript. This research was supported by a National Science Foundation Graduate Fellowship and a Pacific Northwest Shell Club Scholarship to RC, and grant OCE 9301665 to R. Strathmann.

Literature Cited

Amio, M. 1963. A comparative embryology of marine gastropods, with ecological considerations. *Shimonoskei Univ. Fish. J.* **12:** 15–144.

Bieler, R. 1992. Gastropod phylogeny and systematics. *Annu. Rev. Ecol. Syst.* **23:** 311–338.

Biggelaar, J. A. M. van den. 1996. The significance of the early cleavage pattern for the reconstruction of gastropod phylogeny. Pp. 155–160 in *Origin and Evolutionary Radiation of the Mollusca*, J. D. Taylor, ed. Oxford University Press, Oxford, UK.

Biggelaar, J. A. M. van den, and G. Haszprunar. 1996. Cleavage and mesentoblast formation in the Gastropoda: an evolutionary perspective. *Evolution* **50:** 1520–1540.

Boss, K. J., and A. S. Merrill. 1965. Degree of host specificity in two species of *Odostomia* (Pyramidellidae: Gastropoda). *Proc. Malacol. Soc. London* **36:** 349–355.

Bouchet, P. 1989. A review of poecilogony in gastropods. *J. Moll. Stud.* **55:** 67–78.

Clark, K. 1971. Host texture preference of an ectoparasitic opisthobranch, *Odostomia columbiana* Dall and Bartsch 1909. *Veliger* **14:** 54–56.

Cumming, R. L. 1993. Reproduction and variable larval development of an ectoparasitic snail, *Turbonilla* sp. (Pyramidellidae, Opisthobranchia) on cultured giant clams. *Bull. Mar. Sci.* **52:** 760–771.

Dall, W. H., and P. Bartsch. 1907. The pyramidellid mollusks of the Oregonian faunal area. *Proc. U. S. Natl. Mus.* **33:** 491–534.

Dall, W. H., and P. Bartsch. 1909. A monograph of west American pyramidellid mollusks. *Bull. U. S. Natl. Mus.* **68:** 1–258.

Freeman, G., and J. W. Lundelius. 1992. Evolutionary implications of the mode of D quadrant specification in coelomates with spiral cleavage. *J. Evol. Biol.* **5:** 205–247.

Fretter, V. M., and A. Graham. 1949. The structure and mode of life of the Pyramidellidae, parasitic opisthobranchs. *J. Mar. Biol. Assoc. U.K.* **28:** 493–532.

Fretter, V. M., A. Graham, and E. B. Andews. 1982. The prosobranch molluscs of Britain and Denmark. Part 9—Pyramidellidae. *J. Moll. Stud. Suppl.* **11:** 363–434.

Haszprunar, G. 1988. On the origin and evolution of major gastropod groups, with special reference to the Streptoneura. *J. Moll. Stud.* **54:** 367–441.

Hickman, C. S. 1995. Asynchronous construction of the protoconch/teleoconch boundary: evidence for staged metamorphosis in a marine gastropod larva. *Invertebr. Biol.* **114:** 295–306.

Hoagland, K. E., and R. Robertson. 1988. An assessment of poecilogony in marine invertebrates: phenomenon or fantasy? *Biol. Bull.* **174:** 109–125.

Hoffmann, D. L. 1979. An attachment structure in an epiparasitic gastropod. *Veliger* **22:** 75–77.

Høisæter, T. 1989. Biological notes on some Pyramidellidae (Gastropoda: Opisthobranchia) from Norway. *Sarsia* **74:** 283–297.

Kristensen, J. H. 1970. Fauna associated with the sipunculid *Phascolion strombi* (Montagu), especially the parasitic gastropod *Menestho diaphana* (Jeffreys). *Ophelia* **7:** 257–276.

LaFollette, P. 1979. Observation on the larval development and behavior of *Chrysallida* Carpenter, 1857 (Gastropoda: Pyramidellidae). *West. Soc. Malacol. Annu. Rep.* **10:** 18–23.

Lebour, M. 1932. The eggs and early larvae of two commensal gastropods, *Stilifer stylifer* and *Odostomia eulimoides*. *J. Mar. Biol. Assoc. U.K.* **18:** 117–119.

Lebour, M. 1936. Notes on the eggs and larvae of some Plymouth prosobranchs. *J. Mar. Biol. Assoc. U.K.* **20:** 547–566.

Mikkelsen, P. M. 1996. The evolutionary relationships of Cephalaspidea *s.l.* (Gastropoda: Opisthobranchia): a phylogenetic analysis. *Malacologia* **37:** 375–442.

Minichev, Y. S. 1971. On the biology of some Pyramidellidae of the Possjet Bay of the Sea of Japan. *Acad. Sci. USSR Zool. Inst. Explorations of the Fauna of the Seas* **8:** 221–229 [in Russian].

Nishino, T., S. Nojima, and T. Kikuchi. 1983. Quantitative studies of life history and interspecific relationship of two gastropod species, *Odostomia* sp. (ectoparasite) and *Umbonium* (*Suchium*) *moniliferum* (Lamarck) (host). I. Life history and population dynamics of *Odostomia* sp. *Publ. Amakusa Mar. Biol. Lab. Kyushu Univ.* **7:** 61–67.

Page, L. R. 1994. The ancestral gastropod larval form is best approximated by hatching-stage opisthobranch larvae: evidence from comparative developmental studies. Pp. 206–223 in *Reproduction and Development of Marine Invertebrates*, W. H. Wilson, S. A. Stricker, and G. L. Shinn, eds. Johns Hopkins University Press, Baltimore, MD.

Pelseneer, P. 1914. Ethologie de quelques *Odostomia* et d'un Monstrillide parasite de l'un d'eux. *Bull. Sci. France Belg.* **7:** 1–14.

Powell, E. N., M. E. White, E. A. Wilson, and S. M. Ray. 1987. Change in host preference with age in the ectoparasitic pyramidellid snail *Boonea impressa* (Say). *J. Moll. Stud.* **53:** 285–286.

Rasmussen, E. 1944. Faunistic and biological notes on marine invertebrates. I. The eggs and larvae of *Brachystomia rissoides* (Hanl.), *Eulimella natidissima* (Mont.), *Retusa truncata* (Brug.), and *Embletonia pallida* (Alder and Hancock). (Gastropoda marina). *Vi-*

densk. Medd. Dan. Naturhist. Foren. **107:** 207–233.

Rasmussen, E. 1951. Faunistic and biological notes on marine invertebrates II. The eggs and larvae of some Danish marine gastropods. *Vidensk. Medd. Dan. Naturhist. Foren.* **113:** 201–249.

Robertson, R. 1967. The life history of *Odostomia bisuturalis*, and *Odostomia* spermatophores (Gastropoda: Pyramidellidae). *Year Book Am. Philos. Soc.* **1966:** 368–370.

Robertson, R. 1978. Spermatophores of six eastern North American pyramidellid gastropods and their systematic significance (with the new genus *Boonea*). *Biol. Bull.* **155:** 360–382.

Robertson, R. 1985. Four characters and the higher category systematics of gastropods. *Am. Malacol. Bull. Spec. Ed.* **1:** 1–22.

Strathmann, M. F. 1987. *Reproduction and Development of Marine Invertebrates of the Northern Pacific Coast.* University of Washington Press, Seattle, WA. 670 pp.

Thorson, G. 1946. Reproduction and larval development of Danish marine bottom invertebrates with special reference to the planktonic larvae in the Sound (Oresund). *Medd. Dan. Fisk-Havunders. Ser. Plancton* **4:** 1–523.

Thorson, G. 1950. Reproductive and larval ecology of marine bottom invertebrates. *Biol. Rev.* **25:** 1–45.

White, M. E., E. N. Powell, and C. L. Kitting. 1984. The ectoparasitic gastropod *Boonea* (=*Odostomia*) *impressa*: population ecology and the influence of parasitism on oyster growth rates. *Mar. Ecol.* **5:** 283–299.

White, M. E., C. L. Kitting, and E. N. Powell. 1985. Aspects of reproduction, larval development, and morphometrics in the pyramidellid *Boonea impressa* (=*Odostomia impressa*) (Gastropoda: Opisthobranchia). *Veliger* **28:** 37–51.

Wise, J. B. 1993. Anatomy and functional morphology of the feeding structures of the ectoparasitic gastropod *Boonea impressa* (Pyramidellidae). *Malacologia* **35:** 119–134.

Wise, J. B. 1996. Morphology and phylogenetic relationships of certain pyramidellid taxa (Heterobranchia). *Malacologia* **37:** 443–511.

Reference: *Biol. Bull.* **192:** 253–261. (April, 1997)

Bacterial Endosymbionts in the Gills of the Deep-Sea Wood-Boring Bivalves *Xylophaga atlantica* and *Xylophaga washingtona*

DANIEL L. DISTEL[1] AND SUSAN J. ROBERTS[2]

[1]*Department of Biochemistry, Molecular Biology and Microbiology, University of Maine, Orono, Maine 04469-5735; and* [2]*MB, DCS, NCI, NIH, 9000 Rockville Pike, Bethesda, Maryland 20892*

Abstract. Bacterial endosymbionts found in gill tissues in several bivalve families convert otherwise unavailable energy sources (sulfide, methane, or cellulose) to forms readily metabolized by their hosts. We investigated the existence of such a symbiosis in two species of *Xylophaga* (family Pholadidae). The genus *Xylophaga* includes opportunistic species that are the predominant colonizers of wood at depths greater than 150 m. It has been hypothesized that, like their shallow-water counterparts the shipworms (family Teredinidae), species of *Xylophaga* utilize wood for nutrition. Results from transmission and scanning electron microscopy of *X. atlantica* and *X. washingtona* clearly demonstrate the presence of endosymbionts that resemble the shipworm endosymbionts both morphologically and in their anatomical location within the gills. *Xylophaga* and the teredinids both have a caecum packed with wood chips but lack the dense populations of microorganisms associated with cellulose digestion in termites or ruminants. These observations suggest that *Xylophaga* has evolved a symbiotic solution to wood digestion similar to that seen in shipworms. Hence, the *Xylophaga* symbiosis suggests a mechanism for the conversion of terrestrially derived cellulosic carbon from wood into animal biomass in the deep sea.

Introduction

In 1973 Popham and Dixon (Popham and Dickson, 1973) demonstrated the presence of endosymbiotic bacteria in the gills of wood-boring bivalves of the family Teredinidae, commonly known as shipworms. The role of these symbionts, however, was not elucidated until a decade later when it was shown that the symbiotic bacteria, when cultivated *in vitro*, both digest cellulose and fix atmospheric nitrogen (Waterbury *et al.*, 1983). This novel combination of symbiont metabolic activities is now thought to be essential for the survival of teredinids on a diet composed primarily of wood, a food source that, although rich in carbon and energy, is deficient in nitrogen and cannot be digested by most animals.

Whereas teredinids are the predominant wood-boring bivalves in shallow waters (intertidal to 100 m), bivalves of the subfamily Xylophagainae (family Pholadidae) fill the same niche in the deep oceans, occurring primarily at depths from 150 m to greater than 7000 m (Turner, 1972). Like teredinids, xylophagainids bore into woody substrates, ingest the excavated wood particles, and store them in a specialized caecum formed by an outpocketing of the stomach (Purchon, 1941; Turner, 1973). The role of wood in the diet of *Xylophaga* has not, however, been determined experimentally. On the basis of morphological and ecological arguments, it has been proposed that Xylophagainids derive (1) significant (Purchon, 1941; Turner, 1973), (2) little (Potts, 1923), or (3) no (Yonge, 1937, 1938; Yonge and Thompson, 1976) nutrition from the ingestion of wood.

The utilization of wood by xylophagainids is a subject of considerable ecological interest since wood is abundant in many areas of the deep sea (Wolff, 1979) and the opportunistic Xylophagainae are among the most common colonizers of wood at these depths (Turner, 1973). Hence the deep-sea Xylophagainae could perform a role analogous to that of termites in terrestrial habitats and shipworms in shallow marine habitats by converting the refractory cellulosic carbon deposited in wood and other plant remains to a more readily available form (Turner,

Received 2 October 1996; accepted 3 January 1997.

1973). Both termites (Kane, 1997) and shipworms (Waterbury *et al.*, 1983) utilize cellulolytic and nitrogen-fixing symbionts to survive on wood as the sole food source. In this report we present evidence that bacterial endosymbionts are present in the gill tissue of two species of *Xylophaga*, and that these bacteria appear morphologically similar to the gill endosymbionts previously identified in shipworms.

Materials and Methods

Specimens of *X. washingtona* were collected in pine boards submerged for 2–3 months in Monterey Bay (depth 61 m, coordinates 36°39.8′ N, 121°52.88′ W; courtesy of Dr. E. C. Haderlie, Naval Postgraduate School) or in Scripps canyon off the San Diego coast (depth 274 m, coordinates 32°31′ N, 117°16.5′ W). Specimens of *X. atlantica* were collected from oak boards (1″ × 2″ × 2′ lobster-trap skids) submerged for about 1 year at 80–100 m depth 12 miles off the coast of SW Harbor, Maine. Animals were kept alive in chilled seawater tanks until they were removed from the wood and prepared for microscopy (less than 2 weeks). Animals with an average valve diameter of 3–4 mm were dissected and fixed for 1–1.5 h in 3% glutaraldehyde buffered with 0.1 *M* cacodylate/HCl (pH 7.3) and 0.4 *M* NaCl or 3% glutaraldehyde buffered with 0.1 *M* sodium phosphate (pH 7.4), 3% NaCl, and 4.5% sucrose as in Eckelbarger *et al.* (1990). After fixation the specimens were post-fixed in 1% osmium tetroxide and dehydrated through a graded ethanol series. Specimens for transmission electron microscopy (TEM) were then transferred to propylene oxide and embedded in Epon/Araldite for sectioning. Specimens for scanning electron microscopy (SEM) were fractured under liquid nitrogen after ethanol dehydration and then were critical-point dried from CO_2 and sputter coated with gold. A Phillips CM10 transmission electron microscope and an AMR 1000 scanning electron microscope were used to examine samples.

Both *Xylophaga atlantica* and *Xylophaga washingtona* were used for TEM of the gills and light microscopy of the digestive tract. Similar results were observed with both species. *X. atlantica* was used for SEM of the gills, and *X. washingtona* was used for TEM of the digestive tract.

Results

Gross morphology of the ctenidium

The gross morphology of the gills of *Xylophaga* has been described in detail by Purchon (1941) and will be briefly summarized here. The ctenidia (gills) of Xylophagainae, like those of the Teredinidae, are formed by a single (outer) demibranch on either side of the visceral mass (Fig. 1). The marginal groove is absent, there is no ciliary sorting mechanism, and the labial palps are greatly reduced. These features are shared by most tere-

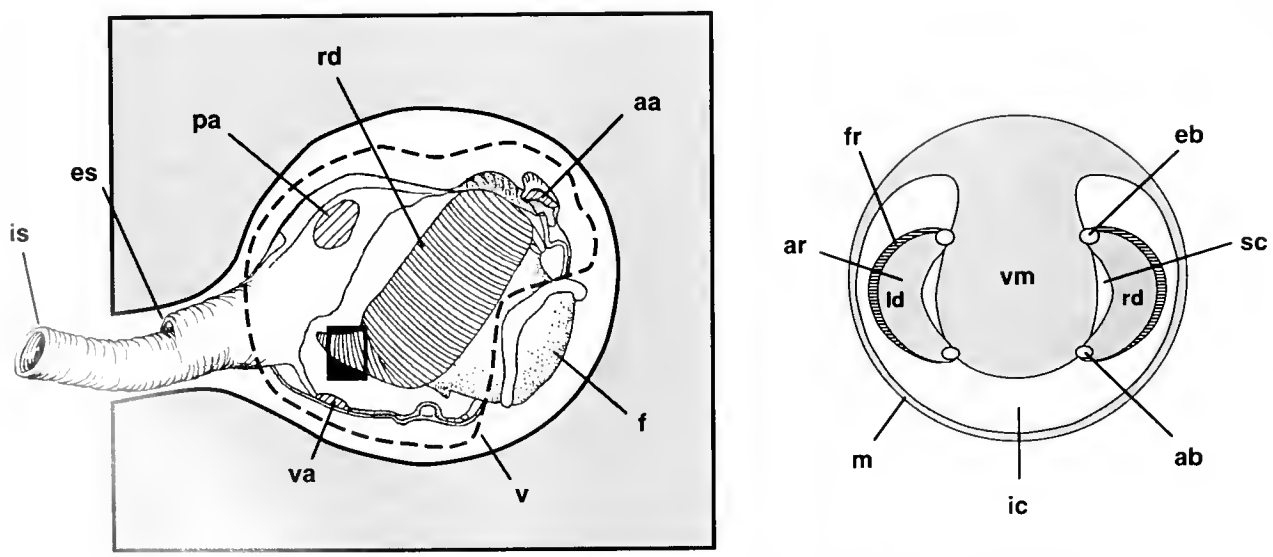

Figure 1. Diagram of *Xylophaga* in sagittal section shown in the burrow (left) and in transverse section (right). aa, anterior adductor muscle; ab, afferent branchial vein; ar, abfrontal region of gill demibranch; eb, efferent branchial vein; es, exhalent siphon; f, foot; fr, frontal region of gill demibranch; ic, infrabranchial chamber of mantle cavity; is, inhalant siphon; ld, left demibranch of gill; m, mantle; pa, posterior adductor muscle; rd, right demibranch of gill; sc, suprabranchial chamber of mantle cavity; va, ventral adductor muscle; v, outline of valves. Boxed area is shown in Figure 2C.

dinids but are divergent from the filter-feeding gill morphology of other lamellibranchs (Purchon, 1941). The ctenidia are connected to the visceral mass dorsally at the efferent branchial vein and ventrally at the afferent branchial vein, forming an arc that separates the mantle cavity into suprabranchial and infrabranchial chambers. Each filament is composed of two distinct regions: a narrow frontal region (fr) and a broad, flattened abfrontal region (ar). As is typical of lamellibranch gills, the frontal region is composed of frontal, laterofrontal, and lateral ciliated cells; a central blood vessel; and supporting connective tissue. The abfrontal region, however, is distinctive, consisting of an extensively developed interlamellar junction that forms a crescent-like sheet bridging the arc of the filament (Fig. 1). The filaments are joined laterally by interfilamentar cellular junctions in the frontal region. Whereas cellular interfilamentar junctions are absent in the abfrontal region, filaments appear to be connected by lateral ciliary junctions in this region (Fig. 2E).

Identification and localization of intracellular bacteria in the ctenidium

In the Xylophagainae, as in other symbiont-bearing bivalves, the frontal region of each gill filament is devoid of symbionts. The most conspicuous cytoplasmic components of the cells of the frontal region include mitochondria, Golgi, endoplasmic reticulum, ciliary structures, centrioles, and glycogen granules. Bacterial symbionts are, however, abundant in the abfrontal region of the ctenidium (Fig. 2D–F and Fig. 3). This region forms a broad, flattened plate composed of two closely appressed single-layered sheets of epithelial cells surrounding a narrow blood sinus.

The epithelium of the abfrontal region consists of two recognizable cell types here referred to as *bacteriocytes* and *intercalary cells* in keeping with terminology in current use for other bivalve symbioses (Fisher, 1990; Frenkiel *et al.*, 1996; Gros *et al.*, 1996). Bacterial endosymbionts are absent from the intercalary cells but dominate the cytoplasm of the bacteriocytes. The symbionts are distributed in clusters throughout the bacteriocytes, with mitochondria infrequently interspersed in the cytoplasm between clusters. Large membrane-bound inclusions, possibly lysosomes or lysosomal residual bodies, also occur in the bacteriocyte cytoplasm (Fig. 3). These inclusions frequently display a biphasic appearance with a granular low-density region and a slightly denser reticulate region that appears to consist of whorled membranes. Some inclusions contain bodies suggestive of partially degraded bacteria. Bacteriocytes and intercalary cells are uniformly distributed in the epithelium of the abfrontal region with about equal frequency. The apical surfaces of both cell types are densely covered with microvilli at points that directly contact the external environment (Fig. 3C).

The bacteriocytes are typically spherical or cylindrical. Their broad basal surfaces compose much of the internal lining of the blood sinus. Intercalary cells, on the other hand, are typically narrow at their basal ends, expanding to a broad and irregular apical surface. Thin sheet-like projections of the apical end of the intercalary cells extend over the apical surfaces of adjacent bacteriocytes, apparently shielding most but not all of the surface of the bacteriocytes from direct contact with the external environment. The outer surface of the abfrontal epithelium is elaborated into a series of larger rounded hummocks (formed by the spherical outline of the bacteriocytes) and smaller papillae (formed by the irregular surfaces of intercalary cells) surrounded by many deep folds and pits (Fig. 2F and Fig. 3A). The inner blood-facing surface of this epithelium also contains numerous invaginations (Fig. 3). These elaborations greatly increase the surface areas that are exposed to blood internally and to seawater externally in the symbiont-containing abfrontal zone.

The endosymbionts are straight to gently curved rods that display a cell-wall morphology typical of gram-negative bacteria and range from 0.4 to 0.7 μm in width and up to 5.0 μm in length (Fig. 3). No conspicuous internal structures, such as the sulfur granules seen in thiotrophic symbionts or the stacked internal membranes seen in methanotrophic symbionts of other bivalve families (Fisher, 1990), are observed in the symbionts of *Xylophaga*.

The symbionts are not in direct contact with the cytoplasm but are contained within membrane-bound vesicles ranging from 10 to 20 μm in diameter. A single vesicle may contain many bacteria. The orientation of symbionts within vesicles is not random. Most symbionts are oriented with their long axes perpendicular to the lateral surface of the filament. Few symbionts are oriented with their long axes parallel to the lateral surface and of those, fewer still align with the frontal-abfrontal axis of the filament. This distribution of orientations is readily observable in both SEM and TEM images.

Extensive examination of TEM images failed to provide evidence of connections between the symbiont-containing vesicles and the external environment. In all sections examined, the vesicular membrane appears distinct from and unconnected to the plasma membrane. Similarly, examination of the exterior surfaces by SEM revealed no evidence of the kind of ducts or openings to the bacteria-containing vesicles that are seen in the symbiont-containing light organs of some luminous fish (Haygood, 1993). Although deep pits and infoldings were observed on the lateral surfaces of the filaments in SEM images, TEM images showed that these are not

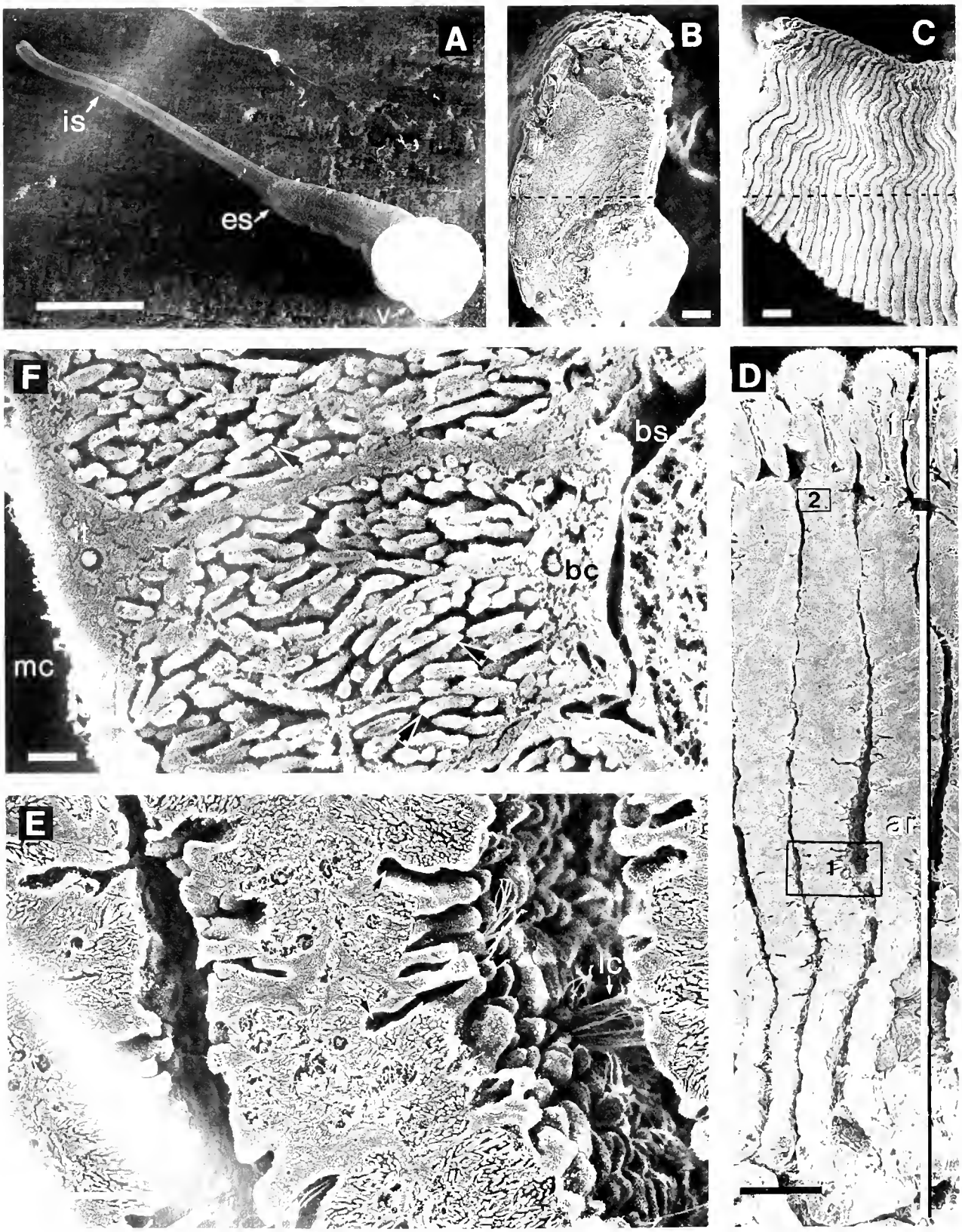

Figure 2. (A) *Xylophaga washingtona* with siphon fully extended. (B–F) Scanning electron micrographs of *X. atlantica* gill. (B) Lateral surface of a gill filament near the posterior tip of the right demibranch. (C) Frontal surface of the right demibranch. (D) Transverse fracture of right demibranch showing three gill

continuous with the symbiont-containing vesicles (Fig. 3C). Hence, at minimum, the bacterial symbionts are separated from the external environment by the plasma membrane, cytoplasm, and vesicular membrane of the host.

Wood and flora of the digestive tract

Xylophaga has a digestive system similar to that described for shipworms, including a large caecum that is typically distended with wood shavings (Fig. 4). The dimensions of the shavings (width and height) match the contours of the dentition on the shell, consistent with the ingestion of wood excavated during burrowing. Wood was the predominant component of the gut contents identifiable at the level of light microscopy. The caecum was the most densely packed space, while the stomach contained dispersed wood fibers. Fibrous material was found in proximity with the crystalline style and at low density in the style sac. Examination of serial thick sections of the guts of several animals failed to reveal any conspicuous community of microorganisms resembling those found in wood-eating insects. Electron microscopy confirmed this observation and further indicated that bacteria are absent from cells of the ciliated epithelium lining the gut and occur only sparsely in the digestive spaces (Fig. 4D–E).

Discussion

The discovery of bacterial endosymbiont populations in a number of marine invertebrate species has been the key to understanding the remarkable ability of these invertebrates to survive on unusual nutrient sources. For example, the identification of cellulolytic, nitrogen-fixing bacteria in the gills of the wood-boring teredinid clams (shipworms) pointed toward an explanation of how these bivalves are able to thrive with wood as their primary food source. This capability, which is quite rare among higher animals, has led to the great success of the Teredinidae as colonizers of wood in coastal marine environments. In the deep oceans, the dominant colonizers of wood and other plant materials are the Xylophagainae (family Pholadidae). Similarities in the gut anatomy and wood-boring habits of the Teredinidae and the Xylophagainae led us to examine whether species of *Xylophaga* maintain similar symbiotic associations. In this report we present morphological evidence for the existence of bacterial endosymbionts in the gill tissue of two of these deep-sea wood-boring bivalves—*Xylophaga atlantica* and *Xylophaga washingtona*.

In many respects, the gill of *Xylophaga* closely resembles the symbiont-containing gills of other bivalves including the Lucinidae, Vesicomyidae, Modiolinae, and Solemyidae (Distel and Felbeck, 1987; Fisher 1990; Frenkiel *et al.*, 1996; Gros *et al.*, 1996). The gill of *Xylophaga* is composed of two regions: a heavily ciliated, symbiont-free frontal region that is like the typical lamellibranch gill structure, and an abfrontal region that appears to be specifically adapted to harbor symbiotic bacteria. The abfrontal region, an extension of the interfilamentar junction, is much broader than the frontal region and composes the bulk of the mass of the gill. The symbionts are completely surrounded by a vacuolar membrane of host origin and lack contact with the external environment. In addition to harboring symbionts, the bacteriocytes contain large membranous structures resembling lysosomes in various stages of development. In some instances, these lysosome-like compartments contain bodies that resemble partially degraded bacteria, which suggests that lysosomal digestion is a mechanism for regulation of the bacterial population.

The symbiont-containing tissue in *Xylophaga* also resembles that of the teredinids. Although teredinid gills are highly modified, the symbionts are found in an anatomically analogous region (Distel *et al.*, 1991). This region is referred to as the gland of Deshayes (Sigerfoos, 1908) in teredinids and corresponds to the interlamellar junction of the fused right and left demibranchs (Turner, 1966; Distel *et al.*, 1991). Bacteriocytes in this tissue contain symbionts that resemble the symbionts of *Xylophaga:* both are gram-negative rods averaging about 0.5 μm in width and up to 5 μm in length, and both lack internal membranes or other conspicuous internal or external structures.

It is striking that xylophagainids and teredinids not only harbor symbionts that are similar in appearance and location, but that they also share similar adaptations to their woody habitats. Both are obligatory wood borers that excavate burrows by using their shells as rasps, ingest the excavated wood shavings, and store the wood parti-

filaments (plane of fracture indicated by dashed lines in B and C). Abfrontal (ar) and frontal (fr) regions indicated by side bar. (E) Detail from box 1 in D, showing deep invaginations (arrows), lateral ciliary tufts (lc), and numerous papillae decorating the lateral surfaces of the abfrontal region. (F) Detail from box 2 in D, showing an intercalary cell (it) and portions of two bacteriocytes (bc). Rod-shaped cells (arrows) within bacteriocytes are symbionts. mc, lumen of mantle cavity; bs, blood sinus; es, exhalent siphon; is, inhalant siphon; v, valve. Scale bars: A, 0.5 cm; B–C, 100 μm; D, 50 μm; E, 10 μm; F, 1.0 μm.

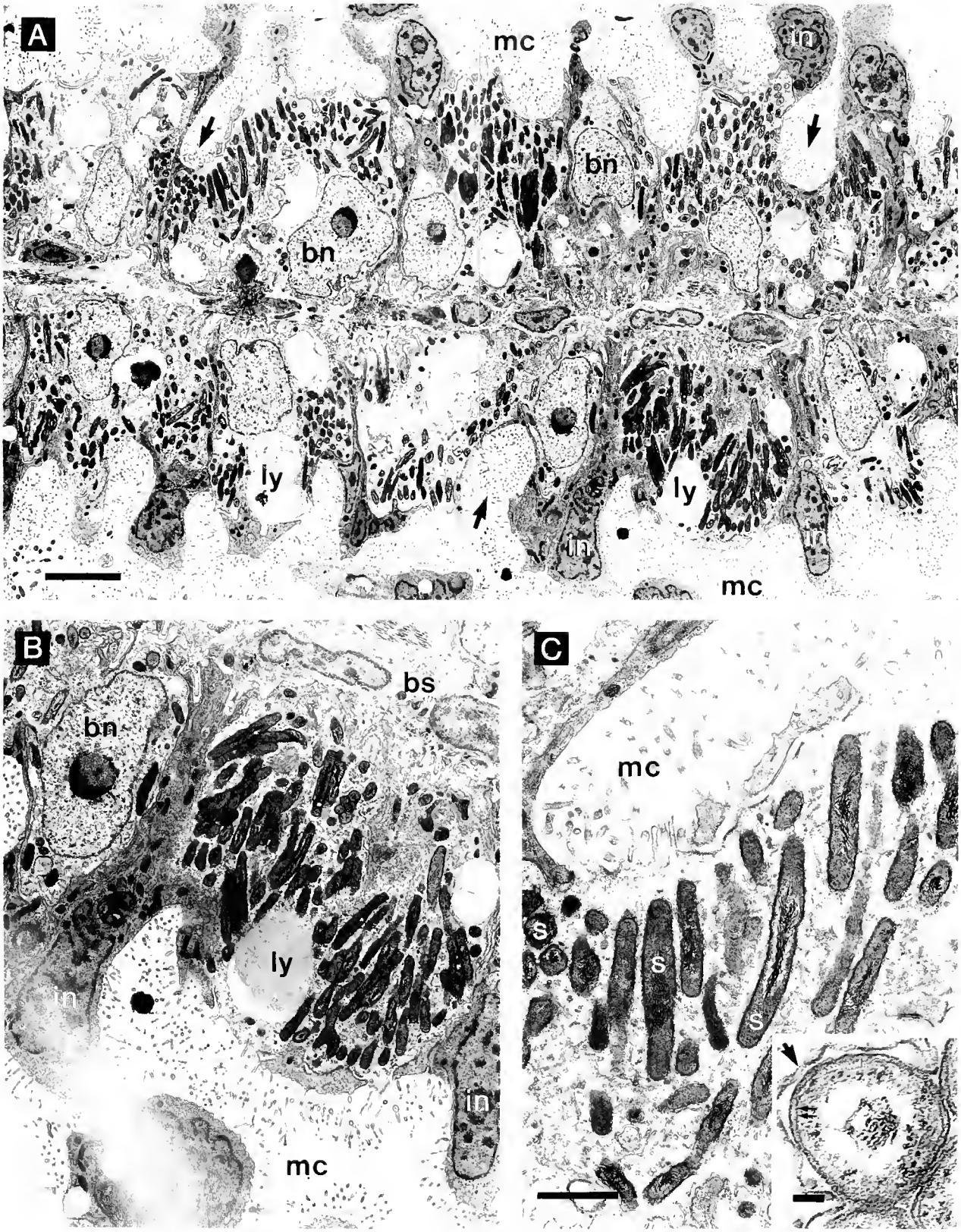

Transmission electron micrographs of a section through the abfrontal region of the gill of
atlantica (A) Low-magnification view of a region comparable to that shown in 2E. Symbionts
lectron-dense rods. Note deep invaginations of the microvillar surface of gill (arrows). (B) Detail

cles in a large caecum prior to passing them through the stomach and gut. Purchon (1941) argued that several features common to the xylophagainid and teredinid digestive systems indicate a departure from reliance on filter feeding and represent specific adaptations to the digestion of wood. These include the lack of a marginal food groove, limited ciliary sorting mechanisms in the ctenidia, reduced labial palps and crystalline style sac, and presence of a wood-storing caecum with ciliated grooves capable of providing a steady stream of wood particles to the stomach.

It is now well established that wood is a primary constituent of the teredinid diet (Gallager *et al.*, 1981), although nutrients may also be obtained from suspension feeding (Mann and Scott, 1985). In fact, at least one shipworm species has been shown to be capable of sustaining normal growth and reproduction with wood as the sole source of particulate nutrients (Gallager *et al.*, 1981). The shipworm symbiont has been cultivated *in vitro* and shown to fix atmospheric nitrogen and secrete cellulolytic, xylanolytic, and proteolytic enzymes (Greene and Freer, 1986; Greene *et al.*, 1988; Greene, 1989, Greene and De Wispeleare, pers. comm.). Although these symbiont activities are appropriate for a wood-based diet and are thought to be critical for the shipworm's success in colonizing woody substrates, no direct evidence exists for their participation in the nutrition of the shipworm hosts.

Since the *Xylophaga* symbiont has not yet been cultivated, the question of whether its metabolic capabilities are similar to those of the shipworm symbiont is unresolved. Hence, it is possible that the two bacteria play different roles in their respective symbioses. For example, the bacterial symbionts in *Xylophaga* may be nitrogen fixing but not cellulolytic, or they may contribute essential nutrients that are absent from wood. On the other hand, phylogenetic analyses based on 16S rRNA sequences indicate that the *Xylophaga* symbiont is the closest relative of the shipworm isolates identified to date (Distel and Roberts, 1996). That finding increases the likelihood that these two symbionts play similar physiological roles.

Although the presence of similar bacteria in the same regions of the gills of the Teredinidae and the Xylophagainae does not demonstrate a common function for the two symbioses, the additional features they have in common—their wood-boring habits and parallel anatomical modifications of the digestive tract—lend support to this hypothesis. To our knowledge, no animal species has yet been demonstrated to utilize wood as a primary nutrient source without the aid of symbiotic microorganisms; thus if wood is the primary dietary constituent of *Xylophaga*, a nutritional role for its symbionts is strongly implicated. If wood is not a primary food source for the xylophagainids (as it is for teredinids), it is difficult to explain the function of the caecum, account for the fact that wood is the principal constituent of the caecal and gut contents, or identify the diet of the xylophagainids. The scarcity of alternative food sources in the deep sea, as well as the notable paucity of bacteria, phytoplankton, and other microorganisms in the gut of *Xylophaga*, seems to preclude the possibilities that *Xylophaga* subsists by filter feeding, by grazing on wood-associated microorganisms, or by utilizing an extracellular symbiotic gut microfauna as do termites and ruminants. Nonetheless, the possibility cannot be ruled out that *Xylophaga* (or the teredinids) produces sufficiently active endogenous cellulases to facilitate wood digestion, as has been suggested for some termites (Breznak and Brune, 1994).

To determine whether the *Xylophaga* symbiosis is cellulolytic, it is necessary to identify the activity of cellulolytic or nitrogen-fixing enzymes in the symbionts, demonstrate the depletion of cellulose in fecal material, and analyze the nutritional utilization of carbon derived from cellulose. These properties have been demonstrated for the shipworm symbiosis, although it is still not clear how the cellulolytic enzymes produced by bacterial endosymbionts in the gill might be transported to the gut where wood digestion must occur. In the teredinids, it has been proposed that a duct in the afferent branchial vein connects the gills to the esophagus (Saraswathy, 1971). Such a duct could serve as a conduit for cellulolytic enzymes; however, the complete vessel was not observed in all species examined, and its existence has not been independently confirmed. Our results indicate that the symbionts of *Xylophaga* (this study) and those of teredinids (unpubl. obs.; Trytek and Allen

---

from lower right quadrant of A, showing a bacteriocyte and portions of two neighboring intercalary cells. (C) Detail from upper left quadrant of A, showing symbionts near the base of a deep lateral invagination. Note that membranes surrounding symbionts are distinct from the microvillar surface of the bacteriocyte plasma membrane. Inset in C shows high magnification of a symbiont cell from *X. washingtona*. Large arrow indicates host-derived membrane of symbiont-containing vesicle. Small arrows indicate double-layered gram-negative cell envelope of the symbiont cell. bs, blood sinus; bn, bacteriocyte nucleus; in, intercalary cell nucleus; ly, lysosome-like granules; mc, lumen of mantle cavity; s, symbionts. Scale bars: A, 5.0 μm, B–C, 1.0 μm; inset, 0.1 μm.

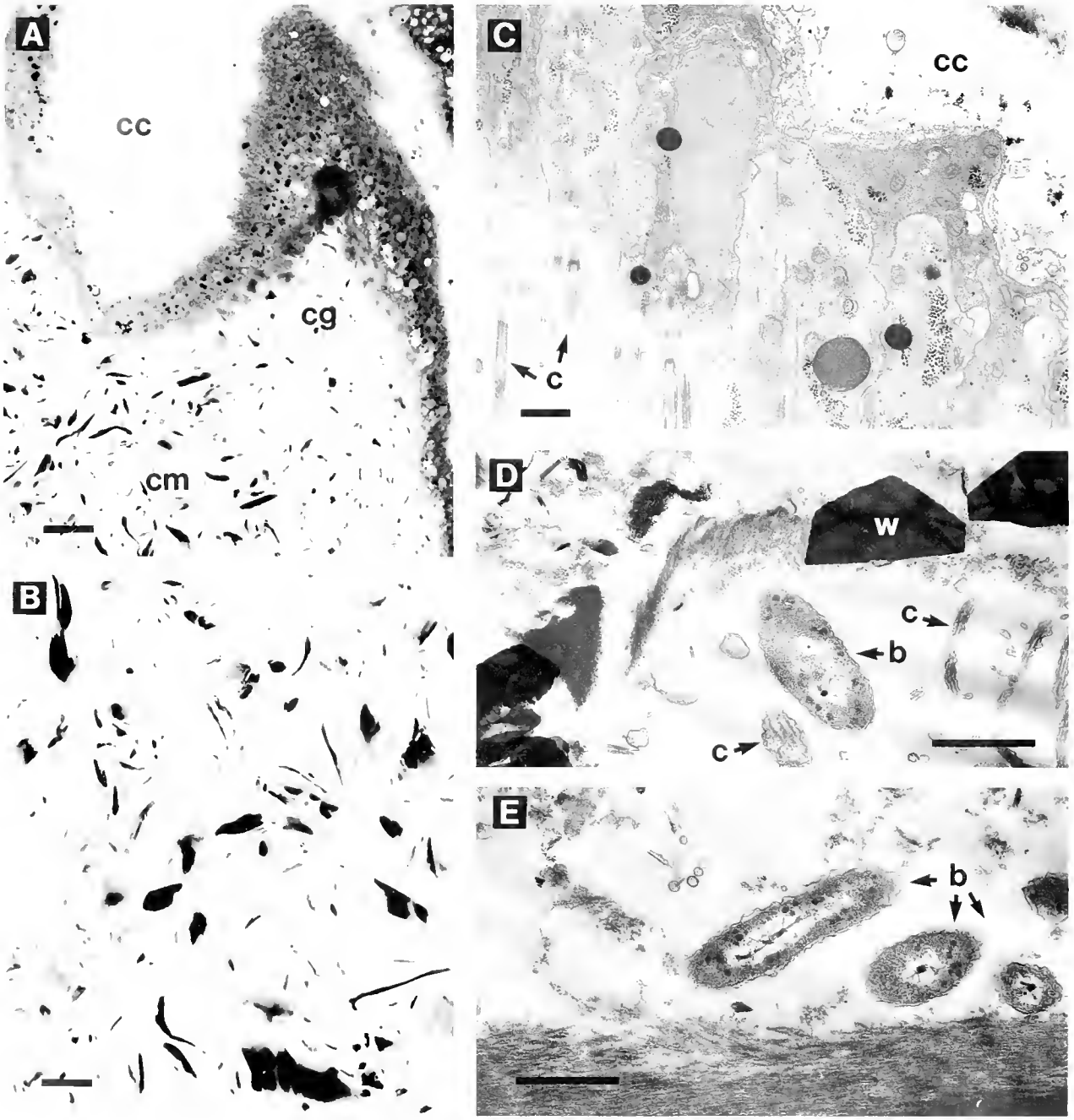

Figure 4. Gut content of *Xylophaga washingtona*. (A) Light micrographs of caecal contents showing ciliated groove (cg) that channels wood shavings into the stomach. (B) Detail of caecal contents from A. Note predominance of wood shavings and absence of algae, fungi, and protozoans. (C–E) Transmission electron micrographs. (C) Ciliated epithelial cells in the region of the caecal wall (ciliated groove) shown in A. The cilia in the lower left face into the lumen of the caecum. No bacteria were observed within the cells of the gut epithelium. (D) One of the rare bacteria seen among the caecal contents. The dark, electron-dense pentagons are wood shavings. (E) Cluster of bacteria observed adjacent to the gastric shield of the stomach. b, bacteria; c, cilia; cc, coelomic cavity; cm, caecum; w, wood. Scale bars: A, 250 μm; B, 150 μm; C–E, 1.0 μm.

(19[illegible] truly intracellular. Consequently, the plausibili[illegible] symbiotic mechanism depends on the demons[illegible] of a pathway whereby enzymes from an intracellular bacterial population are ultimately transported to the lumen of the gut to participate in cellulose degradation.

Acknowledgments

We thank Dr. Ruth D. Turner and Dr. George Somero for helpful discussion and encouragement; Dr. Kevin Eckelbarger, Dr. Nick Holland, and Kelly Edwards for expertise in electron microscopy of marine invertebrates; Wendy Morrill for technical assistance; and Jack Merrill, Ron McConnaughey, and Dr. E. C. Haderlie for aid in collecting specimens. This work was supported by NSF EPSCoR Grant # EHR 91-08766, awards from the Regular Faculty Research and Summer Faculty Research Funds of the University of Maine, Orono, and a research award from the Scripps Industrial Associates.

Literature Cited

Breznak, J. A., and A. Brune. 1994. Role of microorganisms in the digestion of lignocellulose by termites. *Annu. Rev. Entomol.* **39:** 453–487.

Distel, D. L., and H. Felbeck. 1987. Endosymbiosis in the lucinid clams *Lucinoma aequizonata, Lucinoma annulata* and *Lucina floridana*: a reexamination of the functional morphology of the gills as bacteria-bearing organs. *Mar. Biol.* **96:** 79–86.

Distel, D. L., and S. J. Roberts. 1996. Bacterial endosymbionts in the gills of the deep-sea, wood-boring pholad clams *Xylophaga atlantica* and *Xylophaga washingtona*. P. 350 in *Abstracts*. American Society for Microbiology 96th General Meeting, New Orleans, LA. American Society for Microbiology, 1325 Massachusetts Ave., N.W., Washington, DC.

Distel, D. L., E. F. Delong, and J. B. Waterbury. 1991. Phylogenetic characterization and *in situ* localization of the bacterial symbiont of shipworms (Teredinidae: Bivalvia) by using 16S rRNA sequence analysis and oligonucleotide probe hybridization. *Appl. Environ Microbiol.* **57:** 2376–2382.

Eckelbarger, K., B. Bieler, and P. Mikkelsen. 1990. Ultrastructure of sperm development and mature sperm morphology in three species of commensal bivalves (Mollusca: Galeommatoidea). *J. Morphol.* **205:** 63–75.

Fisher, C. R. 1990. Chemoautotrophic and methanotrophic symbioses in marine invertebrates. *Rev. Aquat. Sci.* **2:** 399–436.

Frenkiel, L., O. Gros, and M. Mouëza. 1996. Gill structure in *Lucina pectinata* (Bivalvia:Lucinidae) with reference to hemoglobin in bivalves with symbiotic sulphur-oxidizing bacteria. *Mar. Biol.* **125:** 511–524.

Gallager, S. M., R. D. Turner, and C. J. Berg. 1981. Physiological aspects of wood consumption, growth, and reproduction in the shipworm *Lyrodus pedicellatus* Quatrefages. *J. Exp. Mar. Biol. Ecol.* **52:** 63–77.

Greene, R. V. 1989. A novel, symbiotic bacterium isolated from marine shipworm secretes proteolytic activity. *Curr. Microbiol.* **19:** 353–356.

Greene, R. V., and S. N. Freer. 1986. Growth characteristics of a novel nitrogen-fixing cellulolytic bacterium. *Appl. Environ. Microbiol.* **52(Nov.):** 982–986.

Greene, R. V., H. L. Griffin, and S. N. Freer. 1988. Purification and characterization of an extracellular endoglucanase from the marine shipworm bacterium. *Arch. Biochem. Biophys.* **1(15):** 334–341.

Gros, O., L. Frenkiel, and M. Mouëza. 1996. Gill ultrastructure and symbiotic bacteria in the tropical lucinid, *Linga pensylvanica* (Linné). *Symbiosis* **20:** 259–280.

Haygood, M. G. 1993. Light organ symbioses in fishes. *Crit. Rev. Microbiol.* **19(4):** 191–216.

Kane, M. D. 1997. Microbial Fermentation in Insect Guts. Chap. 8, pp. 231–265 in *Gastrointestinal Fermentation and Ecosystems*, Vol. 1, R. I. Mackie and B. A. White, eds. Chapman and Hall, New York.

Mann, R., and M. G. Scott. 1985. Growth, morphometry, and biochemical composition of the wood boring molluscs *Teredo navalis* L., *Bankia gouldi* (Bartsch), and *Nototerendo knoxi* (Bartsch). *J. Exp. Mar. Biol. Ecol.* **85:** 229–251.

Popham, J. D., and M. R. Dickson. 1973. Bacterial associations in the teredo *Bankia australis* (Lamellibranchia, Mollusca). *Mar. Biol.* **19:** 338–340.

Potts, F. A. 1923. The structure and function of the liver of *Teredo*, the shipworm. *Proc. Camb. Phil. Soc.* **1:** 1–17.

Purchon, R. D. 1941. On the biology and relationships of the lamellibranch *Xylophaga dorsalis* (Turton). *J. Mar. Biol. Assoc. U.K.* **25(1):** 1–39.

Saraswathy, M. 1971. Observations on the structure of the shipworms, *Nausitora hedleyi, Teredo furcifera* and *Teredora pricesae* (Bivalvia: Teredinidae). *Trans. Roy. Soc. Edinb.* **68(14):** 508–562.

Sigerfoos, C. P. 1908. Natural history, organization and late development of the *Teredinidae* or shipworms. *Bull. Bur. Fish.* **37:** 191–231.

Trytek, R. E., and W. V. Allen. 1980. Synthesis of essential amino acids by bacterial symbionts in the gills of the shipworm *Bankia setacea* (Tryon). *Comp. Biochem. Physiol.* **67A:** 419–427.

Turner, R. D. 1966. A Survey and Illustrated Catalogue of the Teredinidae (Mollusca: Bivalvia). The Museum of Comparative Zoology, Harvard University, Cambridge, MA.

Turner, R. D. 1972. A new genus of deep water wood-boring bivalve (Mollusca, Pholadidae, Xylophagainae). *Basteria* **36(2–5):** 98–104.

Turner, R. D. 1973. Wood-boring bivalves, opportunistic species in the deep sea. *Science* **180:** 1377–1379.

Waterbury, J. B., C. B. Calloway, and R. D. Turner. 1983. A cellulolytic-nitrogen fixing bacterium cultured from the Gland of Deshayes in shipworms (Bivalvia: Teredinidae). *Science* **221:** 1401–1403.

Wolff, T. 1979. Macrofaunal utilization of plant remains in the deep sea. *Sarsia* **1(2):** 117–136.

Yonge, C. M. 1937. Evolution and adaptation in the digestive system of metazoa. *Biol. Rev.* **12:** 87–115.

Yonge, C. M. 1938. Recent work on the digestion of cellulose and chitin by invertebrates. *Sci. Prog.* **32:** 638–47.

Yonge, C. M., and T. E. Thompson. 1976. Borers in rock and timber. Chap. 16, pp. 205–219 in *Living Marine Molluscs*. William Collins Sons, London.

Reference: *Biol. Bull.* **192:** 262–278. (April, 1997)

Decline in Pelagic Cephalopod Metabolism With Habitat Depth Reflects Differences in Locomotory Efficiency

BRAD A. SEIBEL, ERIK V. THUESEN[1], JAMES J. CHILDRESS, AND LAURA A. GORODEZKY[2]

Oceanic Biology Group, Marine Science Institute, University of California, Santa Barbara, California 93106

Abstract. The metabolic rates of 33 species of pelagic cephalopods from California and Hawaii were measured and correlated with minimum depth of occurrence. Mean metabolic rates ranged from 0.07 μmol O_2 g^{-1} h^{-1} for the deep-living vampire squid, *Vampyroteuthis infernalis*, to 8.79 μmol O_2 g^{-1} h^{-1} for *Gonatus onyx*, a vertically migrating squid. An individual of *V. infernalis*, which lives within the oxygen minimum layer off California, had the lowest mass-specific metabolic rate ever measured for a cephalopod (0.02 μmol O_2 g^{-1} h^{-1}, 1050 g wet weight). For species collected in sufficient quantity and size range, metabolism was related to body size. Critical partial pressures of oxygen (P_c) were determined for Hawaiian and Californian cephalopods. P_c values for Hawaiian animals were considerably higher than for those taken off California, a trend that corresponds to the higher levels of environmental oxygen in the Hawaiian waters. Buffering capacity (β) of mantle muscle, assayed in eight cephalopod species, was used to estimate the capacity for glycolytic energy production. Mean β ranged from 1.43 slykes for a bathypelagic octopod, *Japetella heathi*, to 77.08 slykes for an epipelagic squid, *Stenoteuthis oualaniensis*. Significant declines with increasing depth of occurrence were observed for both metabolism and β. The decline in metabolic parameters with depth is interpreted as a decreased reliance on locomotory abilities for predator/prey interactions in the light-limited deep sea. The decline in metabolism with depth observed for pelagic cephalopods was significantly steeper than that previously observed for either pelagic fishes or crustaceans. We suggest that since strong locomotory abilities are not a priority in the deep sea, deeper-living cephalopods may rely more heavily on means of locomotion that are more efficient than jet propulsion *via* mantle contractions—means such as fin swimming or medusoid swimming utilizing the arms and extensive webbing present in many deep-living species. The greater efficiency of deeper-living cephalopods may be responsible for the observation that the decline in metabolic rates with depth is more pronounced for pelagic cephalopods than for fishes or crustaceans.

Received 31 January 1996; accepted 18 November 1996.

[1] Present address: The Evergreen State College, Olympia, WA 98505.

[2] Present address: Channel Islands National Marine Sanctuary, 113 Harbor Way, Santa Barbara, CA 93109-231.

Abbreviations: β, buffering capacity; MDO, minimum depth of occurrence; MDdO, minimum depth of daytime occurrence; P_{O_2}, partial pressure of dissolved oxygen; P_c, critical oxygen partial pressure.

Introduction

Cephalopods are morphologically diverse, visually orienting predatory molluscs. The five groups of extant cephalopods—squids (Teuthoidea), cuttlefishes (Sepioidea), octopuses (Octopoda), vampire squids (Vampyromorpha), and the chambered Nautilus (Nautiloidea)—are easily distinguished by morphological characteristics, among which are locomotory adaptations to their habitat (Roper *et al.*, 1984). Locomotory differences are also reflected in an animal's physiological properties. Previous physiological studies on cephalopods have primarily focused on the more commercially important squids, and on the shallow-water octopuses and cuttlefishes (Grieshaber and Gäde, 1976; Baldwin, 1982; O'Dor, 1982; O'Dor and Webber, 1986; Portner *et al.*, 1993).

Some of these animals are among the most metabolically active poikilotherms known (O'Dor and Shadwick, 1989), which stems in part from the inherent inefficiency of jet propulsion. Other studies have investigated the metabolism of *Nautilus* spp. and its ability to withstand low levels of oxygen (O'Dor *et al.*, 1990; Wells *et al.*, 1992; Boutilier *et al.*, 1996). Very little is known, however, about the physiological adaptations of cephalopods to the deep sea. The current study is a comprehensive comparison of the metabolic rates of midwater cephalopods living at depths down to 2 km off California and Hawaii.

Many studies have demonstrated a decline in the metabolic rates of pelagic fishes and crustaceans with increasing habitat depth (Childress, 1975; 1995; Torres *et al.*, 1979; Torres and Somero, 1988; Ikeda, 1988; Cowles *et al.*, 1991). Additional studies found no clear relationship between metabolism and minimum depth of occurrence in chaetognaths and medusae (Thuesen and Childress, 1993a, 1994). Bathypelagic representatives of these groups have metabolic rates comparable to those of their epipelagic counterparts when measured at the same temperature.

Childress and Mickel (1985) put forth the visual interactions hypothesis to explain the decline in metabolic rates of fish and crustaceans with increasing minimum depth of occurrence. They observed that reduced metabolic rates reflect decreased locomotory abilities in many deeper-living groups. They hypothesized that this decrease resulted from relaxed selection for strong locomotory abilities for visually cued predator/prey interactions in the low ambient light levels of the deep sea. Although deep-living fishes and crustaceans do possess well-developed eyes, these are apparently used primarily for interactions *via* bioluminescence (Marshall, 1979), which is a relatively weak, often transient light source. Under these conditions, interactions are likely to take place over short distances that do not require strong locomotory abilities (Marshall, 1979; Herring *et al.*, 1994; Fleisher and Case, 1995). The visual interactions hypothesis is supported by the presence of a decline in metabolic rates of visually orienting pelagic groups (fishes and crustaceans), and by the absence of a decline in non-visually orienting gelatinous organisms (*e.g.*, chaetognaths and medusae).

Cephalopods, like fishes and crustaceans, are highly visual predators that occupy a range of depths and habitats. As such, they are an obvious choice for further testing of the visual interactions hypothesis. In the present study, the oxygen consumption rates of 33 species of pelagic cephalopods were measured and correlated with minimum depth of occurrence. Because of differences in local productivity and ambient oxygen levels between the two regions, comparisons between Hawaiian and Californian animals are used to determine possible effects of oxygen and food availability on metabolic rates. Buffering capacity was assayed to indicate an animal's capacity for anaerobic work (Castellini and Somero, 1981).

Materials and Methods

Cephalopods were captured on nine cruises aboard the R/V *Point Sur* and R/V *New Horizon* between September 1992 and September 1996. Sampling was done primarily in an area 160 km west of Point Conception, California (34° 37′N, 122° 42′W to 34° 30′N, 123° 20′W) and off Oahu, Hawaii (21° 20′N, 158° 20′W to 21° 35′N, 158° 35′W). Animals were collected using an opening/closing Mother Tucker trawl with a 10-m^2 mouth. The net was equipped with a 30-l thermally protecting cod end that reduced mechanical damage and heat shock to animals during recovery (Childress *et al.*, 1978). Ship speed was kept very low (0.5–1 kn) to decrease turbulence and abrasion in the net and to reduce the number of animals collected in the cod end. Upon reaching the surface, specimens were immediately transferred to 5°C seawater and allowed to recover for several hours. Only animals in the best physical condition were selected for physiological study. Animals were identified to species with the aid of several sources (Roper *et al.*, 1984; Sweeney *et al.*, 1992; Young, 1972; Hochberg, pers. comm.; Young, pers. comm.). Voucher specimens were preserved for verification of identifications.

Routine oxygen consumption rates were determined on board ship by allowing individual specimens to deplete the available oxygen in a sealed, water-jacketed chamber filled with filtered seawater containing 50 mg l^{-1} streptomycin (Childress, 1971a). All experiments were carried out at atmospheric pressure because hydrostatic pressure has been shown to have negligible effects on the metabolism of a mesopelagic squid, *Histioteuthis heteropsis* (Belman, 1978), and on several meso- and bathypelagic gelatinous zooplankters (Childress and Thuesen, 1993). Chambers were kept in darkness and, in most cases, the temperature was maintained at 5°C by means of a refrigerated water bath. Rates for individuals of some species were measured at either 2°, 3.5°, 10°, or 15°C and corrected to 5°C either using measured Q_{10} values or according to the methods outlined in Childress *et al.* (1990). The rate of change of the oxygen partial pressure within the respirometer was monitored using a Clark-type oxygen electrode (Mickel *et al.*, 1983) calibrated to air- and nitrogen-saturated seawater before and after each experiment. A magnetic stir pump mixed the water in the respirometry chamber and maintained water flow past the electrode without damage to the animals. Individual respiration experiments lasted from 2 to 24 h. Oxygen concentrations were averaged over 2-min intervals and recorded using a computer-based data

acquisition system. The mean rates of oxygen consumption between partial pressures of 30 and 70 mm Hg were used for comparisons because this allowed a period for the animals to calm down after being introduced to the chamber and ended before oxygen concentrations became limiting. Oxygen consumption rates of the smallest specimens were measured using glass syringes (3–50 ml) as miniature respiration chambers (Thuesen and Childress, 1993a, b) maintained in darkened water baths. Water samples were withdrawn periodically from the incubation syringe through a three-way valve using a gastight syringe, and the new incubation volume was noted. The oxygen content of the water sample was then analyzed using a gas chromatograph.

Oxygen consumption was calculated as micromoles of oxygen consumed per gram wet weight per hour. At sea, immediately following respiration experiments, animals were weighed using a motion-compensated shipboard precision balance system (Childress and Mickel, 1980). For additional comparisons, wet-weight-specific rates of oxygen consumption were corrected by covariance to 10 g by using measured scaling coefficients or an assumed scaling coefficient of −0.20 (Childress *et al.*, 1990). The value of 10 g was chosen because it was the approximate modal weight of the animals measured. Both corrected and unscaled values for mean rates of oxygen consumption are presented in Table I.

Mean rates of oxygen consumption were regressed against habitat depth. Because animals live at a range of depths, minimum depth of occurrence (MDO) was taken as the primary description of habitat depth. MDO is defined as that depth below which 90% of the individuals of a given species are captured in a given region (Childress, 1975). Ten meters was taken as the MDO for animals living at that depth or shallower to avoid distortions in regressions of ln-transformed data. MDO refers to the adult distribution except for species of the genus *Leachia*, as discussed later. For consistency with previous studies, animals that undergo a strong diel vertical migration are considered at their shallowest depth whether day or night. For comparison, regressions against minimum depth of daytime occurrence (MDdO) are also plotted. Both MDO and MDdO are listed in Table I. Estimates of cephalopod depth were based on collections from a variety of studies as well as on personal observations and communications (Pickford, 1946; Roper and Young, 1975; Young, 1978; Lu and Roper, 1979; Roper *et al.*, 1984; Sweeney *et al.*, 1992; James Hunt, MBARI, pers. comm.).

Regulation of oxygen consumption was measured by plotting specific rates of oxygen consumption *versus* partial pressures of oxygen. The critical partial pressure (P_c) was taken as the point at which oxygen consumption was no longer maintained independent of oxygen concentration. The P_c was determined by calculating regression lines for the two distinct parts of the relationship between oxygen consumption and P_{O_2}, the regulated (higher P_{O_2}) segment and the highly sloped (low P_{O_2}) segment. The P_c was designated as the intersection of these two lines.

In vitro buffering capacity (β) of mantle muscle, due to non-bicarbonate buffering compounds, was assayed following the methods of Castellini and Somero (1981). β is defined as the micromoles of base needed to change the pH of the homogenate by 1 pH unit per gram wet weight of muscle tissue. A unit of β is termed a "slyke." Although many cephalopod species use fins for sustained aerobic swimming, most cephalopods rely on mantle musculature for jet propulsion during burst escape responses (Baldwin, 1982). For this reason, and because it usually represents the largest percentage of body mass, mantle tissue was chosen for measurements of buffering capacity. Muscle tissue was homogenized at a dilution of 1:20 (weight:volume) in normal saline (0.9% NaCl). Homogenates were equilibrated to 20°C and stirred continuously during experiments. Homogenates were titrated from pH 6 to 7 using 0.2 *N* NaOH (less concentrated NaOH was used for animals with extremely low buffering capacities to get a sufficient number of points in the titration curve). If the homogenate had an initial pH greater than 6.0, it was acidified by the addition of HCl before the titration. As observed by Castellini and Somero (1981), more weakly buffered muscles yielded curves that tailed upward at pH values near 7.0 and above. In these cases, the linear portion of the curve (usually between pH 6.0 and 6.5) was used for calculating β. An Orion digital research ionalyzer (model 701A) was used with a glass pH electrode for monitoring pH changes. A microburet was used to add the NaOH solution.

All data analyses were performed with Statview II or SuperANOVA statistics programs (Abacus Concepts, Inc., Berkeley, CA). Simple linear regressions, *t* tests, and analysis of covariance (ANCOVA) were used. Mean values given are followed by the standard error. All regressions were carried out on ln-transformed data to linearize the data and maintain consistency with previous studies. The figures, however, are semilog plots. Confidence intervals for regression exponents are at the 95% level, *P* values for regression coefficients are *F* tests. ANCOVA was used to test whether the slopes and elevations of the various relationships were significantly different from zero and from each other. Regression slopes were declared significant when their slopes differed from zero at the 5% confidence level.

Results

The metabolic rates of 33 species of pelagic cephalopods from four orders are presented in Table I. An indi-

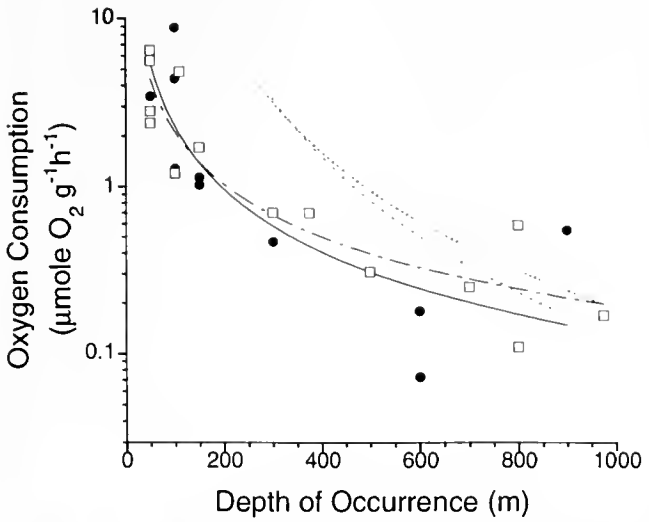

Figure 1. Mean oxygen consumption rates (y = μmol O_2 g^{-1} h^{-1}) of 23 species of pelagic cephalopods as a function of minimum depth of occurrence (x = meters). There is a significant decline in metabolism with minimum depth of occurrence for California (●) species ($y = 707.7x^{-1.25 \pm 0.58}$, $P = 0.001$; $R^2 = 0.68$) and Hawaiian (□) species ($y = 264.0x^{-1.05 \pm 0.55}$; $P = 0.001$; $R^2 = 0.87$). There is also a significant decline in metabolism with minimum depth of daytime occurrence for both Californian (· · ·) species ($y = 1.54*10^8x^{-3.07 \pm 2.33}$; $P = 0.01$; $R^2 = 0.43$) and Hawaiian (· · · ·) species ($y = 1.12*10^8x^{-2.24 \pm 1.65}$; $P = 0.002$; $R^2 = 0.62$). Results of ANCOVA show that there is not a significant difference in the slopes or magnitudes of the regressions of Californian and Hawaiian animals at either MDO or MDdO ($P > 0.4$).

vidual of *Vampyroteuthis infernalis*, which lives within the oxygen minimum layer between 600 and 800 m, had the lowest mass-specific metabolic rate ever measured for a cephalopod (0.02 μmol O_2 g^{-1} h^{-1}, 1050 g wet weight). *V. infernalis* had the lowest mean rate as well (0.07 ± 0.03 μmol O_2 g^{-1} h^{-1}; n = 15, 223.4 g mean wet weight). *Gonatus onyx*, a shallow-living vertical migrator, had a mean metabolic rate of 8.79 μmol O_2 g^{-1} h^{-1}, the highest rate measured in this study. Rates corrected to 10 g of wet weight ranged from 0.06 μmol O_2 g^{-1} h^{-1} for *V. infernalis* measured off Hawaii, to 6.55 μmol O_2 g^{-1} h^{-1} for *Gonatus onyx*. The mean rate presented here for *Histioteuthis heteropsis*, 1.02 ± 0.15 μmol O_2 g^{-1} h^{-1} (0.87 μmol O_2, corrected to 4.25 g for comparison with published values), is comparable to the value of 0.83 μmol O_2 g^{-1} h^{-1}, 4.25 g mean wet weight (Belman, 1978), the only other measurement of this kind available for a midwater cephalopod. Most physiological studies of cephalopods have been done on fast-swimming epipelagic squids that are capable of avoiding midwater trawls. DeMont and O'Dor (1984) reported a metabolic rate of 14 μmol O_2 g^{-1} h^{-1} for *Illex illecebrosus* at rest and 56 μmol O_2 g^{-1} h^{-1} at 100% activity (100-g animal, 13°C measurement temperature). These rates are similar to those observed for *Loligo forbesi* by Boucher-Rodoni and Mangold (1989).

Even with the exclusion of the faster epipelagic squids, a significant decline in mean metabolic rate (y) with MDO (x) was observed for both Californian and Hawaiian pelagic cephalopods (Fig. 1). There was no significant difference in either the slope (ANCOVA; $P = 0.47$) or the elevation (ANCOVA; $P = 0.98$) of the regression lines between Californian ($y = 707.7x^{-1.25 \pm 0.58}$; $P = 0.001$; $R^2 = 0.68$) and Hawaiian ($y = 264.0x^{-1.05 \pm 0.55}$; $P = 0.001$; $R^2 = 0.87$) species. A significant decline in metabolic rate (y) with minimum depth of daytime occurrence (MDdO) was also observed for both Californian and Hawaiian pelagic cephalopods (Fig. 1). Because of the absence of vertical migration among the deepest living species, estimates of daytime depth (x) result in a significantly steeper slope (ANCOVA; $P = 0.002$) for both Californian ($y = 1.54*10^8x^{-3.07 \pm 2.33}$; $P = 0.012$; $R^2 = 0.43$) and Hawaiian ($y = 1.12*10^8x^{-2.24 \pm 1.65}$; $P = 0.002$; $R^2 = 0.62$) regressions.

Normalization of metabolic rates to 10 g wet weight did not have a significant effect on the slopes or elevations of Hawaiian or Californian regressions against MDO or MDdO. The regression of cephalopod metabolism corrected to 10 g against MDO (Fig. 2) had a significantly steeper slope than the slopes for both fishes (ANCOVA; $P = 0.004$) and crustaceans (ANCOVA; $P = 0.001$) (data from Childress, 1975; Torres *et al.*, 1979). This relative steepness is driven both by higher metabolic rates among shallower animals (cephalopods living at 100 m have metabolic rates comparable to fishes and crustaceans living at the surface) and by lower metabolic rates among some deep-living cephalopods. It is interesting that the squids (order Teuthoidea) living below 300 m had significantly higher metabolic rates than other cephalopods (orders Octopoda and Vampyromorpha) (unpaired t test, $P = 0.0001$). The metabolic rates of teuthoids ($y = 117.9x^{-0.86 \pm 0.15}$; $P = 0.0001$; $R^2 = 0.66$) and oetopods with *Vampyroteuthis infernalis* ($y = 16.8x^{-0.74 \pm 0.12}$; $P = 0.0007$; $R^2 = 0.87$) alone still decline with depth with a significantly steeper slope than either fishes or crustaceans.

Several specimens were excluded from the above analyses and are plotted separately (Fig. 3) because small numbers of captures and various life-history characteristics (*i.e.*, ontogenetic vertical migration, or pelagic stages of otherwise benthic animals) make depth distributions and metabolic data difficult to interpret. Inclusion of these species into the regression using roughly estimated MDOs does not significantly alter the slope or elevation of the regression of cephalopod metabolism with minimum depth of occurrence. *Ocythoe tuberculata* and *Amphitretus pelagicus* (both pelagic octopods), planktonic juveniles of the benthic octopus *Octopus rubescens*, and seven species of the family Cranchiidae (Teuthoidea) were among those excluded.

Table I

Metabolic rates and weight and depth data for 33 species of pelagic cephalopods from California and Hawaii

Species	Depth (m)*				Wet weight (g)		MO_2 (μmol O_2 g^{-1} wet wt h^{-1})†		
	MDO	MDdO	*n*	T°C	Range	Mean	Range	Mean ± SE	Corrected
California									
Order Teuthoidea									
Gonatus onyx	100	400	1	5	—	2.30	—	8.79	6.55
Gonatus pyros	100	400	5	5	2.17–31.28	8.58	3.15–7.60	4.38 ± 0.84	3.41
Abraliopsis felis	50	300	1	5	—	0.99	—	3.44	2.16
			1	10	—	0.36	—	6.70	
Octopoteuthis deletron	100	300	1	5	—	8.19	—	1.28	1.22
Histioteuthis heteropsis	150	500	17	5	0.23–36.98	9.99	0.45–2.98	1.02 ± 0.15	0.73
			3	10	0.23–2.85	1.38	1.32–2.5	1.74 ± 0.38	
Histioteuthis hoylei	150	500	1	5	—	8.51	—	1.13	1.09
Chiroteuthis calyx	300	500	11	5	5.87–89.02	38.88	0.15–0.85	0.47 ± 0.07	0.67
Valbyteuthis oligobessa	900	900	1	2	—	25.40	—	0.55	0.66
Family Cranchiidae									
Galiteuthis phyllura	300	500	1	5	—	5.19	—	0.61	0.54
Cranchia scabra	10	10	1	5	—	35.39	—	0.29	0.37
Leachia dislocata	10	300	1	5	—	3.27	—	0.70	0.55
Helicocranchia pfefferi	300	300	6	5	0.15–3.60	0.88	0.41–1.94	0.97 ± 0.22	0.59
Order Octopoda									
Ocythoe tuberculata	10	10	1	5	—	1.21	—	4.17	2.73
Japetella heathi	600	600	11	5	0.84–162.5	35.19	0.03–0.28	0.18 ± 0.03	0.16
			1	10	—	6.32	—	0.48	
Octopus rubescens‡	10		2	5	0.04, 0.08	0.06	7.43–7.53	7.48 ± 0.05	2.78
			3	10	0.07–0.12	0.10	10.19–10.90	10.43 ± 0.23	
Order Vampyromorpha									
Vampyroteuthis infernalis	600	600	15	5	0.41–1050	223.4	0.025–0.41	0.07 ± 0.03	0.09
			1	10	—	4.74	—	0.31	
Hawaii									
Order Sepioidea									
Heteroteuthis hawaiiensis	110	250	1	5	—	5.88	—	4.81	4.31
Order Teuthoidea									
Abraliopsis pacificus	50	300	5	5	0.40–1.90	1.22	1.86–3.94	2.39 ± 0.39	1.63
			2	15	1.89–2.91	2.40	4.96–5.90	5.43	
Enoploteuthis higginsi	50	300	1	5	—	6.47	—	5.59	5.12
Pterygioteuthis microlampas	50	300	1	5	—	0.13	—	6.46	2.71
Octopoteuthis nielseni	100	300	1	2	—	0.13	—	1.20	0.61
Histioteuthis hoylei	150	500	2	5	0.40, 1.27	0.84	1.66–1.77	1.71	1.03
Chiroteuthis imperator	300	500	1	5	—	14.94	—	0.70	0.76
Joubiniteuthis portieri	500	500	3	5	36.00–48.99	41.85	0.20–0.39	0.31 ± 0.06	0.41
Mastigoteuthis famelica	375	675	1	5	—	4.06	—	0.70	0.59
Ctenopteryx siculus	50	625	1	5	—	4.24	—	2.81	2.37
			2	15	1.28, 2.11	1.70	5.07–5.41	5.24	
Bathyteuthis abyssicola	800	800	2	5	1.53, 37.7	19.6	0.56–0.61	0.59	0.59
Family Cranchiidae									
Leachia pacifica	50	50	3	3.5	0.90–2.12	1.52	0.24–1.83	0.81 ± 0.51	0.56
Liocranchia valdivia	500	500	12	5	0.17–21.28	2.92	0.27–1.61	0.56 ± 0.11	0.27
			11	15	0.02–19.0	2.25	1.47–3.47	2.47 ± 0.23	
Megalocranchia fisheri	10	600	1	5	—	47.9	—	0.39	0.54
Cranchia scabra	10	10	1	5	—	6.39	—	0.40	0.37
Order Octopoda									
Japetella diaphana	700	700	12	5	0.02–242	59.49	0.04–0.89	0.25 ± 0.07	0.15
			4	15	0.02–17.15	5.04	0.53–4.04	1.79 ± 0.82	0.52
Eledonella pygmaea	975	975	5	5	2.03–40.00	15.88	0.05–0.43	0.17 ± 0.07	0.18
			6	15	2.00–67.0	24.03	0.08–1.03	0.49 ± 0.11	
Amphitretus pelagicus	300	—	1	5	—	30.3	—	0.10	0.13
Order Vampyromorpha									
Vampyroteuthis infernalis	800	800	1		—	0.5	—	0.11	0.06

* MO_2: mean oxygen consumption rates measured from 70 to 30 mm Hg oxygen partial pressure. Values in the rightmost column are corrected to 10 g wet weight and 5°C (using scaling coefficients and Q_{10} values or assuming a scaling coefficient of −0.20 and a Q_{10} of 2.0).

†MDO: minimum depth of occurrence; MDdO: minimum depth of daytime occurrence.

‡The individuals of *Octopus rubescens* measured here are pelagic juveniles of an otherwise benthic species.

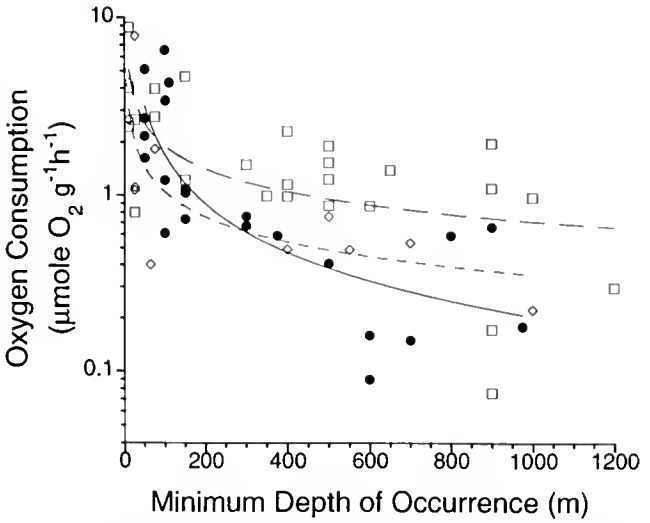

Figure 2. Oxygen consumption rates of cephalopods (●), fish ( ), and crustaceans (□) normalized to 10 g wet weight and 5°C as a function of minimum depth of occurrence. Results of ANCOVA show that the slope of the regression for cephalopods is significantly steeper than for either fish ($P = 0.004$) or crustaceans ($P = 0.001$) (data from Childress, 1973; Torres *et al.*, 1979).

The one specimen of *Ocythoe tuberculata* measured in this study was a male caught in an oblique tow from 2500 m to the surface. The animal's excellent physical condition upon reaching the surface suggests that it was caught at a shallow depth near the end of the trawl, but very little is known about its vertical distribution. It had a metabolic rate of 4.17 μmol O_2 g^{-1} h^{-1}. The specimen of *Amphitretus pelagicus* measured was captured in a closing net at night between 700 and 820 m. There is some evidence that the juveniles of the species are found shallower than the adults, but adults have been captured as shallow as 250 m at night (Roper and Young, 1975). Nothing is known of its daytime distribution. Its metabolic rate (0.10 μmole O_2 g^{-1} h^{-1}) is very close to that of other deep-living pelagic octopods and to *Vampyroteuthis infernalis*.

Seven species of the family Cranchiidae were measured in this study. Limited data and questionable vertical distribution information failed to reveal a significant relationship with depth in these species. *Helicocranchia pfefferi* had the highest corrected (to 10 g wet weight) metabolic rate among the Cranchiidae (0.59 μmol O_2 g^{-1} h^{-1}, $n = 6$), but was not significantly different from other cranchiid species. Because many cranchiids undergo an ontogenetic migration (Young, 1975a, b), MDO was difficult to pinpoint. In the case of *Leachia pacifica* and *Leachia dislocata*, minimum depth refers to the larval habitat. Individuals of this species spend the majority of their lives in epipelagic waters and then migrate suddenly to great depths where maturation and spawning occur (Young, 1975a). The specimens of *L. pacifica* measured in this study were captured in shallow water, so its minimum depth is listed here as 50 m. Certainly for most of its life, *L. pacifica* is subject to the selection regime associated with epipelagic waters. *Galiteuthis phyllura*, *H. pfefferi*, and *Lio-*

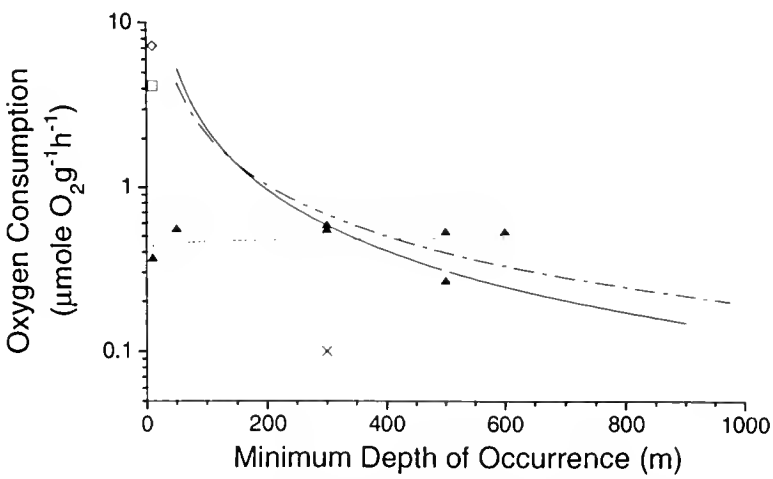

Figure 3. Mean oxygen consumption rates (μmol O_2 g^{-1} h^{-1}) normalized to a wet weight of 10 g (assuming a scaling coefficient of −0.20) of seven species from the family Cranchiidae (▲) as a function of habitat depth (m). The slope of the regression line is not significantly different from zero ($P = 0.57$). The regressions of Californian (——) and Hawaiian (– – –) cephalopods other than cranchiids are plotted as a function of minimum depth of occurrence for comparison (from Fig. 1). *Ocythoe tuberculata* (□) had an oxygen consumption rate of 4.17 μmol O_2 g^{-1} h^{-1}. Paralarval *Octopus rubescens* ( ) had a mean oxygen consumption rate of 7.27 μmol O_2 g^{-1} h^{-1}. *Amphitretus pelagicus* (×) had a metabolic rate of 0.10 μmol O_2 g^{-1} h^{-1}.

Table II

Critical oxygen partial pressures (P_c), weight-specific oxygen consumption rates (MO_2, μmol O_2 g^{-1} wet weight h^{-1}) as a function of body weight (M), and Q_{10} values for bathypelagic cephalopods with different life-history characteristics

Species	P_c 5°C (mm Hg)	Wet weight (g) range	$VO_2 = aM^b$ a;	b (±95% CI, n)	Mean MO_2 (±SE, n) 5°C	10°C	15°C	Q_{10}
California								
Order Teuthoidea								
Abraliopsis felis	—	0.36–0.99	ns	—	3.44 (—, 1)	6.70 (—, 1)	—	3.79
Histioteuthis heteropsis	6.97	0.23–36.98	1.16;	−0.20 (0.09, 17)	1.09*	1.74 (0.38, 3)	—	2.55
Order Octopoda								
Japetella heathi	6.10	0.84–162.5	ns		0.22 (—, 2)	0.48 (—, 1)	—	4.76
Octopus rubescens§	—	0.04–0.12	ns		7.48 (—, 2)	10.43 (0.23, 3)	—	1.94
Order Vampyromorpha								
Vampyroteuthis infernalis	3.10	0.41–1050	0.18;	−0.30 (0.10, 15)	0.11*	0.31 (—, 1)	—	7.90
Hawaii								
Order Teuthoidea								
Abraliopsis pacificus	—	0.40–2.91	ns		2.39 (0.39, 5)	—	5.43 (—, 2)	2.27
Ctenopteryx siculus	—	1.28–4.24	ns		2.81 (—, 1)	—	5.24 (—, 2)	1.86
Liocranchia valdivia	—	0.17–21.28	ns		0.56 (0.11, 12)	—	2.47 (0.23, 11)	4.41
		0.01–0.25†	ns		1.05 (—, 2)	—	2.56 (0.70, 3)	2.43
		0.37–21.3‡	ns		0.47 (0.08, 9)	—	2.43 (0.28, 8)	5.17
Bathyteuthis abyssicola	18.0	—	ns					
Order Octopoda								
Japetella diaphana	18.6	0.02–242	0.24;	−0.27 (0.05, 12)	0.44 (0.11, 6)	—	1.79 (0.82, 4)	4.10
		0.56–2.97†	ns		0.26 (0.01, 3)	—	0.60 (—, 1)	2.31
		17.0–36.0‡	ns		0.11 (—, 2)	—	0.53 (—, 1)	4.82
Eledonella pygmaea	—	2.03–40.0	ns		0.17 (0.07, 5)	—	0.57 (0.14, 5)	3.35

Critical partial pressure of oxygen (P_c) is defined as that partial pressure of oxygen at which oxygen consumption is no longer independent of oxygen concentration. All confidence intervals for scaling coefficients (b) are t tests at the 95% level of significance. Q_{10} values were calculated using rates from similar-sized animals.

* Rates corrected to appropriate weight for Q_{10} measurements using measured scaling coefficients.

† Weight range undergoing ontogenetic descent (captured between surface and 600 m depth).

‡ Adult weight range captured below 600 m depth.

§ Pelagic juveniles stage of an otherwise benthic species.

cranchia valdivia undergo a gradual ontogenetic descent. The specimens measured here were primarily small (10–30 mm mantle length) and are plotted at intermediate depths ranging from 300 to 500 m. *Cranchia scabra* has a very wide distribution. It has been captured from the surface to depths greater than 2000 m. It is plotted here at an MDO of 10 m.

Temperature effects

Metabolic rates were measured at 5°, and either 10° or 15°C for 10 cephalopod species with various life-history characteristics. Q_{10} values are presented in Table II. Q_{10} values were significantly lower for species that undergo diurnal vertical migrations through large temperature changes than for species with permanently deep (cold) habitats (unpaired t test, $P = 0.049$). The mean Q_{10} for vertical migrators was 2.62 ± 0.42 ($n = 4$), which is consistent with temperature responses observed previously for vertically migrating crustaceans (Cowles *et al.*, 1991). The mean Q_{10} for non-migrators was 4.90 ± 0.78 ($n = 5$). Pelagic juveniles of *Octopus rubescens* were excluded from this comparison because nothing is known of their diel movements. The Q_{10} for *O. rubescens* was 1.94. Of the non-migrators, two species are known to undergo ontogenetic migrations from the surface to great depths. *Liocranchia valdivia* and *Japetella diaphana* both migrate from the surface as paralarvae to great depths as subadults. The Q_{10} values measured for individuals captured in the process of migration are similar to those of diurnally migrating cephalopods (2.31, 2.43), whereas the Q_{10} values for deep-living adults are considerably higher (4.82, 5.17). It should be pointed out that the non-migrators (including the adults of ontogenetically migrating species) live in water of about 5°C or below and rarely if ever encounter water as warm as 10°C. Their responses to temperatures of 10°C and above are thus not expected to be adaptive.

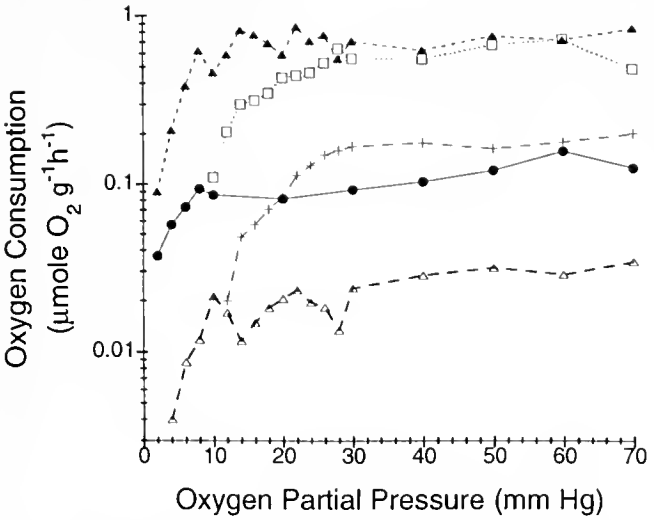

Figure 4. Mean oxygen consumption rates (μmol O_2 g^{-1} h^{-1}) averaged over 2-min intervals as a function of available oxygen (mm Hg) at 5°C. Individuals from five species are plotted. Mean critical partial pressures are 7.2 ± 1.4 mm Hg for *Vampyroteuthis infernalis* (△), 6.1 mm Hg for *Japetella heathi* (●), 21.8 ± 3.2 mm Hg for *Japetella diaphana* (+), 11.99 ± 2.28 mm Hg for *Histioteuthis heteropsis* (▲), and 18.0 for *Bathyteuthis abyssicola* (□).

Regulation

The regulation of oxygen consumption at 5°C was investigated in five species of pelagic cephalopods (Fig. 4). Critical partial pressures of oxygen (P_c) are presented in Table II. *Vampyroteuthis infernalis*, which lives permanently within the well-developed oxygen minimum layer off California, had a mean P_c of 7.2 ± 1.4 mm Hg (n = 6), which is comparable to that of the mysid *Gnathophausia ingens* (Childress, 1968; Sanders and Childress, 1990). One individual of *V. infernalis* demonstrated regulatory abilities down to 3.1 mm Hg, considerably lower than the minimum P_{O_2} of 6 mm Hg found within the California oxygen minimum layer. Similarly, *Japetella heathi*, a bathypelagic octopod found off the California coast, was capable of regulating its oxygen consumption to as low as 6.1 mm Hg (n = 2). *Japetella diaphana* off Hawaii, however, is apparently able to regulate its oxygen consumption to only 21.8 ± 3.2 mm Hg (n = 3), despite a metabolic rate very similar to that observed for *J. heathi* (Table I). *Bathyteuthis abyssicola* from Hawaii regulated to 18 mm Hg (n = 2). The regulatory abilities of *J. diaphana* and *B. abyssicola* are consistent with the minimum value of 20 mm Hg found for the partial pressure of oxygen within the Hawaiian oxygen minimum layer. Regulatory abilities were assessed in four individuals of the vertically migrating squid *Histioteuthis heteropsis* captured off California. The mean critical partial pressure was 11.99 ± 2.28 mm Hg. One individual regulated to 6.97 mm Hg, consistent with oxygen concentrations found at its deeper, daytime habitat.

Buffering capacity

The mean buffering capacities (β) in mantle muscle of eight species of pelagic cephalopods are listed in Table III. β ranged from 1.43 slykes for the Californian bathypelagic octopod *Japetella heathi* to 77.08 slykes for the epipelagic Hawaiian squid *Sthenoteuthis oualaniensis*. Significant scaling relationships could not be derived for any species measured. A significant decline in buffering capacity (y = slykes) with increasing MDO (x = meters) was observed ($y = 275.9x^{-0.67 \pm 0.39}$; $P = 0.004$; $R^2 = 0.85$; Fig. 5). The slope of this regression is significantly lower than the slope of the regression of oxygen consumption with depth (ANCOVA: $P = 0.009$).

Metabolic scaling

Regressions of weight-specific oxygen consumption against wet weight were significant in only three individual species (Fig. 6). *Vampyroteuthis infernalis* had a scaling coefficient, b, of −0.30 ± 0.10 (P = 0.0001; R^2 = 0.75), with weights ranging from 0.41 to 1050.0 g. *Histioteuthis heteropsis* had a scaling coefficient of −0.20 ± 0.09 (P = 0.001; R^2 = 0.50), with weights ranging from 0.23 to 36.98 g. The scaling coefficient found for *Japetella diaphana* was −0.27 ± 0.05 (P = 0.0001; R^2 = 0.95). Weights ranged from 0.02 to 242.17 g. The scaling coefficients for all three of these species are consistent with scaling data available for a wide range of animals (Schmidt-Nielsen, 1983). Sufficient range in size and numbers of *Chiroteuthis calyx* (5.97–89.02 g, n = 11) and *Japetella heathi* (0.84–162.5 g, n = 11) failed to yield a significant scaling relationship. Individuals of *J. heathi* larger than 10 g appear to follow a scaling pattern similar to that of *J. diaphana*, although the relationship was not significant.

There is a significant increase in wet weight (ln y = grams) with increasing MDO (ln x = meters) among the species for which oxygen consumption was measured ($y = 1.22x - 4.08$; $P = 0.0001$; $R^2 = 0.39$). The largest cephalopod measured in this study, an individual of *Vampyroteuthis infernalis* (1050 g), had the lowest metabolic rate measured (0.02 μmol O_2 g^{-1} h^{-1}). We were unable to measure oxygen consumption for the faster epipelagic squids, many of which reach sizes considerably larger than any species reported in the present study. Typical sizes of commercial species range from 0.1 to 1.0 kg (Roper *et al.*, 1984).

Discussion

A decline in metabolic rate with a species' minimum depth of occurrence (MDO) was observed for pelagic

Table III

Buffering capacity (β) of mantle muscle of pelagic cephalopods from California and Hawaii measured at 20°C; wet weight and minimum depth of adult occurrence (MDO) are also given

Species	MDO (m)	*n*	Wet weight (g)		β	
			Range	Mean ± SE	Range	Mean ± SE
California						
Order Teuthoidea						
Gonatus onyx	100	1	—	1.06	—	32.61
Chiroteuthis calyx	300	5	3.43–70.08	36.96	7.43–9.86	8.37
Mastigoteuthis pyrodes	375	2	67.50, 96.98	82.25	8.00, 11.76	9.88
Cranchia scabra	10	2	16.14, 35.38	25.76	14.99, 30.77	22.88
Order Octopoda						
Japetella heathi	600	3	25.50–162.5	86.59	0.94–2.33	1.43 ± 0.45
Order Vampyromorpha						
Vampyroteuthis infernalis	600	13	5.93–600	224.35 ± 52.39	0.86–6.89	3.33 ± 0.45
Hawaii						
Order Teuthoidea						
Sthenoteuthis oualaniensis	10	1	—	110		77.08
Chiroteuthis imperator	300	3	27.7–53.56	40.07 ± 7.50	5.98–9.66	8.03 ± 1.08
Order Octopoda						
Japetella diaphana	700	7	8.96–325.8	119.10 ± 40.06	1.34–2.44	1.67 ± 0.15

cephalopods off California and Hawaii. This decline with increasing MDO is significantly steeper in slope than that observed for pelagic fishes and crustaceans (Fig. 2) (Childress, 1975; Torres *et al.*, 1979). The large decline results from both higher rates among shallower cephalopods and lower rates among many cephalopods living at depth. This means that many deep-living cephalopods have metabolic rates similar to those of midwater jellyfishes (Thuesen and Childress, 1994). The presence of a strong decline in cephalopods, fishes, and crustaceans suggests, however, that the selective factors that influence metabolic parameters are similar at any given depth for all three groups. Buffering capacity has been used in the past to indicate the capacity of muscle tissue for anaerobic work (Castellini and Somero, 1981). Like oxygen consumption, β declined with increasing MDO. This is consistent with the results of Castellini and Somero (1981), who saw lower β values in deep-sea fishes than in either actively foraging pelagic ectotherms or in warm-bodied fishes.

There are many variables confounded with habitat

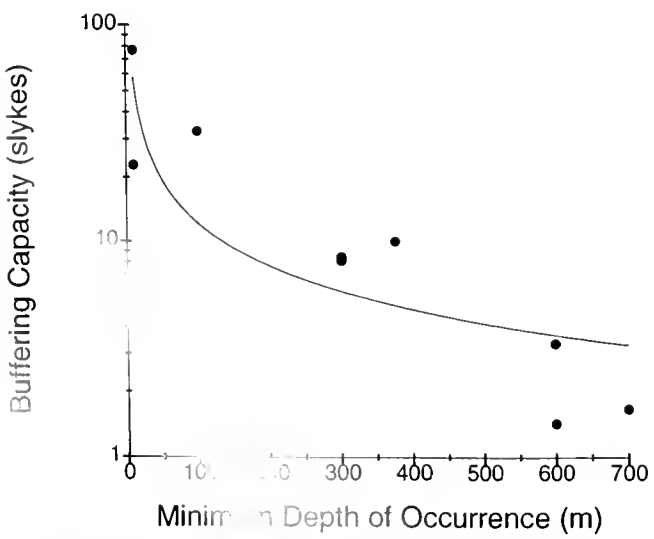

Fig. of min sured fro ($P = 0.004$, r^2 85).

Buffering capacity (slykes) of mantle muscle as a function pth of occurrence in meters for nine cephalopods measrnia and Hawaii. The regression is $y = 275.9x^{-0.67\pm0.39}$

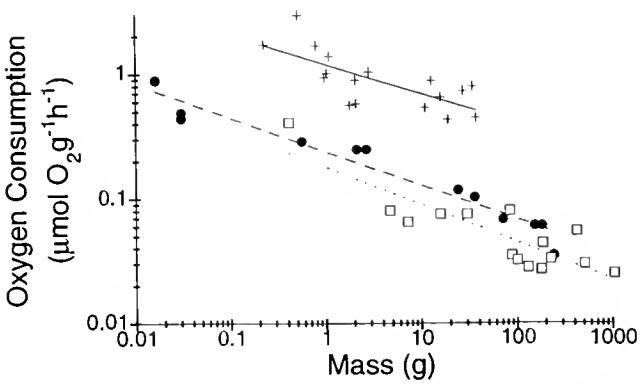

Figure 6. Oxygen consumption rates (μmol O_2 g^{-1} h^{-1}) as a function of wet weight (g). The slope of the regression line is $y = 1.16x^{-0.20\pm0.09}$ ($P = 0.001$; $R^2 = 0.50$) for *Histioteuthis heteropsis* (+), $y = 0.18x^{-0.30\pm0.10}$ ($P = 0.0001$; $R^2 = 0.75$) for *Vampyroteuthis infernalis* (□), and $y = 0.24x^{-0.27\pm0.05}$ ($P = 0.0001$; $R^2 = 0.95$) for *Japetella diaphana* (●).

depth. These include light, productivity, temperature, phylogeny, neutral buoyancy, vertical and horizontal migrations, oxygen concentration, and body size, among others. However, in the discussion below it will become apparent that the decline in metabolic parameters with increasing habitat depth most likely reflects decreased locomotory abilities in deeper-living animals. The steep slope of the regression of cephalopod metabolism with depth relative to that of fishes and crustaceans may reflect the relative efficiencies of locomotion at the surface, where high speeds are required for visually cued predator/prey interactions, and at depth, where sit-and-wait predation strategies are prevalent.

Light and visual interactions

According to the visual interactions hypothesis, reduced reliance on visual predator/prey interactions in the light-limited deep sea decreases selection for locomotory abilities, thus resulting in the lower metabolic rates observed in deep-living fishes, crustaceans, and cephalopods (Childress, 1995). This idea is supported by the presence of a decline in metabolism with depth among these visually orienting groups and the absence of such a decline among organisms that lack eyes (medusae and chaetognaths). That light-limited predator/prey interactions affect animal behavior is not a new idea. Light has long been recognized as a primary controlling factor in the daily movements of midwater organisms (Kerfoot, 1970). Limits on concealment from predation through counterillumination determine daytime depth distribution in some squids and fishes (Young *et al.*, 1980), and young cranchiid squids undergo ontogenetic changes that minimize their visibility at a given light level (Young, 1975b). These cranchiids can also control the orientation of their body and eyes to reduce the size of their own silhouette against surface illumination (Seapy and Young, 1986). The extent to which animals are concealed from visual predators and prey is suggested here to strongly influence the evolution of locomotory abilities and metabolic rates of midwater organisms. The metabolic rate of *Lolliguncula brevis*, which is typically found in complex and shallow coastal waters where opportunities for refuge and crypsis are greater, is half that of the more powerful squid living in open epipelagic waters. It was suggested that *L. brevis* is not required to swim great distances or at high speeds to capture prey or to escape predators (Finke *et al.*, 1996). The metabolic rates of fishes and crustaceans in benthic habitats, where opportunities for refuge and crypsis are greater, do not decline with increasing habitat depth to nearly the extent observed in pelagic animals (Childress *et al.*, 1990). The apparent lack of a decline in metabolic rates among cranchiid squids in the present study is probably a result of concealment from predation through transparency.

Productivity

The food limitation hypothesis suggests that animals living in relatively food-poor environments such as the deep sea have evolved lower metabolic rates as a way of conserving energy (Childress, 1971b; Smith and Hessler, 1974). If this were true, one might expect metabolic rates of deeper-living species to vary from region to region in correlation with surface primary productivity. Contrary to this prediction, comparisons between tropical and temperate regions of differing productivity have shown that among pelagic crustaceans living continuously below 400 m, there is no significant variation in metabolic rate with depth. In fact, shallow-living crustaceans actually have higher metabolic rates in Hawaii than in California where productivity is considerably higher (Cowles *et al.*, 1991). This may indicate an increased demand for strong locomotion for predator/prey interactions over greater distances in the clearer, more strongly illuminated surface waters. No significant differences were found between the slopes or magnitudes of the regressions of metabolism with depth for Californian and Hawaiian cephalopods. Although the magnitudes of the regressions were not significantly different, it may be worth noting that *Vampyroteuthis infernalis* seems (based on small numbers of captures) to come as much as 100 m shallower off California than off Hawaii. Similarly, *Japetella heathi* comes about 100 m shallower off California than does *J. diaphana* off Hawaii (Roper and Young, 1975; Young, 1978). This may reflect differing light regimes between the two regions.

Temperature effects

Temperature generally has large effects on metabolic processes. A 10°C increase in temperature typically causes a doubling of metabolic rate (Q_{10} = 2). Deep-living animals may be expected to have lower metabolic rates on the basis of lower temperatures alone. Donnelly and Torres (1988) report that the decline in aerobic metabolism of midwater fishes and crustaceans with depth in the eastern Gulf of Mexico is no greater than that due to the decrease in temperature. However, the observation that metabolism declines with increasing MDO in the isothermal waters of Antarctica (Torres and Somero, 1988; Ikeda, 1988) seems to eliminate temperature as the primary factor producing lower metabolic rates in the deep sea.

The Q_{10} values measured here (Table II) fall into two groups. Vertical migrators, which experience a wider range of temperatures every day, have typical responses to temperature, but non-migrators have much larger responses. Non-migrators typically live at or near 5°C and rarely, if ever, experience temperatures near 10°C. The responses to temperatures outside the normal range for the species are not expected to be adaptive. A few of the non-

migrators undergo ontogenetic descents through the water column. The young stages experience a wider range of temperatures over a relatively short (though unknown) period of time. Individuals captured during the process of ontogenetic descent have more typical responses to temperature than do the adults of the species. A Q_{10} of approximately 20 would be required to explain the slope of the decline in metabolic rates with depth observed here.

Phylogeny

Harvey and Pagel (1991) warned that interspecific comparisons may be invalid because phylogeny, instead of selection, may have played the greater role in determining the properties of the species. Although there are obvious phylogenetic effects, the observed variation with depth in the metabolism of cephalopods, like that of fishes and crustaceans, is probably not an artifact of phylogeny for two reasons (Childress, 1995). First, the physiological and morphological characteristics of related species seem to diverge as a function of habitat depth. Single genera or families of fishes and crustaceans often occupy the entire depth range studied, and the variation in a characteristic being studied may approach the entire range of variation for such a parameter within a data set (Childress *et al.*, 1990; Cowles *et al.*, 1991). Second, the evidence for convergent evolution among genera, families, and even phyla is strong. The origin of many of these groups lies outside the deep sea and thus can hardly produce a phylogenetic bias. Many deep-living groups share characteristics of chemical composition, general musculature, and physiology that all lead to decreased locomotory abilities. Cowles and Childress (1988) demonstrated directly that bathypelagic mysids have weaker swimming capabilities than do epipelagic species. Enzymatic activities provide evidence for reduced locomotory abilities in deeper-living fishes also (Childress and Somero, 1979; Sullivan and Somero, 1980).

Divergence of related species as a function of habitat depth can be seen at the ordinal level among cephalopods. Epipelagic squids (order Teuthoidea) are extremely active predators, and some are capable of speeds sufficient to propel their bodies out of the water (Cole and Gilbert, 1970). A study on *Illex illecebrosus* reported a respiration rate nearly twice as high as any cephalopod measured in this study (DeMont and O'Dor, 1984). Among the teuthoids measured here, nearly 2 orders of magnitude separate *Gonatus onyx*, a vertical migrator that lives below 100 m, and *Bathyteuthis abyssicola*, which lives continuously below 800 m. Similarly, *Octopus tuberculata* (order Octopoda), believed to be epipelagic, had a metabolic rate nearly 2 orders of magnitude greater than that measured for the pelagic octopods *Argonauta pelagicus* (captured at 700 m) and *Japetella diaphana* (MDO = 700). Convergence of cephalopods with fishes and crustaceans living at similar depths is evidenced by both their morphology and metabolism. Voss (1967) recognized morphological similarities in cephalopods living at a given habitat depth. He observed a decrease in mantle musculature and the appearance of a gelatinous material that formed the bulk of the mantle in deep-living forms. In general, deeper-living cephalopods, like fishes and crustaceans, appeared to be relatively poor swimmers compared to their epipelagic counterparts.

Phylogeny does, however, appear to play at least some role in the evolution of cephalopod metabolism. Deep-living octopods have significantly lower metabolic rates than squids at similar depths. It appears from observations of the musculature (Roper, 1969), gill areas (Madan and Wells, 1996; Seibel and Childress, 1996), and metabolic rates that perhaps *Bathyteuthis abyssicola* leads a more active life than the deep-living octopods and *Vampyroteuthis infernalis*. However, the metabolic rate of *B. abyssicola* is still comparable to that of deep-living fishes with sit-and-wait predation strategies (Cowles and Childress, 1996).

The only family with representatives from a wide range of depths measured in this study is the Cranchiidae. Cranchiids comprise a monophyletic group distinguished from other cephalopods by many unique features (Nixon, 1983; Voss and Voss, 1983) that allow relatively low metabolic rates regardless of habitat depth. Foremost among these is the presence of a coelom, which provides neutral buoyancy (Denton and Gilpin-Brown, 1973; Clarke *et al.*, 1979) and may be contracted to create a flow of water over the gills. The mantle musculature is rarely used and then only for escape responses (Clarke, 1962). All cranchiids are largely transparent (Clarke, 1962; Seapy and Young, 1986), which decreases the selection associated with higher predation risks in higher levels of ambient light (McFall-Ngai, 1990). When disturbed, *Cranchia scabra* is also capable of filling its mantle cavity with seawater, which effectively doubles its volume (shipboard observations). It apparently shares this ability with at least one other cranchiid (Nixon, 1983). This sort of defense mechanism may reduce the need for lengthy escape swimming, and further emphasizes the trend among cranchiids to reduce metabolic costs. The limited data on metabolic rate and vertical distribution suggest that metabolism may be independent of habitat depth within this family (Fig. 3). Inclusion of the cranchiids does not significantly alter the slope or elevation of the regression in Figure 1.

Buoyancy

Many midwater cephalopods possess some means of achieving neutral buoyancy (Denton and Gilpin-Brown,

1973; Clarke, 1988; Clarke *et al.*, 1979; Voight *et al.*, 1994), whereas most epipelagic squids are negatively buoyant and rely on constant swimming for lift. It is conceivable that the metabolic rates of midwater cephalopods might be reduced simply by achieving neutral buoyancy, and that the higher metabolic rates of epipelagic cephalopods result from the added cost of support in the water column. Childress and Nygaard (1974) found, however, that neutral buoyancy in crustaceans does not appear to be a means of conserving energy *per se*. Metabolic rates were not correlated with density at a given depth. In epipelagic waters, locomotion is apparently a greater priority and dictates a high content of protein. Protein, associated with locomotory muscles, provides the density responsible for the negative buoyancy in such epipelagic squids as *Loligo* sp. and *Ommastrephes* sp. (Denton and Gilpin-Brown, 1973). Buoyancy can actually have a detrimental effect on locomotory abilities. Buoyancy organs make animals bulkier, which increases the energy needed for swimming at a given speed (Alexander, 1990; O'Dor and Webber, 1991). Although metabolism and buoyancy are certainly confounding factors, evidence suggests that the need for strong swimming determines the practicality of buoyancy. The energy required for support in the water column may be insignificant compared to an animal's overall activity level (Childress and Nygaard, 1974). However, when locomotion is not a high priority and activity levels are relatively low, the cost of support in the water column may be large relative to that of overall activity. In such situations, neutral buoyancy may be a cost-effective option. Among neutrally buoyant cephalopods there is still a decline in metabolic rates with increasing habitat depth.

Vertical migration

Many organisms undergo daily vertical migrations, spending the daylight hours at greater depths. Because vertical migrators are never exposed to surface daylight conditions, one might expect that light limitation on predator/prey interactions would result in metabolic rates more similar to those of deeper-living non-migrators than of epipelagic non-migrators. In previous studies (Childress and Nygaard, 1974), vertical migrators were considered at their shallowest depth (MDO) because it was the location of their primary food source. Evidence suggests that vertically migrating fishes and crustaceans are more similar in composition to shallow-living than to deep-living non-migrators (Childress and Nygaard, 1974). It was suggested that vertical migrators are essentially epipelagic animals that take refuge during the day at depth. However, *Gonatus* sp. and *Histioteuthis* sp., both vertically migrating cephalopods, have energy contents lower than those of epipelagic squids (Clarke *et al.*, 1985). The lower wet-weight-specific energy contents in some species are believed to be a result of increased water content, suggesting decreased locomotory abilities in those species. As discussed previously, Voss (1967) characterized organisms from various depths on the basis of morphological features such as body musculature, size and shape of fins and mantle, eye size, and skin color. He considered *Histioteuthis* to be a resident of the bathypelagic zone (700–2000 m) along with *Bathyteuthis*. By his criteria, *Gonatus* would have been placed in the mesopelagic zone (200–700 m), at a depth consistent with its deeper daytime habitat. The vast majority of epipelagic cephalopods exhibit some diel movements. Loliginids and ommastrephids (among others) migrate away from the surface during the day. A full moon, the equivalent of daylight at 300 m depth, has been shown to keep some ommastrephids away from the surface at night (Wormuth, 1976). This suggests that vertically migrating cephalopods may be following an isolume to which their metabolic rate may be adapted. The day and night habitats of vertical migrators are distinctly different, and both presumably have strong effects on the physiology of vertically migrating organisms. Both MDO and MDdO reveal a strong decline in cephalopod metabolism with increasing habitat depth (Fig. 1).

Horizontal migration

In addition to migrating vertically, many epipelagic squids migrate long distances horizontally. O'Dor (1992) has suggested that powerful squids have evolved to take advantage of current systems, and that this requires strong swimming and perhaps high metabolic rates as well. The deep sea has relatively weak currents, which may relieve animals from the selective pressures associated with current systems. However, this hypothesis probably applies only to truly large and active predators, all of which are capable of avoiding midwater trawls. Although nothing is known of the horizontal migration patterns of midwater cephalopods, none of the species studied here appear to be powerful swimmers of the caliber discussed by O'Dor (1992). Selection due to strong currents also cannot explain the lack of a decline in metabolism with depth in some phyla (cnidarians and chaetognaths; Thuesen and Childress, 1993a; 1994); patterns of vertical migration through varying current strengths; or differences in metabolic rates observed between Hawaii and California for shallow-water crustaceans (Cowles et al., 1991).

Oxygen minimum layer

Another factor possibly selecting for lower metabolic rates at depth is oxygen concentration. Layers of low oxygen are found throughout the worlds' oceans at depths

between 200 and 1000 m. The oxygen minimum layer off California is particularly well developed. Partial pressures of oxygen reach a minimum of about 6 mm Hg between 600 and 800 m. Fischer and Bottjer (1995) suggest that the oxygen minimum layer provides refuge from large predators and that low oxygen has enforced passivity in animals that live within it. Certainly some larger predators are excluded from hypoxic waters (Carey and Robison, 1980). Reduced predation pressure may allow passive lifestyles. *Vampyroteuthis infernalis* is "oligoaerobic"—found only in low oxygen, with a peak concentration in the oxygen minimum layer (Pickford, 1946, 1952)—and had a metabolic rate of 0.09 μmol O_2 g^{-1} h^{-1}. Species of the genus *Japetella* also live within the oxygen minimum layer off both California and Hawaii and are relatively inactive metabolically. However, the mean metabolic rate of *J. diaphana* off Hawaii, where the oxygen seldom drops below 20 mm Hg, is not significantly higher than that of *J. heathi* off California. Fishes and crustaceans living below the oxygen minimum layer have been shown to have lower metabolic rates than others living directly within (Childress, 1995). This suggests that the low metabolic rates are not a specific adaptation to low oxygen and that passive lifestyles are selected for at great depths regardless of oxygen content.

Some animals possess specific adaptations to the oxygen minimum layer. *Gnathophausia ingens*, a deep-living mysid, has been shown to live aerobically within the minimum layer by being especially effective at extracting oxygen from the water. Its ability to regulate oxygen consumption to P_{O_2} values as low as 3 mm Hg is due in part to its ability to maintain a high ventilatory flow and to remove up to 50%–80% of the oxygen from the inhaled water (Childress, 1968, 1971a; Belman and Childress, 1976). The latter ability appears to stem from a hemocyanin with an unusually high affinity for oxygen and cooperativity of oxygen binding (Sanders and Childress, 1990). Regulation of oxygen consumption was measured in *Japetella diaphana*, *J. heathi*, *Histioteuthis heteropsis*, and *Vampyroteuthis infernalis*. Like *G. ingens*, both *J. heathi* and *V. infernalis* off California can regulate oxygen consumption to at least 6 mm Hg, allowing aerobic living even at the lowest environmental oxygen levels found there. Two individuals of *V. infernalis* regulated successfully below 4 mm Hg. *J. diaphana*, however, regulated oxygen consumption to a mean of 21.8 mm Hg, which corresponds to the minimum environmental P_{O_2} of 20 mm Hg off Hawaii. *Histioteuthis heteropsis*, which migrates into the oxygen minimum layer during the day as previously reported by Belman (1978) to be incapable of regulating to oxygen concentrations required for aerobic living within the minimum layer (P_c = 20.0 mm Hg). In contrast to those earlier studies, in our studies *H. heteropsis* was able to regulate its oxygen consumption to at least 7 mm Hg. The mean critical partial pressure for this species was 11.99 ± 2.28 mm Hg. The lowered metabolism at low temperatures may allow aerobic living for some animals, such as *H. heteropsis*, migrating into the cooler waters of the oxygen minimum layer during the day. Cowles *et al.* (1991) found a strong effect of temperature on the critical oxygen partial pressures of vertically migrating crustaceans. This is consistent with findings by Sanders and Childress (1990) that the oxygen affinity of hemocyanin from several of these species is temperature-dependent and increases greatly at low temperatures.

Oxygen extraction and jet propulsion are incompatible functions in cephalopods (Wells, 1988). To maximize oxygen extraction, water must be passed relatively slowly over the gills and out the jet. Maximization of propulsion requires the ejection of water at a velocity sufficient to generate the required thrust. *Nautilus pompilius*, for example, can extract 20% of the available oxygen from the ventilatory stream at rest, but only 5% or less during active propulsion (Wells and O'Dor, 1991). Epipelagic squids have maximized locomotion and are able to extract oxygen at levels necessary to fuel high speeds only because water flow over the gills increases as swimming speed increases. Circulatory adaptations, including enhanced unloading of oxygen at the tissues and a large positive Bohr shift, allow efficient use of nearly all of the oxygen taken up by the blood (Zammit, 1978). Benthic octopods, on the other hand, have optimized oxygen extraction. The respiratory pigments of octopods have a greater affinity for oxygen than do pigments in the faster squid and sepioid species (Brix *et al.*, 1989). In addition, their slow benthic lifestyle allows a reduction in mantle contractions and a slow flow of water over the gills. The decreased reliance of deep-living cephalopods on locomotory abilities, implied by the decline in metabolism with depth, would, as in benthic octopods, allow a slowing of the ventilatory stream and more efficient extraction of oxygen—adaptations compatible with life in a reduced oxygen environment.

Buffering capacity

Reduced buffering capacities in mantle muscle at depth are further evidence that locomotory abilities are not strongly selected for in the deep sea. A high buffering capacity allows prolonged glycolytic work such as that required for extended burst escape responses. The sit-and-wait predation strategies prevalent through much of the deep sea do not require a high capacity for anaerobic work. Differences in oxygen levels between California and Hawaii might be expected to yield higher short-term anaerobic capacities in animals that live in the lower ox-

ygen habitat. A lesser oxygen supply would more quickly lead to functional anoxia (tissue energy demand outstrips aerobic capacity). However, no difference in β was seen between *Japetella diaphana* and *J. heathi*. Both species, like *Gnathophausia ingens*, appear to have very limited anaerobic abilities. Buffering capacity is believed to be an adaptable parameter that can be altered to match metabolic function (Castellini and Somero, 1981) and has been correlated with tissue capacity for glycolytic energy production in response to functional anoxia (Eberlee and Storey, 1984). The fact that no difference was seen between similar animals in different oxygen environments is evidence that the reduced locomotory abilities are not a response to ambient oxygen levels.

Metabolic scaling

The body size of the pelagic cephalopods measured in this study increased with increasing MDO (largely because the large epipelagic species were not sampled). Because mass-specific metabolism has, with notable exceptions (DeMont and O'Dor, 1984; Thuesen and Childress, 1994), been repeatedly shown to decrease with increasing body mass (Schmidt-Nielsen, 1983), body size could have significant effects on metabolic estimates based on depth of occurrence. Scaling coefficients could be derived for only three species: *Vampyroteuthis infernalis, Japetella diaphana,* and *Histioteuthis heteropsis*. Scaling coefficients for all three ($b = -0.30$, -0.27, and -0.20 respectively) fall within the range of most animals (Schmidt-Nielsen, 1983). Sufficient range in size and numbers failed to yield a significant scaling relationship for *Chiroteuthis calyx*. This is perhaps due to the drastic change in body proportion from the "doratopsis" paralarval stage, a characteristic of this genus, to adulthood (Vecchione *et al.*, 1992). Significant scaling relationships could not be derived for the remaining species, owing either to lack of sufficient numbers of specimens or to insufficient size ranges. Normalizing metabolic rates to 10 g, either by assuming a scaling coefficient of -0.20 (Schmidt-Nielsen, 1983) or by using measured coefficients where possible, did not have a significant effect on the slopes of the regressions with depth. A scaling coefficient of approximately -1.8, based on the increase in body size with depth observed in this study, would be required in order for size to account for the observed variation with depth. A significant increase in body size with depth was observed among the animals for which β was assayed as well. However, no significant size-scaling was observed for buffering capacity.

Locomotory efficiency

Packard (1972) compared fish and cephalopod "modes of life" and distinguished these organisms from crustaceans and other molluscs in terms of their "great ability to travel." He observed that functionally, squid are fish. But many deep-living cephalopods actually have much lower metabolic rates than do fishes or crustaceans living at similar depths. The slope of the regression of 10-g-corrected oxygen consumption with MDO is steeper for cephalopods than for both fishes and crustaceans (Fig. 2). The metabolic rates of *Vampyroteuthis infernalis* and the deep-living pelagic octopods are more comparable to those of similar-sized scyphomedusae (Thuesen and Childress, 1994) than to those of fishes or crustaceans. Although the rates of deep-living squids are similar to those of fish with sit-and-wait predation strategies (Cowles and Childress, 1996), shallow squids have higher rates than do fish or crustaceans at similar depths. The slope of the regression of metabolism with depth is steeper for teuthoids and octopods, considered separately, than for fishes and crustaceans. More efficient locomotion among deeper-living cephalopods may be responsible for this difference. Shallow-living cephalopods rely extensively on jet propulsion to gain high speeds. Because the energy required for thrust increases with the velocity squared, high-speed jet propulsion is inherently inefficient (Vogel, 1994). Yet most shallow-living squids retain jet propulsion as the primary means of locomotion (Baldwin, 1982; Hoar *et al.*, 1994). Hoar *et al.* (1994) did note, though, that the slower coastal species such as the loliginids use their fins, which are large, more actively than do the oceanic ommastrephids, which use their smaller fins as rudders during extremely high-speed swimming.

Deep-living cirrate octopods have been observed using the arms and web to swim in a manner similar to the "bell-swimming" of medusae (Vecchione and Roper, 1991). *Cirrothauma murrayi* relies very heavily on fins for locomotion (Aldred *et al.*, 1983). It has also been seen using the arms and web as a "balloon" for defense, eliminating costly escape swimming (Boletzky *et al.*, 1992). *Vampyroteuthis infernalis, Chiroteuthis calyx,* and *Histioteuthis heteropsis,* among others, have been observed swimming primarily with fins (James Hunt, pers. comm.). Fin- and bell-swimming are cost efficient compared to jet propulsion by means of mantle contractions, due to reduced speeds (reduced drag) and to the large water masses (relative to body mass) being processed (Vogel, 1994). Although their morphology suggests that *Octopoteuthis* spp. (MDO = 100 m) rely heavily on fins for swimming, limited video footage shows *O. deletron* swimming with slow contractions of the mantle while holding the large fins curved over the body so that water passes beneath them (James Hunt, pers. comm.). The metabolic rates of *O. deletron* and of *O. nielseni* are low compared to those of other squids at similar depths. Perhaps the curious fin posture provides static lift that re-

duces the metabolic costs associated with support in the water column. This species also attains considerable size, which would deter predation (Roper *et al.*, 1984). Again, among the cranchiids, where transparency has alleviated much of the need for high-speed swimming, mantle contractions are rarely used for locomotion (Clarke, 1962).

Morphology and limited shipboard observations indicate that some deep-living cephalopods do utilize jet propulsion as a primary means of locomotion. At extremely low speeds, jet propulsion may not be so costly, which might explain the existence of slow jetters such as jellyfish and salps (Vogel, 1994). It might also explain the extremely low metabolic rates of deep-living pelagic octopods. These organisms process large amounts of water through a relatively large funnel opening, resulting in efficient, low-speed swimming. It is also possible that they utilize the arms and web for bell-swimming, much as the cirrate octopods do. There is tremendous diversity in the swimming behaviors of pelagic cephalopods but, perhaps because high speeds are not a priority in the deep sea, a more efficient means of locomotion is desirable.

Despite differences in their locomotory efficiencies, buoyancy mechanisms, and structural compositions, fishes, crustaceans, and cephalopods show similar metabolic trends with depth; these trends probably reflect the presence of highly evolved eyes in these groups. The results presented here emphasize the importance of differential selection for locomotory abilities with habitat depth in determining the metabolic rates of organisms. Available evidence implicates vision as a selective factor strongly affecting the evolution of locomotory abilities. Although one may intuitively suspect food availability or low oxygen, the declines in both oxygen consumption rates and pH buffering capacity of locomotory muscles with depth in pelagic cephalopods point to a different conclusion. These factors support the hypothesis that the extent to which visual predator/prey interactions occur is largely responsible for the decline in metabolic rates of visually orienting, midwater organisms with increasing minimum depth of occurrence. Although cephalopods have often been compared with fishes in discussions of ecology and locomotion, we conclude that pelagic cephalopods living in the deep sea might be more appropriately compared with medusae in these contexts.

Acknowledgments

We thank F.G. Hochberg and A.L. Alldredge for constructive comments on the manuscript. We are grateful to captains, crews, and scientists aboard the research vessels *New Horizon* and *Point Sur* for their assistance at sea. Thank R.E. Young and J. Hunt for informative discussions concerning midwater cephalopods, and C. Braby, M. Kelly, T. vanMeeuen, J. Freytag, and B. Rabkin for their assistance at sea, in the laboratory, or both. Research was supported by NSF grants OCE-9415543 and OCE-9115551 to J.J. Childress.

Literature Cited

Aldred, R. G., M. Nixon, and J. Z. Young. 1983. *Cirrothauma murrayi* Chun, a finned octopod. *Philos. Trans. R. Soc. Lond. B* **301:** 1–54.

Alexander, R. M. 1990. Size, speed and buoyancy adaptations in aquatic animals. *Am. Zool.* **30:** 189–196.

Baldwin, J. 1982. Correlations between enzyme profiles in cephalopod muscle and swimming behavior. *Pac. Sci.* **36:** 349–356.

Belman, B. 1978. Respiration and the effects of pressure on the mesopelagic vertically migrating squid *Histioteuthis heteropsis*. *Limnol. Oceanogr.* **23:** 735–739.

Belman, B. W., and J. J. Childress. 1976. Circulatory adaptations to the oxygen minimum layer in the bathypelagic mysid *Gnathophausia ingens*. *Biol. Bull.* **150:** 15–37.

Boletzky, S. V., M. Rio, and M. Roux. 1992. Octopod 'ballooning' response. *Nature* **356:** 199.

Boucher-Rodoni, R., and K. Mangold. 1989. Respiration and nitrogen excretion by the squid *Loligo forbesi*. *Mar. Biol.* **103:** 333–338.

Boutilier, R. G., T. G. West, G. H. Pogson, K. A. Mesa, J. Wells, and M. J. Wells. 1996. *Nautilus* and the art of metabolic maintenance. *Nature* **382:** 534–536.

Brix, O., A. Bardgard, A. Cau, A. Colosimo, S. G. Condo, and B. Giardina. 1989. Oxygen-binding properties of cephalopod blood with special reference to environmental temperatures and ecological distribution. *J. Exp. Zool.* **252:** 34–42.

Carey, F. G., and B. H. Robison. 1980. Daily patterns in the activities of swordfish, *Xiphias gladius*, observed by acoustic telemetry. *Fish. Bull.* **79:** 277–292.

Castellini, M. A., and G. N. Somero. 1981. Buffering capacity of vertebrate muscle: correlations with potentials for anaerobic function. *J. Comp. Physiol.* **143:** 191–198.

Childress, J. J. 1968. Oxygen minimum layer: vertical distribution and respiration of the mysid *Gnathophausia ingens*. *Science* **160:** 1242–1243.

Childress, J. J. 1971a. Respiratory adaptations to the oxygen minimum layer in the bathypelagic mysid *Gnathophausia ingens*. *Biol. Bull.* **141:** 109–121.

Childress, J. J. 1971b. Respiratory rate and depth of occurrence of midwater animals. *Limnol. Oceanogr.* **16:** 104–106.

Childress, J. J. 1975. The respiratory rates of midwater crustaceans as a function of depth occurrence and relation to the oxygen minimum layer off Southern California. *Comp. Biochem. Physiol.* **50A:** 787–799.

Childress, J. J. 1995. Are there physiological and biochemical adaptations of metabolism in deep-sea animals? *Trends Ecol. Evol.* **10:** 30–36.

Childress, J. J., and T. J. Mickel. 1980. A motion compensated shipboard precision balance system. *Deep-Sea Res.* **27A:** 965–970.

Childress, J. J., and T. J. Mickel. 1985. Metabolic rates of animals from the hydrothermal vents and other deep-sea habitats. *Biol. Soc. Wash. Bull.* **6:** 249–260.

Childress, J. J., and M. H. Nygaard. 1974. The chemical composition and relative buoyancy of midwater crustaceans as a function of depth off Southern California. *Mar. Biol.* **27:** 225–238.

Childress, J. J., and G. N. Somero. 1979. Depth related enzymic activities in muscle, brain and heart of deep-living pelagic marine teleosts. *Mar. Biol.* **52:** 273–283.

Childress, J. J., and E. V. Thuesen. 1993. The effect of hydrostatic

pressure on the metabolic rates of six species of gelatinous zooplankton. *Limnol. Oceanogr.* **38:** 665–670.

Childress, J. J., A. T. Barnes, L. B. Quetin, and B. H. Robison. 1978. Thermally protecting cod ends for recovery of living deep-sea animals. *Deep-Sea Res.* **25:** 419–422.

Childress, J. J., D. L. Cowles, J. A. Favuzzi, and T. J. Mickel. 1990. Metabolic rates of benthic deep-sea decapod crustaceans decline with increasing depth primarily due to the decline in temperature. *Deep-Sea Res.* **37:** 929–949.

Clarke, A., M. R. Clarke, L. J. Holmes, and T. D. Waters. 1985. Calorific values and elemental analysis of eleven species of oceanic squids (Mollusca: Cephalopoda). *J. Mar. Biol. Assoc. U.K.* **65:** 983–986.

Clarke, M. R. 1962. Respiratory and swimming movements in the cephalopod *Cranchia scabra*. *Nature* **196:** 351–352.

Clarke, M. R. 1988. Evolution of buoyancy and locomotion in recent cephalopods. *Mollusca* **12:** 203–213.

Clarke, M. R., E. J. Denton, and J. B. Gilpin-Brown. 1979. On the use of ammonium for buoyancy in squids. *J. Mar. Biol. Assoc. U.K.* **59:** 259–276.

Cole, S. K., and D. L. Gilbert. 1970. Jet propulsion of squid. *Biol. Bull.* **138:** 245–246.

Cowles, D. L., and J. J. Childress. 1988. Swimming speed and oxygen consumption in the bathypelagic mysid *Gnathophausia ingens*. *Biol. Bull.* **175:** 111–121.

Cowles, D. L., and J. J. Childress. 1996. Aerobic metabolism of the anglerfish *Melanocetus johnsoni*, a deep-pelagic marine sit-and-wait predator. *Deep-Sea Res.* **42:** 1631–1638.

Cowles, D. C., J. J. Childress, and M. E. Wells. 1991. Metabolic rates of midwater crustaceans as a function of depth of occurrence off the Hawaiian Islands: food availability as a selective factor? *Mar. Biol.* **110:** 75–83.

DeMont, M. E., and R. K. O'Dor. 1984. The effects of activity, temperature and mass on the respiratory metabolism of the squid, *Illex illecebrosus*. *J. Mar. Biol. Assoc. U.K.* **64:** 535–543.

Denton, E. J., and J. B. Gilpin-Brown. 1973. Floatation mechanisms in modern and fossil cephalopods. *Adv. Mar. Biol.* **11:** 197–268.

Donnelly, J., and J. J. Torres. 1988. Oxygen consumption of midwater fishes and crustaceans from the eastern Gulf of Mexico. *Mar. Biol.* **97:** 483–494.

Eberlee, J. C., and K. B. Storey. 1984. Buffering capacities of the tissues of marine molluscs. *Physiol. Zool.* **57:** 567–572.

Finke, E., H. O. Portner, P. G. Lee, and D. M. Webber. 1996. Squid (*Lolliguncula brevis*) life in shallow waters: oxygen limitation of metabolism and swimming performance. *J. Exp. Biol.* **199:** 911–921.

Fischer, A. G., and D. J. Bottjer. 1995. Oxygen-depleted waters: a lost biotope and its role in ammonite and bivalve evolution. *N. Jb. Geol. Palaont. Abh.* **195:** 133–146.

Fleisher, K. J., and J. F. Case. 1995. Cephalopod predation facilitated by dinoflagellate luminescence. *Biol. Bull.* **189:** 263–271.

Grieshaber, M., and G. Gäde. 1976. The biological role of octopine in the squid, *Loligo vulgaris* (Lamarck). *J. Comp. Physiol.* **108:** 225–232.

Harvey, P. H., and M. D. Pagel. 1991. *The Comparative Method in Evolutionary Biology*. Oxford University Press, New York. 239 pp.

Herring, P. J., P. N. Dilly, and C. Cope. 1994. The bioluminescent organs of the deep-sea cephalopod *Vampyroteuthis infernalis* (Cephalopoda: Vampyromorpha). *J. Zool. Lond.* **223:** 45–55.

Hoar, J. A., E. Sim, D. M. Webber, and R. K. O'Dor. 1994. The role of fins in the competition between squid and fish. Pp. 27–43 in *Mechanics and Physiology of Animal Swimming*. L. Maddock, Q. Bone, and J. M. V. Rayner, eds. Cambridge University Press, New York.

Ikeda, T. 1988. Metabolism and chemical composition of crustaceans from the Antarctic mesopelagic zone. *Deep-Sea Res.* **35:** 1991–2002.

Kerfoot, W. B. 1970. Bioenergetics of vertical migration. *Am. Nat.* **104:** 529–546.

Lu, C. C., and C. F. E. Roper. 1979. Cephalopods from deepwater dumpsite 106 (western Atlantic): vertical distribution and seasonal abundance. *Smithson. Contrib. Zool.* **288:** 1–36.

Madan, J. J., and M. J. Wells. 1996. Why squid breathe easy. *Nature* **380:** 590.

Marshall, N. B. 1979. *Developments in Deep-Sea Biology*. Blandford Press, Poole, England. 566 pp.

McFall-Ngai, M. J. 1990. Crypsis in the pelagic environment. *Am. Zool.* **30:** 175–178.

Mickel, T. J., L. B. Quetin, and J. J. Childress. 1983. Construction of a polarographic oxygen sensor in the laboratory. Pp. 81–89 in *Polarographic Oxygen Sensors*. E. Gnaiger and H. Forstner, eds. Springer-Verlag, Berlin.

Nixon, M. 1983. *Teuthowenia megalops*. Pp. 233–247 in *Cephalopod Life Cycles*. P. R. Boyle, ed. Academic Press, London.

O'Dor, R. K. 1982. The respiratory metabolism and swimming performance of the squid, *Loligo opalescens*. *Can. J. Aquat. Sci.* **39:** 580–587.

O'Dor, R. K. 1992. Big squid in big currents. *S. Afr. J. Mar. Sci.* **12:** 225–235.

O'Dor, R. K., and R. E. Shadwick. 1989. Squid, the olympic cephalopods. *J. Ceph. Biol.* **1:** 33–54.

O'Dor, R. K., and D. M. Webber. 1986. The constraints on cephalopods: why squid aren't fish. *Can. J. Zool.* **64:** 1591–1605.

O'Dor, R. K., and D. M. Webber. 1991. Invertebrate athletes: tradeoffs between transport efficiency and power density in cephalopod evolution. *J. Exp. Biol.* **160:** 93–112.

O'Dor, R. K., J. Wells, and M. J. Wells. 1990. Speed, jet pressure, and oxygen consumption relationships in free-swimming *Nautilus*. *J. Exp. Biol.* **154:** 383–396.

Packard, A. 1972. Cephalopods and fish: the limits of convergence. *Biol. Rev.* **47:** 241–307.

Pickford, G. E. 1946. *Vampyroteuthis infernalis* Chun, an archaic dibranchiate cephalopod. I: Natural history and distribution. *Dana-Rep.* **29:** 1–40.

Pickford, G. E. 1952. The Vampyromorpha of the Discovery expeditions. *Discovery Rep.* **26:** 197–210.

Portner, H. O., D. M. Webber, R. K. O'Dor, and R. G. Boutilier. 1993. Metabolism and energetics in squid (*Illex illecebrosus*, *Loligo pealei*) during muscular fatigue and recovery. *Am. J. Physiol.* **265:** R157–R165.

Roper, C. F. E. 1969. Systematics and zoogeography of the worldwide bathypelagic squid *Bathyteuthis* (Cephalopoda: Oegopsida). *U.S. Nat. Mus. Bull.* Washington D.C. **291.**

Roper, C. F. E., and R. E. Young. 1975. Vertical distribution of pelagic cephalopods. *Smithson. Contrib. Zool.* **209:** 1–51.

Roper, C. F. E., M. J. Sweeney, and C. E. Nauen. 1984. *FAO Species Catalogue. Vol. 3. Cephalopods of the World. An Annotated and Illustrated Catalogue of Species of Interest to Fisheries*. 277 pp.

Sanders, N. K., and J. J. Childress. 1990. Adaptations to the deep-sea oxygen minimum layer: oxygen binding by the hemocyanin of the bathypelagic mysid, *Gnathophausia ingens* Dohrn. *Biol. Bull.* **178:** 286–294.

Schmidt-Nielsen, K. 1983. *Animal Physiology: Adaptation and Environment*. Cambridge University Press, Cambridge. 619 pp.

Seapy, R. R., and R. E. Young. 1986. Concealment in pipelagic pterotracheid heteropods (Gastropoda) and cranchiid squids (Cephalopoda). *J. Zool.* **210:** 137–147.

Seibel, B. A., and J. J. Childress. 1996. Deep-breathing cephalopods? *Nature* **384:** 421.

Smith, K. L., and R. R. Hessler. 1974. Respiration of benthopelagic fishes: *in situ* measurements at 1230 m. *Science* **184:** 72–73.

Sullivan, K. M., and G. N. Somero. 1980. Enzyme activities of fish skeletal muscle and brain as influenced by depth of occurrence and habits of feeding and locomotion. *Mar. Biol.* **60:** 91–99.

Sweeney, M. J., C. F. E. Roper, K. M. Mangold, M. R. Clarke, and S. V. Boletzky. 1992. "Larval" and juvenile cephalopods: a manual for their identification. *Smithson. Contrib. Zool.* **513:** 282.

Thuesen, E. V., and J. J. Childress. 1993a. Enzymatic activities and metabolic rates of pelagic chaetognaths: lack of depth-related declines. *Limnol. Oceanogr.* **38:** 935–948.

Thuesen, E. V., and J. J. Childress. 1993b. Metabolic rates, enzyme activities, and chemical compositions of some deep-sea pelagic worms, particularly *Nectonemertes mirabilis* (Nemertea; Hoplonemertinea) and *Poeobius meseres* (Annelida; Polychaeta). *Deep-Sea Res.* **140:** 937–951.

Thuesen, E. V., and J. J. Childress. 1994. Respiratory rates and metabolic enzyme activities of oceanic California medusae in relation to body size and habitat depth. *Biol. Bull.* **187:** 84–98.

Torres, J. J., and G. N. Somero. 1988. Vertical distribution and metabolism in antarctic mesopelagic fishes. *Comp. Biochem. Physiol.* **90B:** 521–528.

Torres, J. J., B. W. Belman, and J. J. Childress. 1979. Oxygen consumption rates of midwater fishes as a function of depth of occurrence. *Deep-Sea Res.* **26A:** 185–197.

Vecchione, M., and C. F. E. Roper. 1991. Cephalopods observed from submersibles in the Western North Atlantic. *Bull. Mar. Sci.* **49:** 433–445.

Vecchione, M., B. H. Robison, and C. F. E. Roper. 1992. A tale of two species: tail morphology in paralarval *Chiroteuthis* (Cephalopoda: Chiroteuthidae). *Proc. Biol. Soc. Wash.* **105(4):** 683–692.

Voight, J. R., H. O. Portner, and R. K. O'Dor. 1994. A review of ammonia-mediated buoyancy in squids (Cephalopoda: Teuthoidea). *Mar. Fresh. Behav. Physiol.* **25:** 193–203.

Vogel, S. 1994. *Life in Moving Fluids.* Second Edition. Princeton University Press, Princeton. 467 pp.

Voss, G. L. 1967. The biology and bathymetric distribution of deep-sea cephalopods. *Stud. Trop. Oceanogr.* **5:** 511–535.

Voss, N. A., and R. S. Voss. 1983. Phylogenetic relationships in the cephalopod family Cranchiidae (Oegopsida). *Malacologia* **23(2):** 397–426.

Wells, M. J. 1988. Oxygen extraction and jet propulsion in cephalopods. *Can. J. Zool.* **68:** 815–824.

Wells, M. J., and R. K. O'Dor. 1991. Jet propulsion and the evolution of the cephalopods. *Bull. Mar. Sci.* **49:** 419–432.

Wells, M. J., J. Wells, and R. K. O'Dor. 1992. Life at low oxygen tensions: the behaviour and physiology of *Nautilus pompilius* and the biology of extinct forms. *J. Mar. Biol. Assoc. U.K.* **72:** 313–328.

Wormuth, J. H. 1976. The biogeography and numerical taxonomy of the oegopsid squid family Ommastrephidae in the Pacific Ocean. *Bull. Scripps Inst. Oceanogr. Univ. Calif.* **23.**

Young, R. E. 1972. The systematics and areal distribution of pelagic cephalopods from the seas off southern California. *Smithson. Contrib. Zool.* **97:** 1–159.

Young, R. E. 1975a. *Leachia pacifica* (Cephalopoda, Teuthoidea): spawning habitat and function of the brachial photophores. *Pac. Sci.* **29:** 19–25.

Young, R. E. 1975b. Transitory eye shapes and the vertical distribution of two midwater squids. *Pac. Sci.* **29:** 243–255.

Young, R. E. 1978. Vertical distribution and photosensitive vesicles of pelagic cephalopods from Hawaiian waters. *Fish. Bull.* **76:** 583–615.

Young, R. E., E. M. Kampa, S. D. Maynard, F. M. Mencher, and C. F. E. Roper. 1980. Counterillumination and the upper depth limits of midwater animals. *Deep-Sea Res.* **27A:** 671–691.

Zammit, V. A. 1978. Possible relationship between energy metabolism of muscle and oxygen binding characteristics of haemocyanin of cephalopods. *J. Mar. Biol. Assoc. U.K.* **58:** 421–424.

Reference: *Biol. Bull.* **192:** 279–289. (April, 1997)

Plasticity in the Sclerites of a Gorgonian Coral: Tests of Water Motion, Light Level, and Damage Cues

JORDAN M. WEST

Section of Ecology and Systematics, Corson Hall, Cornell University, Ithaca, New York 14853-2701

Abstract. The gorgonian coral *Briareum asbestinum* contains skeletal elements (sclerites) that vary in length and density within and among local populations. Data from previous work suggested that the sclerite compositions of colonies may be altered in response to environmental cues such as predator damage, water motion, and light level. To test these hypotheses, colonies from shallow reefs were transplanted to racks at a single location where the three environmental factors of interest were artificially manipulated. After 9–14 weeks of growth, sclerite morphologies and densities had not changed in response to shading or to water-motion reductions that mimicked deep-water conditions. However, colonies did respond significantly to two types of simulated predator damage. Following tip amputation, sclerites in the regenerated tips of damaged colonies were shorter and more dense than in the controls. In contrast, mid-branch scarring caused colonies to produce longer sclerites at lower densities. Since long sclerites deter feeding by predatory snails, the increase in sclerite length in response to scarring of mid-branch regions may function as an inducible defense.

Introduction

Phenotypic plasticity—or differential phenotypic expression of a genotype under varying environmental conditions—has been a subject of increasing interest to evolutionary ecologists since Bradshaw's (1965) extensive review (*e.g.*, Bradshaw, 1974; Via and Lande, 1985; Schlichting, 1986; Stearns, 1989; Scheiner, 1993). Although plasticity can be nonadaptive or maladaptive, researchers have been primarily interested in adaptive plasticity as a mechanism by which organisms cope with changing environments. Adaptive plasticity is especially well documented in plants, for which the literature contains numerous examples of induced responses to physical factors such as shade (Turesson, 1920), desiccation (Harlan, 1945), soil fertility (Sorensen, 1954), temperature (Mooney and West, 1964), and water stress (Roy and Mooney, 1982). Bradshaw (1965) reasoned that plasticity should often be favored in plants because they are sessile organisms whose autotrophic lifestyle requires that they inhabit relatively open spaces where they may be exposed to environmental extremes. When the scale of temporal variability is shorter than the lifespan of the organism, or where spatial variability is at a scale smaller than the dispersal range of the organism, adaptive plasticity is a viable strategy.

In marine habitats, sessile colonial invertebrates, such as scleractinian and gorgonian corals, share many characteristics with plants. Colonies are permanently sessile, often with upright branched growth forms (Barnes, 1987); and many corals depend on symbiotic algae (zooxanthellae) for a large proportion of their energy (Muscatine, 1974; Muscatine *et al.*, 1975; Svoboda, 1978; Sebens, 1987) and are thus largely autotrophic. In addition, populations with wide distributions are routinely exposed to variation in abiotic factors such as light level (McCloskey and Muscatine, 1984; Miles, 1991), wave exposure (de Weerdt, 1981; Sebens, 1984), and sedimentation rate (Foster, 1979). Indeed, variation in colony morphology or physiology in response to temperature, depth, or water movement has been documented in sponges (Bavestrello *et al.*, 1993), scleractinian corals (Wijsman-Best, 1974; Foster, 1979; Lesser *et al.*, 1994), and gorgonian corals (Grigg, 1972; West *et al.*, 1993).

In both plants and corals, inducible defenses represent a special category of adaptive plasticity that involves biotic rather than abiotic cues. Defined as environmentally triggered phenotypic responses that defend against spe-

Received 18 September 1996; accepted 6 February 1997.

Present address: University of Washington, Friday Harbor Laboratories, 620 University Road, Friday Harbor, Washington 98250.

cific biotic selective agents (Adler and Harvell, 1990), inducible defenses have emerged as prominent phenomena only in the past 20 years. A variety of plant responses to real or simulated herbivore damage include increased morphological defenses such as spines or resistant growth forms (Young, 1987; Lewis *et al.*, 1987) and production of physicochemical deterrents such as polyphenolic compounds, alkaloids, or silica (McNaughton and Tarrants, 1985; Schultz, 1988; Van Alstyne, 1988; Baldwin and Ohnmeiss, 1993). Among colonial invertebrates, various species respond to the presence of competitors by producing agonistic weaponry such as digestive filaments, stolons, or sweeper tentacles (Ivker, 1972; Francis, 1973; Lang, 1973; Wellington, 1980; Sebens and Miles, 1988; Harvell and Padilla, 1990; Miles, 1991). However, although predator-induced defenses, such as spines and helmets, have been documented in various clonal freshwater invertebrates (*e.g.*, Gilbert and Stemberger, 1984; Havel, 1986), examples of induced defenses against predators in colonial marine invertebrates (Harvell, 1984) are surprisingly rare.

In the Caribbean coral *Briareum asbestinum* (Gorgonacea), both biotic and abiotic environmental agents may contribute to plastic variation in skeletal features. Unlike the hard corals with their massive calcium carbonate skeletons, gorgonian corals consist of a central axis surrounded by an outer cortex of a soft, polyp-bearing matrix, the structural integrity of which is maintained by small (0.2–1.2 mm), calcitic skeletal elements (sclerites) (Fig. 1). Within and among local populations, *B. asbestinum* colonies vary significantly in the mean lengths and densities of their sclerites. Furthermore, a reciprocal transplant of colonies between shallow and deep sites indicated that sclerite morphology is phenotypically plastic in response to one or more environmental cues (West *et al.*, 1993; West, 1996).

One such cue may be damage from predators. In addition to skeletal support, sclerites fulfill a second role as structural defenses against predators. *B. asbestinum* contains ichthyodeterrent, diterpene secondary compounds (Pawlik *et al.*, 1987), and predation by fishes appears to be min[illegible] (C. D. Harvell, unpubl. data). However, the gastropo[illegible]*phoma gibbosum* is a major predator of gorgonian[illegible] (Kinzie, 1970; Lasker and Coffroth, 1988; Lasker[illegible]1988) and is an important source of damage to *B. a[illegible]um* (Hazlett and Bach, 1982). *Cyphoma gibbosum* [illegible]ains biotransformation enzymes capable of detoxifying *B. asbestinum* allelochemicals (Vrolijk and Targett, 1992) and consumes artificial foods containing *B. asbestinum* extracts and pure compounds just as readily as it consumes control foods (C. D. Harvell, unpubl. data). Therefore, the sclerites of *B. asbestinum* may be its only defense against this predator, such that differences in skeletal composition will correlate with the ability of colonies to deter snail feeding (West *et al.*, 1993; West, 1996). As sclerites increase in size, they render artificial foods less palatable to *C. gibbosum* (Van Alstyne and Paul, 1992; West *et al.*, 1993; West, 1996). Hence, the inducibility of long, defensive sclerites as a reaction to damage would be a potentially advantageous plastic response.

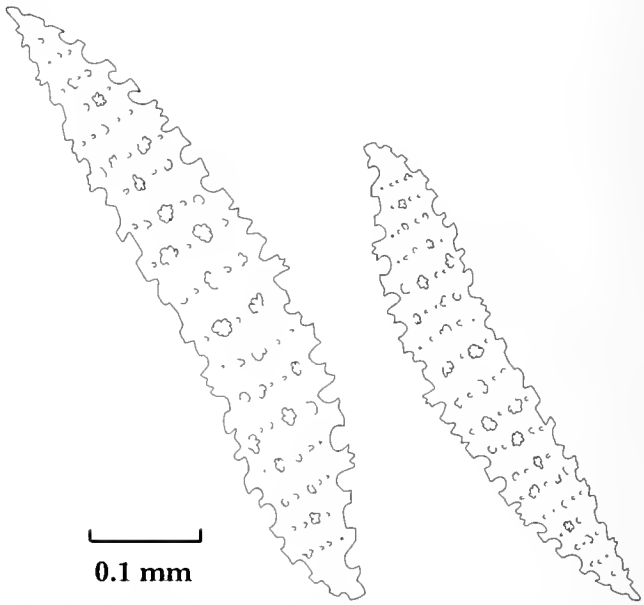

Figure 1. *Briareum asbestinum* Diagram of typical sclerites, showing the 23% difference in mean sclerite length that is inducible and affects snail feeding (West, 1996). Colonies within the same local population can differ in mean sclerite length by as much as 32% (West, 1996).

In addition to biotic induction, sclerite plasticity among *B. asbestinum* populations may also be cued by changing abiotic conditions. At two islands in the Caribbean, colonies of *B. asbestinum* are distributed along a depth gradient of 1–30 m. At the shallow end of the gradient, sclerites are short and of high density, whereas deep colonies contain sclerites that are long and of low density. Sclerite length and density within colonies are negatively correlated, such that colonies with both long and densely packed sclerites do not occur (West *et al.*, 1993; West, 1996). Although biotic induction by a patchily distributed predator could account for variability within sites, the pattern of increasing sclerite length with depth cannot be explained solely by the presence of predators. Snails are indeed present at all of my study sites, but their densities and damage actually decrease with depth, whereas sclerite length increases with depth (West, 1996; C. D. Harvell, unpubl. data). Hence, larger-scale patterns of sclerite variability with depth may be generated by abiotic environmental factors.

Along the depth cline, declining light penetration and

water motion both show some degree of correlation with sclerite variation (West, 1996). Both factors might affect skeletal composition in different ways and might function as cues that induce a plastic response in sclerite length and density. Observed correlations between sclerite variation and percent penetration of photosynthetically active radiation (West, 1996) may be related to effects of light on colony growth rates (C. D. Harvell, unpubl. data), because gorgonians depend on their symbiotic zooxanthellae for most of their energy (Sebens, 1987). In addition, strong correlations between sclerite variation and water motion (West, 1996) may relate to the function of sclerites as skeletal support structures. The sclerites of *B. asbestinum* act as rigid reinforcing points of attachment within the soft matrix, providing resistance to deformation; both smaller sclerites and greater densities of sclerites confer greater stiffness (Wainwright *et al.*, 1976; Koehl, 1982; Palumbi, 1986). Therefore, colonies may display depth-related shifts in skeletal composition according to water motion and light level cues.

In this study, I tested the ability of one biotic agent (predator damage) and two abiotic factors (water motion and light) to induce skeletal modifications in the soft coral *B. asbestinum*. Because the large collections needed for this work would have denuded the sparsely populated deep reefs at my sites, I focused on shallow-water *B. asbestinum*. To examine separately the effect of each type of cue, two large transplant experiments were conducted in which colonies from a shallow population were grown on racks at a single site where water motion, light, and damage were manipulated under controlled conditions. I hypothesized that shallow-water colonies subjected to reduced water motion and reduced light (simulating deep-water conditions) and colonies subjected to mechanical scarring (simulating predator damage) should respond in each case by producing longer sclerites at lower densities compared to controls.

Materials and Methods

Experiment I: water motion and damage

To assess whether differences in water motion and simulated predator damage would induce plastic changes in sclerite composition, I conducted a transplant experiment at San Salvador, Bahamas, from 1 June to 3 August, 1991. Branches from a shallow (1–3 m) population of *Briareum asbestinum* were transplanted to racks on which they reattached themselves and grew as independent new colonies. The racks were arrayed at a single location where water motion and damage were varied. The 12 racks were constructed according to a design modified from West *et al.* (1993). Each rack consisted of an acrylic plate, dimensions 30.0 × 23.0 × 2.5 cm, that snapped into an aluminum angle frame. Each plate accommodated 12 (2 rows of 6) colonies, each inserted into a recessed well and secured with cushioned cable ties to an acrylic post.

The racks were rigidly affixed to cement blocks at a shallow (3 m) site that exposed the colonies to high-energy waves and surge. Water motion was reduced inside half of the racks by clear, small-mesh (0.20 mm) nylon screening that was attached to form walls 15 cm tall (Fig. 2). Water motion inside control and walled racks was quantified by recording the percent dissolution of plaster of Paris (a water-motion index) using methods adapted from Muus (1968), Doty (1971), Day (1977), Bushek (1988), and Jokiel and Morrissey (1993). For this integrated relative measure of water movement due to current velocities and turbulence (Doty, 1971), I measured the weight loss of five replicate plaster domes (24 g) for each rack type over a 24-h period (see West, 1996, for a more detailed description). When compared with measurements made at various other *B. asbestinum* habitats, the reduction in water motion between walled and control racks was found to be similar to differences in water motion between colonies growing deep within crevices and colonies out on the open reef flat. Naturally occurring *B. asbestinum* colonies from these habitat types differ significantly in sclerite composition (West, 1996).

All racks were fitted with clear, large-mesh (2.5 cm) roofs that afforded protection from disturbance by fishes without affecting light penetration. Furthermore, placement of the racks in a sand patch several meters from the reef prevented discovery of the colonies by benthic predators (confirmed through weekly monitoring). Light measurements with a quantum/radiometer/photometer (LI-185B with LI-192SB underwater sensor; LI-COR, Inc., Lincoln, Nebraska) showed that penetration of photosynthetically active radiation (PAR) was the same inside and outside of walled and control racks. During the experiment, the walls and roofs were scrubbed regularly with a stiff brush to remove fouling organisms.

The effects of damage due to simulated predation or breakage were tested by assigning each colony to one of three damage treatments: (1) control; (2) scar; and (3) tip amputation (Fig. 2). The controls were left undamaged. The scar treatment simulated damage by *Cyphoma gibbosum* (Gastropoda), a predator that is typically found on the middle region of colony branches (Harvell and Suchanek, 1987; Gerhart, 1990), where it can rasp the cortex as deep as the axis (Harvell and Suchanek, 1987; West, 1996). Hence, starting about 3 cm from the tip and working downward, I damaged the mid-regions of colonies by gouging them to the axis to create a 1- × 3-cm scar. Finally, tip amputation involved severing the top 1 cm of the colony to simulate predation or breakage. *Briareum asbestinum* is a preferred prey species of *Her-*

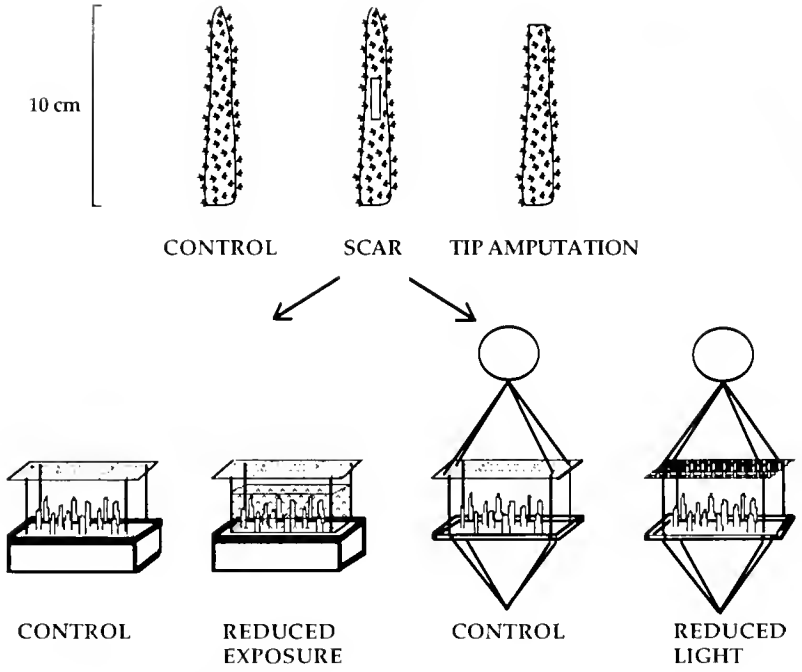

Figure 2. Design of transplant experiments to test sclerite plasticity in *Briareum asbestinum*. Damage types: control = undamaged, scar = 1- × 3-cm gouge, tip = 1-cm tip amputation. Experiment I (exposure and damage): control and reduced exposure racks. Experiment II (light and damage): control and reduced light racks.

modice carunculata (Polychaeta), which commonly feeds by a characteristic removal of branch tips (Vreeland and Lasker, 1989). Thus, tip removal may be similar to the damage inflicted on colonies by worms. Yet, tip removal also lays bare a cross-sectional area of the colony, so amputation also mimics the end product of breakage resulting from heavy wave action. The original cortex material from each scar or tip amputation was preserved in 70% ethanol for later analysis.

Because the number of samples was large, the experiment was set up over 2 days. Each day, 72 undamaged branches, 10 cm long, were collected from a shallow (1–3 m) reef of high wave energy. To maximize the genetic diversity of the collection, divers swam linearly along the reef and sampled single branches from colonies that were separated from any others by at least 3 m. After collection, the branches were suspended in flow-through mesh bags from the side of the boat at the nearby transplant site. They were then assembled onto racks (equal numbers of damage types, randomized with respect to rack position) inside large containers of seawater in the boat, and each completed rack was immediately conveyed to the transplant site below. Virtually all branches began extending their polyps within 2 h of transplantation. Within a few weeks, the branches had attached themselves to the racks and were growing as independent colonies. The colonies were allowed to heal and grow for 9 weeks, and survival exceeded 95%. During the experiment, more than 50% of the colonies increased in height by 0.1–1.5 cm; and all survivors showed positive growth in the sense that they produced new cortex material that encrusted their supportive posts and ties, filled in their scars, and covered over their tip wounds. At the end of 9 weeks, the colonies were collected and preserved in 70% ethanol until they could be processed in the laboratory.

Experiment II: light and damage

To test the effects of reduced light and colony damage, another transplant experiment was conducted from 7 February to 20 April, 1991. The methods were the same as those described for experiment I with the following modifications. Branches were collected from throughout a shallow, relatively calm bay and transplanted to a 12-m location nearby. The colonies were subjected to the same three types of damage and were distributed similarly within the racks, but instead of walls, half of the racks were fitted with roofs made of a double layer of dark window screening (Fig. 2). This screening (1-mm

mesh) reduced the light levels typical of 12-m depth to light levels typical of 30-m depth (J. Miles, pers. comm., calibrated with Li-Cor light meter). The other half of the racks (controls) were fitted with roofs made of clear nylon netting (2.5-cm mesh) to discourage disturbance by fishes without affecting light penetration. The roofs were scrubbed regularly to remove fouling organisms.

To prevent access by benthic predators, the racks were floated about 2 m above the reef flat with steel cables and subsurface buoys. Because the racks could move with the currents, the effects of water motion were moderated. Positive growth of the transplanted colonies was similar to that of experiment I, and colony survival again exceeded 95%. After 14 weeks, the colonies were preserved in 70% ethanol until they were processed in the laboratory.

Sclerite measures

At the end of each experiment, subsets of 1–3 colonies per damage type per rack were measured. Sclerite lengths were recorded in the laboratory with the MORPHOSYS image analysis program (Meacham and Duncan, 1990; version 1.26). For colonies subjected to scarring or tip amputation, both the original cortex material collected when the colonies were damaged ("before" sample) and newly regenerated material from the healed wound ("after" sample) were analyzed. In experiment I, a mid-branch cortex sample from the side opposite the scar ("opposite" sample) was also analyzed to see whether the response to scarring was regionwide. Hence, cortex material was sampled from the following regions of the colonies: (1) tip region of damaged colonies, before and after amputation; (2) mid-branch region of damaged colonies, before, after, and opposite the scars; and (3) mid-branch and tip regions of control colonies at the end of the experiment (after).

For sclerite length measurements, cortex subsamples were taken from the edges of scars before and after healing, from original and healed tips at a distance of 1 cm down from the apex, and from the same locations (by distance from the apex) in the controls. In each case, two small (3–4 mm^3) cortex samples were excised, and the organic matter was dissolved away with a solution of 2.6% sodium hypochlorite. The isolated sclerites were rinsed and distributed in their entirety across six slides (three slides per tissue sample). Video images of the first 4 intact sclerites encountered per slide were measured, for a mean of 24 sclerites per region per colony.

From the same regions of the colonies, the proportion of cortex weight consisting of sclerites (the sclerite weight fraction, a measure of density) was estimated according to Harveli and Suchanek's (1987) protocol. From mid-branch regions, a 1- × 3-cm cortex scraping at the edge of the original scar (or from the middle region of the control) was taken, and from tip regions, the distal 1 cm of cortex material was used in all cases. The samples were separately dried for 24 h at 60°C and weighed; a drying test on a subset of samples showed that they did not continue to lose weight after 24 h. Each sample was then ashed in a muffle furnace at 450°C for 1 h. This process burned the organic matter away, but left the sclerites intact (Harvell and Suchanek, 1987). The sclerite weight fraction was calculated as the proportion of the total cortex weight consisting of sclerites (ash weight/dry weight).

Statistical analyses

All length and weight fraction distributions were normal and homoscedastic, so groups were compared using parametric tests. The "after" data from experiments I and II were subjected to split-unit (or split-plot) analysis of variance (Neter *et al.*, 1990). Blocks, which tested for microenvironmental effects within the experimental site, consisted of pairs of adjacent racks (units), one unit being a control rack while the other was a reduced exposure (experiment I) or reduced light (experiment II) rack. Within racks, individual colonies (subunits) received the different damage treatments. Because previous work had indicated that different regions within colonies may differ in sclerite composition (West, 1996), mid-branch and tip regions were examined separately. Hence, for each experiment, four split-unit analyses were performed: (1) mid-branch sclerite length; (2) mid-branch sclerite weight fraction; (3) tip sclerite length; and (4) tip sclerite weight fraction. Because the Unit*Damage term was not significant in any of the analyses ($P > 0.29$ in all cases), it was removed from the model and its sum of squares was pooled with the error sum of squares for final calculation of F-statistics (Neter *et al.*, 1990).

Mid-branch and tip-damage responses detected in the split-unit ANOVAs were confirmed through comparison of "before" and "after" material from within damaged colonies. Both before and after measurements were taken for each mid-damaged or tip-damaged colony, and my *a priori* expectation was that after and before samples would differ in the same direction as would the after and control samples; hence, I analyzed the before and after data using paired one-tailed t-tests. Data from opposite the scars (experiment I only) were also compared to before data using a paired one-tailed t-test.

In both experiments, the different contrasts of interest involved multiple comparisons and contained variables that lacked independence from variables in other tests (*e.g.*, sclerite length and sclerite weight fraction are from the same colony; control mid-branch and control tip are from the same colony). Hence, a sequential Bonferroni correction for multiple tests was performed (Holm,

1979; Rice, 1989). The sequential Bonferroni method is less conservative and more powerful than the standard Bonferroni method yet still restricts the probability of a type-I error for the entire test as well as each step of the test to $\alpha = 0.05$ (Holm, 1979; Rice, 1989).

Results

Damage

In both experiments I and II, mean sclerite length increased 23% in regenerated mid-branch scars (see Fig. 1), whereas sclerite weight fraction decreased 2.3% (Fig. 3). The increase in sclerite length was significant for the after and control comparisons of the split-unit ANOVAs (Tables I, II) as well as for the before and after paired comparisons (Fig. 3A). Mean sclerite weight fraction decreased in cortex material after scar damage, but the effect was statistically significant only for the before and after comparison of experiment II (Tables I, II; Fig. 3B). Thus, simulated predator damage did alter the average lengths and (in one case) the average weight fractions of *B. asbestinum* sclerites. Moreover, the mid-branch increase in sclerite length was not restricted to newly formed cortex material within the healed scars. Sclerites

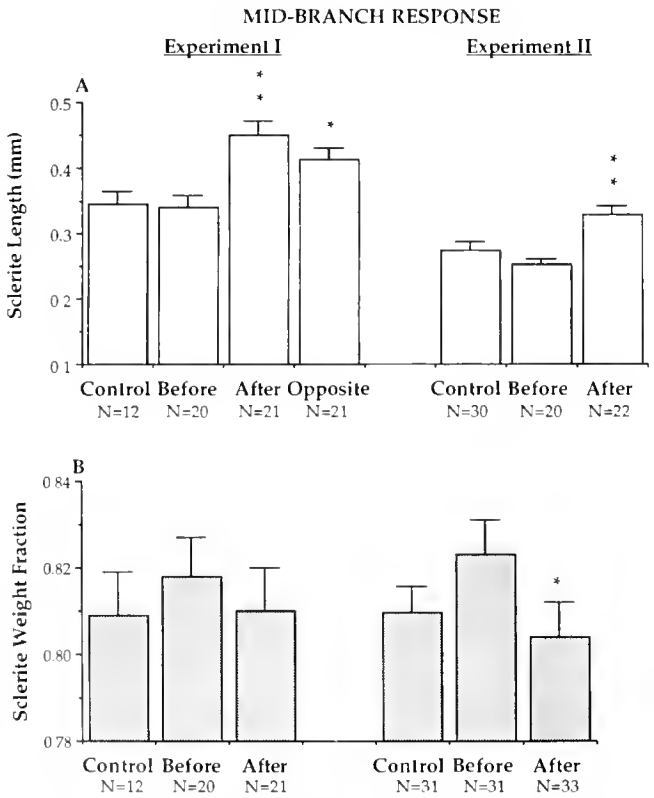

Figure 3. *Briareum asbestinum.* Response of colony mid-branch regions to simulated predator damage: (A) mean sclerite lengths (mm); and (B) mean sclerite weight fractions. Error bars are 1 standard error. Groups: control = undamaged mid-branch tissue at end of experiment; before = original mid-branch tissue gouged at start of experiment; after = regenerated mid-branch scar tissue at end of experiment; opposite = tissue from opposite the scar, sampled at the end of the experiment. The sample sizes for paired *t*-tests are indicated by the *n* values of the before groups. Under sequential Bonferroni adjustment, **denotes significance of both the control *versus* after group comparison and the before *versus* after paired *t*-test; *denotes significance of the paired *t*-test only.

Table I

Summary of split-unit analyses of variance on sclerite length and sclerite weight fraction for Briareum asbestinum *in experiment I (June–August 1991)*

Comparison region	Source	*P* value: Length	*P* value: Wt. fraction
Tip	Block	0.954	0.040
	Exposure	0.465	0.294
	Block * Exposure	0.201	0.946
	Damage	0.062	0.742
Mid-branch	Block	0.284	0.340
	Exposure	0.388	0.240
	Block * Exposure	0.663	0.896
	Damage	0.005*	0.939

Note: Tip region: comparison of protected to exposed colony tips and comparison of damaged colony tips to undamaged control tips; mid-branch region: comparison of protected to exposed mid-regions and comparison of damaged colony mid-regions to undamaged control mid-regions. Blocks (pairs of adjacent racks) test for microenvironmental effects. *denotes significance under sequential Bonferroni adjustment.

Table II

Summary of split-unit analyses of variance on sclerite length and sclerite weight fraction for Briareum asbestinum *in experiment II (February–April 1991)*

Comparison region	Source	*P* value: Length	*P* value: Wt. fraction
Tip	Block	0.870	0.294
	Shading	0.977	0.433
	Block * Shading	0.286	0.126
	Damage	0.005*	0.971
Mid-branch	Block	0.666	0.532
	Shading	0.191	0.865
	Block * Shading	0.348	0.092
	Damage	0.003*	0.559

Note: Tip region: comparison of shaded to unshaded colony tips and comparison of damaged colony tips to undamaged control tips; mid-branch region: comparison of shaded to unshaded mid-regions and comparison of damaged colony mid-regions to undamaged control mid-regions. Blocks (pairs of adjacent racks) test for microenvironmental effects. *denotes significance under sequential Bonferroni adjustment.

from material opposite the scar were also significantly longer than the sclerites before damage (Fig. 3A), indicating that this length response was regionwide.

The response to tip removal was opposite to that of mid-branch scarring. Colonies subjected to tip amputation produced new tips that contained sclerites that were up to 16% shorter and made up 2.5% more of the total cortex weight (Fig. 4). The significant difference between tips after damage and control tips is reflected in the damage term of the split-unit ANOVA for experiment II (Table IIA). The difference between damaged tips and controls was not statistically significant in experiment I (Table IA; Fig. 4A). However, within colonies, both experiments showed a significant decrease in sclerite length from before to after damage (Fig. 4A). Increases in mean weight fraction in healed tips were statistically significant only for the before and after comparison of experiment I (Tables I, II; Fig. 4B).

Water motion

Dissolution of plaster of Paris domes over 24 h showed that water motion inside the walled racks was significantly reduced compared to water motion within control racks ($P = 0.01$, unpaired t test; Fig. 5). The magnitude of the reduction was similar to water-motion differences measured for colonies growing within crevices versus on the open reef flat at a variety of sites around San Salvador (Fig. 5). Such microhabitat differences have been correlated with significant sclerite variation, with microprotected colonies containing longer sclerites at lower densities than microexposed colonies (West, 1996).

When colonies from a shallow site of high-energy waves and surge were shielded from water motion within the walled racks, their sclerites did not differ from the sclerites of control colonies after 9 weeks. This result was consistent for both mid-branch and tip regions of colonies (Table I). In summary, the skeletal composition of *Briareum asbestinum* colonies was not modified in response to the degree and duration of water-motion reductions tested here.

Light

In experiment II, shallow-water colonies were subjected to greatly reduced light levels by shading them with dark screens that had been previously determined to reduce the light levels typical of 12 m to those typical of 30 m (J. Miles, pers. comm.). After 14 weeks, shaded colonies did not differ significantly from unshaded controls in either sclerite length or sclerite weight fraction. This result was consistent for both mid-branch and tip regions of colonies (Table II). Thus, as with water motion, there was no indication that the light reductions tested in this experiment triggered a plastic response in sclerite composition.

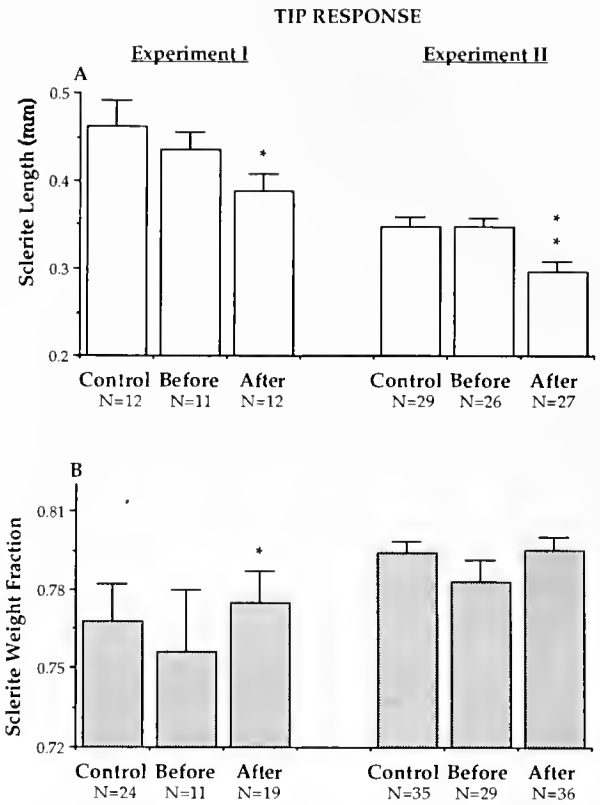

Figure 4. *Briareum asbestinum.* Response of colony tip regions to simulated predator damage: (A) mean sclerite lengths (mm); and (B) mean sclerite weight fractions. Error bars are 1 standard error. Groups: control = undamaged tips at end of experiment; before = original tips amputated at start of experiment; after = regenerated tips at end of experiment. The sample sizes for paired t-tests are indicated by the n values of the before groups. Under sequential Bonferroni adjustment, **denotes significance of both the control *versus* after group comparison and the before *versus* after paired t-test; *denotes significance of the paired t-test only.

Discussion

Environmental cues

Briareum asbestinum colonies responded to one of the three types of environmental cues tested in this study. Simulated predator damage caused clear and significant changes in sclerite morphology, and these changes actually reversed patterns of sclerite length that were observed in colonies without mid-branch or tip damage. Samples collected from naturally growing colonies in the field display a consistent pattern in which the sclerites are longer at the tips of colonies than at the basal regions; similarly, the experimental controls contained longer sclerites at the tips than at the mid-branch regions (Fig.

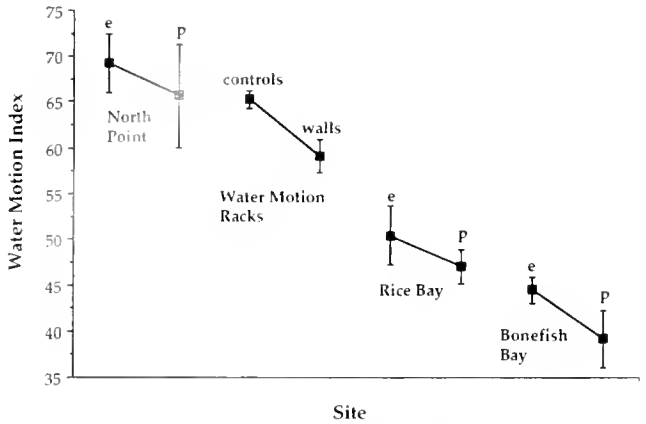

Figure 5. Comparison of mean water-motion index (percent dissolution of plaster of Paris domes over 24 h) for walled and control experimental racks and for other *Briareum asbestinum* sites of similar depth (1–4 m) (n = 4–5 domes in all cases). Error bars are one standard error. p = protected microhabitat (where colonies are growing within sheltered crevices), e = exposed microhabitat (where colonies are growing on the open reef flat).

6). In contrast, sclerite length decreased in regenerated tips and increased in mid-branch scars, such that the usual pattern of variation within undamaged branches was fully reversed (Fig. 6). Furthermore, sclerite length increased not only within mid-branch scars, but also in material located on the opposite side of the colony from the actual wound. Hence, this is a regionwide response that likely affects the entire band of cortex material surrounding a scar.

These mid-region increases in mean sclerite length are more likely due to sclerite turnover than to the simple addition of many long sclerites. If the average length of sclerites was shifted by the accumulation of very long sclerites without the loss of any small sclerites, then we would expect to see greater variances associated with scar means than with control means and higher sclerite weight fractions within scars than in controls. Instead, scarred colonies have length variances that are comparable to controls, and they have reduced weight fractions (Fig. 3).

In general, the changes in sclerite weight fraction reflected the previously observed negative correlation between sclerite length and sclerite density. Weight fraction tended to decrease as sclerite length increased within [illegible]d scars, and the opposite was true for regenerated t[illegible]wever, for each region (tip and mid-branch), the d[illegible]induced change in weight fraction was statistically [illegible]ficant for only one out of six contrasts tested. Nev[illegible]s, the significant weight fraction responses that w[illegible]tected, when combined with the dramatic and cor[illegible]changes in sclerite length (16%–23%) observed, p[illegible]strong evidence of plasticity.

In contrast to the damage responses, there was no indication that the sclerites of shallow-water colonies were altered in response to the abiotic cues of reduced water motion or reduced light. Depth-related sclerite variation may therefore include a component of genetic differentiation. With its ability to reproduce asexually through fragmentation (Brazeau, 1989) and its brooded, negatively buoyant larvae (Brazeau and Lasker, 1990), *B. asbestinum* is probably relatively philopatric. Indeed, an electrophoretic study performed concurrently with this work indicates significant genetic differentiation between shallow and deep populations (Brazeau and Harvell, 1994). Yet there is also some indication that sclerites are altered in response to wounds that mimic breakage (see discussion below), and reciprocal transplantation revealed a plastic change in sclerites with very extreme differences in depth (West *et al.*, 1993). Here, I tested the more usual variation in light and water motion that colonies in highly populated shallower environments encounter. As such, the exposure and light treatments applied to *B. asbestinum* over 9–14 weeks did not induce significant changes in sclerite length or sclerite weight fraction. Further testing is warranted to determine whether a longer duration of acclimation could eventually result in plastic shifts in sclerite composition.

Ecological and evolutionary implications

When colony tips regenerate, the new cortex contains sclerites of decreased length and increased weight frac-

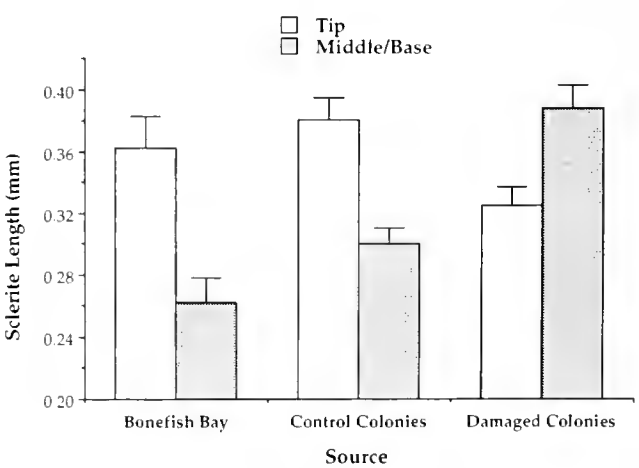

Figure 6. *Briareum asbestinum.* Comparison of mean sclerite length (mm) in different regions of naturally growing colonies *versus* experimental colonies. Source groups: Bonefish Bay = samples from tip and base regions of colonies (n = 16) growing naturally near the transplant sites, Control Colonies = samples from tip (n = 41) and mid-branch (n = 42) regions of pooled experimental controls, Damaged Colonies = samples from regenerated tips (n = 39) and healed mid-branch scars (n = 43) of pooled damage treatments. Error bars are 1 standard error.

tion. Since tip amputation is a characteristic feeding mode of the worm *Hermodice carunculata*, then perhaps increased sclerite densities are an induced defense that makes feeding difficult for worms, or renders the food less palatable (Vreeland and Lasker, 1989). This hypothesis seems unlikely for the following reasons. First, *H. carunculata* does not feed exclusively on colony tips, but also feeds on middle regions of *B. asbestinum* branches (Vreeland and Lasker, 1989) where the response to damage is a *decrease* in sclerite density. Second, Vreeland and Lasker (1989) found no relationship in this predator between preferences for particular gorgonian species and the ash content (sclerite density) of those species. Finally, *H. carunculata* routinely feeds on milleporid fire corals (Witman, 1988), and one hungry worm in the laboratory attempted to engulf the tip of a plastic pen cap (pers. obs.). Hence, a 2.5% increase in sclerite weight fraction at colony tips would probably be a poor defense against this predator.

Instead, the plasticity of sclerites in colony tips after amputation may be a response that decreases further breakage. Survival is lower for small fragments than for larger fragments in other gorgonians (Lasker, 1990), thus breakage of *B. asbestinum* colonies may result in partial mortality as water motion abrades loose branch fragments against the reef. In addition, Gerhart (1990) found that fouling by epibionts such as algae is a serious problem for gorgonian colonies that have suffered major damage such as the baring of large wounded areas at scars or break points. For these reasons, it may be advantageous for colonies to cover such wounds with new cortex material that is fortified against further breakage through increased packing of smaller sclerites.

Biomechanical assays using both artificial and real tissues have indicated that small sclerites at high densities confer greater stiffness than longer and more sparsely packed sclerites (Koehl, 1982). This may be because small sclerites at high densities provide more surface area for tissue attachment and also leave smaller spaces consisting solely of deformable soft matrix. In more recent work, Koehl (1996) has also shown that the strength and toughness of sclerite-reinforced materials increases—and then decreases—with increasing sclerite density. Biomechanical testing of actual *B. asbestinum* branches is needed to determine whether the tip response renders the surrounding matrix stronger and tougher, or more brittle and breakable. A finding of increased strength and toughness in regenerated tips would support the hypothesis that the observed sclerite modifications function in colony reinforcement. This hypothesis could be further tested by breaking additional colonies at the mid-branch region instead of the tip region and observing their response. To adopt a fortification response of shorter, denser sclerites at mid-branch, colonies would have to be capable of reversing the scar-induced sclerite shifts detected in this study (see below).

At the mid-branch region, *B. asbestinum* colonies respond dramatically to mechanical scarring, producing sclerites that are 23% longer. The middle region of colonies is the typical feeding location of the snail *Cyphoma gibbosum* (Harvell and Suchanek, 1987; Gerhart, 1990), and longer sclerites have been shown to reduce snail feeding significantly (West *et al.*, 1993; West, 1996). At St. Croix (U.S. Virgin Islands), *B. asbestinum* colonies from two habitats contain sclerites that differ in length by about 22% (see Fig. 1), and individuals of *C. gibbosum* that are given a choice feed at a higher rate and spend more time on the colonies with shorter sclerites than on those with longer sclerites (West, 1996). It is unlikely that this effect is due solely to chemistry because *C. gibbosum* has gorgonian-detoxifying enzymes (Vrolijk and Targett, 1992) and appears indifferent to *B. asbestinum* extracts in sclerite-free artificial foods (C. D. Harvell, unpubl. data). Conversely, artificial food assays that employed isolated sclerites in the absence of chemistry have indicated that this predator is significantly deterred by long sclerites (West *et al.*, 1993; West, 1996). Hence, the production of 23% longer sclerites in the mid-branch regions of scarred San Salvador colonies may represent an induced defense.

Harvell (1984) hypothesized that predator-induced defenses should be favored in clonal taxa that suffer intermittent, unpredictable nonfatal encounters with predators. *Cyphoma gibbosum* frequently causes significant damage to colonies of *B. asbestinum*, but it seldom completely kills them (Kinzie, 1970; Birkeland and Gregory, 1975). At shallow sites of greatest snail activity, the average amount of surface area scarred per *B. asbestinum* colony can approach 30% (West, 1996). Although the tenure time of individual *C. gibbosum* on particular gorgonian colonies averages only about 10 days (Harvell and Suchanek, 1987), snails tend to form aggregations that have been observed to stay together in a localized area (and even on a single colony) for up to 4 months (Kinzie, 1970; Birkeland and Gregory, 1975; Hazlett and Bach, 1982; Gerhart, 1986). Therefore, colonies within such a feeding area may be grazed upon multiple times, by multiple snails, over a period of weeks to months. Meanwhile, *B. asbestinum* in areas adjacent to large snail aggregations may be virtually free of predator damage (pers. obs.). Experiments on feeding behavior have shown that when given a choice, *C. gibbosum* tends to move off of colonies containing long sclerites and onto colonies containing short sclerites (West, 1996). Therefore, production of snail-deterrent sclerites by *B. asbestinum*, occurring over a period of months, would be an appropriate and advantageous defensive response.

A potential cost to this induced defense may relate

once again to the effects of changes in skeletal composition on the biomechanical behavior of colonies. Tissues that contain long sclerites at low densities will be less stiff and more elastic than tissues with short sclerites at high densities. In the region of a shift to long, sparse sclerites, a branch will indeed be in little danger of breaking due to brittleness; yet too great a propensity for pliability might itself be disadvantageous. A branch that is too soft may not be able to support the optimal orientation for light or prey capture, and excessive bending and swaying of the colony in waves and surge could lead to damage as tissue is abraded against adjacent coral heads. If so, this may explain why long sclerites are an induced rather than a constitutive defense.

The evolution of adaptive plasticity is favored in many plants and corals because of their distributions across changing habitats and their inability to escape extreme environmental conditions through movement (Bradshaw, 1965). In plants, inducible chemical and morphological defenses against predators have been widely reported (Schultz, 1988). In colonial invertebrates such as bryozoans, gorgonians, and scleractinians, it is morphological defenses against competitors rather than against predators that have been most widely documented (Adler and Harvell, 1990). Examples of predator-induced defenses have been uncommon in colonial invertebrates and have been cited only for temperate bryozoans (Harvell, 1984). Now, *B. asbestinum* may represent a new example of a tropical colonial invertebrate with an inducible defense against a predator. Another gorgonian (*Plexaurella dichotoma*) also responds to snail damage by increasing both the size and density of its sclerites (Nowlis, West, and May, unpubl. data). These results for two different genera of gorgonians suggest that the functioning of sclerites as an inducible defense may be widespread in this order of corals.

Acknowledgments

This project benefited from suggestions and field assistance from C. D. Harvell, A.-M. Walls, D. F. Shapiro, J. Nov[illegible] S. Lewis, and S. Nolon. Statistical advice was provide[illegible] L. Buttel and S. J. Schwager. I thank C. D. Harvell, [illegible]ber, N. J. Hairston, Jr., R. Strathmann, the FHL dis[illegible]n group, and two anonymous reviewers for constr[illegible]omments on the manuscript. This research was sup[illegible]y grants from the Mellon Foundation, the Ameri[illegible]useum of Natural History, the Houston Underwater [illegible] Club (Seaspace), Sigma Xi Grants-in-Aid of Research (national chapter), and the Cornell Graduate School to J. M. West, and NSF grant OCE 90-012034 to C. D. Harvell.

Literature Cited

Adler, F. R., and C. D. Harvell. 1990. Inducible defenses, phenotypic variability and biotic environments. *TREE* **5(12):** 407–410.

Baldwin, I. T., and T. E. Ohnmeiss. 1993. Alkaloidal responses to damage in *Nicotiana* native to North America. *J. Chem. Ecol.* **19(6):** 1143–1153.

Barnes R. D. 1987. *Invertebrate Zoology.* Saunders, New York.

Bavestrello, G., M. Bonito, and M. Sara. 1993. Influence of depth on the size of sponge spicules. *Sci. Ma.* **57(4):** 415–420.

Birkeland, C., and B. Gregory. 1975. Foraging behavior and rates of feeding of the gastropod, *Cyphoma gibbosum*. *Bull. Nat. Hist. Mus. Los Angeles Co.* **20:** 57–67.

Bradshaw, A. D. 1965. Evolutionary significance of phenotypic plasticity in plants. *Adv. Genet.* **13:** 115–155.

Bradshaw, A. D. 1974. Environment and phenotypic plasticity. *Brookhaven Symp. Biol.* **25:** 75–94.

Brazeau, D. A. 1989. A male-biased sex ratio in the Caribbean octocoral, *Briareum asbestinum*: sex ratio evolution in clonal organisms. Doctoral Dissertation, State University of New York at Buffalo, NY.

Brazeau, D. A., and C. D. Harvell. 1994. Genetic structure of local populations and divergence between growth forms in a clonal invertebrate, the Caribbean octocoral *Briareum asbestinum*. *Mar. Biol.* **104:** 465–474.

Brazeau, D. A., and H. R. Lasker. 1990. Sexual reproduction and external brooding by the Caribbean gorgonian *Briareum asbestinum*. *Mar Biol* **104:** 465–474.

Bushek, D. 1988. Settlement as a major determinant of intertidal oyster and barnacle distributions along a horizontal gradient. *J. Exp. Mar. Biol. Ecol.* **122:** 1–18.

Day, R. W. 1977. The ecology of settling organisms of the coral reef at Heron Island, Queensland. Doctoral Dissertation, University of Sydney, Australia.

de Weerdt, W. H. 1981. Transplantation experiments with Caribbean *Millepora* species, including some ecological observations on growth forms. *Bijdr. Dierkd.* **51:** 1–9.

Doty, M. S. 1971. Measurement of water movement in reference to benthic algal growth. *Bot. Mar.* **14:** 32–35.

Foster, A. B. 1979. Phenotypic plasticity in the reef corals *Montastraea annularis* (Ellis & Solander) and *Siderastrea siderea* (Ellis & Solander). *J. Exp. Mar. Biol. Ecol.* **39:** 25–54.

Francis, L. 1973. Intraspecific aggression and its effects on the distribution of *Anthopleura elegantissima* and some related anemones. *Biol. Bull.* **144:** 73–92.

Gerhart, D. J. 1986. Gregariousness in the gorgonian-eating gastropod *Cyphoma gibbosum*: tests of several possible causes. *Mar. Ecol. Prog. Ser.* **31:** 255–263.

Gerhart, D. J. 1990. Fouling and gastropod predation: consequences of grazing for a tropical octocoral. *Mar. Ecol. Prog. Ser.* **62:** 103–108.

Gilbert, J. J., and R. S. Stemberger. 1984. *Asplanchna*-induced polymorphism in the rotifer *Keratella slacki*. *Limnol. Oceanogr.* **29:** 1309–1316.

Grigg, R. W. 1972. Orientation and growth form of sea fans. *Limnol. Oceanogr.* **17(2):** 185–192.

Harlan, J. R. 1945. Cleistogamy and chasmogamy in *Bromus carinatus* Hook, and Arn. *Am. J. Bot.* **32:** 66–72.

Harvell, C. D. 1984. Predator-induced defense in a marine bryozoan. *Science* **224:** 1357–1359.

Harvell, C. D., and D. Padilla. 1990. Inducible morphology, heterochrony and size hierarchies in a colonial invertebrate monoculture. *Proc. Natl. Acad. Sci. USA* **87:** 508–512.

Harvell, C. D., and T. S. Suchanek. 1987. Partial predation on tropical gorgonians by *Cyphoma gibbosum* (Gastropoda). *Mar. Ecol. Prog. Ser.* **38:** 37–44.

Havel, J. 1986. Predator-induced defenses: a review. Pp. 263–278 in *Predation: Direct and Indirect Impacts on Aquatic Communities.*

W. C. Kerfoot and A. Sih, eds. University Press of New England, Hanover, NH.

Hazlett, B. A., and C. E. Bach. 1982. Distribution pattern of the Flamingo Tongue Shell (*Cyphoma gibbosum*) on its gorgonian prey (*Briareum asbestinum*). *Mar. Behav. Physiol* **8**: 305–309.

Holm, S. 1979. A simple sequentially rejective multiple test procedure. *Scand. J. Stat.* **6**: 65–70.

Ivker, F. 1972. A hierarchy of histo-incompatibility in *Hydractinia echinata*. *Biol. Bull.* **143**: 162–174.

Jokiel, P. L., and J. I. Morrissey. 1993. Water motion on coral reefs: evaluation of the 'clod card' technique. *Mar. Ecol. Prog. Ser* **93**: 175–181.

Kinzie, R. A. 1970. The ecology of the gorgonians (Cnidaria: Octocorallia) of Discovery Bay, Jamaica. Doctoral Dissertation, Yale University, New Haven, CT.

Koehl, M. A. R. 1982. Mechanical design of spicule-reinforced tissue: stiffness. *J. Exp. Biol.* **98**: 239–267.

Koehl, M. A. R. 1996. Mechanical design of sclerite-reinforced skeletons. *Am. Zool.* **36(5)**: 55A.

Lang, J. C. 1973. Interspecific aggression by scleractinian corals. II. Why the race is not only to the swift. *Bull. Mar. Sci.* **23**: 260–279.

Lasker, H. R. 1990. Clonal propagation and population dynamics of a gorgonian coral. *Ecology* **71(4)**: 1578–1589.

Lasker, H. R., and M. A. Coffroth. 1988. Temporal and spatial variability among grazers: variability in the distribution of the gastropod *Cyphoma gibbosum* on octocorals. *Mar. Ecol. Prog. Ser.* **43**: 285–295.

Lasker, H. R., M. A. Coffroth, and L. M. Fitzgerald. 1988. Foraging patterns of *Cyphoma gibbosum* on octocorals: the roles of host choice and feeding preference. *Bull. Mar. Biol. Lab. Woods Hole* **174**: 254–266.

Lesser, M. P., V. M. Weis, M. R. Patterson, and P. L. Jokiel. 1994. Effects of morphology and water motion on carbon delivery and productivity in the reef coral, *Pocillopora damicornis* (Linnaeus): diffusion barriers, inorganic carbon limitation, and biochemical plasticity. *J. Exp. Mar. Biol. Ecol.* **178**: 153–179.

Lewis, S. M., J. N. Norris, and R. B. Searles. 1987. The regulation of morphological plasticity in tropical reef algae by herbivory. *Ecology* **68(3)**: 636–641.

McCloskey, L. R., and L. Muscatine. 1984. Production and respiration in the Red Sea coral *Stylophora pistillata* as a function of depth. *Proc. R. Soc. Lond. Ser. B* **222**: 215–230.

McNaughton, S. J., and J. L. Tarrants. 1985. Grass leaf silicification: natural selection for an inducible defence against herbivores. *Proc. Natl. Acad. Sci. USA* **80**: 790–791.

Meacham, C. A., and T. Duncan. 1990. *Morphosys* version 1.26. University Herbarium, University of California, Berkeley, CA.

Miles, J. 1991. Inducible agonistic structures in the tropical corallimorpharian, *Discoma sanctithomae*. *Biol. Bull.* **180**: 406–415.

Mooney, H. A., and M. West. 1964. Photosynthetic acclimation of plants of diverse origin. *Am. J. Bot.* **51**: 825–827.

Muscatine, L. 1974. Endosymbiosis of cnidarians and algae. Pp. 359–395 in *Coelenterate Biology*, L. Muscatine and H. M. Lenhoff, eds. Academic Press, New York.

Muscatine, L., R. R. Pool, and R. K. Trench. 1975. Symbiosis of algae and invertebrates: aspects of the symbiont surface and the host-symbiont interface. *Trans. Am. Microsc. Soc.* **94(4)**: 450–469.

Muus, B. J. 1968. A field method for measuring "exposure" by means of plaster balls. *Sarsia* **34**: 61–68.

Neter, J., W. Wasserman, and M. H. Kutner. 1990. *Applied Linear Statistical Models*. Richard D. Irwin, Inc., Boston, MA.

Palumbi, S. R. 1986. How body plans limit acclimation: responses of a demosponge to wave force. *Ecology* **67(1)**: 208–214.

Pawlik, J. R., M. T. Burch, and W. Fenical. 1987. Patterns of chemical defense among Caribbean gorgonian corals: a preliminary survey. *J. Exp. Mar. Biol. Ecol.* **108**: 55–66.

Rice, W. 1989. Analyzing tables of statistical tests. *Evolution* **43(1)**: 223–225.

Roy, J., and H. A. Mooney. 1982. Physiological adaptation and plasticity to water stress of coastal and desert populations of *Heliotropium curassavicum*. *Oecologia* **52**: 370–375.

Scheiner, S. M. 1993. Genetics and evolution of phenotypic plasticity. *Annu. Rev. Ecol. Syst.* **24**: 35–68.

Schlichting, C. D. 1986. The evolution of phenotypic plasticity in plants. *Annu. Rev. Ecol. Syst.* **17**: 667–693.

Schultz, J. C. 1988. Plant responses induced by herbivores. *TREE* **3(2)**: 45–49.

Sebens, K. P. 1984. Water flow and coral colony size: interhabitat comparisons of the octocoral *Alcyonium siderium*. *Proc. Natl. Acad. Sci. USA* **81**: 5473–5477.

Sebens, K. P. 1987. Coelenterata. Pp. 55–120 in *Animal Energetics*, T. J. Pandian and F. J. Vernberg, eds. Academic Press, San Diego, CA.

Sebens, K. P., and J. C. Miles. 1988. Sweeper tentacles in a gorgonian octocoral: morphological modifications for interference competition. *Biol. Bull.* **175**: 378–387.

Sorensen, T. 1954. Adaptation of small plants to deficient nutrition and a short growing season. Illustrated by cultivation experiments with *Capsella bursapastoris* (L.). *Med. Botan. Tidsskrift* **51**: 339–361.

Stearns, S. C. 1989. The evolutionary significance of phenotypic plasticity. *Bioscience* **39(7)**: 436–445.

Svoboda, A. 1978. *In situ* monitoring of oxygen production and respiration in Cnidaria with and without zooxanthellae. Pp. 75–82 in *Physiology and Behavior of Marine Organisms*, D. S. McLusky and A. J. Berry, eds. Permagon Press, New York.

Turesson, G. 1920. The cause of plagiotrophy in maritime shore plants. *Lunds Univ. Arsskr. Avd. 2 (NF)* **16(2)**: 1–33.

Van Alstyne, K. L. 1988. Herbivore grazing increases polyphenolic defenses in the intertidal brown alga *Fucus distichus*. *Ecology* **69(3)**: 655–663.

Van Alstyne, K. L., and V. J. Paul. 1992. Chemical and structural defenses in the sea fan *Gorgonia ventalina* effects against generalist and specialist predators. *Coral Reefs* **11**: 155–159.

Via, S., and R. Lande. 1985. Genotype-environment interaction and the evolution of phenotypic plasticity. *Evolution* **39(3)**: 505–522.

Vreeland, H. V., and H. R. Lasker. 1989. Selective feeding of the polychaete *Hermodice carunculata* Pallas on Caribbean gorgonians. *J. Exp. Mar. Biol. Ecol.* **129**: 265–277.

Vrolijk, N. H., and N. M. Targett. 1992. Biotransformation enzymes in *Cyphoma gibbosum* (Gastropoda: Ovulidae): implications for detoxification of gorgonian allelochemicals. *Mar. Ecol. Prog. Ser.* **88**: 237–246.

Wainwright, S. A., W. D. Biggs, J. D. Currey, and J. M. Gosline. 1976. *Mechanical Design in Organisms*. Edward Arnold, London.

Wellington, G. M. 1980. Reversal of digestive interactions between Pacific reef corals: mediation by sweeper tentacles. *Oecologia* **47**: 340–343.

West, J. M. 1996. Skeletal variation in the Caribbean coral *Briareum asbestinum* (Gorgonacea): pattern and process across environmental gradients. Doctoral Dissertation, Cornell University, Ithaca, NY.

West, J. M., C. D. Harvell, and A.-M. Walls. 1993. Morphological plasticity in a gorgonian coral (*Briareum asbestinum*) over a depth cline. *Mar. Ecol. Prog. Ser.* **94**: 61–69.

Wijsman-Best, M. 1974. Habitat-induced modification of reef corals (Faviidae) and its consequences for taxonomy. *Proc. 2nd Int. Coral Reef Symp.* **2**: 217–228.

Witman, J. D. 1988. Effects of predation by the fire worm *Hermodice carunculata* on milleporid hydrocorals. *Bull. Mar. Sci* **42**: 446–458.

Young, T. P. 1987. Increased thorn length in *Acacia depranolobium*—an induced response to grazing. *Oecologia* **71**: 436–438.

Reference: *Biol. Bull.* **192:** 290–299. (April, 1997)

Life-History Variation in a Colonial Ascidian: Broad-Sense Heritabilities and Tradeoffs in Allocation to Asexual Growth and Male and Female Reproduction

PHILIP O. YUND, YVETTE MARCUM[1], AND JOHN STEWART-SAVAGE

Department of Biological Sciences, University of New Orleans, New Orleans, Louisiana 70148

Abstract. Intraspecific variation in life-history strategy provides a valuable opportunity for examining how natural selection acts on life-history variants to mold reproductive strategies. Evaluating the consequences of selection requires knowledge of the range of phenotypic variation in life histories, the extent to which variation is genetically based, and possible correlations among different traits that might constrain or promote the effect of selection on individual traits. We explored life-history variation in the colonial ascidian *Botryllus schlosseri* (a cyclical hermaphrodite) by growing clonal replicates of 18 genotypes in a common-garden experiment. Colonies of this species have previously been shown to vary in egg production and growth rate. We demonstrate that genotypes also vary in sperm production, which is manifested as variation in testis size. We then calculate broad-sense heritabilities for a suite of life-history traits and demonstrate correlations among traits that suggest a three-way tradeoff in resource allocation to asexual growth and sexual reproduction *via* male and female function. This correlation structure suggests that selection cannot act independently on individual life-history traits.

Introduction

Marine habitats tend to subject organisms to unique selective pressures that are reflected in the life-history strategies that evolve in this environment (Hendler, 1975; Strathmann *et al.*, 1984; McEdward and Coulter, 1987; Emlet *et al.*, 1987; Strathmann, 1990). For free-spawning marine invertebrates, fertilization *via* the release of sperm into the water column may lead to distinctive selective pressures on life-history strategies (Ghiselin, 1987; Strathmann, 1990). In particular, recent field experiments and assays of fertilization success in nature have suggested that selection *via* fertilization processes may profoundly influence both the quantity of gametes produced and specific attributes of those gametes (reviewed in Levitan, 1995; Levitan and Petersen, 1995).

Because many species exhibit little apparent intraspecific variation in life-history strategy, comparative studies among taxa have contributed immensely to the study of the evolution of marine invertebrate life histories (*e.g.*, Menge, 1975; Strathmann and Strathmann, 1982; Eckelbarger and Watling, 1995). However, selection actually acts on variation within a species, and some marine species do exhibit substantial intraspecific variation in different life-history characters (*e.g.*, Hughes and Hughes, 1986; Grosberg, 1988; Yund, 1991; Cohen and Strathmann, 1996). These variable taxa yield particularly valuable opportunities for evaluating the action of natural selection on life-history variants.

Evaluating the consequences of natural selection on intraspecific variation in life-history traits requires three types of information: first, which life history traits exhibit phenotypic variation, and hence can potentially be subject to selection; second, for each variable trait, what is the extent to which phenotypic variation is genetic; third, since selection ultimately acts on the total phenotype and not just on independent traits, are there positive and negative correlations among traits. Correlations among traits could either constrain or promote the effect of selection acting on each individual trait (Lande and Arnold, 1983).

We present data from a common-garden experiment with the colonial ascidian *Botryllus schlosseri*, a cyclical

Received 3 October 1996; accepted 3 January 1997.

[1] Current address: School of Veterinary Medicine, Louisiana State University, Baton Rouge, LA 70803.

hermaphrodite, that addresses these three points. Colonies of this species are known to vary in growth rate, terminal size, and egg production (Grosberg, 1982, 1988; Chadwick-Furman and Weissman, 1995). We demonstrate additional variation among genotypes in sperm production and reproductive cycle duration, and estimate broad-sense heritabilites for all five of these traits. Finally, we explore possible correlations among traits to assess the potential for selection to act independently on individual traits.

Materials and Methods

Study species

Botryllus schlosseri, a colonial ascidian with a cosmopolitan distribution, is common on firm substrata in the shallow subtidal zone of New England waters (Gosner, 1971). Colonies are composed of asexually produced zooids arranged in clusters, or systems, with all zooids in a system sharing a common exhalant siphon. All zooids in the colony synchronously undergo an asexual cycle of zooid replacement in which a new generation of zooids (buds) forms between the existing generation of zooids (Milkman, 1967). Over a period of about 6–12 d, these buds grow and expand, and then take over the function of the previous generation of zooids, which are quickly resorbed. Colonies grow as long as bud production exceeds the number of zooids in the current generation, and growth continues until colonies reach a terminal size (generally associated with the onset of sexual reproduction), which is then maintained over a number of subsequent asexual cycles (Boyd *et al.*, 1986; Grosberg, 1988).

Sexual reproduction begins when colonies exceed a minimum size (Harvell and Grosberg, 1988). Eggs brooded by each new generation of zooids are fertilized at the time of take-over, when the zooids' siphons first open and admit water to the atrial chambers. Sperm release does not begin until about 1–2 d after ovulation, effectively preventing self-fertilization (Milkman, 1967; Yund and McCartney, 1994). Because sexual reproduction is linked to the asexual zooid replacement cycle, colonies cycle between male and female function.

Relationship between testis cross-sectional area and sperm count

When colonies are grown in culture on glass substrata, variation in sperm production is readily apparent as variation in testis size (viewed from the underside; pers. obs.). To facilitate monitoring a number of colonies and to permit repeated sampling of individuals over time, we needed an assay of sperm production that was relatively quick and nondestructive. Consequently, we assayed sperm production as testis cross-sectional area. To validate this approach, we first tested for a correlation between testis cross-sectional area and the number of sperm in individual testes. We used an ocular micrometer to measure the length and width of 27 mulberry-shaped testes in zooids of different colonies and then surgically removed each measured testis from its zooid. All testes were sampled at the time of maximum size during the reproductive cycle (day 2–3 by the criteria of Milkman, 1967). Each testis was removed by making a longitudinal incision in the wall of the zooid, lifting the testis with forceps, and cutting the connective tissue attached to the underside of the testis. Excised testes were preserved in 2% glutaraldehyde in buffered seawater and later macerated in 100 μl of seawater by five gentle grinds with a glass rod. The number of mature spermatozoa in each testis was estimated as the mean of four hemocytometer counts of the sperm suspension. We analyzed these data by examining the correlation between mean sperm count and testis cross-sectional area (calculated as the length multiplied by the width of each testis).

Common-garden experiment

We examined life-history variation among 18 *B. schlosseri* genotypes by growing clonal replicates in a flowing seawater system at the University of Maine's Darling Marine Center. Colonies used in this experiment were initially collected from widely spaced ($\approx$10–20 m. apart) locations within a field population located in 3 to 8 m of water (MLW) on the western shore of Carlisle Island in the Damariscotta River, Maine (adjacent to the experimental field site of Yund and McCartney, 1994; Yund, 1995; Atkinson and Yund, 1996). Field-collected colonies were subdivided and explanted onto glass microscope slides (2.5 $\times$ 7.6 cm), with between 5 and 11 replicate colonies established for each genotype.

The 18 genotypes selected for inclusion in the common-garden experiment were chosen on the basis of initially possessing less than three eggs per bud. Although this criterion restricted us to exploring only a subset of the total life-history variation in this population, this limitation was necessary in order for us to collect data on each colony over a series of asexual or sexual cycles. Genotypes with higher egg production were present (although rare) in this population, but such colonies typically die after one brooding cycle (Grosberg, 1988).

The experiment began on 20 June 1994, when all colonies were trimmed to an average of 33.5 zooids ($\pm$1.9 SE) arranged in two or three systems of zooids. Colonies were housed in a vertical position in acrylic racks, with neighboring slides separated by 1.3 cm. The racks were placed in a single large, shallow tank (130 $\times$ 100 $\times$ 9 cm) in the flowing seawater system. Racks had no fixed position within the tank, but systematic posi-

tional effects are unlikely because racks were moved and relocated daily throughout the experiment. Similarly, colonies were shuffled among positions within racks about once a week (at the time of each data collection). No supplemental food was added, because past experience indicated that colonies have reasonably high growth and fecundity under these culture conditions.

Data on colony size (number of zooids), growth rate (number of buds), egg production (number of eggs per bud for a subsample of 10 buds), and sperm production (testis cross-sectional area for a subsample of 10 testes in 5 zooids) were collected for each surviving colony (some replicates died before the end of the experiment) once during each asexual or sexual cycle for seven cycles, beginning the week of 27 June. Colonies were viewed from either the top (colony size) or bottom (all other variables) under a dissecting microscope. Testis cross-sectional area was calculated by measuring the length and width of testes with an ocular micrometer at 25 × magnification. Testes measurements were standardized within each asexual or sexual cycle by sampling within the window of maximum testis size (day 2–3 by the criteria of Milkman, 1967). Testes measurements and bud counts were performed on 5 and 10 zooids (respectively) widely scattered throughout the colony to prevent possible biases from positional effects within colonies. For a subset of eight genotypes, we also directly assayed variation in sperm production by excising three testes from each of three replicate colonies in cycle 6 and estimating the number of mature sperm in each testis as the mean of four hemocytometer counts of a 100-μl dilution of the macerated testis (as described in the preceding section). For each colony, we also recorded the time (number of days) required to complete each asexual and sexual cycle. Comparison of these values permits an assessment of variation in cycle duration among genotypes.

Life-history data were analyzed through a series of ANOVAs performed with a computer software package (JMP, SAS Institute, Cary, NC). Unequal sample sizes among genotypes and sample dates due to the death of some replicate colonies and values missed during data collection necessitated an unbalanced design. Similar analyses were conducted for six dependent variables: eggs per bud, buds per zooid (calculated by dividing the number of buds by the number of zooids in each colony in each cycle), testis cross-sectional area, sperm count in cycle 6, terminal size (the maximum number of zooids produced by each colony), and cycle duration. All analyses included the random effects 'genotype' and 'replicate within genotype', except for the analysis of terminal size which did not include a 'replicate' effect because there was only a single size value for each replicate colony. Analyses for the four dependent variables eggs per bud, buds per zooid, testis cross-sectional area, and cycle duration included 'cycle' as an effect and were performed as repeated measures ANOVAs by testing 'cycle' with respect to the random effects. The 'genotype' by 'cycle' interaction effect was omitted from these models due to inadequate sample sizes in some cells. Data collection for the two dependent variables terminal size and sperm count during cycle 6 was restricted to a single cycle, and hence no 'cycle' effect could be included in these models.

Variance components from these analyses were used to calculate the clonal repeatability of each life-history trait (a form of broad-sense heritability; Falconer, 1981). The component of variance attributable to the 'genotype' effect was used as an estimate of genetic variance and was divided by the sum of all variance components, which provides an estimate of total phenotypic variance (Falconer, 1981). We also recorded the range of genotype means and least square means (which adjust for a 'cycle' effect in four of the six analyses) for each life-history trait, and calculated the magnitude of variation in each trait by dividing the highest genotype least square mean by the lowest. Finally, we explored possible univariate and multivariate correlations among life-history traits. First, we calculated Pearson product-moment correlations among genotype least square means for each possible set of paired traits. For a subset of three of the traits (eggs per bud, testis area, and buds per zooid) we also calculated partial correlation coefficients and employed a principal components analysis to characterize the dimensionality of the three-way relationship.

Results

Relationship between testis cross-sectional area and sperm count

Testis cross-sectional area, calculated as testis length multiplied by width, was highly correlated with the actual number of mature spermatozoa in each testis (Fig. 1; $r = 0.71$, $P < 0.001$). Testes are three-dimensional objects, and so variation in cross-sectional area alone (a two-dimensional measurement) might be expected to scale nonlinearly with actual sperm counts. However, there is no evidence of a nonlinear relationship between these variables (Fig. 1). Nonlinear functions fit to these data yielded substantially lower correlation coefficients than the linear function (exponential, $r = 0.52$; power, $r = 0.48$; logarithmic, $r = 0.62$). Either variation in testis thickness (the third, unmeasured dimension) is minimal, or the effect of this aspect of variation in testis volume on sperm counts is negligible within the size range measured in this study.

Genotypic variation and clonal repeatabilities of life-history traits

All six life history traits assayed in this study varied greatly among genotypes (Table I). The effect of geno-

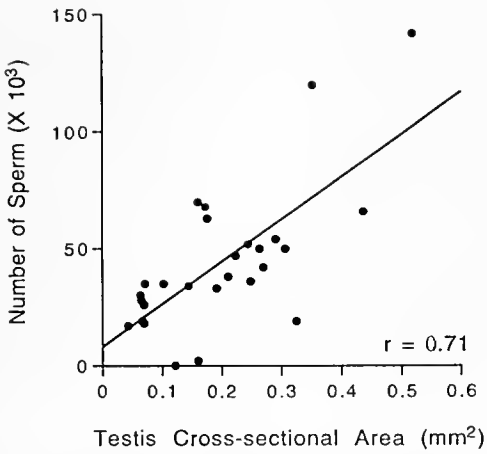

Figure 1. The relationship between testis cross-sectional area and number of mature spermatozoa within 27 testis measured and excised from different colonies.

type was extremely significant ($P < 0.0001$) in all six analyses. In contrast, the effect of replicate nested within genotype (an indicator of environmental variance) was not significant in four out of the five analyses in which it was included (Table I). Testis cross-sectional area was the only trait that exhibited significant variation among replicate colonies within a genotype, though the magnitude of the replicate effect was only about half that of the genotype effect (Table I). In all four analyses for which data were collected in multiple asexual and sexual cycles, the effect of cycle was also highly significant (Table I). Averaged across all genotypes, the number of eggs per bud and testis cross-sectional area both initially increased over the first two reproductive cycles and then declined in the final two cycles (Table II). The number of buds per zooid decreased over subsequent cycles as colonies approached a terminal size (Table II). Cycle duration fluctuated over subsequent cycles with no apparent pattern (Table II).

The temporal patterns of life-history traits can be better appreciated by examining the performance of three sample genotypes, chosen to represent the extremes of life-history strategy present among experimental colonies (Fig. 2). All three genotypes exhibited high initial growth rates and then leveled off at a maximum size (Fig. 2; number of zooids), but the high-growth genotype (Fig. 2C) grew more rapidly than the other two (Fig. 2A, B) and never completely ceased growing. Egg production generally increased over subsequent cycles, but substantial variation was present between adjacent cycles (Fig. 2; eggs per bud). Finally, though sperm production generally increased over subsequent cycles (Table II), sperm production in the high-sperm-production genotype actually decreased over time (Fig. 2A; testis area), a pattern that was repeated for the second highest sperm-production genotype in this study (unpubl. data). All of the lower sperm-production genotypes either increased sperm production over time or remained more-or-less constant (Fig. 2B, C).

Clonal repeatabilities calculated from variance components from these analyses varied widely among traits (Table III). The two variables with the highest expected environmental component to variance (buds per zooid and cycle duration) had the lowest clonal repeatabilities (Table III). The relatively high clonal repeatability for actual sperm counts may be due to a combination of sampling in a single cycle, limiting data collection to only eight genotypes, and utilizing a higher resolution sampling technique (in comparison to testis cross-sectional area), all of which could have reduced environmental variance.

Although all six life-history traits varied significantly among genotypes (Table I), the magnitude of that variation differed greatly among traits (Table III). Cycle duration exhibited the least variation, with the least square mean for the slowest genotype only 40% greater than that

Table I

ANOVA results for the six life-history variables

Source	df	Sum of squares	*F*	*P*
A. Dependent: Eggs per bud				
Genotype	17	199.1	38.9	0.0001
Replicate [Genotype]	123	34.4	0.7	0.9979
Cycle	6	78.4	30.4	0.0001
B. Dependent: Testis cross-sectional area				
Genotype	17	21.8	11.4	0.0001
Replicate [Genotype]	93	11.3	1.7	0.0005
Cycle	6	8.6	19.9	0.0001
C. Dependent: Sperm count in cycle six				
Genotype	7	183,698	28.7	0.0001
Replicate [Genotype]	16	14,609	1.0	0.4781
D. Dependent: Buds per zooid				
Genotype	17	16.7	9.3	0.0001
Replicate [Genotype]	107	10.6	0.7	0.9958
Cycle	6	115.1	150.8	0.0001
E. Dependent: Terminal colony size (number of zooids)				
Genotype	17	39,101	9.0	0.0001
F. Dependent: Cycle duration				
Genotype	17	116.6	13.0	0.0001
Replicate [Genotype]	106	44.7	0.3	0.9999
Cycle	5	136.1	22.1	0.0001

Note: All analyses contain genotype as a random main effect. Analyses for all dependent variables except for terminal colony size contain replicate nested within genotype as a second random main effect. Analyses for all dependents except for terminal colony size and sperm count in cycle 6 contain cycle as an additional main effect. These four analyses were performed as repeated measures by testing the cycle effect with respect to the random effects.

Table II

Cycle effects for the four life-history variables measured over subsequent asexual and sexual cycles

Cycle number	Eggs per bud	Testis area	Buds per zooid	Cycle duration
1	1.12	0.64	2.25	—
2	1.63	0.99	1.85	6.74
3	1.61	0.78	1.11	8.10
4	2.01	0.79	1.01	7.22
5	2.21	0.99	1.08	7.06
6	1.57	0.80	0.96	7.78
7	1.34	0.58		8.17

Note: Least square means, adjusted for genotype and replicate nested within genotype effects, are reported for each cycle. Cycle duration values are missing for the first cycle because the start of the cycle preceded the initiation of data collection. Similarly, buds per zooid data are missing for cycle seven because the number of zooids was not counted in what would have been the eighth cycle.

of the fastest genotype (Table III). Thus, although we were able to detect significant variation in cycle duration among genotypes, the magnitude of variation in this trait relative to other life-history traits is comparatively minor. The other five variables exhibited variation in genotype least square means ranging from more than a factor of 2 (buds per zooid) to almost a factor of 5 (sperm count in cycle six; Table III).

Correlations among life-history variables—genotype means

Two pairs of correlations among the six life-history traits that we measured exist because the pairs of variables measure traits produced by the same or very similar underlaying processes. First, for the subset of eight genotypes for which we actually counted sperm in cycle 6, this variable was highly correlated with genotype least square means for testis cross-sectional area (Table IVA). Because the two variables just represent two different ways of measuring sperm production, this correlation is to be expected and conveys little biological information (beyond confirming the relationship between testis size and sperm number; see Fig. 1). Secondly, genotype least square means for growth rate (buds per zooid) were significantly correlated with genotype means for terminal size (Table IVA). Again, genotypes with higher growth rates (adjusted for variation among cycles) should in general attain a larger terminal size. These two correlations are assumed to be biologically relatively trivial, and the remainder of our presentation considers only one of each of these two pairs of variables (genotype least square means for testis cross-sectional area and buds per zooid, since these two traits are measured at the zooid level and adjusted for variation among cycles).

Of the remaining four life-history variables, genotype least square means for cycle duration were not significantly correlated with genotype least square means for any of the other variables (Table IVA). Since the magnitude of variation in cycle duration was so much smaller than for the other three variables (Table III), correlations might exist that could be detected only with much larger sample sizes. Alternatively, variation in cycle duration may be truly independent of other life-history traits.

The genotype least square means of the three remaining variables, which represent allocation to female repro-

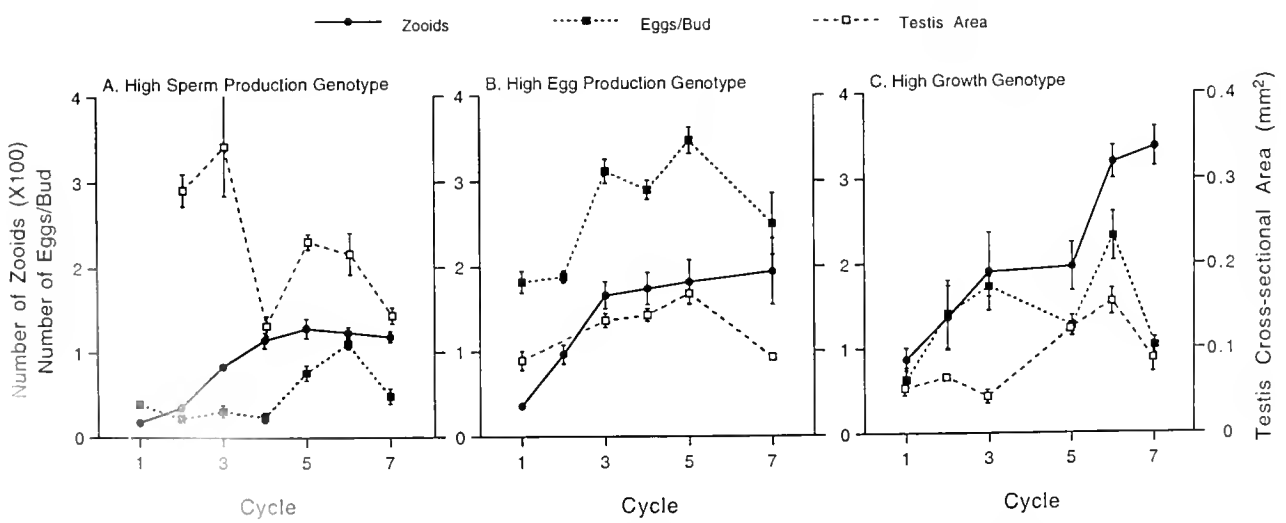

Figure 2. Growth and sexual reproduction trajectories for three of the more extreme *Botryllus schlosseri* genotypes in this study. Average eggs per bud, colony size, and testis cross-sectional area are plotted against cycle number. Error bars represent 1 standard error. (A) A high-sperm-production genotype. (B) A high-egg-production genotype. (C) A high-growth genotype.

Table III

Clonal repeatabilities, genotype ranges, genotype least square means ranges (adjusting for cycle effects in four of the variables), and the magnitude of genotype least square means variation (highest genotype value divided by lowest genotype value) for the six life-history variables

Variable	Clonal repeatability	Genotype means		Genotype least square means		
		Highest	Lowest	Highest	Lowest	Magnitude
Eggs per bud	0.47	2.63	0.68	2.77	0.62	×4.5
Testis area (mm^2)	0.42	0.23	0.08	0.25	0.07	×3.5
Sperm count ($\times 10^3$)	0.75	196.4	42.0	196.4	42.0	×4.7
Buds per zooid	0.21	1.89	0.99	1.92	0.79	×2.4
Terminal size	0.57	338.3	78.3	338.3	78.3	×4.3
Cycle duration	0.20	8.19	6.33	8.68	6.28	×1.4

duction (eggs per bud), male reproduction (testis cross-sectional area), and asexual growth (buds per zooid) at the zooid level, exhibit somewhat more complex correlations. First, there are significant negative univariate correlations between buds per zooid and both eggs per bud and testis area (Table IVA). In contrast, the correlation between eggs per bud and testis area is virtually zero (Table IVA). However, the partial correlation coefficients between each pair of traits (which in each case adjust for the effect of the third variable) suggest a much stronger relationship in three-dimensional space. All three partial correlations are much more strongly negative than the respective univariate correlations, especially the partial correlation between eggs per bud and testis area (Table IVB). This pattern suggests a negative, three-way correlation among these three variables that is consistent with a tradeoff in resource allocation among male, female, and asexual reproduction.

These negative correlations can also be examined by visualizing the relationships among these variables in three dimensions (Fig. 3). The data points fall primarily on a plane that intersects the egg per bud, testis cross-sectional area, and buds per zooid axes at relatively high values (Fig. 3). A principal components analysis provides an additional assessment of the dimensionality of this data cloud (Table V). The first two principal components have relatively high eigenvalues and in combination explain more than 92% of the variance in the data set (Table V). The third principal component has a low eigenvalue and explains less than 8% of the variance (Table V). This result indicates that the data points cluster

Table IV

Correlations among genotype least square means

	Testis area	Sperm count	Buds per zooid	Terminal size	Cycle duration
A. Univariate (Pearson's product moment) correlation coefficients between each pair of variables (all pairs)[1]					
Eggs per bud	0.01 NS	−0.21 NS	−0.59**	−0.34 NS	−0.06 NS
Testis area		−0.87**	−0.48*	−0.46 NS	0.12 NS
Sperm count			−0.41 NS	−0.30 NS	0.02 NS
Buds per zooid				0.52*	0.19 NS
Terminal size					−0.09 NS
B. Partial correlation coefficients among the three zooid-level variables[2]					
Eggs per bud	−0.48*		−0.67**		
Testis area			−0.59**		

Note: $*P < 0.05$; $**P < 0.01$; NS = Not Significant.

[1] $n = 18$ genotypes in all comparisons (16 df) except those involving sperm count in cycle 6 for which $n = 8$ (6 df).

[2] $n = 18$ in each comparison (15 df). These values represent the correlations between each pair of variables after adjusting for the effect of the third variable.

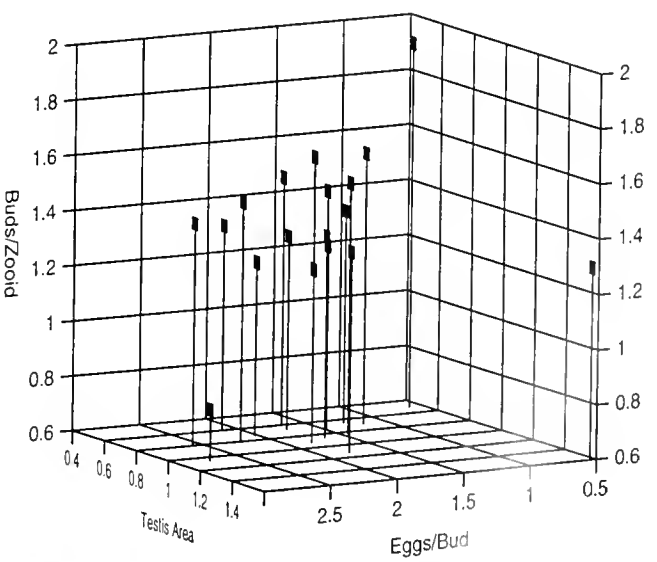

Figure 3. The three-dimensional relationship among genotype least square means for eggs per bud, testis cross-sectional area, and buds per zooid. Values for the 18 genotypes fall near a plane that slopes downward from the upper back to the lower front of the figure.

Table V

Principal components analysis of the three-way relationship among eggs per bud, testis cross-sectional area, and buds per zooid

	Principal components		
	PC 1	PC 2	PC 3
Eigenvalue	1.77	0.99	0.24
Percent of variance	59.00	33.04	7.96
Cumulative percent of variance	59.00	92.04	100.00
Eigenvector loadings			
Eggs per bud	0.55	−0.63	0.55
Testis area	0.45	0.78	0.44
Buds per zooid	−0.71	0.00	0.71

Note. The first two principal components explain most of the variance in the data and are heavily loaded on the three variables, indicating that the data points fall largely on a plane that represents a three-way tradeoff in allocation to male, female, and asexual reproduction (see text for details). Because there are only three variables in the analysis, the third principal component is completely determined by the first two; it has to explain all of the remaining variance. However, the very low magnitude of the third component is not inevitable, and it is the relative magnitude of the three principal components that describes the planar nature of the relationship among the three primary variables.

mainly on and around a plane defined by the first two principal components. The first principal component is most heavily loaded (negatively) on the variable buds per zooid, whereas the second principle component is heavily loaded on eggs per bud (negatively) and testis cross-sectional area (positively; Table V). Again, the principal components analysis demonstrates a three-way negative correlation among traits associated with male, female, and asexual reproduction.

Discussion

Genetic and environmental variation

As previously reported for other populations (Grosberg, 1988; Chadwick-Furman and Weissman, 1995), *B. schlosseri* colonies in the Damariscotta River exhibited a great deal of variation in egg production and growth rate (Table III). In addition, we found colonies to be highly variable in sperm production, with the highest sperm-production genotype yielding 4.7 times as many sperm per testis as the lowest sperm-production genotype (Table III). Variation in sperm production is reflected in the size of testes, and measurement of testis cross-sectional area provides a reasonable nondestructive estimate of actual sperm production (Fig. 1).

In contrast to a previous study (Grosberg, 1982, 1988), we found significant variation in reproductive cycle duration among genotypes. Since a colony's growth rate in reality is a function of both bud production per zooid and cycle duration, the existence of genotype-specific cycle duration suggests that caution must be used in comparing colony growth rates on the basis of budding rates alone. However, the magnitude of variation in cycle duration is relatively small compared to variation in bud production (Table III), and cycle duration does not appear to be correlated with other life-history traits. Consequently, for many purposes the inclusion of information on cycle duration may only increase variance in growth rates.

To assess temporal patterns in four of the life-history variables, we were forced to exclude genotypes with very high egg production from our common-garden experiment. Colonies with higher levels of egg production than those included here typically exhibit semelparous reproduction and then die (Grosberg, 1988), precluding the collection of data on subsequent asexual and sexual cycles. Consequently, our value for the magnitude of variation in egg production (Table III) somewhat underestimates the total variation in this natural population. Qualitatively, however, total variation in egg production in the Damariscotta River still appears to be quite a bit lower than in the Eel Pond at Woods Hole (Grosberg, 1988). Although we have collected colonies that produced up to 6 eggs per bud, colonies with egg production > 3 eggs per bud appear to be rare at all times of the year (unpubl. data). In contrast, colonies producing 8 to 12 eggs per bud dominate populations in the Eel Pond in early summer (Grosberg, 1988). Although we know that we underestimated total phenotypic variation in egg production, we can only speculate on the effect that excluding higher egg producers may have had on our estimates of variation in other life-history traits. If the negative correlations among male, female, and asexual reproduction (Fig. 3, Tables IV and V) are maintained across higher levels of egg production, then the range of variation in the other life-history traits may have been affected as well. Consequently, our range estimates for life-history traits (Table III), though demonstrating a large degree of variation in this population, are likely to be conservative. However, the correlation structure itself may be altered if more extreme genotypes are included in the analysis (Grosberg, 1988).

Following colonies through subsequent asexual and sexual cycles allowed us to evaluate temporal trends in female (eggs per bud), male (testis cross-sectional area), and asexual (buds per zooid) reproduction as well as cycle duration (Table II). All colonies were sexually mature when collected from the field, so the temporal patterns reported here do not simply reflect the onset of reproduction. In particular, significant variation in egg and sperm production among subsequent cycles suggests that estimates of reproductive output based on observations of a single cycle, even of sexually mature colonies, should be interpreted with caution. Additionally, the different tem-

poral patterns exhibited by different genotypes (Fig. 2) are suggestive of genotype by cycle interaction effects, which we could not explicitly test because of inadequate sample sizes in some cells. The temporal component of variation in life-history strategy in *B. schlosseri* merits a more detailed examination.

All six life-history variables that we measured exhibited significant variation among genotypes (Table I), with clonal repeatabilities (a form of broad-sense heritability) ranging from 0.20 to 0.75 (Table III). These broad-sense heritability estimates may include some forms of environmental variance, and so set an upper limit for the proportion of additive genetic variance (Falconer, 1981). Although the relatively large magnitude of most of our broad-sense heritability estimates suggests a large genetic component to phenotypic variation, environmental effects are also likely to be substantial. Grosberg (1988) has previously demonstrated that food levels can significantly alter both asexual growth rates and egg production levels in *B. schlosseri*. The temporal patterns that we observed in egg and sperm production among reproductive cycles (Table II) may reflect temporal variation in planktonic food availability. In particular, the decrease in reproductive output during the last two cycles coincided with a previously reported seasonal decrease in phytoplankton in the Damariscotta River (Incze *et al.*, 1980). Likewise, temporal patterns in cycle duration (Table II) may be due to variation in water temperature (Grosberg, 1982). Clearly, the results reported here do not constitute a definitive statement about the genetic basis of these life-history traits. Breeding experiments will ultimately be necessary to estimate narrow-sense heritabilities.

The terminal sizes of colonies in our study were substantially smaller than those reported in other studies that did not employ clonal replication (Grosberg, 1988; Chadwick-Furman and Weissman, 1995; etc.). Either colonies in the Damariscotta River cease growth at a smaller size than colonies in some other populations (Monterey Bay and the Eel Pond), or our estimates of terminal size were affected by subdividing colonies to produce clonal replicates. Field colonies in the Damariscotta River appear to frequently attain a larger size than those in our study (pers. obs.), lending credence to the latter interpretation. Although subdivision may have affected our absolute values for terminal size, all genotypes were subdivided, and hence the terminal size of subdivided colonies should nevertheless yield a valid estimate of the relative performance of each genotype.

Correlations and selection

The six life-history variables that we measured were not independent of one another. In addition to a couple of correlations between variables that measure the same or similar traits (testis cross-sectional area and sperm counts, growth rate and terminal size), we found negative partial correlations among genotype least square means for male (testis cross-sectional area), female (eggs per bud), and asexual (buds per zooid) reproduction (Table IV). The three-dimensional relationship of these variables (Fig. 3) and the results of a principal component analysis (Table V) both suggest a three-way tradeoff among these variables. Although this three-dimensional relationship is greatly strengthened by the inclusion of the three most extreme genotypes, the remaining 15 genotypes still cluster around a plane (Fig. 3) and display the same basic relationship.

One element of this multivariate correlation appears to differ slightly from the result previously reported by Grosberg (1982), who found no correlation within iteroparous colonies between asexual growth (buds per zooid) and female reproduction assayed as eggs per bud (male reproduction was not assayed). However, Grosberg (1982) did detect a negative correlation between asexual growth and lifetime egg production, which is another assay of female reproduction. Strikingly, the correlation between asexual growth and female reproduction (assayed as eggs per bud) became strongly positive when semelparous genotypes were also included in the analysis (Grosberg, 1982, 1988).

The existence of negative correlations alone indicates little about the proximate causes of life-history tradeoffs. Surgical manipulation of gamete production and growth patterns (Grosberg, 1988) could be employed to explore possible physiological mechanisms underlaying these negative correlations. However, the correlation structure that we detected is consistent with a simple energetic tradeoff in allocation to male, female, and asexual reproduction. Although a tradeoff in allocation between male and female reproduction is a common assumption of sex-allocation models for hermaphrodites (Charnov, 1979, 1982), this assumption has rarely been empirically evaluated. Although the likely consequence of a shift in resource allocation between male and female reproduction is relatively straightforward, variation in allocation to asexual reproduction has potentially more complex ramifications. Asexual reproduction increases the number of zooids in a colony and hence is likely to fundamentally alter the future energy budget of a colony by determining total food intake. Could increased allocation to asexual growth at the expense of current sexual reproduction be associated with increased sexual reproduction effort at some later point in colony ontogeny? Again, temporal allocation patterns of different genotypes (genotype by cycle interactions) merit further consideration.

The negative correlations among male, female, and asexual reproduction that we detected have important

implications for evaluating the possible consequences of selection on these life-history traits. These negative correlations are based on genotype least square means, and so represent broad-sense genetic correlations roughly comparable to estimates based on family mean values in breeding studies (Via, 1986). To the extent that these broad-sense genetic correlations reflect narrow-sense genetic correlations, they indicate that selection cannot act independently on these three traits. A change in fitness *via* increased allocation to one form of reproduction will be balanced by reduced allocation, and hence presumably reduced fitness, *via* the other two modes of reproduction. In this scenario, selection would result in evolutionary change if fitness advantages due to increased allocation to one mode of reproduction more than offset fitness costs due to decreased allocation to the other two modes.

The selective pressures acting on life-history traits in *B. schlosseri* are not completely understood. Overgrowth by colonies of the con-familial *Botrylloides diegense* has been suggested to select against semelparous, high-egg-production genotypes of *B. schlosseri* in the Eel Pond at Woods Hole (Grosberg, 1982, 1988), and this introduced spatial competitor has also been present in the Damariscotta River since the late 1970s (Yund and Feldgarden, 1992). Selection *via* fertilization processes may also be important, especially in favoring different production levels of male and female gametes (Levitan, 1995; Levitan and Petersen, 1995). For example, ecological situations in which males compete for fertilizations (Yund and McCartney, 1994) or levels of egg fertilization are sperm limited (Levitan, 1995) could both result in selection for increased production of sperm (Yund, 1997). The relaxation of those conditions would in turn favor increased allocation to egg production due to tradeoffs in allocation.

Acknowledgments

T. Miller and the other staff members of the University of Maine's Darling Marine Center made this work possible, and R. Grosberg provided valuable comments on correlations among life-history traits in *B. schlosseri*. Financial support was provided by the National Science Foundation (OCE-92-02805 and OCE-94-16548).

Literature Cited

Atkinson, O. S., and P. O. Yund. 1996. The effect of variation in population density on male fertilization success in a colonial ascidian. *J. Exp. Mar. Biol. Ecol.* **195:** 111–123.

Boyd, H. C., S. K. Brown, J. A. Harp, and I. L. Weissman. 1986. Growth and sexual maturation of laboratory-cultured Monterey *Botryllus schlosseri*. *Biol. Bull.* **170:** 91–109.

Chadwick-Furman, N. E., and I. L. Weissman. 1995. Life histories and senescence of *Botryllus schlosseri* (Chordata, Ascidiacea) in Monterey Bay. *Biol. Bull.* **189:** 36–41.

Charnov, E. L. 1979. Simultaneous hermaphroditism and sexual selection. *Proc. Natl. Acad. Sci.* USA **76:** 2480–2484.

Charnov, E. L. 1982. *The Theory of Sex Allocation.* Princeton University Press, Princeton, New Jersey.

Cohen, C. S., and R. R. Strathmann. 1996. Embryos at the edge of tolerance: effects of environment and structure of egg masses on supply of oxygen to embryos. *Biol. Bull.* **190:** 8–15.

Eckelbarger, K. J., and L. Watling. 1995. Role of phylogenetic constraints in determining reproductive patterns in deep-sea invertebrates. *Invertebr. Biol.* **114:** 256–269.

Emlet, R. B., L. R. McEdward, and R. R. Strathmann. 1987. Echinoderm larval ecology viewed from the egg. Pp. 55–136 in M. Jangoux and J. M. Lawrence, eds. *Echinoderm Studies.* Vol. 2. Balkema, Rotterdam.

Falconer, D. S. 1981. *Introduction to Quantitative Genetics* (2nd ed.). Longman, Essex, England.

Ghiselin, M. T. 1987. Evolutionary aspects of marine invertebrate reproduction. Pp. 609–665 in A. C. Giese, J. S. Pearse, and V. B. Pearse, eds. *Reproduction of Marine Invertebrates: Seeking Unity in Diversity.* Boxwood Press, Pacific Grove, CA.

Gosner, K. L. 1971. *Guide to the Identification of Marine and Estuarine Invertebrates. Cape Hatteras to the Bay of Fundy.* John Wiley, New York.

Grosberg, R. K. 1982. Ecological, genetical, and developmental factors regulating life history variation within a population of the colonial ascidian *Botryllus schlosseri* (Pallas) Savigny. Thesis. Yale University, New Haven, CT.

Grosberg, R. K. 1988. Life-history variation within a population of the colonial ascidian *Botryllus schlosseri*. I. The genetic and environmental control of seasonal variation. *Evolution* **42:** 900–920.

Harvell, C. D., and R. K. Grosberg. 1988. The timing of sexual maturity in clonal animals. *Ecology* **69:** 1855–1864.

Hendler, G. 1975. Adaptational significance of the patterns of ophiuroid development. *Am. Zool.* **15:** 691–715.

Hughes, D. J., and R. N. Hughes. 1986. Life history variation in *Celleporella hyalina* (Bryozoa). *Proc. Royal Soc. London Ser.* **B228:** 127–132.

Incze, L. S., R. A. Lutz, and L. Watling. 1980. Relationship between effects of environmental temperature and seston on growth and mortality of *Mytilus edulis* in a temperate northern estuary. *Mar. Biol.* **57:** 147–156.

Lande, R., and S. J. Arnold. 1983. The measurement of selection on correlated characters. *Evolution* **37:** 1210–1226.

Levitan, D. R. 1995. The ecology of fertilization in free-spawning invertebrates. Pp. 123–156 in L. McEdward, ed. *Ecology of Marine Invertebrate Larvae.* CRC Press, Boca Raton, FL.

Levitan, D. R., and C. Petersen. 1995. Sperm limitation in the sea. *Trends Ecol. Evol.* **10:** 228–231.

McEdward, L. R., and L. K. Coulter. 1987. Egg volume and energetic content are not correlated among sibling offspring of starfish: implications for life history theory. *Evolution* **41:** 914–917.

Menge, B. 1975. Brood or broadcast? The adaptive significance of different reproductive strategies in the two intertidal sea stars *Leptasterias hexactis* and *Pisaster ochraceus*. *Mar. Biol.* **31:** 87–100.

Milkman, R. 1967. Genetic and developmental studies on *Botryllus schlosseri*. *Biol. Bull.* **132:** 229–243.

Strathmann, R. R. 1990. Why life histories evolve differently in the sea. *Am. Zool.* **30:** 197–207.

Strathmann, R. R., and M. F. Strathmann. 1982. The relationship be-

tween adult size and brooding in marine invertebrates *Am Nat* **119:** 91–101.

Strathmann, R. R., M. F. Strathmann, and R. H. Emson. 1984. Does limited brood capacity link adult size, brooding, and simultaneous hermaphroditism? A test with the starfish *Asterina phylactica*. *Am Nat.* **123:** 796–818.

Via, S. 1986. Genetic covariance between oviposition preference and larval performance in an insect herbivore. *Evolution* **40:** 778–785.

Yund, P. O. 1991. Natural selection on hydroid colony morphology by intraspecific competition. *Evolution* **45:** 1564–1573.

Yund, P.O. 1995. Gene flow via the dispersal of fertilizing sperm in a colonial ascidian (*Botryllus schlosseri*): the effect of male density. *Mar Biol* **122:** 649–654.

Yund, P. O. 1997. The effect of sperm competition on the relationship between sperm production and reproductive success in a marine invertebrate. *Ecology* In press.

Yund, P. O., and M. Feldgarden. 1992. Rapid proliferation of histocognition alleles in populations of a colonial ascidian. *J. Exp. Zool.* **263:** 442–452.

Yund, P. O., and M. A. McCartney. 1994. Male reproductive success in colonial invertebrates: competition for fertilizations. *Ecology* **75:** 2151–2167.

Reference: *Biol. Bull.* **192:** 300–308. (April, 1997)

Compound Eye Fine Structure in *Paralomis multispina* Benedict, an Anomuran Half-Crab From 1200 m Depth (Crustacea; Decapoda; Anomura)

EISUKE EGUCHI[1], MARI DEZAWA[2], AND V. BENNO MEYER-ROCHOW[3]

[1]*Department of Biology, Yokohama City University, 22-2 Seto, Kanazawa-ku, Yokohama 236, Japan, from Japan Marine Science and Technology Center (JAMSTEC), Natsushima-cho, Yokosuka, 237, Japan;* [2]*Department of Anatomy, School of Medicine, Chiba University, Inohana, Chuo-ku, Chiba 260, Japan; and* [3]*Department of Biology (Section Animal Physiology), University of Oulu, SF-90570 Oulu, Finland*

Abstract. Fully grown, unsexed specimens of the anomuran half-crab *Paralomis multispina* Benedict were obtained from a depth of 1200 m, and the eyes of three individuals were prepared for light and electron microscopy. In their outer appearance the compound eyes of *Paralomis* resemble those of common shallow-water half-crabs (*e.g., Petrolisthes*), but facets in *Paralomis* were about 3 times larger in diameter (*i.e.*, 60 μm) and at least twice as long. Interommatidial angles ranged from 3° to 5°. The proximal width of the crystalline cone in *Paralomis* was 10 times that of its equivalent in the *Petrolisthes* eye, and the rhabdom—although only twice as long—had a radius that was 7 times greater distally and 4 times greater proximally. A clear-zone between cones and rhabdom was not developed, and cross sections of crystalline cones revealed rounded rather than square profiles. A distal retinula cell (R8) was absent, and all regular retinula cells (R1–R7) protruded microvilli of about 0.11 μm diameter in many (and not only two) directions. A maximum rhabdom occupation ratio of 85% was found in the *Paralomis* retinula, whereas in the shallow-water half-crabs the comparable figure was 35%. *Paralomis* featured a wide, rhabdomless space between basement membrane and proximal rhabdom ends; the space was occupied by reflecting cells. Primary screening pigment cells and their dark granules were present; secondary screening pigment cells, however, were replaced by reflecting cells. The anatomical modifications in the *Paralomis* eye are consistent with habitat-related adaptations seen in the eyes of other benthic and slow-moving deep-water crustaceans, but not with those of euphausiids. We conclude that the eye of *Paralomis* functions as an apposition eye, designed to maximize photon capture, especially from point sources (*i.e.*, bioluminescence) rather than extended sources. We estimate that the *Paralomis* eye is at least 150 times more sensitive to light than the eye of shallow-water *Petrolisthes*.

Received 19 June 1996; accepted 18 November 1996.

Introduction

Animals that live in or colonize greater oceanic depths face three major physical challenges (Marshall, 1957; Thorson, 1972): (a) atmospheric pressure increases by 1 with every 10 m of water; (b) ambient light levels become progressively reduced, and the spectral composition of the downwelling light changes as depth increases; and (c) the temperature of the water falls as the distance to the surface increases, except in the polar oceans (where bottom temperatures may actually lie a few degrees above those of the surface) and near hydrothermal vents.

The eyes of animals are usually attuned to the photic conditions under which they operate (Forward *et al.*, 1988), but environmental temperature and pressure also influence certain structural and functional parameters of photoreception through their effects on membrane fatty acid content and composition (Cossins and Macdonald, 1989; Sebert *et al.*, 1992; Kashiwagi *et al.*, 1996). Based

on a number of light microscopical (Beddard, 1890; Welsh and Chace, 1937, 1938; Zharkova, 1970, 1975; Bursey, 1975) and electron microscopical studies of deep-water crustacean eyes (Elofsson and Hallberg, 1977; Ball, 1977; Hallberg, 1977; Meyer-Rochow and Walsh, 1977, 1978; Hallberg *et al.*, 1980; Gaten *et al.*, 1992; Gaten, 1994; Nuckley *et al.*, 1996), certain general trends concerning their anatomy and performance in relation to depth have become apparent.

Bath pelagic and benthic species of depths exceeding 1000 m usually exhibit small and degenerate eyes (similar to those of species known from marine caves (Meyer-Rochow and Juberthie-Jupeau, 1987). Crustaceans inhabiting zones above 1000 m, on the other hand, frequently possess adaptations such as enlarged ommatidia, more voluminous rhabdoms, presence of retinal reflectors, *etc.*, to improve the efficiency of photon capture. Often such adaptations enhance overall sensitivity at the expense of acuity, but in cases where acuity apparently suffers little degradation, regional eye modifications and special optical designs may be employed as, for instance, in the Euphausiaceae (Land *et al.*, 1979; Hiller-Adams and Case, 1984). Most euphausiids, however, are luminescent and thus not necessarily representative of other groups of crustaceans. For that reason and the fact that few species of deep-sea crustaceans have had their photoreceptors studied, we decided to examine the eyes of the anomuran decapod half-crab *Paralomis multispina* from a depth of 1200 m and compare them with those of shallow-water anomurans investigated earlier (Eguchi *et al.*, 1982; Meyer-Rochow *et al.*, 1990; Gaten, 1994).

Materials and Methods

Several unsexed specimens of *Paralomis multispina* Benedict (Decapoda, Anomura, Galatheoidea) with carapace widths ranging from 5 to 11 cm and maximum body lengths (from head to tail) of 11.5 cm (Fig. 1a) were obtained in March 1992. Collections were made from the "Hatsushima seep" (Ohta *et al.*, 1987) at a depth of 1200 m about 5 km off Hatsushima Island in Sagami Bay (Shizuoka Prefecture, Japan) during a cruise of the manned research submersible *Shinkai 2000* (JAMSTEC). The half-crabs themselves are not considered to be thermophilic, although they occurred in association with the giant clam *Calyptogena soyae*, vestimentiferan tube worms, gastropods, and polychaetes (Hashimoto *et al.*, 1987) in an area that was characterized by an extremely high methane content. The half-crabs were picked up from the seafloor with remotely controlled artificial arms and put in a basket attached to the outside of the submersible. It took about 1 h for the submersible, with the collected animals, to reach the surface at about 1700 h.

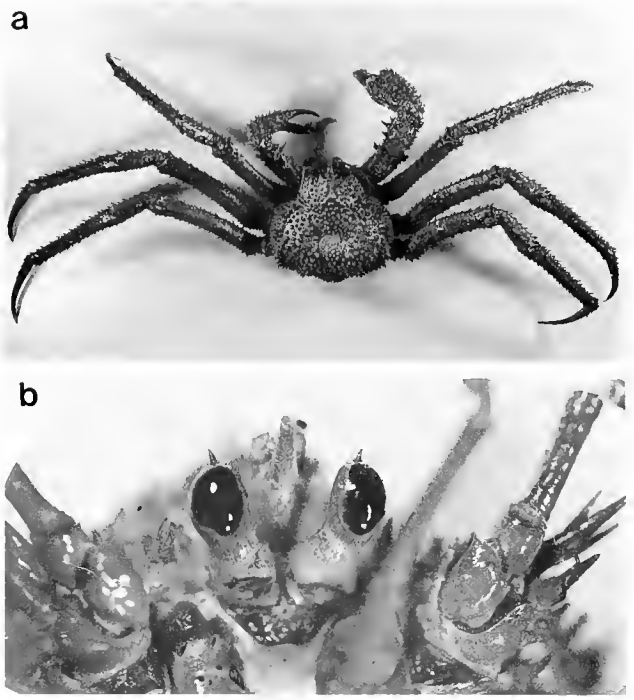

Figure 1. Photographs of *Paralomis multispina*. (a) Dorsal view of specimen with carapace width of 11 cm and legs 30 cm long. (b) Close-up of head region with pair of eyestalks and black shiny eyes, each measuring about 4 mm in length in this specimen.

During capture, the animals were exposed to 10,000–20,000 lux bright sunlight for about 20 min, but immediately after they had been hauled on board the mothership *Natsushima*, the compound eyes of three individuals were fixed for 12 h at 4°C in 2% glutaraldehyde and 2% paraformaldehyde solution, buffered to a pH of 7.3 with 0.1 *M* cacodylate buffer. The dissections were carried out under dim red light to minimize further exposure to light and structural damage (*cf.* Meyer-Rochow, 1994). After a brief wash in buffer, the specimens were postfixed for 2 h in 2% OsO_4 solution, using the same buffer as before, and dehydrated in a graded series of acetone before being embedded in Epon 812. Ultrathin sections, cut with a diamond knife, were picked up on uncoated 200-mesh copper grids and stained with uranyl acetate and lead citrate for a few minutes. Observations were carried out under a JEM 1200EX transmission electron microscope, operated at 80 kV.

Results

In their external appearance the compound eyes of the deep-sea anomuran *Paralomis multispina* (Fig. 1b) resemble those of other common anomuran shore-crabs (*e.g.*, genus *Petrolisthes:* Eguchi *et al.*, 1982; Meyer-Ro-

chow *et al.*, 1990), but overall the eyes are considerably larger. They are oval in outline and measure 3.5 × 2.5 mm in an individual of about 10 cm carapace width. Each eye sits at the tip of an eyestalk that is 4–5 mm thick and 12 mm long; thus inter-eye distances and the precise location of the eyes in space are to a certain extent variable. Ommatidial numbers increase with age: whereas a specimen with a carapace length of 5 cm has about 1500 facets, some 2400 were counted in a specimen with a carapace width of 10 cm.

Interommatidial angles apparently do not change significantly with age and measure about 3°–5°. Figure 2 provides a comparison between the ommatidia, shown in identical scale, of a shallow-water anomuran and the deep-water species *Paralomis multispina*. Biometrical

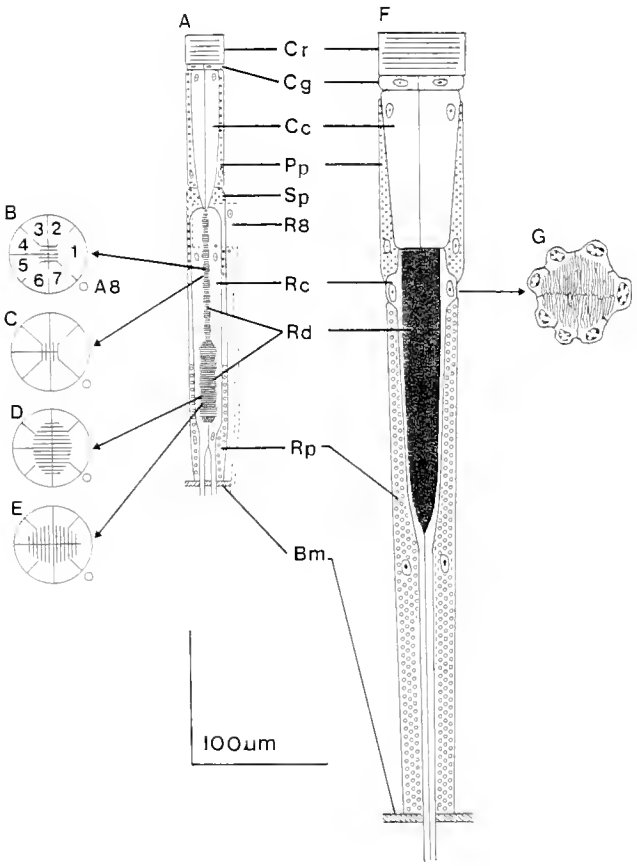

Figure 2. D[illegible] comparable ommatidia of *Petrolisthes* sp. (A–E), found in s[illegible]r, and *Paralomis multispina* (F, G), found in the deep-sea at t[illegible]itive scale. A8 = axon of distal retinula cell R8; Bm = basem[illegible]rane; Cc = crystalline cone; Cg = corneagenous cell; Cr = c[illegible] R8 = distal retinula cell; Rc = retinula cell; Rh = rhabdom; Rp = [illegible]flecting pigment cell; Sp = screening pigment. (A) longitudinal section; (B, C) cross sections at the level of two bands in the distal layers of the rhabdom; (D, E) cross sections of adjacent bands in the proximal rhabdom layers. (F) longitudinal section; (G) cross section at distal rhabdom layers.

data of the constituent parts of one representative central ommatidium of the compound eye of the two crustaceans are given in Table I. From Figure 2 and Table I it is evident that the ommatidium of the deep-sea half-crab is much larger than that of the shallow-water species, even if differences in body size are taken into consideration.

Dioptric apparatus

A single facet of the eye of *Paralomis* is about 3 times larger in diameter and has a corneal lens that is 1.8 times thicker than that of a comparable shallow-water *Petrolisthes*. No significant difference between the two types could be detected, however, in the 200 µm thick periodic layers, revealed in longitudinal sections of the cornea along the optic axis. Two corneagenous cells, not noticeably different from those of *Petrolisthes* or any other decapod crustacean, occupied the space between cornea and cone.

The crystalline cone of *Paralomis* tapered only very gently and retained a much wider proximal diameter (Fig. 3a) than that of *Petrolisthes*. Whereas in *Petrolisthes*, cross sections through distal and central regions of the cone displayed square profiles and a content of electron-dense material, sections through the cone of *Paralomis* at corresponding levels exhibited rather circular outlines and a content of much looser consistency (Fig. 3b). When related to overall ommatidial length, the dioptric apparatus in the eye of *Paralomis* (though greatly enlarged in diameter) occupied significantly less space than the equivalent structure in the eye of the shallow-water *Petrolisthes*.

Retinula and rhabdom

In the eyes of other anomuran species—for example, *Petrolisthes* spp. (Eguchi *et al.*, 1982; Meyer-Rochow *et al.*, 1990) and *Munida* spp. (Bursey, 1975; Gaten, 1994)—a distal retinula cell (R8) with four cytoplasmic lobes occupies the tier between the crystalline cone and the seven regular retinular cells, but in *Paralomis* an ommatidial retinula is composed of only seven regular cells (1–7) and lacks the distal eighth cell. The distal end of the rhabdom is thus made up of seven regular retinula cells, which are in contact with the proximal end of the crystalline cone. It is in this region that the mottled retinula cell nuclei, with a maximum diameter of 7.5 µm, can be found.

The rhabdoms in *Paralomis* are extraordinarily well developed and occupy up to 85% of the available cytoplasmic space in the distal and central regions of the retinula (Fig. 4). The estimated membrane surface of an ommatidial rhabdom of *Paralomis* (231 × 10^4), calcu-

Table I

Comparison of biometrical data (in μm) of ommatidia in the shallow-water Petrolisthes sp. *and the deep-sea* Paralomis multispina

	Petrolisthes	*Paralomis*	*Para/Petro*	Remarks
Cornea				
diameter	21	60	2.9	
thickness	16	28	1.8	
Crystalline cone				
distal diameter	20	56	2.8	length of a square side
prox. diameter	4	40	10.0	
length	110	110	1.0	
Ommatidial retinula				
length	60	390	2.6	
diameter	20	40	2.0	
Rhabdom				
diameter at nuclear layer	3.5	25	7.1	
diameter at proximal layer	3 × 8*	18	3.7	*rectangular
length	50	210	1.9	
thickness of one band	7	4–7	0.6–1.0	
diameter of one microvillus	0.08	0.11	1.4	
area of rhabdom membrane	8.5×10^4	231×10^4	27.2	total surface of microvilli/ommatidium
Rhabdom occupation ratio (%)				
distal and central region	12	85	6.3	
proximal region	35	45	1.3	
Distance from rhabdom end to BM	12	180	15.0	
Interommatidial angle	4–6°	3–5°	*ca.* 0.9	
Sensitivity	0.23	34.7	151	relat. sensitivities (after Land, 1981)

lated from the data in Table I, is about 27 times larger than that of *Petrolisthes* (8.5×10^4). Another comparison could be made with *Limulus*, which—even though it is not a crustacean—has a compound eye (Fahrenbach, 1969) superficially similar to that of *Paralomis*, but with rhabdom occupation ratios generally lower than 10%. On the other hand, the hydrothermal vent shrimp *Rimicaris exoculata* occurs in a habitat similar to that of *Paralomis*, but its eye is highly aberrant, with volume densities of rhabdoms reaching 70%–80% (O'Neill *et al.*,

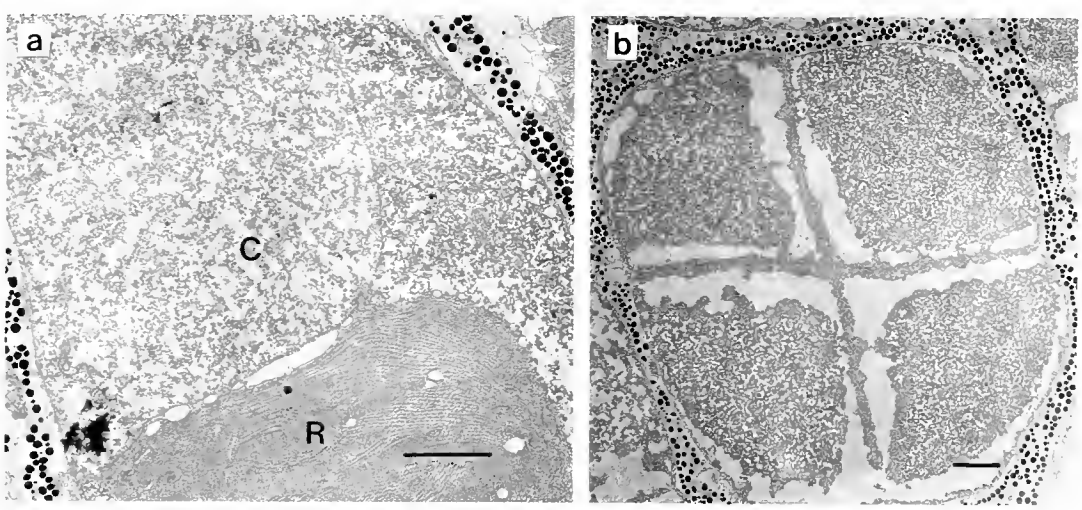

Figure 3. The deep-sea half-crab *Paralomis multispina*. (a) Longitudinal section through the proximal region of the crystalline cone and the distal tip. C = crystalline cone; R = rhabdom. Scale bar = 5 μm. (b) Cross section through proximal part of crystalline cone with its four components. Numerous screening pigment granules surround the crystalline cone. Scale bar = 5 μm.

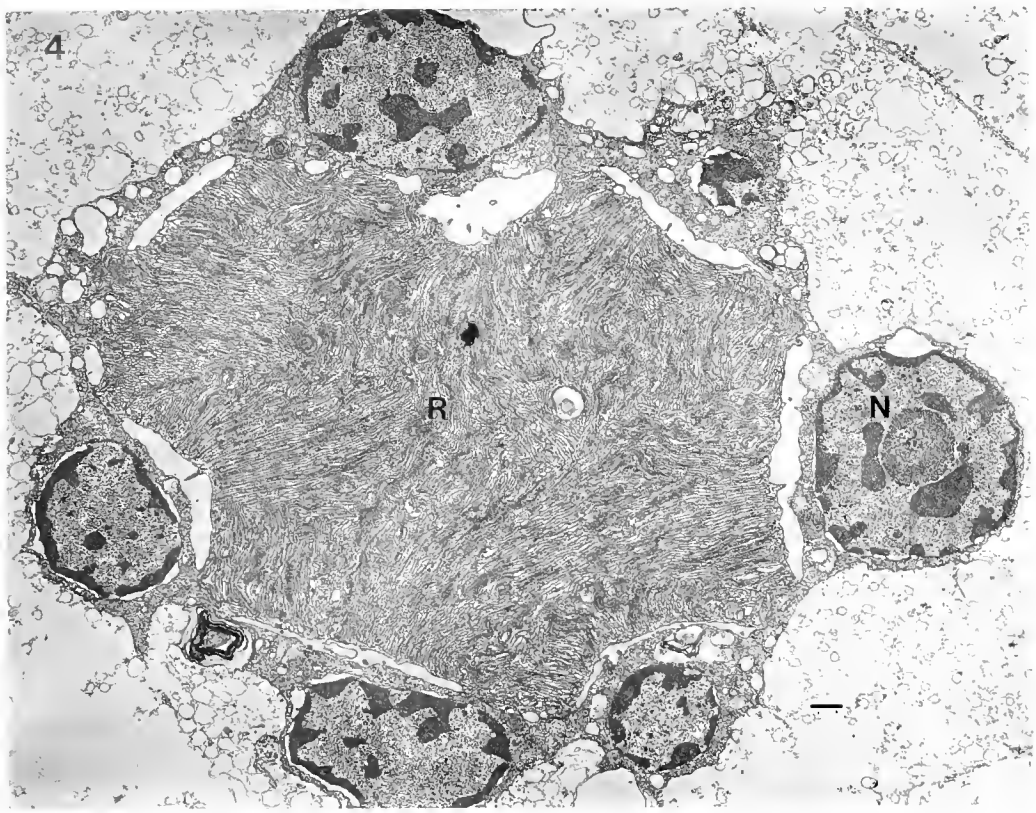

Figure 4. Cross section of rhabdom at the retinula cell nuclear layer. Almost the entire cytoplasmic space of the retinula cells is occupied by the rhabdomeres. N = nucleus of retinula cell; R = rhabdom. Scale bar = 1 μm.

1995). The retinula cells do not form proper rhabdoms in the proximal region; instead they gradually turn into slender axonal processes (Fig. 5).

Longitudinal sections reveal that the regular "bands," so typical for the rhabdoms of other decapods (including those of the shallow-water anomuran species), are almost lost in *Paralomis* and are replaced by microvilli running in many directions. This gives the rhabdom a somewhat irregular, disorderly appearance. Individual microvilli in *Paralomis* (Fig. 6) were thicker (0.11 μm) than those of fully grown shallow-water *Petrolisthes* (0.08 μm: Eguchi *et al.*, 1982; Meyer-Rochow and Reid, 1996). This difference has to be interpreted with caution, since it is known from other crustacean eyes (*e.g.*, *Orchomene* sp.: Meyer-Rochow, 1981; *Mysis relicta*: Lindström *et al.*, 1988) that rhabdom microvilli have a tendency to swell and increase diameter when suddenly exposed to very bright light.

A core-filament, usually identifiable in the lumen of a rhabdom microvillus of the crustacean eye, was [illegible] or fragmented into smaller pieces (Fig. 7). Some rhabdom microvilli exhibited flattened or swollen structures in the place where core-filaments with their associated side-arms should have been. Since core-filaments and their associated side-arms in compound eyes are fragile and easily destroyed by irradiation with bright light (Blest *et al.*, 1982; Tsukita *et al.*, 1988), their disruption in our material could stem from the brief exposure to sunlight during capture.

Screening pigment

The eye of *Paralomis* lacks secondary pigment cells; two primary pigment cells are found around the crystalline cones and contain spherical electron-opaque pigment grains of about 0.4 μm in diameter (Fig. 3a). The density of these granules seems not to differ from that of granules in the shallow-water half-crabs, but screening pigment granules in the retinula cells are far less numerous in *Paralomis*. In place of secondary pigment cells are an unknown number of cells presumed to contain reflecting granules.

Reflecting pigment

The distance between the proximal end of the rhabdom and the basement membrane of an ommatidium is relatively short in *Petrolisthes* and other shallow-water

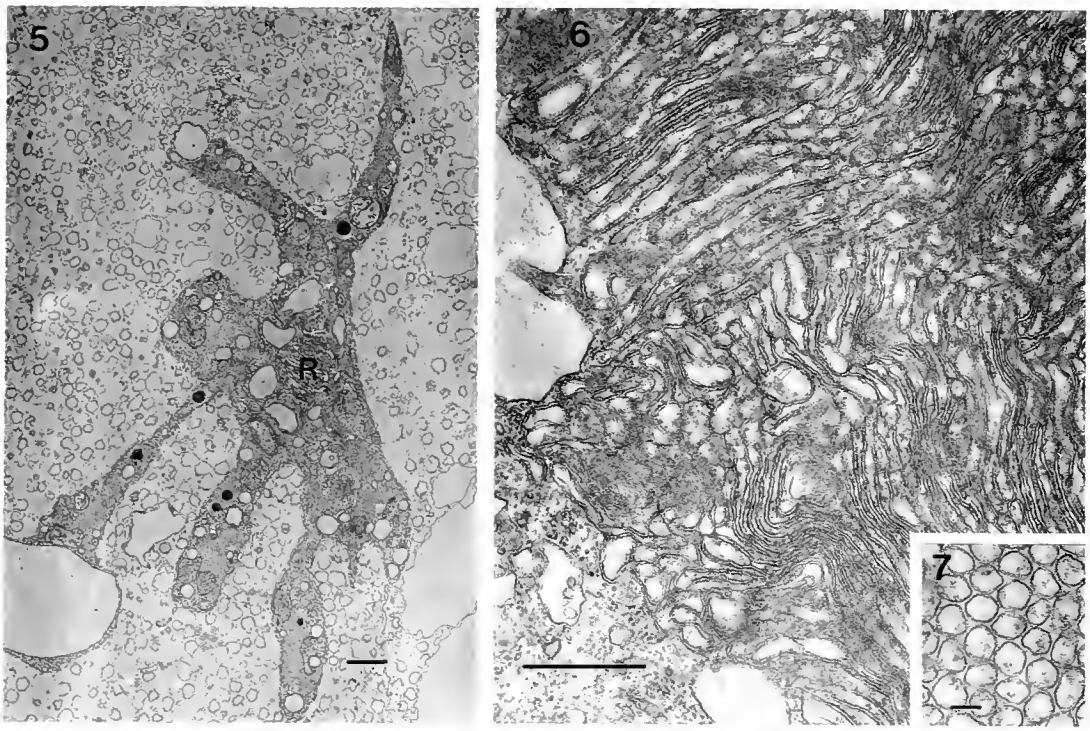

Figure 5. Cross section through proximal retinal layer. A small rhabdom (R) is seen at the center of a cluster of seven retinula cells. A few scattered screening pigment granules are visible in some of the retinula cells. Well-developed reflecting pigment cells fill the interommatidial spaces. Scale bar = 1 μm.

Figure 6. Cross section through a segment of a retinula cell demonstrating the multidirectional orientation of microvilli in the rhabdom. Scale bar = 1 μm.

Figure 7. Higher magnification of transversely cut microvilli of the rhabdom. Note that core-filaments are lost in some of the microvilli. Scale bar = 0.1 μm.

decapods. In *Paralomis*, however, this same distance is strikingly long (*ca.* 180 μm). In the proximal layer, the retinula cells become slender as shown in Figure 5. The space thus made available is filled with enormously developed cells containing large amounts of reflecting pigments. The extensions of the reflecting pigment cells, which are easily identifiable by their innumerable 0.3-μm-wide vesicles, penetrate between the retinula cells of individual ommatidial units, thus apparently increasing their effectiveness in reflecting light towards the more distally placed rhabdom.

Discussion

Eguchi *et al.* (1982) suggested that anomuran half-crabs of the superfamily Galatheoidea possess reflecting superposition eyes. Research by Meyer-Rochow *et al.* (1990) on the galatheid *Petrolisthes elongatus* and by Gaten (1994) on *Munida rugosa* lent further support to this notion, but specified that this was true only for the dark-adapted eye; in the light-adapted state apposition optics were used. It is generally assumed that superposition eyes are more useful than apposition eyes in dim light, for the former are typical of many nocturnal crustaceans and deep-sea forms.

It is, therefore, a little surprising to find that the eye of the deep-sea anomuran galatheid *Paralomis multispina* (a) lacks a wide clear-zone, which is normally considered a prerequisite for any form of superposition vision (Land, 1981), and (b) possesses roundish rather than regular, square cones, which are an essential requirement for reflecting superposition (Land, 1976; Vogt, 1980). The species does, however, exhibit other kinds of modifications that are more in keeping with adaptations to an extremely dim environment: compared with the shallow-water half-crabs of the genus *Petrolisthes* (Eguchi *et al.*, 1982; Meyer-Rochow *et al.*, 1990), in *Paralomis* the corneal diameter is three times greater, and cone as well as rhabdom diameters are even more enlarged (Table I). The reflecting tapetum on the proximal side of the retinula is massively developed, and it is evident that the eye is designed to maximize photon capture. The fine-struc-

tural disruptions and larger diameters of the rhabdom microvilli seen in *Paralomis* are almost identical to those reported from the eyes of deep-water amphipods from the Antarctic (Meyer-Rochow, 1981) and are most likely caused by the exposure to bright light during capture. Indirectly the disruptions thus point to a high absolute sensitivity to light, but at the same time they obscure signs for or against membrane shedding (*cf.* Chamberlain and Barlow, 1984).

On the basis of the definition that Land (1981) provided for "absolute sensitivity," we calculated sensitivities of light-adapted eyes of *Paralomis* and those of shallow-water *Petrolisthes:* the eye of *Paralomis* was 150 times more sensitive. The comparison is based on the assumptions that the extinction coefficient (k) is the same for the two species and that the types and densities of pigments found in the rhabdoms are identical (*cf.* discussion in Ziedins and Meyer-Rochow, 1990). If one assumes a superior photopigment content in the dark-adapted *Paralomis* eye and considers thermal noise reduction at low environmental temperatures (Aho *et al.*, 1988), the overall sensitivity advantage of *Paralomis* over *Petrolisthes* to extended light sources may be even higher.

If the lack of a clear-zone is real and not artifactual (clear-zones in the superposition eyes of deep-sea decapods can easily collapse and, on account of their fragility and delicateness, may remain undetected as shown by Nilsson, 1990), the closer approximation of the massively developed rhabdom to the much wider dioptric elements, in combination with the backing of a tapetum from behind, could be interpreted as an adaptation to improve sensitivity, especially to point sources. The shortening of both cornea and cone, relative to the overall length of one ommatidium, and the loss of the orderly arrangement of microvilli in the rhabdom also point toward an adaptation to minimize photon loss and maximize photon capture (Laughlin *et al.*, 1975). The considerably greater rhabdom-occupation ratio in the eye of *Paralomis* as compared with the shallow-water species not only allows more photopigment molecules to be packed into the visual membranes, but also indicates low energy demand and slow cellular metabolism, both adaptations that are extremely useful in the deep-sea environment (Elofsson and Hallberg, 1977).

In the shallow-water *Petrolisthes elongatus* the eye enlarges as the half-crab grows; ommatidia are added and sensitivity to both extended and point sources increases. *P. elongatus* uses vision to detect and approach hiding places (Meyer-Rochow and Meha, 1994). Since signs of eye regression in adult *Paralomis* are missing, we must assume that the general growth pattern resembles that of *Petrolisthes.* This, however, raises the question of what *Paralomis* could possibly see at a depth of 1200 m, the "limit" beyond which sunlight can no longer be detected (Clarke and Kelly, 1964). Biological light sources, however, abound at this depth (Omori, 1974), and it may well be in the interest of a benthic, sedentary detritus and filter feeder to notice them. Any visual signal adult *Paralomis* could possibly be interested in would almost never come from below, and this could explain the lack of regional eye specializations seen in so many mesopelagic shrimps (Gaten *et al.*, 1992).

We know nothing about the spectral sensitivity of *Paralomis,* but the visual pigments of eight other anomuran species all exhibit a single absorption peak in the bluegreen region of the spectrum (Cronin and Forward, 1988). Ziedins and Meyer-Rochow (1990) electrophysiologically measured spectral sensitivity peaks of dark- and light-adapted eyes of *P. elongatus* and also found them to lie in the bluegreen part of the spectrum. Since even the eyes of the hydrothermal vent species *Rimicaris exoculata,* which are strongly modified morphologically (O'Neill *et al.*, 1995), possess a sensitivity peak in the bluegreen (Johnson *et al.*, 1995), we do not expect the eyes of *Paralomis* to differ in this respect. However, the lack of secondary screening pigments and retinula cell 8 in *Paralomis* suggests that the eye of *M. rugosa,* for example, is less well adapted to the greatest depth of its range (shallow water down to 1250 m: Gaten, 1994) than that of *Paralomis. M. rugosa* appears to be a relative "newcomer" to the deep-sea, while *Paralomis* has been exploiting that habitat for a longer evolutionary period. How much longer is hard to say, but Nuckley *et al.* (1996) speculate that a hydrothermal vent shrimp with modified eyes may have "migrated from the surface possibly in the last 5,000–10,000 years" and over that period evolved its present eye morphology.

In conclusion, the hypertrophied rhabdoms in the eye of *Paralomis,* the loss of the orderly microvillus arrangement, the reduction of the cytoplasmic component of the retinula cells, the massively developed layer of reflecting vesicles in the proximal half of the retinula, and (considering overall ommatidial length) the relative shortening of the dioptric elements coincident with greatly enlarged diameters in the eye of *Paralomis* are all consistent with depth-related adaptations seen also in the eyes of deep-sea mysids (Elofsson and Hallberg, 1977), amphipods (Hallberg *et al.*, 1980; Meyer-Rochow *et al.*, 1991), and to some extent other benthic decapods (Hiller-Adams and Case, 1985) and mesopelagic shrimps (Gaten *et al.*, 1992). However, the eyes of deep-water euphausiids (Hiller-Adams and Case, 1988) are least similar to those of *Paralomis* and this, we believe, has to do with (a) the widespread ability of euphausiids to produce light, (b) the greater mobility and pelagic lifestyles of euphausiids,

and (c) the longer evolutionary period euphausiids have had to adapt their photoreceptors to the deep-sea environment.

Acknowledgments

We thank the *Shinkai 2000* operation team and the Japan Marine Science and Technology Center (JAMSTEC) (Natsushimacho, Yokosuka, Japan) for their kind offer to assist in the procurement of the material. We also wish to acknowledge that through the constructive criticism of two anonymous referees we were able to improve the paper.

Literature Cited

Aho, A. C., K. O. Donner, C. Hyden, L. O. Larsen, and T. Reuter. 1988. Low retinal noise in animals with low body temperatures allows high visual sensitivity. *Nature* **334:** 348–350.

Ball, E. E. 1977. Fine structure of the compound eyes of the midwater amphipod *Phronima* in relation to behaviour and habitat. *Tissue Cell* **9:** 251–536.

Beddard, F. E. 1980. On the minute structure of the eye in some shallow-water and deep-sea species of the isopod genus *Acturus*. *Proc. Zool. Soc. Lond.* **26:** 365–375.

Blest, D., S. Stowe, and W. Eddy. 1982. Cytoskeleton in rhabdomeral microvilli of blowflies. *Cell Tissue Res.* **223:** 553–573.

Bursey, C. R. 1975. The microanatomy of the compound eye of *Munida irrasa* (Decapoda: Galatheidae). *Cell Tissue Res.* **160:** 505–514.

Chamberlain, S. C., and R. B. Barlow, Jr. 1984. Transient membrane shedding in *Limulus* photoreceptors: control mechanisms under natural lighting. *J. Neurosci.* **4:** 2792–2810.

Clarke, G. L., and M. G. Kelly. 1964. Variation in transparency and in bioluminescence on longitudinal transects in the western Indian Ocean. *Bull. Inst. Oceanogr. (Monaco)* **64:** 1–20.

Cossins, A. R., and A. G. Macdonald. 1989. The adaptation of biological membranes to temperature and pressure: fish from the deep and cold. *J. Bioenerg. Biomembr.* **21:** 115–135.

Cronin, T. W., and R. B. Forward. 1988. The visual pigments of crabs. I. spectral characteristics. *J. Comp. Physiol. A* **162:** 463–478.

Eguchi, E., T. Goto, and T. H. Waterman. 1982. Unorthodox pattern of microvilli and intercellular junctions in regular retinular cells of the porcellanid crab *Petrolisthes*. *Cell Tissue Res.* **222:** 493–513.

Elofsson, R., and E. Hallberg. 1977. Compound eyes of some deep-sea and fiord mysid crustaceans. *Acta Zool. (Stockh.)* **58:** 169–177.

Fahrenbach, W. H. 1969. The morphology of the eyes of *Limulus*—II. Ommatidia of the compound eye. *Z. Zellforsch.* **93:** 451–483.

Forward, R. B., T. W. Cronin, and J. K. Douglass. 1988. The visual pigments of crabs. II. environmental adaptations. *J. Comp. Physiol. A* **162:** 479–490.

Gaten, E. 1994. Geometrical optics of a galatheid compound eye. *J. Comp. Physiol. A* **175:** 749–759.

Gaten, E., P. M. J. Shelton, and P. J. Herring. 1992. Regional morphological variations in the compound eyes of certain mesopelagic shrimps in relation to their habitat. *J. Mar. Biol. Assoc. UK* **72:** 61–75.

Hallberg, E. 1977. The fine structure of the compound eyes of mysids (Crustacea: Mysidacea). *Cell Tissue Res.* **184:** 45–65.

Hallberg, E., H. Nilsson, and R. Elofsson. 1980. Classification of amphipod compound eyes—the fine structure of the ommatidial units (Crustacea, Amphipoda). *Zoomorphology* **94:** 279–306.

Hashimoto, J., T. Tanaka, S. Matsuzawa, and H. Hotta. 1987. Surveys of the deep-sea communities dominated by the giant clam *Calyptogena soyae* along the slope foot of Hatsushima Island, Sagami Bay. *JAMSTECTR Deepsea Res.* **3:** 37–51.

Hiller-Adams, P., and J. F. Case. 1984. Optical parameters of euphausiid eyes as a function of habitat depth. *J. Comp. Physiol.* **154:** 307–318.

Hiller-Adams, P., and J. F. Case. 1985. Optical parameters of the eyes of some benthic decapods as a function of habitat depth. *Zoomorphology* **105:** 108–113.

Hiller-Adams, P., and J. F. Case. 1988. Eye size of pelagic crustaceans as a function of habitat depth and possession of photophores. *Vision Res.* **28:** 667–680.

Johnson, M. L., P. M. J. Shelton, P. J. Herring, and S. Gardner. 1995. Spectral responses from the dorsal organ of a juvenile *Rimicaris exoculata* from the TAG-hydrothermal vent site. *Bridge Newslett.* **8:** 38–42.

Kashiwagi, T., V. B. Meyer-Rochow, K. Nishimura, and E. Eguchi. 1996. Fatty acid composition and ultrastructure of photoreceptive membranes in the crayfish *Procambarus clarkii* under conditions of thermal and photic stress. *J. Comp. Physiol. B:* In press.

Land, M. F. 1976. Superposition images are formed by reflection in the eyes of some oceanic decapod Crustacea. *Nature* **263:** 764–765.

Land, M. F. 1981. Optics and vision in invertebrates. Pp. 471–492 in *Vision in Invertebrates* (Handbook of Sensory Physiology, Vol. VII/6B), H. Autrum, ed. Springer, New York.

Land, M. F., F. A. Burton, and V. B. Meyer-Rochow. 1979. The optical geometry of euphausiid eyes. *J. Comp. Physiol.* **130:** 49–62.

Laughlin, S. B., R. Menzel, and A. W. Snyder. 1975. Membranes, dichroism and receptor sensitivity. Pp. 237–262 in *Photoreceptor Optics*, A. W. Snyder and R. Menzel, eds. Springer, New York.

Lindström, M., H. Nilsson, and V. B. Meyer-Rochow. 1988. Recovery from light-induced sensitivity loss in the eye of the crustacean *Mysis relicta* in relation to temperature: a study of ERG-determined V/log I relationships and morphology at 4°C and 14°C. *Zool. Sci.* **5:** 743–757.

Marshall, N. B. 1957. *Tiefseebiologie*. VEB, Jena, Germany.

Meyer-Rochow, V. B. 1981. The eye of *Orchomene* sp. cf. *O. rossi*, an amphipod living under the Ross Ice Shelf (Antarctica). *Proc. R. Soc. Lond. B Biol. Sci.* **212:** 93–111.

Meyer-Rochow, V. B. 1994. Light-induced damage to photoreceptors of spiny lobsters and other crustaceans. *Crustaceana* **67:** 97–111.

Meyer-Rochow, V. B., and J. Juberthie-Jupeau. 1987. An electron microscope study of the eye of the cave mysid *Heteromysoides cotti* from the Island of Lanzarote (Canary Isl.). *Stygologia* **3:** 24–34.

Meyer-Rochow, V. B., and W. P. Meha. 1994. Tidal rhythm and the role of vision in shelter-seeking behaviour of the half-crab *Petrolisthes elongatus* (Crustacea: Anomura). *J. R. Soc. NZ* **24:** 423–428.

Meyer-Rochow, V. B., and W. A. Reid. 1996. Does age matter in studying the crustacean eye? *J. Comp. Physiol. B.* In press.

Meyer-Rochow, V. B., and S. Walsh. 1977. The eyes of mesopelagic crustaceans I. *Gennadas* sp. (Penaeidae). *Cell Tissue Res.* **186:** 87–101.

Meyer-Rochow, V. B., and S. Walsh. 1978. The eyes of mesopelagic crustaceans III. *Thysanopoda tricuspidata* (Euphausiaceae). *Cell Tissue Res.* **195:** 59–79.

Meyer-Rochow, V. B., D. Towers, and I. Ziedins. 1990. Growth patterns in the eye of *Petrolisthes elongatus* (Crustacea; Decapoda; Anomura). *Exp. Biol.* **48:** 329–340.

Meyer-Rochow, V. B., H. Stephan, and S. D. Moro. 1991. Morphological and anatomical observations on the hairy eyes of males and females of the marine amphipod *Dulichia porrecta* (Crustacea, Amphipoda, Podoceridae). *Boll. Zool.* **58:** 59–69.

Nilsson, D.-E. 1990. Three unexpected cases of refracting superposition eyes in crustaceans. *J. Comp. Physiol. A* **167:** 71–78.

Nuckley, D. J., R. N. Jinks, B.-A. Battelle, E. D. Herzog, L. Kass, G. H. Renninger, and S. C. Chamberlain. 1996. Retinal anatomy of a new species of bresiliid shrimp from a hydrothermal vent field on the mid-atlantic ridge. *Biol. Bull.* **190:** 98–110.

Ohta, S., H. Sakai, A. Taira, K. Ohwada, T. Ishii, M. Maeda, K. Fujioka, T. Saino, K. Kogure, T. Gamo, Y. Shirayama, T. Furuta, T. Ishizuka, K. Endow, T. Sumi, H. Hotta, J. Hashimoto, N. Handa, T. Masuzawa, and M. Horikoshi. 1987. Report on multi-disciplinary investigations of the *Calyptogena* communities at the Hatsushima site. *JAMSTECTR Deepsea Res.* **3:** 52–65.

Omori, M. 1974. The biology of pelagic shrimps. Pp. 233–324 in *Advances in Marine Biology*, F. S. Russel and M. Yonge, eds. Academic Press, New York.

O'Neill, P. J., R. N. Jinks, E. D. Herzog, B.-A. Battelle, L. Kass, G. H. Renninger, and S. C. Chamberlain. 1995. The morphology of the dorsal eye of the hydrothermal vent shrimp, *Rimicaris exoculata*. *Visual Neurosci.* **12:** 861–875.

Sebert, P., B. Simon, and L. Barthelemy. 1992. Fluidite membranaire et allometrie: interet ecophysiologique. *Bull. Soc. Ecophysiol.* **17:** 115–120.

Thorson, G. 1972. Erforschung des Meeres—eine Bestandsaufnahme. Kindler, Munich.

Tsukita, S., S. Tsukita, and G. Matsumoto. 1988. Light induced structural changes of cytoskeleton in squid photoreceptor microvilli detected by rapid-freeze method. *J. Cell Biol.* **106:** 1151–1160.

Vogt, K. 1980. Die Spiegeloptik des Flusskrebsauges. *J. Comp. Physiol.* **135:** 1–19.

Welsh, J. H., and F. A. Chace. 1937. Eyes of deep-sea crustaceans I. Acanthephyridae. *Biol. Bull.* **72:** 57–74.

Welsh, J. H., and F. A. Chace. 1938. Eyes of deep-sea crustaceans II. Sergestidae. *Biol. Bull.* **74:** 364–375.

Zharkova, I. S. 1970. Reduction of the organs of vision in deep-sea mysids. *Zool. Zh.* **49:** 685–693.

Zharkova, I. S. 1975. Reduction of organs of sight in deep-water Isopoda, Amphipoda, and Decapoda. *Zool. Zh.* **54:** 200–208.

Ziedins, I., and V. B. Meyer-Rochow. 1990. ERG-determined spectral and absolute sensitivities in relation to age and size in the halfcrab *Petrolisthes elongatus* (Crustacea; Decapoda; Anomura). *Exp. Biol.* **48:** 319–328.

Reference: *Biol. Bull.* **192:** 309–320. (April, 1997)

Heat-Shock Protein Expression in *Mytilus californianus:* Acclimatization (Seasonal and Tidal-Height Comparisons) and Acclimation Effects

DEIRDRE A. ROBERTS, GRETCHEN E. HOFMANN[1], AND GEORGE N. SOMERO[2]

Department of Zoology, Oregon State University, Corvallis, Oregon 97331-2914

Abstract. Heat-shock protein (hsp) expression was examined in gill of field-acclimatized and laboratory-acclimated mussels (*Mytilus californianus*) from the Oregon coast. Endogenous levels of heat-shock proteins in the 70-kDa class (hsp70 isoforms) and profiles of induction temperature for newly synthesized hsp70 were measured in freshly field-collected specimens as functions of location height in the intertidal and season, and in mussels after 7 weeks of laboratory thermal acclimation. There were significant differences in endogenous levels of hsp70 as functions of season and collection height. Strong induction of new hsp70 synthesis occurred at body temperatures within the range measured in field specimens. Profiles of hsp70 thermal induction varied significantly with season, but not with height of collection. In contrast to the large differences in hsp70 expression between winter- and summer-acclimatized mussels, no differences related to temperature occurred in the differently acclimated mussels. The differences found between the effects of field acclimatization and laboratory thermal acclimation suggest that the stress response is modulated by environmental factors in addition to body temperature. Thus, caution is required in extrapolating from laboratory acclimation studies to acclimatization effects in field populations. The seasonal and tidal-height variations in the heat-shock response are discussed in the context of energy costs of protein turnover.

Received 4 June 1996; accepted 30 January 1997.

[1] Direct correspondence to Dr. Hofmann at the Department of Biology, University of New Mexico, Albuquerque, NM 87131-1091.

[2] Current address: Hopkins Marine Station, Stanford University, Pacific Grove, CA 93950-3094.

Introduction

All but one species so examined have been found to synthesize heat-shock proteins (hsps) in response to exposure to temperatures of a few to several degrees Celsius above those normally experienced by the organism (Craig, 1985; Bosch *et al.*, 1988; Welch, 1993; Parsell and Lindquist, 1993; Becker and Craig, 1994). At temperatures near the upper limit of thermal tolerance, hsps may be the major, and in some cases the only, proteins synthesized (Morimoto *et al.*, 1990). The presence of the heat-shock response across taxa suggests an ancient origin for the response (Gupta and Singh, 1992). In addition, many studies suggest that hsps play a critical role in thermal tolerance at the cellular level (for review see Parsell and Lindquist, 1994). The recognition that some hsps are members of a broad class of proteins termed molecular chaperones—proteins that prevent improper aggregation of structurally non-native proteins and assist in correct protein folding and compartmentalization—has helped to clarify the potential roles of hsps in response to heat stress. Thus, hsps prevent aggregation of heat-damaged proteins in the cell, and therefore may indirectly assist in restoring the native structure of proteins that are reversibly damaged by high temperatures (Wiech *et al.*, 1992; Jakob *et al.*, 1993; Parsell and Lindquist, 1993; Becker and Craig, 1994; Hartl, 1996).

Although major advances have been made using isolated cell lines and unicellular organisms to resolve the mechanisms by which molecular chaperones function and by which their synthesis is regulated, relatively few studies have examined the heat-shock response in organisms in their natural habitats, in which thermal stress may greatly vary in time and space. Studies of the heat-

shock response in natural populations are important for several reasons, including (1) determining what temperatures are in fact sufficiently high to induce the response under natural habitat conditions; (2) characterizing the plasticity of the response (*e.g.*, changes in induction temperatures and endogenous levels of hsps) in concert with variation in seasonal thermal regimes; and (3) establishing the relative magnitude of the heat-shock response in conspecifics exposed to different thermal regimes in their distinct microhabitats. In view of the high fraction of metabolism directed to protein synthesis and protein turnover (Hawkins and Bayne, 1992), all of this information could be useful in developing models of ecological energetics—for example, in understanding the energy cost of existence in the face of fluctuating temperatures. Further understanding of the heat-shock response could be especially important in developing and refining conceptual models in community ecology. These would include models of environmental stress, distribution and zonation, and diversity gradients, which invoke the importance of sublethal abiotic stress in determining organisms' distribution limits, competitive relationships, and life-history strategies (Menge and Olson, 1990; Bertness and Callaway, 1994).

As part of a broad study of the physiological ecology of temperate, rocky intertidal invertebrates, we have examined several attributes of the heat-shock response in the California mussel, *Mytilus californianus*. The rocky intertidal zone exposes its inhabitants, especially sessile species like *M. californianus*, to wide ranges of temperature, as well as to desiccating conditions, wave-exposure stress, variations in access to oxygen and nutrients, and high levels of UV radiation (Newell, 1979). Variation in physical condition occurs both seasonally and as a function of height in the intertidal zone. In general, the high-intertidal zone is characterized by more extreme abiotic conditions than the low-intertidal zone, due to wider fluctuations in temperature and greater exposure to aerial conditions during tidal cycles.

Mytilus californianus is an appropriate species for studies of natural variation in the heat-shock response with season and microhabitat location of conspecifics. *Mytilus* spp. are a prominent component of many temperate, wave-swept rocky shores (Seed and Suchanek, 1992). *Mytilus californianus* occurs along the Pacific coast of North America from Alaska to Baja California (Morris *et al.*, 1980), and the upper and lower limits of its beds typically define the boundaries of the mid-intertidal zone (Suchanek, 1978). The lower limit of the *M. californianus* zone is primarily determined by biotic interactions, predation and competition (Paine, 1966, 1974), whereas the upper limit is generally considered to be most influenced by physical constraints involving temperature and desiccation (Seed and Suchanek, 1992). Harger (1970) found that *M. californianus* at higher tidal heights had decreased growth rates and attained smaller maximal sizes than conspecifics found lower in the intertidal zone.

We examined the heat-shock response in *Mytilus californianus* to determine how it varies with season and with microhabitat location. Two characteristics of the response were studied: the temperatures at which hsp induction occurs and the endogenous levels of hsps. We focused on hsps of the 70-kDa size class (*i.e.*, hsp70 isoforms) and found that both attributes of the heat-shock response change significantly with season, and that the concentration of hsp70 in high- and low-intertidal individuals of *M. californianus* also differs significantly. We performed a companion laboratory study of thermal acclimation to determine whether temperature *per se*, independent of other environmental factors like aerial exposure, influenced variations in the heat-shock response. We discuss these results in the context of the expression of heat-shock proteins in organisms under ecologically relevant habitat conditions and in relation to how laboratory acclimation studies may obscure the complete range of expression patterns found in field-acclimatized organisms.

Materials and Methods

Acclimatization studies: field collections and body-temperature measurements

Mytilus californianus (shell length 60–80 mm) was collected at Strawberry Hill on the central Oregon coast (44° 15′N, 127° 07′W) in July of 1993, and in February, March, May, June, and August of 1994. Collections were performed on a single day each month. In February, mussels were collected from a mid-intertidal site. In all other months, mussels were collected from low- and high-intertidal sites corresponding to the lower and upper limits of the *M. californianus* zone at Strawberry Hill. For the heat-shock induction experiments, freshly collected mussels were transported to the laboratory in ambient-temperature seawater (8° to 12°C) within 4–6 h of collection. In the laboratory, mussels were kept at 10°C in tanks of recirculating seawater and used in hsp induction experiments within 1–3 days of collection.

Samples of gill tissue for solid-phase immunochemical quantification of hsp70 levels (western blotting) were collected in July 1993 and February 1994. In the field, gill lamellae were dissected from mussels gathered at the high- and low-intertidal sites at the beginning and end of the emersion period, during the more extreme low tide on the collection day. The tissue samples were immediately frozen on aluminum blocks chilled on dry ice, transported to the laboratory on dry ice, and stored at −70°C until processed for protein electrophoresis and western blotting.

The body temperatures of mussels at the field collec-

tion sites were measured with a thermocouple connected to a hand-held digital thermometer (Omega Inc.). The probe was inserted into a small hole drilled through a valve, and temperatures were recorded at intervals of about 20 min throughout the emersion period. Between measurements, the holes were plugged with modeling clay to prevent evaporative water loss.

Acclimation studies: field collections and acclimation procedure

Specimens were collected at Strawberry Hill on 15 May 1994, during low tide. Gill-tissue samples for western analysis were collected from mussels dissected in the field, as described above. Mussels for acclimation experiments ($n = 125$) were haphazardly selected from a mid-intertidal rock bench, within an area of about 4 m^2. Mussels were transported to the laboratory in ambient-temperature seawater (12°C) within several hours of collection and immediately placed in a tank with recirculating seawater at 13°C. The next day, the mussels were divided into four tanks, each containing 30 mussels. One tank was maintained at 13°C and the other three tanks were adjusted to one of three temperatures, 10°, 17°, or 20°C, at a rate of 2°C per day. All tanks were maintained for 7 weeks after acclimation temperatures (10°, 13°, 17°, and 20°C) were reached. Mussels were fed an algal concentrate mixture (Algae Preserve Diet 'B'; Coast Seafoods Co., Bellevue, WA) every 4 days.

Heat-shock-protein induction experiments

For the field-acclimatization studies, hsp induction experiments were conducted on freshly collected mussels in February, March, May, June, and August of 1994. For the laboratory-acclimation studies, hsp induction experiments were conducted in May 1994 on freshly field-collected mussels and in July 1994, at the end of the 7-week acclimation period, on mussels acclimated to temperatures of 10°C, 13°C, 17°C and 20°C. All induction experiments were conducted with gill tissue because of the ease with which several similar fragments of this tissue could be obtained from each individual, and because of the ability of gill to take up dissolved amino acids from the medium. Whole gill lamellae were dissected from mussels held in chilled seawater. The lamellae were cut into small fragments weighing about 200 mg. These fragments, one for each temperature tested, were immediately placed into 500 μl of incubation medium (Hepes-buffered artificial seawater [20 m*M* Hepes, 7.57 m*M* $(NH_4)_2SO_4$, 375 m*M* NaCl, 9.35 m*M* KCl, 2.7 m*M* $NaHCO_3$, 17.95 m*M* Na_2SO_4, 37.7 m*M* $MgCl_2$-$6H_2O$, 8 m*M* $CaCl_2$-$2H_2O$, 10 m*M* glucose]) in 1.5-ml microcentrifuge tubes that had been pre-equilibrated at the heat-exposure temperatures. Immediately prior to the addition of gill, 5 μl of ^{35}S-labeled methionine and cysteine (Trans-35, ICN Radiochemicals) was added to the incubation medium. Gill fragments were radiolabeled for 2 h at the following temperatures: 10°, 13°, 17°, 20°, 23°, 25°, and 28°C. During the incubation period, gill fragments were aerated frequently by blowing a stream of air onto the surface of the incubation medium with sufficient force to stir the medium and oxygenate the buffer. After the incubation period, gill fragments were rinsed in 2 vol of nonradioactive incubation medium and then either frozen immediately on dry ice or processed for protein electrophoresis.

Protein electrophoresis and fluorography

Gill fragments from hsp induction experiments were placed in microcentrifuge tubes containing 300 μl of lysis buffer (32 m*M* Tris-HCl, pH 6.8; 2% sodium dodecyl sulfate (SDS) with 1 m*M* phenylmethylsulfonylfluoride (PMSF), a protease inhibitor, added immediately before use), and boiled for 2 min. Samples were then homogenized with a Teflon pellet pestle, boiled again for 5 min, and homogenized a second time. The homogenates were centrifuged at 16,000 $\times$ *g* in a microcentrifuge for 15 min. The supernatants were removed and the radioactivity, in counts per minute (CPM), of a 10-μl fraction of each sample was determined with a liquid scintillation counter; the remainder of the sample (about 200 μl) was stored at −20°C.

Proteins in the supernatants were separated by electrophoresis on 12% polyacrylamide gels in an SDS-buffer system (Laemmli, 1970). For ease of comparison and consistency, all of the samples (one gill fragment at each of the heat-exposure temperatures) from an individual mussel were analyzed on a single gel. Each sample was loaded in equivalent counts, approximately 600,000 CPM per lane. Gels were electrophoresed with 20 mA current for about 3.5 h, fixed for 1 h in an aqueous solution of 10% acetic acid and 30% methanol, and then incubated in EN^{3}HANCE (NEN) according to the manufacturer's protocol. Dried gels were exposed to film (Kodak X-OMAT) at −70°C for 15 h. After the film was developed, protein bands were analyzed with a densitometer (Molecular Dynamics), and the relative intensity and size of bands were quantified using ImageQuant software (Molecular Dynamics).

We measured the amount of newly synthesized protein (radioactivity) in a given band with a volume quantification procedure in ImageQuant, which calculated the intensity and the area of the band. The hsp bands were normalized relative to a non-heat-induced, strongly labeled 46-kDa protein band within the same sample lane to eliminate the variation in background labeling between samples. All comparisons of amounts of newly synthesized hsp70 were made relative to the amounts of newly synthesized 46-kDa protein ("relative amounts of

hsp70 synthesis"), for reasons given below. Normalization to the 46-kDa protein is appropriate because our objective was to estimate the temperatures at which enhanced synthesis of hsp70 relative to other size classes of proteins occurred, regardless of whether the change in relative synthesis rates was due to enhanced synthesis of hsp70 or to reduced synthesis of proteins, such as the 46-kDa protein, not induced at high temperatures. At the highest incubation temperatures, synthesis of proteins other than hsps was reduced. This observation was consistent with a defining characteristic of the heat-shock response: preferential synthesis of hsps over normal cellular proteins at abnormally high temperatures. Thus, the ratio of hsp70: 46-kDa protein could potentially increase as a result of an increase in hsp70 synthesis, a decrease in synthesis of the 46-kDa protein, or both. Our analysis of newly synthesized proteins therefore is appropriate for determining when hsp70 synthesis is induced by heat stress, even though this autoradiographic procedure cannot provide an estimate of the absolute amount of new hsp70 that is synthesized. Another reason for normalizing to the 46-kDa protein is the need to control for temperature effects on rate processes (Q_{10} effects). It could be argued that increases in hsp synthesis with rising temperature could simply be a consequence of Q_{10} effects on the rate of protein synthesis, and not a result of thermal induction of the heat stress response *per se*. By normalizing synthesis of hsp70 to synthesis of a non-heat-induced protein, we eliminated potential artifacts due to Q_{10} effects on synthesis rates.

For the graphical representations, but not for the statistical analyses, the relative amounts of hsp70 synthesized were normalized to the corresponding value at 10°C within each gel (*i.e.*, within each mussel), so that among the autoradiographs (*i.e.*, among the mussels) the relative intensities of hsp70 at 10°C were equivalent. This temperature is within the range of ambient seawater temperatures recorded at Strawberry Hill, and from preliminary experiments was shown not to induce synthesis of hsps in this population of *M. californianus*. By standardizing the relative intensity values for hsp70 to this common temperature, we could make graphical comparisons of the heat-shock response between sites and on a seasonal basis.

Hsp70 western blotting

ndogenous hsp70 levels in gill samples were quanti- th immunoblotting techniques. For the field stud- dissected in the field in July 1993 and February e used; for the acclimation experiments in the lab gills dissected in the field in May 1994 and from 's acclimated to 10°C and 20°C for 7 weeks were use ll fragments dissected from mussels in the field and fr n immediately were homogenized in lysis buffer, following the same protocol used on samples for the induction experiment. Equivalent amounts of protein (5 μg) were electrophoresed on 7% or 7.5% SDS-polyacrylamide gels. This amount of protein was determined to be within the linear range of detection for the final immunochemical detection step (data not shown; see Hofmann and Somero, 1995). After electrophoresis, separated proteins were transferred from the gel to a nitrocellulose membrane *via* a semi-dry transfer blot apparatus (Owl Scientific). Transfers were conducted for 1.5 h at 115 mA with a transfer buffer containing 25 m*M* Tris base, 192 m*M* glycine, and 20% methanol. The nitrocellulose membrane was hydrated for 3 h prior to transfer, and the filter paper used to sandwich the membrane and gel was saturated in transfer buffer. After the transfer, the membrane was blocked overnight in blocking solution (5% nonfat dry milk, 0.02% thimerosal, in phosphate-buffered saline (PBS: 10 m*M* sodium phosphate, 150 m*M* NaCl, pH 7.4)) and then rinsed three times for 10 min in PBS containing 0.1% Tween-20. The membrane was then sequentially incubated in solutions of rat monoclonal anti-hsp70 antibody (hybridoma 7.10; provided by Dr. Susan Lindquist of the University of Chicago), bridging antibody (rabbit anti-rat IgG; Vector Laboratories) and Protein A-horseradish peroxidase (HRP) conjugate (Bio-Rad). These methods are more fully described in Hofmann and Somero (1995). The enhanced chemiluminescence detection method (ECL detection reagents; Amersham) was used to visualize proteins that cross-reacted with the anti-hsp70 antibody. In order to compare multiple western blots, a biotinylated ECL molecular weight marker was run on each gel and visualized by adding a streptavidin-HRP incubation after the Protein A-HRP incubation step (see Hofmann and Somero, 1995). For individual western blots, the intensity of the ECL marker was used to standardize the intensities of the hsp70 bands. The chemiluminescent signal was detected according to the manufacturer's instructions, using pre-flashed Hyperfilm-ECL X-ray film (Amersham). Exposure times of the blot to the film were typically 5–15 s. Relative amounts of hsp70 were then quantified with densitometry and ImageQuant software.

Statistical analysis

SAS (SAS Institute Inc.) and SYSTAT (Systat Inc.) software programs were used for the statistical analyses. In induction experiments with field-acclimatized mussels, we compared the relative level of newly synthesized hsp70 in relation to incubation temperature, tidal height, and time of collection (*i.e.*, month). Using ANOVA techniques, incubation temperature (TEMP), collection time (MONTH), and tidal height of collection site (HEIGHT) were designated as factors, or main effects (*i.e.*, independent variables), and the relative level of newly synthe-

sized hsp70 was designated as the response variable (*i.e.*, dependent variable). Because individual mussels were divided into separate gill fragments, *subunits*, in the induction experiments, a split-plot ANOVA was used (Sokal and Rohlf, 1981). MONTH and HEIGHT were *unit* (whole mussel) level effects, and TEMP was a *subunit* (gill fragment) level effect. A variable to designate "among whole mussel variation" (MUSS) was also included in the analysis. In this case, the null hypothesis was that the variation in hsp70 synthesis was random, and not due to TEMP, MONTH, or HEIGHT. Because the relative level of newly synthesized hsp70 was calculated as a ratio, and because exploratory data analyses revealed unequal variances, these data were log-transformed prior to running the analysis. A similar model was used to analyze the results of the hsp induction experiments with the laboratory-acclimated mussels. We were interested in comparing the relative level of newly synthesized hsp70 in relation to incubation temperature and acclimation treatment (pre-acclimation (field), 10°, 13°, 17°, and 20°C acclimation). Incubation temperature (TEMP) and acclimation treatment (ACCLTRT) were the independent variables, and the relative level of newly synthesized hsp70 was the dependent variable.

ANOVA was also used to analyze the results of the hsp70 western blotting. For the field studies, the relative level of endogenous hsp70 was the dependent variable, and collection season, tidal height, and collection time were the independent variables. For the laboratory acclimation studies, the relative level of endogenous hsp70 was the dependent variable, and acclimation treatment was the independent variable (Sokal and Rohlf, 1981). The Bonferroni correction procedure (Systat) was used for *post hoc* multiple comparisons (Schlotzhauer and Littell, 1987).

Results

Tissue temperatures of mussels in the field

Internal tissue temperatures of attached mussels during emersion at low tide were recorded seasonally at Strawberry Hill, using mussels from both high- and low-intertidal sites. Tissue temperatures in May and July ranged from about 9° to 28°C. Tissue temperatures on a day in July 1993 are shown in Figure 1 (top). Tissue temperatures were above 18°C for 2.5 h during emersion at the high site and for less than 30 min at the low site. Temperature data from a day in May 1993 (Fig 1, bottom) show that tissue temperatures were above 18°C for about 3.5 h at both sites. The temperatures of the low-site animals reached slightly higher peak values than conspecifics at the high site.

These data indicate the potential range and variability in tissue temperatures, but because measurements were only made over discrete time intervals around low tide, and because weather conditions (*e.g.*, wind, cloud cover) can fluctuate immensely on a daily basis, the data should not be interpreted to represent general seasonal patterns. In addition, these data show the unpredictable nature of the temperature ranges experienced by mussels on any given day. The time of day of the lowest low tide each day during spring tides varies seasonally; in the fall and winter the extreme low tides are in the early evening and night, and in the spring and summer the extreme low tides are in the early to mid morning (*1995 Tide Tables for the Pacific Coast of North and South America*, NOAA, US Dept. of Commerce).

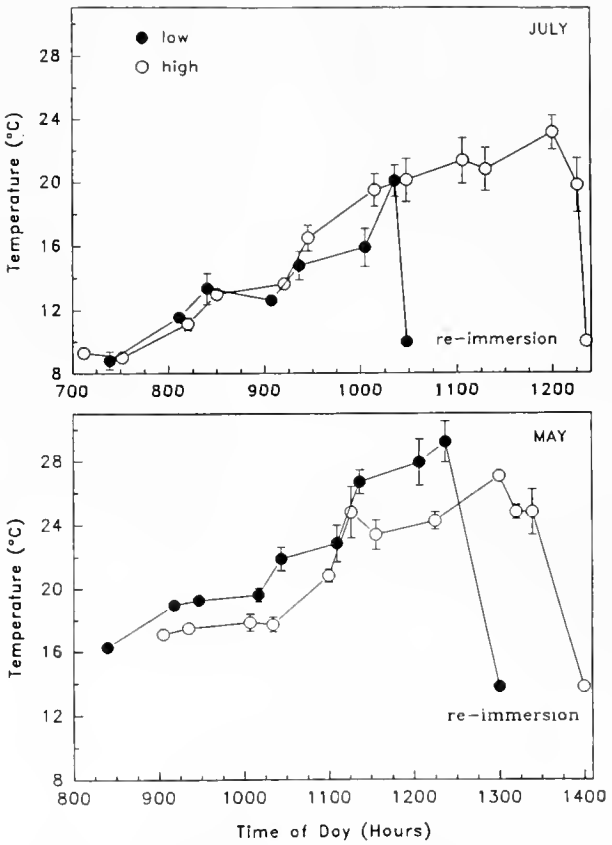

Figure 1. *In situ* tissue temperatures of *Mytilus californianus* in relation to time of day over a single low-tide emersion period in July (top) and May (bottom) 1993, at high- and low-intertidal sites at Strawberry Hill, Oregon. Each point represents the mean temperature of 5 mussels. Error bars are ±1 standard error of the mean.

Heat-shock-protein induction profiles

General patterns of newly synthesized proteins in field-acclimatized mussels. Experiments on induction of heat-shock proteins were conducted on freshly field-collected mussels in February, March, May, June, and August of 1994. In most cases, direct visual analysis of labeled protein bands revealed a clear profile of hsp induction: as

incubation temperature increased, the relative intensities of bands representing newly synthesized proteins changed markedly, with bands of molecular mass corresponding to major classes of heat shock proteins showing the strongest increase in intensity (Fig. 2). The most prominent bands of heat-inducible protein were of apparent M_r 68–74 kDa and 31.5 kDa—bands that we assume to represent heat shock proteins of the 70-kDa and 30-kDa classes. These bands were faint or absent at temperatures below 20°C, and exhibited a marked increase in intensity and width at temperatures of 23°C and higher (Fig. 2). The appearance of two strong bands with M_r values near 70 kDa indicated *de novo* synthesis of more than one hsp70 isoform (Fig. 2). Other protein bands, whose synthesis was not induced by heat, were consistently present in all samples and at all temperatures tested. Most notable were two bands of 39 and 46 kDa (Fig. 2). However, synthesis of these non-heat-induced proteins decreased at 25° and 28°C, temperatures at which hsp synthesis remained strong.

Seasonal and tidal-height patterns in hsp70 induction profiles. In February, in mussels collected from a mid-intertidal site, there was a significant increase in the relative amount of hsp70 synthesis at 23°, 25°, and 28°C as compared to synthesis at lower temperatures (Fig. 3; ANOVA, $P < 0.001$ in all cases). Between 23° and 28°C there was a twofold increase in the relative amount of hsp70 synthesized, and synthesis levels at 28°C were about four times higher than at 10°, 17°, and 20°C (Fig. 3). The importance of normalizing hsp70 synthesis to the 46-kDa protein to determine induction temperatures is illustrated by comparing data in Figures 2 and 3. Although Figure 2 appears to show an increase (induction) in hsp70 synthesis at 20°C, when the 70-kDa band is normalized to the 46-kDa band (Fig. 3) no change in the relative amount of hsp70 synthesis is found until 23°C.

Beginning in March, hsp induction experiments were performed on mussels collected at high- and low-intertidal sites, to examine site location and seasonal effects on patterns of hsp synthesis. The overall trends in the March and February specimens were similar: a strong increase in relative synthesis of hsps of both general size classes occurred at 23°C, and hsp70 levels were about fourfold higher at 28°C than at temperatures of 20° and lower (Fig. 4). In March, the relative magnitude of the response was somewhat elevated in the low-intertidal

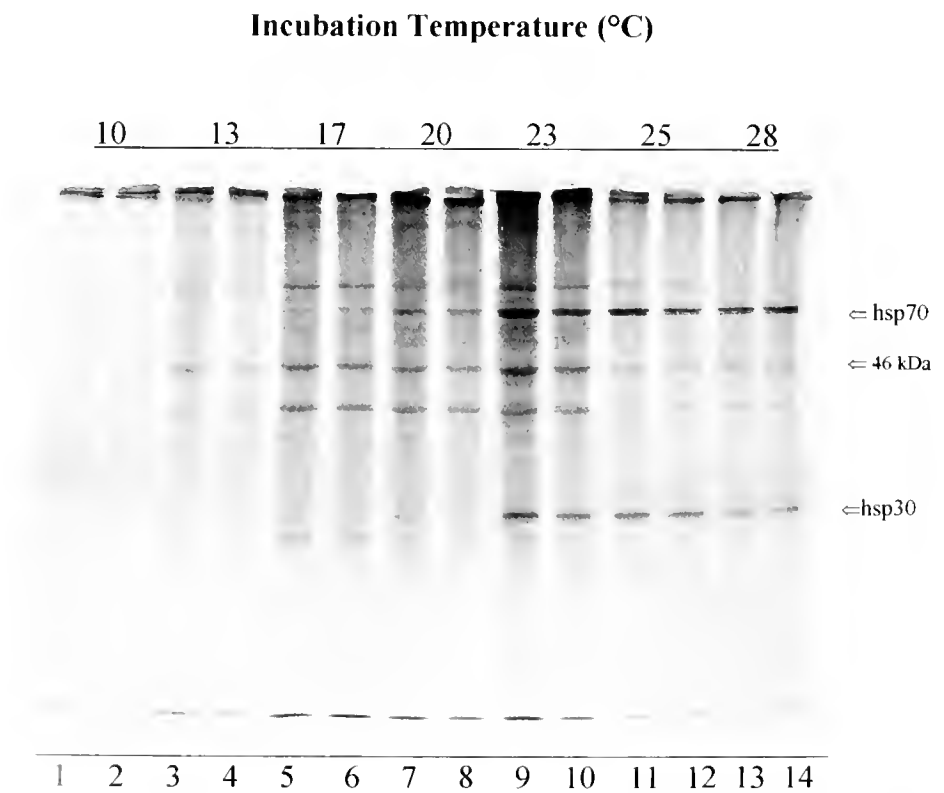

Figure 2. Autoradiograph from an experiment on the induction of heat shock proteins in *Mytilus californianus*. Fragments of gill tissue from a single individual (collected in February 1994) were radiolabeled with a mixture of ^{35}S-methionine and ^{35}S-cysteine for 2 h. Samples were loaded on a 12% polyacrylamide gel in duplicate; approximately 600,000 CPM per lane were loaded. Lanes 1–2, 10°C; lanes 3–4, 13°C; lanes 5–6, 17°C; lanes 7–8, 20°C; lanes 9–10, 23°C; lanes 11–12, 25°C; lanes 13–14, 28°C.

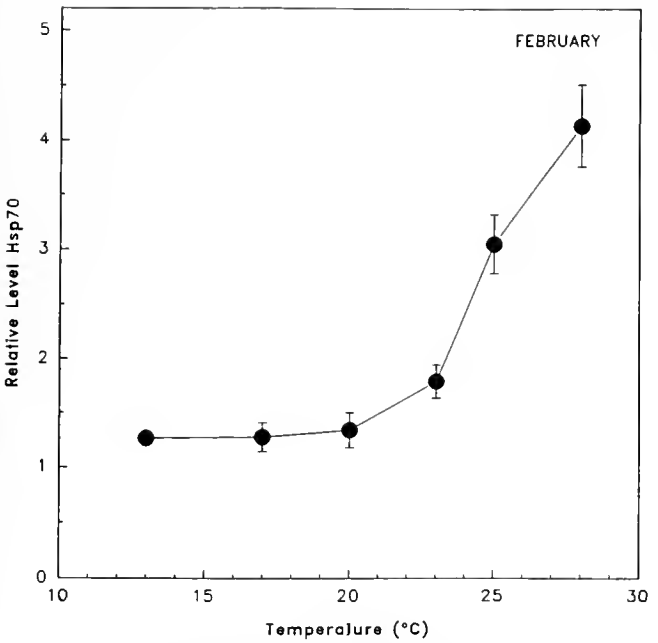

Figure 3. Hsp induction in gill of *Mytilus californianus* in relation to incubation temperature. Mussels were collected in February 1994 from a mid-intertidal site at Strawberry Hill. Each point represents the mean relative level of newly synthesized hsp70 of 6 mussels; error bars are ±1 standard error of the mean.

mussels as compared to the high-intertidal mussels at all temperatures, although this difference was not significant (Fig. 4). The induction profiles in the May samples are similar to those in February and March, although there was an overall reduction in the magnitude of the response. The June samples showed a further dampening of the induction response (note that 13° and 17°C were not tested in the June collection; Fig. 4), and in the August samples there was no longer a sharp induction profile in either the high or low samples (note that 13°C was not tested; Fig. 4).

A split-plot ANOVA indicated that incubation temperature (TEMP, $P < 0.0001$), collection month (MONTH, $P < 0.0007$), and the interaction term between temperature and collection month (MONTH * TEMP, $P < 0.0001$) were statistically significant in explaining variation in relative amounts of new synthesis of hsp70. There was significant individual variability in hsp70 expression among individual mussels (MUSS (MONTH * HEIGHT), $P < 0.0001$), but the tidal height of the collection site was not significant in the model (HEIGHT, $P < 0.7470$).

Hsp70 synthesis patterns in laboratory-acclimated mussels. Freshly collected (= pre-acclimation) specimens of mid-intertidal *M. californianus* collected in May 1994 exhibited an hsp70 expression pattern (data not shown) similar to that observed with high- and low-in-

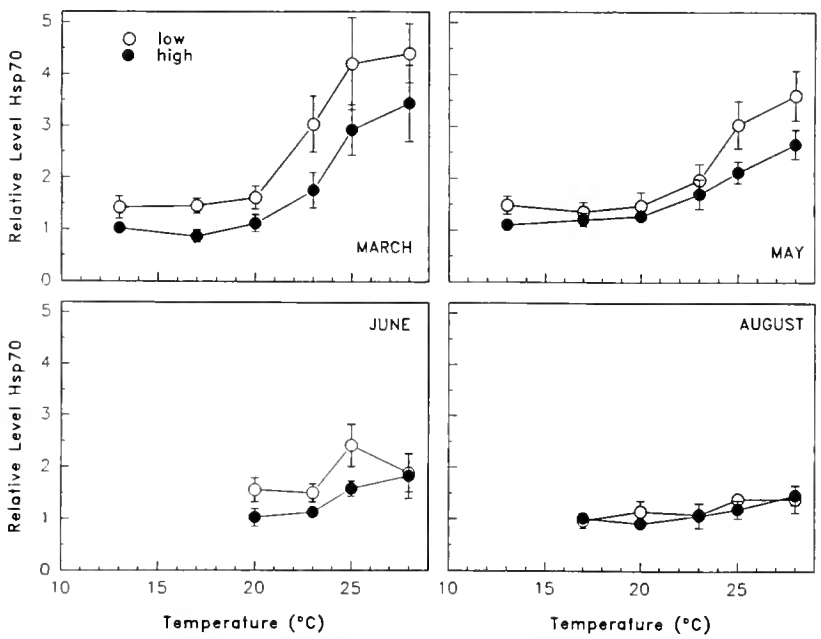

Figure 4. Hsp70 induction in gill of *Mytilus californianus* in relation to incubation temperature in field-collected mussels in March, May, June, and August 1994, from high- and low-intertidal sites at Strawberry Hill. Points represent means: March low, $n = 5$; March high, $n = 4$; May low, $n = 8$; May high, $n = 8$; June low, $n = 5$; June high, $n = 4$; August low, $n = 3$; August high, $n = 3$. Error bars are ±1 standard error of the mean.

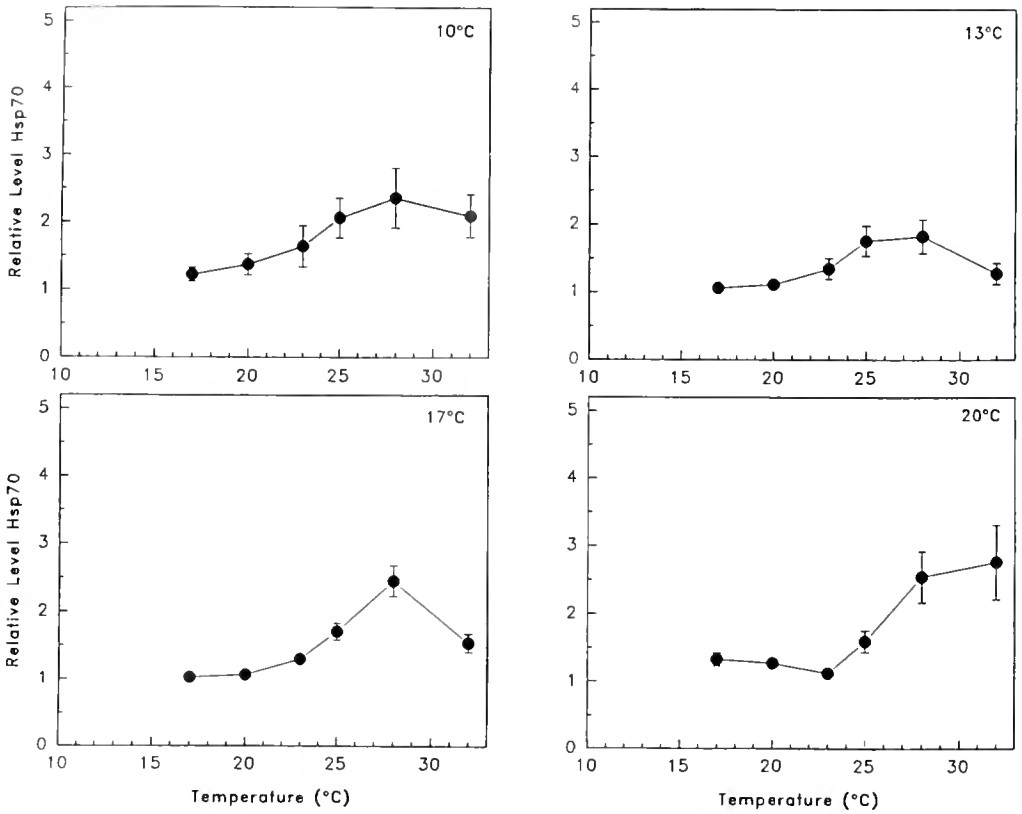

Figure 5. Hsp70 induction in gill of laboratory-acclimated *Mytilus californianus* in relation to temperature. Mussels were collected in May 1994 from a mid-intertidal site at Strawberry Hill and acclimated in the laboratory for 7 weeks. Each point represents the mean relative level of newly synthesized hsp70; error bars are ±1 standard error of the mean. Sample sizes were 10°C-acclimation, $n = 5$; 13°C-acclimation, $n = 6$; 17°C-acclimation, $n = 7$; 20°C-acclimation, $n = 7$.

tertidal mussels from the same month (Fig. 4): amounts of newly synthesized hsp70 were relatively constant and low between 10°C and 20°C, but between 20°C and 25°C there was a sharp increase in synthesis of hsp70. The amounts of newly synthesized hsp70 at 25°C and 28°C were more than three times the levels at 10°C and 13°C.

A comparison of these data with results from the temperature-acclimated mussels (Fig. 5) revealed several differences. Overall, the relative magnitude of the amount of newly synthesized hsp70 was reduced in the mussels acclimated to 10°, 13°, and 17°C, when compared to the pre-acclimation mussels (compare May data in Fig. 4 with data in Fig. 5). In all but the 20°C-acclimated specimens, the relative amount of new hsp70 synthesis was maximal at 28°C and decreased at the highest incubation temperature, 32°C. Protein synthesis in the 20°C-acclimated mussels was more resistant to high temperature, and no decrease in hsp70 synthesis was noted at 32°C. Acclimation had no consistent effects on the temperature at which a significant increase in hsp70 synthesis first occurred.

The split-plot ANOVA model showed that acclimation treatment (ACCLTRT, $P < 0.0001$), temperature (TEMP, $P < 0.0001$), and the interaction between these two factors (ACCLTRT * TEMP, $P < 0.0001$) explained a significant portion of the variation in relative levels of newly synthesized hsp70. This model also shows that the variation in response among individual mussels was significant ($P < 0.0052$).

Endogenous hsp70 levels: constitutive and heat-induced isoforms

Western blotting with a rat monoclonal anti-hsp70 antibody was used to measure the relative amounts of hsp70 present in field-acclimatized *M. californianus* over the low-tide emersion period, in high- and low-intertidal populations, and in summer- and in winter-acclimatized specimens (Fig. 6). For quantification and comparison, the hsp70 bands were divided into two groups of isoforms; a lower molecular mass group (LMM-hsp70, apparent M_r: 66–68 kDa) and a higher molecular mass group (HMM-hsp70, apparent M_r: 69–73 kDa). These two molecular-mass classes may include both constitutively synthesized isoforms of 70-kDa chaperones (hsp70 cognates = hsc70) and heat-induced isoforms (hsp70s)

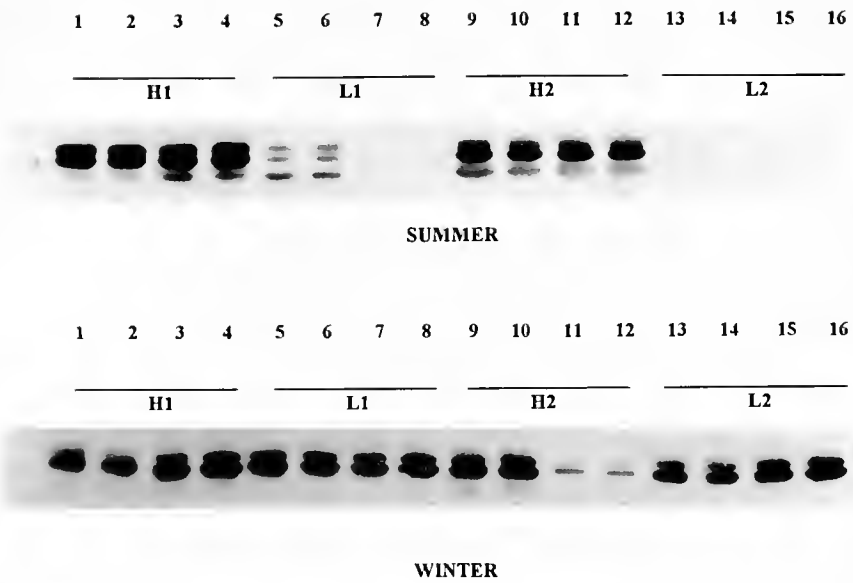

Figure 6. Western blot analysis of hsp70 isoforms in gill tissue of summer- and winter-acclimatized *Mytilus californianus*. Mussels were collected at high- and low-intertidal sites just as the water was receding (H1 and L1, respectively) and just prior to re-immersion (H2 and L2, respectively). Lanes were loaded with equal amounts of protein (5 μg), and immunodetection was performed using ECL reagents. Two samples from each site were loaded in duplicate (*e.g.*, lanes 1 and 2 are the same sample). It should be noted that one individual (H2 in Winter) displayed significantly lower levels of endogenous hsp70; the reason for this difference is unknown.

because this anti-hsp 70 antibody reacts with both types of 70-kDa isoforms.

As shown in Figure 7, there were no significant differences in hsp70 levels over a single low-tide emersion period in either the high- (H1, H2) or low- (L1, L2) intertidal sample, in either the summer or winter collections. However, distinct seasonal and tidal height differences, both in the quantity and banding pattern of hsp70 proteins, were observed (Fig. 7). The relative amount of LMM-hsp70 isoforms was significantly greater in the high-intertidal mussels than in the low-intertidal mussels in the summer collection ($P < 0.01$). In the winter, there was no significant difference in the amount of LMM-hsp70 in the gill of high- and low-intertidal mussels (Fig. 7a). Within the high-intertidal site, there were significantly higher levels of LMM-hsp70 isoforms in the summer than in the winter ($P < 0.01$). Within the low site, there were no significant seasonal differences.

Consistent with the patterns shown by LMM-hsp70, the amount of HMM-hsp70s in summer was significantly higher in the high-intertidal mussels than in the low-intertidal mussels (Fig. 7b; $P < 0.01$). However, within the high-intertidal site, there were no significant differences seasonally, and within the low intertidal site, the amount of HMM-hsp70 was higher in winter than in summer.

Using western analysis, we also compared hsp70 levels in the pre-acclimation group of field-collected mussels (May 1994), and in the laboratory-acclimated mussels after 7 weeks of acclimation to either 10° or 20°C (data not shown). There were no significant differences among any of these three treatment groups for either the LMM or HMM forms of hsp70.

Discussion

In situ *tissue temperatures and expression of heat-shock proteins*

The tissue temperatures recorded *in situ* during emersion at all seasons frequently reached levels at which increased synthesis of hsp70 was observed in the *in vitro* labeling studies (Figs. 1–4). These observations, in concert with the seasonal and tidal-height variations observed in endogenous levels of hsp70 (Figs. 6 and 7), show that the heat-shock response is likely to be induced in mussels at all seasons, but particularly during summer when low tides typically occur during midday. Because the intensity of thermal stress is due to the product of temperature multiplied by duration of exposure, mussels in the higher regions of the intertidal zone experience greater heat stress, even though the absolute tissue temperatures reached during emersion on hot days may not differ between high- and low-intertidal individuals (Fig. 1). Other data support our conclusion that tissue temperatures of mussels frequently become high enough to induce the heat-shock response. Elvin and Gonor (1979) recorded tissue temperatures ranging from 0° to 34°C in *M. californianus* on the Oregon coast. Hofmann and

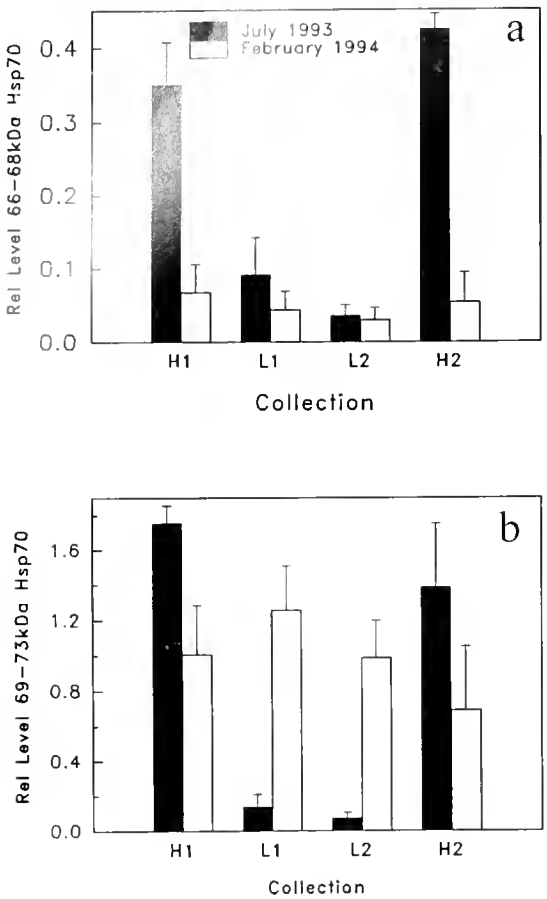

Figure 7. Mean relative level of low molecular mass (66–68 kDa) hsp70 isoforms (a) and high molecular mass (69–73 kDa) hsp70 isoforms (b) in *Mytilus californianus* gill in relation to intertidal collection site, over a low-tide emersion period in summer and in winter. H and L designate samples from high and low sites, respectively; 1 and 2 designate samples collected at the beginning and end, respectively, of the period of emersion. Error bars are ±1 standard error of the mean (n = 5).

Somero (1995) reported tissue temperatures as high as 32°C during emersion of *M. trossulus* during midday low tides in coastal intertidal sites on San Juan Island, Washington. These data on body temperature, taken in conjunction with the hsp induction profiles presented here and in other studies of intertidal invertebrates (Hofmann and Somero, 1995, 1996), highlight how important stress-protein expression may be to eurythermal ectotherms, such as intertidal invertebrates, for tolerance of fluctuations in environmental temperature and the development of seasonal thermotolerance (Coleman *et al.*, 1995).

Seasonal patterns: induction profiles and endogenous levels of heat-shock proteins

The results of the *in vitro* labeling experiments showed that patterns of hsp expression varied significantly over the 7-month period of the field experiment (Figs. 3, 4; $P < 0.0007$). Two observations illustrate the plasticity of the stress response in field organisms. First, there was significant seasonal variation in the induction profiles with respect to induction temperatures and the magnitude of new synthesis of hsp70 isoforms (Figs. 3 and 4). In gill from mussels sampled in February and March, hsp70 synthesis was strongly induced at temperatures greater than 20°C. By May, the induction response was dampened, and this trend continued in June and August. Thus, in what may appear to be a paradoxical trend, the amount of new synthesis of hsp70 was lowest in the months when average temperatures during emersion were likely to be highest.

Few other studies have examined seasonal changes in the heat-shock response. In an estuarine goby fish, *Gillichthys mirabilis*, the induction temperature for synthesis of hsp90 increased from 28°C in winter-acclimatized fish to 32°C in summer-acclimatized fish (Dietz and Somero, 1992). The plasticity observed in invertebrates (this study) and fishes (Dietz and Somero, 1992) in the induction of hsp synthesis indicates that the regulation of hsp expression is not a genetically fixed characteristic of an organism, but is instead a trait subject to acclimatization.

The second type of plasticity noted in the field-acclimatization experiment was the strong effect of season on endogenous levels of hsp70 isoforms (Figs. 6 and 7). During summer, when the highest body temperatures during emersion are likely, the levels of the LMM isoforms of hsp70 were significantly elevated over levels measured in winter mussels in the high-intertidal location, but not at the lower site (Fig. 7; see below). For the HMM isoforms of hsp70, summer levels were significantly elevated in mussels from the high-intertidal site as compared to levels in mussels from the low-intertidal site (Fig. 7). The seasonal changes noted in endogenous levels of hsp70 isoforms may provide a partial explanation (but see below) for the seemingly paradoxical result found in the induction experiments—namely, the dampened induction response noted in summer specimens. The higher levels of hsp70 isoforms maintained in summer may be a type of "anticipatory" adaptation to the likelihood of increased thermal stress in these months. Higher endogenous levels of hsps may preclude the need for induction of new hsp synthesis in concert with emersion during the tidal cycle.

Tidal height patterns: induction profiles and endogenous levels

No significant differences were found in the induction profiles of mussels from high- and low-intertidal sites (Fig. 4), even though the endogenous levels of hsp70 isoforms in the two groups were significantly different (Fig. 7). In summer, the levels of LMM and HMM hsp70 were

significantly higher in mussels from the high site than in individuals from the low site, an observation consistent with greater amounts of thermal stress in the high intertidal individuals. In winter, for both isoforms of hsp70, high- and low-site mussels had the same hsp70 levels. These data show that the temperatures at which new synthesis of hsp70 isoforms is induced are not established entirely by the endogenous levels of hsp70. One reason for the observed lack of a consistent correlation between endogenous levels of hsp70 isoforms and induction temperature may be that the data from the western analysis includes both constitutively expressed and heat-induced isoforms of hsp70, whereas the data from *in vitro* labeling primarily represents new synthesis of the heat-inducible isoforms. A clearer understanding of the correlation between endogenous levels of an hsp and the induction temperature for new hsp synthesis thus requires the ability to to distinguish between constitutively expressed and heat-induced isoforms, something our antibody analysis did not do.

Studies with other intertidal invertebrates have also observed differential expression of stress proteins as a function of intertidal location. The limpet *Collisella scabra*, which occurs relatively high in the intertidal zone, expressed more isoforms of hsp70 and hsp60 than a congener, *C. pelta*, which occurs lower in the intertidal in shaded surge channels (Sanders *et al.*, 1991). In the sea anemone *Anemonia viridis*, intertidally occurring individuals have higher constitutive levels of a low molecular weight hsp than do anemones from subtidal collections (Sharp *et al.*, 1994). In *M. trossulus*, intertidal populations had higher endogenous levels of hsp70 than subtidal populations (Hofmann and Somero, 1995).

Acclimation patterns: induction profiles and endogenous levels of heat-shock proteins

The acclimation experiments were conducted to determine whether the seasonal acclimatizational effects noted in induction profiles and endogenous levels of hsp70 could be mimicked through cold- and warm-acclimation in the laboratory. That is, the acclimation experiments were designed to test the hypothesis that changes in temperature alone were responsible for seasonal acclimatization of the heat-shock response. Our data refute this hypothesis. The induction profile data (Fig. 5) show that the warm- and cold-acclimated mussels had indistinguishable heat-shock responses. Both acclimation groups exhibited a relatively attenuated response, with maximal increases in hsp70 synthesis of no more than about 2.5-fold, in contrast with the greater than 4-fold increases seen in winter-acclimatized mussels (Figs. 3 and 4). Similarly, no significant differences were found between pre-acclimation, 10°-, and 20°C-acclimated groups in the endogenous levels of LMM and HMM hsp70 isoforms.

The differences that distinguish the results of the acclimation and acclimatization experiments with *M. californianus* raise caveats about the design and interpretation of heat-shock experiments. Particularly for sessile intertidal species like *M. californianus*, which encounter a variety of emersion-related stresses, including those due to desiccation and anaerobiosis, it may be unrealistic to assume that temperature is the only, or even the primary, stress that necessitates the heat-shock (stress) response. A common signal for hsp induction is the appearance in the cell of unfolded proteins (Ananthan *et al.*, 1986; Parsell and Lindquist, 1993). In addition to thermal stress, changes in intracellular ionic strength and pH during emersion could affect protein structure and, thereby, induce the synthesis of heat-shock proteins. Because the mussels in the acclimation experiment were continuously submerged, stresses due to desiccation and anaerobiosis were not present. Therefore, acclimation to a single environmental variable, for example, temperature, may not lead to a heat-shock response that mimics the response occurring under *in situ* conditions.

General conclusions

Synthesis of stress proteins, like all protein synthesis, is expensive in terms of the energy budget of an animal (Creighton, 1993). Hawkins (1991) has estimated the costs of protein synthesis to constitute 20%–25% of the energy budget of the bay mussel, *Mytilus edulis*. This cost represents an additional energy burden because stress proteins do not directly contribute to increases in growth or reproduction, and because under stress conditions they may be synthesized preferentially, such that other proteins critical for the normal functioning of the organism are either synthesized at reduced rates or not synthesized at all. Furthermore, the function of stress proteins may require considerable ATP turnover; refolding of a protein may consume in excess of 100 ATP molecules (Creighton, 1991; Martin *et al.*, 1991; Parsell and Lindquist, 1993). The extent to which different intensities of thermal stress found in high- and low-intertidal sites impact protein synthesis and growth is not known. However, significant differences in growth rates (Menge *et al.*, 1994) and in capacity for protein synthesis as indicated by RNA:DNA ratios (Dahlhoff and Menge, 1996) have been found between mussels in different tidal locations at Strawberry Hill. Although these height-related differences may be due in large measure to variation in food availability from site to site (Dahlhoff and Menge, 1996), other explanations are possible. The data also are consistent with the conjectures that the heat shock response can exact a measurable toll on the energy budgets of organisms (Krebs and Loeschcke, 1994; Coleman *et al.*, 1995), and that thermal damage to proteins could play a key role in defining the habitat ranges of marine species (Somero, 1995).

Acknowledgments

We thank Dr. Susan Lindquist for providing the antibodies used in this study. Team Mussel was supported by an OSU Zoological Research Fund Award to DAR, an NSF Marine Biotechnology Postdoctoral Fellowship to GEH, and NSF grant IBN 9206660 to GNS.

Literature Cited

Ananthan, J., A. L. Goldberg, and R. Voellmy. 1986. Abnormal proteins serve as eukaryotic stress signals and trigger the activation of heat shock genes. *Science* **232:** 522–524.

Becker, J., and E. A. Craig. 1994. Heat-shock proteins as molecular chaperones. *Eur. J. Biochem.* **219:** 11–23.

Bertness, M. D., and R. Calloway. 1994. Positive interactions in communities. *Trends Ecol. Evol.* **9:** 191–193.

Bosch, T. C. G., S. M. Krylow, H. R. Bode, and R. E. Steele. 1988. Thermotolerance and synthesis of heat shock proteins: these responses are present in *Hydra attenuata* but absent in *Hydra oligactis*. *Proc. Natl. Acad. Sci. USA* **85:** 7927–7931.

Coleman, J. S., S. A. Heckathorn, and R. L. Hallberg. 1995. Heat-shock proteins and thermotolerance: linking molecular and ecological perspectives. *Trends Ecol. Evol.* **10:** 305–306.

Craig, E. A. 1985. The heat shock response. *CRC Crit. Rev. Biochem* **18:** 239–280.

Creighton, T. E. 1991. Unfolding protein folding. *Nature* **352:** 17–18.

Creighton, T. E. 1993. *Proteins: Structure and Molecular Properties,* 2nd. ed. W. H. Freeman, San Francisco.

Dahlhoff, E. P., and B. A. Menge. 1996. Influence of phytoplankton concentration and wave exposure on the ecophysiology of the California mussel *Mytilus californianus*. *Mar. Ecol. Prog. Ser.* **144:** 97–107.

Dietz, T. J., and G. N. Somero. 1992. The threshold induction temperature of the 90-kDa heat shock protein is subject to acclimatization in eurythermal goby fishes (genus *Gillichthys*). *Proc. Natl. Acad. Sci. USA* **89:** 3389–3393.

Elvin, D. W., and J. J. Gonor. 1979. The thermal regime of an intertidal *Mytilus californianus* Conrad population on the central Oregon coast. *J. Exp. Mar. Biol. Ecol.* **39:** 265–279.

Gupta, R. S., and B. Singh. 1992. Cloning of the HSP70 gene from *Halobacterium marismortui:* relatedness of archaebacterial HSP70 to its 24 eubacterial homologs and a model for the evolution of the HSP70 gene. *J. Bacteriol.* **174:** 4594–4605.

Harger, J. R. E. 1970. The effect of wave impact on some aspects of the biology of sea mussels. *Veliger* **12:** 401–414.

Hartl, F. U. 1996. Molecular chaperones in cellular protein folding. *Nature* **381:** 571–580.

Hawkins, A. J. S. 1991. Protein turnover: a functional appraisal. *Funct. Ecol.* **5:** 222–233.

Hawkins, A. J. S., and B. L. Bayne. 1992. Physiological interrelations and the regulation of production. Pp. 171–222 in *The Mussel* Mytilus: *Ecology, Physiology, Genetics and Culture,* E. Gosling, ed. Dev. Aquac. Fish. Sci. 25, Elsevier, Amsterdam.

Hofmann, G. E., and G. N. Somero. 1995. Evidence for protein damage at environmental temperatures: seasonal changes in levels of ubiquitin conjugates and hsp70 in the intertidal mussel *Mytilus trossulus*. *J. Exp. Biol.* **198:** 1509–1518.

Hofmann, G. E., and G. N. Somero. 1996. Protein ubiquitination and stress protein synthesis in *Mytilus trossulus* occurs during recovery from tidal emersion. *Molec. Mar. Biol. Biotech.* **5:** 175–184.

Jakob, U., M. Gaestel, K. Engel, and J. Buchner. 1993. Small heat shock proteins are molecular chaperones. *J. Biol. Chem.* **268:** 1517–1520.

Krebs, R. A., and V. Loeschcke. 1994. Costs and benefits of activation of the heat shock response in *Drosophila melanogaster*. *Funct. Ecol.* **8:** 730–737.

Laemmli, E. K. 1970. Cleavage of structural proteins during the assembly of the head of bacteriophage T4. *Nature* **356:** 683–689.

Martin, J., T. Langer, R. B. Boteva, A. Schramel, A. L. Horwich, and F.-U. Hartl. 1991. Chaperonin-mediated protein folding at the surface of groEL through a 'molten globule'-like intermediate. *Nature* **352:** 36–42.

Menge, B. A., E. L. Berlow, C. A. Blanchette, S. A. Navarrete, and S. B. Yamada. 1994. The keystone species concept: variation in interaction strength in a rocky intertidal habitat. *Ecol. Monogr.* **64:** 249–286.

Menge, B. A., and A. M. Olson. 1990. Role of scale and environmental factors in regulation of community structure. *Trends Ecol. Evol.* **5:** 52–57.

Morimoto, R. I., A. Tissieres, and C. Georgopoulos. 1990. *Stress Proteins in Biology and Medicine.* Cold Spring Harbor Laboratory Press, New York.

Morris, R. H., D. P. Abbott, and E. C. Haderlie. 1980. *Intertidal Invertebrates of California.* Stanford University Press, Stanford, CA.

Newell, R. C. 1979. *Biology of Intertidal Animals,* 3rd ed. Marine Ecological Surveys, Faversham, UK.

Paine, R. T. 1966. Food web complexity and species diversity. *Am. Nat.* **118:** 65–75.

Paine, R. T. 1974. Intertidal community structure: experimental studies on the relationship between a dominant competitor and its principal predator. *Oecologia* **15:** 93–120.

Parsell, D. A., and S. Lindquist. 1993. The function of heat-shock proteins in stress tolerance: degradation and reactivation of damaged proteins. *Annu. Rev. Genet.* **27:** 437–496.

Parsell, D. A., and S. Lindquist. 1994. Heat shock proteins and stress tolerance. Pp. 457–494 in *The Biology of Heat Shock Proteins and Molecular Chaperones,* R. I. Morimoto, A. Tissieres, C. Georgopoulos, eds. Cold Spring Harbor Laboratory Press, New York.

Sanders, B. M., C. Hope, V. M. Pascoe, and L. S. Martin. 1991. Characterization of the stress protein response in two species of *Collisella* limpets with different temperature tolerances. *Physiol. Zool.* **64:** 1471–1489.

Schlotzhauer, S. D., and R. C. Littell. 1987. *SAS System for Elementary Statistical Analysis.* SAS Institute, Inc., Cary, NC.

Seed, R., and T. H. Suchanek. 1992. Population and community ecology of *Mytilus.* Pp. 87–169 in *The Mussel* Mytilus: *Ecology, Physiology, Genetics and Culture,* E. Gosling, ed. Dev. Aquac. Fish. Sci. 25., Elsevier, Amsterdam.

Sharp, V. A., D. Miller, J. C. Bythell, and B. E. Brown. 1994. Expression of low molecular weight HSP70 related polypeptides from the symbiotic sea anemone *Anemonia virdis* Forskall in response to heat shock. *J. Exp. Mar. Biol. Ecol.* **179:** 179–193.

Sokal, R. R., and F. J. Rohlf. 1981. *Biometry,* 2nd ed. W. H. Freeman, San Francisco.

Somero, G. N. 1995. Proteins and temperature. *Annu. Rev. Physiol.* **57:** 43–68.

Suchanek, T. H. 1978. The ecology of *Mytilus edulis* L. in exposed rocky intertidal communities. *J. Exp. Mar. Biol. Ecol* **31:** 105–120.

Wiech, H., J. Buchner, R. Zimmerman, and U. Jakob. 1992. Hsp90 chaperone protein folding *in vitro*. *Nature* **358:** 169–170.

Welch, W. J. 1993. How cells respond to stress. *Sci. Am.* (May): 56–64.

Reference: *Biol. Bull.* **192:** 321–331. (April, 1997)

The Route of Ion and Water Movements Across the Gill Epithelium of the Freshwater Shrimp *Macrobrachium olfersii* (Decapoda, Palaemonidae): Evidence From Ultrastructural Changes Induced by Acclimation to Saline Media

JOHN C. McNAMARA[1] AND ALICE GONÇALVES LIMA[2]

[1]*Departamento de Biologia, FFCLRP, Universidade de São Paulo, Ribeirão Preto 14040-901 SP, Brasil; and* [2]*Departamento de Fisiologia, Instituto de Biociências, Universidade de São Paulo, São Paulo, Brasil*

Abstract. The ultrastructure of the pillar cells in the gill lamellae of the freshwater shrimp *Macrobrachium olfersii* was examined to evaluate the routes of salt and water movement across the gill epithelium and into the hemolymph. Alterations were morphometrically quantified in shrimp maintained in fresh water (FW, <0.5‰ salinity) and after acclimation to saline media (21‰ or 28‰ salinity). The tissue interface between the hemolymph and the external medium consists exclusively of the thin apical flange regions of the pillar cells, the upper membrane of which is highly amplified by dense microvilli and overlain by a thin cuticle. The lower flange membrane, bathed by the hemolymph, is smooth and not invaginated. Contiguous flanges are strongly bound by junctional structures including desmosomes and septate junctions. The basal surface of the pillar cell perikaryon is linked to the adjacent septal cells through many basolateral junctions. The septal cell plasmalemma is abundantly and deeply invaginated, each infolding enclosing numerous mitochondria; these characteristics are typical of salt-transporting machinery. After shrimps were acclimated to saline media for 10 days, the thickness of the pillar cell flanges was significantly reduced (from 1.3 to $\approx$0.4 μm), as was the height (from 0.8 to 0.3 μm) and density (from 4.0 to $\approx$ 1.8 microvilli/μm) of the apical microvilli. This reduction in the apical surface area of the pillar cells appears to lead to decreased ionic permeability, concomitant with a reduction in Na^+/K^+-ATPase activity, thus limiting Na^+ uptake. In contrast to the brachyurans, in which the respiratory and ion-transporting mechanisms are differentially located in the anterior and posterior gills, in palaemonid shrimps the pillar cells apparently play a dual role: ions move preferentially through ion transporters in the microvilli above the pillar cell perikaryon, while respiratory gases are exchanged through the fine flange regions in contact with the hemolymph.

Received 6 May 1996; accepted 20 December 1996.

Introduction

Salt uptake in hyperosmoregulating, freshwater decapods and in hyper-regulating, euryhaline brachyurans experimentally exposed to dilute media takes place primarily through the gill tissues (see Mantel and Farmer, 1983; Gilles and Péqueux, 1986; Freire and McNamara, 1995, for discussion and references).

In brachyurans, specific ion-transporting regions of the posterior gills account for much of this salt uptake, while the anterior gills appear to be responsible mainly for respiratory gas exchange (Péqueux, 1995). Such salt-transporting gills exhibit a typical microanatomy: the highly flattened, cuticle-bounded gill lamellae essentially consist of a continuous layer of epithelial cells enclosing a narrow hemolymph space; linked pairs of sustaining pillar cells extend across this space between the opposing epithelial sheets, their apical flanges often forming part of the epithelium (Mantel and Farmer, 1983; Taylor and

Taylor, 1986; Maina, 1990). The apical surfaces of the epithelial cells are characteristically amplified by membrane infoldings in the form of leaflets, whereas the basolateral membranes are deeply invaginated and associated with mitochondria (Copeland, 1968; Copeland and Fitzjarrell, 1968; Gilles and Péqueux, 1985; Maina, 1990). A fenestrated, partial intralamellar septum, which bisects the gill lamella into two symmetrical portions, may be present (Barra *et al.*, 1983; see Taylor and Taylor, 1992, for review).

The apical infolding system of the gill epithelial cells of decapod crustaceans undergoes structural reorganization in response to short-term exposure or acclimation to salinities different from that predominant in the habitat (Bubel, 1976; Compère *et al.*, 1989; see Taylor and Taylor, 1992; Freire and McNamara, 1995, for review and references). After exposure to dilute media, the apical leaflets and microvilli become more numerous and elaborate, and an extracellular, subcuticular compartment enlarges due to osmotic swelling (Gilles and Péqueux, 1985). During short- and medium-term exposure (hours to days) to concentrated media, the apical infolding system is disrupted and regresses while the subcuticular space disappears (see Shires *et al.*, 1994; Péqueux, 1995). The apical region of the epithelial cells thus appears to represent a labile, primary barrier to osmotic alteration deeper within the gill tissue.

The routes by which salt uptake is effected in the gills of hyperosmoregulating, freshwater palaemonid shrimps have received very little attention. Although phyllobranchiate palaemonid gill is comparable to the brachyuran gill in gross morphology, very little is known about its fine structure (*cf.*, Nakao, 1974; Doughtie and Rao, 1978; see Taylor and Taylor, 1992); ultrastructural studies of the effects of acclimation to saline media on the apical infolding system are entirely lacking. Freire and McNamara (1995) analyzed the gill structure of *Macrobrachium olfersii*, a representative freshwater palaemonid shrimp. Each flattened hemilamella constitutes a narrow hemolymph-filled space delimited by the flanges of two opposing layers of pillar cells, the bases of which adjoin in the mid-region of the lamella. A layer of septal cells, continuous with the pillar cell bases, divides the intralamellar space into two parallel compartments, forming a lattice-like series of lacunae through which the hemolymph flows. The epithelium forming the hemolymph-water interface thus consists exclusively of the expanded apical flanges of the pillar cell perikarya. The upper membranes of these flange cells are modified to form an extensive system of microvilli, although the lower flange surfaces and perikarya show no membrane-amplifying features that would suggest salt transport. This role has been assumed by the cells of the intralamellar septum, the plasma membranes of which are extensively invaginated and rich in associated mitochondria. Other cell types are rare within the septum.

This relocation of the salt-transporting machinery—from the basolateral membranes of epithelial cells whose apical surfaces are in direct contact with the cuticle adjacent to the external medium, in the brachyurans, to the intralamellar septum, surrounded on both surfaces by flowing, Na^+-rich hemolymph, in the freshwater palaemonids—poses several engaging questions in terms of the physical routes by which salt might be transported across the gill tissue to the hemolymph. The present study thus examines the ultrastructure of the pillar cells, particularly their apical microvilli and junctions, in the gills of *Macrobrachium olfersii*, a strongly hyperosmoregulating, freshwater palaemonid shrimp (McNamara, 1987). Gills were examined both in animals maintained in fresh water (<0.5‰ salinity) and in those acclimated to media considered to be strongly saline (21‰ and 28‰ salinity) for this species.

Materials and Methods

Adult female specimens of *Macrobrachium olfersii*, measuring 4 to 6 cm in total length, were collected some 2 km from the mouth of the Paúba Stream on the southern coast of São Paulo State, Brazil. In the laboratory, the shrimps were maintained in 250-l aquaria in water from the collection site (fresh water [FW], <0.5‰ salinity) and were fed 3 times a week with fish, beef, and carrot.

To examine the effects of exposure to saline media on gill ultrastructure, groups of shrimps in stage $C\text{-}D_0$ of the molt cycle were acclimated to salinities of <0.5‰, 21‰, or 28‰ (20, 630, and 840 mOsm/kg H_2O; 5, 287, and 383 mEq Na^+/l; 5, 335, and 447 mEq Cl^-/l, respectively) over a 10-day period. Salinities, verified using an optical refractometer, were prepared by diluting seawater with FW from the collection site.

After the acclimation period, the ventral nerve cord was severed, the eyestalks and rostrum were removed, and the shrimps were perfused through the ventral abdominal sinus with primary fixative at the rate of 1 ml/min for 10 min. The sixth gill was then dissected, the middle third was removed and bisected, and the two portions, each comprising about 15 lamellae, were placed in primary fixative on ice for 2 h.

The primary fixatives for the different groups of acclimated shrimps were adjusted according to the hemolymph osmolality measured for each group. For shrimps maintained in FW, the fixative consisted of (in millimoles) paraformaldehyde (200), glutaraldehyde (250), sodium cacodylate (100); and Na^+ (28), K^+ (8), Ca^{++} (25), and Mg^{++} (4) as chlorides (effective osmolality 360 mOsm/kg H_2O, pH 7.3). The effective osmolalities (565 and 725 mOsm/kg H_2O) of the fixatives for shrimps

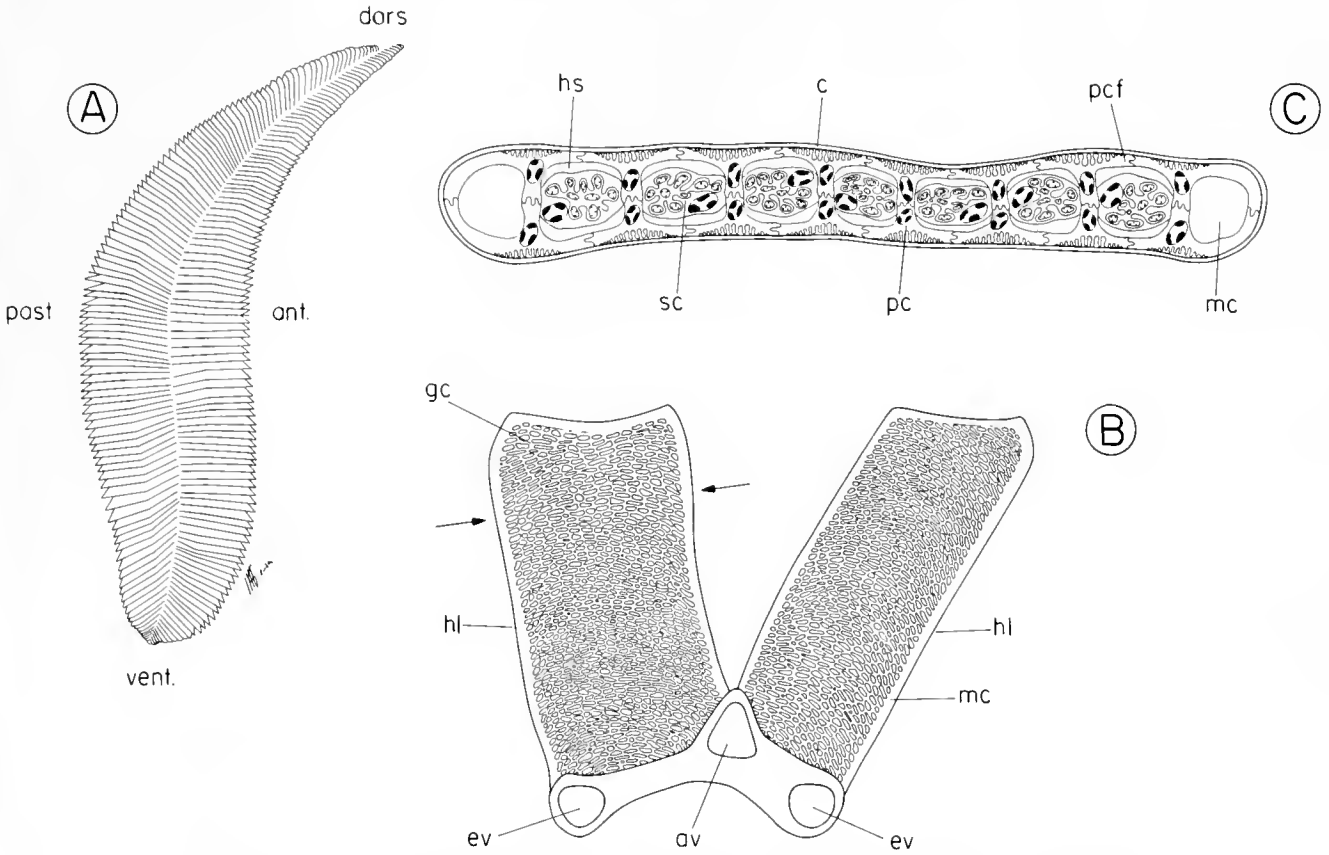

Figure 1. A summary and location diagram showing the general anatomy of the sixth, right posterior gill (A) and of a constituent gill lamella (B) in the freshwater shrimp *Macrobrachium olfersii*. Hemolymph flows from the lateral efferent vessels (ev), through the outer marginal canals (mc), across the hemilamella (hl) by way of the gill capillaries (gc) to the inner marginal canals, and back through the central afferent vessel (av). (C) A cross section of the hemilamella (between arrows in B) reveals the lattice-like organization of the gill tissue, resulting from the semi-regular arrangement of opposing pillar cells (pc). The perikarya of the pillar cells are surrounded by hemolymph spaces (hs) and abut the lateral regions of the median, intralamellar, septal cells (sc). The fine pillar cell flanges (pcf), in contact with the thin cuticle (c), form the primary epithelial interface between the hemolymph and the external medium.

acclimated to saline media of 21‰ and 28‰ were adjusted by using final NaCl concentrations of 140 and 225 m*M*, respectively.

The gill fragments were then rinsed (3 × 5 min) in the respective buffer solutions alone on ice (composition as above, less the aldehydes) and post-fixed in 1% osmium tetroxide in the same buffer systems for 1.5 h on ice.

The fragments were dehydrated in a graded ethanol series (65 min total), transferred into propylene oxide (2 × 15 min), infiltrated overnight, and embedded in Araldite 6005 resin. Thick sections were cut with glass knives at 0.5 μm thickness on a Porter-Blum Sorvall MT2 ultramicrotome, stained with 1% methylene blue and 1% azur II in 1% aqueous borax, and photographed using Kodak T-Max 100 ASA film on a Nikon AFX II photomicroscope. Thin sections of 50–80 nm thickness prepared similarly were stained with aqueous uranyl acetate and Reynolds' (1963) lead citrate and examined at an accelerating voltage of 80 kV in a Jeol 100-CX electron microscope.

The effects of acclimation to the experimental media (<0.5‰, 21‰, or 28‰) were evaluated morphometrically using as criteria the alterations induced in the thickness (in micrometers) of the intralamellar septal cells and the pillar cell flanges; and the height (in micrometers) and numerical density (as microvilli/micrometer of apical membrane) of the apical microvilli on the pillar cells. Measurements were made on between 10 and 15 micrographs of sections taken at random in a plane transverse to the long axis of the gill lamellae (see Fig. 1, and Freire and McNamara, 1995) from 3 to 5 shrimp for each saline medium. The material was photographed at 8000 to 10,000× and the negatives were printed at a final magnification of 25,000×.

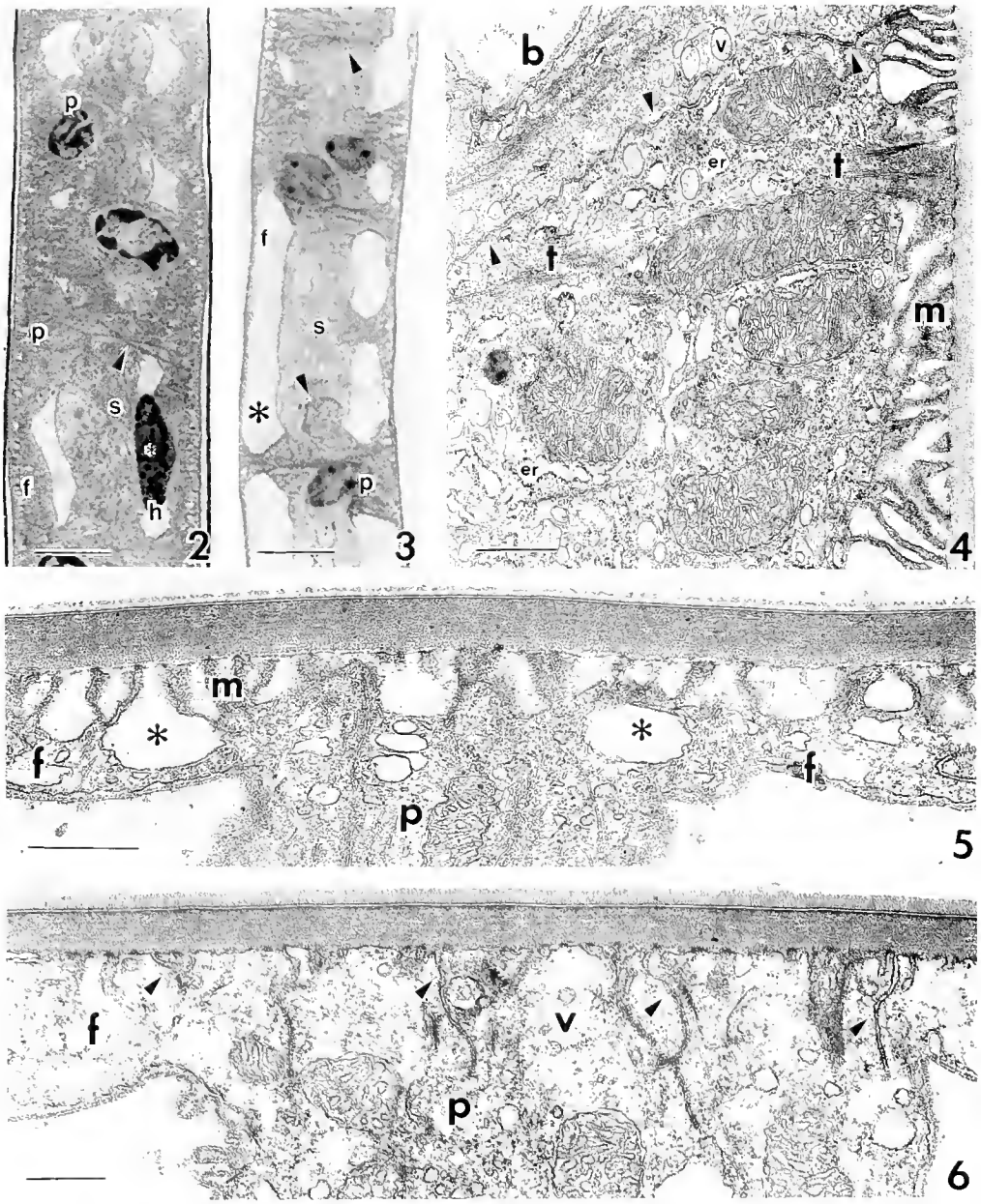

Figure 2. Thick (0.5 μm), epoxy section, taken transversely to the long axis of a gill lamella from *Macrobrachium olfersii* acclimated to fresh water (FW, < 0.5‰), showing the pillar cell perikarya (p) and thick flanges (f) below the subcuticular space. The intralamellar septum (s) adjoins the pillar cell perikarya (arrowhead). A hemocyte (*) is present in the hemolymph space (h). Scale bar = 10 μm.

Figure 3. Thick, epoxy section taken transversely to the long axis of a gill lamella from *M. olfersii* acclimated to seawater (SW) 28‰ for 10 days. The marked reduction in thickness of the pillar cell flanges (f) and septal cells (s) results in extensive hemolymph spaces (*). There is a distinct difference in cytoplasmic density (arrowheads) between the dark pillar (p) and light septal cells (s). Scale bar = 10 μm.

Figure 4. Transmission electron micrograph of a thin section taken transversely to the long axis of a gill lamella from *M. olfersii* in FW, showing the apical cytoplasm directly above the perikarya of two adjacent pillar cells, separated by a long, junctional complex (arrowheads). Apical microvilli (m), numerous vesicles (v), mitochondria, cisternae of rough endoplasmic reticulum (er), and microtubule bundles (t) are present. A basal lamina (b) separates the pillar cell membrane from the hemolymph space. Scale bar = 0.7 μm.

Figure 5. Electron micrograph of the apical region of a pillar cell perikaryon (p) and the bases of its lateral flanges (f) in a section taken transversely to the long axis of a gill lamella from *M. olfersii* acclimated to SW 21‰ for 10 days. The reduction in the height and numerical density of the apical microvilli (m) and in the thickness of the flanges is evident. The subcuticular space (*) between and below the microvilli is still present. Scale bar = 0.75 μm

Morphometric measurements were made using a transparent test overlay consisting of parallel line segments each 1 cm in length, equally spaced at 1-cm intervals (Weibel *et al.*, 1966; Freire and McNamara, 1995). To measure the thickness of the septal cells, the test system was placed perpendicularly to the plane of the gill cuticle; valid transects were represented by single planes in which the line segments intersected both cell margins. To estimate the thickness of the pillar cell flanges, valid transects were single planes in which a line segment intersected at least one cell margin.

The heights of the apical microvilli were sampled both in the region above the pillar cell body and in the mid-flange region. The test system was placed parallel to the plane of the microvilli, and the heights of all microvilli intersecting one of the extremities of each line segment were measured. A height of 1 mm on the micrograph was considered to be the minimum length criterion representing a single microvillus.

The numerical density of the apical microvilli was also sampled in the same regions of the pillar cells. A second test system comprising a straight line 125 mm in length (equivalent to 5.0 μm at 25,000×) was placed over the micrograph at random, although parallel to the plane of the cuticle. All microvilli lying directly above the plane of the test line were counted.

All data were tested for normality of distribution using the Kolmogorov-Smirnov test. Non-normal data were normalized by transformation using the inverse function. Single- or two-factor analyses of variance were then performed to detect the effect of acclimation salinity on the various response variables. This was followed by multiple means testing, using the Student-Newman-Keuls test, when an effect was found. The data on microvillus height could not be normalized by transformation and were analyzed nonparametrically with the Friedman two-factor and Kruskal-Wallis one-factor analyses of variance. Differences between groups were located using the Wilcoxon-Mann-Whitney U test. All tests were performed using a minimum significance level of $P = 0.05$. The data are presented in the text as the mean ± 1 SEM (n) unless otherwise indicated.

Results

Figure 1, a diagram of the localization and general morphology of the gill lamella in *M. olfersii*, illustrates the organization of the gill tissue into a semiregular latticework of pillar and septal cells within the lamella. The present study focuses particularly on the ultrastructure of the flange and perikaryon regions of the pillar cells, which form the principal epithelial barrier between the hemolymph and the external medium.

Fine structure of the gill tissue in shrimps acclimated to fresh water

Pillar cells. The electron-dense pillar cells are highly differentiated epithelial cells constituted by two distinct regions: the pillar cell perikaryon, 7.8 ± 1.4 μm (n = 10) in height by 9.1 ± 5.8 μm (n = 14) in width (Fig. 2); and the pillar cell flange, a fine, roughly elliptical, radial, apical expansion of the perikaryon (Fig. 2), 56 ± 10 μm (n = 3) in diameter and 2.86 ± 0.16 μm (n = 6) in thickness near the perikaryon.

The apical membrane of the pillar cells, overlain by the fine gill cuticle [249.0 ± 4.4 nm (n = 10) thickness], is folded into an extensive system of microvilli (Fig. 4) that are organized into small tufts of from 4 to 8 villi (Fig. 7). These 10-nm diameter, cylindrical projections of the apical cytoplasm (Fig. 8) are frequently arranged into regularly spaced, often hexagonal, units and measure roughly 700 nm in height. The distribution and height of the microvilli are not uniform over the pillar cell surface: they are longer (Table 1) and numerically more dense (Fig. 13) above the perikaryon (Fig. 4) than in the outer flange region (Fig. 9). A distinct subcuticular space, consisting mainly of the deeper invaginations between the tufts of microvilli (Figs. 2 and 7) and of large vesicles lying near the apical membrane (Fig. 9), is apparently continuous with these invaginations.

The electron-dense subapical cytoplasm immediately above the perikaryon (Fig. 4) contains numerous small vesicles; polyribosomes; mitochondria, frequently disposed with their long axes parallel to that of the perikaryon; cisternae of rough endoplasmic reticulum; and bundles of 23-nm diameter microtubules that insert into the base of each tuft of microvilli (Fig. 4). The nucleus occupies the basal region of the pillar cell perikaryon (Fig. 2), which is coupled to the adjacent cells of the intralamellar septum by regions of thick, basolateral junctions (Fig. 12). These junctions consist of a wide (109.3 ± 35.5 nm) intercellular space of variable form and length. The space, which contains granular material, leads to often complex, although limited, interdigitations between the plasmalemmae of the two cell types (Fig. 12, insert).

Figure 6. Electron micrograph of the apical region of a pillar cell perikaryon (p) and bases of its flanges (f) from *M. olfersii* acclimated to SW 28‰ for 10 days. The apical microvilli and subcuticular space have disappeared completely, being replaced by a few invaginations of the plasma membrane (arrowheads). Numerous vesicles (v) and mitochondria are present in the subapical cytoplasm. Scale bar = 0.4 μm.

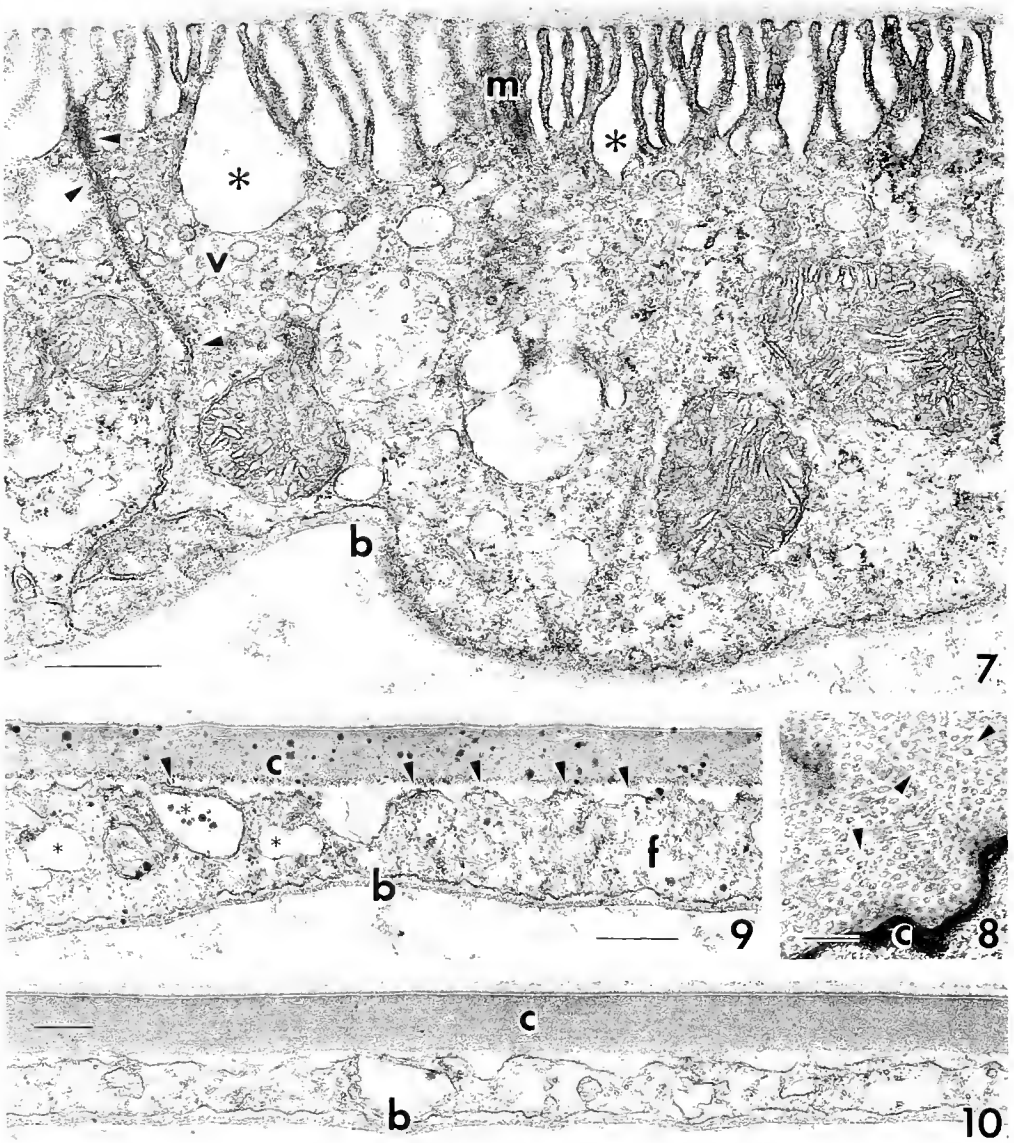

Figure 7. Transmission electron micrograph of a section taken transversely to the long axis of a gill lamella from *Macrobrachium olfersii* in FW, showing a region of the pillar cell flange, near the perikaryon, in junctional contact (arrowheads) with a flange from an adjacent pillar cell. Well developed, apical microvilli (m) are evident below the thin gill cuticle, as are numerous apical microvesicles (v), mitochondria, and the basal lamina (b) separating the uninvaginated, lower plasma membrane from the hemolymph. Subcuticular spaces (*) are present among and below the microvilli. Scale bar = 0.7 μm.

Figure 8. Thin section taken slightly obliquely to and just below the base of the gill cuticle (c) from *M. olfersii* in FW, demonstrating that the apical infolding system is constituted by microvilli (arrowheads) rather than leaflets, seen here in transverse section. Scale bar = 0.7 μm.

Figure 9. Extreme, lateral region of a fine, pillar cell flange (f), distant from the perikaryon, underlain by basal lamina (b) from *M. olfersii* in FW. The apical microvilli (arrowheads) have virtually disappeared below the cuticle (c), and only a few vesicles of the subcuticular space (*) and microtubules are present in the granular cytoplasm. Scale bar = 0.5 μm.

Figure 10. Extreme, lateral region of an apical, pillar cell flange, distant from the perikaryon, in the gill epithelium from *M. olfersii* acclimated to SW 21‰ for 10 days. No apical microvilli are distinguishable below the cuticle (c), and only a very thin layer of cytoplasm containing a few microtubules is visible above the basal lamina (b) and underlying hemolymph space. Scale bar = 0.3 μm.

Table I

Effect of acclimation to saline media for 10 days on various morphometric characteristics analyzed in the gill lamellae of the freshwater shrimp Macrobrachium olfersii

Characteristic	Acclimation salinity (‰)		
	<0.5	21	28
Thickness of pillar cell flange (μm)	1.30 ± 0.20 (11)	[a]0.34 ± 0.04 (10)	[a]0.40 ± 0.05 (11)
Density of microvilli in pillar cell flange	[b]4.00 ± 0.50 (11)	[b]2.70 ± 0.40 (12)	[bcd]1.00 ± 0.40 (12)
Density of microvilli above pillar cell perikaryon	6.20 ± 0.40 (12)	5.00 ± 0.20 (12)	[c]4.00 ± 0.60 (12)
Thickness of septal cell (μm)	7.80 ± 0.50 (10)	7.10 ± 0.50 (10)	6.50 ± 0.60 (13)

Data are given as mean values ± SEM (n). Numerical densities are expressed as the number of microvilli per micrometer of linear apical membrane.

[a] $P \leq 0.05$ compared to control thickness in 0 ‰; [b] $P \leq 0.05$ compared to values for perikaryon; [c] $P \leq 0.05$ compared to value for flange in 0 ‰; [d] $P \leq 0.05$ compared to value for flange in 21 ‰; [e] $P \leq 0.05$ compared to value for perikaryon in 0 ‰.

The apical flange region of the pillar cells becomes attenuated and thinner as the distance from the perikaryon increases, attaining only 1.38 ± 0.30 μm (n = 6) in thickness at the extreme margins (Fig. 9). The number and height of the microvilli and organelles likewise decrease markedly; the mitochondria exhibit no specific orientation. Like the pillar cell perikaryon (Fig. 4), the entire lower surface of the pillar cell flange is underlain by a fibrous basal lamina (Figs. 7 and 9), thickness 92.8 ± 11.0 nm (n = 8), that separates it from the hemolymph space. The plasma membrane of this lower surface is not folded or amplified in any way.

The regions of contact between adjacent pillar cell flanges constitute highly structured junctional complexes (Figs. 7 and 11). These typically comprise a short, dense desmosome of 287.4 ± 30.2 nm (n = 6) length, followed by an extensive septate junction of about 1.5 μm in length, and a long region of simple apposition of the two cell membranes, separated by a constant narrow distance of 17.8 ± 1.7 nm (n = 10).

Intralamellar septal cells. The electron-lucent septal cells, 12.0 ± 0.7 μm (n = 10) in thickness (Figs. 2 and 3), make contact with the hemolymph over most of their surface, which is greatly amplified and is characterized by many invaginations of the plasmalemma; these penetrate deeply into and extensively throughout the septal cell cytoplasm and appear to individually envelop each of the numerous ovoid mitochondria present within the cytoplasm (Fig. 12). The membrane infoldings define an extracellular space of constant width (22.0 ± 0.7 nm, n = 10) and maintain contact with the hemolymph. Typically, a single septal cell connects the bases of two adjacent pillar cells, its lateral ends interdigitating in a restricted manner with their basolateral membranes (Fig. 12, insert). Golgi bodies and glycogen granules are frequently found in the septal cells.

Ultrastructural and morphometric alterations induced in the gill tissue of shrimps acclimated to saline media

Various ultrastructural alterations appear in the pillar cells of the gill lamellae of *M. olfersii* after acclimation to the two saline media (21‰ and 28‰) for 10 days. Qualitatively similar, these modifications comprise substantial reductions in the thickness of the pillar cell flanges (Figs. 3 and 10) and in the height and density of the apical microvilli, both in the region above the pillar cell perikarya (Figs. 5 and 6) and in the attenuated flange regions (Fig. 10). In 21‰ salinity, the microvilli lose their characteristic tuft-like arrangement (Fig. 5), and the associated microtubule bundles are less evident. In 28‰, the microvilli are virtually absent, and only a few invaginations of the apical membrane are evident (Fig. 6).

There is a more subtle reduction in the thickness of the intralamellar septal cells (Fig. 3, *cf.* Fig. 2), the structural organization of which is maintained. With the reduction in thickness of the pillar cell flanges, and to a lesser extent of the intralamellar septal cells, there is a corresponding, marked increase in the volume of the hemolymph lacunae (Fig. 3, *cf.* Fig. 2).

These qualitative ultrastructural alterations were quantified through morphometrical evaluation; the principal findings for normally distributed data are presented in Table I. Figure 13 presents the data on the height of the apical microvilli for which a normal distribution could not be obtained.

Discussion

In the gill epithelium of *Macrobrachium olfersii*, the apical surface of the pillar cells is highly amplified by an extensive system of microvilli (type 2, see Cioffi, 1984). This system is found principally above the perikaryon, becoming attenuated in the extreme lateral regions. The lower surface of the pillar cell flange is not invaginated or associated with mitochondria, and it does not appear to be involved in active transport and salt movement. This is in strong contrast to the epithelial cells of the gill in brachyurans (Gilles and Péqueux, 1983), penaeids (Couch, 1977; Foster and Howse, 1978), and amphipods (Kikuchi *et al.*, 1993; Kikuchi and Matsumasa, 1995; Shires *et al.*, 1994). In these crustaceans, Na^+/K^+-ATPases are typically associated with the basolateral infold-

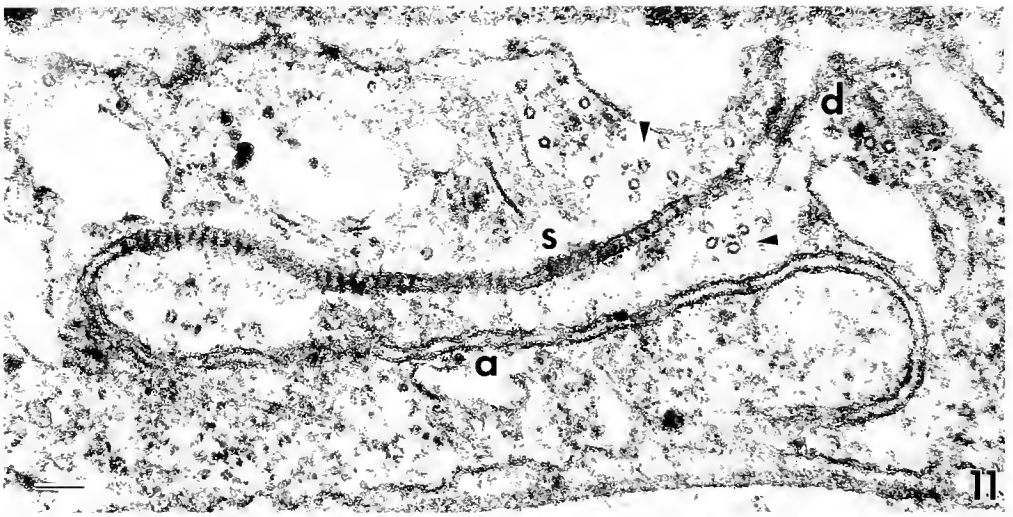

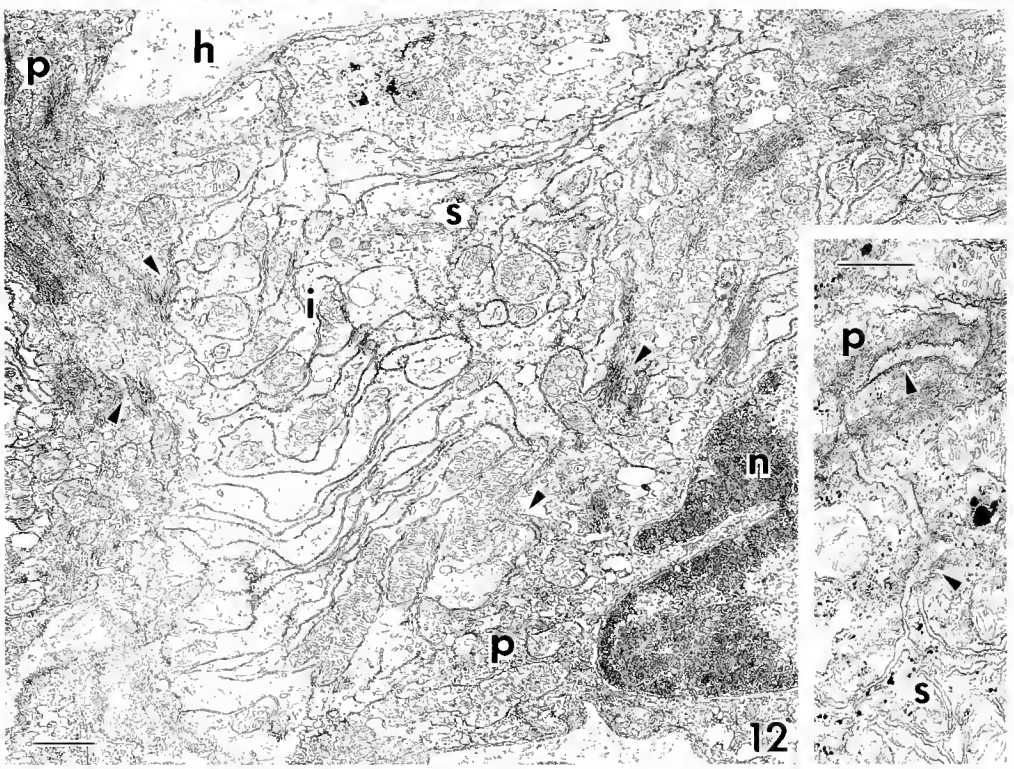

Figure 11. Detail of a characteristic junctional complex between the extreme, lateral flange regions of adjacent pillar cells from *Macrobrachium olfersii* in FW. The sequence of a small desmosome (d), septate junction (s) and region of close membrane apposition (a) is typical. Small groups of microarrowheads) are loosely associated with the apical region of the junction. Scale bar = 100 nm.

2. Transverse section of a gill lamella from *M. olfersii* in FW, showing a complex region of ...een the bases of two electron dense, pillar cell perikarya (p) and an electron lucent cell in the ... septum (s), characterized by extensive, deep invaginations (i) of the plasma membrane associ... ...chondria. Areas of dense, basolateral junctional complexes (arrowheads) link the two cell types ... nucleus (n), hemolymph space (h). Scale bar = 1.0 μm. Insert: Detail of a thick, basolateral ... arrowheads) between an interlamellar septal cell (s) and an abutting pillar cell (p), showing abund... finely granular material in the wide extracellular space. Scale bar = 0.5 μm.

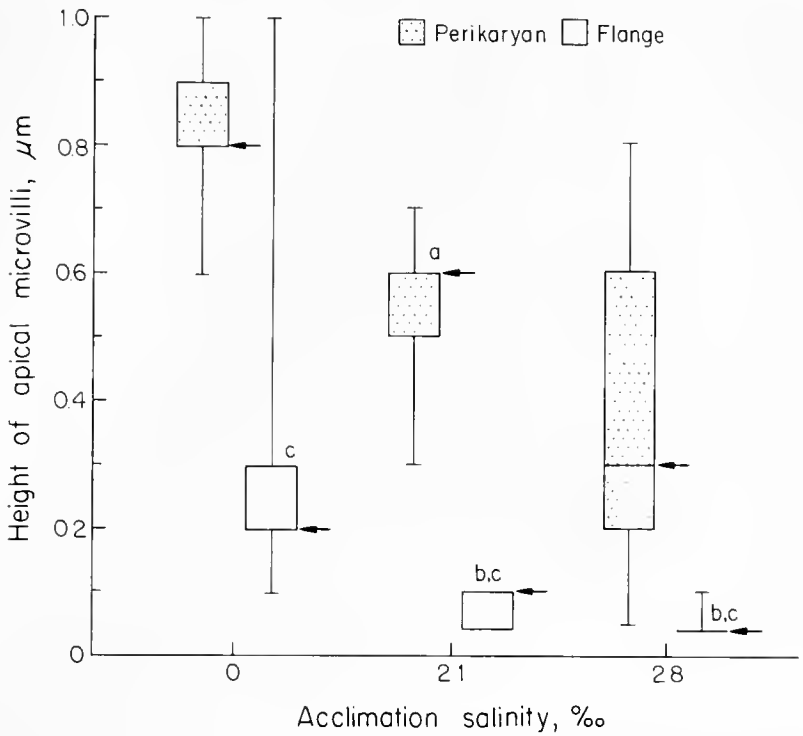

Figure 13. The effect of acclimation salinity (<0.5‰, 21‰, and 28‰) on the height of the apical microvilli in the region immediately above the pillar cell perikarya and in the extreme flange regions. The non-normally distributed data are given as the median values (arrows); the upper and lower box boundaries indicate the interquartile range; and the whiskers depict the minimum and maximum values. $^{a}P < 0.05$ compared to value for perikaryon in fresh water (< 0.5‰), $^{b}P < 0.05$ compared to value for flange in fresh water, $^{c}P < 0.05$ compared to respective values for perikarya in same salinities.

ings of the epithelial cells (see Towle, 1984; Towle and Kays, 1986; Taylor and Taylor, 1992) and actively drive salt uptake from the external medium directly into the hemolymph up a Na^+ gradient across the epithelium (see Péqueux, 1995, for review).

The differential distribution of the apical microvilli in *M. olfersii* attests to a dual role for the pillar cells in the regulatory physiology of the gill. The principal ion movements across the apical membrane occur through ion exchangers like the Na^+/NH_4^+ (Armstrong *et al.*, 1981) and Cl^-/HCO_3^- (Péqueux, 1995) counter transporters most likely present in the membranes of the long, dense microvilli located immediately above the pillar cell perikaryon, the region closest to the basolateral junctions with the septal cells. The exchange of respiratory gases, however, would be preferentially effected through the far less amplified surface of the shorter, less dense microvilli in the very thin, extreme flange regions that form a cytoplasmic barrier only 1.4 μm in thickness, directly above and in contact with the hemolymph space. This situation contrasts sharply with that known for brachyurans, in which respiratory gas-exchange functions predominate in the anterior gills, while ion transport mechanisms are more restricted to the posterior gills (Péqueux, 1995).

The notable reductions in the height and numerical density of the microvilli on the apical surface of the pillar cells, and in the thickness of the flanges, which occur as a result of acclimation to saline media in *M. olfersii*, are qualitatively similar to the modifications seen in the gill epithelia of a variety of osmoregulating crustaceans in response to exposure to either hyper- or hypo-osmotic media. In the brachyuran crabs *Eriochier sinensis* and *Carcinus maenas* acclimated to fresh water and 30% seawater, respectively, the apical infolding system becomes deeper and more pronounced, as does the subcuticular space (Gilles and Péqueux, 1985, 1986). In the latter crab, the depth of the basolateral invaginations and the number of mitochondria also appear to increase, with a closer degree of apposition between them (Compère *et al.*, 1989).

In the marine shrimp *Penaeus aztecus* exposed to a dilute medium of 0.9‰, the apical membranes of the epithelial cells become highly and deeply infolded compared to those of shrimps kept in seawater (Foster and

Howse, 1978). In this penaeid and *P. duorarum* (Couch, 1977) and *P. vannamei* (Taylor and Taylor, 1992, Fig. 25A), and in the palaemonid *Palaemonetes pugio* (Doughtie and Rao, 1978), the pillar cell perikarya appear to constitute part of the intralamellar septum. However, no changes seem evident in the septal cells of *P. aztecus* after low-salinity exposure (Foster and Howse, 1978). In *M. olfersii*, subtle changes in septal cell morphometry do occur after high-salinity acclimation: the number of membrane invaginations interposed between adjacent mitochondria increases, as does the surface density (square micrometers of membrane surface per cubic micrometer of cytoplasm) of the septal cells and the mitochondrial volume fraction; the mitochondrial profiles also become more elongate (Freire and McNamara, 1995).

In one of the few studies directly comparable to the present report (Shires *et al.*, 1994), a marked reduction occurred in the height and organization of the apical lamellae in the gill epithelial cells of the amphipod *Gammarus duebeni* within 1 h of exposure to seawater; the mitochondria relocated to the cell center and appeared to lose their intimate contact with both the apical and basolateral membrane systems. These alterations were transient, however, as the lamellae appeared to reorganize after 10–16 h.

These various data demonstrate the labile nature of the apical infoldings of the epithelial and pillar cells in the gill lamellae of osmoregulating crustaceans. The membrane surface area of this primary interface between the external medium and the hemolymph increases markedly during the acclimation of marine decapods to dilute media, and is notably decreased in freshwater Crustacea acclimated to saline media. This membrane system may thus serve primarily to modulate apical permeability by regulating the density of constituent ion-exchange molecules. In contrast, the system of basolateral infoldings and mitochondria in the epithelial cells of marine decapods appears largely unresponsive to decreased salinity; in freshwater Crustacea, exposure to saline media produces subtle alterations in membrane surface area and stacking, and in the location of the mitochondria.

The data on *M. olfersii*, both from shrimps maintained in fresh water (FW) and in those acclimated to saline media, also provide pertinent information about the routes of ion and water movements into the hemolymph through the gill tissue. In FW-acclimated shrimps, the gill epithelium appears to be a tight epithelium, well protected from paracellular water and ion movements by extensive and characteristic junctions—constituted by a small desmosome and a lengthy septate junction—between adjacent pillar cell flanges. These junctions are similar to those found in the gill epithelia of the freshwater amphipods *Sternomoera yezoensis* (Kikuchi *et al.*, 1993) and *Gammarus duebeni* (Shires *et al.*, 1994). The absence of mitochondria and infoldings of the basolateral membrane strongly suggests that the lower flange regions are not involved in active salt movement in *M. olfersii*.

However, the ultrastructure of the intralamellar septal cells, with their deep and numerous invaginations intimately associated with mitochondria, is typical of an active, salt-transporting epithelium in crustaceans and in a variety of invertebrate tissues (see Cioffi, 1984; Péqueux, 1995). Sites of Na^+/K^+-ATPase activity, demonstrated ultracytochemically, are present on the cytoplasmic surface of the leaflets of this extensive membrane system in *M. olfersii* (Torres and McNamara, 1996); their activity would be fueled by ATP furnished directly by the abundant adjacent mitochondria. In FW-acclimated shrimps, the activity of the Na^+/K^+-ATPases in the membrane invaginations of the septal cells creates the driving force for net Na^+ uptake from the freshwater medium across the apical membranes of the pillar cells into the perikarya. Na^+ would then pass through the extensive intercellular junctions between the base of the pillar cell perikarya and the lateral ends of the intralamellar septal cells into the septal cell cytoplasm, and from there directly into the hemolymph *via* the Na^+/K^+-ATPases in the membrane invaginations. Corroborating this proposed route of ion movement, Lima *et al.* (1997) have shown a significant reduction in Na^+/K^+-ATPase activity in preparations of gill membrane vesicles from *M. olfersii* after acclimation to saline media (21 and 28‰ salinity) for 20 days. This observation suggests a reduction in the number of ATPase molecules in these membranes available for active Na^+ transport.

The alterations occurring at the apical pillar cell interface, and other changes in the characteristics of the intralamellar septal cells, including the reduction in Na^+/K^+-ATPase activity, thus appear to reflect the structural transformations underlying the molecular mechanisms of long-term adaptation to hyperionic media in freshwater palaemonids, particularly those that restrict the uptake of Na^+.

Acknowledgments

This study represents part of an MSc thesis submitted by AGL to the Departamento de Fisiologia/IBUSP; it was financed by a research grant to JCM (FAPESP 91/2467-2) and a post-graduate scholarship (FAPESP 90/3807-9). The authors thank Drs. João Lunetta (CEBIMAR), Sergio Oliveira (DHE/ICB), and Valder de Melo (DM/FMRP) for access to essential facilities; José Augusto Maulin (DM/FMRP) for photographic work; and Marcos Ribeiro de Souza (FFCLRP) for the line drawing.

Literature Cited

Armstrong, D. A., K. Strange, J. Crowe, A. Knight, and M. Simmons. 1981. High salinity acclimation by the prawn *Macrobrachium rosenbergii*: uptake of exogenous ammonia and changes in endogenous nitrogen compounds. *Biol. Bull.* **160:** 349–365.

Barra, J.-A., A. Péqueux, and W. Humbert. 1983. A morphological study on gills of a crab acclimated to fresh water. *Tissue Cell* **15:** 583–596.

Bubel, A. 1976. Histological and electron microscopical observations on the effects of different salinities and heavy metal ions on the gills of *Jaera nordmanni* (Rathke) (Crustacea, Isopoda). *Cell Tiss. Res.* **167:** 65–95.

Cioffi, M. 1984. Comparative ultrastructure of arthropod transporting epithelia. *Am. Zool.* **24:** 139–156.

Compère, Ph., S. Wanson, A. Péqueux, R. Gilles, and G. Goffinet. 1989. Ultrastructural changes in the gill epithelium of the green crab *Carcinus maenas* in relation to external salinity. *Tissue Cell* **21:** 299–318.

Copeland, D. E. 1968. Fine structure of salt and water uptake in the land crab *Gecarcinus lateralis*. *Am. Zool.* **8:** 417–432.

Copeland, D. E., and A. T. Fitzjarrell. 1968. The salt absorbing cells in the gills of the blue crab (*Callinectes sapidus* Rathbun) with notes on modified mitochondria. *Z. Zellforsch.* **92:** 1–22.

Couch, J. A. 1977. Ultrastructural study of lesions in gills of a marine shrimp exposed to cadmium. *J. Invertebr. Pathol.* **29:** 267–288.

Doughtie, D. G., and K. R. Rao. 1978. Ultrastructural changes induced by sodium pentachlorophenate in the grass shrimp, *Palemonetes pugio*, in relation to the molt cycle. Pp. 213–250 in *Pentachlorophenol: Chemistry, Pharmacology, and Environmental Toxicology*, Vol. 12, K. R. Rao, ed. Plenum Press, New York.

Foster, C. A., and H. D. Howse. 1978. A morphological study on gills of the brown shrimp, *Penaeus aztecus*. *Tissue Cell* **10:** 77–92.

Freire, C. A., and J. C. McNamara. 1995. Fine structure of the gills of the fresh-water shrimp *Macrobrachium olfersii* (Decapoda): effect of acclimation to high salinity medium and evidence for involvement of the intralamellar septum in ion uptake. *J. Crustac. Biol.* **15:** 103–116.

Gilles, R., and A. Péqueux. 1985. Ion transport in crustacean gills: physiological and ultrastructural approaches. Pp. 136–158 in *Transport Processes, Iono- and Osmoregulation*, R. Gilles and M. Gilles-Biallien, eds. Springer-Verlag, Berlin.

Gilles, R., and A. Péqueux. 1986. Physiological and ultrastructural studies of NaCl transport in crustacean gills. *Bol. Zool.* **53:** 173–182.

Kikuchi, S., M. Matsumasa, and Y. Yashima. 1993. The ultrastructure of the sternal gills forming a striking contrast with the coxal gills in a fresh-water amphipod (Crustacea). *Tissue Cell* **25:** 915–928.

Kikuchi, S., and M. Matsumasa. 1995. Pereopodal disk: a new type of extrabranchial ion-transporting organ in an estuarine amphipod, *Melita setiflagela* (Crustacea). *Tissue Cell* **27:** 635–643.

Lima, A. G., J. C. McNamara, and W. R. Terra. 1997. Regulation of hemolymph osmolytes and gill Na^+/K^+-ATPase activities during acclimation to saline media in the freshwater shrimp *Macrobrachium olfersii* (Wiegmann, 1836) (Decapoda, Palaemonidae). *J. Exp. Mar. Biol. Ecol.* In press.

Maina, J. N. 1990. The morphology of the gills of the freshwater African crab *Potamon niloticus* (Crustacea: Brachyura: Potamonidae): a scanning and transmission electron microscopic study. *J. Zool.* **221:** 499–515.

Mantel, L. H., and L. L. Farmer. 1983. Osmotic and ionic regulation. Pp. 53–161 in *The Biology of Crustacea*, Vol. 5, *Internal Anatomy and Physiological Regulation*, L. H. Mantel, ed. Academic Press, New York.

McNamara, J. C. 1987. The time course of osmotic regulation in the freshwater shrimp *Macrobrachium olfersii* (Wiegmann) (Decapoda, Palaemonidae). *J. Exp. Mar. Biol. Ecol.* **107:** 245–251.

Nakao, T. 1974. Electron microscopic study of the open circulatory system of the shrimp, *Caridina japonica*. I. Gill capillaries. *J. Morphol.* **144:** 361–380.

Péqueux, A. 1995. Osmotic regulation in crustaceans. *J. Crustac. Biol.* **15:** 1–60.

Reynolds, E. S. 1963. The use of lead citrate at high pH as an electron-opaque stain in electron microscopy. *J. Cell Biol.* **17:** 208–212.

Shires, R., N. J. Lane, C. B. Inman, and A. P. Lockwood. 1994. Structural changes in the gill cells of *Gammarus duebeni* (Crustacea, Amphipoda) under osmotic stress: with notes on microtubules in association with the septate junctions. *Tissue Cell* **26:** 767–778.

Taylor, H. H., and E. W. Taylor. 1986. Observations of valve-like structures and evidence for rectification of flow within the gill lamellae of the crab *Carcinus maenas* (Crustacea, Decapoda). *Zoomorphology* **106:** 1–11.

Taylor, H. H., and E. W. Taylor. 1992. Gills and lungs: the exchange of gases and ions. Pp. 203–293 in *Microscopic Anatomy of Invertebrates*, Vol. 10, *Decapod Crustacea*, F. W. Harrison and A. G. Humes, eds. Wiley-Liss, Inc., New York.

Torres, A. H., and J. C. McNamara, 1996. Localização ultracitoquímica da ATPase Na^+/K^+-dependente em células de brânquia e glândula antenal do camarão de água doce *Macrobrachium olfersii*. IV Simpósio de Iniciação Científica da Universidade de São Paulo, Abstracts, p. 132.

Towle, D. W. 1984. Membrane-bound ATPases in arthropod ion-transporting tissues. *Am. Zool.* **24:** 177–185.

Towle, D. W., and W. T. Kays. 1986. Basolateral localization of $Na^+ + K^+$-ATPase in gill epithelium of two osmoregulating crabs, *Callinectes sapidus* and *Carcinus maenas*. *J. Exp. Zool.* **239:** 311–318.

Weibel, E. R., G. S. Kistler, and W. F. Scherle. 1966. Practical stereological methods for morphometric cytology. *J. Cell Biol.* **30:** 23–28.

Reference: *Biol. Bull.* **192:** 332–339. (April, 1997)

Effect of Salinity on Ionic Shifts in Mesohaline Scyphomedusae, *Chrysaora quinquecirrha*

DAVID A. WRIGHT[1] AND JENNIFER E. PURCELL[2]

University of Maryland System, Center for Environmental and Estuarine Studies, [1]Chesapeake Biological Laboratory, Solomons, Maryland 20688-0038, and [2]Horn Point Environmental Laboratory, Cambridge, Maryland 21613

Abstract. Mesohaline populations of the scyphomedusae *Chrysaora quinquecirrha* are found in salinities ranging from 5‰ to 25‰. Osmotic and ionic adjustments within this salinity range were investigated using *C. quinquecirrha* ephyrae budded from polyps in the laboratory and young medusae collected from the mid-salinity region of the Patuxent River, Maryland. When medusae were transferred from 20‰ salinity to lower salinities (8‰, 12‰), concentrations of sodium and magnesium in tissue and mesogleal fluid fell rapidly and approached those of dilute seawater within 6 hours. There was some recovery of these levels relative to the 8‰ medium, and they were significantly higher than the dilute seawater concentration after 1 week. Tissue concentrations of calcium showed no evidence of being regulated, whereas potassium was strongly regulated such that levels did not fall significantly following transfer of medusae to lower salinities. However, after 1 week, the concentration of potassium in mesogleal fluid approached that of the dilute medium. Extracellular space measured by direct blotting and weighing or using ^{35}S was about 40%. As a result, estimates for intracellular potassium were revised to 17 $mM\ l^{-1}$. The concentration of potassium in tissue remained stable following transfer to lower salinity, despite a substantial osmotic influx of water. This influx was measured as >20% gain in body weight over 24 h following transfer of medusae from 16‰ to 8‰. Mesogleal fluid was slightly hypo-osmolar to the medium at 15% and 20‰ and slightly hyperosmolar to the medium at 5‰ and 12‰. Sulfate concentrations in mesogleal fluid were 66%–70% those of the external medium. Medusae died or were unable to achieve positive buoyancy at 5‰, which is probably very close to a lower salinity limit for *C. quinquecirrha* in the mesohaline Chesapeake Bay.

Received 28 May 1996; accepted 13 January 1997.

Introduction

Most members of the phylum Cnidaria are marine. Only a few hydrozoans (*e.g., Craspedacusta*) live in fresh water. Some cnidarians occur in low-salinity waters, but species diversity decreases sharply with decreased salinity (Dumont, 1994). In Chesapeake Bay, medusae of the scyphozoan *Chrysaora quinquecirrha* are unusual in tolerating salinities as low as 5‰; the scyphistomae (polyps) are not found where salinities are less than 7‰ and thrive at 10‰ to 25‰ (Cargo and Schultz, 1966, 1967). Purcell (unpubl. data) has determined that asexual reproduction in *C. quinquecirrha* in the mesohaline Chesapeake Bay is limited by both low (<5‰) and high (>25‰) salinities. Differences in reproduction at different salinities may result in part from the physiological cost of salinity adjustment; *i.e.*, energy required for volume regulation may detract from that available for reproductive effort.

Mills (1984) found that a variety of marine hydromedusae and ctenophores adjusted osmotically within a few hours to abrupt changes in salinity between 23‰ and 38‰. Most species tested were able to osmoconform to this salinity range. However, salinity of 19‰ was usually lethal to animals normally found at a salinity of 30%. In experiments using Percoll to change the density but not the tonicity of seawater, medusae made no buoyancy adjustments. Therefore, Mills (1984) concluded that the process was passive osmotic accommodation to the salinity changes, not active density regulation. Studies such as those of Schick (1973) have suggested that amino acids play an important role in maintaining cellular volume

in osmotically stressed cnidarians. In freshwater forms, however, sodium and potassium extrusion followed by water loss from cells (Benos and Prusch, 1972) seems to provide the principal means of regulating cellular volume. Webb *et al.* (1972) examined free amino acids (FAA) in scyphistomae of three species of scyphomedusae, including *C. quinquecirrha.* They found that although FAA concentrations increased linearly with increasing salinity, they were only 0.9% to 4.6% of the total osmotically active substances in the scyphistoma and could not account for its osmotic balance. In summary, there is evidence for both active and passive osmotic processes in pelagic cnidarians.

Little work has been done on ionic regulation in pelagic cnidarians. Robertson (1949) summarized some earlier work on *Aurelia aurita* medusae, showing that the ionic composition of the medusae was not the same as that of the surrounding water and thus suggesting that the medusae can actively control their ionic composition. The finding that sulfate ions were particularly low stimulated interest in the exclusion of heavy ions, specifically sulfate, as a mechanism of buoyancy control in gelatinous zooplankton (Denton and Shaw, 1962; Mackay, 1969; Bidigare and Biggs, 1980; Mills and Vogt, 1984). Mackay (1969) described a saturable, probably active, sulfate transport mechanism with K_m values of 17 to 22 mM l^{-1} in two species of hydromedusae. Bidigare and Biggs (1980) determined that active sulfate loss from the ctenophore *Beroe cucumis* could be compensated by isosmotic chloride exchange. The current research investigated changes in tissue and mesoglea osmolality and cation levels in *C. quinquecirrha* medusae at different salinities. Results were considered in light of salinity-related changes in body size and extracellular space determined either directly or using sulfate.

Materials and Methods

Medusae between 1 and 2 g wet weight (25–30 mm bell diameter) were obtained from the Patuxent River, Maryland, and acclimated in 40-l aquaria containing 16‰ Patuxent River water for 1 wk before experiments. Medusae were fed *Artemia salina* nauplii during the acclimation periods, but they were not fed during experimental treatments unless otherwise stated. Ephyrae were budded from scyphistomae at 20‰ in the laboratory.

Cation measurements

Medusae were netted out of holding tanks, blotted dry in a standardized manner using laboratory wipes, and weighed by introducing them to tared individual polyethylene beakers containing 400 ml of experimental medium. In the two experiments reported here, medusae were transferred from 20‰ to 8‰ and 12‰ at time = 0 h. Six animals were prepared for immediate analysis, and six animals from each treatment were sampled at 6 h, 24 h, and 7 d. Animals were lifted from beakers with large plastic forceps, blotted dry on laboratory wipes, and weighed in plastic weighing dishes. The bell and tentacles were then separated, and the mesoglea was allowed to drain into the weighing dish. A 50-μl sample of mesogleal fluid was pulled into a hematocrit tube and then expelled into a small Nalgene vial containing 200 μl of Ultrapure concentrated nitric acid. A weighed amount of tentacular tissue (50–100 mg) was stored in Nalgene vials with 500 μl of nitric acid. Water samples from each beaker were collected at the end of each experiment and stored in Nalgene vials with 100 μl of nitric acid. When digestion was complete, all samples were diluted with nanopure water and refrigerated until analysis.

Sodium, potassium, calcium, and magnesium were analyzed using flame atomic absorption spectrophotometry. Lanthanum chloride was used to offset anionic interference with calcium and magnesium analyses.

Effect of salinity on osmolality of mesogleal fluid

Medusae were acclimated for 1 wk at salinities of 5‰, 12‰, 15‰, and 20‰. Mesogleal fluid from both bell and tentacles was drawn into calibrated hemocrit tubes and osmotic pressure determined using a Wescor 5500 vapor pressure osmometer. Osmotic pressure was also measured in the corresponding samples of external media. Osmolality in media and mesogleal fluid was expressed per kilogram, based on weight determinations made of both samples.

Size and weight changes in ephyrae and medusae

Ephyrae used for experiments were 2–3 mm in diameter; others, fed on *Artemia* nauplii, were grown to greater sizes for determinations of diameter and weight. A binocular microscope equipped with a micrometer eyepiece was used to measure diameters; a Cahn microbalance was used for weights. Weights of ephyrae used in experiments were estimated from a regression curve relating empirical measurements of diameter and wet weight over a range of animal sizes.

Medusa weights were determined directly by removing animals from the media, rinsing and blotting them lightly to remove surface water and gastrovascular fluid, and transferring them to a plastic weighing tray on a top-pan balance. To estimate the relative contributions of mesogleal fluid and tissue to total medusa weight, eight medusae were weighed as above. Then the bell and tentacles were separated and weighed. The bell and tentacles were next sliced into small pieces, thoroughly blotted with laboratory wipes, and reweighed; this weight was subtracted from the total wet weight to estimate the

mesogleal fluid weight. No correction was made for the fibrous component of the mesoglea, which was included in the tissue weight. Some contamination of the mesogleal fluid component by gastrovascular fluid may have occurred, but most of the latter was removed by the initial blotting. Finally the residue was dried thoroughly and reweighed to obtain a percentage solid material.

During salinity transfer experiments, we observed weight losses that were probably caused by starvation. To better understand the role of starvation in weight loss, a single controlled feeding experiment was conducted using ephyrae fed cultured rotifers (*Brachionis*). The diameters of 24 ephyrae acclimated to a salinity of 20‰ were measured. The animals were placed into individual multi-wells containing 2 ml of 20‰ water. The ephyrae were divided into three feeding groups: unfed, 5 rotifers d^{-1}, and 10 rotifers d^{-1}. At 24 h, the ephyrae were measured, their water was changed, and the appropriate number of rotifers was added to each well. Measurements were repeated at 48 h, and growth was recorded as the mean daily increase in ephyra diameter.

Sulfate in medusa tissue

Weighed tissue samples were dissolved in Ultrapure concentrated nitric acid and diluted with nanopure water. Total sulfate was determined with a Dionex ion chromatograph. Sulfate exchange was measured using $Na_2{}^{35}SO_4$. Small medusae were exposed to radioisotope for periods up to 60 h. The exposure medium had a salinity of 16‰, with $Na_2{}^{35}SO_4$ added to a specific activity of 250 μCi/mM SO_4. After isotope exposure the medusae were netted, then triple rinsed, blotted, and weighed. The specific activity of sulfate in the animals was recorded as a percentage of the specific activity of the external medium. ^{35}S was measured with a Packard Tricarb 4000 series liquid scintillation counter.

Statistics

Statistical differences between the mean ionic concentrations of tissue and seawater were tested using t-tests with significance determined at the 5% level. Paired t-tests were used to evaluate osmolality differences between mesoglea and medium in individual replicates ($P < 0.05$). A line of best bit fit through ^{35}S exchange data was estimated using an iterative (NLIN) hyperbolic regression program (SAS).

Results

Cation concentrations in tissue and mesogleal fluid

Ionic concentrations in tissue and mesogleal fluid generally underwent similar changes when medusae were transferred from a salinity of 20‰ to either 8‰ (experiment 1, Fig. 1) or 12‰ (experiment 2, Fig. 2). Following the transfer of animals from 20‰ to either 8‰ or 12‰, sodium concentrations in tissue and mesogleal fluid were characterized by a rapid drop over the initial 6 h to levels approaching those seen in the external media (Figs. 1A, 2A). Mesogleal sodium also fell, but much slower in the 12‰ medium; at 8‰, the tissue Na concentration made an apparent "recovery" after 1 wk, to a level higher than that of the external medium.

Tissue potassium concentration in animals held at 20‰ was at least twice the corresponding seawater concentration and was generally maintained at levels between 11 and 14 mM kg^{-1} over a period of a week in both experiments. However, in experiment 2, tissue potassium in control (20‰) animals rose to a mean level of 17 mM kg^{-1}. Tissue potassium levels represented a differential of at least 12 mM kg^{-1} compared with the most dilute medium (2 mM kg 1^{-1}). In experiment 1 the initial concentration of potassium in mesogleal fluid was significantly higher than at 20‰ ($P < 0.05$). When animals were transferred from 20‰ to 8‰, mesogleal potassium fell to a concentration similar to that of the initial medium (20‰) but significantly higher than the 8‰ medium (Fig. 1B). After a subsequent rise at 24 h it fell again, but remained significantly higher than the 8‰ medium after 1 wk. On transfer from 20‰ to 12‰ (experiment 2), mesogleal potassium concentration showed no significant dilution and remained consistently higher than that of the 12‰ medium over 1 wk. Tissue potassium levels did not change significantly following the transfer of medusae to either 8‰ (Fig. 1B) or 12‰ (Fig. 2B).

In animals transferred from 20‰ to 8‰, concentrations of calcium in both tissue and mesogleal fluid fell after 6 h (Fig. 1C). Thereafter, mesogleal calcium concentration remained significantly higher than concentrations in tissue or in the external medium. Overlap of standard deviations associated with calcium levels of the medium at 20‰ and 12‰ (Fig. 2C) rendered calcium data from experiment 2 equivocal.

Magnesium levels in both salinity transfer experiments showed trends similar to those of calcium. Following transfer of animals from 20‰ to either 8‰ (Fig. 1D) or 12‰ (Fig. 2D), magnesium levels in tissue remained consistently higher than in mesogleal fluid. Both tissue and mesogleal magnesium concentrations remained higher than those of dilute external media for a period of a week.

Transference of medusae from 20‰ to 5‰ caused all animals to fall to the bottom of the experimental beakers. Three out of six medusae began to disintegrate within 36 h; one was unhealthy but alive after 3 days, and two were swimming weakly near the bottom of the beakers. No ionic data were recorded from these animals.

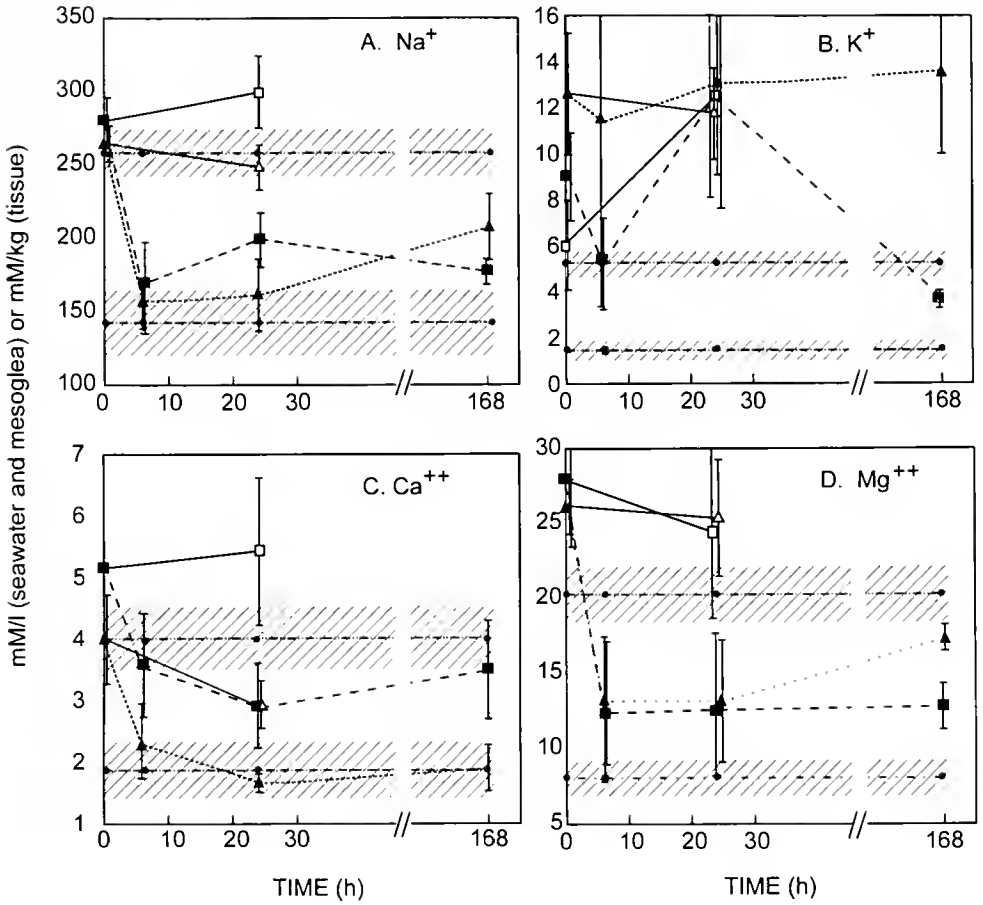

Figure 1. Ion concentrations in mesogleal fluid and tissue of *Chrysaora quinquecirrha* medusae transferred from 20‰ salinity to 8‰. (A) sodium, (B) potassium, (C) calcium, (D) magnesium. Each symbol represents the mean ± 1 SD of six animals. Solid symbols represent ion concentrations in animals transferred from higher to lower salinity at $t = 0$: squares = mesogleal fluid, triangles = tissue. Open squares and triangles represent concentrations in mesogleal fluid and tissue respectively, in animals maintained at 20‰. Dotted horizontal lines represent the mean ionic concentrations of the media in experimental containers (upper = control, lower = treatment) at the end of the experiments; shaded areas represent ±1 SD.

Effect of salinity change on body and tissue weight

All of the foregoing measurements of ionic shifts should be considered against changes in tissue hydration resulting from osmosis. Several experiments were carried out to quantify this phenomenon, although it proved difficult to obtain consistent results. Typical results indicate a wide variation in weight change, even over 24 h (Fig. 3). Changes in salinity from 16‰ to 8‰ resulted in body weight increases between 10% and 15% in whole medusae over 24 h, at which time their body weight was >30% higher than control animals. The time course of the subsequent weight loss was reflected by a concomitant loss in weight of medusae maintained in 16‰ for 1 wk.

Some of this weight loss could have been due to lack of food during the experiments. The diameter of unfed ephyrae in a 48-h controlled feeding experiment was reduced at a daily rate of 2.3% ± 20.5% (SD) (Fig. 4). Ephyra size was positively related to food; diameters increased by 10.6% ± 13.8% d^{-1} in those fed 5 rotifers d^{-1} and by 29.2% ± 25.4% d^{-1} in those fed 10 rotifers d^{-1}.

Osmolality of mesogleal fluid

The osmolality of mesogleal fluid and corresponding seawater was measured in medusae acclimated for 1 wk in 5‰, 12‰, 15‰, and 20‰ (Fig. 5). All animals at 12‰–20‰ exhibited overlap between seawater and mesogleal osmolality, although paired *t*-tests indicated that the osmolality of mesogleal fluid was significantly lower than that of the corresponding external medium at 15‰ and 20‰ ($P < 0.05$). Conversely, animals at 5‰ and 12‰ had significantly higher mesogleal osmolality than that of seawater.

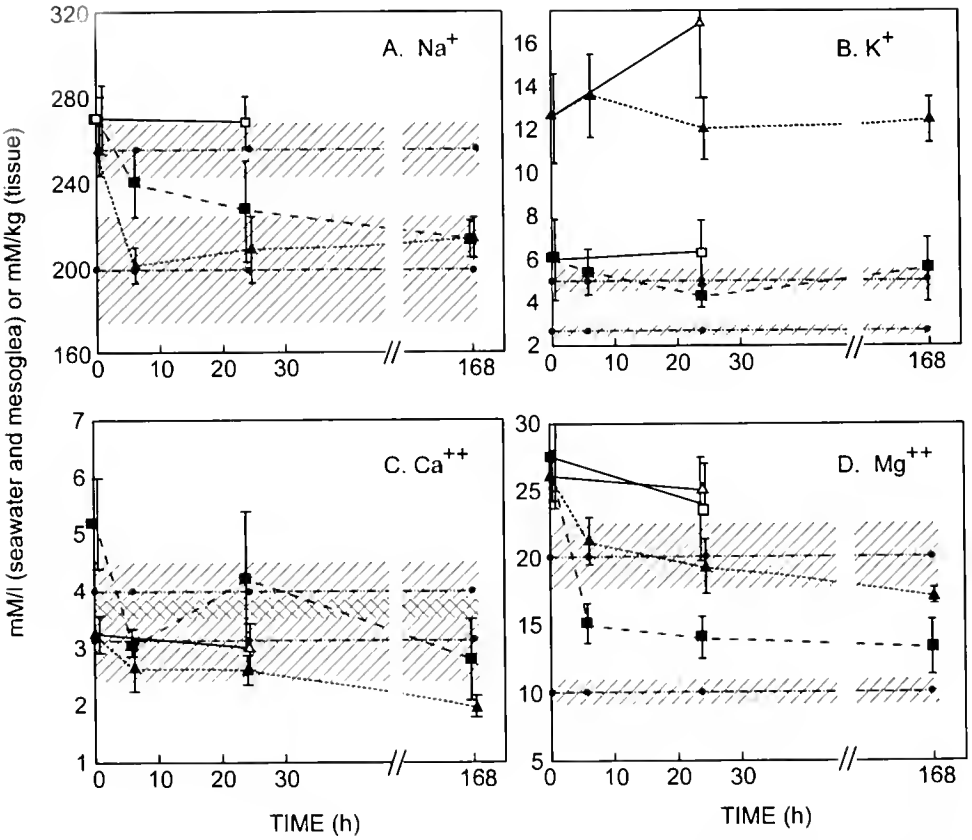

Figure 2. Ion concentrations in mesogleal fluid and tissue of *Chrysaora quinquecirrha* medusae transferred from 20‰ salinity to 12‰. (A) sodium, (B) potassium, (C) calcium, (D) magnesium. Symbols as in Figure 1.

Sulfate

^{35}S exchange at a salinity of 16‰ was complete in about 40 h (Fig. 6) and indicated a freely exchanging component representing about 40% of the total weight. This corresponded closely to the "mesogleal space" of 43% that was estimated from direct measurement of whole medusa bell and tentacular tissue weight (Fig. 7). The sulfate concentrations in mesogleal fluid of medusae acclimated to 20‰, 16‰, and 12‰ are shown in Table I. In all cases mesogleal sulfate levels were significantly lower than the external medium.

Mills (1984) found that the mesoglea of *Aequorea victoria* hydromedusae maintained for 24 h at equilibrium in salinities between 23‰ and 28‰ was generally hypoosmolar to the corresponding external medium, although differences between seawater and mesoglea were very small at the lower end of the salinity range. A similar pattern was seen here, although between 15‰ and 12‰ *Chrysaora quinquecirrha* mesoglea switched from being hypo-osmolar to hyperosmolar relative to the external medium. Although there is some overlap in the osmolalities of seawater and mesogleal fluid at salinities between 12‰ and 20‰, paired *t*-tests involving individual replicates reveal significant differences in each case. Nevertheless, differences between mesogleal fluid and seawater remained very small, and *C. quinquecirrha* appeared to be an osmoconformer throughout this range.

Of the ions measured, the most clearly regulated was potassium. Total tissue potassium concentration was approximately 13 mM kg^{-1} and remained stable following transference of medusae from a salinity of 20‰ to 8‰ or 12‰. The apparent rise in tissue potassium in control animals (maintained at 20‰) in experiment 2 (Fig. 2B) was unexplained but did not differ significantly from the corresponding tissue levels in 12‰. The potassium concentration in mesogleal fluid appeared more variable, and values of 8.8 mM kg^{-1} and 6 mM kg^{-1} were recorded at $t = 0$ in experiments 1 and 2. Transference of medusae from 20‰ to 8‰ resulted in fluctuating mesogleal concentrations, including an apparent rise in mesogleal potassium 24 h after the salinity change (Fig. 1B).

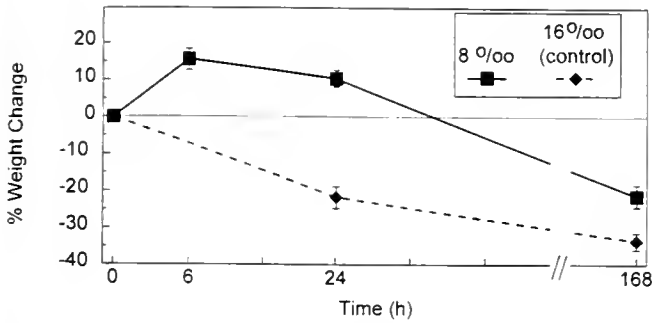

Figure 3. Weight changes in *Chrysaora quinquecirrha* medusae following transfer from 16‰ salinity to 8‰ over 1 week. Means ± 1 SD for eight animals.

This elevation in mesogleal potassium concentration was seen only after the larger salinity change (20‰ to 8‰), and it is possible that osmotic shock may have resulted in a transient increase in cellular potassium permeability or, perhaps, in some cell damage leading to potassium contamination of the mesogleal fluid. A further possibility is that potassium may be actively extruded from cells to mitigate cellular hydration, as has been demonstrated in the freshwater hydromedusa *Craspedacusta sowerbyi* (Fleming and Hazelwood, 1967; Hazelwood *et al.*, 1970). However, in *Craspedacusta*, sodium was also involved (Hazelwood *et al.*, 1970). There is no significant evidence of sodium involvement in volume regulation in *C. quinquecirrha*, and amino acid regulation is probably more important in this regard (Wright, unpubl. data). In the euryhaline sea anemone *Diadumene leucolena*, Pierce and Minasian (1974) demonstrated that volume regulation was achieved through the regulation of the intracellular amino acid pool.

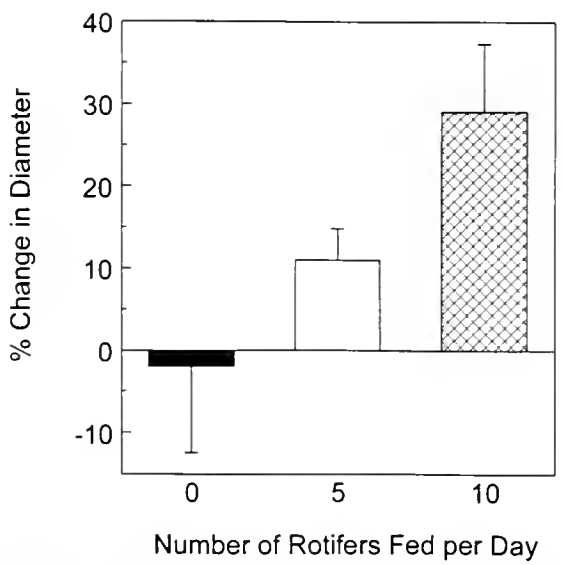

Figure 4. Effect of food ration on size of *Chrysaora quinquecirrha* ephyrae over a 48-h period as determined by measurement of diameter.

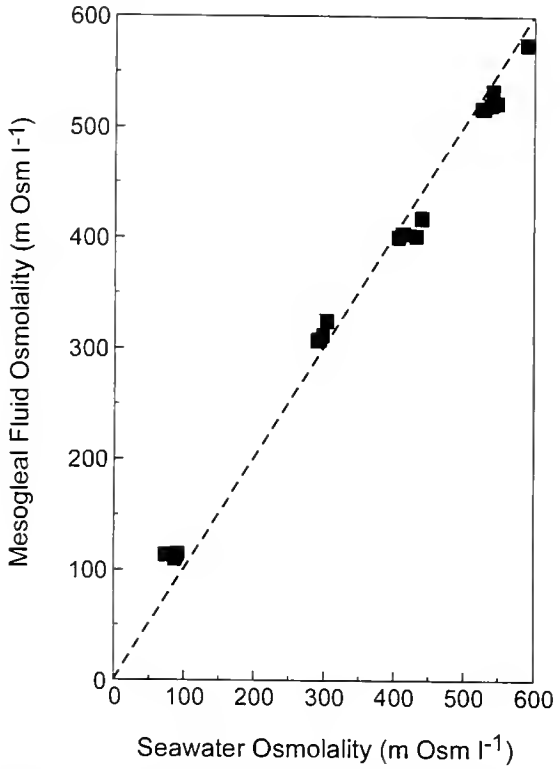

Figure 5. Osmolality of mesogleal fluid and external medium in *Chrysaora quinquecirrha* medusae acclimated for 1 week in salinities of 5‰, 12‰, 15‰, and 20‰. Six individuals were measured at each salinity except for 5‰, where $n = 5$. Some symbols overlay others.

The coincidence of measured sulfate space and our physical determination of extracellular fluid indicated an extracellular space of about 40% in *C. quinquecirrha*. Using this figure and a concentration of 7.4 mM kg^{-1} for mesoglea potassium, one can determine a corrected value for intracellular potassium. The corrected esti-

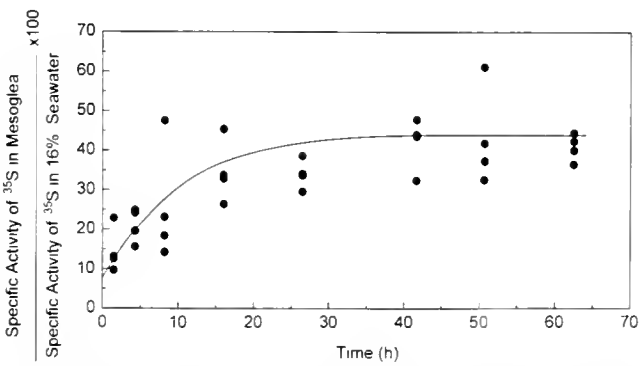

Figure 6. Sulfate exchange in *Chrysaora quinquecirrha* medusae. Exchange was determined as the percentage internal ^{35}S specific activity *versus* external ^{35}S specific activity over 63 h.

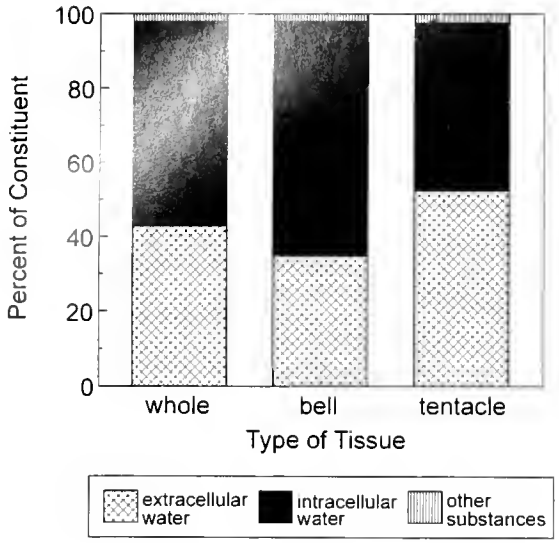

Figure 7. Mesogleal fluid space in bell, tentacles, and whole medusae of *Chrysaora quinquecirrha*. The space, expressed as a percentage of all constituents, was measured directly by weighing the components. "Other substances" refers to dry residue following final drying and reweighing.

mate of 17 mM kg^{-1} calculated in this way is intermediate between the mean values of 10.6 mM kg^{-1} and 29.5 mM kg^{-1} determined by Steinbach (1963) for intracellular potassium in the hydroids *Chlorohydra viridissima* and *Hydra littoralis* in freshwater media. Sulfate space shows considerable variation both within and between species of hydromedusae. Mills and Vogt (1984) reported the sulfate space to be between 10% and 80% in six species of marine hydromedusae. They found that equilibration times varied between <4 h for *Aglantha digitale* and about 85 h for *Mitrocoma cellularia*. The current estimate of 40% sulfate space for *C. quinquecirrha*, with an apparent equilibration time of about 40 h, falls more or less in the middle of this range. At salinities between 20‰ and 12‰, sulfate in the mesogleal fluid of *C. quinquecirrha* is maintained at concentrations lower than those of the external media. Similar results were obtained by Newton and Potts (1993), who reported mesogleal sulfate levels of 40% and 52% of seawater levels in *Cyanea capillata* and *Rhizostoma pulmo* respectively.

In both experiments 1 and 2, there was evidence that the magnesium concentrations in tissue and mesogleal fluid were maintained at levels above that of the external medium. Following transfer of medusae from 20‰ to 12‰, magnesium was substantially diluted in tissue and mesogleal fluid, yet even 7 d after the salinity change, remained significantly higher than the concentration of the dilute medium (Fig. 2D). A similar phenomenon was seen following transfer from 20‰ to 8‰ (Fig. 1D). The concentration of sodium also remained significantly ($P < 0.05$) higher in tissue than in the 8‰ medium.

Dilution resulting from water influx obviously contributed to the fall in tissue ions in most cases. Weight changes in medusae transferred to lower salinities indicated that water influx reached 10%–20% of total body weight within the first 24 h following transfer. But tissue concentrations of sodium, magnesium, and calcium in animals transferred from 20‰ to 8‰ fell by more than 40% in the first 6 h, indicating that diffusional losses of these ions were at least as important as increased tissue hydration in explaining these losses. The apparent subsequent "recovery" of tissue sodium and magnesium to levels above those of the dilute medium suggests that, although these ions may not be actively regulated, the tissue is not freely permeable to them. It is also possible that tissue permeability to these ions changes after the initial osmotic shock. The relative stability of tissue potassium, despite the osmotic swelling, emphasizes the efficiency of the mechanism that regulates cellular potassium in *C. quinquecirrha*.

The degree to which medusae of *C. quinquecirrha* behave like osmometers with changing salinity is difficult to exactly quantify in view of the likely influence of food on weight changes. The controlled feeding experiment illustrated that lack of feeding may account for a weight loss greater than 20% over a 24-h period. This supports the data shown in Fig. 3B. If results from 8‰ animals are corrected for controls (16‰), the 24-h weight change due to osmotic stress may exceed 30%. Medusae of *Aurelia aurita* and *C. quinquecirrha* also decreased in diameter when unfed (Hamner and Jenssen, 1974; Rosen and Purcell, unpubl. data).

In studies conducted here, medusae were able to achieve at least neutral buoyancy in all salinities except one—at 5‰ they remained on the bottom of experimental containers. Bidigare and Biggs (1980) suggested a role for sulfate in adjusting buoyancy in jellyfish. They showed that, by active elimination of more than half of its body SO_4 relative to seawater, the ctenophore *Beroe cucumis* could neutralize its protein mass and achieve neutral buoyancy in dilute seawater. It was postulated that sulfate elimination was offset by isosmotic replacement by chloride. Our data show sulfate concentrations

Table I

Sulfate concentrations in mesogleal fluid of Chrysaora quinquecirrha *medusae adapted to different salinities for 48 h*

Salinity ‰	Seawater sulfate concentration (mM/l)	Mesogleal sulfate concentration (mM/l)	Mesogleal sulfate as percentage seawater
20	13.2	9.1	69
16	9.7	6.8	70
12	7.9	5.2	66

to be consistently lower in tissue of *C. quinquecirrha* than in the external media, but there was no indication of a change in tissue:medium sulfate ratio on transfer of medusae from higher to lower salinity. Therefore, we conclude that *C. quinquecirrha* does not regulate buoyancy by excluding sulfate ions. These medusae are strong swimmers and perhaps would not benefit substantially from ionic buoyancy compensation.

Our results suggest the possibility that medusae of *Chrysaora quinquecirrha* are unable to regulate volume or buoyance at salinities <5‰. This agrees with the distribution of polyps and medusae *in situ* (Cargo and Schultz, 1966, 1967) and with laboratory experiments on asexual reproduction (Purcell *et al.*, unpubl. data).

Acknowledgments

This research was funded by NSF grant OCE-9019404. We thank H. Lemke, G. Aldridge, and T. Lewis for assistance with experiments. University of Maryland, Center for Environmental and Estuarine Studies Contribution No. 2793.

Literature Cited

Benos, D., and R. Prusch. 1972. Osmoregulation in fresh-water *Hydra*. *Comp. Biochem. Physiol.* **43A:** 165–171.

Bidigare, R. R., and D. C. Biggs. 1980. The role of sulfate exclusion in buoyancy maintenance by siphonophores and other oceanic gelatinous zooplankton. *Comp. Biochem. Physiol.* **66A:** 467–471.

Cargo, D. G., and L. P. Schultz. 1966. Notes on the biology of the sea nettle, *Chrysaora quinquecirrha*, in Chesapeake Bay. *Chesapeake Sci.* 7: 95–100.

Cargo, D. G., and L. P. Schultz. 1967. Further observations on the biology of the sea nettle and jellyfishes in the Chesapeake Bay. *Chesapeake Sci.* **8:** 209–220.

Denton, E. J., and T. I. Shaw. 1962. The buoyancy of gelatinous marine animals. *J. Physiol.* **161:** 14–15.

Dumont, H. J. 1994. The distribution and ecology of the fresh- and brackish-water medusae of the world. *Hydrobiologia* **272:** 1–12.

Fleming, W. R., and D. H. Hazelwood. 1967. Ionic and osmoregulation in the freshwater medusa *Craspedacusta sowerbyi*. *Comp. Biochem. Physiol.* **23:** 911–915.

Hamner, W. M., and R. M. Jenssen. 1974. Growth, degrowth, and irreversible cell differentiation in *Aurelia aurita*. *Am. Zool.* **14:** 833–849.

Hazelwood, D. H., W. T. W. Potts, and W. R. Fleming. 1970. Further studies on the sodium and water metabolism of the freshwater medusa, *Craspedacusta sowerbyi*. *Z. Vgl. Physiol.* **67:** 186–191.

Mackay, W. C. 1969. Sulfate regulation in jellyfish. *Comp. Biochem. Physiol.* **30:** 481–488.

Mills, C. E. 1984. Density is altered in hydromedusae and ctenophores in response to changes in salinity. *Biol. Bull.* **166:** 206–215.

Mills, C. E., and R. G. Vogt. 1984. Evidence that ion regulation in hydromedusae and ctenophores does not facilitate vertical migration. *Biol. Bull.* **166:** 216–227.

Newton, C., and W. T. W. Potts. 1993. Ionic regulation and buoyancy in some planktonic organisms. *J. Mar. Biol. Assoc. U.K.* **73:** 15–23.

Pierce, S. K., and L. L. Minasian, Jr. 1974. Water balance of a euryhaline sea anemone, *Diadumene leucolena*. *Comp. Biochem. Physiol.* **49A:** 159–167.

Robertson, J. D. 1949. Ionic regulation in some marine invertebrates. *J. Exp. Biol.* **26:** 182–200.

Shick, J. M. 1973. Effects of salinity and starvation on the uptake and utilization of dissolved glycine by *Aurelia aurita* polyps. *Biol. Bull.* **144:** 172–179.

Steinbach, H. B. 1963. Sodium, potassium and chloride in selected hydroids. *Biol. Bull.* **124:** 322–336.

Webb, K. L., A. L. Schimpf, and J. Olmon. 1972. Free amino acid composition of scyphozoan polyps of *Aurelia aurita*, *Chrysaora quinquecirrha* and *Cyanea capillata* at various salinities. *Comp. Biochem. Physiol.* **43B:** 653–663.

CONTENTS

Volume 192 Number 3

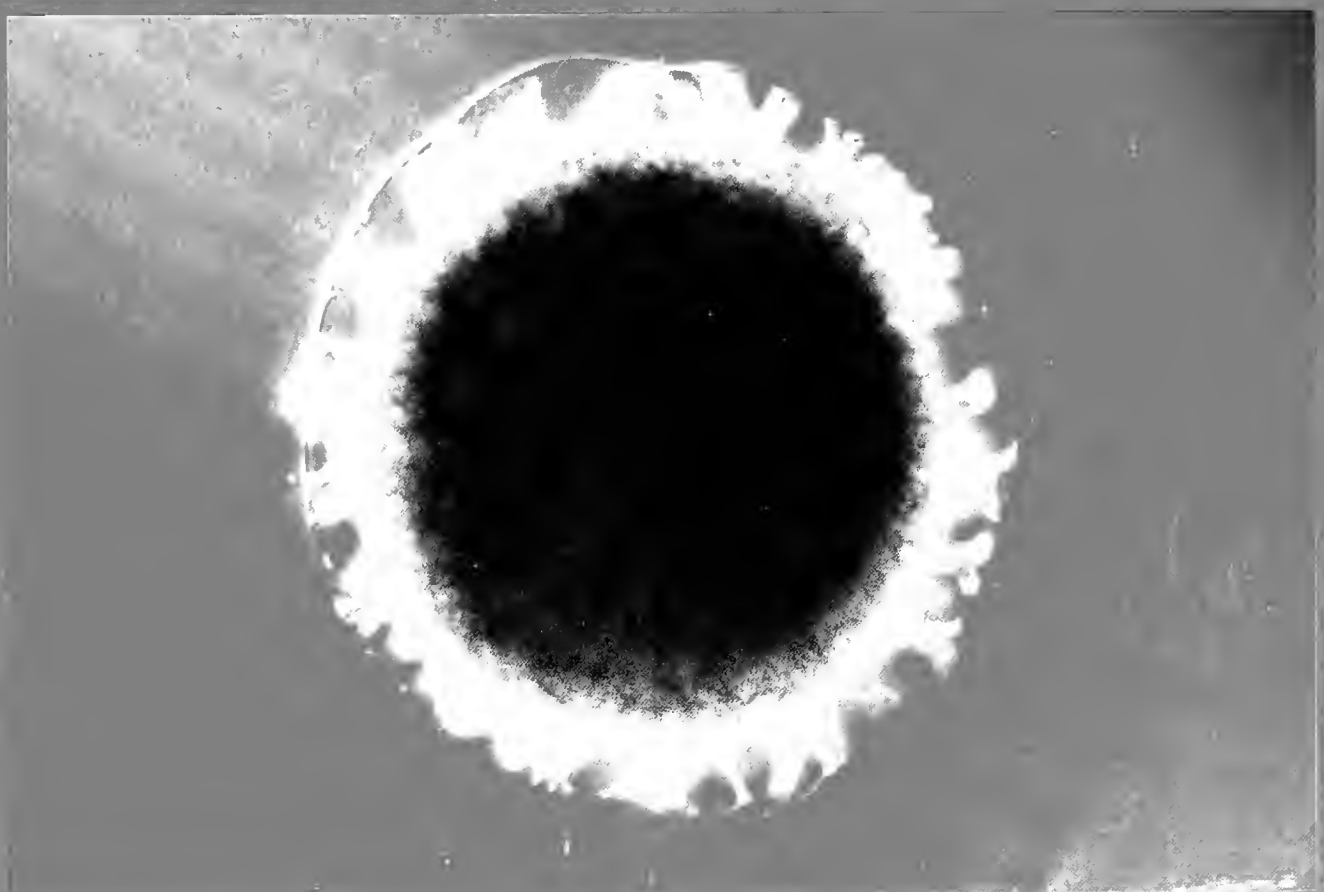

JUNE, 1997

THE BIOLOGICAL BULLETIN

PUBLISHED BY
THE MARINE BIOLOGICAL LABORATORY

JUNE, 1997

Printed and Issued by
LANCASTER PRESS, Inc.
3575 HEMPLAND ROAD
LANCASTER, PA

Cover

Embryo of *Hydra vulgaris* encased in a multilayered cuticle adorned with ornate spines. The embryo remains in the cuticle for varying lengths of time. At hatching, the cuticle breaks open and a hatchling emerges head-end first. See Martin *et al.*, this issue.

CONTENTS

THE BIOLOGICAL BULLETIN

THE BIOLOGICAL BULLETIN is published six times a year by the Marine Biological Laboratory, 7 MBL Street, Woods Hole, Massachusetts 02543.

Subscriptions and similar matter should be addressed to Subscription Manager, THE BIOLOGICAL BULLETIN, Marine Biological Laboratory, 7 MBL Street, Woods Hole, Massachusetts 02543. For 1997, a lower rate is available to individual subscribers (as distinguished from libraries and institutions). Single numbers: $40 for libraries; $20 for individuals. Subscription per volume (three issues): $97.50 for libraries; $50 for individuals. Subscription per year (six issues, two volumes): $195 for libraries; $100 for individuals.

Communications relative to manuscripts should be sent to Michael J. Greenberg, Editor-in-Chief, or Pamela L. Clapp, Managing Editor, at the Marine Biological Laboratory, 7 MBL Street, Woods Hole, Massachusetts 02543. Telephone: (508) 289-7428. FAX: 508-457-1924. E-mail: pclapp@mbl.edu.

http://www.mbl.edu/BiologicalBulletin/

The home page for the electronic companion to THE BIOLOGICAL BULLETIN—*the Marine Models Electronic Record*—and other BIOLOGICAL BULLETIN publications is available on the World Wide Web at the address shown above.

THE BIOLOGICAL BULLETIN is indexed in bibliographic services including *Index Medicus* and MEDLINE, *Chemical Abstracts, Current Contents, CABS (Current Awareness in Biological Sciences),* and *Geo Abstracts.*

Printed on acid free paper,
effective with Volume 180, Issue 1, 1991.

POSTMASTER: Send address changes to THE BIOLOGICAL BULLETIN, Marine Biological Laboratory, 7 MBL Street, Woods Hole, MA 02543.

Periodicals postage paid at Woods Hole, MA, and additional mailing offices.
ISSN 0006-3185

INSTRUCTIONS TO AUTHORS

The Biological Bulletin accepts outstanding original research reports of general interest to biologists throughout the world. Papers are usually of intermediate length (10–40 manuscript pages). A limited number of solicited review papers may be accepted after formal review. A paper will usually appear within four months after its acceptance.

Very short, especially topical papers (less than 9 manuscript pages including tables, figures, and bibliography) will be published in a separate section entitled "Research Notes." A Research Note in *The Biological Bulletin* follows the format of similar notes in *Nature.* It should open with a summary paragraph of 150 to 200 words comprising the introduction and the conclusions. The rest of the text should continue on without subheadings, and there should be no more than 30 references. References should be referred to in the text by number, and listed in the Literature Cited section in the order that they appear in the text. Unlike references in *Nature,* references in the Research Notes section should conform in punctuation and arrangement to the style of recent issues of *The Biological Bulletin.* Materials and Methods should be incorporated into appropriate figure legends. See the article by Lohmann *et al.* (October 1990, Vol. **179**: 214–218) for sample style. A Research Note will usually appear within two months after its acceptance.

The Editorial Board requests that regular manuscripts conform to the requirements set below; those manuscripts that do not conform will be returned to authors for correction before review.

1. ***Manuscripts.*** Manuscripts, including figures, should be submitted in triplicate. (Xerox copies of photographs are not acceptable for review purposes.) The submission letter accompanying the manuscript should include a telephone number, a FAX number, and (if possible) an E-mail address for the corresponding author. The original manuscript must be typed in no smaller than 12 pitch or 10 point, using double spacing (*including* figure legends, footnotes, bibliography, etc.) on one side of 16- or 20-lb. bond paper, 8½ by 11 inches. Please, no right justification. Manuscripts should be proofread carefully and errors corrected legibly in black ink. Pages should be numbered consecutively. Margins on all sides should be at least 1 inch (2.5 cm). Manuscripts should conform to the *Council of Biology Editors Style Manual,* 5th Edition (Council of Biology Editors, 1983) and to American spelling. Unusual abbreviations should be kept to a minimum and should be spelled out on first reference as well as defined in a footnote on the title page. Manuscripts should be divided into the following components: Title page, Abstract (of no more than 200 words), Introduction, Materials and Methods, Results, Discussion, Acknowledgments, Literature Cited, Tables, and Figure Legends. In addition, authors should supply a list of words and phrases under which the article should be indexed.

2. ***Title page.*** The title page consists of a condensed title or running head of no more than 35 letters and spaces, the manuscript title, authors' names and appropriate addresses, and footnotes listing present addresses, acknowledgments or contribution numbers, and explanation of unusual abbreviations.

3. ***Figures.*** The dimensions of the printed page, 7 by 9 inches, should be kept in mind in preparing figures for publication. We recommend that figures be about 1½ times the linear dimensions of the final printing desired, and that the ratio of the largest to the smallest letter or number and of the thickest to the thinnest line not exceed 1:1.5. Explanatory matter generally should be included in legends, although axes should always be identified on the illustration itself. Figures should be prepared for reproduction as either line cuts or halftones. Figures to be reproduced as line cuts should be unmounted glossy photographic reproductions or drawn in black ink on white paper, good-quality tracing cloth or plastic, or blue-lined coordinate paper. Those to be reproduced as halftones should be mounted on board, with both designating numbers or letters and scale bars affixed directly to the figures. All figures should be numbered in consecutive order, with no distinction between text and plate figures and cited, in order, in the text. The author's name and an arrow indicating orientation should appear on the reverse side of all figures.

Color: The Biological Bulletin will publish color figures and plates, but must bill authors for the actual additional cost of printing in color. The process is expensive, so authors with more than one color image should—consistent with editorial concerns, especially citation of figures in order—combine them into a single plate to reduce the expense. On request, when supplied with a copy of a color illustration, the editorial staff will provide a pre-publication estimate of the printing cost.

4. ***Tables, footnotes, figure legends, etc.*** Authors should follow the style in a recent issue of *The Biological Bulletin* in preparing table headings, figure legends, and the like. Because of the high cost of setting tabular material in type, authors are asked to limit such material as much as possible. Tables, with their headings and footnotes, should be typed on separate sheets, numbered with consecutive Roman numerals, and placed after the Literature Cited. Figure legends should contain enough information to make the figure intelligible separate from the text. Legends should be typed double spaced, with consecutive Arabic numbers, on a separate sheet at the end of the paper. Footnotes should be limited to authors' current addresses, acknowledgments or contribution numbers, and explanation of unusual abbreviations. All such footnotes should appear on the title page. Footnotes are not normally permitted in the body of the text.

5. ***Literature cited.*** In the text, literature should be cited by the Harvard system, with papers by more than two authors cited as Jones *et al.*, 1980. Personal communications and material in preparation or in press should be cited in the text only, with author's initials and institutions, unless the material has been formally accepted and a volume number can be supplied. The list of references following the text should be headed Literature Cited, and must be typed double spaced on separate pages, conforming in punctuation and arrangement to the style of recent issues of *The Biological Bulletin*. Citations should include complete titles and inclusive pagination. Journal abbreviations should normally follow those of the U. S. A. Standards Institute (USASI), as adopted by BIOLOGICAL ABSTRACTS and CHEMICAL ABSTRACTS, with the minor differences set out below. The most generally useful list of biological journal titles is that published each year by BIOLOGICAL ABSTRACTS (BIOSIS List of Serials; the most recent issue). Foreign authors, and others who are accustomed to using THE WORLD LIST OF SCIENTIFIC PERIODICALS, may find a booklet published by the Biological Council of the U.K. (obtainable from the Institute of Biology, 41 Queen's Gate, London, S.W.7, England, U.K.) useful, since it sets out the WORLD LIST abbreviations for most biological journals with notes of the USASI abbreviations where these differ. CHEMICAL ABSTRACTS publishes quarterly supplements of additional abbreviations. The following points of reference style for THE BIOLOGICAL BULLETIN differ from USASI (or modified WORLD LIST) usage:

A. Journal abbreviations, and book titles, all underlined (for *italics*)

B. All components of abbreviations with initial capitals (not as European usage in WORLD LIST *e.g., J. Cell. Comp. Physiol.* NOT *J. cell. comp. Physiol.*)

C. *All* abbreviated components must be followed by a period, whole word components *must not* (*i.e., J. Cancer Res.*)

D. Space between all components (*e.g., J. Cell. Comp. Physiol.*, not *J.Cell.Comp.Physiol.*)

E. Unusual words in journal titles should be spelled out in full, rather than employing new abbreviations invented by the author. For example, use *Rit Vísindafjélags Islendinga* without abbreviation.

F. All single word journal titles in full (*e.g., Veliger, Ecology, Brain*).

G. The order of abbreviated components should be the same as the word order of the complete title (*i.e., Proc.* and *Trans.* placed where they appear, not transposed as in some BIOLOGICAL ABSTRACTS listings).

H. A few well-known international journals in their preferred forms rather than WORLD LIST or USASI usage (*e.g., Nature, Science, Evolution* NOT *Nature, Lond., Science, N.Y.; Evolution, Lancaster, Pa.*)

6. ***Reprints, page proofs, and charges.*** Authors receive their first 100 reprints (without covers) free of charge. A $25 surcharge will be added for each 100 reprints (including the first 100) of articles that include color illustrations. Additional reprints may be ordered at time of publication and normally will be delivered about two to three months after the issue date. Authors (or delegates for foreign authors) will receive page proofs of articles shortly before publication. They will be charged the current cost of printers' time for corrections to these (other than corrections of printers' or editors' errors). Other than these charges for authors' alterations, *The Biological Bulletin* does not have page charges.

VOLUME CONTENTS

No. 1, February 1997

CELL BIOLOGY

DEVELOPMENT AND REPRODUCTION

IMMUNOBIOLOGY

ECOLOGY AND EVOLUTION

THE FUTURE OF AQUATIC RESEARCH IN SPACE: NEUROBIOLOGY, CELLULAR AND MOLECULAR BIOLOGY

MECHANOSENSITIVITY

PLANT BIOLOGY

NEUROBIOLOGY/SENSORY BIOLOGY

No. 2, April 1997

NEUROBIOLOGY AND BEHAVIOR

PHYSIOLOGY

No. 3, June 1997

RESEARCH NOTE

DEVELOPMENT AND REPRODUCTION

NEUROBIOLOGY AND BEHAVIOR

PHYSIOLOGY

* * *

Reference: *Biol. Bull.* **192:** 341–344. (June, 1997)

Scallop Shells Exhibit Optimization of Riblet Dimensions for Drag Reduction

ERIK J. ANDERSON, PATRICK S. MACGILLIVRAY, AND M. EDWIN DEMONT*

Biology Department, St. Francis Xavier University, Antigonish, Nova Scotia, Canada B2G 2W5

Drag reduction by streamwise surface grooves, or riblets, has been observed by engineers and has been suggested to apply to certain biological systems. Drag reductions as high as 8% have been observed (1), leading to practical nautical and aeronautical applications (2, 3, 4). The shells of several species of scallop, including Placopecten magellanicus, *display riblets arranged radially, and therefore roughly parallel to the flow during swimming (Fig. 1a). The dimensions of these riblets on particular scallops fall within the region necessary for drag reduction at experimentally measured swimming speeds. Moreover, the actual spacing of the riblets gradually migrates into the theoretically optimal spacing region as shell length increases beyond 40 mm (Figs. 2, 3). Specimens of* P. magellanicus *40 to 80 mm in length demonstrate the greatest swimming ability (5); our data strongly suggest that streamwise riblets may be a contributing factor to the swimming success in scallops of this size range.*

The giant scallop, *Placopecten magellanicus*, was the subject of a recent comprehensive work on the hydrodynamics and energetics of locomotion (6, 7, 8, 9). Scallops utilize a jet-propulsion system in swimming: water is taken in when the shells open, and the valve-like velum traps a volume of water between the shells which is expelled in two jets adjacent to the hinge as the shells clap shut. The scallop is therefore propelled through the water gape-leading, hinge-trailing, at speeds up to about 0.55 m/s, the swimming speed common to scallops 65 mm in ventral-dorsal length, L_s (5). Their swimming ability enables scallops to escape from predators, such as starfish, and, as some suggest, to migrate with the seasons (5). Certainly if the latter behavior were a significant part of the scallop life cycle, development of drag-reducing structural features would not be surprising.

Recent years have seen the application of streamwise grooves, or riblets, to aircraft and the hulls of racing boats as a means of drag reduction and, therefore, enhanced speed capability and decreased energy requirements. The mechanism involves a reduction in the surface shear stress arising from a turbulent boundary layer. Similar grooves in aquatic organisms may offer the same advantage (3, 4, 10, 11). We examined about 440 species of bivalves from 60 families representing over 160 genera and found that, with the exception of 7 genera, radial riblets of dimensions similar to those in *P. magellanicus* occur almost exclusively in swimming bivalves (observed in 16 genera). The *Limidae*, which swim hinge first, in the direction opposite to that of the scallop, also exhibit radial riblets.

Theoretical and experimental work by fluid engineers has elucidated the function and efficacy of riblets (12, 13) with drag reductions of 3%–8% observed in various systems, from flat plates, to the hulls of racing boats (2), the surfaces of aircraft (3), and the skin of sharks (3, 4, 10, 11). Though riblet function is still not fully understood, researchers have put forth a theory, based on the organization of surface vortices, to explain the drag-reducing mechanism. According to the theory, there is a reduction in the component of drag arising from a particular high shear occurrence generated by the action of so-called hairpin vortex tubes. In turbulent boundary layers, hairpin-shaped vortex tubes occur near the surface, oriented so the bend of the hairpin is downstream and the two prongs of the hairpin are pointed upstream and aligned roughly parallel to the flow. As the bend of the hairpin is swept further downstream, the remaining vortex tubes move toward each other in a spanwise direction, which

Received 2 December 1996; accepted 14 April 1997.

* Author for correspondence.

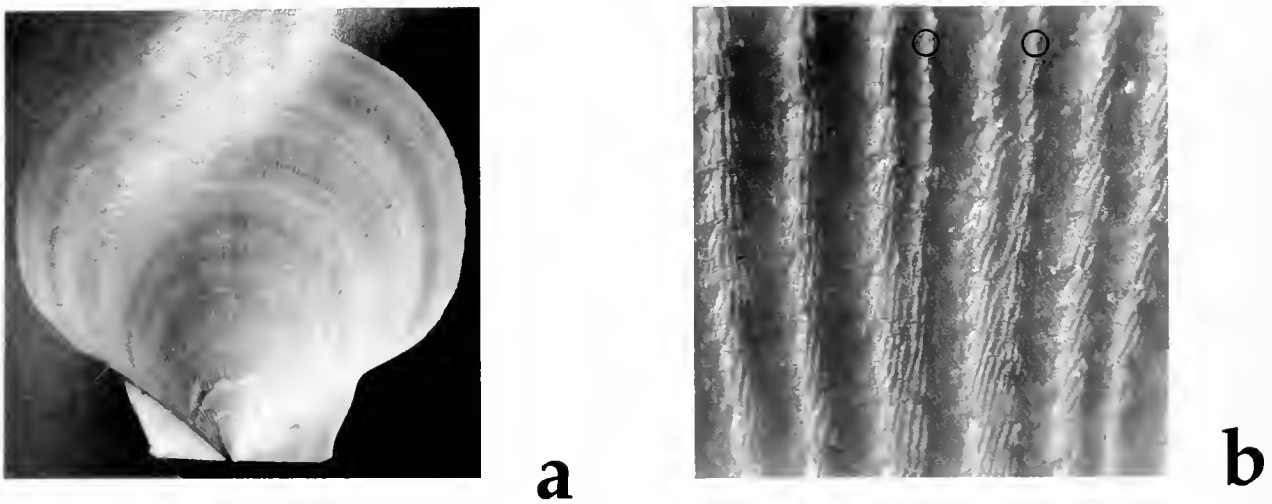

Figure 1. Photographs of riblets on the scallop *Placopecten magellanicus*. (a) Whole shell. Shell length, L_s = 63 mm. (b) Magnified image of riblets. Note the two newly added riblets marked with circles. For scale, the distance between the two circles is 1 mm.

ultimately results in a downwash of fluid onto the surface. This phenomenon is known as near-wall burst. Riblets may inhibit this spanwise movement by organizing adjacent surface vortex tubes into streamwise corridors and thus restricting the vortex tubes from interacting to cause near-wall burst.

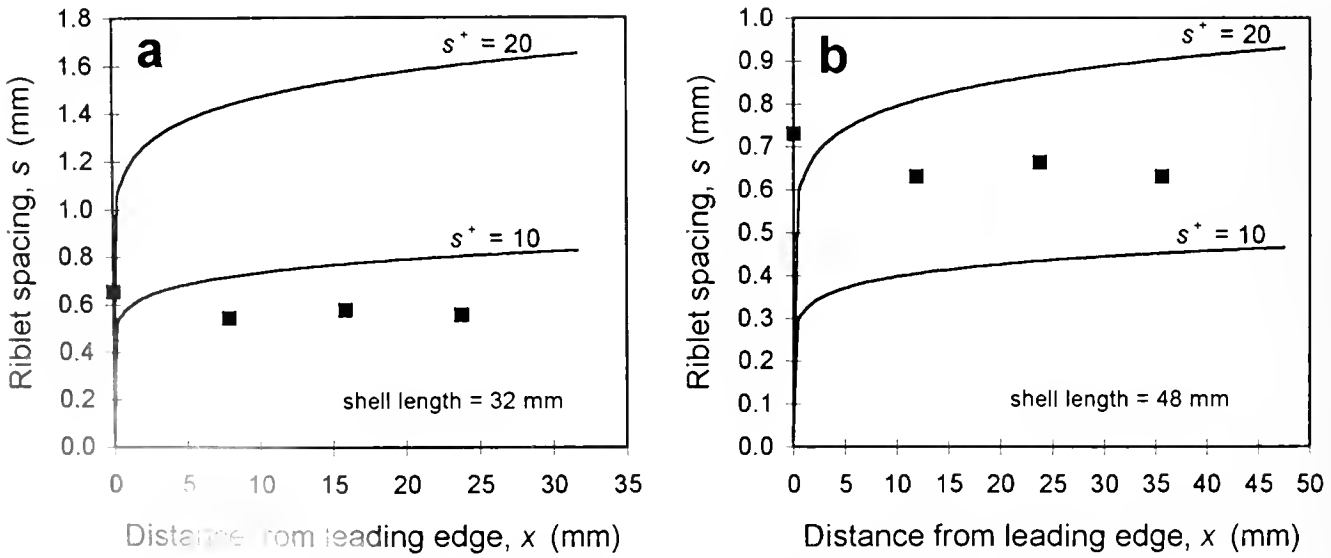

Figure 2. Real riblet spacings (squares), at positions x = 0, 0.25L_s, 0.5L_s, and 0.75L_s, plotted against distance from the leading edge of the shell, from two representative scallops: (a) L_s = 32 mm; (b) L_s = 48 mm. The solid lines represent the boundaries of the optimal riblet spacing region for riblet-based drag reduction, which is specific to each scallop on the basis of shell length and swimming speed (Eqs. 1 and 2). A series (n = 20) of *P. magellanicus* shells of L_s from 10 mm to 90 mm was used in this study. Arcs were established at positions x = 0, 0.25L_s, 0.5L_s, and 0.75L_s over the central 30 degree sector of each shell, and the number of riblets on each arc was counted; Bioquant OS/2 image analysis software was used for positioning and counting. Real riblet spacings were calculated by dividing the arc length, $l_{arc} = \pi(L_s - x)/6$, at each of the four positions by the number of riblets on the arc. Swimming velocities, needed to calculate peak shear stresses (Eq. 2), vary significantly with shell length and were taken from published data obtained from film of *P. magellanicus* swimming *in situ* (5). Note that despite the radial pattern of riblets, spacing remains relatively constant due to riblet addition. Note also that the spacing measurements move into the optimal region between s^+ = 10 and s^+ = 20 as shell length increases from 32 mm to 48 mm.

Riblet spacing for optimal drag reduction can be determined from the following expression,

$$s = \nu s^+ \sqrt{\frac{\rho}{\tau_w}} \qquad \text{(Eq. 1)}$$

where s is actual riblet spacing, ν is the kinematic viscosity of the fluid, s^+ is a dimensionless expression of riblet spacing for which the range 10–20 has been determined to be optimal (11, 14), τ_w is the wall shear stress due to the flow, and ρ is the fluid density. The equation is simply a rearrangement of the standard expression for a dimensionless length parameter, in terms of ν, τ_w and ρ. Such dimensionless parameters are used in fluid dynamics for the reason that, in general, any two systems with the same s^+ value will behave similarly, though values of actual spacing, s, may differ. Wall shear stress for the swimming scallop was determined from the equation for flow over a flat plate with a turbulent boundary; the equation was obtained through the standard practice of applying the momentum integral equation to a $^1/_7$ power velocity profile,

$$\tau_w = \frac{1}{2}\rho U^2 \frac{0.0594}{Re_x^{1/5}} \quad Re_x = \frac{Ux}{\nu} \qquad \text{(Eq. 2)}$$

where U is the flow velocity over the scallop, Re_x is the length (or local) Reynolds number, and x is the distance measured along the line bisecting the valve, starting from the most ventral edge of the valve (*i.e.*, the leading edge of the scallop). Due to the shell curvature, the shear would be slightly higher than the equation predicts for the leading section of the scallop. A turbulent boundary layer is assumed on the basis of Reynolds numbers close to the transition between laminar and turbulent flow; an early breakdown of the laminar boundary layer is probably triggered by the combined effects of leading edge roughness and the rapid clapping of the leading edge of the scallop during swimming.

The average riblet spacing as a function of distance from the leading edge was determined for each scallop observed, then plotted together with the theoretically predicted optimal riblet spacing for $s^+ = 10$ and $s^+ = 20$ (Fig. 2). At smaller shell lengths, the actual riblet spacing data fall below the optimal region (Fig. 2a). Since scallops of lengths up to about 30 mm are attached to the ocean bottom by byssal threads (5), there would be no advantage for optimized riblet spacing in these smaller scallops. At a shell length of about 50 mm—the size at which *P. magellanicus* exhibits the greatest swimming speed (in body lengths per second)—the actual riblet spacing data fall near the center of the optimal region for riblet-based drag reduction (Fig. 2b). When the riblet spacing at $x = 0.5L_s$ for each scallop observed is plotted against shell length, the riblet spacing on scallop shells larger than 40 mm remains in the optimal region (Fig. 3). Moreover, the higher Reynolds numbers, $Re = 2.0$–4.0×10^4, at these larger scallop sizes, increase the likelihood of transition from laminar to turbulent boundary flow. Thus, scallops of the size reported to swim most vigorously are highly favored for riblet-based drag reduction, suggesting an optimization of shell design. Research on *P. magellanicus* reveals that scallops larger than 80 mm are generally less active swimmers due to inferior hydrodynamic characteristics and heavy bodies (5, 7). Scallops of this size are also commonly covered with embionts which reduce swimming ability.

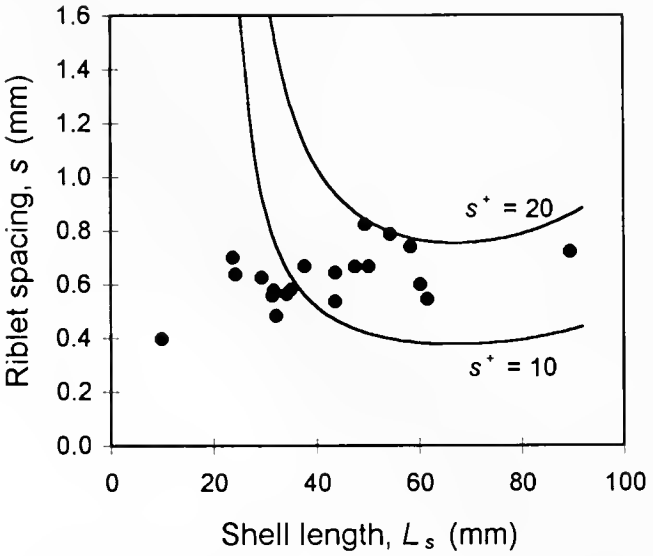

Figure 3. Real riblet spacing at position $x = 0.5L_s$ plotted against shell length. The plot compares the riblet spacings of the entire series ($n = 20$) of shells observed at the same relative position on each shell. Thus, each data point (circle) is produced from the spacing data of a different shell. The solid lines are the predicted optimal riblet spacing for $s^+ = 10$ and $s^+ = 20$, at $x = 0.5L_s$ using swimming speeds corresponding to the given shell lengths (5). Notice that as shell length increases past 40 mm, the data points enter the optimal region.

An equally impressive aspect of riblet design in these scallops is best introduced by examining the equations for determining optimal riblet spacing, s. Combining equations 1 and 2 reveals that optimal riblet spacing is inversely proportional to distance from the leading edge to the $^1/_{10}$ power. Therefore, as the optimal curves show (Fig. 2), the best arrangement would be to have, at the leading edge of an object ($x = 0$), narrow spacing which gets wider as you move toward the trailing edge ($x = L_s$). The radial pattern of the scallop riblets, which has its vertex at the trailing edge, would be the opposite of this optimal arrangement if it were not for the fact that riblets are added to the pattern, by intercalation, as the scallop grows (Fig. 1b); *i.e.*, there are more riblets at the leading edge than near the vertex. Shells showed an average of 3 to 4 times as many riblets at the leading edge as at $x = 0.75L_s$. For example, in a shell 54 mm in length, riblet

spacing decreases, from 0.79 mm at $x = 0.75L_s$, to a surprising 0.66 mm at the leading edge ($x = 0$). In contrast, if the scallop did not add riblets, the geometrically calculated spacing would be 0.33 mm at the leading edge. If the riblet spacing were maintained by intercalation, the riblet spacing data from scallops could not remain within the optimal spacing region for riblet-based drag reduction. Of the 37 species of nonswimming bivalves observed to have shells with radial riblets, none added riblets except 12 species of ribbed mussels and 7 species of *Arcidae, Glycymeridae,* and *Psammobiidae.* Although there are surely more bivalves with this trait, the occurrence and addition of riblets does not appear to be widespread; yet this characteristic is fairly common in the scallops and limids.

The combination of the correlation of optimal riblet spacing with previously observed swimming capability and the maintenance of riblet spacing by intercalation implies that the apparent fine-tuning of riblet spacing on *P. magellanicus* is functionally significant.

Acknowledgments

This research was funded by an NSERC (Canada) research grant to M.E.D. P.S.M. was supported by an NSERC Summer Research Scholarship. We thank R. Antonia (The University of Newcastle) for his valuable comments and suggestions throughout this study, A. Anderson (St. F. X.) for the use of his image analysis equipment, the Nova Scotia Museum of Natural History for opening their bivalve collection to us, E. Kechington at the Department of Fisheries and Oceans for sending specimens, and collector M. Le Quement for his contribution of bivalves from Brittany. We thank also J. Flynn (Dalhousie), W. Quinn (St. F.X.) and S. Vogel (Duke) for reading the manuscript.

Literature Cited

1. **Walsh, M. J., and L. M. Weinstein. 1978.** Drag and heat transfer on surfaces with longitudinal fins. *AIAA Paper* 78–1161.
2. **Bushnell, D. M., and K. J. Moore. 1991.** Drag reduction in nature. *Annu. Rev. Fluid Mech.* **23:** 65–79.
3. **Moin, P., and J. Kim. 1997.** Tackling turbulence with supercomputers. *Sci. Am.* **276(1):** 62–68.
4. **Mullins, J. 1997.** Secrets of a perfect skin. *New Sci.* **153(2065):** 28–31.
5. **Dadswell, M. J., and D. Weihs. 1990.** Size-related hydrodynamic characteristics of the giant scallop *Placopecten magellanicus* (Bivalvia: Pectinidae). *Can. J. Zool.* **68:** 778–785.
6. **Cheng, J.-Y., and M. E. DeMont. 1996.** Hydrodynamics of scallop locomotion: unsteady fluid forces on clapping shells. *J. Fluid Mech.* **317:** 73–90.
7. **Cheng, J.-Y., and M. E. DeMont. 1996.** Jet-propelled swimming in scallops: swimming mechanics and ontogenic scaling. *Can. J. Zool.* **74:** 1734–1748.
8. **Cheng, J.-Y., I. G. Davison, and M. E. DeMont. 1996.** Dynamics and energetics of scallop locomotion. *J. Exp. Biol.* **199:** 1931–1946.
9. **Vogel, S. 1997.** Squirt smugly, scallop. *Nature* **385:** 21–22.
10. **Reif, W.-E. 1982.** Morphology and hydrodynamic effects of the scales of fast swimming sharks. *Neues. Jahrb. Geol. Paleontol.* **164:** 184–187.
11. **Bechert, D. W., G. Hoppe, and W.-E. Reif. 1985.** On the drag reduction of shark skin. *AIAA Paper* 85–0546.
12. **Kline, S. J., W. C. Reynolds, F. A. Schraub, and P. W. Runstadler. 1967.** The structure of turbulent boundary layers. *J. Fluid Mech.* **30:** 741–773.
13. **Djenidi, L., and R. A. Antonia. 1993.** Riblet flow calculation with a low Reynolds number k-ϵ model. *Appl. Sci. Res.* **50:** 267–282.
14. **Walsh, M. J. 1982.** Turbulent boundary layer drag reduction using riblets. *AIAA Paper* 82–0169.

Reference: *Biol. Bull.* **192:** 345–363. (June, 1997)

Embryogenesis in Hydra

VICKI J. MARTIN[1], C. LYNNE LITTLEFIELD[2,3,4], WILLIAM E. ARCHER[1], AND HANS R. BODE[2,3]

[1]*Department of Biological Sciences, University of Notre Dame, Notre Dame, Indiana 46556;* [2]*Developmental Biology Center and* [3]*Department of Developmental and Cell Biology, University of California at Irvine, Irvine, California 92717; and* [4]*Department of Cell and Molecular Biology, Tulane University, New Orleans, Louisiana 70118*

Abstract. Embryogenesis in hydra includes a variable period of dormancy; and this period, as well as subsequent stages through hatching, takes place within a thick cuticle that hinders observation. Thus, although the early stages of development have been well-characterized qualitatively, the middle and later stages are only poorly understood. Here, we provide a detailed description of the stages of embryogenesis, including the time required to traverse each of the stages, and the changes that occur in the type and number of cells throughout the stages. The events of cleavage and gastrulation occur within the first 48 h. Cleavage is holoblastic and unipolar and leads to a single-layered coeloblastula. Gastrulation occurs by ingression and is followed by the deposition of the thick cuticle. Thereafter, during the variable period of dormancy ranging from 2–24 weeks, little occurs; the important events are the conversion of the outer layer into an ectoderm and the appearance of the interstitial cell lineage. During the last 2 days before hatching, the endoderm and gastric cavity form, while stem cells of the interstitial cell lineage proliferate and differentiate into neurons, nematocytes, and secretory cells. Finally, the cuticle cracks, and the hatchling enlarges and emerges from the cuticle as a functional animal. The formation of the gastric cavity and the hatching of the embryo are both explicable in terms of the osmotic behavior of the animal and the hydrostatic forces generated by this behavior. Characteristics of development that are common to hydra and triploblastic phyla are presented.

Received 15 November 1996; accepted 26 March 1997.

Introduction

Hydra, like all cnidarians, arose very early in evolution. Its diploblastic body plan is therefore simple, as is its embryogenesis. A comparison of this simple embryogenesis with those of the more complex triploblastic metazoans would reveal those features that are common to all animals. And a further investigation of those common features should then uncover basic genetic mechanisms underlying development. The Hox genes, for example, play an important role in specifying morphological regions in insects and vertebrates—and these genes also occur in cnidarians (Schierwater *et al.*, 1991; Murtha *et al.*, 1991; Schummer *et al.*, 1992); *Cnox-2* is a Hox gene that is involved in maintaining the adult pattern of hydra (Shenk *et al.*, 1993a, b). Identifying these regulatory genes and understanding their roles in development will depend on a detailed knowledge and understanding of hydra embryogenesis.

The epithelial cells in the adult hydra are constantly proliferating, changing their relative position along the body axis, and differentiating. Thus the patterning processes that maintain the form of the animal are continuously active in the adult as well as the embryo (Campbell, 1967a, b; Otto and Campbell, 1977). The effects of the patterning processes on cells and tissues are well understood, and current efforts are focused on understanding their molecular bases. The processes that set up the pattern in the embryo could be the same, overlap with, or differ from those maintaining pattern in the adult. Resolving this uncertainty in hydra will require a precise description of embryogenesis.

After more than a century of study, the early stages of hydra embryogenesis—cleavage through cuticle

formation—have been well described qualitatively (Kleinenberg, 1872; Brauer, 1891; Tannreuther, 1908; Kanev, 1952; Tardent, 1966). But the stages have not been timed, and neither the rates of cell division nor the number of cells in each stage have been measured. In contrast to the early stages of embryogenesis, the later ones are poorly understood; a single report (Brauer, 1891) provides a rough outline of the events, but detail is lacking. This lack of information is due to four factors. First, many strains of hydra species do not produce gametes under culture conditions in the laboratory. Second, most cultured strains and species also have low hatching rates. Third, the early and late stages of embryogenesis are separated by a period of dormancy that is extremely variable (2–52 weeks). Finally, a thick cuticle covers the embryo through most of embryogenesis; thus development is difficult to examine during the dormant period or during the final stages leading to hatching.

We have taken advantage of two strains, one female and one male, that produce gametes continuously in the laboratory. Although the hatching time remains quite variable, the number of embryos produced is high and the hatching rate is close to 100%. We could therefore describe the stages of development in detail; we could also time them and quantify the cell populations during embryogenesis.

Materials and Methods

Culture of adult hydra and embryos

Most analyses were carried out with two strains. One was PA1, a female strain of *Hydra vulgaris*, isolated from a pond on the Haverford College campus near Philadelphia, Pennsylvania, by Dr. Carolyn Teragawa. The other, CA7, a male strain of *Hydra vulgaris*, was isolated by Drs. Lynne Littlefield and Carolyn Teragawa at Boulder Creek, near Susanville, California. Both strains were maintained in the laboratory for 3 years before the current studies were undertaken. Some analyses were carried out with the male E2 and female A5 strains, which were derived from crosses of PA1 and CA7. All strains were cultured in hydra medium, which consisted of a commercial spring water (Arrowhead) supplemented with 1 m*M* $CaCl_2$. Animals were maintained at 15°C with a light/dark regime of 12 hours light and 12 hours dark; they were fed once a week with the nauplii of the brine shrimp, *Artemia salinas* (San Francisco Brand), and the medium was changed three times per week. Under these culture conditions, the males produced sperm most of the time. Individual females produced one-to-several eggs at roughly monthly intervals, and often a culture of females produced eggs simultaneously.

To obtain fertilized eggs, six male hydra bearing testes and 50 female hydra bearing eggs were cultured together in 100 ml of hydra medium. The males were removed weekly and replaced with new males bearing testes; 50–100 fertilized eggs, identified by the initiation of cleavage, were harvested. In most cases, the strands attaching the embryo to the parent were cut with a surgical knife and the detached egg was transferred to a petri dish (60 mm × 15 mm) containing hydra medium. In other cases, females carrying fertilized eggs were transferred to a fresh dish containing hydra medium, and the embryos were allowed to develop while still attached. Cultures of 20 embryos or 20 females bearing embryos were maintained at 15°C, and the medium was replaced daily. Embryos were cultured until they hatched, unless used for experiments at some point during embryogenesis.

Analysis of embryonic stages

Video microscopy. Progress through the stages of embryogenesis was monitored on live embryos in two ways. For the early stages of development, embryos from the fertilized egg to the early cuticle stages were continuously monitored with a time-lapse video recorder (JVC BR-9000U) mounted on a dissecting microscope (Olympus SZH) and attached to a Sony Trinitron color monitor (model KX-2501). One frame per second was recorded over 3 days. Second, the entire process of embryogenesis, from fertilized egg to hatching, was monitored with an optical disc recorder (Panasonic) attached to a Wild dissecting microscope and a Sony color monitor. One frame per 15 seconds was recorded over 30 days. The resultant time-lapse films were viewed and analyzed at playback speeds 10-100 times normal speed.

Histology. At various stages from early cleavage to hatchlings, embryos or young animals were fixed and sectioned to examine their histological structure. The embryos were fixed in Lavdowsky's fixative (ethanol: formalin: acetic acid: water in the ratios of 50:10:4:40), either for 60 min at room temperature or, for embryos with a cuticle, overnight at 4°C. Embryos at the last stage—bilayer formation, which occurs 2 days before hatching—and young hatchlings were relaxed in 2% urethane in hydra medium for 30 s prior to fixation. Fixed embryos and hatchlings were dehydrated through an ascending alcohol series (25%–100% ethanol), rinsed for 20 min in a 1:1 mixture of 100% ethanol and tertiary butyl alcohol, incubated overnight in tertiary butyl alcohol, and then infiltrated and embedded in Paraplast Plus paraffin (Fisher Scientific). Serial sections (10 μm) of embryos and hatchlings were prepared, mounted on glass slides, and stained with Schiff's reagent, toluidine blue, or hematoxylin and eosin. The stained sections were observed and photographed with a Zeiss compound microscope.

Scanning electron microscopy. Relaxed hatchlings and

embryos at various stages were fixed for 90 min with glutaraldehyde (2.5% in 10 m*M* Millonig's phosphate buffer, pH 7.2), and then rinsed three times for 15 min each in 10 m*M* Millonig's buffer. While in buffer, some samples were cut transversely with a straightedged razor blade. Samples were postfixed for 60 min in 2% osmium tetroxide in 10 m*M* Millonig's buffer, and then rinsed three times in 10 m*M* Millonig's buffer. Subsequently, they were dehydrated through a graded series of ethanols to 100%, critical-point dried with CO_2, mounted on metal stubs, and sputter-coated with gold-palladium for 1 min in a Denton sputter-coater. Samples were examined and photographed with a scanning electron microscope (JEOL JSM T-300) operated at 25 kV.

Quantification of cell numbers and types. Individual embryos were submerged in 50 μl of maceration fluid (acetic acid:glycerol:water in the ratios of 1:1:26; David, 1973) and maintained at 5°C for 2–3 days. For eggs and embryos up to the cuticle stage, the cell suspension was gently agitated with a stream of air blown through a microcapillary pipette. The cells dispersed in this way were postfixed with 8% formaldehyde and transferred to a gelatin-coated slide. A piece of fishline coated with 1% Tween 80 was used to spread the cells evenly over a 1 × 1–2 cm^2 area of the slide. For later stages (post-cuticle formation), individual embryos were placed on a gelatin-coated slide in a drop of maceration fluid, and the cuticle was removed with sharpened forceps. This often caused some of the larger embryonic cells to be sheared as they were extruded through the opening in the cuticle layer. Nevertheless, the cells were postfixed with formaldehyde and spread on a gelatin-coated slide as described above. The cells from early and late stages were dried on a slide warmer (40°C) overnight.

To aid in distinguishing embryonic cells (or the nuclei released when cells were sheared) from the nurse cells that are present in eggs and embryos at all stages through to hatching, macerated cells were stained with a 2.5 μg/ml solution of DAPI (4,6 diamidino-2-phenylindole-2HCl; Accurate Scientific and Chemical Corp.) in 10 m*M* $MgCl_2$/McIlvaine buffer (18 m*M* citric acid, 164 m*M* Na_2PO_4, pH 7.0) for 30 min and rinsed in 10 m*M* $MgCl_2$/McIlvaine buffer. The cells were examined microscopically at 375× and classified using terminology established for cell types of adult hydra (David, 1973; Campbell and Bode, 1983). Classification criteria were based on nuclear morphology (examined with epifluorescence) for cells at early stages of embryogenesis and on both nuclear and cell morphology (viewed with phase optics) for cells at later stages.

Hydroxyurea treatment

To block cell division during gastrulation, blastulae were exposed to 10 m*M* hydroxyurea (HU) in hydra medium for 6–12 h at 15°C. Thereafter, the embryos were washed three times in hydra medium and allowed to develop in hydra medium until hatching. Some embryos (controls and treated) were fixed and processed for DAPI staining to determine if the treatment blocked cell division during the time of treatment. In detail, embryos were fixed in Lavdowsky's fixative for 60 min, rinsed in hydra medium, incubated for 5 min in DAPI, washed three times for 10 min each in phosphate buffered saline (PBS), mounted in glycerin:PBS (3:1), and examined with epifluorescence. The number of nuclei per embryo was scored. Some HU-treated embryos were processed for histology immediately after gastrulation as described above.

Immunocytochemical detection of mesoglea and interstitial cells

Hydra embryos (all stages of development) and hatchlings were examined for the presence of interstitial cells and mesoglea. The monoclonal antibody MG52 (kindly provided by Michael Sarras), which recognizes laminin (Sarras *et al.*, 1991), was used to detect the presence of mesoglea. CP4, a monoclonal antibody that recognizes cells of the interstitial cell lineage (Javois and Bode, unpubl. data), was used to identify cell types of this lineage. Indirect immunofluorescence was used for visualization.

The procedure used for immunocytochemistry was a modification of the one described by Dunne *et al.* (1985). Animals were fixed for 60 min in Lavdowsky's fixative, washed three times for 15 min each in PBT (PBS containing 0.25% Triton-X), and incubated overnight at 4°C in blocking serum (PBS containing 10% neonatal calf serum [Irvine Scientific] and 0.1% sodium azide). Thereafter, antibody diluted in PBS (1:100 dilution of CP4 ascites fluid or a 1:20 dilution of MG52 tissue culture supernatant) was added to the samples, and they were incubated overnight at 4°C. Subsequently, samples were washed two times for 10 min each in PBT followed by a 30-min rinse in PBT. Then, samples were incubated in a 1:50 dilution of FITC-conjugated goat anti-mouse Ig's (Boehringer-Mannheim) in blocking serum for 30 min in the dark at 22°C. Samples were washed three times for 10 min each in PBT and counterstained in 0.01% Evans blue in PBT for 10 min. Finally, animals were washed ten times for 2 min each in PBT, rinsed twice in PBS, and mounted on slides in 3:1 glycerin:PBS containing 0.5% *n*-propyl gallate, and examined with epifluorescence.

Results

Aspects of oogenesis

In hydra, an egg forms in the following manner (Honegger, 1981; Honegger *et al.*, 1989; Littlefield, 1994).

Stem cells located in the ectoderm, whose only differentiation products are oocytes and nurse cells, continuously enter the gamete differentiation pathway. Under the appropriate environmental conditions they complete traversal of the pathway, and the products, which have the morphology of large interstitial cells, accumulate in the ectoderm. One of these interstitial cells forms an oocyte that increases in mass by engulfing or fusing with large numbers of the remaining interstitial cells, referred to as nurse cells. As the oocyte grows in mass, it distends and eventually ruptures the ectoderm (Fig. 1). Thereafter, the ectoderm recedes around the edge of the egg to form the egg cup, a raised ring of tissue at the base of the egg (Fig. 2).

Once an egg is exposed to the medium, meiosis and fertilization occur. The egg nucleus, which is located at the distal end of the cell, the point furthest from the body column of the parent, undergoes meiosis I and II, resulting in the formation of three polar bodies (Honegger, 1981). Thereafter, in the female strain used here, the egg has to be fertilized within 2 h for normal embryogenesis to occur. After 2 h the addition of fresh sperm did not result in the initiation of cleavage divisions. Instead the egg began to swell and eventually disintegrated.

The nurse cells engulfed by the developing oocyte during oogenesis remain in the egg throughout embryogenesis as spherical, refractile cells with pycnotic nuclei (Zihler, 1972; Honegger *et al.*, 1989) (see Fig. 11). They are located within the cytoplasm of all cells until cuticle formation; thereafter, they persist in many of the epithelial cells until hatching. They occur in large numbers, ranging from 2000–9000 per embryo, with an average of 4500.

Stages of embryogenesis

1. Cleavage. Fertilization occurs at the distal end of the egg, which is the end farthest from the adult body column. The distal end is also the future head of the animal. This was established by marking the distal end with a vital dye and finding that the head was stained in the resulting hatchling. Cleavage in hydra embryos is holoblastic and unipolar; that is, the cleavage furrow progresses inward from one side of each cell. The first meridional division is initiated at the distal end of the embryo and moves in a distal-proximal direction perpendicular to the axis of the parent (Figs. 3 and 4).

The second cleavage division, which begins shortly before the first is complete, also occurs in a distal-proximal direction and is perpendicular to the first one. The two divisions result in four equal-sized blastomeres (Fig. 5). As the first cleavage furrow bisects the egg, small microvilli, or filopodia, form in the region immediately behind the leading edge of the furrow (Fig. 4). These microvilli, which also occur in the next cleavage divisions, appear to hold the forming blastomeres together. Occasionally the blastomeres separate at the two-cell stage, or less frequently at the four-cell stage, resulting in the development of two or four embryos in a single egg cup.

The third division is equatorial, starting at the side of the embryo closest to the head of the adult. The furrow occurs somewhat closer to the distal end of the embryo, resulting in two tiers of unequal-sized blastomeres (Fig. 6). Because the furrow starts at one end, the division of the four blastomeres is asynchronous. Thereafter, the cleavage divisions are very irregular. They occur asynchronously and the division planes are often oblique, yielding unequal-sized blastomeres. Cells near the distal end are generally smaller than those at the proximal end (Fig. 7).

By the fourth to fifth cleavage division, a cavity begins to form in the interior of the cell mass (Fig. 11), while the surface remains uneven (Fig. 8). Over the next 2 h the cavity enlarges to its final size. The shape of the embryo smooths out into a spherical shell (Fig. 9), which is organized in a single cell layer surrounding the blastocoel (Fig. 10). At this point, the embryo has reached the blastula stage and consists of 64–128 cells (ave. = 76 ± 47 cells, Table I). Each cell is filled with about 40 nurse cells (Fig. 11). Since each cell division lasts about 60 min, the blastula stage is reached within 6 to 8 h of fertilization.

2. Gastrulation. Gastrulation occurs by ingression. Shortly after the blastula is formed, individual cells begin elongating and extending their basal surfaces into the blastocoel (Figs. 15 and 16). Simultaneously, the lateral contacts with neighboring cells are reduced and eventually severed, resulting in these blastomeres moving into the blastocoel. The process of ingression occurs in about 2 to 4 h; when it is completed, the embryo consists of an outer layer of columnar cells and a central mass of unorganized spherical cells (Figs. 12, 17, 18). There are nurse cells in all blastomeres, although many more in the cells of the inner cell mass (Fig. 12). No cavity remains, and the embryo is somewhat compacted.

Ingression begins at the distal end and proceeds in a wave traveling across the embryo in a proximal direction. It is accompanied by a transient inward distortion of the surface of the blastula as cells ingress. This distortion apparently involves considerable force—an embryo detached from its parent will actually roll over the surface of the culture dish as ingression takes place.

During gastrulation, the number of cells increases roughly fourfold, from 76 ± 47 to 315 ± 200 (Table I). The fact that cell division occurs while cells are accumulating in the blastocoel suggests delamination as an alternative explanation for generating cells in the cavity. If

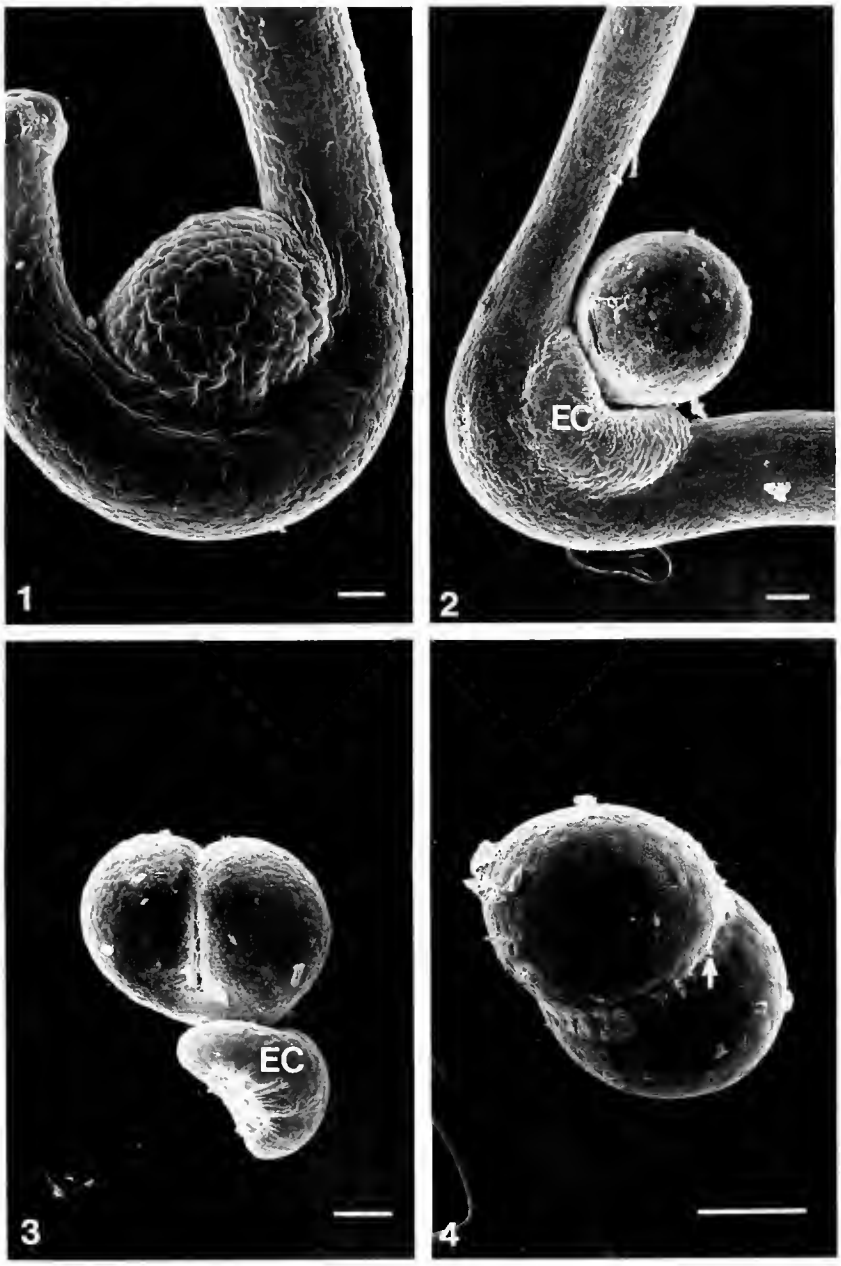

Figure 1. Hydra forming an egg. As the egg increases in size, it distends the overlying ectoderm of the parent. The ectoderm has not yet ruptured. Bar = 100 μm.

Figure 2. Hydra egg that has broken through the ectoderm. This developing egg is loosely attached to the parent at the egg cup (EC). Bar = 100 μm.

Figure 3. Hydra egg undergoing first cleavage. Note the distinctive heart shape created by unilateral furrowing. EC, egg cup. Bar = 100 μm.

Figure 4. Two-cell stage. Microvilli (arrow) form in the region of the cleavage furrow and may help hold the blastomeres together. Bar = 100 μm.

the plane of cell division were parallel to the surface of the embryo, cell division would result in one daughter remaining at the surface while the other would be in the interior. To distinguish between delamination and ingression, embryos were treated with hydroxyurea (HU) for 6 h covering the period of gastrulation. HU blocks cell division in hydra (Bode, 1983). In HU-treated embryos, gastrulation, the subsequent development of the embryo, and the resulting hatchlings were all normal. The only differences were two. One was that the cells of

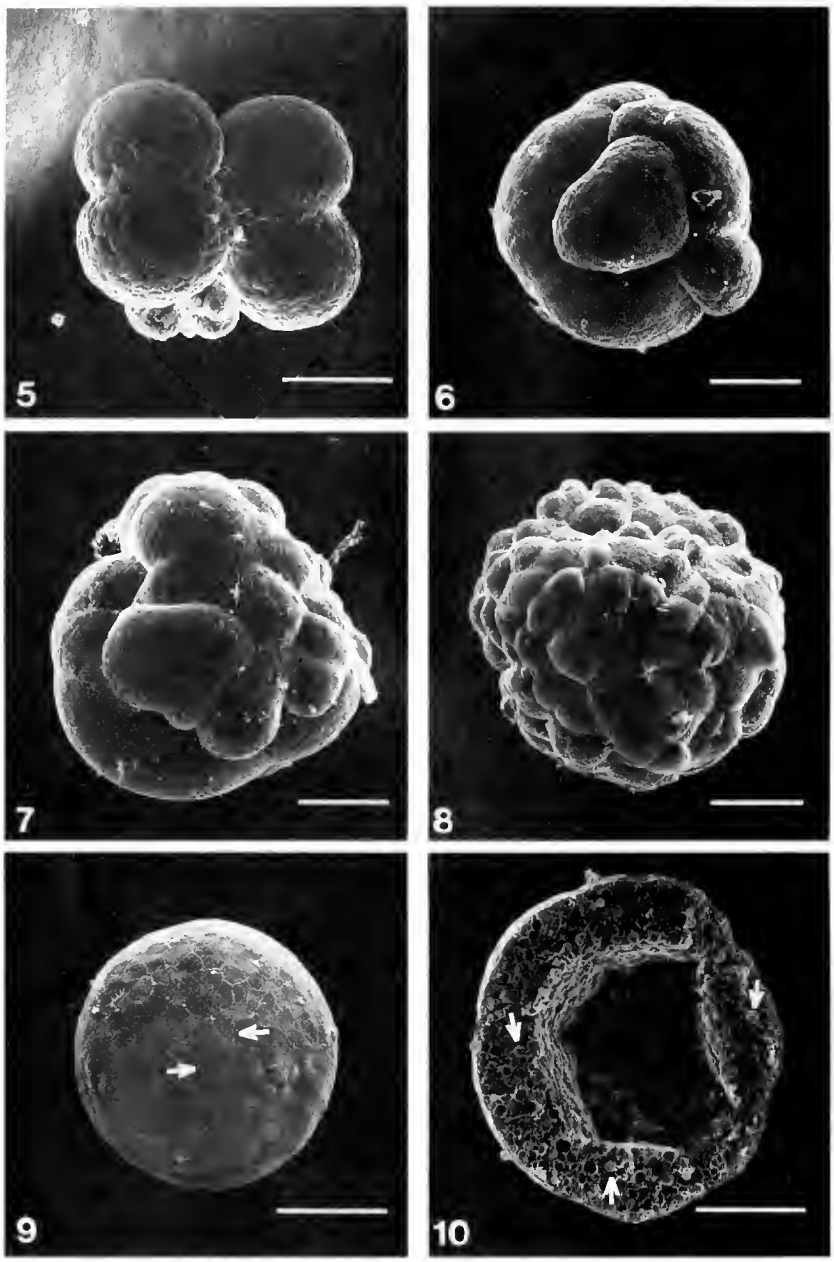

Figure 5. Four-cell embryo. Bar = 100 μm.

Figure 6. Forming eight-cell embryo of hydra showing two unequal-sized tiers of cells. Bar = 100 μm.

Figure 7. Mid-cleavage embryo. Note the unequal size of the blastomeres. Cells at the distal end are smaller than those at the proximal end. Bar = 100 μm.

Figure 8. Late cleavage stage. The cells are more uniform in size and resemble a morula. Bar = 100 μm.

Figure 9. Coeloblastula. Note the microvilli (arrows) that delineate the margins of the cells. Bar = 100 μm.

Figure 10. Cross-section of the coeloblastula. Note the single layer of cells surrounding the blastocoel. These cells contain many nurse cells (arrows). Bar = 100 μm.

g[illegible] the treated animals were somewhat larger than [illegible] (compare Figs. 12 and 13), as would be expected [illegible] vision had been interrupted. The other was that [illegible] of cells did not increase during gastrulation in the treated animals. Thus, ingression of cells, not delamination, is the most likely explanation for the origin of the interior cells.

Gastrulation is complete by 8 to 12 h postfertilization,

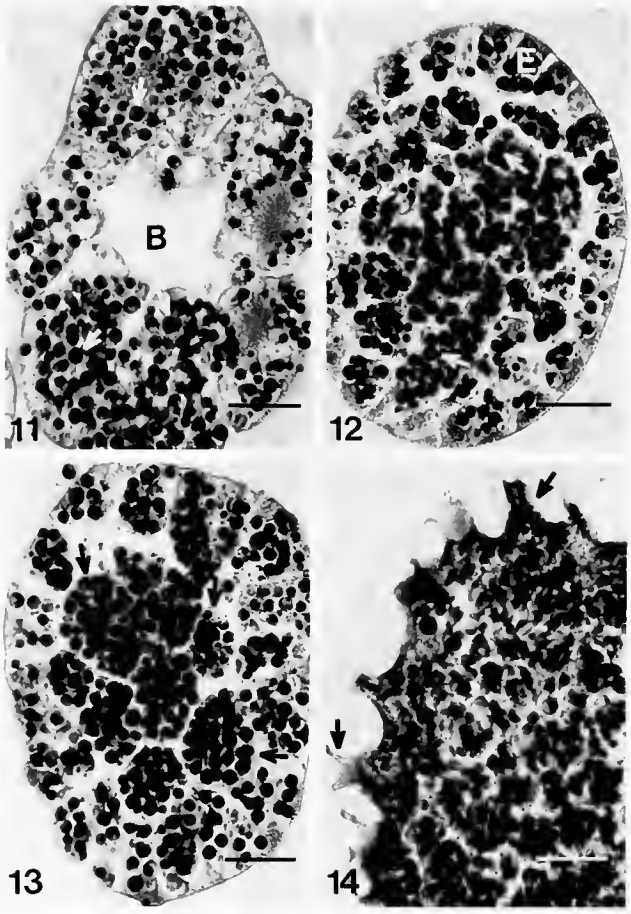

Figure 11. Histological section of the morula. Note the forming blastocoel (B) and the darkly stained nurse cells (arrows) within the blastomeres. Bar = 100 μm.

Figure 12. Gastrula of control embryo. A central mass of cells filled with darkly stained nurse cells (arrows) is surrounded by an outer epithelial layer (E). Bar = 100 μm.

Figure 13. Gastrula of hydroxyurea-treated embryo. Note the large cells (arrows) filled with nurse cells. Bar = 100 μm.

Figure 14. Cuticle deposition in a control embryo. Cells of the outer layer exhibit filopodia (arrows) extended into the outside medium. Cuticle material is deposited around the filopodia, producing spines. Bar = 100 μm.

or about 2 to 4 hours after the blastula is formed. Thereafter, little activity is visible for the next 10–12 h.

3. Cuticle formation. The next stage involves the formation of the cuticle, a thick protective outer layer that is also commonly referred to as the embryotheca. About 20 h after fertilization, the cells of the outer layer begin to extend filopodia into the surrounding medium (Fig. 14). Cuticular material is deposited in layers around the filopodia and on the apical surfaces of the cells (Fig. 19). Three hours later the material has built up to the point that spines are visible. Over the next 18–24 h, material is continually deposited, producing a multilayered structure over the surface of the embryo (Figs. 20 and 21) with ornate spines 25–50 μm long (Fig. 22) forming where filopodia were located. Towards the end of this period, the filopodia are retracted and the resulting channels filled with cuticular material. The process is complete 40–48 h postfertilization.

Cuticle deposition commonly starts on the proximal side in the egg cup and slowly progresses around the embryo in a distal direction. In general, the final distribution of material is somewhat asymmetric, with the cuticle being thickest (~60 μm) at the proximal end and thinnest (~45 μm) at the distal end. Once this process is complete, a second, very thin, membranous layer is deposited by the outer cell layer beneath the cuticle (Fig. 24). Thereafter, the embryo detaches from the parent, although detachment occurs occasionally at any point from the two-cell stage onward. The time of detachment has no bearing on the progress of embryogenesis.

4. Cuticle stage. Unlike the early and late stages of embryogenesis, the middle stage is of undefined length, ranging in the laboratory from 2–24 weeks. It is thought to correspond to an overwintering period of the embryo in nature. Two important events occur during this stage: the cells of the outer layer acquire characteristics of the epithelial cells of the adult ectoderm; and the cells of the interstitial cell lineage first appear.

Shortly after cuticle formation is complete, the outer layer is observed to consist primarily of smaller squamous epithelial cells, most of which are devoid of nurse cells (Figs. 23 and 24). In contrast, the interior cells are irregular in shape and all contain nurse cells (Fig. 25). A change in nuclear morphology is correlated with the appearance of these smaller epithelial cells. In macerates,

Table I

Increase in number of blastomeres and epithelial cells through embryogenesis

Stage	Time after fertilization	Number of epithelial cells[1] (± 1 SD)
Blastula	6–8 h	76 ± 47
Gastrula	8–12 h	315 ± 200
Cuticle formation	20 h	400 ± 200
Cuticle	40 h	370 ± 120
Cuticle	6 d	440 ± 160
Cuticle	11 d	420 ± 200
Bilayer[2]		3000 ± 100
Hatchling		2830 ± 1080

[1] Through 144 h, the cells are blastomeres and all are included. Thereafter, epithelial cells are counted, but cells of the interstitial cell lineage are not. Sample size = 5–13.

[2] Bilayer embryos are analyzed 2 days before hatching. Bilayer and hatchling data are from embryos with a diameter of 400 μm.

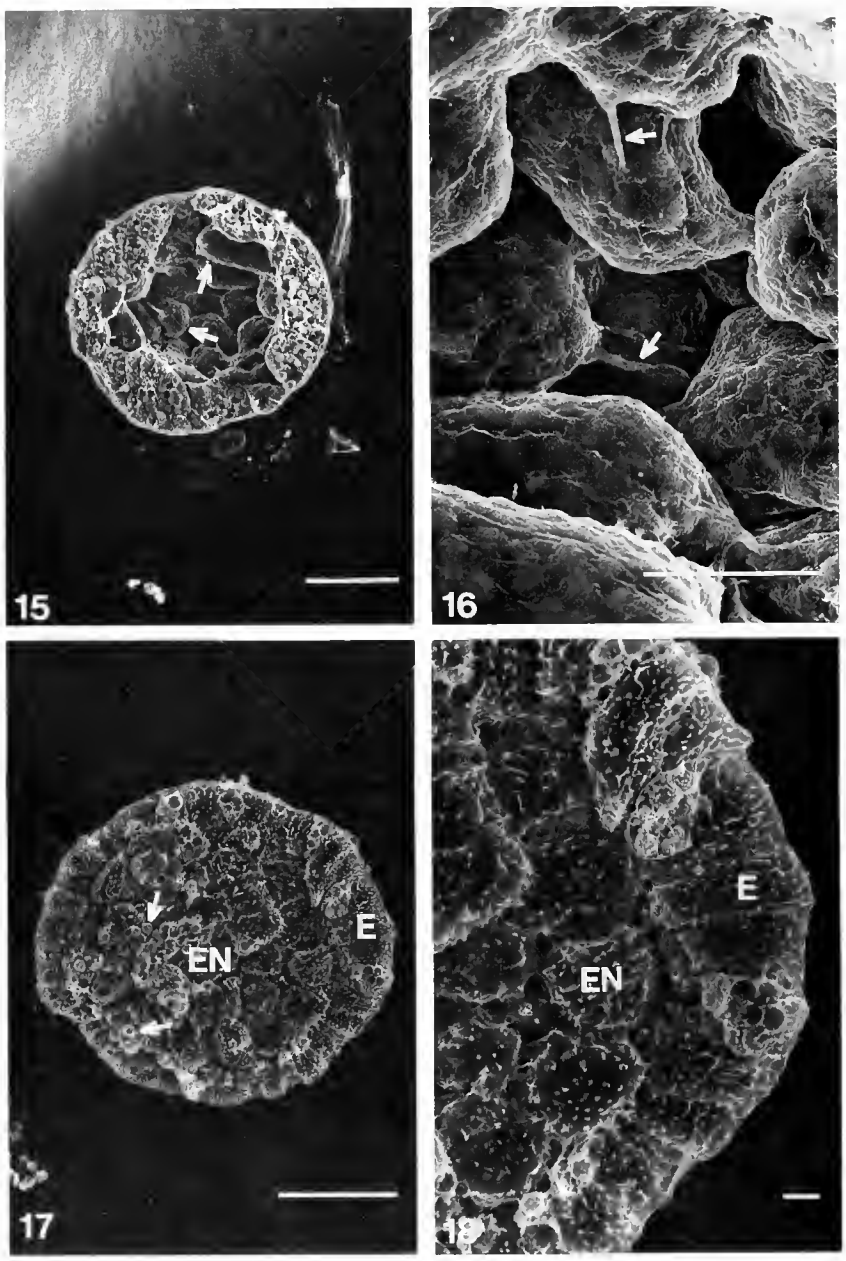

Figure 15. Cross-section of a hydra blastula showing cells (arrows) ingressing into the blastocoel from all sides. Bar = 100 μm.

Figure 16. Cells ingressing into the blastocoel during gastrulation (enlargement of Fig. 15). Individual cells extending filopodia (arrows) detach from their neighbors, move into the blastocoel, and fill it. Bar = 100 μm.

Figure 17. Cross-section of a control hydra gastrula. The outer layer of cells (E) will give rise to the epidermis of the adult polyp, while some of the cells of the inner mass (EN) will contribute to the gastrodermis of the adult. Nurse cells (arrows) are abundant in the inner layer of cells. Bar = 100 μm.

Figure 18. Cross-section of a control gastrula. Note the outer layer of columnar-shaped cells (E) that surround the central spherical cells (EN). A mesoglea is not detected between the outer and inner cells. Bar = 10 μm.

tic nuclei of blastomeres of the gastrula and early cuticle stages are large and amorphous. By 6 days postfertilization and 4 days after cuticle formation is complete, some of the cells are much smaller and have nuclei that resemble those of the epithelial cells of adults. They have a prominent nucleolus and a clear cytoplasm. Thus, by

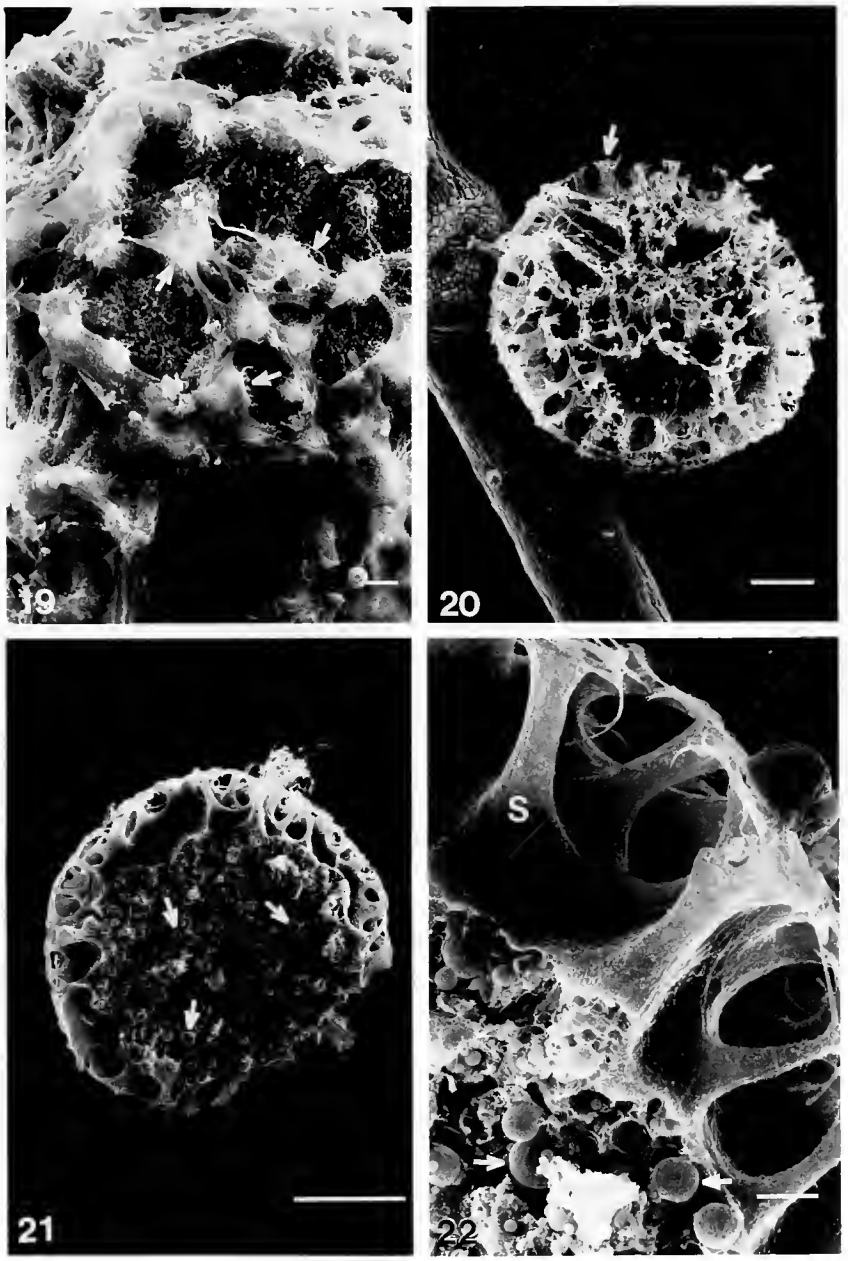

Figure 19. Early cuticle stage. Cuticular material (arrows) is deposited on the apical surfaces of the cells and around filopodia that project from the outer cells. Bar = 10 μm.

Figure 20. Hydra embryo with fully developed cuticle. The cuticle is adorned with thick spines (arrows). Bar = 100 μm.

Figure 21. Cross-section of a cuticulated embryo. A thick cuticle is tightly attached to an outer thin layer of squamous cells (not visible here). The interior of the embryo contains spherical cells rich in nurse cells (arrows). Bar = 100 μm.

Figure 22. Enlargement of cuticle spines (S) and nurse cells (arrows) of a cuticulated embryo. Bar = 10 μm.

this stage the outer layer becomes morphologically similar to the epithelium of the adult ectoderm.

The second event is the appearance of interstitial cells. All nonepithelial cells in hydra are part of the interstitial cell lineage. It consists of a population of interstitial cells, some of which are multipotent stem cells, and four classes of differentiation products: neurons, nematocytes, secretory cells, and gametes (Bode, 1996). During

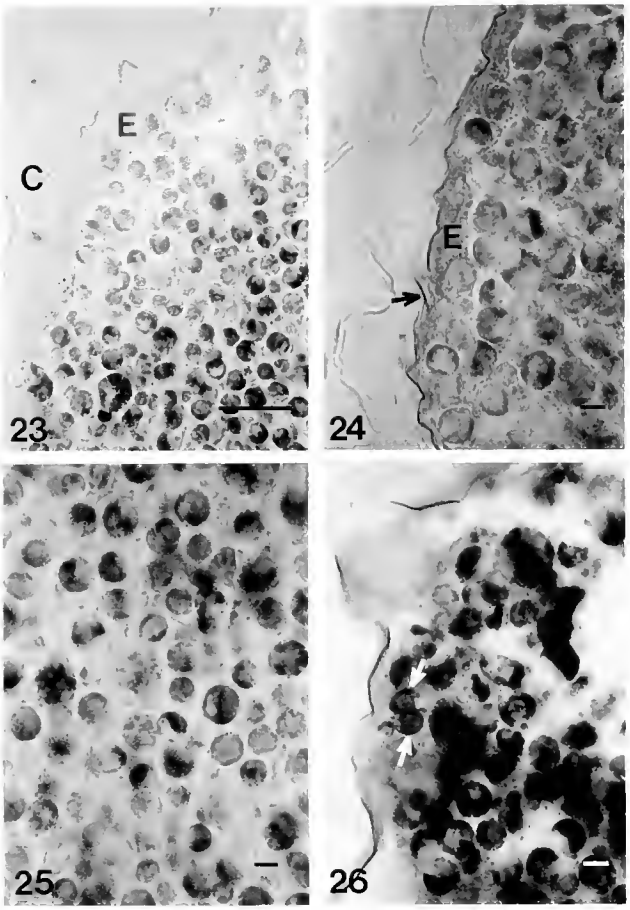

Figure 23. Early cuticle stage. The outer layer of lightly staining cells (E) is flattened against the cuticle (C). Nurse cells (darkly staining) fill the central mass of cells. Bar = 50 μm.

Figure 24. Mid-cuticle stage. Note the flattened squamous-like cells of the outer layer (E) and the inner membranous layer (arrow) of the cuticle. Bar = 10 μm.

Figure 25. Central mass of cells, containing nurse cells, of a cuticle stage embryo. Bar = 10 μm.

Figure 26. Young interstitial cells (arrows) among cells of the outer layer. Bar = 10 μm.

the first 6 days of embryogenesis, the morphology of the cells is either large with amorphous nuclei or epithelial in character. By 11 days postfertilization, however, another distinct change has occurred in a subpopulation of the cells. Much smaller cells with a morphology of the large and small interstitial cells of the adult have appeared (Fig. 26). Most of these cells are found among the epithelial cells of the thin outer layer (Fig. 26), and some are also observed in the inner mass of cells. As shown in Table II, most of these cells are large interstitial cells.

5. *Bilayer formation.* During this last stage of embryogenesis, two epithelial layers separated by a basement membrane are formed; these closely resemble the cell layers of the adult animal. Because the cuticle stage is of variable length, the timing of the onset of bilayer formation is not easy to predict. However, the fact that an embryo is in the final stage is signaled by a clear morphological change that occurs 2 days before hatching. In general, the embryo is opaque due to the refractility of the several thousand nurse cells in the cytoplasm of the embryonic cells. Two days before hatching the outer edge of the embryo becomes translucent. The thin outer layer of squamous cells devoid of nurse cells becomes thicker, consisting of columnar epithelial cells and large numbers of interstitial cells (Figs. 27 and 28). Between the 11-day postfertilization stage and the bilayer stage, the number of interstitial cells increases markedly (Table III). When sections are treated with the antibody CP4, which specifically recognizes large interstitial cells, the majority of stained cells appear in the outer layer (Fig. 29). In addition, the small interstitial cells (cell types derived from the large interstitial cells) appear in substantial numbers (Tables II and III). Small numbers of neurons and nests of nematoblasts are also observed. At this point, the layer closely resembles the ectoderm of the adult.

The formation of the ectoderm must precede the formation of the endoderm because the outer layer is clearly defined 2 days before hatching, while the cells in the interior remain in an unorganized mass (Fig. 27). Once the ectoderm has formed, some of the cells of the interior mass line up along the ectoderm and change in shape from spherical to columnar (Fig. 30). This alignment occurs simultaneously in different parts of the embryo, and the enlarging aligned regions of the developing endoderm fuse into a complete spherical layer. As this occurs, spaces appear among the cells within the interior cell mass (Figs. 28 and 30). These spaces enlarge and coalesce with time, thereby forming the gastric cavity. When these processes are complete, two layers have formed (Figs. 31 and 32). Most of the cells of the inner mass have become part of the endoderm, although some remain in the cavity and later appear to degenerate. The cells of the inner layer have the typical appearance of endodermal epithelial cells of the adult in that one or more cilia protrude from their surfaces into the gastric cavity (Fig. 32).

The last step is the formation of the mesoglea, the basement membrane that separates the two layers in the adult. Like the basement membranes found in higher metazoans, this structure is mainly composed of collagen IV, fibronectin, laminin, and heparan sulfate proteoglycan (Sarras *et al.*, 1991). Whole embryos at different stages of development were stained with the monoclonal antibody MG52, which recognizes the laminin component of mesoglea. Embryos at the blastula, gastrula, cuticle deposition, and early presumptive ectoderm stages did not stain with the antibody, indicating that the mesoglea had not yet been synthesized (data not shown). Embryos in which both layers had formed showed staining

Table II

Relative increase in the population sizes of the cell types of the interstitial cell lineage during embryogenesis

Stage[1]	Number of cells of a cell type/epithelial cell				
	Large interstitial cells	Small interstitial cells	Nematoblasts + Nematocytes	Neurons	Secretory cells
Cuticle (6 d pf)	—	—	—	—	—
Cuticle (11 d pf)	0.33	0.06	—	—	—
Bilayer	0.61	0.40	0.023	—	0.013
Hatchling (0–5 h)	0.52	0.58	0.13	0.025	0.058
Hatchling (2–20 h)	0.49	0.61	0.70	0.11	0.12
Adult[2]	0.64	0.70	1.32	0.25	0.27

[1] pf = postfertilization.
[2] Data from Bode *et al.*, 1973.

between the layers where the mesoglea normally forms (Fig. 33). The endodermal layer need not be complete for the appearance of the mesoglea, which begins to form shortly after the endodermal cells align on the ectoderm. With the formation of the mesoglea, the overall structure of the embryo is complete.

6. *Hatching.* Once the bilayer has formed, the embryo begins to pulsate rhythmically and continues to do so until hatching is complete. As the embryo pulsates, perforations and channels appear in the cuticle, forming a honeycomb pattern and suggesting that the structure is beginning to break down (Fig. 34). Within 24 h of the formation of the two epithelial layers, the cuticle cracks open on its thinnest side, the original distal side of the embryo where the head forms. To confirm that the crack was always on the distal side, embryos that had formed a cuticle were detached from the parent, embedded in soft agar with known orientation, and incubated in hydra medium. These embryos hatched in the agar, and in each case the cuticle opened at the distal end. Furthermore, the head end of the hatchling always came out first.

Once the cuticle opens, the spherical embryo continues its pulsatile contractile activity and begins to elongate and emerge from the cuticle (Fig. 35). For the next 2.5 h the periodic elongations and contractions continue, and the shape changes from a compact sphere to an elongate cylinder 550–700 μm in length. During the early stages of hatching, the embryo is still enveloped in the membrane that was laid down at the beginning of the cuticle stage, but as the embryo enlarges, the membrane ruptures. This results in increased activity of the hatchling as it frees itself of membrane and cuticle.

The apical end of the hatchling undergoes dramatic morphological changes during the final stages of hatching. Before the membrane ruptures, the apical end has the shape of a smooth dome (Fig. 35). Within as short a period as 15 min after rupture, the apical end narrows into a conical shape, and one to five tentacle primordia evaginate in a ring below the apical tip (Fig. 36). At this point, the head of the hatchling is morphologically complete and resembles that of a mature bud. The foot is also completely functional. Once free of the cuticle, the hatchling is able to stick to the surface of the petri dish. This ability is also found in adult hydra, and indicates the presence of functional mucous-producing cells in the foot region.

Other signs that the hatchling is essentially fully functional are apparent. The body column elongates and contracts, indicating that the muscle processes of the epithelial cells in each of the layers are fully developed. Further, the nerve net that coordinates the contractile activity must have formed. The hypostome, the dome above the ring of tentacles in the head, contains the mouth. In adults, treatment with glutathione results in opening of the mouth, mimicking a feeding response (Lenhoff, 1983). A freshly hatched hydra treated with glutathione opens its mouth, indicating that the mouth is fully formed and functional. When the hypostome is touched with a brine shrimp larva the mouth opens and the larva is ingested, and then digested. Because the tentacles are short upon hatching, capture of brine shrimp larvae is difficult. But within 2 days of hatching, after the tentacles have grown in length, the hatchling is fully capable of capturing shrimp larvae and feeding itself. Hence, the nematocytes necessary for the capture of the shrimp, the mucous cells of the head, which are inferred to be involved in ingestion, and the gland cells necessary for digestion have all formed. All of these activities indicate that the hatchling has a full complement of the somatic cell types found in an adult. As shown in Table II, the cell composition of a hatchling less than a day old is rapidly approaching that of an adult, which confirms the inference from the behavior of the young animal.

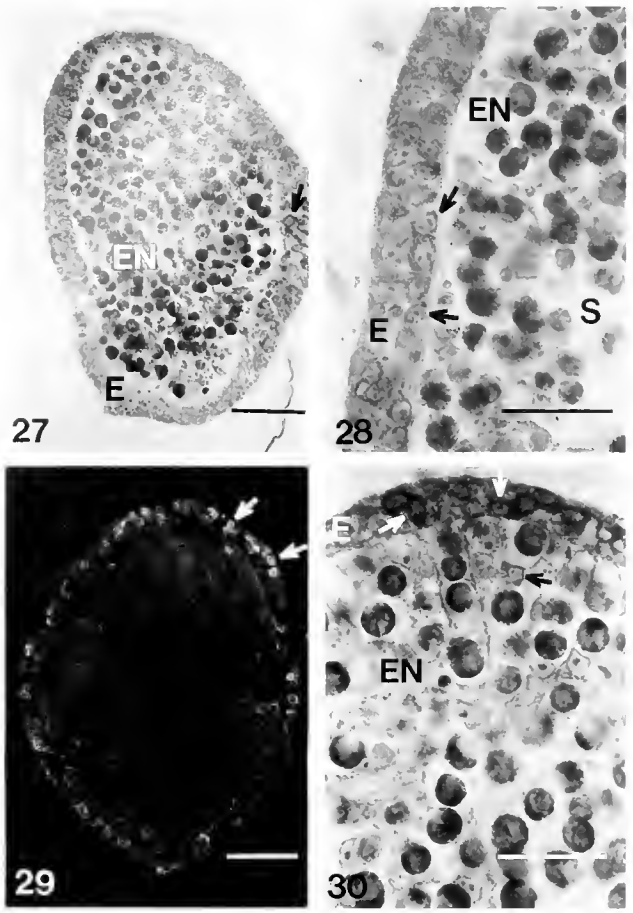

Figure 27. Early bilayer stage. An outer layer (E, future ectoderm) of columnar cells and interstitial cells (arrow) surround an unorganized mass of interior cells (EN, future endoderm). Bar = 100 μm.

Figure 28. Forming endoderm (EN) of a bilayer embryo. As the endodermal epithelial cells line up along the ectoderm (E), spaces (S) appear among the interior mass of cells. Note the interstitial cells (arrows) in the outer layer. Bar = 50 μm.

Figure 29. Bilayer stage stained with CP4 monoclonal antibody. A large number of labeled interstitial cells (arrows) are seen in the outer epithelial layer. Bar = 100 μm.

Figure 30. Bilayer stage. An outer ectoderm (E) and inner endoderm (EN) are complete. Interstitial cells (arrows) are found in both layers. Bar = 50 μm.

Discussion

Timing of embryological events

Because the body plan of hydra is simple, the events of embryogenesis are few when compared to the development of the body plans of more complex metazoans. The early events can be summarized as shown in Figures 37–39. After fertilization, the cleavage divisions lead to the formation of a single-layered blastula. Gastrulation is due to the ingression of cells from the blastula layer into the cavity until it is filled. Thereafter, a thick protective outer layer of cuticle and a thin inner membranous layer are laid down around the embryo (Fig. 40). During the prolonged cuticle stage, the major events are the conversion of the outer layer of blastomeres into a layer closely resembling the adult ectoderm and the appearance of the interstitial cell lineage (Figs. 41–43). In the final days before hatching, the endoderm, the mesoglea separating the two layers, and the gastric cavity form (Figs. 43 and 44).

When kept in the laboratory at a constant temperature of 15°C, embryos of the species used here complete development at any time from 2 weeks to 6 months. Yet, this is not an accurate reflection of the time required to undergo the events of embryogenesis. From fertilization through the completion of cuticle formation requires 40 to 48 h. The time from the appearance of the translucent stage, indicating a fairly complete ectoderm at the onset of the bilayer stage, until hatching is also about 48 h. The very large variable period occurs during the cuticle stage. In its normal freshwater habitats, the embryo is inactive during this period of embryogenesis.

There are indications that the actual time required for embryogenesis may be much shorter. Other authors (Kanaev, 1952) have noted that fertilized eggs can hatch in 13–14 days. We found that 5%–10% of the embryos hatched in about 2 weeks, but the percentage increased to 40%–50% if the embryos were subjected to electroporation at 5 days postfertilization (P. Bode, pers. obs.). These results suggest that, in addition to the 2 days at the beginning and 2 at the end of embryogenesis, the cuticle stage can be traversed in about 9 to 10 days. Because relatively few embryonic events occur during this stage compared to the beginning and end of embryogenesis, it is unclear whether this amount of time is obligatory.

The two epithelial cell lineages form sequentially

The development of both epithelial lineages involves relatively few steps. A hatchling derived from a large embryo (~400 μm in diameter) has about 3000 epithelial cells (see Table III). Most of the cell divisions giving rise to this population occur at the very beginning of embryogenesis. In the approximately 10 h from the fertilized egg through gastrulation, the cell number increases to about 300 cells, with each of the eight to nine cell divisions lasting about an hour. Thereafter, the rate of cell division slows down dramatically. In the next 10 h before cuticle formation begins, some of the cells undergo another division and raise the number to about 400 cells. Since the interstitial cells most likely arise by asymmetric cell divisions of blastomeres in the cuticle stage, one can consider the 400 blastomeres at the beginning of cuticle formation to be the direct precursors of the 3000 epithelial cells of the hatchling. This implies that these blastomeres, or later as epithelial cells, un-

Table III

Changes in cell composition during embryogenesis

Stage	Epithelial cells	Large interstitial cells	Small interstitial cells	Nematoblasts + Nematocytes	Neurons	Secretory cells
Blastula	76	—	—	—	—	
Gastrula	315	—	—	—	—	—
Cuticle formation	400	—	—	—	—	—
Cuticle (40 h)	370	—	—	—	—	—
Cuticle (6 d)	440	—	—	—	—	—
Cuticle (11 d)	420	140	25	—	—	—
Bilayer	3000	1830	1230	70	—	40
Hatchling (0–5 h)	2830	1470	1640	370	70	160
Hatchling (2–20 h)	2830	1390	1730	1980	310	340

Data for epithelial cells are from Table I. The number of cells of the interstitial cell lineages are calculated from the numbers of epithelial cells and the ratios of interstitial cell lineage cell type to epithelial cells from Table II.

dergo only another two to three divisions. And, if the minimum hatching time is about 13–14 days, about ten cell divisions occurred in the first day, and the remaining two to three occurred in the last 12–13 days.

The outer layer of blastomeres formed at gastrulation will give rise to the ectoderm. After ingression is complete, these cells still contain nurse cells, although they are fewer and mostly located near the basal portions of the cells (Fig. 39). In animals whose hatching time was not artificially reduced, a distinct change occurs by 6 days postfertilization. The outer layer next to the cuticle consists of a layer of squamous cells devoid of nurse cells (Fig. 41). In addition, the morphology of the nuclei of these cells changes from the amorphous nucleus of a blastomere to the clear nucleus, characterized by a prominent nucleolus, of an adult epithelial cell. This layer most likely arose from blastomeres of the outer layer undergoing a division parallel to the surface and giving rise to the squamous cells next to the outer cuticle and deeper, somewhat larger, cells that contain nurse cells.

The next distinct change in this layer occurs 2 days before hatching when the ectodermal layer becomes

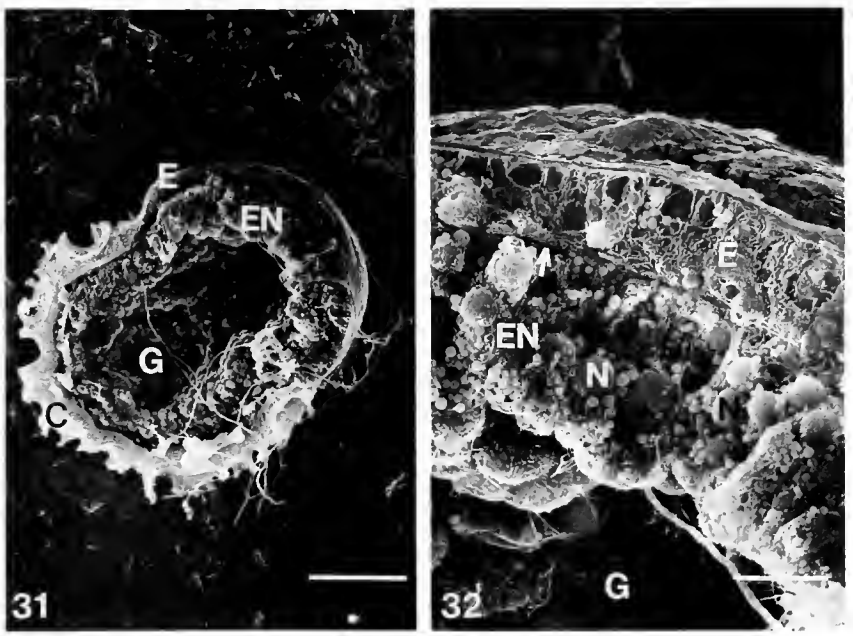

Figure 31. Cross-section of a bilayer stage embryo. Two distinct layers (E, EN) surrounding a gastric cavity (G) are visible. C, cuticle. Bar = 100 μm.

Figure 32. Bilayer stage embryo. A distinct ectoderm (E) and endoderm (EN) are separated by a mesoglea (arrow). Nurse cells (N) are found in the cells of the endoderm. G, gastric cavity. Bar = 10 μm.

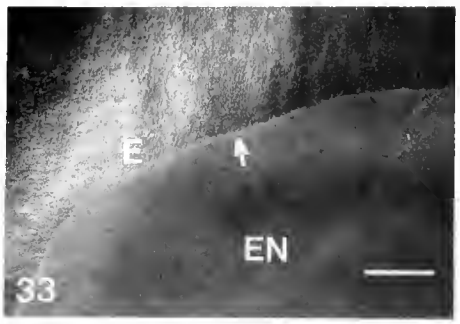

Figure 33. Mesoglea (arrow) of the bilayer stage stained with an anti-laminin monoclonal antibody, MG52. E, ectoderm; EN, endoderm. Bar = 50 μm.

translucent. The layer becomes two to three times thicker, with the ectodermal cells changing from squamous to columnar in shape. The increased width and the absence of the opaque nurse cells render the layer translucent. This change may occur primarily because of the rapid accumulation of cells of the interstitial cell lineage among the cells of the outer layer during the bilayer stage. Since the surface area of this layer is constant, the increasing mass of the interstitial cells may force the epithelial cells to undergo the observed shape change. At this point the outer layer is very similar to the adult ectoderm.

At the bilayer stage when the ectoderm is mostly complete, the definitive endoderm is nonexistent. The cells that will form the endoderm are still a disorganized mass in the interior of the embryo. Between the bilayer stage and hatching 2 days later, many of these cells begin to align themselves on the overlying ectoderm, changing in shape from roughly spherical to columnar (Figs. 43 and 44). This alignment occurs independently in several places, with the enlarging patches merging and fusing into a complete endodermal layer. These cells still contain large numbers of nurse cells and will do so for several days after hatching. The role of the nurse cells is unclear, although the most probable explanation is that they provide a source of nutrients.

The last step in the development of the two epithelial layers is the formation of the mesoglea between them (Figs. 43 and 44). This occurs after the alignment of the endodermal cells with the overlying ectodermal cells. Evidence in adult animals indicates that both layers are involved in the formation of the mesoglea (Epp *et al.*, 1986; Sarras *et al.*, 1993). Most likely the same process occurs here.

These events lead to the formation of two layers separated by a basement membrane. An unanswered question concerns the changes in these epithelia that will lead to formation of the head and foot. Shortly after hatching, tentacles emerge from the apical dome, and upon stimu-

Figure 34. Degenerating cuticle just prior to hatching. Perforations and channels (arrows) appear in the cuticle, producing a honeycomb pattern. Bar = 10 μm.

Figure 35. Hydra hatchling emerging from the cuticle. Arrow indicates a dome-shaped anterior head. Bar = 100 μm.

Figure 36. Hydra hatchling with four tentacle bumps. Bar = 100 μm.

lation with glutathione, the mouth opens. In addition, once free of the cuticle, the hatchling sticks to the surface, indicating that it has a fully formed foot. When do the epithelia undergo the changes that set up the tissue for these morphogenetic and differentiation events?

Development of the interstitial cell lineage

All nonepithelial cells in hydra are part of the interstitial cell lineage. The formation of this lineage occurs in parallel with the development of the two epithelial layers. Large interstitial cells are rare or absent at 6 days postfertilization, but are present by 11 days (Tables II and III). Since large interstitial cells are considerably smaller than blastomeres, the simplest explanation is that some of the blastomeres undergo asymmetric cell divisions to generate the interstitial cells. Though such divisions were not observed directly here, Noda and Kanai (1980) reported them in another species of hydra, *Pelmatohydra robusta*, and Fennhoff (1980) described similar divisions in *Tubularia crocea*, a marine relative of hydra.

Where do these asymmetric cell divisions take place? Noda and Kanai (1980) placed them at the base of the outer layer, and Fennhoff (1980) localized them in the central mass of cells. In our study there is clear evidence of large interstitial cells in the thin outer layer where the epithelial cells are devoid of nurse cells. However, some cells in the interior mass of cells also have the morphology of interstitial cells. Results of the CP4 staining in bilayer stage embryos (Fig. 29) indicate that most of the interstitial cells are in the ectoderm, and some are in the

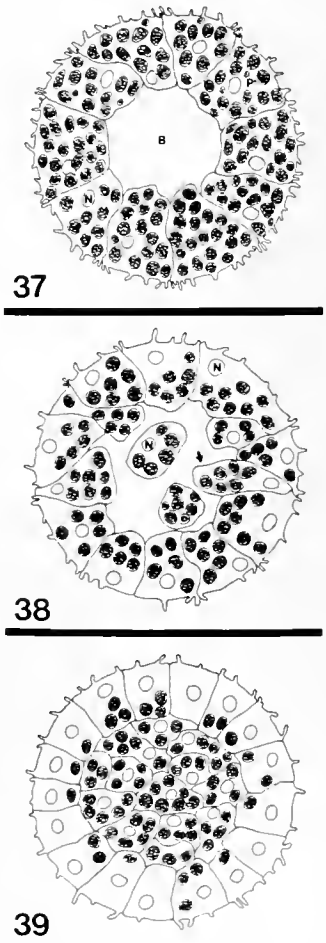

Figure 37. Coeloblastula. A single layer of cells filled with darkly colored nurse cells (P) surround a fluid-filled blastocoel (B). N, nucleus.

Figure 38. Cells ingressing (arrow) into the blastocoel during early gastrulation. As cells move to the interior they elongate, detach from their neighbors, and round up once in the filling blastocoel. N, nucleus.

Figure 39. Embryo at the completion of gastrulation. An outer layer of columnar cells has formed; within these cells the nurse cells are found at the basal tips. Spherical cells filled with nurse cells occupy the center of the embryo. A blastocoel is obliterated.

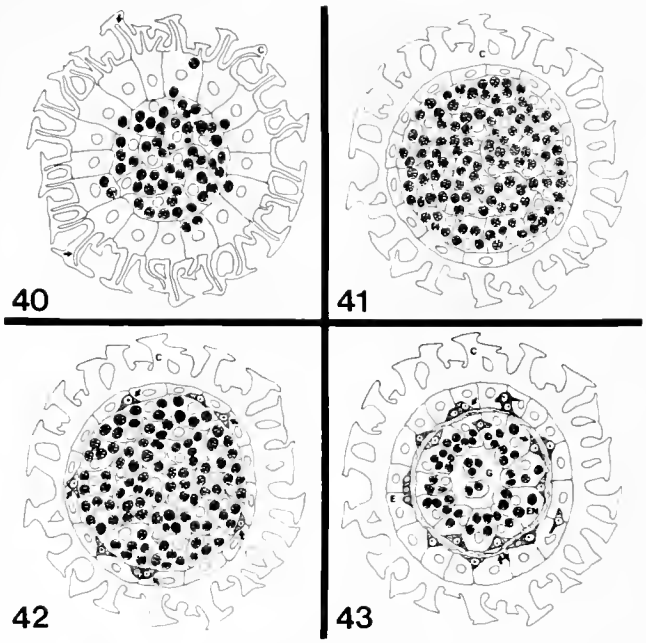

Figure 40. Early cuticle stage of hydra. The cells of the outer layer extend tiny filopodia (arrows) upon which cuticle material is deposited. Note that the darkly colored nurse cells have accumulated in the central cells. C, cuticle.

Figure 41. Embryo a few days after cuticle deposition is completed. Note that the outer layer of cells has flattened against the cuticle (C) to assume a squamous-like morphology. Nurse cells are virtually absent from the outer layer. Spherical cells containing numerous nurse cells fill the center of the embryos. The cuticle is thick and bears beautiful geometric spines. Filopodia of the outer cells have been retracted.

Figure 42. Mid-cuticle stage of hydra. Interstitial cells (arrows) arise in the outer layer. Cells of the outer layer have a flattened, squamous morphology. The inner cells are spherical and filled with nurse cells; no nurse cells remain in the ectoderm. C, cuticle.

Figure 43. Bilayer stage. The two layers, the ectoderm (E) and the endoderm (EN), are distinct and are separated by a mesoglea (double arrows). A forming gastric cavity (G) is present. Interstitial cells (single arrows) are found in both germ layers. C, cuticle.

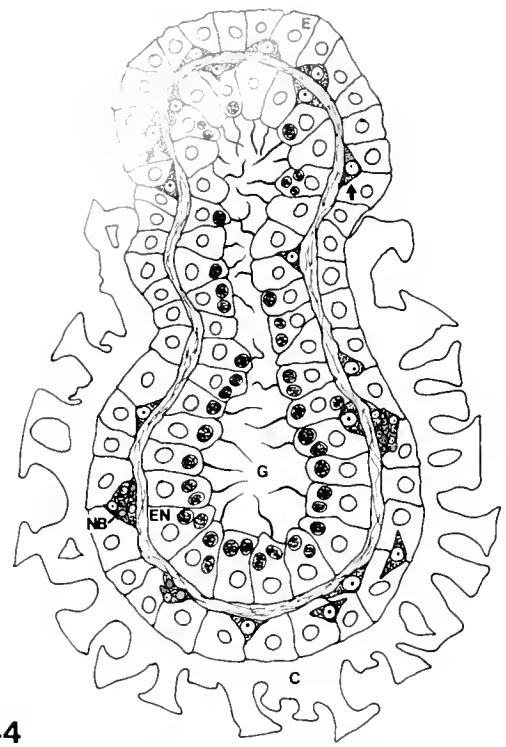

Figure 44. Emerging hatchling. As the cuticle (C) breaks open, the hatchling exits head-end first. The cells of the ectoderm (E) and endoderm (EN) expand, and the gastric cavity (G) increases in size. Interstitial cells (single arrows) are abundant in both layers, and clusters of nematoblasts (NB) (differentiating nematocytes) are found in the ectoderm.

endoderm. Since interstitial cells can migrate (Martin and Archer, 1986; Teragawa and Bode, 1990), it is quite plausible that they arise in both areas and that most eventually migrate into the ectoderm.

The development of the population of the interstitial cell lineage can be conveniently examined in three stages: the cuticle and bilayer stages and shortly after hatching. The large interstitial cells, which contain the multipotent stem cells (David and Murphy, 1977), arise during the cuticle stage, appearing between 6 and 11 days postfertilization. At 11 days the ratio of large interstitial cells to epithelial cells is 0.3: 1.0, and rises to 0.5: 1.0 by the time of hatching (Table II). In the adult, this ratio of these two ever-growing populations is maintained at 0.65: 1.0 (Bode *et al.*, 1973). These results imply that the population of large interstitial cells arises, grows, and approximates the adult ratio of large interstitial cells to epithelial cells during the cuticle stage. Whether the population of large interstitial cells reaches this size primarily by the division of a few interstitial cells that arise by asymmetric divisions, or whether most arise from asymmetric divisions is not known.

During the cuticle stage, most of the large interstitial cells are involved in proliferation. By the bilayer stage, however, a substantial fraction are differentiating, as measured in terms of the small interstitial cells, which are the dividing intermediates of the neuron and nematocyte pathways (David and Gierer, 1974). Shortly after hatching, fully differentiated neurons, nematocytes, and secretory cells appear; within a day there are substantial numbers of all three classes of these differentiation products. Since the time required for the three classes of differentiation products to traverse the differentiation pathways is equal to, or considerably longer than, the length of the bilayer stage, large interstitial cells must have begun entering the differentiation pathways late in the cuticle stage. Within a day after hatching, when the first wave of differentiation is complete, the ratios of the populations of these differentiation products to epithelial cells have reached half those found in adult animals (Table II).

In summary, the interstitial cell lineage develops in a straightforward manner. Large interstitial cells, perhaps all stem cells, appear during the cuticle stage and proliferate. Starting one-to-several days before the bilayer stage, these cells enter the three differentiation pathways in large numbers, resulting in the formation of numbers of neurons, nematocytes, and secretory cells within a day after hatching. Thus, this initial round of differentiation results in a cell composition that is close to that of the normal adult.

A mechanism for the formation of the gastric cavity and hatching

Unexplained so far is how the gastric cavity forms, and how an embryo emerges from the cuticle during hatching. Both events are probably part of a single process that is related to the osmotic behavior of the animal and the hydrostatic forces generated by this behavior.

There is a considerable difference in osmolarity between the external environment and the cytosol of the cells of an adult hydra (Lilly, 1955). Since the two environments are separated only by a plasma membrane, water is continually transported from the surrounding medium into, and through, the cells of the two epithelial layers into the gastric cavity. The increasing volume of the gastric cavity is periodically reduced as the animal contracts, thereby expelling fluid through the mouth.

Observations of developing aggregates indicate that both layers are necessary for this transport. When viable cells obtained by dissociating whole hydra are centrifuged into a pellet, or aggregate, the aggregate will develop into a normal animal (Gierer *et al.*, 1972). Initially, ectodermal epithelial cells migrate to the surface, forming an epithelium. Thereafter, endodermal epithelial cells align themselves on the ectoderm and form patches

of epithelium, which eventually coalesce into a complete endoderm. Internal spaces of fluid first form directly behind the patches of endodermal epithelium (Sawada, 1994), which suggests that the transport of water from the surrounding medium into the interior requires both the ectodermal and endodermal layers.

A similar process occurs during embryogenesis. During the bilayer stage, as the endodermal layer forms, fluid-filled spaces appear among the internal cells; these eventually coalesce into the gastric cavity. Because the size of the cavity becomes substantially larger than the volume of the space occupied by the interior cells at the beginning of the bilayer stage, it is unlikely that the cavity arises simply by the ordering of these cells into a layer. Instead, it is more likely that the formation of the gastric cavity and the subsequent hatching are due to the transport of water into the internal space. This could happen in the following manner.

By the bilayer stage, the cuticle has developed cracks. Because the cuticle is thinnest at the distal end where the head will form, it is likely that water seeps through the cuticle in significant quantities in this location first, and is transported into the interior of the embryo. That the gastric cavity is first visible as an elipse-shaped space near the distal end is consistent with this view. As the cuticle weakens, increasing amounts of water are transported into the gastric cavity from all over the surface of the embryo. This increases the hydrostatic pressure of the cavity, which in turn increases the pressure on the weakening cuticle. Eventually the cuticle cracks at the thinnest, and thus, weakest, point, which is at the distal end where the head is forming. With the embryonic surface now in direct contact with the surrounding medium, even more water is transported across the epithelial layers. Without the restraint of an intact cuticle at the distal end, the ever-increasing hydrostatic pressure in the gastric cavity distends the epithelial layers. Hence, the embryo slowly emerges through the crack in the cuticle like an inflating balloon, increasing in size as it emerges. Once liberated, the hatchling is at least twice the size it was just before hatching.

Another effect of water transport is taking place at the same time. Adult ectodermal epithelial cells have vacuoles that make up 90%–95% of the cell volume (Campbell, 1985). The size of these vacuoles is inversely correlated with the ion concentration of the surrounding medium (Trenkner *et al.*, 1973). Shortly before hatching, the ectodermal epithelial cells have no, or small, vacuoles. As water enters the late stage embryo during prehatching and hatching, the ectodermal cells begin to form vacuoles and increase in size. The resulting increase in the size of the ectoderm as a whole acts synergistically with the increasing volume of the gastric cavity to force the hatchling out of the cuticle.

Embryogenesis in hydra and deuterostomes shares several characteristics

The evolutionary distance is considerable between the diploblastic, radially symmetrical cnidaria and the triploblastic bilateral phyla of both deuterostomes and protostomes. Yet, in examining the evolutionary conservation of developmental processes and mechanisms, it is useful to compare the features of embryogenesis in hydra, or cnidaria in general, with those of other phyla. A tentative conclusion is that embryogenesis in hydra has a number of features that are characteristic of deuterostomes.

The cleavage pattern of hydra is radial for the first three divisions, becoming irregular thereafter. Both are characteristic of some vertebrates, such as amphibians. The resulting hydra blastula is a spherical shell consisting of a single layer of cells surrounding a blastocoel, as is found in sea urchins. And, as with many deuterostomes, hydra embryos are regulative during early cleavage stages. The two cells resulting from the initial cleavage sometimes separate, with each blastomere developing individually into a normal animal. Each of these embryos is half the size of the original egg. Occasionally, the cells resulting from the first two cleavage divisions separate to form four embryos with one-fourth the volume of the original egg. They too undergo normal embryogenesis and yield normal hatchlings.

In many deuterostomes, gastrulation occurs by involution or invagination of parts of the blastula. The same is true for some cnidarians, as many scyphozoans and anthozoans gastrulate by invagination (Hyman, 1940; Berrill, 1949; Chia and Spaulding, 1972). Other cnidarians use ingression for gastrulation; hydra clearly uses this process (Hyman, 1940). The endoderm and mesoderm of the chick embryo are also formed by ingression, as are the primary mesenchyme cells of the sea urchin embryo.

Another interesting feature is that, like vertebrates, hydra has several stem cell systems that arise during embryogenesis. Both the ectoderm and the endoderm of hydra are epithelial stem cell systems; they are similar to the epidermis and intestinal epithelium of vertebrates in that all consist of stem cells and differentiation products. Even more striking is the hydra interstitial cell system, which has many similarities to the hemopoietic system of the mouse. In both cases the cells of the tissue are migratory, and a multipotent stem cell gives rise to a number of differentiation products.

Finally, the cnidaria are usually considered to be diploblastic animals with an ectoderm and an endoderm, but no mesoderm. They may, in fact, have a primitive mesoderm. The interstitial cell lineage is a separate lineage even though it is physically intermingled with the

cells of the other two layers. Like many mesodermal tissues, this interstitial cell lineage is mesenchymal rather than epithelial in character. Moreover, in some cnidarians there are clusters of the interstitial cell lineage in the mesoglea, suggesting the beginnings of a physical separation of a mesoderm "precursor" from the other two layers.

Conclusion

This study provides a clearer understanding of the sequence and timing of embryonic events in hydra, the changes in cell population sizes, and the development of the three cell lineages that constitute the adult animal. We are now in a better position to examine the expression pattern of a variety of genes that have been isolated in hydra, and thereby investigate the relationship among the patterning processes that govern embryogenesis, budding, and maintenance of the form of the adult body.

Acknowledgments

The authors thank Lydia Gee for her technical assistance, Jason VanLieshout for the line drawings, and Pat Bode, Ann Grens, Andy Shenk, Robert Steele, and Hiroshi Shimizu for providing help and suggestions throughout the course of these studies. We thank Michael Sarras, University of Kansas Medical Center, for supplying the monoclonal antibody to hydra mesoglea, and we are grateful to Beverly Marcum, California State University at Chico, for the use of her time-lapse video system. This work was supported in part by NIH grants HD24511 (HRB) and HD27173 (HRB), NSF grants DCB-8702212 (VJM), DCB-8711245 (VJM), DUE-9552116 (VJM), DCB-8819247 (CLL), and funds from the Jesse Jones Foundation (VJM).

Literature Cited

Berrill, N. 1949. Developmental analysis of scyphomedusae. *Biol. Rev.* **24:** 393–410.

Bode, H. 1983. Reducing populations of interstitial cells and nematoblasts with hydroxyurea. Pp. 291–294 in *Hydra: Research Methods*, H. Lenhoff, ed. Plenum Press, New York.

Bode, H. 1996. The interstitial cell lineage of hydra: a stem cell system that arose early in evolution. *J. Cell Sci.* **109:** 1155–1164.

Bode, H., S. Berking, C. David, A. Gierer, H. Schaller, and E. Trenkner. 1973. Quantitative analysis of cell types during growth and morphogenesis in hydra. *Wilhelm Roux' Arch.* **171:** 269–285.

Brauer, A. 1891. Über die entwicklung von hydra. *Z. Wiss. Zool.* **52:** 167–216.

Campbell, R. 1967a. Tissue dynamics of steady state growth in *Hydra littoralis* I. Pattern of cell divisions. *Dev. Biol.* **15:** 487–502.

Campbell, R. 1967b. Tissue dynamics of steady state growth in *Hydra littoralis* II. Patterns of tissue movement. *J. Morphol.* **121:** 19–28.

Campbell, R. 1985. Tissue architecture and hydroid morphogenesis: the role of locomotory traction in shaping the tissue. Pp. 221–238 in *The Cellular and Molecular Biology of Invertebrate Development*, R. Sawyer and R. Showman, eds. Univ. of South Carolina Press, Columbia.

Campbell, R., and H. Bode. 1983. Terminology for morphology and cell types. Pp. 5–14 in *Hydra: Research Methods*, H. Lenhoff, ed. Plenum Press, New York.

Chia, F-S., and J. Spaulding. 1972. Development and juvenile growth of the sea anemone, *Tealia crassicornis*. *Biol. Bull.* **142:** 206–218.

David, C. 1973. A quantitative method for maceration of hydra tissue. *Wilhelm Roux' Arch.* **171:** 159–268.

David, C., and A. Gierer. 1974. Cell cycle kinetics and development of *Hydra attenuata*. III. Nerve and nematocyte differentiation. *J. Cell Sci.* **16:** 359–375.

David, C., and S. Murphy. 1977. Characterization of the interstitial stem cells in hydra by cloning. *Dev. Biol.* **58:** 372–383.

Dunne, J., L. Javois, L. Huang, and H. Bode. 1985. A subset of cells in the nerve net of *Hydra oligactis* defined by a monoclonal antibody: its arrangement and development. *Dev. Biol.* **109:** 41–53.

Epp, L., I. Smid, and P. Tardent. 1986. Synthesis of the mesoglea by ectoderm and endoderm in reassembled hydra. *J. Morphol.* **189:** 271–279.

Fennhoff, F. 1980. Embryonic development of *Tubularia crocea* Agassiz with special reference to the formation of the interstitial cells. Pp. 127–131 in *Developmental and Cellular Biology of Coelenterates*, P. Tardent and R. Tardent, eds. Elsevier North-Holland, Amsterdam.

Gierer, A., S. Berking, H. Bode, C. David, K. Flick, G. Hansmann, H. Schaller, and E. Trenkner. 1972. Regeneration of *Hydra* from reaggregated cells. *Nat. New Biol.* **239:** 98–101.

Honegger, T. 1981. Light and scanning electron microscopic investigation of sexual reproduction in *Hydra carnea*. *Int. J. Invertebr. Reprod. Dev.* **3:** 245–255.

Honegger, T., D. Zürrer, and P. Tardent. 1989. Oogenesis in *Hydra carnea*: a new model based on light and electron microscopic analysis of oocyte and nurse cell differentiation. *Tissue Cell* **21:** 381–393.

Hyman, L. 1940. *The Invertebrates: Protozoa through Ctenophora* McGraw-Hill Book Company, New York.

Kanaev, I. 1952. Hydra (in Russian). Izd. Akad. Nauk SSR, Moscow-Leningrad.

Kleinenberg, N. 1872. *Hydra* Eine Anatomisch-entwicklungsgeschichtliche Untersuchung. Leipiz, pp. 1–90.

Lenhoff, H. 1983. Labeling with gaseous $^{14}CO_2$ or by feeding on radioactive tissues. Pp. 193–196 in *Hydra: Research Methods* H. Lenhoff, ed. Plenum Press, New York.

Lilly, S. 1955. Osmoregulation and ionic regulation in hydra. *J. Exp. Biol.* **32:** 423–429.

Littlefield, C. 1994. Cell-cell interactions and the control of sex determination in hydra. *Semin. Dev. Biol.* **5:** 13–20.

Martin, V., and W. Archer. 1986. Migration of interstitial cells and their derivatives in a hydrozoan planula. *Dev. Biol.* **116:** 486–496.

Murtha, M., J. Leckman, and F. Ruddle. 1991. Detection of homeobox genes in evolution and development. *Proc. Natl. Acad. Sci. USA* **88:** 10711–10715.

Noda, K., and C. Kanai. 1980. An ultrastructural observation on the embryogenesis of *Pelmatohydra robusta*, with special reference to "germinal dense bodies." Pp. 127–131 in *Developmental and Cellular Biology of Coelenterates*, P. Tardent and R. Tardent, eds. Elsevier North-Holland, Amsterdam.

Otto, J., and R. Campbell. 1977. Tissue economics of hydra: regula-

tion of cell cycle, animal size and development by controlled feeding rates. *J. Cell Sci.* **28:** 117–132.

Sarras, M., M. Madden, X. Zhang, S. Gunwar, J. Huff, and B. Hudson. 1991. Extracellular matrix (mesoglea) of *Hydra vulgaris* I. Isolation and characterization. *Dev. Biol.* **148:** 481–494.

Sarras, M., X. Zhang, J. Huff, M. Accavitti, P. St. John, and D. Abrahamson. 1993. Extracellular matrix (mesoglea) of *Hydra vulgaris* III. Formation and function during morphogenesis of hydra cell aggregates. *Dev. Biol.* **157:** 383–398.

Sawada, Y. 1994. Regeneration of hydra from dissociated cell aggregates. Proceedings of the 33rd NIBB Conference: approaches to the cellular and molecular mechanisms of regeneration. Okazaki, Japan, p. 28.

Schierwater, B., M. Murtha, M. Dick, F. Ruddle, and L. Buss. 1991. Homeoboxes in cnidarians. *J. Exp. Zool.* **260:** 413–416.

Schummer, M., I. Scheurlen, C. Schaller, and B. Galliot. 1992. HOM/HOX homeobox genes are present in hydra (*Chlorohydra viridissima*) and are differentially expressed during regeneration. *EMBO J.* **11:** 1815–1823.

Shenk, M., H. Bode, and R. Steele. 1993a. Expression of Cnox-2, a HOM/HOX homeobox gene in hydra, is correlated with axial pattern formation. *Development* **117:** 657–667.

Shenk, M., L. Gee, R. Steele, and H. Bode. 1993b. Expression of Cnox-2, a HOM/HOX gene, is suppressed during head formation in hydra. *Dev. Biol.* **160:** 108–118.

Tannreuther, G. 1908. The development of hydra. *Biol. Bull.* **14:** 261.

Tardent, P. 1966. Zur sexualbiologie von *Hydra attenuata* (Pall.) *Rev. Suisse Zool.* **73(2):** 357–380.

Teragawa, C., and H. Bode. 1990. Spatial and temporal patterns of interstitial cell migration in *Hydra vulgaris*. *Dev. Biol.* **138:** 63–81.

Trenkner, E., K. Flick, G. Hansmann, H. Bode, and P. Bode. 1973. Studies on hydra cells in vitro. *J. Exp. Zool.* **185:** 317–326.

Zihler, J. 1972. Zur gametogenese und befruchtungsbiologie von Hydra. Wilhelm Roux' Arch. **169:** 239–267.

Reference: *Biol. Bull.* **192**: 364–374. (June, 1997)

Laboratory Culture of the Sepiolid Squid *Euprymna scolopes:* A Model System for Bacteria–Animal Symbiosis

ROGER T. HANLON[1], MICHAEL F. CLAES[2,*], SUSAN E. ASHCRAFT[1], AND PAUL V. DUNLAP[3,*]

[1]*Marine Resources Center, Marine Biological Laboratory, Woods Hole, Massachusetts 02543;* [2]*Marine Science Center, Northeastern University, Nahant, Massachusetts 01908; and* [3]*Department of Biology, Woods Hole Oceanographic Institution, Woods Hole, Massachusetts 02543*

Abstract. The small Hawaiian sepiolid *Euprymna scolopes*, with its symbiotic luminous bacterium *Vibrio fischeri*, was cultured through one complete life cycle in 4 months. Paralarval squid hatchlings were actively planktonic for the first 20–30 days, after which they settled and assumed the typical adult mode of nocturnal activity and diurnal quiescence. Squids were aggressive predators that preferred actively swimming prey up to 2–4 times their size; the only diet that yielded good survival and rapid growth for paralarvae was large adult mysids. Survival to settlement was 73% on this diet, whereas it was 0%–17% on controls and three other diets. Paralarvae initially lacked both detectable luminescence and *V. fischeri* cells in their incipient light organs; all remaining stages produced luminescence, and their light organs were colonized by apparently pure cultures of $>10^5$ *V. fischeri* typical of *E. scolopes* symbiont strains. Survival from settlement to sexual maturity was 76%. Mating and egg laying commenced at 2 months, yet attempts to culture the next laboratory generation of hatchlings were not as successful. The results indicate that the host organism of this symbiosis can soon be cultured with consistency through its brief life cycle, thus opening new avenues of research into developmental aspects of this symbiosis.

Introduction

The symbiotic association between the Hawaiian sepiolid *Euprymna scolopes* and the bioluminescent bacterium *Vibrio fischeri* has been developed into an experimental marine model in cell and molecular biology (Wei and Young, 1989; McFall-Ngai and Ruby, 1991; Ruby and McFall-Ngai, 1992). Various strains of *Vibrio fischeri* (both natural and mutant) have been cultured so that components of the symbiotic association can be manipulated experimentally (*e.g.*, Boettcher and Ruby, 1990; Ruby and Asato, 1993; Graf *et al.*, 1993; Dunlap *et al.*, 1995). However, full development of this marine model system has been hampered by the inability to culture the host organism—the squid—completely through its life cycle with some degree of consistency and standard methodology.

Euprymna scolopes is a very small species that is endemic to the Hawaiian Islands, where it spends much of its life buried in the sand. There have been no field studies of its behavior and life cycle, so most of what is known comes from laboratory studies (Singley, 1983). Of particular interest is how these small squids might use their relatively huge light organ in their daily lives.

Since the mid-1980s, several teams of researchers have studied details of the symbiosis by bringing wild-caught adults to the laboratory, allowing them to mate and lay eggs, and then using the hatchling squids (*i.e.*, the paralarvae) to explore the infection process as well as the initial development of the light organ. However, thus far investigators have been unable to examine events beyond the first week posthatching because the squid paralarvae deplete their internal yolk supplies by that time and perish; several unreported rearing attempts in the 1990s have failed. Nevertheless, before this model system was developed, *Euprymna* had been reared from

Received 14 November 1996; accepted 4 March 1997.

*Present address: Center for Marine Biotechnology, University of Maryland Biotechnology Institute, Baltimore, Maryland 21202.

eggs through a portion of its life cycle. *Euprymna berryi* was reared to 2 months in Korea by Choe and Oshima (1963) and Choe (1966). Arnold *et al.* (1972) reared 10 *E. scolopes* (from a starting number of 26) to 28 days, and two survived to 202 days without reproducing. Singley (1983) reared 13 of 16 *E. scolopes* to 28 days and one to 120 days, although its reported length was very small (<4 mm mantle length). The encouraging results of Arnold *et al.* (1972) and Singley (1983) on *E. scolopes*, coupled with the rapid development of this symbiosis model system in the last 5 years, led us to initiate the trials reported here. The overall goal was to develop standard methods for culturing *Euprymna* and to learn aspects of its biology that would enhance its successful culture in captivity. We hypothesized that behavioral features related to feeding would be most important to the successful culture of *Euprymna* hatchlings through the paralarval stage, as they have proved to be in many other squid species (*e.g.*, Boletzky and Hanlon, 1983; Yang *et al.*, 1986; Hanlon *et al.*, 1989; Hanlon, 1990; Lee *et al.*, 1994).

Although we hope to eventually culture successive generations of this small, fast-growing cephalopod, a near-term goal is to develop a method for rearing aposymbiotic hatchlings (*i.e.*, those deprived of the bacterium) through most of the life cycle, so that cellular and molecular aspects of the complex development of the symbiosis can be studied in even greater detail. We report here our initial findings that *Euprymna scolopes* can be cultured through its brief life cycle under controlled laboratory conditions, and we highlight some of the more important needs of this species in captivity. We also describe our observations on some critical features of the behavior of this species, including multiple effects of light and some aspects of reproductive biology that require future experimentation.

Materials and Methods

The term "paralarvae" is used to describe young squids from hatching to about 3 weeks of age; it accurately distinguishes the behavior of hatchlings from that of juveniles and adults (see details in Young and Harman, 1988). *Euprymna scolopes* is a member of the family Sepiolidae in the order Sepioidea (according to the nomenclature of Voss, 1977), which includes cuttlefish. The term "squid" is commonly applied to some sepioids, although true squids are members of the order Teuthoidea.

Brood stock acquisition and egg care

Adults were collected on Oahu, Hawaii, and shipped via airfreight to the Marine Resources Center of the Marine Biological Laboratory in Woods Hole, Massachusetts. Squids were shipped individually in 3-l plastic bags containing 1.5 l of natural seawater. The seawater was filtered to 10 μm, heavily aerated, and spiked with 1 g/l tris buffer; the remaining 1.5 l of each bag was filled with oxygen and the bags were fitted in insulated shipping boxes. The total time spent in these bags by each squid was typically 21 hours. When the bags arrived at the laboratory, the temperature was slightly depressed (down to 18°–19°C), the salinity was 31–32 ppt, the concentration of dissolved oxygen was 7–11 mg/l, the pH was 8.29–8.41, and the levels of ammonia and nitrite were low (however, colorimetric reading were often impossible due to interference from ink in the bags). Ammonia was measured with LaMotte kits that are based on the salicylate method and colorimetric analysis. Nitrite and nitrate were measured with Hach kits that also used colorimetric methods; the precision of the ammonia and nitrite methods is ±0.01 mg/l, and the lowest sensitivity is 0.05 mg/l.

Adult males were housed individually, and females individually or in pairs, in small chambers (25 cm × 33 cm; water depth 18 cm) and were fed *ad libitum* with live shrimp (*Palaemonetes* sp. or *Crangon* sp.). Each chamber had 10 cm of crushed coral sand for the squids to bury in.

Mating was induced once per week by transferring one male into a female's chamber overnight. To avoid damaging the squid they were transported in small clear glass vials of water rather than in nets. Transferred males always mated, and eggs were generally laid the night after the male was removed. In the trials reported here, five females and three males produced 13 clutches of eggs, but we used only five clutches for the culture trials.

It was essential that eggs be handled as little as possible so that they would develop fully and not hatch prematurely. The key was to keep temperature, salinity, pH, nitrogen levels, and light cycles as steady as possible, and to keep disturbance at a minimum (not bumping tanks, changing light levels, inspecting eggs, *etc.*). Adults were kept in closed, recirculating seawater systems to ensure that water quality was consistent. Eggs laid on coral fingers were left on the coral and moved to aerated mesh containers. Eggs laid on the flat tank wall were gently scraped from the wall with a glass slide; they generally came off as a single unit, which was then transferred to a mesh container. Eggs were never exposed to air, and an airstone was placed into each mesh container adjacent to the eggs so that water was constantly circulating near them. The eggs were kept in the same water that adults had laid them in.

Rearing chambers and seawater systems

The actual rearing chamber for each paralarval rearing trial was a circular black container, 25 cm in diameter,

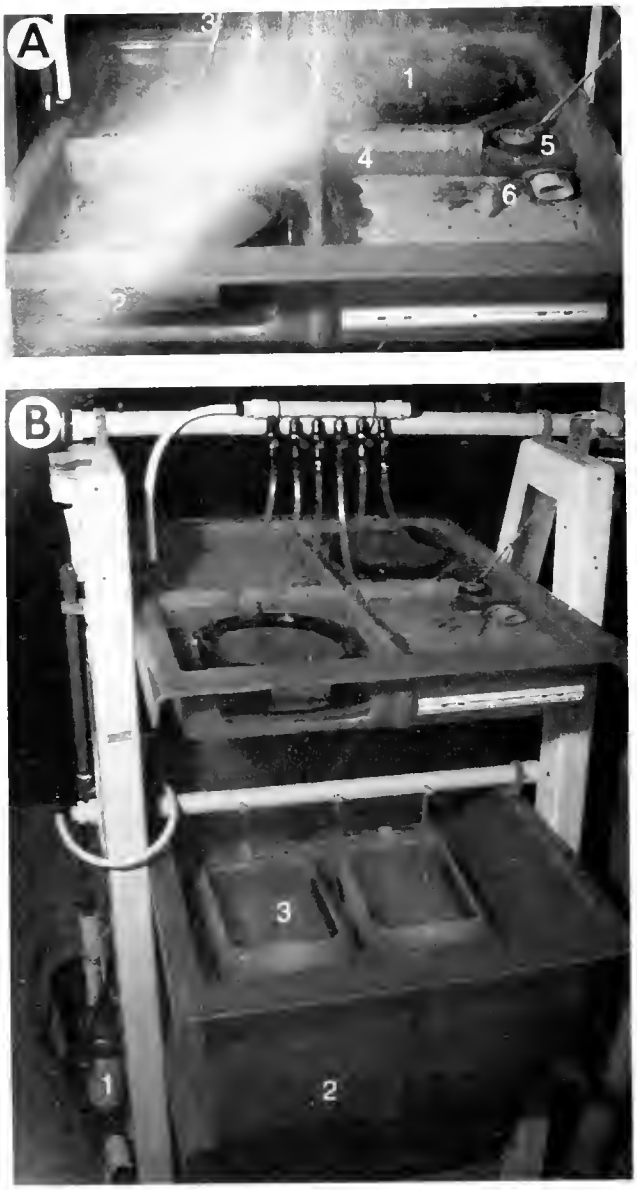

Figure 1. The culture tanks for *Euprymna scolopes*. (A) Each paralarval rearing chamber (1) held 30 squids and had a viewing port (2). Water flowed in through two tubes (3) in each chamber and exited vertically through the sand-covered sieve bottom, then flowed horizontally through mesh screens (4) to the drain (5). The white ruler is the standard 12 inches. (B) The complete closed system and A-frame, showing the filter apparatus (1), the location of the biological filter substrate (2) and the chambers for maintaining adults and for mating (3).

with a 200-μm-mesh screen bottom (Fig. 1). The chamber was immersed in a seawater tray tank to achieve shallow water depths of only 3–6 cm. Water flowed into the top through rubber tubing and flowed out through the mesh bottom. The two inflow tubes were arranged along the edge to create a gentle circular water flow, which helped keep the hatchlings and prey items away from the sides. A thin layer of sand coated the mesh bottom.

Two small seawater systems were used in the Marine Resources Center: one was a completely recirculating system of 340 l, and the other was an open system of 600 l. Local Woods Hole water was the original source, and this water was passed through a 1-μm filter and heated to about 23°C. The closed system consisted of an A-frame with a shallow tray tank for the rearing experiments above (70 cm × 78 cm × 9 cm deep) and a deeper tank below to house the biological filter. The biological filter was composed of crushed oyster shell with an undergravel filter; the oyster shell was 15 cm deep and spread over an area of 5250 cm^2. The water was then pumped through a canister with a particulate filter and then through activated carbon and a UV filter. The flow rate was about 22 l/min, and about 30% of the water was replaced weekly. The open system was constructed similarly, with a top tray size of 76 cm × 130 cm × 9 cm deep and a tank below with 9956 cm^2 crushed oyster shell as a substitute substrate. The open system was only used for some squids after Day 49 to help reduce crowding. Immersion heaters in each system helped maintain temperature. Water quality was checked two or three times per week and ammonia, nitrite, and nitrate were determined according to the methods listed above.

The tanks were situated 3 m from a window that provided indirect natural light. Overhead fluorescent fixtures provided indirect light on a 12:12 light cycle. The typical light level falling on the tray tanks was 2–8 $W\,m^{-2}$ μA.

One small trial (n = 8 squids) was performed in a semi-closed seawater system at the Marine Science Center of Northeastern University. Natural seawater was used in an A-frame that held a total of 350 l. Crushed coral was the biological filter, and no other UV or charcoal system was used. Lighting was by direct overhead incandescent bulbs (50 cm away) on a 12:12 cycle. The paralarvae were reared in a black circular PVC chamber (20 cm in diameter, 20 cm in height) with 150-μm-mesh sides and a bare plastic bottom.

For behavioral observations, the top trays were fitted with glass panels for horizontal viewing into portions of the round rearing chambers. Observations were made from the side and also from the top of the tanks, and night observations were accomplished with a night-vision device that amplified existing dim light. A very weak red light was aimed at the ceiling to produce a soft glow of reflected light in the room (approximately 0.3 W m^{-1} μA). A video camera (Sony HiBand 8 mm) was used to record behavior; the night-vision device could be fit to the front of the camcorder to record nocturnal behavior.

Hatchlings, stocking densities, and foods

Most embryos hatched in the first 2 h of the dark cycle, and individuals were transferred with a turkey baster to the culture chamber. For individual 30-day feeding trials, 30 hatchlings were stocked in each round rearing chamber. The exceptions were one trial in which 50 hatchlings were stocked and one trial in which only 8 hatchlings were taken to the Nahant laboratory. By day 50, squids were removed from the small round chambers and the juveniles were reared in the divided tray tanks, each of which had dimensions of 35 by 39 cm.

Food items included live zooplankton, crustaceans, and larval fishes. Mysid shrimps of the genera *Mysidopsis* and *Neomysis*, and larval fishes, *Menidia beryllina*, were commonly used. The term "postlarval mysids" was applied to those that were newly hatched from the brood sacks of females (Lussier *et al.*, 1988). They were of body lengths 0.5–1.5 mm, whereas adult mysids were typically 4–10 mm long. Hatchlings were fed 1–5 times per day between 0700 and 2300 to ensure adequate food availability. Progressively larger shrimp (*Crangon* and *Palaemonetes*) were provided to juvenile and adult squids as they grew.

Luminescence measurement and quantification of symbiotic bacteria

Light produced by hatchlings, juveniles, and subadults was detected qualitatively with a Turner 20e luminometer (Sunnyvale, CA). Individual live animals were placed in 5 ml (50 ml for subadult animal) of filter-sterilized (0.2-μm pore size) natural seawater in 30-ml glass scintillation vials (300-ml glass beaker for subadult animal, placed in a foil-lined funnel to channel light into the luminometer detector), and the light produced was recorded for 30 s. Three measurements were taken. The data reported (as arbitrary light units, LU, per animal) are the highest of the light levels detected for each animal.

V. fischeri cells colonizing the animal light organ were quantified by plate counts using a seawater complete agar (SWC; Nealson, 1978). To minimize the presence of surface-associated bacteria, hatchlings and juveniles were removed from culture tanks in a minimal volume of seawater and rinsed by three passages in 5 ml of filter-sterilized seawater in autoclave-sterilized scintillation vials. The animals were then homogenized in a 15-ml Ten Broeck tissue homogenizer with 1 ml of filter-sterilized seawater. The homogenate was serially diluted and plated in quadruplicate on SWC agar plates, which were incubated at room temperature for 24 h before colonies were counted. For subadults, the light organ was removed aseptically and homogenized and handled as above. Representative colonies of bacteria arising on the spread-plates, which were uniform in appearance for those animals that produced light, were confirmed to be *V. fischeri* strains that characteristically colonize light organs of *E. scolopes* (Boettcher and Ruby, 1990; Dunlap *et al.*, 1995) by (i) their production of luminescence, although at a very low level in culture, (ii) their luminescence response to the *V. fischeri* autoinducer-producing, nonluminous strain MJ-203, and (iii) their effect on the luminescence of the autoinducer nonproducing strain MJ-215 (Kuo *et al.*, 1994; Kuo *et al.*, 1996).

Results

Hatching success, water quality, and system design

An essential improvement that led to successful culture was providing a very stable environment so that embryos developed to full term and did not hatch prematurely. Failure to do this affected early trials adversely. Temperature, light, and pH were nearly constant, and the nitrogen levels were kept within standard limits (*i.e.*, 0.10 mg/l for ammonia and nitrite, 20 mg/l nitrate; Spotte, 1973; Hanlon, 1990). Hatching occurred after about 18–22 days at 21–23°C. Particular care was taken not to bump the tank or handle the eggs during the last days of development. A sample check under a dissection microscope indicated that hatchlings had no external yolk amidst the arms, and normal amounts of internal yolk along the midgut (Arnold *et al.*, 1972).

Concentrations of ammonia (NH_3) and nitrite (NO_2) remained near the recommended levels of 0.10 mg/l except for two brief spikes of ammonia to 0.40 mg/l on day 22 and 0.20 mg/l on day 71, and one brief spike of nitrite to 0.20 mg/l on day 46. No mortalities or unusual behavior could be correlated with these spikes. Nitrate (NO_3) levels were very low throughout the trials, ranging from 1 to 4 mg/l, well below the recommended level of 20 mg/l. The pH always stayed above 8.0, and salinity ranged from 30 to 37 ppt although the mean was near 35 ppt. Temperature ranged from 21 to 25°C, but on one occasion the temperature in the Northeastern University tank decreased slowly to 4°C during the night. The temperatures were returned to 21°C in the course of 5 h. All of these tropical Hawaiian squids survived!

The utility of a shallow rearing chamber was evident; in particular it helped concentrate prey organisms for the very young squids. The system also allowed easy visual inspection of the tank, including the behavior of the squids and their food sources.

Behavior of paralarvae and juveniles

The paralarvae in this study showed two notable behavioral features: (i) they were strong swimmers, especially compared to other cephalopod hatchlings of com-

parable size; and (ii) they were alternately active and planktonic as well as benthic for the first month post-hatching. The first [illegible] was validated in field observations when RTH observed the hatchlings and juveniles in their natural [illegible] in Hawaii in August 1995. Very small squid [illegible] dart towards prey 20 cm away in only a second [illegible] a large distance for a paralarval cephalopod.

Diurnal paralarval swimming activity is illustrated in Figure 2. There were many squids swimming during the day in both the unsuccessful and successful feeding trials. Nevertheless, even the youngest hatchlings spent a large proportion of their day buried in the sand substrate. By day 30 in our trials, all of the squids remained benthic during the day like the adults. At all phases of the life cycle, the squids were active throughout the night (only occasional observations were made from midnight to 0600 h). The behavior of juveniles was seemingly identical to that of adults: they remained buried in the sand during the day and hunted for prey at night.

At all life stages, *Euprymna* tolerated high densities. By the time the squids had settled (*ca.* 30 days) and grown for a total of 40–50 days, their density was quite high considering that they were still in the small round rearing chambers. At this time some were transferred to an adjacent tank system, and in both systems the squids were distributed into rectangular sections measuring 35 × 39 cm with a sand substrate of about 1–2 cm. There were no cases of cannibalism, which is common in many cephalopods.

Unlike the squid in most of the trials, the group of eight taken to Northeastern University were given no sand substrate. These squids never sat on the bottom but swam all the time. After 2–3 weeks, they settled on the bare PVC bottom; the five squids that survived in this system were brought to Woods Hole and reared with others to adulthood.

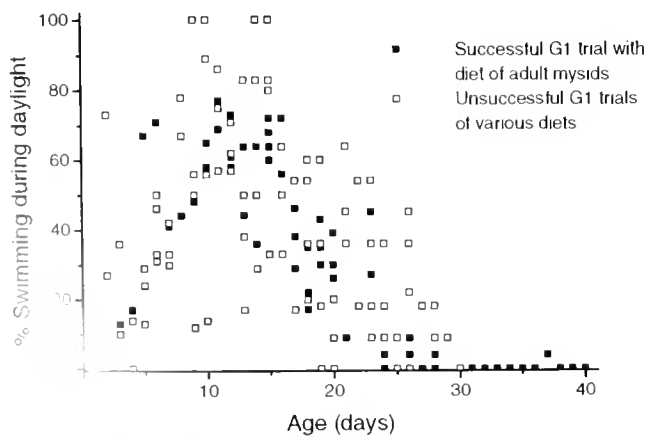

Figure 2. Paralarval swimming behavior, indicating the percentage of squids that was actively swimming during daylight hours. After 30 days all squids remained benthic during the day.

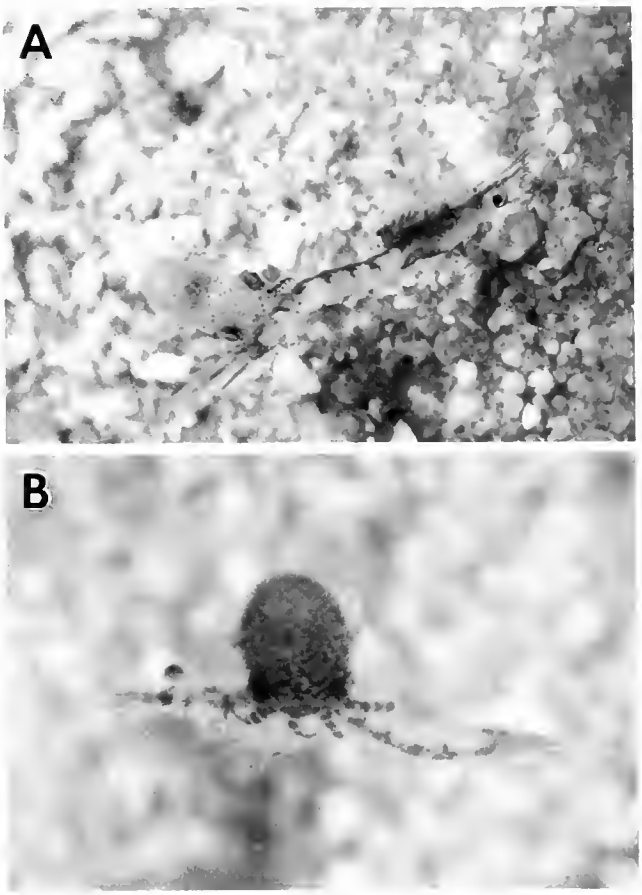

Figure 3. Predation by paralarval squids. (A) A 15-day-old paralarva subduing a very large mysid, which it ate successfully. (B) A 7-day-old paralarva eating a mysid and holding it in a typical position at mid-carapace.

Feeding

Substantial effort was devoted to studying the feeding behavior of squids, the swimming behavior of various prey, and the interactions of predator and prey. The most important finding was that hatchlings of *Euprymna scolopes* are voracious predators that prefer very large prey relative to their own size. As indicated in Figure 3, it was common for hatchlings to successfully attack and ingest prey that were much larger than themselves. Conversely, they were capable of eating very small prey, on the order of 0.5 mm. Hatchlings were already strong swimmers and could easily make vigorous forward attacks of 12 body lengths in 1 s (as measured from videotape). Field observations at night in Hawaii also confirmed this strong swimming ability.

To assess different preferences, six diets were tried for

the critical paralarval period of 1–30 days post-hatching. Figure 4 indicates the clear results: large adult mysids were preferred and also produced the best survival; 22 of 30 squids survived to settlement. These mysids were usually stocked at levels of about 2–4 per squid, but the numbers fluctuated a great deal. Control animals received no food and all died by day 8, as did all 30 squids provided with a smorgasbord of live zooplankton. Postlarval mysids, which were expected to be the best food, produced poor results too; only 5 of 50 squids survived to settlement. When postlarval mysids and larval fishes were provided together, the mortality was initially high but stabilized within a week; 5 of 30 squids survived to settlement. Similar results were obtained with irregular mixed diets that consisted of postlarval mysids and fishes, as well as zooplankton and adult mysids; only 4 of 30 survived to settlement. It is worth emphasizing that food was presented in abundance in every case, and for all but a few of the 30 days in each trial.

The behavior of squids during active periods (*i.e.*, when in the water column) seemed to be related solely to foraging. Very rarely was a prey item attacked near the substrate. Generally the squids preferred to strike upward, which often required that they descend under the prey, then move rapidly towards it at about a 45 degree vertical angle. Because their two tentacles were not evident until about 25 days post-hatching, squids used their eight arms to grasp the prey. Feeding was clearly stimulated by the addition of prey items to the tank; possibly the increased motion and swimming activity of prey was enough of a stimulus to provoke more attack attempts by squids. For this reason it is advisable to feed squids many times per day rather than once or a few times. Mysids were clearly preferred, even when other prey such as fish larvae were present in the tank in far greater quantities. Squids were commonly observed to make 2–8 strikes at mysids before a successful capture. Usually a large mysid was held at mid-carapace (Fig. 3B), and it is possible that the squids were biting through the dorsal nerve cord to immobilize the mysid. We occasionally saw two squids eating the same large mysid and, more rarely, one squid attacking a mysid while in the process of eating another; this occurred only with the smaller postlarval mysids. Extremely large mysids (*e.g.*, more than 4 times the size of squids) were not eaten and probably disrupted the squids in small chambers.

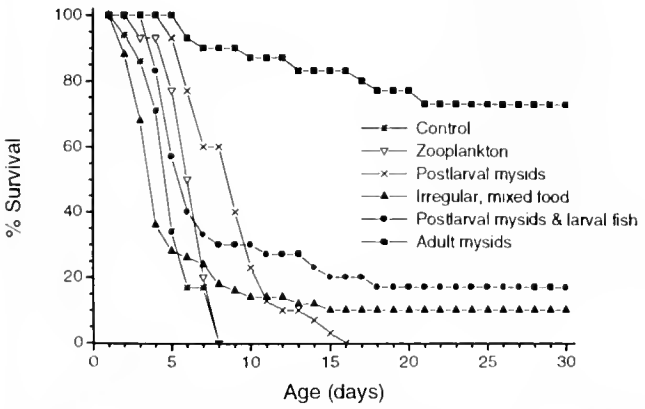

Figure 4. Survival on different diets during the 1-month paralarval period.

Paralarval squids showed considerable interest in fish larvae (*Menidia*) on some days. But the *Menidia* larvae seemed to present problems for capture, and survival of squids on this diet was poor. For example, on day 27, squids were presented with fishes that were nearly 12 mm long. The squids strongly pursued the fish larvae, yet often made 4–6 unsuccessful strikes and sometimes as many as 20; recall that squids of this age and size were well developed and strong swimmers. In a typical feeding, only 1–3 squids would have a fish 15 min after 30–40 fishes were added and 30 attacks were observed. By contrast, if 30 shrimp (*Crangon*) were placed in the same tank, commonly 8 squids would have successfully captured one within 5 min. It was often observed that squids could not hold onto a fish even when they made contact, suggesting that the suckers were not able to grasp the fish well. Once captured, fish were harder to subdue than shrimp; it took on the order of 2–3 min, as compared with 10–30 s for shrimp. When a fish was being eaten, the stomach of the squid was black and highly visible compared to a much less distinct dark color when shrimp were ingested.

Food densities varied greatly due to variable food supply. However, in the early weeks, about 2–4 large adult mysids were supplied to each squid in trial 1. These mysids, which were about 1–3 times the average body length of the very young squids, were generally eaten in the course of 24 h. By days 35–40, these squids were being fed a combination of adult mysids and *Crangon* shrimp (1.0–1.5 cm length) at a level of 5–6 times as many prey as predator; the tanks appeared very crowded when the food was first put in. By day 52, 15 juvenile squids were being fed about 20 *Crangon* (1.5 cm length) and 100 large mysids.

Paralarval squids foraged throughout day and night, but this was not quantified by counting the number of attacks on prey per unit time. After settling to the adult behavior mode by day 30, all squids foraged at night, and food was generally added to tanks late in the day and cleaned out the following morning. Juveniles and adults continued to feed vigorously on prey that were generally their own size or larger.

Lighting levels appeared to be important to successful feeding: lower light enhanced feeding, whereas bright light seemed to retard it. For example, when tops were

placed over the rearing chamber during the day, the reduced light level stimulated feeding. Very dark overcast days also resulted in [illegible] squids spending more time foraging and f[illegible] light in the rearing chambers was arrange[illegible] individual squids could view prey objects in [illegible]ing light against a black background, and this [illegible] increased the contrast of the prey organism.

Growth, age, maturity, and mortality

Growth was rapid and adult sizes were reached in about 2 months. Figure 5 illustrates growth in mantle length and wet weight over the culture period. Hatchlings ranged from 1.6 to 1.9 mm in mantle length and from 4.2 to 5.8 mg in wet weight. Despite the limited data set (*i.e.*, few points between days 10 and 70) and the highly conservative growth measurements (nearly all taken from freshly dead squids), rapid growth in wet weight through day 83 was still best fit by the exponential equation $y = 0.0033e^{(0.084x)}$. From this function, the instantaneous relative growth rate from hatching to day 83 was an 8.4% increase in weight per day. After day 83, the data were not amenable to curve fitting because growth was very slow and the data were highly variable. The extremely high growth rate of paralarvae is mostly due to the high feeding rate; hatchlings that were feeding on 2–3 very large mysids per day were probably ingesting more than their body weight per day. The length/weight relationship, based upon 41 measurements from hatching to day 133, was expressed by the equation

$$\text{Wet weight in grams} = 0.0015 \times (\text{mantle length in millimeters})^{2.674}$$

The complete life cycle (*i.e.*, from egg to egg) was completed in about 80 days, and the longest-lived squid reached an age of 139 days. As noted in the next section, many squids were sexually mature by 60 days post-hatching. During the paralarval stage, mortality was 27%, then the population stabilized and the remaining mortalities occurred over a protracted period that was marked by reproductive activity. From settling to sexual maturity, mortality was only 24%; thereafter, there was a slow attrition. Early mortalities were probably related to nutrition, but later ones were inexplicable and may have been associated with maturity and "old age" or with some unknown pathogen.

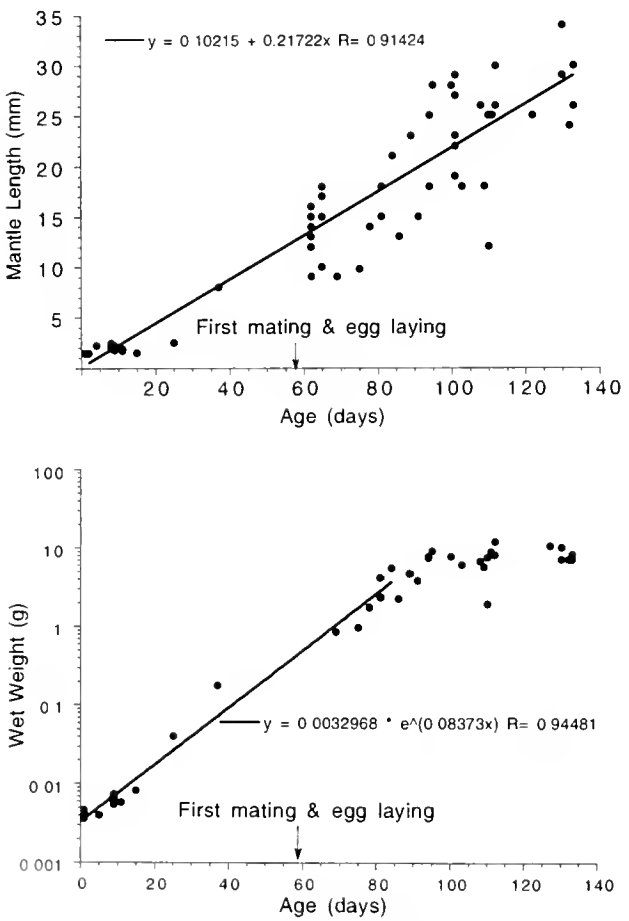

Figure 5. Growth of cultured *Euprymna scolopes*. TOP: Linear plot of mantle length increases versus age. BOTTOM: Wet weight growth was exponential through day 83 ($R = 0.95$). Data for males and females are lumped because identification was not always possible.

Reproduction

Sexual dimorphism is only slightly evident in this species. Males have slightly enlarged suckers on some arms and tend to have slimmer posterior mantles, especially compared to fully mature females whose posterior mantles become broader as they fill with eggs. The testis of the male can sometimes be seen dorsally when all the chromatophores are retracted.

The first eggs were laid on day 58 and the first mating was observed on day 61, when 24 squids were still alive. Mating occurred at night, often just at the onset of darkness. Overall, 16 matings were observed between days 61 and 116; the last squid died on day 139, so that mating occurred over the last one-third to one-half of the brief life cycle. Matings were not controlled in any way and possibly more matings occurred throughout the nights than we observed. Mating (Fig. 6A) seemed to be initiated by the male (bottom), who grasped the female and placed a spermatophore somewhere in her mantle. Mating lasted about 30–50 min in the few cases in which the whole mating was observed. Competition for mates was observed only once: two males grabbed a female, some wrestling followed, then they all moved to corners of the tray tank. One male was removed, but the remaining

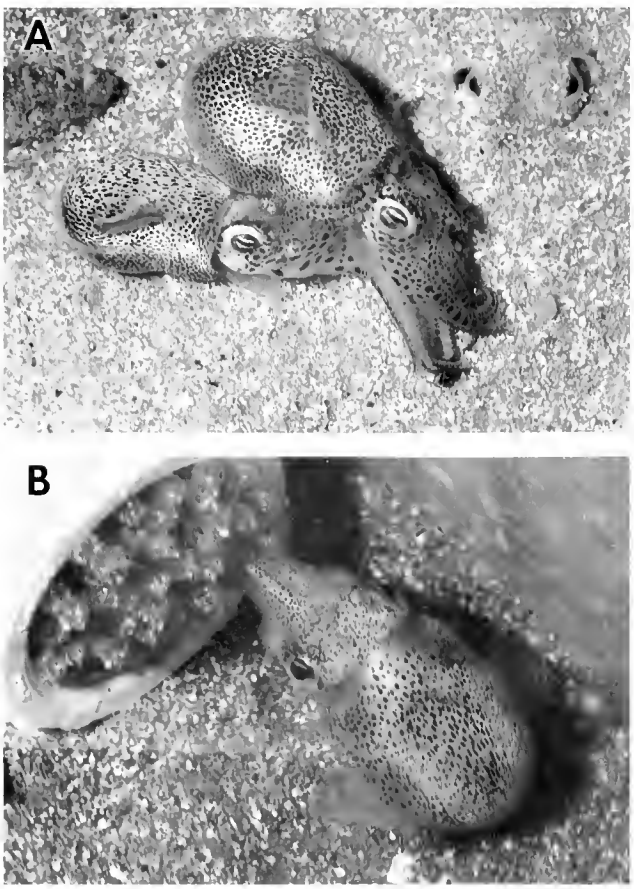

Figure 6. Mating (A) and egg laying (B) by cultured *Euprymna scolopes*. The male grasped the female from underneath and they mated for 30–50 min. Later, the female affixed one egg at a time to a PVC pipe and coated the eggs with sand to camouflage them.

male and female did not mate that night. In this particular case, the female was larger than the males.

Egg laying (Fig. 6B) was observed four times and, curiously, took place in the mornings and often lasted until midday. In total, 13 egg clutches were laid by this generation of adults. Attachment of each egg took 10 s on average, and about 40 s elapsed between the deposition of each egg, so that it took about 25–30 min to lay a clutch of 30 eggs. As usual, the eggs were soon coated with sand that was somehow placed there by the females.

To minimize handling, individual squid were not marked; thus fecundity could be estimated only from the number of eggs laid by individual females. All tray tanks contained males and females in high densities, even when the squids were separated on day 49; *i.e.*, there were 2–3 squids per 35 × 39 cm chamber.

Reestablishment of the bacterial symbiosis in reared squids

To determine whether symbiosis with *V. fischeri* was reestablished in the light organ of the reared squids, hatchlings, juveniles, and subadult animals were examined for the production of light and for the presence of *V. fischeri* cells. The hatchling squids initially lacked luminescence, and no colony-forming units of *V. fischeri* were detected in their nascent light organs. By day 5, however, the animals were luminous, and their light organs contained 10^5 or more *V. fischeri* cells (Table I). Figure 7 illustrates bacterial cells in the light organ of a reared squid.

Discussion

We have identified three essential keys for successful laboratory culture of *Euprymna scolopes:* (i) the eggs must be provided with conditions that lead to complete embryonic development, thus rendering fully competent hatchlings; (ii) water quality must be good, and the tank configuration and lighting must be tailored to the specific needs and behavior of the species; and (iii) the proper type and quantity of prey organism must be provided. Observations in the sea as well as in the laboratory indicated that *E. scolopes* was a voracious predator for its size, and that relatively large prey were preferred.

Because our main interest in culturing *E. scolopes* is to advance the use of this model of symbiosis, it was also important to demonstrate that laboratory animals were competent to receive bacteria in a manner similar to that of wild-caught *Euprymna*. Our results are consistent with previous demonstrations that hatchlings initially are aposymbiotic and that they acquire symbiotic strains of *V. fischeri*, and consequently produce light, within about a day of hatching (Wei and Young, 1989; McFall-Ngai and Ruby, 1991). Furthermore, squids that had reached the juvenile benthic and subadult stages also produced luminescence, and their light organs contained increasingly larger populations of *V. fischeri* (Table I; Fig. 7).

Table I

Re-establishment of bacterial symbiosis in cultured Euprymna scolopes

Animal stage	Approximate size (mm)	Animal light production[1]	Symbiont CFU[2]
Hatchling (Day 0–1) (Planktonic)	2 × 2	not detected (n = 5)	not detected (n = 5)
Paralarval (Day 5) (Planktonic)	2.5 × 2	44 3.2	6.0×10^5 5.0×10^5
Juvenile (Day 15) (Benthic)	4 × 3	220	8.0×10^6
Juvenile (Day 30) (Benthic)	7 × 4.5	16	2.0×10^7
Subadult (Day 130)	35 × 20	640	8.0×10^7

[1] LU (arbitrary light units) per animal.
[2] Symbiont CFU = colony-forming units of *Vibrio fischeri*

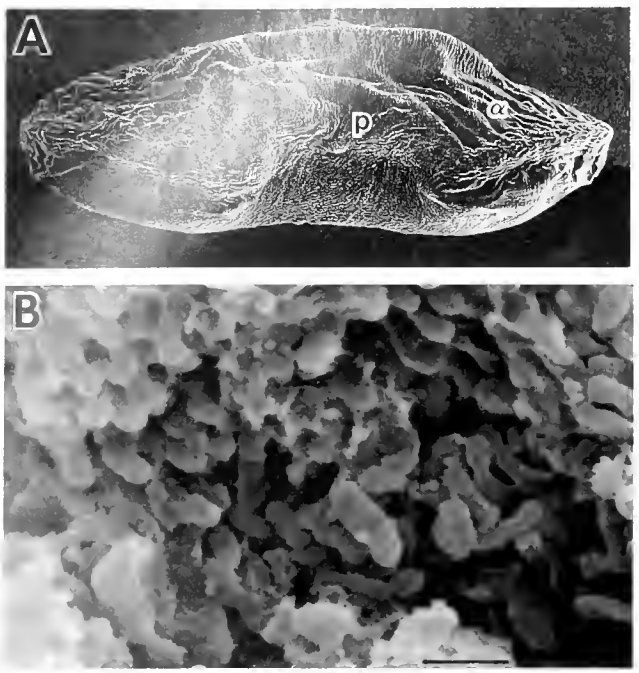

Figure 7. (A) Scanning electron micrograph of half the light organ of a mature, cultured squid. Letter "p" indicates the pore. Symbol indicates the approximate region of interest shown in panel B. (B) High magnification of *Vibrio fischeri* cells within the internal cavity of the distal end of the light organ. Bar is 1 μm.

Behavior, life cycle, and laboratory culture comparisons

It has been found repeatedly that teuthoid and sepioid squids are visual predators that generally prefer actively swimming prey (*e.g.*, Boletzky *et al.*, 1971; Boletzky and Boletzky, 1973; Boletzky, 1974; Boletzky and Hanlon, 1983; Yang *et al.*, 1986; Hanlon *et al.*, 1989; Hanlon, 1990; Lee *et al.*, 1994). The peculiar decapod arrangement of eight arms and two tentacles allows capture and ingestion of both very small and unusually large prey. Nevertheless, as observed in many of the studies just cited, many seemingly good prey items are not preferred by paralarval squids, thus diets must be determined experimentally. It was predictable that *E. scolopes* would ingest mysids given the enormous success of this diet for other squids (studies cited above) and cuttlefish (Forsythe *et al.*, 1994) and the results of rearing work on *E. berryi* (Choe and Oshima, 1963; Choe, 1966) and *E. scolopes* (Arnold *et al.*, 1972; Singley, 1983). It was *not* predictable that *E. scolopes* paralarvae would prefer such large prey and only survive well on them as compared to mysids of other sizes. However, field observations made with a night-vision device by RTH in Hawaii indicated that very young *E. scolopes* were exceptionally strong swimmers that could jet forward at great lengths. Laboratory video in this experiment documented forward attacks of at least 12 body lengths in about a second, a feat that small squids such as *Loligo* cannot perform.

How might the paralarvae live in nature? Our study indicates that their activity patterns are flexible compared with those of adults (Fig. 2). They can bury in the sand like adults, yet they are surprisingly strong swimmers that can capture prey with a very rapid forward attack and avoid predators by combining a swift backwards jet escape with inking. We did not see any evidence that the light organ was used by paralarvae, juveniles, or adults in our study, despite many observations at night. It seems unlikely that paralarvae commonly use the light organ while seeking prey because we probably would have observed it through the viewing ports in the side of the tray tanks (Fig. 1). A more plausible use for the bioluminescence would be in defense against predators from below, when *Euprymna* of any life stage are higher in the water column. Since the organ is directed downward, it probably is used to eliminate or interrupt the squid's shadow against the downwelling light.

Euprymna scolopes has one of the shortest life cycles of any cephalopod (Boyle, 1983), mainly as a result of its rapid exponential growth, the warm temperatures it lives in, and its small adult size. The fast exponential growth through day 83 is typical for many squids; since first mating and egg laying were seen at about day 60, we expected that growth would slow substantially soon thereafter, which it did. The shortest life cycle reported for a cephalopod is in the small tropical species *Idiosepius pygmaeus:* statolith ring analysis indicates that this species matures in 1.5–2.0 months and lives only about 79 days (Jackson, 1989); this species was not cultured in the laboratory. *E. scolopes* is relatively easy to rear because of the large strong hatchlings and their propensity for mysid shrimps. Close relatives of *E. scolopes* share rapid growth, small size, and preference for mysids. *Euprymna berryi* was reared to 2 months by Choe and Oshima (1963) and Choe (1966); four species of *Sepiola* and two of *Sepietta* were reared by similar techniques by Boletzky *et al.* (1971); *Sepietta oweniana* was cultured by Summers and Bergstrom (1981); and *Rossia macrosoma* was reared to 8 months by Boletzky and Boletzky (1973). Only *E. scolopes*, however, lives in warm water, which accelerates growth (Forsythe and Van Heukelem, 1987) and promotes a short life cycle. Could these techniques be applicable to *Euprymna morsei* from Japan and to similar sepioids with light organs?

Behavioral and physiological factors that require future attention

Now that progress has been achieved with the paralarval stages, the next logical stage is to focus on reproductive behavior. Practically nothing is known about the mating system of any member of the subfamily Sepioli-

nae (*e.g.*, Boletzky *et al.*, 1971; Boletzky, 1975; Moynihan, 1983; also reviewed by Hanlon and Messenger, 1996), and optimal conditions for brood stock management will have to be determined before "normal" reproductive behavior and high fecundity can be expected. The density of adults, the diet, the light cycle (especially gradual changes that imitate natural changes), the combinations of females and males and the nature of their pairings, agonistic behavior, courtship, and any form of sperm competition will all influence mating, egg laying, and the quality of the progeny. The matings observed in this study averaged 35 min; Moynihan (1983) and Singley (1983) reported matings of 25–80 min. These long mating times combined with the presence of a seminal receptacle (called the pharetra, located internally near the opening of the oviduct) strongly suggest the possibility of sperm competition behavior among males. A practical problem is to determine how many adult squids must be maintained as brood stock under optimal conditions (physical and social) to ensure sufficient genetic diversity in subsequent generations.

A misbalance in the mating system can put stress on the females, resulting in poor egg production, low fertilization rates, and thus poor hatching rates or lack of vigor in the progeny. Crowded laboratory conditions in cuttlefish and loliginid squids can lead to forced copulations of females (J.G. Boal, pers. comm., 1996) and a disruption of the mating system. Lack of attention to these key issues in reproduction is one reason why most cephalopods cultured in captivity have not been cultured through multiple generations. Another sepioid, the cuttlefish *Sepia officinalis*, is the one cephalopod that has successfully been cultured through many generations (Forsythe *et al.*, 1994), and is currently in the 14th laboratory generation at the University of Texas Medical Branch in Galveston.

The second-generation hatchlings in this culture trial did not do well, but no obvious cause was detected. Because we had no access to a control group of hatchlings from wild-caught adults, we were unable to determine whether the problem lay with our techniques or with a lack of vigor in the first filial generation. We also had no certain clues to the cause of the mortalities that occurred throughout the trials, although several of the adults had whitish patches of ulceration that are common in many laboratory-reared cephalopods (Hanlon and Forsythe, 1990). Certainly other factors should be analyzed more closely—for example, different light cycles and types of substrates (*cf.*, Shears, 1988)—to see how they affect the health and well being of squid in captivity.

Future possibilities for this marine model of symbiosis

The immediate application of our culture techniques is in exploring new questions about the developmental biology of this symbiosis. The light organ requires bacteria before it can develop (Montgomery and McFall-Ngai, 1994), and the bacteria need the light organ to become luminescent (Boettcher and Ruby, 1990). On one hand, the ability to culture the host organism—the squid—opens the prospect of studying late development of the light organ, although it first requires that the paralarvae be reared in the absence of the bacteria. On the other hand, one can now address issues of involvement of bacteria in developmental programs at the level of tissue, organ, and whole animal.

The longer-term application of *Euprymna scolopes* culture is to develop this species into a genetic model. This is not a trivial task, but *E. scolopes* has characteristics that favor success. Unlike other cephalopods, this species is small and short-lived, and each female usually lays its clutch of eggs in a single night and in a discrete clutch, so that parentage and reproductive success can be assessed.

Acknowledgments

We are grateful for advice from John Arnold, Alan Kuzirian, Bill Mebane, Richard Young, Ned Ruby, and Margaret McFall-Ngai. Alan Kuzirian helped produce the fine SEMs in Figure 7, and John Forsythe helped with the growth analysis. Kurt Fiedler collected adults for us in Hawaii. Bill Mebane, Janice Hanley, Louis Kerr, and David Remsen of the MBL provided essential logistical support. We thank the Aquatic Resources Division of the MBL, Springborn Laboratories (MA), Aquatic Research Organisms (NH), the Marine Biomedical Institute (TX), Dave Bengston (RI), and especially Ray Lewis of Aquatic Indicators (FL) for help in providing food organisms. Roxanna Smolowitz performed necropsies of dead squids. This work was partially funded by NSF Grant MCB 94-08266 to PVD.

Literature Cited

Arnold, J. M., C. T. Singley, and L. D. Williams-Arnold. 1972. Embryonic development and post-hatching survival of the sepiolid squid *Euprymna scolopes* under laboratory conditions. *Veliger* **14:** 361–364.

Boettcher, K. J., and E. G. Ruby. 1990. Depressed light emission by symbiotic *Vibrio fischeri* of the sepiolid squid *Euprymna scolopes*. *J. Bacteriol.* **172:** 3701–3706.

Boletzky, S. v. 1974. Elevage de Céphalopodes en aquarium. *Vie Milieu* **24(2-A):** 309–340.

Boletzky, S. v. 1975. The reproductive cycle of Sepiolidae (Mollusca, Cephalopoda). *Pubbl. Staz. Zool. Napoli* **39, Suppl.:** 84–95.

Boletzky, S. v., M. V. v. Boletzky, D. Frösch, and V. Gatzi. 1971. Laboratory rearing of Sepiolinae (Mollusca, Cephalopoda). *Mar. Biol.* **8(1):** 82–87.

Boletzky, S. v., and V. v. Boletzky. 1973. Observations on the embryonic and early post-embryonic development of *Rossia macrosoma* (Mollusca, Cephalopoda). *Helgol. Wiss. Meeresunters.* **5:** 135–161.

Boletzky, S. v., and R. T. Hanlon. 1983. A review of the laboratory

maintenance, rearing and culture of cephalopod molluscs. *Mem Natl. Mus. Vic.* **44:** 147–187.

Boyle, P. R. 1983. *Cephalopod Life Cycles, Vol. I. Species Accounts.* Academic Press, London.

Choe, S. 1966. On the rearing, habits of the fry, and growth of some cephalopods. *Mar. Sci.* **16:** 330–347.

Choe, S., and [illegible]. 1963. Rearing of cuttlefishes and squids. *Nature* **197:** [illegible].

Dunlap, P. V., K. Kita-Tsukamoto, J. Waterbury, and S. M. Callahan. 1995. Isolation and characterization of a visibly luminous variant of *Vibrio fischeri* strain ES114 from the sepiolid squid *Euprymna scolopes*. *Arch. Microbiol.* **164:** 194–202.

Forsythe, J. W., and W. F. Van Heukelem. 1987. Pp. 135–155 and 203–204 in *Cephalopod Life Cycles, Vol. II Comparative Reviews*, P. R. Boyle, ed. Academic Press, New York.

Forsythe, J. W., R. H. DeRusha, and R. T. Hanlon. 1994. Growth, reproduction and life span of *Sepia officinalis* (Cephalopoda: Mollusca) cultured through seven consecutive generations. *J. Zool. (Lond.)* **23:** 175–192.

Graft, J., P.V. Dunlap, and E. G. Ruby. 1993. Effect of transposon-induced motility mutations on colonization of the host light organ by *Vibrio fischeri*. *J. Bacteriol.* **176:** 6986–6991.

Hanlon, R. T. 1990. Maintenance, rearing and culture of teuthoid and sepioid squids. Pp. 35–62 in *Squid as Experimental Animals*, D. L. Gilbert, W. J. Adelman, Jr., and J. M. Arnold, eds. Plenum Press, New York.

Hanlon, R. T., and J. W. Forsythe. 1990. Diseases of Mollusca: cephalopoda: I.1. Diseases caused by microorganisms; 1.3 Structural abnormalities and neoplasia. Pp. 23–46 in *Diseases of Marine Animals. Vol. III. Cephalopoda to Urochordata*, O. Kinne, ed. Biologische Anstalt Helgoland, Hamburg.

Hanlon, R. T., and J. B. Messenger. 1996. *Cephalopod Behaviour* Cambridge University Press, Cambridge, U.K.

Hanlon, R. T., W. T. Yang, P. E. Turk, P. G. Lee, and R. F. Hixon. 1989. Laboratory culture and estimated life span of the eastern Atlantic squid, *Loligo forbesi Steenstrup*, 1856, (Mollusca: Cephalopoda). *Aquacult. Fish. Manage.* **20:** 15–34.

Jackson, G. D. 1989. The use of statolith microstructures to analyze life-history events in the small tropical cephalopod *Idioteuthis pygmaeus*. *Fish. Bull.* **87:** 265–272.

Kuo, A., N. V. Blough, and P. V. Dunlap. 1994. Multiple *N*-acyl-homoserine lactone autoinducers of luminescence in the marine symbiotic bacterium *Vibrio fischeri*. *J. Bacteriol.* **176:** 7558–7565.

Kuo, A., S. M. Callahan, and P. V. Dunlap. 1996. Modulation of luminescence operon expression by *N*-octanoyl-homoserine lactone in *ainS* mutants of *Vibrio fischeri*. *J. Bacteriol.* **178:** 971–976.

Lee, P. G., P. E. Turk, W. T. Yang, and R. T. Hanlon. 1994. Biological characteristics and biomedical applications of the squid *Sepioteuthis lessoniana* cultured through multiple generations. *Biol. Bull.* **186:** 328–341.

Lussier, S. M., A. Kuhn, M. J. Chammas, and J. Sewall. 1988. Techniques for the laboratory culture of *Mysidopsis* species (Crustacea: Mysidacea). *Envir. Toxicol. Chem.* **7:** 969–977.

McFall-Ngai, M. J., and E. G. Ruby. 1991. Symbiont recognition and subsequent morphogenesis as early events in an animal-bacterial mutualism. *Science* **254(5037):** 1491–1494.

Montgomery, M. K., and M. McFall-Ngai. 1994. Bacterial symbionts induce host organ morphogenesis during early postembryonic development of the squid *Euprymna scolopes*. *Development* **120:** 1719–1729.

Moynihan, M. 1983. Notes on the behaviour of *Euprymna scolopes* (Cephalopoda: Sepiolidae). *Behaviour* **85:** 25–41.

Nealson, K. H. 1978. Isolation, identification, and manipulation of luminous bacteria. *Methods Enzymol.* **57:** 153–166.

Ruby, E. G., and L. M. Asato. 1993. Growth and flagellation of *Vibrio fischeri* during initiation of the sepiolid squid light organ symbiosis. *Arch. Microbiol.* **159:** 160–167.

Ruby, E. G., and M. J. McFall-Ngai. 1992. A squid that glows in the night, development of an animal-bacterial mutualism. *J. Bacteriol.* **174:** 4865–4870.

Shears, J. 1988. The use of a sand-coat in relation to feeding and diel activity in the sepiolid squid *Euprymna scolopes*. *Malacologia* **29:** 121–133.

Singley, C. T. 1983. *Euprymna scolopes*. Pp. 69–74 in *Cephalopod Life Cycles*, Vol. 1, P. R. Boyle, ed. Academic Press, New York.

Spotte, S. H. 1973. *Marine Aquarium Keeping* Wiley, New York.

Summers, W. C., and B. Bergstrom. 1981. Cultivation of the sepiolid squid, *Sepietta owenana*, and its ecological significance. *Am. Zool.* **20:** 927.

Voss, G. L. 1977. Present status and new trends in cephalopod systematics. Pp. 49–60 in *The Biology of Cephalopods, Symposia of the Zoological Society of London 38* M. Nixon and J. B. Messenger, eds. Academic Press, London.

Wei, S. L., and R. E. Young. 1989. Development of symbiotic bacterial bioluminescence in a nearshore cephalopod, *Euprymna scolopes*. *Mar. Biol.* **103:** 541–546.

Yang, W. T., R. F. Hixon, P. E. Turk, M. E. Krejci, W. H. Hulet, and R. T. Hanlon. 1986. Growth, behavior, and sexual maturation of the market squid, *Loligo opalescens*, cultured through the life cycle. *Fish. Bull.* **84:** 771–798.

Young, R. E., and R. E. Harman. 1988. 'Larva', 'paralarva' and 'subadult' in cephalopod terminology. *Malacologia* **29:** 201–207.

Reference: *Biol. Bull.* **192:** 375–387. (June, 1997)

Post-Hatching Development of Circular Mantle Muscles in the Squid *Loligo opalescens*

THOMAS PREUSS, ZORA N. LEBARIC, AND WILLIAM F. GILLY

Hopkins Marine Station, Department of Biological Sciences, Stanford University, Pacific Grove, California 93950

Abstract. Post-hatching development of the circular muscles in the mantle of squid was studied morphometrically to identify structural changes and to quantify hyperplasia and hypertrophy of the muscle fibers. Superficial, mitochondria-rich (SMR) fibers and central, mitochondria-poor (CMP) fibers are present at hatching. Although both fiber types increase in size and, even more so, in number during post-hatching development, CMP fibers increase at a much higher rate than do SMR fibers. As a result, the relative proportion of SMR to CMP fibers shifts from about 1:1 in a hatchling to about 1:6 in an 8-week-old animal; it then apparently remains constant to adulthood. These structural changes are consistent with developmental changes in muscular activity. During slow, jet-propelled swimming, 1-week-old animals show mantle contractions that have twice the relative amplitude and frequency of those in adults. The presence of Na-channel protein in mantle muscle was detected biochemically by using site-directed antibodies; the protein was found to be preferentially expressed in CMP fibers. These results suggest that SMR fibers are an important source of locomotory power at hatching, but become progressively less important during the first 8 weeks of development as CMP fibers assume the dominant role in jet locomotion.

Introduction

Jet propulsion in squids is caused by the antagonistic action of circular and radial mantle muscles in connection with two layers of stiff, collagenous tunics and a network of intermuscular connective tissue fibers (Ward and Wainwright, 1972; Bone *et al.*, 1981; Gosline *et al.*, 1983; Kier, 1988; Wells, 1988). The circular muscle mass, responsible for producing thrust during jet propulsion, is divided into three layers, largely on the basis of the relative mitochondrial content of individual muscle fiber types. Two thin layers of superficial mitochondria-rich, oxidative fibers on the outer and inner mantle surface enclose a much thicker layer of mitochondria-poor, glycolytic fibers in the central zone (Bone *et al.*, 1981; Mommsen *et al.*, 1981). In light of these structural and metabolic differences, it has been proposed that the superficial layers are active during respiration and slow jet-propelled swimming, whereas the central circular fibers, presumed to be innervated by the giant axon system, power the jet-escape and rapid locomotion (Bone *et al.*, 1995). In general agreement with these ideas, recent electrophysiological studies have revealed that at least two classes of circular muscle fibers can be distinguished on the basis of their electrical properties and that some of the circular fibers, presumably those innervated by giant axons, display Na-channel-based excitability (Gilly *et al.*, 1996).

Jet propulsion, mantle mechanics, and mantle structure have been well studied in adult squid, but relevant work on hatchlings and developing juvenile squid is comparatively limited (Zuev, 1966; v. Boletzky, 1982, 1987; O'Dor *et al.*, 1986; Moltschaniwskyj, 1994, 1995; Matsuno, 1987). Although squid begin actively swimming by jet propulsion as soon as they hatch (Packard, 1969), the full flexibility and fine coordination of the locomotor system is lacking (Gilly *et al.*, 1991; Chen *et al.*, 1996). The aim of the present study was to analyze the maturation of the mantle musculature during post-

Received 2 December 1996; accepted 3 April 1997.

Abbreviations: CMP = central mitochondria-poor muscle fibers; DML = dorsal mantle length; GFL = giant fiber lobe; SMR = superficial mitochondria-rich muscle fibers; SR = sarcoplasmic reticulum.

hatching development and to identify structural and functional characteristics of the different types of muscle fiber associated with jet-propelled locomotion. In pursuit of that goal, we combined three approaches. First, anatomical and morphometric methods at light- and electron-microscopic levels were used to reveal structural changes as squid mature from hatchlings to adults. Second, the kinematics of mantle contractions in free-swimming animals were investigated to shed light on functional characteristics of locomotion at different maturity stages. Third, biochemical analysis of the presence of Na-channel protein in superficial and central fibers provided a tool to characterize the location and abundance of putative fast-twitch fibers in the developing mantle musculature.

Our results indicate that superficial, mitochondria-rich (SMR) fibers are an important source of locomotory power at hatching but become progressively less important during the first 8 weeks after hatching. Over this same period, central, mitochondria-poor (CMP) fibers increase in number until they contribute most of the overall mantle muscle mass and play the dominant role in jet locomotion.

Materials and Methods

Experimental animals

Loligo opalescens was collected in Monterey Bay, California, between August and November of 1995. Animals were maintained at Hopkins Marine Station in circular tanks (2.5 m diameter; 1 m deep) plumbed with flow-through natural seawater. Spawning typically occurred in these tanks within 3–5 days of collecting the squid. Clusters of egg cases were removed and cultured at the Monterey Bay Aquarium, Monterey, California, in flow-through circular 320-l tanks (temperature range 13–16°C) until natural hatching occurred. During the first 10 weeks, squid received a diet, *ad libitum,* of brine shrimp nauplii (*Artemia salina*) enriched with algae and Super Selco (a nutrient medium rich in lipids, fatty acids, and vitamins; produced by Artemia Systems N. V., Belgium). Copepods (*Acartia* sp.) and mysids (*Acanthomysis* sp.) were added to the diet when available (about twice per week).

Mantle anatomy

The anatomy of the mantle musculature was examined by light microscopy (LM) and transmission electron microscopy (TEM). Prior to dissection, all animals were anesthetized for 20 min in 7.5% $MgCl_2$ diluted 1:1 in oxygenated seawater and then killed by decapitation. Tissue for fixation was removed from adult squid within 1 day after collection. Blocks of mantle muscle were cut parallel to the main body axis and taken from an anterodorsal region close to the stellate ganglion of five adults with dorsal mantle lengths (DML) between 80 and 140 mm. For studies of hatchling and juvenile squid, six healthy looking animals that displayed vigorous swimming capability were collected for fixation weekly over a 10-week period. These animals were fixed whole, and smaller tissue samples for ultrastructural analysis of the mantle muscles were taken after fixation. In all animals (except hatchlings), the skin was carefully removed before fixation.

For LM, the tissue was fixed in 4% paraformaldehyde in filtered seawater for 3–5 days at 4°C, dehydrated in graded ethanol, and either infiltrated with paraffin under vacuum or embedded in plastic (JB4; Polysciences, Inc.). Thick sections (6–10 μm) and semithick sections (2–4 μm) were cut and stained with conventional histological stains and viewed with an Olympus BH-2 microscope.

For TEM, the tissue samples were fixed in 0.065 *M* sodium phosphate buffer (pH 7.4) with 3% glutaraldehyde, 0.5% tannic acid, and 6% sucrose for 8 h at 4°C (first 15 min at room temperature), rinsed in 0.065 *M* sodium phosphate buffer without sucrose, and postfixed in a 1:1 mix of 0.13 *M* cacodylate buffer (pH 7.2) with 2% potassium ferrocyanide and 2% osmium tetroxide for 40 min at 4°C. Thereafter, the tissue was rinsed in 0.065 *M* cacodylate buffer, dehydrated in graded ethanol, and infiltrated overnight (10–12 h) in resin (LR White; Sigma). For sectioning, the blocks were oriented to obtain transverse, sagittal, and tangential sections of the circular mantle muscles. Thin (0.8–1 μm) and ultrathin (gray-silver) sections were obtained in alternating section series, thereby collecting ultrathin sections every 4–6 μm in hatchlings and juveniles and every 50–60 μm in adults. Up to five consecutive section series were collected in this manner. Thin sections were stained with toluidine blue and examined with an Olympus BH-2 microscope. Ultrathin sections were collected onto Formvar-coated mesh and slot grids (Electron Microscopy Sciences), stained either with a saturated aqueous uranyl acetate solution and Reynolds' lead citrate or with 2% phosphotungstic acid, and examined with Phillips EM 201 or EM 401 electron microscopes. The magnification stops were calibrated with a diffraction grating replica (Ted Pella, Inc.).

For morphometric analysis of the muscle fibers, a computer-aided image analysis program (NIH-Image 1.60) was used on a Power Macintosh 7100/80 computer. TEM micrographs of muscle fibers were digitized at 600-dpi resolution using a scanner (Microtek ScanMaker II_{HR}), and stored on a magneto-optical drive (Pin-

nacle Tahoe 230 MB). In addition, LM video-images were obtained using an Olympus BH-2 microscope equipped with a CCD B/W camera (Sony SSC-M374), and selected frames were digitized with a high-resolution video capture card (Scion LR-3).

Measurements were taken on longitudinal mantle sections (*i.e.*, on a cross section of the circular muscle fibers). Two measurements of each muscle fiber visible in a given electron micrograph were taken: (i) the total cross-sectional area of a single muscle fiber and (ii) the area occupied by its mitochondrial core. The difference between these values approximates the remaining myofilament area; this value also includes cytoplasm and sarcoplasmic reticulum (SR). Additional measurements were taken in selected micrographs to determine the cross-sectional area (and the calculated diameter) of synaptic vesicles in nerve processes.

Mantle kinematics

A dorsal view of freely swimming juvenile (1-week-old) and adult squid in their respective holding and rearing tanks was filmed with a high-resolution CCD B/W video camera (Sony SSC-M374) mounted above the tanks on a remote controlled panning motor (Prinz Power-Panner 430-62), and recorded on a Sony Hi-8 recorder (EVO-9700). Single video-frame analysis of digitized video sequences was carried out using the image analysis system described above. The mantle diameter was measured at its widest point (the anterior mantle end in juveniles and about $^1/_3$ from the anterior mantle end in adults) in successive, enlarged video images (calibrated by dorsal mantle length). To compare mantle diameter dimensions in animals of different size, the fractional mantle diameter was calculated by defining the largest diameter in a given measurement sequence as 100%.

Biochemistry

Production of antibodies. Two antibodies (one polyclonal and one monoclonal) directed against distinct regions of a putative squid sodium channel encoded by the cDNA GFLN1 (Rosenthal and Gilly, 1993) were used. mRNA corresponding to this gene is expressed widely throughout the squid nervous system (Liu and Gilly, 1995).

Polyclonal antisera (produced in collaboration with Dr. S.R. Levinson, University of Colorado) were raised against a bacterial fusion protein that contained amino acids (aa) 483-576 of the predicted GFLN1 sequence. These residues compose the C-terminal half of the cytoplasmic linker between domains I and II. Construction of the fusion protein is described in detail elsewhere (Rosenthal, 1996). Polyclonal antisera ($Ab_{483\text{-}576}$) were affinity-purified using the soluble fraction of the fusion protein coupled to an affinity column (AminoLink, Pierce) according to manufacturer's protocol.

A monoclonal antibody ($mAb_{1305\text{-}21}$) was produced in collaboration with J. Burkhard and S. L. Feng, University of California, San Francisco. This antibody was directed against a synthetic peptide (synthesized by the Protein and Nucleic Acid Facility, Stanford University, Stanford, CA) corresponding to aa 1305-1321 of the GFLN1 sequence. These residues make up the part of the cytoplasmic linker between domains III and IV that is well conserved in most sodium channels (Gordon *et al.*, 1988).

Preparation of protein samples. Specificity of the antibodies was tested with tissue samples of cleaned giant axons and giant fiber lobes (GFL) taken from adult squid. Animals were rapidly decapitated before tissues were dissected in cold, Ca-free artificial seawater (480 m*M* NaCl, 10 m*M* $MgCl_2$, 5 m*M* EGTA, 10 m*M* HEPES, pH 7.4) for biochemical analysis. Segments of stellar nerves were ligated and cleaned by manually stripping off the small nerve fibers under microscopic observation until only the giant axon and its Schwann-cell sheath remained. Cleaned axons were cut at both ends and immediately placed in ice-cold lysis buffer containing proteinase inhibitors (Knudson *et al.*, 1989). Several axons were pooled, homogenized in the same buffer, and centrifuged at $1500 \times g$ for 10 min at 4°C. The supernatant was then used for protein-concentration analysis (bicinchoninic acid assay; Pierce, Rockford, IL) and for immunoblotting. Giant fiber lobe, brain, and cornea tissues were dissected and homogenized in the lysis buffer as described above. The resulting supernatant was centrifuged at $100{,}000 \times g$ for 30 min at 4°C to form a crude membrane pellet. This pellet was resuspended in lysis buffer for determination of protein concentration and for immunoblotting.

Muscle samples were obtained from animals anesthetized in 0.5% urethane in artificial seawater and dissected in cold, Ca-free artificial seawater. Thereafter, all muscle tissue was processed as described for giant fiber lobes (see above). To test for Na-channel protein within individual layers of circular mantle muscle, tissue samples from superficial and central layers were dissected and processed separately (outer and inner superficial layers were pooled). To test for the presence of Na-channel protein in the mantle muscle mass during post-hatching development, samples were taken from skinned mantles of hatchling and juvenile squid at four maturity stages (3 days, 2 weeks, 3 weeks, and 14 weeks) and from adults.

Immunoblotting. Protein samples (10 μg of total protein per lane) were separated by standard SDS-PAGE electrophoresis using 5% gels and transferred to nitrocel-

lulose. Nonspecific binding of the antibodies was minimized by pretreating the nitrocellulose with 10% nonfat dry milk in PBS (0.38 *M* Na_2HPO_4, 0.02 *M* NaH_2PO_4, 0.1 *M* NaCl) at pH 7.4. Affinity-purified antibodies were diluted as specified in the figure legends. Undiluted hybridoma supernatant was used as a source of monoclonal antibody. Goat anti-rabbit or goat anti-mouse secondary antibodies conjugated to horseradish peroxidase (Sigma) were used at 1:5000 dilution in conjunction with an enhanced chemiluminescence detection system (Renaissance, Du Pont NEN Research Products). For control experiments with blocked $Ab_{483-576}$, purified antiserum was incubated overnight at 4°C with the fusion protein antigen at a concentration of 0.1 mg/ml.

Results

Structural aspects of muscle fiber maturation

Squid hatchlings (1–2 days old) already possess the overall organization of radial and circular muscle fibers shown by adults (Bone *et al.*, 1995). Profiles of two distinct types of circular muscle fibers are visible in a longitudinal mantle section (Fig. 1A). Layers of superficial, large-diameter fibers on the outer and inner mantle surface enclose a central layer composed of fibers of smaller diameter. The superficial fibers and the central fibers differ in their mitochondrial content. In any given cross section, superficial mitochondria-rich (SMR) fibers often contain several large mitochondria, whereas central mitochondria-poor (CMP) fibers rarely display more than a single small one (Fig. 1). In both fiber types, the mitochondria are surrounded by loosely packed myofilaments (Fig. 1B, C). Myofilaments are rather poorly organized at this time, and sizable areas of cytoplasm without myofilaments are common. Similarly, the SR network is poorly developed and organized at this stage, with only a few SR tubules scattered among the myofilaments (Fig. 1B, C). Fibers of both types display very large nuclei (Fig. 1A).

By 8 weeks after hatching, several of the above characteristics show signs of substantial maturation. In addition to their difference in size and mitochondrial content (see also below), SMR and CMP fibers now clearly display differences in the organization of their myofilaments and SR (Fig. 2). The myofilament density increases considerably in both fiber types, but CMP fibers show a much thicker myofilament zone, both in absolute size and in relation to the mitochondrial core (Figs. 2B, 2C, and 3). Moreover, myofilaments in each fiber type are now organized in a characteristic manner. In cross sections of CMP fibers, myofilaments are divided by the SR and the Z-bodies into radially oriented, trapezoidal blocks (Fig. 2C). In the same sections, SMR fibers lack such divisions, and the myofilaments form a continuous ring around the central mitochondrial core (Fig. 2B). This difference between CMP and SMR fibers was found in cross sections examined at all maturity stages from week 1 on.

Longitudinal sections confirm the difference in width of the myofilament zone in relation to the mitochondrial core of the two circular fiber types (Fig. 3). These sections also reveal differences in myofilament staggering in the two fiber types. In CMP fibers, the myofilaments and Z-bodies form an oblique pattern across the fiber, which characterizes them as regular, obliquely striated muscles similar to those in other cephalopods (Gonzalez-Santander and Garcia-Blanco, 1972; Amsellem and Nicaise, 1980, Kier, 1985). In contrast, the myofilaments and Z-bodies of SMR fibers are lined up nearly in register across the fiber (Fig. 3). Although the appearance of the SMR fibers in cross section and longitudinal section is suggestive of cross striation rather than oblique striation, further morphological studies are necessary to clarify this point. The degree of myofilament staggering in a given section depends on the sectioning angle and on the degree of contraction of the muscle fiber (Rosenbluth, 1972; Kier 1985).

In all maturity stages, numerous profiles of neuronal processes containing round, clear vesicles were found (Fig. 4). These processes contact CMP and SMR muscle fibers at presumptive chemical synapses with clefts about 20 nm wide (Fig. 4C). A rich, ramifying network of these processes exists within the zone of CMP fibers, and individual processes appear to contact multiple fibers (Fig. 4A, B). Within the SMR fiber zone, nerve processes are less prominent and appear to run in grooves of the muscle fibers (Fig. 4D). The cross-sectional areas of synaptic vesicles were measured at a magnification of 240,000 on scanned micrographs, and vesicle diameters were calculated by assuming a spherical shape. Vesicles from processes associated with SMR fibers (mean diameter of 39 nm ± 0.7 SEM) are significantly smaller than those from processes associated with CMP fibers (mean diameter of 45.8 nm ± 0.6 SEM). These values are significantly different by Student's *t* test ($df = 225$, $P < 0.005$).

Quantitative aspects of muscle fiber maturation

In longitudinal sections, the circular mantle muscle mass is divided by bands of radial fibers into rectangular muscle segments (Figs. 1A and 2A). The dimensions of such a muscle segment, in a given section, can be described by (i) its thickness (*i.e.*, the distance between the outer and inner tunics) and (ii) its width (*i.e.*, the distance between two successive radial-fiber bands). Horizontal sections through the entire body of a juvenile showed that the thickness and the width of the muscle segments

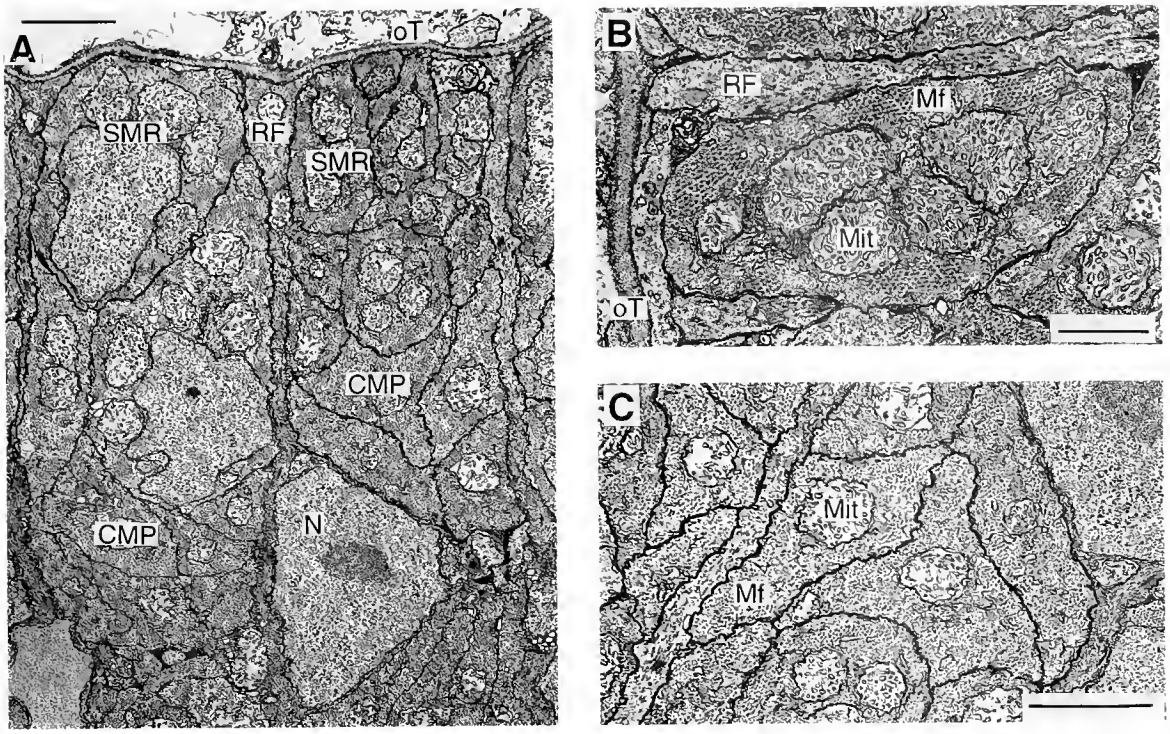

Figure 1. Transmission electron micrographs of superficial (outer) and central layers of mantle muscle from a squid hatchling (1–2 days old). (A) Cross section of circular muscle fibers showing the outer layer composed of 1–2 superficial mitochondria-rich fibers (SMR) and half of the central zone composed of mitochondria-poor fibers (CMP). Radial fibers (RF; cut longitudinally) divide mantle muscle into rectangular segments. N = nucleus; oT = outer tunics. Scale bar = 2 μm. (B) Cross section of a single SMR fiber. Many large mitochondria (Mit) are located in the central core. Mf = myofilaments. Scale bar = 1 μm. (C) Cross section of several CMP fibers. Usually one mitochondrion is located in the central core of an individual CMP fiber. Note the irregular shape of CMP fibers and the lack of any myofilament organization. Scale bar = 2 μm.

vary considerably along the mantle. The thickest and widest segments are found about one-third of the way from the anterior mantle end, whereas more anterior and posterior segments become progressively thinner and narrower. Transverse mantle sections, on the other hand, show almost no variation in the thickness of the muscle segments in a given section, although segments become very narrow dorsally at the location of the pen. In light of these results, the mantle region that contains the thickest muscle segments was chosen for analyzing the growth of the mantle muscle, and two animals of each age group with similar dorsal mantle length (DML) were studied.

In adults, muscle segments from this same area of the mantle were analyzed. Although adult animals were part of a spawning population, only very robust males that showed no sign of skin damage or senescence were studied. We therefore consider it unlikely that any selective "deconstruction" of the mantle muscle mass took place prior to fixation (Giese, 1969; O'Dor and Wells, 1978).

A muscle segment in a hatchling (2 mm DML) encloses the profiles of about 20–22 circular muscle fibers, of which 12–14 are CMP fibers (*i.e.*, ≈ 60%). During growth, the number of fibers enclosed in a single muscle segment increases considerably, but SMR and CMP fibers increase at different rates (Fig. 5). By 8 weeks (12 mm DML), the number of CMP fibers has increased about 10-fold, whereas the number of SMR fibers increases only 2.5-fold (Fig. 5A). Thus, the relative proportion of CMP fibers increases during growth (Fig. 5B), and by week 8, about 84% of the fibers in a muscle segment are CMP fibers. This proportion is comparable to that derived from analysis of a single muscle segment in a mature animal (110 mm DML; muscle segment 2.8 × 0.12 mm), which revealed a total of about 12,000 circular fibers, 86% of which were CMP fibers (Fig. 5A, B).

Morphometric measurements on the ultrastructural level for developing CMP fibers are summarized in Figure 6A. Mean cross-sectional area of CMP fibers doubles between 1 week and 8 weeks of age and increases by a

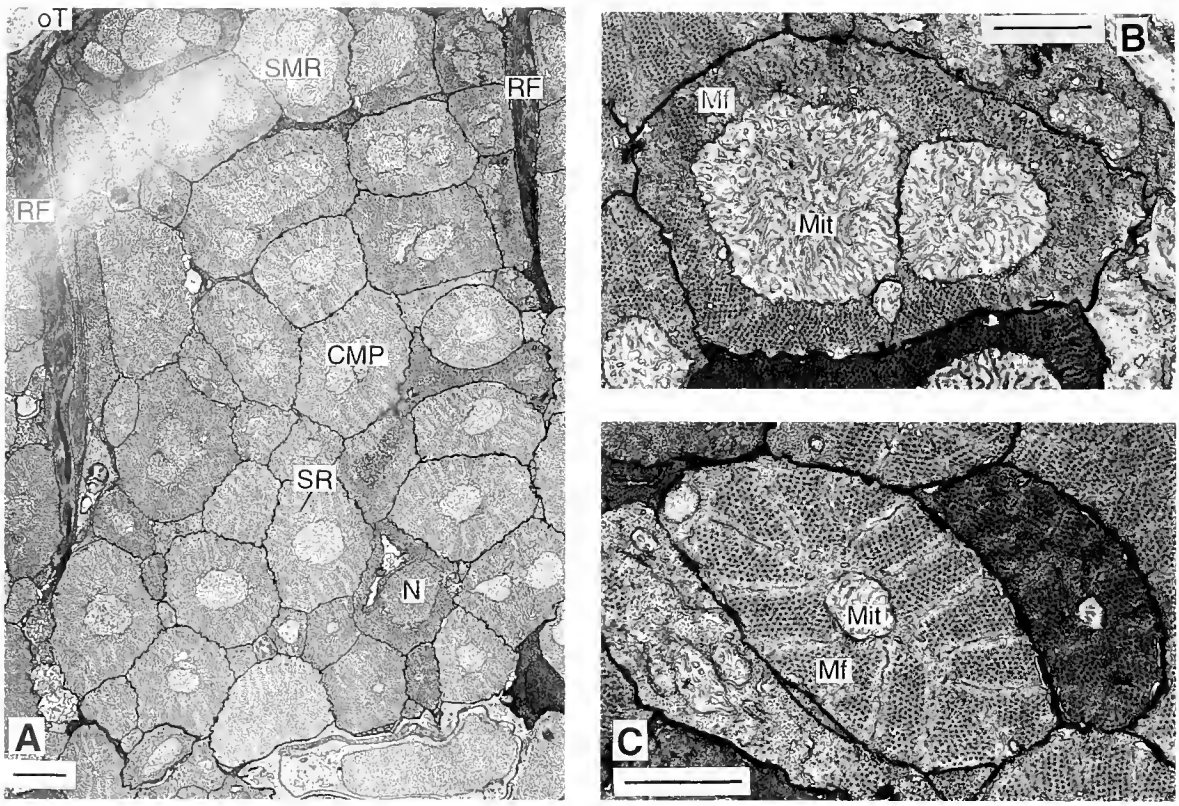

Figure 2. Transmission electron micrographs of superficial (outer) and central layers of mantle muscles from a juvenile squid (8 weeks old). (A) Cross section of circular muscle fibers showing the outer layer composed of several SMR fibers and part of the central zone composed of CMP fibers. Radial fibers (RF) are cut longitudinally. CMP fibers show a well-developed sarcoplasmic reticulum (SR). oT = outer tunics. Scale bar = 2 μm. (B) Cross section of a single SMR fiber. A continuous ring of myofilaments (Mf) surrounds a massive core of large mitochondria (Mit). Scale bar = 1 μm. (C) Cross section of a single CMP fiber. The myofilament area is divided into trapezoidal blocks by SR and Z-bodies. Only a small proportion of the fiber is occupied by mitochondria (Mit). Scale bar = 1 μm.

total of 3- to 4-fold in mature animals. This increase in fiber cross-sectional area is almost exclusively due to an increase in the filament and SR area. The mitochondrial core contributes relatively little to the absolute fiber size and, moreover, does not grow in proportion to the rest of the fiber. As a consequence, the relative area occupied by the mitochondrial core in CMP fibers decreases during growth from 16.3% ± 0.6% SEM in 1-week-old animals to 6% ± 0.3% SEM in adults.

In Figure 6B, results of the same ultrastructural analysis are presented for SMR fibers. The mean cross-sectional area of SMR fibers shows a pattern of increase similar to that described above for CMP fibers, although the absolute fiber area is much larger in SMR fibers (Fig. 6A, B left). Growth in SMR fibers, however, reflects a substantial increase in both the filament and SR area and the mitochondrial core. As a result, the proportional area occupied by the mitochondrial core in SMR fibers remains more-or-less constant at about 40%.

Functional maturation of circular muscle fibers in locomotion

The anatomical data described above indicate that the circular muscle of the mantle changes in composition during post-hatching maturation. At hatching, SMR and CMP fibers contribute almost equally to the circular mantle mass. Subsequent growth is mostly due to an increase in the contribution of CMP fibers, and the relative contribution of SMR fibers to the mantle mass in an adult is only about 14%. These structural changes suggest that the mantles of hatchlings and adults may have different contractile and endurance properties. For example, the endurance capabilities of SMR fibers should be manifested in respiration-related slow swimming (Bone *et al.*, 1995) or hovering (Zuev, 1966), and their relative contribution to jet-propelled locomotion should be most apparent at the earliest stages of maturation. To test this idea, we compared the kinematics of mantle

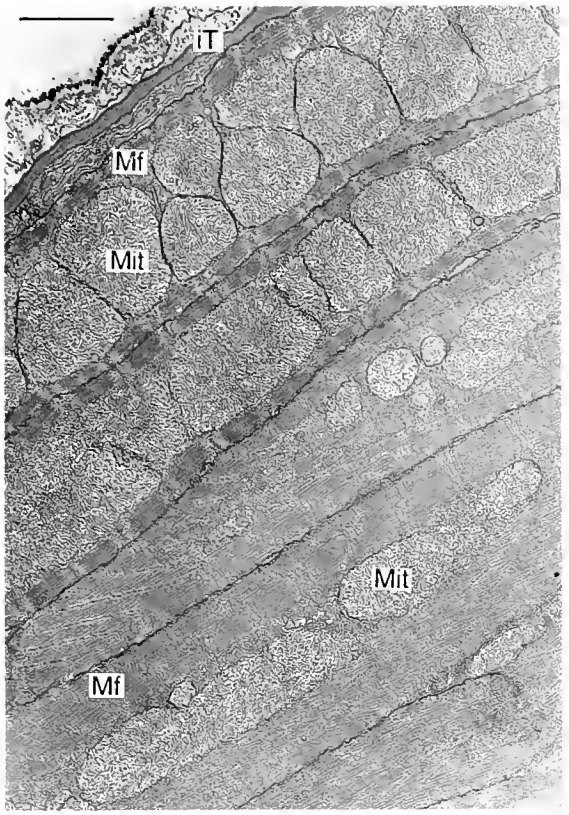

Figure 3. Transmission electron micrograph of mantle muscle fibers from a juvenile squid (8 weeks old). Longitudinal section of circular muscle fibers showing portions of two SMR fibers and three CMP fibers. Note the differences in mitochondrial content and in myofilament (MF) staggering angle between SMR and CMP fibers. Mit = mitochondria; iT = inner tunics. Scale bar = 2 μm.

contractions in freely swimming 1-week-old and adult squid during hovering behavior.

Adults and juveniles show quite different locomotor behavior during hovering. Adults move slowly back and forth, either in a slightly head-down or head-up position, due to gentle jets and undulatory fin movements. Juveniles, on the other hand, continuously bob up and down in a definite head-down position. Although juveniles beat their very small fins rapidly (up to 16 Hz), locomotion at this stage is apparently driven primarily by jetting. Comparison of the mantle kinematics in Figure 7 shows that hovering juveniles (2.5 mm DML) produce jets about twice as frequently (2.7 Hz) as do adults (1.3 Hz). In addition, the fractional change in mantle diameter in juveniles (≈32%) is about three times that in adults (≈12%; Fig. 7).

Identification of Na-channel protein in developing mantle muscle

Both Na-channel antibodies described in this study were produced against predicted sequence for the putative squid Na channel encoded by the cDNA GFLN1 (Rosenthal and Gilly, 1993). mRNA corresponding to GFLN1 is expressed throughout the squid nervous system, particularly in neurons, including those of the GFL, whose axons are large, long, or both (Liu and Gilly, 1995). These tissues were therefore used to test the specificity of the Na-channel antibodies.

Results of the monoclonal antibody $mAb_{1305\text{-}21}$ with GFL and cleaned axon samples are shown in Figure 8A. A prominent band with an apparent molecular weight of about 250 kD is present in both lanes. Control experiments with secondary antibody alone gave no signal (not illustrated). Similar results were obtained using the polyclonal antibody $Ab_{483\text{-}576}$ with GFL samples (Fig. 8B). In this case, a control experiment employing blocked-$Ab_{483\text{-}576}$ (see Methods) demonstrates specificity. The specificity of these antibodies for Na-channel protein is also supported by the fact that both antibodies give similar results, even though they are directed against two distinct portions of the protein encoded by GFLN1.

As detected by the polyclonal antibody, a specific (*i.e.*, blockable) Na-channel band centered around 210–220 kD is prominent in protein samples derived from mantle muscle (Fig. 8C). The monoclonal antibody also recognizes a comparable band in muscle tissue (not illustrated). Thus, it appears that Na-channel protein is relatively abundant in mantle muscle tissue.

Results obtained with a control tissue expected to show minimal Na-channel protein are also shown in Figure 8C. The cornea of the eye is a simple arrangement of a layer of epithelial cells supported by a transparent layer of muscle fibers (unpubl. obs.). Whole-cell patch clamp recordings made, using established methods (Gilly *et al.*, 1990, 1996), from enzymatically dissociated cells from both layers failed to reveal the presence of any voltage-gated Na currents (unpubl. results); the immunoblot results also fail to reveal a strong Na-channel band (Fig. 8C). The weak bands in the cornea lane may arise from axonal membrane, because the muscle fiber layer of the cornea presumably is innervated. These bands are blocked in the control experiment (Fig. 8C).

Electrophysiological recordings of Na currents in circular muscle fibers of squid mantle have been reported, and it was proposed that the muscle fibers with Na currents were small-diameter, CMP fibers (Gilly *et al.*, 1996). To test this idea, mantle tissue was dissected from an adult squid (see Methods) to provide samples of pure CMP circular fibers (plus radial fibers) and samples containing SMR fibers (plus contaminating CMP fibers as well as radial fibers). The results of an immunoblot with these samples are shown in Figure 9. The Na-channel band is most prominent in the central-zone sample,

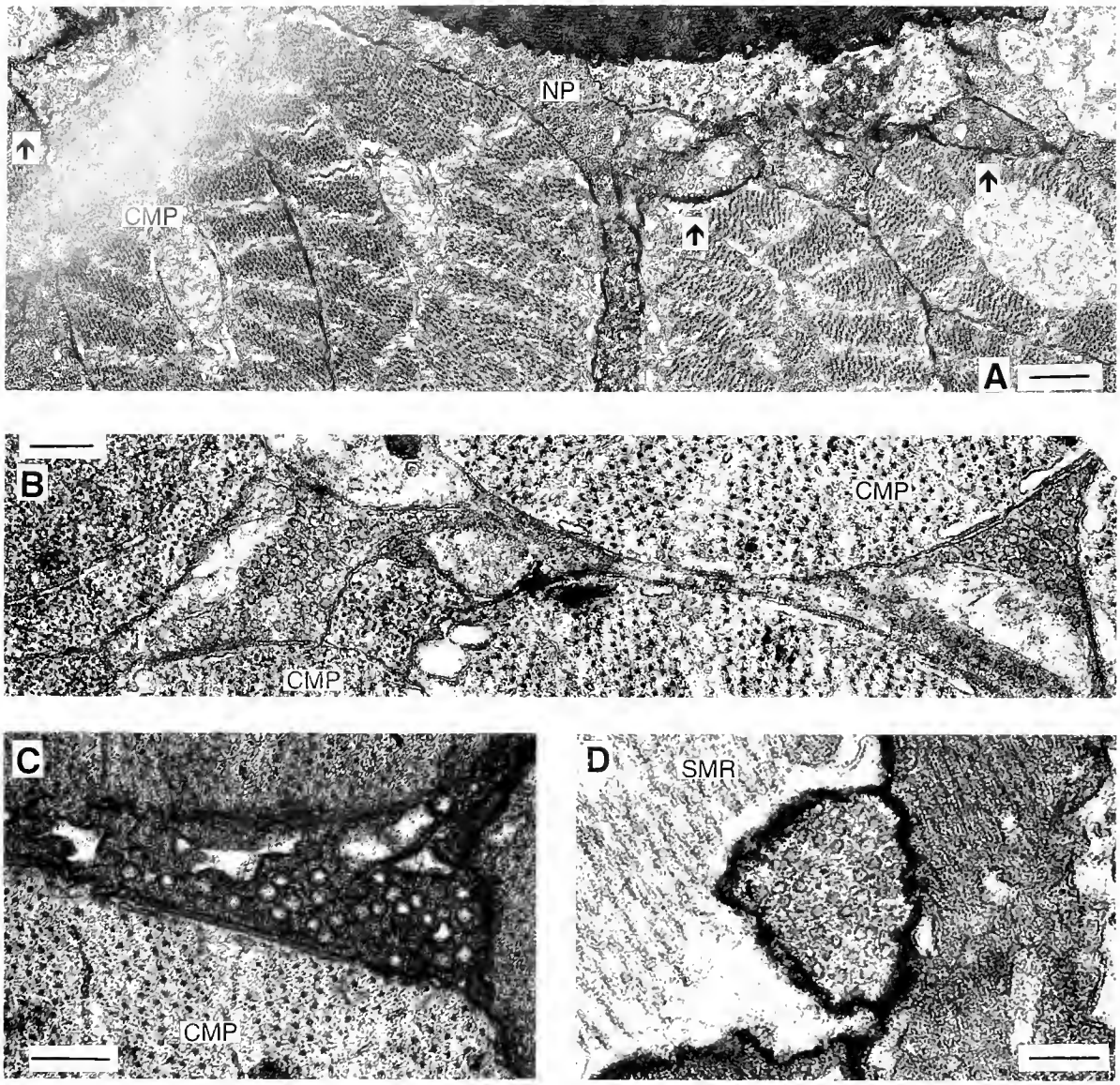

Figure 4. Transmission electron micrographs of synaptic profiles contacting circular mantle muscle fibers (juvenile; 8 weeks old). (A and B) Longitudinal mantle section (circular fibers in cross section). A nerve process (NP) runs within the central muscle layer and forms putative synaptic contacts (arrows) onto several CMP fibers. Note the relatively large dimensions of the synaptic profiles in relation to the size of the muscle fiber. (C) Neuromuscular junction onto a CMP fiber. The synaptic profile is filled with round, clear vesicles. (D) Synaptic profile running within a groove of an SMR fiber. Scale bars = 0.5 μm for A, and 0.2 μm for B–D.

much weaker in the superficial (inner/outer) sample, and quite strong in the whole-mantle sample.

If Na channels are preferentially expressed in CMP fibers, the relative abundance of Na-channel protein in whole-mantle samples should increase during the post-hatching period of maturation described in this study. Mantle samples were therefore collected from squid during this period and processed for immunoblotting. Results in Figure 10 confirm the predicted pattern. The muscle-type Na-channel band of low apparent molecular weight (relative to the neuronal form detected in brain; see also Fig. 8A) increases steadily in intensity between days 3 and 100 post-hatching. At this latter time, the band is comparable to that in the adult squid. Because each lane in Figure 10 was loaded with the same amount of protein, these results strongly suggest that the

relative abundance of Na-channel protein in mantle muscle is increasing during maturation.

Discussion

Comparison of the histology of the circular muscle of squid mantle during development from hatchling to adult reveals large changes in the size and number of the muscle fibers. Moreover, clear changes in the relative proportions of the different types of fiber are associated with maturation; these, in turn, affect mantle kinematics and jet-propelled locomotion.

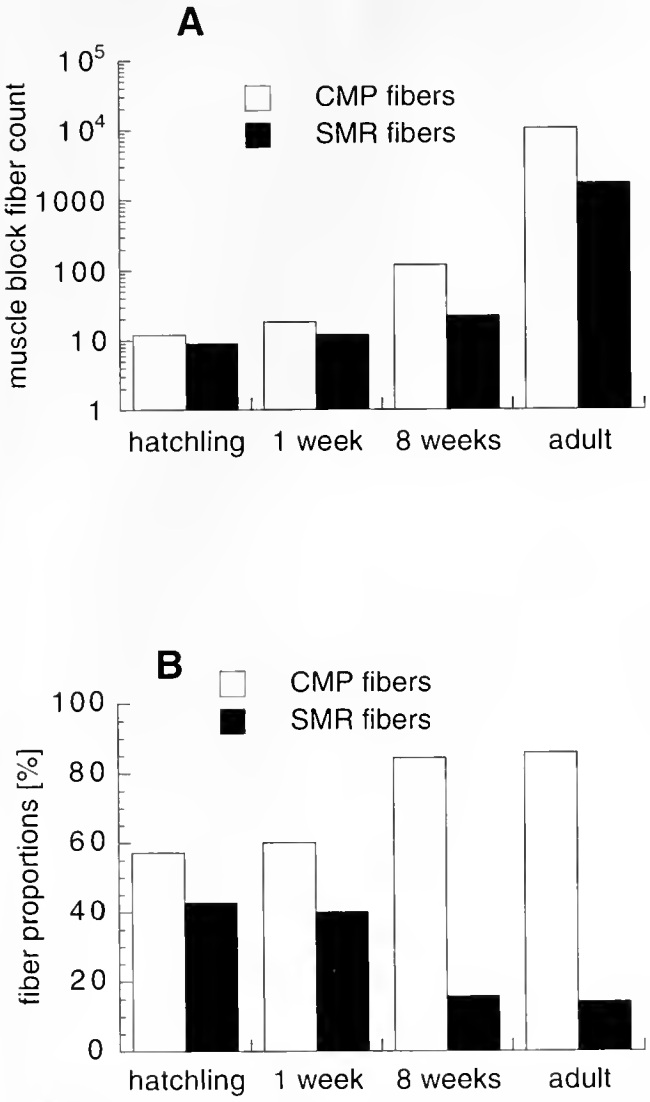

Figure 5. Recruitment of CMP and SMR fibers during mantle growth. (A) Absolute fiber counts are from individual muscle segments from hatchling, 1-week-old, 8-week-old, and adult squid. (B) Histogram of relative proportion of SMR and CMP fibers at different maturity stages.

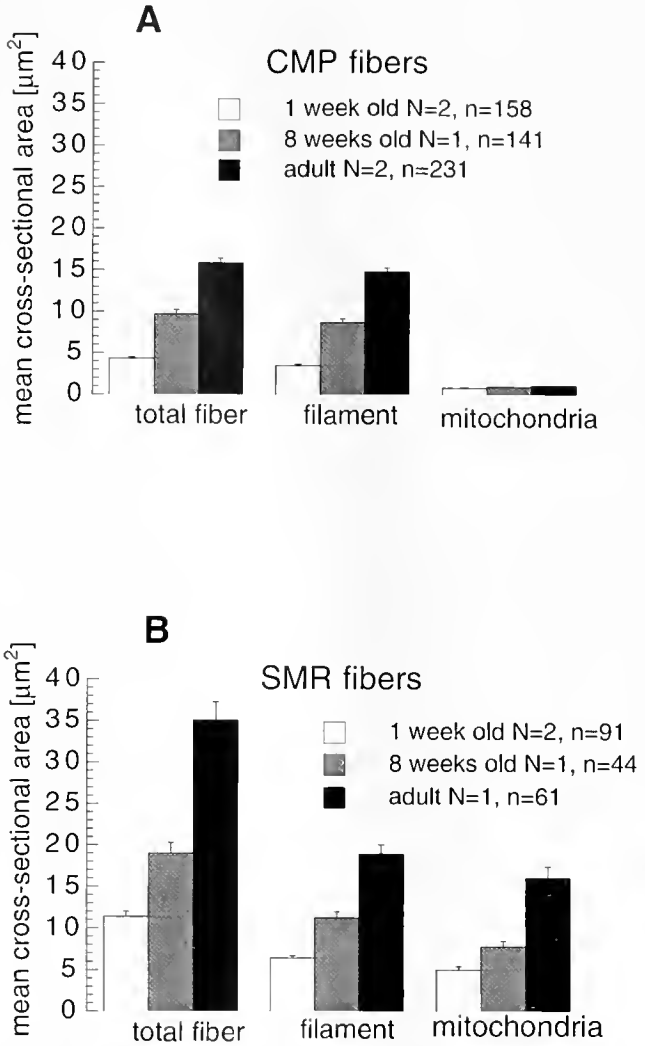

Figure 6. Characteristics of muscle fiber growth in CMP (A) and SMR (B) fibers. Individual histograms are given for the total cross-sectional fiber area, the filament and SR area, and the area occupied by the mitochondrial core for three maturity stages (means ± SEM; N = number of animals; n = number of measurements).

Mantle growth in squid is due to an increase in the size of existing muscle fibers (hypertrophy) and to recruitment of new fibers (hyperplasia). The extensive increase in fiber number in a single muscle segment, however, suggests that the latter mechanism is dominant in overall growth, and may also be responsible for the rapid somatic growth rates reported in squid (Forsythe and Van Heukelem, 1987). Similar growth mechanisms have been found in other squid (Moltschaniwskyj, 1994) and in teleost fish (Weatherley *et al.*, 1988).

On an ultrastructural level, hypertrophy in both SMR and CMP fibers is based on a steady increase in the number of myofilaments and, in the case of SMR fibers, the

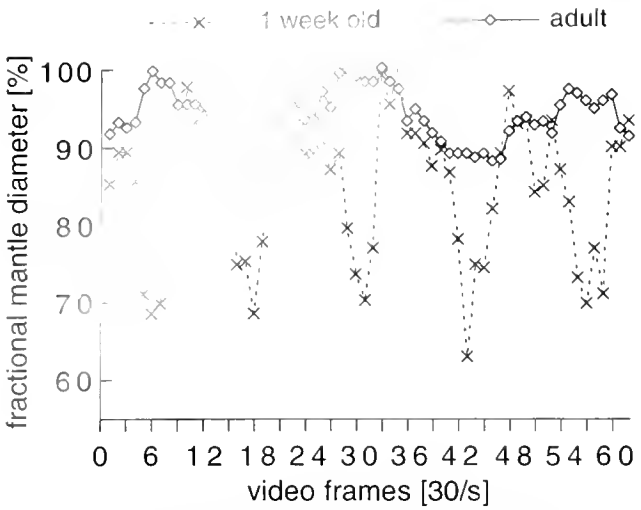

Figure 7. Mantle kinematics analyzed from video recordings of hovering or slow-swimming adult and juvenile squid. Mantle diameter was measured at the widest point (dorsal view), and the fractional mantle diameter was calculated by defining the largest diameter in a given measurement sequence as 100%. Time resolution is 30 frames/s.

size of the mitochondrial core. CMP fibers, however, show a selective hypertrophy of the myofilament and SR area and thus add a disproportional amount of force-generating capability at the individual fiber level. Nevertheless, hypertrophy of individual muscle fibers is limited by physiological constraints. For example, fibers requiring rapid excitation-contraction coupling in the absence of a transverse tubular system need to be small in diameter (Bone and Ryan, 1973; Bone *et al.*, 1995). This constraint would especially affect the presumptive fast-twitch CMP fibers with their high myofilament volume-to-surface ratio (Fig. 2). Such limitations on fiber diameter would indeed necessitate extensive recruitment of new CMP fibers (Fig. 5) to maintain rapid muscular responses as an animal grows throughout development.

Two biochemical results described in this paper support the idea that at least some CMP fibers display Na-channel-based excitability. Such excitability is consistent with the hypothesis that these are fast-twitch fibers responsible for all-or-none mantle contractions (Young, 1938; Gilly *et al.*, 1996). The first supporting evidence is that Na-channel protein is primarily expressed in the CMP fiber layer. Second, the increase of Na-channel protein seen in developing mantle is comparable to the selective hypertrophy and hyperplasia of CMP muscle fibers as shown by histology. The Na-channel band in muscle tissue is of lower apparent molecular weight than that detected in neuronal tissue (Figs. 8–10), and this suggests that a distinct Na-channel isoform exists in muscle. The exact relationship of this Na channel to the GFLN1-derived channels, which have a predicted core-polypeptide mass of 203 kD, is currently unknown.

Nerve terminals have been previously described in the mantle of other squid (Bone *et al.*, 1981, 1982, 1995) and

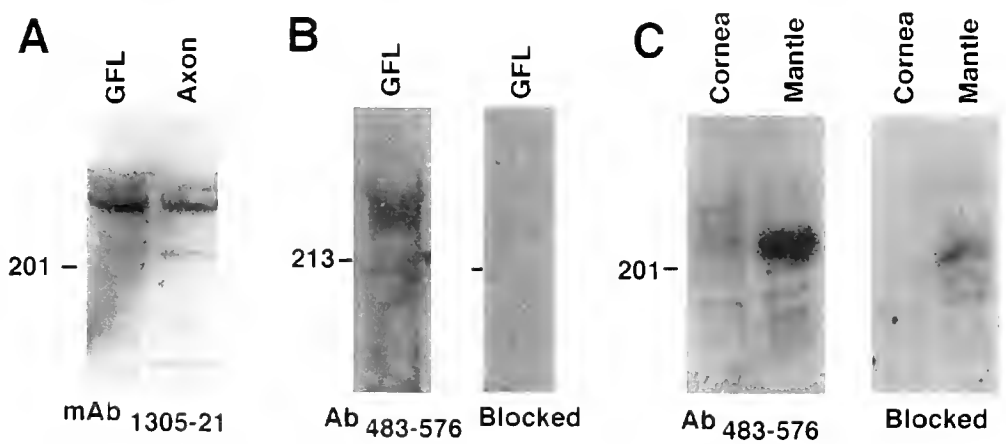

Figure 8. Specificity of Na-channel antibodies determined with immunoblots of samples of giant fiber lobe (GFL), cleaned giant axon, cornea, and mantle muscle. (A) $mAb_{1305-21}$ was used as undiluted hybridoma supernatant. Secondary goat anti-mouse antibody dilution was 1:5000. (B) $Ab_{483-576}$ was used at 1:1000 dilution, while dilution of secondary goat anti-rabbit antibody was 1:10,000. (C) $Ab_{483-576}$ used at 1:2000, dilution of secondary goat anti-rabbit antibody was 1:5000. Samples were prepared as described and separated on 5% SDS-PAGE gels. Each lane was loaded with 10 μg of total protein. Following transfer and antibody incubation, bands were detected by chemiluminescence reagent. A 260–280 kD band is detected in GFL and clean axon by monoclonal (A) and polyclonal (B) antibodies. A specific 210–220 kD band is present in mantle muscle, but not in cornea tissue (C). Blocking control was carried out as described in Methods.

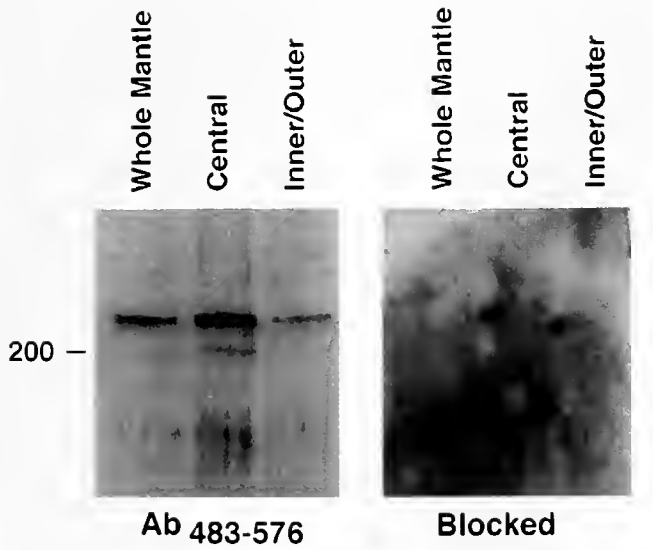

Figure 9. Identification of Na-channel protein in different layers of mantle muscle. Mantle muscle blocks were dissected to represent CMP fibers, SMR fibers, and whole mantle samples. $Ab_{483-576}$ was used at 1:1000 dilution; secondary goat anti-rabbit antibody dilution was 1:5000. Blocking control was prepared as described in Methods. Each lane was loaded with 10 μg of total protein. A 210–220 kD blockable band is detected in all samples. The band is most prominent in the CMP fiber sample, weaker in the SMR fiber sample, and strong in the whole-mantle sample. Although the CMP sample contains no SMR fibers, the SMR sample does contain some CMP fibers.

in other muscles of *Sepia* and *Octopus* (Graziadei, 1966). Although there is no direct evidence, the likely functional relationship between giant axons and CMP fibers (see above) and the large size of the neuronal processes contacting multiple CMP fibers (Fig. 4A, B) suggest that these processes may be the terminal branches of the giant axons. The origin of the terminal branches found within the SMR fibers remains unknown. Nevertheless, the detection of distinct size populations of vesicles in nerve profiles associated either with CMP or SMR fibers is consistent with the idea that different types of motor axons innervate the two fiber types (Bone *et al.*, 1981).

Muscle fiber recruitment takes place at different rates in CMP and SMR fibers during maturation; *i.e.*, the relative proportions of SMR to CMP fibers change progressively from 1:1 in hatchlings to 1:6 in adults. SMR fibers possess a high relative abundance of mitochondria (Figs 1–3) and a high content of oxidative enzymes (Mommsen *et al.*, 1981), which suggests that hatchlings and juveniles may have a higher demand for aerobic, fatigue-resistant muscles than do adults. This is consistent with our findings that the frequency and extent of mantle contractions during hovering (slow swimming) are substantially higher in juveniles than in adults (Fig. 7). These differences undoubtedly reflect the fact that juveniles are more negatively buoyant than adults (Zuev, 1966), and that, in contrast to adults, fin beating plays only a minor role during hovering (and for locomotion in general; v. Boletzky, 1982; Hoar *et al.*, 1994).

The disproportional increase of CMP fibers, on the other hand, suggests a higher demand for acceleration power in adults than in juveniles. It is clear that CMP fibers are necessary to produce the fast and powerful mantle contractions required for the high accelerations seen during escape- and attack-jets in all maturity stages (Gilly *et al.*, 1991). Indeed, Packard (1969) showed that acceleration power increases during development in *Loligo* (*i.e.*, an increase of power per unit weight of mantle muscle during escape-jets), which would be consistent with the disproportional increase of CMP fibers described in the present study.

The disproportional increase of CMP fibers may also reflect metabolic constraints due to the restricted capacity of hemocyanin to deliver oxygen (Wells, 1983; O'Dor *et al.*, 1990). This might effectively limit the proportion of aerobic SMR fibers in the mantle that can be supplied with oxygen (O'Dor, 1988), despite the heavy vascularization of this layer (Bone *et al.*, 1981). Even considering the fact that SMR fibers can be supplied with oxygen directly by diffusion through the skin (Wells and Wells, 1983; Pörtner, 1994), the size of the SMR fiber layer that

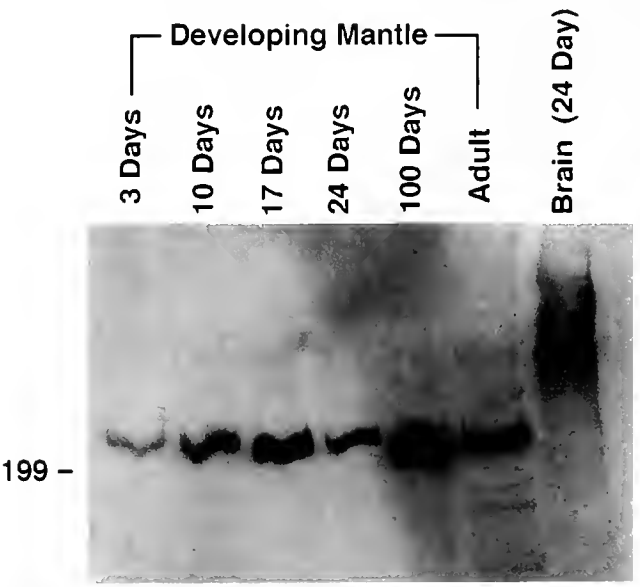

Figure 10. Apparent increase in abundance of Na-channel protein in developing mantle muscle. Mantle samples were collected from maturing squid and processed as described. In addition, a brain sample was included. $Ab_{483-576}$ was used in 1:1000 dilution, secondary antibody dilution was 1:5000. Each lane was loaded with 10 μg of total protein. The muscle samples show a 210–220 kD band of increasing intensity, whereas the brain sample shows a 260–280 kD band.

can thus be ventilated will be restricted. These constraints would again favor the recruitment of anaerobic CMP fibers during growth.

A final factor influencing the different ratios of SMR and CMP fibers found in hatchlings and adults pertains to growth-related changes in the forces acting on the body of a squid during jet-propelled swimming such as drag, thrust, and acceleration (Johnson *et al.*, 1972). Indeed, hatchlings and adults live at regimes of low and high Reynolds number respectively (Hoar *et al.*, 1994; Moltschaniwskyj, 1995); which, in turn, determines the relative importance of viscous and inertial effects on the hydrodynamic resistance to motion (Blake, 1983). For example, the movement of hatchlings ceases almost immediately when jet-propelled thrust stops, whereas adults coast over a considerable distance with a single jet (unpubl. data). These observations are consistent with the idea that viscous forces dominate over inertial forces in hatchlings and vice versa in adults. Thus, to cover any distance efficiently, hatchlings have to jet continuously because they cannot coast and therefore have a higher demand for aerobic, fatigue-resistant muscles than do adults.

Increasing size, on the other hand, places an additional constraint on the developing mantle muscle if rapid acceleration is to be maintained during growth. Inertial resistance is proportional to body mass, which increases as the third power of DML. Driving muscle force, on the other hand, is proportional to myofilament cross-sectional area, which increases with the square of DML (Daniel and Webb, 1987). Consequently, a disproportionate increase in fast-twitch CMP fibers would lead to a greater driving force for a given body size and, by tending to compensate for the increased inertial resistance as an animal grows, would help to maintain proper accelerations during escape- and attack-jets.

Acknowledgments

This material is based upon work supported by the National Institutes of Health under Grant No. NS-17510-14 and by the National Science Foundation under Grant No IBN-9631511. We are also grateful to Gilbert Van Dykhuizen and Reginald C. Gary (Monterey Bay Aquarium, California) for providing juvenile squid and to Dr. M. W. Denny for helpful comments on the manuscript.

Literature Cited

Amsellem, J., and G. Nicaise. 1980. Ultrastructural study of muscle cells and their connections in the digestive tract of *Sepia officinalis* L. *J. Submicrosc. Cytol.* **12(2):** 219–231.

Blake, R. W. 1983. *Fish Locomotion.* Cambridge University Press, Cambridge.

Boletzky, S. v. 1982. Developmental aspects of the mantle complex in coleoid cephalopods. *Malacologia* **23(1):** 165–175.

Boletzky, S. v. 1987. Juvenile behaviour. Pp. 45–60 in *Cephalopod Life Cycles—Volume II—Comparative Reviews,* P. R. Boyle, ed. Academic Press, London.

Bone, Q., and K. P. Ryan. 1973. The structure and innervation of locomotor muscles of salps (Tunicata: Thalicea). *J. Mar. Biol. Assoc. U. K.* **53:** 873–883.

Bone, Q., A. Pulsford, and A. D. Chubb. 1981. Squid mantle muscle. *J. Mar. Biol. Assoc. U. K.* **61:** 327–342.

Bone, Q., A. Packard, and A. L. Pulsford. 1982. Cholinergic innervation of muscle fibres in squid. *J. Mar. Biol. Assoc. U. K.* **62:** 193–199.

Bone, Q., E. R. Brown, and M. Usher. 1995. The structure and physiology of cephalopod muscle fibers. Pp. 301–329 in *Cephalopod Neurobiology,* N. J. Abbott, R. Williamson, and L. Maddock, eds. Oxford University Press, New York.

Chen, D. S., G. Van Dykhuizen, J. Hodge, and W. F. Gilly. 1996. Ontogeny of copepod predation in juvenile squid *(Loligo opalescens). Biol. Bull.* **190:** 69–81.

Daniel, T. L., and P. W. Webb. 1987. Physical determinants of locomotion. Pp. 343–369 in *Comparative Physiology: Life in Water and On Land,* P. Dejours, L. Bolis, C. R. Taylor, and E. R. Weibel, eds. IX-Liviana Press, Padova.

Forsythe, J. W., and W. F. Van Heukelem. 1987. Growth. Pp. 135–156 in *Cephalopod Life Cycles—Volume II—Comparative Reviews,* P. R. Boyle, ed. Academic Press, London.

Giese, A. C. 1969. A new approach to the biochemical composition of the mollusc body. *Oceanogr. Mar. Biol. Annu. Rev.* **7:** 175–229.

Gilly, W. F., M. T. Lucero, and F. T. Horrigan. 1990. Control of the spatial distribution of sodium channels in giant fiber lobe neurons of the squid. *Neuron* **5:** 663–674.

Gilly, W. F., B. Hopkins, and G. O. Mackie. 1991. Development of giant motor axons and neural control of escape responses in squid embryos and hatchlings. *Biol. Bull.* **180:** 209–220.

Gilly, W. F., T. Preuss, and M. B. McFarlane. 1996. All-or-none contraction and sodium channels in a subset of circular muscle fibers of squid mantle. *Biol. Bull.* **191:** 337–340.

Gonzalez-Santander, R., and E. S. Garcia-Blanco. 1972. Ultrastructure of the obliquely striated or pseudostriated muscle fibers of the cephalopods: *Sepia, Octopus* and *Eledone. J. Submicrosc. Cytol.* **4:** 233–245.

Gordon, D., D. Merrick, D. A. Wollner, and W. A. Catterall. 1988. Biochemical properties of sodium channels in a wide range of excitable tissues studied with site-directed antibodies. *Biochemistry* **27:** 7032–7038.

Gosline, J. M., J. D. Steeves, A. D. Harman, and M. E. DeMont. 1983. Patterns of circular and radial muscle activity in respiration and jetting of the squid *Loligo opalescens. J. Exp. Biol.* **104:** 97–109.

Graziadei, P. 1966. The ultrastructure of the motor nerve endings in the muscles of cephalopods. *J. Ultrastruct. Res.* **15:** 1–13.

Hoar, J. A., E. Sim, D. M. Webber, and R. K. O'Dor. 1994. The role of fins in the competition between squid and fish. Pp. 27–43 in *Mechanics and Physiology of Animal Swimming,* L. Maddock, Q. Bone, and J. M. V. Rayner, eds. Cambridge University Press, New York.

Johnson, W., P. D. Soden, and E. R. Trueman. 1972. A study in jet propulsion: an analysis of the motion of squid, *Loligo vulgaris. J. Exp. Biol.* **56:** 155–165.

Kier, W. M. 1985. The musculature of squid arms and tentacles: ultrastructural evidence for functional differences. *J. Morphol.* **185:** 223–239.

Kier, W. M. 1988. The arrangement and function of molluscan mus-

cle. Pp. 211–252 in *The Mollusca, Vol. II Form and Function*, E. R. Trueman and M. R. Clarke, eds. Academic Press, San Diego.

Knudson, C. M., N. Chandhari, A. H. Sharp, J. A. Powell, K. G. Beam, and K. P. Campbell. 1989. Specific absence of the α subunit of the dihydropyridine receptor in mice with muscular dysgenesis. *J. Biol. Chem.* **264:** 1345–1348.

Liu, T. I., and W. F. Gilly. 1995. Tissue distribution and subcellular localization of Na^+ channel mRNA in the nervous system of the squid *Loligo opalescens*. *Recept. Channels* **3:** 243–254.

Matsuno, A. 1987. Ultrastructural studies on developing oblique-striated muscle cells in the cuttlefish, *Sepiella japonica* Sasaki. *Zool. Sci.* **4:** 53–59.

Moltschaniwskyj, N. A. 1994. Muscle tissue growth and muscle fibre dynamics in the tropical loliginid squid *Photololigo sp.* (Cephalopoda: Loliginidae). *Can. J. Fish. Aquat. Sci.* **51:** 830–835.

Moltschaniwskyj, N. A. 1995. Changes in shape associated with growth in the loliginid squid *Photololigo sp.* morphometric approach. *Can. J. Zool.* **73:** 1335–1343.

Mommsen, T. P., J. Ballantyne, D. MacDonald, J. Gosline, and P. W. Hochachka. 1981. Analogues of red and white muscle in squid mantle. *Proc. Natl. Acad. Sci. USA* **78:** 3274–3278.

O'Dor, R. K. 1988. Limitations on locomotor performance in squid. *J. Appl. Physiol.* **64(1):** 128–134.

O'Dor, R. K., and M. J. Wells. 1978. Reproduction versus somatic growth: hormonal control in *Octopus vulgaris*. *J. Exp. Biol.* **77:** 15–31.

O'Dor, R. K., E. A. Fny, P. L. Helm, and N. Balch. 1986. The locomotion and energetics of hatchling squid, *Illex illecebrosus*. *Amer. Malacol. Bull.* **4(1):** 55–60.

O'Dor, R. K., H. O. Pörtner, and R. E. Shadwick. 1990. Squid as elite athletes: locomotory, respiratory, and circulatory integration. Pp. 481–503 in *Squid As Experimental Animals*, D. L. Gilbert, W. J. Adelman, and J. M. Arnold, eds. Plenum Press, New York.

Packard, A. 1969. Jet propulsion and the giant fibre response of *Loligo*. *Nature* **221:** 875–877.

Pörtner, H. O. 1994. Coordination of metabolism, acid-base regulation and hemocyanin function in cephalopods. *Mar. Fresh. Behav. Physiol.* **25:** 131–148.

Rosenbluth, J. 1972. Obliquely striated muscle. Pp. 389–419 in *The Structure and Function of Muscle—Vol. 1*, G. H. Bourne, ed. Academic Press, New York.

Rosenthal, J. J. C. 1996. Molecular identification of the ion channels underlying the action potential in the squid giant axon. Ph. D. Thesis, Department of Biological Sciences, Stanford University.

Rosenthal, J. J. C., and W. F. Gilly. 1993. Amino acid sequence of a putative sodium channel expressed in the giant axon of the squid *Loligo opalescens*. *Proc. Natl. Acad. Sci. USA* **90:** 10026–10030.

Ward, D. V., and S. A. Wainwright. 1972. Locomotory aspects of squid mantle structure. *J. Zool. (Lond.)* **167:** 437–449.

Weatherley, A. H., H. S. Gill, and A. F. Lobo. 1988. Recruitment and maximal diameter of axial muscle fibers in teleosts and their relationship to somatic growth and ultimate size. *J. Fish Biol.* **33:** 851–859.

Wells, M. J. 1983. Circulation in cephalopods. Pp. 239–290 in *The Mollusca, Vol 5*, K. M. Wilbur, ed. Academic Press, London.

Wells, M. J. 1988. Mantle muscle and mantle cavity in cephalopods. Pp. 287–300 in *The Mollusca—Form and Function*, E. R. Trueman and M. R. Clarke, eds. Academic Press, San Diego.

Wells, M. J., and J. Wells. 1983. The circulatory response to acute hypoxia in *Octopus*. *J. Exp. Biol.* **104:** 59–71.

Young, J. Z. 1938. The functioning of the squid giant nerve fibres of the squid. *J. Exp. Biol.* **15:** 170–185.

Zuev, G. V. 1966. Characteristic features of the structure of cephalopod molluscs associated with controlled movements. *Fisheries Research Board of Canada Translation Series No. 1011 1968.*

Reference: *Biol Bull* **192**: 388–398. (June, 1997)

Fine Structure of the Apical Ganglion and Its Serotonergic Cells in the Larva of *Aplysia californica*

RENÉ MAROIS[1,*] AND THOMAS J. CAREW[2]

[1]*Interdepartmental Neuroscience Program and* [2]*Departments of Biology and Psychology, Yale University, New Haven, Connecticut 06520*

Abstract. The apical ganglion is a highly conserved structure present in various marine invertebrate larvae. Although one of the hallmarks of this ganglion is the presence of serotonergic cells, little is known about the structure and function of these cells. We have examined this ganglion in larvae of the marine mollusc *Aplysia* with light- and electron-microscopic immunocytochemistry. The results indicate that the cellular composition of the apical ganglion of *Aplysia* is very similar to that of other opisthobranchs. It consists of three classes of sensory cells (ampullary, para-ampullary, and ciliary tuft cells) and of other nerve cell types. Almost a third of the cells in the apical ganglion of *Aplysia* are serotonergic, and these can be divided into two classes: three para-ampullary and two interneuronal cells. All of the serotonergic cells extend an axon into the central nervous system. The variety of sensory and serotonergic cell types suggests that each type processes distinct attributes of the sensory environment. We argue that the apical ganglion, by virtue of its serotonergic cells, is well-suited to play important roles in the integration of sensory information to achieve proper motor adaptation to variable seawater conditions.

Introduction

One of the most highly conserved neuronal structures across phyla is the apical ganglion (AG) (Nielsen, 1994). Also referred to as the apical sensory organ, the apical organ, or the cephalic sensory organ, the AG has so far been extensively described in the embryos, larvae, or both of cnidarians (Chia and Koss, 1979; Fukui, 1991), turbellarians (Lacalli, 1982; 1983), polychaetes (Lacalli, 1981; 1984), molluscs (Bonar, 1978; Chia and Koss, 1984; Page, 1992, Tardy and Dongard, 1993; Kempf and Page, 1995); brachiopods (Hay-Schmidt, 1992); phoronids (Hay-Schmidt, 1989; Lacalli, 1990), echinoderms (Bisgrove and Burke, 1986; Chia *et al.*, 1986; Nakajima, 1988; Nakajima *et al.*, 1993), and hemichordates (Dautov and Nezlin, 1992). A homologous structure may also occur in cephalochordates (Lacalli, 1994; Lacalli *et al.*, 1994). Although the precise function of this organ remains to be determined, its subcellular and cellular structures, as well as its superficial anterior position just above the mouth, have led to the suggestion that the AG is likely to be involved in sensing ambient water conditions during locomotion, feeding, and metamorphosis (Bonar, 1978; Chia and Koss, 1984).

Despite considerable variations in their fine structure, the apical ganglia of all species examined to date appear to share two characteristics: first, the presence of modified epithelial or subepithelial cells that give rise to an external tuft of nonmotile cilia; and second, the presence of serotonergic cells (Bisgrove and Burke, 1986, 1987; Nakajima, 1988; Hay-Schmidt, 1990, 1992, 1995; Kempf *et al.*, 1991; Nakajima *et al.*, 1993; Moss *et al.*, 1994; Lacalli, 1994; Kempf and Page, 1995). Despite their pervasive nature, very little is known of the structure, identity, and functions of the serotonergic neurons in the apical ganglion.

The present study describes the fine structure of the AG and its serotonergic cells in the larva of the marine mollusc *Aplysia californica*. In addition to shedding some light on the biology of the serotonergic (5HT) cells, this detailed study of the serotonergic constituents of the AG also aims at achieving a better understanding of the functions of this anatomical structure. This work is also the first to describe the presence of an apical ganglion in

Received 7 October 1996; accepted 12 April 1997.

* Present address: Department of Diagnostic Radiology, Yale University School of Medicine, New Haven, CT 06520-8042.

Aplysia. Surprisingly, despite the fact that this animal has been a favorite preparation of neurobiologists and the focus of a number of neurodevelopmental studies (Saunders and Poole, 1910; Kriegstein, 1977a, b; Schacher *et al.*, 1979a, b; Jacob, 1984), the apical ganglion has hitherto gone unnoticed in *Aplysia*.

Some of the results presented in this paper have been previously reported in abstract form (Marois *et al.*, 1992, 1993).

Materials and Methods

Mariculture

Animals were collected and maintained as described in Marois and Carew (1997a). Seven-day-old embryos (7 days after oviposition), hatchlings (9 days after oviposition), and 2-day-old larvae (11 days after oviposition) were used in this study. In addition, older (Stage 2 and 3) larvae were used for histological characterization and localization of the apical ganglion. The animals were staged according to the criteria of Kriegstein (1977a).

Immunocytochemistry (ICC)

All the immunocytochemical and ultrastructural techniques were performed as described in Marois and Carew (1997a). The specificity of the serotonin antibody used has been previously demonstrated (Marois and Carew, 1997a). The results are based on semi-thin and ultra-thin sectioning of the apical ganglion of at least 10 animals, and on whole-mount processing of at least 50 animals.

Whole-mount immunocytochemistry. Animals were first anesthetized in a $MgCl_2$ solution isotonic to seawater for 5 min at room temperature (rt), followed by 8 min on ice. Animals were then immersed in three changes of ice-cold fixative solution (4% paraformaldehyde in Millonig's phosphate buffer saline [PBS]) for 30 min, and then left in the fixative solution at 4°C for an additional 2.5 h (total fixation time: 3 h). After five 4-min washes in PBS, Stage 1–6 larvae were exposed to trypsin (Type 1, Sigma, St. Louis, MO, 0.1% in PBS for 5 to 15 min at rt) and specimens were then immersed in 4% Triton X-100 (TX-100) in PBS for 1 h, rinsed in PBS, exposed to 10% EDTA in PBS for 45 min at rt to decalcify the shell, and rinsed in PBS. This was followed by pre-incubation in 2% goat serum (GS), 0.5% TX-100 in PBS for 1 h at 4°C, and by a primary (1°) Ab incubation (rabbit anti-serotonin, Incstar, Stillwater, MN; 1:650 in pre-incubation serum) for 2.5 days at 4°C on a shaker. The animals were then rinsed in PBS, pre-incubated in 2% GS in PBS for 1 h at 4°C, and immersed in secondary (2°) Ab solution (fluorescein isothiocyanate [FITC]-linked goat anti-rabbit IgG, Sigma, St. Louis, MO, 1:50 in PBS with 2% GS, 0.5% TX-100) for 2.5 h at 4°C, and rinsed in PBS. The specimens were mounted in a 3:1 glycerine:PBS solution, viewed under FITC optics (excitation filter, 480 nm; barrier filter, 520 nm) on a Nikon Optiphot-2 microscope, and photographed with Ilford XP2 400 or Kodak Ektachrome 400 film.

Sectioned tissue immunocytochemistry. Embryos and larvae were prepared as above, with the following modifications. 2° Ab (goat anti-rabbit IgG, Cappel; 1:50 in 2% GS, 0.5% TX-100 in PBS for 2 h at rt), and 3° Ab (rabbit peroxidase anti-peroxidase (PAP), Cappel; 1:50 in 2% GS, 0.5% TX-100 in PBS for 2 h at rt). Following the PBS rinses after the 3° Ab solution, the animals were processed for horseradish peroxidase (HRP) reaction (15 min in 0.05% DAB in PBS at rt; followed by 45 min in 0.005% H_2O_2, 0.05% DAB in PBS), rinsed in PBS, and dehydrated in an alcohol series (50, 70, 80, 95, and 3× 100% ethanol), and infiltrated in Epon (3× propylene oxide (PO); 2:1 PO:Epon; 1:2 PO:Epon, and pure Epon). A few animals were not processed for ICC and instead were stained with the Richardson's solution (Richardson *et al.*, 1960). All animals were sectioned on a Sorvall MT-2 ultramicrotome. Sections were viewed under a Nikon Optiphot-2 microscope and photographed with Kodak T-MAX 100 film.

Immuno-electron microscopy

Embryos or larvae were anesthetized as described above. They were fixed for 30 min on ice and then for 3 h at 4°C on a shaker in 4% paraformaldehyde, 0.12% glutaraldehyde, 20% sucrose in Millonig's phosphate buffer (PB). After PBS rinses, the animals were decalcified in 10% EDTA in PBS (PB with 0.9% NaCl) for 45 min at rt, exposed to 1% NaH_2B_4 in PBS for 1 h at rt, rinsed in PBS, exposed to 0.05% trypsin for 15 min, and rinsed in PBS. This was followed by freeze-thawing: the animals were first immersed at 4°C for 2 h in cryoprotectant (25% sucrose, 10% glycerol in 0.1 *M* PB), then subsequently dipped in liquid N_2-cooled iso-pentane and in liquid N_2, and rinsed in PBS. The 1°, 2°, and tertiary (3°) Ab incubations were performed as for sectioned tissue ICC except that the pre-incubations lasted 2 h and no TX-100 was present in the pre-incubation and incubation solutions. The HRP reaction was performed as for sectioned tissue ICC, except that a metal-enhanced DAB substrate was used (Pierce, Rockford, IL; 45–60 min incubation followed by PBS rinses). The animals were subsequently osmicated in 2% OsO_4 in PBS for 1 h at rt on a shaker, and dehydrated and infiltrated in Epon as described for sectioned tissue ICC. Serial silver and gold sections were cut on a Sorvall MT-2 microtome and collected serially on either Formvar-coated slot copper grids or Thin-200 copper grids (EMS, Fort Washington, PA).

The sections were viewed under a Philips 300 or Zeiss EM-10 transmission electron microscope at 80 kV.

Ultrastructure (SEM)

Animals were anesthetized as described above and fixed in 2.5% glutaraldehyde, 20% sucrose in 0.1 *M* PB for 30 min on ice followed by 2.5 h at 4°C on a shaker. After several PBS rinses, animals were osmicated, rinsed in PBS, decalcified in 10% EDTA in PBS, rinsed in PBS, and dehydrated and infiltrated as described above. Silver and gold sections were cut and collected as described above. The grids were then stained for 12–15 min in 3% uranyl acetate and for 5 min in 0.3% lead citrate, and viewed as described above.

Results

General observations

The veliger of *Aplysia californica* possesses an apical ganglion (AG), located above and between the cerebral ganglia (Figs. 1, 2). It sits atop the cerebral commissure and is composed of 15 to 20 cells, many of which are heavily ciliated (Fig. 2). Since this structure is strikingly similar to the AG in the nudibranch *Rostanga pulchra* (Chia and Koss, 1984), we have adopted the same nomenclature to describe the components of this ganglion in *Aplysia*. As in *Rostanga*, three major types of cells were observed in the AG of *Aplysia:* (1) four ampullary cells with large, heavily ciliated lumina; (2) three para-ampullary cells that extend one or two cilia from their apical surface; and (3) two ciliary tuft cells that project numerous long cilia from their apical surface. All of these cells send anterior apical projections that follow one of three tracts (left, right, and medial tracts) to reach the epithelial surface (Fig. 3). In addition to these cell types, the AG contains a few posterior cells that do not have any apical projections, and a dense neuropilar region located posterior and medial to all of these cells (Fig. 2B). This neuropil is in contact with the underlying cerebral commissure (Fig. 2A). Immunocytochemical staining for serotonin reveals that five cells of the AG are serotonergic (the three para-ampullary cells and two posterior cells; Fig. 4A). These are the only serotonergic cells in the entire CNS of the newly hatched *Aplysia* veliger (Marois and Carew, 1997a).

Fine structure of the major cell types in the AG

Ampullary cells. These are four centrally positioned cells, each containing a large lumen densely populated with cilia (Figs. 2, 3A, 4B). Posteriorly the cells border the neuropilar region, while anteriorly their cytoplasm funnels to a constricted neck to expand again as a swelling at the epithelial surface (Figs. 3A, 4B). Numerous microvili and one or two cilia protrude externally from these swellings (Figs. 3A, 4B). These apical cilia are distinct from the cilia in the lumen. The latter are entirely contained inside the lumen and do not pierce through the epithelial surface (Figs. 3A, 4B). The bases of these internal cilia are anchored into the cytoplasm of the ampullary cells (Fig. 3B). None of the ampullary cells are serotonergic.

Para-ampullary cells. This set of three cells surround-

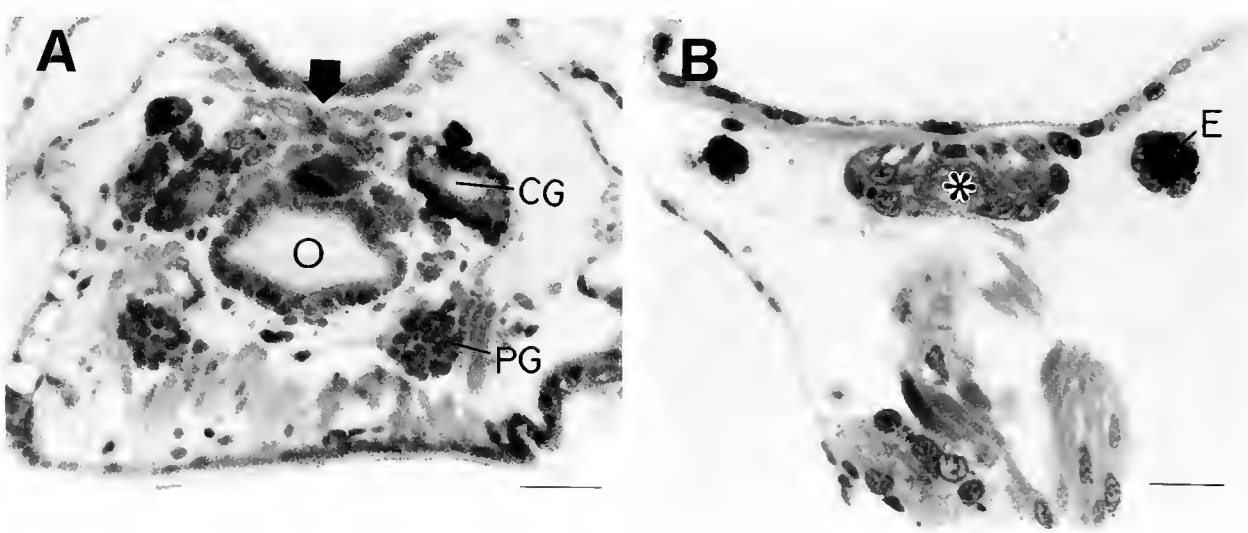

Figure 1. Position of the apical ganglion (AG) in *Aplysia* veligers. (A) Cross-section of a Stage 2 larva showing the AG (arrow) between the cerebral ganglia (CG) and above the oesophagus (O). (B) Horizontal section through the AG (asterisk). E, eye; PG, pedal ganglion. Scale bar: A, 20 μm; B, 15 μm.

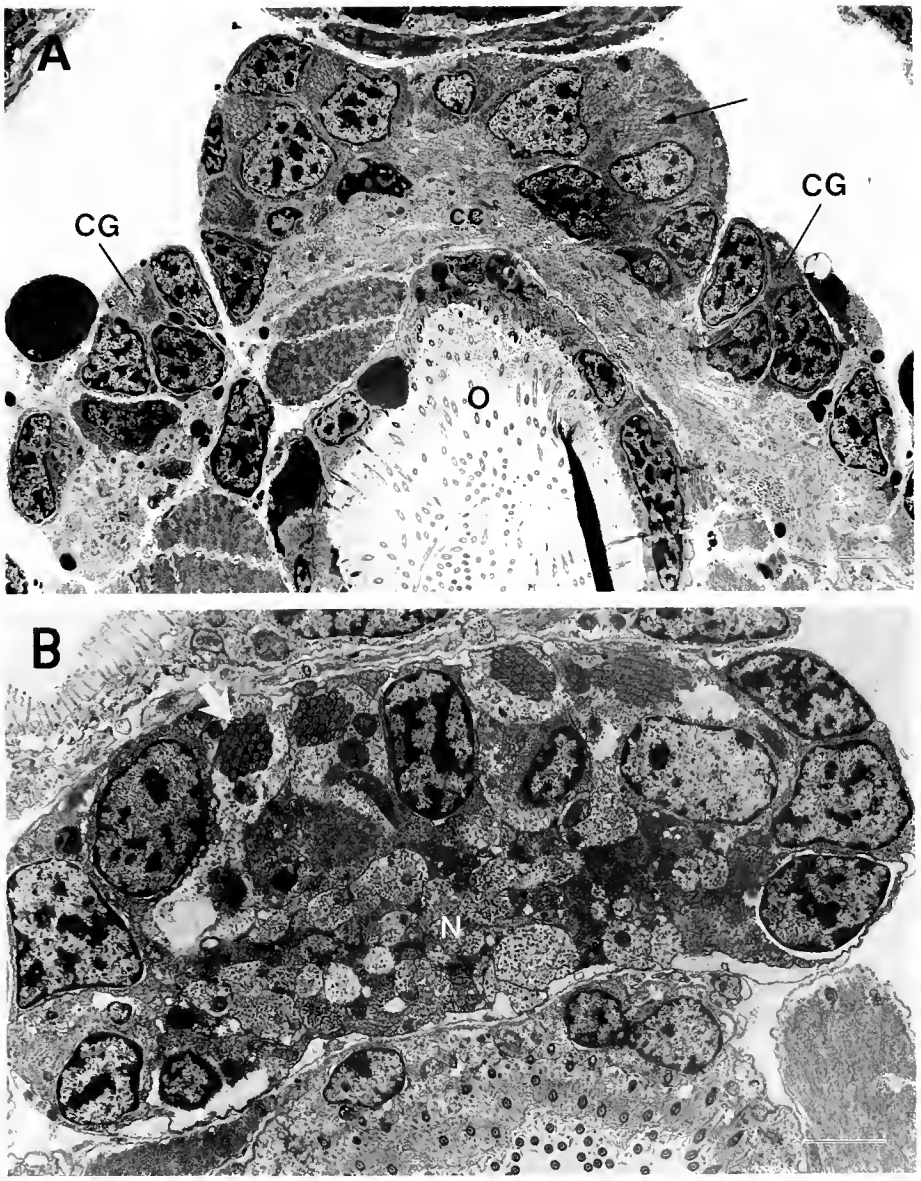

Figure 2. Ultrastructure of the apical ganglion. (A) Cross-section shows the AG above the cerebral commissure (cc) and between the cerebral ganglia (CG). Note the cilia (arrow) in the ampullary cells. (B) Horizontal section through the AG. Anterior is up. Note ciliary bundles (white arrow) inside the ampullary cells and a neuropil (N) posterior to these cells. O, oesophagus. Scale bar: A and B, 2 μm.

ing the ampullary cells is immunoreactive for serotonin: two of the cells are laterally positioned, and the third is centrally located between the two pairs of ampullary cells (Fig. 4A). These cells correspond to the para-ampullary cells of *Rostanga* (Chia and Koss, 1984). Each para-ampullary cell sends an anterior projection to the epithelial surface of the apical ganglion (Figs. 4, 5, 6). The projections of the lateral pair follow the lateral tracts (Figs. 4, 6), whereas the projection of the median cell emerges from the ventral side of the cell and bends anteriorly to reach the epidermal surface beneath the central tract (Fig. 5B). These three processes enlarge at the epithelial surface. From the swellings, one or two short, curly cilia extend into the external environment (Figs. 3A, 4B, 5A). The swellings also contain numerous mitochondria (Figs. 3A, 4B) and bear microvili (Fig. 3A). These expansions are linked together and to the adjacent epithelial cells by zonula adherens (Fig. 3A). In addition to their anterior projections, each of these three cells also sends a projection into the central neuropil (Fig. 4A), which appears to be heavily populated with serotonergic fibers (Fig. 5A). The distant target tissues of these central neu-

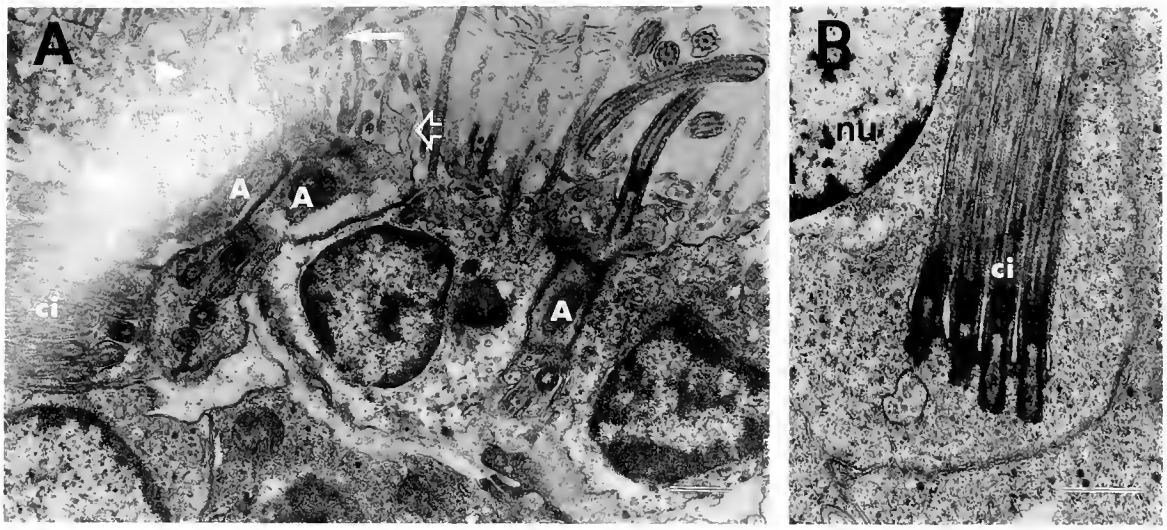

Figure 3. Cilia in the apical ganglion. Horizontal sections, anterior is up. (A) The apical projections of the AG cells follow tracts to the epithelial surface. The left lateral tract consists of two ampullary cell processes (A) and one para-ampullary cell process (P); the median tract has a single ampullary cell projection (A). The apical swellings of these projections extend cilia (arrow) and microvili (open arrow). The swellings are linked to each other and to the adjacent epithelial cells with zonula adherens (arrowheads). An ampullary cell contains an internal ciliary bundle (ci). (B) A ciliary bundle (ci) is attached to the cytoplasm of an ampullary cell. m, mitochondria; nu, nucleus. Scale bar: A, 0.5 μm; B, 0.5 μm.

ropilar projections have been described elsewhere (Marois and Carew, 1997b). Under conventional electron microscopy, the cytoplasm of the para-ampullary cells appears very granular and contains lipid yolk droplets, mitochondria, and small (40–60 nm) clear and dense-core vesicles (Fig. 4C). Unlike the ampullary cells, the para-ampullary cells do not contain lumina densely packed with cilia.

Ciliary tuft cells. A bilateral pair of rectangular cells is located at the anterior and ventral edge of the AG (Fig. 6). Each cell sends a cytoplasmic projection anteriorly into the lateral tracts, underneath the projections of the ampullary and para-ampullary cells. After narrowing in the lateral tracts, the projections expand considerably at the apical surface of the AG (Fig. 7). At least five long cilia emerge from each of these two large apical swellings (Figs. 6, 7). These cilia are anchored to the swellings by long ciliary rootlets and dense basal bodies (Fig. 7). Mitochondria are found at the bases of the cilia. The swellings are linked by zonula adherens to epidermal cells, to the serotonergic swelling of the unpaired median para-ampullary cell, and to each other.

Other serotonergic and non-serotonergic cells. There are six to eight other cells in the AG at hatching. Two of them are immunoreactive for serotonin (Figs. 4A, 6). These 5HT cells are located immediately posterior and slightly medial to the lateral pair of para-ampullary serotonergic cells (Figs. 4A, 6). Each of these cells extends a single process into the neuropil of the AG (Fig. 4A). Since these cells have not been identified in *Rostanga* (Chia and Koss, 1984) and since they do not extend any apical projections, they are referred to as serotonergic interneurons. Little is known about the remaining cells of the AG except that they do not appear to have any apical processes and are not immunoreactive for serotonin. The structure of the apical ganglion and of its principal cellular constituents in *Aplysia* is summarized in Figure 8.

Discussion

General structure of the AG of Aplysia *and other gastropods*

The AG of *Aplysia* is strikingly similar to the apical ganglion of the opisthobranch *Rostanga pulchra* (Chia and Koss, 1984). They both have the same number and major types of cells: four ampullary cells, three para-ampullary cells, and two ciliary tuft cells. The only notable difference is that the cell bodies and apical projections of the ciliary tuft cells are ventral to the other cells in the AG of *Aplysia*, but they seem to occupy a dorsal position in *Rostanga* (Chia and Koss, 1984).

It is intriguing that the structure of the AG in both *Aplysia* and the nudibranch *Rostanga* (Chia and Koss, 1984) differs markedly from that of another nudibranch, *Phestilla sibogae* (Bonar, 1978): Ciliary tuft cells, characterized by apical projections having many long, deeply rooted cilia, appear to be absent in *Phestilla*. Neverthe-

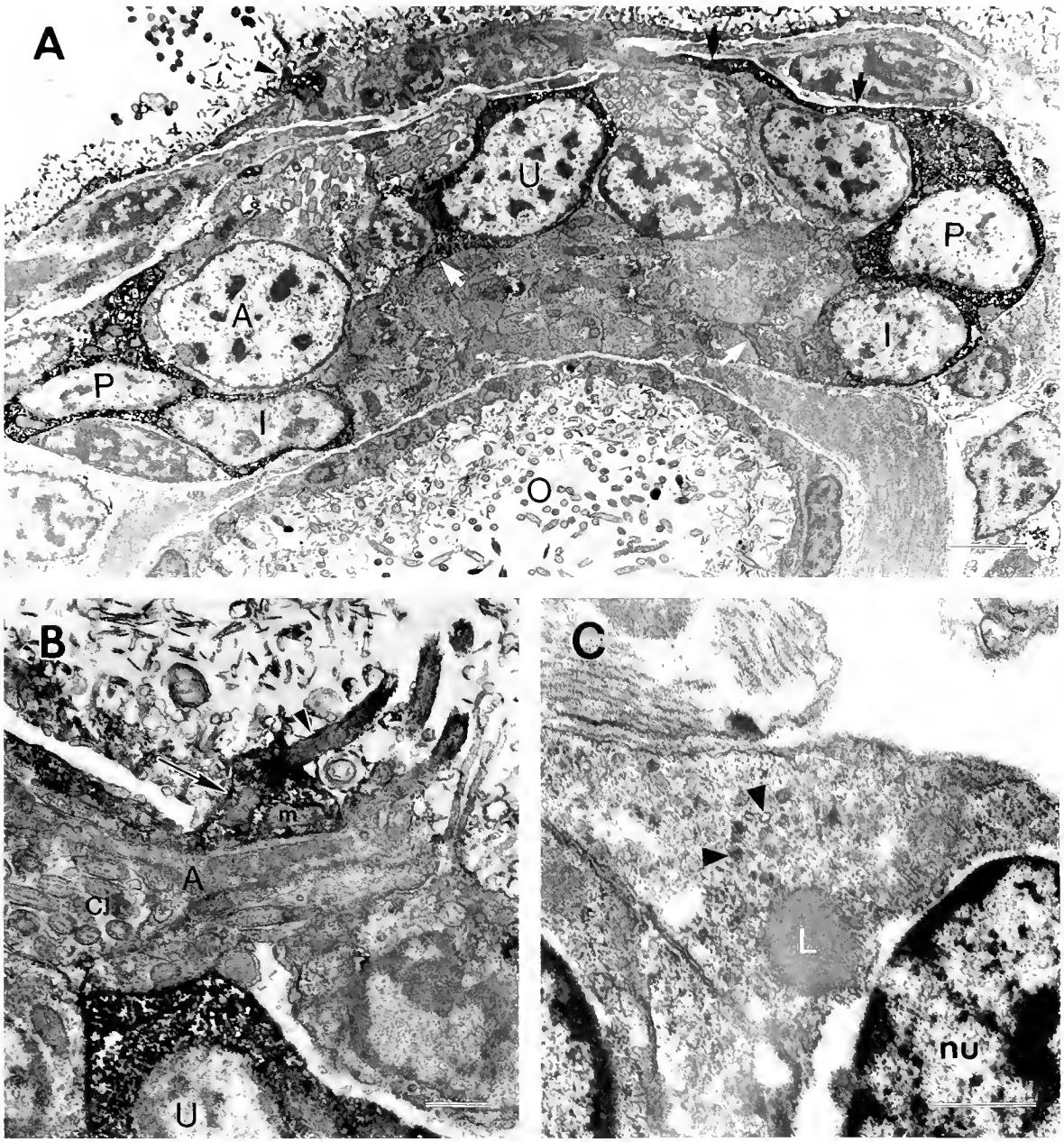

Figure 4. Serotonergic cells of the apical ganglion. Horizontal sections, anterior is up. (A) The lateral (P) and unpaired median (U) para-ampullary cells are serotonergic. Two interneurons (I) posterior to the lateral para-ampullary cells are also serotonergic. Note the apical projection (small black arrows) of a para-ampullary cell, the apical swelling of another (black arrowhead), and the central projections (small white arrows) of a para-ampullary cell and an interneuron. (B) Apical swelling (arrow) of a serotonergic para-ampullary cell. A cilium (arrowhead) extends from the external surface of the swelling. Note the cilia (ci) and apical process of the adjacent ampullary cell (A). (C) Fine structure of a para-ampullary cell processed for conventional electron microscopy. The cytoplasm contains lipid yolk droplets (L), and clear and dense-core vesicles (arrowheads). A, ampullary cell; ci, ciliary bundle; O, oesophagus; nu, nucleus; U, unpaired median para-ampullary cell. Scale bar: A, 2 μm; B 0.5 μm; C, 0.5 μm.

less, other cell types appear structurally similar to those of *Aplysia*. Thus, the ampullary cells of *Aplysia* and *Rostanga* are very similar to the flask-shaped cells of *Phestilla* (Bonar, 1978), with the notable difference that the ciliary bundles in *Phestilla* are not restricted to the lumen but extend to the surface of the animal. Likewise,

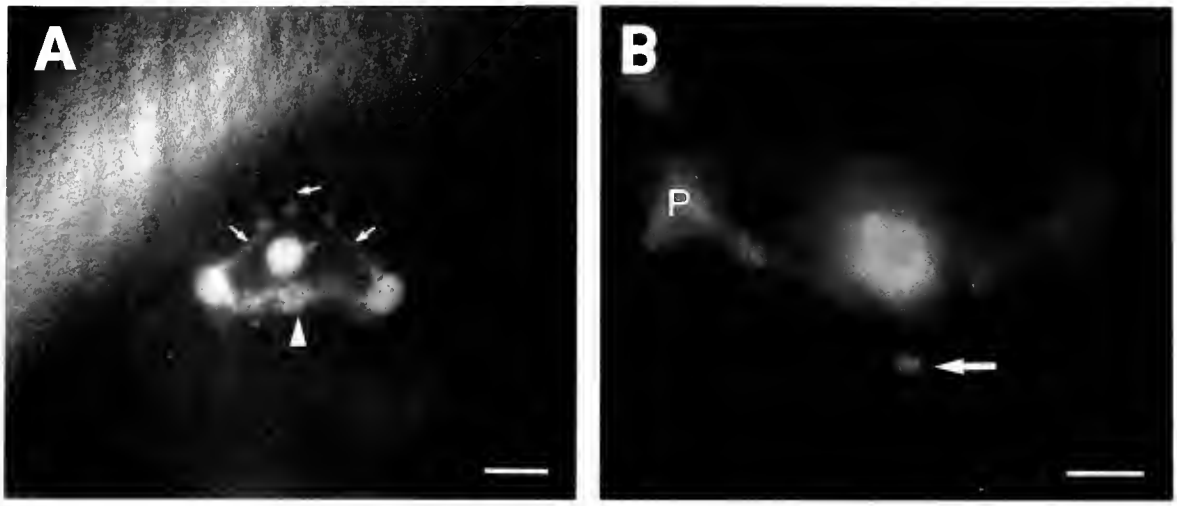

Figure 5. Serotonergic cells of the apical ganglion. (A) Dorsal view, anterior is up. Whole-mount immunocytochemistry in a late-stage embryo shows central projections in the neuropil (arrowhead) and apical projections with terminal cilia (small arrows) of the para-ampullary cells. (B) Frontal whole-mount ICC shows the apical projection terminating as a swelling (arrow). P, para-ampullary cell. Scale bar: A, 10 μm; B, 5 μm.

Figure 6. Oblique horizontal section through the apical ganglion showing two serotonergic para-ampullary (P) cells and interneurons (I) and a ciliary tuft cell (asterisk). Note the apical projection (arrowheads) of a para-ampullary cell, and the long cilia (arrow) of a ciliary tuft cell. O, oesophagus. Scale bar: 2 μm.

the cells referred to as support cells in *Phestilla* (Bonar, 1978) strongly resemble the para-ampullary cells of *Rostanga* and *Aplysia*. They surround the flask-shaped cells, and each has a narrow process extending to the surface and giving rise to microvilli and one or two cilia. Although the striking similarities between the AG cells of

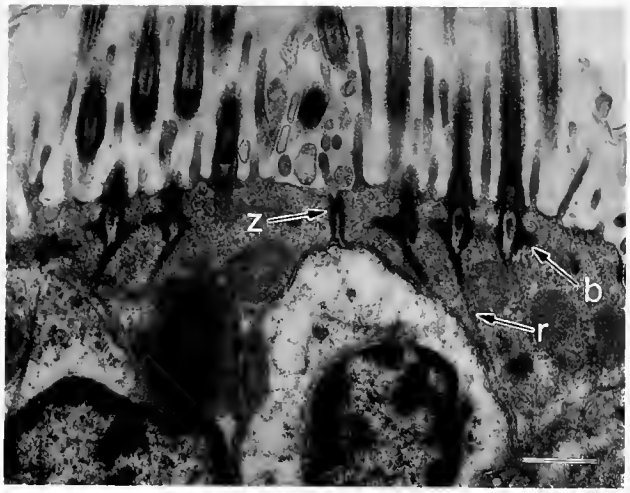

Figure 7. Apical projections of the ciliary tuft cells. Horizontal section, anterior is up. b, basal bodies of cilia; r, rootlet of cilia; z, zonula adherens. Scale bar, 0.5 μm.

Rostanga, Phestilla, and *Aplysia* suggest that these structures are truly homologous, more detailed phyletic studies of the AG in various prosobranchs and opisthobranchs are required before the homology is demonstrated conclusively.

Functions of the ciliated cells of the apical ganglion

The morphology of the three ciliated cell types of the AG is very similar to the known morphology of epithelial chemoreceptor and mechanoreceptor cells in sensory organs of adult *Aplysia* and other invertebrates and vertebrates (Laverack, 1974; Wright, 1974; Emery and Audesirk, 1978; Altner and Prillinger, 1980; Dorsett, 1986). In addition, ultrastructural examinations of the cilia of apical ganglion cells have consistently indicated that, unlike the motile cilia of the velar cells, these cilia are nonmotile: They have a 9 + 2 microtubular arrangement lacking the dynein arms that confers motility to the cilia (Bonar, 1978; Dorsett, 1986; Nakajima, 1988). Taken together, these findings strongly suggest that the ciliated cells of the AG are sensory cells. The additional finding that these ciliated cells can be classified into three morphological groups in *Aplysia* and *Rostanga* implies that each class may serve a distinct sensory function. Chia and Koss (1984) have proposed that in *Rostanga* the internal ciliary bundles of the ampullary cells have a role in vibration or pressure detection, the long numerous cilia of the ciliary tuft cells act as distance chemoreceptors, and the short curly cilia of the para-ampullary cells act as contact chemoreceptors. Although only the para-ampullary cells were examined for central axonal projections in the present study, in *Rostanga* the three cell types extend axons into the AG neuropil (Chia and Koss, 1984). These results suggest that information about the veliger's aquatic surroundings is first gathered by the primary sensory ciliated cells of the AG and subsequently conveyed to the CNS of the animal.

Serotonergic cells in the apical ganglion of Aplysia *and other gastropods*

Despite the notable differences in the structure of the AG across phyla, when serotonergic neurons have been looked for in this organ, they have invariably been found. Serotonergic neurons have been observed in the AG or apical region of the nudibranch *Berghia* (Kempf *et al.,* 1991; Kempf and Page, 1995), the prosobranch *Haliotis* (Barlow and Truman, 1992), phoronids (Hay-Schmidt, 1990), polychaetes (Hay-Schmidt, 1995), brachiopods (Hay-Schmidt, 1992) and various echinoderms (Moss *et al.,* 1994; Bisgrove and Burke, 1986; 1987; Nakajima, 1988; Nakajima *et al.,* 1993). In addition, serotonergic neurons are associated with the extreme anterior end of the amphioxus nerve cord (Holland and Holland, 1993), a region postulated to be derived from the apical organ of invertebrate ancestors (Lacalli, 1994; Lacalli *et al.,* 1994). However, it is difficult to compare the fine structure of the serotonergic cells of *Aplysia* with those of other species because these other studies have predominantly been limited to a whole-mount, light microscopic level of analysis. Nevertheless, serotonergic cells with the gross morphology of the para-ampullary cells of *Aplysia* (a short apical projection and a basal axonal process) have been observed in the apical organs of some echinoderms (Bisgrove and Burke, 1986; 1987; Nakajima, 1988), and serotonergic cells extending only basal processes, similar to the serotonergic interneurons of *Aplysia,* have been observed in polychaete and brachiopod larvae (Hay-Schmidt, 1992; 1995). Although these findings could be interpreted as indicating that the two classes of serotonergic cells observed in *Aplysia* may be differentially represented in other phyla, an examination of the fine structure of the 5HT cells in these other animal groups may reveal instead that they do not correspond to either of the two serotonergic classes in *Aplysia.*

Functions of the serotonergic cells in the AG

The serotonergic cells make up about a third of the entire cellular population of the AG. This sheer number suggests that serotonergic cells are important components of the AG. Furthermore, the distinct morphology of the para-ampullary and interneurons suggests that these two types of serotonergic cells serve different functions. As mentioned above, the three para-ampullary serotonergic cells are probably sensory (Chia and Koss, 1984). Because the serotonergic interneurons do not possess an apical process or any cilia, it is unlikely that they

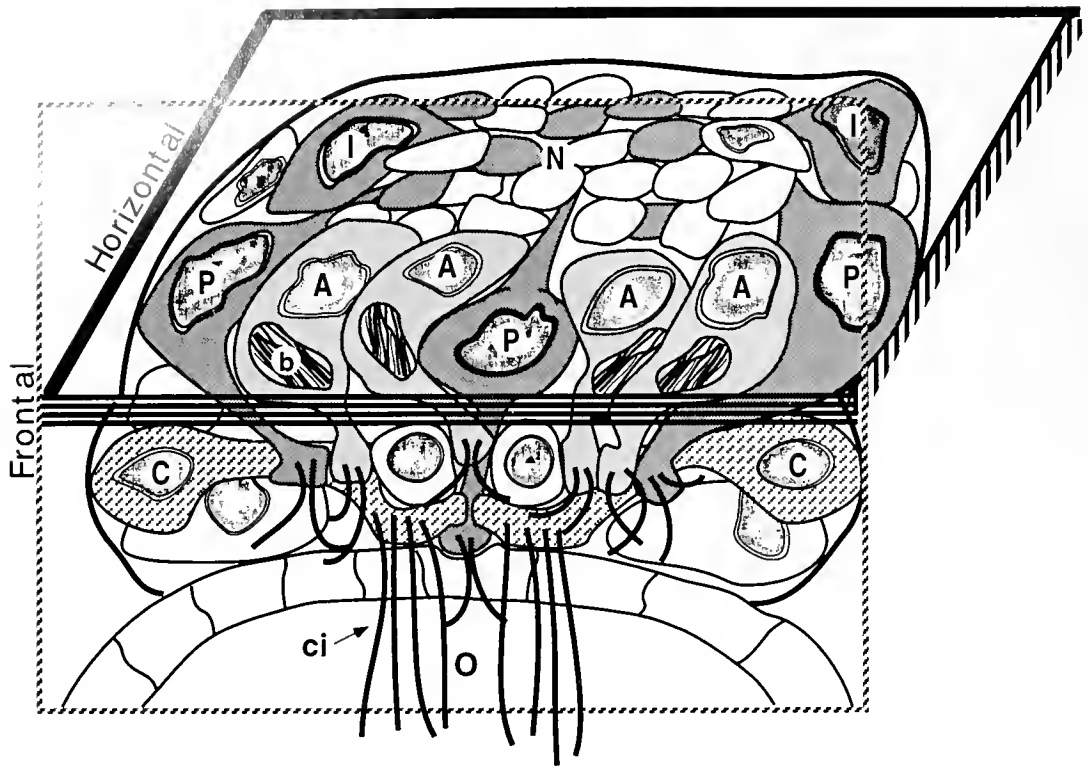

Figure 8. Schematic diagram of the apical ganglion of larval *Aplysia*. The diagram illustrates both horizontal and frontal plane views. The three para-ampullary (P) and the two interneuron (I) cells are serotonergic. All 5HT cells send projections into the neuropil (N). The ampullary (A) and the ciliary tuft (C) cells are also illustrated. Except for the 5HT interneurons, all the labeled cell types extend apical processes to the surface of the animal. See text for details. ci, cilia; b, ciliary bundle; O, oesophagus.

act as sensory receptors. Instead, they may act as interneurons along the information pathway that links the AG to the rest of the CNS and to effector tissues. These cells, as well as the para-ampullary cells, extend an axonal process into the AG neuropil and the cerebral commissure; these processes subsequently course in various directions to reach and innervate muscles, nerve cells, and ciliated cells of the velum (Marois and Carew, 1997b). There is circumstantial evidence that the para-ampullary cells provide the serotonergic input to the velum and the interneurons innervate the CNS of *Aplysia* (Marois and Carew, 1997b). There is also biochemical evidence from bath-application experiments that serotonin exerts a potent modulatory effect on ciliary activity and locomotion of various molluscs (Koshtoyants *et al.*, 1961; Diefenbach *et al.*, 1991; Marois and Hofstadter, unpubl. obs.). Given that these velar cells are directly contacted by serotonergic varicosities (Marois and Carew, 1997b), it is very likely that the modulatory effects of 5HT on ciliary beating are mediated by these serotonergic synapses. Thus, the serotonergic cells of the AG cannot be regarded as strictly sensory or interneuronal since they appear to have direct effector functions on ciliary activity, and probably on muscular and neuronal activity as well.

These findings suggest that the serotonergic cells in larval *Aplysia* are multimodal neurons involved in the modulation of ongoing physiological and behavioral activity (see Marois and Carew, 1997b). Although there is evidence from studies on the gastropod *Ilyanassa* that serotonin may also be involved in the induction of metamorphosis (Levantine and Bonar, 1986; Leise, 1996; Couper and Leise, 1996), no comparable effect has been observed in *Aplysia* and other gastropods (Morse *et al.*, 1979; Hadfield, 1984; Coon *et al.*, 1985; Marois and Hofstadter, unpubl. obs.).

In conclusion, this study, together with other recent work (Marois and Carew, 1997a, b), has begun to reveal the anatomical and functional properties of the serotonergic system in the apical ganglion of the gastropod *Aplysia*. However complex the functions of the serotonergic cells may turn out to be, they probably represent only a fraction of the roles played by the entire apical ganglion. The AG may therefore be best regarded as a complex nerve center for the regulation of larval-specific behaviors, integrating sensory information to achieve

proper motor adaptation to variable environmental conditions. Thus, more than simply a sensory structure, the apical organ is a *bona fide* neuronal ganglion.

Acknowledgments

We thank Isabel Gauthier for assistance with the drawing. This work was financially supported by an NSERC (Canada) pre-doctoral fellowship to R.M. and by NSF grant IBN9221117 and NIMH Merit Award R01-MH-14-1083 to T.J.C.

Literature Cited

Altner, H., and L. Prillinger. 1980. Ultrastructure of invertebrate chemoreceptors, thermoreceptors and hydroreceptors and its functional significance. *Int. Rev. Cytol.* **67:** 69–140.

Barlow, L. A., and J. W. Truman. 1992. Patterns of serotonin and SCP immunoreactivity during metamorphosis of the nervous system of the red abalone, *Haliotis rufescens*. *J. Neurobiol.* **23:** 829–844.

Bisgrove, B. W., and R. D. Burke. 1986. Development of serotonergic neurons in embryos of the sea urchin, *Strongylocentrotus purpuratus*. *Dev. Growth Differ.* **28:** 569–574.

Bisgrove, B. W., and R. D. Burke. 1987. Development of the nervous system of the pluteus larva of *Strongylocentrotus droebachiensis*. *Cell Tissue Res.* **248:** 335–343.

Bonar, D. B. 1978. Ultrastructure of a cephalic sensory organ in larvae of the gastropod *Phestilla sibogae* (Aeolidacea, Nudibranchia). *Tissue Cell* **10:** 153–165.

Chia, F. S., and R. Koss. 1979. Fine structural studies of the nervous system and the apical organ in the planula larva of the sea anemone *Anthopleura elegantissima*. *J. Morphol.* **160:** 275–298.

Chia, F. S., and R. Koss. 1984. Fine structure of the cephalic sensory organ in the larva of the nudibranch *Rostanga pulchra* (Mollusca, Opisthobranchia, Nudibranchia). *Zoomorphology* **104:** 131–139.

Chia, F. S., R. D. Burke, R. Koss, P. V. Mladenov, and S. S. Rumrill. 1986. Fine structure of the doliolaria larva of the feather star *Florometra serratissima* (Echinodermata: Crinoidea), with special emphasis on the nervous system. *J. Morphol.* **189:** 99–120.

Coon, S. L., D. B. Bonar, and R. M. Weiner. 1985. Induction of settlement and metamorphosis of the Pacific oyster, *Crassostrea gigas* (Thunberg) by L-DOPA and catecholamines. *J. Exp. Mar. Biol. Ecol.* **94:** 211–221.

Couper, J. M., and E. M. Leise. 1996. Serotonin injections induce metamorphosis in larvae of the gastropod mollusc *Ilyanassa obsoleta*. *Biol. Bull.* **191:** 178–186.

Dautov, S. Sh., and L. P. Nezlin. 1992. Nervous system of the *Tornaria* larva (Hemichordata: Enteropneusta). A histochemical and ultrastructural study. *Biol. Bull.* **183:** 463–475.

Diefenbach, T. J., N. K. Koehncke, and J. I. Goldberg. 1991. Characterization and development of rotational behavior in *Helisoma* embryos: role of endogenous serotonin. *J. Neurobiol.* **22:** 922–934.

Dorsett, D. A. 1986. Brain to cells: the neuroanatomy of selected gastropod species. Pp. 101–187 in *The Mollusca (Vol. 9): Neurobiology and Behavior Part 2*, A. O. D. Willows, ed. Academic Press, New York.

Emery, D. G., and T. E. Audesirk. 1978. Sensory cells in *Aplysia*. *J. Neurobiol.* **9:** 33–46.

Fukui, Y. 1991. Embryonic and larval development of the sea anemone *Haliplanella lineata* from Japan. *Hydrobiologia* **216/217:** 137–142.

Hadfield, M. G. 1984. Settlement requirements of molluscan larvae: new data on chemical and genetic roles. *Aquaculture* **39:** 283–298.

Hay-Schmidt, A. 1989. The larval nervous system of *Phoronis muelleri*. *Zoomorphology* **108:** 333–351.

Hay-Schmidt, A. 1990. Catecholamine-containing, serotonin-like and FMRFamide-like immunoreactive neurons and processes in the nervous system of the early actinotroch larva of *Phoronis vancouverensis* (Phoronida): distribution and development. *Can. J. Zool.* **68:** 1525–1536.

Hay-Schmidt, A. 1992. Ultrastructure and immunocytochemistry of the nervous system of the larvae of *Lingula anatina* and *Glottidia* sp. (Brachiopoda). *Zoomorphology* **112:** 189–205.

Hay-Schmidt, A. 1995. The larval nervous system of *Polygordius lacteus* Scheinder, 1868 (Polygordiidae, Polychaeta): immunocytochemical data. *Acta Zool.* **76:** 121–140.

Holland, N. D., and L. Z. Holland. 1993. Serotonin-containing cells in the nervous system and other tissues during ontogeny of a lancelet, *Branchiostoma floridae*. *Acta Zool.* **74:** 195–204.

Jacob, M. H. 1984. Neurogenesis in *Aplysia californica* resembles nervous system formation in vertebrates. *J. Neurosci.* **4:** 1225–1239.

Kempf, S. C., and L. Page. 1995. Development of the apical serotonergic complex in opisthobranch larvae. *Larval Biol. Meet. Abstr.* **2:** 20.

Kempf, S. C., A. Saini, and A. Jones. 1991. The ontogeny of neuronal systems expressing SCP-like and serotonin-like antigens in *Berghia verrucicornis*. *Soc. Neurosci. Abstr.* **17:** 1356.

Koshtoyants, K. H. S., A. G. Buznikov, and B. N. Manukhin. 1961. The possible role of 5-hydroxytryptamine in the motor activity of some marine gastropods. *Comp. Biochem. Physiol.* **3:** 20–26.

Kriegstein, A. R. 1977a. Stages in the post-hatching development of *Aplysia californica*. *J. Exp. Zool.* **199:** 275–288.

Kriegstein, A. R. 1977b. Development of the nervous system of *Aplysia californica*. *Proc. Natl. Acad. Sci. USA* **74:** 375–378.

Lacalli, T. C. 1981. Structure and development of the apical organ in trochophores of *Spirobranchus polycerus*, *Phyllodoce maculata* and *Phyllodoce mucosa* (Polychaeata). *Proc. R. Soc. Lond. B* **212:** 381–402.

Lacalli, T. C. 1982. The nervous system and ciliary band of Müller's larva. *Proc. R. Soc. Lond. B* **217:** 37–58.

Lacalli, T. C. 1983. The brain and central nervous system of Müller's larva. *Can. J. Zool.* **61:** 39–51.

Lacalli, T. C. 1984. Structure and organization of the nervous system in the trochophore larva of *Spirobranchus*. *Philos. Trans. R. Soc. Lond. B Biol. Sci.* **306:** 79–135.

Lacalli, T. C. 1990. Structure and organization of the nervous system in the actinotroch larva of *Phoronis vancouverensis*. *Philos. Trans. R. Soc. Lond. B Biol. Sci.* **327:** 655–685.

Lacalli, T. C. 1994. Apical organs, epithelial domains, and the origin of the chordate central nervous system. *Am. Zool.* **34:** 533–541.

Lacalli, T. C., N. D. Holland, and J. E. West. 1994. Landmarks in the anterior central nervous system of amphioxus larvae. *Philos. Trans. R. Soc. Lond. B Biol. Sci.* **344:** 165–185.

Laverack, M. S. 1974. The structure and function of chemoreceptor cells. Pp. 1–48 in *Chemoreception in Marine Organisms*, P. T. Grant and A. M. Mackie, eds. Academic Press, New York.

Leise, E. M. 1996. Selective retention of the fluorescent dye DASPEI in a larval gastropod mollusc after paraformaldehyde fixation. *Micros. Res. Tech.* **33:** 496–500.

Levantine, P. L., and D. B. Bonar. 1986. Metamorphosis of *Ilyanassa obsoleta*: natural and artificial inducers. *Am. Zool.* **26:** 14A.

Marois, R., and T. J. Carew. 1997a. Ontogeny of serotonergic neurons in *Aplysia californica*. *J. Comp. Neurol.* In press.

Marois, R., and T. J. Carew. 1997b. Projection patterns and develop-

mental functions of serotonergic cells in larval *Aplysia californica*. *J. Comp. Neurol. In press.*

Marois, R., P. Hofstadter, and T. J. Carew. 1993. Birthdate and identification of serotonergic cells in embryonic and larval *Aplysia*. *Soc. Neurosci. Abstr.* **19:** 1287.

Marois, R., G. M. Kelly, S. Hockfield, and T. J. Carew. 1992. An ultrastructural study of serotonergic cells in the CNS of embryonic and larval *Aplysia*. *Soc. Neurosci. Abstr.* **18:** 1471.

Morse, D. E., N. Hooker, H. Duncan, and L. Jensen. 1979. Gamma-aminobutyric acid, a neurotransmitter, induces planktonic abalone larvae to settle and begin metamorphosis. *Science* **204:** 407–410.

Moss, C., R. D. Burke, and M. C. Thorndyke. 1994. Immunocytochemical localization of the neuropeptide S1 and serotonin in larvae of the starfish *Pisaster ochraceus* and *Asterias rubens*. *J. Mar. Biol. Assoc. U.K.* **74:** 61–71.

Nakajima, Y. 1988. Serotonergic nerve cells of starfish larvae. Pp. 235–239 in *Echinoderm Biology, Proceedings of the Sixth International Echinoderm Conference*, R. D. Burke, P. V. Mladenov, P. Lambert, and R. L. Parsley, eds. Balkema, Rotterdam.

Nakajima, Y., R. D. Burke, and Y. Noda. 1993. The structure and development of the apical ganglion in the sea urchin pluteus larvae of *Strongylocentrotus droebachiensis* and *Mespilia globulus*. *Dev. Growth Differ.* **35:** 531–538.

Nielsen, C. 1994. Larval and adult characters in animal phylogeny. *Am. Zool.* **34:** 492–501.

Page, L. R. 1992. New interpretation of a nudibranch central nervous system based on ultrastructural analysis of neurodevelopment in *Melibe leonina* I. Cerebral and visceral loop ganglia. *Biol. Bull.* **182:** 348–365.

Richardson, K. C., L. Jarrett, and E. H. Finke. 1960. Embedding in epoxy resins for ultrathin sectioning in electron microscopy, *Stain Technol.* **35:** 313–323.

Saunders, A. M. C., and M. Poole. 1910. The development of *Aplysia punctata*. *Q. J. Microsc. Sci.* **55:** 497–539.

Schacher, S., E. R. Kandel, and R. Woolley. 1979a. Development of neurons in the abdominal ganglion of *Aplysia californica*. I. Axosomatic synaptic contacts. *Dev. Biol.* **71:** 163–175.

Schacher, S., E. R. Kandel, and R. Woolley. 1979b. Development of neurons in the abdominal ganglion of *Aplysia californica*. II. Non-neural support cells. *Dev. Biol.* **71:** 176–190.

Tardy, J., and S. Dongard. 1993. Le complexe apical de la véligère de *Ruditapes philippinarum* (Adams et Reeve, 1850) Mollusque Bivalve Vénéridé. *Biol. Mar.* **316:** 177–184.

Wright, B. R. 1974. Sensory structure of the tentacles of the slug, *Arion ater* (Pulmonata, Mollusca) 2. Ultrastructure of the free nerve endings in the distal epithelium. *Cell Tissue Res.* **151:** 245–257.

Reference: *Biol. Bull.* **192:** 399–409. (June, 1997)

Serotonin and Dopamine Have Opposite Effects on Phototaxis in Larvae of the Bryozoan *Bugula neritina*

ANTHONY PIRES[1] AND ROBERT M. WOOLLACOTT[2]

[1]*Department of Biology, Dickinson College, Carlisle, Pennsylvania 17013; and* [2]*Department of Organismic and Evolutionary Biology, Harvard University, Cambridge, Massachusetts 02138*

Abstract. Adult colonies of the bryozoan *Bugula neritina* release short-term anenteric larvae that initially are strongly photopositive. Over the course of several hours larvae lose their initial photopositivity and either become photonegative or alternate between positive and negative phototaxis. We report that newly released photopositive larvae rapidly become photonegative upon exposure to 10^{-6}–10^{-5} *M* serotonin or its metabolic precursor, 5-hydroxytryptophan. This behavior was not observed in two congeners of *B. neritina*, nor in larvae of three other species of bryozoans and seven species from four additional phyla. Antibodies to serotonin label cells in the region of the equatorial nerve-muscle ring and in two tracts extending from the apical disc to this ring. In a separate series of experiments, larvae treated with dopamine (10^{-7}–10^{-5} *M*) significantly prolonged their photopositive period. This effect was also obtained with the D_2 dopamine receptor agonist, quinpirole (10^{-6}–10^{-5} *M*). HPLC analysis determined that newly released photopositive larvae contained 0.120 pmol dopamine/μg protein. These findings implicate serotonin and dopamine as important neurochemical regulators of phototaxis in larvae of *B. neritina*.

Introduction

Regulation of the vertical distributions of pelagic larvae of marine invertebrates is most likely restricted to the vectoral factors of current velocity, light direction, and gravity (Crisp, 1984). Of these, most is known about the influence of light. Studies of the role of phototaxis in larval behavior were pioneered by Thorson (1964), who documented the photic responses exhibited by larvae of 141 species of shallow-water benthic marine invertebrates from 11 phyla. In Thorson's survey, the most frequently observed response to light was for larvae to be initially positively phototactic (82%). Only 6% responded negatively to light throughout larval life, and only 12% were indifferent to light. In 76% of the cases examined, larvae that were initially photopositive became photonegative before the end of the larval period. Apparently, an ontogenetically regulated switch governing the sign of phototaxis is found in larvae of many species. Positive phototaxis early in the larval period may bring larvae up into the water column and facilitate dispersal; later negative phototaxis may bring them down to the substratum where settlement occurs. In addition to changes in phototaxis during development, environmental signals may influence phototactic behavior of larvae (see Crisp, 1984; Young and Chia, 1987, for reviews). Factors such as temperature, salinity, light intensity, ionic shock, pH, exposure to chemical cues from settlement-specific substrates, and pollutants all have been implicated in environmentally induced changes in phototaxis.

Despite the wide phylogenetic distribution and ecological significance of larval phototaxis, very little is known about the internal mechanisms responsible for generating and modulating this behavior. This lack of knowledge stands in contrast to current understanding of the neural bases of stereotyped behaviors in many adult invertebrates. Although that literature is far too extensive

Received 11 February 1997; accepted 7 April 1997.

Abbreviations: 5HT, serotonin; 5HTP, 5-hydroxytryptophan; DA, dopamine; DHBA, 3,4-dihydroxybenzylamine; DDW, deionized distilled water; HPLC, high-pressure liquid chromatography; MBL-ASW, MBL artificial seawater; MPB, Millonig's phosphate buffer; PBS+, phosphate-buffered saline containing 0.1% Triton X-100 and 0.1% NaN_3.

to review here, it is important to point out a common theme that has emerged in the last two decades: Many behaviors are initiated, maintained, altered, or terminated by the action of monoamine or peptide modulators on neural networks (see reviews by Harris-Warrick and Marder, 1991; Katz, 1995). Examples involving monoamines include initiation of swimming in an annelid (Willard, 1981; Mangan *et al.*, 1994); modulation of phototaxis, swimming, respiration, and feeding in gastropods (Crow and Forrester, 1986; McClellan *et al.*, 1994; Syed *et al.*, 1990; Wieland and Gelperin, 1983; Kyriakides and McCrohan, 1989); starting and stopping flight in an insect (Claassen and Kammer, 1985); and switching of body postures and modulation of pyloric motor output in decapod crustaceans (Livingstone *et al.*, 1980; Flamm and Harris-Warrick, 1986).

Although evidence has been presented for the existence of neuroactive monoamines in the larvae of many marine invertebrates—including hydrozoans (McCauley, 1995; Walther *et al.*, 1996), a nemertean (Hay-Schmidt, 1990a), a polychaete (Hay-Schmidt, 1995), bivalve and gastropod molluscs (Coon and Bonar, 1986; Goldberg and Kater, 1989; Marois and Carew, 1990; Barlow and Truman, 1992; Pires *et al.*, 1992), several echinoderms (Toneby, 1980; Burke, 1983; Burke *et al.*, 1986; Bisgrove and Burke, 1986, 1987; Nakajima, 1987, 1988; Thorndyke *et al.*, 1992), brachiopods (Hay-Schmidt, 1992), phoronids (Hay-Schmidt, 1990b,c), a hemichordate (Dautov and Nezlin, 1992), and a cephalochordate (Holland and Holland, 1993)—less is known of the roles of these compounds in the mediation or modulation of larval behaviors. Monoamines have been implicated in the control of metamorphosis in a variety of taxa including hydrozoans (McCauley, 1995; Walther *et al.*, 1996), polychaetes (Biggers and Laufer, 1992; Okamoto *et al.*, 1995), gastropods (Couper and Leise, 1996; Pires *et al.*, 1995), bivalves (Coon and Bonar, 1987; Bonar *et al.*, 1990; Chevolot *et al.*, 1991; Kingzett *et al.*, 1990), a barnacle (Yamamoto *et al.*, 1996), and an echinoid (Burke, 1983). Effects of monoamines on ciliary locomotion have also been reported. Bath-applied dopamine (DA) induces ciliary reversal and backward swimming in some echinoid plutei (Lacalli and Gilmour, 1990; Mogami *et al.*, 1992), while serotonin (5HT) increases the speed of forward swimming (Mogami *et al.*, 1992). Serotonin also accelerates ciliary beat frequency in encapsulated embryos of the gastropod *Helisoma trivolvis*, while DA has no effect (Diefenbach *et al.*, 1991; Goldberg *et al.*, 1994). However, no data have been published on the regulation of larval phototaxis by monoamines or any other neuroactive substances.

Bryozoans are excellent material for experimental studies of larval phototaxis because most species retain their early developmental stages and, on stimulus of light, release larvae that generally settle within a few hours of eclosion. Cohorts of larvae all released within a few minutes of each other can thus be obtained. Ryland (1976, 1977) reviewed in detail the early studies of the phototactic behavior of bryozoan larvae, and several important conclusions come from these studies. First, a range of responses to light are possible, depending on the species. During the course of its larval existence an individual could remain neutral to light throughout; react positively throughout; change from positive to negative or positive to partial negative; and change from positive to alternation between positive and negative (Ryland, 1960). Second, in larvae of *Bugula flabellata* and *B. turrita*, it is possible to artificially force a switch in photic response with agents such as elevated pH, hypotonic seawater, or CuCl (Lynch, 1947). Third, in larvae of *Cryptosula pallassiana*, a rise in temperature decreases the photopositive phase, but the amount of illumination has no effect on the rate of change in sign of the response to light (Ryland, 1962). Furthermore, Ryland observed that pipetting larvae also results in an immediate change from positive to negative phototaxis.

Larvae of many species with phototactic responses possess pigmented epidermal structures that, on the basis of anatomical criteria, are assumed to be photoreceptors (Ryland, 1976, 1977). Not all species with larvae that orient to light have pigmented "eyespots," however (Ryland, 1960); in these species, other specialized epidermal cell types are hypothesized to be photoreceptors (Zimmer and Woollacott, 1989). To date, all pigmented ocelli of bryozoan larvae examined at the ultrastructural level have been based on a sensory cell with an elaboration of multiple cilia that are thought to be the receptoral organelles (Woollacott and Zimmer, 1972; Hughes and Woollacott, 1978, 1980; Reed *et al.*, 1988).

We selected *Bugula neritina* for detailed investigation of the monoaminergic control of phototaxis in the larvae of marine bryozoans. *B. neritina* is cosmopolitan in temperate to tropical waters and is often abundant in specific locales at certain times of the year. Larvae of *B. neritina* are barrel-shaped and about 300 μm in diameter. General features of larval anatomy and events in metamorphosis are well documented for this species (Woollacott and Zimmer, 1971, 1972, 1978; Reed and Woollacott, 1982, 1983). The motive force for swimming is provided by the coordinated beating of the cilia of some 300 elongate coronal cells that form the extensive lateral surface of the larva. Two pigmented "eyespots" are situated on the posterior surface, and these connect with a neural plate in the apical disc by way of an underlying equatorial nerve-muscle ring. Larvae are strongly photopositive on release and with time either

change to photoneutral or alternate between photopositive and photonegative.

We report that 5HT and its immediate metabolic precursor, 5-hydroxytryptophan (5HTP), rapidly caused photopositive larvae of *B. neritina* to become photonegative. Antibodies to 5HT label cells with processes that are associated with the apical disc and extend orally to the equatorial nerve-muscle ring. In contrast, we show that DA and the D_2 DA receptor agonist quinpirole prolonged photopositivity in newly released larvae, and we present chromatographic data to confirm the presence of endogenous DA. We also report qualitative observations on the effects of 5HT and DA on the photic behavior of larvae from five other species of bryozoans and from seven species in four additional phyla. These results demonstrate that the responses observed in *B. neritina* to 5HT and DA are generalizable neither to larvae of congeners nor to a broad range of marine invertebrate larvae.

Materials and Methods

Behavior of larvae of Bugula neritina

Sexually mature colonies of *Bugula neritina* (Linnaeus) 1758 were collected in 1993, during February and March, from the sides of floating docks and other submerged objects in the Indian River near the Smithsonian Marine Station at Link Port, Fort Pierce, Florida. Colonies were maintained in 2-gal aquaria provided with aeration. Release of larvae was initiated by exposing colonies to sunlight following an overnight period of dark adaptation.

Phototaxis experiments were conducted in MBL artificial seawater (MBL-ASW, Cavanaugh, 1956) with the salinity adjusted to habitat level (20‰). Phototactic behavior of larvae was assessed in the presence of 5-hydroxytryptamine hydrochloride (serotonin, 5HT, Sigma); 5-hydroxy-L-tryptophan (5HTP, Sigma); 3-hydroxytyramine hydrochloride (dopamine, DA, Sigma); (±)-SKF-38393 (a D_1 DA receptor agonist, Research Biochemicals Inc.); and (−)-quinpirole hydrochloride (a selective D_2 DA receptor agonist, Research Biochemicals Inc.). Twenty milliliters of MBL-ASW served as the control in all experiments. Drugs were dissolved and diluted directly into MBL-ASW. Final working solutions were in 20-ml volumes and contained 10^{-5}, 10^{-6}, 10^{-7}, or 10^{-8} *M* concentrations of the drug.

Experiments were conducted in glass Stender dishes with a capacity of 30 ml and an inside diameter of 4.5 cm. Larvae were transferred into dishes by pipetting, usually carrying over about 0.2–0.3 ml of Indian River water. It was not feasible to accurately determine the number of larvae being transferred; consequently, dishes contained unequal numbers of larvae. The number of larvae varied from 20 to 78 per dish, but 25 to 35 was the most common range of values. Pipetting did not affect the responses of larvae of *B. neritina* to light; this result is contrary to the observations of Ryland (1962) with larvae of another bryozoan, *Cryptosula pallasiana*. A 4-ft GE F400CW cool white fluorescent lamp was used as the light source. Dishes containing larvae were placed on white paper 3 in. from the light. Photon flux was measured with a LI-COR model LI-1000 light meter equipped with a detector calibrated for air and measuring between 400 and 700 nm. Irradiance measurements were made in air and ranged between 4.76×10^{15} and 5.78×10^{15} photons/s/cm^2 along the length of the tube. The gradient across the dishes was 6.69×10^{15} to 4.88×10^{15} photons/s/cm^2. Temperature remained within 1°C over the course of individual experiments and ranged from 20°C to 23°C over the course of all experiments.

The number of larvae in the half of the dish that was closest to the light was counted at designated time intervals throughout an experiment. Total numbers of larvae were then counted and the data converted to percentages. A repeated-measures ANOVA was used on arcsin-transformed data to determine whether significant differences existed among treatments, and a Fisher probability least significant difference test was used to localize where these differences, if any, resided (Statview 4.0, Abacus Concepts).

Behavior of other marine invertebrate larvae

The phototactic responses of larvae of 12 additional species of marine invertebrates were evaluated qualitatively (Table I). Some of these studies were conducted at the Museum of Comparative Zoology in Cambridge, Massachusetts, and others at the Kewalo Marine Laboratory in Honolulu, Hawaii. In all cases, 5HT and DA were applied at a concentration of 10^{-5} *M*. As above, 20-ml volumes in 30-ml Stender dishes were used. A combination of fluorescent and natural light was employed, but irradiance was not quantified. Responses of larvae were gauged qualitatively.

Scanning electron microscopy

Larvae of *Bugula neritina* were fixed in 1% OsO_4 in seawater for 30 min, rinsed in distilled water, and dehydrated in a graded series of acetone. Specimens were critical-point dried in CO_2, gold-palladium coated, and examined with an AMR 1000 scanning electron microscope.

Immunohistochemistry

The immunohistochemical protocol was adapted from that of Kempf *et al.* (1987). Larvae were fixed for 1 h at

room temperature in 4% paraformaldehyde containing 0.14 *M* NaCl and 0.2 *M* Millonig's phosphate buffer (MPB). After fixation, larvae were washed twice in MPB (10 min each). They were then washed in deionized distilled water (DDW) and dehydrated through an ethanol series to xylene (30%, 50%, 80%, 95%, 100%, 100%, xylene, 10 min each), then rehydrated through the same series back to DDW. This procedure increases tissue permeability to antibodies. Larvae were then washed twice (10 min each) in 20 m*M* phosphate-buffered saline in 0.15 *M* NaCl, pH 7.3, containing 0.1% Triton X-100 and 0.1% NaN_3 (PBS+). Subsequent steps were carried out on a shaker table at 4°C. Larvae were incubated for 4 h in a blocking medium consisting of 5% heat-inactivated goat serum in PBS+, then incubated overnight in primary antibody solution. This was a 1:325 dilution (in blocking medium) of polyclonal rabbit anti-5HT (Incstar #20080). A batch of larvae was treated overnight with blocking medium instead of primary antibody solution, as a control for specificity of immunofluorescent labeling. All larvae were then washed four times with PBS+ over a 12-h period, and incubated overnight in the secondary antibody solution. Secondary antibodies were goat anti-rabbit immunoglobulin G conjugated to fluorescein isothiocyanate (Organon-Teknica-Cappel #12121671), diluted 1:300 in blocking medium. Following treatment with secondary antibody, larvae were again washed four times with PBS+ over a 12-h period, then mounted in a Tris-buffered (pH 9.5) glycerol medium containing 4% *n*-propyl gallate (Giloh and Sedat, 1982). Larvae were examined and photographed under UV epi-illumination.

Chromatographic analysis of dopamine

DA content of larvae was analyzed by high-pressure liquid chromatography (HPLC) with electrochemical detection. Homogenization of larvae and extraction of catecholamines differed only in a few details from the methods of Coon and Bonar (1986). Approximately 75 μl of packed larvae was concentrated by gentle centrifugation and homogenized in a glass tissue grinder on ice in 1.0 ml of 0.4 *N* perchloric acid with 4 m*M* reduced glutathione, 4.7 m*M* EGTA, and 100 n*M* 3,4-dihydroxybenzylamine (DHBA, Sigma) as an internal standard. The homogenate was centrifuged at 15,000 × *g* for 5 min. Two 400-μl aliquots were transferred to 10 × 75 mm glass tubes for extraction of catecholamines over alumina (Anton and Sayre, 1962). To each tube was added 600 μl DDW, 50 mg alumina, and 1 ml extraction buffer (1.5 *M* Tris plus 50 m*M* Na_2 EDTA, pH 8.6). Tubes were agitated 10 min by inversion. Alumina was washed twice with DDW, transferred to microcentrifuge filter assemblies (Rainin #39-402), and catechols were eluted with 200 μl 0.1 *N* perchloric acid. This extract was injected directly into the HPLC system (standard injection volume 80 μl). Each extraction therefore provided enough material for two full sample injections; the remaining material from each extraction was used in smaller injections to help confirm the DA peak while varying the organic content of the mobile phase and "spiking" the chromatographic standards mix (see below). The recovery efficiency of the DHBA internal standard (64%–68%) was calculated for each extraction and used to correct the endogenous catecholamine data from that extraction.

Separation of catecholamines was accomplished by HPLC with an Alltech #28922 Adsorbosphere catecholamine column (100 × 4.6 mm, 3 μm C-18 reverse phase packing). The aqueous portion of the mobile phase contained 100 m*M* monochloroacetic acid, 1.3 m*M* Na_2 EDTA, and 1.3 m*M* sodium octyl sulfate adjusted to pH 3.00–3.05 with NaOH (85 m*M* final concentration). To this was added 1%–5% (v/v) acetonitrile. Flow rate was set at 1.0 ml/min.

Catecholamines were detected with an EG & G/Princeton Applied Research #400 amperometric electrochemical detector with glassy carbon working electrode set at an oxidizing potential of 700 mV against a Ag/AgCl reference electrode (Riggin and Kissinger, 1977; Krstulovic, 1982). Oxidation current range was set at 10 or 20 nA full-scale for the smaller peaks in the first part of the chromatogram, and at 50 nA for DA, which eluted later and was present at higher concentration. Detector output was low-pass filtered (1.0-s time constant) and sent to a Beckman #427 integrator which printed chromatograms and calculated peak areas and retention times.

The DA chromatogram peak was identified by comparing its retention time to that of authentic DA at various concentrations of acetonitrile (1%–5%). A standard curve of DA peak area as a function of amount injected was used to quantify DA concentration in larval homogenates. Reported values of larval DA are derived from the mean of two 80-μl injections, one from each extraction, run at the acetonitrile concentration (5%) that yielded best resolution of the DA peak. Dopamine concentration was expressed as picomoles of free base per microgram of protein. Protein content of the homogenate was assayed by the Coomassie blue dye-binding method (Bradford, 1976) with bovine serum albumin as the standard (Bio-Rad kit, #500-0002).

Results

Monoamine modulation of phototactic behavior of larvae of Bugula neritina

Preliminary experiments conducted during June 1992 in Honolulu, Hawaii, established in a qualitative fashion

that the addition of exogenous 5HT at 10^{-5} *M* concentration brought about an immediate transformation from positive to negative phototaxis in newly released larvae of *B. neritina*. At that time, stocks of adult colonies were insufficient to provide the quantities of larvae needed for a full experimental analysis, but the response was reconfirmed in Hawaiian *B. neritina* during May 1993.

The effects of 5HT and, subsequently, DA on phototaxis were evaluated in detail in February and March 1993 in Fort Pierce, Florida, where a large supply of sexually mature colonies was available.

The effect of 5HT on the percentage of positively phototactic larvae was evaluated at concentrations of 10^{-5}, 10^{-6}, 10^{-7}, and 10^{-8} *M* over a 140-min period (Fig. 1A). In controls without applied 5HT, the percentage of larvae remaining photopositive decreased from a mean of 88% to 70% over the 140-min period. There was no significant difference from the control in experimental treatments with 10^{-8} *M* exogenous 5HT. However, the decrease in photopositivity seen after 140 min in larvae treated with 10^{-7}, 10^{-6}, and 10^{-5} *M* 5HT was much greater than that seen in controls ($P < 0.05$ for 10^{-7} *M*; $P < 0.02$ for 10^{-6} and 10^{-5} *M* 5HT). The change from photopositive was especially rapid at 10^{-6} and 10^{-5} *M* concentrations. At these concentrations, most larvae switched to photonegative within about 1 min after the addition of 5HT; in every trial at 10^{-5} *M* all larvae were photonegative after 110 min. Parallel studies of change in sign of phototaxis were conducted using 5HTP, the immediate metabolic precursor of 5HT (Fig. 1B). Results of these studies documented a shift in phototaxis even more dramatic than that observed with 5HT. The decrease in percentage of positively phototactic larvae after 140 min was significantly greater at 10^{-5}, 10^{-6}, and 10^{-7} *M* 5HTP than in control trials ($P < 0.02$). The response to 5HTP was also more rapid at the higher concentrations than was the response to 5HT at those same concentrations.

The effect of DA on the percentage of positively phototactic larvae was assessed at 10^{-5}, 10^{-6}, 10^{-7}, and 10^{-8} *M* concentrations over a 240-min period (Fig. 2A). In controls lacking exogenous DA, the percentage of larvae remaining photopositive decreased from a mean of 83% to 41% over 240 min. The addition of DA at 10^{-7}, 10^{-6}, and 10^{-5} *M* levels caused more larvae to remain photopositive than in the untreated controls ($P < 0.02$). Larvae treated with 10^{-5} *M* DA did not show any appreciable loss of positive phototaxis up to 240 min after application of DA. The response of larvae of *B. neritina* to DA was qualitatively reconfirmed using Hawaiian material in May 1993. Application of the D_1 DA receptor agonist SKF-38393 had no significant effect on phototactic

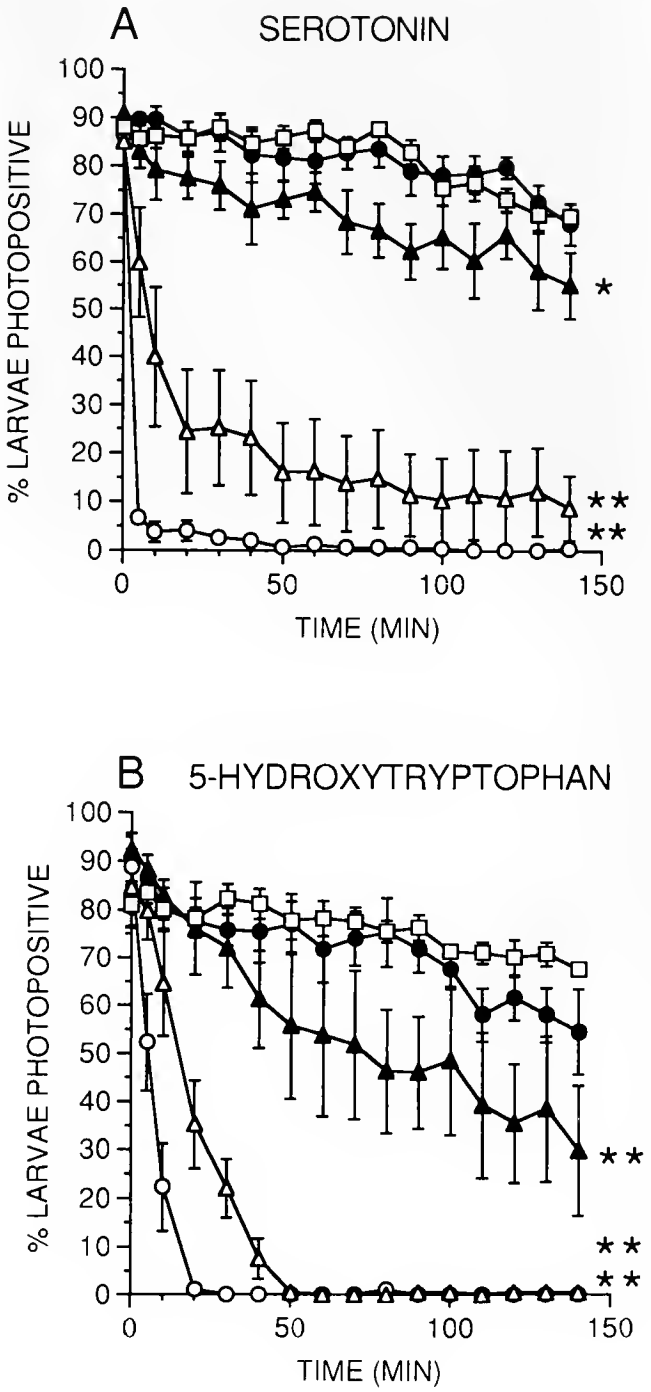

Figure 1. Percentage of larvae of *Bugula neritina* that were photopositive after timed exposure to varying concentrations of (A) serotonin and (B) 5-hydroxytryptophan. Each point represents the mean (±1 SEM) of 5 (A) or 4 (B) replicate trials. Open circles, 10^{-5} *M*; open triangles, 10^{-6} *M*; filled triangles, 10^{-7} *M*, filled circles, 10^{-8} *M*; squares, control. Single and double asterisks indicate significant differences from control at $P < 0.05$ and $P < 0.02$.

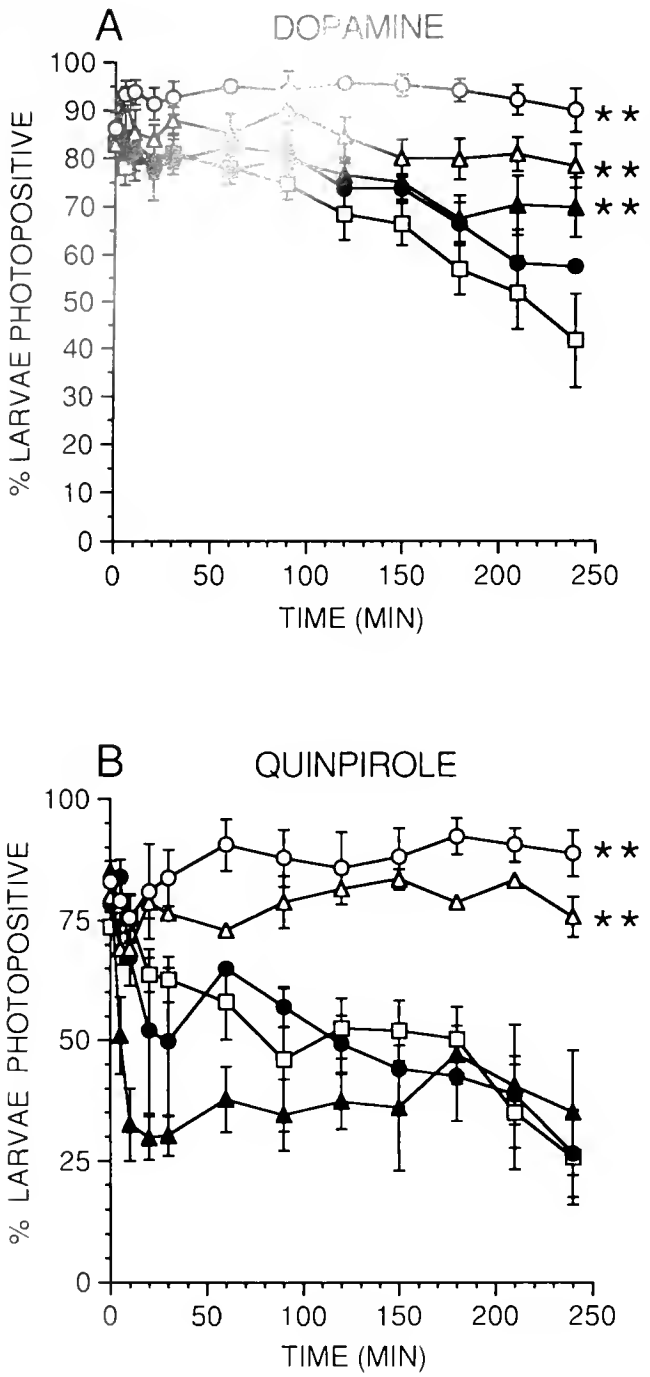

Figure 2. Percentage of larvae of *Bugula neritina* that were photopositive after timed exposure to varying concentrations of (A) dopamine and (B) quinpirole. Each point represents the mean (±1 SEM) of [illegible] trials. Explanation of symbols as in Figure 1.

[illegible] of larvae of *B. neritina* at concentrations of 10^{-5} to [illegible], but was clearly toxic to the larvae. The D_2 DA receptor agonist quinpirole, however, mimicked the effect of DA in prolonging positive phototaxis. The percentage of photopositive larvae was significantly greater after 240 min in quinpirole treatments of 10^{-5} and 10^{-6} *M* than in the untreated controls ($P < 0.02$, Fig. 2B). Application of quinpirole at 10^{-7} and 10^{-8} *M* produced an initial decrease in the percentage of photopositive larvae compared with the controls, but the difference was no longer significant after 240 min.

Localization of serotonin

Larvae of *B. neritina* have two pigmented eyespots situated in two depressions on the posterior lateral surface of the larva (Fig. 3). The lateral surfaces of the larva are formed by heavily ciliated cells of the corona, the larval locomotory organ. An apical disc complex with a central neural plate is situated at the aboral pole of the larva.

Immunolocalization of 5HT was achieved in larvae of *B. neritina*, but the procedure resulted in distortion of larvae and made precise determination of sites of the reaction difficult (Fig. 4). Strong 5HT-like immunoreactivity is evident, however, in the region of the equatorial nerve-muscle ring and in two tracts extending from the apical disc to this ring. These tracts are in a position occupied by a nerve-muscle tract extending from the roof of the metasomal sac and equatorial nerve-muscle ring to the neural plate in the center of the apical disc. The equatorial nerve-muscle ring underlies the two posterior lateral pigmented eyespots. No fluorescence above background was observed in control larvae in which the anti-5HT primary antibody was omitted.

Chromatographic analysis of dopamine

Reversed-phase HPLC of two alumina extracts of a homogenate of newly released larvae of *B. neritina* yielded chromatograms that included several peaks, including one that was identified as DA on the basis of its co-elution with authentic DA over a range of mobile-phase acetonitrile concentrations (Fig. 5). The two extractions resulted in DA values of 516 and 481 pmol/homogenate; these were averaged and divided by the total soluble protein content of the homogenate to yield a final estimate of larval DA content of 0.120 pmol/μg protein. Dihydroxyphenylalanine and norepinephrine may also be present in larvae of *B. neritina* (Fig. 5): all chromatograms showed at least a partially resolved peak corresponding to each of these monoamines, but we did not have enough material to justify reporting quantitative values.

Comparative analysis of larval phototaxis

We examined the effects of 5HT at 10^{-5} *M* concentration, and in some cases 10^{-5} *M* DA as well, on phototaxis

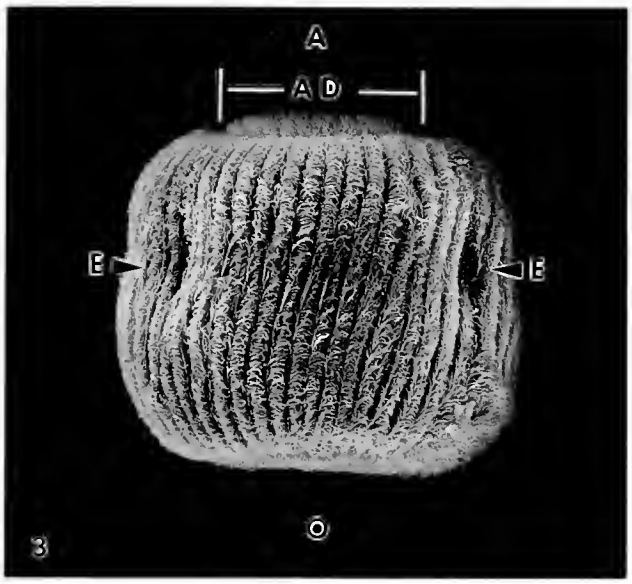

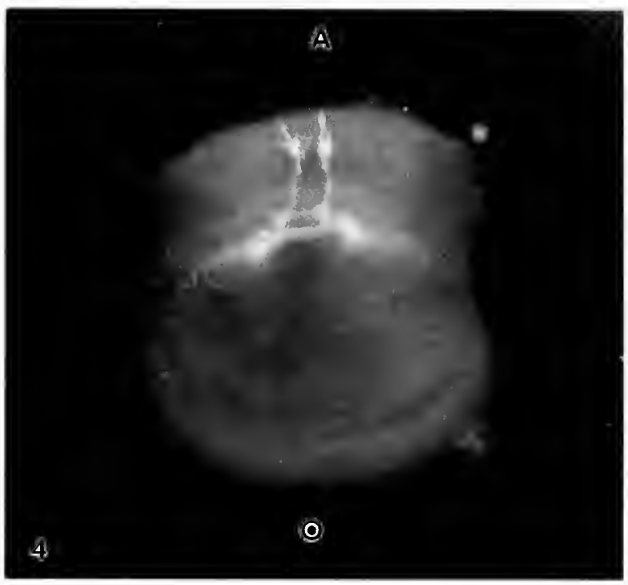

Figure 3. Scanning electron micrograph of *Bugula neritina* larva taken from lateral view. The metachronal waves of cilia mark the locations of the strap-like elongated coronal cells that together form the larval locomotory organ. Depressions in which the two pigmented eyespots (E) are situated are visible on the posterior lateral surface. The opening of the metasomal sac marks the oral pole (O) of the larva, and the ciliated apical disc (AD) is located at the aboral pole (A). ×200

Figure 4. Light photomicrograph of 5HT-like immunoreactivity in larva of *Bugula neritina*, with orientation of larva positioned to match that in Figure 3. Fluorescence is associated with position of equatorial nerve-muscle tract that underlies eyespots and is continuous with two fluorescent tracts that extend into apical disc. ×200

of larvae from a number of species (Table I). Although the analysis was based exclusively on a qualitative evaluation of responses to the addition of these monoamines, we were unable to document a pattern similar to that observed in *B. neritina* in larvae from two congeners and three additional species of bryozoans. In a broader survey we did not detect any effects of monoamines on phototaxis of larvae of one copepod crustacean, one gastropod, two demosponges, and two ascidians. The larvae of the gastropod *Phestilla sibogae*, however, did present increased motility and greater positive phototaxis when exposed to 10^{-5} *M* 5HT.

Discussion

Bath-application of 10^{-5} *M* or 10^{-6} *M* 5HT rapidly induced negative phototaxis in newly released photopositive larvae of *B. neritina* (Fig. 1A). A similar response was obtained with the same concentrations of 5HTP, the immediate metabolic precursor of 5HT, although the onset of negative phototaxis took about 10–15 min longer with 5HTP than with 5HT (Fig. 1B). This result is consistent with the notion that serotonergic cells may take up exogenous 5HTP and convert it to 5HT, thus augmenting releasable endogenous stores of that neuromodulator. In the gastropod *Lymnaea stagnalis*, injection of 5HT activates rhythmic shell movements; the same motor program can be obtained by injection of 5HTP, which also increases levels of 5HT and firing of serotonergic neurons (Kabotyanski *et al.*, 1992).

Dopamine, when bath-applied in concentrations from 10^{-7} *M* to 10^{-5} *M*, prolonged the initial period of photopositivity in larvae of *B. neritina* (Fig. 2A). This effect was mimicked by the mammalian D_2 DA receptor agonist quinpirole (Fig. 2B) at 10^{-6} *M* and 10^{-5} *M*. The sharp initial decrease in the percentage of photopositive larvae seen after treatment with 10^{-7} *M* quinpirole, contrasted with enhancement of phototaxis at higher concentrations, may reflect interactions with more than one class of DA receptor; no pharmacological profiles of bryozoan DA receptors are available.

Under normal laboratory conditions, larvae of *B. neritina* remain photopositive for 2–3 h (see controls in Fig. 2), then make a transition to a state in which they alternate between positive and negative phototaxis (Ryland, 1960), and eventually may become photonegative (Mawatari, 1951). Lynch (1947) never observed negative phototaxis in this species under normal laboratory conditions of lighting, temperature, and salinity, but he was able to induce larvae to become photonegative by

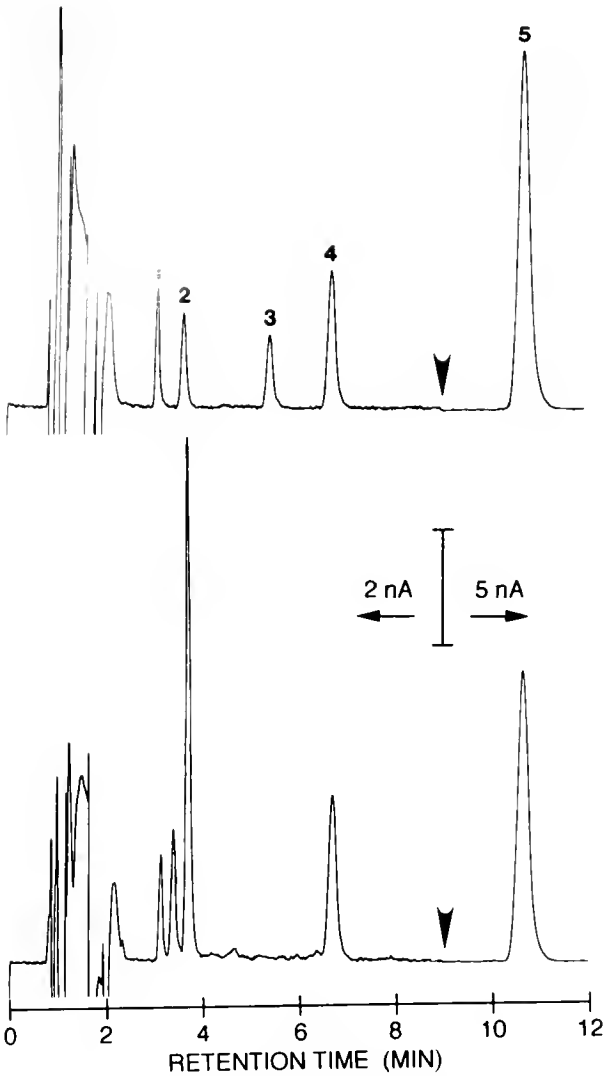

Figure 5. Separation of catecholamines by HPLC with electrochemical detection. Upper trace: chromatogram of catecholamine standards mixture (3.2 pmol each of [1] dihydroxyphenylalanine, [2] norepinephrine, [3] epinephrine; 6.4 pmol [4] DHBA; 64 pmol [5] DA). Lower trace: chromatogram of alumina extract of homogenate of newly released larvae of *Bugula neritina*. Current scale changes at time marked by vertical arrows.

exposing them to intense light. He inferred from distributions of adult colonies in the field that most larvae in nature are probably photonegative at the time of settlement and metamorphosis.

It is possible that 5HT and DA are neurochemical effects of an ontogenetic switch in the sign of phototaxis, mediating peripheral cilioexcitatory and both peripheral and central cilioinhibitory roles, respectively of serotonin and dopamine, have been described in the gill epithelium of the bivalve *Mytilus edulis* (Catapane *et al.*, 1978; [illegible] *et al.*, 1986). However, such mechanisms are probably not adequate to explain the aminergic control of cilia-driven phototaxis documented in this report. Because 5HT and DA exert opposite effects on the sign of phototaxis when applied homogeneously to the entire animal, it seems more likely that they modulate the interaction between photoreceptor organs and the ciliated coronal cells that are the effectors of phototaxis (Woollacott and Zimmer, 1972). Larvae of *B. neritina* always swim with the aboral pole directed forward, while rotating clockwise about the oral-aboral axis. In both positive and negative phototaxis the sensory feedback to the larva's locomotion should operate to equalize the light input to the two laterally situated photoreceptor organs; this would keep the oral-aboral axis parallel to the direction of the light stimulus. The crucial difference between positive and negative phototaxis is expected to be in the larva's course-correction mechanism. In positive phototaxis, asymmetric illumination of the two photoreceptor organs should result in inhibition of cilia on the more-illuminated side, or excitation of cilia on the less-illuminated side (Woollacott and Zimmer, 1972). To achieve negative phototaxis, the opposite course-correction strategy would be required: inhibition of cilia on the less-illuminated side, or excitation of cilia on the more-illuminated side.

If phototaxis is synaptically mediated by cells of the equatorial nerve-muscle ring, as has been suggested on anatomical grounds (Woollacott and Zimmer, 1972), one can propose that a functional "rewiring" of the phototaxis control system might be accomplished by monoamine neuromodulators. That is, whether a light stimulus to a photoreceptor organ excites or inhibits a given population of cilia might depend on the neuromodulatory milieu of the synapses in the phototaxis control system. In the pyloric network of the stomatogastric ganglion of the lobster *Panulirus interruptus,* the qualitative pattern of functional connections between identified neurons has been shown to depend critically upon the modulatory neurohormonal environment of the circuit (Johnson *et al.*, 1995). In two instances DA actually reverses the sign of an identified mixed chemical/electrical synaptic connection, enhancing chemical inhibition and reducing electrical coupling so that the net synaptic interaction changes from excitatory to inhibitory (Johnson *et al.*, 1993).

Although we have demonstrated clear and dramatic effects of bath-applied 5HT and DA on the photic behavior of larvae of *B. neritina,* participation of endogenous 5HT and DA in the control of phototaxis remains to be established. However, such roles for these amines seem quite likely. Processes of 5HT-immunoreactive cells are localized in the equatorial nerve-muscle ring (Fig. 4), where they are situated to modulate the interactions be-

Table I

Change in phototactic swimming behavior of initially photopositive larvae to exogenously applied monoamines (10^{-5} M)

Phylum	Species	Larval type	Phototaxis examined	Monoamine	Response	Source	Date
Arthropoda	*Acartia tonsa*	Nauplius	Positive	5HT	None	North Atlantic	11/93
Bryozoa	*Amathia distans*	Coronate	Positive	5HT	None	Honolulu, HI	5/93
				DA	None		
	Bugula neritina	Coronate	Positive	5HT	Abrupt switch to negative	Honolulu, HI	6/92
					Abrupt switch to negative	Fort Pierce, FL	2/93
					Abrupt switch to negative	Honolulu, HI	5/93
				DA	Slows switch to negative	Fort Pierce, FL	2/93
					Slows switch to negative	Honolulu, HI	5/93
	Bugula stolonifera	Coronate	Positive	5HT	None	Woods Hole, MA	9/93
	Bulgula turrita	Coronate	Positive	5HT	None	Woods Hole, MA	9/93
	Hippopodina feegeensis	Coronate	Positive	5HT	None	Honolulu, HI	5/93
				DA	None		
	Schizoporella sp.	Coronate	Positive	5HT	None	Honolulu, HI	5/93
Mollusca	*Crepidula fornicata*	Veliger	Neutral	5HT	None	Woods Hole, MA	11/93
				DA	None		
	Phestilla sibogae	Veliger	Positive	5HT	>motility, >positive taxis	Honolulu, HI	5/93
				DA	None		
Porifera	*Aplysilla* sp.	Parenchymella	Positive	5HT	None	Honolulu, HI	8/94
	Halichondria coerulea	Parenchymella	Neutral	5HT	None	Honolulu, HI	8/94
Urochordata	*Ascidia ceratodes*	Tadpole	Positive	5HT	None	Monterey, CA	11/93
				DA	None		
	Ciona intestinalis	Tadpole	Positive	5HT	None	Boston, MA	11/93
				DA	None		

tween the putative photoreceptoral organs and the coronal effectors of locomotion (Woollacott and Zimmer, 1972). Dopamine was not localized in the present study, but amounts of DA per microgram of total protein in newly released larvae of *B. neritina* are within the range reported for molluscan larvae, in which DA has been implicated in the control of settlement (Coon and Bonar, 1986; Bonar *et al.*, 1990) and metamorphosis (Pires *et al.*, 1992; Pires *et al.*, 1995).

It is indeed puzzling that newly released photopositive larvae of *B. stolonifera* and *B. turrita* were unresponsive to 10^{-5} *M* bath-applied 5HT. It may be that in these species the conditions that would permit 5HT to influence phototaxis do not apply early in larval life, or at all. Resolution of this issue will require detailed neurochemical and behavioral investigations across the duration of the larval period.

Acknowledgments

This study was made possible through the kindness of M. Hadfield (Kewalo Marine Laboratory, University of Hawaii, Honolulu, Hawaii) and M. Rice (Smithsonian Marine Station at Link Port, Fort Pierce, Florida), who sponsored our work at their respective facilities. SEM analysis was conducted by E. Seling at the Museum of Comparative Zoology, Harvard University. During this project AP was a postdoctoral fellow supported by NSF Grant # DCB89-03800 to M. Hadfield. Support provided RMW by a Short-Term Visitor Award from the Smithsonian Institution and a Putnam Expedition Grant from the Museum of Comparative Zoology, Harvard University, is gratefully acknowledged. This is contribution number 428 from the Smithsonian Marine Station at Link Port.

Literature Cited

Aiello, E., E. Hager, C. Akiwumi, and G. B. Stefano. 1986. An opioid mechanism modulates central and not peripheral dopaminergic control of ciliary activity in the marine mussel *Mytilus edulis*. *Cell. Mol. Neurobiol.* **6:** 17–30.

Anton, A. H., and D. F. Sayre. 1962. A study of the factors affecting the aluminum oxide-trihydroxyindole procedure for the analysis of catecholamines. *J. Pharmacol. Exp. Ther.* **138:** 360–375.

Barlow, L. A., and J. W. Truman. 1992. Patterns of serotonin and SCP immunoreactivity during metamorphosis of the nervous system of the red abalone *Haliotis rufescens*. *J. Neurobiol.* **23:** 829–844.

Biggers, W. J., and H. Laufer. 1992. Chemical induction of settlement and metamorphosis of *Capitella capitata* Sp. I (Polychaeta) larvae by juvenile hormone-active compounds. *Invertebr. Reprod. Dev.* **22:** 39–46.

Bisgrove, B. W., and R. D. Burke. 1986. Development of serotoner-

gic neurons in embryos of the [illegible]in *Strongylocentrotus purpuratus*. *Dev. Growth Differ.* [illegible]74.

Bisgrove, B. W., and R. D. [illegible] 1987. Development of the nervous system of the plu[illegible] *Strongylocentrotus droebachiensis*. *Cell Tissue Res.* [illegible]

Bonar, D. B., S. [illegible]n, R. M. Weiner, and W. Fitt. 1990. Control of [illegible] and metamorphosis by endogenous and exoge[illegible]cues. *Bull. Mar. Sci.* **46:** 484–498.

Bradford, M[illegible] 1976. A rapid and sensitive method for the quantitation of [illegible]gram quantities of protein utilizing the principle of protein-dye binding. *Anal. Biochem.* **72:** 248–254.

Burke, R. D. 1983. Neural control of metamorphosis in *Dendraster excentricus*. *Biol. Bull.* **164:** 176–188.

Burke, R. D., D. G. Brand, and B. W. Bisgrove. 1986. Structure of the nervous system of the auricularia larva of *Parastichopus californicus*. *Biol. Bull.* **170:** 450–460.

Catapane, E. J., G. B. Stefano, and E. Aiello. 1978. Pharmacological study of the reciprocal dual innervation of the lateral ciliated gill epithelium by the CNS of *Mytilus edulis* (Bivalvia). *J. Exp. Biol.* **74:** 101–113.

Cavanaugh, G. M., ed. 1956. *Formulae and Methods IV of the Marine Biological Laboratory Chemical Room*. Marine Biological Laboratory, Woods Hole, Massachusetts.

Chevolot, L., J.-C. Cochard, and J.-C. Yvin. 1991. Chemical induction of larval metamorphosis of *Pecten maximus* with a note on the nature of naturally occurring triggering substances. *Mar. Ecol. Prog. Ser.* **74:** 83–89.

Claassen, D. E., and A. E. Kammer. 1985. Effects of octopamine, dopamine, and serotonin on production of flight motor output by thoracic ganglia of *Manduca sexta*. *J. Neurobiol.* **17:** 1–14.

Coon, S. L., and D. B. Bonar. 1986. Norepinephrine and dopamine content of larvae and spat of the Pacific oyster, *Crassostrea gigas*. *Biol. Bull.* **171:** 632–639.

Coon, S. L., and D. B. Bonar. 1987. Pharmacological evidence that alpha-1 adrenoceptors mediate metamorphosis of the Pacific oyster, *Crassostrea gigas*. *Neuroscience* **23:** 1169–1174.

Couper, J. M., and E. M. Leise. 1996. Serotonin injections induce metamorphosis in larvae of the gastropod mollusc *Ilyanassa obsoleta*. *Biol. Bull.* **191:** 178–186.

Crisp, D. J. 1984. Overview of research on marine invertebrate larvae, 1940–1980. Pp. 103–126 in *Marine Biodeterioration: An Interdisciplinary Study*, J.D. Costlow and R.C. Tipper, eds. Naval Institute Press, Annapolis, Maryland.

Crow, T., and J. Forrester. 1986. Light paired with serotonin mimics the effect of conditioning on phototactic behavior of *Hermissenda*. *Proc. Natl. Acad. Sci. USA* **83:** 7975–7978.

Dautov, S. S. II, and L. P. Nezlin. 1992. Nervous system of the tornaria larva (Hemichordata: Enteropneusta). A histochemical and ultrastructural study. *Biol. Bull.* **183:** 463–475.

Diefenbach, T. J., N. K. Koehncke, and J. I. Goldberg. 1991. Characterization and development of rotational behavior in *Helisoma* embryos: role of endogenous serotonin. *J. Neurobiol.* **22:** 922–934.

Flamm, R. E., and R. M. Harris-Warrick. 1986. Aminergic modulation in lobster stomatogastric ganglion. I. The effects on motor pattern and activity of neurons within the pyloric circuit. *J. Neurophysiol.* 55: 847–865.

Gr[illegible]n, H. J., and J. W. Sedat. 1982. Fluorescence microscopy: reduced [illegible]bleaching of rhodamine and fluorescein protein conjugates by n-propyl gallate. *Science* **217:** 1252–1255.

Go[illegible], L., and S. B. Kater. 1989. Expression and function of the [illegible]transmitter serotonin during development of the *Helisoma* n[illegible]. *Dev. Biol.* **131:** 483–495.

Goldb[illegible] J. I., N. K. Koehncke, K. J. Christopher, C. Neumann, and T. J. Diefenbach. 1994. Pharmacological characterization of a serotonin receptor involved in early embryonic behavior of *Helisoma trivolvis*. *J. Neurobiol.* **25:** 1545–1557.

Harris-Warrick, R. M., and E. Marder. 1991. Modulation of neural networks for behavior. *Annu. Rev. Neurosci.* **14:** 39–57.

Hay-Schmidt, A. 1990a. Catecholamine-containing, serotonin-like, and neuropeptide FMRFamide-like immunoreactive cells and processes of the nervous system of the pilidium larva (Nemertini). *Zoomorphology* **109:** 231–244.

Hay-Schmidt, A. 1990b. Distribution of catecholamine-containing, serotonin-like and neuropeptide FMRFamide-like immunoreactive neurons and processes in the nervous system of the actinotroch larva of *Phoronis muelleri* (Phoronida). *Cell Tissue Res.* **259:** 105–118.

Hay-Schmidt, A. 1990c. Catecholamine-containing, serotonin-like, and FMRFamide-like immunoreactive neurons and processes in the nervous system of the early actinotroch larva of *Phoronis vancouverensis* (Phoronida): distribution and development. *Can. J. Zool.* **68:** 1525–1536.

Hay-Schmidt, A. 1992. Ultrastructure and immunocytochemistry of the nervous system of the larvae of *Lingula anatina* and *Glottidia* sp. (Brachiopoda). *Zoomorphology* **112:** 189–205.

Hay-Schmidt, A. 1995. The larval nervous system of *Polygordius lacteus* Scheinder, 1868 (Polygordiidae, Polychaeta): immunocytochemical data. *Acta Zool.* **76:** 121–140.

Holland, N. D., and L. Z. Holland. 1993. Serotonin-containing cells in the nervous system and other tissues during ontogeny of a lancelet, *Branchiostoma floridae*. *Acta Zool.* **74:** 195–204.

Hughes, R. L., Jr., and R. M. Woollacott. 1978. Ultrastructure of potential photoreceptoral organs in the larva of *Scrupocellaria bertholetti* (Bryozoa). *Zoomorphologie* **91:** 225–234.

Hughes, R. L., Jr., and R. M. Woollacott. 1980. Photoreceptors of bryozoan larvae (Cheilostomata, Cellularioidea). *Zool. Scr.* **9:** 129–138.

Johnson, B. R., J. II. Peck, and R. M. Harris-Warrick. 1993. Dopamine induces sign reversal at mixed chemical-electrical synapses. *Brain Res.* **625:** 159–164.

Johnson, B. R., J. II. Peck, and R. M. Harris-Warrick. 1995. Distributed amine modulation of graded chemical transmission in the pyloric network of the lobster stomatogastric ganglion. *J. Neurophysiol.* **74:** 437–452.

Kabotyanski, E. A., W. Winlow, D. A. Sakharov, L. Bauce, and K. Lukowiak. 1992. 5-hydroxytryptophan elicits sustained CPG activity for rhythmic shell movements in *Lymnaea stagnalis*. *Soc. Neurosci. Abstr.* **18:** 531.

Katz, P. 1995. Intrinsic and extrinsic neuromodulation of motor circuits. *Curr. Opin. Neurobiol.* **5:** 799–808.

Kempf, S. C., B. Masinovsky, and A. O. D. Willows. 1987. A simple neuronal system characterized by a monoclonal antibody to SCP neuropeptides in embryos and larvae of *Tritonia diomedea* (Gastropoda, Nudibranchia). *J. Neurobiol.* **18:** 217–236.

Kingzett, B. C., N. Bourne, and K. Leask. 1990. Induction of metamorphosis of the Japanese scallop *Patinopecten yessoensis* Jay. *J. Shellfish Res.* **9:** 119–124.

Krstulovic, A. M. 1982. Investigations of catecholamine metabolism using high-performance liquid chromatography: analytical methodology and clinical applications. *J. Chromatogr.* **229:** 1–34.

Kyriakides, M. A., and C. R. McCrohan. 1989. Effect of putative neuromodulators on rhythmic buccal motor output in *Lymnaea stagnalis*. *J. Neurobiol.* **20:** 635–650.

Lacalli, T. C., and II. J. Gilmour. 1990. Ciliary reversal and locomotory control in the plutcus larva of *Lytechinus pictus*. *Phil. Trans. R. Soc. Lond. B.* **330:** 391–396.

Livingstone, M. S., R. M. Harris-Warrick, and E. A. Kravitz. 1980. Serotonin and octopamine produce opposite postures in lobsters. *Science* **208:** 76–79.

Lynch, W. R. 1947. The behavior and metamorphosis of the larva of *Bugula neritina* (Linnaeus): experimental modification of the length of the free-swimming period and the responses of the larvae to light and gravity. *Biol. Bull.* **92:** 115–150.

Mangan, P. S., G. A. Curran, C. A. Hurney, and W. O. Friesen. 1994. Modulation of swimming behavior in the medicinal leech. III. Control of cellular properties in motor neurons by serotonin. *J. Comp. Physiol. A* **175:** 709–722.

Marois, R., and T. J. Carew. 1990. The gastropod nervous system in metamorphosis. *J. Neurobiol.* **21:** 1053–1071.

Mawatari, S. 1951. The natural history of a common fouling bryozoan, *Bugula neritina* (Linnaeus). *Misc. Rep. Res. Inst. Nat. Resour. (Tokyo)* **20:** 47–54.

McCauley, D. W. 1995. Serotonin mediates metamorphosis in planulae of the hydrozoan *Phialidium gregarium*. *Am. Zool.* **35:** 112A.

McClellan, A. D., G. D. Brown, and P. A. Getting. 1994. Modulation of swimming in *Tritonia:* excitatory and inhibitory effects of serotonin. *J. Comp. Physiol. A.* **174:** 257–266.

Mogami, Y., K. Watanabe, C. Ooshima, A. Kawano, and S. A. Baba. 1992. Regulation of ciliary movement in sea urchin embryos: dopamine and 5-HT change the swimming behaviour. *Comp. Biochem. Physiol. C* **101:** 251–254.

Nakajima, Y. 1987. Localization of catecholaminergic nerves in larval echinoderms. *Zool. Sci.* **4:** 293–299.

Nakajima, Y. 1988. Serotonergic nerve cells of starfish larvae. Pp. 235–239 in *Echinoderm Biology,* R.D. Burke, P.V. Mladenov, P. Lambert, and R.L. Parsley, eds. Balkema, Rotterdam.

Okamoto, K., N. Watanabe, A. Watanabe, and K. Sakata. 1995. Induction of larval metamorphosis in serpulid polychaetes by L-DOPA and catecholamines. *Fish. Sci.* **61:** 69–74.

Pires, A., S. L. Coon, and M. G. Hadfield. 1992. Analysis of catecholamines and DOPA in a gastropod larva. *Am. Zool.* **32:** 119A.

Pires, A., M. G. Hadfield, and J. A. Skiendzielewski. 1995. Depletion of dopamine is accompanied by inhibition of metamorphosis in two gastropods. *Am. Zool.* **35:** 10A.

Reed, C. G., and R. M. Woollacott. 1982. Mechanisms of rapid morphogenetic movements in the metamorphosis of the bryozoan *Bugula neritina* (Cheilostomata, Cellularioidea). I. Attachment to the substrate. *J. Morphol.* **172:** 335–348.

Reed, C. G., and R. M. Woollacott. 1983. Mechanisms of rapid morphogenetic movements in the metamorphosis of the bryozoan *Bugula neritina* (Cheilostomata, Cellularioidea). II The role of dynamic assemblages of microfilaments in the pallial epithelium. *J. Morphol.* **177:** 127–143.

Reed, C. G., J. M. Ninos, and R. M. Woollacott. 1988. Bryozoan larvae as mosaics of multifunctional ciliary fields: ultrastructure of the sensory organs of *Bugula stolonifera* (Cheilostomata: Cellularioidea). *J. Morphol.* **197:** 127–145.

Riggin, R. M., and P. T. Kissinger. 1977. Determination of catecholamines in urine by reverse-phase liquid chromatography with electrochemical detection. *Anal. Chem.* **49:** 2109–2111.

Ryland, J. S. 1960. Experiments on the influence of light on the behavior of polyzoan larvae. *J. Exp. Biol.* **37:** 783–800.

Ryland, J. S. 1962. The effect of temperature on the photic responses of polyzoan larvae. *Sarsia* **6:** 41–48.

Ryland, J. S. 1976. Physiology and ecology of marine bryozoans. *Adv. Mar. Biol.* **14:** 285–443.

Ryland, J. S. 1977. Taxes and tropisms of bryozoans. Pp. 411–436 in *Biology of Bryozoans,* R.M. Woollacott and R.L. Zimmer, eds. Academic Press, New York.

Syed, N. I., A. G. M. Bulloch, and K. Lukowiak. 1990. *In vitro* reconstruction of the respiratory central pattern generator of the mollusk *Lymnaea. Science* **250:** 282–285.

Thorndyke, M. C., B. D. Crawford, and R. D. Burke. 1992. Localization of a SALMFamide neuropeptide in the larval nervous system of the sand dollar *Dendraster excentricus. Acta Zool.* **73:** 207–212.

Thorson, G. 1964. Light as an ecological factor in the dispersal and settlement of larvae of marine bottom invertebrates. *Ophelia* **1:** 167–208.

Toneby, M. 1980. Dopamine in developing larvae of the sea urchin *Psammechinus miliaris* Gmelin. *Comp. Biochem. Physiol. C* **65:** 139–142.

Walther, M., U. Ulrich, M. Kroiher, and S. Berking. 1996. Metamorphosis and pattern formation in *Hydractinia echinata,* a colonial hydroid. *Int. J. Dev. Biol.* **40:** 313–322.

Wieland, S. J., and A. Gelperin. 1983. Dopamine elicits feeding motor program in *Limax maximus. J. Neurosci.* **3:** 1735–1745.

Willard, A. 1981. Effects of serotonin on the generation of the motor program for swimming by the medicinal leech. *J. Neurosci.* **1:** 936–944.

Woollacott, R. M., and R. L. Zimmer. 1971. Attachment and metamorphosis of the cheilo-ctenostome bryozoan *Bugula neritina* (Linné). *J. Morphol.* **134:** 351–382.

Woollacott, R. M., and R. L. Zimmer. 1972. Fine structure of a potential photoreceptoral organ in the larva of *Bugula neritina* (Bryozoa). *Z. Zellforsch. Mikrosk. Anat.* **123:** 458–169.

Woollacott, R. M., and R. L. Zimmer. 1978. Metamorphosis of cellularioid bryozoans. Pp. 49–63 in *Settlement and Metamorphosis of Marine Invertebrate Larvae,* F.-S. Chia and M.E. Rice, eds. Elsevier North-Holland, New York.

Yamamoto, H., A. Tachibana, S. Kawaii, K. Matsumura, and N. Fusetani. 1996. Serotonin involvement in larval settlement of the barnacle, *Balanus amphitrite. J. Exp. Zool.* **275:** 339–345.

Young, C. M., and F.-S. Chia. 1987. Abundance and distribution of pelagic larvae as influenced by predation, behavior, and hydrographic factors. Pp. 385–463 in *Reproduction of Marine Invertebrates. Volume IX. General Aspects: Seeking Unity in Diversity,* A.C. Giese, J.S. Pearse, and J.B. Pearse, eds. Blackwell Scientific Publ, Palo Alto, CA and The Boxwood Press, Pacific Grove, CA.

Zimmer, R. L., and R. M. Woollacott. 1989. Intercoronal cell complex of larvae of the bryozoan *Watersipora arcuata* (Cheilostomata: Ascophora). *J. Morphol.* **199:** 151–164.

Reference: *Biol. Bull* **192**: 410–417. (June, 1997)

Role of Chemical Signals in the Orientation Behavior of the Sea Star *Asterias forbesi*

PAUL A. MOORE AND DEBORAH M. E. LEPPER

Laboratory for Sensory Ecology, Department of Biological Sciences, Bowling Green State University, Bowling Green, Ohio 43403

Abstract. The importance of chemical signals as foraging and orientation cues has been demonstrated for many marine organisms. It is still unclear whether sea stars use chemical signals during orientation and whether chemoreception occurs in the absence of macroscale flow. To determine whether the sea star *Asterias forbesi* can perceive chemical signals in the absence of flow and what role such signals play in orientation and foraging behavior, we tested the orientation behavior of sea stars to prey and nonprey items under conditions of nondirectional flow. Prey items were whole and broken clams (*Mercenaria mercenaria*) and mussels (*Mytilus edulis*); the nonprey item was squid flesh. *Asterias forbesi* showed the ability to successfully locate odor sources irrespective of the type of odor. Only in trials with the broken clam did the animals reveal an initial directional choice towards the odor source. There were significant changes in the movement rates and heading angles during orientation for all three stimuli. In addition, orientation paths were different for each of the chemical stimuli tested. From these results, we conclude that sea stars can detect and respond to chemicals in the absence of macroscale flow. Orientation paths appear to be more of a taxis, in which heading is directly guided by the stimulus field.

Introduction

Asteroids are marine benthic invertebrates found in abundance in the littoral and subtidal zones of most shorelines. Most asteroids are carnivores and can play a significant role as keystone predators in these habitats (Feder and Christensen, 1966; Jangoux, 1982). Prey items consist of large epifaunal species including gastropods, various bivalves, and some crustaceans, typically barnacles (Feder and Christensen, 1966; Jangoux, 1982). Some species show food preferences that are not due exclusively to prey availability (Christensen, 1957; Jangoux, 1982). The sensory mechanisms that asteroids use to forage for prey have been debated for a number of years.

Most of the previous research, focusing on the chemosensory or mechanosensory abilities of asteroids, has resulted in mixed conclusions. Sloan and Campbell (1982) have reported evidence for olfaction in some species, while concluding that others have no such abilities. Other researchers have shown that olfaction is important for foraging (McClintock and Lawrence, 1981; McClintock *et al.*, 1984; Valentincic, 1985; Valentincic and Ota, 1985). In addition, chemical orientation also has been seen in both field (Christensen, 1957) and laboratory settings (Castilla, 1972a; Castilla and Crisp, 1970; Rochette *et al.*, 1994). Conversely, it was noted that *A. rubens* showed an avoidance response to damaged or spawning prey and living predators in the static-flow Y-maze and the flow tank (Castilla and Crisp, 1970). *Crossaster papposus* was observed to be attracted to prey extracts by choosing the arm in a Y-maze in which the extract was added. They also avoided the extract of carnivorous conspecifics by moving downstream (Sloan and Northway, 1982). However, orientation to live oysters, mussels, and nudibranchs could not be demonstrated in other instances (Sloan and Campbell, 1982).

Many of these studies were done in flow tanks (Castilla, 1972b; Castilla and Crisp, 1970; Sloan and Northway, 1982; Zafiriou, 1972; Zafiriou *et al.*, 1972), to which sea stars show a positive rheotaxis (Valentincic, 1983). Observed movement toward the odor source may or may not have been mediated by chemical stimulation but

Received 27 November 1996; accepted 3 March 1997.

may have been strictly a response to water flow. Avoidance responses in these situations may be negative rheotaxis, initiated by the presence of the chemical signal. Behavioral trials with no macroscale flows can help eliminate the possibility of rheotaxis but may have some confounding factors due to small-scale water dynamics in the tank. Sea stars, when excited by a food item in the aquarium, often pass directly by it or turn away just as they near it (Feder and Christensen, 1966). These behavioral results could be interpreted as being a result of small-scale circulation patterns within the aquarium.

The spatial distribution of chemical signals in marine environments is determined by the hydrodynamics of the environment. In most marine habitats, turbulent diffusion is the major force that disperses chemicals. Whether in air or water, turbulent odor concentrations in plumes are heterogeneous when measured at fast temporal and small spatial scales (air: Murlis and Jones, 1981; Murlis *et al.,* 1991; water: Atema, 1985; Moore and Atema, 1988, 1991; Zimmer-Faust *et al.,* 1988). The exact nature of concentration fluctuations within any habitat depends on the interaction between the size of the turbulent eddies and the size of the odor plume. As a result of these interactions, animals using chemical signals to locate potential prey items will experience different stimulus patterns in different flow regimes (Moore *et al.,* 1994). Thus, if changes in behavior occur simultaneously with changes in flow, it is often difficult to determine whether those changes are due to the differences in the chemical signal or the mechanical signal. In previous work, mechanical and chemical signals were presented simultaneously (Castilla, 1972b; Castilla and Crisp, 1970; Rochette *et al.,* 1994; Sloan and Northway, 1982; Zafiriou, 1972; Zafiriou *et al.,* 1972). To determine which source of information is important in orientation behavior, it is important to separate these two sources of information during orientation trials.

Marine animals use many different behavioral mechanisms to orient to a chemical source. Categories for orientation behaviors have been based on a variety of criteria, including locomotor output, distribution and number of sensory receptors, and information available to and used by the animal (Bell, 1984; Dusenbery, 1992; Kennedy, 1986; Preface for Bell and Cardé, 1984; Schöne, 1984). In a broad sense, it appears that chemical signals either play a direct guidance role (Johnson and Teeter, 1980; Moore *et al.,* 1991; Reeder and Ache, 1980; Rochette *et al.,* 1994), serve to initiate maneuvers that depend on nonchemical stimuli (Mafra-Neto and Cardé, 1994), or can be used in conjunction with mechanical signals (Weissburg and Zimmer-Faust, 1993).

From a sensory perspective, it is important to differentiate between potential sources of directional information. Y-mazes and other choice experiments demonstrate that chemoreception can play a role in directional decisions, but under these conditions, reliable directional information is still provided by the unidirectional flow. Although there are problems of small-scale circulation, the reason for performing experiments in still water is the removal of any directional information provided by macroscale currents. Although it is highly unlikely that flow is completely absent in still-water trials, it is equally unlikely that reliable directional information on the odor source is provided by any small-scale circulation present within the tank.

Chemical cues are apparently important in orientation by *A. forbesi,* but it is still not clear whether chemical signals or mechanical and chemical signals mediate foraging and orientation. The purpose of this study was to demonstrate chemoreception by *A. forbesi* in the absence of directional information provided by macroscale flow and to investigate the role of chemical signals in orientation behavior. We hypothesize that this species of sea star has the ability to use chemical signals in the absence of macroscale flow to successfully orient to potential prey. Thus, still-water trials become crucial for determining the source of information controlling or guiding the orientation of the organism. A better understanding of the chemoreceptive abilities of this sea star and sources of sensory information used in foraging may lead to a broader understanding of intertidal foraging mechanisms in sea stars.

Materials and Methods

Animals

Sea stars, *Asterias forbesi,* were obtained from the Aquatic Resources Division of the Marine Biological Laboratory in Woods Hole, Massachusetts. The animals were wild caught off the coast of Woods Hole and remained in flow-through seawater tanks before shipping to our laboratory. The animals measured 7.5–15.25 cm in diameter and were kept in 35-gallon aquaria, maintained at a salinity of 25‰–30‰, a temperature of 15°–20°C, and a cycle of 12 h light and 12 h dark. An undergravel filter was used for maintaining water quality in the tank, and filtered air was pumped into the system for aeration and circulation. Each sea star was isolated from the others in the aquarium by plastic crating, which allowed water movement between the chambers but separated animals for individual identification. No more than four individuals were housed in a single aquarium. The sea stars were fed once a week at a maintenance level, about 2 g of thawed squid flesh. Any uneaten food was removed from the aquarium after 2 h.

Hard-shelled clams (*Mercenaria mercenaria*) and blue mussels (*Mytilus edulis*) were obtained from the Aquatic Resources Division of the Marine Biological Laboratory

in Woods Hole. Both of these molluscs are common prey items of *A. forbesi* in this area. The clams (5–10 cm in width) and mussels (2–5 cm in width) were placed in a 35-gallon aquarium under the same conditions of salinity, temperature, and light as the sea stars. They were fed suspended algae twice a week for 4 h each time by placing them in beakers with the algae.

Experimental procedure

The testing arena was an acrylic plastic aquarium, dimensions 57.5 cm × 117.5 cm, with a water depth of 5 cm. It was located within the same room as the housing aquaria and under the same lighting conditions. The salinity of the tank was matched to the salinity of the housing aquarium. The bottom of the tank was marked off in a 5-cm grid with the origin (0, 0) at the center of the tank. Between each trial, the tank was rinsed with cold tap water to avoid any chemical contamination from the previous trial. After filling, the tank was allow to sit for at least 1 h before orientation trials were started.

For every trial, the animal was placed at the origin, with its madreporite as a fixed point of reference. Previous observations indicated that handling did not adversely affect the behavior. In trials with a chemical stimulus, the source was placed in a position (x = 0 cm, y = −45 cm) that allowed the sea star to move both toward and away from the stimulus by several body lengths and prevented accidental contact with the source if the animal was only following the contours of the tank walls.

During each 25-min trial, the position of the sea star (determined using the madreporite as a reference) was recorded by eye every 30 s. Animals that did not move for a period of 6 min were rejected. For experimental trials, the chemical stimulus (squid, mussel, or clam) was placed in the tank before the sea star was added. If the animal walked within 5 cm of the stimulus source, the run was considered successful. If the madreporite of the animal was within 5 cm of the odor source, one of the arms would be in contact with the source. By accepting a distance of 5 cm for the madreporite, we had a criterion that was consistent between trials and independent of the arm size of the animals. Control studies were conducted in the same way as experimental trials except that no chemical stimulus was placed in the tank. After each trial, the sea star was returned to its chambered aquarium and any stimulus source discarded.

Stimulus preparation and distribution

In chemical stimulus trials, five stimulus sources were used: squid flesh (a broad-based amino acid source), whole live clam and mussel (potential prey items), and cracked clam and mussel (wounded potential prey items). For the squid stimulus, a 2-g piece of flesh was cut from the body of the squid with a sharp blade. The frozen flesh had been obtained in bulk and was allowed to thaw before use. For whole prey trials, the bivalve was placed in the tank 5 min prior to an orientation run to allow it to begin filtering. For broken prey trials, the bivalve was crushed and left in the tank for 10 min prior to an orientation run. Mussels were prepared by holding the animal directly over the source point and crushing the shell with pliers; clams were placed on plastic wrap, hit with a hammer, and then transferred to the source point. Additional control trials used cleaned and dried empty shells from the clam or mussel. For these trials, an intact shell of each species was recovered from dead individuals in the holding aquarium. The shells were vigorously scrubbed with biodegradable soap and a nylon brush. The shells were then rinsed under tap water for 1 min, soaked in tap water for 1 h, and soaked in dilute bleach (1:10) for 10 min. After this the shells were rinsed under tap water for 1 min, soaked three times for 30 min each in distilled water, and rinsed between each period. Just prior to the trials, the shells were soaked for 30 min in 30‰ salt water.

To qualitatively analyze the spatial movement of chemicals within the testing arena, we used fluorescein dye in gelatin blocks to mimic the spatial distribution of chemicals emanating from the nonliving prey items. Gelatin blocks with 2 g/l of fluorescein dye were placed within the testing arena using the methods outlined above for broken prey items. After 10 min, the spatial distribution of the dye was mapped visually using four broad categories of dye concentration. This process was repeated six times. This qualitative analysis showed that each of the six replicates resulted in a different spatial distribution and that the lowest visible concentration of dye was 35 ± 0.2 cm (SEM) away from the odor source. For each replicate, the distance that 10 individual filaments of dye moved during a 1-min period was recorded as an estimate of the maximum water velocity within the tank. The estimate of the maximum water velocity was 3 ± 0.5 cm/min (SEM) or 0.05 ± 0.008 cm/s for all 60 samples.

Data analysis

The orientation paths from each run were recorded as a single point (x, y) every 30 s as previously described. From these paths, several orientation parameters were analyzed. These included walking speed, net-to-gross ratio (NGR), turning angles, and headings. NGR values were transformed using an arcsine method (specifically, $p' = \text{arcsine } p^{1/2}$, Zar, 1984). Standard ANOVA techniques were used to compare the average value for each parameter between each of the trials. If the ANOVA was significant, it was followed by a *post-hoc* comparison us-

ing a Neuman-Keuls analysis. A linear regression analysis was used to correlate changes in parameter values with distance from source. Distance from the source for regression analysis was the Euclidean distance between the source point (0, 0) and the animal's position within the tank (described above). NGR was calculated by dividing the Euclidean distance from start to finish (net) by the total path length (gross). These values can range from 0 to 1, with 0 being a very circuitous path, and 1 being a linear path. Turn angle was defined as the angle between the path connecting the previous ($t = -1$) position to the present ($t = 0$) position and the path connecting the present to the next ($t = +1$) position (Moore *et al.*, 1991). A sea star's heading was defined as the angle between a straight line towards the source and the direction from the present position to the next position on the track, with an angle of zero pointing directly at the source (Moore *et al.*, 1991). All angles were calculated in a clockwise fashion.

The initial directional choice for each sea star was recorded as the heading angle for initial movement from the starting point. A modification of the Rayleigh's test (The V test) was used to determine whether the heading angles were uniformly distributed around the circle or if there was a significant directionality to the movement (Zar, 1984). For this test, we assumed *a priori* that an angle of zero degrees towards the odor source was expected.

Results

General orientation results

Our criteria for successful orientation resulted in rejection of 52% of the total number of trials. Successful trials resulted in different paths that depended upon the odor source (Fig. 1). Most rejections were due to the animal's inability to locate the odor source; very few of the trials were rejected due to lack of movement by the animal. This high rate of rejection may be due to the unnatural experimental condition of no macroscale flow. Subsequent testing under flowing conditions may produce a higher success rate, but would not allow us to pursue the hypothesis proposed in the introduction.

Orientation to squid flesh

The odor of squid flesh in the test arena caused the animal to modify its walking behavior. This was shown by a significantly slower walking speed in the experimental animals compared with controls (t test, $P < 0.01$, Fig. 2). Sea stars in the presence of odor walked at 0.06 ± 0.01 (SEM) cm/s and control animals at 0.18 ± 0.02 cm/s. In

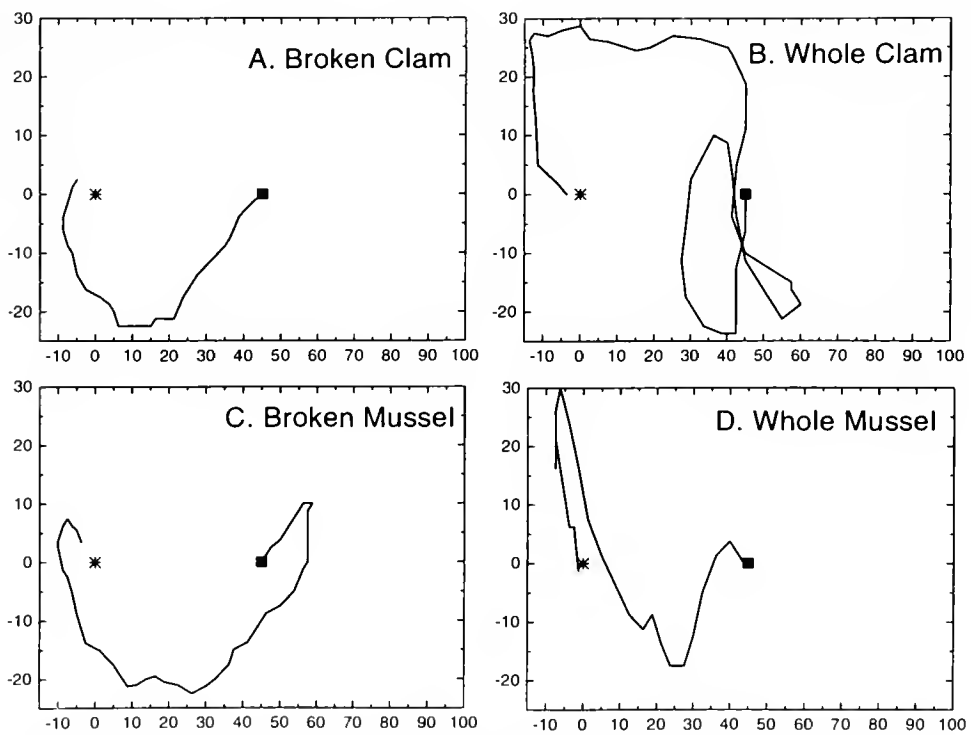

Figure 1. Randomly selected trials for four different sea stars for four different stimuli. Odor sources: (A) broken clam, (B) whole clam, (C) broken mussel, (D) whole mussel. Stimulus source is located at 0,0 (asterisk) and starting point of orientation path is at 45,0 (solid square).

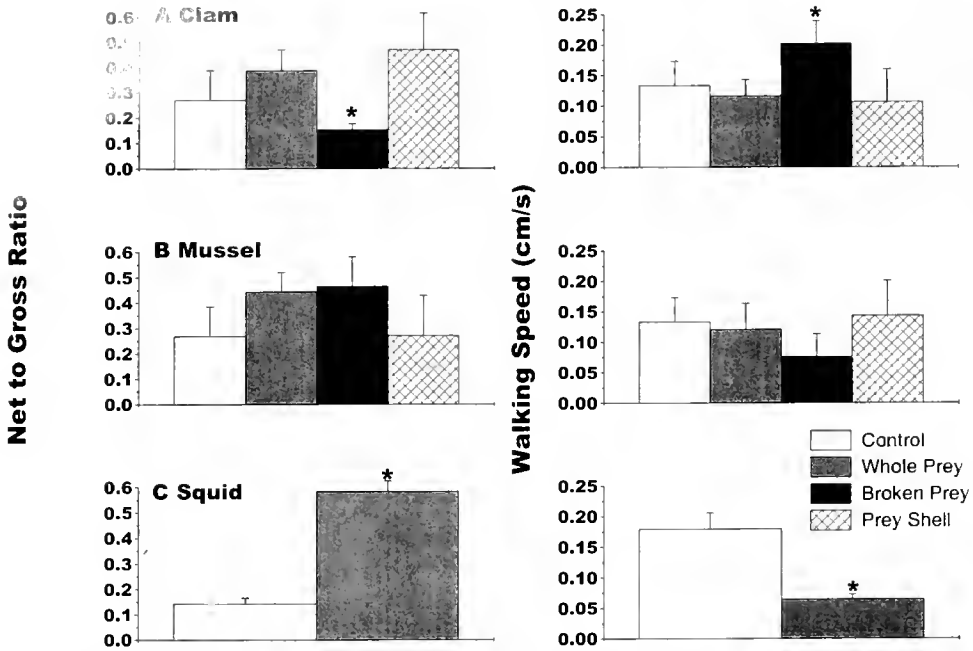

Figure 2. Average (±SEM) net-to-gross ratio and walking speed of sea stars under no odor stimulation (control, blank bar), whole prey (gray bar), broken prey (black bar), and empty prey shell (hatched bar). Prey items: (A) clam, (B) mussel, (C) squid flesh. $n = 14$ for all trials for clam and mussel; $n = 22$ for squid. Asterisk indicates a value that is significantly different from all other values (ANOVA, then Newman-Keuls test, $P < 0.05$).

addition, the paths of sea stars walking during chemical stimulation were more linear than those of control animals. This was shown by a significantly higher NGR in the experimental animals than in the controls (t test, $P < 0.01$, Fig. 2). Experimental animals had an average net-to-gross ratio of 0.58 ± 0.04 (SEM), whereas control animals had ratios of 0.14 ± 0.02. Further analysis of orientation paths showed a significant relationship between heading angles and distance from the odor source (Table I). Sea stars had lower heading angles as they approached the odor source, but this same relationship was not present in the turning angles. Analysis of the initial directionality of sea star orientation to squid flesh showed no significant initial directional choice for either the control or the experimental groups.

Orientation to natural prey items

Clam. Sea stars walked significantly faster when a broken clam was in the test arenas than they did in the other test situations (Fig. 2). There was no difference in walking speeds among the control, whole clam, or empty clam shell trials. Sea stars showed a more circuitous path in the presence of a broken clam than in the other test situations (Fig. 2). There was no difference in NGR among the control, whole clam, or empty clam shell trials. Regression analysis of orientation paths showed a significant relationship between heading angles and distance from the odor source during whole clam stimulation (Table I). As with the squid odor, heading angles during orientation significantly decreased as sea stars approached the odor source. This relationship was absent from heading angles for the control, empty shell, and

Table I

Regression summary of changes in heading and turning angles with distance from odor source

Odor source	Heading angles	Turning angles
Control	N.S.	N.S.
Squid	$y = 37.7 + 0.59\,x^{A}$	N.S.
Whole mussel	$y = 46.0 + 0.52\,x^{B}$	N.S.
Broken mussel	$y = 31.8 + 0.86\,x^{C}$	N.S.
Mussel shell	N.S.	N.S.
Whole clam	$y = 26.2 + 0.82\,x^{D}$	N.S.
Broken clam	N.S.	N.S.
Clam shell	N.S.	N.S.

All regressions were run on the population of sea stars within each trial.

[A] $F(1,393) = 20.1$, $P < 0.05$, $r = 0.22$.

[B] $F(1,348) = 12.5$, $P < 0.05$, $r = 0.18$.

[C] $F(1,194) = 16.4$, $P < 0.05$, $r = 0.28$.

[D] $F(1,120) = 11.4$, $P < 0.05$, $r = 0.30$.

All nonsignificant results had $P > 0.10$.

broken clam situations and was absent from all turning angle analysis. Analysis of the initial directional choices of sea stars during clam stimulation showed a significant directional choice towards the odor source for the broken clam only (The V test, $\mu_0 = 0°$, $u = 2.0$, $P < 0.05$, Fig. 3). All other heading angles were uniformly distributed around the circle, indicating no significant initial heading angle.

Mussel. Sea stars did not alter either their walking speed or the NGR in any of the trials involving either mussels, broken mussels or empty mussel shells when compared to control values (Fig. 2). There was a significant change in heading angles for both the whole and broken mussel trials. Sea stars significantly decreased their heading angles as they approached the odor source (Table I). This relationship was absent from heading angles for the control and empty mussel shell and was absent from all turning angle analysis. Analysis of the initial directional choices of sea stars during mussel stimulation showed that there was not a significant directional choice towards the odor source for any of the odor stimulations (Fig. 4).

Discussion

In previous orientation studies using sea stars, it has been difficult to differentiate between a true chemically mediated response, in which the animal is responding only to the odors, and a combination of chemically and mechanically mediated responses. In fact, Rochette *et al.* (1994) showed conclusively that *Leptasterias polaris* has a strong orientation response to current in both the presence and absence of chemical stimulation. The orientation behavior that results from multiple inputs of chemosensory and mechanosensory information could be due to a range of orientation strategies from a chemically triggered rheotaxis to a flow-triggered chemotaxis (for a review of different orientation strategies, see Shöne, 1984). This study demonstrates three results concerning the chemosensory abilities of *A. forbesi*. First, this species perceives and responds to chemical signals in the absence of macroscale flow. Many previous studies on both the foraging and orientation behavior of other sea stars have been in flow tanks (Castilla, 1972b; Castilla and Crisp, 1970; Sloan and Northway, 1982; Zafiriou, 1972; Zafiriou *et al.*, 1972). In many of these situations, the sea stars show a positive rheotaxis (Valentincic, 1983), and it is not clear whether they are responding to the macroscale flow, to the chemical, or to both.

Second, we demonstrate that *A. forbesi* is capable of locating odor sources without the aid of external directional cues provided by macroscale flow. The analysis of the orientation paths shows that orientations are probably a response to information from the chemical signal within the experimental arena. Several features of the orientation paths reveal an orientation strategy that may be a taxis (as defined in both Dusenbery, 1992, and Schöne, 1984). Using these definitions, a taxis is an orientation that is a result of biased or directed turns with respect to some aspect of the stimulus field. This would result in decreased heading angles as the organism approached the odor source. As has been demonstrated for other sea stars (Rochette *et al.*, 1994), and suggested for *A. forbesi* under different flow conditions (Dale, 1996), these animals use concentration differences as measured at the tips of different arms to guide orientation to food sources. This is a tropotactic response, in which the orientation path is guided by simultaneous information obtained by spatially separate sensory cells. If *A. forbesi* is performing a tropotaxis by comparing different concentrations at the tips of its arms, we would expect to find some initial directional decisions towards the odor source and decreased heading angles as the animal approached the source.

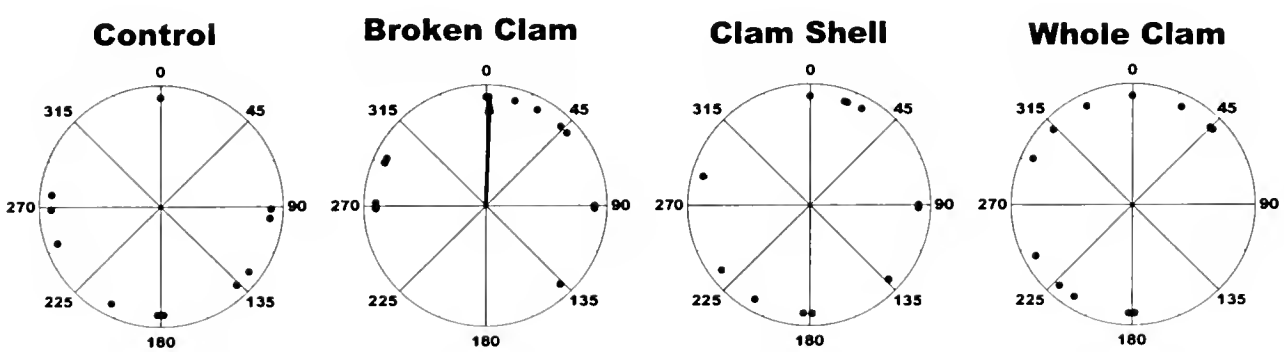

Figure 3. Initial directional choices for sea stars during different odor stimulations for clam sources. Solid dots represent heading angle in relation to odor source for the first movement of the animal. Significant mean angles are indicated by a solid black arrow, V test. All other groups were uniformly distributed around the circle; $n = 14$ for all groups.

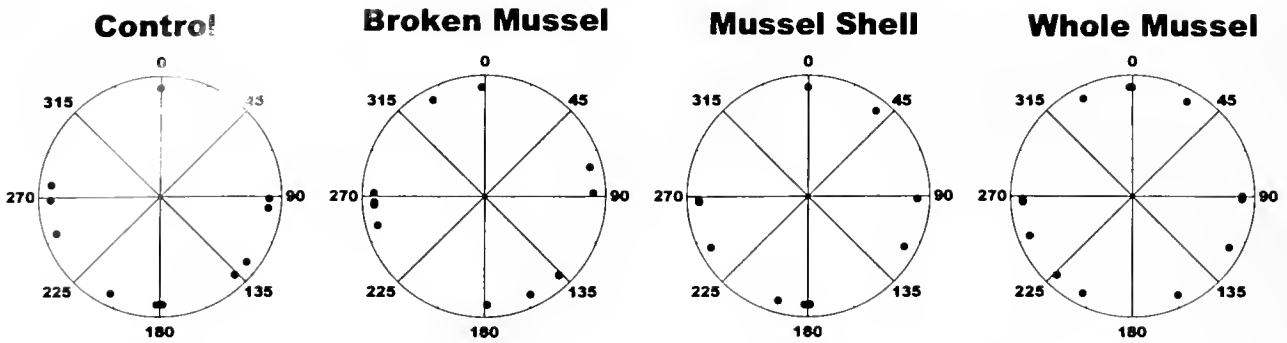

Figure 4. Initial directional choices for sea stars during different odor stimulations for mussel sources. Solid dots represent heading angle in relation to odor source for the first movement of the animal. There were no significant mean angles in any of the groups, indicating that the initial headings were uniformly distributed around the circle; $n = 14$ for all groups.

We found changes in the orientation paths to be a function of distance from the odor source. For all of our stimulus conditions except one, we found that the heading angle relative to the odor source decreased as an animal approached the odor source. In other words, as it approached the odor source, the animal began to walk in a straighter line towards the source. Since we did not find similar results with the control or shell studies, we conclude that the locomotory output of the animal is influenced by the chemical stimulus whether it is perceived spatially or temporally. In addition, walking speed and turning angles did not change as a function of distance. Although these results are consistent with either orientation mechanism, we feel that the behavioral patterns of our animals in the absence of macroscale flow are more compatible with a taxis-based orientation strategy then with a kinesis strategy (as defined by Dusenbery, 1992). This finding is similar to that of Rochette *et al.* (1994), who convincingly demonstrated that other species of sea stars were capable of showing directed responses, but that these directional choices were dependent upon their physiological state (starved *vs.* fed) and the ambient current flow. Their finding may be due to decisions based on dual sensory information (that is, from both the odor signal and ambient conditions of macroscale flow), whereas we provided mainly chemosensory cues.

Third, *A. forbesi* responded differently to the various stimulus sources by having distinct walking patterns for each of the stimulus conditions. During stimulation with squid flesh, the sea stars walked slower, in a straighter line, with a characteristic decrease in heading angle as they approached the odor source. The sea stars walked faster and had a more circuitous path only for the broken clam and showed only the characteristic changes in heading angles for the mussel stimulus. Different locomotory outputs may indicate either that these animals can perceive and identify different prey items or that the outputs are responses to concentration differences between stimulus sources. Since we neither quantified the stimulus patterns nor analyzed the chemical composition under the different treatments, it is difficult to make any definite conclusions based on the differences in locomotion.

Many researchers have studied chemical orientation in marine animals. Animal models include fish (Kleerekoper, 1967; Kleerekoper *et al.*, 1969) and decapod crustaceans (Moore *et al.*, 1991; Reeder and Ache, 1980; Weissburg and Zimmer-Faust, 1993). These studies have shown that the spatial and temporal distribution of chemical signals plays an important part in the orientation ability of these animals. It has also been shown that animals can have different responses to different odors. Certainly, for sea stars, some odors trigger an attraction and other odors an avoidance (Castilla and Crisp, 1970; Sloan and Northway, 1982). Similar findings have been recorded for the mud snail (Atema and Burd, 1975). All of these results taken together show that marine organisms can have different behavioral responses for different chemical sources, but it has yet to be shown whether a single animal has distinct orientation strategies for different odors.

In summary, *A. forbesi* has chemosensory responses in the absence of macroscale flow and can locate the source of odors using only chemosensory information. It is still unclear whether these animals strictly use a chemotaxis or a kinesis strategy and whether they use both spatial and temporal sampling of concentrations to guide orientation to the odor source. In addition, the sea stars show different orientation paths for different odors. Further research is needed to determine whether these animals have different orientation strategies that are prey dependent.

Acknowledgments

The authors thank Dr. Steve Vessey for reading an earlier version of this manuscript and three anonymous re-

viewers for insightful comments. This research is supported by NSF grant OCE-9596270.

Literature Cited

Atema, J. 1985. Chemoreception in the sea: adaptation of chemoreceptors and behavior to aquatic stimulus conditions. *Soc. Exp. Biol. Symp.* **39:** 387–423.

Atema, J., and G. D. Burd. 1975. A field study of chemotactic responses of the marine mud snail *Nassarius obsoletus*. *J. Chem. Ecol.* **1:** 243–251.

Bell, W. J. 1984. Chemo-orientation in walking insects. Pp. 93–106 in *Chemical Ecology of Insects*, W. J. Bell and R. T. Cardé, eds. Sinauer Associates, Sunderland, MA.

Bell, W. J., and R. T. Cardé. 1984. *Chemical Ecology of Insects*. Sinauer Associates, Sunderland, MA.

Castilla, J. C. 1972a. Responses of *Asterias rubens* to bivalve prey in a Y-maze. *Mar. Biol.* **12:** 222–228.

Castilla, J. C. 1972b. Avoidance behavior of *Asterias rubens* to extracts of *Mytilus edulis*, solutions of bacteriological peptone, and selected amino acids. *Mar. Biol.* **15:** 236–245.

Castilla, J. C., and D. J. Crisp. 1970. Responses of *Asterias rubens* to olfactory stimuli. *J. Mar. Biol. Assoc. U.K.* **50:** 829–847.

Christensen, A. M. 1957. The feeding behavior of the seastar *Evasterias troschelii* Stimpson. *Limnol. Oceanogr.* **2:** 180–197.

Dale, J. H. 1996. Co-ordination of chemosensory orientation in the starfish, *Asterias forbesi*. *Chem Senses Abstr.* (in press).

Dusenbery, D. B. 1992. *Sensory Ecology: How Organisms Acquire and Respond to Information*. W.H. Freeman, New York.

Feder H., and A. M. Christensen. 1966. Aspects of asteroid biology. Pp. 87–127 in *Physiology of Echinodermata*, R. A. Boolootian, ed. Interscience, New York.

Jangoux, M. 1982. Food and feeding mechanisms: Asteroidea. Pp. 117–159 in *Echinoderm Nutrition*, M. Jangoux and J. M. Lawrence, eds. Balkema, Rotterdamm.

Johnsen, P. B., and J. H. Teeter. 1980. Spatial gradient detection of chemical cues by catfish. *J. Comp. Physiol. A* **140:** 95–99.

Kennedy, J. S. 1986. Some current issues in orientation to odour sources. Pp. 11–25 in *Mechanisms in Insect Olfaction*, T. L. Payne, M. C. Birch, and C. E. J. Kennedy, eds. Claredon Press, Oxford.

Kleerekoper, H. 1967. Some aspects of olfaction in fish, with special reference to orientation. *Am. Zool.* **7:** 385–295.

Kleerekoper, H., A. M. Timms, G. F. Westlake, F. B. Davy, T. Malar, and V. M. Anderson. 1969. Inertial guidance system in the orientation of the goldfish (*Carassius auratus*). *Nature* **223:** 501–502.

Mafra-Neto, A., and R. T. Cardé. 1994. Fine scale structure of pheromone plumes modulates upwind orientation of flying moths. *Nature* **369:** 142–144.

McClintok, J. B., T. S. Klinger, and J. M. Lawrence. 1984. Chemoreception in *Lucidia clathrata* (Echinodermata: Asteroidea): qualitative and quantitative aspects of chemotactic responses to low molecular weight compounds. *Mar. Biol* **84:** 47–52.

McClintok, J. B., and J. M. Lawrence. 1981. An optimization study on the feeding behavior of *Lucidia clathrata* Say (Echinodermata: Asteroidea). *Mar. Behav. Physiol.* **10:** 167–181.

Moore, P. A., and J. Atema. 1988. A model of a temporal filter in chemoreception to extract directional information from a turbulent odor plume. *Biol. Bull.* **174:** 355–363.

Moore, P. A., and J. Atema. 1991. Spatial information in the three-dimensional fine structure of an aquatic odor plume. *Biol. Bull.* **181:** 408–418.

Moore, P. A., N. Scholz, and J. Atema. 1991. Chemical orientation of lobsters, *Homarus americanus*, in turbulent odor plumes. *J. Chem. Ecol* **17:** 1293–1307.

Moore, P. A., M. J. Weissburg, J. M. Parrish, R. K. Zimmer-Faust, and G. A. Gerhardt. 1994. Spatial distribution of odors in simulated benthic boundary layer flows. *J. Chem. Ecol.* **20:** 255–279.

Murlis J., and C. D. Jones. 1981. Fine-scale structure of odour plumes in relation to insect orientation to distant pheromone and other attractant sources. *Phys. Ent.* **6:** 71–86.

Murlis, J., M. A. Willis, and R. T. Cardé. 1991. Odour signals: patterns in space and time. Pp. 6–17 in *Proceedings of the Tenth International Symposium on Olfaction and Taste*, K. Døving, ed. Graphic Communication System, Oslo.

Reeder, P. B., and B. W. Ache. 1980. Chemotaxis in the Florida spiny lobster, *Panulirus argus*. *Anim. Behav.* **28:** 831–839.

Rochette, R., J.-F. Hamel, and J. H. Himmelman. 1994. Foraging strategy of the asteroid *Leptasterias polaris*: role of prey odors, current and feeding status. *Mar. Ecol. Prog. Ser.* **106:** 93–100.

Shöne, H. 1984. *Spatial Orientation*. Princeton University Press, Princeton, NJ.

Sloan, N. A., and A. C. Campbell. 1982. Perception of food. Pp. 3–23 *Echinoderm Nutrition*, M. Jangoux and J. M. Lawrence, eds. Balkema, Rotterdam.

Sloan N. A., and S. M. Northway. 1982. Chemoreception by the asteroid *Crossaster papposus* (L). *J. Exp. Mar. Biol. Ecol.* **61:** 85–98.

Valentincic, T. 1983. Innate and learned responses to external stimuli in asteroids. Pp. 111–137 *Echinoderm Nutrition*, M. Jangoux and J. M. Lawrence, eds. Balkema, Rotterdam.

Valentincic, T. 1985. Behavioral study of chemoreception in the sea star *Marthasterias glacialis*: structure-activity relationships of lactic acid, amino acids, and acetylcholine. *J. Comp. Physiol. A* **157:** 537–545.

Valentincic, T., and D. Ota. 1985. Comparison of chemical senses in the sea star *Marthasterias glacialis* with chemical senses in some fishes. Pp. 563–569 in *Echinodermata. Proceedings of the Fifth International Echinoderm Conference*, B. F. Keegan and B. D. S. O'Connor, eds. Balkema, Rotterdam.

Weissburg, M. J., and R. K. Zimmer-Faust. 1993. Life and death in moving fluids: hydrodynamic effects on chemosensory-mediated predation. *Ecology* **74:** 1428–1443.

Zafiriou, O. 1972. Response of *Asterias vulgaris* to chemical stimuli. *Mar. Biol.* **17:** 100–107.

Zafiriou, O., K. J. Whittle, and M. Blumer. 1972. Response of *Asterias vulgaris* to bivalves and bivalve tissue extracts. *Mar. Biol.* **13:** 137–145.

Zar, J. H. 1984. *Biostatistical Analysis*, second edition. Prentice Hall, Englewood Cliffs, NJ.

Zimmer-Faust, R. K., J. M. Stanfill, and S. B. Collard, III. 1988. A fast, multichannel fluorometer for investigating aquatic chemoreception and odor trails. *Limnol. Oceanogr.* **33:** 1586–1595.

Reference: *Biol. Bull.* **192:** 418–425. (June, 1997)

Behavioral Modes Arise From a Random Process in the Nudibranch *Melibe*

AMANDA E. SCHIVELL[1], SAMUEL S.-H. WANG[2], AND STUART H. THOMPSON[3]

Department of Biological Sciences and the Hopkins Marine Station, Stanford University, Pacific Grove, California 93950

Abstract. Stochastic analysis was applied to observations of spontaneous behavior in the carnivorous mollusc *Melibe leonina*. Six behaviors were defined that could be easily recognized on inspection and it was found that transitions between each of these behaviors could be fully described by a first-order random process without memory of past behavioral choices. The behaviors are organized by frequency of transition into two modes, a feeding mode and a resting mode. Transitions within modes are more likely than transitions between modes, and the feeding and resting modes are linked by a preferred pair of behavioral transitions. The amount of time spent in the feeding mode is positively correlated with body size, but the average length of a feeding episode is independent of size. This suggests that body size regulates the probability of entry into feeding behavior but does not influence the basic pattern of feeding. In the presence of food the animals express nearly continuous feeding behavior, suggesting that food reduces the probability of exiting the feeding mode. This model of spontaneous behavior in *Melibe* is used to form hypotheses amenable to further exploration through neurophysiological experiments.

Introduction

Analysis of animal behavior provides the background necessary for studies of the underlying neural circuitry and circuit function. Such analysis sometimes permits useful predictions to be made about specific properties of the underlying neural networks—for example, the extent to which stochastic processes in the nervous system influence the ordering of behaviors in a sequence (Heiligenberg, 1973). Molluscs have been used to advantage by neuroethologists because the relatively limited behavioral repertoires and accessible nervous systems of these animals permit investigation of synaptic connections between identified neurons (Davis *et al.*, 1974; Kandel, 1976; Gelperin, 1983; Willows, 1985; Getting, 1989). Most studies have concentrated on reflex or conditioned responses evoked by stimuli presented in defined patterns, an approach that simplifies the design of electrophysiological experiments. Important generalizations about the organization of small neural networks have emerged from such studies, including the idea that animal behaviors are organized in hierarchies of successively more dominant or more strongly commanded responses (Tinbergen, 1951; Davis *et al.*, 1977; Getting, 1989).

Concentration on evoked and conditioned behavior ignores, however, the phenomenon of unstimulated behavioral choice (Lorenz, 1981). We recorded the temporal sequence of behaviors in the nudibranch *Melibe leonina* as it evolved spontaneously in the absence of overt stimulation, then used standard techniques of random-process analysis to model this behavioral sequence (Chatfield and Lemon, 1970). Our results lead to several conclusions. (1) In the absence of overt stimuli, the choice of behavior is well described by a first-order random process. (2) Consideration of the transition probabilities of this process indicates that spontaneous behaviors in *Melibe* fall into two behavioral modes. (3) There is a preferred transition that links the behavioral modes. (4) The presence of strong stimuli such as food organisms influences the individual transition probabilities. Fi-

Received 2 December 1996; accepted 28 February 1997.

[1] Present address: Dept. of Zoology, University of Washington, Seattle, WA

[2] Present address: Dept. of Neurobiology, Bryan Research Bldg., Duke University Medical Center, Durham, NC 27710.

[3] Author to whom correspondence should be addressed.

nally, (5) physiological parameters, such as body size, also influence behavioral transition probabilities.

Melibe is well suited to this study. We were able to define a set of six canonical behaviors that are easily recognized on inspection. Transitions between these behaviors were infrequent and could be adequately scored by making observations at 15-min intervals. This permitted us to examine behavioral transitions over an extended time period and to perform replicate sets of observations. Furthermore, the *Melibe* central nervous system is suitable for microelectrode and optical recording methods for monitoring cellular activity in identified neurons in restrained whole animal preparations (Willows, 1973; Cohen *et al.*, 1991). This provides the opportunity to study mechanisms of spontaneous behavioral expression at the level of neural networks.

Materials and Methods

Melibe leonina, a carnivorous nudibranch of the family Tethyidae, is distinguished by an extended oral veil used in prey capture (Agersborg, 1923). Two groups of 10 animals were studied between 1 and 29 May. Adult specimens weighing 40–250 g were collected from the *Macrocystis* kelp forest in Monterey Bay, California. The animals were held in 45-liter tanks supplied with continuously flowing sand-filtered seawater for 2–28 days before observations were begun. Changes in motivation were minimized by allowing the animals to acclimate to the experimental tanks and by simulating a natural environment. No correlation was found between the number of days in captivity and the behavioral pattern. For observation, animals were placed in five identical 17-liter acrylic plastic tanks provided with flowing sand-filtered seawater and a frond of kelp. The tanks rested on sea tables in a roofed aquarium building where they were protected from direct sun and rain but exposed to natural cycles of light and temperature. Methylene blue dye was injected into the first right ceratum of one animal of the two animals in each tank to facilitate identification. The animals were fed every other day at the same time with the same amount of their natural food, live mysid shrimp collected from the wild. The animals were otherwise left undisturbed for eight days of observation, which included four nonfeeding days from each group.

We define six behaviors that occur frequently but without overlap in the absence of overt stimulation (Fig. 1). Together they account for greater than 90% of the activity in the observation tanks. The behaviors are distinguished by characteristic body postures involving the oral hood, the rhinophore processes, and the cerata, as well as by the presence or absence of pedal locomotion. The six behaviors are as follows: (1) Feeding (F): rhythmic extension and contraction of the oral hood in a casting motion through the water (Hurst 1968; Watson and Trimarchi, 1992). (2) Open hood (OH): full extension of the oral hood with the cerata and rhinophore processes extended. (3) "Alert"/processes extended posture (AL): oral hood partially closed with the oral tentacles tucked inside, cerata and rhinophore processes extended. (4) Roaming/open hood (R/OH): OH behavior combined with pedal locomotion. (5) Roaming/processes extended (R/AL): AL behavior combined with pedal locomotion. (6) Resting (RST): locomotion absent, hood closed and held against the substrate, cerata contracted against the sides of the body, rhinophore processes folded down.

Several other behaviors occurred too infrequently for analysis. These included (1) pedal locomotion in the RST posture; (2) the "crumple" reflex, an alarm response elicited by tactile or vibratory stimuli and characterized by forceful contraction of most of the body wall musculature (Scott, 1990); (3) swimming; (4) egg-laying. Copulation was observed occasionally but was not scored independently because the six behaviors we followed occurred at the same frequency independent of copulation.

Observations were made at 15-min intervals for 6 hours a day beginning between 0800 and 1200 h. During preliminary studies, we observed behavior continuously for periods of several hours. By parsing the data into time periods of varying duration, we determined that a 15-min sample interval is adequate to capture behavioral transitions. Observations from one nonfeeding day for the 10 animals in group 1 are tabulated in Figure 2. It is apparent that behavior changes infrequently and that individuals tend to perform the same behavior over several time points. On feeding days the animals spent about 80% of their time performing feeding behavior (F), indicating that the presence of prey organisms has a powerful influence on behavioral choice (Watson and Trimarchi, 1992; Watson and Chester, 1993). Analysis was limited to nonfeeding days in order to include a more diverse range of behaviors and to obtain observations under relatively constant physiological conditions.

Results

The frequency of occurrence of each of the 36 possible behavioral transitions, including consecutive occurrences of the same behavior, was tallied by observing behavior at 15-min intervals. The data are expressed in Table I as transition probabilities for each of two replicate, 4-day experiments. The sum of the transition probabilities from a given starting behavior is normalized to 1.0. The predominance of certain one-step transition probabilities over others suggests that the six behaviors can be grouped into two distinct behavior modes (Fig. 3). Behaviors F, OH, and R/OH form the feeding mode, while

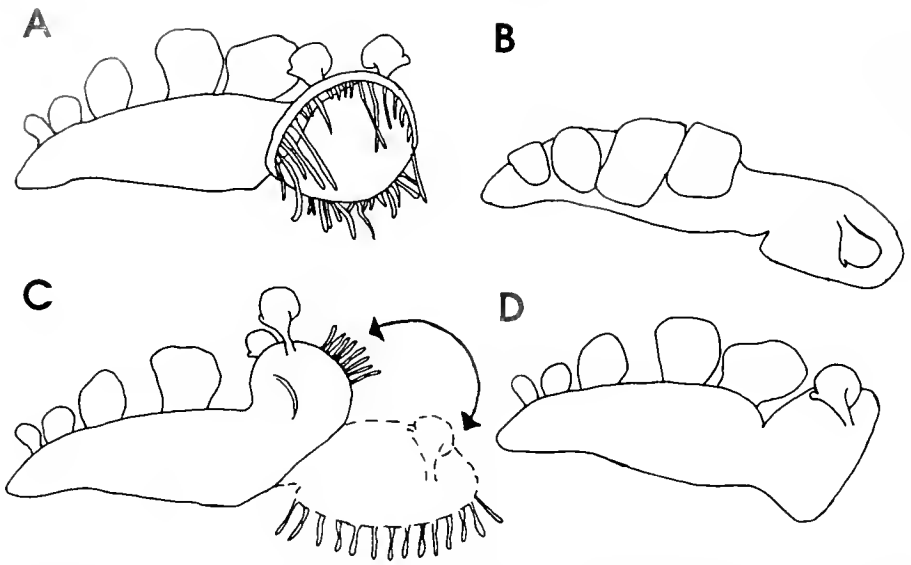

Figure 1. Body postures during six behaviors: (A) Open hood (OH) and roaming/open hood (R/OH) behaviors. (B) Resting (RST) behavior. (C) Feeding (F) behavior. (D) "Alert"/processes extended (AL) and roaming/alert (R/AL) behaviors.

behaviors RST, AL, and R/AL form the resting mode. This grouping of behaviors is based on the observation that transitions among mode elements occur much more frequently than transitions to behaviors outside of the mode. The frequencies of intermode transitions are listed in Table II. This qualitative observation is borne out by calculating between-mode transition frequencies for all possible ways of grouping the six behaviors into two modes. The correct mode structure will give fewer between-mode transitions than any other grouping.

There are 25 ways to structure two modes: 10 in which each mode contains three behaviors, and 15 in which one mode contains two behaviors and the other contains four. For data set 1, the number of between-mode transitions for the mode structure proposed in Figure 3 was 145, whereas between-mode transitions for the other possible groupings ranged from 267 to 389. This supports the behavioral relationships diagrammed in Figure 3. According to this analysis, animals stay in one mode for an average of 1 hour and 11 minutes (5.2 observation intervals) before switching to the other.

Transitions between modes occur most frequently between behaviors OH and AL in either direction. The OH to AL transition accounts for 35% of all transitions from

THURSDAY, MAY 9, 1991, 0900-1500 hrs

interval #

animal I.D. #	1	2	3	4	5	6	7	8	9	10	11	12	13	14	15	16	17	18	19	20	21	22	23	24	25
1A	R/OH	F	F	F	F	F	F	F	F	F	F	F	F	F	F	F	F	F	F	F	F	F	F	F	F
4B	OH	OH	F	F	OH	R/OH	F	OH	OH	AL	OH	OH	F	F	OH	OH	OH	OH	OH	OH	AL	OH	OH	OH	F
2A	R/OH	F	AL	R/AL	RST	AL	R/AL	RST	RST	R/OH	AL	OH	AL	OH	OH	OH	R/OH	RST	OH	R/AL	RST	RST	RST	RST	R/OH
2B	RST	R/OH	OH	R/AL	AL	AL	R/AL	AL	CR	RST	RST	R/AL	RST	RST	RST	R/AL	CR	AL	RST	RST	AL	RST	RST	RST	R/AL
3A	RST	OH	R/AL	OH	OH	OH	OH	OH	OH	OH	OH	OH	OH	OH	OH	OH	RST	OH	R/OH	OH	OH	R/OH	F	OH	F
3B	RST	RST	RST	RST	AL	AL	R/AL	AL	AL	AL	AL	AL	R/AL	R/AL	AL	R/AL	R/AL	AL	R/AL	AL	AL	R/AL	R/AL	R/OH	R/AL
4A	R/OH	RST	OH	RST	R/OH	OH	OH	OH	OH	OH	OH	OH	AL	OH	OH	AL	AL	AL	OH	AL	AL	S	AL	OH	OH
1B	RST	RST	RST	RST	RST	RST	RST	RST	RST	RST	RST	RST	RST	RST	RST	RST	RST	RST	RST	AL	RST	RST	RST	RST	RST
5A	F	F	R/OH	R/OH	RST	R/AL	RST	R/AL	OH	OH	R/OH	RST	R/OH	AL	R/OH	R/AL	OH	R/OH	R/AL	AL	RST	RST	OH	R/OH	RST
5B	RST	RST	RST	AL	AL	AL	AL	AL	AL	AL	AL	AL	AL	AL	AL	AL	R/AL	AL	R/AL	RST	AL	AL	R/AL	R/AL	RST

Figure 2. Sample data set from one full day of observations. Observations of each of 10 animals were made at 15-min intervals for 6 h. The duration of a behavior in continuous intervals is referred to as its dwell time. An example of a seven-interval dwell time in the open hood (OH) behavior can be seen in animal 4A from intervals six to twelve. Abbreviations: Feeding (F), open hood (OH), "Alert"/processes extended posture (AL), roaming/open hood (R/OH), roaming/processes extended (R/AL), resting (RST), crumple (CR), and swimming (S).

Table I

Transition probabilities between all behaviors for both sets of data

SET 1

Starting behavior	Ending behavior: F	OH	R/OH	AL	R/AL	RST
F	**0.597**	**0.223**	**0.095**	0.038	0.019	0.028
OH	**0.183**	**0.486**	**0.115**	0.101	0.014	0.101
R/OH	**0.299**	**0.253**	**0.218**	0.080	0.151	0.226
AL	0.041	0.142	0.027	**0.473**	**0.122**	**0.196**
R/AL	0.085	0.149	0.085	**0.298**	**0.149**	**0.234**
RST	0.040	0.081	0.054	**0.117**	**0.054**	**0.664**

SET 2

Starting behavior	Ending behavior: F	OH	R/OH	AL	R/AL	RST
F	**0.459**	**0.208**	**0.138**	0.101	0.075	0.019
OH	**0.188**	**0.370**	**0.087**	0.268	0.043	0.043
R/OH	**0.293**	**0.200**	**0.227**	0.093	0.120	0.067
AL	0.065	0.094	0.039	**0.526**	**0.101**	**0.175**
R/AL	0.135	0.122	0.135	**0.446**	**0.122**	**0.041**
RST	0.005	0.020	0.010	**0.256**	**0.054**	**0.655**

Each row of probabilities totals 1.00. Probabilities for transitions occurring within a behavioral mode are given in boldface.

the feeding to the resting mode, and the AL to OH transition accounts for 30% of transitions from the resting to the feeding mode. None of the 16 other possible between-mode transitions accounted for more than 15% of the transitions in either direction.

Individual variability

The time spent in each behavior varied a great deal between individual animals. As a measure of this variability, we calculated coefficients of variation (CV) for the number of transitions from a behavior back to itself (*i.e.*, F → F) using the second set of 10 animals. The CV ranged from 64% to 157%. Some of the variability can be linked to a physiological correlate. For example, we found that body weight and time spent in the feeding mode are positively correlated ($r = 0.87$; Fig. 4). An 80-g individual spent 10% of the time in the feeding mode as compared to 80% for a 250-g animal. A similar correlation exists between size and time spent in the feeding (F) behavior within the feeding mode. The 250-g animal spent 58% of the total time in F, but the 80-g animal did not exhibit this behavior at all. This bias on both inter- and intramodal transition probabilities may reflect a difference in the nutritional needs of small *vs.* large animals and is worthy of further study. We did not find a correlation between body size and average dwell time in the F behavior in the absence of food organisms. This suggests that large animals enter feeding behavior more often than small ones, but that the duration of feeding episodes is about the same once feeding begins. Although body size has little effect on feeding dwell time, this pa-

Table II

Transition probabilities within and between modes

	Probability that the next transition is to: Feeding mode	Resting mode
Starting from:		
Feeding mode	0.79	0.21
Resting mode	0.18	0.82

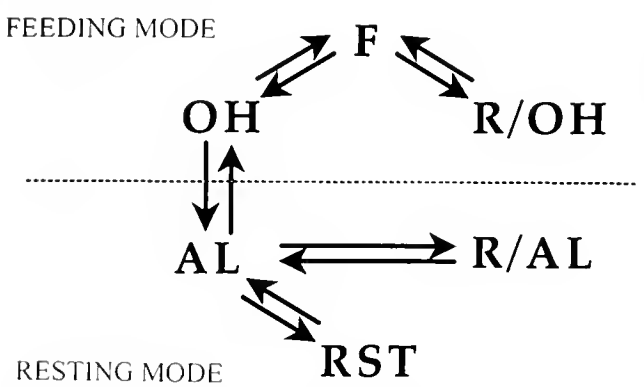

Figure 3. Feeding and resting modes. Arrows indicate the 10 most frequent transitions between different states. The mode structure minimizes intermode transitions; all other possible mode arrangements were considered (see text).

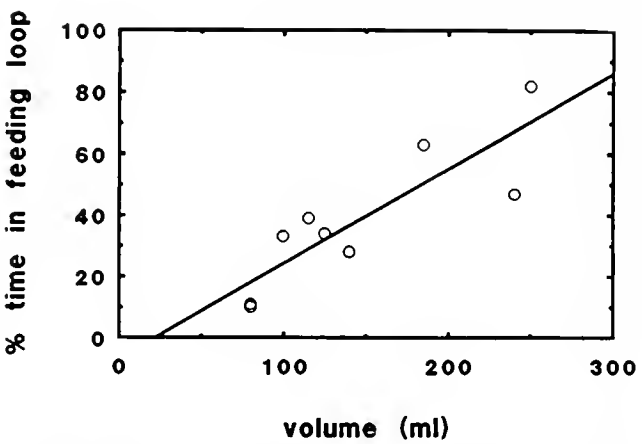

Figure 4. Body size and total time spent in the feeding mode are correlated. Data taken from set 2. Total time in the feeding mode from Figure 3 was calculated by counting the total number of intervals spent in feeding mode behaviors. Body volume was determined by water displacement. The correlation coefficient is $r = 0.87$.

rameter is influenced by the presence of food; Watson and Trimarchi (1992) have shown that dwell time varies inversely with the concentration of available prey.

Two-step transition probabilities

A sequence of behavioral acts is stochastic if the transition from one behavior to the next is independent of preceding behavioral changes. If this is so, the frequency of two-step transitions observed experimentally should match the transition frequencies predicted from a two-step stochastic model. Expected probabilities for two-step transitions were calculated from the measured one-step probabilities following the equation $P(a \rightarrow b \rightarrow c) = P(a \rightarrow b) * P(b \rightarrow c)$, where a, b, and c represent any of the six canonical behaviors. Behavioral observations from the 10 individuals in each data set were pooled and used to tabulate the probability of occurrence of each of the 216 possible two-step behavioral transitions. Transitions from four of the six possible starting behaviors occurred frequently enough to permit this extensive analysis (F, OH, AL, and RST). The expected and observed probabilities were placed in 6×6 matrices for comparison. The matrices for starting behavior a = AL from data set 2 are tabulated and plotted in Figure 5. The expected and observed three-dimensional plots of behavioral frequency show peaks and valleys at the same positions and with approximately the same amplitudes.

We attempted to test the significance of differences between the expected and observed 6×6 matrices by calculating chi-square values. When the two data sets were treated separately, chi-square scores ranged from 42.5, for set 2, starting behavior AL, to 62.9 for set 1, starting behavior F. When both sets of data were pooled, chi-square scores ranged from 66.5 to 81.5. All the chi-square values were significant by standard tests using 25 degrees of freedom ($P < 0.001$ to $P < 0.01$). The chi-square statistic is known to be unreliable, however, in the case of behavior-sequence matrices with cells containing low values (Chatfield and Lemon, 1970), and the two-step transition matrices we tabulated have a number of cells with values of 0. Also, variation in transition rates was high among individuals (CV for F → F as high as 157%), which adds to the chi-square score. The presence of this type of added uncertainty is demonstrated by the fact that higher scores result when data from two periods of observation are pooled. Instead of a chi-square test, Chatfield and Lemon (1970) suggest selecting the most frequent sequences and comparing expected and observed values by inspection. The plots of Figure 5 follow that principle and show that the two-step transition predictions match the observations fairly well.

Behavioral dwell-time distributions

We defined behavioral dwell time as the duration of a continuous single bout of the same behavior. This is equivalent to the 'interval distribution' (Heiligenberg, 1973) or the 'hazard function' (Cox and Lewis, 1966) but differs in that exits into any other behavioral state are allowed. Dwell-time histograms for four of the six behaviors are plotted in Figure 6. If behavioral choice is determined stochastically, the distribution of dwell times will be exponential. R/OH and R/AL behaviors did not occur frequently enough to permit dwell-time analysis. OH and AL dwell times were exponentially distributed. F dwell times were also exponentially distributed, with the exception of a few lengthy episodes. The presence of longer episodes has implications for the organization of the feeding neural network and suggests that the network may be modulated by stimuli such as the presence of stray food organisms or by a long-lasting effect of food presented on the previous day (Watson and Chester, 1993). The RST dwell-time histogram was best fit by the sum of two exponentials. This suggests two possibilities: first, there may be two resting states which have independent transition probabilities but are indistinguishable by observation; alternatively, the transition probabilities for exiting RST may vary with time spent in the RST behavior.

Discussion

These observations demonstrate that spontaneously evolving sequences of behavioral transitions in *Melibe leonina* are stochastic such that the probability of a given transition is independent of preceding ones. At the same time, behavior is organized by the fact that transitions between behaviors within a mode are more likely than transitions between behaviors in different modes. This creates a *cul-de-sac* within the transition-probability matrix so that one behavior pattern can only be reached by way of another. As a result, the organization is not inconsistent with hierarchical models of behavioral organization like that proposed by Tinbergen (1951) since specific stimuli might move the animal into a mode in which certain behaviors are more likely than others even though the individual transition probabilities are constant and independent. This view is supported by evidence that the neural circuits underlying spontaneous behavioral choice are influenced by external cues such as the presence of prey and by physiological signals correlated with body size.

Spontaneous behavior in *Melibe* demonstrates two features characteristic of a stochastic system. First, the two-step transition probabilities predicted from consideration of measured single-step transition frequencies closely match the two-step frequencies observed experimentally. This shows that behavioral transitions are influenced by the starting behavior but not by previous behaviors. Second, for three of the four behaviors for which

EXPECTED

		c					
	a=AL	F	OH	AL	R/OH	R/AL	RST
	F	8.8	4.1	2.1	2.6	1.5	0.3
	OH	5.3	10.3	7.3	2.3	1.2	1.2
b	AL	10.0	14.4	81.2	6.2	15.5	27
	R/OH	3.2	2.3	1.2	2.6	1.5	0.9
	R/AL	4.1	3.5	13.2	4.1	3.5	1.2
	RST	0.3	1.2	13.2	0.6	2.6	33.7

OBSERVED

		c					
	a=AL	F	OH	AL	R/OH	R/AL	RST
	F	5	4	6	0	4	1
	OH	5	7	9	5	0	2
b	AL	10	12	96	3	12	27
	R/OH	1	2	2	4	2	1
	R/AL	3	2	14	3	5	1
	RST	0	0	11	2	5	27

Figure 5. Top. Expected and observed two-step transitions with data from starting behavior AL (set 2). Expected numbers were calculated from single-step transition frequencies using the equation $P(a \rightarrow b \rightarrow c) = P(a)P(a \rightarrow b)P(b \rightarrow c)$ (see text). Bottom, 3-D plots corresponding to the expected and observed two-step transition matrices.

there was sufficient data to evaluate behavioral dwell-time distributions, dwell times were distributed exponentially. This supports a model based on independent and unvarying transition probabilities. The dwell-time distribution for the exception, the RST behavior, was best fit by the sum of two exponentials. This result might be explained by the existence of two resting states with different average duration. We were unable to identify multiple resting states but, like sleep and quiescent behavior in other animals, the two states may have a different neurophysiological basis while appearing identical to the observer. Another possible interpretation is that the exit probability from RST decreases with time spent in the RST state, perhaps reflecting a decrease in arousal. The data are not sufficient to evaluate these possibilities, but they raise questions of a general nature that might be accessible to neurophysiological investigation in *Melibe*.

A property that emerges from a consideration of the transition-probability matrix is that spontaneous behavior can be interpreted as a series of jumps between two modes named the *feeding mode* and the *resting mode*. This grouping of behaviors follows directly from the one-step transition probabilities and the observation that transits within modes are far more probable than transits between modes. It is a robust conclusion based on over 1900 observations of transitions, far more than the 360 ($10\ n^2$) required to analyze a repertoire of n behaviors (Fagen and Young, 1978). This organization represents a way in which higher order structure can be generated by a coupled system of first-order random processes.

The probability of transitions between modes did not fluctuate during 6 h observations, but this period is short relative to the life span of the animal. Preliminary data suggest that transition frequencies do change with maturation and that juveniles demonstrate both a different repertoire of behaviors and different frequencies of transitions between the behaviors they share with adults (S.E. Gelber, pers. comm.). In addition, Watson and Trimarchi (1992) have shown that the presence of prey organisms, sensed in response to chemical and tactile cues (Watson and Chester, 1993), influences feeding dwell

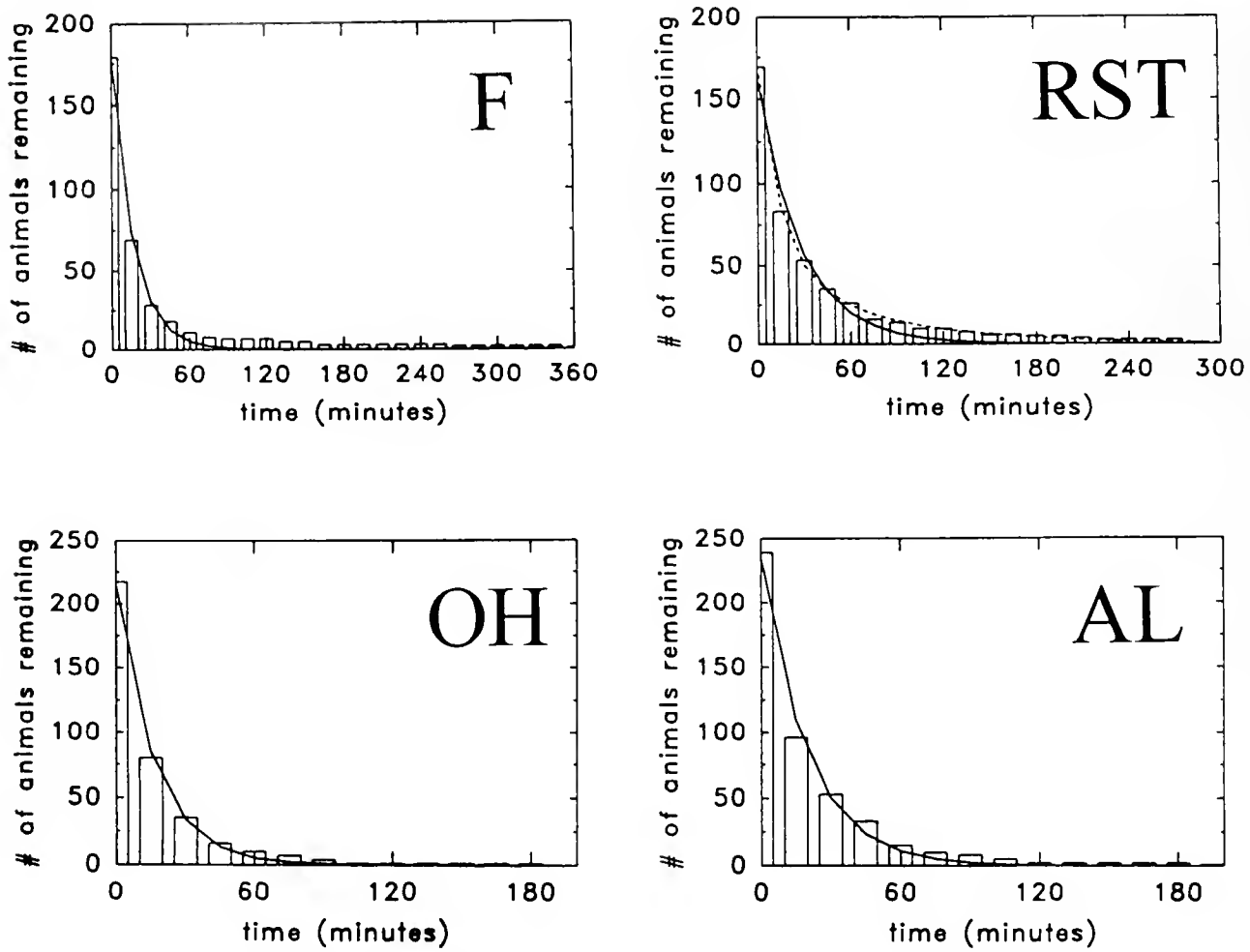

Figure 6. Dwell-time histograms for feeding (F), open hood (OH), resting (RST), and alert-processes extended (AL) behaviors. The OH and AL distributions are fit by exponentials (solid curve), consistent with the exit from these behaviors being random. The feeding (F) dwell-time distribution is also approximately exponential, except for outlying points that account for 1% of the data. The outlying points with long dwell times may reflect behavior driven by external stimulation. Two fits are plotted for the resting (RST) data, a single exponential (solid line) and the sum of two exponentials (dashed line). All distributions were fitted using a nonlinear least-squares method.

time in a fashion that is graded with the concentration of prey.

A particular pair of behavioral transitions, OH↔AL, acts as a gateway between the feeding and resting behavior modes. The OH and AL behaviors share features of body posture such as the positions of the rhinophores and cerata, but they different in oral hood posture. The change between behavior modes, therefore, is bridged by a relatively small postural adjustment, but it signals a long-term change in the animal's behavior pattern. A neurophysiological interpretation is that slight but measurable shifts in the activities of neurons involved in OH and AL behaviors can result in a stable, lasting shift in motor-system function.

Increased body size is correlated with an increase in time spent feeding, but the average dwell time of feeding episodes is independent of size. This suggests that the probability of entering feeding behavior increases with body size. Conversely, it is apparent that the presence of food organisms decreases the probability of exit from feeding but does not have a clear effect on entry into feeding behavior. If we assume that separate entry and exit circuits govern transitions into and out of the feeding state, it should be possible to measure changes in excitability in those circuits that correspond to the behavioral observations. One simple and testable prediction is that body size modulates the entry circuit, while the presence of food modulates the exit circuit. Modulation of the exit circuit by food could confer competitive advantage by maximizing foraging efficiency in the face of a variable

food supply. Such shifts in behavioral transition probabilities might be mediated by neuromodulatory or hormonal effects that cause a dynamic restructuring of neural networks by influencing either postsynaptic excitability or the amplitudes of synaptic potentials (Getting, 1989; Katz *et al.*, 1994).

Neuronal circuits that mediate behavior in *Melibe* can be studied with intracellular recording in a whole-animal preparation using techniques pioneered by Willows (1973) and Getting (1981). Using this preparation, we have made progress in elucidating the networks involved in swimming locomotion and feeding movements of the oral hood; Cohen *et al.* (1991) have succeeded in using optical imaging techniques to monitor activity simultaneously in dozens of neurons in the *Melibe* buccal ganglion. Neurophysiological methods are available, therefore, to study changes in neuronal function that are correlated with behavioral choice. The behavioral model developed here provides a framework for the interpretation of physiological experiments.

Acknowledgments

We thank Russ Fernald for comments and R.C. Rao for original artwork. We also thank the staff of the Hopkins Marine Station. Supported by NSF grant 9021217 (S.H.T) and the Lerner-Gray Fund for Marine Research (S. S.-H. W.).

Literature Cited

Agersborg, H. P. K. 1923. The morphology of the nudibranchiate mollusc *Melibe* (syn. *Chioraera leonina* (Gould.)). *Q. J. Microsc. Sci.* **67:** 508–592.

Chatfield, C., and R. E. Lemon. 1970. Analysing sequences of behavioral events. *J. Theor. Biol.* **29:** 427–445.

Cohen, L. B., W. Watson, J. Trimarchi, C. X. Falk, and J.-Y. Wu. 1991. Optical measurement of activity in the *Melibe leonina* buccal ganglion. *Soc. Neurosci. Abstr.* **17:** 1593.

Cox, D. R., and P. A. Lewis. 1996. *The Statistical Analysis of Series of Events.* p. 276, Methuen, London.

Davis, W. J., G. J. Mpitsos, M. V. S. Siegler, J. M. Pinneo, and K. B. Davis. 1974. Neuronal substrates of behavioral hierarchies and associative learning in *Pleurobranchaea. Am. Zool.* **14:** 1037–1050.

Davis, W. J., G. J. Mpitsos, J. Pinneo, and J. L. Ram. 1977. Modification of the behavioral hierarchy of *Pleurobranchaea. J. Comp. Physiol. A:* **117:** 99–125.

Fagen, R. M., and D. Y. Young. 1978. Temporal patterns of behaviors: durations, intervals, latencies, and sequences. Pp. 79–114 in: *Quantitative Ethology*, P.W. Colgan, ed. John Wiley & Sons, New York.

Gelperin, A. 1983. Neuroethological studies of associative learning in feeding control systems. Pp. 189–205 in: *Neuroethology and Behavioral Physiology—Roots and Growing Points.* F. Huber and H. Markl, eds. Springer-Verlag, New York.

Getting, P. A. 1981. Mechanisms of pattern generation underlying swimming in Tritonia. I. Neuronal network formed by monosynaptic connections. *J. Neurophysiol.* **46:** 65–79.

Getting, P. A. 1989. Emerging principles governing the operation of neural networks. *Annu. Rev. Neurosci.* **12:** 184–204.

Heiligenberg, W. 1973. Random processes describing the occurrence of behavioral patterns in a cichlid fish. *Anim. Behav.* **21:** 169–182.

Hurst, A. 1968. The feeding mechanism and behavior of the opisthobranch *Melibe leonina. Symp. Zool. Soc. Lond.* **22:** 151–166.

Katz, P. S., P. A. Getting, and W. N. Frost. 1994. Dynamic neuromodulation of synaptic strength intrinsic to a central pattern generator circuit. *Nature* **367:** 729–731.

Kandel, E. R. 1976. *Cellular Basis of Behavior.* p. 727. W.H. Freeman and Company, San Francisco.

Lorenz, K. Z. 1981. *The Foundations of Ethology.* p. 380. Springer-Verlag, New York.

Scott, D. L. 1990. The shrug response in *Melibe leonina:* behavioral and neurophysiological observations. Unpublished ms. on file at Hopkins Marine Station library, Pacific Grove, CA.

Tinbergen, N., 1951. *The Study of Instinct.* p. 228. Clarendon Press, Oxford.

Watson, W. H., III, and J. Trimarchi. 1992. A quantitative description of *Melibe* feeding behavior and its modulation by prey density. *Mar. Behav. Physiol.* **19:** 183–194.

Watson, W. H., III, and C. M. Chester. 1993. The influence of olfactory and tactile stimuli on the feeding behavior of *Melibe leonina* (Gould, 1852) (Opisthobranchia: Dendronotacea). *Veliger* **36(4):** 311–316.

Willows, A. O. D. 1973. Interactions between brain cells controlling swimming in a mollusc. Pp. 233–247 in: *Neurobiology of Invertebrates.* J. Salanki, ed. Plenum, New York.

Willows, A. O. D., ed. 1985. *The Mollusca: Neurobiology and Behavior, Part 1.* Academic Press, Inc, Orlando.

Reference: *Biol. Bull.* **192:** 426–443. (June, 1997)

Physiological Variation Among Clonal Genotypes in the Sea Anemone *Haliplanella lineata:* Growth and Biochemical Content

MICHAEL G. McMANUS[1], ALLEN R. PLACE[2], AND WILLIAM E. ZAMER[1]

[1]*Department of Biology, Lake Forest College, 555 N. Sheridan Rd., Lake Forest, Illinois 60045; and* [2]*Center of Marine Biotechnology, University of Maryland Biotechnology Institute, Suite 236 Columbus Center, 701 E. Pratt St., Baltimore, Maryland 21202*

Abstract. We have explored physiological variability among clonal genotypes from a single population of the sea anemone *Haliplanella lineata* located at Indian Field Creek, Virginia. Information about the correlation between physiological variability and genetic differences may provide a foundation for a mechanistic understanding of the breadth of adaptation of individual genotypes (*i.e.*, the nature of "general purpose genotypes") and of the concept of localized adaptation in clonal anemones. Anemones from three clones (A, B, C) were fed measured rations of adult *Artemia*, after which growth, absorption efficiency, and net growth efficiency were determined. Biochemical constituents were measured in the tissue of this group of anemones as well as in the tissue of anemones from the same clones that had fed *ad libitum* on *Artemia* nauplii. Anemones from the different clones did not differ significantly in growth, or gravimetric absorption or growth efficiencies, but significant differences were found in biochemical composition. Regardless of feeding regime and diet composition, clone B anemones consistently had lower tissue averages of triacylglycerols, fatty acids, sterol and wax esters, glycerol ethers, and carbohydrates than did clone A and clone C anemones. As a result of differences in the carbohydrate and lipid constituents, the energetic content of tissues from clone B anemones that had been fed rations was significantly lower than the energetic content of tissues of anemones from clone C. This clonal pattern in biochemical composition and energetic content may be due to differences in substrate absorption among anemones from the different clones, to differences in metabolic rate, or to a combination of both. Because anemones from this population may encyst in mucus and stop feeding when water temperatures are less than 10°C, the genotypic differences in storage lipids and carbohydrate may have implications for the winter survivorship of clone B anemones in this population.

Received 29 August 1996; accepted 12 April 1997.

Introduction

Many species of sea anemones reproduce asexually, resulting in the production of genetically identical individuals in natural populations. Local populations may consist of a single clone (*e.g.*, the actinian *Haliplanella lineata;* Shick, 1976; Shick and Lamb, 1977), or they may be composed of many clones and approach the genetic diversity expected for a sexually outcrossing population (see Shick, 1991, pp. 270–277). Such differences in population genetic structure may have multiple causes. For example, monoclonal populations may result from genetic founder effects (*i.e.*, settlement of a single adult or planula larva, followed by asexual proliferation), followed by competitive exclusion of other clonal genotypes (Ayre, 1982, 1983, 1995; Hoffmann, 1986). Alternatively, monoclonal populations could result from the settlement of multiple genotypes, followed by differential selection leading to the elimination of all but one highly locally adapted genotype (see Ayre, 1985, 1995). Multiclonal populations could result from the asexual proliferation of multiple genotypes that have the same relative fitness, although formal tests of

fitness differences among clonal genotypes are rare (Ayre, 1995).

On theoretical grounds, asexual reproduction may be viewed as a means of preserving and increasing the size of locally adapted multiple-locus (*i.e.*, clonal) genotypes (Williams, 1975), and a number of researchers have provided evidence consistent with this theoretical prediction of local adaptation (see especially, Ayre, 1985, 1995). However, the functional basis for such local adaptation has not been explored. Indeed, Shick (1991) points out that studies yielding evidence of local adaptation have not tested whether locally adapted clones exist in any other localities, *i.e.*, the extent to which any single clone is a broadly adapted, "general purpose genotype" (Shick, 1976; Shick and Lamb, 1977).

Although the ecological physiology of sea anemones is rather well-studied (*cf.* Shick, 1991), there have been surprisingly few investigations of physiological variation among clonal genotypes present in individual populations or individual habitats within populations of asexually reproducing anemones (*e.g.*, Shick and Dowse, 1985). Such information could provide the initial basis for a mechanistic understanding of localized adaptation, and for determining whether natural selection or genetic founder effect is more important to the genetic structure of these populations. Of particular note in this context is a study by Shick and Dowse (1985), who concluded, on the basis of an examination of literature data on sea anemones, that intraclonal variance in a variety of physiological measurements is smaller than interclonal variance in these traits, and that the variance for some traits could be explained largely by clonal identity. Thus they provided strong evidence of genetically correlated performance variability. However, much of their work focused on comparisons of variances between geographically separated monoclonal and multiclonal populations of the same species, or between genetically diverse populations of one species and monoclonal populations of another species. Although many studies have persuasively shown that localized adaptation of clones occurs (*e.g.*, Ayre 1985, 1995; Sebens, 1981; Zamer and Shick, 1989), such comparisons reflect the fact that few studies have directly examined physiological variation among clonal genotypes collected from a single population or habitat, and maintained under the same environmental conditions so as to remove acclimation effects on performance.

Some field-based studies have provided limited evidence for physiological variation among clonal genotypes within and between populations. For example, Jennison (1979) interpreted differences in tissue lipid among clones of the anemone *Anthopleura elegantissima* to be the result of either genetically encoded differences in lipid metabolism or micro-environmental differences in food availability between clones at a single field site. Differences in reproductive characteristics between high- and low-intertidal clones of *A. elegantissima* were attributed to higher temperatures in the upper intertidal (Sebens, 1981), the likeliest explanation, but the possibility remains that these clones were genetically adapted to the different habitats in this single population.

More persuasive evidence of localized genetic adaptation among anemone clones comes from controlled experimental studies. When acclimated to common conditions, high-intertidal clones of *A. elegantissima* exhibit different physiological energetic characteristics (*e.g.*, absorption efficiency, net growth efficiency) than low-intertidal clones of this anemone; these results were interpreted to mean that adaptive, genetic divergence of the clones had occurred in response to low food availability in the upper intertidal zone (Zamer, 1986; Zamer and Shick, 1987, 1989). Ayre (1985) showed that local clones of the anemone *Actinia tenebrosa* had greater capacities for asexual reproduction than did transplanted foreign clones; he concluded that highly localized adaptation of the clones had occurred in colonies of the anemone that were only 2–4 km apart. And Shick *et al.* (1979) transplanted clones of the anemone *H. lineata* from a Rhode Island population to a Maine population site and observed 100% mortality of the transplants. These investigators also interpreted their results to mean that the separate populations were genetically distinct and contained locally adapted clones. However, little information about functional diversity among clones within any single habitat or population is available from the aforementioned studies. More recently, variation in performance traits among clones has been explored in polyps of the jellyfish *Aurelia aurita* (Keen and Gong, 1989), in the corallimorpharian *Corynactis californica* (Chadwick and Adams, 1991), and in the anemone *A. elegantissima* (Tsuchida and Potts, 1994).

Genetic variation in growth among individual organisms has been examined generally by two approaches. The first, quantitative genetics, statistically partitions phenotypic variance among relatives (*e.g.*, parents, offspring, half-siblings) into genetic and environmental components (Falconer, 1989). This approach has successfully documented significant genetic variation and genotype-environment interactions in growth in a number of shellfish species (Jones *et al.*, 1996; Rawson and Hilbish, 1991). Such studies cannot, however, address the physiological mechanisms underlying genetic variation in growth (*cf.* Clark, 1990; Koehn, 1991), and therefore cannot provide relevant information about the mechanisms of localized adaptation among clones of sea anemones.

The second approach is physiological energetics,

which focuses on performance traits that constitute the energy and materials budgets of an organism (*e.g.*, Hilbish and Koehn, 1985; Hawkins *et al.*, 1986; Zamer and Shick, 1987; 1989; Koehn and Bayne, 1989; Present and Conover, 1992). We have taken this approach to examine physiological variation among clonal genotypes in the eurytolerant sea anemone *H. lineata* collected from a single population. The present paper focuses on growth and on the biochemical content of the tissue. The balanced energy equation (Winberg, 1956) has been used as a conceptual framework in examining variation in organismal performance. Bayne and Newell (1983) expressed the equation as

$$Pg + Pr = C \cdot AE - (R_m + R_r)$$

where Pg is somatic production (growth), Pr is reproductive production (gametes), C is energy consumed, AE is the efficiency with which consumed energy is absorbed, R_m is the metabolic cost of body maintenance, and R_r includes all other metabolic costs (Koehn and Bayne, 1989). Variation in growth among individuals can originate from differences in the components of the balanced energy equation, such as metabolic costs, consumption, and absorption efficiency (Koehn and Bayne, 1989; Present and Conover, 1992).

Haliplanella lineata is a widely distributed, colonizing species, which in natural populations rapidly increases in numbers by asexual reproduction and may disappear from an area suddenly (Shick, 1976). Although this species is extremely euryhaline and eurythermal (Shick, 1976), sudden disappearances have been attributed to the existence of one or only a few clonal genotypes in populations and to environmental factors that exceed genetically based tolerance limits (Shick, 1976; Shick *et al.*, 1979). Although sexually reproducing populations occur in Japan (Fukui, 1991), North American and laboratory populations of *H. lineata* reproduce only asexually, mainly by longitudinal fission (Johnson and Shick, 1977; Minasian, 1979), and the species can be classified as an agametic, cloning anemone (Hughes, 1989; Carvalho, 1994).

A physiological advantage of studying anemones that reproduce exclusively by asexual fission is that sexual reproduction (Pr) is eliminated from consideration of energy balance, simplifying the analysis. The animal is easily cultured in the laboratory, and the rate of longitudinal fission may be increased by maintaining the anemones at relatively high temperatures (Minasian, 1979; Minasian and Mariscal, 1979; Zamer and Mangum, 1979), so that large numbers of genetically identical clonemates are obtained easily. It is this latter feature, and the eurytolerant nature of the animal, that affords an ecophysiological and genetic advantage, in that clonemates may be studied at a variety of relevant environmental conditions. Using this approach we can replicate our physiological measurements on genetically identical individuals. Eventually, to better understand localized adaptation in this species, we can study the physiological characteristics of clonal genotypes from separate populations. We will also be able to partition physiological variation in *H. lineata* into genetic (comparisons among anemones from different clones) and nongenetic (comparisons within each clone) components (Shick and Dowse, 1985; Vrijenhoek, 1994).

In this study genetic variation in growth was examined in anemones from different clones, all of which were fed similar, measured food rations, thereby eliminating consumption differences in the energy balance equation as a source of variation in growth. In terms of physiological energetics we asked: Do growth, absorption efficiency, and growth efficiency differ among anemones from different clones? Because genetic variation in physiological energetics has been associated with differences in lipid and protein metabolism in some organisms (Medrano and Gall, 1976a, b; Hawkins *et al.*, 1986), we examined the biochemical composition of the ration-fed anemones from the different clones. Finally, we measured the biochemical composition of tissues from anemones that were fed *Artemia* nauplii to test whether consumption differences associated with the capture of suspended prey could affect any of the biochemical patterns.

Materials and Methods

Collection and maintenance

In October 1990, individuals of *H. lineata* were collected from Indian Field Creek, a tributary of the York River in Virginia (37°16′ N, 76°33′ W), and shipped by air to our laboratory at Lake Forest College. Anemones were collected from tens of square meters at the site (C. P. Mangum, pers. comm.), so that this original sample was likely to have included a representative sampling of clones in this population. At the time of collection, water temperature was about 20°C (C.P. Mangum, pers. comm.). Salinity ranges from 15–18 parts per thousand (ppt) at this site (W.E.Z., pers. obs., and C.P. Mangum, pers. comm.), and surface water temperature ranges annually from about 5°C to 27°C (Coast and Geodetic Survey, 1960, as cited in Sassaman and Mangum, 1970). Air temperatures to which the anemones are exposed at low tide may reach 30°–32°C during the summer, and may be near freezing during the winter (C. P. Mangum, pers. comm.).

Each anemone was placed in its own beaker (30 ml) containing 16 ppt seawater (Instant Ocean), held at room temperature (15°–25°C), and fed *Artemia* nauplii (San Francisco Bay brand) *ad libitum* every other day.

Under these conditions, most anemones underwent repeated longitudinal fission. Fission products within individual beakers constitute a separate genetic lineage, and were eventually transferred to individual "stock" aquaria (9.5 l), where the separate lineages are currently maintained under continuous immersion in recirculating filtered seawater. Other maintenance conditions are the same as stated above.

Anemones from each of the aquaria were genotyped by using starch gel electrophoresis at five polymorphic loci [superoxide dismutase (SOD), isocitrate dehydrogenase 1 (IDH 1), glucose-6-phosphate isomerase (GPI), octopine dehydrogenase (ODH), and 6-phosphogluconate dehydrogenase (6Pgdh)] with standard gel electrophoresis techniques that will be described elsewhere (Zamer, unpubl. data). Based on the five polymorphic loci, five unique, multiple-locus genotypes, designated as A, B, C, D, E, and referred to hereafter as clones, were detected among the different lineages of anemones. For most of the work described below, three clones (A–C) were used.

Anemones from these different clones were acclimated in monoclonal aquaria (9.5 l) in an incubator at 15°C for at least 5 weeks prior to the experiments. At this temperature these anemones do not readily undergo longitudinal fission, but they do grow. All acclimation and experimental conditions described in this paper included continuous immersion of the anemones.

Growth experiment

In 1994 we initiated a controlled growth experiment using anemones from our stock cultures. Sixty-five anemones from clones A, B, and C were selected from the stock cultures so as to minimize any size differences among the clones (Table I). Sample sizes were n = 13, 26, and 26, in clones A, B, and C, respectively (unequal sample size was due to the slow rate of fission by clone A anemones in the stock aquaria). Before weighing each anemone, adhering debris was removed, and the gastrovascular water was removed to absorbent paper by applying gentle pressure to the body wall with a small spatula. Anemones were allowed to attach to individual 15-ml plastic beakers, which were then floated on the surface of monoclonal aquaria at 15°C. Anemones were fed *Artemia* nauplii in the aquaria by submerging the beakers.

From the 65 anemones, an initial group of 25 was chosen for calculation of dry-to-wet-mass regressions. Each anemone in this initial group (n = 5, 10, and 10 respectively for clones A, B, and C) was removed from its beaker, sliced longitudinally to release all gastrovascular water, rinsed briefly with deionized water to remove salts, and blotted. The anemones were dried at 50°C for 24 h, cooled to room temperature in a desiccator, and weighed to the nearest 0.01 mg. For each of the clones, the dry mass of the anemones in the initial group was regressed on their wet mass (previous paragraph). Clonal regression equations were used to estimate the starting dry mass from the wet mass of the remaining individual anemones in each clone. These dry mass estimates were used in the growth experiment, and the size range of initial anemones was selected to ensure that the estimates were interpolations and not extrapolations of the regressions (Weisburg, 1985).

The 40 remaining anemones used in the growth experiment (hereafter called the experimental anemones) were attached to individual glass beakers that were randomly assigned to one of two 38-l aquaria maintained at 15°C and filled with 24 l of 16-ppt salt water. Anemones were randomly assigned to a position on the floor of each aquarium. The box filter in each aquarium was moved once a day to a different corner of the aquarium to prevent any bias in airflow and filtration. These aquaria served as experimental blocks, which minimized any effects of temperature heterogeneity within the incubator.

Each experimental anemone received a daily ration of frozen adult *Artemia* (San Francisco Bay brand) for the next 10 days. For the first 2 days, the size of the ration was 6% of the estimated starting dry mass of each anem-

Table I

Anemone size (in milligrams)

Clone	n	Initial Wet Mass	n	Initial Dry Mass (Regression-Estimated)	n	Final Dry Mass
A	13	66.1 (50.5, 86.7)	8	10.96 (7.67, 15.67)	8	14.30 (10.46, 19.53)
B	26	62.7 (48.5, 81.2)	16	8.96 (6.54, 12.28)	16	11.98 (9.00, 15.94)
C	26	63.5 (52.1, 77.4)	16	10.46 (8.45, 12.99)	16	14.45 (11.51, 18.16)

The values for the size variables are the back-transformed means with their 95% confidence limits in parentheses. Based on analysis of variance for each variable, clonal identity did not have a significant effect on anemone size (initial wet mass P = 0.96, initial dry mass P = 0.56, final dry mass P = 0.46).

one. To make the weighing of the *Artemia* easier, the ration size was increased to 8.5% for the remaining 8 days. Each ration was placed on the oral disk of each anemone to ensure that it was ingested. On the following day, egesta produced from each anemone was removed a few hours prior to that day's feeding. The daily egesta for each anemone was rinsed with deionized water to remove salts and stored on a weigh boat in a desiccator. Egesta obtained from individual anemones was pooled over the 10-day experiment, dried at 50°C, and then weighed. The pooled egesta mass was used in the calculation of gravimetric absorption efficiency for each anemone (see below). On the day following collection of the last egesta, "blotted" wet mass (described below) and dry mass (described earlier) were determined for each of the 40 experimental anemones.

Physiological energetics

The relative growth (RGR) of the experimental anemones was calculated as: RGR = [(final dry mass − estimated starting dry mass)·(estimated starting dry mass)$^{-1}$] × 100%. Gravimetric absorption efficiency [A_g, (g ingested − g egested)·(g ingested)$^{-1}$ × 100%] and net growth efficiency [K_2, g growth·(g absorbed ration)$^{-1}$ × 100%] were calculated as in Zamer (1986).

Biochemical analyses and energetic content

Tissue hydration, and protein, carbohydrate, and lipid content of tissues were measured. Tissue hydration was calculated for the initial and experimental groups of anemones as: (blotted wet mass − dry mass)·(blotted wet mass)$^{-1}$ × 100%. Blotted wet mass (mean ± SE = 83.1 ± 4.55 mg) was obtained on anemones after cutting their body walls to express gastrovascular cavity water, rinsing to remove salts, and blotting as described previously for the initial group of anemones.

After the dry mass of an anemone was measured, the material was placed in a shell vial, ground with a glass rod, and stored at −70°C. Total protein and carbohydrate was measured in samples (3.1–8.4 mg) of oven-dried tissue sonicated in 500 μl of deionized water. An 800-μl volume of cold 10% trichloroacetic acid (TCA) was added to a 200-μl aliquot of the homogenate, the sample was kept on ice for 10 min and swirled every 5 min, then centrifuged at 4500 × g at 2°C for 30 min. The supernatant was discarded, and the tube containing the precipitated protein was inverted and drained for 1 h at room temperature. The protein was then dissolved in 1.0 ml of 10% sodium hydroxide (NaOH). Two 200-μl aliquots of this protein solution were removed and each was mixed with 400 μl of 10% NaOH and 1.4 ml of deionized water. Microbiuret (Itzhaki and Gill, 1964) determinations of protein were made on this solution. Bovine serum albumin is an inappropriate standard for estimating protein content in sea anemones (Zamer *et al.*, 1989). Protein was isolated from anemones (kept in the stock aquaria) representing all five clones, using the procedures of Zamer *et al.* (1989). This *Haliplanella* protein was dissolved in 10% NaOH and used as the standard.

Total carbohydrate was isolated from the remaining 300 μl of homogenate as described in Zamer *et al.* (1989) and quantified spectrophotometrically using the method of Dubois *et al.* (1956). The relatively mild wet biochemical methods that we used to isolate carbohydrate do not cleave the carbohydrate residues from glycoproteins associated with collagen in anemones (Zamer *et al.*, 1989). Consequently, this source of structural carbohydrate was not included in our measurements of carbohydrate content of the tissues.

Total lipid was extracted from 1.4–6.0 mg of oven-dried tissue by using a modified Bligh and Dyer (1959) technique with methylene chloride and methanol as the solvents (Carlson, 1985). Lipid class composition was measured by thin-layer chromatography/flame ionization detection (TLC/FID) on an Iatroscan TH-10 TLC/FID Analyzer (Iatron Laboratories, Tokyo, Japan). About 20 μg of lipid from each extracted lipid sample was spotted onto activated S-III chromarods in duplicate in 1–2 μl of methylene chloride:methanol (1:1) for TLC/FID lipid class analysis. As controls for both lipid class retention time and FID efficiency, we included with each sample analysis two chromarods, which were spotted with a standard mixture of phosphatidyl choline, cholesterol, triolein, 1-*O*-hexadecyl-2-3-dipalmitoyl-rac-glycerol (glycerol ethers) and cholesteryl oleate in proportions similar to those found in anemone samples, as determined by a preliminary analysis of the samples. Rods spotted with lipids were prefocused twice in chloroform:methanol (1:1), then developed in hexane:diethyl ether:formic acid (85:15:0.1) for 45 min. Racks containing the chromarods were then dried at 100°C for 5 min before being scanned. Developed chromarods were scanned at 30 cm·min^{-1}. Gas flow rates for hydrogen and air were 190 ml·min^{-1} and 2.0 l·min^{-1}, respectively. Peak areas for each lipid component were quantified by using a Hewlett Packard 3390A integrator.

Standard curves from 0 to 20 μg were created for phospholipids, sterols, fatty acids, triacylglycerols, glycerol ethers, sterol esters, and wax esters. The specific lipid used to represent each lipid class and the r^2 value for each standard curve are as follows: phospholipids (phosphatidyl choline), r^2 = 0.992; sterols (cholesterol), r^2 = 0.996; fatty alcohols (hexadecanol), r^2 = 0.998; fatty acids (oleic acid), r^2 = 0.985; triacylglycerols (triolein), r^2 = 0.984; glycerol ethers. (1-*O*-hexadecyl-2-3-dipalmitoyl-rac-glycerol), r^2 = 0.992; sterol esters (cholesteryl oleate), r^2

= 0.987 and wax esters (cetyl oleate), $r^2 = 0.914$. Sterol and wax esters are not resolved in the solvent system used. Periodic checks of area responses for standards indicated that standard errors of replicates were less than 3% of mean values in all cases. Total lipid was estimated by summing peak areas for each of the lipid classes.

Anemones in the experimental group were of sufficient size so that enough tissue was available for protein, carbohydrate, and lipid measurements, including the six lipid classes. The masses (in milligrams) of protein, lipid, and carbohydrate in each experimental anemone were multiplied by their corresponding specific enthalpy of combustion ($\Delta_c h$, $kJ \cdot g^{-1}$; Gnaiger, 1983), and the products were summed to estimate tissue energetic content (in kilojoules) of each anemone.

Anemones in the initial group, which were fed nauplii and used for estimating starting dry mass, had only enough tissue for determination of lipid class content. Therefore, in two other experimental groups (X and Y), we measured biochemical composition of tissues of anemones. These two groups of anemones were maintained simultaneously (in this case for over 5 weeks) in a single set of five monoclonal aquaria under the same conditions of feeding, temperature, and salinity as the initial group of anemones. Anemones in groups X and Y consisted of individuals from all five clones (A, B, C, D, and E), and were attached to the surfaces of the aquaria; unlike the anemones in the initial and experimental groups, they were not confined to beakers. The initial group of anemones and anemones in groups X and Y allowed us to test for the effects of clonal identity on biochemical composition when *H. lineata* consumed suspended nauplii as opposed to rations of frozen adult *Artemia*. Protein, carbohydrate, and tissue hydration were measured on the group X anemones; ash content and tissue hydration were measured on group Y anemones. Ash content was determined after the dried anemone tissue was combusted at 500°C for 6 h in a muffle furnace.

Statistical analysis

Relative growth, gravimetric absorption efficiency, and gravimetric net growth efficiency of the experimental anemones were analyzed with a randomized block analysis of variance (ANOVA) (Steel and Torrie, 1980). The categorical factors were block, represented by the two aquaria, and clone. Relative growth was arcsine transformed, whereas gravimetric absorption efficiency required a logit transformation (Cox and Snell, 1992) to meet the assumptions of the analysis. Gravimetric net growth efficiency did not require any transformation. Based on regression analysis, these three physiological energetic traits did not vary with body size.

Tissue hydration (percent) was measured on anemones from all four data sets: initial, experimental, and groups X and Y. The analysis of tissue hydration for the experimental anemones followed the randomized block design. Tissue hydration was examined by using an analysis of covariance (ANCOVA) for anemones in the other three data sets because significant regression slopes showed size-dependence, which was not the case for the experimental group. Tissue hydration in all cases was arcsine transformed, and the covariate, dry mass of the anemones, was transformed using natural logarithms.

All the biochemical variables (protein, carbohydrate, total lipid, and the six lipid classes) were initially expressed as proportions of the dry mass of tissue samples. These biochemical variables were "scaled up" (and expressed in milligrams) by multiplying the proportions by the dry mass of each anemone. The estimate of ash was made from an entire anemone, not from a tissue sample, so "scaling up" of that variable (milligrams of ash) was not needed. All the biochemical response variables, ash and anemone dry mass were transformed using natural logs.

Next, to acknowledge the metabolic relationships and potential covariance among similar dependent variables (*e.g.*, protein, carbohydrate, and lipid in tissues of experimental anemones), all of which had dry mass as a covariate, we grouped such variables and initially analyzed them with a multivariate analysis of covariance (MANCOVA; Huitema, 1980). This set of analyses also guards against over-interpretation of only a series of univariate analyses for these same variables. We used MANCOVA to analyze the effect of clone on protein, carbohydrate, and total lipid in experimental anemone tissue; the effect of clone on the six lipid classes in tissues of initial and experimental anemones; and the effect of clone on protein and carbohydrate content in tissues of group X anemones. When a MANCOVA resulted in a significant effect of clone on the group of dependent variables being analyzed, we proceeded with a series of ANCOVA, in which the effect of clone was examined for individual dependent variables having dry mass as covariate. Block and clone were the categorical variables for the experimental group of anemones for all these analyses. Clone was the only categorical variable for the other data sets (initial group, and groups X and Y) in all of these analyses.

The energetic contents of the experimental anemones were size-dependent, so they were analyzed with an ANCOVA. Block and clone were the categorical variables, and the natural log of dry mass was the covariate. No transformation was necessary for energetic content.

When ANOVA or ANCOVA resulted in a significant effect of clone on a dependent variable, we employed unplanned multiple comparison procedures (Day and Quinn, 1989). For the ANOVAs, all pairwise compari-

sons of means were made with the Tukey-Kramer procedure, which adjusts for unequal sample sizes (Day and Quinn, 1989). In the case of significant clonal effects from ANCOVAs, the Bryant-Paulson-Tukey (BPT) procedure was used to compare the size-adjusted means (Huitema, 1980). The BPT procedure takes into account that these size-adjusted means are not statistically independent due to the use of a pooled regression slope (Day and Quinn, 1989).

The relationship between the amount of water in the anemones (measured as the difference between blotted wet mass and dry mass; in milligrams) and the amount of total lipid (in milligrams) in the experimental and initial anemones was examined by partial correlation analysis, which measures the correlation between this pair of variables, keeping anemone body size constant (Sokal and Rohlf, 1981).

In the tables, the clonal means are presented with their 95% confidence limits (CL), and in the graphs, the clonal means are presented with their 95% confidence intervals (CI). For the size-independent variables (physiological energetic traits and tissue hydration of experimental anemones), their transformed means and standard errors were used to calculate the 95% CL, the means and 95% CL were back-transformed, and these values are reported here (Sokal and Rohlf, 1981, p. 419). The untransformed means for gravimetric absorption efficiency are presented. For the size-dependent variables (tissue hydration for the initial, X, and Y groups of anemones, and all the biochemical data) transformed, size-adjusted means, and their size-adjusted standard errors (Sokal and Rohlf, 1981, p. 525) were used to calculate 95% CL, and both means and confidence limits were then back-transformed. We present these back-transformed values of means and confidence intervals. The significant differences from the unplanned multiple comparison procedures, Tukey-Kramer or BPT, are indicated on the graphs, where different lowercase letters indicate significantly different clonal means.

Results

Physiological energetics

Our comparison of the physiological energetics of the anemones from the different clones revealed substantial intraclonal variation. Average relative growth for the ration-fed anemones was 35% (Fig. 1), and the effect of clone was not significant ($F_{2,36} = 1.3$, $P = 0.29$). The initial dry mass and final dry mass averages did not differ significantly among the clones ($F_{2,37} = 0.60$, $P = 0.56$, $F_{2,36} = 0.80$, $P = 0.46$, respectively; Table I). Nor was there a significant effect of clone on gravimetric absorption efficiency ($F_{2,26} = 0.36$, $P = 0.70$), for which clonal averages ranged between 92.7% and 93.5%. The clonal

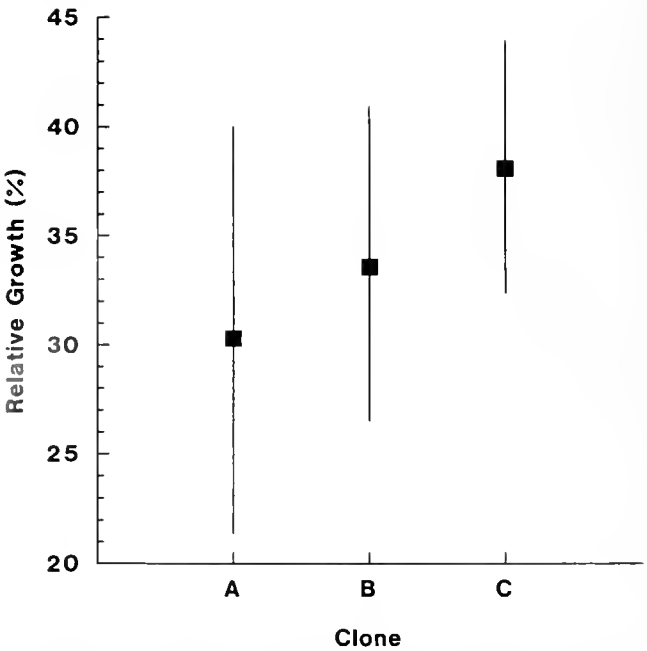

Figure 1. Relative growth, expressed as a percentage of the estimated initial dry mass, of the experimental anemones fed frozen adult *Artemia* rations. The filled squares are the clonal, back-transformed means, and the vertical bars are 95% confidence intervals (CI). The clonal sample sizes were $n_A = 8$, $n_B = 16$, and $n_C = 16$. Growth did not vary among the clones ($P = 0.29$).

pattern in net growth efficiency (K_2) was similar to that for relative growth. Clonal averages for K_2 were 40.4%, 43.8%, and 51.3% for clones A, B, and C, respectively. There was no significant effect of clone on K_2 ($F_{2,26} = 1.9$, $P = 0.16$).

Tissue hydration and lipid content

At the biochemical level of organization, interclonal variation was frequently greater than intraclonal variation. Clonal genotype significantly affected biochemical content in the experimental anemones, as revealed by a MANCOVA in which carbohydrate, protein, and lipid values were analyzed collectively (Wilks' $\lambda = 0.33$, $F_{6,32} = 7.6$, $P < 0.001$).

Tissue hydration differed significantly among clones of the experimental anemones ($F_{2,36} = 15.2$, $P < 0.001$), with those from clone B having the highest average (Fig. 2A). The effect of clone accounted for 43% of the variation in tissue hydration. For the initial group, anemones from the three clones also differed significantly in tissue hydration ($F_{2,21} = 14.8$, $P < 0.001$); anemones from clone B had the highest average at 84.5% (Fig. 2B). Tissue hydration was not significantly different among the anemones from the five clones of group X ($F_{4,34} = 2.4$, $P = 0.07$; Table II), but it was in group Y anemones ($F_{4,24}$

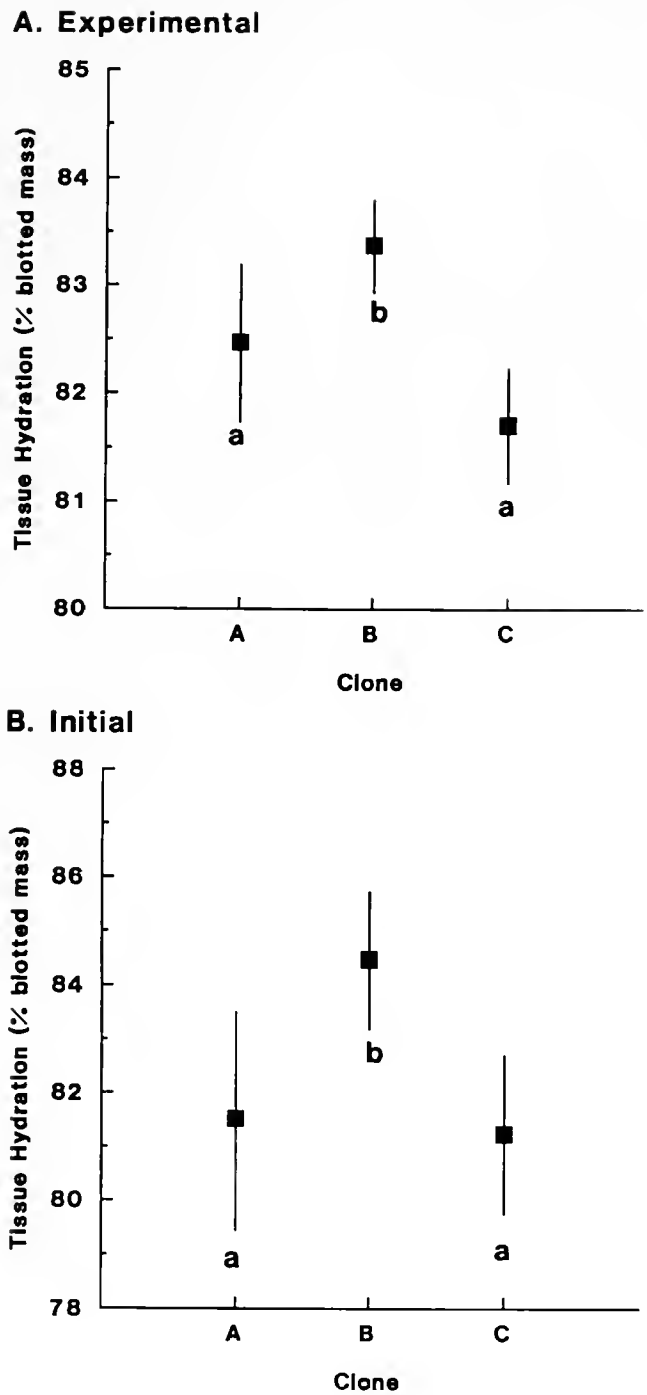

Figure 2. Tissue hydration, expressed as a percentage of the blotted wet mass, of the experimental (A) and initial (B) anemones. Clonal averages that do not share the same lowercase letter are significantly different from one another ($P \leq 0.05$). For the experimental anemones (A), the Tukey-Kramer procedure was used, and the symbols and sample sizes are as described in Figure 1. For the initial anemones (B), the Bryant-Paulson-Tukey (BPT) procedure was used, and the filled squares are the size-adjusted, back-transformed means, and the vertical bars are the 95% CI. For the initial anemones, tissue hydration was calculated for an anemone with an average dry mass of 8.40 mg. The clonal sample sizes for the initial anemones are $n_A = 5$, $n_B = 10$, and $n_C = 10$.

Table II

Tissue hydration for group X and Y anemones

Clone	Group X Tissue Hydration (%)	Group Y Tissue Hydration (%)
A	82.3 (81.6, 83.0)	81.8 (81.0, 82.6)
B	82.3 (81.6, 83.0)	82.2 (81.4, 83.0)
C	81.0 (80.3, 81.8)	81.6 (80.8, 82.5)
D	81.6 (80.8, 82.4)	81.5 (80.4, 82.6)
E	82.1 (81.3, 82.8)	83.1 (82.2, 84.1)

For each of the five clones, the sample sizes are $n = 8$ in group X and $n = 6$ in group Y. All values are the size-adjusted, back-transformed means and their 95% confidence limits. Tissue hydration was calculated for an anemone with an average dry mass of 8.73 mg for group X and 17.80 mg for group Y.

$= 2.8$, $P = 0.048$; Table II). However, in group Y none of the pairwise comparisons among clonal means were significant.

The amount of water and lipid (both in milligrams) in tissues of the experimental anemones showed an inverse relationship that was significant according to the partial correlation analysis ($r = -0.34$; $r_{0.05,\,35df} = -0.32$). The effect of clone was significant on the amount of total lipid ($F_{2,35} = 3.3$, $P = 0.05$; Fig. 3A), which composed 15.5% of the dry mass, on average, of the experimental anemones. On the basis of the Tukey-Kramer procedure, none of the pairwise comparisons were significant. For the initial group of anemones, amounts of tissue water and total lipid were not significantly correlated (partial correlation coefficient $= -0.30$, $r_{0.05,\,22df} = -0.40$). Also, initial anemones from the three clones were not significantly different in the amount of total lipid ($F_{2,21} = 2.8$, $P = 0.08$; Fig. 3B). Total lipid constituted 20.4% of the dry mass, on average, of the initial anemones.

The analysis of the individual lipid classes proved more informative than the examination of total lipid. Overall, lipid class content differed significantly among clones of both the experimental anemones (Wilks' $\lambda = 0.245$, $F_{12,60} = 5.10$, $P < 0.001$) and the initial group of anemones (Wilks' $\lambda = 0.107$, $F_{12,32} = 5.48$, $P < 0.001$). In general, anemones from clone B had less lipid than anemones from clones A and C. The three clones of experimental anemones differed significantly in the amounts of triacylglycerols ($F_{2,35} = 4.3$, $P = 0.02$; Fig. 4A), sterol esters and wax esters ($F_{2,35} = 7.3$, $P = 0.002$; Fig. 5A), glycerol ethers ($F_{2,35} = 15.1$, $P < 0.001$; Fig. 6A), and free fatty acids ($F_{2,35} = 5.5$, $P = 0.009$; Fig. 7A). In the initial anemones, clonal identity significantly affected levels of triacylglycerols ($F_{2,21} = 3.9$, $P = 0.04$; Fig. 4B), glycerol ethers ($F_{2,21} = 8.3$, $P = 0.002$; Fig. 6B), and free fatty acids ($F_{2,21} = 4.3$, $P = 0.03$; Fig. 7B).

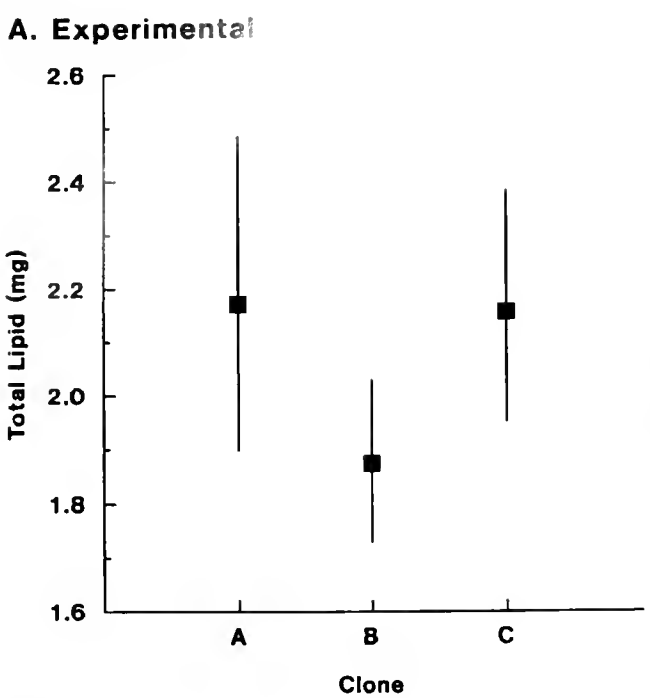

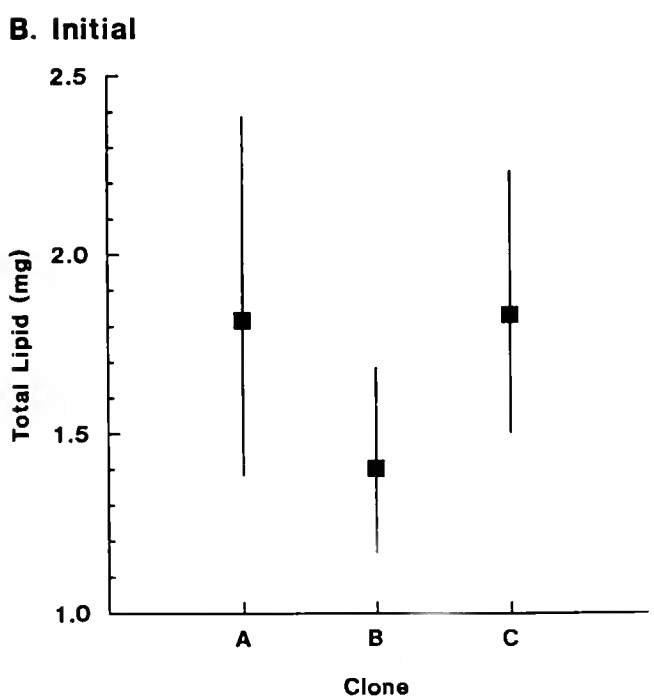

Figure 3. (A) Total lipid (mg) in the experimental anemones. Filled squares are size-adjusted, back-transformed means, and the vertical bars are the 95% CI. Sample size is as described in Figure 1. Total lipid was calculated for an anemone with an average dry mass of 13.38 mg. Clonal identity significantly affected total lipid ($P = 0.05$). (B) Total lipid (mg) in the initial anemones. Symbols and sample size are as described in Figure 2B. Total lipid was calculated for an anemone with an average dry mass of 8.40 mg. Clone did not significantly affect total lipid ($P = 0.08$).

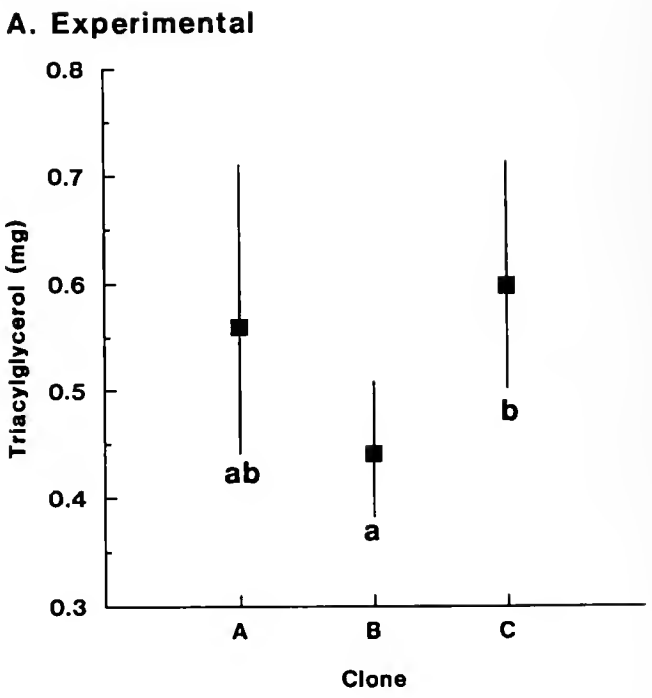

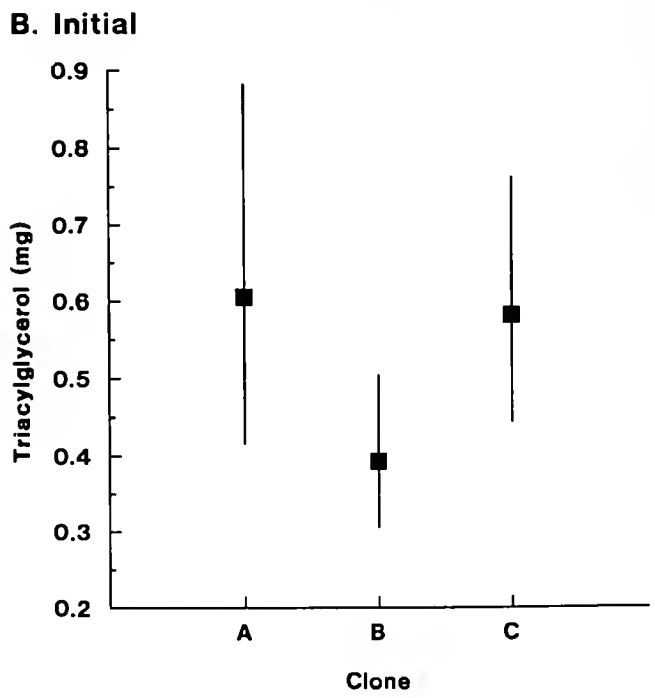

Figure 4. Triacylglycerol (mg) in the experimental (A) and initial (B) anemones. Clonal averages that do not share the same lowercase letter are significantly different from one another ($P \leq 0.05$) based on the BPT procedure. (A) Symbols for the experimental anemones are as described in Figure 3A, and sample size as described in Figure 1. Triacylglycerol was calculated for an anemone with an average dry mass of 13.38 mg. (B) Symbols and sample size for the initial anemones are as described in Figure 2B. Triacylglycerol was calculated for an anemone with an average dry mass of 8.40 mg. Clone significantly affected triacylglycerol content in experimental ($P = 0.002$) and initial anemones ($P = 0.004$).

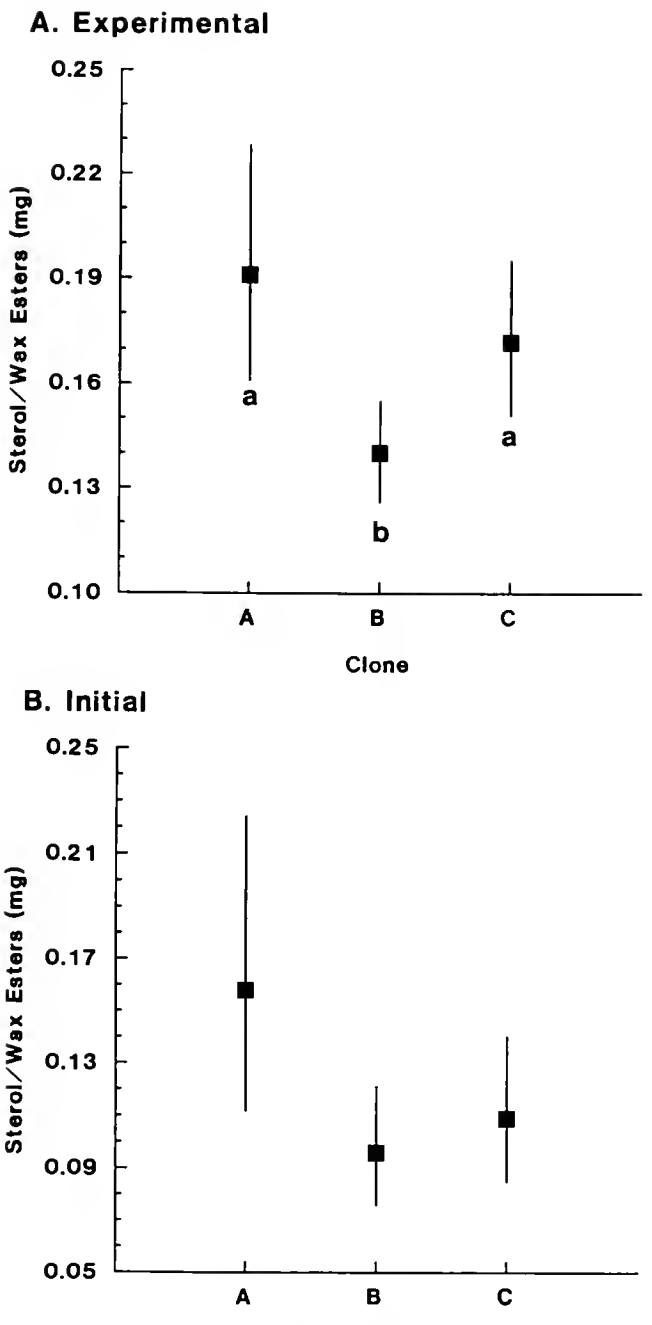

Figure 5. Sterol esters and wax esters (mg) in the experimental (A) and initial (B) anemones. Symbols and sample sizes of experimental and initial anemones are as described in Figure 4. Clone significantly affected sterol and wax ester content in experimental anemones ($P = 0.002$), but not in initial anemones ($P = 0.25$).

On average, experimental anemones from clone B had 35.6% less triacylglycerol than anemones in clone C (Fig. 4A), and clone B anemones in the initial group had the lowest levels of triacylglycerol (Fig. 4B). However, comparison of the average amount of triacylglycerol between clones B and C in the initial group yielded a generalized Studentized range statistic ($Q_{P(0.05,3,2,21)} = 3.47$) from the BPT procedure (Huitema, 1980) that was not significant ($Q_{P(crit)} = 3.67$).

Among the experimental anemones, those in clone B

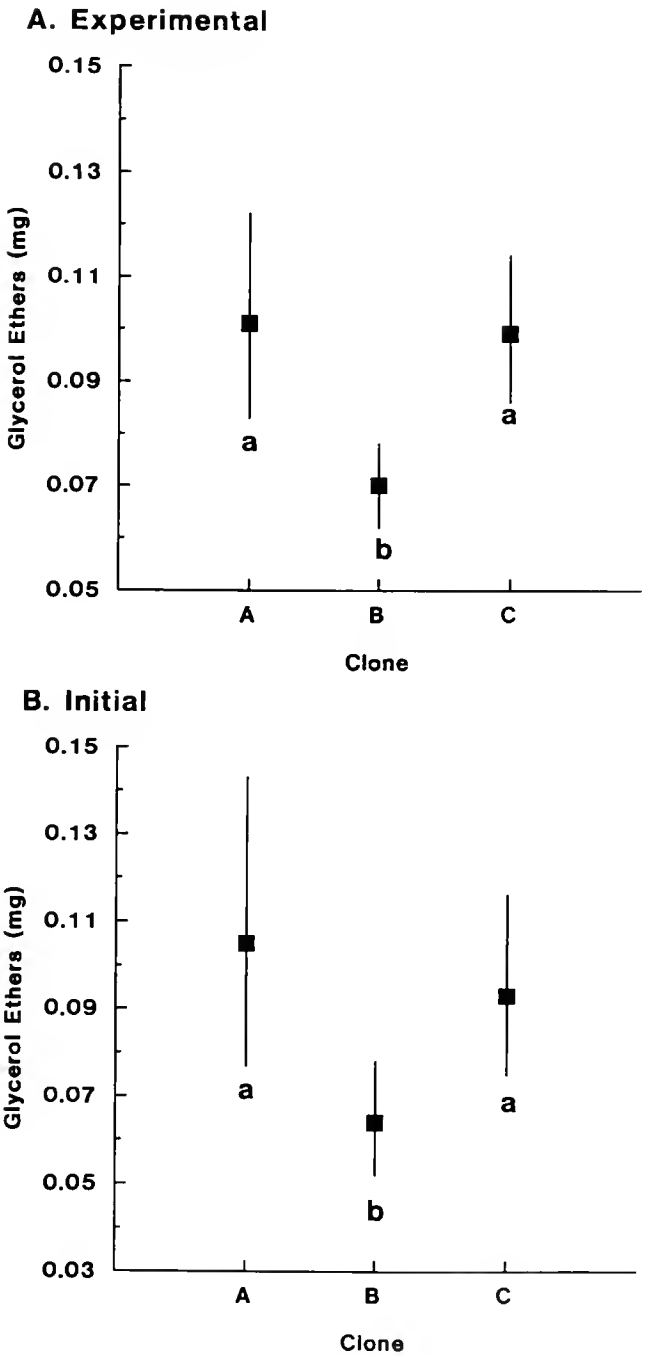

Figure 6. Glycerol ethers (mg) in the experimental (A) and initial (B) anemones. Symbols and sample sizes of experimental and initial anemones are as described in Figure 4. Clone significantly affected glycerol ether content in experimental ($P < 0.001$) and initial anemones ($P = 0.002$).

had the lowest amount of sterol esters and wax esters, averaging 36.4% less than anemones in clone A and 22.5% less than anemones in clone C (Fig. 5A). Although the effect of clone was significant on the amount of sterol esters and wax esters in the initial group of anemones ($F_{2,21} = 3.8$, $P = 0.04$; Fig. 5B), an outlier, the maximum value for sterol esters and wax esters, was identified, and dropping this value resulted in no detectable effect of clone ($F_{2,20} = 1.5$, $P = 0.25$).

Similar patterns were found for glycerol ethers and free fatty acids in both experimental and initial anemones. In the experimental group of anemones, clone B anemones had at least 41% less glycerol ethers than anemones in clones A and C (Fig. 6A), and they had 36% less free fatty acids than anemones in clone C (Fig. 7A). Among initial anemones, clone B anemones had 64% less glycerol ethers than anemones in clone A, and 45% less than anemones in clone C (Fig. 6B). And free fatty acids in initial clone B anemones were 62% less than the value in anemones in clone C (Fig. 7B).

Sterol content did not vary among the clones of experimental anemones ($F_{2,35} = 0.20$, $P = 0.82$; Fig. 8A), or among clones of the initial anemones ($F_{2,21} = 2.6$, $P = 0.10$; Fig. 8B). Similarly, there was no effect of clone on the amount of phospholipids for the experimental anemones ($F_{2,35} = 0.45$, $P = 0.64$; Fig. 9A) or the initial anemones ($F_{2,21} = 0.92$, $P = 0.41$; Fig. 9B).

Carbohydrate, protein, and ash contents

Clones of experimental anemones differed significantly in tissue carbohydrate content ($F_{2,33} = 27.0$, $P < 0.001$), which constituted 6.7% of anemone dry mass, on average (Fig. 10A). Carbohydrate, like lipid, was lowest in anemones from clone B—on average, 24% less than that of anemones in clones A and C (Fig. 10A). In group X anemones, a MANCOVA revealed significant clonal effects on protein and carbohydrate contents (Wilks' $\lambda = 0.43$, $F_{8,52} = 3.4$, $P < 0.001$), and univariate analysis of carbohydrate content showed that clonal identity affected levels of this biochemical class ($F_{4,27} = 5.0$, $P = 0.004$; Fig. 10B). Anemones in clones A and C had higher amounts of carbohydrate than anemones in clones B, D, and E, and the latter clones had similar levels (Fig. 10B). Carbohydrate constituted, on average, 8.3% of the dry mass among group X anemones.

The clonal pattern for the amount of protein in the experimental anemones resembled that seen for relative growth, with anemones in clone A having the lowest amount and those in clone C the highest amount (Fig. 11A). Like relative growth, the amount of protein in the experimental anemones showed no significant effect of clone ($F_{2,34} = 1.7$, $P = 0.19$). Protein constituted the bulk of the anemone's dry mass, averaging 69.2%. For group X anemones, the ranking of lowest to highest amount of protein was the same as for the experimental anemones. The effect of clone was not significant on amount of pro-

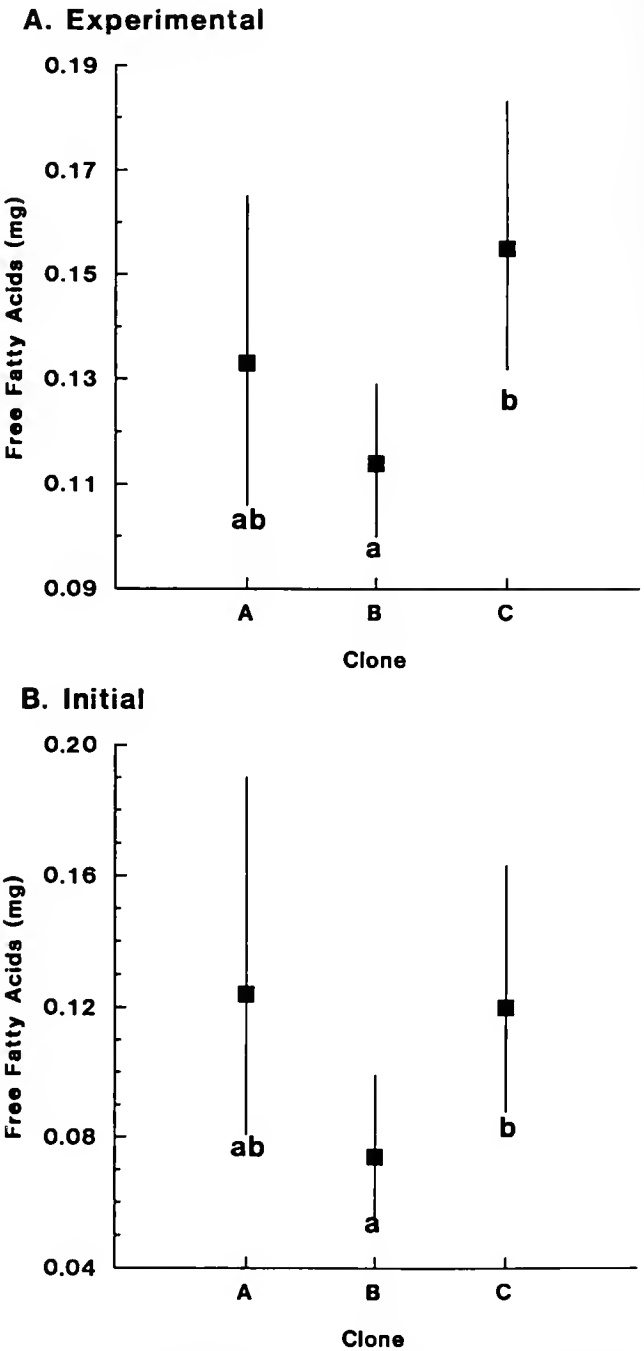

Figure 7. Free fatty acids (mg) in experimental (A) and initial (B) anemones. Symbols and sample sizes of experimental and initial anemones are as described in Figure 4. Clone significantly affected free fatty acid content in experimental ($P = 0.009$) and initial ($P = 0.03$) anemones.

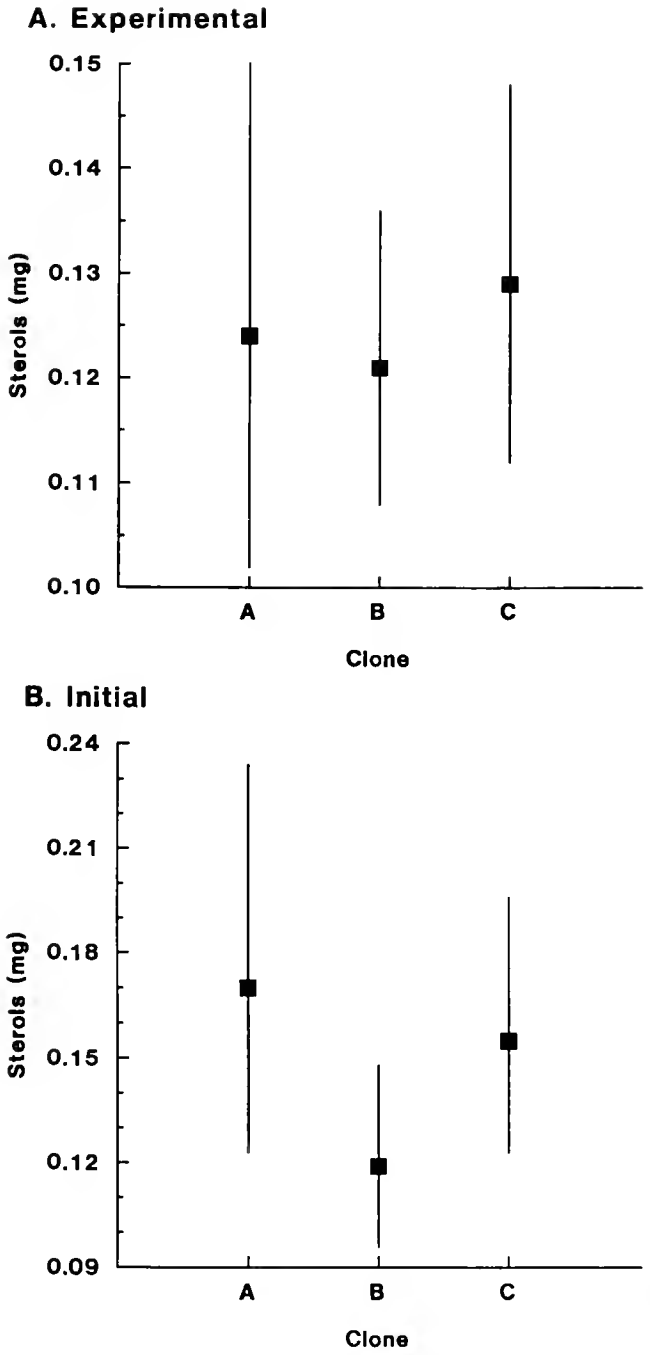

Figure 8. Sterol (mg) in experimental (A) and initial (B) anemones. Symbols and sample sizes of experimental and initial anemones are as described in Figure 4. Clone had no significant effect on sterol content of experimental ($P = 0.82$) or initial ($P = 0.10$) anemones.

tein in group X anemones ($F_{4,28} = 1.2$, $P = 0.34$; Fig. 11B), and protein composed, on average, 77.8% of the anemone dry mass.

On average, ash constituted 8.6% of the dry mass of an anemone (group Y; Table III). Clonal genotype did not affect ash content ($F_{4,23} = 1.5$, $P = 0.24$; Table III). The

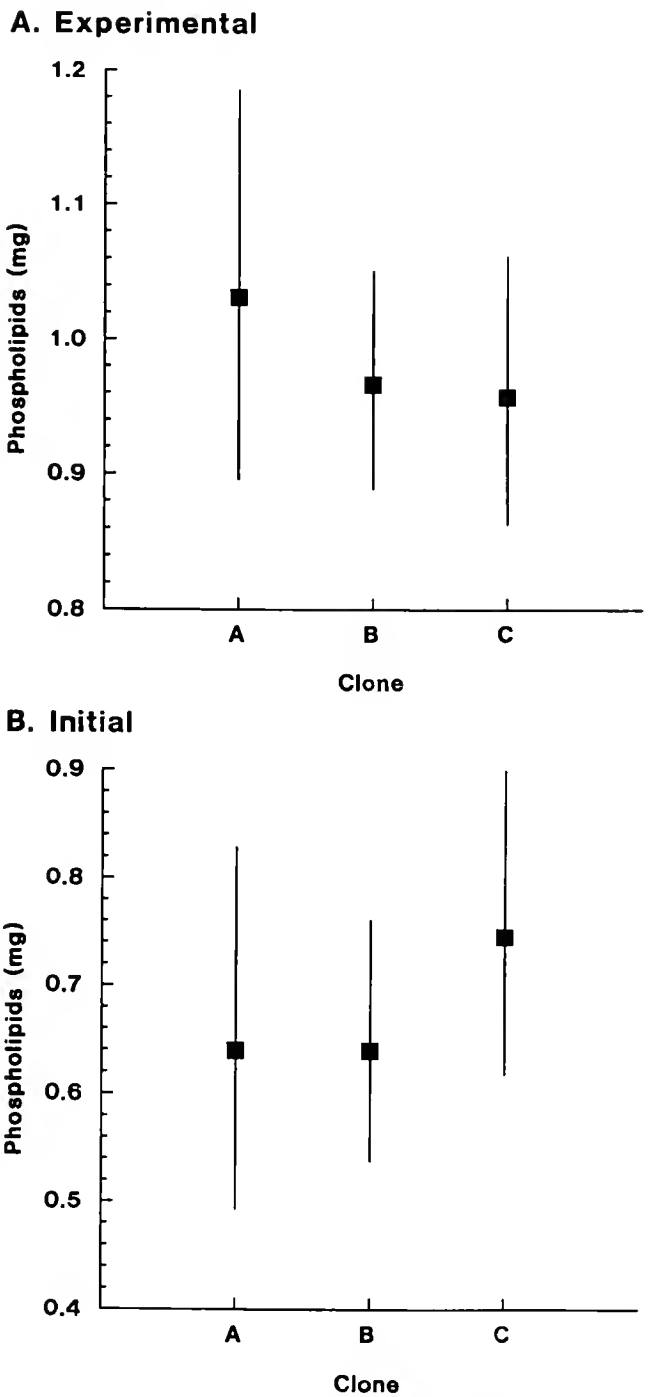

Figure 9. Phospholipids (mg) in experimental (A) and initial (B) anemones. Symbols and sample sizes of experimental and initial anemones are as described in Figure 4. Clone had no significant effect on phospholipid content of experimental ($P = 0.64$) or initial ($P = 0.41$) anemones.

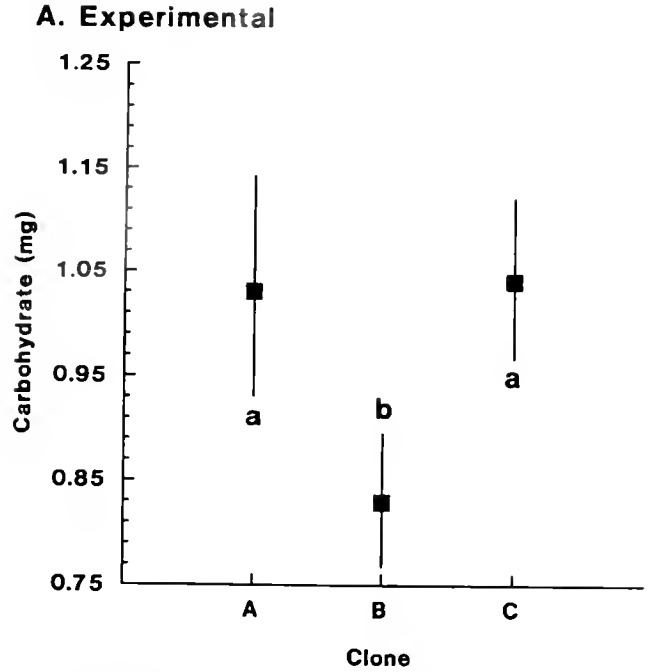

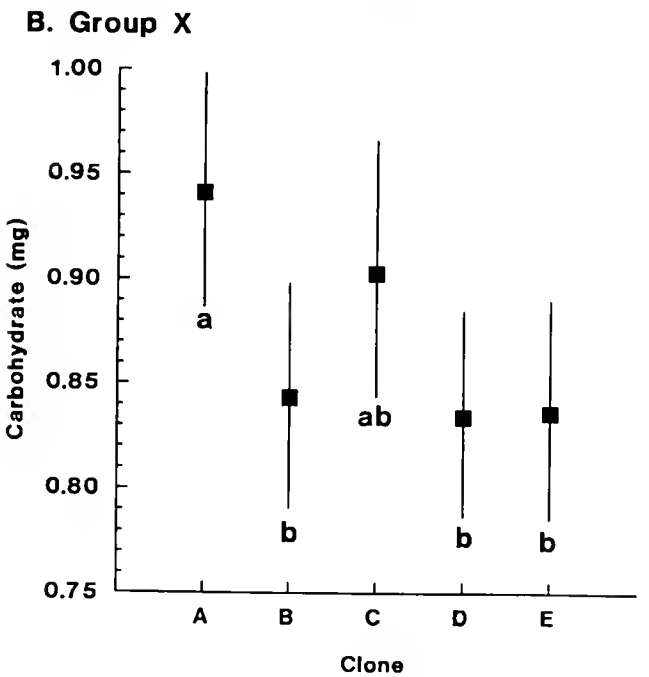

Figure 10. Carbohydrate (mg) in experimental (A) and group X anemones (B). Clonal averages that do not share the same lowercase letter are significantly different from one another based on the BPT method ($P \leq 0.05$). (A) Symbols for the experimental anemones are as described in Figure 3A, and clonal sample sizes are $n_A = 8$, $n_B = 14$, and $n_C = 16$. Carbohydrate was calculated for an anemone with an average dry mass of 14.37 mg. (B) The filled squares for group X anemones are the size-adjusted, back-transformed means, and vertical bars are 95% confidence intervals. Clonal sample sizes are $n_A = 6$, $n_B = 6$, $n_C = 6$, $n_D = 8$, and $n_E = 7$. Carbohydrate was calculated for an anemone with an average dry mass of 10.47 mg. Carbohydrate content was significantly different among clones of experimental anemones ($P < 0.001$) and among clones of the group X anemones ($P = 0.004$).

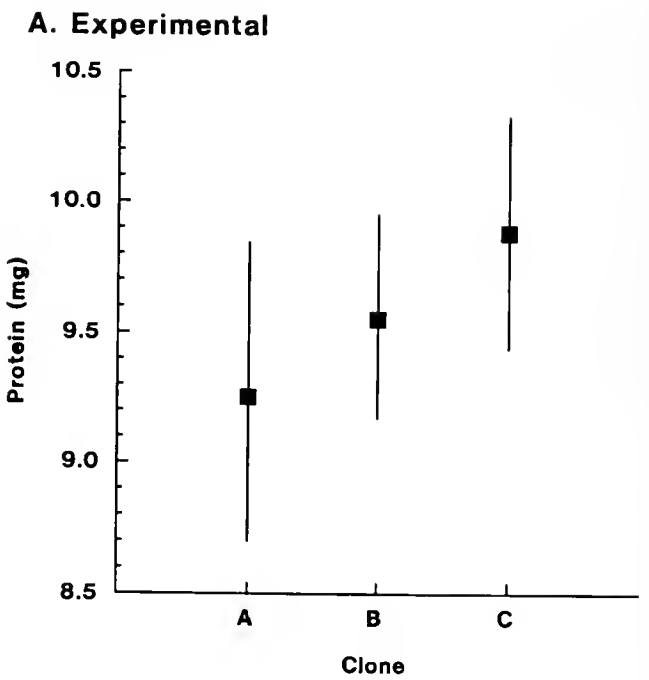

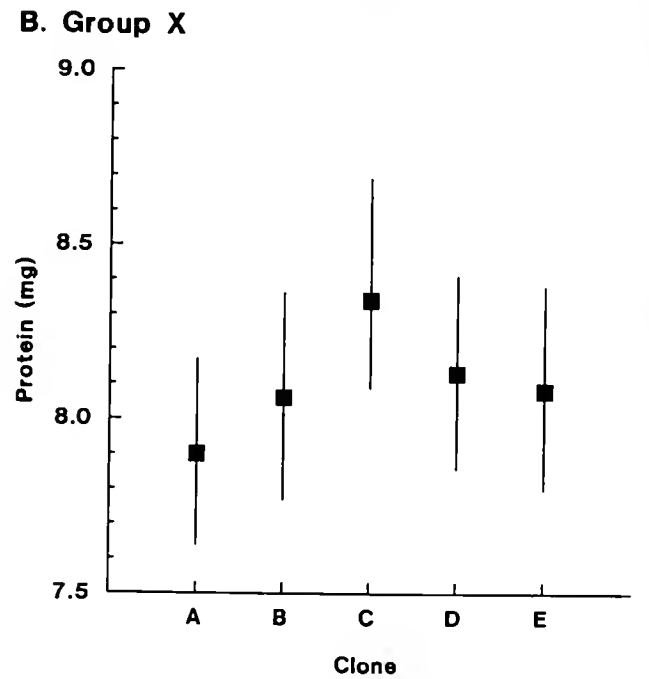

Figure 11. Protein (mg) in the experimental (A) and group X anemones (B). (A) Symbols for the experimental anemones are as described in Figure 3A. Clonal sample sizes are $n_A = 8$, $n_B = 15$, and $n_C = 16$. Protein was calculated for an anemone with an average dry mass of 13.96 mg. (B) Symbols for the group X anemones are as in Figure 10B. Clonal sample sizes are $n_A = 6$, $n_B = 6$, $n_C = 7$, $n_D = 8$, and $n_E = 7$. Protein was calculated for an anemone with an average dry mass of 10.45 mg. Protein was not significantly different among clones of either experimental ($P = 0.19$) or group X ($P = 0.34$) anemones.

Table III

Ash content of group Y anemones

Clone	Ash (mg)
A	1.44 (1.33, 1.55)
B	1.51 (1.41, 1.61)
C	1.46 (1.36, 1.57)
D	1.57 (1.44, 1.72)
E	1.61 (1.49, 1.75)

The sample size is $n = 6$ for all of the clones except clone A, where $n_A = 5$. All values are the size-adjusted, back-transformed means and their 95% confidence limits. Ash content was calculated for an anemone with an average dry mass of 17.83 mg.

amount of ash in *H. lineata* is comparable to the 9.1% ash content in the sea anemone *A. elegantissima* fed *Artemia* nauplii in the laboratory (Zamer, 1986).

Energetic content

Tissue energetic content (in kilojoules), as calculated from biochemical composition, differed significantly among the three clones of experimental anemones ($F_{2,33} = 5.6$, $P = 0.008$). The average energetic content of anemones from clone B was 17% less than that of anemones from clone C (Fig. 12).

Discussion

We observed a consistent, significant pattern of genetic variation in tissue hydration, carbohydrate content, and the content of several lipid classes among clones of *H. lineata*. The same clonal differences occurred in anemones from the two feeding regimes. Compared to anemones from clones A and C, clone B anemones consistently had lower averages for the lipid and carbohydrate contents of their tissues, and higher values for tissue hydration. Similar to clone B, anemones from clones D and E had less carbohydrate in their tissues than anemones from clone A (Fig. 10B). The net result of these differences in tissue constituents was lower energetic content in tissues of clone B anemones.

Although the similarity in clonal pattern for the tissue constituents between nauplii-fed and ration-fed anemones may reflect the relatively short duration of the growth experiment (10 days of ration feedings) compared with the extended acclimation of the nauplii-fed anemones (groups X and Y; more than 5 weeks), the experimental anemones (ration fed) tended to contain less protein (69.2%) and carbohydrate (6.7%) than the anemones in group X (average protein and carbohydrate contents: 77.8% and 8.3%, respectively), which were fed *ad libitum* on suspensions of *Artemia* nauplii. Thus biochemical composition responded to the change in feeding regime during the 10-day experimental period. Changes in biochemical constituents in tissues of *A. elegantissima* also were evident after just 6 days of feeding on even smaller rations (1% of dry body mass) of adult *Artemia* (Zamer, 1986; Zamer and Shick, 1989), and the same trend in protein and carbohydrate content was found between groups of *A. elegantissima* that were fed adults and nauplii of *Artemia* (Zamer, 1986; Zamer and Shick, 1989). Clearly, cnidarian biochemical composition can be altered by differences in diet composition and feeding frequency (Szmant-Froelich and Pilson, 1980; Fitt and Pardy, 1981; Zamer and Shick, 1989).

Yet despite this trend in biochemical content associated with the different feeding regimes in our study, we observed overriding and repeatable clonal patterns in biochemical composition of the tissues of *H. lineata*. We cannot convincingly argue that the 10-day period of feeding on adult *Artemia* was sufficient time to remove a clonal pattern in biochemical content differences that could have been established by clonal differences in tentacular capture of suspended prey. However, the similar and rapid changes in protein and carbohydrate that occur when both *H. lineata* and *A. elegantissima* are switched from nauplii to ration feeding suggest that the persistent pattern of clonal differences observed under both feeding regimes is not the result of prey capture differences, but rather the result of differences in meta-

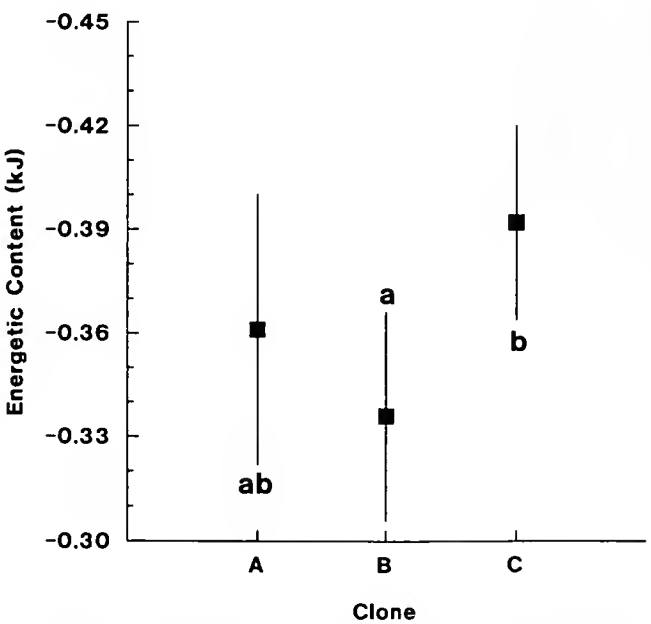

Figure 12. Energetic content, in kilojoules, of the experimental anemones, with symbols as described in Figure 3A. Clonal sample sizes are $n_A = 8$, $n_B = 14$, $n_C = 16$. Energetic content, calculated for an anemone with an average dry mass of 14.37 mg, was significantly different among clones of the experimental anemones ($P = 0.008$).

bolic rates or food conversion efficiencies among the separate clones of *H. lineata* (see below).

The high amounts of storage lipids and carbohydrate in anemones in clones A and C compared to anemones in clone B is the same pattern of genetic covariation in these biochemical classes that has been found in different genetic lines of *Drosophila melanogaster* (Clark and Keith, 1988; Clark, 1990) and in different species of *Drosophila* (Clark and Wang, 1994). Mechanisms that may produce this covariation include genetic modulation of the activities of enzymes associated with lipid and carbohydrate pathways of metabolism (Clark and Keith, 1988), and such genetic modulation of metabolic pathway performance has been associated with genotypes at the glucose-phosphate isomerase locus in the anemone *Metridium senile* (Zamer and Hoffmann, 1989). Alternatively, clone B anemones may have been unable to absorb energy from the digested rations as well as anemones from the other two clones. Differential substrate-specific absorption has been demonstrated in anemones (Zamer and Shick, 1989), and could produce differences in the biochemical and energetic content of their tissues. Low amounts of carbohydrate and lipid in tissues of clone B anemones resulted in low values for the calculated energetic content of these tissues, even though anemones in clone B received the same rations as anemones in clones A and C.

The lower energetic content of clone B anemones derives primarily from the lower levels of what may be considered energy-storage forms of lipid: fatty acids, triacylglycerols, and sterol esters and wax esters. All of these lipid classes have been associated with energy storage in anemones (*e.g.*, Pollero, 1983; Hill-Manning and Blanquet, 1979). We know of no data concerning the turnover of glycerol ethers in tissues of sea anemones, but given the low levels of this class of lipids in clone B anemones, we infer that it may also be a storage form.

In contrast, sterol (with cholesterol being the principal sterol in the anemone *Actinostola callosa;* Bergmann *et al.*, 1956) and phospholipids (often considered to be important as structural or membrane classes) are not variable among the three anemone clones examined here. These results indicate that storage of energy in the form of lipid is somehow impaired in clone B anemones.

In this context, we also note the inverse relationship between tissue water and total lipid in the experimental anemones. Small differences in tissue hydration have been reported between high- and low-intertidal individuals of *A. elegantissima* and between continuously immersed individuals of *H. lineata* and those maintained under fluctuating immersion conditions (Shick, 1991; Johnson and Shick, 1977). In both cases, anemones periodically exposed to air have slightly higher tissue hydration. In *A. elegantissima* freshly collected from upper and lower intertidal areas, a significant difference in lipid content was not observed, although high-shore specimens tended to have lower lipid than low-shore ones, consistent with the inverse relationship between tissue hydration and lipid content found in this study for *H. lineata*. Shick (1991) also points out that tissue hydration may be genetically correlated, given that variance in tissue hydration is significantly greater in multiclonal populations of *H. lineata* than in monoclonal ones (Shick and Dowse, 1985). Our findings of significant differences in tissue hydration among clones of *H. lineata* are consistent with this observation.

No genetic variation in tissue protein was detected among the anemones. Likewise, none was found for the flour beetle *Tribolium castaneum*, either in genetic lines selected for 21-day pupa weight or in control, unselected, genetic lines (Medrano and Gall, 1976a). Protein content in *H. lineata* is less variable than carbohydrate or lipid. For the experimental anemones ($n = 38$), the coefficient of variation of protein was 8.3%, whereas it was 15.4% for carbohydrate and 19.1% for lipid. Although our static measurements of protein were not different among our anemone clones, genetic variation has been associated with nitrogen metabolism, protein turnover rate, and physiological energetics of the blue mussel *Mytilus edulis* (Hilbish and Koehn, 1985; Hawkins *et al.*, 1986).

The physiological energetic values reported here for *H. lineata* are within typical ranges for sea anemones (Shick, 1991), and the experimental anemones from clones A, B, and C did not differ in the traits of relative growth, absorption efficiency, and net growth efficiency, which are all expressed gravimetrically. Recently, Tsuchida and Potts (1994) also reported that, in two separate feeding experiments, clonal identity had no effect on weight change in *A. elegantissima*. Differences in absorption efficiencies and net growth efficiencies have been detected among clones of *A. elegantissima* from different shore levels (Zamer, 1986), and those differences could not be erased by acclimation to common conditions. However, variation among clones within each tidal regime was not examined in that study. *A. elegantissima* had an average gravimetric absorption efficiency of 69.6% (Zamer, 1986), compared to 93% measured for *H. lineata* in this study. The net gravimetric growth efficiencies for these two species are about 45% (*cf.* Zamer, 1986). The relative growth reported here for *H. lineata* is about 15% greater than that measured in *A. elegantissima* (Zamer, 1986), but the difference is probably due to the larger rations received by *H. lineata* in this study (6%–8.5% of dry body mass compared to 4%–5.6% for *A. elegantissima*).

The lack of clonal differences in these components of the energy budget does not necessarily mean that the genotypes of *H. lineata* are equivalent in their physiologi-

cal energetics. First, an examination of energetically expressed absorption and net growth efficiencies, in which the energy content (rather than mass) of tissue growth, rations, and egesta are used in the calculations of these quantities, may reveal features of the physiological energetics of these clones that are not apparent from the present analysis of gravimetric values (*cf.* Zamer, 1986). The similar average body masses of anemones in all three clones examined (Table 1), in combination with both the low energetic content of the tissues of clone B anemones and the similar growth rates in anemones among these clones, is circumstantial support for the hypothesis that *energetic* values for net growth efficiency may be more informative than the present gravimetric ones.

Moreover, estimates of the biochemical content of food and egesta, which are values needed for determining energetic contents of these substances, may also be used to test one hypothesis concerning the differences in biochemical and energetic content of the tissues from anemones in the three clones. If we find the biochemical composition of the egesta to be the same, regardless of clonal genotype, then we can eliminate the differential-substrate-absorption hypothesis as an explanation for differences in the biochemical content of tissue.

Second, metabolic rate was not measured in the present study. If clone B anemones have a higher metabolic rate, on average, than anemones in clones A and C, then a greater proportion of the absorbed ration would be catabolized for maintenance, and consequently less energy would be stored in the tissues. In comparing clone B anemones acclimated to 25°C with anemones in clone C at the same temperature, we have observed consistently higher rates of longitudinal fission and smaller average body mass in clone B animals (Zamer, unpubl. data). The metabolic rate in clone B anemones may be elevated owing to greater costs associated with higher fission rate at 25°C. But we do not know whether elevation of metabolic rate underlies the low energetic content of clone B anemone tissues at 15°C. Genetic variation in metabolic rate, measured as oxygen consumption, has been detected among selected and control lines of *T. castaneum* (Medrano and Gall, 1976b), among *D. melanogaster* lines selected for desiccation resistance and control lines (Hoffmann and Parsons, 1989a; 1989b), in bivalves differing in multiple-locus heterozygosity (Bayne, 1987), in common garter snake (*Thamnophis sirtalis*) offspring from different families (Garland, 1994), and among strains and populations of the deer mouse *Peromyscus maniculatus* that differed in α-chain hemoglobin genotypes (Chappell and Snyder, 1984). Such variation in metabolic rate can be manifested as variation in maintenance efficiency, specifically in the rate of protein turnover (Hawkins *et al.*, 1986). Our ongoing experiments are aimed at determining energetically expressed values for absorption efficiency and growth and measuring oxygen uptake rates among anemones from our different clones. These studies will yield information about the mechanisms underlying the present clonal differences in physiological energetic traits as well as additional data on genetically correlated physiological variation.

In addition to providing these two mechanistic hypotheses, our study of the physiological variation that is associated with clonal genotype potentially has implications for the relative fitness of anemones from the different clones. At 10°C in the laboratory, individuals of *H. lineata* commonly encyst in mucous secretions, and in Indian Field Creek encysted and nonencysted individuals occur in the winter when the surface water temperature is below 10°C (Sassaman and Mangum, 1970). Although metabolic rate is correspondingly low at this temperature, and is likely to be even less in encysted compared to nonencysted individuals, survivorship of encysted anemones probably depends on reserves of storage lipid and carbohydrate. During extended encystment, anemones from clone B, which have less of these reserves at 15°C, may have lower survivorship than anemones in clones A and C, which have more of these reserves. The relationship between individual variation in the physiological characteristics of organisms and the variation among organisms in fitness is an essential component of organismal performance (Pough, 1989).

Acknowledgments

Thanks to Mike Lynch for assistance in the lipid analysis, to M. Amsler for doing the electrophoresis, and to C.P. Mangum for collecting the anemones at Indian Field Creek. This research was supported by NSF grant DCB-9057315 to W. E. Z. This is contribution No 294 from the Center of Marine Biotechnology, University of Maryland Biotechnology Institute. Versions of this manuscript benefitted from comments by C. O. Deetz, A. T. Weglinski, and two anonymous reviewers.

Literature Cited

Ayre, D. J. 1982. Inter-genotype aggression in the solitary sea anemone *Actinia tenebrosa*. *Mar. Biol.* **68:** 199–205.

Ayre, D. J. 1983. The effects of asexual reproduction and inter-genotypic aggression on the genotypic structure of populations of the sea anemone *Actinia tenebrosa*. *Oecologia (Berl.)* **57:** 158–165.

Ayre, D. J. 1985. Localized adaptation of clones of the sea anemone *Actinia tenebrosa*. *Evolution* **39:** 1250–1260.

Ayre, D. J. 1995. Localized adaptation of sea anemone clones: evidence from transplantation over two spatial scales. *J. Anim. Ecol* **64:** 186–196.

Bayne, B. L. 1987. Genetic aspects of physiological adaptation in bivalve molluscs. Pp. 169–189 in *Evolutionary Physiological Ecology*, P. Calow, ed. Cambridge University Press, New York.

Bayne, B. L., and R. C. Newell. 1983. Physiological energetics of ma-

rine molluscs. Pp. 407–515 in *The Mollusca*, Volume 4, Physiology, Part 1, A. S. M. Saleuddin and K. M. Wilbur, eds. Academic Press, New York.

Bergmann, W., S. M., Creighton, and W. M. Stokes. 1956. Contributions to the study of marine products. XL. waxes and triglycerides of sea anemones. *J. Org. Chem.* **21:** 721–728.

Bligh, E. G., and W. T. Dyer. 1959. A rapid method of total lipid extraction and purification. *Can. J. Biochem. Physiol.* **37:** 911–917.

Carlson, L. A. 1985. Extraction of lipids from human whole serum and lipoproteins and from rat liver tissue with methylene chloride-methanol: a comparison with extraction with chloroform-methanol. *Clin. Chim. Acta* **149:** 89–93.

Carvalho, G. R. 1994. Genetics of aquatic clonal organisms. Pp. 291–323 in *Genetics and Evolution of Aquatic Organisms*, A. R. Beaumont, ed. Chapman and Hall, London.

Chadwick, N. E., and C. Adams. 1991. Locomotion, asexual reproduction, and killing of corals by the corallimorpharian *Corynactis californica*. *Hydrobiologia* **216/217:** 263–269.

Chappell, M. A., and L. R. G. Snyder. 1984. Biochemical and physiological correlates of deer mouse α-chain hemoglobin polymorphisms. *Proc. Natl. Acad. Sci. USA* **81:** 5484–5488.

Clark, A. G. 1990. Genetic components of variation in energy storage in *Drosophila melanogaster*. *Evolution* **44:** 637–650.

Clark, A. G., and L. E. Keith. 1988. Variation among extracted lines of *Drosophila melanogaster* in triacylglycerol and carbohydrate storage. *Genetics* **119:** 595–607.

Clark, A. G., and L. Wang. 1994. Comparative evolutionary analysis of metabolism in nine *Drosophila* species. *Evolution* **48:** 1230–1243.

Coast and Geodetic Survey. 1960. Surface water temperature and salinity Atlantic Coast North and South America. C. & G. S. Publication 31-1, 76 pp. Government Printing Office, Washington, DC.

Cox, D. R., and E. J. Snell. 1992. *Analysis of Binary Data.* Chapman and Hall, New York.

Day, R. W., and G. P. Quinn, 1989. Comparisons of treatments after an analysis of variance in ecology. *Ecol. Monogr.* **59:** 433–463.

Dubois, M., K. A. Gilles, J. K. Hamilton, P. A. Rebers, and F. Smith. 1956. Colorimetric method for determination of sugars and related substances. *Anal. Chem.* **28:** 350–356.

Falconer, D. S. 1989. *Introduction to Quantitative Genetics.* Wiley, New York.

Fitt, W. K., and R. L. Pardy. 1981. Effects of starvation, light and dark on the energy metabolism of symbiotic and aposymbiotic sea anemones, *Anthopleura elegantissima*. *Mar. Biol.* **61:** 199–205.

Fukui, Y. 1991. Embryonic and larval development of the sea anemone *Haliplanella lineata* from Japan. *Hydrobiologia* **216/217:** 137–142.

Garland, T., Jr. 1994. Quantitative genetics of locomotor behavior and physiology in a garter snake. Pp. 251–277 in *Quantitative Genetic Studies of Behavioral Evolution*, C. R. B. Boake, ed. The University of Chicago Press, Chicago.

Gnaiger, E. 1983. Appendix C. Calculation of energetic and biochemical equivalents of respiratory oxygen consumption. Pp. 337–345 in *Polarographic Oxygen Sensors: Aquatic and Physiological Applications*, E. Gnaiger and H. Forstner, eds. Springer, New York.

Hawkins, A. J. S., B. L. Bayne, and A. J. Day. 1986. Protein turnover, physiological energetics and heterozygosity in the Blue Mussel, *Mytilus edulis*: the basis of variable age-specific growth. *Proc. R. Soc. Lond. B Biol. Sci.* **229:** 161–176.

Hilbish, T. J., and R. K. Koehn. 1985. The physiological basis of natural selection at the *lap* locus. *Evolution* **39:** 1302–1317.

Hill-Manning, D. N., and R. S. Blanquet. 1979. Seasonal changes in the lipid[illegible] the sea anemone, *Metridium senile* (L.) *J. Exp. Mar. Biol. Ecol.* **5:** 249–257.

Hoffmann, A. A., and P. A. Parsons. 1989a. An integrated approach to environmental stress tolerance and life-history variation: desiccation tolerance in *Drosophila*. *Biol. J. Linn. Soc.* **37:** 117–136.

Hoffmann, A. A., and P. A. Parsons. 1989b. Selection for increased desiccation resistance in *Drosophila melanogaster*: additive genetic control and correlated responses. *Genetics* **122:** 837–845.

Hoffmann, R. J. 1986. Variation in contributions of asexual reproduction to the genetic structure of populations of the sea anemone *Metridium senile*. *Evolution* **40:** 357–365.

Hughes, R. N. 1989. *A Functional Biology of Clonal Animals.* Chapman and Hall, New York.

Huitema, B. E. 1980. *The Analysis of Covariance and Alternatives.* Wiley, New York.

Itzhaki, R. F., and D. M. Gill. 1964. A micro-biuret method for estimating proteins. *Anal. Biochem.* **9:** 401–410.

Jennison, B. L. 1979. Annual fluctuations of lipid levels in the sea anemone *Anthopleura elegantissima* (Brandt, 1835). *J. Exp. Mar. Biol. Ecol.* **39:** 211–221.

Johnson, L. L., and J. M. Shick. 1977. Effects of fluctuating temperature and immersion on asexual reproduction in the intertidal sea anemone *Haliplanella luciae* (Verrill) in laboratory culture. *J. Exp. Mar. Biol. Ecol.* **28:** 141–149.

Jones, R., J. A. Bates, D. J. Innes, and R. J. Thompson. 1996. Quantitative genetic analysis of growth in larval scallops (*Placopecten magellanicus*). *Mar. Biol.* **124:** 671–677.

Keen, S. L., and A. J. Gong. 1989. Genotype and feeding frequency affect clone formation in a marine cnidarian (*Aurelia aurita* Lamarck 1816). *Funct. Ecol.* **3:** 735–745.

Koehn, R. K. 1991. The cost of enzyme synthesis in the genetics of energy balance and physiological performance. *Biol. J. Linn. Soc.* **44:** 231–247.

Koehn, R. K., and B. L. Bayne. 1989. Towards a physiological and genetical understanding of the energetics of the stress response. *Biol. J. Linn. Soc.* **37:** 157–171.

Medrano, J. F., and G. A. E. Gall. 1976a. Growth rate, body composition, cellular growth, and enzyme activities in lines of *Tribolium castaneum* selected for 21-day pupa weight. *Genetics* **83:** 379–391.

Medrano, J. F., and G. A. E. Gall. 1976b. Food consumption, feed efficiency, metabolic rate, and utilization of glucose in lines of *Tribolium castaneum* selected for 21-day pupa weight. *Genetics* **83:** 393–407.

Minasian, L. L., Jr. 1979. The effect of exogenous factors on morphology and asexual reproduction in laboratory cultures of the intertidal sea anemone, *Haliplanella luciae* (Verrill) (Anthozoa:Actinaria) from Delaware. *J. Exp. Mar. Biol. Ecol.* **40:** 235–246.

Minasian, L. L., and R. N. Mariscal. 1979. Characteristics and regulation of fission activity in clonal cultures of the cosmopolitan sea anemone, *Haliplanella luciae* (Verrill). *Biol. Bull.* **157:** 478–493.

Pollero, R. J. 1983. Lipid and fatty acid characterization and metabolism in the sea anemone *Phymactis clematis* (Dana). *Lipids* **18:** 12–17.

Pough, F. H. 1989. Organismal performance and Darwinian fitness: approaches and interpretations. *Physiol. Zool.* **62:** 199–236.

Present, T. M. C., and D. O. Conover. 1992. Physiological basis of latitudinal growth differences in *Menidia menidia*: variation in consumption or efficiency. *Funct. Ecol.* **6:** 23–31.

Rawson, P. D., and T. J. Hilbish. 1991. Genotype-environment interaction for juvenile growth in the hard clam *Mercenaria mercenaria* (L.). *Evolution* **45:** 1924–1935.

Sassaman, C., and C. P. Mangum. 1970. Patterns of temperature adaptation in North American Atlantic coastal actinians. *Mar. Biol.* **7:** 123–130.

Sebens, K. P. 1981. Reproductive ecology of the intertidal sea anemones *Anthopleura xanthogrammica* (Brandt) and *A. elegantissima*

(Brandt): body size, habitat, and sexual reproduction. *J. Exp. Mar. Biol. Ecol* **54:** 225–250.

Shick, J. M. 1976. Ecological physiology and genetics of the colonizing actinian *Haliplanella luciae*. Pp. 137–146 in *Coelenterate Ecology and Behavior*, G. O. Mackie, ed. Plenum Publishing, New York.

Shick, J. M. 1991. *A Functional Biology of Sea Anemones*. Chapman and Hall, New York.

Shick, J. M., and H. B. Dowse. 1985. Genetic basis of physiological variation in natural populations of sea anemones: intra- and interclonal analyses of variance. Pp. 465–479 in *Proceedings of the Nineteenth European Marine Biology Symposium*, P. E. Gibbs, ed. Cambridge University Press, U. K.

Shick, J. M., R. J. Hoffmann, and A. N. Lamb. 1979. Asexual reproduction, population structure, and genotype-environment interactions in sea anemones. *Am. Zool.* **19:** 699–713.

Shick, J. M., and A. N. Lamb. 1977. Asexual reproduction and genetic population structure in the colonizing sea anemone *Haliplanella luciae*. *Biol. Bull.* **53:** 604–617.

Sokal, R. R., and F. J. Rohlf. 1981. *Biometry*. W. H. Freeman and Co., San Francisco.

Steel, R. G. D., and J. H. Torrie. 1980. *Principles and Procedures of Statistics*. McGraw-Hill, New York.

Szmant-Froelich, A., and M. E. Q. Pilson. 1980. The effects of feeding frequency and symbiosis with zooxanthellae on the biochemical composition of *Astrangia danae* Milne Edwards and Haime 1849. *J. Exp. Mar. Biol. Ecol.* **48:** 85–97.

Tsuchida, C. B., and D. C. Potts. 1994. The effects of illumination, food and symbionts on growth of the sea anemone *Anthopleura elegantissima* (Brandt, 1835). I. Ramet growth. *J. Exp. Mar. Biol. Ecol.* **183:** 227–242.

Vrijenhoek, R. C. 1994. Unisexual fish: model systems for studying ecology and evolution. *Annu. Rev. Ecol. Syst.* **25:** 71–96.

Weisberg, S. 1985. *Applied Linear Regression*. John Wiley and Sons, New York.

Williams, G. C. 1975. *Sex and Evolution*. Princeton University Press, Princeton, NJ.

Winberg, G. C. 1956. Rate of metabolism and food requirements of fishes. *Fish. Res. Board Can. Trans. Ser.* **194:** 1–202.

Zamer, W. E. 1986. Physiological energetics of the intertidal sea anemone *Anthopleura elegantissima* I. Prey capture, absorption efficiency and growth. *Mar. Biol.* **92:** 299–314.

Zamer, W. E., and R. J. Hoffmann. 1989. Allozymes of glucose-6-phosphate isomerase differentially modulate pentose-shunt metabolism in the sea anemone *Metridium senile*. *Proc. Natl. Acad. Sci. USA* **86:** 2737–2741.

Zamer, W. E., and C. P. Mangum. 1979. Irreversible nongenetic temperature adaptation of oxygen uptake in clones of the sea anemone *Haliplanella luciae* (Verrill). *Biol. Bull.* **157:** 536–547.

Zamer, W. E., and J. M. Shick. 1987. Physiological energetics of the intertidal sea anemone *Anthopleura elegantissima*. II. Energy balance. *Mar. Biol.* **93:** 481–491.

Zamer, W. E., and J. M. Shick. 1989. Physiological energetics of the intertidal sea anemone *Anthopleura elegantissima*. III. Biochemical composition of body tissues, substrate-specific absorption, and carbon and nitrogen budgets. *Oecologia* **79:** 117–127.

Zamer, W. E., J. M. Shick, and D. W. Tapley. 1989. Protein measurement and energetic considerations: comparisons of biochemical and stoichiometric methods using bovine serum albumin and protein isolated from sea anemones. *Limnol. Oceanogr.* **34:** 256–263.

Reference: *Biol. Bull.* **192**: 444–456. (June, 1997)

Oxidative Stress in the Symbiotic Sea Anemone *Aiptasia pulchella* (Carlgren, 1943): Contribution of the Animal to Superoxide Ion Production at Elevated Temperature

CALVIN M. NII AND LEONARD MUSCATINE

Department of Biology, University of California, Los Angeles, California 90095-1606

Abstract. Production of superoxide ions within tissues of the symbiotic sea anemone *Aiptasia pulchella* was detected using SOD-inhibitable cytochrome *c* reduction and quantified by SOD-inhibitable reduction of nitro blue tetrazolium (NBT). Intact aposymbiotic and symbiotic specimens of *A. pulchella* produced superoxide in response to acute, sublethal thermal stress. Neither light nor inhibition of symbiont photosynthesis by (3,4-dichlorophenyl)-1,1-dimethylurea (DCMU) affected superoxide production. The time course of superoxide ion production strongly resembled the time course of increased dark respiration by intact anemones, suggesting that the effect of elevated temperature on host mitochondria may account for increased superoxide production. Interestingly, freshly isolated algae (FIZ) did not release superoxide ions in response to elevated temperature, and net oxygen production decreased greatly in both intact symbiotic anemones and in FIZ within 20 minutes after temperature elevation. These results show that oxidative stress in *A. pulchella* is primarily an animal response, and suggest that the presence of symbiotic algae, although sufficient to cause hyperoxia, is not necessary for the appearance of oxidative stress in these anemones at elevated temperature.

Introduction

Elevated temperature can adversely affect the stability of symbioses between cnidarians and symbiotic dinoflagellates and result in bleaching (Glynn, 1990). Cnidarian bleaching may be manifest as a decline in the population density of the symbiotic algae (Fisk and Done, 1985; Hoegh-Guldberg and Smith, 1989), a reduction in the amount of chlorophyll *a* (Coles and Jokiel, 1977; Kleppel *et al.*, 1989; Porter *et al.*, 1989; Szmant and Gassman, 1990) and accessory pigments (Kleppel *et al.*, 1989) per alga, or both (Glynn and D'Croz, 1990; Lesser *et al.*, 1990). While the loss of symbionts *per se* has been described at the organismic level (Gates *et al.*, 1992; Brown *et al.*, 1995), there are few experimental studies of the cellular or molecular mechanism of cnidarian bleaching.

Oxidative stress is thought to play a role in bleaching (Lesser and Shick, 1989; Lesser *et al.*, 1990; Shick *et al.*, 1991, Shick *et al.*, 1995; Lesser, 1996). Active oxygen species may be produced within the algae and within the host in response to a combination of elevated seawater temperature and high levels of photosynthetically active radiation (PAR) or ultraviolet radiation (Lesser and Shick, 1989; Lesser *et al.*, 1990; Dykens *et al.*, 1992). Symbiotic dinoflagellates may respond by exhibiting increased activities of the protective enzymes superoxide dismutase (SOD) and catalase (CAT; Lesser and Shick, 1989; Lesser *et al.*, 1990; Shick *et al.*, 1991; Matta and Trench, 1991; Shick *et al.*, 1995). Production of hydroxyl radicals in the light has been detected in homogenates of both symbiotic and aposymbiotic anemones and in isolated symbiotic algae (Dykens *et al.*, 1992). Yet, the explicit source of active oxygen species in the intact symbioses under stress conditions is still unknown.

Active oxygen species could originate from the interaction of molecular oxygen from symbiont photosynthesis and electrons from animal tissue sources (Dykens and Shick, 1982, 1984; Dykens, 1984; Dykens *et al.*,

Received 26 July 1996; accepted 27 February 1997.

1992), or from oxidants (O_2^- and H_2O_2) produced within the algae and released to host tissues (Lesser and Shick, 1989; Lesser *et al.*, 1990). Lesser *et al.* (1990) also hypothesized that active oxygen species from algae may signal the bleaching response in symbiotic cnidarians.

Whereas the foregoing observations emphasize oxygen production and univalent reduction in algae, oxygen derived from the ambient medium may also undergo univalent reduction in the animal. About 4% of the total oxygen that is consumed by animal mitochondria during aerobic respiration undergoes a further univalent reduction to form superoxide ion (Boveris and Cardenas, 1982), and exposure to elevated temperature increases superoxide ion production in animal mitochondria (Burdon *et al.*, 1990).

In this study, we demonstrate that oxidative stress is concomitant with acute, sub-lethal thermal stress in the tropical sea anemone *Aiptasia pulchella*, and that at elevated temperature, increased superoxide production represents primarily an animal response.

Materials and Methods

Animal collection and maintenance

The symbiotic sea anemone *Aiptasia pulchella* (Carlgren, 1943) was collected from reef flats near the Hawaii Institute of Marine Biology, Kaneohe, Hawaii, and transported to the University of California, Los Angeles. These anemones were maintained in 1.5-liter glass bowls containing natural seawater (Redondo Beach, CA; 33‰, pH 8.3) and kept in a temperature (26° ± 1°C) and light-controlled (70 $\mu E/m^2/s$; 12 h light/12 h dark) incubator. Anemones were fed three times weekly with freshly hatched *Artemia* nauplii. Unless stated otherwise, artificial seawater ("FSW"; 33‰, pH 8.3, Tropic Marin) filtered through glass fiber filters (Whatman GF/C) was used in all experiments. All chemicals were obtained from Sigma (St. Louis, MO).

Aposymbiotic anemones were generated by chilling symbiotic *A. pulchella* in 4°C seawater for 4 h and then maintaining them in darkness at 26° ± 1°C (Steen and Muscatine, 1987). The anemones lost about 99% of their algae within 1 week after "cold shock," but were not used in experiments until they had been maintained in darkness for at least 10 weeks. Aposymbiotic anemones were fed three times weekly with *Artemia* nauplii, but those used in the hyperoxia experiments were fed twice weekly with adult *Artemia*.

Algae-free tissue homogenates from individual animals were prepared by homogenizing a single specimen of *A. pulchella* in 1.0 ml FSW on ice and removing the algae by centrifugation (IEC; 500 × *g*) for 2 or 3 min. The supernatant containing the algae-free animal tissue homogenate was decanted, brought to a final volume of 2.0 ml with FSW, and kept on ice briefly until needed. A 0.2-ml aliquot of the homogenate was removed for measurement of soluble protein.

Freshly isolated symbiotic dinoflagellates (FIZ; *Symbiodinium pulchrorum*, Banaszak *et al.*, 1993) were prepared by homogenizing an anemone in 2 ml FSW and then centrifuging this homogenate at 500 × *g* for 2–3 min. The supernatant was discarded, and the algal pellet was washed by suspension and centrifugation up to five times until it was free of nearly all animal contamination. Samples were then taken for algal cell counts.

Assay for superoxide ions in intact host tissues by NBT reduction

Superoxide ions were measured by the reduction of nitro blue tetrazolium (NBT) to its diformazan derivative (formazan; Seidler, 1991; Thom *et al.*, 1993). Formazan production was quantified by a modification of the methods used by Chacon and Acosta (1991). NBT formazan was first isolated by homogenization of an intact anemone in 1.0 ml FSW in a glass tissue grinder. The homogenate was then centrifuged (IEC; 500 × *g*), and the supernatant was removed and saved for measurement of soluble protein. NBT formazan crystals remained as a thin bluish layer above the algal pellet. Pellet and formazan were then transferred to a 1.5-ml plastic microfuge tube and then extracted in 1.0 ml of 80% or 95% ethanol at 4°C for at least 60 min to remove algal pigments that interfere with the spectrophotometric measurement of the ethanol-insoluble NBT formazan. Complete removal of algal pigments was verified by spectrophotometric examination (between 400 and 800 nm) of the ethanolic extract.

The extracted suspension was then centrifuged (Fisher microcentrifuge; 5000 × *g*) to pellet the ethanol-insoluble formazan crystals. The ethanol supernatant and residual algae were then discarded and replaced by 1.0 ml of dimethylformamide (DMF) to dissolve the formazan. Dissolution was accelerated by sonication (Branson; four 15-s pulses at 35 W) and the absorbance of the resulting bluish solution was then measured spectrophotometrically at 550 nm. The concentration of formazan was then calculated from the measured absorbance and the molar extinction coefficient of the NBT formazan (ϵ = 30,000). Results are expressed as nmol NBT formazan produced per milligram of soluble animal protein.

Specificity of the NBT assay for superoxide ions

Separate volumes (2.0 ml) of animal homogenate were prepared as described above. After removing 0.2 ml for soluble protein analysis, four 0.3-ml samples were used in NBT reduction experiments. These were performed in microfuge tubes (1.5 ml). A series of four treatments

was performed: samples with animal homogenate only (control); samples with Cu-Zn SOD only (from bovine erythrocytes; 50-500 U); samples with both SOD and 1 m*M* diethyldithiocarbamate (DDC), a copper chelator that inhibits SOD activity *in vivo* (Enger and Kensler, 1985); and samples with DDC only. DDC did not reduce NBT in control experiments.

The reaction mixtures consisted of animal homogenate (0.3 ml), NBT dissolved in FSW (0.3 ml, to a final concentration of 10^{-4} *M*), 1 m*M* DDC, and 100 U Cu-Zn SOD to a final reaction volume of 1 ml. The residual volume in treatments that omitted SOD, DDC, or both was made up with FSW (0.4 ml). Control treatments contained only animal homogenate and NBT; FSW was added to achieve the final reaction volume.

The NBT was added last to the sample mixture to initiate the reaction. Reaction mixtures were incubated in darkness for 60 min, including a 5-min centrifugation ($5000 \times g$) to isolate any NBT formazan produced. Formazan was quantified using the methods described above. The results are expressed as the percent stimulation or inhibition of NBT reduction (per milligram of soluble animal protein) by SOD, DDC, or both compared with control samples (no SOD/DDC).

The effect of SOD concentration on NBT reduction in animal homogenates was investigated by adding 50 to 500 U Cu-Zn SOD to a mixture (final volume = 1.0 ml) containing animal homogenate (0.3 ml) and NBT dissolved in FSW (0.3 ml; final NBT concentration = 10^{-4} *M*).

Cytochrome c *reduction assay for superoxide production*

Cytochrome *c* reduction was used as an independent assay for superoxide production in algae-free tissue homogenates of symbiotic *A. pulchella*. The tissue homogenates were prepared by homogenizing three to five symbiotic anemones in a reaction buffer (0.5 m*M* potassium phosphate, 0.1 m*M* EDTA, pH 7.8) and then separating the algae from the homogenate by centrifugation as described above. The soluble protein content of the homogenate was adjusted to 5 mg/ml by dilution with reaction buffer. The homogenate was maintained briefly at room temperature until needed. The cytochrome *c* reduction assay used was modified from the method of Flohé and Otting (1984). Briefly, the reaction mixture (total volume 1.5 ml) contained 0.5 m*M* potassium phosphate buffer (pH 7.8), 0.1 m*M* EDTA and 20 μM acetylated cytochrome *c*. The latter is refractory to reduction by mitochondrial cytochrome *c* oxidases (Azzi *et al.*, 1975). To verify the efficacy of this modified assay, we used xanthine oxidase (0.2 U/ml) and 50 μM xanthine to generate superoxide in the reaction medium, causing reduction of cytochrome *c*. Cytochrome *c* reduction was determined by measuring the change in absorbance at 550 nm using a UV-VIS spectrophotometer (Uvikon) fitted with temperature-controlled cuvette holders. The cuvette holders were connected to a recirculating water bath maintained at 26° ± 1°C. The addition of 1, 10, or 100 U Cu-Zn SOD to the reaction mixture inhibited cytochrome reduction by 55%, 95%, and 98% respectively. Superoxide production by tissue homogenates was determined by substituting 100 μl of tissue homogenate for the xanthine and xanthine oxidase. To verify the assay specificity for superoxide ions, Cu-Zn SOD (10, 20, 50, or 100 U) was added to inhibit cytochrome *c* reduction in reaction mixtures containing homogenates.

NBT reduction by intact symbiotic and aposymbiotic anemones

Symbiotic and aposymbiotic anemones of similar oral disc diameter (~1 cm) and column height (~1.5 cm) were placed in 15-ml glass test tubes containing 2.5 ml FSW and allowed to attach to the bottom of the tube. Groups of 12 anemones were pre-incubated in light (300 $\mu E/m^2/s$) or dark at ambient temperature (26°C) for at least 1 h before the start of an experiment. Another group was pre-incubated in FSW containing 0.5 m*M* (nominal concentration) 3-(3,4-dichlorophenyl)-1,1-dimethylurea (DCMU) at ambient temperature. Preliminary experiments (n = 3) showed that DCMU did not affect dark respiration in intact symbiotic and aposymbiotic animals or in FIZ, but did inhibit photosynthetic oxygen production in the light (300 $\mu E/m^2/s$) in intact symbiotic animals and FIZ.

The FSW used for pre-incubations was discarded from each tube and replaced with 2.5 ml FSW containing 1.2×10^{-4} *M* NBT pre-warmed to the desired temperature (either 26° or 32°C). All anemones were incubated in the presence of NBT at the desired temperature for an additional 60 min. DCMU-treated anemones were exposed to 0.5 m*M* DCMU during the 60 min incubation with NBT at the desired temperature. The elevated temperature condition was set at 32°C because this is a sublethal (and environmentally relevant) temperature that evokes bleaching in *A. pulchella* (C. B. Mahnke and L. Muscatine, unpubl.).

Incubations in light were carried out by placing the test tubes containing the anemones in the reservoir of a circulating water bath (Neslab) illuminated by six 40 W fluorescent tubes (Sylvania "Cool-White"; 300 $\mu E/m^2/s$) and maintained at the desired incubation temperature. Dark incubations were conducted in a photographic darkroom illuminated only by a safelight (Kodak). After the incubations were completed, the seawater containing the NBT in each test tube was replaced by an equal vol-

ume of fresh seawater and the anemones were allowed to expand in the dark or in the light for about 30–45 min before formazan production and soluble protein content were measured.

The effect of pO_2 *on NBT reduction in intact anemones*

Hyperoxic conditions were established by bubbling 50 ml of FSW (33‰; pH 8.3) with a gas mixture containing 67% O_2, 32.97% N_2, and 0.03% CO_2 at 26°C for 60 minutes (Matta and Trench, 1991). The oxygen content of the FSW bubbled with this gas mixture was determined using a microcathode oxygen electrode (Strathkelvin Instruments). The oxygen content of the hyperoxic medium was 13.88 ml O_2/l (466 mmHg). This value is comparable to the pO_2 measured in tissues of symbiotic anemones in the light (Shick and Brown, 1977; Dykens and Shick, 1982). To control for the effect of bubbling, normoxia (4.75 ml O_2/l, 160 mmHg) was achieved by bubbling 50 ml of FSW with ambient air for 60 min.

Nine aposymbiotic *A. pulchella* were allowed to acclimate to either hyperoxic or normoxic conditions for 1 h in darkness with continuous bubbling in a 50-ml Erlenmeyer flask. The FSW containing 10^{-4} *M* NBT was prebubbled with the special gas mixture or with air for 60 min to establish either hyperoxic or normoxic conditions. A 1-h NBT reduction experiment as described earlier was then conducted with these animals in darkness. The flasks were bubbled continuously with the special gas mixture or with ambient air to maintain hyperoxic or normoxic conditions during the experiment.

NBT reduction by freshly isolated algae

A sample of FIZ containing 10^6 cells was transferred to a 10-ml test tube and centrifuged to pellet the cells. The algae were then resuspended with 2.5 ml of FSW containing 10^{-4} *M* NBT, preheated to the desired temperature. Six replicate tubes were incubated under the experimental conditions at either ambient or elevated temperature either in darkness or in the light.

Enzyme analyses

The activities of superoxide dismutase (Cu-Zn SOD and Mn SOD) and catalase (CAT) in symbiotic and aposymbiotic host tissues were determined using the methods of Lesser *et al.* (1990). The single modification was that host tissue homogenates were prepared in ice-cold 0.01 *M* phosphate buffer containing 400 m*M* NaCl (pH 8.3) and 0.1 m*M* phenylmethyl sulfonyl fluoride (PMSF).

Oxygen flux in intact anemones at ambient and elevated temperature

Dark respiration rates of intact symbiotic anemones were measured at time = 1, 20, and 60 min at both 26°C and 32°C using the method described by Hoegh-Guldberg and Smith (1989) with two modifications. First, the incubation chamber (15 ml) used for these measurements was connected to a circulating water bath set at either 26°C or 32°C. Second, between each oxygen measurement the electrode was briefly removed from the chamber and then replaced to prevent hypoxia within the chamber.

The effect of acute temperature elevation on anemone dark respiration was studied in an individual anemone after a 1-h incubation period at 26°C. The FSW in the chamber was immediately replaced with FSW preheated to 32°C, and host dark respiration was then measured over the next 60 min as described above. The FSW in the incubation chamber was changed every 15 min with a fresh volume of FSW preheated to 32°C. The anemone was then sacrificed by homogenization in 2 ml of FSW. The algae were separated from the animal tissue by centrifugation (500 × *g*) and the supernatant containing algal-free animal homogenate was then decanted and saved for analysis of soluble protein. Dark respiration rates for intact anemones are reported as microliters of O_2 consumed per hour per milligram of soluble protein (μl O_2/h/mg soluble animal protein). The soluble protein content of animal homogenates was determined using the method of Bradford (1976).

To determine the effect of acute temperature elevation on algal photosynthesis *in hospite,* oxygen flux in intact symbiotic anemones was measured in the light (300 μE/m^2/s) at ambient (26°C) and elevated temperature (32°C). First, rates of dark respiration photosynthesis for intact animals were measured at 26°C. The FSW used for these initial measurements was then replaced by FSW preheated to 32°C, and changes in the O_2 concentration were monitored for another 60 min in the light after 1, 20, and 60 min. After 60 min, the light was turned off and a final measurement of dark respiration was made.

Oxygen flux in freshly isolated algae at ambient and elevated temperature

Algae (10^6 cells) from a single anemone were resuspended in 3 ml of FSW and placed in the incubation chamber. Oxygen flux in freshly isolated algae was measured at both 26°C and 32°C over a 60-min incubation period as described for intact animals. After dark respiration and photosynthesis were measured at 26°C, 3 ml of algal suspension in the incubation chamber was removed and the algae were isolated by centrifugation (500 × *g*). The supernatant (FSW) was discarded and the algal

pellet was resuspended in 3 ml of FSW preheated to 32°C. This suspension was then returned to the incubation chamber for oxygen flux measurements in the light (300 $\mu E/m^2/s$) for another 60 min at 32°C. Algal dark respiration was measured at the beginning and end of the 60-min period. Oxygen flux for freshly isolated algae is expressed as $\mu l\ O_2/h/10^6$ cells. The concentration of FIZ was determined using a hemacytometer (Spencer Brightline) and the mean of eight separate cell counts.

Statistical analyses

Nonparametric statistical methods were used for all analyses because some data subsets within the same experiment were heteroscedastic (F_{max} test, (Sokal and Rohlf, 1981) and Kolmogorov-Smirnoff analysis (Zar, 1984)). Homoscedastic data sets were also analyzed using parametric methods; in these cases, parametric and nonparametric analyses led to identical conclusions.

Formazan production by anemones was evaluated for the effects of temperature, light, and "condition" (symbiotic versus aposymbiotic) by a nonparametric three-way analysis of variance (Zar, 1984). The effect of DCMU on NBT reduction in intact symbiotic and aposymbiotic anemones was evaluated separately because DCMU effects were investigated only in the light and not in darkness. Including DCMU results would cause an unbalanced analysis of the results obtained for the other treatments (light/temperature/condition). Treatment effects were evaluated at a significance level of 0.05.

Where significant treatment effects occurred, a nonparametric multiple comparison test based on a modification of the Kruskal-Wallis method (Zar, 1984) was applied at the 0.05 significance level to identify individual differences among data sets. The Mann-Whitney *U*-test was used to determine differences in antioxidant enzyme activities of symbiotic and aposymbiotic animal tissue homogenates and in NBT reduction by aposymbiotic anemones subjected to normoxia or hyperoxia.

Results

Superoxide ion specifically reduces NBT

To determine if superoxide ions specifically reduced NBT, we measured the effect of SOD on NBT reduction in algae-free tissue homogenates of *A. pulchella*. The addition of 100, 250, or 500 U Cu-Zn SOD to reaction mixtures inhibited NBT reduction by more than 95% (Fig. 1).

Conversely, the addition of DDC, an SOD inhibitor, to the reaction mixture increased NBT reduction by nearly 100% in mixtures that contained no SOD and in mixtures that contained 100 U SOD (Fig. 2). Neither DDC nor SOD caused NBT reduction in controls. These results strongly suggest that superoxide ion is the primary reductant of NBT in these homogenates.

We also used the SOD-inhibitable reduction of acetylated cytochrome *c* as an independent method to verify superoxide ion production in algae-free *A. pulchella* tissue homogenates. The homogenates reduced acetylated cytochrome *c* at rates comparable to positive control experiments in which superoxide ions were generated enzymatically using purified xanthine oxidase and xanthine. Xanthine oxidase reduced cytochrome *c* at a rate of 0.040 ± 0.004 absorbance units/min. *A. pulchella* tissue homogenates reduced cytochrome *c* at a rate of 0.035 ± 0.008 absorbance units/min. The addition of 10 U SOD to homogenates decreased the rate of cytochrome *c* reduction by 35% (0.023 ± 0.006 absorbance units/min). SOD added in excess of 10 U (20, 50, 100, or 200 U) did not cause any further inhibition of cytochrome *c* reduction (0.025 ± 0.005 absorbance units/min). These results show that superoxide ions are produced in algae-free *A. pulchella* tissue homogenates, despite the presence of native SOD, which interferes with the assay. These results also indicate that cytochrome *c* reduction by homogenates may still occur by alternate mechanisms.

Some studies have reported that elevated pO_2 may affect NBT reduction *in vitro* (Auclair and Voisin, 1985, Seidler and Van Noorden, 1994). To determine the effect of elevated pO_2 on NBT reduction by anemones *in vivo*, we imposed hyperoxia on aposymbiotic *A. pulchella* in darkness and then conducted an NBT reduction experiment at ambient temperature (26°C). As there was no significant difference in NBT reduction between apo-

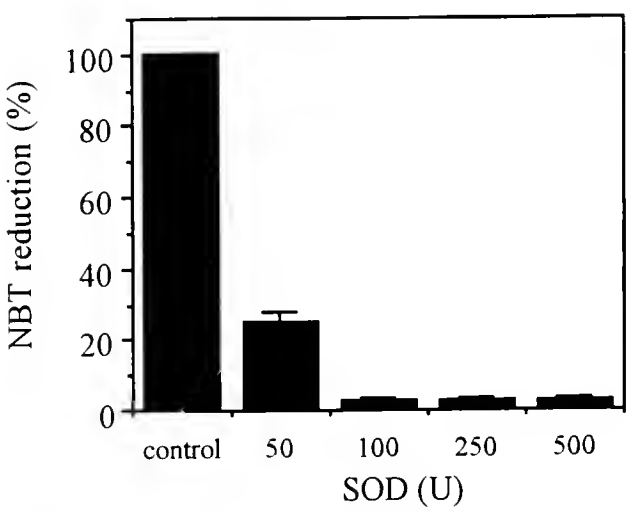

Figure 1. The effect of SOD concentration on NBT reduction in algae-free *Aiptasia pulchella* tissue homogenates. Six anemones were homogenized individually. From each homogenate a sample was taken for NBT reduction at each SOD concentration. Each bar represents the mean ± SD of the six samples.

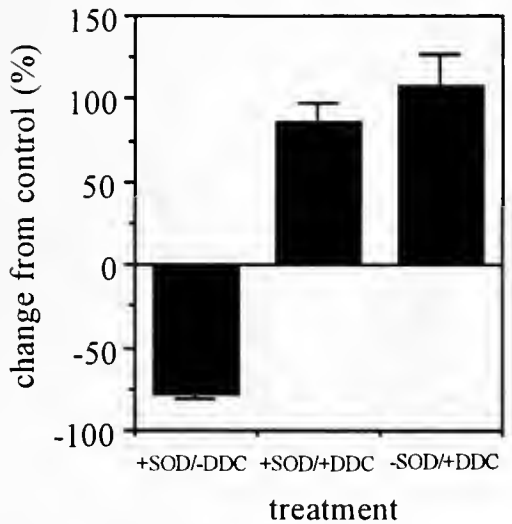

Figure 2. The effect of 1 m*M* DDC on NBT reduction by algae-free *Aiptasia pulchella* tissue homogenates. Six anemones were homogenized individually. From each homogenate a sample was taken for NBT reduction under the following conditions: +SOD/−DDC; +SOD/+DCC; and −SOD/+DDC. Controls contained neither DDC nor SOD. Each bar represents the mean ± SD of the percent increase or decrease in NBT reduction compared to controls determined for the six samples.

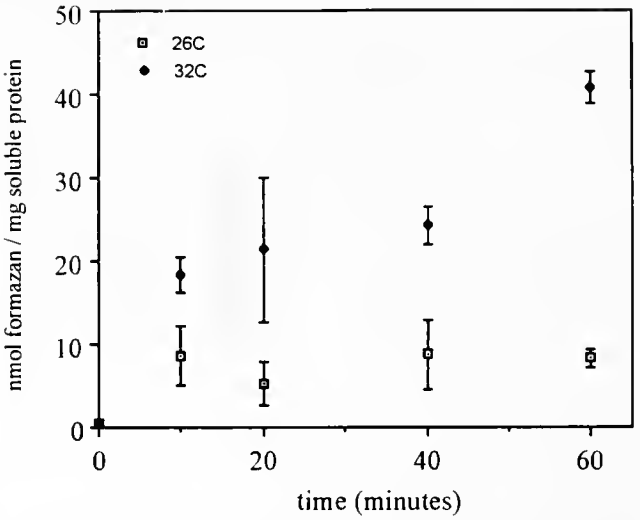

Figure 4. Time course of NBT reduction by symbiotic *Aiptasia pulchella* at 26° and 32°C. Two groups of 12 anemones were selected for a 60-min NBT reduction experiment at either ambient (26°C) or elevated (32°C) temperature. Three anemones at each temperature were sacrificed 1, 20, 40 and 60 min after starting the experiment, and the amount of NBT formazan produced by each anemone was measured. Each point represents the mean ± SD for three anemones per time point.

symbiotic anemones under hyperoxia or normoxia (Mann-Whitney *U*, $P > 0.10$; Fig. 3), it appears that elevated pO_2 does not influence NBT reduction by these organisms.

Acute thermal stress causes oxidative stress in intact symbiotic anemones

To determine if acute thermal stress causes oxidative stress in intact symbiotic anemones, we measured the production of NBT formazan in the animal tissues of anemones exposed to ambient (26°C) and elevated temperature (32°C). A 60-min incubation was sufficient to resolve differences in NBT reduction between control anemones and those exposed to acute thermal stress (Fig. 4).

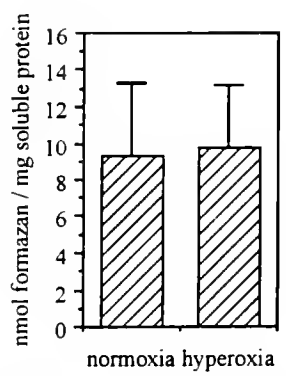

Figure 3. The effect of hyperoxia on NBT reduction by aposymbiotic *Aiptasia pulchella*. Groups of three anemones were acclimated to either normoxia or hyperoxia for 60 min in darkness at 26°C. A 60-min NBT reduction experiment using these anemones was then conducted under normoxia or hyperoxia. The amount of NBT formazan produced by each anemone was then measured. Each bar represents the mean ± SD for nine anemones per treatment.

Temperature had a significant effect on formazan production by symbiotic anemones (ANOVA, $P < 0.001$). Symbiotic *A. pulchella* produced significantly more formazan at 32°C in both darkness and light, and in the presence of DCMU than at 26°C (Fig. 5). Neither light (ANOVA, $P > 0.25$) nor DCMU (ANOVA, $P > 0.25$) had a significant effect on formazan production in intact anemones at either ambient or elevated temperature. Except for the significant interaction between light and temperature (ANOVA, $P < 0.05$), there were no significant interactions between temperature, light, and "condition" (ANOVA, all $P > 0.10$) in either intact symbiotic or aposymbiotic anemones. These results show that acute thermal stress increases superoxide ion production and that the increase may be independent of the presence of algae.

Is oxidative stress an "animal" rather than an "algal" phenomenon?

To further investigate the observation that symbiotic algae may be sufficient but not necessary for oxidative

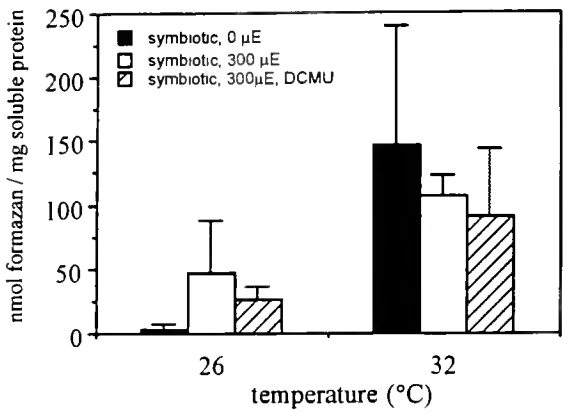

Figure 5. Superoxide production by symbiotic *Aiptasia pulchella* at ambient (26°C) and elevated (32°C) temperature in darkness, in light, and in light in the presence of 0.5 m*M* DCMU. Groups of six anemones were used in each treatment. A 60-min NBT reduction experiment was then conducted under each defined condition, after which the amount of formazan produced by each anemone was measured. Each bar represents the mean ± SD for six anemones per treatment.

stress to occur in these anemones, aposymbiotic *A. pulchella* were exposed to FSW containing 10^{-4} *M* NBT in both darkness and light at both ambient and elevated temperature. Figure 6 shows that temperature had a significant effect on formazan production by intact aposymbiotic anemones (ANOVA, $P < 0.001$): in darkness and light these anemones produced significantly more formazan at elevated temperature (Kruskal-Wallis, $P < 0.001$). Neither light nor DCMU had a significant effect in aposymbiotic anemones (ANOVA, $P > 0.50$ and $P > 0.25$, respectively). Interestingly, at ambient temperature, formazan production in darkness was significantly higher by aposymbiotic anemones than by symbiotic anemones in darkness (Kruskal-Wallis, $P < 0.01$).

Do symbiotic algae release superoxide ions?

Because NBT does not penetrate intact algae and remains in the external medium (Nii, unpubl. obs.), it can be used to measure the possible release of superoxide ion by FIZ.

To determine if symbiotic algae release superoxide ions, FIZ from *A. pulchella* were incubated in FSW containing 10^{-4} *M* NBT under the following incubation conditions: ambient and elevated temperature; darkness or light; and with or without DCMU. If superoxide ions are released by the algae, these radicals should then reduce NBT present in the external medium. NBT can detect the presence of superoxide ions in nanomolar concentration (>5 nmol; Auclair and Voisin, 1985). However, formazan was not detected in the external medium under any of the incubation conditions (data not shown). If these algae released superoxide ions under these experimental conditions, the amount was less than 5 nmol.

SOD and CAT activity in symbiotic and aposymbiotic A. pulchella

To determine if differences in NBT reduction were related to the ability of the host to detoxify potential oxidants, the specific activities of Cu-Zn SOD, Mn SOD, and CAT were measured in animal homogenates prepared from symbiotic and aposymbiotic *A. pulchella*. The specific activities of Cu-Zn SOD (Mann-Whitney *U*; $P < 0.05$, Fig. 7), Mn SOD (Mann-Whitney *U*, $P < 0.05$, Fig. 7), and CAT (Mann-Whitney *U*, $P < 0.05$, Fig. 8) were significantly higher in aposymbiotic anemones than in symbiotic ones. The specific activity of CAT was an order of magnitude higher in aposymbiotic *A. pulchella*. These results suggest that aposymbiotic anemones may be subject to chronic oxidative stress.

The effect of acute thermal stress on oxygen flux by intact anemones and FIZ

In a 60-min incubation, acute thermal stress immediately increased the dark respiration rate of intact symbiotic anemones more than twofold (Fig. 9). Further, the time course of the rate increase (Q_{10} = 14.1) resembled the apparent time course of NBT reduction (Q_{10} = 34.2) by anemones at elevated temperature (Fig. 4).

Net oxygen flux in intact anemones was relatively constant in the light at ambient temperature (26°C; Table 1). However, within 20 min of the initiation of acute ther-

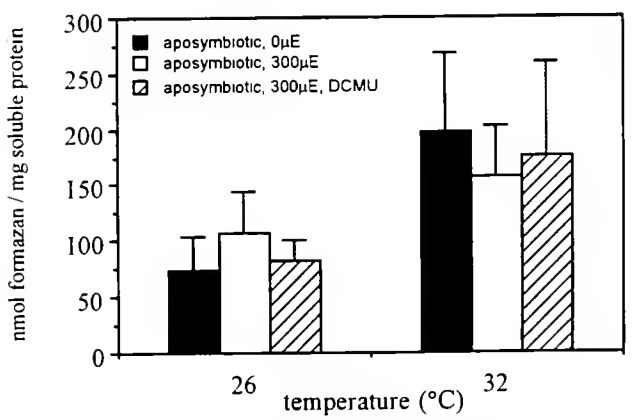

Figure 6. Superoxide production by aposymbiotic *Aiptasia pulchella* at ambient (26°C) and elevated (32°C) temperature in darkness, in light, and in light in the presence of 0.5 m*M* DCMU. Groups of six anemones were used in each treatment. A 60-min NBT reduction experiment was then conducted under each defined condition, after which the amount of formazan produced by each anemone was measured. Each bar represents the mean ± SD for six anemones per treatment.

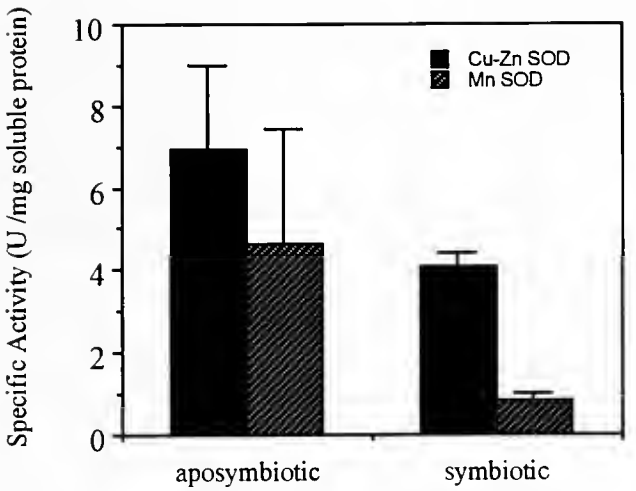

Figure 7. Specific activities (U/mg soluble protein) of Cu-Zn SOD and Mn SOD in symbiotic and aposymbiotic *Aiptasia pulchella*. Six anemones were homogenized individually. From each homogenate, samples were taken for SOD measurement. Each bar represents the mean ± SD of the six homogenates.

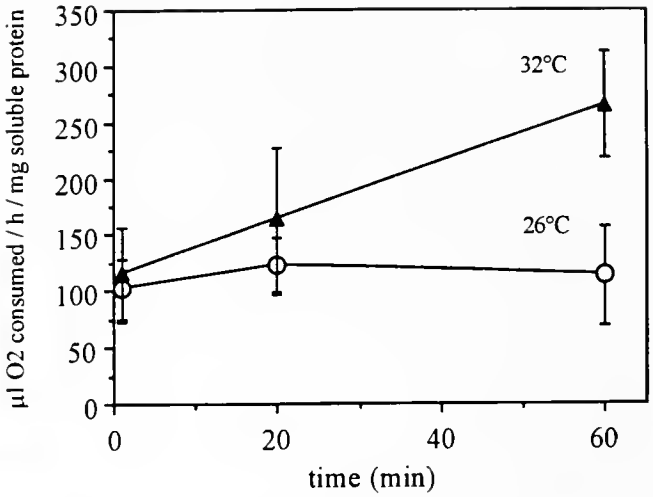

Figure 9. Time course of the dark respiration response of intact anemones to acute thermal stress. Dark respiration by an individual anemone was measured first at 26°C over 60 min (at 1, 20, and 60 min). The 26°C seawater was then immediately replaced with seawater preheated to 32°C. Dark respiration was then measured for another 60 min at 32°C (at 1, 20, and 60 min). Each point represents the mean ± SEM for three anemones.

mal stress, net oxygen production by intact anemones ceased (32°C; Table I). After 60 min, intact anemones began to consume oxygen in the light at rates comparable to their dark respiration rates at elevated temperature (Table I).

Net oxygen flux in FIZ also decreased dramatically within 20 min after exposure to elevated temperature (Table I). This decrease was accompanied by an increase in dark respiration. There was considerable variability in the mean response of FIZ to elevated temperature. In three of the five experiments performed, net oxygen consumption in the light began within 20 min of exposing the FIZ to elevated temperature. Although net oxygen production was observed in the two remaining experiments, the rates were <20% of the net flux at ambient temperature. Further, in two of the five experiments, dark respiration rates increased more than fivefold at elevated temperature. These results suggest that the molecular oxygen produced by algae during acute thermal stress is mostly consumed by the algae themselves.

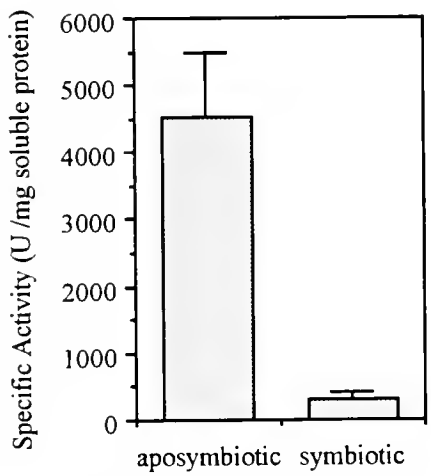

Figure 8. Specific activity (U/mg soluble protein) of CAT in symbiotic and aposymbiotic *Aiptasia pulchella*. Six anemones were homogenized individually. From each homogenate, samples were taken for CAT measurement. Each bar represents the mean ± SD of the six homogenates.

Discussion

Acute thermal stress causes oxidative stress in intact anemones

Our results show that superoxide ions are produced within symbiotic and aposymbiotic specimens of *Aiptasia pulchella* in response to acute thermal stress. Interestingly, production of superoxide ions at elevated temperature was not affected by exposing anemones to light and DCMU. Moreover, net oxygen production in the light ceases when either intact anemones or FIZ are subjected to acute thermal stress. These results strongly suggest that, in response to acute thermal stress, oxidative stress in *A. pulchella* is largely an animal rather than an algal phenomenon. Symbiotic algae are sufficient but not necessary for the manifestation of oxidative stress in host tissues at elevated temperature.

Table I

Net oxygen flux for intact Aiptasia pulchella *and freshly isolated* Symbiodinium pulchrorum, *in light (300 μE/m²/s) and darkness, exposed to ambient (26°C) and acutely elevated (32°C) temperature*

Process	Temperature (°C)	Time after exposure	Net oxygen flux* (mean ± 1 SEM) Intact anemones[1] (μl O_2/h/mg soluble protein)	Net oxygen flux* (mean ± 1 SEM) Freshly isolated algae[2] (μl O_2/h/10^6 cells)
Photosynthesis	26°		58.80 ± 13.95	8.49 ± 0.59
	32°			
		0 min	12.75 ± 2.10	9.14 ± 5.30
		20 min	−10.95 ± 4.50	2.63 ± 3.66
		60 min	−38.85 ± 9.60	2.02 ± 2.70
Dark respiration	26°		−14.70 ± 4.80	−5.55 ± 0.96
	32°		−39.30 ± 8.40	−8.68 ± 2.50

*A negative value indicates net oxygen consumption.
[1] $N = 3$.
[2] $N = 5$.

Superoxide production in animal tissues

Despite the caveats regarding tissue homogenates (Dykens *et al.*, 1992; Verde and McCloskey, 1996), we measured superoxide production in *A. pulchella* tissue homogenates by using two independent methods (SOD-inhibitable NBT and cytochrome *c* reduction), and we find evidence to support the interpretation that superoxide ion is the primary reductant of NBT in these anemones. The inhibition of NBT reduction by SOD and increase in NBT reduction in the presence of the inhibitor, DDC, is consistent with this interpretation. Further, because *A. pulchella* tissue itself exhibits SOD activity, both methods (NBT or cytochrome *c* reduction) may actually underestimate the amount of superoxide ion produced either in homogenates or in intact animals due to SOD interference with each assay. We also observed that the addition of the SOD did not completely inhibit cytochrome *c* reduction. This result is not entirely surprising considering the complex, dynamic nature of tissue homogenates. Although acetylated cytochrome *c* has been shown to resist reduction specifically by mitochondrial cytochrome *c* reductases (Azzi *et al.*, 1975), other reductases released during homogenization may still reduce cytochrome *c* under the assay conditions.

The effect of molecular oxygen on NBT reduction in intact anemones

The reduction in photosynthetic oxygen production by intact symbiotic anemones and by FIZ at elevated temperature argues against the possible confounding effects of molecular oxygen on NBT reduction. Molecular oxygen is thought to compete with NBT for reductants (*i.e.* electrons; see Halliwell and Gutteridge, 1987, for a discussion of this hypothetical phenomenon), which may result in a decreased and therefore inaccurate estimation of NBT reduction by superoxide ions. However, the evidence for the existence of such competition is equivocal (Seidler, 1991). In this study, we demonstrate empirically that elevated pO_2 does not affect NBT reduction in aposymbiotic *A. pulchella* during imposed hyperoxia (Fig. 3). We attribute the lack of hyperoxic enhancement in these aposymbiotic anemones primarily to their increased antioxidant enzyme activity (compared to symbiotic anemones).

We noticed that the magnitude of NBT reduction in the aposymbiotic anemones used in the hyperoxia experiment was lower than that in other experiments (Figs. 3 and 6). This is probably due in part to differences in the antioxidant enzyme activities present in aposymbiotic *A. pulchella*, as well as to differences in the soluble protein content of the aposymbiotic specimens used in the different experiments. The animals used in the hyperoxia experiment contained similar amounts of protein, but this amount was up to 10 times higher than that in animals used in other experiments. This difference may be due in part to changes in the maintenance regime for aposymbiotic anemones (*i.e.*, feeding on *Artemia* adults rather than nauplius larvae), as well as to poorly understood variation in these artificially generated aposymbiotic animals. Nevertheless, under these conditions, tissue-specific NBT reduction by aposymbiotic anemones was three times that of symbiotic anemones at ambient temperature.

Symbiotic algae do not release superoxide

The lack of detectable NBT reduction by FIZ incubated in FSW containing NBT preheated to the identical temperatures used in whole-animal experiments (26°

and 32°C) indicates that, at least *in vitro*, little (<5 nmol), if any, superoxide ion is released by the algae to the medium during acute thermal stress. Although it is possible that other oxidant species such as hydrogen peroxide (H_2O_2) may be released from the algae during environmental stress (Lesser *et al.*, 1990, Lesser, 1996a), three observations argue against this conjecture: (1) algae exhibit robust antioxidant activity (Lesser and Shick, 1989; Matta and Trench, 1991); (2) transport of superoxide ions is relatively slow (Fisher, 1987); and (3) oxidant species are highly reactive (Dykens *et al.*, 1992). Tytler and Trench (1988) did not detect the release of H_2O_2 from cultured symbionts *in vitro*, although H_2O_2 can cross biological membranes more readily than superoxide ions (*cf.* Lesser, 1996). Our short-term, acute stress experiments with *S. pulchrorum* do not exclude the possibility that exposure to chronic stress may cause symbiotic algae to release oxidants directly (Lesser *et al.*, 1990). However, there is yet no published evidence that oxidants are released directly by symbiotic algae under any defined condition (Lesser, 1996).

Does hyperoxia contribute to oxidative stress in intact anemones during thermal stress?

Hoegh-Guldberg and Smith (1989) observed greatly reduced net oxygen production in intact corals exposed to chronic temperature stress, and Iglesias-Prieto *et al.* (1992) showed that in cultured *Symbiodinium*, net oxygen flux decreases precipitously *in vitro* at nonlethal temperatures exceeding 31°C. In the present study, at elevated temperature, net oxygen production in anemones and FIZ ceases, probably because of impairment of photosynthetic electron transport at or near the reaction center of PSII (Warner *et al.*, 1996). As photosynthetic oxygen production is greatly reduced, any oxidative stress attributed directly to hyperoxia in symbiotic anemone tissues (Dykens and Shick, 1982) is also greatly reduced. Our results show that, whereas symbiotic algae may contribute to hyperoxia, they are not required for the evocation of oxidative stress in these anemones at elevated temperature.

On the other hand, it remains unclear from our data whether photosynthesis has actually ceased at elevated temperature as it is not possible to measure oxygen flux due to photosynthesis and respiration in the light simultaneously (Table 1). Net oxygen flux could be reduced, in part, by the increase in dark respiration of the host (Fig. 9). That is, the oxygen produced within the algae could be consumed by the algae before it diffuses into host tissues. However, a very low, but positive, net oxygen flux was sometimes observed in FIZ during exposure to elevated temperature (Table 1). This observation suggests that oxygen production may still occur within the algae at elevated temperature, but may be largely masked by the increase in algal respiration.

At ambient temperature, the slightly elevated production of superoxide ions by symbiotic anemones in the light compared with those in darkness is probably due to hyperoxia generated in the host cytoplasm as a result of algal photosynthesis (Shick and Brown, 1977; Dykens and Shick, 1982). However, hyperoxia cannot account for oxidative stress in aposymbiotic anemones during acute thermal stress in darkness or light. These results suggest that superoxide ion production may be limited by the supply of electrons or other excitatory inputs such as photodynamic effects (Valenzano and Pooler, 1987; Dykens *et al.*, 1992; Lesser, 1996) that can participate in univalent reduction of available molecular oxygen, rather than by the supply of molecular oxygen itself.

Do aposymbiotic anemones experience chronic oxidative stress?

We observed that superoxide ion production by aposymbiotic *A. pulchella* in darkness at ambient temperature was significantly higher than superoxide ion production by symbiotic anemones under the same conditions (Figs. 5 and 6). To account for this observation, we assessed the activities of the antioxidant enzymes superoxide dismutase (SOD) and catalase (CAT) in aposymbiotic versus symbiotic *A. pulchella*. We found significant differences in the specific activities of Cu-Zn SOD, Mn SOD, and CAT between the two forms of the anemone. The specific activity of Mn SOD was fivefold higher in aposymbiotic anemones. The MnSOD activity in aposymbiotic *A. pulchella* is much higher than MnSOD activity reported for other eukaryotic organisms (Asada *et al.*, 1980), including symbiotic dinoflagellates (Lesser and Shick, 1989; Matta and Trench, 1991). The CAT activities measured using a spectrophotometric method were very similar to CAT activities measured previously using a polarigraphic method (Tytler and Trench, 1988). Like Tytler and Trench (1988), we also found that the specific activity of CAT was an order of magnitude higher in aposymbiotic specimens.

At present, we find it difficult to explain the increased MnSOD activity observed in aposymbiotic *A. pulchella*. The increase may represent one of potentially many, and as yet uncharacterized, physiological changes which occur in *A. pulchella* when it is rendered aposymbiotic due to cold shock. Overexpression of MnSOD in aposymbiotic individuals may be a response to increased heterotrophy or may reflect an increase in mitochondrial density. The former explanation is difficult to reconcile as Asada *et al.* (1977) found that *Euglena gracilis* raised phototrophically has almost three times the SOD activity of *E. gracilis* raised heterotrophically. The latter expla-

nation also seems unlikely because the protein-specific dark respiration rates for symbiotic and aposymbiotic *A. pulchella* are very similar (Nii, unpubl.). We infer from the increased MnSOD and CAT activities in aposymbiotic *A. pulchella* that these anemones may manifest chronic (oxidative) stress, although the origin of this condition is still unknown.

The origin of increased superoxide production at elevated temperature

The dark respiration rate of symbiotic *A. pulchella* triples under acute thermal stress (Fig. 9). The time course of host dark respiration over 60 min (Fig. 9) resembles the time course of formazan production by anemones at elevated temperature (Fig. 4). The Q_{10} values calculated for the respective processes are very different, but both reflect the acute sensitivity of each process to elevated temperature. These observations suggest that increased respiration by the animal host may contribute to an increase in the rate of electron leakage from mitochondrial electron transport and may account, in part, for the increased production of superoxide ions (Burdon *et al.*, 1990; Richter *et al.*, 1995; Garcia-Ruiz *et al.*, 1995; Van-Fleteren and De Veese, 1996).

Our results also suggest that in these anemones, superoxide is produced primarily within the host. Animal cells have many sites of superoxide generation (Bendich, 1989). Production of superoxide ion has been localized between complexes I and III of the mitochondrial electron respiratory chain at the sites of NADH dehydrogenase (Krishnamoorthy and Hinkle, 1988; Turrens and Boveris, 1980) and ubiquinone (Nohl and Jordan, 1984). Other potential sites for active oxygen production in the host cell include the respiratory chain enzymes NADH-ubiquinone reductase and NADH-cytochrome b_5 reductase, xanthine oxidase, and the lipid metabolism enzymes NADPH-cytochrome P_{450} reductase and δ-9-desaturase (Bendich, 1989).

How are oxidative stress and cnidarian bleaching related?

Direct comparison between our results using NBT and other studies of oxidative stress in symbiotic cnidarians is difficult, largely because of differences in the species; contrast between intact animals, FIZ and cultured algae; and dissimilarities in the methods used in recent studies attempted *in vivo*. On the basis of enhanced antioxidant enzyme activities in symbiont and host, Lesser *et al.* (1990) concluded that elevated temperature caused oxidative stress and bleaching in *Palythoa caribaeorum*. Dykens *et al.* (1992), using a methane sulfinic acid bioassay for hydroxyl radicals *in vivo*, found greater oxidant production within the symbionts (*S. californium*) of *Anthopleura elegantissima* than in host tissues. They also observed enhanced hydroxyl radical production in *S. californium* due to chronic UV radiation exposure, but did not investigate the effects of elevated temperature in either the symbiont or the host. More recently, Lesser (1996) measured increased production of superoxide ion and hydrogen peroxide in cultured algae (*S. bermudense* from *Aiptasia pallida*) due to chronic elevated temperature and UV radiation; specific fluorochromes were used for each oxidant species. Using these observations as a point of departure, we now advance the hypothesis that oxidative stress may also represent an animal response to acute thermal stress, and we suggest that the symbiont may not necessarily be required for oxidative stress to occur under these conditions.

The link between oxidative stress and cnidarian bleaching is still unknown. The production of active oxygen species can lead to a number of damaging effects, including the peroxidation of membrane lipids (Gutteridge, 1987) or the direct disruption of cell adhesion molecules by oxygen radicals. Such damage may then lead to release of host cells (Gates *et al.*, 1992). As the host animal alone may manifest oxidative stress—that is, without the contribution of photosynthetic oxygen by symbiotic algae—oxidative stress originating in host cells may explain the correlation observed between high rates of colony respiration and thermal bleaching in reef corals (Jokiel and Coles, 1990; P. Edmunds, in prep.). The inherent susceptibility of host cells themselves to oxidative stress may be an important mechanistic link between temperature stress and cnidarian bleaching.

Acknowledgments

We thank Drs. J. Dykens, P. Edmunds, R. Gates, M. Lesser, J. M. Shick, R. K. Trench, and three anonymous reviewers for critically evaluating earlier versions of the manuscript, and D. Nii for editorial assistance. This work was supported by NSF grant OCE # 9115834.

Literature Cited

Asada, K., S. Kanematsu, and K. Uchida. 1977. Superoxide dismutases in photosynthetic organisms: absence of the cuprozinc enzyme in eukaryotic algae. *Arch. Biochem. Biophys.* **179:** 243–256.

Asada, K., S. Kanematsu, S. Oka, and T. Hayakawa. 1980. Phylogenic distribution of superoxide dismutase in organisms and in cell organelles. Pp. 136–153 in *Chemical and Biochemical Aspects of Superoxide and Superoxide Dismutase*, J.V. Bannister and H.A.O. Hill, eds. Elsevier/North-Holland, Amsterdam.

Auclair, C., and E. Voisin. 1985. Nitroblue tetrazolium reduction. Pp. 123–132 in *CRC Handbook of Methods for Oxygen Radical Research*, R.A. Greenwald, ed. CRC Press, Boca Raton, FL.

Azzi, A., C. Montecucco, and C. Richter. 1975. The use of acetylated ferricytochrome *c* for the detection of superoxide radicals produced in biological membranes. *Biochem. Biophys. Res. Commun.* **65:** 597–603.

Banaszak, A. T., R. Iglesias-Prieto, and R. K. Trench. 1993. *Scrippsiella velellae* sp. nov., Peridiniales and *Gloedinium viscum* sp. nov., Phytodiniales, dinoflagellate symbionts of two hydrozoans (Cnidaria). *J. Phycol.* **29:** 517–528.

Bendich, A. 1989. Antioxidant nutrients and immune functions: an introduction. Pp. 1–12 in *Antioxidant Nutrients and Immune Functions*, A. Bendich, M. Phillips, and R. Tengerdy, eds. Pergamon Press, New York.

Boveris, A., and E. Cardenas. 1982. Production of superoxide radicals and hydrogen peroxide in mitochondria. Pp. 15–30 in *Superoxide Dismutase*, L.W. Oberly, ed. CRC Press, Boca Raton, FL.

Bradford, M. M. 1976. A rapid and sensitive method for the quantitation of microgram quantities of protein utilising the principle of protein-dye binding. *Anal. Biochem.* **72:** 248–254.

Brown, B. E., M. D. A. Le Tissier, and J. C. Bythell. 1995. Mechanisms of bleaching deduced from histological studies of reef corals sampled during a natural bleaching event. *Mar. Biol.* **122:** 655–66.

Burdon, R. H., V. Gill, and C. Rice Evans. 1990. Active oxygen and heat shock protein induction. Pp. 19–25 in *Stress Proteins*, M.J. Schlesinger, M.G. Santoro, and E. Garaci, eds. Springer-Verlag, Heidelberg.

Chacon, E., and D. Acosta. 1991. Mitochondrial regulation of superoxide by Ca^{2+}: an alternate mechanism for the cardiotoxicity of doxorubicin. *Toxicol. Appl. Pharmacol.* **107:** 117–128.

Coles, S. L., and P. L. Jokiel. 1977. Effects of temperature on photosynthesis and respiration in hermatypic corals. *Mar. Biol.* **43:** 209–216.

Dykens, J. A. 1984. Enzymic defenses against oxygen toxicity in marine cnidarians containing endosymbiotic algae. *Mar. Biol. Lett.* **5:** 291–301.

Dykens, J. A., and J. M. Shick. 1982. Oxygen production by endosymbionts control superoxide dismutase activity in their animal host. *Nature* **297:** 579–580.

Dykens, J. A., and J. M. Shick. 1984. Photobiology of the symbiotic sea anemone, *Anthopleura elegantissima:* defenses against photodynamic effects, and seasonal photoacclimitization. *Biol. Bull.* **167:** 693–697.

Dykens, J. A., J. M. Shick, C. Benoit, G. R. Buettner, and G. W. Winston. 1992. Oxygen radical production in the sea anemone *Anthopleura elegantissima* and its endosymbiotic algae. *J. Exp. Biol.* **168:** 219–241.

Enger, P. A., and T. W. Kensler. 1985. Effects of a biomimetic superoxide dismutase on complete and multistage carcinoma in mouse skin. *Carcinogenesis* **6:** 1167–1172.

Fisher, A. B. 1987. Intracellular production of oxygen-derived free radicals. Pp. 34–39 in *Oxygen Radicals and Tissue Injury*, B. Halliwell, ed. Federation of American Studies for Experimental Biology, Bethesda, MD.

Fisk, T. A., and T. J. Done. 1985. Taxonomic and bathymetric patterns of bleaching in corals, Myrmidon Reef (Queensland). *Proc. Fifth Intl. Coral Reef Congr.* **6:** 149–154.

Flohé, L., and F. Otting. 1984. Superoxide dismutase assays. Pp. 93–104 in *Methods in Enzymology*, L. Packer, ed. Academic Press, New York.

Garcia-Ruiz, C., A. Colell, A. Morales, N. Kaplowitz, and J.C. Fernandez-Checa. 1995. Role of oxidative stress generated from the mitochondrial electron transport chain and molecular glutathione status in loss of mitochondrial function and activation of transcription factor nuclear factor-kappa B: studies with isolated mitochondria and rat hepatocytes. *Mol. Pharmacol.* **48:** 825–834.

Gates, R. D., G. Baghdasarian, and L. Muscatine. 1992. Temperature stress causes host cell detachment in symbiotic cnidarians: implications for coral bleaching. *Biol. Bull.* **182:** 324–332.

Glynn, P. W. 1990. Coral mortality and disturbances to coral reefs in the tropical eastern Pacific. Pp. 55–126 in *Global Ecological Consequences of the 1982-83 El Nino-Southern Oscillation*, P.W. Glynn, ed. Elsevier, Amsterdam.

Glynn, P. W., and L. D'Croz. 1990. Experimental evidence for high temperature stress as the cause of El-Nino coincident coral mortality. *Coral Reefs* **8:** 181–192.

Gutteridge, J. M. C. 1987. Lipid peroxidation: some problems and concepts. Pp. 9–19 in *Oxygen Radicals and Tissue Injury*, B. Halliwell, ed. Federation of American Societies for Experimental Biology, Bethesda, MD.

Halliwell, B., and J. M. C. Gutteridge. 1987. *Free Radicals in Biology and Medicine, 2nd Edition.* Blackwell, London, p. 75.

Hoegh-Guldberg, O., and G. J. Smith. 1989. The effect of sudden changes in temperature, light and salinity on population density and export of zooxanthellae from the reef corals *Seriatopora hystrix* and *Stylophora pistillata*. *J. Exp. Mar. Biol. Ecol.* **129:** 279–303.

Iglesias-Prieto, R., J. L. Matta, W. A. Robins, and R. K. Trench. 1992. Photosynthetic response to elevated temperature in the symbiotic dinoflagellate *Symbiodinium microadriaticum* in culture. *Proc. Natl. Acad. Sci. USA* **89:** 10302–10305.

Kleppel, G. S., R. E. Dodge, and C. J. Reese. 1989. Changes in pigmentation associated with the bleaching of stony corals. *Limnol. Oceangr.* **34:** 1331–1335.

Krishnamoorthy, G., and P. C. Hinkle. 1988. Studies on the electron transfer pathway, topography of iron sulfur centers and sites of coupling in NADH-Q oxido-reductase. *J. Biol. Chem.* **263:** 566–575.

Lesser, M. P. 1996. Elevated temperature and ultraviolet radiation cause oxidative stress and inhibit photosynthesis in symbiotic dinoflagellates. *Limnol. Oceangr.* **41:** 271–283.

Lesser, M.P., and J.M. Shick. 1989. Effects of irradiance and ultraviolet radiation on photoadaptation in the zooxanthellae of *Aiptasia pallida:* primary production, photoinhibition and enzymatic defenses against oxygen toxicity. *Mar. Biol.* **102:** 243–255.

Lesser, M. P., W. R. Stochaj, D. W. Tapley, and J. M. Shick. 1990. Bleaching in coral reef anthozoans: effects of irradiance, ultraviolet radiation and temperature on the activities of protective enzymes against active oxygen. *Coral Reefs* **8:** 225–232.

Matta, J. L., and R. K. Trench. 1991. The enzymatic response of the symbiotic dinoflagellate *Symbiodinium microadriaticum* (Freundenthal) to growth under varied oxygen tensions. *Symbiosis* **11:** 31–45.

Nohl, H., and W. Jordan. 1984. The biochemical role of ubiquinone and ubiquinone-derivatives in the generation of hydroxyl radicals from hydrogen peroxide. Pp. 155–160 in *Oxygen Radicals in Chemistry and Biology*, W. Bors, M. Saran, and D. Tait, eds. Walter de Gruyter, Berlin.

Porter, J. W., W. K. Fitt, H. J. Spero, C. S. Rogers, and M. W. White. 1989. Bleaching in reef corals: physiological and stable isotopic responses. *Proc. Natl. Acad. Sci. USA* **86:** 9342–9346.

Richter, C., V. Gogvadze, R. Laffranchi, R. Schalpbach, M. Schweizer, M. Suter, P. Walter, and M. Yaffee. 1995. Oxidants in mitochondria: from physiology to diseases. *Biochim. Biophys. Acta* **1271:** 67–74.

Seidler, E. 1991. The tetrazolium-formazan system: design and histochemistry. *Progr. Histochem. Cytochem.* **24:** 1–86.

Seidler, E., and C. J. F. Van Noorden. 1994. On the mechanism of tetrazolium salts with special reference to the involvement of tetrazolium radicals. *Acta Histochem.* **96:** 43–49.

Shick, J. M., and W. I. Brown. 1977. Zooxanthellae-produced O_2 promotes sea anemone expansion and eliminates oxygen debt under environmental hypoxia. *J. Exp. Zool.* **201:** 149–155.

Shick, J. M., M. P. Lesser, and W. R. Stochaj. 1991. Ultraviolet radiation and photooxidative stress in zooxanthellate anthozoa: the

sea anemone *Phyllodiscus semoni* and the octocoral *Clavularia* sp. *Symbiosis* **10:** 145–173.

Shick, J. M., M. P. Lesser, W. C. Dunlap, W. R. Stochaj, B. E. Chalker, and J. Wu Won. 1995. Depth-dependent responses to solar ultraviolet radiation and oxidative stress in the zooxanthellate coral *Acropora microphthalma*. *Mar. Biol.* **122:** 41–51.

Sokal, R. R., and F. J. Rohlf. 1981. *Biometry, 2nd edition.* W.H. Freeman, New York. 859 pp.

Steen, R. G., and L. Muscatine. 1987. Low temperature evokes rapid exocytosis of symbiotic algae by a sea anemone. *Biol. Bull.* **172:** 246–263.

Szmant, A. M., and N. J. Gassman. 1990. The effects of prolonged bleaching on the tissue biomass and reproduction of the reef coral *Montastrea annularis*. *Coral Reefs* **8:** 217–224.

Thom, S. M., R. W. Horobin, E. Seidler, and M. R. Barer. 1993. Factors affecting the selection and use of tetrazolium salts as cytochemical indicators of microbial viability and activity. *J. Appl. Bacteriol.* **74:** 433–443.

Turrens, J. F., and A. Boveris. 1980. Generation of superoxide anion by the NADH dehydrogenase of bovine heart mitochondria. *Biochem. J.* **191:** 501–507.

Tytler, E. M., and R. K. Trench. 1988. Catalase activities in cell-free preparations of various invertebrate hosts. *Symbiosis* **5:** 247–254.

Valenzano, D. P., and J. P. Pooler. 1987. Photodynamic action. *BioScience* **37:** 270–276.

VanFleteren, J. R., and A. DeVreese. 1996. Rate of aerobic metabolism and superoxide rate production in the nematode *Caenorhabditis elegans*. *J. Exp. Zool.* **274:** 93–100.

Verde, E. A., and L. R. McCloskey. 1996. Carbon budget studies of symbiotic cnidarian anemones—evidence in support of some assumptions. *J. Exp. Mar. Biol. Ecol.* **195:** 161–171.

Warner, M. E., W. K. Fitt, and G. W. Schmidt. 1996. The effects of elevated temperature on the photosynthetic efficiency of zooxanthellae *in hospite* from four different species of reef coral: a novel approach. *Plant Cell and Environ.* **19:** 291–299.

Zar, J. H. 1984. *Biostatistical Analysis, 2nd edition.* Prentice-Hall, Englewood Cliffs, N.J. 718 pp.

INDEX

D

E

F

G

H

I

J

K

L

M

N

O

P

R

S

T

U

V

W

X

Y

Z

Time gain through flexibility

The new LEICA DM RB/E microscope for biological and medical applications is a complete innovation in modern microscopy. With its new infinity optics it is prepared for all contrast techniques.

Due to the integrated modular design it can be exactly tailored to your personal criteria simply by adding the necessary components.

The unique motor focus with coded septuple objective nosepiece makes work highly efficient – you'll be amazed at the amount of time you save.

DAS Mikroskop LEICA DM RB/E stands for:

- *Superb results even in the border regions of the spectrum*
- *Optimum contrast and extremely high resolution*

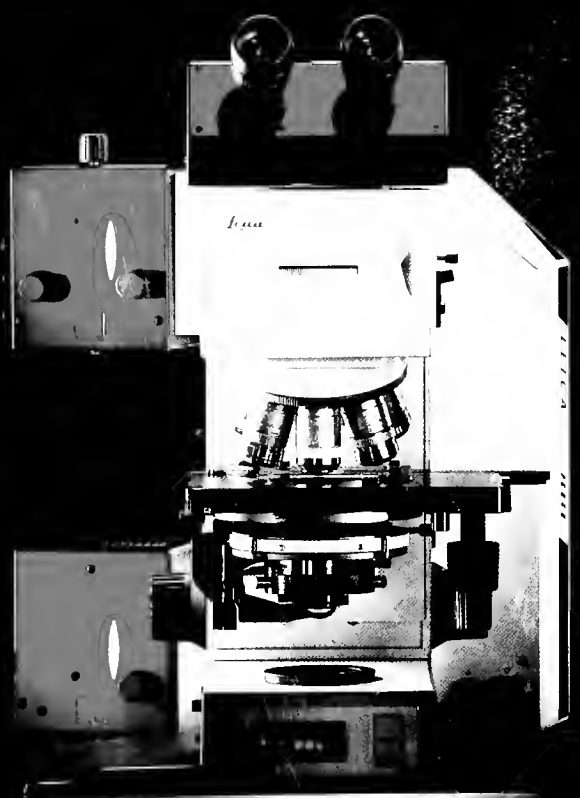

w.leica.com

Leica